AD-A154 031 PROPAGATION INFLUENCES ON DIGITAL TRANSMISSION SYSTEMS: 1/6
PROBLEMS AND SOLU..(U) ADVISORY GROUP FOR AEROSPACE
RESEARCH AND DEVELOPMENT NEUILLY.. J H BLYTHE
UNCLASSIFIED 08 JUN 84 AGARD-CP-363 F/G 17/2 NL

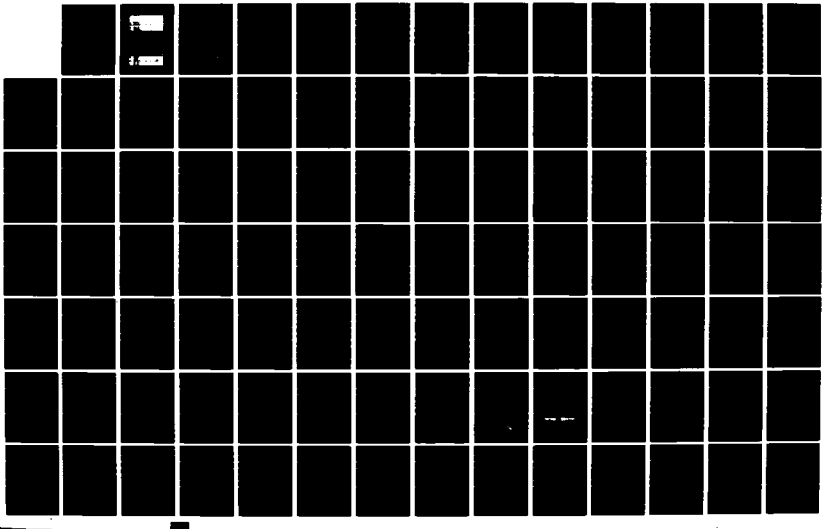

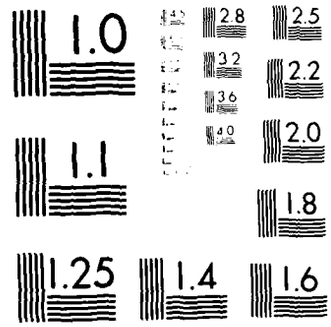

MICROCOPY RESOLUTION TEST CHART

REPRODUCED AT GOVERNMENT EXPENSE

AGARD-CP-363

AGARD

ADVISORY GROUP FOR AEROSPACE RESEARCH & DEVELOPMENT

7 RUE ANCELLE 92200 NEUILLY SUR SEINE FRANCE

AGARD CONFERENCE PROCEEDINGS No.363

Propagation Influences on Digital Transmission Systems: Problems and Solutions

NORTH ATLANTIC TREATY ORGANIZATION

DISTRIBUTION AND AVAILABILITY
ON BACK COVER

DTIC
ELECTE
JAN 30 1985

85 01 14 147

NORTH ATLANTIC TREATY ORGANIZATION

ADVISORY GROUP FOR AEROSPACE RESEARCH AND DEVELOPMENT

(ORGANISATION DU TRAITE DE L'ATLANTIQUE NORD)

AGARD Conference Proceedings No.363

PROPAGATION INFLUENCES ON DIGITAL TRANSMISSION SYSTEMS – PROBLEMS AND SOLUTIONS

Edited by

Dr John H.Blythe

DTIC
ELECTE
JAN 25 1985
A

Papers presented at the Electromagnetic Wave Propagation Panel Symposium held in Athens, Greece, 4–8 June 1984.

THE MISSION OF AGARD

The mission of AGARD is to bring together the leading personalities of the NATO nations in the fields of science and technology relating to aerospace for the following purposes:

Exchanging of scientific and technical information;

Continuously stimulating advances in the aerospace sciences relevant to strengthening the common defence posture;

Improving the co-operation among member nations in aerospace research and development;

Providing scientific and technical advice and assistance to the North Atlantic Military Committee in the field of aerospace research and development;

Rendering scientific and technical assistance, as requested, to other NATO bodies and to member nations in connection with research and development problems in the aerospace field;

Providing assistance to member nations for the purpose of increasing their scientific and technical potential;

Recommending effective ways for the member nations to use their research and development capabilities for the common benefit of the NATO community.

The highest authority within AGARD is the National Delegates Board consisting of officially appointed senior representatives from each member nation. The mission of AGARD is carried out through the Panels which are composed of experts appointed by the National Delegates, the Consultant and Exchange Programme and the Aerospace Applications Studies Programme. The results of AGARD work are reported to the member nations and the NATO Authorities through the AGARD series of publications of which this is one.

Participation in AGARD activities is by invitation only and is normally limited to citizens of the NATO nations.

The content of this publication has been reproduced
directly from material supplied by AGARD or the authors.

Published October 1984

Copyright © AGARD 1984
All Rights Reserved

ISBN 92-835-0367-8

Printed by Specialised Printing Services Limited
40 Chigwell Lane, Loughton, Essex IG10 3TZ

THEME

As digital transmission systems become more widespread, and as data rates continually increase, the problems posed by propagation effects become more severe, and are the subject of much current research. This research, scattered amongst the NATO nations, is being conducted in frequency bands and for systems which are of great military importance. For example, at HF there is a need for air-ground communication links at 2.4 kbps and above which is a difficult technical problem because of multipath effects and man-made interference, as well as naturally occurring noise effects. In the VHF/UHF bands ECM resistant systems are being developed, the performance of which will be strongly influenced by propagation effects, such as jammer detection range and hence jammer reaction time, etc. In the microwave bands, line-of-sight and troposcatter are used extensively on trunk routes which will increasingly become digital links. At the moment the propagation problems, particularly multipath, are not well codified and the best technical solutions are not clear.

The meeting reviewed propagation effects which have an influence on the performance of digital systems, including: noise level and system sensitivities to noise; man-made interference types and system sensitivities to man-made interference; and multipath effects, dispersion, fading rates medium coherent bandwidth, channel models, and system sensitivities to these effects. The meeting also reviewed systems designed to counter the above effects, including the various kinds of adaptive systems, and assessed the performance improvements which they can provide. The Avionics Panel assisted in the preparation of this Symposium.

* * * *

Au fur et à mesure que les systèmes de transmission numérique se généralisent et que s'accroissent les débits de données, les effets de la propagation posent des problèmes plus critique qui font l'objet d'une somme considérable de recherches. Ces recherches, reparties entre les pays de l'OTAN, sont menées dans des bandes de fréquence et pour des systèmes qui présentent une importance extrême au plan militaire. C'est ainsi que, dans le domaine des ondes décamétriques, la nécessite de liaisons air-sol a 2,4 kbps et plus s'impose, ce qui crée un délicat problème technique en raison des échos, des interférences créées par l'homme, ainsi que des effets des bruits naturels. Dans les bandes d'ondes métriques et décimétriques sont actuellement développés des systèmes résistants aux contre-mesures électroniques dont le fonctionnement sera fortement influencé par les effets de la propagation tels que portée de détection — d'où temps de réaction — des brouilleurs, etc. Dans les bandes de micro-ondes, il est largement fait appel à la ligne de visée et à la diffusion troposphérique le long des itinéraires principaux qui deviendront de plus en plus des liaison numériques. Pour le moment, les problèmes que pose la propagation, en particulier celle qui s'effectue sous plusieurs angles, ne sont pas bien codifiés et les meilleurs solutions techniques n'apparaissent pas clairement.

Au cours de la réunion étaient examinés les effets de la propagation sur le fonctionnement des systèmes numériques; entre autres: niveaux de bruit et sensibilité des systèmes au bruit; types d'interférences créées par l'homme et sensibilité des systèmes à ces types d'interférences; échos, dispersion, taux d'affaiblissement, largeur de bande cohérente moyenne, modèles de canaux et sensibilité des systèmes à ces effets. Etaient également étudiés les systèmes adaptifs, en même temps qu'étaient évaluées les améliorations de fonctionnement que permettent ces systèmes. Le Panel d'Avionique apportait son concours à la préparation de ce Symposium.

Accession For
NTIS
DTIC TAB

INTRODUCTION

Papers presented at the meeting covered all aspects of the theme, so that these Conference Proceedings present a rather comprehensive survey of the current state of the art. It cannot be claimed that all the problems have been solved definitively, but a wide range of possible techniques were described, and it is clear that system designers have a rich set of resources at their disposal.

The meeting was arranged in a number of sessions, each with its own Session Chairman, and these Proceedings follow the same arrangement. Papers in each Session are preceded by a Session Summary, provided by the Session Chairman, which will enable readers to obtain quickly an overview of papers in the Session. The first paper in each Session (except IIB) was an invited Review Paper. Each paper was followed by a period of discussion, some of which is given here using for the most part Question and Answer sheets provided by the individuals concerned. In a few cases it was necessary to edit tape recordings. Following each Session (except Session I) a more general discussion took place, and this has been reproduced verbatim as far as possible, using a tape recording, with the editing necessary in the conversion from the spoken word to the written word. The editor hopes that this process has not distorted the speakers' thoughts but it is felt that the inclusion of this informal material, containing a number of interesting suggestions, will enhance the value of this volume, to participants and non-participants alike.

J.H.BLYTHE
Editor

ELECTROMAGNETIC WAVE PROPAGATION PANEL

Chairman: Dr J.H.Blythe
Communications Research Lab.
Marconi Research Centre
West Hanningfield Road, Gt Baddow
Chelmsford, Essex, CM2 8HN
UK

Deputy Chairman: Dr H.Soicher
US Army Communications
Electronic Cmd
Center for Communications
Systems
Attn. DRSEL-COM-RN-1
Fort Monmouth N.J. 07703
USA

TECHNICAL PROGRAMME COMMITTEE

Dr J.H.Blythe (Co-Chairman)
Marconi Research Centre
Great Baddow
Chelmsford, CM2 8HN
UK

Dr W.Utlaut (Co-Chairman)
Director, ITS/NTIA
Department of Commerce
Boulder, CO 80303
USA

COMMITTEE

Dr F.J.Diamond, US
Prof. C.Goutelard, FR
Prof. A.N.Ince, TU
Dr E.W.Lampert, GE
Ir. J.T.Neessen, NE
Prof. S.M.Scheggi, IT

HOST NATION COORDINATOR

Dr Mavrokoukoulakis
Technology Research Centre, KETA
Delta Falirou
Palaion Faliron
Athens
Greece

PANEL EXECUTIVE

Lt. Colonel L.B.Russell
AGARD-OTAN
7, rue Ancelle
92200 Neuilly-sur-Seine
France
Telephone: (1) 745 0810 Telex: 610176 F

From US and Canada
AGARD-NATO
APO New York 09777

CONTENTS

	Page
THEME	iii
INTRODUCTION	iv
MEETING AND PANEL OFFICIALS	v

	Reference
SESSION I – PROPAGATION CONSTRAINTS TO RELIABLE DIGITAL COMMUNICATIONS	
CHAIRMAN'S SUMMARY	CSI
LIMITS OF THE PROPAGATION MEDIUM WITH RESPECT TO DIGITAL SIGNAL TRANSMISSION by E.W.Lampert	1
PROPAGATION OF WIDE BANDWIDTH SIGNALS IN A TROPOSPHERIC DUCTING MEDIUM by N.K.Uzunoğlu	2
DIGITAL DATA COMMUNICATIONS OVER MICROWAVE RADIO CHANNELS by J.Salz	3
THE AIR-TO-AIR COMMUNICATIONS by P.N.Edraos	4
PROPAGATION INFLUENCES ON THE PERFORMANCE OF A REDUCED BANDWIDTH QUADRATURE PHASE SHIFT KEYED DIGITAL RADIO SYSTEM by J.E.Doble	5
EQUATORIAL TRANS-IONOSPHERIC PROPAGATION CONDITIONS AFFECTING DIGITAL COMMUNICATIONS by J.Aarons	6
PROPAGATION EFFECTS ON THE DOPPLER FREQUENCY SHIFT OF SATELLITE TRANSMISSIONS by G.H.Millman and M.C.Arabadjis	7
INFLUENCE DE LA PROPAGATION DANS LES FAISCEAUX HERTZIENS NUMERIQUES par J.Bursztejn	8
THE IMPACT OF PROPAGATION EFFECTS ON THE DESIGN OF HIGH CAPACITY DIGITAL MICROWAVE LINKS IN THE 18 GHz FREQUENCY BAND by L.van der Hoek, A.Mawira and J.Neessen	9

SESSION II A – RECENT PROGRESS IN PROPAGATION MEASUREMENTS AND PROPAGATION MODELS	
CHAIRMAN'S SUMMARY*	CSIIA
A REVIEW OF ATMOSPHERIC MULTIPATH MEASUREMENTS AND DIGITAL SYSTEM PERFORMANCE by R.W.Hubbard	10
THE COMMUNICATIONS THROUGH FORESTED PROPAGATION CHANNELS by A.Schneider	11
MULTIPATH AND DOPPLER OBSERVATIONS DURING TRANSATLANTIC DIGITAL HF PROPAGATION EXPERIMENTS by B.W.Remisch, K.Bibl, M.Ahmed, H.Soicher, F.Gorman and J.C.Jodogne	12

* Not available at time of printing.

Reference

AN IONOSPHERIC MODE DETECTION SYSTEM FOR HF DATA COMMUNICATIONS APPLICATION
by I.B.Jones and P.L.Hayhurst 13

WIDEBAND LINE-OF-SIGHT CHANNEL MEASUREMENTS AND SIMULATION: APPLICATION TO DIGITAL RADIO LINKS
by R.Valentin and K.Metzger 14

DESIGN CRITERIA FOR LIMITED SCAN ANTENNAS AT DIGITAL MICROWAVE LINE OF SIGHT LINKS
by L.P.Lighthart 15

DISCUSSION OF SESSION II A DIIA

SESSION II B – RECENT PROGRESS IN PROPAGATION MEASUREMENTS AND PROPAGATION MODELS

CHAIRMAN'S SUMMARY CSIIB

A COMPARISON BETWEEN PREDICTED AND MEASURED PROPAGATION LOSS IN THE VHF/UHF RANGE IN RUGGED TERRAIN
by K.Besserudhagen, N.Klippenberg and M.Norland 16

SOME PROPAGATION EXPERIMENTAL RESULTS ON PROTECTION TECHNIQUES FOR LINE-OF-SIGHT DIGITAL SYSTEMS
by F.Fabbri 17

SYSTEME DE MESURE DES CARACTERISTIQUES DU CANAL IONOSPHERIQUE POUR LES TRANSMISSIONS NUMERIQUES
par Y.M.Le Roux, L.Bertel, J.P.Jolivet, P.Lassudrie-Duchesne et H.Rouault 18

MESURES DE PROPAGATION EN ZONE URBAINE A 900 MHz POUR L'ETABLISSEMENT D'UN SYSTEME RADIOMOBILE NUMERIQUE
par C.Havel and A.Maloberti 19

MEASUREMENTS AND PREDICTIONS OF MULTIPATH DISPERSION FOR TROPOSCATTER LINKS
by R.Larsen 20

DISCUSSION OF SESSION II B DIIB

SESSION III – CHANNEL SIMULATION

CHAIRMAN'S SUMMARY CSIII

DIGITAL SIMULATION OF COMMUNICATIONS CHANNELS: AN OVERVIEW
by J.C.Holtzman and K.S.Shanmugan 21

LOS MICROWAVE CHANNEL SIMULATION – A SURVEY OF MODELS, REALIZATIONS AND NEW CONCEPTS
by J.A.Hoffmeyer and W.J.Hartman 22

SIMULATION OF THE PERFORMANCE OF ADAPTIVELY CONTROLLED NAVSTAR ANTENNAS IN BATTLEFIELD SCENARIOS
by F.Klinker and O.B.M.Pietersen 23

AN HF SIMULATOR FOR USE WITH REAL TIME CHANNEL EVALUATION SYSTEMS
by J.Dawson 24

ETUDE THEORIQUE D'UN SIMULATEUR DYNAMIQUE D'EVANOUISSEMENTS SELECTIFS POUR FAISCEAUX HERTZIENS NUMERIQUES
par A.Bouidene et P.Vandamme 25

DISCUSSION OF SESSION III DIII

Reference

SESSION IV – SIGNAL PROCESSING TECHNOLOGY

CHAIRMAN'S SUMMARY — CSIV

ADAPTIVE SIGNAL PROCESSING FOR RADIO COMMUNICATIONS
by P.Monsen — 26

FAST SYNCHRONISATION MODEM FOR THE SPREAD-SPECTRUM COMMUNICATION SYSTEM
by R.Skaug and H.Olaisen — 27

A TECHNICAL SOLUTION TO FADINGS IN SATELLITE DIGITAL TRANSMISSIONS
by G.Losquadro and A.Lorenzoni — 28

Paper 29 withdrawn

TIME AND SPACE DOMAIN FILTERING FOR IMPROVED HF COMMUNICATION
by R.N.Smith and R.L.Moses — 30

OVERVIEW OF RADC ADAPTIVE ANTENNA DEVELOPMENTS FOR COMMUNICATIONS
by J.A.Graneiro, C.J.Lavera and J.R.Periard — 31

TRANSMISSION ASYNCHRONE A FORT ETALEMENT DE SPECTRE
par M.Schilliger et C.Leloup — 32

Paper 33 withdrawn

DISCUSSION OF SESSION IV — DIV

SESSION V – SIGNALLING AND SOUNDING SCHEMES FOR RELIABLE DIGITAL COMMUNICATIONS

CHAIRMAN'S SUMMARY — CSV

A REVIEW OF TRANSMISSION AND CHANNEL EVALUATION TECHNIQUES FOR DIGITAL COMMUNICATION SYSTEMS
by M.Darnell — 34

Paper 35 withdrawn

MODEM A CODES PSEUDO-ORTHOGONAUX: RESULTATS EXPERIMENTAUX
par F.Chavand, D.Desage, C.Goutelard et J.P.Van Uffelen — 36

CODAGE CORRECTEUR D'ERREURS POUR MODEM AUTO ADAPTATIF, RESULTATS THEORIQUES ET EXPERIMENTAUX
par F.Chavand, C.Goutelard et S.Harari — 37

A MICROPROCESSOR CONTROLLED PARALLEL MODEM WITH EDPSK
by H.F.Buding — 38

TRANSMISSION DE DONNEES SERIE A GRAND DEBIT SUR CANAL HF
par J.P.Van Uffelen et A.Deconche — 39

FAST DATA AND VOICE TRANSMISSION FOR MOBILE SERVICES WITH HIGH IMMUNITY AGAINST MULTIPATH AND CO-CHANNEL INTERFERENCE
by U.Langewellpott — 40

"NARROWBAND" SPREAD SPECTRUM SYSTEMS
by K.H.Anneeke and M.Ottka — 41

EFFECTIVE MILLIMETERWAVE TRANSMISSION UNDER SEVERE MULTIPATH CONDITIONS
by U.Schulz and G.Hofgen — 42

DISCUSSION OF SESSION V — DV

LIST OF PARTICIPANTS — P

SUMMARY OF SESSION I

PROPAGATION CONSTRAINTS TO RELIABLE DIGITAL COMMUNICATIONS

by

Prof. C.Goutelard
Session Chairman

La session I a été consacrée aux contraintes de la propagation sur la qualité des transmissions numériques.

Au cours de cette session les différents auteurs et les intervenants ont abordé quatre points fondamentaux:

- les phénomènes physiques de la propagation et leur manifestation au niveau des systèmes,
- la définition et la modélisation des canaux,
- l'importance du choix des signaux
- les solutions techniques utilisables compte tenu de l'état de l'art.

Dans la première conférence le Docteur E.W.Lampert a développé son exposé à partir de trois phénomènes fondamentaux de la propagation qui affectent le signal: le rapport signal/bruit, les trajets multiples et les fadings, le bruit et les interférences. Ces facteurs sont discutés dans les différentes gammes de fréquences et des illustrations concrètes étayent cette présentation. L'auteur conclut en signalant l'importance relative de ces différents facteurs et de leurs conséquences sur l'élaboration des systèmes.

Deux exposés à caractère théorique ou général ont ensuite été présentés.

La communication du Docteur Uzunoğlu a porté sur un travail théorique de propagation d'un signal large bande dans les conduits troposphériques. A partir de la théorie électromagnétique de la propagation, et en tenant compte de la polarisation des ondes, l'auteur établit par la transformée de Fourier inverse la réponse du canal à une modulation PSK. Il présente alors pour différents canaux, des résultats numériques de probabilités d'erreurs. Les résultats théoriques sont utilisables dans un grand nombre de configurations.

Le Docteur J.Salz, lui, a traité d'un problème général de transmissions numériques micro ondes à travers un canal affecté d'un fading sélectif. L'influence des trajets multiples y est examinée à partir du modèle de Rummler et l'auteur évalue les performances d'une modulation QAM en introduisant un indice d'efficacité qui lui sert de référence. Un système de prédistorsion à l'émission est proposé dans une solution auto-adaptive pour améliorer la qualité de la transmission.

Deux exposés on été consacrés aux liaisons terre-satellites.

Celui du Docteur J.Aarons traite des effets ionosphériques sur les transmissions satellite-terre dans la région équatoriale. Cette étude est orientée vers les gammes de fréquence utilisées dans les liaisons maritimes. L'auteur présente un ensemble important de mesures qu'il relie aux anomalies de l'ionosphère équatoriale ainsi que des statistiques sur ces phénomènes. Les solutions techniques susceptibles d'améliorer les transmissions sont ensuite examinées.

Le Docteur G.H.Millman présente une étude sur les erreurs introduites par la réfraction des ondes dans l'ionosphère sur le décalage doppler dans les liaisons satellite-terre. Dans une première étude théorique l'auteur examine séparément les effets de l'ionosphère et de la troposphère.

L'effet de la fréquence de l'onde qui agit de façon inverse dans l'ionosphère et la troposphère est étudié. Les résultats de l'étude, présentés pour différentes trajectoires de satellites, sont utilisables comme données de base.

Deux exposés sont consacrés aux systèmes de transmission numériques par ondes troposphériques ou en vision directe.

Monsieur J.Bursztejn a présenté une méthode de détermination des paramètres permettant d'effectuer la prédiction de la qualité des liaisons hertziennes par diffusion troposphériques et à vue directe à 7 GHz. Cette étude qui s'appuie sur un ensemble de mesures effectuées sur des liaisons réelles conduit à des formules empiriques dont l'auteur montre la validité. L'application de cette étude permet d'évaluer le dimensionnement, les dispositifs à mettre en oeuvre pour atteindre les qualités souhaitées.

Le Docteur J.E. Doble a présenté, quant à lui, un système de transmissions numériques dans la bande 6 GHz utilisant une modulation quadriphase à bande réduite. Une expérimentation de deux ans sur une liaison de 51 km et utilisant différentes diversités de réception fournit les résultats de base. L'auteur discute de l'efficacité des méthodes et des systèmes utilisables pour augmenter la robustesse de la transmission vis-à-vis des trajets multiples, du fading et du bruit.

Deux auteurs présentent des communications sur les systèmes opérant à des fréquences supérieures à 10 GHz.

Le Docteur J.Neessen traite dans son exposé des effets de la propagation sur les systèmes de transmission numériques à haut débit à 18 GHz. A partir d'un modèle de propagation proposé par l'auteur, les paramètres significatifs qui affectent la qualité de la liaison sont examinés et leur influence discutée en vue d'une prédiction. Les résultats sont confrontés aux mesures effectuées sur deux liaisons expérimentales.

Le Docteur P.N.Eldiasy s'est intéressé aux problèmes de transmission air-air à faible probabilité d'interception. Il présente une étude effectuée dans la gamme EHF en utilisant pour cela des fréquences situées dans les bandes d'absorbtion de l'oxygène atmosphérique, plus précisément dans la bande des 60 GHz. Les contraintes de la propagation sont d'abord analysées et les systèmes et leurs performances sont examinés pour un certain nombre de situations et en tenant compte de l'état de l'art.

Cette première session a donc joué un rôle introductif important dans ce congrès en redéfinissant spontanément son objectif qui couvrant, par sa couverture, la plupart de ses horizons et en établissent d'emblée une large discussion.

EFFECTS OF THE PROPAGATION MEDIUM ON DIGITAL SIGNAL TRANSMISSION

by Ernst W. Lampert
Siemens-Aktiengesellschaft
Hofmannstraße 51
8000 München 70, FRG

SUMMARY

The effects of the propagation medium are more pronounced in digital communication systems than in analog ones, in particular when considering single channel systems. The quality parameters: bit-error-rate and link availability are affected not only by the received signal level but also by multipath propagation which may result in frequency selective fading or just in a too low signal level when changing the modulation in a variable system or signal fading when the medium is time variable. While fading decreases the available ratio of links (within short or long time intervals), frequency selective fading causes irreducible interference and distortion which results in classical systems in an irreducible error rate.

In the HF frequency region, HF- up to SHF different propagation modes are dominant, propagation effects have to be discussed individually for each region. In HF for short distances ground waves show no multipath effect, however, when the skywave becomes dominant over long distances, the received signal is the sum of several discrete multipath components which may have differential delays up to 5 ms.

In the UHF, SHF region the multipath behavior is almost continuous in the terrestrial, mobile scenario and the maximum of the delay spread depends on the area to be covered by the system. In airborne communication the specular reflected signals interfere with the direct path, so that frequency selective fading is introduced.

For LOS-links the typical multipath geometry is presented and data for coherence bandwidth and fading rate are given.

Tropospheric scatter can only be used in digital FDM-systems. It is shown that present systems are rather power limited than interference limited. In digital troposcatter systems selective fading due to the mutual differential delay of the modal components is a limiting factor especially in digital systems. Delay spread specifications are discussed with respect to geometry and layer structure.

Apart from the well known effect that the quality of the received signal is influenced by interference, which can be either man-made, such as noise in general or ignition noise in particular. Other sources of interference are multiple users of the same channel or jammer sources, the effectivity of both depend on the applied modulation methods.

1. Introduction

The paper starts from the basic properties of the electromagnetic wave propagation medium with respect to digital signal transmission, it is intended to point out why there are differences with respect to analog transmission and in what cases the phenomena may be treated alike.
Generally, digital transmission is felt to be more tolerant against interference and distortion. This tolerance is however not merely an attribute of the link but also related to source and sink. In analog systems the whole transmission and reception, eye and ear are involved and therefore information can be interpreted in the brain, as in transmission usually a fair share of redundancy is contained. - In modern digital transmission systems, especially when encrypted and also furthermore source and sink are data processing equipment the requirements for correct transmission have to be more stringent.

The quality of a link is usually described in terms of the errors produced while transmitting information. Most frequently this is done by the bit-error-rate (ber). In most cases this figure cannot fully describe a channel when burst properties are present and also in conjunction with bursty interference. We then have periods of relatively few errors, followed by blocks with an error rate of almost 0.5, a situation which is not tolerated by data transmission equipment because of their data protocols (e.g. HDLC within computer to computer communication).

Another important effect is the fact that whether a link outage occurs because of the lack of signal power, or because of time dispersion, or lack of synchronization in coherent modulation systems is of great significance, the system designer should be able to separate the effects in order to improve the system performance.

2. Basic Propagation Effects

The basic propagation effects are perturbations in the received signal strength, a parameter which is of importance for the type of service transmission. Often it is claimed that there is a difference between analog and digital transmission (particularly with voice!) The difference between analog and digital transmission is based on what is regarding the fading of the channel. The characteristics of the different media have to be presented in terms of measurable figures, which then can be used by the system designer.

Besides fading, interference is important. In the case of noise, the effectiveness of the thermal receiver noise is the result of the received signal strength and therefore will not be dealt with separately. Atmospheric noise (spherics and man-made noise in the HF-region and above are very much dependent on the propagation effects. This also applies to the general problem of cochannel interference.

DISCUSSION

L.Boithias, Fr

Compte tenu de l'etendue extremement grande (10 a 10) de la gamme des valeurs numeriques de parametres de propagation (retards de propagation, debits binaires), y a t'il des possibilites d'aide mutuelle entre les techniques utilisees dans les differentes gammes de frequences?

Author's Reply

Hopefully, during this conference, people dealing with different problems of, e.g. SHF-LOS or HF, will find that because they both have to cope with multipath, they find that these are methods which can have a rather general usage.

C.Goutelard, Fr

Les trajets multiples sont toujours traites comme des signaux parasites. En fait ce sont des sources redondantes que l'on peut utiliser et des etudes theoriques montrent qu'ils permettent de reduire le taux d'erreurs. Disposez-vous d'informations sur ce sujet?

Author's Reply

In principle one always can make positive use of multipath signal components as long as one can separate them from each other, i.e. in a frequency selection situation. Making use of the RAKE-receiver principle a reduction in fading margin up to 10dB seems to be realistic.

[illegible]	[illegible]	[illegible]	[illegible]	[illegible]	[illegible]
[illegible]	[illegible]	[illegible]	[illegible]	[illegible]	[illegible]
[illegible]	[illegible]	[illegible]	[illegible]	[illegible]	[illegible]
[illegible]	[illegible]	[illegible]	[illegible]	[illegible]	[illegible]
[illegible]	[illegible]	[illegible]	[illegible]	[illegible]	[illegible]

[illegible] Relevant effects for different scenarios

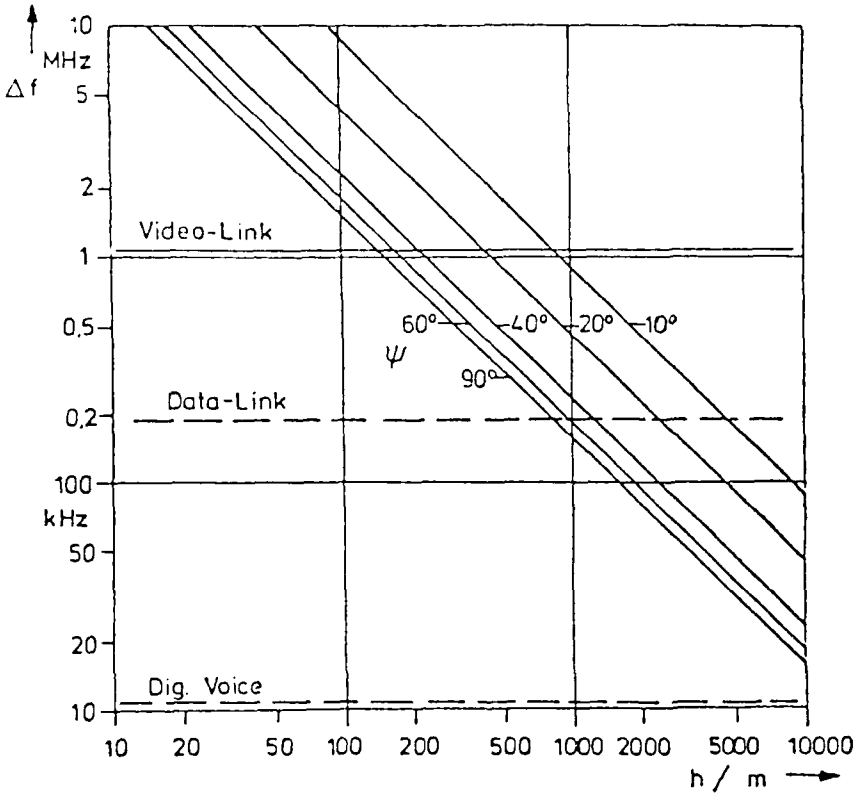

Fig. 8 maximum data rate for air-ground links using elassical modulation

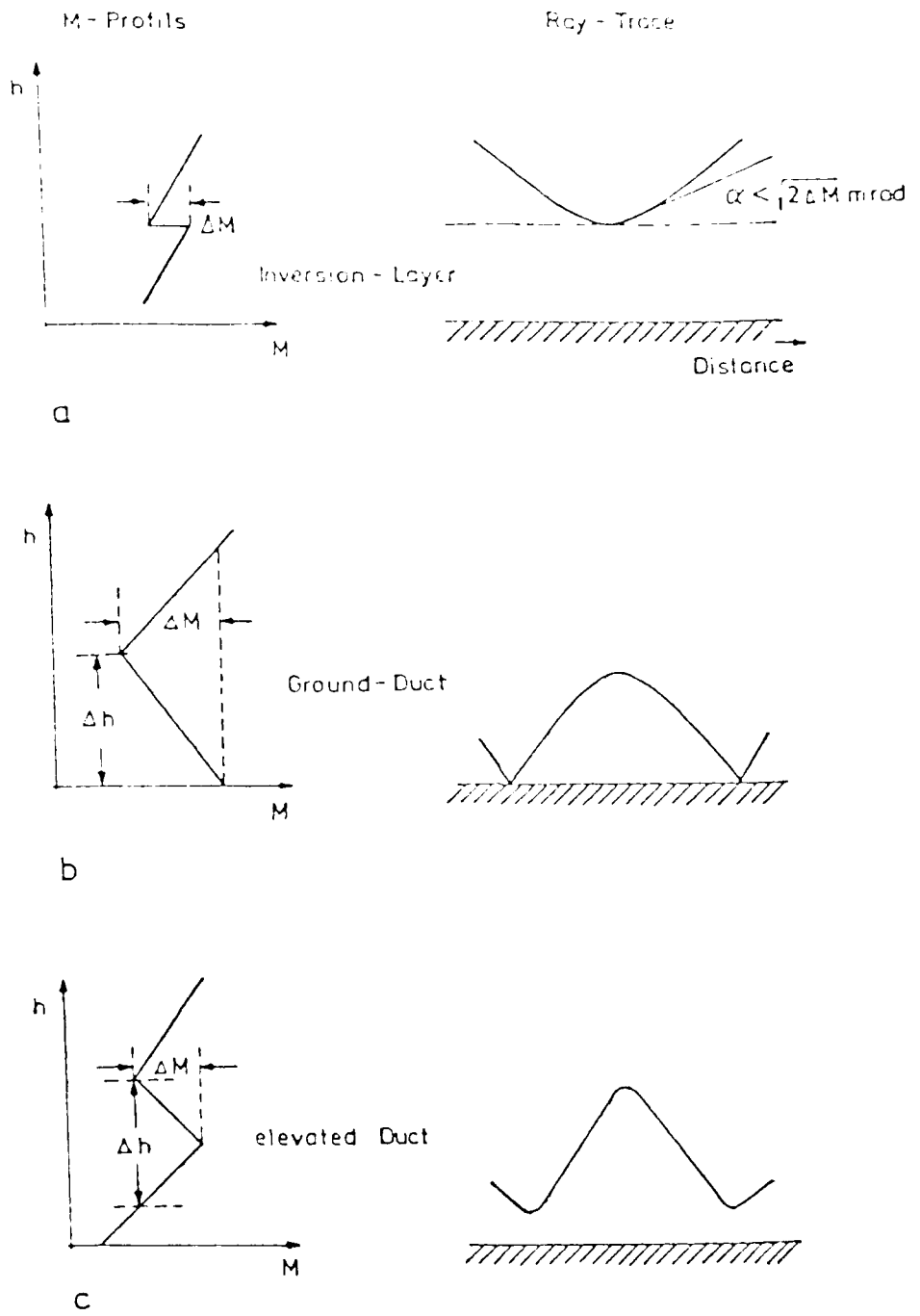

Fig. 7 Inversion Layer and duct effects in the lower troposphere

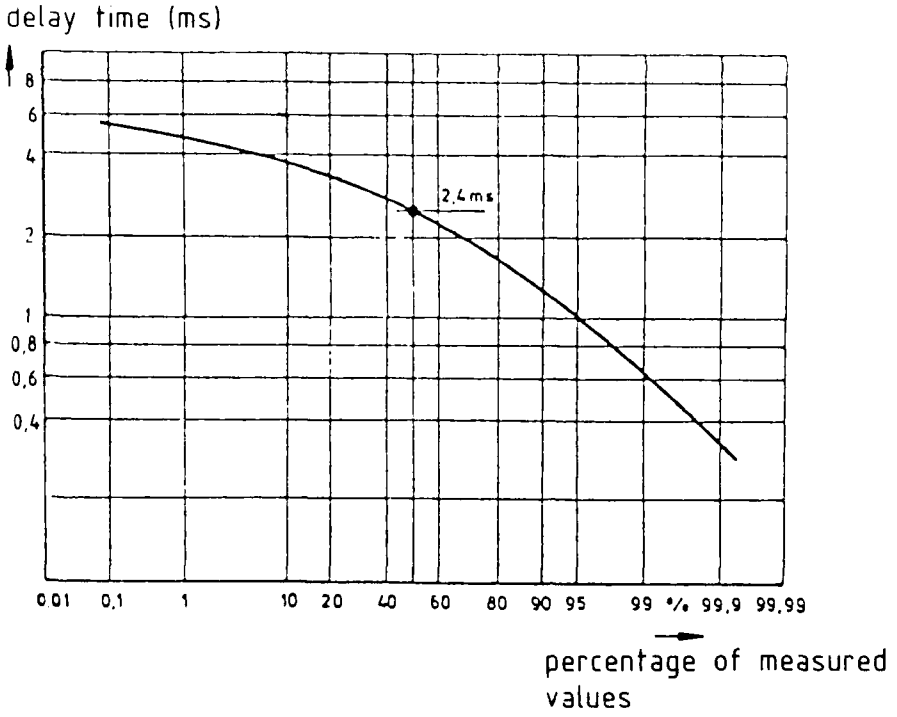

Fig. 5 probability distribution of multipath differential time delay over long distance HF links, (8)

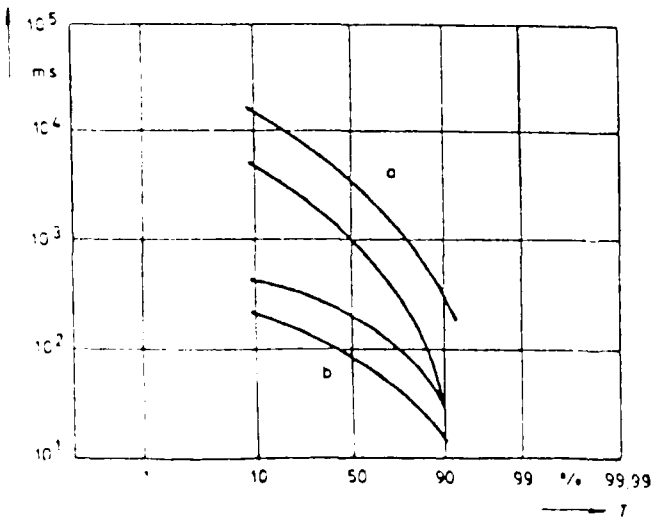

Fig. 6 Probability distribution for fade duration, (8)
a) 0dB below average power
b) 25dB below average power

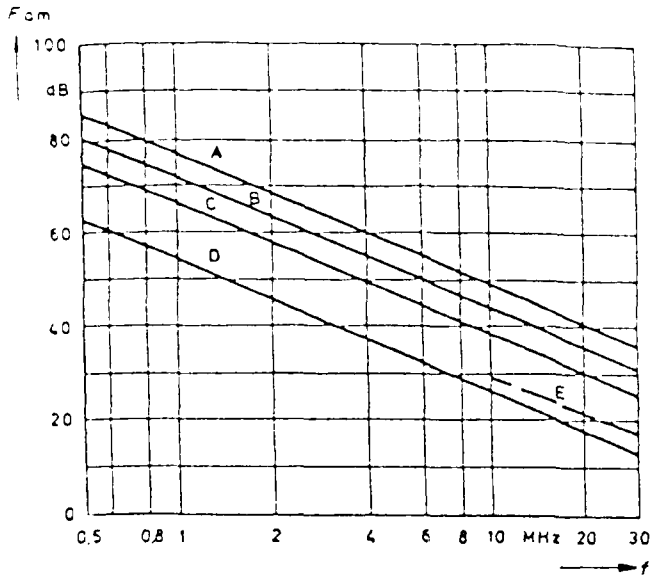

Fig. 2 spectral distribution of atmospheric and man made noise
A urban industry
B suburban
C rural
D remote areas
E cosmic noise

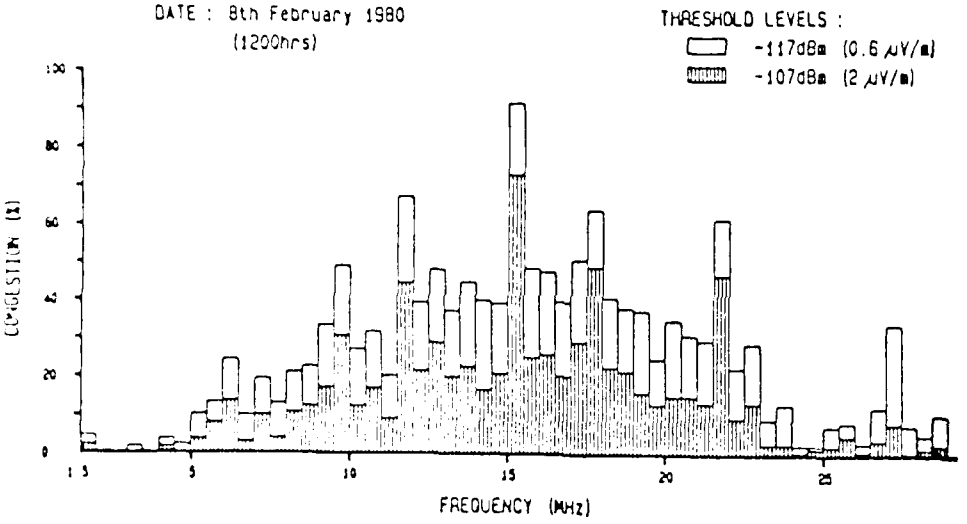

Fig. 3 Example of spectrum congestion histogram in HF, (4)

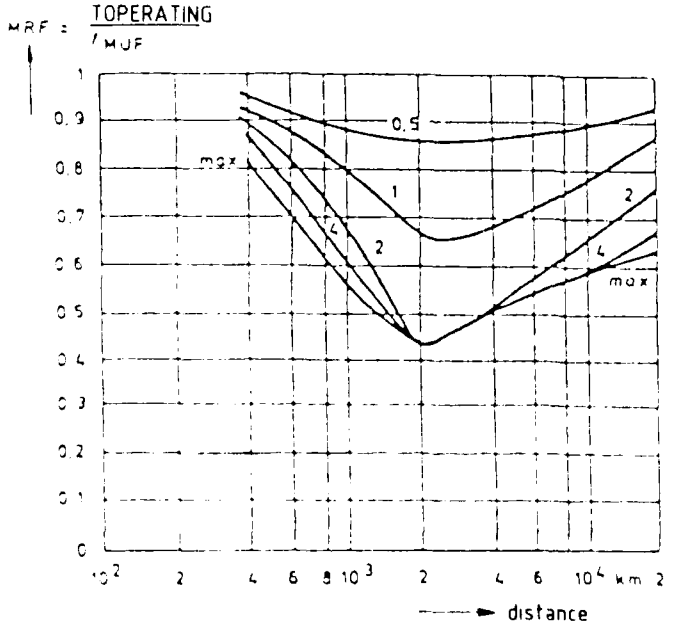

Fig. 4 Multipath reduction factor, (5)

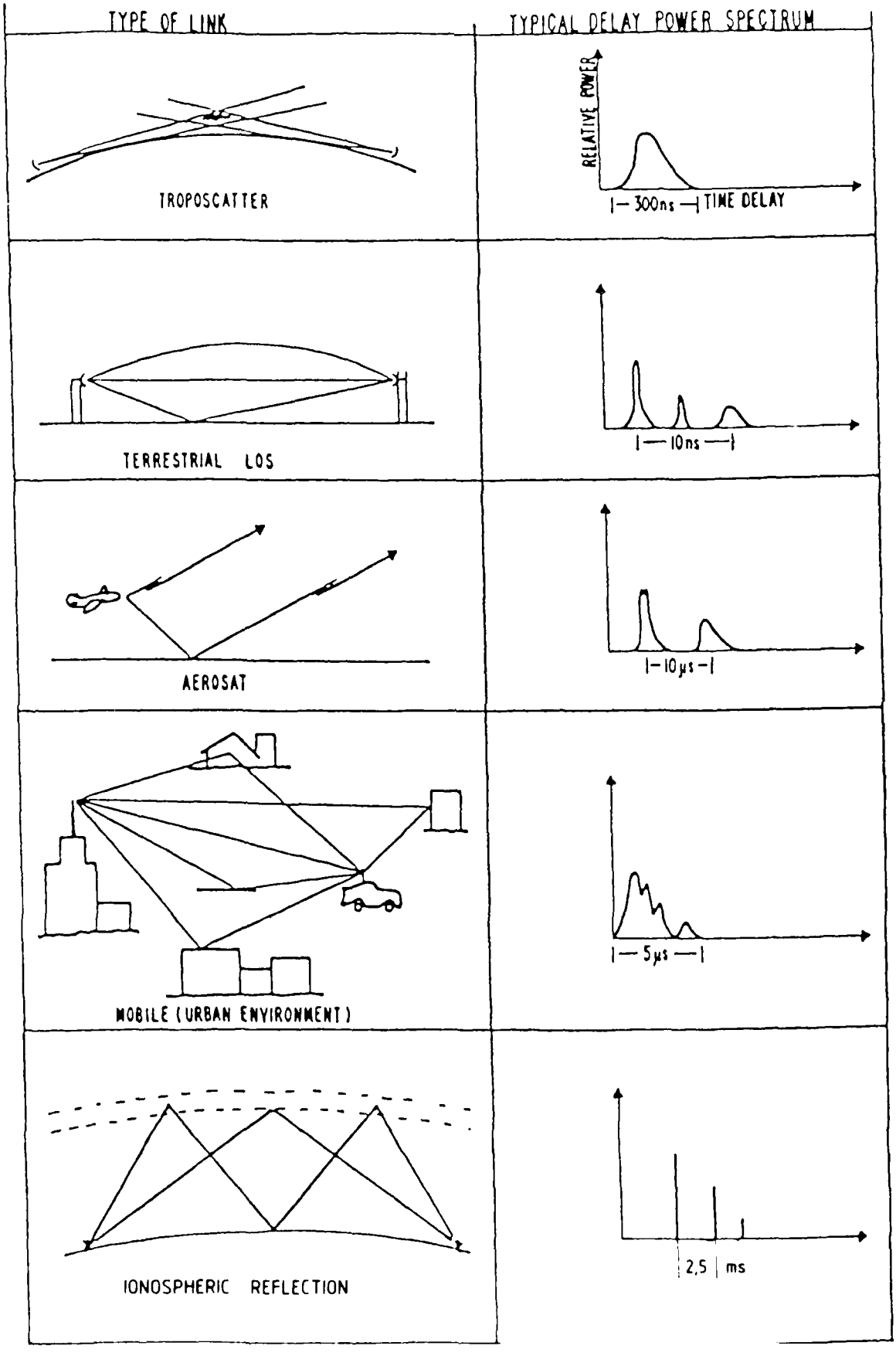

Fig 1 Typical delay power spectra, (15)

11) Beckmann, P. and Spizzichino, A. — The Scattering of Electromagnetic Waves from Rough Surfaces, Macmillan, New York 1963

12) Hortenbach, K.J. — Die statistischen Eigenschaften der Feldstärkeschwankungen auf Satelliten-Flugzeug-Funkstrecken in verschiedenen Höhen über unregelmäßigem Gelände Dissertation Techn. Hochschule Aachen 1977

13) Barrick, D.E. — Rough Surface Scattering Based on the Specular Point Theory IEEE Trans. AP-16, No 4, July 1968, pp. 449 - 454

14) Fitzgerrard — Radio Wave Propagation, 1974

15) Linfield, R.F. — Radio Channel Capacity Limitations. ECAC, North Severn, Annapolis, MD. 21402, Nov. 1977

16) Strohbehn, J.W. and Clifford, S.F. — The Theory of Microwave Line-of-Sight Propagation Through a Turbulent Atmosphere, IEEE Trans. AP-18, March 1970, pp. 264 - 274

17) Lebow, I.L. et al — Satellite Communications to Mobile Platforms Proc. IEEE, vol. 59, No 2, Feb. 1971, pp. 139 - 156

18) [illegible] — [illegible] Spacecraft Survivability Aviation Week & Space technology, August 4, 1975, pp. 41 - 42

19) CCIR-Rpt. 238-3 — Vol. V Propagation in Non-ionized Media Para XIV Plenar Assembly Kyoto 1978

20) NBS-Report 1018 — Transmission Loss Predictions for Troposheric Communication Circuits, National Bureau of Standards, 1967

21) Kennedy, R.S. — A Comparison of Measured and Calculated Frequency Correlation Functions over 4.6 and 7.6 GHz Troposcatter Paths IEEE Trans. COM-20, April 1972, pp. 173 - 178

22) Pelle, E.A. — A Troposcatter Channel Model IEEE Trans. COM-17, April 1969, pp. 130 - 137

23) Ince, A.N. — Interception of Signals Transmitted via Meteor Trails, AGARD-CP 244, pager 19

24) Brown, D.W. and Williams, H.P. — The Performance of Meteor-Burst-Communications at Different Frequencies, AGARD-CP 244, paper 24

25) Retting, J.D. — An Analysis of Meteor Burst Communications for Military Application, IEEE COM-28, Sept. 1980, pp. 1591 - 1601

For estimating the traffic theory of a meteor burst link, up to now data of a known system are used and scaled to the new environment. It is therefore useful to know that in the STC comet system (25) over a distance of 1000 km 200 W transmitters have been used to transmit data in bursts with a rate of 2000 baud (FSK). The system used an ARQ modem (based on 7 bit characters) and obtained an average throughput over a 24 h interval of about 150 baud, i.e. a duty cycle of 7.5 % (24).

With meteor scatter, too, antenna gain and transmitter power are not interchangeable numbers as the beamwidth of the antennas has to be wide enough to illuminate the whole area where suitably oriented trails are likely to occur. For a 1000 km link this value is about 50° (23).

Recent publications suggest that the intervals between usable meteor trails are distributed in a poisson process (25).

$$P_n(t) = \frac{(t/t_{1A})^n}{n!} \exp.\ (-t/t_{1A}) \qquad (5)$$

Where $P_n(t)$ is the probability that exactly n bursts occur during time interval t and t_{1A} is the average time interval between bursts. t_{1A} can be calculated using measured data of a reference system along with the following scaling equation (24):

$$t_{1A} = t_{1AR} \cdot \frac{G_T}{G_{TR}} \cdot \frac{G_R}{G_{RR}} \cdot \frac{R}{R_R} \cdot \frac{P_T}{P_{TR}}^{-0.6} \cdot \left(\frac{f}{f_R}\right)^{2.4} \qquad (6)$$

$G_{T,R}$	antenna gain of transmitter/receiver
R	range
P_T	transmitter power
f	HF-frequency

Index R denotes the parameters of the reference system, for the COMET-System these would be; $G_T = G_R = 10$ dB, $P_T = 200$ W, R = 2 kbit/s, f = 37,5 MHz, $t_{1A} = 4$ s, whereby t_{1AR} has to be corrected when the range is different from the reference system (25).

Although the data rate within a burst is limited because of dispersion, this restriction has not yet become visible as the power level in the system still limits the transmitted bitrate and not the distortion (neglection of tailends of underdense trails).

From the measured data it can be seen that considerable delay times can be involved in the transmission of a certain message, in particular when its length approaches the order of several hundred bits additional processing may be required in the terminal.

4. Conclusion

It has been shown that in present radio channels multipath is an important limiting factor for the transmission of high speed digital signals whereby the model showed are individually depending on the scenario. Noise and Interference however should not be ignored as their character is decisive upon the engineering means to combat them for transmitting digital signals.

5. Literature

1)	CCIR-Report 258-2	Man made radio noise, Geneva 1974
2)	Hagn, G.H. and Shepherd, N.A.	Man made electromagnetic noise from unintentional radiators: a summary; in AGARD Conf. Proc. 159 on Electromagnetic Noise Interference and Compatibility, 21. - 25. Oct 1974, Paris
3)	AGARD Conf. Proc.332	Propagation Aspects of Frequency sharing Interference and System Diversity, 18. - 22. Oct. 1982 Issy-les-Moulineaux, France
4)	Bott, E.R. et al.	Occupancy Measurements across the entire HF-Spectrum, in (3)
5)	Davies, K.	Ionospheric Radio Propagation National Bureau of Standards, Boulder NBS-Monograph 81
6)	AGARD Conf. Proc.13	Oblique Ionospheric Radiowave Propagation, Editor T.B. Jones, June 1969, Technivision Services
7)	Barney, D.K.	The effect of multipath distortion on the choice of operating frequencies for high-frequency communication circuits, Trans IRE, AP-7, p.398
8)	Fetting, H. and Voigt, K.	Schwunddauer und Schwundhäufigkeit bei Kurzwellenübertragungsstrecken, Nachr.-techn.Ztg. 17 (1964) Heft 2, S. 57 - 62
9)	Fehlhaber, L. and [illegible]	Effects of Nocturnal Ground-Based Temperature Inversion Layers on Line-of-Sight Radio Links AGARD Conf. Proc. 208, EM Propagation Characteristics of Surface Materials and Interference Aspects
10)	Sasaki, Y. and Akiyama, T.	Multipath Delay Characteristics on Line-of-Sight Microwave Radio Systems From IEEE, COM-27, No. 12, Dec. 1979, pp. 1876 - 1880

- Man made scattering phenomena might also be exploited in future tactical communications. Chaff, i.e. a multitude of thin conductive foils can be distributed in certain areas of the atmosphere. When operating with the appropriate frequency the dipols resonate and scatter incoming radio waves. However chaff clouds will fade away within hours. - In the ionosphere irregularities can be produced by heating up certain areas of this layer by emitting high power radio waves with approximately the plasma frequency in vertical direction from the ground. The produced irregularities however are closely related to the geomagnetic field direction in the heated area and scattering will only be effective in directions perpendicular to the magnetic field direction.

General aspects

In scatter propagation the received signal is the sum of a multitude of wave components originating form the different areas. It is convenient to think of distinct scattering particles, f.i. blobs of differing dielectric constant although some discussions have to be based on a continuum of scatterers. The wave components are to some extent independent from each other and therefore an incoherent summation of the many component waves takes place at the receiver. As the scatterers are moving, the relative phase of the component waves will, too. The received signal therefore fluctuates.

The short term amplitude statistic of tropospheric and chaff produced scatter is rayleigh. The mean power level is in all cases very much dependent on the scatter angle.

Troposcatter

Troposcatter has become an established technique for transmitting analogue multichannel voice and TV signals. One of the largest systems operating in Europe in the NATO-ACE-HIGH-System, linking together the North of Norway and Turkey, which shows its importance in military communication. Methods for calculating the link budget may be found in CCIR-Rept. 238-3 (19) and NBS-Report 101 (20), nevertheless the calculated values may be by up to 10 dB in error.

As the scatter signal is the summation of many independent components multipath produces severe restrictions for the system. To get an estimate of the value of the correlation bandwidth of the channel quite often it is derived from the maximum possible delay time difference in the system using the 3 dB antenna beamwidth and geometric reasoning.

This however produces very conservative values shich may be too small by more than a factor 2. This comes from the fact that the scatter efficiency of the common volume is decreasing with height. (21) Bello (22) has calculated the delay power spectrum of scatter links using the complete antenna pattern and a reciprocal height dependance of the scatter efficiency. Comparisons of calculations with this method and experiments have shown that measured values of B_c are usually smaller than those calculated according to Bello (21).

While in the past the coherence bandwidth has been considered being the most important limiting factor for broad band signal transmissing, R&D work over the last decade has shown that one can take advantage of the fact that when exceeding the correlation bandwidth the individual spectral components fade independently. Using sophisticated diversity combiners it could therefore be more advantageous to use high bandwidths. The equipment however then has to become adaptive. Because the fading frequency increases both with RF frequency and the average vertical velocity of turbulence, so problems increase with frequency.

Actual measurements however show that the highest fading frequency associated with very deep fading occurs when aircraft fly through the common volume (30 dB and 50 Hz). As the aircraft has a very large scatter cross section it is already effective when it approaches the outer etch of the common volume. This can then result in a very pronounced multipath with delay differences of several µs.

Meteor Burst Communication

Meteor bursts can be used to bridge distances between 800 km and 1500 km using frequencies in the VHF band between 30 MHz and 100 MHz (3, 4, 5). Billions of ionized meteortrails are produced daily by meteors with a mass range of 10^{-7} to more than 10 grams in a height between 80 to 120 km.

To use a particular meteor trail for transmission, geometric reflection conditions have to be established between the trail, a rod of ionization, and transmitter A and receiver B. The meteor trail therefore has to be located on a prolate spheroid with A, B being foci. In contrast to troposcatter the ray projection onto the earth surface is essentially not restricted to the great circle. In general reflections occur not on that path, because of the inevitable tilt of the trail with respect to the earth surface. Usually the reflection points are located at so-called hot spots which are located about 5° to 10° off the great circle path.

The ionized trails of a meteor are generated in a height of about 80 km. After having been generated the electrons will diffuse into the neighborhood thereby reducing the electron density in the trail. A meteor trail has therefore only a restricted lifetime, which is shorter for higher frequencies as here higher electron densities are required to cause an appreciable effect. The lifetime depends also on its actual location with respect to path, particular angle of reflection and distance between transmitter and trail.

Although the earth is exposed continuously to a multitude of very small meteors, a continuously available communication channel cannot be established using meteor trail reflection, as only in a small percentage of time a suitably oriented meteor of adequate characteristics will be present. The channel is therefore to be probed continuously and when a trail is present the previously information can be transmitted with as high a speed as possible, whereby the message length should not exceed the lifetime of the trail (about 0.5 s).

The use of digital signal transmission in conjunction with spread-spectrum modulation however could improve the situation because now signal summation and subtraction can be averaged keeping multipath degradation within acceptable limits.

Antennas for LOS radio relay links are always of very high directivity, so that ground reflections can be suppressed. Therefore in the SHF-region comperatively high coherence bandwidths are obtained. (250 MHz and beyond).

Above about 10 GHz multipath is no more the most relevant propagation factor. Absorption effects especially due to water vapor and also scatter due to rain become noticable, degrading mostly the field strength.

6.5 Extremely High Frequencies (30 GHz to 300 GHz, λ = 1 cm to 0,1 cm)

It is not only attenuation because of molecular resonance and rain which becomes appreciable now, but also free space loss reaches higher values. Antennas with 40 dB gain therefore seems to be a general necessity, resulting in a beamwidth of only 1.5°. In radio relay links either tracking systems or very stable masts are required and are range limiting factors. Atmospheric scintillations become appreciable causing timevariable focusing and defocusing effects on the wave (16).

The region around 60 GHz gains more and more attraction because it seems to be possible to establish links over short distance and at the same time to make use of the high absorption in order to shield the communication system from the outside world. Further investigations seems to be necessary when applying very high datarate systems as not much is known about signal dispersion in that region.

f. Satellite links

Satellite communication is principally possible at frequencies above the highest ionospheric reflection frequency, i.e. above 50 MHz. When asking for optimum frequency ranges, it should be borne in mind that as the satellite is to illuminate a particular area on the earth, so its antenna gain has a fixed upper bound which is frequency dependent. The same is true for terminals on the earth which when mobile can only use low gain antennas, with say ≈ 3 dB gain. As the sensitivity of a mobile terminal is limited, this results in the rule, to use an as low as possible frequency, because of the increasing free space attenuation (20 lg (f) dB).

Compared to radio relay links data transmission may occur with much higher speed when using high gain antennas, as usually the elevation of the transmission path is above 10°, which prevents the ground reflected wave from causing severe limitations of correlation bandwidth.

In the VHF band, however, quite a lot of regular ionospheric effects have to be taken into account, limiting the performance. In the UHF band they have almost died out, and one is only faced with ionospheric scintillations causing amplitude and phase fluctuations. Although, from wave propagation point of view, frequencies between 500 and 1000 MHz seem to be optimum (17). SHF has to be used when services using bandwidths up to 100 MHz are required. This however then requires sophisticated equipment which can only be installed in larger terminals.

Because of the lack of unoccupied bands, frequencies above 10 GHz will be applied by future systems. The propagation medium is the critical factor as in terrestrial communications particularly precipation causes attenuation, noise and depolarization. EHF has been used in intersatellite communication (LES 8,9) (18) where such restrictions posed f. i. by the 60 GHz oxygen band do not exist and could even preserve those links from terrestrial interference.

g. Scatter links

As most of our communication links are set up between terminals on the earth surface (or no more than 1000 m above) the LOS condition is a severe restriction. When not using space borne relay stations, i.e. satellites, electromagnetic (E.M.) wave scattering is the only way to overcome the LOS restriction. Irregularities in the composition of the atmosphere with relevance to E.M. wave parameters produce an energy transfer offset from the streight LOS propagation direction.

In the earth atmosphere such irregularities have been observed in:

- the troposphere (lowest atmospheric layer up to 10000 m).
  Here turbulence is always created by wind shear - wind velocity is smaller at the close proximity to the ground compared to regions further up - and the thermal temperature gradient with height.
  The changing weather, in particular cold fronts and thunderstorms, produce turbulence. Along with this turbulence irregularities in the dielectric constant are produced and from these areas we get scattered waves. The associated propagation mode is called troposcatter and is used to bridge distances mainly between 100 km and 300 km (up to 700 km) and can be applied with frequencies in the UHF and SHF bands.

From the higher atmospheric layers no scattering has been observed apart from the ionosphere. This layer (composed of several sublayers) is mainly used as a mirror for RF-signals (HF up to 30 MHz). However this mirror becomes transparent for higher frequencies than the MUF (maximum usable frequency) which may vary according to distance, time of day and year between 4 MHz and 34 MHz. However scattering effects have been observed above these frequencies originating from two different mechanisms.

- Ionoscatter is a propagation mode produced by variations in the electron contents of D and lower E-layer. Apart from this effect a very bursty signal with higher power level has been observed which originates from signals scattered at the ionized trails of meteors when passing the ionosphere. This propagation mode is called meteor burst scatter. Of these two modes only the latter is of greater relevance to the communications engineer.

1.2 Very-High-Frequency Band (30 MHz to 300 MHz, λ = 10 m to 1 m)

Similar data rates compared to the HF-band may be transmitted in the VHF region. Propagation takes place in the line-of-sight (LOS) mode using also diffraction and is therefore restricted to relatively short ranges. The propagation characteristics depends on the troposphere as well as the boundaries of the medium, in this case earth, source and sink.
While the VHF-band design may take into account the stable propagation mode other modes may occur. In the lower VHF-region (f < 100 MHz) sporadic ionospheric E-layer reflection may be present. In mobile communication systems this may lead to multipath conditions with differential delays up to 4.5 ms.

Tropospheric layering also has to be considered in particular inversion layers as they produce a bilinear refraction index profile with height. Such a jump of the modified refractivity index M leads to total reflection as long as the grazing angle γ is below a certain limit $\gamma_g = \sqrt{2 \cdot \Delta M}$. Fig. 7 gives an overview. Rohlmann, D. and Illers, J. (9) have discussed these effects in detail. Multipath situations because of tropospheric layering are important in LOS radio relay links because they cannot be suppressed with antennas of high directivity, as the inversion layer height may vary according to weather conditions. In the LOS-scenarios two situations have to be distinguished. When source and sink both are located at the lower edge of the inversion layer one ray propagates below the layer the other inside the ducting layer. The maximum differential time delay however occurs when source and sink both are below the ducting layer. The direct ray arriving at the receiver is then interfering with a second ray which penetrates into the ducting layer and is bent again towards the earth.
Sakani and Arayama (10) discussed both scenarios in detail and showed that timedelay differences well above 1 µs can occur in an appreciable time percentage.
They also showed that tropospheric layer reflection is of less importance for slant path conditions.

In air-air and air-ground communication scenarios beside the direct ray the ground reflected ray has to be considered. This leads to deep fades when transmitter and receiver are moving. Because of the different time delay selective fading resp. intersymbol interference is produced. So the maximum symbol rate on the path is limited as shown in Fig. 8. The curve indicates the dependence of the maximum data rate on the height of the terminal above the reflecting plane and the grazing angle.

When considering a rough ground surface, the average specular reflection coefficient is reduced, however fluctuates heavily (11). The resulting field strength of the receiver now still shows the regular distribution but has a Rice distribution in amplitude (12). The fading pattern therefore will become slightly irregular but the order of magnitude of the fading depth will still remain. The same is true for the effective transmission bandwidth.

The effect of the rough surface in the avionic scenario has been classified rigorously by Hortenbach (12) showing that the conditions for air-ground communication are essentially not altered. The adverse effects of multipath decrease the higher transmitter and receiver are located above the rough ground for a given grazing angle (specular point scattering theory (13)).

The situation is different for the terrestrial mobile radio channel. Here usually diffraction and terrain scattering are responsible for signal transmission as in many cases the direct line of sight is obstructed. The fixed services are generally well planned with guaranteed unobstructed first fresnel zone (14)).
With respect to the multipath situation we have to distinguish between urban and rural situations.
In urban scenarios, the received signal is composed from many reflected signals from buildings in the vicinity of the receiver. The amplitude distribution will therefore be Rayleigh around a local mean, which varies log-normal in the area, as far away reflectors usually are completely shielded. The multipath delay spread reaches values up to 4 µs while the delay power distribution can extend to 10 µs. When moving, doppler shift will occur, which is proportional to the carrier frequency and the velocity of the vehicle. At 1 GHz doppler spectra have been measured with a half width of 70 Hz when moving with a velocity of about 60 km/h (15).

In a rural environment the reflector causing multipath conditions may be quite away from receiver and transmitter causing much higher differential delays however still with sufficient signal strength. In such an environment the maximum transmission rate should as a rule of thumb not exceed values beyond

$$B \prec \frac{2 \cdot 10^3}{d/1\ km} \quad \text{baud}$$

where d is the diameter of the coverage zone of the system.

1.3 Ultra-High-Frequency-Band (300 MHz to 3 GHz, λ = 1 m to 0.1 m)

In the UHF-band tropospheric reflections occur. Considering the terrestrial scenario, the propagation differs from the one in the VHF. However as the wavelength is smaller the freespace loss is higher and also the Doppler frequency will be higher when moving through the interference pattern and also the width of the Doppler-Power-Spectrum of the signal will be wider.

Diffraction on the direct line-of-path will result in higher values of [illegible] and the diffraction propagation loss is less [illegible]. However the [illegible] is higher. Therefore the [illegible] is smaller. Another variability of the mean field strength within a certain area.

1.4 Super-High-Frequencies (3 GHz to 30 GHz, λ = 10 cm to 1 cm)

The SHF is already different to use the upper part of the UHF band for mobile services (omnidirectional radiation). The SHF band is mostly used for fixed services or for mobile services transmitting only small [illegible] data that is less susceptible to fading.

In the HF-band the noise due to atmospherics varies according to daytime, season and geographic location because of varying ionospheric condition. Man made noise also shows variations of this kind which are due to varying business activity.

With man made noise we have to distinguish between a general stationary background level and bursts, e.g. due to ignition. Ignition noise has to be considered in all mobile communication systems. It is of highly impulsive nature and spreads over much of the frequency spectrum. In heavy traffic even at 3 GHz noise spikes can occur which are more than 40 dB above receiver noise level in 100 kHz bandwidth (2). Ignition noise seems to be very much dependent on the individual vehicle and relatively few modeles exist which have not adequate by checked against experimental data.

5. Interference

In HF region interference due to an "overdense" usage of the band is a common source of degradation, which often is of more importance than multipath distortion. Gott et al (4) made extensive measurements of the congestion of the HF-band, Fig. 3. The data presented there refer to a 1 kHz-band. Keeping in mind that for a good signal transmission the signal to interference ratio should be at least 10 dB within the used band, therefore signal levels at the receiver input above -100 dBm are required when using 2.4 kbit/s serial transmission to overcome interference. As in HF each user tries to use a frequency around the maximum usable frequency (MUF) in the area of optimum propagation conditions, the interchannel interference tends to be worst case.

In VHF and above inter and co-channel interference is very important for mobile users and tactical LOS radio relay links. The variability originates from varying atmospheric conditions in particular ducting and superrefraction. In 1982 AGARD has devoted a complete Symposium to propagation aspects of frequency sharing, interference and systemdiversity (3).

6. Propagation effects in the frequency bands of interest

The different scenarios presented require the use of a suitable frequency band. In a survey on propagation effects it seems to be an efficient way of classification, to continue the discussion in terms of the frequency bands.

6.1 HF-band (1,5), 3 to 30 MHz; λ=(200 m) 100 m to 10 m

Wave propagation in this band is characterized by two particular modes. The ground wave is still of sufficient strength to overcome distances up to 50 km using frequencies below 5 MHz. No multipath is present, if no interference with other propagation modes occurs. As the range of the ground wave is limited due to its 40 lg (d/λ) dB dependance of the transmission loss (d = distance), the skywave is the dominant mode for overcoming long distances, as long as this wave has the appropriate frequency to be reflected by the ionosphere. So it is a unique means of communications all over the world without an artificial relay.

As the electron density of the refracting ionospheric layer show diurnal, seasonal and sunspot cycle variations, the maximum usable frequency (MUF) for reflection does so, too. For short distance communication the MUF varies between 3 MHz and 10 MHz at noon. But this does not mean that at daytime a broader frequency band can be used for communication, as then the D-layer will absorb a considerable amount of signal power (up to 25 dB at a free-spea pathloss of about 100 dB) (5). That means that a relatively narrow band of some MHz is available which is moving in its center frequency. As MUF and LUF (the lowest usable frequency, because of D-layer absorption) are proportional to the secants of the angle of incidence longer distances require a frequency band with a higher center frequency than smaller distances. This problem can be solved by using the correct frequency range and an appropriate transmitter power. Because of the complex structure of the ionosphere and the possibility of multiple reflection between the ionospheric mirror and the earth surface multipath propagation will always be a significant effect which results in time and frequency selective fading as layer heights and electron densities show regular and random time-variability (6).

The propagation medium may involve:

a) multiple hop propagation
   Even with short links the reflection from the earth is quite often not to be neglected.

b) multiple layer propagation

c) low and high angle ray interference in oblique propagation close to the junction frequency (5)

d) both ordinary and extraordinary ray.

... (7) has calculated the principal time delay bounds for the ionospheric propagation path in terms of the ratio operationally used radio frequency and the momentary FOT-MUF. The resulting nomogram, Fig. 4a shows that only when working very close to the actual MUF, time delay values less than 0.5 ms will occur. In general up to 4 ms have to be taken into account. In most cases only two rays are involved in the interference mechanisms producing frequency selective fading with relative attenuation peaks up to ... which are spaced quite regularly in frequency according to their propagation delay time difference, see also Fig. ... Fig. 5 shows the probability distribution for a particular multipath differential time delay derived from measurements over long links (6 000 - 7 000km). Because of the time dependent height variations of the layers, these attenuation peaks move in frequency through the channel with a speed up to ... Hz/s. When using slow data rate channels this effect reflects only in a time selective fading of the signal envelope. Fig. 6 shows measured values for the probability distribution of fadedurations, an important parameter for the design of error correcting codes in HF.

The study of different digital transmission equipment, have shown that the following phenomena have to specifically looked at:

- field strength conditions
- fading, broadband and selective, multipath interference and its time distribution
- noise and interference.

As far as possible data with respect to these phenomena will be given on which system design can be based.

Fading in radio channels is caused by time and/or frequency dispersion which distorts multifrequency signals waveforms in usually not completely predictably and continuously changing manner.
We distinguish between time and frequency dispersion. Time dispersion causes the information pulse to spread when it passes the medium. It can be of different origin. The propagation medium can have a frequency dependent complex refraction index caused by the electron content or rain, water vapor or oxygen resulting in amplitude or phasevariations in the considered frequency band. When the time dispersion is caused by the signals propagating along different paths of unequal delay we speak of multipath. The resulting multipath spread causes frequency selective fading which produces distortion especially intersymbol interference. The time dispersion is characterized by its delay power spectrum or in the frequency domain the frequency autocorrelation function. While often it is sufficient to use a single characteristic parameter of these functions i.e. the delay spread or the coherence bandwidth to characterize the channel.

Frequency dispersion originates from the timevariability of the channel parameters and causes time selective fading. It is characterized by the frequency power spectrum. When its mean value differs from that of the transmitted signal a doppler shift is present. The center of gravity of the frequency power spectrum is called doppler spread.

In most cases of interest the one or the other type of dispersion dominates. If the [illegible] rate of the transmitted signal is very wide compared to the doppler spread, the channel is treated being like flat. It may be also frequency flat if its bandwidth is small compared to the coherence bandwidth of the channel. The signal then passes the channel apparently undistorted and the channel is then called a flat-flat channel.

3. Scenarios

It has been found that it is very useful to distinguish between the following propagation modes:

1. ground wave propagation
2. skywave with ionospheric refraction
3. terrestrial line-of-sight propagation and diffraction
4. [illegible]
5. [illegible] burst scatter

[illegible] are restricted to the lower frequency region (HF), 3, 4 and 5 to the higher frequency bands (HF and above). Of the complete presently available radio spectrum, VLF, LF and MF are excluded from this discussion as these bands are mainly used for other purposes but communication or they are required by broadcast services. The relevant frequency range starts above 1,5 MHz, with the extended HF-band.
It can be agreed upon that between mobile units HF, VHF and optical frequencies can only be used for digital communication under special preconditions and are usually preserved for stationary services. Also experience has shown that the prevailing problems in HF-wave propagation depends very much on the geometrical and topographical scenario. Therefor the following distinction will be made:

air - air
air - ground
satellite
terrestrial systems, radio
terrestrial systems, fixed

For these scenarios in table 1 the relevant frequency regions, propagation modes and associated [illegible] are shown.
For different propagation modes fig. 1 shows the type of delay power spectrum to be expected and the [illegible] values.

4. Noise

[illegible] only the signal is given in the propagation medium but further, unwanted signals are present at the receiver, such as intergrading carriers, unwanted noise signals are present because of [illegible], man made noise and extraterrestrial sources. A spectral distribution is shown in fig. 2 (1).

As the noise is also propagated predominantly by ground wave, the horizontal component of the overall [illegible] is usually much smaller than the vertical component.
Assuming that the equipment has a noise figure below 10 dB, it is obvious that only in the HF-band the [illegible] is important. In the region below 10 MHz it dominates all other sources [illegible] and [illegible] are used.

PROPAGATION OF WIDE BANDWIDTH SIGNALS IN A TROPOSPHERIC DUCTING MEDIUM

Nikolaos K. Uzunoglu

Hellenic Nany Technology Development Office (GETEN)
Cholargos, Athens, Greece

A B S T R A C T

The propagation properties of wide bandwidth signals transmitted through a tropospheric ducting medium are examined analytically. A flat earth model with a perfect surface conductivity (sea surface) is taken. The refractive index profile $n(h)$ is assumed a stepwise function of the height h. Horizontal and vertical polarized waves are treated in parallel by employing similar procedures. The corresponding boundary value problems are solved by using spectral representations for the primary antenna and induced fields. Guided and radiated mode contributions are then computed by applying approximate asymptotic integration techniques under a continuous wave (cw) excitation. The behavior of wide bandwidth signals propagating in a tropospheric duct is examined in terms of the inverse Fourier transformation of the cw field expressions. Several geometries are considered such as both transmitting and receiving antennas being inside the tropospheric waveguide or the opposite. Particular attention is given to the case when communication path crosses the waveguide ceiling. In order to determine the influence of the multipath propagation, occuring inside the ducting medium, into a real communication link a Phase shift keying (PSK) modulation is considered. Numerical results are given for several tropospheric ducting media in terms of the bit error rate.

1. INTRODUCTION

The use of wide bandwidth signals is assuming increasing importance in line of sight (LOS) communication links for several reasons such as the transmission of high bit rate signals and the use of spread spectrum modulation techniques. Instead of the conventionally used 3 KHZ bandwidth signals to transmit 2,5 Kbps information flow, signal bandwidths of the order of 1 MHZ bandwidths are proposed to obtain a processing of the order of 25dB. The experience of the past fourty years in operating Ionospheric High Frequency communication channels has shown that multipath phenomena can result in a severe intersymbol interference problem on data links. In general the maximum attainable transmission rate over long ionospheric links is 100 to 200 bps. Considering the similarities between an ionosphere-earth waveguide geometry and a tropospheric ducting medium one should expect quite similar phenomena in principle.

It is a well known fact that there are two extreme cases in multipath propagation depending on the comparisons of the effective signal bandwidth $\mathcal{B}$ with the differential delays $\Delta\tau$ observed in the communication channel. In particular if $\mathcal{B} > 1/\Delta\tau$ then we have a selective type fading. Otherwise if $\mathcal{B} < 1/\Delta\tau$ then the multipath phenomena are observed mainly as averaging phenomena resulting into a Rayleigh type fading for randomly varying channels. In this paper we consider selective type fading as this could be observed for signals propagating in a tropospheric ducting medium.

The propagation in tropospheric ducts have been examined in the past 40 years extensively in the literature[1,2,3]. Several approaches such as the equivalent earth radius, the Watson transformation, the WKB and the geometrical optics techniques have been used to treat the propagation in tropospheric ducts. Interesting phenomena are observed in radar systems associated with the propagation in ducts. Until now mostly reported ducting phenomena are associated with extraordinary radar coverages. In this paper, the effects of the phase distortions for short duration signals are treated.

2. COMPUTATION OF THE FIELD STRENGTH

The tropospheric ducting medium is modelled with a refractive index profile described mathematically as:

$$n^2(z) = \begin{cases} \epsilon_1 , & 0 < z < h \\ 1 , & h < z < +\infty \end{cases} \qquad (1)$$

where h is the duct height, z is the vertical coordinate and $\epsilon_1 > 1$ is the dielectric constant of the tropospheric duct medium. The whole space is assumed magnetically homogeneous with a magnetic permeability $\mu = \mu_0$. Although this assumed profile is a rather crude approximation to the real refractive index profiles in the troposphere, nevertheless it has been used in the past to describe tropospheric propagation phenomena as the basic ducting mechanism is retained in the model. The simplicity of the $n(z)$ distribution results into simple analytic formulas for the field distributions. In figure 1 the propagation geometry is shown, where an antenna radiating a continuous wave of frequency $\omega = 2\pi f$ is located at $x = x_0, z = z_0 < h$. Two type antennas are considered that are: (a) a vertical electric dipole and (b) a vertical magnetic dipole corresponding to vertical and horizontal polarizations respectively. The analysis is proceeded in parallel for both kind sources.

Assuming an $\exp(+j\omega t)$ time dependence, the electromagnetic field can be described in terms of the Hertz potentials Π and M as follows[4]

$$E_x = \frac{\partial^2 M}{\partial y \partial x} + \frac{\partial^2 \Pi}{\partial x \partial z} \qquad \mu_0 H_x = \frac{k_0^2 n^2(z) \partial \Pi}{\omega \partial y} + \frac{\partial^2 M}{\partial x \partial z}$$

(2a)

where $k_0 = \omega\sqrt{\varepsilon_0\mu_0}$ is the free space wave number. Both Π and M satisfy the Helmothz equation

$$\nabla^2\Pi + k_0^2 n^2(z)\Pi = 0 \tag{2b}$$

in the absence of primary sources. Assume Π_o, M_o be the quantities associated with primary sources located inside the ducting medium.

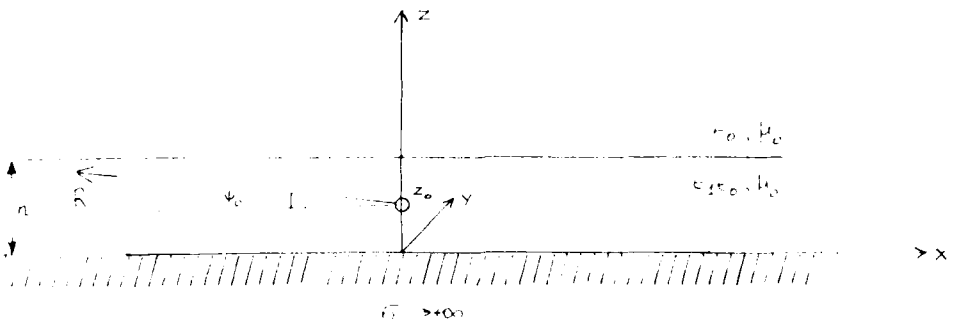

Fig. 1. Tropospheric Ducting Medium Geometry

For example, if the source is a vertical electric dipole we have

$$\Pi_o = \frac{p}{4\pi\varepsilon_0\varepsilon_1}\,\frac{e^{-ik_1R}}{R}, \qquad M_o = 0 \tag{3}$$

and if the source is a vertical magnetic dipole

$$\Pi_o = 0, \qquad M_o = \frac{m}{4\pi}\,\frac{e^{-ik_1R}}{R} \tag{4}$$

where $\varepsilon_1 = \varepsilon_r\varepsilon_0$ is the distance from the dipole to the observation point, p and m are the electric and magnetic moments respectively. Let Π_1, M_1 be the potentials of the induced fields inside the ducting medium and Π_2, M_2 those of the transmitted to the outer region $z > h$. The boundary of the ducting medium is assumed of perfect conductivity and therefore from eq.(1) it is deduced that

$$\Pi_2 = -\Pi_1 \quad \text{at } z = h, \qquad M_2 = M_1 \quad \text{at } z = h \tag{5}$$

At the $z = 0$ ducting and free space regions interface plane the continuity of the E_x, H_y, E_y, H_x components are satisfied if,

$$\Pi_1 = \Pi_2, \qquad \frac{\partial(\Pi_o + \Pi_1)}{\partial z} = \frac{\partial\Pi_2}{\partial z}$$

$$M_1 = M_2, \qquad \frac{\partial M_1}{\partial z} = \frac{\partial M_2}{\partial z} \tag{6}$$

Using the well known Fourier transform of the scalar Green function, eqs.(3) and (4) can be

$$\Pi_1 = \int\int \Pi_1(z, k_x, k_y)\, e^{-i(k_x x + k_y y)}\, dk_x\, dk_y$$

$$M_1 = \int\int M_1(z, k_x, k_y)\, e^{-i(k_x x + k_y y)}\, dk_x\, dk_y \tag{7}$$

where $k_x = k_1\cos\theta$, $k_y = k_1\sin\theta$ and $r = x\hat{x} + y\hat{y}$

The substitution of the wave equation (2) for the Π_1, Π_2 and M_1, M_2 functions can be written as follows:

$$\Pi_1 = \frac{P}{4\pi} \int_{-\infty}^{+\infty} d\lambda_x \int_{-\infty}^{+\infty} d\lambda_y \left(B_1 e^{\mu_1 z} + B_2 e^{-\mu_1 z} \right) e^{i\lambda \cdot r} \tag{8a}$$

$$\Pi_2 = \frac{P}{4\pi} \int_{-\infty}^{+\infty} d\lambda_x \int_{-\infty}^{+\infty} d\lambda_y \; C_1 e^{-\mu_0 (z-h)} e^{i\lambda \cdot r} \tag{8b}$$

$$M_1 = \frac{m}{4\pi} \int_{-\infty}^{+\infty} d\lambda_x \int_{-\infty}^{+\infty} d\lambda_y \left(D_1 e^{\mu_1 z} + D_2 e^{-\mu_1 z} \right) e^{i\lambda \cdot r} \tag{9a}$$

$$M_2 = \frac{m}{4\pi} \int_{-\infty}^{+\infty} d\lambda_x \int_{-\infty}^{+\infty} d\lambda_y \; C_2 e^{-\mu_0 (z-h)} e^{i\lambda \cdot r} \tag{9b}$$

where $\mu_0 = (\lambda^2 - k_0^2)^{1/2}$ and B_1, B_2, C_1, D_1, D_2, C_2, are unknown coefficients to be determined.

In writing the solution for the outer region ($z > h$) the Sommerfeld-Müller radiation conditions have been incooperated. Therefore considering the radiation condition in eqs. (7), (8b) and (9b) and the $\exp(i\omega t)$ time dependence it is concluded that on the (λ_x, λ_y) plane the square roots μ_1, μ_0 should be defined as:

$$Re(\mu_1) > 0 \quad , \quad Im(\mu_1) > 0 \tag{10a}$$

$$Re(\mu_0) > 0 \quad , \quad Im(\mu_0) > 0 \tag{10b}$$

In order to determine the unknown coefficients in eqs. (8a)-(9b) it is necessary to substitute eqs. (7)-(9b) into the boundary conditions given by eqs. (5) and (6). Following a lengthy but straightforward algebra the following results are obtained:

for the electric dipole

$$B_1(\lambda) = q_e \frac{(1 - \epsilon_1 \mu_0 / \mu_1) \cosh(\mu_1 z_0) e^{-\mu_1 h}}{\Delta_e(\lambda)} \tag{11a}$$

$$B_2(\lambda) = q_e \frac{\cosh(\mu_1 (z_0 - h)) - \epsilon_1 \frac{\mu_0}{\mu_1} \sinh(\mu_1 (z_0 - h))}{\Delta_e(\lambda)} \tag{11b}$$

$$C_1(\lambda) = q_e \frac{2\epsilon_1 \cosh(\mu_1 z_0)}{\Delta_e(\lambda)} \quad , \quad q_e = -\frac{1}{2 2\pi \epsilon_0 \epsilon_1} \tag{11c}$$

and for the magnetic pole:

$$D_1(\lambda) = q_m \frac{(1 - \mu_0 / \mu_1) \sinh(\mu_1 z_0) e^{-\mu_1 h}}{\Delta_m(\lambda)} \tag{12a}$$

$$D_2(\lambda) = q_m \frac{-\cosh(\mu_1 (z_0 - h)) + \frac{\mu_0}{\mu_1} \sinh(\mu_1 (z_0 - h))}{\Delta_m(\lambda)} \tag{12b}$$

$$C_2(\lambda) = q_m \frac{2 \sinh(\mu_1 z_0)}{\Delta_m(\lambda)} \quad , \quad q_m = -\frac{1}{2 2\pi} \tag{12c}$$

where $\Delta_e(\lambda) = \epsilon_1 \mu_0 \cosh(\mu_1 h) + \mu_1 \sinh(\mu_1 h)$ (13a)

$\Delta_m(\lambda) = \mu_1 \sinh(\mu_1 h) + \mu_0 \cosh(\mu_1 h)$ (13b)

This completes the formal solution for the electromagnetic problem. However the obtained solutions, being in the form of infinite integrals are not easily convertable to numerical data which is required for practical purposes. To this end, it is necessary to device analytical techniques and to proceed at least approximately with the computation of the integrals given in eq. (8a)-(9b).

Consider first the computation of the (8a). The integrand function $(B_1 e^{\mu_1 z} + B_2 e^{-\mu_1 z})$ is a function only of the $\lambda = (\lambda_x^2 + \lambda_y^2)^{1/2}$ variable. Then substituting the expansion

$$e^{i\lambda \cdot r} = \sum_{m=-\infty}^{+\infty} i^m J_m(\lambda \rho) e^{im(\theta - \theta_0)}$$

with [illegible] into eq. (8a) and by integrating from [illegible] to 2π one obtains

$$H_1 = \frac{P}{2} \int_{\lambda=0}^{+\infty} d\lambda\, J_0(\lambda\rho)\,(B_1 e^{\mu_1 z} + B_2 e^{-\mu_1 z}) \tag{14a}$$

Instead of the Bessel function $J_0(\lambda\rho)$ it is possible to substitute

$$J_0(\lambda\rho) = \frac{1}{2}\,(H_0^{(1)}(\lambda\rho) + H_0^{(2)}(\lambda\rho)) \tag{14b}$$

and since $H_0^{(1)}(-\lambda\rho) = H_0^{(2)}(\lambda\rho)$ eq.(14a) can be written as,

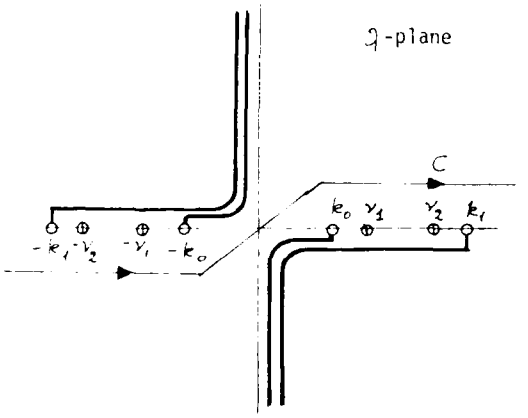

Fig. 2. Complex λ-plane.

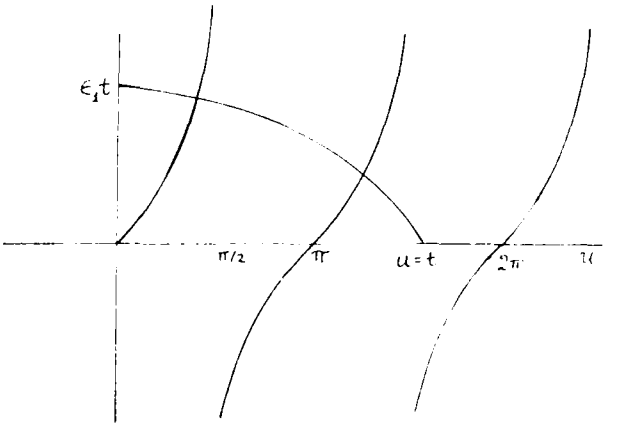

Fig. 3. Graphical solution of eq. (16).

$$H_1 = -\frac{P}{4} \int_{\lambda=-\infty}^{+\infty} H_0^{(2)}(\lambda\rho)\,[B_1(\lambda) e^{\mu_1 z} + B_2(\lambda) e^{-\mu_1 z}]\,\lambda\, d\lambda \tag{15}$$

In Fig. 2. the contour of integration (C) is shown for the integral of eq. (15). In order to have a single valued function for the square roots μ_1, μ_0 it is necessary to define appropriate branch cut lines in the λ-plane. These cuts are shown in Fig. 2. This particular choice of the branch lines insures the radiation condition (eq.(15)) to be satisfied on the C contour [5]. Examination of the $B_1(\lambda)$, $B_2(\lambda)$ functions shows that there are finite number singularity points due to the roots of the equation $\Delta_e(\lambda) = 0$. These roots are real and are located symmetrically in the regions $[-k_1, -k_0]$ and $[k_0, k_1]$. Substituting the auxilliary variables $u = \mu_1 h$ and $t^2 = (k_0 h)^2(\epsilon_1 - 1)$ into eq.(13a) the singularity points are determined by solving the transendental equation

$$\epsilon_1 (t^2 - u^2)^{1/2} = u \tan(u) \tag{16}$$

In Fig.3 we show the graphical solution of eq.(16). The number of roots N_e depends upon the parameter $t = k_0 h \sqrt{\epsilon_1 - 1}$ and can be computed from

$$N_e = [t/\pi] + 1 \tag{17}$$

where $[x]$ is the integer part of x. Each of the roots correspond to a surface wave guided along the dielectric waveguide that is formed by the stepwise refractive index profile defined in eq. (1).

3. FIELD INSIDE THE DUCT

In practical communication problems the distance ρ (see Fig. 1) between the transmitter and receiver is very large in comparison with the radiation wavelength $2\pi/k_0$. The same is not true for the z-coordinate for terrestrial communication links and it is not possible to compute the integral in eq. (15) for the far field region by applying the "stationary phase" approximate integration technique. It has been shown that it is necessary to use the steepest descent approach[6]. However if one is interested for the field strength inside the waveguide this can be computed by considering only the surface wave contributions. Indeed if the steepest descent approach is used it is shown that the contribution to the integral of eq. (15) arise in the form of a superposition of surface waves and radiation fields. The former waves being two dimensional waves attenuates as $1/\sqrt{\rho}$ while the radiated waves as $1/\rho$. Therefore if both the transmitter and receiver are inside the duct the field strength is computed by taking into account only the surface wave poles. After some algebra, the final result is obtained in the following form

$$E_\varphi = \frac{[illegible]}{2} \sum_{i=1}^{N_e} \gamma_i^2 H_1^{(2)}(\gamma_i \rho)\, b_1(\gamma_i)\, e^{-(\gamma_i \gamma_i z)} + b_2(\gamma_i)\, e^{-(\gamma_i \gamma_i z)} \tag{18}$$

where [illegible] for [illegible].

Following a similar procedure for the magnetic dipole excitation we obtain the following result for the vertical magnetic field,

$$\mu_o H_z = m \frac{\pi i}{2} \sum_{i=1}^{N_m} \gamma_i^2 H_o^{(2)}(\gamma_i \rho) \left(d_1(\gamma_i) e^{i q(\gamma_i) z} + d_2(\gamma_i) e^{-i q(\gamma_i) z} \right) \qquad (19)$$

where now the surface wave numbers are determined from the roots of the equation $\Delta_m(\lambda) = 0$, N_m is the number of roots and

$$d_j(\gamma_i) = \lim_{\lambda \to \gamma_i} \left((\lambda - \gamma_i) D_j(\lambda) \right)$$

As $\rho \to \infty$, the Hankel function in eqs (18) and (19) can be replaced with the asymptotic expansion:

$$H_o^{(2)}(\gamma_i \rho) \cong \left(\frac{2}{\pi \gamma_i \rho} \right)^{1/2} e^{-i(\gamma_i \rho - \pi/4)} \qquad (20)$$

4. COMPUTATION OF THE FIELD FOR THE REGION $z > h$

In this case, the field should be computed by substituting eqs. (11c) (12c) into (8b), (9b) respectively. Again we consider the vertical electric dipole first. The Π_2 potential function after transforming the integration variables into cylindrical coordinates and by using eq. (14b) can be written as:

$$\Pi_2 = \frac{I}{4} \int_{\lambda=0}^{+\infty} \frac{\lambda}{\mu_o} d\lambda \, H_o^{(2)}(\lambda \rho) \, C_1(\lambda) e^{-\mu_o (z-h)} \qquad (21)$$

The residue contributions due to the surface wave poles gives leaking waves because of the $e^{-\mu_o(z-h)}$ term. Then the surface waves and the radiation field could have comparable contributions. Therefore it is necessary to consider both kind contributions. To this end use is made of the steepest descent technique. Substitute for the integration variable $\lambda = -k_o \cos\alpha$ and define $\mu_o = i k_o \sin\alpha$, $\alpha = \xi + i\eta$. Then in the new complex a-plane the integration path is shown with the Ca where the location of the surface wave poles is also indicated. Introducing the spherical coordinates $\rho = R\cos\psi_o$, $z - h = R\sin\psi_o$ and by using eq.(20) the Π_2 potential function is written as:

$$\Pi_2 = \frac{I}{4\pi} \int_{Ca} d\alpha \, F(\alpha) \, e^{i k_o R \cos(\alpha + \psi_o)} \qquad (22a)$$

where $F(\alpha) = k_o \sin\alpha \left(\frac{2}{\pi k_o \rho \cos\alpha} \right)^{1/2} C_1(-k_o \cos\alpha) \, e^{i\pi/4}$ (22b)

The stationary point of the integrand function in eq. (22) is determined from $\sin(\alpha + \psi_o) = 0$ or $\alpha = -\psi_o$. The steepest descent path Cs (see Fig. 4) is obtained from the conditions: $\mathrm{Re}\{\cos(\alpha + \psi_o)\cos(i\eta)\} = 0$ or $\cos(\xi + \psi_o)\cosh(\eta) = -1$ subject to $\mathrm{Im}\{\cos(\alpha + \psi_o)\} < 0$. It is possible to apply the Cauchy theorem to compute the integral in eq. (22) for the contour $Ca, T_2, (-Cs), T_1$ (see Fig. 4). The integrand function vanishes exponentially on the T_1 and T_2 paths and then from eq. (22)

$$\Pi_2 = \frac{I}{2} \sum_{\substack{\text{Enclosed} \\ \text{surface} \\ \text{wave poles}}} \mathrm{Res}_{\lambda = \gamma_i} \left(F(\alpha) \right) e^{i(\gamma_i \rho - \mu_o(\gamma_i)(z-h))} \qquad (23)$$

$$+ \int_{Cs} d\alpha \, F(\alpha) \, e^{i k_o R \cos(\alpha + \psi_o)}$$

In order to compute the integral on the C_s path we follow the well known procedure[5]. If however $\psi_o \sim 0$, which is the most interesting case in practice, then care should be taken for the approximation of the F function around the α_s on the steepest descent path. Indeed if the elevation angle ψ_o (see Fig. 1) is sufficiently small the surface wave poles are in the vicinicity of the stationary point. Then as we introduce into the integral of the eq. (23) $\alpha = \alpha_s + q e^{i\pi/4}$ for points $\alpha \sim \alpha_s$ on the Cs contour the functions appearing under the integral sign are expanded as:

$$\cdots \qquad (24)$$

$$\cdots \quad \text{(Taylor series)} \qquad (25)$$

where $\cdots$

and $\cdots$

The approximate steepest descent integral then takes the form

$$\int_{C} F(\alpha) e^{-ik_0 R\cos(\alpha+\psi_0)} d\alpha \approx \int_{C_s} F(\alpha) e^{-ik_0 R\cos(\alpha+\psi_0)} d\alpha + \sum_{i=1}^{N_p} \frac{\gamma_i}{\alpha-\alpha_i} \Bigg) e^{\frac{\pi i}{2}} k_0 R \tag{26}$$

or computing[7] the definite integrals and substituting the $F(\alpha)$ function from eq. (22b) and (11c) we obtain the final result:

$$\int_{C_s} F(\alpha) e^{-ik_0 R\cos(\alpha+\psi_0)} d\alpha = e^{-ik_0 R + i\frac{\pi}{4}} \left(\frac{2\pi}{k_0 R}\right)^{1/2} G(\alpha_s) + \pi i \sum_{i=1}^{N_p} \gamma_i e^{ik_0 \frac{(\alpha_s-\alpha_i)^2}{2}} \operatorname{erfc}\left(\mp i \sqrt{\frac{k_0 R}{2}} (\alpha_s-\alpha_i)\right) \tag{27}$$

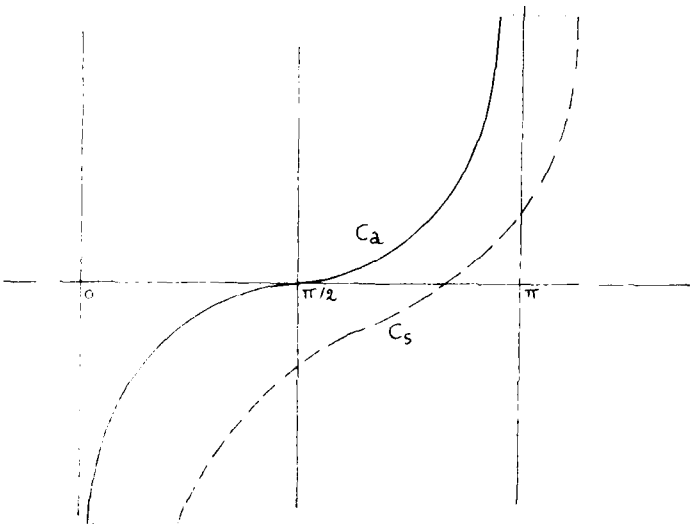

Fig. 4. Complex α-plane

5. ANALYSIS OF MULTIPATH DISTURBANCES IN A TROPOSPHERIC DUCT FOR A PSK SYSTEM

The results obtained in the preceding sections concern the electromagnetic field under a continuous wave excitation. Consider the case of the eq. (18) which can be rewritten as

$$E_z(r,\omega) = \sum_{i=1}^{N_p} A_i(\omega) e^{-\gamma_i(\omega) r} e^{-j\omega t} \tag{28}$$

where

$$A_i = \frac{1}{\sqrt{2\pi}} \frac{1}{\sqrt{a}} \frac{\gamma_i k_0^2 (1+\varepsilon_1^{-1})\sqrt{\gamma_i k_0}}{1+\varepsilon_0\gamma_i^2 - \gamma_i k_0^2 (1+\varepsilon_1^{-1})} \cdot \gamma_i^{-\frac{1}{2}} F_1(\gamma_i^2 / \gamma_i k_0^2) \tag{29}$$

is a real number.

It is evident that the amplitudes of the surface waves A_i and the propagation constants γ_i are functions of the cw frequency ω. In case of transmission of information instead of a cw transmission a signal of finite bandwidth B should be radiated from the transmitter. If $B \ll 1$, as it is in most cases, then $\gamma_i(\omega)$ can be expanded around the center frequency $\omega = \omega_c$ as follows:

$$\gamma_i(\omega) = \gamma_i(\omega_c) + \left(\frac{d\gamma_i}{d\omega}\right)_{\omega=\omega_c} (\omega-\omega_c) + \frac{1}{2}\left(\frac{d^2\gamma_i}{d\omega^2}\right)_{\omega=\omega_c} (\omega-\omega_c)^2 + \ldots \tag{30}$$

where $\gamma_i'(\omega_o) = \partial \gamma_i(\omega)/\partial\omega\,|_{\omega=\omega_o}$ is the group delay and when $|\omega-\omega_o|/\omega_o \ll 1$ The corresponding real field in the time domain is computed easily and is written as

$$E_z(\rho,z,t) = \sum_{i=1}^{Ne} A_i(\omega_o)\, \sin(\omega_o t - \gamma_i(\omega_o)\rho)\; p(t-\gamma_i'(\omega_o)\rho) \qquad (31)$$

This shows that the signal arriving to the receiver consists of several surface waves. For each surface wave the propagation delay is given by $\gamma_i'(\omega_o)\rho$ and the corresponding phase notation by $\gamma_i(\omega_o)\rho$ The notation $p(t-\gamma_i'(\omega_o)\rho)$ is to indicate the delay of the electric dipole moment signal in the time domain. The modulation signal can be expressed with a time domain wave-form as

$$v(t) = \sum_{n=-N}^{N} a_n\, g(t-nT)$$

where T is the bit transmission period, $2N$ is the number of bits, for a PSK signal $a_n = \pm 1$ and

$$g(t) = \begin{cases} 1 & 0 \le t < T \\ 0 & \text{otherwise} \end{cases}$$

The electric dipole moment is propotional to the antenna current. Then $p(t) = C\, v(t)$, with C being a constant depending on the antenna type and transmitted power level. In addition to the useful information signal we always have the additional Gaussian channel noise affecting the communication link. According to these considerations the signal at the receiver I.F Channel output can be written as

$$S(t) = \kappa \sum_{i=1}^{P} A_i \sin(\omega t - \gamma_i\rho) \sum_n a_n g(t-nT-\gamma_i'\rho) + \xi(t)\sin(\omega t) + \eta(t)\cos(\omega t) \qquad (32)$$

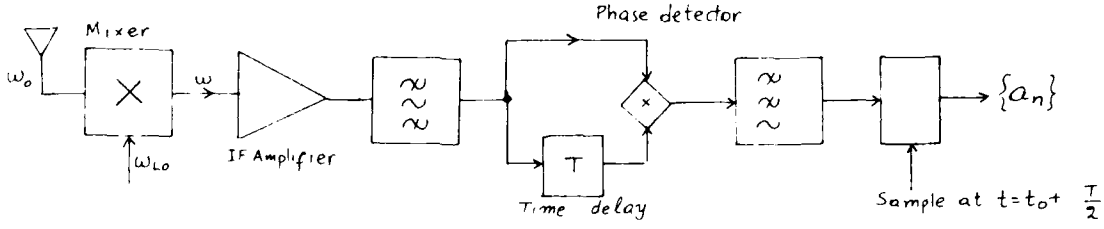

Fig. 5. Block diagram of the demodulation process.

where κ is a propotionality constant, $P = Ne$ or N_m and $(\xi^2(t)+\eta^2(t))^{1/2}$ is the noise envelope in the I.F. filter output.

In most practical cases a differential modulation scheme is used. A simplified block diagram of a such receiver is shown in Fig. 5. The output from the phase detector after the low pass filtering is written as:

$$\begin{aligned}
\frac{1}{\kappa}\langle S(t)S(t-T)\rangle = {} & \sum_{i=1}^{P}\sum_{j=1}^{P} A_i A_j \cos((\gamma_j-\gamma_i)\rho+\omega_c T) \sum_n \sum_m a_n a_m\, g(t-nT-\gamma_i'\rho)\, g(t-(m+1)T-\gamma_j'\rho) \\
& + \big(\xi(t)\xi(t-T) + \eta(t)\eta(t-T)\big)\cos(\omega_c T) \\
& + \big(\xi(t)\eta(t-T) - \eta(t)\xi(t-T)\big)\sin(\omega_c T) \\
& + \Big(\sum_{i=1}^{P} A_i \cos(\omega_c T - \gamma_i\rho)\sum_n a_n g(t-nT-\gamma_i'\rho)\Big)\xi(t-T) \\
& + \Big(\sum_{i=1}^{P} A_i \sin(\omega_c T - \gamma_i\rho)\sum_n a_n g(t-nT-\gamma_i'\rho)\Big)\eta(t-T) \\
& + \Big(\sum_{j=1}^{P} A_j \cos(\omega_c T + \gamma_j\rho)\sum_m a_m g(t-(m+1)T-\gamma_j'\rho)\Big)\xi(t) \\
& + \Big(\sum_{j=1}^{P} A_j \sin(-\omega_c T - \gamma_j\rho)\sum_m a_m g(t-(m+1)T-\gamma_j'\rho)\Big)\eta(t)
\end{aligned} \qquad (33)$$

If $\omega_c T = 2\pi L$ (L integer multiplier) and if the decision for the transmitted bit is done with sampling at the time instants $t = t_o + T/2$, $t_o + 3T/2$, $t_o + 5T/2$ the sampler output is written as

where [illegible] the final result is written as:

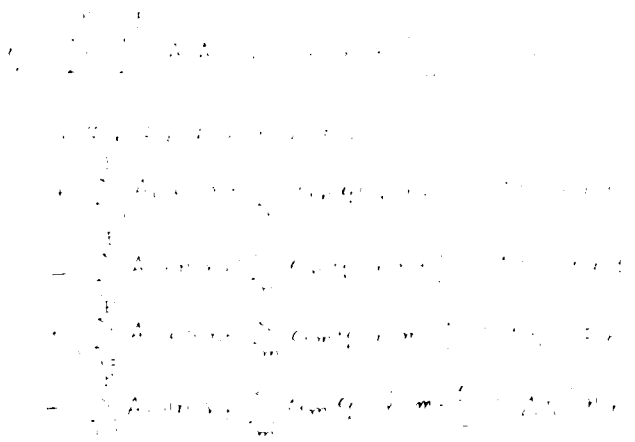

(34)

where [illegible] and [illegible] is the differential delay.

It should be emphasized that the assumption of sampling in the middle of the bit period increases the suceptibility of the PSK demodulation to multipath fading. Examining eq. (34) we can distinguish two extreme cases:

(a) When [illegible], then intersymbol interference phenomena are neglible. The existence of multipath propagation is exhibited in the form of constructive or destructive interference.

(b) When [illegible] then a strong intersymbol interference or otherwise known as selective fading is observed.

In this paper we are interested for the (b) type phenomena. However it is directly evident that if [illegible] the communication channel is highly dispersive and adaptive equalization could be utilized to reduce the selective fading. This results into a complex receiver design and it will not be treated further. In the rest part of this paper we focus our attention to the case when [illegible] i.e. each bit interacts with the next transmitted bit. Under this assumption the summation over the m and n integers in eq.(34) can be reduced to the integer values [illegible] and [illegible]. Furthermore introducing some new random variables

$$w_1 = \sum_{i=1}^{P} A_i \cos(\gamma_i \rho) \left(a_{\ell} g\left(\frac{3}{2}T - \Delta\tau_i\right) + a_{\ell} g\left(\frac{T}{2} - \Delta\tau_i\right) \right) + \xi(\ell)$$

$$w_2 = \sum_{i=1}^{P} A_i \cos(\gamma_i \rho) \left(a_{\ell-1} g\left(\frac{3}{2}T - \Delta\tau_i\right) + a_{\ell} g\left(\frac{T}{2} - \Delta\tau_i\right) \right) + \xi(\ell-1)$$

$$w_3 = \sum_{i=1}^{P} A_i \cos(\gamma_i \rho) \left(a_{\ell} g\left(\frac{3}{2}T + \Delta\tau_i\right) + a_{\ell-1} g\left(\frac{T}{2} - \Delta\tau_i\right) \right) + \eta(\ell)$$

$$w_4 = \sum_{i=1}^{P} A_i \cos(\gamma_i \rho) \left(a_{\ell-2} g\left(\frac{3}{2}T - \Delta\tau_i\right) + a_{\ell-1} g\left(\frac{T}{2} - \Delta\tau_i\right) \right) + \eta(\ell-1)$$

and the complex random variables

$$z_1 = w_1 + jw_3 \qquad z_2 = w_2 + jw_4$$

eq. (34) can be written in compact form as

$$z = \mathrm{Re}\{z_1 z_2^*\} = w_1 w_2 + w_3 w_4$$

In order to compute the probability of error for each transmitted bit an assumption should be made for the communication protocol for the differentially coherent phase shift keying. If [illegible] then the transmitted bit [illegible] is mark (0^0 phase shift) and if [illegible] then it is space (180^0 phase shift). Therefore the conditional error probabilities are written as

[illegible] $\mathrm{Prob}(\mathrm{Re}\{z_1 z_2^*\} < 0)$

and

$$P_E = \frac{1}{4} \sum_{a_{\ell-2}=-1}^{+1} \left(P_\varepsilon(a_\ell=+1, a_{\ell-1}=+1 | a_{\ell-2}) + P_\varepsilon(a_\ell=-1, a_{\ell-1}=+1 | a_{\ell-2}) \right)$$

The probability of $Re(z_1 z_2^*) < 0$ is computed from the well known result of the DPSK theory[8]. Applying this formulation to our problem we arrive to the following results:

$$Prob(Re(z_1 z_2^*) < 0) = \frac{1}{2} \left[1 - Q(\sqrt{B}, \sqrt{A}) + Q(\sqrt{A}, \sqrt{B}) \right]$$

where

$$B = \frac{\alpha_1^2}{\sigma^2}, \qquad A = \frac{\alpha_2^2}{\sigma^2}$$

$$\alpha_1 = \left| \sum_{i=1}^{P} A_i e^{j\gamma_i p} \left[a_{\ell-1} \left(g(\tfrac{3}{2}T - \Delta\tau_i) + g(\tfrac{T}{2} - \Delta\tau_i) \right) + a_\ell \, g(\tfrac{T}{2} - \Delta\tau_i) + a_{\ell-2} g(\tfrac{3}{2}T - \Delta\tau_i) \right] \right|$$

$$\alpha_2 = \left| \sum_{i=1}^{P} A_i e^{j\gamma_i p} \left[a_{\ell-1} \left(g(\tfrac{3}{2}T - \Delta\tau_i) - g(\tfrac{T}{2} - \Delta\tau_i) \right) + a_\ell \, g(\tfrac{T}{2} - \Delta\tau_i) - a_{\ell-2} g(\tfrac{3}{2}T - \Delta\tau_i) \right] \right|$$

$$\sigma^2 = \langle \xi_\ell^2 \rangle = \langle \xi_{\ell-1}^2 \rangle = \langle \eta_\ell^2 \rangle = \langle \eta_{\ell-1}^2 \rangle$$

and

$$Q(\omega_1, \omega_2) = \int_{\omega_2}^{+\infty} x \, dx \, \exp\left(-\frac{\omega_1^2 + x^2}{2} \right) I_0(\omega_1 x)$$

is tne Q-function of the probability theory.

6. NUMERICAL RESULTS

Numerical computations have been performed using the theory of the previous sections. In the following computations the tropospheric duct height is taken h=100m, the relative electric constant is $\varepsilon_1 = 1.000120$ and propagation is considered for f=1GHz and f=3GHz transmission frequencies for vertical polarized waves. In fig.6 the error probability Pe is given vs. the signal to noise ration (S/N) for the f=1GHz frequency and a path length of 100km where the number of participating modes is $N_e=7$. The surface waves are grouped in two packets in terms of the differential delay which are $\Delta\tau = 14.81$ ns and 23.96 ns for 100km. According to this there are three different bit transmission rate regions with different corresponding Pe vs. (S/N) behavior. These regions are $T < 2 \times 14.81 = 29.62$ ns, $29.62\text{ns} < T < 2 \times 23.96 = 47.92$ and $T > 47.92$ ns When $T < 29.62$ ns the $P_e = 0.5$ independently of the (S/N) ratio and when $T > 47.92$ ns the Pe dependence to the (S/N) ratio is the same with the ideal DPSK modulation case.

In fig. 7 results are given for the same tropospheric duct path for a higher frequency f=3GHz where the number of surface waves is Ne=19. The variation of the Pe with the bit transmission rate is an interesting one. Observe that for the assumed tropospheric path of 100km maximum available bandwidth is $1/80\text{ns} \approx 12$ MHz at f=3GHz transmission frequency.

7. CONCLUSIONS

The multipath propagation in tropospheric duct media is treated analytically. Analytical expressions are developed for the probability of error Pe versus signal to noise ratio (S/N) for a differentially coherent Phase Shift Keying Communication system. Numerical results have been computed for several cases. The results of these computations reveals the restrictions that are impos on Digital Radios by the multipath propagation in tropospheric ducting media.

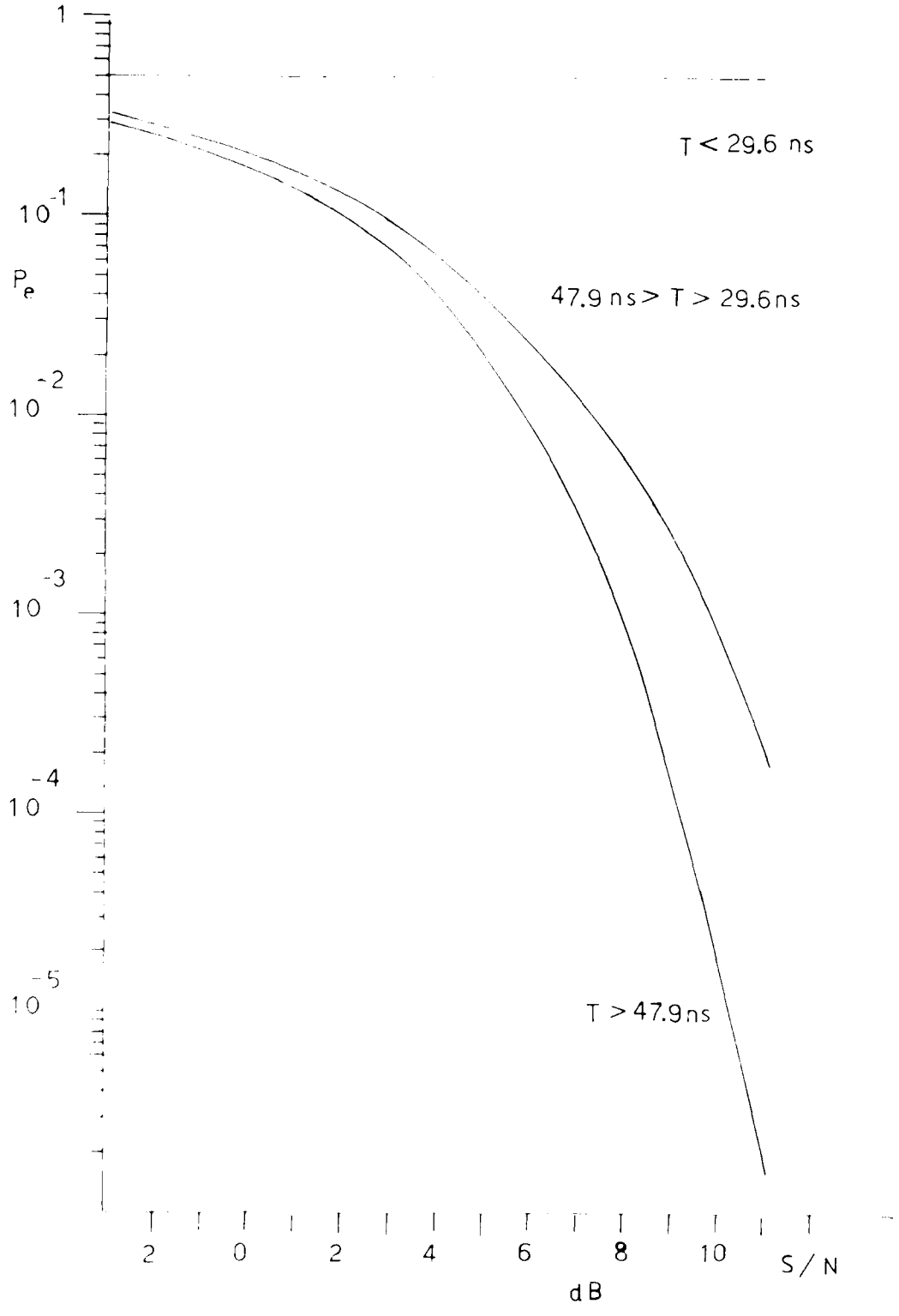

Fig. 6 Probability of error (Pe) vs. (S/N) for several T bit periods at f 1GHz, the propagation path is 100km, h 100m and ϵ_1 1.00012

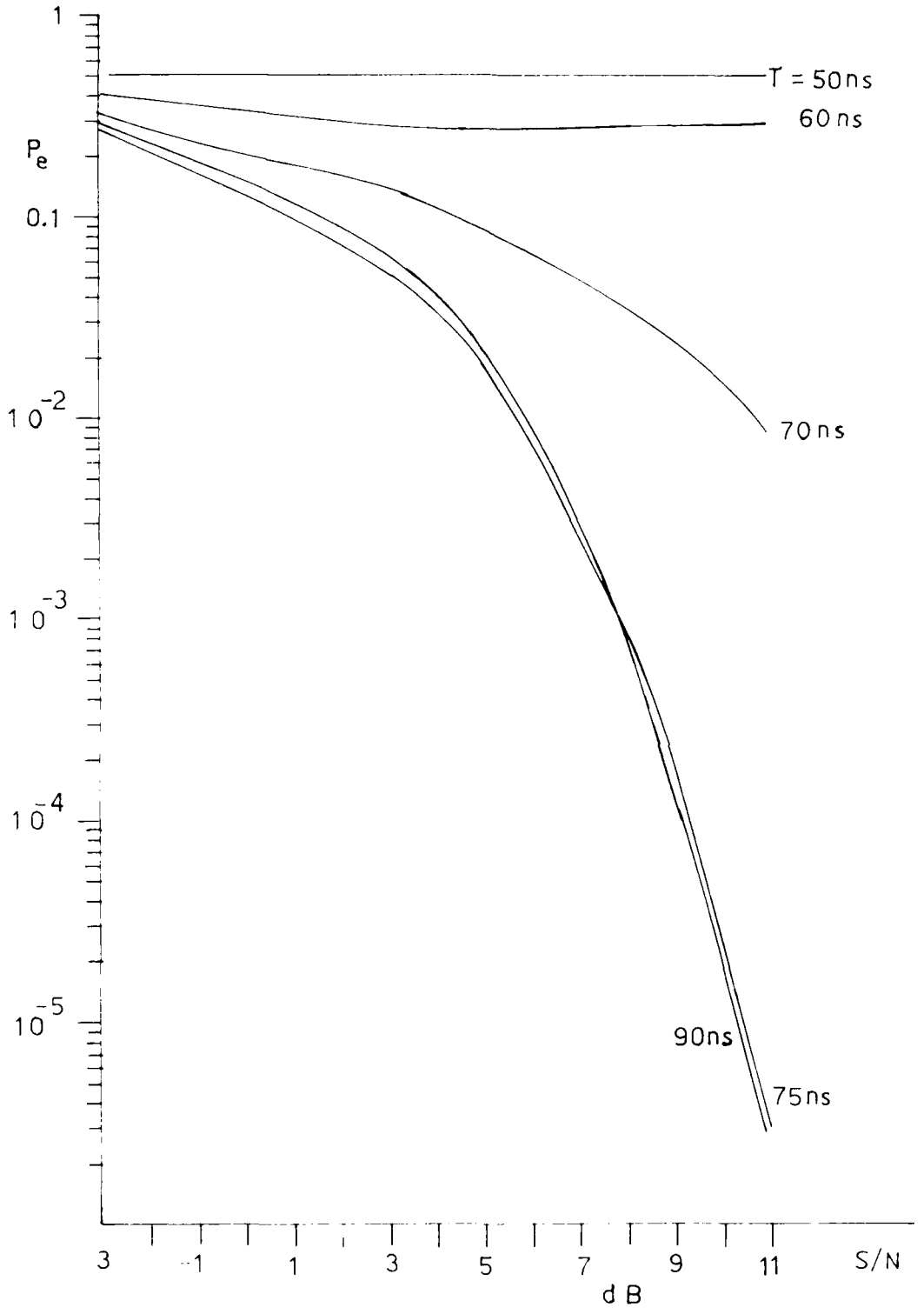

Fig. 7 Pe vs. (S/N) for various T bit Periods at f = 3GHz, the propagation medium is the same with fig. 6.

REFERENCES

1.- C.L. Pekeris,"Asymptotic solutions for the normal modes in the theory of microwave propagation",J. Appl. Phys.,VOL. 17,pp. 1108-1124,(1946).

2.-J.B. Smyth and L.G. Trolese, "Propagation of Radio Waves in the Lower Troposphere", Proc. I.R.E., vol. 35,pp.1198-1202,(1947).

3.- P.K. Arora and J.R. Wait, "Refraction theories of radio wave propagation through the troposphere - A review ",vol. 13,pp. 599-600, (1978).

4.- J.S. Jones, Theory of Electromagnetism, Pergamon Press, London (1964) (Chapter 6)

5.- R.E. Collin, Field Theory of Guided Waves, Mc Graw Hill, New York (1960),(Chapter 11).

6.- A. Baños, Dipole Radiation in the Presence of a Conducting Half - Space, Pergamon Press, Oxford, (1966), (Chapter 3).

7.- Ref.6 page 22.

8.- M. Schwartz, W.R. Bennet and S. Stein, Communication Systems and Techniques, Mc Graw-Hill, New York,(1966),(Chapter 8).-

DIGITAL DATA COMMUNICATIONS OVER MICROWAVE RADIO CHANNELS

J. Salz
AT&T Bell Laboratories
Crawford Hill Laboratory
Holmdel, NJ 07733

ABSTRACT

A major contribution to system outage in a terrestrial digital radio channel is deep fading of the frequency transfer characteristic, which in addition to causing a precipitous drop in received signal-to-noise ratio (s/n) also causes signal dispersion that can result in severe intersymbol interference. Because the temporal variation of the channel is slow compared to the signaling rate, the information theoretic channel capacity and the "Efficiency Index" in bits/cycle - a figure-of-merit we use for the communication techniques considered - can be viewed as random processes.

Based on an established mathematical model for fading channels, we estimate the probability distribution of channel capacity and the distribution of efficiency indices for different communications techniques. A crucial obstacle to achieving these rates is the nonlinear distortion introduced by power amplifiers. We also describe a method for coping with this nonlinear distortion.

I. INTRODUCTION

Fading of terrestrial digital radio channels owing to multipath reception is a prime cause of system outage. For a specific hop a mathematical model of these fades has been developed by W. D. Rummler[1,2] from measurements of the channel frequency power transfer characteristic over time. The radio channel has a time-varying frequency characteristic, with additive Gaussian noise; however, the temporal variations are slow in comparison to the data symbol rate so that the characteristics can be represented as a random ensemble of static power transfer functions. The presence of additive noise implies that each member of the ensemble is limited to a maximum rate of transmission of data, depending on the communication method. For each specific communication technique, the stochastic nature of the channel makes it meaningful to consider the probability distribution of data rates that can be supported at a certain bit-error-rate objective.

High bit rates are achieved with multilevel signaling or, with a modulation technique referred to as Quadrature Amplitude Modulation (QAM). The use of this technique, however, has been inhibited by the amplitude (AM/AM) and phase (AM/PM) nonlinearities present in r-f power amplifiers.

Here we also discuss the problem of adaptive predistortion linearization. We describe a transmitter-based recursive algorithm for predistorting the signal constellation, thereby rendering a virtually linear transmitter. The algorithm operates in real-time and is data-directed. The predistortion is accomplished within a digital memory, which is used to generate the desired baseband signal.

II. THE EQUALIZED QAM SYSTEM-IDEALIZED MODEL

The use of equalizers to mitigate the effects of ISI and noise in voiceband data transmission is by now standard. We are thus led to consider the application of these techniques in digital data transmission over the radio channel where slowly varying frequency-selective fading is the predominant impairment.

Our analyses are based on the digital communications model depicted in Figure 1. To appreciate the applicability and generality of this baseband model to digital radio communications, we observe that, for any bandpass linear channel, the output waveform, when the input is any linearly modulated data wave, can be represented as

$$s(t) = \mathrm{Re}\left\{\sum_n a_n h(t - nT + t_0) \exp\left[i(2\pi f_0 t + \phi)\right]\right\} .$$

where Re $\{\cdot\}$ stands for the "real part". The data symbol $\{a_n\}$ transmitted at T-second intervals, are statistically independent and assume complex values. The overall equivalent baseband impulse response, h(t), is also complex-valued. The real part represents the in-phase response, while the imaginary part is the quadrature component. The frequency, f_0, is the carrier frequency, ϕ is the carrier phase, and, t_0 is the timing phase. Ideal demodulation with a known carrier frequency f_0 and carrier phase ϕ implies a translation of the received bandpass signal to baseband. The real part of the resulting complex signal represents the in-phase modulation, while the imaginary part is the quadrature modulation. This then is the rationale, in addition to economics of notation, for using the complex baseband model depicted in Figure 1.

We now discuss various functions and notations. Without loss of generality we assume that the complex data symbols, $a_n + ib_n$, take values on a set of positive and negative odd integers with equal probability. Accordingly,

$$E a_n = 0 \text{ and } E\{a_n^2\} = 2\,\frac{L^2 - 1}{3}$$

where $E\{\cdot\}$ denotes mathematical expectation and L (even) is the maximum number of data levels assumed by a_n and b_n. Thus, in QAM, L^2 data points are available for conveying information and the source therefore generates

$$R = \frac{\log_2 L^2}{T} \text{ bits/sec} . \tag{1}$$

For a given channel bandwidth, W, the efficiency index is defined as

$$I = R/W = \frac{2 \log_2 L}{WT} \text{ bits/cycle} . \tag{2}$$

The relationship among P_e probability of error, s/n, W, T and $H(\omega)$ is rather complicated, and is discussed in detail in Reference 3.

The fading radio channel is characterized by a slowly varying linear filter whose baseband equivalent complex impulse response is the Fourier transform of the transfer function $H(\omega)$, shifted to zero frequency:

$$h(t) = h_1(t) + ih_2(t) = \int_{-2\pi W}^{2\pi W} H(\omega)\, e^{i\omega t}\, \frac{d\omega}{2\pi} .$$

At the receiver the filtered complex noise process, $\nu(t) = \nu_1(t) + i\nu_2(t)$, is assumed to be white Gaussian with $\nu_1(t)$ independent of $\nu_2(t)$ and each possessing a double-sided spectral density $N_0/2$. Thus,

$$E\{\nu(t)\nu^*(t)\} = E\nu_1^2(t) + E\nu_2^2(t)$$

$$= N_0 \delta(0) .$$

where $\delta(\cdot)$ is the Dirac delta function. The average transmitted signal power, P_0, for the ideal transmitting filter can easily be calculated. However, for our purposes a more relevant quantity is the received signal power

$$P = K^2 P_0 = 2\,\frac{L^2 - 1}{3}\,\frac{K^2}{T^2} ,$$

where K^2 is a constant that includes the effects of amplifiers, antennas, and the unfaded channel loss. Also, the added average noise power in the Nyquist band, $W = 1/2T$, is

$$P_n = \frac{N_0}{T} .$$

Thus the emitted received s/n, is

$$s/n = 2\,\frac{L^2 - 1}{3}\,\frac{K^2}{N_0}\,\frac{1}{T} . \tag{3}$$

The receiver structure under consideration consists of a perfect demodulator followed by a matched filter with complex response $W(t)$, a sampler, a decision device, and a timing circuit. The design of an optimum receiver entails the selection of $W(t)$ and the timing for a particular channel. Since the channel characteristics are usually unknown to the receiver, these components must be determined adaptively.

To characterize the function of the receiver, consider the signal sample at the output of the matched filter,

$$z_n = \sum_k h_{n-k} a_k + \nu_n , \tag{4}$$

where $h_{n-k} = h(nT - kT)$ is the overall sampled impulse response and z_n is the Gaussian

Noise Temperature

The receiver noise temperature is the sum of the effective temperatures of the antenna, transmission line, preamplifier and succeeding stages; here, the primary contribution is due to the preamplifier; a secondary contribution due to the antenna and transmission line, and a minor contribution due to the succeeding stages. The receiver system effective noise temperature (referenced to the preamplifier input) is given by[22]:

$$T_e = aT_A + T_O(1 - a) + T_1 + \sum_{n=2}^{M} \frac{T_n}{G_{n-1}}$$

where a is transmitter line transmission coefficient (0.7 @ 1 dB);
T_A is the antenna effective noise temperature (290°K);
T_O is the physical temperature of the transmission line (290°K);
T_1 is the noise temperature of the preamplifier (1150°K @ 7 dB);
T_M is the noise temperature of the succeeding M_{th} stage and
G_{M-1} is the gain preceding the M_{th} stage.

Using the above inputs, the receiver effective temperature is estimated at approximately 1500°K. The major noise temperature contributions are those prior to, and including, the preamplifier; subsequent stages are not a major contribution, due to the reciprocal gain function.

Receiver Noise Figure

The receiver noise figure F is given by the equation[23]:

$$F = (1 + T_e/T_O)$$

For the effective temperature T_e of 1500°K above, the noise figure for the baseline receiver is estimated at 6 (absolute number), or 8 dB.

Receiver Noise Input

The receiver noise input can be given by the thermal relation, using the effective noise temperature:

$N_{th} = \kappa T_e B$, where k is Boltzmann's constant at -198.6 dBm/°K/Hz,
T_e is the effective noise temperature at 1500°K, and
B is the receiver noise bandwidth at (nominally) 20 KHz.

Equivalently, the noise input can be derived from the physical temperature, using the expression:

$$N_{th} = K T_O B F.$$

For the systems under consideration here, the thermal noise input is:

16 Kbps: N_{th} = -122 dBm

2.4 Kbps: N_{th} = -130 dBm

LINK BUDGET CALCULATIONS

Maximum Allowable Attenuation

The link power-budget calculations determine maximum allowable attenuation, according to:

$ATTN_{max}$ = Effective Radiated Power - Thermal noise - Margins

= $- N_{th} + P_{PA} + G_{TX} + G_{RX} - S/N - LINKMARGIN$ by reordering and substituting.

The following system baseline calculations and parameters are determined from the above relationships:

PARAMETER	SYMBOL	16 KBPS		2.4 KBPS	
Receiver Noise Temperature	T_e	1500	deg K	1500	deg K
Receiver Noise Figure	F	8	dB	8	dB
Data Rate	D	16	Kbps	2.4	Kbps
Detection Bandwidth	B	32	KHz	4.8	KHz
Thermal Noise Power	N_{th}	-122	dBm	-130	dBm
Transmitter Power Amplifier	P_{PA}	40	dBm	40	dBm
Transmitter Antennna Gain	G_{TX}	0	dB	0	dB
Receiver Antenna Gain	G_{RX}	0	dB	0	dB
Signal-to-Noise Requirement	S/N	9	dB	9	dB
Link Margin Allowance	LINKMARGIN	9	dB	9	dB
Maximum Allowable Attenuation	$ATTN_{max}$	144	dB	152	dB

Sweep Time:

The sweep time is calculated by finding the dwell time in each scanning bandwidth sample, and multiplying by the number of bandwidths to be sampled:

$$t_{sweep} = \text{time/sample} \times \text{number of samples}$$

$$= \text{bits/sample} \times \text{time/bit} \times \frac{\text{swept bandwidth}}{\text{sampling bandwidth}}$$

$$= \text{bits/sample} \times \frac{1}{\text{data BW}} \times \frac{\text{IF BW}}{\text{detection BW}}$$

For 2-bit sampling, using 2.4 Kbps data rate as worst-case:

$$t_{sweep} = 2 \text{ bits}/(2.4 \times 10^3) \text{ bits/sec} \times 480 \text{ Khz}/4.8\text{Khz}$$

$$= 80 \text{ msec.}$$

Acquisition Probability

Acquisition probability, P_{acq}, is determined by the probability-of-detection per sweep. The acquisition probability for any number of sweeps, i, is given by:

$$P_{acq} = 1 - (P_{miss})^i$$

$$= 1 - (1 - P_D)^i$$

The following list of acquisition probabilities over an integral number of sweeps is generated for 2.4 Kbps data, and P_D of 85% and 60%:

Sweeps	Time	P_{acq} (P_D @ 85%)	P_{acq} (P_D @ 60%)
1	80 msec	0.85	0.6
2	160	0.9775	0.84
3	240	0.9966	0.936
4	320	0.9995	0.9744

A few sweeps may be sufficient to satisfy acquisition requirements for a system as here discussed.

Tracking

Tracking requirements are defined by the short-term oscillator instabilities, and by the Doppler rate of frequency shift, or frequency slew. For systems with high Doppler in close passage, it is obvious that the slew can be extremely high, as determined by the separation distance, and the velocity-vector differences. The Doppler time-rate of change, or Doppler slew, can significantly impacts tracking circuit performance. The slew is essentially proportional to relative platform acceleration. This acceleration can be caused by actual aircraft change in velocity, or by apparent platform velocity change due to time-variation in the geometric situation. In the first case, the slew will be relatively slow, in the second, geometric conditions can change extremely rapidly in close passing situations, and it is easily conceivable that the Doppler slew can exceed circuit frequency tracking capability. Tracking capability for coherent demodulation is also affected by phase-noise generated by the oscillators.

Frequency Offset Contribution

Frequency offset in detection circuits will result in signal loss, and affect link-margin calculations. Loss margins of 1, 2, and 3 dB correspond to signal phase offsets of roughly 40°, 50°, and 60° respectively. We allow a 1 dB loss in the link margin, corresponding to a 10% offset in the tracking circuits.

[illegible] Wide-band Bandwidths

Link Margin

Link margin allowance (LINKMARGIN) for the baseline is estimated as follows:

Transmitter line loss	1 dB
RF switch loss	0.5 dB
Rain/fog allowance	3 dB
Receiver line loss	1 dB
RF switch loss	0.5 dB
Frequency tracking loss	1 dB
Link Margin Allowance	7 dB

Demodulation

A trade-off analysis is required to determine best type of demodulation between coherent and non-coherent; this analysis has not been performed. Due to the possibility of rapid phase-fluctuations through a turbulent atmosphere, we assume non-coherent FSK demodulation for the baseline.

Probability of Error

LPC decoding is considered satisfactory at 10^{-2} bit-error-rate. This translates to a minimum signal-to-noise requirement of 9 dB for non-coherent FSK detection (7 dB for coherent FSK)[20]. In a Rayleigh fading channel the S/N requirement for noncoherent detection rises to 20 dB; link margin allowance of this magnitude may not be available for this application, and system performance might be marginal under these conditions. The fading issue, therefore, is critical to these considerations.

Probability of Detection

The probability of detection (P_D) is estimated at 85%, for a non-coherent detection S/N requirement of 9 dB[21]. In the case of Rayleigh fading, the detection probability for 9 dB S/N reduces to 60%. The figures for detection probability were derived on the basis of 10^{-2} false-alarm probability (P_{FA}). Under fading conditions, to maintain the 85% P_D figure quoted above, and for 10^{-2} P_{FA}, the S/N requirement rises from 9 dB to 14 dB. Again, fading may considerably affect system performance.

Acquisition

Acquisition time must not impact significantly into message time. The acquisition time depends on the detection probabilities, the sweep time of the scanning-receiver, and the ratio of total swept bandwidth to scanning bandwidth. There is a maximum bound to the swept, or IF, bandwidth determined by acquisition-time requirements. It is of little consequence whether the bandwidth is determined by oscillator uncertainty/instability, or Doppler shift (the major difference between them is that increased oscillator instability may cause increase in phase noise).

There is a difference between the acquisition bandwidth and the detection bandwidth. The detection bandwidth is, for FSK, that which passes through one of a pair of filters, each centered on a different FSK frequency (for simplicity, we consider the detection bandwidth of a signal at a data-rate D Kbps as equivalent to null-to-null bandwidth, 2D KHz, of a $\sin^2 x/x^2$ spectrum). The acquisition-channel bandwidth, however, must be capable of detecting either signal at any time. This involves an ambiguity, as to whether the first detected signal (Fig. 4a) is in the upper or lower frequency state, since the other FSK frequency may be either higher or lower than that first detected. The acquisition channel must be able to handle this ambiguity; this involves an increase in total bandwidth for the acquisition channel. We assume, for our first example, the offset of the FSK frequency shift centered at the first null (Fig. 4b). For this offset, the total acquisition bandwidth of 4D is the farthest null-to-null bandwidth of the combined signals, including any ambiguity. If the frequency offset is centered at the second null for purposes of decreasing bit error, the acquisition bandwidth would be 6D (Fig. 4c).

This problem for a scanning receiver is a consequence of the indeterminacy in location of an offset signal, on detection of the first signal. Superficially, it could be presumed that a scanning receiver could acquire on one frequency only, with a penalty of 3 dB due to loss of detected envelope power in the alternate frequency state. This is precluded here by the acquisition requirements. Since the sampling time of a few bits is so short, it is well within possibility that a single-frequency acquisition circuit, with a filter bandwidth equal to the null-to-null bandwidth of a single frequency state, could miss both signals during a sweep, by sampling when the signal is in the opposite state. This problem might be handled by a set of three filters in the acquisition circuit, each with bandwidth equivalent to the detection-bandwidth, and offset by the FSK frequency difference. Acquisition strategy then would involve detection of the first frequency using the center-tuned filter, providing detection capability at either higher/lower frequency by the remaining filters.

a. First detected signal

b. Upper/Lower FSK Possibilities (1-D Spacing)

c. Upper/Lower FSK Possibilities (2-D Spacing)

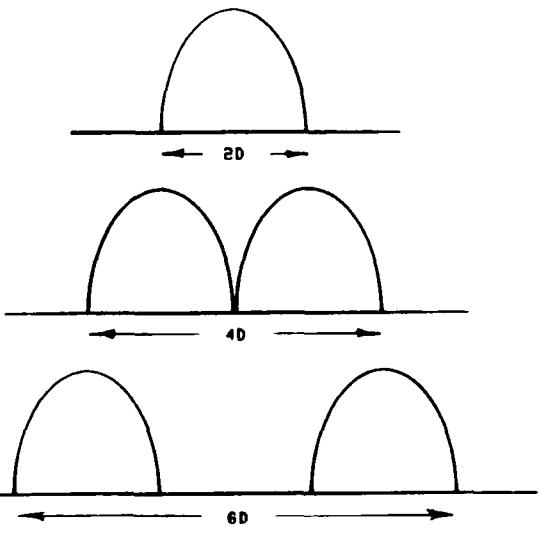

FIGURE 4. ACQUISITION BANDWIDTH

Transmission Line

At 50 GHz, the loss rate of WR-19 EHF waveguide is 0.05 dB/inch or 0.02 dB/cm[18]. To reduce transmission line loss, lines should be as short as possible; transmitter amplifier sections and receiver front ends should be positioned close to the antennas. Assuming short-length lines, we allow approximately 1 dB loss in the line from the power amplifiers to the antenna, in addition to 0.5 dB loss in the rf switch. Low loss amounts for line loss are allowed from the antenna to the receiver preamplifier.

Antennas

A major difference between air-to-air applications and others is the antenna coverage problem to maintain communications throughout operations. Aircraft will of necessity undergo many geometrical orientations during operations. In addition, aircraft formations usually utilize altitude differences between aircraft. Transmission or reception between aircraft from any single point on the aircraft may experience blockage, due to the fuselage, wings and stores. Since communications are required throughout operations, it is necessary to implement antenna design to provide maximum geometrical coverage. This requirement is reflected in use of wide-beam/low-gain antennas only, and in top and bottom antenna mounting on the aircraft. The best antenna type appears to be the discone, for azimuthal-omnidirectional pattern, combined with circular polarization, to partially correct for misalignment between airborne platforms due to arbitrary orientation of aircraft during maneuvers. Although it will not completely solve this problem, top and bottom antenna placement will alleviate blockage to a large extent. However, top and bottom antenna placement complicates the implementation of EHF, due to the lossy nature of transmission line at these frequencies. Design of the EHF system would necessitate that transmitter amplifier units, including the RF switch, and receiver front ends be close to, or integral with, each antenna unit.

Signal Interference

A consequence of transmission from multiple antennas, interference between the signals may occur at the receiver antenna, resulting in reduced capability. In order to reduce this interference, the fields of view should have minimum overlap. This might be accomplished by antenna design to restrict overlap in the vertical plane of vision, or by positioning the bottom antenna such that the aircraft body and stores could restrict the field of view, the field of view of the bottom antenna being primarily in a downward direction, and restricting lateral pattern-overlap. The top antenna would provide coverage to the side and upward.

In considering the interference problem in a different manner, multiple signal interference may be resolved by decorrelation (diversity) processes in space, time, frequency, or message structure (coding). It is conceivable that spatial decorrelation occurs as a matter of course due to the large wavelength spacing between top and bottom-mounted antennas, or because of transmission through different atmospheric paths in a turbulent medium. We have not yet considered this aspect in depth yet, to estimate whether spatial decorrelation in this context occurs. If interference exists, and spatial diversity does not occur, then the other diversity techniques as mentioned above must be considered, with attendant system complexity. However, due to time/bandwidth limitations, code-diversity does not appear feasible; emphasis therefore would be on frequency-diversity by offsetting frequencies between top and bottom antennas, and on time-diversity by alternate switching between antennas (the use of time-diversity would involve a 3 db loss in average signal power).

Receiver

A digital FFT receiver is probably optimal, but not practicable at the present state-of-art. An FFT receiver should eventually be considered with regard to this, or similar, applications.

Preamplifiers, Mixers

Present state-of-the art capability for EHF preamplifier-mixers with regard to noise figure is in the 6-7 dB range[19]; we use the higher figure in our calculations here.

IF Bandwidth

The IF bandwidth is determined by the sum of oscillator frequency uncertainties (both transmitter and receiver), Doppler frequency uncertainties, and the data bandwidth. Assuming elimination of all oscillator uncertainty, there is still an irreducible frequency uncertainty due to Doppler shift, on the order of 100 KHz or greater, corresponding to Doppler shift at EHF. Justification of oscillator accuracy better than Doppler uncertainty can not be made at this point, and the baseline requirements for oscillator accuracy use this as a bound. For these considerations, we estimate aircraft in-line approach/withdrawal at Mach 1 each, giving Doppler shifts at 60 GHz of ±120 KHz, resulting in an allowance for Doppler shift of 240 KHz. An equivalent allowance is made for oscillator frequency uncertainty; this is within presently-obtainable accuracy capability. The total IF bandwidth is the sum of the two, plus the detection bandwidth. The detection bandwidth is determined by link-budget requirements; both 16 Kbps and 2.4 Kbps data rates are initially used in the calculations. Detection bandwidths for these rates are 32 KHz and 4.8 Khz respectively, corresponding to the null-to-null frequency-separation (2D, or twice the data rate) of a $\sin^2 x/x^2$ spectrum. The IF bandwidths for these rates are then:

Data Rate:	Doppler	+	Uncertainty	+	Data BW	=	IF BW
16 Kbps	240 KHz	+	240 KHz	+	32 KHz	=	512 KHz
2.4 Kbps	240 KHz	+	240 KHz	+	4.8 KHz	=	485 KHz

Oscillators: Frequency Accuracy

In considering oscillator frequency accuracy/stability requirements, we base our considerations on present UHF capability: the accuracy of the present airborne AN/ARC-164 UHF voice radio. The following list[14] indicates ARC-164 accuracies for its various component units, UHF percentage accuracies, and the EHF equivalent absolute accuracies corresponding to these percentages.

AN/ARC-164 Unit	Accuracy	UHF Percentage	EHF Equivalent
Transmitter	± 500 Hz	$\pm 2 \cdot 10^{-6}$	± 100 KHz
Main Receiver	± 1.5 KHz	$\pm 5 \cdot 10^{-6}$	± 300 KHz
Guard Receiver	± 5 KHz	$\pm 2 \cdot 10^{-5}$	± 1 MHz

There is a factor of 200 between the UHF and EHF frequency bands, and we shall consider whether frequency accuracy/stability factors must be correspondingly improved for successful operation: whether present UHF percentage accuracies suffice for EHF, or whether frequency accuracy must be upgraded proportionally. If present absolute accuracy requirements are translated to EHF, the best present crystal oscillators would be needed. This would impact the system with regard to size and weight, warm-up time, and, as always, cost. This accuracy problem shall be discussed further with regard to receiver IF bandwidth.

An even more critical problem is that of oscillator stability. Any oscillator used for generation of EHF, whether generated at EHF, or at a lower frequency and multiplied up to EHF, will be subject to instabilities which will significantly affect modulation type, bandwidth, etc. These instabilities can be corrected to some extent by phase-locking; it may be necessary to correct instability even further by more complicated means (cavity-locking, for example). Oscillator stability requirements are dependent on modulation type, and modulation bandwidth. The area of voltage regulation is also very important, in any discussion of oscillator stability; voltage regulation and voltage-stability requirements must also be considered with regard to impact on frequency accuracy/stability.

Voice Encoding

The baseline considers two voice digital encoding rates: 16 Kbps and 2.4 Kbps. 16 Kbps encoding is a straightforward A/D sampling process; 2.4 Kbps encoding uses a linear predictive coding (LPC) algorithm, representing sampled speech as a set of parameters, including frequency, loudness, etc. At the receiver, the 2.4 Kbps digital stream is processed and restored to analog speech. Encoders/decoders (vocoders) for 16 and 2.4 Kbps speeech are standard items in present inventory.

Modulation

With regard to type of modulation, that is, in choosing between amplitude, phase, or frequency modulations, we have spoken above of the possibility of amplitude/phase distortions in the signal by passage through a turbulent atmosphere. Also, for a scanning receiver, such as seems to be necessary here because of the large Doppler/detection bandwidth ratio, acquisition processes require a constant envelope, otherwise there is a possibility of failure to lock during acquisition. Since amplitude/phase modulations may involve some difficulties, the alternative is some type of frequency modulation.

In accordance with our design philosophy, the modulation chosen is the least-complicated capable of performing the required communications functions. Narrowband FSK is preferred on the basis of simplicity, cost, and bandwidth utilization efficiency. In FSK, the carrier switches between predetermined frequencies either by modulating one oscillator, or by switching between two oscillators. Primarily, applicable FSK forms are binary noncoherent FSK, binary coherent FSK, and quaternary FSK.

Generally, a channel with B Hz bandwidth will allow from B to 2B binary pulses per second to be transmitted over the channel. Alternately, if 1/T pulses are to be transmitted, the bandwidth required ranges from a minimum of 1/T Hz to 2/T Hz, depending on pulse shape. Multilevel signalling allows corresponding higher bit rates to be transmitted over the channel. The system bandwidth is essentially twice the frequency deviation. In narrowband FM, where the deviation is defined by the data bandwidth, the system bandwidth can approach the data bandwidths of 1/T to 2/T[15].

Amplifiers/Power Combining

EHF solid-state amplifiers are negative-resistance diodes, such as Gunn or IMPATT devices, the IMPATT (Impact Avalanche and Transit Time: a p-n junction diode reverse-biased to avalanche for oscillation and amplification) structure being the most common presently used. Silicon and gallium arsenide can both be used for IMPATTs; silicon has better frequency performance and reliability than arsenide. Although gallium arsenide is at present the most popular material, it is not considered very suitable for low-noise applications. Effort is being expended on indium phosphide for low noise EHF amplification. Solid-state devices are recommended for airborne applications, although lower in power-output than tubes. The use of tubes (TWTs, EIAs, EIOs) appears to be inappropriate for airborne use on the basis of size, weight, and cost considerations.

Individual amplifiers can be combined to provide more power. For present EHF solid-state CW power amplifier capability of approximately 1.25 watts/unit[16,17], linear power-combining could provide up to 5 watts of EHF. Linear combining of more than four amplifier units is difficult; radial-geometry is recommended for further combining. There is no inherent upper limit for radial combining, but we hesitate to recommend combining of more than eight power amplifiers, again, on the basis of complexity, cost, etc. This could provide up to 10 watts of EHF RF CW power, and this estimate is used for the baseline calculations. Unless some breakthrough is accomplished in EHF solid-state amplification techniques, it appears that power shall be limited to this approximate level.

The Doppler shift is the difference between transmitted and received signals, where +, −, denote approach or withdrawal, respectively:

$$f_D = \pm f_{TX}(v/c)$$

For rapid calculations, the following approximate expression can be used to estimate Doppler shift from the transmitted frequency:

f_D = ± 1 Hz/Mach number relative velocity/MHz frequency

For relative velocities of Mach 2 or greater, which can occur for the condition of two aircraft, each approaching or withdrawing at Mach 1, Doppler shifts at EHF may be more than 100 KHz, depending on velocity-vector difference conditions. It is interesting to note that, because of the velocities between an emitter and any receivers, received signals are Doppler-displaced by some frequency shift from the transmitted signal; depending on the vector-differences between the various transmitter-receiver links, a given transmitted signal received at widely-separated receivers may be on different frequencies. These received signals, originated by a single transmission, may effectively be on different channels with respect to each other, depending on the detection bandwidth. This Doppler-shift characteristic poses some interesting features with regard to narrowband transmission, reception, and exploitation.

Doppler Slew

The Doppler rate-of-change, or slew, impacts tracking circuit requirements, and is obtained by taking the differential of the Doppler-shift equation, considering vector-difference conditions. Maximum slew can be calculated by evaluating the differential at passage. Assuming parallel motion for simplicity,

$$f_D = \pm (v/c) f_{TX} \cos\theta$$

$$= + (v/c) f_{TX} (x/(x^2 + d^2)^{1/2})$$

$$df_D/dt = \pm (v/c) f_{TX} ((x^2 + d^2)^{1/2} dx/dt - x\, d/dt (x^2 + d^2)^{1/2}) / (x^2 + d^2)$$

$$= + (v^2/d) f_{TX} \text{ at } x = 0$$

$$= + (v/d) f_D$$

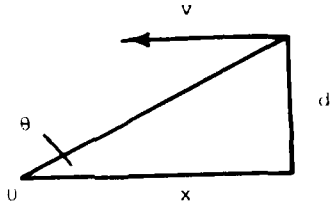

The maximum rate of Doppler slew at EHF can be estimated by the following example: assuming Mach 2 relative velocity (approximately 2.6 Km/Sec) at a separation of 1 km, the slew is approximately 80 KHz/sec.

SYSTEM DESCRIPTION

Figure 1 is a functional block diagram of the baseline system. The EHF capability can be considered an add-on subsystem extension to other communication systems, or it can be considered in a stand-alone capacity. In an integrated voice/data communication system, the interface point between the EHF RF subsystem(s) and the system modem would be most appropriate after the voice/data encoding point. For the present, we consider a stand-alone EHF system.

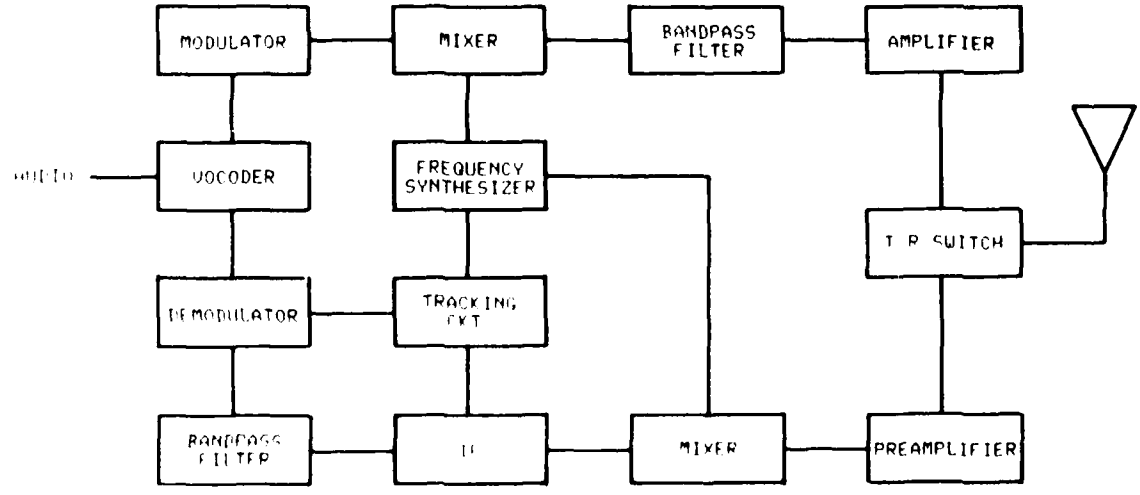

FIGURE 1. SIMPLIFIED FUNCTIONAL BLOCK DIAGRAM

A baseline communications system is discussed that can be implemented within the technological state-of-art, offering communications protection against stand-off signal exploitation systems. This is accomplished by choosing frequencies which provide both communication-link capability at short ranges, and, beyond these projected communication ranges, experience high absorption. Effective communication range at any given frequency is determined by atmospheric absorption being less than maximum allowable attenuation as estimated by link-budget calculations. To a large extent, the effective communication range for any frequency is determined by the straight-line portion of the attenuation curve, close to the free-space value, where oxygen absorption is not of major significance. Stand-off range capability, or the range beyond which a system is effectively protected, is determined by the region of high cumulative oxygen absorption; this region is above the point where the attenuation curve sharply departs from the free-space value. Beyond this point, any nominal range increase requires enormous increase in system capability, and may not be considered to be productive use of available resources.

OTHER PROPAGATION EFFECTS

Rain and Fog

Rain and fog are considered as they present an additional absorption mechanism for EHF. Rain attenuation increases with frequency, and with rate of precipitation; fog attenuation increases with frequency, and with vapor density. Allowance for rain/fog attenuation is made in the link margin; values given are derived from empirical data. Other effects which may be significant, such as depolarization, are not explicitly considered; since the data is empirical, depolarization effects should be implicitly included. In the 50-60 GHz band, EHF rain/fog attenuation rates are, roughly[12]:

Condition	Moisture	Attenuation in dB/km
Light fog	0.25 g/m^3	0.5
Light rain	1.25 mm/hr	1
Medium rain	2.5 mm/hr	2
Heavy fog	1 g/m^3	2
Heavy rain	5 mm/hr	3

A simple exponential model for rain attenuation is used in the link margin calculations, using the above coefficients to estimate power loss. Due to the relatively short ranges involved, a uniform rain distribution with distance is assumed. For the link power budget calculations, rain/fog margin is estimated at 5 dB to allow for short-range communications through light fog or rain.

Fading and Fluctuations

The type of fading experienced over the propagation channel significantly affects the link calculations, with regard to the error probabilities. Due to the time-varying nature of the channel, amplitude and phase fluctuations may be experienced. The air-to-air situations involve high dynamic situations and a turbulent propagation channel. Amplitude fluctuations may be caused by specular signal multipath interference conditions; phase fluctuations may be caused by signal transmission through the turbulent atmosphere surrounding the aircraft. (Fading/interference due to ambient-atmospheric multipath is neglected here.) The platforms are moving many wavelengths per detection frame, and it remains to be determined whether the fading is fast or slow with regard to signal bandwidth, which would affect the signal statistics. We have not yet estimated the magnitude of these effects, but we expect this issue to impact significantly on type of modulation, signal statistics, link margins, etc.

THE BASELINE SYSTEM

General Considerations

In order to make the link power-budget calculations, a baseline system is proposed, representative of the current technological state-of-art. The configuration of this baseline system is discussed, system operational parameters are determined, link power-budget calculations are performed, the baseline system performance is assessed for a variety of situations, and recommendations are made with regard to system configuration. Our baseline system philosophy has been to utilize the simplest of choices with regard to characterization/specification, and to test these choices against suggested operational conditions. If it is evident that the choices initially selected on the basis of simplicity are not appropriate, other more complex choices can then be considered.

Doppler Shift

At EHF, aircraft velocities are sufficient to produce significant Doppler shifts. The formula for Doppler-shifted received frequency[13] is:

$$f_{RX} = f_{TX}((1 - v/c)/(1+ v/c))^{\frac{1}{2}}$$

Expanding the denominator and cancelling, the received frequency can be approximated by:

$$f_{RX} = f_{TX}(1 - v/c)$$

EHF PROPAGATION MODEL

The electromagnetic-wave attenuation in the EHF frequency region is due to the absorption characteristics of the oxygen and water vapor molecules in air. The emphasis here is on oxygen absorption in the 50-70 GHz frequency band; the oxygen molecules absorb energy in this band at discrete frequencies as a consequence of their magnetic dipole resonant structure. At low altitudes, the absorption line-spectrum of molecular oxygen is broadened, due to minute energy transfers as a consequence of collisions, resulting in a continuous attenuation band. As altitude increases the molecular collisions decrease due to atmospheric rarefaction, resulting at very high altitudes in discrete absorption lines at the resonance frequencies.

The initial work in the definition of EHF propagation in the atmospheric oxygen absorption band was done by Van Vleck[1,2] during World War II. The Van Vleck absorption model has since been updated by Meeks and Lilley[3], Carter, Mitchell, and Reber[4,5], and Rosenkranz[6], among others. More recently, the propagation model has been investigated by Liebe[7,8,9], resulting in a more accurate model, and a computer program for that model. That work was reported at the 1982 AGARD/EPP Propagation Symposium[10].

The work reported here is based on tabular data from the Reber, Mitchell, Carter model developed in the 1968-69 period[11]. This propagation model is admittedly simplified, but sufficient for our present purpose. The model does have limitations, however, that must be considered: water vapor absorption due to the electric dipole structure of the water molecule, "...is generally negligible compared to oxygen absorption in the 50-to-70 GHz region". This is acceptable for the present, but it is preferable that water vapor absorption be included, as Liebe has done.

The computations used in this paper are to be considered as approximate. Because of the tabular nature of our data, interpolations are used for attenuation rate values at intermediate frequencies and altitudes, and numerical results presented here are not to be used for engineering design. Extreme precision was not a factor; this was justified on the basis of simplicity and computational rapidity, and was considered adequate for the purposes of this investigation. Our conclusions will be largely valid, although we would not utilize our calculations for communications system engineering design.

The characteristic EHF attenuation rate vs. frequency is seen in the inset to Figure 1. Tabular EHF attenuation-rate data is used to develop a set of curves of total attenuation vs. range, such as that given in Figure 2. The curves can be parametric with respect to frequency, as here, or with altitude. It is seen that cumulative oxygen absorption eventually becomes important, causing significant increase in attenuation over that of free space. In order to determine communication system capability, these curves are overlaid by the maximum allowable system attenuation values (see sample maximum attenuation at 150 dB) determined by the power budget calculations for the systems under consideration, to determine whether the attenuation experienced is greater or less than the communication system can withstand. Given a specific frequency, it can be determined by the intersection of the link-budget estimate with the atmospheric attenuation curve what range a system can operate over, or alternatively, what frequency should be used to provide operation over a given range.

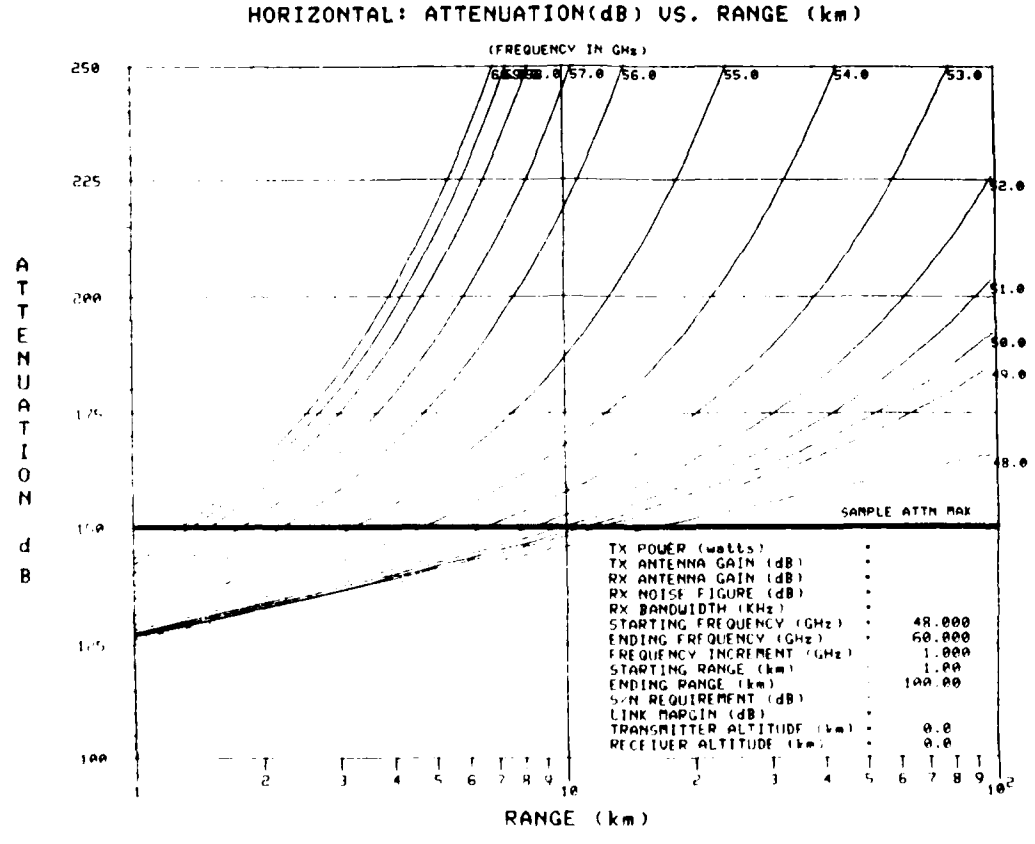

FIGURE 2. TOTAL HORIZONTAL ATTENUATION VS. RANGE (ALTITUDE: SEA LEVEL)

EHF AIR-TO-AIR COMMUNICATIONS

Peter N. Edraos
Rome Air Development Center
Griffiss Air Force Base, NY, USA 13441

SUMMARY

The use of the EHF oxygen-absorption frequency band for low-detectability air-to-air communications has been proposed at various times; this presentation deals with considerations in the development of such an EHF short-range air-to-air communications system. The protection to the communications system is provided by the cumulative oxygen absorption characteristics of the atmosphere. System considerations are dealt with parametrically; the effects of aircraft velocity, altitude, antenna coverage, transmitter power, and so forth, are discussed with regard to impact on range, frequency, acquisition time, data rate, etc. A baseline system is submitted; link power budget calculations are made for the baseline, resulting in estimates for maximum allowable attenuation; system performance is assessed for a number of situations. Emphasis is on communications and the problems involved in the design and implementation of an EHF air-to-air digital voice system, concentrating on the propagation influences and constraints.

INTRODUCTION

This paper deals with a digital voice communications system that is strongly influenced by the propagation channel - in fact, the propagation characteristics of the channel are the only rationale for its consideration. The problems in the design and implementation of the system are discussed, and approaches to their solution proposed.

The use of the EHF oxygen-absorption frequency band for low-detectability air-to-air communications has been proposed at various times; this presentation deals with considerations in the development of such an EHF short-range air-to-air communications system, protected against detection and jamming. The emphasis in this presentation is on communications, and the problems involved in the design and implementation of an EHF air-to-air digital voice system, concentrating on the propagation influences and constraints. Problem areas are discussed, including estimates as to the effect of these problems on system performance, and the factors that must be considered in system development. A number of problems are unique to airborne applications, as a consequence, for example, of aircraft velocities and orientations, antenna siting, transmission-line attenuation, etc.

Air-to-air communications systems presently operate in the UHF/VHF/HF frequency bands of the electromagnetic spectrum, which, because of low-loss RF propagation at these frequencies, makes it simple for relatively distant stand-off electronic systems to detect, jam or otherwise exploit these transmissions. In the EHF band, electromagnetic absorption is comparatively high and varies with frequency, and this is capitalized upon to limit the effectiveness of stand-off exploitation equipment. With reference to Figure 1, EHF frequency assignments would be set such that detection/jamming equipment operating at ranges longer than the communications link would operate under high-attenuation penalties; the handicap on standoff exploitation equipments due to atmospheric attenuation would render them largely ineffective, forcing utilization of more critical resources, or increased risk at more exposed positions.

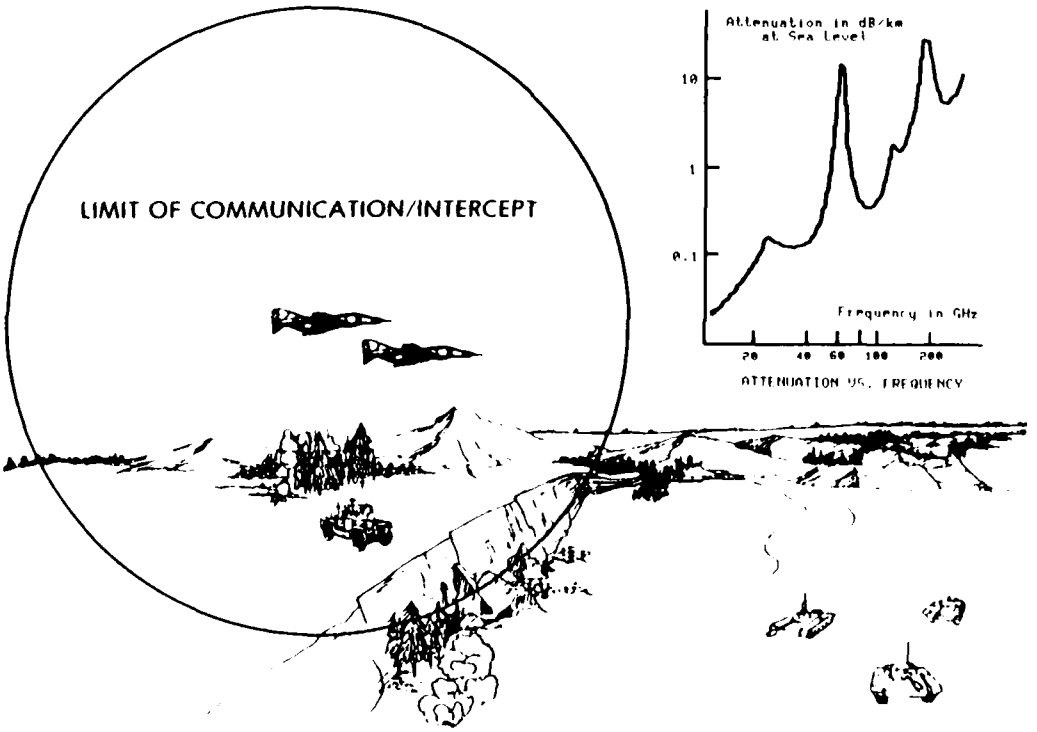

FIGURE 1. CONCEPT: EHF AIR-TO-AIR COMMUNICATIONS

DISCUSSION

C.Goutelard, Fr

Dr Salz, you have indicated the use of convolutional codes and the Viterbi algorithms. Could you discuss the use of block codes and convolutional codes.

Author's Reply

It turns out that everything you can do with block codes you can do with convolutional codes, exept simpler, so that convolutional codes with reasonable constraint lengths and a Viterbi decoder are very effective nowadays.

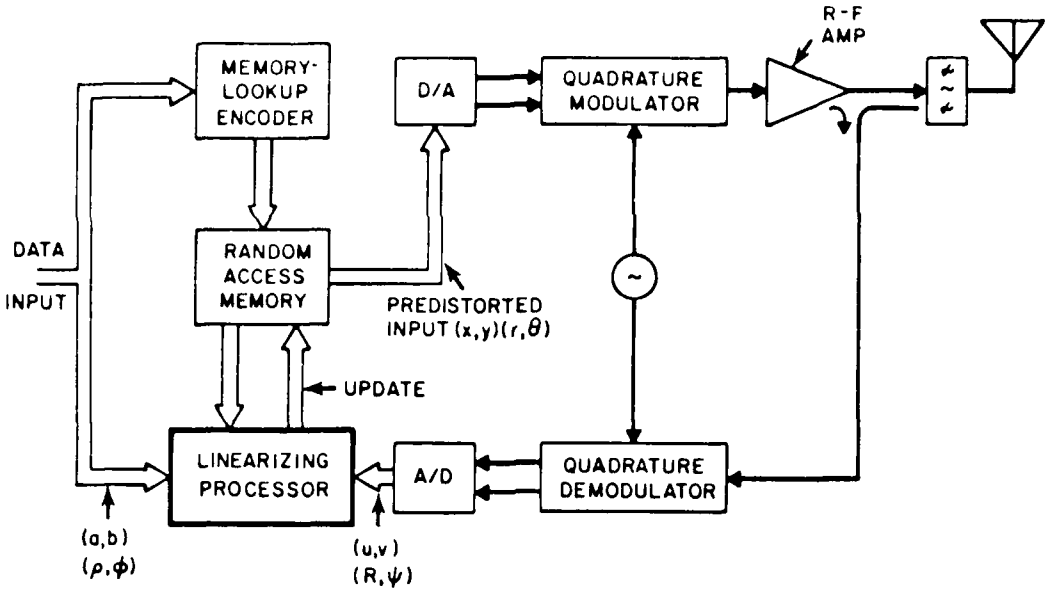

FIGURE 2 - SCHEMATIC REPRESENTATION OF THE ADAPTIVE, DIGITAL PREDISTORTION LINEARIZER.

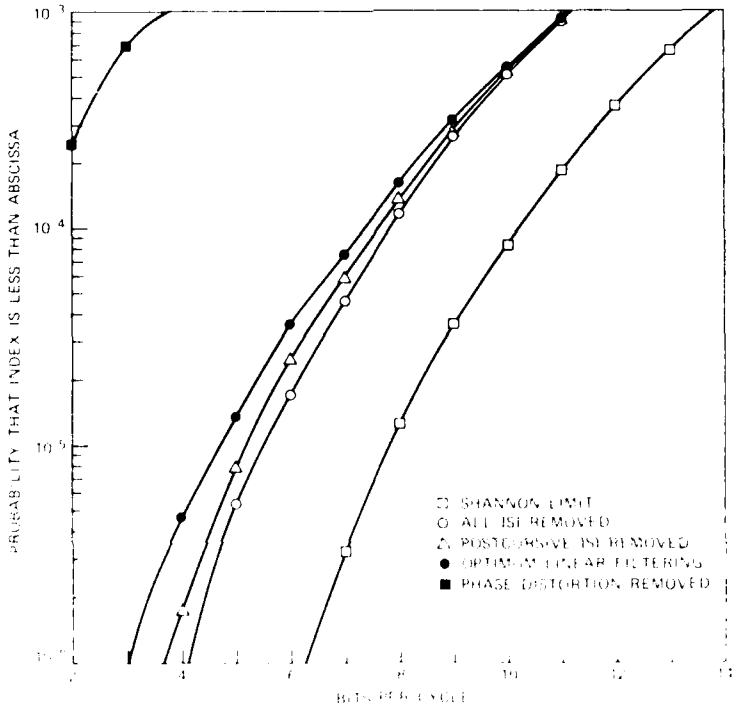

that F_{DF} is displaced over two bits per cycle to the right of F_{MF}, while F_{DH} is displaced substantially to the left of F_{LIN}.

The plot for the equalizer that inverts the channel is not shown as it is not perceptibly different from that for the optimum linear equalizer. This is expected since the optimum linear filter is essentially inverting the channel at the high signal-to-noise ratios we are considering.

We have examined the sensitivity of $F(I, P_e, \cdot)$ to P_e. The sensitivity is especially critical at the low error rates needed for data (as opposed to voice) transmission. An asymptotic analysis shown that, for large $\cdot$, the curves translate to the left in $\cdot$ inverse with a $\log_2 N$ shift, where 10^{-N} is the P_e objective. This insensitivity is an illustration of the well-known result[6] that once a pulse code modulation (PCM) operating point is achieved it takes a very small improvement to make the error rate an order of magnitude smaller. In fact, if at some operating data rate the probability of error turns out to be 10^{-5} - 10^{-6}, one should be able to design an error-correcting code of small redundancy and moderate complexity that could improve the error rate by several orders of magnitude.

A detailed examination of the sensitivity to signal-to-noise ratio reveals that the degradation in all cases is roughly 1/3 bit/cycle/dB.

REFERENCES

[1] W. D. Rummler, "A New Selective Fading Model: Application to Propagation Data", B.S.T.J. 58, No. 5 (May-June 1979), pp. 1032-71.

[2] W. D. Rummler, "More on the Multipath Fading Channel Model", IEEE Trans. Commun., COM-29, No. 3 (March 1981), pp. 346-52.

[3] G. J. Foschini and J. Salz, "Digital Communications over Fading Radio Channels", B.S.T.J. (February 1983), Vol. 62.

[4] B. R. Saltzberg, "Intersymbol Interference Error Bounds with Application to Ideal Bandlimited Signaling", IEEE Trans. Inform. Theory, IT-14, No. 4, (July 1968), pp. 563-8.

[5] A. A. M. Saleh and J. Salz, "Adaptive Linearization of Power Amplifier Nonlinearity in Digital Radio Systems", B.S.T.J. 62 (April 1983), No. 4.

[6] B. M. Oliver, J. R. Pierce and C. E. Shannon, "The Philosophy of PCM", Proc. IEEE, (November 1948), pp. 1324-31.

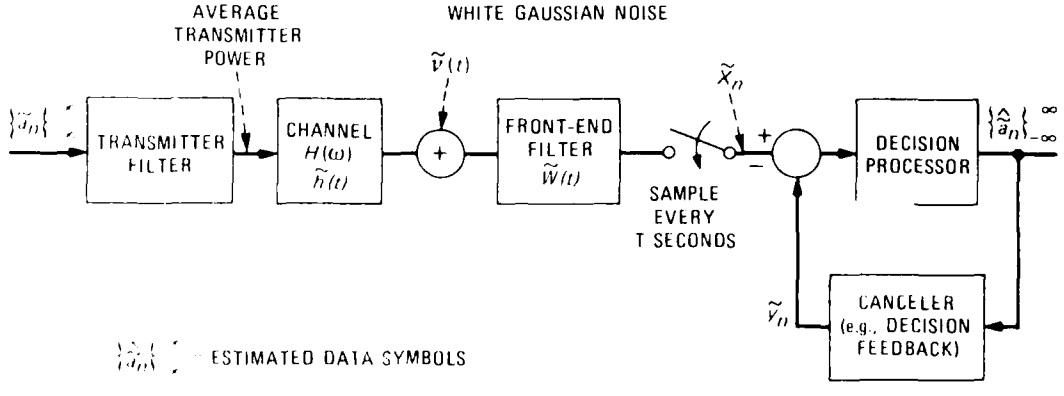

FIGURE 1 - COMPLEX BASEBAND MODEL FOR QAM DATA TRANSMISSION

where:

i. [illegible] with B an exponential random variable with mean 3.8.

ii. The parameter, [illegible], is a log normal random variable with dependence on the parameter, b. Specifically, [illegible] = $1/10^{A/20}$, where A is normal with a mean of $24.6(B^4 + 500)/(B^4 + 800)$dB and a standard deviation of 5 dB.

iii. The phase, [illegible], is independent of a and b and has a constant density on each section [illegible] and [illegible] with P[illegible] = 5xP[illegible].

iv. The scale factor [illegible] is a constant = 6.31 nanoseconds.

In the model, the channel is in the faded state for 8060 seconds in a normal heavy fading month. Thus the channel can be viewed as being in one of the two states where:

Nonfaded state = 0.99689

Faded state (Rummler model operative) = 0.00311 .

In the sequel we employ this model to estimate the outage distributions for various transmission methods.

V. A DESCRIPTION OF THE TRANSMITTER LINEARIZER

A block diagram of a QAM transmitter with the proposed predistortion linearizer is shown in Figure 2. A random-access memory (RAM) contains the predistorted value of the in-phase and quadrature voltages of each point on the QAM constellation. A gray-coding encoder obtains each input data symbol and generates the RAM addresses of the desired signal point. The corresponding stored predistorted voltage values are converted to analog voltages using a pair of digital-to-analog (D/A) converters. These voltages drive a quadrature modulator, which generates the desired predistorted RF signal for the duration of the input symbol. That signal is then amplified, filtered and transmitted.

To update the RAM information, the amplifier output is sampled by a directional coupler, and demodulated using the same local oscillator used for the modulator, which eliminates the need for carrier recovery. The output in-phase and quadrature signals of the demodulator are converted to digital form using a pair of analog-to-digital (A/D) converters. A linearizing processor, which is the heart of the linearizer, receives this information, compares it with the input data, and computes the predistortion error. A recursive algorithm, which is discussed in Reference 5 uses the error to update the voltage values in the RAM corresponding to the particular data point under consideration. Note that each point on the signal constellation is updated separately. Thus, the linearizer can support any desired constellation.

The proper operation of the linearizer as described above assumes that the amplifier is memoryless, and requires that the signal not be filtered before the power amplifier. Thus, all pulse shaping and filtering must be performed by the combination of the post-amplifier, RF bandpass filter and the receiver filters. The former filter should be designed just to meet FCC (or other) emission rules for square input pulses.

VI. PRINCIPAL RESULTS

For the purpose of presenting our results we need the following notation for the outage distributions:

[illegible]: phase distortion removed

[illegible]: [illegible] linear equalization

[illegible]: [illegible] intersymbol interference (ISI) removed

[illegible]: all ISI removed (matched filter bound)

[illegible]: information theory limit (Shannon).

The efficiency index distributions were computed for 30-MHz channels assuming an ideal transmitter linearizer. Strictly speaking, the notion of an index in bits per cycle is [illegible] (the probability distribution of bits per cycle) would change if calculated at 20 MHz or at 40 MHz. However, by calculation we established that, for the purposes of the discussion that follows, treating F(I) as invariant over the 20- to 40-MHz practical bandwidths is an adequate approximation.

The most striking features of the outage distribution functions F(I; P_0, .) are exhibited in Figure 3. The beneficial effects of adaptive equalization are apparent. The three equalization schemes yield roughly similar results; however, as one looks more closely at the extreme outage tail, F_{LIN}, F_{DF}, and F_{MF} begin to depart from each

noise-input sample. Ideally the canceler strives to synthesize the value

$$y_n = \sum_{k \in S} r_k s_{n-k} \qquad (5)$$

and to subtract it from (4) where the set of integers S is defined as $S = \{k : k = -N_1, \ldots, -1, 1, \ldots, N_2\}$. The canceler's ability to synthesize these values presumes that some past ($k = 1, \ldots, N_2$) and or future ($k = -1, \ldots, -N_1$) transmitted data symbols are perfectly detected and, that the set of complex numbers, r_k, are adaptively estimated.

The front-end filter, W(t), is usually determined adaptively by minimizing the mean-squared error (MSE) between the sample, $x_n - y_n$, and the expected data symbol s_n:

$$MSE[N_1, N_2, W(t)] = E\,|x_n - y_n - s_n|^2 , \qquad (6)$$

and the optimum filter, W(t), is then chosen to achieve

$$(MSE)_0 = \min_{W(t)} MSE[N_1, N_2, W(t)] = MSE[N_1, N_2, W_0(t)] . \qquad (7)$$

Since MSE is a quadratic functional of W(t), a unique minimum can always be found. It is natural to represent the linear filter W(t) by a transversal structure and in practice, the search for the minimum is accomplished by varying the taps of this filter until a minimum of the time average of the squared error is found. To realize such a filter, estimates of the transmitted data symbols must be used.

III. SYSTEM PERFORMANCE

To get at the efficiency index of a system, the error rate as a function of data rate for any choice of the canceler set, S, and front-end filter W(t), must be explicitly expressed. Exact relationships are not tractable for the simplest of systems and so we employ upperbounds. For the systems under consideration, we obtain exponentially tight inequalities. We adopt a bounding procedure introduced by B. Saltzberg[4] to analyze the error rate in an unequalized baseband system. We extended Saltzberg's approach to our systems.

From Section II we have $I = 2\log_2 L$ and $\sigma^2(L) = [(L^2 - 1)/3]$. These two equations in conjunction with the P_e formulas (see Reference (3)) enable us to determine I as a function of the P_e objective, σ, the channel, and the equalization scheme. Specifically,

$$I = \log_2 \left[\frac{G(H, \sigma)}{\sigma \sqrt{\ln(P_e^2/2)}} + 1 \right] ,$$

where $G(H, \sigma)$ is a function that depends on the communication method. With the channel response considered to be a random function, I is a random variable, and we can determine its probability distribution function for each communication scheme. The quantities σ and P_e are parameters of the distribution.

It can be shown that the information theory bound on communications efficiency is

$$I = \int_f \log_2 [1 + |H(f)|^2 \sigma^2] , \qquad (8)$$

where as before $H(f)$ is the channel frequency characteristics and where the integral is over a frequency band of size 2W.

IV. MODEL FOR THE FADING CHANNEL

Now we describe the model for the frequency-selective fading. This model for the random functions $H(f)$ is due to W. D. Rummler[1,2] and is based on measurements of a 26.4-mile hop between Palmetto and Atlanta, Georgia. The measurements of fades were made on a 30.3-MHz channel situated in the 6-GHz band during the heavy fading month of June (1974).

In the model, the $|H(f)|^2$ functions are 6-dB-depth sections of scaled, displaced cosine waves. Specifically, conditional on a fade occurring

$$|H(f)|^2 = \sigma^2 [1 + b^2 - 2b \cos(\quad + \quad)] ,$$

Figure 5 is the absorption-curve chart of Figure 1, with the superposition of the baseline attenuation allowances. Considering detection bandwidth based on utilization of a 16 Kbps digital voice modem, operation is relatively ineffective, either because of lack of capability to propagate over any significant range, or because of lack of protection, as determined by stand-off range estimation. That is, there is little extra attenuation due to oxygen absorption, and thus little protection against exploitation systems. Considering detection bandwidths based on utilization of a 2.4 Kbps digital voice modem, EHF communications can be accomplished at reasonably practical ranges, and yet the absorption properties of atmospheric attenuation can be utilized to limit stand-off signal exploitation capability.

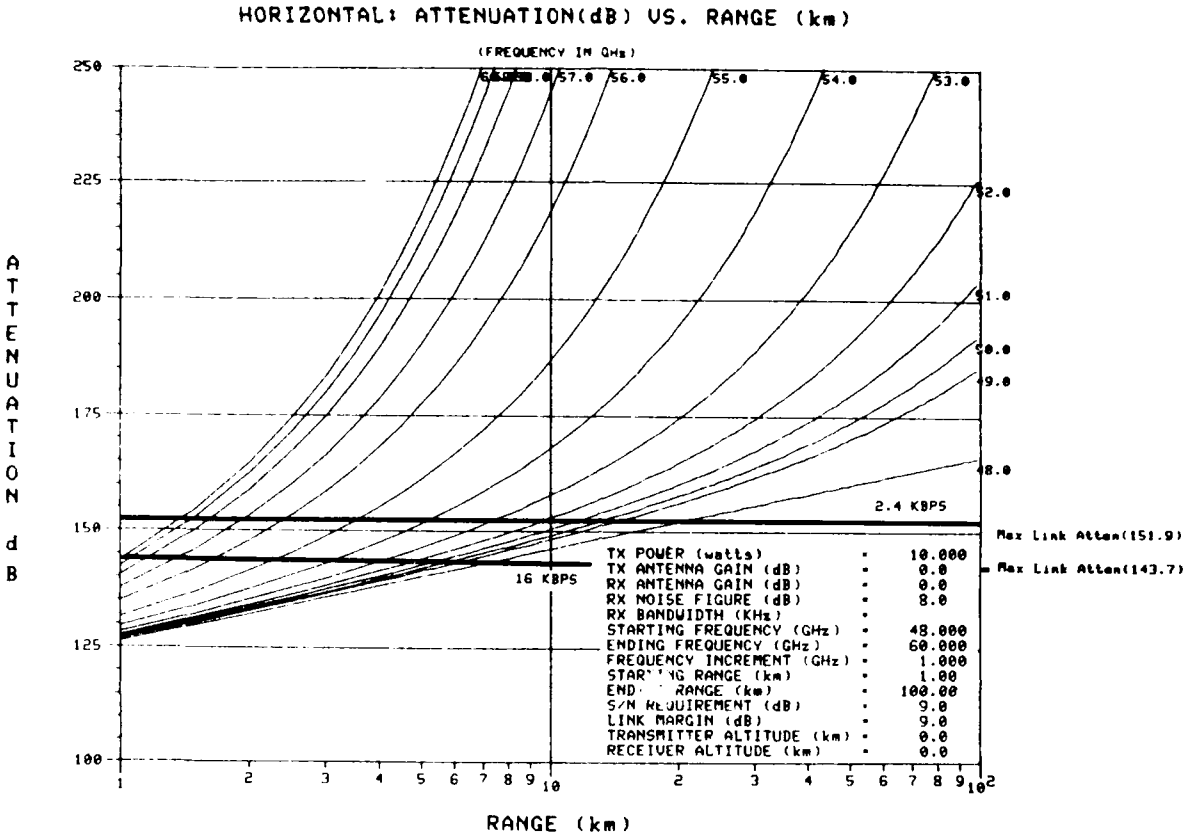

FIGURE 5. BASELINE SYSTEM LINK BUDGET OVERLAY ON TOTAL ATTENUATION (ALTITUDE: SEA LEVEL)

Communication performance can be further improved by decreasing detection bandwidth; 800 bps and 400 bps vocoders are at present being investigated for application to digitized voice communications. Results to date are promising, but for the applications here, there is an impact on acquisition time requirements, in that the time required to acquire may be too long for mission requirements. In any case, although under investigation, vocoders in the 400-800 bps range are not presently available. Therefore, a 2.4 Kbps vocoder is subsequently considered for the baseline system.

If we consider utilizing detection bandwidths on the order of the IF bandwidth, as presently used for some systems, we see that this is not effective; attenuation prevents communications at essentially all practical ranges. The systems referred to satisfy link-budget requirements by use of high-gain antennas; our application does not allow this. Here, the baseline communication-system operation must of necessity be narrowband-detection in a wideband environment determined by the frequency uncertainties. A scanning receiver is therefore required, utilizing a detection bandwidth much less than the total bandwidth scanned, corresponding to frequency uncertainty.

MISSION PHASES

Communication Areas

A baseline EHF tactical air-to-air communications system has been defined, and the link power budget calculations performed to determine maximum allowable attenuation. The system is now assessed in a number of different mission situations, to qualitatively evaluate its performance. Communication requirements may differ during various portions of a mission. These portions may be:

Approach Phase

Entry into Engagement Area

Mutual Aircraft Support during Engagement

Withdrawal Phase

Protection may be needed at some point in the overall mission for other types of exploitation-resistant communications: for instance, during refueling, for IFF, etc.

Approach

Figure 6 is the superposition of the maximum allowable attenuation for the 2.4 Kbps baseline system on the total-attenuation curves for horizontal communications at an altitude of 2 km*.

For low-detectability approach through the rear area, it can be assumed that the aircraft are flying at low altitudes to prevent radar detection, that communication ranges between the aircraft in formation are relatively short, that aircraft velocities are approximately the same, and that the flight is fairly well-ordered with regard to aircraft alignment. Due to this relatively well-ordered, uniform and stable geometry, this is probably the easiest situation to analyze. The primary communication-protection consideration during this part of the mission is to prevent detection during approach, and can be considered as concluded when the aircraft are within visual sighting capability. Considering aircraft ground clearance requirements, a representative value for penetration altitude is estimated here at 2 km, as input to the performance evaluation.

* All altitudes are referenced to mean sea level.

Entry

Figure 7 is the superposition of the maximum allowable attenuation for the 2.4 Kbps baseline system on the total-attenuation curves for slant-range communications between altitudes of 2 km and 0 km (sea level).

As the aircraft enter into the forward area, communication-protection consideration changes; low-detectability in this area is irrelevant, the aircraft are within visual sighting capability. Jam-resistant communications are required in this phase between aircraft for coordination, and for instructions from forward air control units. During this phase, the aircraft may still be in fairly well-ordered conditions, although more maneuvering may be expected. A factor here is the time needed to transfer message content, which depends on the effective communication range, relative velocity between aircraft, or between aircraft and stationary forward air-control ground units, transmitter power, any available antenna gain, etc. Available message time may easily be calculated by determining the effective comunication range, and dividing by the aircraft velocity. Another factor in these communications is the Doppler shift between aircraft and forward air control. In close-passage situations, Doppler slew may be at rates sufficient to cause unlocking of tracking circuits.

Engagement

Figure 8 is the superposition of the maximum allowable attenuation for the 2.4 Kbps baseline system on the total-attenuation curves for horizontal communications at an altitude of 8 km.

As the aircraft progress into the area of conflict, the communications protection requirement is still jam-resistance, but the geometrical situation is altered; this situation is the most difficult to analyze: aircraft velocities are high; aircraft orientation is random; altitudes, and altitude differences are widely varying, etc. This is the most vulnerable portion of the mission, and thus the most communications-critical; maximum communication range is required for effective mutual support. It is also during this phase that Doppler-offsets may considerably affect the communications/exploitation situation.

Withdrawal

Figure 9 is the superposition of the maximum allowable attenuation for the 2.4 Kbps baseline system on the total-attenuation curves for slant-range communications between altitudes of 8 km and 0 km (sea level).

As the aircraft exit from the forward area, communications may be required for mission and status reporting, either to forward air control units, or to more rearward echelons. A long-range rearward link might utilize low-data-rate digital information to report status, as indicated here, instead of digitized voice. Because of the length of this link to the rear, communication-protection capability based on any range discriminant, such as the oxygen-absorption mechanism used here, is invalid; for this case, the link cannot be protected by means of EHF, and transmissions must of necessity be outside the oxygen-absorption band. Any communication protection to this link must be supplied by other means such as frequency-hopping, direct-modulation pseudonoise spread-spectrum,directional antennas, power control, etc.

Also, in this case, and although we have not indicated it in the figures or the baseline calculations, it is reasonable to expect that some amount of antenna gain would be available for this particular link. This can easily be factored into the figure as it stands.

Communications Assessment

Any detailed communications assessment must of course rest on actual communications mission requirements; any comments we have at this point are qualitative and highly subjective. First, the low-detectable approach mode, proposed heretofore, seems feasible within the present state-of-art. This feasibility is based on the well-ordered flight conditions during the approach phase; thus any available antenna gains (generally, nominally 3 dB) could be utilized; Doppler shifts are relatively low, etc. Conditions become slightly more difficult during the entry phase: Doppler may be fairly high due to relative motion between incoming aircraft and forward air control elements, but aircraft attitude may still be fairly stable. Maximum communications difficulty occurs during the engagement phase: aircraft geometries may be completely disordered; we have assumed 0 dB antenna gain during this phase; certainly nothing precludes antenna gains of less than this. During the withdrawal phase, conditions again become more stable.

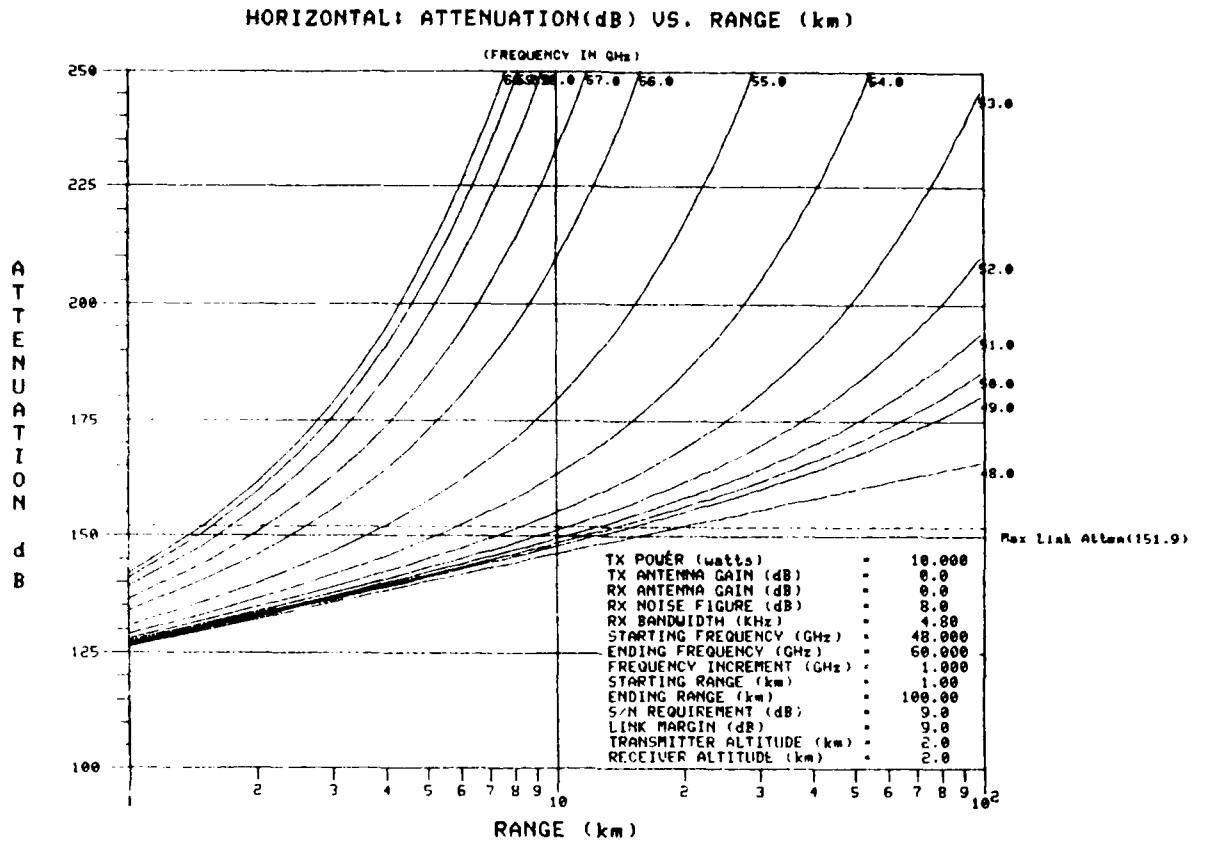

FIGURE 6. APPROACH: HORIZONTAL COMMUNICATIONS (ALTITUDE: 2 KM)

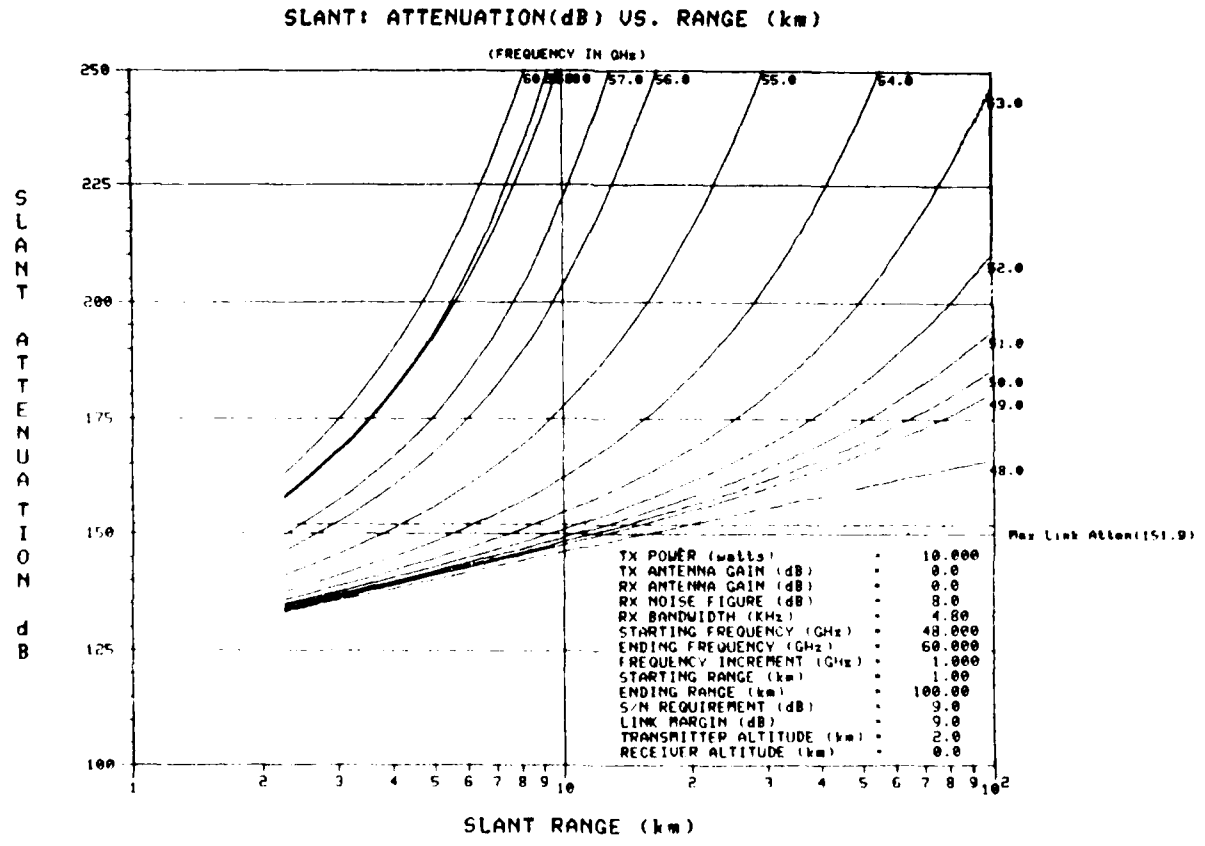

FIGURE 7. ENTRY: SLANT-RANGE COMMUNICATIONS (ALTITUDES: 2 KM/0 KM)

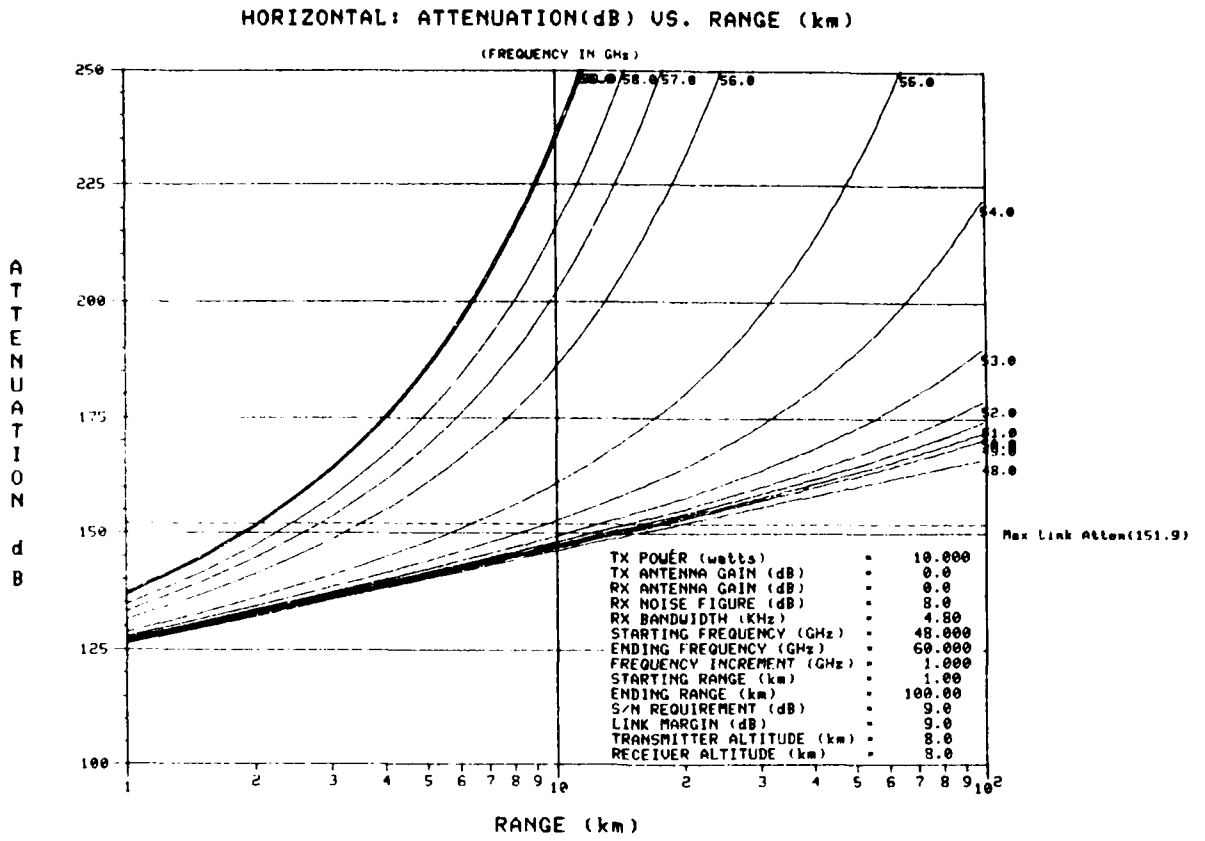

FIGURE 8. ENGAGEMENT: HORIZONTAL COMMUNICATIONS (ALTITUDE: 8 KM)

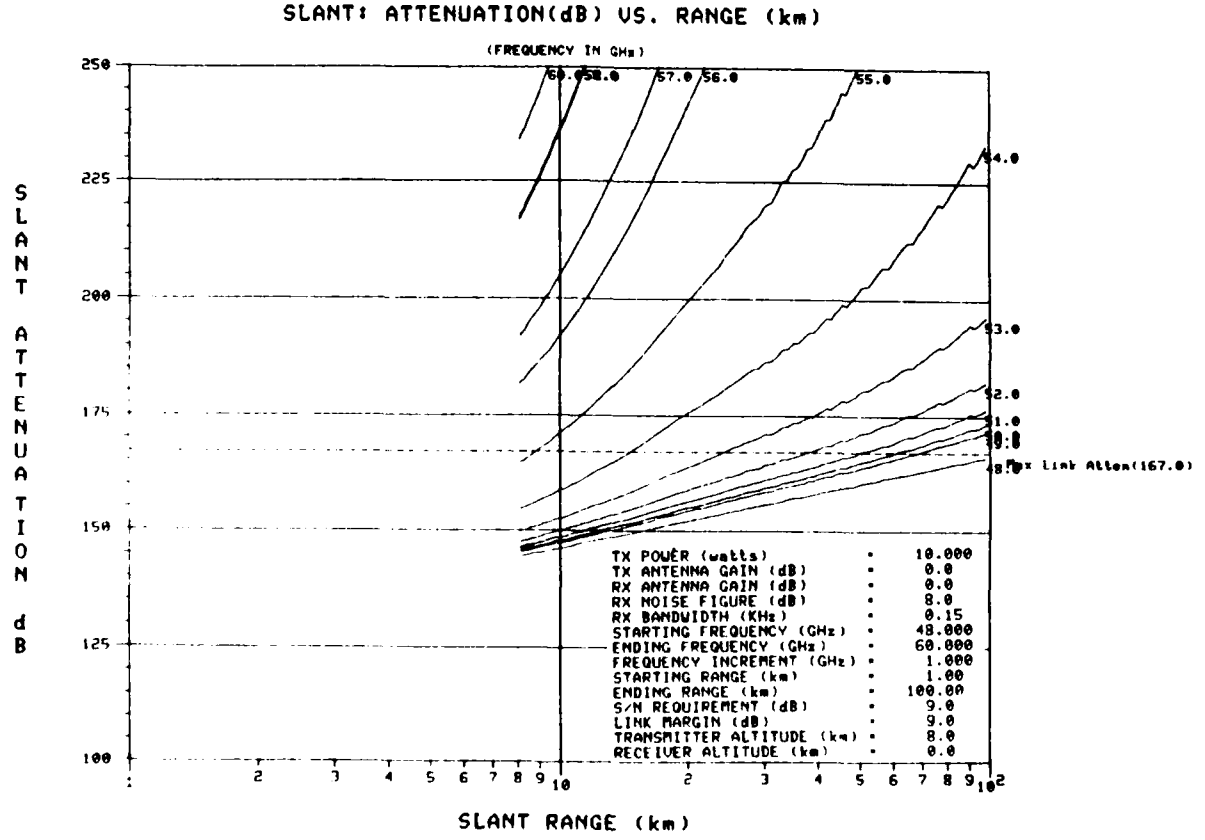

FIGURE 9. WITHDRAWAL: SLANT-RANGE COMMUNICATIONS (ALTITUDES: 8 KM/0 KM)

OTHER CONSIDERATIONS

Problem Areas

Major areas of concern with the present technological state-of-art, as it pertains to this area are:

Component reproducibility
Frequency stability
Solid state power amplification
Power combining
Oscillator/amplifier noise figures
Voltage stability
Acquisition/tracking circuit control/linearity/resolution
Transmission line losses
Transmitter/receiver filters
Fading
Phase coherence through turbulent atmosphere
Narrow-band voice encoding/decoding
Airborne antenna coverage
Frequency accuracy
Frequency allocations

Frequency Allocations

Present frequency allocations are as follows[24]:

FREQ BAND	INTERNATIONAL	UNITED STATES
42.5 - 43.5	FIXED - SATELLITE - ASTRONOMY	FIXED - SATELLITE - ASTRONOMY
43.5 - 47	MOBILE - SATELLITE - NAVIGATION	MOBILE - SATELLITE - NAVIGATION
47 - 47.2	AMATEUR	AMATEUR
47.2 - 50.2	FIXED - SATELLITE - MOBILE	FIXED - SATELLITE - MOBILE
50.2 - 50.4	FIXED - SATELLITE - MOBILE - SPACE	FIXED - SATELLITE - MOBILE - SPACE
50.4 - 51.4	FIXED - SATELLITE - MOBILE	FIXED - SATELLITE - MOBILE
51.4 - 54.25	SATELLITE - SPACE RESEARCH	SATELLITE - SPACE RESEARCH - ASTRONOMY
54.25- 58.2	FIXED - MOBILE - SATELLITE - SPACE	FIXED - MOBILE - SATELLITE -SPACE
58.2 - 59	SATELLITE - SPACE RESEARCH	SATELLITE - SPACE RESEARCH - ASTRONOMY
59 - 64	FIXED - MOBILE - INTERSATELLITE	FIXED - MOBILE - INTERSATELLITE
64 - 65	SATELLITE - SPACE RESEARCH	SATELLITE - SPACE RESEARCH - ASTRONOMY
65 - 66	SATELLITE - SPACE REASEARCH	SATELLITE - SPACE RESEARCH
66 - 71	MOBILE - SATELLITE - NAVIGATION	MOBILE - SATELLITE - NAVIGATION

Communications above 60 GHz.

If transmission in the 50-60 GHz frequency band is precluded by frequency management, operation in the frequencies between 60-70 GHz can be considered. Referring back to Figure 1, the attenuation rate is roughly symmetric about the main oxygen absorption peak at 60 GHz. Effectively, operation would be similar as operation in the 50-60 GHz band, with some important differences. First, the magnitude of the Doppler shifts and the Doppler rates of change would be increased proportional to frequency increase; this would necessitate reconsideration of the system bandwidth/acquisition parameters. Second, system implementation would be more difficult, due to the increase in mechanical-design tolerance requirements. Third, solid state CW power capability decreases rapidly as one exceeds 50 GHz; it would be difficult to achieve the necessary solid-state power levels.

Conferencing

The issue of conferencing, allowing reception of multiple simultaneous transmissions, presents a problem. Present airborne communications utilizing amplitude modulation automatically offer this capability, in that out of a number of signals that are received, all are processed and presented to the listener, and a desired signal is then mentally selected out of this complex of signals. With digital systems, however, this capability is more difficult to achieve. Digital modem aquisition of multiple simulataneous signals is not a trivial problem; although it can be accomplished, it essentially requires parallel operation of multiple loops, thus considerably increasing compexity and cost.

CONCLUSION

We have attempted to present a balanced estimate of the feasibility of applying EHF frequencies for protection of air-to-air communications from signal exploitation, and to determine the practicality of this approach with regard to the technological state-of-art, with regard to impact on installation, operations, cost, and so forth. With regard to the low-detectability approach phase, the technology for this capability may be within the present state-of-art; although some special design must be performed, implementation of this mode should be straightforward. With regard to the mutual support mode, and the other modes discussed, the capability is more difficult to achieve; this is based on estimations of system requirements for communication range, antenna coverage, and acquisition time, and considering present limitations in state-of-art with regard to amplifiers, transmission lines, frequency tracking circuitry, oscillator stabilities/offsets/control, etc. Any development program must consider penalties involved in achieving system requirements, with regard to trade-off of EHF system capability vs cost. Considering the problems, the question as to whether the development of EHF technology for protected air-to-air communications is a viable proposition will depend on the capability of EHF as compared to alternative technology that can offer effective communications-protection capability.

REFERENCES

1. Van Vleck, J.H., The Absorption of Microwaves by Oxygen, Physical Review, 71(7), Apr. 1, 1947, 413-424.

2. Van Vleck, J.H., The Absorption of Microwaves by Uncondensed Water Vapor, Physical Review, 71(7), Apr. 1, 1947, 425-433.

3. Meeks, M.L., and A.E. Lilley, The Microwave Spectrum of Oxygen in the Earth's Atmosphere, Journal of Geophysical Research, 68(6), Mar. 15, 1963, 1683-1703.

4. Carter, C.J., R.L. Mitchell, and E.E. Reber, Oxygen Absorption Measurements in the Lower Atmosphere, Journal of Geophysical Research, 73(9), May 15, 1968, 3113-3120.

5. Reber, E.E, Absorption of the 4- to 6-Millimeter Wavelength Band in the Atmosphere, Journal of Geophysical Research, 77(21), Jul. 20, 1972, 3831-3845.

6. Rosenkranz, P.W., Shape of the 5mm Oxygen Band in the Atmosphere, IEEE Trans. Antennas and Propagation, AP-23(4), Jul. 1975, 498-506.

7. Liebe, H.J., G.G. Gimmestad, and J.D. Hopponen, Atmospheric Oxygen Microwave Spectrum - Experiment versus Theory, IEEE Trans. Antennas and Propagation, AP-25(3), May 1977, 327-335.

8. Liebe, H.J., and J.D. Hopponen, Variability of EHF Air Refractivity with respect to Temperature, Pressure, and Frequency, IEEE Trans. Antennas and Propagation, AP-25(3), May 1977, 336-345.

9. Liebe, H.J., Modelling Attenuation and Phase of Radio Waves in Air at Frequencies below 1000 GHz, Radio Science, 16(6), Nov-Dec 81, 1183-1199.

10. Liebe, H.J., The Atmospheric Propagation Medium Between 45 and 75 GHZ, AGARD: Proceedings of the 30th Symposium, Propagation Effects of ECM Resistant Systems in Communications and Navigation, Copenhagen, 1982, AGARD CP-331.

11. Reber, E.E., R.L. Mitchell and C.J. Carter, Oxygen Absorption in the Earth's Atmosphere, Microwave Journal, 12(11), Nov. 1969, 75-81.

12. Dudzinsky, S.J., Jr., RAND Corp., Atmospheric Effects on Terrestrial Millimeter-Wave Communications, 1974, DARPA R-1335-ARPA.

13. ITT, Reference Data for Radio Engineers, 6th ed., Indianapolis, H.W. Sams, 1979, 33-9.

14. Magnavox Electronic Systems Co., AN/ARC-164, Magnavox document FWD 80-3478A, p. 9.

15. Schwartz, M., Information, Transmission, Modulation, and Noise, 3rd ed., New York, McGraw-Hill, 1980, Chapter 4.

16. Beislmaier, H., C. DeSantis and N.J. Wilson, State of the Art of Solid State and Tube Transmitters, Microwave Journal, 26(10), Oct. 1983, 46-48.

17. Ying, R.S., Mm Solid State Transmitter Sources Come of Age, Microwave Systems News, 12(10), Oct. 1982, 91-99.

18. Hughes Aircraft Co., Chart: Guide to Millimeter Waves.

19. Watkins, E.T., GaAs FET Amp Uses one-Quarter Micron Gate Heralding MIC Opportunities at up to 60 GHz, Microwave Systems News, 13(13), Dec. 1983, 52-62.

20. Whalen, A.D., Detection of Signals in Noise, New York, Academic Press, 1971, Chapter 7.

21. ibid.

22. Hughes Aircraft Company, Millimeter Wave System Calculator.

23. Schwartz, ibid., Chapter 5.

24. National Telecommunications and Information Administration, Tables of Frequency Allocations and Other Extracts From: Manual of Regulations and Procedures for Federal Radio Frequency Management, 1980, Revised May 1983.

ACKNOWLEDGEMENT

The author gratefully acknowledges the contributions of Alan Akins, Joe Rozman, and John DeVincentis in planning and programming the computer analysis used in this paper.

DISCUSSION

E.W.Lampert, Ge

In your link budget you showed antenna gain values of 0 dB; do you feel that this is realistic or should one not have an extra link margin because of antenna lobing?

Author's Reply

Antenna gain values of 0 dB were used as a compromise estimate for the few examples shown. The actual airborne antenna structure would probably be a discone type with circular polarization, as we have indicated in the preprint. These antennas would have the familiar toroid pattern, with an uniform pattern in the azimuthal plane. Nominally, such antenna would have a 3 dB polarization gain azimuthally, but since the aircraft would experience variations in orientation, this optimistic figure cannot be used. We used 0 dB as an estimate, hopefully it is not too optimistic. During the approach phase, when aircraft are in well-ordered formation, antenna gain may in fact be positive. If one is more pessimistic, one can easily adjust the attenuation value found by the link-budget calculation, and determine a new set of intersections with the attenuation-versus-range curves to arive at a shorter value for communication range.

E.W.Lampert, Ge

The problem you attacked in the beginning was that in the 60 GHz region you are much better off concerning enemy jamming and detection. On the other hand, when you have to put in a big link margin because of antenna lobing, you lose that advantage because the jammer does not have to have such a high link availability.

Author's Reply

If we operate in the 54—57 GHz region, there is a high oxygen absorption beyond 20 km range. If we assume that we are entering a combat area, we will be detected at a range of 10—20 km, by optical means. We think that the high range of oxygen provides a sufficient margin. The assumed antenna gains are just a starting point for the calculation.

PROPAGATION INFLUENCES ON THE PERFORMANCE OF A REDUCED BANDWIDTH QUADRATURE PHASE SHIFT KEYED DIGITAL RADIO SYSTEM.

by
J E Dobie
British Telecom Research Laboratories
Martlesham Heath
Ipswich IP5 7RE
UK

SUMMARY

British Telecom are running a field-trial of a spectrally efficient (4.2 bits/Hz) Reduced Bandwidth Quadrature Phase Shift Keyed system for the lower 6 GHz and 4 GHz bands, in a part of the UK that is subject to above average multipath activity. The experiment has been running for around two years and this paper describes some of the observations made during this period, the improvements made to the antennas, and the methods likely to be used in predicting system performance in other locations.

The current method of predicting multipath fading is examined, and found wanting in its application to digital system planning. An alternative is put forward and an example given of its use.

1 INTRODUCTION

British Telecom (BT) have an extensive FDM-FM microwave trunk network operating in the 2, 4, 6 and 11 GHz bands. Much of the equipment in the lower 6 GHz band is due for replacement over the next few years, and since BT is moving towards an all digital network and new equipment is installed on the basis of a 10-20 year working life, it would not be economical to install further analogue equipment.

Digital equipment has already been installed on some 11 GHz links, using a four-level QPSK system with an interleaved (alternate polarisation) frequency plan. Such a configuration does not provide the same traffic capacity as would the analogue alternative, so work has been concentrated on the implementation of a spectrally efficient system for use in other bands, starting with the lower 6 GHz and following up with the 4 GHz band. In co-operation with GEC plc, a Reduced Bandwidth Quadrature Phase Shift Keyed (RBQPSK) system has been designed and is currently undergoing field-trials at the BT Research Laboratories (BTRL) in East Anglia. For the purpose of high spectral efficiency, the system has been designed to operate in the co-frequency cross-polar frequency re-use mode.

2 FIELD-TRIAL

The field trial is being carried out on a 51 km path in the worst multipath environment in the UK, utilising towers of the existing microwave network, although operating over a path for which a direct link did not previously exist. The channels are configured such that one operates with co-frequency and adjacent channel interferers, while the orthogonally cross-polarised co-frequency channel has no adjacent channels present. By this means the effects of the two sources of interference can be better controlled.

Measurements are made for non-diversity operation and for two levels of height diversity. A schematic of the experiment is shown in figure 1. The comprehensive data recording system allows one second sampling of age level, cross-polar discrimination (XPD), and bit-error ratios (BER) to be made for channel 2 (both polarisations) in both diversity and non-diversity configurations. In addition, a 1 MHz slot filter in the horizontally polarised channels allows comparison to be made between the wideband and narrowband fading distributions as determined from the age voltage measurement. During periods of multipath activity all of the one second samples are recorded onto a Winchester disc for later processing. When no activity is observed, the sampling continues at the same rate, but recording is restricted to just one sample set per minute. By this means the Winchester disc is capable of holding at least two weeks of data during a severe multipath period. The second sampling of the system is initiated by detection of errors in any channel or a combination of change of age level together with a degradation of XPD performance exceeding given thresholds. A thirty second period without detection of any error conditions will reset the system to the one-minute recording mode of operation.

In addition to the above, a channel, offset from the system simulation, is equipped with a microwave link analyser. A video recording system, triggered by fades exceeding a given threshold, then provides a record of activity within this channel during periods of multipath activity, thus allowing later analysis of the factors that would effect the system performance under working conditions. The recordings obtained have proved very useful in determining the behaviour of notches within a channel in terms of growth and progression across the channel, and also the proportion of fades that change between minimum and non-minimum phase states.

Initial results showed the RBQPSK system to be very robust in the presence of multipath distortion, the principal factor affecting the outage performance being degradation of the XPD under fading conditions. Consequently the emphasis of the work has

[illegible] permissible. The cause is considered to be due to very stable [illegible] with the height of the transmit antenna thereby causing beam splitting. [illegible] is exacerbated by the fact that with normal spacing of the receiving diversity antennas, diversity offers little in the way of improvement. This stable [illegible] thought to be a rare event in East Anglia, and measures to minimise the effect [illegible] considered necessary. However, in locations where stable ducting could be a problem, [illegible] the use of increased diversity antenna spacing and/or transmit diversity are techniques that may offer a solution. The severity of the events observed can be judged from the fact that outage in the first five months of 1983 was less than 72 seconds, while for June and July it was 301 and 271 seconds respectively. It must be emphasised that this was purely a problem of deep fading in excess of the flat-fade margin and not a function of the system design.

5.3 Adjacent Channel Interference

In the static situation this has been accounted for in the determination of the system XPD requirements. During multipath fading there will be some change in the relative levels due to the notch shape. However with the limited range of delays that can affect the system, the contribution from this source is considered to be negligible.

6 SYSTEM OUTAGE CALCULATION

We have established that for an average year in the UK, the outage on the BBGPSK system can be determined by analysis of the flat or - XPD correlation and multipath [illegible] points. The additional loading to these two factors are interwoven, but if we treat them as independent events then what we get is a prediction that is pessimistic by a few percent.

6.1 Contribution due to XPD Degradation

We will look first at a method for predicting outage due to the XPD problem and then simply add this with any brought about by the multipath distortion. Figure 2 represents the system XPD-CPA requirement onto which combinations of flat and frequency selective fading, for certain antenna clear-sky XPDs, can be superimposed. However if we have a flat fading situation, then with an antenna having a good XPD performance, there should be no degradation in XPD. Thus flat fading is represented by horizontal movement across the diagram. With frequency selective fading there will, ideally, be one-to-one relationship between XPD and CPA. Thus this type of fading is represented by a diagonal line on the diagram.

Taking a clear-sky XPD of, for example, 40 dB, we can determine the possible degree of selective fading that the system can tolerate, for various amounts of flat fading. In this example shown by the heavy line, with 10 dB of flat fading present, the system is capable of withstanding around 21 dB of selective fading without exceeding the 10^{-3} error ratio. Repeating this exercise over a range of values, we can build up the diagram of [illegible], which shows the limit of possible operation of the system for a given value of [illegible] XPD without exceeding the 10^{-3} error ratio.

If we then draw in the joint cumulative probability contours of flat and selective [illegible] we can ascertain the lowest value of joint probability for [illegible] completely to the left of our XPD characteristic. This [illegible] the outage due to XPD degradation. (Since the joint [illegible] and the XPD characteristic are not identical they could be allowed to [illegible] the outage requirement). With due regard for the overall [illegible] approach the method can nevertheless be recommended.

6.2 [illegible] Contribution

[illegible] outage due to multipath distortion, we have found that the [illegible] is very small indeed. The basic assessment is [illegible] the characteristics of possible notch depth against delay, (a [illegible] and the idealised system signature level against [illegible], we can observe where the two cross and by integrating and [illegible] the resultant outage. In the case of the BBGPSK [illegible] zero outage, indicating a zero contribution to the [illegible]. However, there are two special situations that must be taken into account. [illegible] of the two-path situation for certain delays, results in [illegible] being situated at minima of the interference field [illegible] we find ourselves virtually in a non-diversity situation. [illegible] the minimum delay level parameter. This situation [illegible] enter into the prediction method. The second [illegible] the fact that many deep notches have been observed to change [illegible] minimum-phase states. Such behaviour is not unexpected [illegible], the two vectors concerned will be in anti-phase and of near [illegible], and it is obvious that slight changes in their relative amplitudes [illegible] reversal of the group-delay characteristic. In changing state, [illegible] the odd infinite notch situation and thus add to the outage [illegible]. This is not a situation that can be catered for in the prediction method, [illegible] it must be borne in mind when analysing individual events affecting a system. It is [illegible] a system that can tolerate notches in excess of, say, 20 dB must expect [illegible] of minimum and non-minimum phase group-delay characteristics.

Acknowledgement is made to the Director of Research of the British Telecommunications plc for permission to publish this paper.

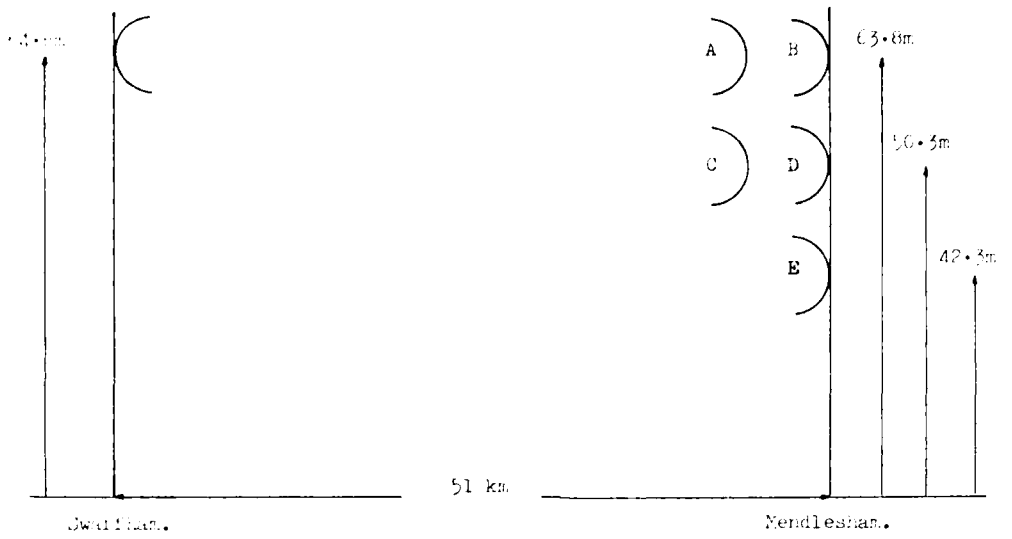

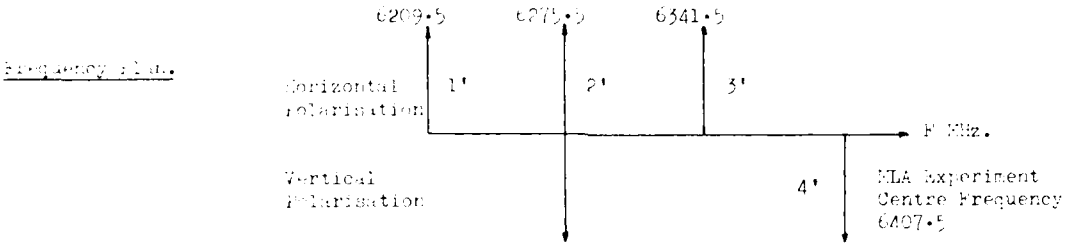

Frequency Plan.

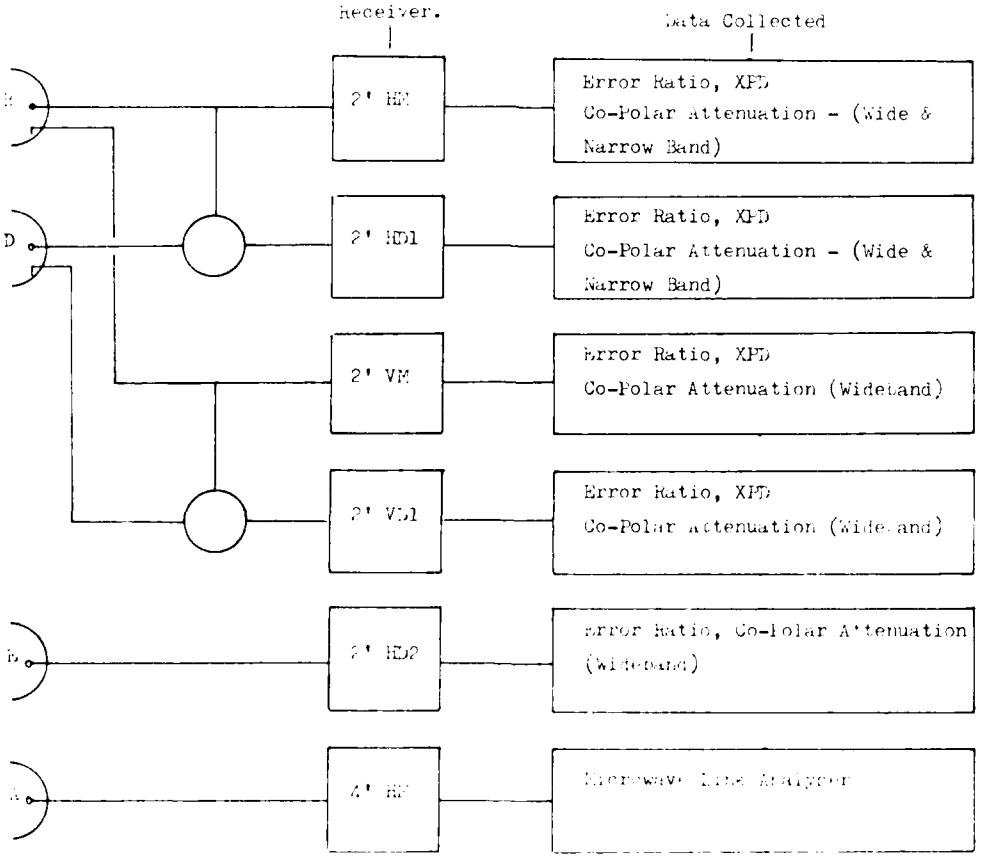

Figure 1.

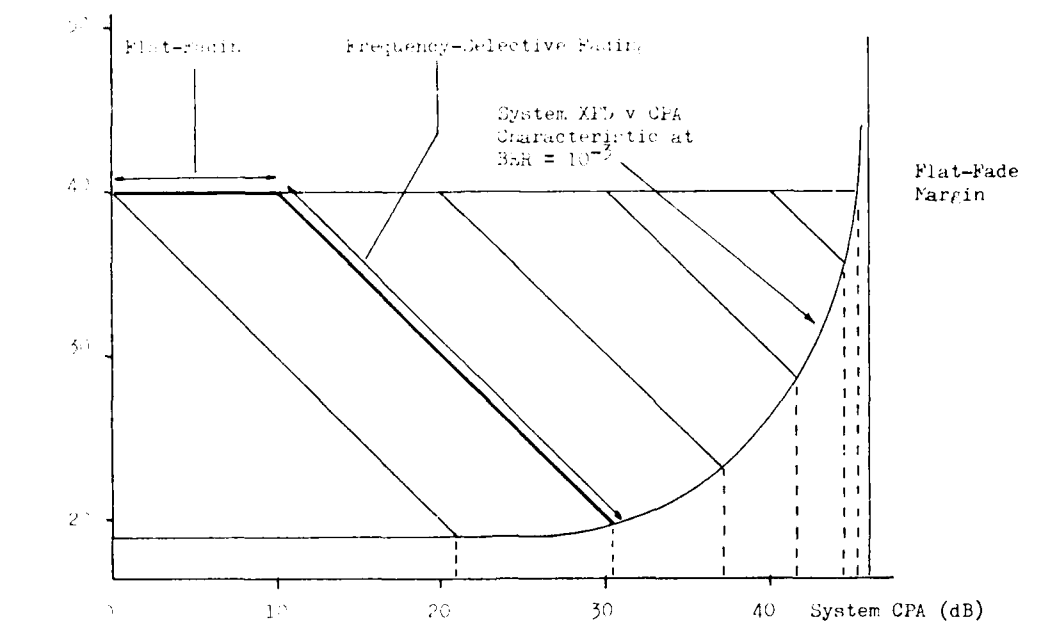

Figure 2.

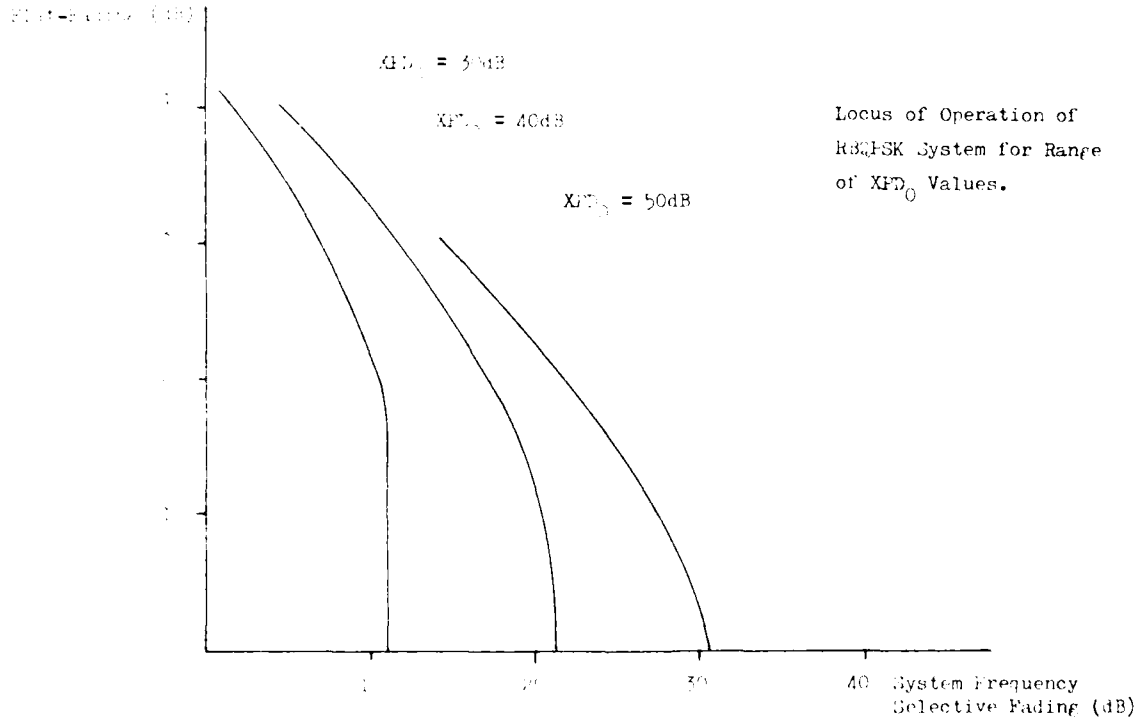

Figure 4.

DISCUSSION

R.Valentin, Ge

Could you please comment on the relative advantages or disadvantages of the RBQPSK-modulation compared to other digital modulation methods like QPRS and 16 QAM. The spectral efficiency is one factor, the signal-to-noise or E_b/N_o ratio is another one when dealing with these modulation schemes. How big is the difference in practice in the signal-to-noise ratio required for a given BER of a RBQPSK system compared to a "normal" QPSK system?

Author's Reply

The main features of the RBQPSK system are

(1) The spectral efficiency

(2) The robustness of the system in the presence of multipath activity due to the "built-in" two-stage adaptive feedback system to counteract the inherent intersymbol interference of the system. Thus much of the system outage is determined by the XPI performance of the antennas employed.

As a measure of the effectiveness of the adaptive equalisation in combatting multipath activity, when an RBQPSK demodulator was fitted to an 11 GHz QPSK system, the outage was reduced by a factor of at least 6.

We are monitoring the performance of a 16 QAM system on the same route as the RBQPSK experiment, but this has not been running for sufficient time for us to give a meaningful comparison of results.

I am sorry, but I cannot answer the question re signal-to-noise ratio for given BER. I am a propagationist not a systems engineer, but will arrange for the information to be sent to you.

R.W.Hubbard, US

(1) What was the diversity spacing during the power fading event?

(2) What was used to estimate the small delay values during multipath fading?

Author's Reply

(1) For first diversity level – 13.5 metres; for second level 21.5 metres.

(2) (a) From analysis of video recordings of the Microwave Link Analyser. (b) From an experimental programme of curve fitting to a 500 MHz swept frequency experiment 1972–75.

J.A.Hoffmeyer, US

You commented that minimal and non-minimal phase fading are equally probable. What is the basis of this assertion?

Author's Reply

The equiprobability of minimal and non-minimal phase fading applies only to *deep* fading, where in a two-path situation the components are of near equality in amplitude and hence any slight change in relative amplitude will change the classification of the fade. This has been observed to happen in the MLA experiment.

PROPAGATION EFFECTS ON THE DOPPLER FREQUENCY SHIFT OF SATELLITE TRANSMISSIONS

George H. Millman
Michael C. Arabadjis
General Electric Company
Syracuse, New York 13221, U.S.A.

SUMMARY

The refraction phenomenon in the troposphere and the ionosphere causes an error in the Doppler frequency shift of radio transmissions emitted from a nonstationary satellite and received on the ground. Estimates are made of the Doppler error for various atmospheric and solar-geophysical conditions and are applicable for frequencies in the VHF-UHF range and above.

1. INTRODUCTION

Electromagnetic waves when transmitted through a medium, such as the troposphere or the ionosphere, whose dielectric constant or index of refraction is a varying function of the path, undergo a change in the direction of propagation or refractive bending. Because of the refraction phenomenon, an error is introduced in the Doppler frequency shift of radio transmissions emanating from satellites and in the determination of the radial velocity of space-borne vehicles. The error results from the fact that the direction of the refracted ray at the spacecraft differs slightly from the unrefracted line-of-sight direction.

In this paper, estimates are made of the characteristics of the Doppler frequency shift and the errors that can be encountered in the reception of transmissions from satellites traversing circular-polar orbits, an elliptical-polar orbit and an orbital path of small inclination at geosynchronous altitude.

2. THEORETICAL CONSIDERATIONS

2.1 DOPPLER EFFECTS

The frequency of a radio signal emitted from a transmitter on a space vehicle and received on the earth experiences an apparent shift. The phenomenon which is referred to as the Doppler effect occurs because of the relative motion between the source of transmission and the stationary receiver terminal.

The Doppler effect can be expressed by the relationship

$$f_d = -\frac{f}{c} V \cos \psi \tag{1}$$

where f_d is the frequency difference between the apparent reflected frequency, f', and the transmitted frequency, f, c is the free space velocity and V is the satellite velocity. As shown in Figure 1, ψ is the angle between the satellite velocity vector and the direct path (i.e., line-of-sight direction).

Because of the refractive characteristics of the troposphere and the ionosphere, an error is introduced in the determination of the Doppler frequency shift. The error in the Doppler frequency difference is given by

$$\Delta f_d = -\frac{f}{c} \Delta V \cos \psi \tag{2}$$

where it is assumed that f and ψ are errorless quantities.

The term, $\Delta V \cos \psi$, is the component of the satellite velocity error in the direction of the line-of-sight path. According to Figure 1, this term is given by

$$\Delta V \cos \psi = V_D - V_R \tag{3}$$

where

$$V_D = V \cos \psi \tag{4}$$

$$V_R = V \cos \phi \tag{5}$$

and where ϕ is the angle between the velocity vector and the ray path. It is noted that V_D and V_R are the components of the satellite velocity projected along the direct path and the ray path, respectively.

It follows from Equations (3) through (5) that Equation (2) can be rewritten as

$$\Delta f_d = -\frac{f}{c} V \left[\cos \psi - \cos \phi\right] \tag{6}$$

DISCUSSION

G.H.Millman, US

Your discussion pertains to irregularities which induce amplitude scintillation. Have you considered irregularities which are associated with phase scintillation?

Author's Reply

The irregularities in the F layer produce both phase and amplitude fluctuations. The digital outages noted in equatorial measurements could all be explained by amplitude fading. It is certainly possible that phase fluctuations could affect certain modulation systems.

B.W.Reinisch, US

You stated the irregularities in the F-region have the size of a Fresnel zone. Did you mean to say that the observed scintillations at a given signal frequency are caused by Fresnel size irregularities?

Author's Reply

The F-region irregularities which produce the predominant effect on trans-ionospheric transmissions are of the Fresnel wavelength $[\alpha (\lambda Z)^{\frac{1}{2}}]$ although the smaller scale irregularities have an important effect on the spectra of the fluctuations.

C.Goutelard, Fr

Vous signalez que la diversité temporelle avec le codage est la seule qui puisse être utilisée dans le problème que vous venez d'exposer. Entendez-vous par là un entrelacement de codes ou une répétition des messages?

Author's Reply

Code interleaving is the only practical method of dealing with a changing medium (the irregularity structure) since repetition might only bring new errors; the receiver of the message would then have to decide as to which characters were in error.

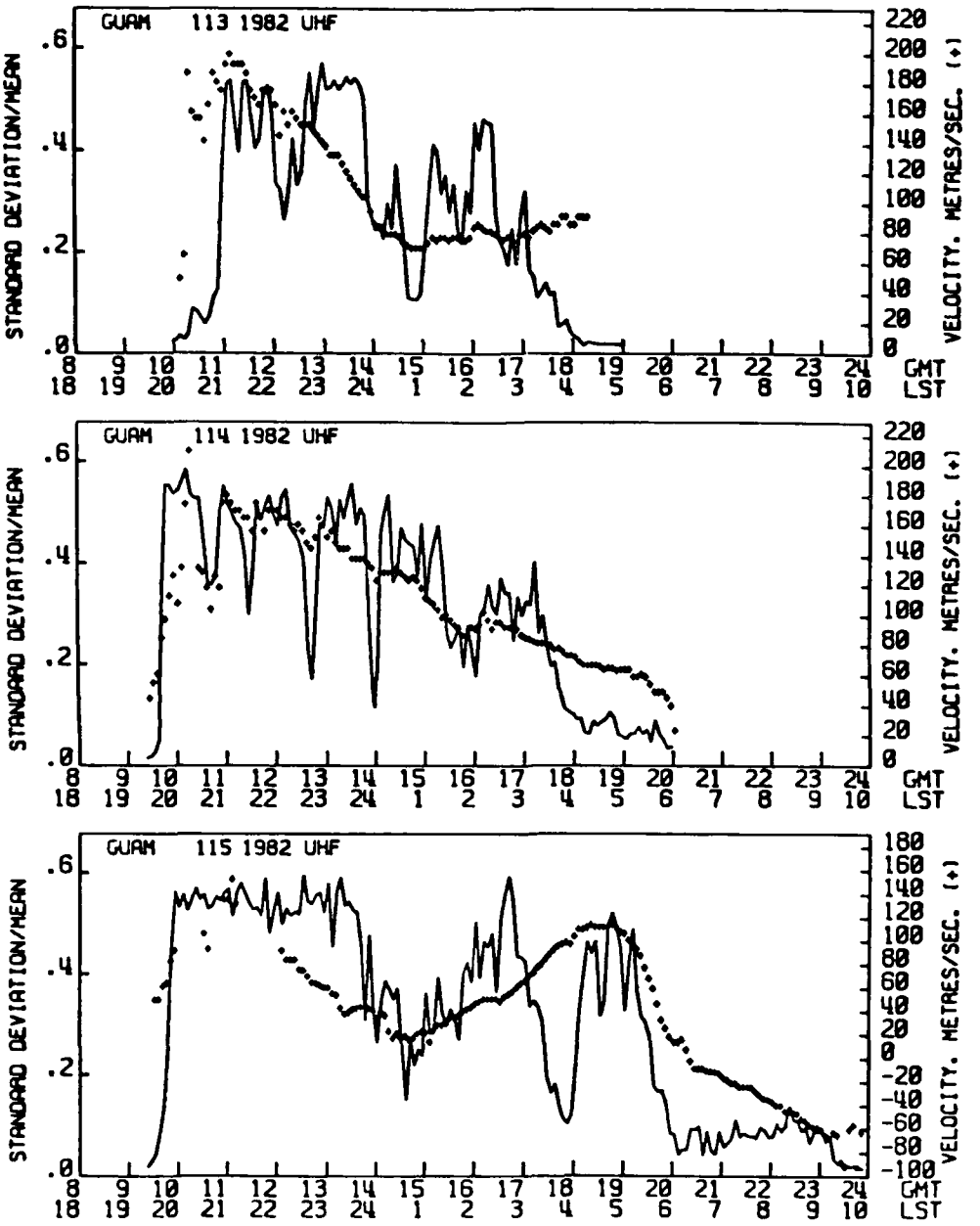

Figure 12: Scintillation levels at 250 MHz as taken close to the magnetic equator (Guam). Periods of relatively low level can be noted before midnight on days 113 and 114 (Paulson,1982).

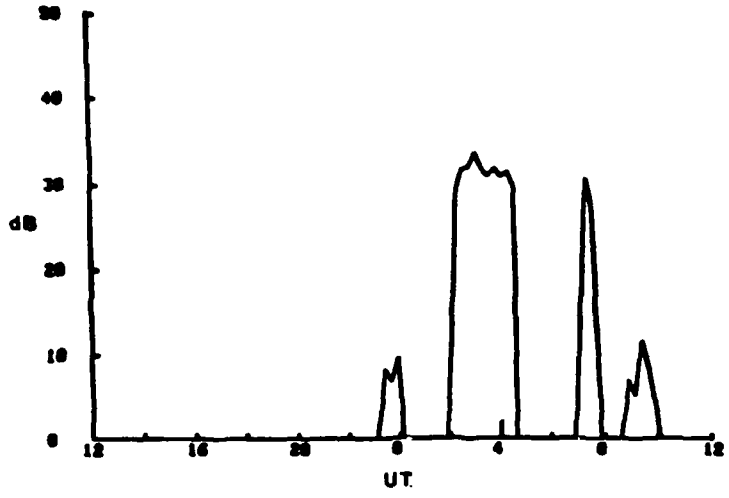

Figure 11: Observed max-min AGC from USNS Hayes at magnetic latitude 21° with geographic latitude -38°S and longitude 57.5°W; January 28, 1981

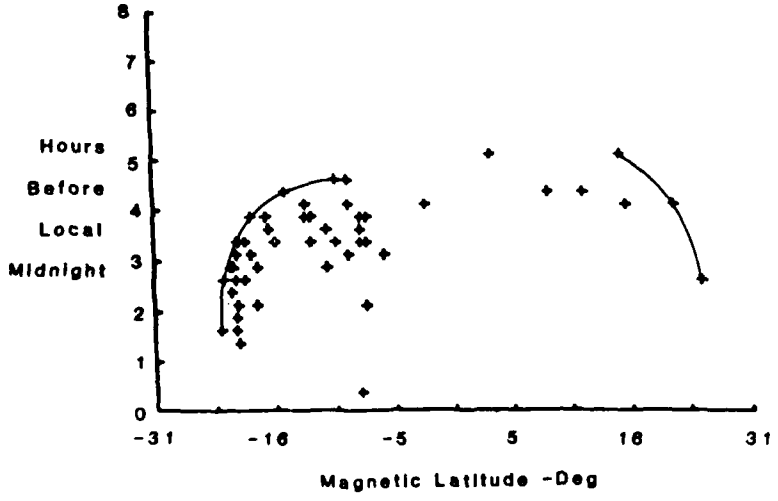

Figure 13: Time advance (prior to local midnight) at which 20 dB scintillation was observed. The outer ring of observations is connected to denote the first appearance of strong scintillation at various magnetic dip angles (Goodman and Martin, 1982)

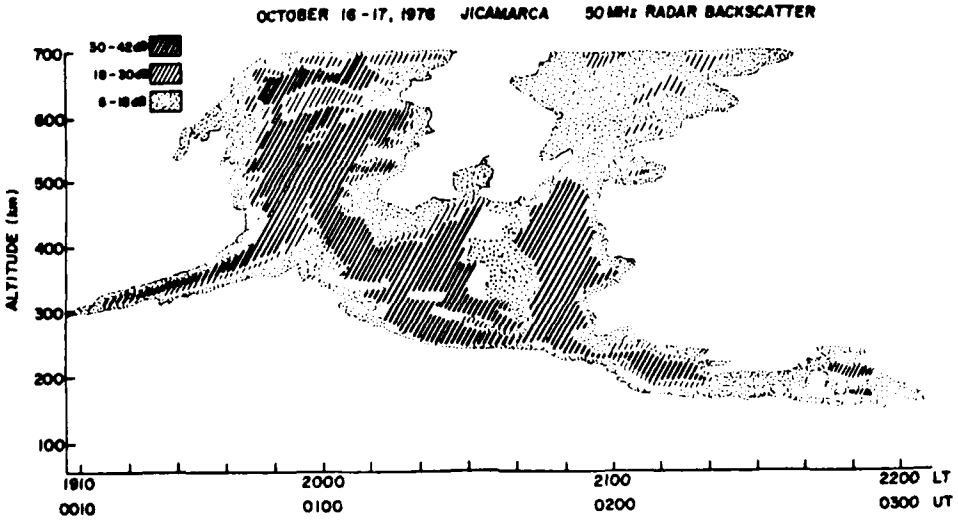

Figure 9: 50 MHz radar backscatter power map of nighttime irregularities obtained at Jicamarca on 16-17 October 1976 (Basu and Aarons, 1977; map from data supplied by J.P.McClure)

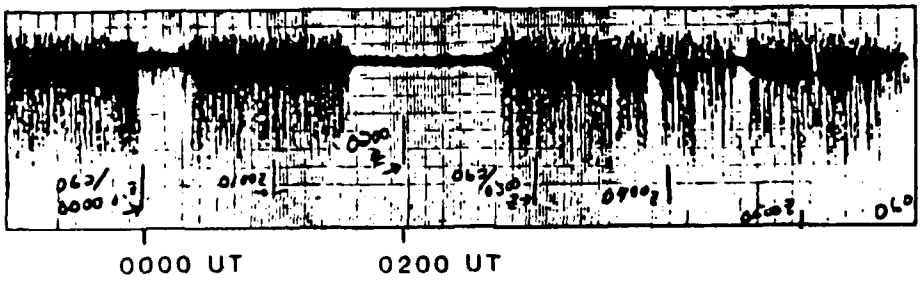

[illegible] 10. VLF/LF Waves [illegible] observations at 10° magnetic [illegible] path, max sun [illegible] 35 dB, March 1-2, 1981.

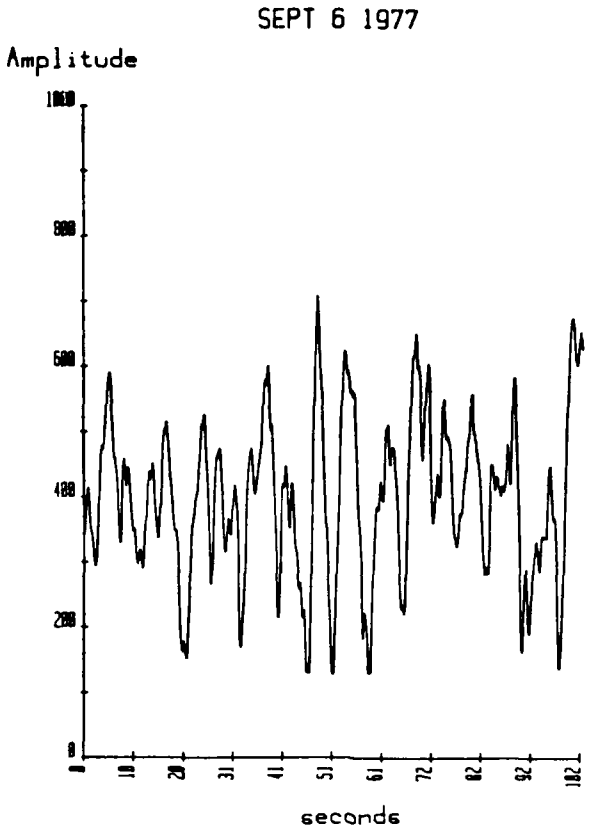

Figure 8a: Amplitude recordings of signals taken at Natal (similar to those in 6a)

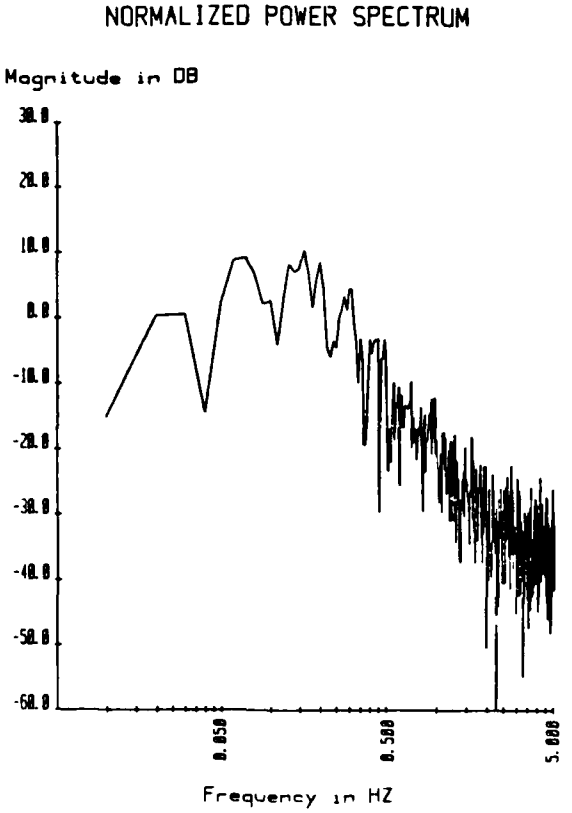

Figure 8b: Normalized power spectrum of recording shown in 8a

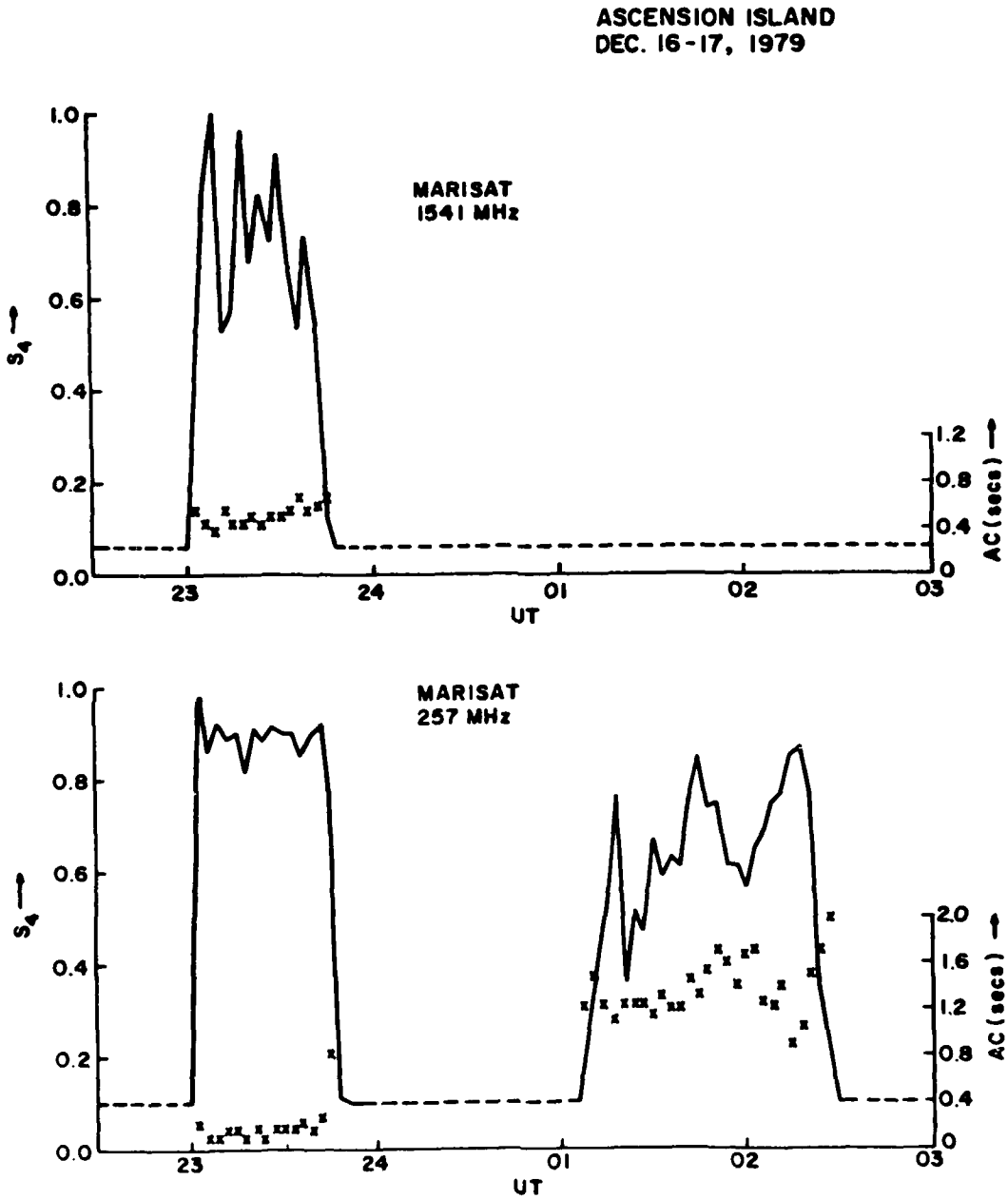

Figure 7: Temporal variations of MARISAT recordings at Ascension Island (Basu et al, 1983)

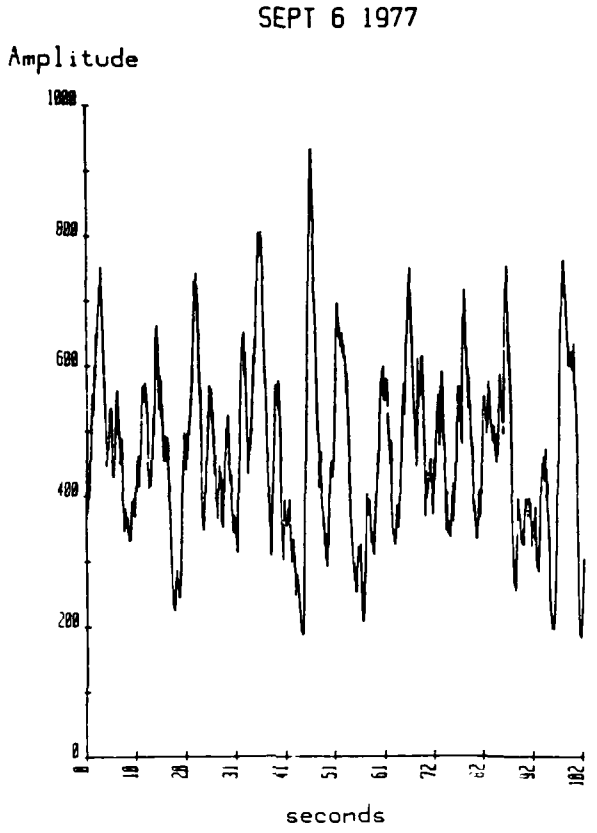

Figure 6a: Amplitude recordings of signals taken at 258 MHz at Natal , Brazil (Yeh et al,1981)

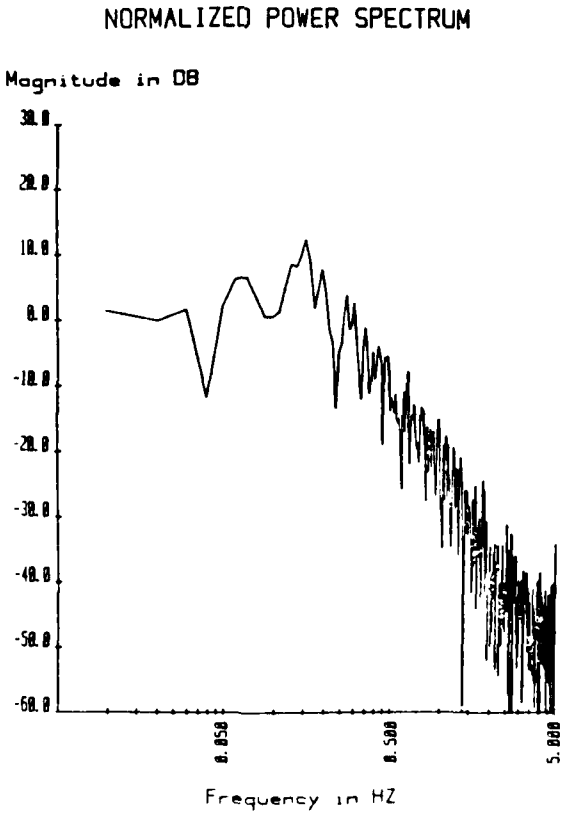

Figure 6b: Normalized power spectrum of recording shown in 6a

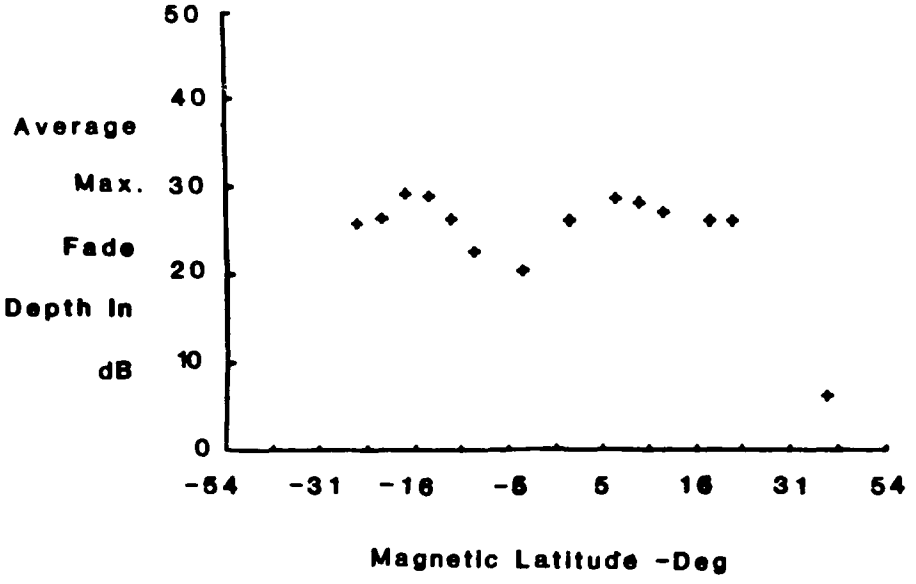

Figure 3: Average maximum UHF fade depth versus magnetic latitude from cruise of USNS Hayes (Goodman and Martin, 1982).

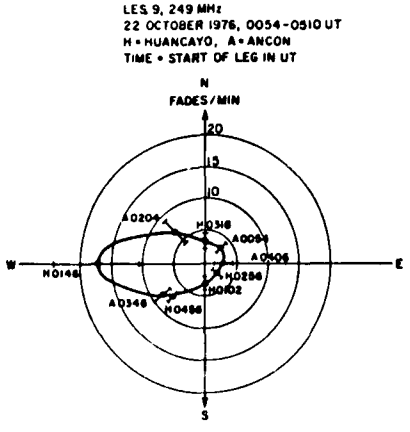

Figure 4: Fading rate as a function of aircraft heading, (J. Buchau, personal communication).

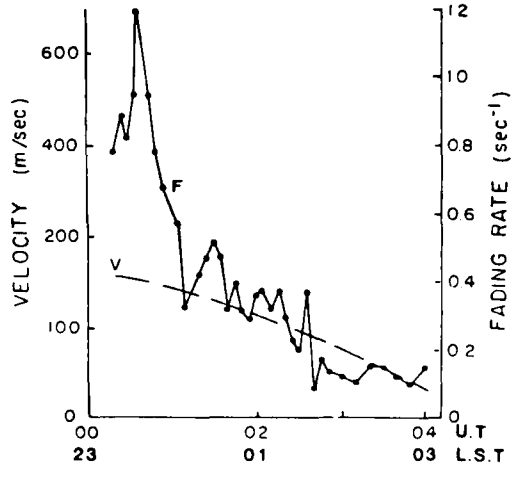

Figure 5: Velocity and fading rate during one night; observations at Natal, Brazil. Slower rates occur in the post-midnight time period (Yeh et al, 1981).

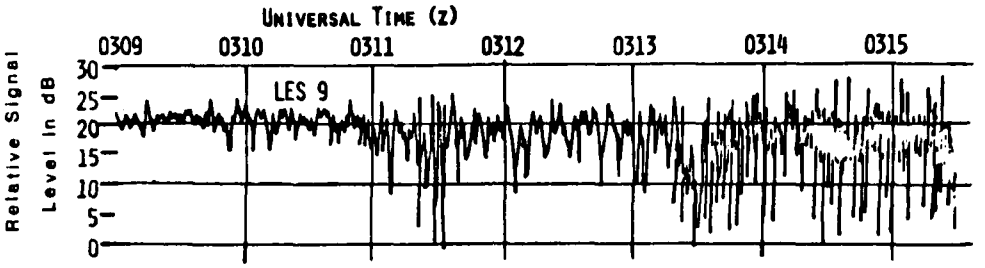

**FADING ON 250 MHz (LES-9)
OBSERVED ON AFAL
AIRCRAFT OCT. 19, 1976**

Figure 1: Samples of scintillation fading data taken in AFAL Aircraft. Quiet signal level is of the order of 20 dB. Fades to noise at 0 dB and below can be noted (A. Johnson, personal communication).

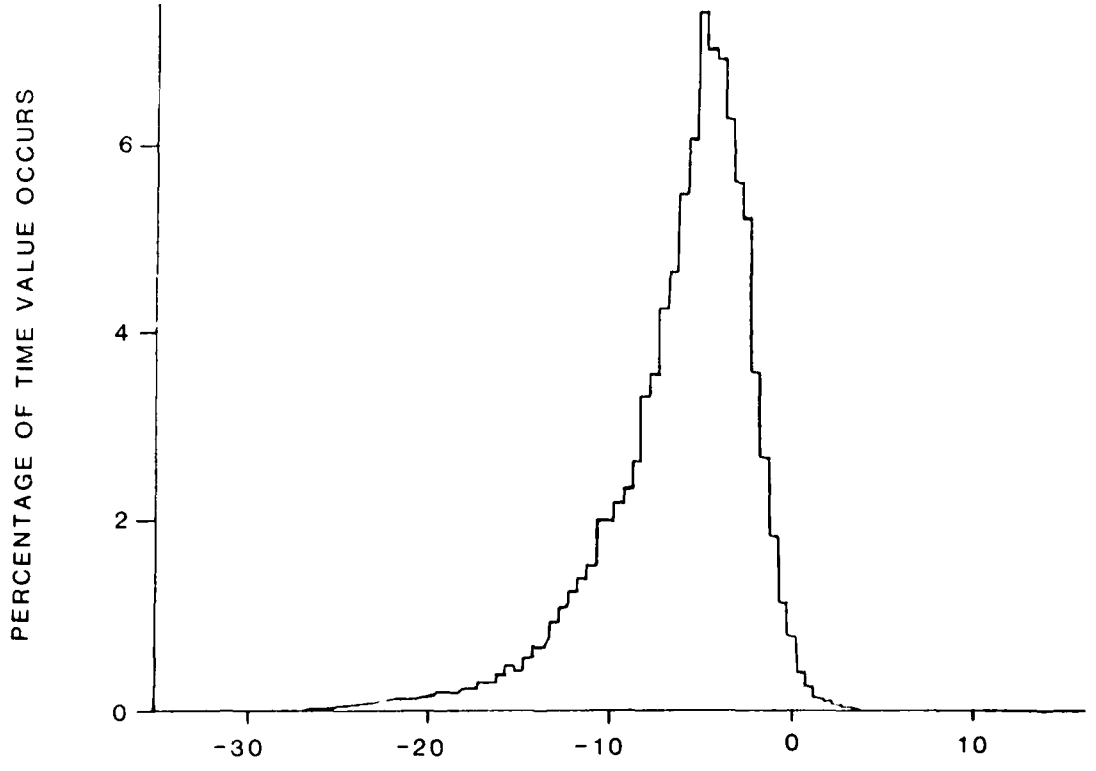

Figure 2: Histogram of scintillation fading data giving percentage of time signal is equal or or less than abscissa (A. Johnson, personal communication).

BIBLIOGRAPHY

Aarons, J. (1982) Global morphology of ionospheric scintillations, Proc. IEEE 70, 360-378.

Basu, Santimay and J. Aarons (1977) Equatorial irregularity campaigns, Air Force Geophysics Laboratory TR-77-0264, Hanscom AFB, MA.

Basu, Santimay and S. Basu (1981) Equatorial scintillations-a review, J. Atmos. and Terr. Phys. 43, 473-489.

Basu, Sunanda, S. Basu, J.P. McClure, W.B. Hanson, and H.E. Whitney (1983) High resolution topside in situ data of electron densities and VHF/GHz scintillations in the equatorial regions, J. Geophys. Res. 88, 403-415.

Goodman, J.C. and A.J. Martin (1982) A summary of propagation studies undertaken by the 1981 expedition of the USNS Hayes, Naval Research Laboratory Report 4720 NRL, Washington, D.C.

Johnson, A. (1980) Propagation anomalies affecting airborne satellite communications, AGARD Conference Proceedings 284- Propagation effects in space/earth paths, AGARD Paris, France.

Ossakow, S.I. (1981) Spread-F theories-a review, J. Atmos. Terr. Phys. 43, 437-452.

Paulson, M.R. (1982) Equatorial scintillations of satellite signals and the drift characteristics of the scintillation, Naval Oceans Systems Command TN 1183 16 August 1982. NOSC, San Diego, CA.

Yeh, K.C. and C.H. Liu (1982) Radio wave scintillations in the ionosphere, Proc. IEEE 70, 324-359.

Yeh, K.C., J.P. Mullen, J.R. Medeiros, R.F. da Silva and R.T. Medeiros (1981) Ionospheric scintillation observations at Natal, J. Geophys. Res. 86, 7527-7532.

ACKNOWLEDGEMENTS: The author acknowledges support from the Office of Naval Research. Shipboard strip-chart recordings of FLEETSATCOM were kindly provided by J.M. Goodman and A.J. Martin of the Naval Research Laboratory.

One can note however that the irregularities at 700 km show a gap between 2020 and 2040. The lines of force of the earth's magnetic field that are associated with the 700 km point come down to 250 km in the anomaly region. Thus irregularities seen at 700 km and higher over the magnetic equator are the only irregularities observed directly overhead at Ascension Island. Between 2020 and 2040 therefore it is possible to have extremely low levels of fading. As illustration of this, 250 MHz records are shown (Figure 10) where gaps between the high intensity scintillations are observable (Goodman and Martin, 1982). Levels in dB for another day are shown in Figure 11. At the magnetic latitude of the observations (10 and 21) there are periods of one hour between the larger structures. The gaps are also noted at lower frequencies.

Even at the magnetic equator for example in data from Guam (Figure 12 from Paulson, 1981) there are blocks of time when scintillation levels are low (note low periods in Days 113 and 114, 1982). In this illustration the velocity can be noted to slow down as the night progresses towards morning. However there are times (0100 LST on Day 115) when the velocity may increase after having slowed down.

5.2 TIME OF EFFECTS

The basic time sequence of the irregularity patches is that the plume forms within an hour after sunset, rises into the higher altitudes during formation and then moves eastward (for the most part). Scintillation effects at the receiving sites will therefore vary. If the signals which are to be retransmitted are scintillating then mitigation using morphology is inadequate. However if only the receivers are affected then a knowledge of the temporal variation of scintillation is important. Since the plume rises with velocities which may reach over 200 meters per second (Ossakow, 1981) the signals would appear later in the regions distant from the magnetic equator. This has been shown in the shipborne experiment of Goodman and Martin (1982) where high scintillation levels are noted around the midnight time period when the ship was distant from the equator compared to earlier hours when the ship was near the magnetic equator.

5.3 OTHER MITIGATION TECHNIQUES

Johnson (1980) has covered mitigation techniques, finding frequency diversity impractical for separations less than 100 MHz and space diversity needing separations of .5 to 1.0 km for the most part.

Time diversity, utilizing the measured real time channel chacteristics to develop the coding to be used, appears to be the most practical method of mitigating the deep fades of scintillation activity. Modems and coding methods could be utilized in conjunction with the geophysical characteristics of irregularity patches to minimize the effect of the small scale irregularities on digital communications.

Another possible mitigation technique is to utilize multiple satellites thus supplying a diversity of paths for the signal. This would yield time differences of up to a few hours as well as utilize the individual behavior of different sectors. The obliquity of the paths however, cutting through several patches, should be taken into consideration.

To determine the effects of scintillation on digital transmissions, power spectra and fading characteristics should be examined. Both the power spectra and the fading statistics must be assessed as they change as a function of time, latitude, frequency etc. We will attempt to outline some results to date and to give references for additional information. A single histogram of scintillation fading data at 250 MHz is given in Figure 2. The 250 MHz aircraft data shows the percentage of time that the fading amplitude equaled the abcissa. The data in Figures 1 and 2 were taken near the magnetic equator during a period of low solar activity. From a series of observations of 250 MHz scintillations using the USNS HAYES, Goodman and Martin (1982) were able to contrast the average maximum of fade depth in dB across the anomaly region with the region near the magnetic equator. This is shown in Figure 3.

3. FADING RATE

Analogue records such as shown in Figure 1 appear to encompass a relatively narrow band of frequencies; in general the zero crossings are not greatly variable when observing on the ground over a time span of 5 minutes. Basically the small scale irregularities with Fresnel wavelengths of several hundred meters are moving eastward across the trans-ionospheric path. An aircraft moving with the ionospheric F layer wind pattern would experience lower fading rates than an aircraft moving against the wind. Figure 4 (J.Buchau, personal communication) shows the increase in rate as a function of aircraft heading. The fading rate is a function however of both the velocity of the ionospheric wind and the strength of the irregularities. With strong scattering the pattern on the ground is not the pattern of the irregularity motion across the path; additional components are created and the fading rate increases. In Figure 5 (Yeh et al, 1981) the fading rate is much higher earlier in the evening than later. The velocity however changed slowly. For strongly scattered signals therefore the velocity is only one component of the fading rate.

4. SPECTRA OF EQUATORIAL SCINTILLATIONS

The more accurate measure of the signal characteristics is of course the fading spectrum. Amplitude measurements taken at Natal, Brazil at 250 MHz such as shown in Figure 6a (Yeh et al., 1981) were analyzed with the normalized power spectra shown in Figure 6b. It is these spectra that the designer of modems must utilize. The problem is that the spectra vary as a function of strength of the irregularities, frequency, time, and location of site. Just as in all systems therefore the limits of requirements must be established.

Perhaps the most direct way of showing the variations as a function of time and frequency would be to illustrate the scintillation amplitude changes as a function of frequency as well as the changes in the auto-correlation function as a function of both time and frequency. In the illustration of reduced data shown in Figure 7 (Basu et al., 1983), amplitude scintillations at 257 MHz were saturated from 2200 LST (2300 UT) to 2245 LST; the 1.54 GHz scintillations are very high but are at times not saturated. The autocorrelation falls to .5 at about .6 seconds. Very strong scattering was produced at 257 MHz however and the autocorrelation fell to .1 seconds from 0110-0220 UT. In the post-midnight time period scintillations were less than 1 dB at 1.54 GHz but were considerable at 257 MHz. The autocorrelation function was of the order of 1.2 seconds for 257 MHz in the post- midnight time period. From the viewpoint of correcting errors in digital communications, differing characteristics of each frequency have to be met in correction methods even during the same night.

Subtle differences in spectra can be noted between the illustrations given in Figure 6a and 6b (Yeh et al., 1981) and Figures 8a and 8b. The second set can be seen to have higher frequency components than the first set; this is shown distinctly by the increased level of the high frequency components in the spectra of the Figure 8 set. These are relatively similar spectra. The differences emerge more strongly when slow and deep fading take place -- sometimes simultaneously (early hours of the morning). Both spectra and their simplified forms, fading rates, show the effects of the velocity decreasing as a function of time as the night progresses, moving on occasion to a westerly velocity in the early morning hours.

5. MINIMIZING THE EFFECTS OF EQUATORIAL SCINTILLATION

5.1 PATCH STRUCTURE

The nature of the formation of the plumes and their dimensions allow for a method of "inserting information" between the patches. In Figure 9 the coherent radar returns observed in Jicamarca, Peru show a typical structure (Basu and Aarons, 1977, from data supplied by J.P. McClure). The cross section of the irregularities as shown by the backscatter return plus an understanding of the geophysics of irregularities allows us an opportunity to minimize the effect of scintillations. The irregularity patch can be pictured as a banana oriented magnetic North-South, its long dimension at times extending over one or two thousand kilometers north and south of the of the magnetic equator. The structures shown in Figure 9 appear overhead as scattered signals at 1920 Local Standard Time. Scattered signals disappear at 2200. At frequencies greater than 1 GHz one would observe scintillations from 1945 to 2010. Scintillations would also appear between 2030 and 2050. Overhead at Jicamarca, Peru, on the magnetic equator, trans-ionospheric signals in the VHF-UHF range would be affected between 1920 and 2200 LST.

EQUATORIAL TRANS-IONOSPHERIC PROPAGATION CONDITIONS AFFECTING DIGITAL COMMUNICATIONS

Jules Aarons
Department of Astronomy
Boston University
725 Commonwealth Ave.
Boston, Mass. 02215 USA

SUMMARY

In the region within ± 20° of the magnetic equator, irregularities in the F layer of the ionosphere have a deteriorating effect on satellite transmissions, analogue and digital. Ionospheric effects have been observed at frequencies to 7 GHz although the fade levels (in the worst case) at that frequency are no greater than 2 dB. However fades of 10 dB have been noted on 4 GHz in worst case statistics. Systems using frequencies affected by the irregularities are proliferating and include communications at 250 MHz and 400 MHz, navigational systems at 1.2 GHz and 1.6 GHz and commercial maritime communications systems at 1.5 GHz. There is need to assess the strength, morphology, and spectral characteristics of the trans-ionospheric transmissions in order to mitigate fading in a trans-ionospheric digital system. The morphology and signal statistics of equatorial scintillations have recently been reviewed (Aarons, 1982 and Yeh and Liu, 1982). During years of high solar flux, the anomaly regions of the equatorial region (regions of high electron density near 20 magnetic latitude) experience extremely high levels of fading during the hours from one hour after sunset to midnight. Maximum activity takes place during the equinoctial months although there are differences in behavior of various longitudinal sectors. In years of low solar flux the anomaly regions do not experience deep fading of the level noted although fades of 6 dB at the magnetic equator have been noted at 1.5 GHz during years of low solar flux. Typical amplitude spectra from regions on the magnetic equator and in the anomaly region are given at frequencies varying from 250 MHz to 1.5 GHz. Spectra vary as a function of the strength of irregularities, frequency, local time and location of site. Data are given to allow the designer of modems to determine the range of fading. Saturated signals as well as weakly scattered signals can be noted. The system designer will be urged to utilize times of low scintillation levels between large scale patches of irregularities to transmit information redundantly. Away from the magnetic equator and at times at the magnetic equator the patches may produce deep fading which will last for an hour and then give 5-30 minutes of time when no irregularities are in the trans-ionospheric path. High data rates can be utilized in these periods. While the forecasting of the structure of the patches and the pauses is difficult the general characteristics of the irregularity structure should allow for programming information even during those months when maximum scintillation activity exists.

1. INTRODUCTION

In the region within ± 20° of the magnetic equator, irregularities in the F layer of the ionosphere have a deteriorating effect on satellite transmissions, analogue and digital. Ionospheric effects have been observed at frequencies to 7 GHz although the fade levels (in the worst case) at that frequency are no greater than 2 dB. However fades of 10 dB have been noted on 4 GHz in worst case statistics.

Systems using frequencies affected by the irregularities are proliferating and include transmissions at 250 MHz, navigational systems at 1.2 GHz and 1.6 GHz, and commercial maritime communications systems at 1.5 GHz. The need therefore to assess the strength, morphology, and spectral characteristics of the trans-ionospheric transmissions is important if one is to deal with the fading in a trans-ionospheric digital system.

The morphology of equatorial scintillations has recently been reviewed (Aarons, 1982) and the signal statistics involved in scintillation observations have also been reviewed (Yeh and Liu, 1982). During years of high solar flux such as experienced between 1979 and 1981 the anomaly regions of the equatorial region (regions of high electron density near 20° magnetic latitude) experience extremely high levels of fading during the night hours from one hour after sunset to midnight (the worst case statistics given above come from the anomaly region). Maximum activity is for the most part in the equinoxes although there are differences in behavior of various longitude sectors. In years of low solar flux the anomaly regions do not experience deep fading of the level noted although fading of 6 dB peak to peak at the magnetic equator has been noted at 1.5 GHz during years of low solar flux.

2. FADING CHARACTERISTICS RELEVANT TO DIGITAL COMMUNICATIONS

Fluctuations of signal are due to the passage of irregularities across the trans-ionospheric path. The scale size of the irregularities is determined by the Fresnel wavelength which in the case of transmissions from 100 MHz to 4 GHz is of the order of hundreds of meters. While this is the dominant size, there are strong shorter wavelength irregularities; these are responsible for a high frequency component of the scintillations. Fast recordings of scintillation amplitude appear as shown in Figure 1 (A. Johnson, personal communication). It can be seen that even with signal to noise margins of 10-20 dB above noise, there are times when the signal level falls to a point where digital information will be lost in the fade.

Expressions for the angles ψ and ϕ can be derived utilizing the vector analysis approach. It is assumed that the velocity, V and the directions D,(direct path) and R (ray path), are unit vectors. Thus the scalar product of the vectors $\vec{V}$ and $\vec{D}$ and $\vec{V}$ and $\vec{R}$ are

$$\vec{V} \cdot \vec{D} = |V||D| \cos \psi = \cos \psi \tag{7}$$

$$\vec{V} \cdot \vec{R} = |V||R| \cos \phi = \cos \phi \tag{8}$$

According to Figure 1, the vectors, $\vec{V}$, $\vec{D}$ and $\vec{R}$ can be represented by the unit vectors (i, j, k) along the X (east), Y (north) and Z (zenith) axes:

$$\vec{V} = i \sin \alpha \sin A_V + j \sin \alpha \cos A_V + k \cos \alpha \tag{9}$$

$$\vec{D} = i \sin \gamma \sin A_R + j \sin \gamma \cos A_R + k \cos \gamma \tag{10}$$

$$\vec{R} = i \sin (\gamma + \Delta E_s) \sin A_R + j \sin (\gamma + \Delta E_s) \cos A_R + k \cos \gamma \tag{11}$$

It is noted that $\vec{D}$ is in the Z - $\vec{R}$ plane and that α is the angle between the Z-axis and $\vec{V}$, A_V is the azimuth angle of $\vec{V}$ measured from geographic north at the satellite location, A_R is the azimuth angle of $\vec{R}$ measured from geographic north at the satellite location, γ is the angle between the Z-axis and $\vec{D}$ and ΔE_s is the angle between $\vec{D}$ and $\vec{R}$.

Substituting Equations (9) and (10) in Equation (7) yields

$$\cos \psi = \sin \alpha \sin A_V \sin \gamma \sin A_R + \sin \alpha \cos A_V \sin \gamma \cos A_R + \cos \alpha \cos \gamma \tag{12}$$

Similarly, when substituting Equations (9) and (11) in Equation (8), it follows that

$$\cos \phi = \sin \alpha \sin A_V \sin (\gamma + \Delta E_s) \sin A_R + \sin \alpha \cos A_V \sin (\gamma + \Delta E_s) \cos A_R + \cos \alpha \cos (\gamma + \Delta E_s) \tag{13}$$

For the two-dimensional case in which $A_R - A_V = 0$ or 90°, Equations (12) and (13) simplify to

$$\cos \psi = \cos (\gamma - \alpha) \tag{14}$$

$$\cos \phi = \cos \left[(\gamma + \Delta E_s) - \alpha \right] \tag{15}$$

When substituting Equations (12) and (13) in Equation (5), the Doppler frequency difference error becomes

$$\Delta f_d = -\frac{f}{c} V \left\{ \sin \alpha \left[\sin \gamma - \sin (\gamma + \Delta E_s) \right] \cos \left(A_R - A_V \right) + \cos \alpha \left[\cos \gamma - \cos (\gamma + \Delta E_s) \right] \right\} \tag{16}$$

An expression for the angles, ΔE_s and γ, can be readily derived from Figure 2 which illustrates the angular deviation of a ray due to the refractive effects of the medium.

It can be shown utilizing Snell's Law for spherically stratified surfaces and the law of sines that

$$\Delta E_s = \cos^{-1} \left[\frac{r_o}{r_o + h_s} \cos (E_o - \Delta E) \right] - \cos^{-1} \left[\frac{n_o r_o}{n_s (r_o + h_s)} \cos E_o \right] \tag{17}$$

where n_o and n_s are the refractive indices at the ground and space vehicle, respectively, r_o is the radius of the earth (6371 km) and ΔE is the refraction angle error corresponding to the apparent elevation angle, E_o, and satellite altitude, h_s.

The angle, γ, is derivable from the law of sines and is given by

$$\gamma = \sin^{-1}\left[\frac{r_o}{r_o + h_s}\cos\left(E_o - \Delta E\right)\right] \tag{18}$$

In determining an expression for the angle α, it is necessary to consider the orientation of the satellite's velocity vector with respect to the zenith as indicated in Figure 3. It can be shown from simple trigonometric considerations that

$$\alpha = \tan^{-1}\left\{\frac{\sin\theta}{\cos\theta - \dfrac{r_o + h_{s1}}{r_o + h_{s2}}}\right\} \tag{19}$$

where θ is the earth's central angle measured between the two satellite positions, p_1 and p_2. The parameters h_{s1} and h_{s2}, are the altitudes of the satellite at p_1 and p_2, respectively.

For small angle θ, Equation (19) simplifies to

$$\alpha \approx \tan^{-1}\left\{\frac{D}{h_{s2} - h_{s1}}\right\} \tag{20}$$

where D is the distance travelled by the satellite as projected onto the minimum altitude.

It is noted that

$90° < \alpha \leq 180°$ for $h_{s1} > h_{s2}$

$\alpha = 90°$ for $h_{s1} = h_{s2}$

$0° \leq \alpha < 90°$ for $h_{s1} < h_{s2}$

The $h_{s1} \approx h_{s2}$ condition occurs for a satellite in a circular orbit.

The angle, A_R, which is the bearing angle of the propagation direction, i.e. ray path, at the satellite is given in Figure 4 which depicts the satellite geometry projected on the earth's surface. It can be readily shown from spherical trigonometry that

$$A_R = \cos^{-1}\left\{-\cos A \cos\left(\lambda_s - \lambda_o\right) + \sin A \sin\left(\lambda_s - \lambda_o\right) \sin L_o\right\} \tag{21}$$

where A is the bearing of the satellite (with respect to geographic north) as measured at the observation site, L_o is the latitude of the observation site, and λ_s and λ_o are the longitudes of the satellite and observation site, respectively.

Figure 5 displays the bearing of the satellite orbital velocity vector, A_V, as projected on the earth's surface. It should be evident that A_V can be expressed by the function

$$A_V = \cos^{-1}\left\{\frac{\sin L_2 - \cos\theta \sin L_1}{\sin\theta \cos L_1}\right\} \tag{22}$$

where L_1 and L_2 are the latitudes of the satellite at times t_1, and t_2, respectively. The parameter θ, the earth central angle, is given by

$$\theta = \cos^{-1}\left\{\sin L_1 \sin L_2 + \cos L_1 \cos L_2 \cos\left(\lambda_2 - \lambda_1\right)\right\} \tag{23}$$

where λ_1 and λ_2 are the longitudes of the satellite at times t_1 and t_2, respectively. It is noted that the angle θ in Equations (22) and (23) is identical to that in Equation (19).

2.2 TROPOSPHERIC EFFECTS

As indicated in Equation (17), the angle, ΔE_s, is a function of n_o, the refractive index at the earth's surface and ΔE, the angular deviation, i.e., the elevation angle error.

The tropospheric index of refraction, n, can be expressed in terms of the functions

$$N \quad (n - 1) \times 10^6 \tag{24}$$

and

$$N \quad \frac{a}{T}\left(p + \frac{b\epsilon}{T}\right) \tag{25}$$

where N is the refractivity, T is the air temperature (° K), p is the total pressure (mb) and ϵ is the partial pressure of water vapor (mb). According to Smith and Weintraub (1953), the constants, a and b, are 77.6° K/mb and 4610 K, respectively.

It should be noted that the above expression for the refractivity of air is independent of frequency in the 100- to 30,000-MHz range. The first term in Equation (25), ap/T, applies to both optical and radio frequencies, and is often referred to as the dry term. The second term, $ab\epsilon/T^2$, which is the wet term, is the water vapor relationship required only at radio frequencies.

The tropospheric angular deviations used in the ΔE_s estimation were determined by the stratified layer method (Millman, 1958). The basic assumption which this mathematical approach embodies is that the atmosphere is considered to be stratified into spherical layers with a constant refractive index in each layer.

Since the refractive index is independent of frequency, the tropospheric elevation angle errors are also frequency independent.

The index of refraction model used in the computations was the CRPL Reference Refractivity Atmosphere - 1958. As described by Bean and Dutton (1966), the refractivity model is given by

$$N(h) \quad N_o + \left(h - h_o\right) \Delta N \tag{26}$$

where N_o is the surface refractivity and h_o is surface height above mean-sea-level. This expression is valid for $h_o \leq h \leq (h_o + 1)$ km. The parameter, ΔN, is defined by

$$N \quad -7.32 \exp\left(0.005577\ N_o\right) \tag{27}$$

For the region defined by $(h_o + 1) \leq h \leq 9$ km, the refractivity decays as

$$N(h) \quad N_1 \exp\left[-c\left(h - h_o - 1\right)\right] \tag{28}$$

where N_1 is the value of N at 1 km above the surface and

$$c \quad \frac{1}{8 - h_o} \log_e\left(\frac{N_1}{105}\right) \tag{29}$$

Above 9-km altitude, the exponential decay is of the form

$$N(h) \quad 105 \exp\left[-0.1424\ (h - 9)\right] \tag{30}$$

It is seen that, at an altitude of 30 km, the refractivity decreases to a value of approximately 5 N-units.

2.3 IONOSPHERIC EFFECTS

The ΔE_s term specified in Equation (17) is also a function of the index of refraction at the satellite altitude, in addition to the elevation angle error introduced by the ionosphere.

The index of refraction in the ionosphere can be expressed by the relationship

$$n = \left[1 - \left(\frac{\omega_N}{\omega}\right)^2\right]^{1/2} \quad \left[1 - \frac{N_e e^2}{\epsilon_o m_e \omega^2}\right]^{1/2} \tag{31}$$

where ω_N is the angular plasma frequency of the medium (rad/sec), N_e is the electron density (electrons/m^3), e is the electron charge (1.6×10^{-19} C), m_e is the electron mass (9.1×10^{-31} kg), ϵ_o is the electric permittivity of free space ($10^{-9}/36\pi$ F/m) and ω ($=2\pi f$) is the angular frequency of the incident wave (rad/sec).

It is noted that the ionospheric refractive index is also a function of both the electron collision frequency and the earth's magnetic field. For frequencies on the order of 10 MHz and above, and at altitudes greater than 80 km, the effect of the collision frequency term on the index of refraction is negligible (Davies, 1965).

The electron density at the peak of the F2 layer which is generally at an altitude on the order of 300-350 km, could attain a value as high as 3×10^{12} electrons/m^3. For this condition, the index of refraction at 100 MHz evaluates to 0.9987. The ionospheric refractive index tends toward unity as the electron density decreases and as the frequency increases. In other words, it is valid to assume that, above 100 MHz, the index of refraction at the satellite altitude can be neglected in the ΔE_s computations.

The elevation angle error imposed by the ionosphere can be expressed in terms of the range error, ΔR, by the function (Millman and Reinsmith, 1974)

$$\Delta E = \frac{(R + r_o \sin E_o)\, r_o \cos E_o}{\left[h_i (2 r_o + h_i) + (r_o \sin E_o)^2 \right]} \frac{\Delta R}{R} \tag{32}$$

where R is the range to the satellite, E_o is the apparent elevation angle of the satellite and h_i is the altitude at which the median electron content, i.e., integrated electron density, along the ray path occurs. The altitude applicable to h_i is, for the most part, between approximately 300 and 450 km. For the calculations presented in this paper, a value of 400 km is assumed for h_i.

For high elevation angles, i.e., $r_o \sin E_o > R$, the angular error simplifies to

$$\Delta E \approx \cot E_o \frac{\Delta R}{R} \tag{33}$$

For low elevation angles and long ranges, i.e., $R > r_o \sin E_o$, Equation (32) reduces to

$$\Delta E \approx \frac{\cos E_o}{2h_i} \Delta R \tag{34}$$

The range error, i.e., the increase in path length, due to the ionosphere can be defined by (Millman, 1980)

$$\Delta R \quad \frac{e^2}{8\pi^2 \epsilon_o m_e f^2} \int_0^s N_e \, ds = \frac{e^2}{8\pi^2 \epsilon_o m_e f^2} \overline{\sec \gamma} \quad N_t \tag{35}$$

where ds is the differential distance along the transmission path, N_t is the electron content, i.e. the integrated electron density in a vertical column up to the satellite altitude, and γ is the angle between the ray path and the zenith.

The parameter, sec γ, which is the obliquity factor accounting for the slant path geometry, is given by

$$\sec \gamma \quad \frac{r_o + h}{\left\{ (r_o + h)^2 - \left[r_o \cos \left(E_o - \Delta E \right) \right]^2 \right\}^{1/2}} \tag{36}$$

It is noted that the angle γ in this expression is similar to that defined by Equation (18). In evaluating Equations (35) and (36), an average value for sec γ is assumed where h 400 km and ΔE 0.

An examination of Equations (32) and (35) reveals that the ionospheric refraction - elevation angle errors are inversely proportional to the frequency squared, and directly proportional to the electron content.

The presence of the ionosphere, in addition to imposing an error in the Doppler frequency shift by virtue of the refractive bending of the ray path, introduces a perturbation in the observed frequency. Since the frequency of a wave

is related to the time derivative of the phase or phase path length, it can be readily shown that the nonrelativistic Doppler frequency shift, f_d, in the ionosphere can be described by the relationship (Millman, 1980)

$$f_d = -\frac{f}{c}\frac{ds}{dt} - \frac{e^2}{8\pi^2 c \epsilon_o m_e f}\frac{d}{dt}\int_0^s N_e \, ds \qquad (37)$$

The first term in Equation (37) describes the Doppler frequency shift for an object moving in free space and is identical to Equation (1). The second term basically defines the frequency shift imposed by the ionosphere. It is seen that the Doppler shift is a function of the time derivative of the electron content along the propagation path to the object and is inversely proportional to the frequency.

3. DISCUSSION

3.1 ORBITAL TRAJECTORIES

For this analysis, the propagation effects on the Doppler shift of satellite transmissions were determined on the assumption that the receiving system was located at Boston, Massachusetts (42.5°N, 289°E).

It was assumed that a satellite was traversing (1) a circular polar orbit at an altitude of 500 km and 1000 km and (2) an elliptical polar orbit with an eccentricity of 0.379, an apogee of 10,000 km and a perigee of 1000 km. The projection on the earth's surface of the perigee point coincided approximately with the geographic latitude of Boston.

In addition, a satellite was assumed to be in a geosynchronous orbit (at 35,870-km altitude) with an 8° inclination and stationed at 265.5°E longitude, midway between Boston and Los Angeles (34°N, 242°E).

The ground tracks of a satellite in a geosynchronous orbit and in a circular polar orbit at an altitude of 1000 km are shown in Figure 6. The five passes of the elliptical polar orbit evaluated in this paper were approximately identical to the circular polar orbit illustrated in Figure 6. For the 500-km altitude circular polar orbit, the equatorial crossing of the satellite, i.e., longitude of the ascending node (LAN), occurred at 269°E, 279°E, 289°E, 299°E and 309°E. The longitude of the ascending node of 289°E corresponds to the longitude of Boston.

The elevation angle as observed from Boston for a satellite in a circular polar orbit at an altitude of 1000 km is shown in Figure 7. Although the satellite crossed the equator at the same longitude of Boston, the maximum elevation angle is on the order of only 73°, mainly because of the earth's rotation.

Figure 8 is a plot of the elevation angle, as observed from Boston and Los Angeles, for a satellite at geosynchronous altitude. For Boston, the elevation angle of the satellite varies between approximately 28° and 43°, while for Los Angeles, the angle varies between 36° and 51°. The difference in the elevation angles is attributed to the difference in the latitudes of two locations.

The Doppler frequency shift at a frequency of 100 MHz as observed from Boston for a satellite in a 1000-km altitude circular polar orbit and in an elliptical polar orbit are presented in Figures 9 and 10, respectively. The Doppler shift is a maximum for a satellite with a LAN of 289°E and a minimum with a LAN of 259°E. When neglecting the effects of the propagation media, the maximum Doppler shift is on the order of 2118 Hz for the circular orbit, as compared to about 2520 Hz for the elliptical orbit.

It is seen that the Doppler shift is positive for a satellite approaching Boston and negative as it recedes from Boston. Zero Doppler occurs at the point of closest approach. For a satellite in a circular polar orbit at 500-km altitude, the maximum Doppler shift at 100-MHz frequency evaluates to 2354 Hz as compared to 2118 Hz for a satellite at an altitude of 1000 km. It is noted that at 100 MHz, the maximum Doppler frequency shift of transmissions from the satellite in the geosynchronous orbit is about 17 Hz.

3.2 TROPOSPHERIC EFFECTS

According to Equations (16), (17) and (18), the Doppler frequency error is a function of ΔE, the ground elevation angle error induced by the refraction phenomenon. The parameter, ΔE, for an altitude of 1000 km is presented in Figure 11 as a function of surface refractivity and elevation angle. It is evident that the angular bending error increases with increasing surface refractivity and with decreasing elevation angle.

It is noted that the elevation angle error is also a function of altitude. At 1° elevation angle and a surface refractivity of 320 N-units, ΔE evaluates to 8.06, 8.22 and 8.53 mrad at 500 km, 1000 km and geosynchronous altitude, respectively. The effect of altitude on the magnitude of ΔE diminishes as the elevation angle increases. For example, at 15° elevation angle, the value of ΔE at the three altitudes approaches 1.15, 1.16, and 1.17 mrad, respectively.

Figure 12 depicts the tropospheric Doppler error at 100 MHz for the 1000-km circular polar orbit. The Doppler error is about 0.50 Hz for a surface refractivity of 320 N-units and increases to about 0.67 Hz for a surface refractivity of 400 N-units. At 10 GHz, the Doppler error would increase to 50 and 67 Hz, respectively.

The interesting feature to note in Figure 12 is that the Doppler error is a maximum at the two extremes of the orbital pass. According to Figure 7, this corresponds to the lowest elevation angle. An examination of Figures 7 and 12 also reveals that, as the elevation angle increases, the Doppler error decreases, and that the error is less than 0.1 Hz for elevation angles greater than about 25°.

The effect of satellite altitude on the Doppler error is demonstrated in Figure 13. It is clearly evident that, for a given elevation angle, the error varies inversely with altitude. The disclosure that the altitude - Doppler error inverse relationship also applies to the elliptical orbit is unexpected. It was anticipated that the Doppler error would follow in the same manner as the data in Figures 9 and 10. That is, a satellite in an extreme elliptical orbit imparts a greater Doppler frequency shift than one in an 1000-km altitude circular orbit.

With regard to the geosynchronous orbit, the maximum Doppler error at 100 MHz is approximately 1.2×10^{-4} Hz for a surface refractivity of 320 N-units.

3.3 IONOSPHERIC EFFECTS

The ionospheric refraction angle error, used in this analysis, is shown in Figure 14. The calculations are based on a frequency 100 MHz and a vertical electron content of 10^{18} electrons/m^2. An interesting feature of this plot is that, at a constant altitude of 1000 km, the error increases with elevation angle, attaining a maximum value of 8.3 mrad at about 5°. In the case of the troposphere, however, the elevation angle error monotonically decreases with elevation angle as indicated in Figure 11.

Figure 15 is a plot of the Doppler error at 100 MHz that occurs when ionospheric refraction effects are taken into account. The calculations apply to a satellite in a circular polar orbit at 1000-km altitude. It is of interest to note that the error varies cyclically as the satellite traverses its orbital pass. This is in contrast to Figures 12 and 13 which depict the Doppler errors induced by the troposphere.

As shown in Figure 15, for a LAN of 289°E, the Doppler error maximizes at a relative time of approximately 280 and 740 sec which, according to Figure 7, correspond to an elevation angle of about 25°. It is evident that the elevation angle at which the maximum Doppler error occurs is dependent on the LAN of the orbital pass. It can be readily deduced that, for an LAN of 259°E and 319°E, the elevation angles of the maximum Doppler error are about 5° and 9°, respectively.

The ionospheric Doppler frequency errors for a satellite in an elliptical polar orbit, illustrated in Figure 16, are less than those of a satellite in a circular polar orbit shown in Figure 15. These results are in agreement with the tropospheric data presented in Figure 13.

For the geosynchronous orbit, the maximum Doppler error at 100 MHz is on the order of 2×10^{-2} Hz, the calculations being based on an electron content of 10^{18} electrons/m^2.

The effect of a change in frequency and electron content on the Doppler error is illustrated in Figure 17. It is seen that, when the frequency is decreased to 50 MHz, the Doppler error increases by a value ranging between 1.5 and 2. The variation is a function of the elevation angle, the maximum taking place in the vicinity of the point of closest approach.

When the electron content is increased by an order of magnitude, there is an increase in the Doppler error by a factor of 5 to 10. The range of values is also attributed to the elevation angle dependency.

It is noted that, for a satellite in a circular polar orbit at an altitude of 1000 km, the maximum ionospheric Doppler error at 100 MHz is a factor of about 15 larger than that due in the troposphere. At a frequency of 1000 MHz, the ratio of the two contributions reduces to 0.15. The reduction is due to the fact that the tropospheric Doppler error is directly proportional to frequency, and that the ionospheric error is approximately inversely proportional to frequency.

The frequency shift resulting from a change in the vertical electron content along the satellite orbit, as described in Equation (37), is not considered in detail in this paper. However, it is estimated that, in the presence of a traveling ionospheric disturbance (TID) which is a large-scale electron-density perturbation in the F-region of the ionosphere, a Doppler shift perturbation of 0.14 Hz could occur at a frequency of 100 MHz (Millman, 1980). The calculations are based on an ambient electron content of 10^{18} electrons/m^2 and on a TID with a horizontal velocity of 200 m/sec, a dimension of 150 km and a modulation of 2% on the ambient electron content.

4. CONCLUSIONS

The refraction phenomenon in the troposphere and the ionosphere introduces an error in the Doppler frequency shift of satellite transmissions.

The Doppler error imposed by the troposphere is directly proportional to frequency while, in the case of the ionosphere, the error is approximately inversely proportional to the frequency and approximately directly proportional to the vertical electron content.

Under average tropospheric and ionospheric conditions, i.e., surface refractivity equal to 320 N-units and electron content equal to 10^{18} electrons/m^2, the tropospheric contribution to the Doppler error is predominant for frequencies on the order of 400 MHz and above. Below about 400 MHz, the ionospheric refraction effects are prevalent.

The Doppler effects can be compensated for, to some extent, when the angular bending and the space vehicle velocity are known. Estimates of the angular bending due to the troposphere can be made to a fair degree of accuracy, from measurements of the surface refractivity. For the ionosphere, the vertical electron content data can be used for the estimation of the refraction angle error.

5. REFERENCES

Bean, B.R. and E.J. Dutton, "Radio Meteorology," National Bureau of Standards Monograph 92, U.S. Government Printing Office, Washington, DC, 1966.

Davies, K., "Ionospheric Radio Propagation," National Bureau of Standards Monograph 80, U.S. Government Printing Office, Washington, DC, 1965.

Millman, G.H., "Atmospheric Effects on VHF and UHF Propagation," Proceedings IRE, Vol. 46, pp 1492-1501, August 1958.

Millman, G.H., "Ionospheric Electron Content Effects on Earth-Space Radio Propagation - A Review," General Electric Technical Information Series Report No. R80EMH11, December 1980.

Millman, G.H. and G.M. Reinsmith, "An Analysis of the Incoherent Scatter - Faraday Rotation Technique for Ionospheric Propagation Error Correction," General Electric Technical Information Series Report No. R74EMH2, February 1974.

Smith, E.K. and S. Weintraub, "The Constants in the Equation for Atmospheric Refractive Index at Radio Frequencies," Proceedings IRE, Vol. 41, pp 1035-1037, August 1953.

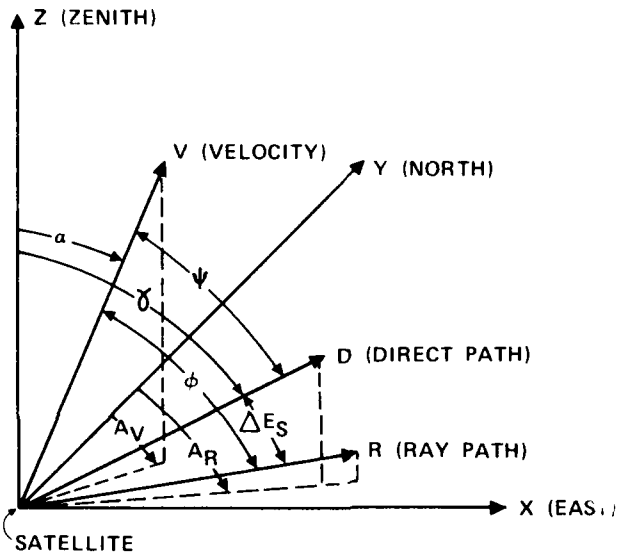

Figure 1. Satellite Velocity Geometry

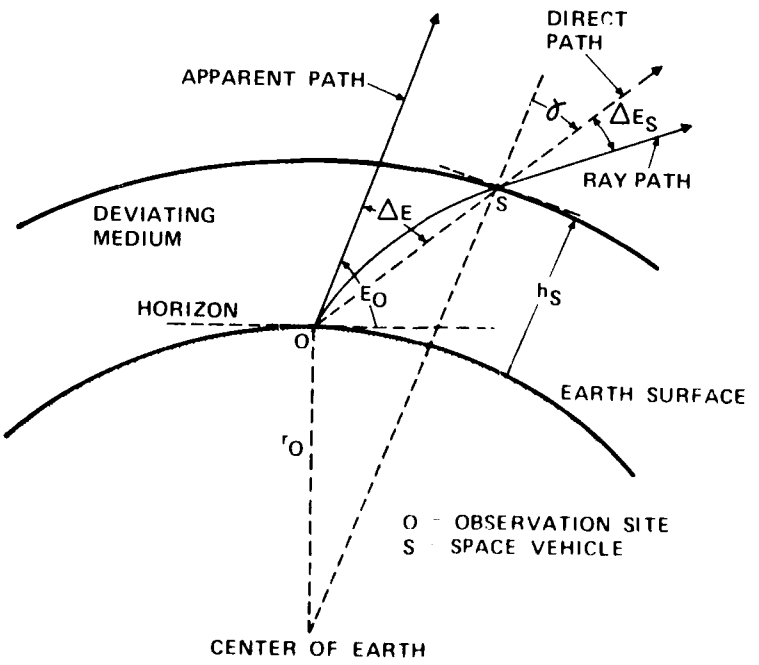

Figure 2. Deviation of Ray Path at Space Vehicle Position

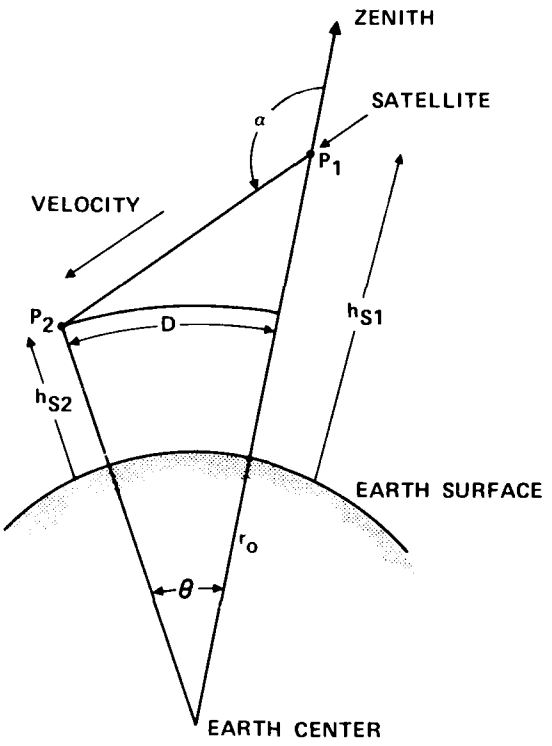

Figure 3. Orientation of Satellite Velocity Vector with Respect to the Zenith

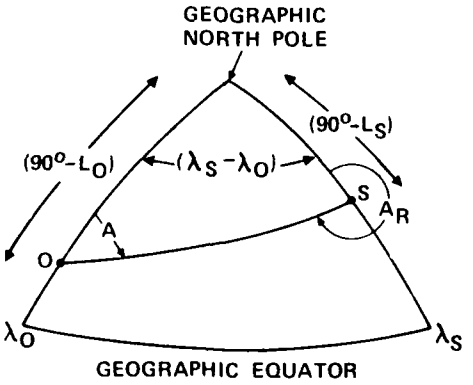

O = OBSERVATION SITE
L_O = OBSERVATION SITE LATITUDE
λ_O = OBSERVATION SITE LONGITUDE
S = SATELLITE
L_S = SATELLITE LATITUDE
λ_S = SATELLITE LONGITUDE

Figure 4. Satellite and Observation Site Geometry

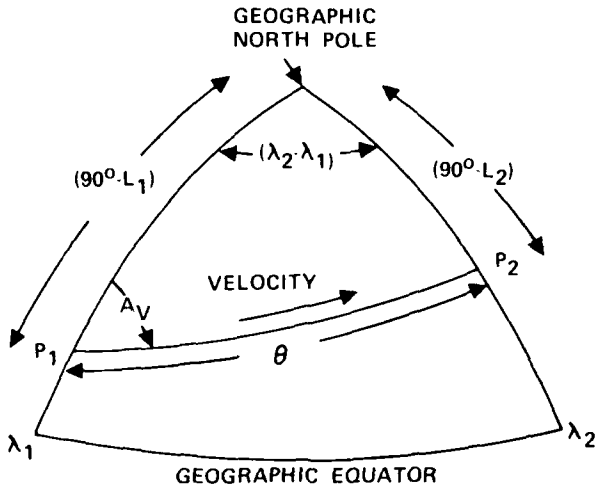

P_1 = SATELLITE LOCATION AT TIME t_1 P_2 = SATELLITE LOCATION AT TIME t_2

L_1 = P_1 LATITUDE L_2 = P_2 LATITUDE

λ_1 = P_1 LONGITUDE λ_2 = P_2 LONGITUDE

Figure 5. Bearing of the Satellite Orbital Velocity Vector

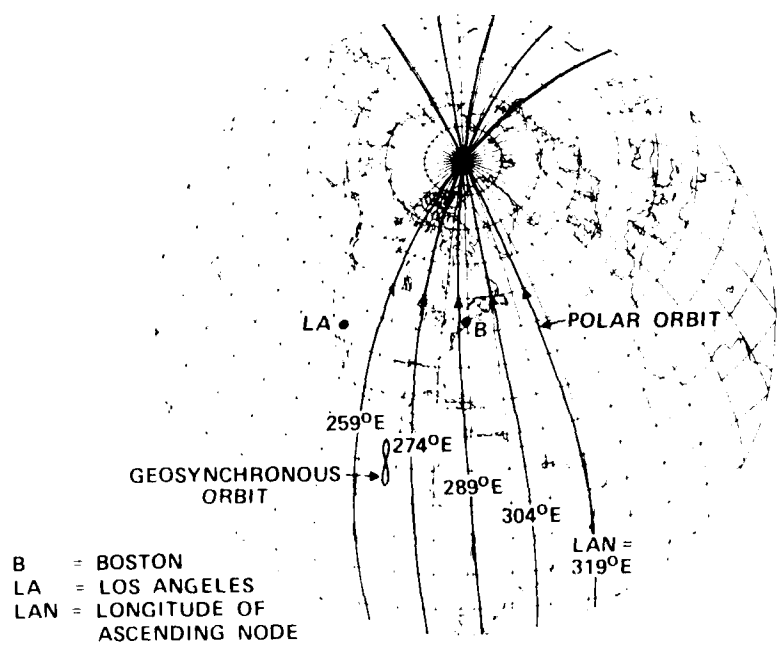

Figure 6. Ground Tracks of a Satellite at Geosynchronous Altitude and in a Circular Polar Orbit at an Altitude of 1000 km

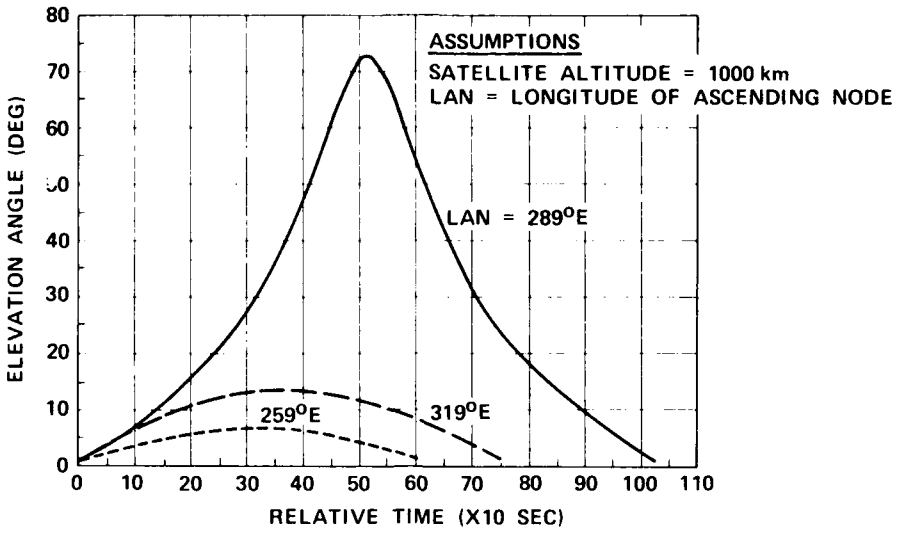

Figure 7. Elevation Angle as Observed from Boston for a Satellite in a Circular Polar Orbit

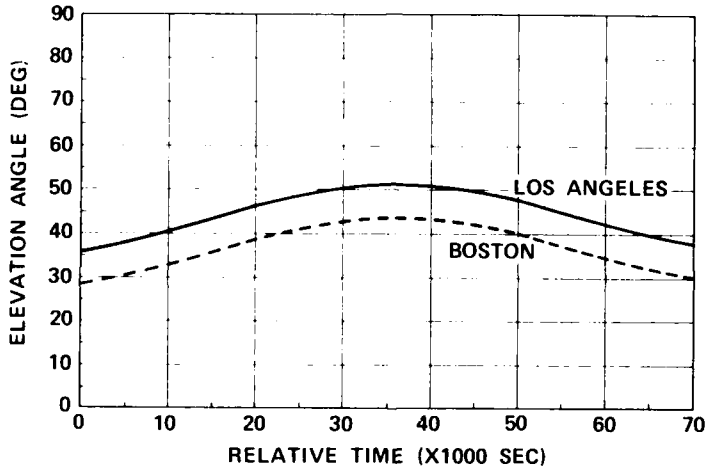

Figure 8. Elevation Angle as Observed from Boston and Los Angeles for a Satellite at Geosynchronous Altitude

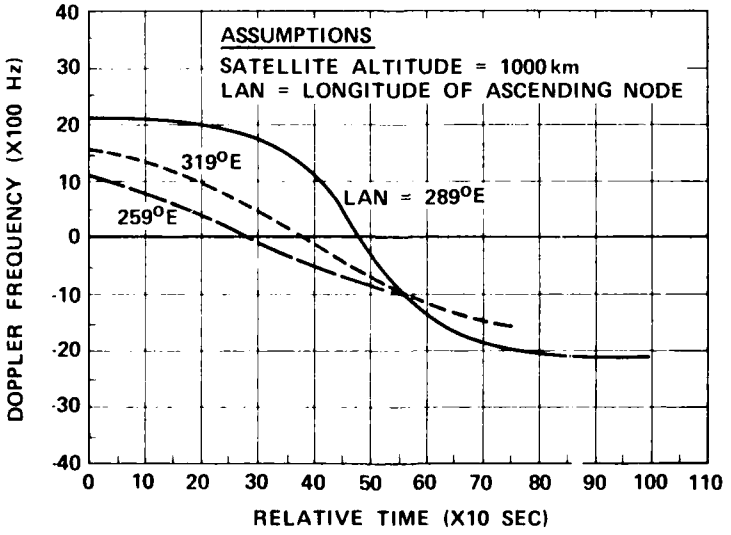

Figure 9. Doppler Frequency Shift at 100 MHz as Observed from Boston for a Satellite in a Circular Polar Orbit

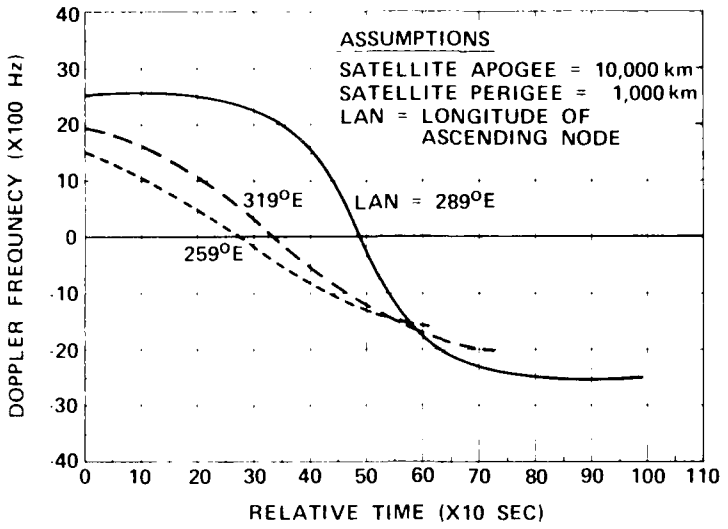

Figure 10. Doppler Frequency Shift at 100 MHz as Observed from Boston for a Satellite in an Elliptical Polar Orbit

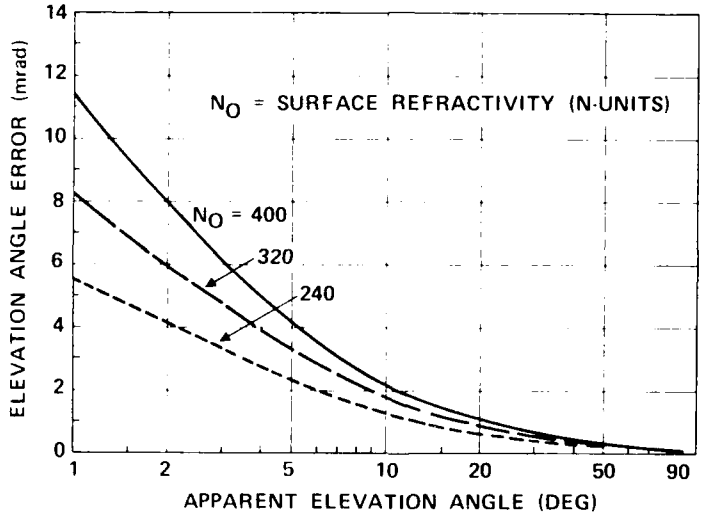

Figure 11. Tropospheric Elevation Angle Error at 1000-km Altitude Based on CRPL Reference Atmosphere - 1958

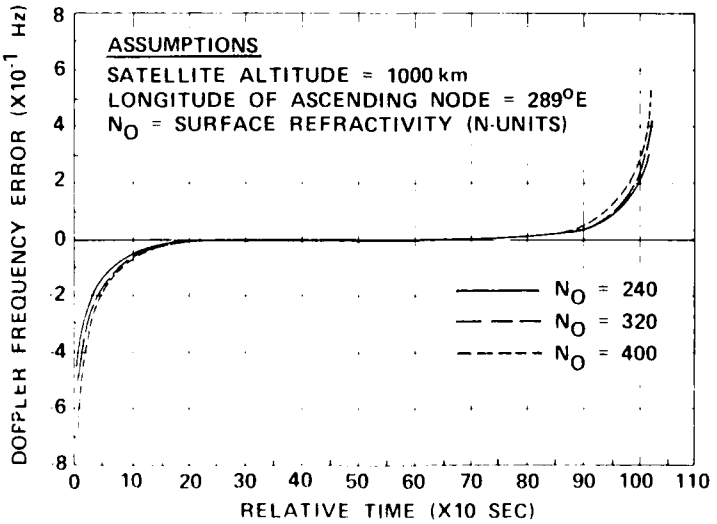

Figure 12. Tropospheric Doppler Frequency Error at 100 MHz as Observed from Boston for a Satellite in a Circular Polar Orbit

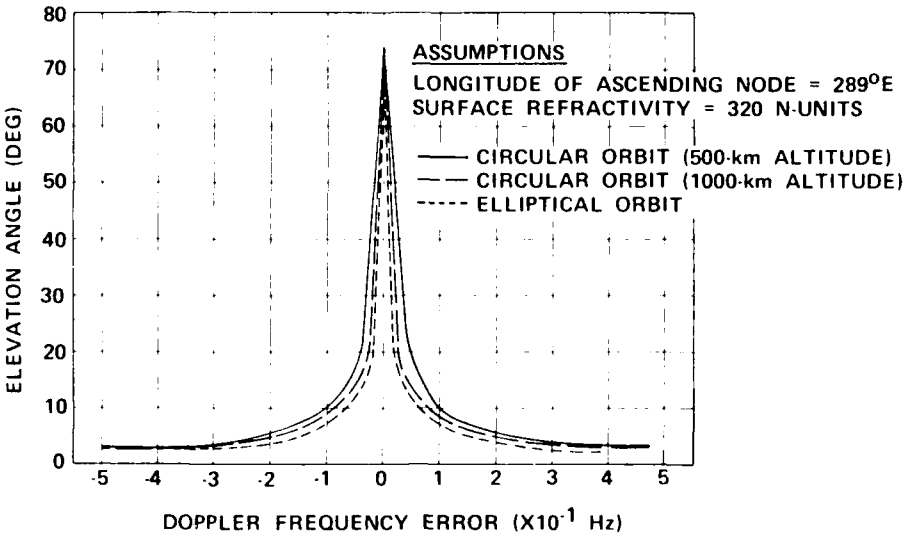

Figure 13. Tropospheric Doppler Frequency Error at 100 MHz as Observed from Boston for a Satellite in Circular and Elliptical Polar Orbits

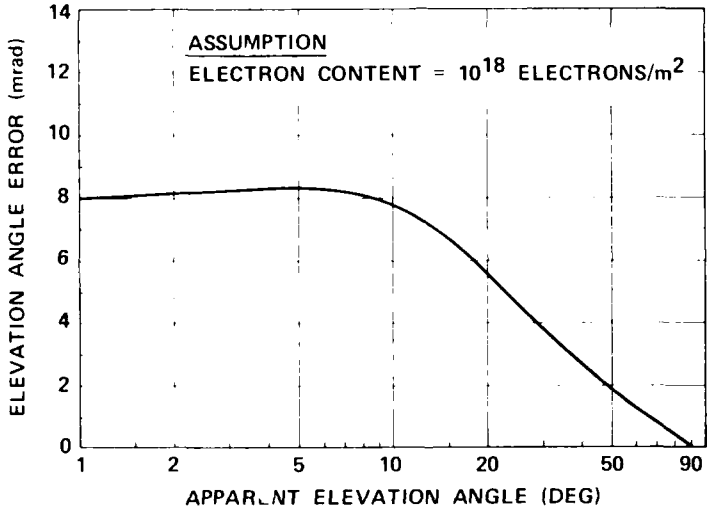

Figure 14. Ionospheric Elevation Angle Error at 1000-km Altitude, 100 MHz

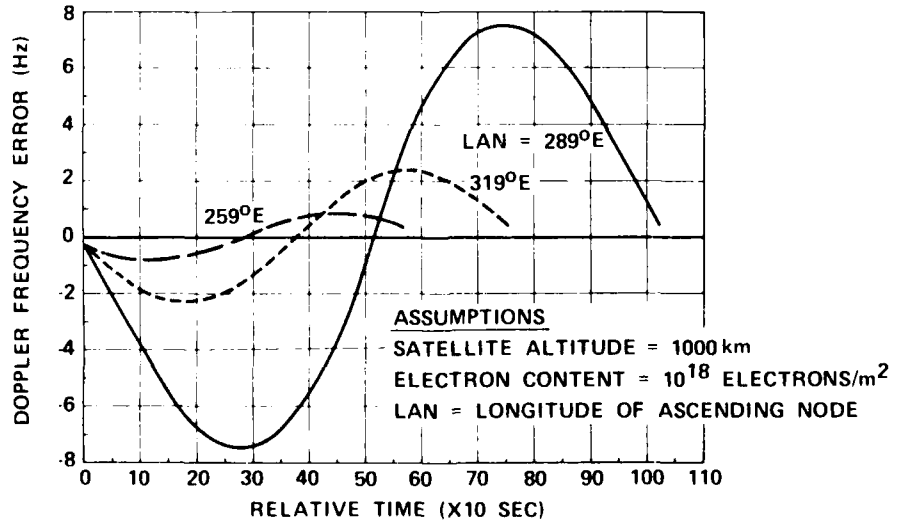

Figure 15. Ionospheric Doppler Frequency Error at 100 MHz as Observed from Boston for a Satellite in a Circular Polar Orbit

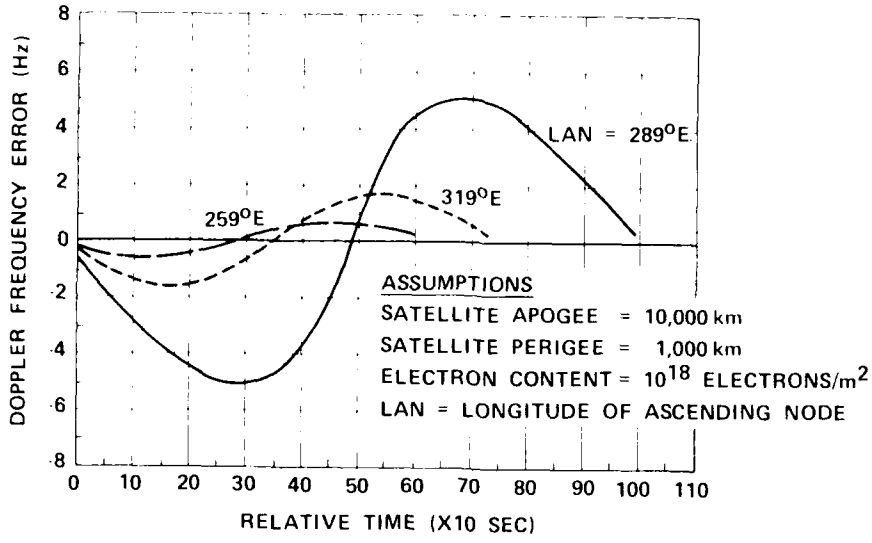

Figure 16. Ionospheric Doppler Frequency Error at 100 MHz as Observed from Boston for a Satellite in an Elliptical Polar Orbit

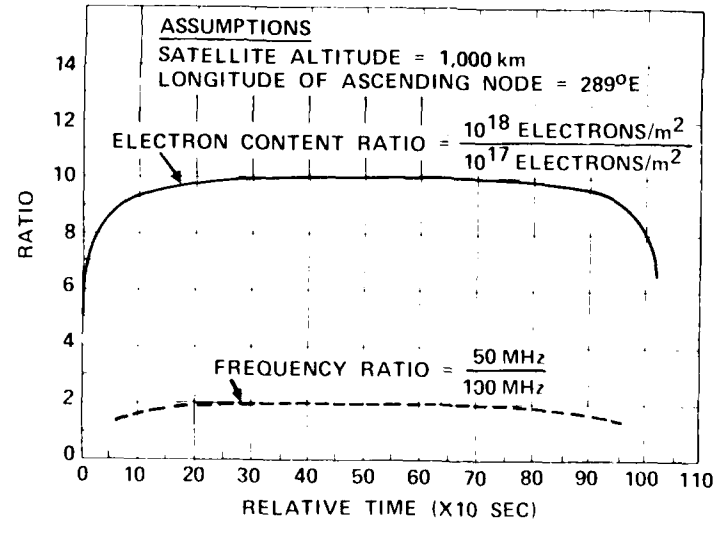

Figure 17. Ratio of Ionospheric Doppler Frequency Error as Observed from Boston for a Satellite in a Circular Polar Orbit

DISCUSSION

L.Bertel, Fr

Vous nous avez presente une Figure 14 montrant l'erreur sur l'angle d'élévation *en fonction* de l'angle apparent d'elevation et sur cette figure nous constatons qu'il y a un maximum à peu près pour 10°.

Comment pouvez-vous expliquer physiquement ce maximum et avez-vous une raison qui permet d'interpreter cette courbe?

Author's Reply

What we think is the horizon in the ionosphere is actually about 5° higher than we think it is. This is one of the factors which enters into maximizing errors at that particular elevation angle.

AD-A154 031 PROPAGATION INFLUENCES ON DIGITAL TRANSMISSION SYSTEMS: 2/6
PROBLEMS AND SOLU..(U) ADVISORY GROUP FOR AEROSPACE
RESEARCH AND DEVELOPMENT NEUILLY.. J H BLYTHE
UNCLASSIFIED 08 JUN 84 AGARD-CP-363 F/G 17/2 NL

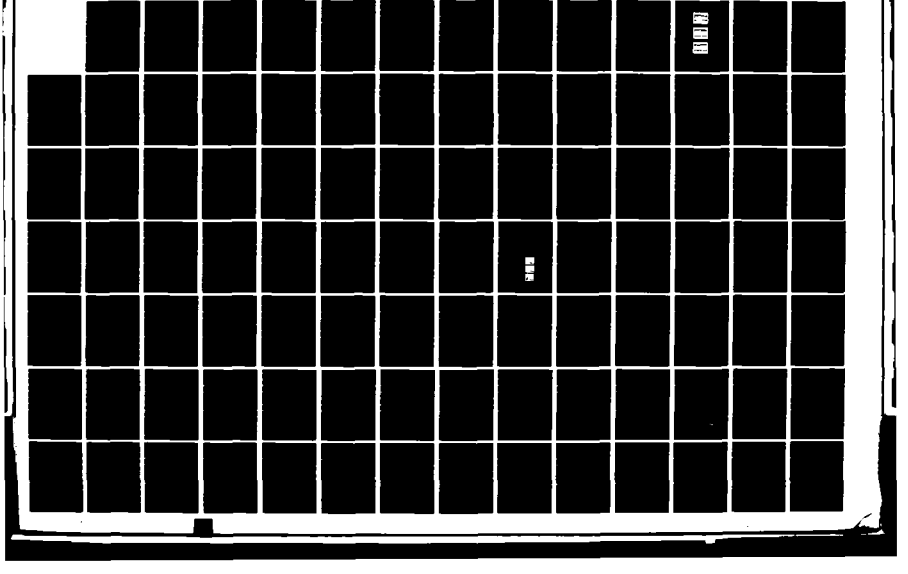

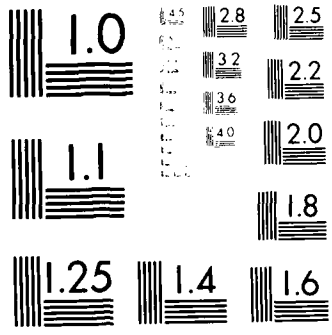

MICROCOPY RESOLUTION TEST CHART

NATIONAL BUREAU OF STANDARDS-1963-A

INFLUENCE DE LA PROPAGATION DANS LES FAISCEAUX HERTZIENS NUMERIQUES

J. BURSZTEJN
THOMSON-CSF
55, rue Greffulhe
92301, Levallois-Perret
France

INTRODUCTION

Dans cette communication, nous présentons les méthodes de détermination des paramètres qui permettent la prédiction de la qualité des liaisons hertziennes à diffusion troposphérique et à vue directe.

La première partie traite des faisceaux hertziens à diffusion troposphérique. A partir des expérimentations faites par THOMSON - CSF, on détermine la bande de cohérence, paramètre essentiel de la transmission numérique par diffusion troposphérique.

La seconde partie traite, dans les faisceaux hertziens à vue directe, des effets des troubles de la propagation tant du point de vue de la dépolarisation que des évanouissements sélectifs. On présente des résultats expérimentaux permettant de chiffrer la sensibilité des matériels et partant de prédire la qualité des liaisons.

LES LIAISONS PAR DIFFUSION TROPOSPHERIQUE

La figure n° 1 représente une liaison par diffusion troposphérique.

Elle est caractérisée par l'angle de diffusion θ, l'angle de site émission βe, l'angle de site réception βr, l'angle d'ouverture des antennes α et Re rayon radioélectrique de la terre (4/3 Ro), d est la distance entre antennes.

CALCUL DE LA VALEUR MEDIANE ANNUELLE DE L'AFFAIBLISSEMENT DE TRANSMISSION

Le rapport 238.2 du CCIR donne une formule permettant le calcul de cette valeur (NBS 1967)

$$L(50) = 30 \log f - 20 \log d + F(\theta d) - Gp - V(de) \quad dB$$

avec f = fréquence en megahertz

La distance angulaire θ (en radian) est l'angle formé par les rayons à l'horizon radioélectrique dans le plan du grand cercle qui contient les antennes et pour les conditions atmosphériques médianes.

d est la distance entre les antennes en km

Gp est le gain effectif total des antennes en propagation troposphérique

$$G_p = G_E + G_R - Lgp$$

V(de) est un facteur de correction qui, en fonction de la distance équivalente de, tient compte des divers types de climat.

Des abaques complémentaires permettent, à partir de la valeur mediane annuelle ainsi calculée, de déterminer l'affaiblissement de la transmission pour d'autres pourcentages du temps.

LARGEUR DE BANDE TRANSMISSIBLE

Les diverses hétérogénéités qui produisent la propagation par diffusion créent autant de trajets de propagation différents, variables en nombre et en temps de transmission.

Si l'émetteur transmet un signal de la forme :

$$a_o = A_o \sin(\omega_o t + \varphi_o)$$

le signal reçu sera alors de la forme :

$$a = A(t) \sin\left[\omega_o (t + T(t)) + \varphi_o\right]$$

A(t) représente un terme de modulation d'amplitude et ω_o T(t) un terme de modulation de phase.

Ce sont les variations rapides de ces deux termes qui déterminent la sélectivité du conduit par diffusion troposphérique et qui limitent la capacité de transmission numérique.

La sélectivité est déterminée par la bande de cohérence qui est, par définition, l'écart en fréquence de deux porteuses dont les amplitudes des champs ont un coefficient d'autocorrélation de 0,4.

EVALUATION EXPERIMENTALE DE LA SELECTIVITE D'UNE LIAISON PAR DIFFUSION TROPOSPHERIQUE

Le tableau de la figure n° 2 résume les expérimentations faites par THOMSON-CSF sur 15 liaisons à diffusion troposphérique.

Pour chacune des liaisons, numérotées de 1 à 15, on a indiqué la distance, la fréquence, l'angle de site et la baisse de gain d'antenne en diffusion troposphérique.

La bande de cohérence indiquée est la valeur médiane : valeur dépassée pendant plus de 50 % du temps.

D'autres expérimentations ont été faites sur une liaison dont les caractéristiques sont les suivantes :

- distance géographique : 134,3 km
- angle de site
  - émission : - 1,6 mrd
  - réception : - 0,5 mrd
- puissance émise : 1 kW
- fréquence : 6 375 MHz
- diamètre des antennes
  - émission : 3,6 m
  - réception : 3 m

A l'aide d'un appareil de mesures du type " Analyseur de faisceaux hertziens ", on a fait un enregistrement cinématographique de la modulation d'amplitude et de la distorsion du temps de propagation de groupe.

On a pu ainsi, en temps réel, visualiser la bande de cohérence.

La figure n° 3 représente quelques-unes des images les plus caractéristiques. Le décalage de 10 ms entre deux traces consécutives permet d'imaginer, sur ces images fixes, les vitesses de variation.

On notera que les variations rapides des évanouissements sélectifs peuvent atteindre des amplitudes de 35 dB en 150 ms et que la distorsion du temps de propagation de groupe est négative ou positive.

Ces remarques sont importantes pour la conception des modulateurs - démodulateurs auto-adaptatifs.

EVALUATION EMPIRIQUE DE LA BANDE DE COHERENCE

La compilation des résultats des expérimentations ont permis de dégager des formules empiriques donnant :

- la valeur médiane de la bande de cohérence $B_{50\ \%}$

- l'écart type b

$$B_{50\ \%} = \frac{9.87 \quad L_{gp}}{f\,\theta^{2}\ d^{1.65}}$$

$$b = \frac{B_{50\ \%}}{B_{84\ \%}} = \frac{1.883}{(\theta\, d)^{0,17}}$$

avec les conditions de validité suivante :

$$135 < d < 270 \text{ km}$$
$$0,9 < f < 7,6 \text{ GHz}$$
$$1,7 < \theta_d < 11$$
$$L_{gp} \geqslant 0,4\ f$$

Climat continental tempéré

Co indice $N_S \sim 320$

Altitude des terminaux < 200 m

Les formules proposées conduisent à des résultats s'écartant de moins de 1 dB des valeurs relevées.

PREDICTION DE LA BANDE DE COHERENCE DEPASSEE PENDANT X % DU TEMPS

On l'obtient en supposant une distribution log. normale

$$B_X = B_{50} \times 10^{G(x)}$$

ou encore

$$B_X = \frac{9,87 \; L\,gp}{f\theta^2 \; d^{1.65}} \times \left[\frac{(\theta d)^{0,17}}{1,883}\right]^{G(X)}$$

avec

X	1	10	50	90	99	99,9
G (X)	-2,326	-1,286	0	1,286	2,326	3,1

ou encore

$$B_X = B_{C\ MIN}\ (X\ \%) \times \left[L\,gp \times \frac{4,7}{f}\right]$$

La courbe de la figure n° 4 donne les variations de $B_{C\ MIN}$ (X %) en fonction de la distance et pour différentes valeurs de X.

La courbe de la figure n° 5 donne les variations du terme correctif correspondant à l'accroissement de la bande de cohérence dû à la baisse de gain d'antenne. On a pris en compte plusieurs valeurs du diamètre des antennes.

Exemple d'utilisation des courbes

Hypothèses :

une liaison de d = 200 km à f = 4,7 GHz
diamètre des antennes $\emptyset$ = 8 m
angles de site nuls

Déterminer la bande de cohérence dépassée à 99 % du temps B_{99} .

De la courbe n° 5, on trouve : $L\,gp \times \frac{4,7}{f} = 9,5$

De la courbe n° 4, on détermine : $B_{C\ MIN}$ (99 %) = 0,265 MHz

L'application de la formule précédente donne alors :

$$B_{99} = 9,5 \times 0,265 = 2,5 \text{ MHz}$$

D'autres présentations peuvent être faites. Elles consistent, par exemple, à déterminer la bande de cohérence en fonction de la fréquence.

La figure n° 6 prend comme hypothèse des antennes de $\emptyset$ = 5 m de diamètre, la distance étant prise comme paramètre.

La figure n° 7 faite pour une distance de 225 km prend le diamètre des antennes comme paramètre.

Ces courbes permettent de déterminer la fréquence pour laquelle la bande de cohérence est optimale.

Pour une liaison de 200 km, faite avec des antennes de Ø = 5 m, la bande de cohérence optimale est obtenue pour une fréquence de 5 GHz.

LES LIAISONS A VUE DIRECTE

L'efficacité spectrale est une contrainte essentielle des faisceaux hertziens à vue directe. Dans les systèmes à longue distance, le trafic à écouler nécessite des efficacités spectrales de l'ordre de 4 Bit/s / Hz. On est alors conduit à utiliser des modulations plurivalentes du type MAQ 16 ou même MAQ 64.

Les largeurs de la bande occupée et la complexité des modulations rend la transmission très sensible aux troubles de la propagation.

Trois types de troubles doivent être pris en compte :

- les évanouissements par trajets multiples entrainant un accroissement du bruit thermique,
- la diminution du découplage de la polarisation entrainant une augmentation du niveau des interférences,
- la sélectivité des évanouissements par trajets multiples entrainant une augmentation de l'interférence intersymbole.

C'est la connaissance des statistiques d'apparition de ces troubles, qui entraine le dimensionnement des éléments à mettre en œuvre pour atteindre la qualité requise par le CCIR Avis 594.

Pour le conduit numérique fictif de référence (2500 km)

	pendant plus de 1 % d'un mois quelconque	pendant plus de 0,05 % d'un mois quelconque
T.E.B. inférieur à	10^{-7}	10^{-3}

ACCROISSEMENT DU BRUIT THERMIQUE

La statistique des évanouissements par trajets multiples est donnée dans le rapport 338-3 du CCIR.

$$\text{Prob.}(m \geqslant mo) \times mo = k F^{\alpha} D^{\beta}$$

avec

m = profondeur de l'affaiblissement

F = fréquence de la porteuse radioélectrique, en GHz

D = longueur du bond radioélectrique en km

k = cœfficient dépendant de la climatologie et de la géographie
Pour le Nord-Ouest de l'Europe, $k = 1{,}4 \times 10^{-8}$

$\alpha \sim 1$

$\beta \sim 3$

En toute rigueur, il faut également prendre encompte les affaiblissements supplémentaires dûs aux hydrométéores, mais leur effet est négligeable pour les fréquences inférieures à 10 GHz.

LE DECOUPLAGE DE LA POLARISATION

On a constaté sur le découplage de polarisation à distance (X P D) des diminutions considérables par rapport à sa valeur en espace libre.

Plusieurs interprétations ont été fournies ; effet de la réfraction, effet du rayonnement diffus en provenance du sol ou, pour les fréquences élevées, influence de la géométrie des gouttes de pluie.

Une loi statistique a été dégagée permettant la prédiction de la valeur de XP

$$XPD = \alpha - \beta M \quad \text{dB}$$

M est l'affaiblissement de la propagation

α est fonction de la fréquence, de la longueur du bond et des antennes

β est voisin de l'unité.

La figure n° 8 montre la variation de α en fonction de la longueur du bond.

On distingue deux parties : une loi en D^6 pour les longueurs inférieures à 20 km, une loi en D^2 au delà.

SELECTIVITE DES EVANOUISSEMENTS

La figure n° 9 issue du CCIR Genève 1982 montre la dispersion du taux d'erreur sur les bits en fonction de la profondeur des évanouissements. Elle illustre l'effet des évanouissements sélectifs par comparaison avec l'affaiblissement non sélectif.

Pour la liaison considérée de longueur 42,5 km, au débit de 45 Mbit/s, en modulation MDP 8, le taux d'interruption à $\tau \geqslant 10^{-3}$ a été de 2.10^{-4} au lieu de 2.10^{-6} escompté pour une marge de 11 dB. Cette perte d'un facteur 100 sur la disponibilité est dûe à la sélectivité des évanouissements par trajets multiples. L'interprétation de ce résultat est que, pendant les périodes troublées, le signal reçu est la combinaison vectorielle de plusieurs rayons ayant suivi des chemins différents. Il en résulte que la principale cause de dégradation est l'interférence intersymbole.

MESURE DE LA SENSIBILITE DES MATERIELS AUX EVANOUISSEMENTS SELECTIFS

RUMMLER a proposé un modèle permettant de comparer entre eux les performances des faisceaux hertziens numeriques. Il consiste à effectuer en laboratoire la mesure de la signature.

La figure n° 10 montre le schéma de la manupulation. Entre l'émetteur et le récepteur, un jeu de coupleurs permet de simuler un modèle à deux rayons.

(signal N, signal R retardé de τ)

Le déphaseur φ o positionne la fréquence de l'évanouissement ; les atténuateurs règlent l'amplitude de la sélectivité.

On relève la courbe S (f), lieu des points où le taux d'erreur est égal à 10^{-3}.

La formule suivante donne une approximation de l'interruption relative due aux évanouissements sélectifs

$$Po, REL. = \int e^{-\frac{S(f)}{3,8}} df$$

La figure n° 11 montre les signatures relevées en laboratoire sur quatre matériels

	140 Mbit/s	Modulation MAQ 16
	140 Mbit/s	Modulation MDP 8
2 x	34 Mbit/s	Modulation MDP 8
	34 Mbit/s	Modulation MDP 4

Si l'on prend comme référence le temps de coupure du système 140 Mbit/s, Modulation MAQ 16 on trouve :

	140 Mbit/s	Modulation MDP 8	Po x $\frac{1}{1,35}$
2 x	34 Mbit/s	Modulation MDP 8	Po x $\frac{1}{5}$
	34 Mbit/s	Modulation MDP 4	Po x $\frac{1}{200}$

DISPOSITIFS MIS EN OEUVRE POUR ATTEINDRE LES OBJECTIFS DE QUALITE

Afin de diminuer les effets des évanouissements sélectifs, des dispositifs complémentaires sont associés aux faisceaux hertziens numériques à vue directe. Ils sont d'autant plus nécessaires que la capacité est élevée.

Ce sont :

- les correcteurs fréquentiels en fréquence intermédiaire,
- les égaliseurs temporels.

La figure n° 12 permet, à partir du relevé de la signature, de chiffrer le gain obtenu par l'emploi de ces dispositifs. Elle a été faite sur un équipement à 140 Mbit/s fonctionnant en MAQ 16.

La comparaison des deux releves permet de chiffrer le gain à environ 200.

En cas de besoin, l'emploi de la diversité d'espace fournit une amélioration supplémentaire.

CONCLUSION

La numérisation de l'information à transmettre a rendu les faisceaux hertziens, tant troposphériques que à vue directe, plus sensibles aux troubles de la propagation.

La connaissance des statistiques de ces troubles permettra de dimensionner les dispositifs à mettre en œuvre afin d'atteindre les qualités requises. On utilisera, suivant le besoin, la diversité d'espace ou de fréquence et des équipements auto-adaptatifs.

REFERENCES

- Avis et rapports du CCIR
  Genève 1982

- Evaluation expérimentale de la sélectivité d'une liaison par diffusion troposphérique
  COLLIN et MARGUINAUD
  Revue Technique THOMSON-CSF - Mars 1979

- Evaluation empirique de la bande de cohérence en diffusion troposphérique
  COLLIN
  Revue Technique THOMSON-CSF - Septembre 1979

- Digital radio outage due to selective fading - LUNDGREN et RUMMLER
  BSTT - Vol. 58, 5,1073 - 1100

- Transmission de signaux numériques à haut débit par faisceaux hertziens
  LEGENDRE
  Doc. THOMSON-CSF

- Selectivity predictions for troposcatter links
  COLLIN
  3rd Military Microwaves conference proceedings - M.M. 80

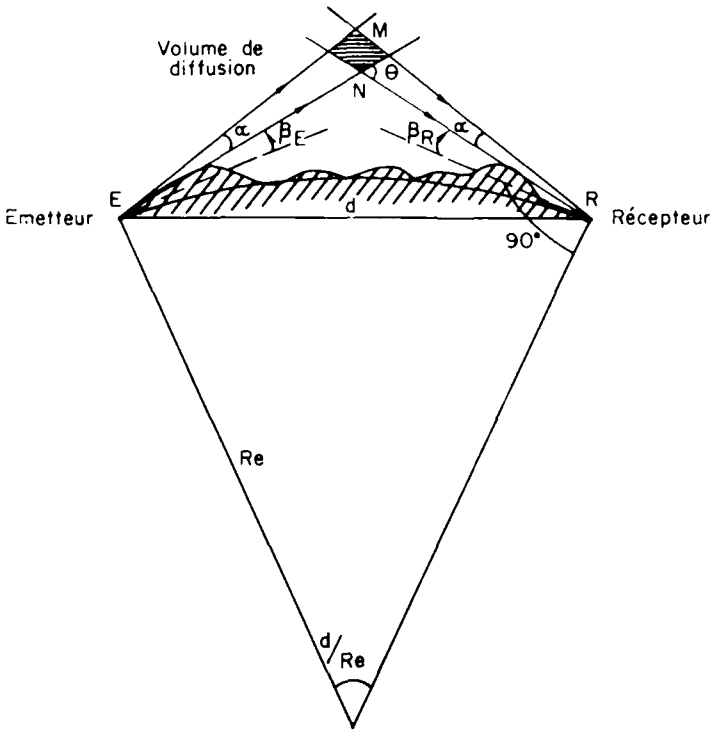

Fig. n° 1 — θ, angle de diffusion ; β_E, angle de site émission ; β_R, angle de site réception ; α, angle d'ouverture des antennes ; R_e, rayon radioélectrique de la terre (4/3 R_o)

$$\theta = \beta_E + \beta_R + \frac{d}{R_e}$$

LIAISON	DISTANCE (km)	FREQUENCE (GHz)	θ (mrd)	Lg p (dB)	BANDE DE COHERENCE MESUREE B50% (MHz)
1	134,3	6,4	13,2	3,4	9,9
2	140	4,6	13,9	1,8	3,1
3	140	7,6	13,9	3,5	3,3
4	199	4,6	38,2	7,4	1,8
5	199	7,6	38,2	11,1	2
6	192	4,6	22,2	3,3	2,4
7	192	7,6	22,2	6	2,6
8	163	4,6	16,7	2,1	3,4
9	163	7,6	16,7	4,4	3,7
10	138,4	4,8	41,7	5,2	1,93
11	138,4	4,8	41,7	6,9	2,55
12	271	4,7	39	16,8	2,05
13	271	0,9	36	2	1,59
14	271	0,9	36	1,9	1,42
15	271	4,7	36	15,8	2,27

Fig n° 2

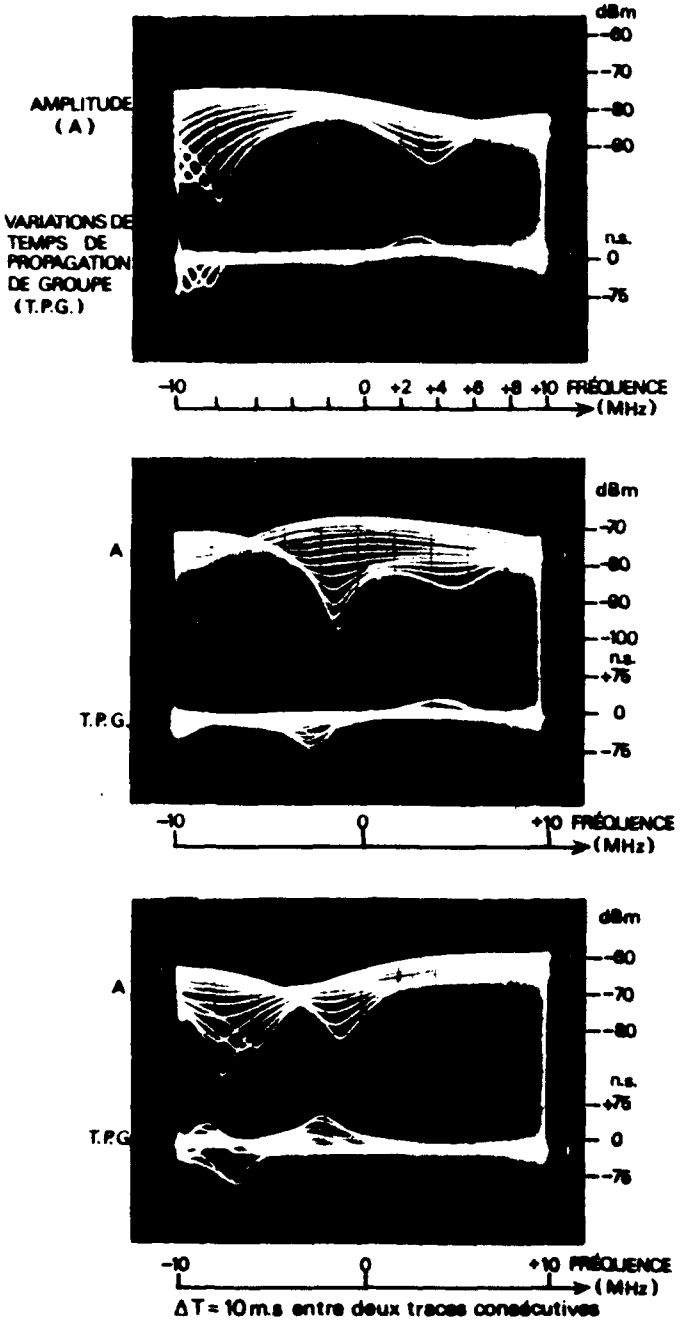
AMPLITUDE
(A)
VARIATIONS DE
TEMPS DE
PROPAGATION
DE GROUPE
(T.P.G.)
dBm
-60
-70
-80
-90
n.s.
0
-75
-10
0
+2
+4
+6
+8
+10
FRÉQUENCE
(MHz)
A
T.P.G.
dBm
-70
-80
-90
-100
n.s.
+75
0
-75
-10
0
+10
FRÉQUENCE
(MHz)
A
T.P.G.
dBm
-60
-70
-80
n.s.
+75
0
-75
-10
0
+10
FRÉQUENCE
(MHz)
ΔT = 10 m.s entre deux traces consécutives

Figure n°3

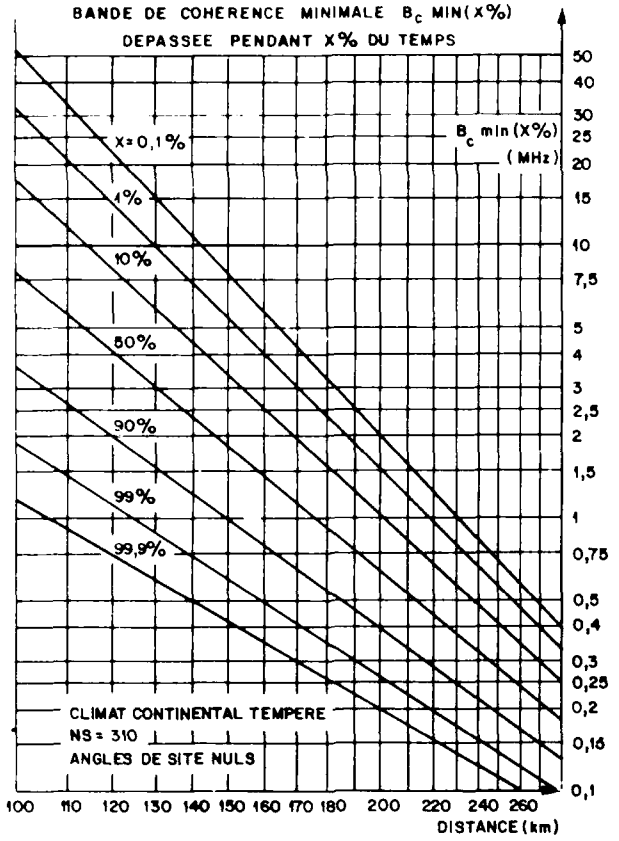
BANDE DE COHERENCE MINIMALE B_c MIN(X%)
DEPASSEE PENDANT X% DU TEMPS
X=0,1%
1%
10%
50%
90%
99%
99,9%
B_c min (X%)
(MHz)
50
40
30
25
20
15
10
7,5
5
4
3
2,5
2
1,5
1
0,75
0,5
0,4
0,3
0,25
0,2
0,16
0,1
CLIMAT CONTINENTAL TEMPERE
NS = 310
ANGLES DE SITE NULS
100 110 120 130 140 150 160 170 180 200 220 240 260
DISTANCE (km)

Fig. n°4

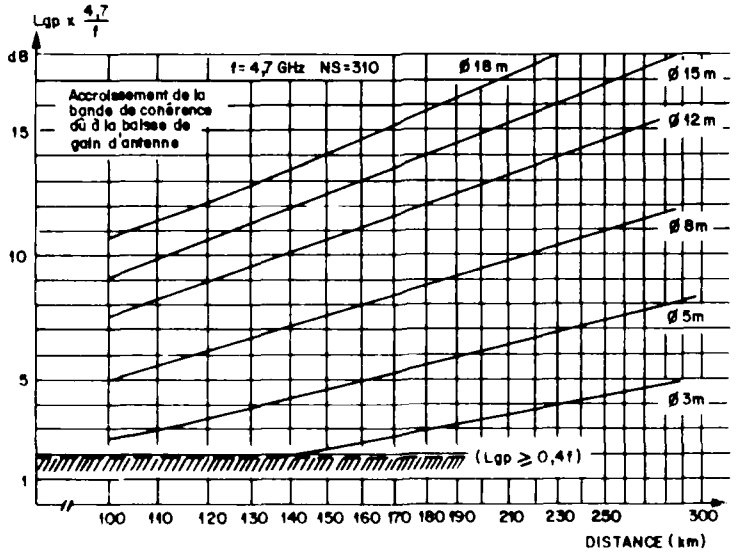
Lgp x 4,7/f
dB
f = 4,7 GHz NS=310
Ø 18 m
Ø 15 m
Ø 12 m
Ø 8m
Ø 5m
Ø 3m
Accroissement de la bande de cohérence dû à la baisse de gain d'antenne
(Lgp ≥ 0,4f)
15
10
5
1
100 110 120 130 140 150 160 170 180 190 210 230 250 300
DISTANCE (km)

Fig n°5

B DE COHER Ø = 5M

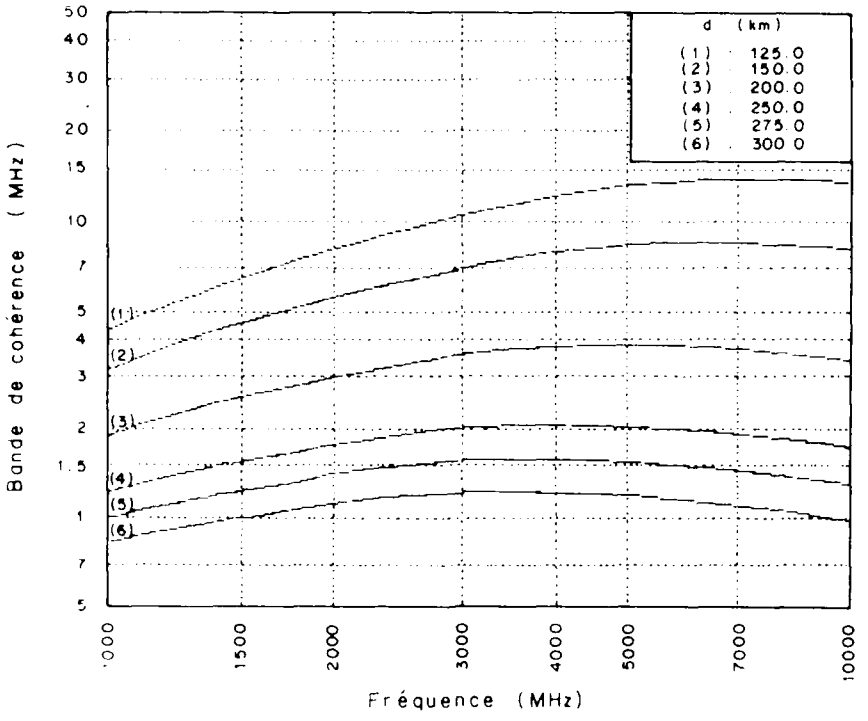

Fig. n°6

B DE COHER. 225 km

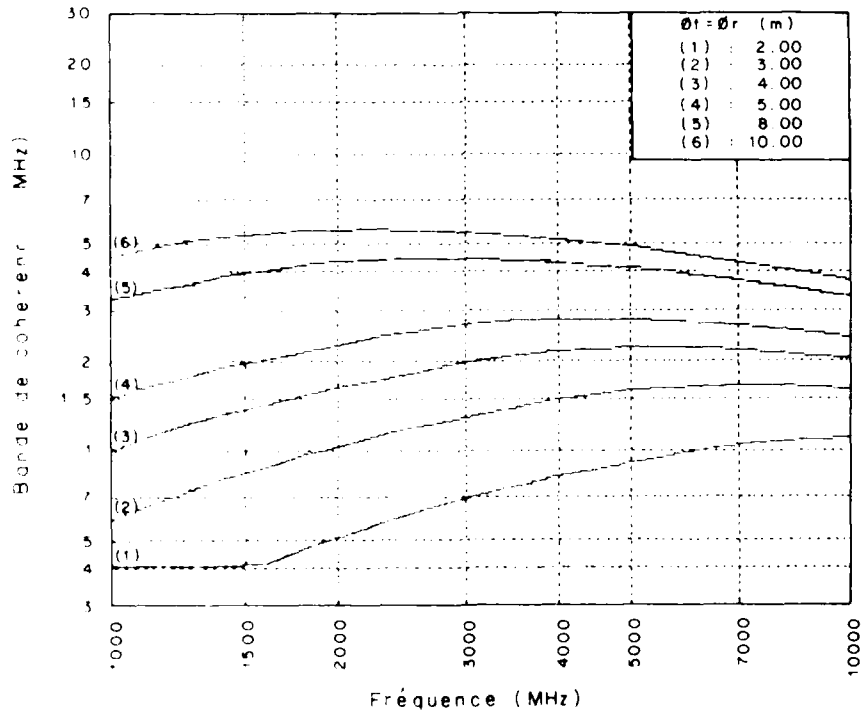

Fig. n° 7

... error detection and error detecting equipment

... of the pseudo random bit streams to be transmitted is achieved by ... self-synchronizing scramblers. A logical "0" is supplied at the input of ... In this way, errors generated on the radio link are easily detected at the receive side ... by self-synchronizing descramblers. The number of sections of these circuits is ... seven or ten.
... extension, inherent to this kind of scramblers, impairs the accuracy in the case of ... errors. This effect is combatted by the application of output feed back at the ... descrambler. This feedback is disabled if burst errors occur by means of a synchronization ... circuit. In this way the accuracy is mainly determined by the error measuring ... equipment.

... bit error ratio and attenuation measurement equipment

... parameters are measured on a short term basis: the bit error ratio is determined by ... the time necessary for the occurrence of 12 errors (50% accuracy with 90% ... assuming a Poisson distribution), this time varies from 8.6 µs (high BER) up to ... 36 s. Meanwhile the attenuation is measured every 0.1 s (accuracy 0.5 dB). The ... measuring times are generally much smaller than the event durations. The last measurement ... value of the calibrated automatic gain control (AGC) voltage. All measurement values ... are collected. In fact this way of proceeding makes it possible to determine a number of ... points of the cumulative distribution function in an efficient way. Table 2 presents the ... parameters of the measuring system described above.

TABLE 2: Key parameters measuring system

type of measurement	BER	AGC
measuring range	$2.3\ 10^{-9} - 10^{-2}$ (66 dB)	0-32 dB
number of classes	11 + 2	8 + 1
class size increment	6 dB	4 dB
integration time	36 s - 8.6 µs	0.1 s

... during rainy conditions

... the nominal value of the carrier to noise ratio C/N_{th} will be ... attenuation values which is assumed to be constant across the receiver ... that the attenuation statistic and the flat fade characteristic ... the bit error ratio statistics.
... the nominal value of the carrier to noise ratio is reduced by ... attenuation and cross-polarization.

...

... is derived from measurements on ... show a 16 dB/decade slope for the ... performance. For a given ... attenuation in horizontal and vertical ... location (1.5), A_0 is in the range ...

... rain attenuation statistics, ... statistics presented in figure 2. The ... an offset of about 1 dB - the ... highest values of attenuation for

[illegible] attenuation [Blevis, 1965]. Analysis of the chart recordings of the observed [illegible] indicate the regular occurrence of such effects, often at the end of a rain [illegible] a typical attenuation of about 3 dB is observed, which subsequently decreases with a [illegible] of about 15 minutes. Such phenomena have been reported also elsewhere [illegible].

The average value of the antenna cross-polarization discrimination ratio across the [illegible] bandwidth has been derived from spot measurements. The resulting values are in [illegible] 1. The antennas with the best cross-polarization characteristics have been installed [illegible] lowest link (PS5). The overall value of the cross-polarization discrimination ratio [illegible] the link during nominal conditions to be used in equation (3.11), is estimated from [illegible] values of XPI of the transmitting and receiving antennas assuming power addition of [illegible] corresponding cross-polarization components.

[illegible] characteristics of cochannel interference

[illegible] the power I of the cross-polarization signal is related to an equivalent [illegible] noise power N_I, yielding the same bit error ratio as the power I. The relation [illegible] to equation (2.11) can be modified to:

$$\frac{C}{N_I} = \frac{C}{I} - 10 \log K \quad \text{dB}$$

where C/I is the carrier to interference ratio.

[illegible] have been carried out to determine the value of K over the BER range of [illegible], using two modems similar to those installed in the 18 GHz links. As the relation [illegible] between the C/I and the carrier to thermal noise power ratio is known, the value of K can [illegible] as a function of the BER with C/I as a parameter. The results of these [illegible] are in figure 10 and show values of K less than 1. A value of K [illegible] is considered to be appropriate for the analysis further on.

[illegible] multipath

[illegible] during multipath events the assumption of flat fade conditions is not [illegible] frequency selective fading may cause a severe degradation of the performance of high [illegible] digital radio systems. However, this degradation is expected to be less [illegible] over links of relatively short path length due to the limited values of the [illegible] time delay for the time percentages of actual interest. In section 5 the [illegible] results will show that distortion effects due to multipath can be [illegible] for the [illegible] links [illegible].

[illegible] OF SYSTEM CHARACTERISTICS

[illegible] characteristics of the 18 GHz 2 x 140 Mbit/s radio system are [illegible] during the "free of rain" period 1984-1985. These measured characteristics [illegible] will be used to validate the transmission model of section 3.

[illegible] parameters

[illegible] of the [illegible] equipment is important to [illegible] the accuracy of the measured [illegible] interpreted by the measurement principles involved. The equipment [illegible] consists of the following items:

- [illegible],
- [illegible],
- [illegible],
- [illegible],
- [illegible].

[illegible] the first two items together as well as the [illegible].

and XPI_o = 42 dB, the average residual XPD as observed during non-faded conditions. The measured 90° curve is very close to the curve predicted by equation (3.11).

4. RADIO EQUIPMENT PARAMETERS

For the prediction of the overall system characteristics using the transmission model introduced in section 2, the values of the relevant equipment parameters are required. In this section the parameters of the 18 GHz equipment are presented, which has been used for the communication experiments.
The 280 Mbit/s signal to be transmitted on each radio channel is formatted by two independent 140 Mbit/s streams. These two streams are supplied to the 4 PSK modulator via differential encoding equipment. Such 280 Mbit/s signal is transmitted for both polarizations. At the receiving side the horizontally polarized signal is demodulated and one of the two 140 Mbit/s streams is analyzed by measuring equipment. The vertically polarized signal serves as a cochannel interferer and may cause an additional degradation of the performance of the horizontally polarized channel, when the value of the XPI is reduced due to rain or multipath.
The attenuation of the horizontally and vertically polarized signals is derived from the calibrated automatic gain control voltage (AGC) of the receiver. So the attenuation values obtained correspond to the average value of the attenuation within the receiver bandwidth.

4.1 Flat fade characteristics

According to equation (2.8) an important parameter to be known is the carrier to thermal noise power ratio (C_o/N_{th}) during nominal conditions. The measured values of this parameter are in TABLE 1 for the paths of interest in this paper. The values are for the horizontally polarized channels, but for the vertically polarized channels differences less than 0.5 dB have been experienced.

TABLE 1: Radio equipment characteristics

		path 2	path 3
path length	(km)	8.5	13.5
centre frequency	(GHz)	18.470	18.930
transmitter power	(dBm)	22.5	22.5
nominal receiver power C_o	(dBm)	-37.0	-41.2
thermal noise power N_{th}	(dBm)	-83.0	-83.5
(C_o/N_{th})	dB	46	42.3
antenna XPD	dB	35	38

The relation between the bit error ratio (BER) and the carrier to thermal noise power ratio is determined by laboratory experiments. However, for practical applications it is more useful to perform such measurements in the links after installation. This is done by the insertion of an RF attenuator at the receiving side during nominal conditions. In this way the relation between the value of the inserted attenuation and the value of the BER is found. The results of these measurements appear as curve a) in figures 14 and 17. This curve will be called the flat fade characteristic and refers to flat fade conditions without cochannel interference. In fact, the value of the attenuation corresponds to the reduction of the carrier to thermal noise power ratio (C_o/N_{th}) to yield a defined value of the bit error ratio.

4.2 Antenna characteristics

The antennas installed have a diameter of 1.2 m and are of the Cassegrain type. The aperture of these antennas is covered with a radome to provide protection against weather effects. However, at the frequencies used water on the radome may be expected to produce

3.3.1 Attenuation due to multipath

In the past a large amount of propagation data relative to attenuation due to multipath has been collected in a large number of countries. However, the prediction of attenuation due to multipath is not well developed. CCIR recommends the following equation to be used (CCIR, 1982, Report 338) as the prediction for the fraction of time $p(A_M)$ during the worst month that a defined value of attenuation A_M is exceeded:

$$p(A_M) = 1.4 \cdot 10^{-8} \cdot f \cdot d^{3.5} \cdot 10^{-A_M/10} \qquad (3.9)$$

where the frequency f in GHz and the path length d in km. In figure 6 the measured curve, as observed during a one year period in the 19 GHz microwave link, is compared with the predicted curve according to equation (3.9). The correspondence between the two curves is surprisingly close.

Observations made in the 19 GHz microwave link show that on an instantaneous basis quite large differences can occur between the attenuation for horizontal and vertical polarizations. This can be seen from figure 7 which gives the 90, 50 and 10 percentile points of the differential attenuation $\Delta A_M = A_M^H - A_M^V$ as a function of the attenuation A_M^H.

3.3.2 Dispersion due to multipath

During multipath conditions the transfer function of the propagation medium is dependent on the frequency. This frequency dependence of the amplitude and group delay with the RF bandwidth of wideband digital systems may cause the additional degradation of the performance due to distorsion.
In general, the transfer function during multipath conditions relates to the relative amplitude and time delay of the interfering electromagnetic waves. For the maximum time delay τ_m, the following expression provides an estimation [C. Jakes, ICC, 1978]:

$$\tau_m = 1.1 \cdot 10^{-4} \cdot d^3 \quad \text{ns} \qquad (3.10)$$

where d is the path length in km. For path lengths less than about 15 km the maximum time delay according to equation (3.10) will be less than about 0.5 ns.
Several models and expressions to describe the multipath transfer function have been proposed (CCIR, 1983, Report 338). However, no expression is available, which relates the characteristics of the multipath transfer function to local radiometeorological data or the climatology.

3.3.3 Cross-polarization due to multipath

The isolation condition according to equation (2.6) is verified, using measured data obtained in the 19 GHz propagation experiment. The results are in figure 8, where the 90, 50 and 10 percentile points of the conditional distribution of $A_M^V + XPI_M^V$ are given as a function of $A_M^H + XPI_M^H$. The measured 50% curve is very close to the curve corresponding to $XPD_M = XPI_M$. Hence we find that the majority of datapoints lies around 42 dB. This means that the result $XPD_M = XPI_M$ may be applied, if the received co-polar power during multipath activity is the same for both polarizations ($C_o^H = C_o^V$).

For prediction purposes it is common to express XPD_M or XPI_M as a function of the attenuation A_M. The following expression is reported by CCIR (CCIR, 1982, Report 338):

$$XPD_M = XPD_o + Q - A_M \quad \text{dB} \qquad (3.11)$$

where XPD_o is the residual XPD during non-faded conditions and Q relates - not clearly defined - to the slope of the cross-polarized antenna pattern. In figure 9 the measured data are presented as obtained during propagation measurements in the 19 GHz microwave link. The measured curve is compared with the curve according to equation (3.11) with Q = 0

The effective reduction coefficient r_{eff} relates to the reduction coefficient r_{av} as defined by equation (3.1), but is also a function of the exponent α in equation (3.4). For values of α nearly equal to 1, as appropriate for the frequency band concerned, r_{eff} is approximated very well by r_{av} [Mawira, AIAA, 1984].

The anisotropy of the rainy propagation medium results in a differential attenuation ΔA_R between horizontal and vertical polarization. In figure 3 the measured values of ΔA_R are presented as observed during 25 major rain events in the 19 GHz microwave link. This figure gives the 90, 50 and 10 percentile points of the conditional cumulative distribution of ΔA_R as a function of A_R^H [De Haas, IEE, 1983]. The relation between ΔA_R and A_R^H as derived from the CCIR formula for polarization scaling [CCIR, 1982, Report 338]:

$$A_R^V = \frac{300.A_R^H}{335 + A_R^H} \quad dB \tag{3.5}$$

is drawn in figure 3 and is very close to the measured 50% curve.

3.1.3 Cross-polarization due to rain

The symmetry condition according to equation (2.6) is verified, using measured data obtained in the 19 GHz propagation experiment. The results are presented in figure 4, where the 90, 50 and 10 percentile points of the conditional distribution of $A_R^V + XPI_R^V$ are given as a function of $A_R^H + XPI_R^H$. The measured 50% curve is very close to the curve corresponding to equation (2.6). This means that the equality $XPD_R = XPI_R$ may be applied, if the received copolar power during nominal conditions is the same for both polarizations:

$$C_o^H = C_o^V \quad dBW \tag{3.6}$$

For prediction purposes it is common to express XPD_R or XPI_R as a function of the attenuation A_R. The following expression has been reported [Olsen et., 1978, A&P Japan] at frequency f (GHz):

$$XPD_R = 0.0053\sigma_\theta^2 - 20 \log|\sin(2\theta_e)| + 30 \log f - 23 \log (A_R) \quad dB \tag{3.7}$$

where σ_θ is the spreading and θ_e the effective value of the canting angle of the raindrops on the path. CCIR recommends the use of a simplification of equation (3.7):

$$XPD_R = U_o + 30 \log f - 20 \log (A_R) \quad dB \tag{3.8}$$

where an average value of U_o of about 15 dB is proposed, with a lower bound of 9 dB [CCIR, 1994, Report 338]. In figure 5 the measured data are presented as obtained during propagation measurements in the 19 GHz microwave link. The measured equiprobable curve is compared with the CCIR curve according to equation (3.8) and the curve derived from equation (3.7) using $\sigma_\theta = 20°$ and $\theta_e = 3°$ (see section 3.1.1). Figure 5 shows that equation (3.7) forms a somewhat better fit to the measured data, bearing in mind that the results of the measurements are of limited accuracy for attenuations exceeding about 0.05%.

3.2 Effects due to multipath

In general, propagation models for the prediction of attenuation and cross-polarization due to multipath are not based on detailed radiometeorological data, which relate to the local characteristics of the propagation medium and the terrain. However, the application of high capacity digital microwave links requires the precise knowledge about the joint statistics of the relative amplitude and time delay of the interfering waves, which relate to the local radiometeorological conditions. Although some information is available and new research programmes are underway as in the Netherlands, one may not expect that sufficiently detailed information is available within a few years.

limited period of registration at Nederhorst den Berg. However, the measured data show a tendency that slightly lower values of the point rainfall intensity may occur in the area around Leidschendam compared to those in the area around Nederhorst den Berg.

For application to the prediction of rain attenuation the horizontal structure of rain is basically described by the expression:

$$r_{av} = \frac{1}{R_o} \cdot \frac{\int_0^d R(s).ds}{d} \qquad (3.1)$$

which is the ratio of the rainfall intensity, averaged along a path of length d (km), to the point rainfall intensity R_o (mm/hr). Using measured data from the two raingauge networks at Leidschendam and Nederhorst den Berg, the following function is found to be suitable:

$$r_{av} = \frac{240}{R_o.d} \cdot \ln\left[1 + \frac{R_o.d}{240}\right] \qquad (3.2)$$

which is a very good approximation to the measured data [Mawira, AIAA, 1984].

Measurements in the Netherlands have shown some experimental evidence in support of the Laws and Parsons raindrop size distribution [Keizer et al, IEE, 1978]. Experiments by the Physics Laboratory TNO, using a distrometer at a location nearby Leidschendam, have indicated that the distribution above can be used for rainfall intensities, corresponding to time percentages of practical interest for the planning of most microwave links.

An important parameter for the prediction of cross-polarization due to rain is the distribution of the canting angle, defined as the angle by which the two orthogonal principal planes of the rainy propagation medium are rotated from the horizontal/vertical planes. Assuming a Gaussian distribution of the canting angle, the observed spreading of the differential attenuation on a 19 GHz microwave link [De Haas, IEE, 1983] indicates that the spreading of the canting angle is about 20 degrees. From the comparison between simultaneously measured cross-polarization for linear and circular polarization on a slant path to the OTS satellite, the conclusion has been drawn that the effective canting angle is about 8 degrees [Mawira, AIAA, 1984].

3.1.2 Attenuation due to rain

In general, the attenuation A_R due to rain on a horizontal path can be expressed by:

$$A_R = \int_0^d \gamma(s).ds \qquad dB \qquad (3.3)$$

where s : the distance along the path (km),
$\gamma(s)$: the specific attenuation (dB/km),
d : the path length (km).

The specific attenuation relates to the rainfall intensity R(s):

$$\gamma(s) = \kappa.R(s)^{\alpha} \qquad dB/km \qquad (3.4)$$

where the values of κ and α are primarily dependent on the frequency, polarization and the raindrop size distribution. Calculated values of κ and α are available [CCIR, 1982, Report 721], assuming the Laws and Parsons raindrop size distribution.

For the prediction of the rain attenuation statistics it is common to use the local point rainfall intensity statistics as a basis. A method to convert point rainfall intensity statistics into rain attenuation statistics is according to the effective pathlength concept:

$$A_R = \kappa.R_o^{\alpha}.d_{eff} = \kappa.R_o^{\alpha}.r_{eff}.d \qquad dB \qquad (3.4)$$

which yields as a suitable modification of equation (3.3).

Using the definitions above one may relate the value of XPI to the value of XPD. If the following condition is met (this condition will be tested in section 3 for rain and multipath):

$$XPI^H + A^H = XPI^V + A^V \quad dB \tag{2.6}$$

the value of XPI relates simply to the value of XPI by:

$$\begin{aligned} XPI^H &= XPI^H + C_o^H - C_c^V \quad dB \\ XPI^V &= XPI^V + C_o^V - C_c^H \quad dB \end{aligned} \tag{2.7}$$

(see also XPI = XPI for $C_o^H = C_o^V$). Using the equations above, equation (2.4) will be modified into:

$$\left(\frac{C}{N}\right) = \left(\frac{C_o}{N_{th}}\right) - A - 10 \log\left[1 + 10^{\frac{\left(\frac{C_o}{N_{th}}\right) - A - XPI + 10 \log K}{10}}\right] dB \tag{2.8}$$

This expression is valid for both polarizations and can be used for the prediction of the carrier to noise ratio, based on the actual values of the equipment and propagation parameters.

Equation (2.8) can be applied directly to flat fading conditions as in the case of rain, and also multipath when distortion effects can be neglected. In general, effects of distortion may be included in equation (2.8) by an extra term to account for any additional degradation.

3. PROPAGATION PARAMETERS

In the preceeding section a transmission model is discussed, which includes propagation parameters. For radio relay systems operating in the 18 GHz band, the dominant propagation phenomena are due to rain and multipath. Effects due to gases are restricted to attenuation which are less than about 2 dB for path lengths of actual interest. Effects due to snow or ice can be neglected, if provisions are made to avoid the collection of snow or ice on the main disk or the radome of the antenna.

3.1 Effects due to rain

For location models for the calculation of attenuation and cross-polarization due to rain certain [illegible] radiometeorological parameters, which relate to the local characteristics of rain. Of these the most important are the point rainfall intensity, data on the [illegible] structure of rain, the raindrop size distribution and the statistics of the [illegible] raindrops. For the accurate calculation of attenuation and cross-[illegible], it is essential that reliable data of these radiometeorological parameters [illegible] location concerned.

[illegible] relative to rain

[illegible] rainfall intensity statistics are the basis for the prediction of the [illegible]. Figure 2 shows the average cumulative distribution of the [illegible] obtained during seven years of measurements by a network of six [illegible] (see Bandam (some 50 km South-West off Nederhorst den Berg). [illegible] are the average cumulative distributions of the point rainfall [illegible] at Nederhorst den Berg during the three years' period of the [illegible] and the values of point rainfall intensity, adopted by CCIR for [illegible] in the Netherlands is attributed (CCIR, 1982, Report 563). As [illegible], the correspondence between the CCIR values and those measured [illegible], bearing in mind the yearly variation of the rainfall characteristics and

As will be discussed later on, rain is the dominant cause of performance impairments due to propagation effects in short-haul radio relay systems, operating in the 18 GHz band. In order to obtain the relevant data on the local characteristics of rain extensive experiments have been carried out by the Dr. Neher Laboratories. These data have been collected during long term measurements by means of raingauge networks, located nearby Leidschendam and Nederhorst den Berg. This set-up allows data to be obtained on the statistics of point rainfall intensity and the horizontal structure of rain (see figure 1).

2. TRANSMISSION MODEL FOR THE PREDICTION OF SYSTEM PERFORMANCE

For the prediction of system performance during fading conditions a transmission model may be used, which relates the relevant equipment and propagation parameters to the quantity, which defines the system performance. For digital systems the appropriate quantity is the bit-error-ratio (BER) or, alternatively, the carrier to noise ratio if the actual relation between the bit-error-ratio and the carrier to noise ratio is known.

In this chapter such transmission model is developed to be used in radio relay systems applying dual polarization in a co-channel arrangement. It is well-known that in such systems the occurring cross-polarization phenomena may cause performance impairments in addition to those due to attenuation, in particular during rainy and multipath conditions. So the total "noisy signal" is the composite of the thermal noise, originating from the receiver, and the cross-polar signal.

In general the characteristics of the cross-polar signal are not identical to those of thermal noise. However, the power I of the cross-polar signal may be expressed by an equivalent thermal noise power N_i, yielding the same bit-error-ratio as the power I of the cross-polar signal:

$$N_i = I + 10 \log K \quad \text{dBW} \tag{2.1}$$

where 10 log K is an equipment parameter. The value of this parameter depends on the equipment characteristics, including the modulation scheme applied. Using this concept, the total noise power N is:

$$N = N_{th} + 10 \log \left[1 + 10^{(N_i - N_{th})/10} \right] \quad \text{dBW} \tag{2.2}$$

where N_{th} is the thermal noise power, originating from the receiver.

The received power C of the copolar signal can be expressed by:

$$C = C_o - A \quad \text{dBW} \tag{2.3}$$

where C_o is the received power of the copolar signal during nominal conditions and A is the copolar attenuation. Combining equation (2.2) and equation (2.3) gives the carrier to noise ratio:

$$\left(\frac{C}{N}\right) = \left(\frac{C_o}{N_{th}}\right) - A - 10 \log \left[1 + 10^{(N_i - N_{th})/10} \right] \quad \text{dB} \tag{2.4}$$

for fading conditions, where no dispersion due to propagation phenomena is encountered within the RF bandwidth of the receiver.

The cross-polar signal levels are expressed in terms of the cross-polarization isolation ratio XPI or the cross-polarization discrimination ratio XPD, which are defined as follows:

$$\begin{aligned} XPI^H &= C^H - I^H = C_o^H - A^H - I^H \quad \text{dB} \\ XPD^H &= C^H - I^V = C_o^H - A^H - I^V \quad \text{dB} \\ XPI^V &= C^V - I^V = C_o^V - A^V - I^V \quad \text{dB} \\ XPD^V &= C^V - I^H = C_o^V - A^V - I^H \quad \text{dB} \end{aligned} \tag{2.5}$$

THE IMPACT OF PROPAGATION EFFECTS ON THE DESIGN OF HIGH CAPACITY DIGITAL MICROWAVE LINKS IN THE 18 GHZ FREQUENCY BAND

L. v.d. Hoek, A. Mawira and J. Neessen
Dr. Neher Laboratories PTT
St. Paulusstraat 4, Leidschendam
The Netherlands

SUMMARY

Propagation effects cause performance impairments in high capacity radio relay links, applying dual polarization. A transmission model is presented, which allows the prediction of system performance during fading conditions. This model includes propagation and equipment parameters, which values depend on the local radiometeorological environment and the actual equipment characteristics. Propagation and communication experiments have been carried out by the Dr. Neher Laboratories, which allow the prediction of system performance in its operational environment at frequencies around 18 GHz. In particular, the paper discusses the effects on the bit-error-ratio as caused by attenuation and cross-polarization due to rain and multipath.

1. INTRODUCTION

The increasing demand for radio transmission capacity necessitates the use of new frequency bands such as the 17.7 to 19.7 GHz band. This 2 GHz broad band is well suited to the operation of high capacity digital radio relay links. However, propagation effects may impose limitations upon the implementation of such links. These limitations depend on the local characteristics of the propagation medium in combination with the characteristics of the communication system applied.

This paper will address particular problems to be met in the frequency band above, especially when dual polarization is applied to increase system capacity. For system design it is of particular importance to know whether the actual system performance during operational conditions corresponds to the predicted system performance as derived from transmission models. Such transmission model is described in section 2. Sections 3 and 4 discuss the propagation and equipment parameters to be used as an input to the transmission model described. Section 5 includes the comparison between the observed and predicted system performance.

Propagation experiments have been carried out on a 16 km path, located in the area around Leidschendam nearby The Hague. The 19 GHz transmitting source is sequentially switched between vertical and horizontal polarization at a switch rate of about 1 kHz. This set-up allows propagation data to be obtained on the attenuation and cross-polarization at both linear polarizations. Further details about the experimental configuration can be found in a previous publication [De Haas et al, IEE, 1983].

In addition communication experiments have been performed on three paths of different length, respectively 6.6, 8.5 and 13.5 km. The systems operate in frequency bands around 18.7 GHz and apply 4 PSK modulation with a capacity of 280 Mbit/s per polarization. The links are located in the area around Nederhorst den Berg, about 50 km North-East off Leidschendam (see figure 1). The registrations include bit-error-ratio and attenuation measurements. Further details about the experimental configuration and the equipment used are given in a previous paper [V.d. Hoek et al, ICC, 1984].

Released to AGARD to publish in all forms. Copyright © 1984 by Dr. Neher Laboratories.

DISCUSSION

J.Hoffmeyer, US

Was the test configuration for measuring equipment signatures implemented at IF or RF?

Réponse d'Auteur

Les mesures de signature ont été faites en hyperfréquence.

A.Schneider, US

Have you compared your empirical results with those predicted by theory (e.g. Bello's, Sunde's, ...) and, if so, what is the result of your comparison?

Réponse d'Auteur

Les comparaisons ont été faites. Le tableau joint indique les résultats.

Bande de cohérence (MHz)						Ecarts (dB) = 10 log $\frac{B_{\text{calculée}}}{B_{50\%\text{ mesurée}}}$			
Liaison	Mesurée $B_{50\%}$	Calculée $B_{50\%}$	Rice B_R	Sunde B_S	$\sqrt{B_R\ B_S}$	Calculée $B_{50\%}$	B_{Rice}	B_{Sunde}	$B_{\sqrt{BR\ BS}}$
1	9,9	9,3	10,4	4	6,4	− 0,3	+ 0,2	− 4	− 1,9
2	3,1	5,75	5,9	2	3,43	+ 2,7 (1)	+ 2,8	− 1,9	+ 0,45
3	3,3	6,75	8,2	3,5	5,36	+ 3,1 (1)	+ 3,95	+ 0,25	+ 2,1
4	1,8	1,75	1,5	0,9	1,16	− 0,14	− 0,8	− 3	− 1,9
5	2	1,6	2,1	1,3	1,65	− 1	+ 0,2	− 1,9	− 0,8
6	2,4	2,45	2,6	1,3	1,84	+ 0,1	+ 0,35	− 2,7	− 1,15
7	2,6	2,7	3,7	2	2,72	+ 0,16	+ 1,5	− 1,15	+ 0,2
8	3,4	3,61	4,2	1,6	2,60	+ 0,25	+ 0,9	− 3,3	− 1,16
9	3,7	4,58	5,8	2,8	4,03	+ 0,90	+ 1,95	− 1,2	+ 0,4
10	1,93	1,82	1,80	0,92	1,30	− 0,25	− 0,3	− 3,2	− 1,8
11	2,55	2,41	2,46	1,43	1,87	− 0,25	− 0,15	− 2,5	− 1,35
12	2,05	2,25	3,33	2,43	2,85	+ 0,40	+ 2,1	+ 0,7	+ 1,45
13	1,59	1,64	0,71	0,28	0,44	+ 0,13	− 3,5	− 7,5	− 5,6
14	1,42	1,57	0,69	0,26	0,42	+ 0,45	− 3,1	− 7,4	− 5,3
15	2,27	2,48	3,61	2,60	3,06	+ 0,40	+ 2	+ 0,6	+ 1,3

L.Boithias, Fr

(1) Les valeurs de la baisse de gain d'antennes indiquées à la figure n° 2 résultent-elles de mesures faites par vous ou d'une courbe du CCIR?

(2) Les courbes de signature (fig.11) semblent peu homogènes. En particulier, les différences très grandes entre les courbes pour 34 et 2 × 34 Mbits/s peuvent-elles être expliquées uniquement par la différence de débit et de type de modulation?

Réponse d'Auteur

(1) La baisse de gain d'antennes indiquée résulte d'une courbe CCIR.

(2) A débit égal et même type de modulation, les dispersions entre les courbes de signature sur différents matériels sont très faibles. Ces comparaisons peuvent être faites pour les 3 débits: 34, 2 × 34 et 140 Mbits/s. Ceci tend bien à prouver que les différences proviennent bien des débits et des types de modulation.

EQUALISEUR TEMPOREL + CORRECTEUR FREQUENTIEL (Lin+Quad)

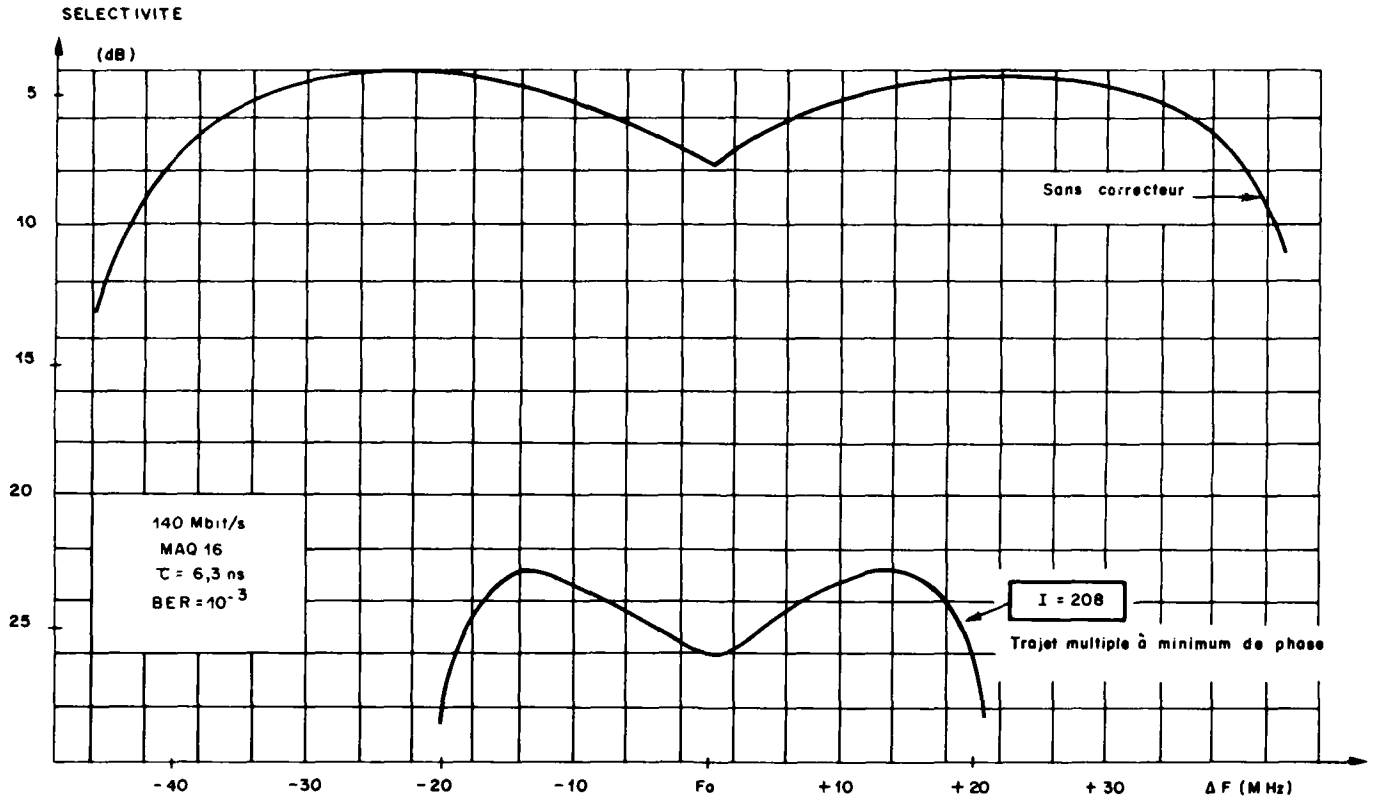

Figure Nº 12

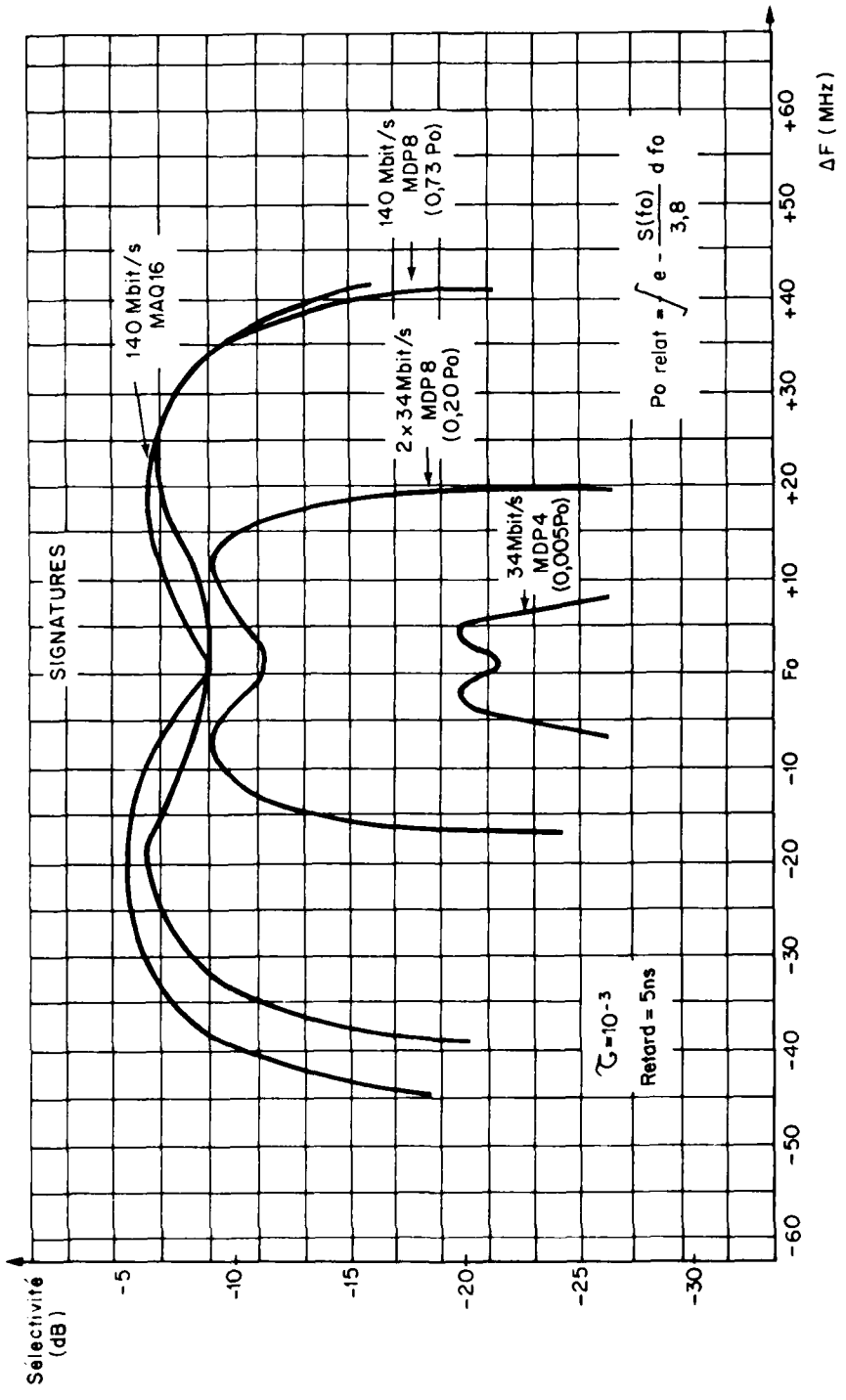
SIGNATURES
Selectivité (dB)
-5
-10
-15
-20
-25
-30
-60
-50
-40
-30
-20
-10
Fo
+10
+20
+30
+40
+50
+60
ΔF (MHz)
140 Mbit/s MAQ16
2 x 34 Mbit/s MDP8 (0,20 Po)
140 Mbit/s MDP8 (0,73 Po)
34 Mbit/s MDP4 (0,005 Po)
τ = 10⁻³
Retard = 5ns
Po relat = ∫ e - S(fo)/3,8 d fo

Fig. n° 11

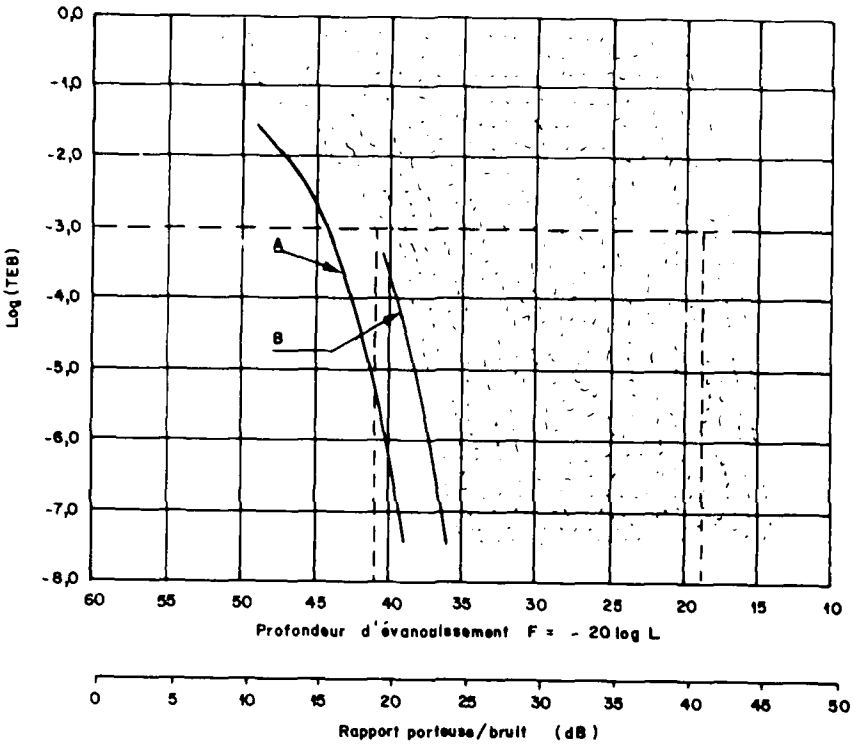

Figure 1 - Exemple de diagramme de dispersion du taux d'erreur.
Chaque point représente un intervalle de mesure d'une seconde.

Fréquence : 4 GHz
Débit binaire : 45 Mbit/s
Modulation : MDP-8 (facteur d'arrondi $\alpha = 0,5$)
Ecartement des canaux : 20 MHz
Longueur des bonds : 42,5 km
A : MDP-8 idéale
B : mesure effectuée pour un évanouissement uniforme

Fig. n°9

EVANOUISSEMENTS SELECTIFS
RESULTAT EXPERIMENTAL
"SIGNATURE"

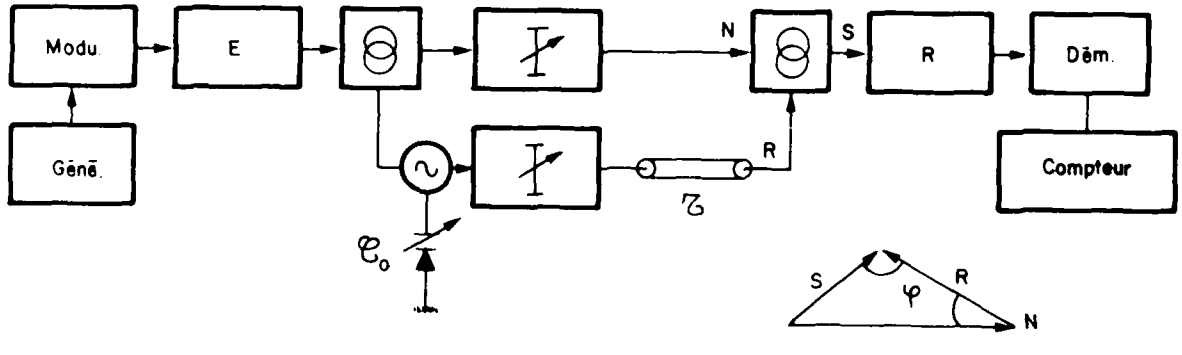

Fig. n°10

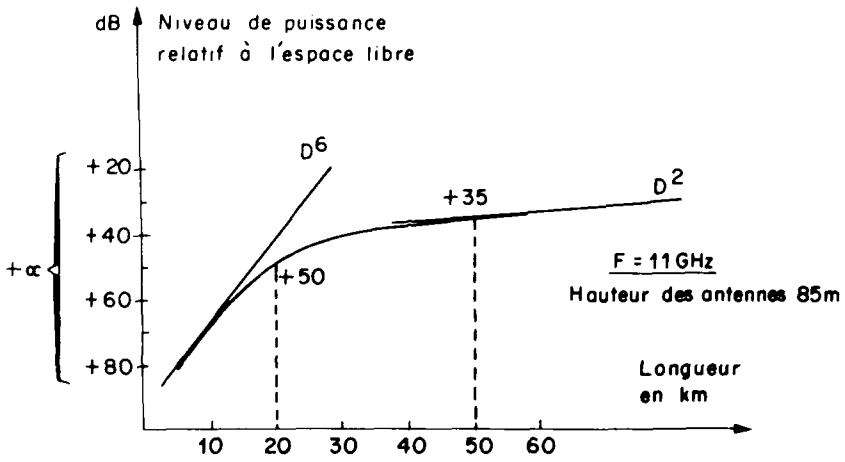
dB
Niveau de puissance
relatif à l'espace libre
+20
+40
+60
+80
+α
D6
D2
+35
+50
F = 11 GHz
Hauteur des antennes 85m
Longueur
en km
10
20
30
40
50
60

Figure N° 8

link 3 where the difference is smaller.
This phenomenon is likely caused by the wetness of the radomes during rain events: unlike the propagation experiment the measurement system does not take this influence into account. Inspection of the strip chart recordings confirms these findings.

5.2.2 Bit error ratio statistics

The cumulative distribution of bit error ratio is shown in figure 13 for links 2 and 3. The curves are quite similar and have a steep slope which may be expected from the attenuation statistics and modem characteristic. Link 2 outperforms the longer link 3 by a factor of 2 because of its 4 dB higher flat fade margin and lower attenuation value for a given percentage of time. This factor can be recovered from the attenuation statistics by comparison of attenuation values with a 4 dB difference. At the 10^{-3} bit error ratio level the curves deviate somewhat because of the occurrence of synchronization loss demanding a switch over to a substitute clock.

The dotted line shows the predicted bit error ratio statistics for link 2 as derived from the predicted attenuation statistics and the predicted relation between attenuation and the bit error ratio according to curve b in figure 14 (see next paragraph). At the 10^{-4} bit error ratio level the predicted and measured time percentage differ by a factor 3. This difference is attributed to the additional attenuation effects due to water on the radomes.

5.2.3 Bit error ratio versus attenuation characteristic

From the measured attenuation and bit error ratio statistics shown before the equi-probability relation between BER and attenuation is derived and presented in figure 14. The flat fade characteristic (curve a) is shown as reference.

The predicted relation between BER and attenuation is calculated by using equation (2.8) and the flat fade characteristic of the system (see section 4). The value of XPI to be used in equation (2.8) is the composite of the contribution $\overline{XPI}_o$ of the antennas and the contribution XPI_R due to rain on the path according the equation (3.8). Assuming power addition the following expression for the value of XPI is applicable:

$$XPI = XPI_R - 10 \log\left[1 + 10^{\frac{XPI_R - \overline{XPI}_o}{10}}\right] \quad dB \qquad (5.1)$$

Using F_{dB} = 4.6 and $\overline{XPI}_o$ = 32 dB the relationship between attenuation and BER is calculated for L_{xt} = 4 dB (the lower bound value in equation (3.8)) and C_o = 15 dB (the average value). The results are shown in figure 14. The measured and predicted values show an excellent correspondence for C_o = 15 dB.
Figure 14 indicates that cross-polarization effects due to rain lead to an additional deterioration of the fade margin of about 1 dB for BER = 10^{-4} as compared to a single polarized system.

5.3 Effects during multipath conditions

The time percentage that a given attenuation is exceeded due to multipath turns out to be a small fraction of that for rain. The contribution of multipath to the attenuation statistics will be considered for link 3, multipath on links 1 and 2 can be neglected.

5.3.1 Attenuation statistics

The cumulative distribution of attenuation due to multipath as obtained from measurements on link 3 is shown in figure 15. The curve shows a slope close to 10 dB/decade which

corresponds to the slope of a Rayleigh distribution for small percentages of time. The differential attenuation appears to be smaller at high attenuation values and higher at lower values of attenuation compared to the results of the propagation experiment shown in figure 7. However, it must be borne in mind that figure 15 shows the cumulative distribution whereas in the case of the propagation experiment the relationship is derived from instantaneous observation i.e. using joint probability statistics.
The dotted line in figure 15 shows the predicted attenuation statistics according to relation (3.9) indicating a higher percentage of time for a given attenuation compared to the measured results. However, the prediction is based on worst month statistics whereas the measured statistics in figure 15 are the average statistics for a three years' period. Furthermore the measured attenuation is the average attenuation across the receiver bandwidth.

5.3.2 Bit error ratio statistics

The measured cumulative distribution of bit error ratio is shown in figure 16. The figure indicates a time percentage of 10^{-4} for a bit error ratio of 10^{-3}, which is a small time percentage compared to that of the high performance standards as recommended by CCIR, 1982, Rec. 594 .

The dotted line in figure 16 shows the prediction of the bit error ratio statistics for link 3 as derived from the predicted attenuation statistics and the predicted relation between attenuation and BER according to curve c in figure 17 (see next paragraph). For BER = 10^{-4} the predicted and measured time percentage differ by a factor 10, mainly caused by the difference between the measured and predicted attenuation statistics in figure 15.

5.3.3 Bit error ratio versus attenuation characteristic

From the measured attenuation and bit error ratio statistics shown before the equiprobability relation between BER and attenuation is derived and presented in figure 17. The flat fade characteristic (curve a) is shown as a reference.
The predicted relation between BER and attenuation is calculated by using equation (2.8) and the flat fade characteristic of the system (see section 4). The value of XPI to be used is according to equation 3.11, which already includes the effect of the antennas. The measured relationship between BER and attenuation is shown in figure 17 for the occurring [illegible] and $\overline{XPD}_o$ = 35 dB (Q = 0).

[illegible] the relatively small distance between curves a and c (about 7 dB), originating [illegible] value (about 35 dB), it is striking that the curve fitting the measuring [illegible] within the two. This implies that the contribution to system degradation [illegible] due to multipath is considered to be of minor importance. According [illegible] distortion due to multipath can be neglected, if the time delay [illegible] rays is less than the critical value which is approximately 0.05 [illegible] at a fade depth of 25 dB for a 4 PSK - 280 Mbit/s system.

[illegible] leading to the critical value of about 0.4 ns. From this [illegible] the occurring time delays are less than 0.4 ns, which is in [illegible] as in paragraph 3.2.2.
[illegible] flat fade margin is eroded by 4 dB for the whole range of BER. [illegible] to cross-polarization phenomena, which are strongly [illegible] the residual XPD of the whole system during non-fading

6. CONCLUSIONS

In the preceeding sections the results from an extensive research programma have been reported, which includes long term propagation and communication experiments. From this experience the following main conclusions are drawn:

1. For the accurate prediction of propagation impairments due to rain the use of local radiometeorological data is essential.
2. The use of radomes to provide weather protection may lead to a substantial increase of the attenuation due to water on the radome.
3. The additional degradation of the fade margin caused by cross-polarization effects due to rain is small.
4. No significant distortion effects due to multipath have been experienced, which is in agreement with the predictions.
5. The time percentage that a defined value of the attenuation due to rain is exceeded is much greater than the corresponding time percentage for multipath attenuation.
6. The additional degradation of the fade margin caused by cross-polarization effects due to multipath may be significant depending on the characteristics of the antennas installed.
7. The transmission model presented is a useful and efficient tool for the prediction of system characteristics, if the local values of the propagation parameters and the actual equipment parameters are known.

It should be noted that the preceeding conclusions are restricted to high capacity digital microwave links of path lengths shorter than about 15 km, operating in the 18 GHz band. Furthermore, these conlusions may not be the same for regions, where different radiometeorological conditions are experienced.

7. ACKNOWLEDGEMENT

The authors are indebted to many colleagues contributing to the experiments for a long period of years. Special thanks are to Philips' Telecommunicatie Industrie B.V. for the cooperation in the communication experiment.

REFERENCES

1) Anderson, I. 1975, IEEE Transactions on Antennas and Propagation, Vol. AP-23, No. 5, pp 610-623.
2) Blevis, B.C., 1965, IEEE Transactions on Antennas and Propagation, Vol. AP-13, No. 1, pp 175-176.
3) CCIR, 1982, Report 563-2, Study Group 5, XV Plenary Assembly, Geneva.
4) CCIR, 1982, Report 721-1, Study Group 5, XV Plenary Assembly, Geneva.
5) CCIR, 1982, Report 338-4, Study Group 5, XV Plenary Assembly, Geneva.
6) CCIR, 1983, Report 338-4 (MOD-I), Study Group 5, Interim Meeting, Geneva.
7) CCIR, 1982, Recommendation 594, Study Group 9, XV Plenary Assembly, Geneva.
8) De Haas J., Mawira A., Neessen J.T.A., Quist J., 1983, International Conference on Antennas and Propagation, Norwich, UK, IEE Conference Publication Nr. 219, pp 224-228.
9) Takes W.C., 1978, Proceedings of the International Conference on Communications, Toronto, pp 47.1.1-47.1.5.
10) Feizer W.P.M.N., Snieder J., De Haan C.D., 1978, IEE Conference on Antennas and Propagation, London, IEE Conference Publication Nr. 169, pp 72-76.
11) Mawira A., Neessen J.T.A., 1984, Proceedings of AIAA 10th Communication Satellite Systems Conference, Orlando-U.S.A., pp 629-639.
12) Olsen R.L., Nowland W.L., 1978, Proceedings of the International Symposium on Antennas and Propagation, Sendai Japan.
13) Van der Hoek L., Kunst M., 1984, Proceedings of the IEEE International Conference on Communications, Amsterdam, pp 1352-1357.

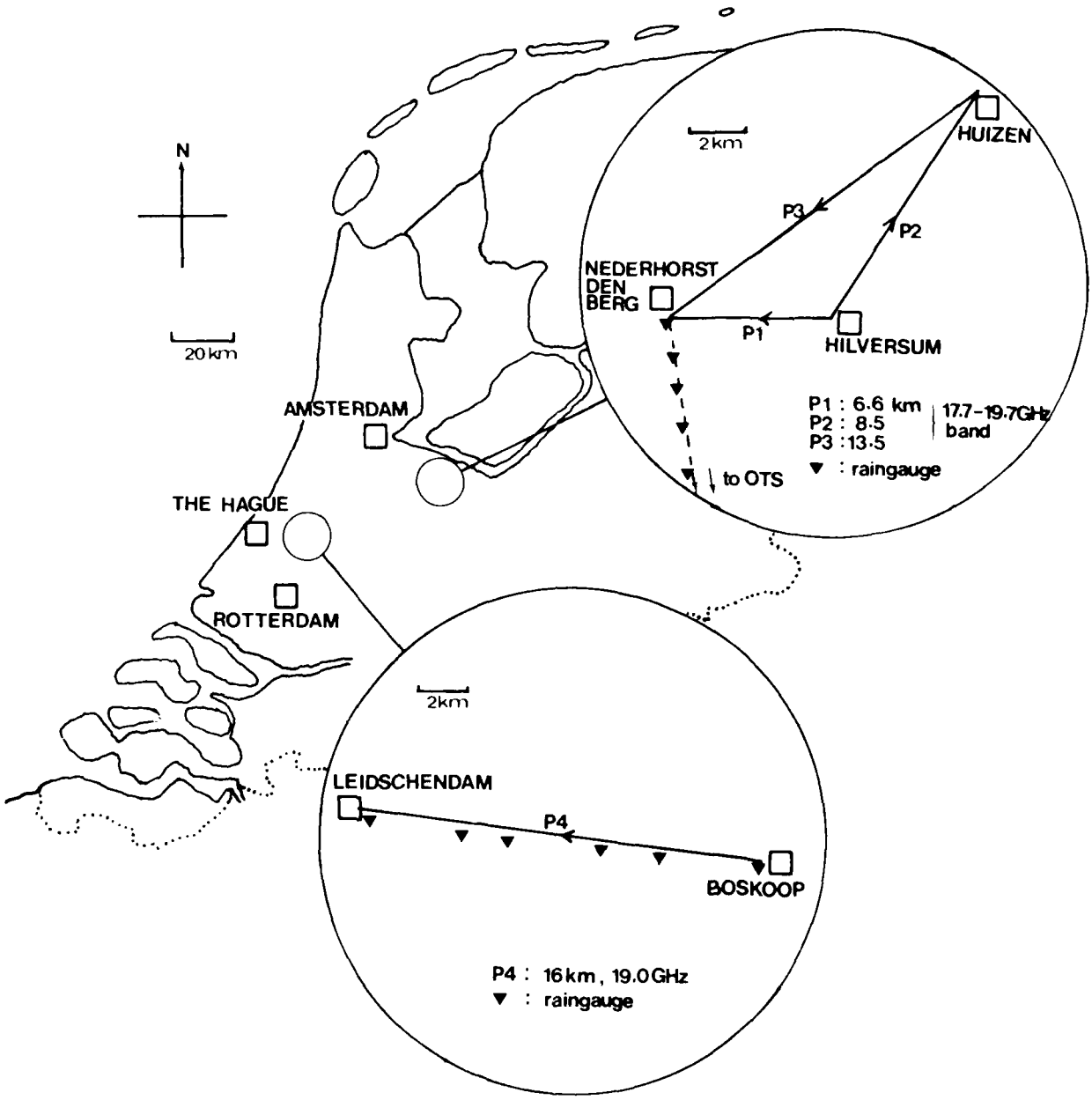

Fig.1 : Location and configuration of the propagation and communication experiments.

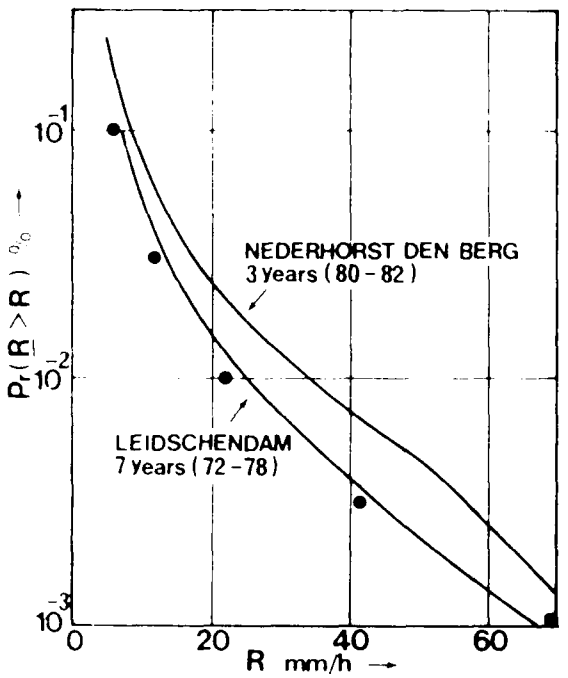

... Measured point rainfall intensity ... statistics ; dots are according ... CCIR.

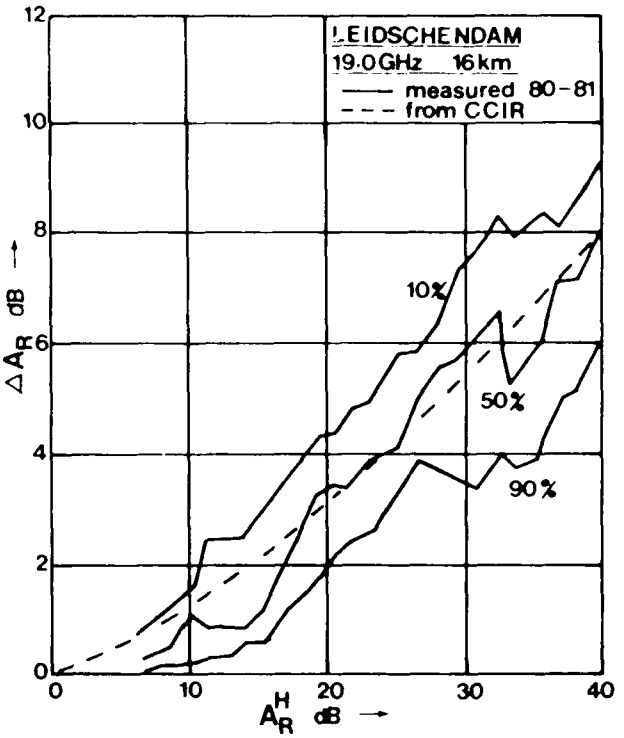

Fig.3 : Differential attenuation versus the attenuation for horizontal polarization during rainy conditions.

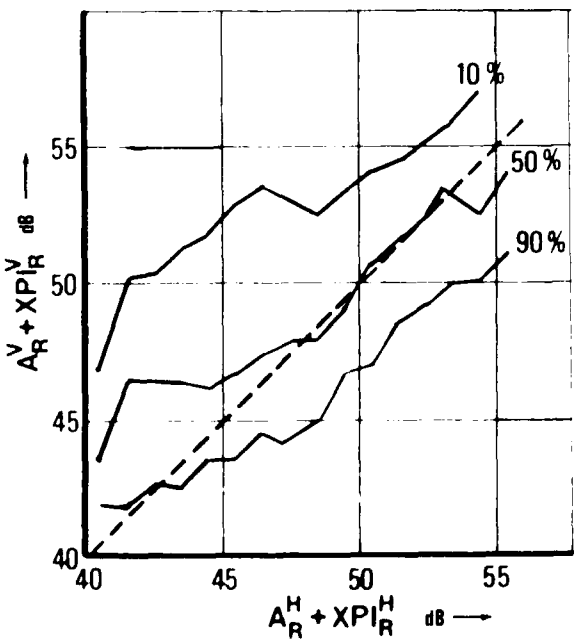

... statistics ...

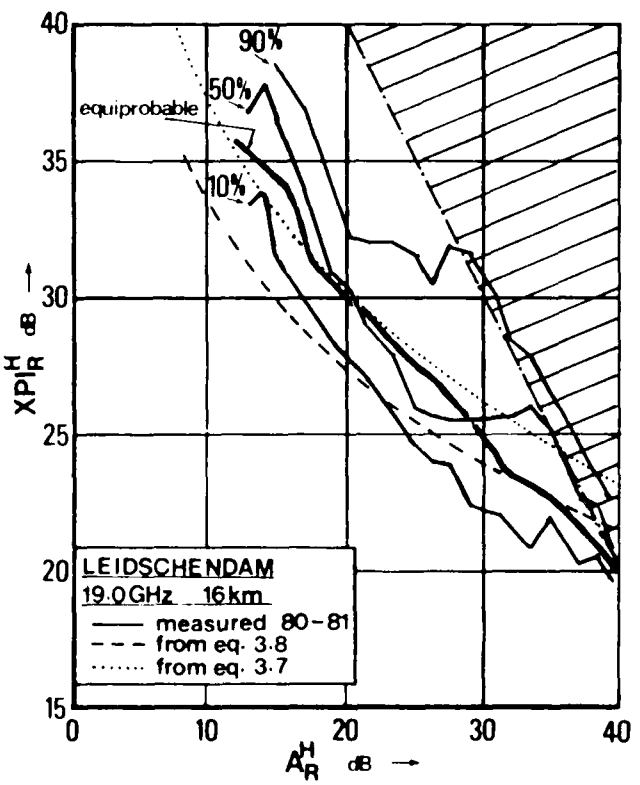

Fig.5 : XPI versus attenuation for rain.

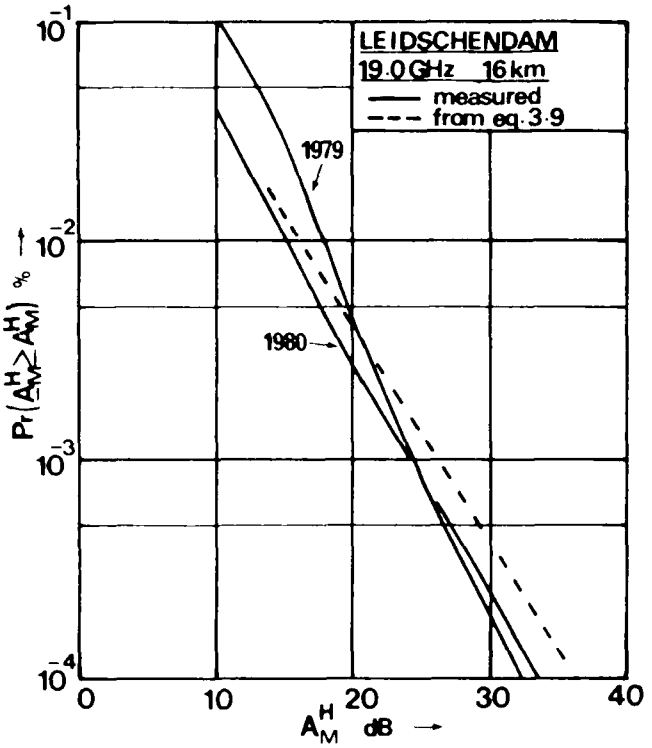

Fig.6 : Measured attenuation statistics due to multipath ; dashed curve is according to CCIR for the worst month.

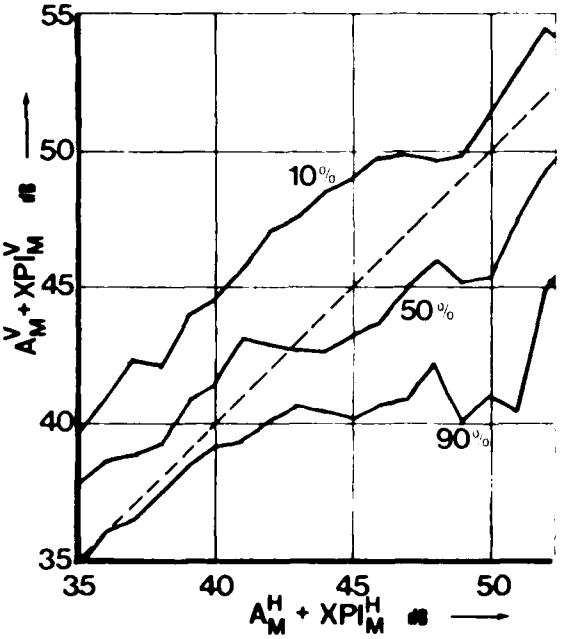

Fig.7 : Testing of the symmetry condition for multipath.

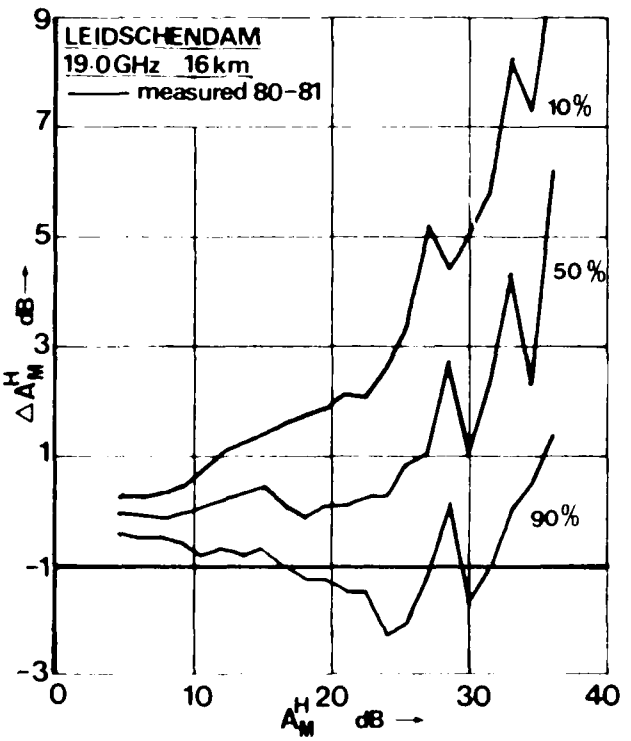

Fig.8 : Differential attenuation versus attenuation for horizontal polarization during multipath conditions.

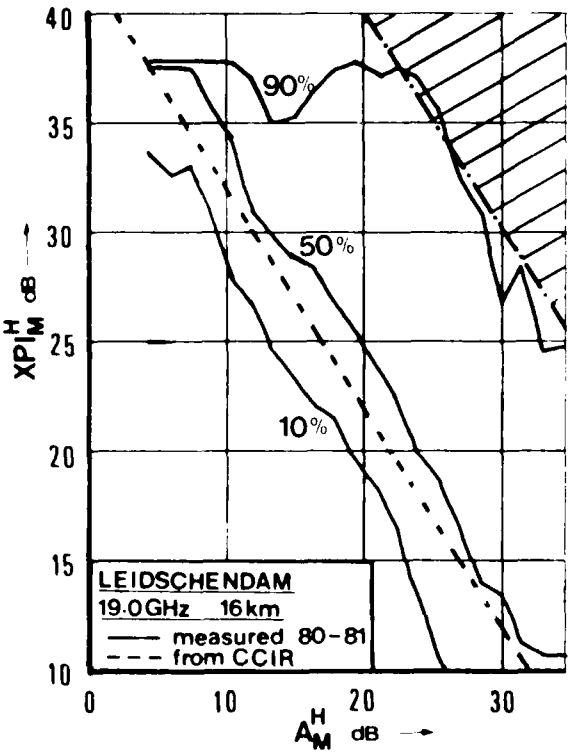

Fig.9 : XPI versus attenuation for multipath.

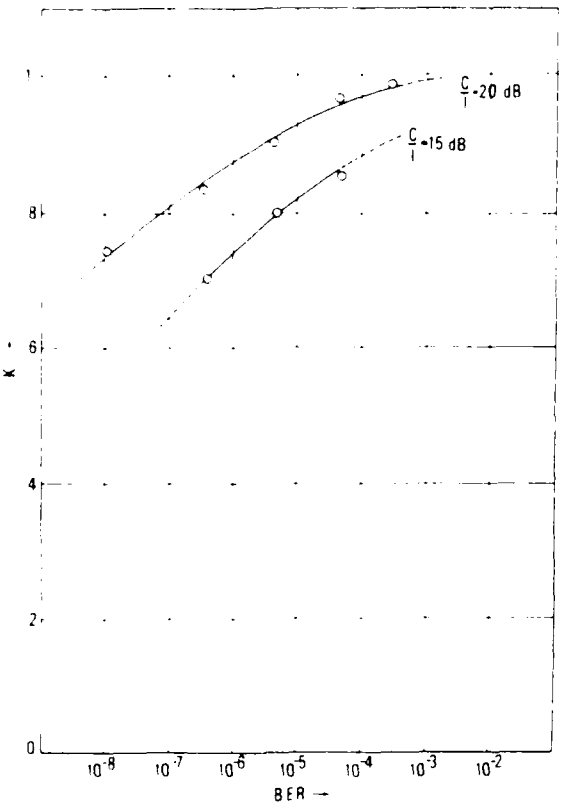

Fig.10 : The parameter k versus BER with the value of C/I as a parameter.

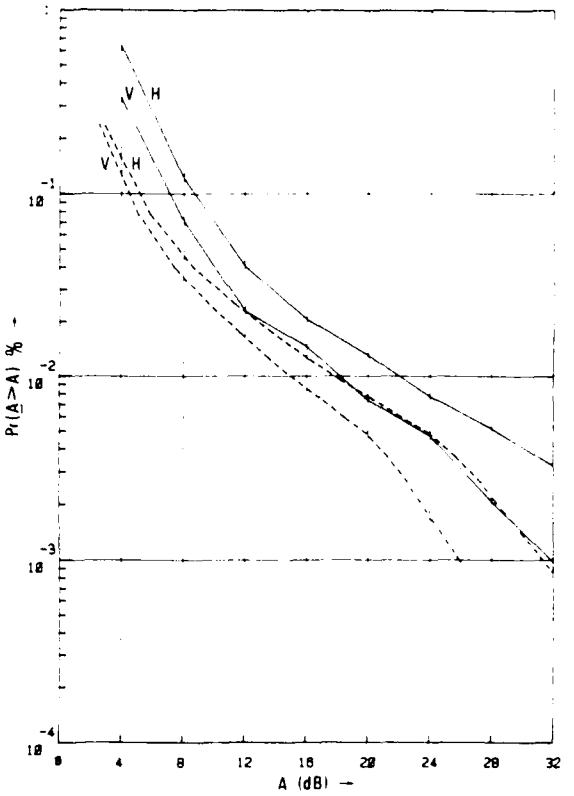

Fig.11 : Predicted (dashed curve) and measured attenuation statistics due to rain for link P2 (8.5 km).

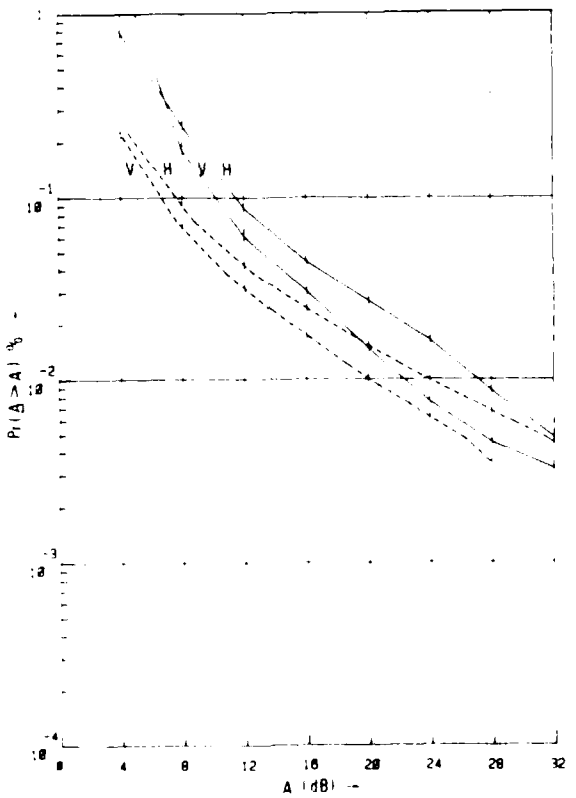

Fig.12 : Predicted (dashed curve) and measured attenuation statistics due to rain for link P3 (13.5 km).

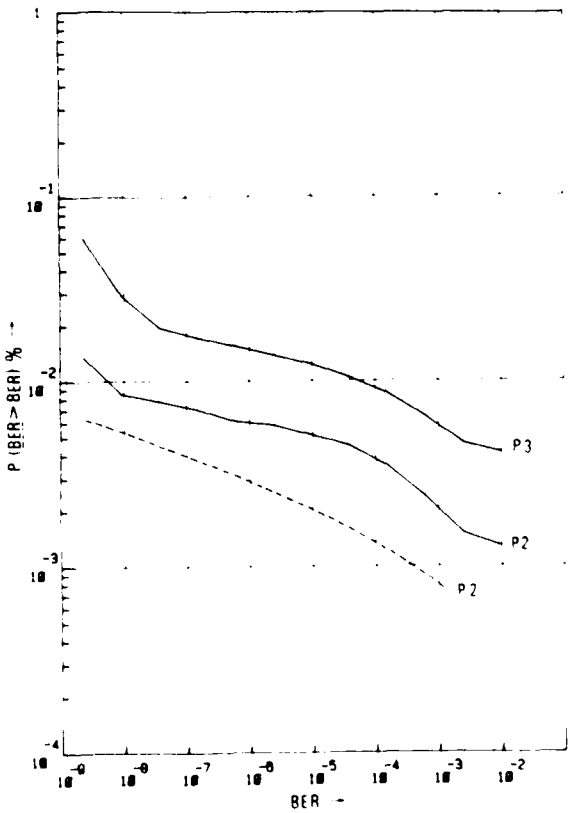

Fig.13 : Predicted (dashed curve) and measured BER statistics due to rain for links P2 and P3.

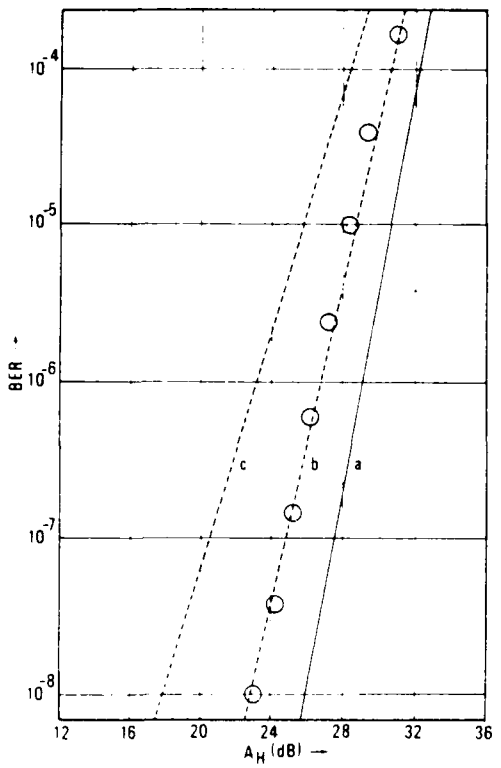

Fig.14 : BER versus attenuation for rain : (a) flat fade characteristic (b) prediction with U_0 = 15 (c) prediction with U_0 = 9 ; dots represent measured data.

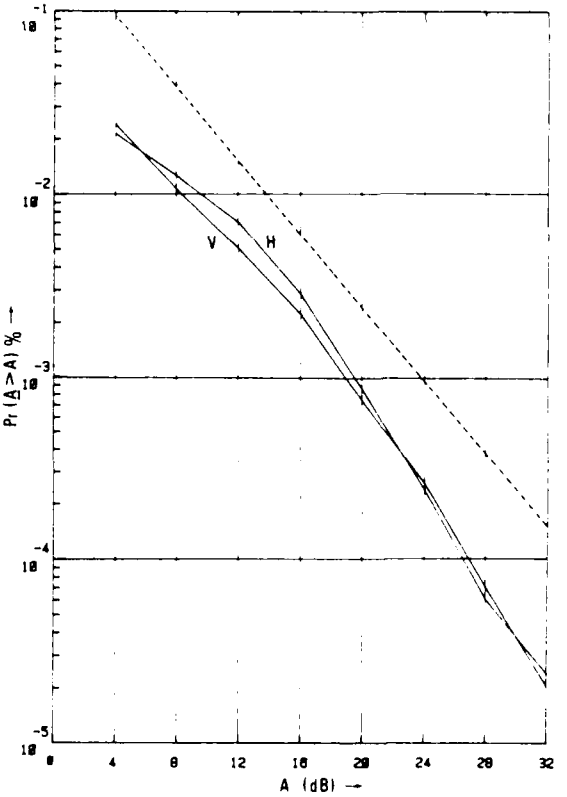

Fig.15 : Predicted (dashed curve) and measured attenuation statistics due to multipath for link P3 (13.5 km).

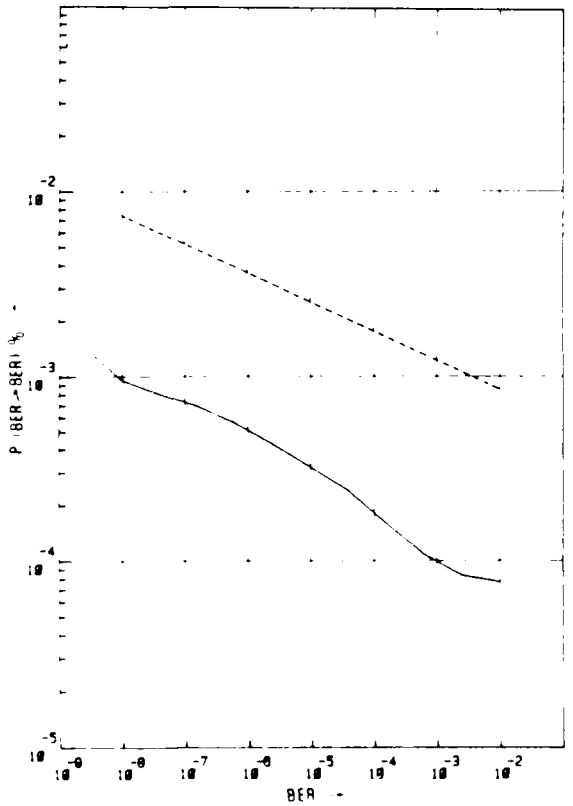

Fig.16 : Predicted (dashed curve) and measured BER statistics due to multipath for link P3 (13.5 km).

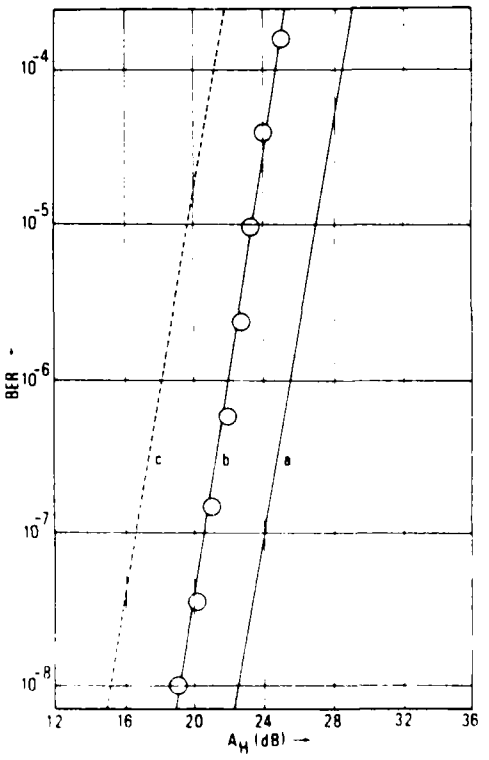

Fig.17 : BER versus attenuation for multipath : (a) flat fade characteristic (b) fit through measured data (c) prediction with XPD_0 = 35 dB.

DISCUSSION

L.Boithias, Fr

La formule 3.9 provenant du CCIR semble s'appliquer, d'après la figure 6, à la liaison considérée (19 GHz et 16 km). Il semble que cet apparent succès résulte d'une compensation de plusieurs erreurs concernant l'effet de la *distance*, l'effet de la *fréquence* et le *facteur numérique* de la formule 3.9:

(a) le terme de distance, en $d^{1.5}$, conduit à des résultats absurdes pour des distances très faibles. Il y a donc une distance minimale pratique de validité.

(b) le terme de fréquence, en F^2, donne une correction indépendante de la distance et du pourcentage de temps. Elle ne peut donc être valable que dans une gamme de fréquences très étroite (la formule a été établie avec des mesures faites principalement à 4 et 6 GHz).

(c) le coefficient numérique ($1.4\ 10^{-7}$) correspond à un *terrain vallonné moyen*, ce qui n'est pas le cas aux Pays-Bas. Aux Pays-Bas ce terme est plus grand.

La bonne concordance entre les mesures et la formule ne peut donc résulter que d'une compensation.

Author's Reply

We used equation (3.9) to show that the existing CCIR prediction technique gives results which are surprisingly close to the measured data — see also Fig.15. It is clear that further evaluation of this technique is required on the basis of *measured* data. The same applies for prediction techniques which are proposed on the basis of theoretical considerations.

A Review of Atmospheric Multipath Measurements and Digital System Performance

Robert W. Hubbard
U.S. Department of Commerce
National Telecommunications and Information Administration
Institute for Telecommunication Sciences
Boulder, Colorado 80303

SUMMARY

This paper discusses the effects of multipath propagation on digital communication systems. It reviews the subject in both recent literature and experiments for information that either describes or defines the phenomenon in terms of the propagation media itself. The performance of digital transmission systems has been studied and reported in recent years in ways that emphasize the multipath problem, but rarely have these experiments included more than a cursory description of the transmission path in terms of the actual multipath structure. In other words, the effects of multipath propagation on system performance are well documented, but a thorough linkage of the transmission channel model to the causes of poor performance is elusive. On the other hand, certain meteorological conditions that create the multipath problem are fairly well understood, and models of these conditions have been developed. In this paper we attempt to bring all of these facets together, and present a morphology that will lead to better understanding and improved performance of digital radio systems.

1. INTRODUCTION

The adverse effects of multipath (or frequency selective) fading in radio transmission have been recognized and measured for several decades. This aspect of radio propagation has been characterized, both qualitatively and quantitatively, in several different ways. Qualitative characteristics were described by such terms as path intermodulation noise for analog systems, and later in terms of intersymbol interference for digital systems. Early quantitative descriptions were based on measurements of coherent bandwidths, signal noise-power ratios, and a variety of other system performance measurements. These terms and parameters reflect a dependence upon the radio system used, and imply multipath effects of the system, as opposed to a direct measurement of the multipath structure within the propagation channel. Since multipath of any form is a multiplicative disturbance, it is a function only of the transmission channel, and is completely independent of the radio system parameters. For this reason, it becomes important to observe and measure parameters of the transmission channel itself and then determine their effects on the performance of systems.

A convenient way of viewing the transmission channel is that of a time-variant linear filter, which relates the output $y(t)$ of a system to the input signal $x(t)$ as [1]

$$y(t) = h(\tau,t) \otimes x(t), \tag{1}$$

where $h(\tau,t)$ is defined as the time-variant impulse response of the channel and $\otimes$ denotes convolution. A corollary in the frequency domain, where the output spectrum is related to that of the input by the product of a time-variant transfer function. The expressions are Fourier transforms of one another. The time domain expression is best for our purposes, as it has been applied to measure multipath characteristics outlined in [2], using instrumentation described in [3] and [4]. Examples of these measurements, made in direct support of performance tests of digital communication systems, are presented later in this paper. The multipath effects of the transmission channel are embodied in these time-varying characteristics.

It is generally acknowledged that multipath effects can be the worst detrimental factor in system performance, particularly for digital systems. One attribute for digital transmission is its ability to overcome additive disturbances and noise in the channel. However, coupled with this is the inherent susceptibility of "catastrophic correlation." It is contrasted to the subjective term of "graceful degradation" applied to analog systems. Early performance tests of digital systems have shown that the error rate floor is rapidly reached due to multipath fading. One example of this fact is presented below. Also, since this form of multipath distortion is a multiplicative effect that is imposed by the channel on the signal, it cannot be overcome with any additive process such as the power budget. Some form of signal processing or bridge must be used to improve performance in a multiplicative channel. Also, to be effective, the signal processing must be capable of following the dynamics of the multipath disturbances and either be cancelled or compensated for. In this paper, we intend to explore the basic characteristics that is inherent to the problem.

2. MULTIPATH IN RADIO PROPAGATION

A review of literature pertaining to the multipath problem in radio propagation reveals an interesting relationship to the introduction of technologies. Some of the earliest studies on LOS microwave propagation were reported in the early 1960's [5,6,7]. The common modulation scheme at that time was frequency division multiplex (FDM). As the FDM channel

[illegible] the multipath effects first became recognized in the wide[illegible]. Since [illegible]M is a nonlinear modulation technique, the [illegible] additional distortions as well as a noise-like signal to be added into the [illegible] overall. It not affect the entire signal significantly, but the intermodulation spectrum affecting only certain voice channels at a time. As the [illegible] used in these systems, the problem became worse. It was never very serious [illegible], however, for these links were relatively short and less dynamic than in longer [illegible] to the user, but rarely did they render the system unusable. When long [illegible] began to many [illegible] program areas and other parts of the world, users began to [illegible] channel problems. Many of these were attributed to path intermodulation and [illegible] the multipath problem shifted from LOS circuits to the troposcatter [illegible] treatments of the troposcatter problem were given in [5] and

[illegible] in analog LOS systems for many years. The use of diversity techniques in [illegible],11] increased over the years and served to alleviate the problem [illegible] systems have an inherent feature that has been labeled as graceful degra[illegible] degrades slowly (shallow slope) as a function of the channel distortions. [illegible] recover rapidly when the disturbance subsides. Probably for these reasons, [illegible] in LOS microwave systems were somewhat dormant during the late 1950's. [illegible], however, the spectral efficiency of microwave systems began to receive attention [illegible] and the advent of microwave allocations for satellite links. To improve [illegible] in analog circuits, baseband signals were expanded. The resultant sys[illegible] resurgence of interest in multipath effects during the latter part of the [illegible] this period, that have been cited in more recent work, are references [illegible] describe this work here, as it is reflected in summaries presented in

[illegible] digital signals for wide-band communications was first seriously considered in [illegible] importance of the multipath problem in LOS applications was essentially over[illegible] the basic studies of digital radios. Theoretical design and analytical practices began [illegible] the analog system, where performance was treated on the basis of signal fade [illegible] versus noise.

[illegible] period, new digital modulation techniques were being considered for the troposcat[illegible] Unlike the early design approaches to the digital LOS system, the path intermodulation in [illegible] was a known problem. It was recognized at the outset in both system design and [illegible]. For example, the digital modems considered as candidates for military troposcatter [illegible] were designed to use the multipath structure to advantage, by providing an intrinsic form of [illegible]. Early propagation and system performance tests included a method to measure and characterize [illegible] spread properties of the channel. In contrast, the digital design and test approaches for the [illegible] did not include any possibility of characterizing the multipath effects. Two [illegible], however, are noted in Section 4.

[illegible] from the late 1960's given above should have alerted the planners and designers of [illegible] microwave systems about what lay ahead in the LOS channel. More evidence of potential transmis[illegible] in this medium was added with another series of papers published in the early 1970's. In [illegible] work, empirical data for the 4, 6, and 11 GHz band provided statistics of inband distortions [illegible] multipath fading. These results were reported in [18], [19], and [20]. The initial measure[illegible] and 6 GHz bands had been reported earlier in [21]. However, if one scans the literature [illegible] digital system designs were discussed in the 1970's, there is little evidence that this problem [illegible] serious one. Without citing any specific papers, we invite a review of the system [illegible] that were presented at the International Communications Conferences in 1976 and 1977. [illegible] the emerging digital systems for LOS applications were discussed in these two conferences. [illegible] protection and measurements were based on the theoretical flat-fading models. Even in [illegible] where diversity combining or sophisticated diversity selection techniques were considered, [illegible] were used. A great deal of attention was given to matters of optimization of filters, pulse [illegible], bit [illegible] processors, and other system parameters such as synchronization and phase-locked loops. [illegible], the [illegible] from interference to a multipath transmission channel was essentially ignored.

[illegible] this apparent oversight could have been that the performance of analog systems was [illegible] acceptable in diversity configurations. Another might have been due to the heavy emphasis [illegible] bits/Hz) in the digital system, and frequency-mask requirements imposed [illegible]. Whatever the reasons for the initial oversight, the problem became quite apparent [illegible] were LOS tests field tests.

[illegible] contributing programs in troposcatter propagation during the 1970's were those of the [illegible] Telecommunications Sciences (ITS), Bell Telephone Laboratories (BTL), the U.S. Air Force, [illegible] Rome Air Development Center (RADC). It is not possible to review all of the work [illegible] this paper, but it will perhaps be useful to chronicle the activities along with [illegible]. We will present more detailed results in Section 4.

[illegible] [illegible] [illegible] [

[illegible] pseudo-random binary signals (PRBS). The PRBS method is shown in [2] to be a transform equivalent to [illegible] spectrum method, and it has a time domain corollary to Eq. (1) as

$$R_{xy}(\tau) = h(\tau,t) \circledast R_{xx}(\tau) , \qquad (2)$$

where $R_{xx}(\tau)$ is the autocorrelation function of the input signal x(t), and $R_{xy}(\tau)$ is the cross-correlation function between the input signal and the output signal y(t) in a linear system. Again, $\circledast$ denotes convolution. Eq. (2) shows that if a test signal (such as a PRBS) that has an impulse-like autocorrelation function is used to probe the linear system, then the cross correlation function describes the impulse response of the system. Since the radio channel is time variant, a "snap shot" of the impulse function is measured over an interval that is short compared with the channel changes.

The PRBS probe uses a dynamic correlation detector in place of the tapped delay line used in the matched RAKE [23,28] receiver. A PRBS tropo probe was first implemented by BTL investigators [24]. Both probing methods have been successfully used in the BTL and Air Force experimental programs to characterize the multipath in troposcatter circuits.

In 1973, the ITS designed and built a channel probe using the PRBS technique for application to the LOS microwave channel. The instrument is described in [3]. It provides a 150 Mb/s transmission rate, yielding an absolute delay resolution of approximately 6.7 ns. However, the practical resolution is on the order of 1 ns. The instrument operates at a fixed frequency of 8.6 GHz, which is in a U.S. Government band, but just slightly above the operation bands. This test frequency was chosen specifically so that the probe could be readily multiplexed into operating systems without interference. The instrument has been applied to a number of multipath experiments [25], and used in direct association with digital performance tests in LOS channels. Results from some of these tests are presented in Sections 5 and 6. More detailed information is contained in [26] and [27].

4. SYSTEM PERFORMANCE MEASUREMENTS IN PRESENCE OF MULTIPATH

4.1 Digital Troposcatter Channel

Multipath intermodulation problems over certain, long troposcatter links was found to be severe in the late 1960's, when the FM systems were used to transmit digital data in the baseband. This was true even for systems that used higher-order space and frequency diversity. A common combiner technique used at the time was that known as maximal-ratio postdetection. Methods proposed to improve the performance of these systems included predetection combining techniques, and the use of angle diversity [28]. In a cooperative program between the BTL, the Raytheon Corp., and the U.S. Air Force, tests were conducted in 1967 and 1968 over an established link between Greenland and Iceland. The results of these tests were summarized individually by the BTL and the Raytheon Corp. in reports to the Air Force [29,30]. It is beyond our scope to discuss these results in detail. It is sufficient to note that new insight was gained relative to digital transmission in this channel, and that these tests led ultimately toward the design features of today's digital troposcatter systems.

Research by the BTL continued for several years in both diversity combining techniques and the application of angle diversity to the troposcatter channel. The work was conducted over an experimental link in the eastern United States. Results from various elements of this research were reported in a group of papers at the International Communications Conference (ICC) in 1971 [31]. The most important results for our purposes were those that conveyed a direct measure of the impulse response over the test channel (noted later). The BTL suspended research on the troposcatter channel around 1972, as the emphasis on long range communications began to shift toward the satellite circuits. The PRBS probe used by the BTL was acquired by the ITS. It was modified and improved, and later used to support the Air Force in continued troposcatter work. Examples of measured data are presented later in this section.

Air Force investigations into troposcatter continued throughout the 1970's, in support of a number of strategic links around the world. Plans were being made to upgrade these links, and to eventually change them to a digital format. Tactical digital troposcatter systems were also under development at this time. Much of the design, test, and evaluation work was conducted by the Rome Air Development Center (RADC). RAKE techniques were used to measure the delay-spread parameters of several links, and results were compared with existing models [9,32,33]. A simple profile of the multipath power as a function of relative delay was found (on the average) to agree quite reasonably with theory. However, both time and spatial variations were found, raising questions and speculations about the structure and dynamics of the scatter mechanism. Some of these are tabulated in a later summary.

A comprehensive report of the Air Force work is given in [34], which also contains an extensive list of other references relevant to the subject. These include the work conducted by the NRDL, which concentrated on the meteorological parameters of the channel. A set of multipath power profiles were derived to characterize a variety of channels. These curves are shown in Figure 1, where each represents a mean or median of the measured characteristics. The 2σ delay-spread value (given for each profile in μs) represents the delay distribution of the power impulse functions, where σ is the standard deviation. These profile data are obtained from the RAKE and PRBS probe instruments mentioned previously.

In 1978, the Air Force established a Joint Tactical Communications Office (JTCO) at Fort Huachuca, AZ. The mission of this office was to develop a test program for the new tactical troposcatter systems (TRI-TAC). In order to assure that the delay-spread parameter of the selected test paths was in accord with the design specifications depicted in Figure 1, arrangements were made with the ITS to conduct impulse response measurements over each path. The tests were conducted in 1979, using the ITS/PRBS probe interfaced with an analog troposcatter system (AN/TRC-97). All of the paths tested were in the southern Arizona region near Fort Huachuca. They ranged in length from 61 km to 355 km, and had varying

[illegible] but not atypical of the benefits being planned or implemented today. Measured results for the [illegible] system's performance over this link are shown in Figure 6 during [illegible] fading. Each data point represents the measured BER and RSL over a 5-minute period. [illegible] scatter plot with respect to the expected performance curve. This [illegible] somewhat surprising at the time, but it has been found to be rather typical of the multipath [illegible] unprotected (nondiversity) digital link. Meteorological data were again used to support [illegible] that ducts caused the periods of deep signal fading and poor performance in [illegible].

[illegible] data obtained from commercially developed systems were first presented at the 1978 ICC [illegible]. Two papers at this conference presented the early results measured by the telephone [illegible] in Canada and the United States. Later versions of these papers, along with one from [illegible], appeared in the IEEE Transactions on Communications in December 1979 (a special issue on digital [illegible]). The Bell Northern Report and the IEEE special issue brought together a significant body of [illegible] on LOS digital transmission. The most important conclusions drawn in this literature are [illegible] in the following.

[illegible] tests of Table 1 conclude that linear amplitude dispersion caused by multipath is the [illegible] factor in degraded performance. Most of the authors also conclude that diversity reception in [illegible] with some form of equalization will be required in the LOS channel to improve its performance. [illegible] tests did not, however, include any measurements that would identify the actual conditions [illegible] transmission channel. The knowledge of such conditions, unfortunately, may be essential to [illegible] the required adaptive techniques.

A general problem noted in these tests is a lack of commonality for the outage criteria used, and [illegible] level that is associated with the specified outage. Most tests were based on a BER [illegible], but the measurement intervals varied, or were not stated. Other results are reported on the [illegible] signal-to-noise (S/N) ratios. These differences make it very difficult to compare results. [illegible], the lack of a channel description renders it impossible to compare the LOS propagation [illegible]. This problem is illustrated in the following discussion, which in part is based on some [illegible] of the above system tests.

[illegible] tests, the in-band dispersion was observed by measuring the relative power in the received signal in narrow-band filters spaced across the signal pass band. The difference in power levels [illegible] of the in-band amplitude dispersion. It was reported that a dispersion on the order [illegible] was sufficient to cause the performance to degrade to a BER>10^{-3}, a slope of only 6 dB [illegible]. The RSL distributions for the test period were compared with calculated statistics [illegible] to be typical of a heavy fading month. The detailed results were as follows:

[illegible]	BER Threshold (1 s Interval)	Time Exceeded	No. of Events	Average Duration	% Time* Above Threshold
[illegible]	1.1 × 10[illegible]	3900 s	195	15 s	99.880
[illegible]	1.2 × 10[illegible]	1000 s	83	12 s	99.958
[illegible]	1.[illegible] × 10[illegible]	1100 s	80	14 s	99.969
[illegible]	1.[illegible] × 10[illegible]	370 s	37	10 s	99.989

[illegible] author.

[illegible] performed by the FCC [27] have shown that performance degradations of this magnitude [illegible] as short a period as one day or less. Thus, we would conclude that the transmission degradation in the above tests was not severe. Reporting test results in terms of a BER in [illegible], but a record of the time that different BER thresholds are exceeded (as above), is a [illegible] becoming more common. For example, a performance measure that is receiving acceptance is [illegible] errored-second (ES), where the number of errors in the second are counted. It has two [illegible], a) the second of time is synchronous with the first error detected, and b) it permits [illegible] to be calculated for any desired BER threshold. If the trend toward [illegible] of the [illegible], it will alleviate the problem of comparing test results.

[illegible] in which these data appear was perhaps the first to consider the "effective fade margin" [illegible] system (other terms such as dispersive, equivalent, and net fade margin are also [illegible] to quantify the difference between the expected flat-fading performance of a [illegible] digital radio performance. The effective fade margin is derived by equating the "outage" of a specified threshold level to the same amount of time in a cumulative rain-depth [illegible] average rain level is exceeded. This concept can be used to some extent to [illegible] performance measurements. However, it is system dependent and obviously very dependent [illegible] threshold selected and the channel conditions. For these reasons, the concept will [illegible] application in performance comparisons.

[illegible] of the tests listed in Table 1 is that reported by Bell Northern Research. Tests [illegible] was conducted in two nondiversity channels, as well as in a space diversity [illegible]. The criteria for outage was selected as a probability of 1.1×10^{-3} [illegible], a proportional factor based on long-haul objectives. The BER threshold was not [illegible] the fraction of bits in error was not stated. The overall performance was summarized in [illegible] improvement factors (ratios of outage probabilities). Since there were no results showing time [illegible] was exceeded, it is not possible to compare the results with the previously discussed [illegible]. The effective fade margins were, however, given for both of these tests, and we examine [illegible].

UHF COMMUNICATIONS THROUGH FORESTED PROPAGATION CHANNELS

by

Allan Schneider
CyberCom Corporation
4105 N. Fairfax Dr.
Arlington, VA 22203

SUMMARY

This paper describes a stochastic radiowave propagation model useful for assessing the effects of forests and other vegetation upon communications signals in the UHF band. The stochastic electromagnetic theory employed as the basis of this model initially considers the forest as an unbounded, discrete random medium of randomly-positioned and oriented circular cylindrical scatterers representing the principal forest constituents (tree trunks are represented as infinitely-long, parallel, circular, dielectric cylinders; leaves as flat circular, dielectric discs). A physically appealing representation for the mean (coherent) field component of the propagating radiowave has been obtained by recognizing that the ensemble of discrete scatterers can be replaced by an equivalent continuous medium described by an effective dyadic permittivity $\underline{\underline{\epsilon}}$. The forest model is then refined by assuring a planar stratified, anisotropic, forest model bounded above by air and below by ground. The associated electromagnetic boundary value problem is solved asymptotically to identify the principal contributions to the mean field: the direct wave, the reflected wave, and the lateral wave. Because the equivalent continuous medium characterized by the effective dyadic permittivity $\underline{\underline{\epsilon}}$ is linear, Fourier transform techniques have been employed to generalize the model so that it accommodates arbitrarily modulated waveforms. The central limit theorem suggests that the fluctuant (incoherent) field component is a Gaussian random process and so can be completely characterized by its intensity (power) and correlation function. The two-frequency correlation function, especially useful in assessing the effectiveness of specific modulation techniques, has been presented for a two-dimensional, unbounded forest of parallel tree trunks illuminated by a parallel line current. In contradistinction to all earlier models, the behavior of the propagating radiowave can be related directly to the biophysical parameters of the forest.

1. INTRODUCTION

One of the most important elements of performance analysis of any radio communications system is an accurate representation of the effects of the communications channel on the transmitted signal. The most important of these effects is undoubtedly signal attenuation, or transmission loss. Of secondary impact is the distortion caused by multipath delays and frequency selective fades which can affect the reliable reception of the signal. The objective of the research reported in this paper is to develop the necessary theory and produce engineering models capable of predicting excess path loss, pulse distortion, and space-frequency correlation functions for UHF communications signals operating in a ground forested environment. This paper reviews progress to date on this research effort.[1]

Viewing the forest as a time-invariant ensemble of randomly positioned and oriented discrete circular scatterers and using the procedures of Twersky[2], the behavior of the time-harmonic radiowave in the forest is first reviewed. The wave equation for the mean (coherent) field propagating through an unbounded forest is used to demonstrate propagation effects resulting from the anisotropic and spatially dispersive character of the equivalent forest medium. The microscopic biophysical parameters of the vegetative constituents are used to derive the relative permittivity and the effective dyadic susceptibility is shown to be useful for describing the equivalent continuous forest medium. Actual statistical data describing trunk and leaf characteristics are discussed and are used in several numerical examples. The model is then used to derive the specific attenuation (attenuation rate) attributable to the mean (coherent) field in tree trunks and leaves.

The next step introduces a more realistic series of models which treat the forest as a stratified continuum, each similar to that of [1], although anisotropic. The models are used to describe the resultant field occurring as a consequence of combined direct, reflected, and lateral wave components and ground reflections. In the final section the analysis is extended through Fourier transform techniques to derive the effects important to communications systems, including pulse response and two-frequency correlation functions. The paper concludes with future plans to improve the models and to conduct experimental measurements to validate the theoretical assumptions.

DISCUSSION

E.W.Lampert, Ge

In your paper you did not discuss effects of aircraft flying across the common volume, at least in Europe. I believe that this is an important factor limiting availability and performance of the channel; do models exist which quantitatively describe this effect?

Author's Reply

I know of no models for this problem. However, this does not mean one does not exist. We have observed the problem for many years. I suppose we must put it in the category with the dynamic unknowns, and hope that it will receive some future attention.

L.Boithias, Fr

(1) A quelle frequence correspondent les resultats de la figure 8?

(2) La figure 10 correspond à des mesures sur un trajet maritime. Comment avez-vous separe les trajets multiples dûs à l'atmosphere de ceux dûs à des reflexions sur la mer?

(3) Avez-vous etudie la relation entre la marge effective d'évanouissement et la longueur du trajet?

Author's Reply

(1) The measurements were all made using the ITS Channel Probe, which operates at 8.6 GHz using a PRBS test signal clocked at 150 MHz.

(2) Reflections from the sea surface on this link, under standard refractivity (k = 4/3), would produce a delay on the order of 2 ns. The geometry of the link and the 10 ft (3 m) parabolas used for the antennas discriminate against this component. We have analyzed the channel probe responses looking for the surface reflection. When it is seen, we find it at levels some 20 to 30 dB below the direct response, and dispersive due to the surface roughness. Thus, it is fairly easy to distinguish the atmospheric component from the surface component.

(3) At this time we have not analyzed all of our data from these tests. We intend to study the relationship noted in your question, and will report on these results at a later time.

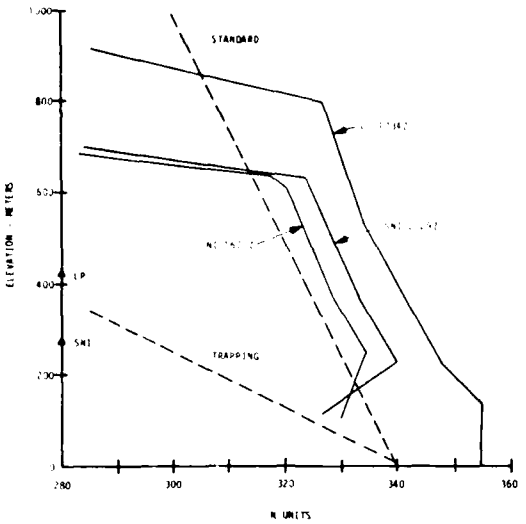

(a) Refractive index profiles measured at the path terminals on 18 August 1981.

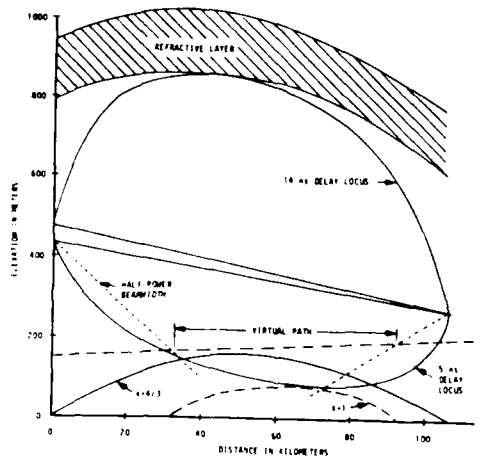

(b) Path profile for the refractive index profiles shown in (a).

Figure 10. Graphical correspondence between measured multipath delay values and the refractive index structure of a LOS over-water path in southern California.

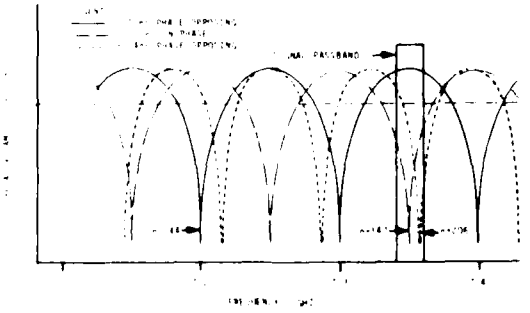

Figure 11. The theoretical frequency transfer functions for a microwave channel with two-ray multipath signals; sketched for a = 1 and b = 0.9 in Eq. (3).

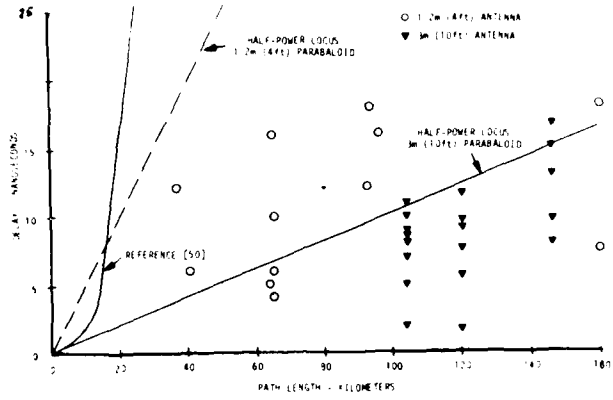

Figure 8. Multipath delay measured over LOS microwave links in Europe and the United States compared with analytical bounds. The boundary from [50] has a cubic dependence on path length; the linear bounds are based on link geometry and antenna beamwidth.

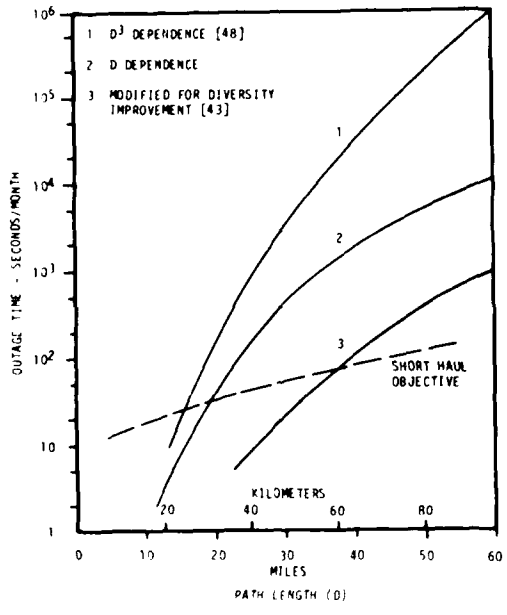

Figure 9. Estimates of the upper bound on digital system performance due to multipath in a LOS microwave channel. Curve 1 is taken from [48]; the other curves are modified as discussed in the text.

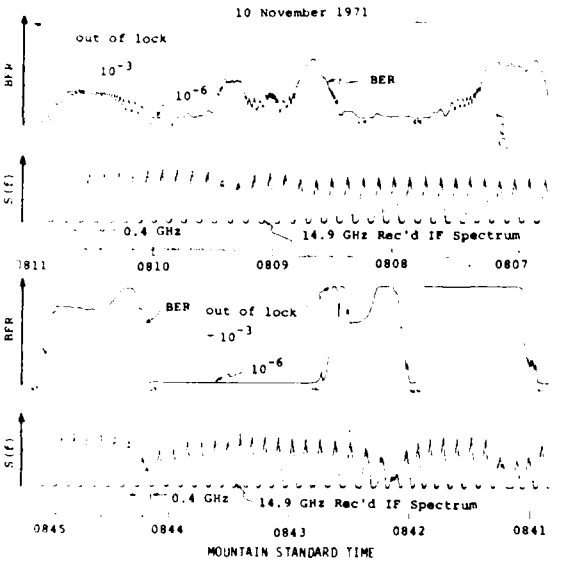

Figure 4. Comparison in real time of the observed BER performance and the IF spectrum of the received signal S(f) for the 400 Mb/s digital transmission tests described in [39].

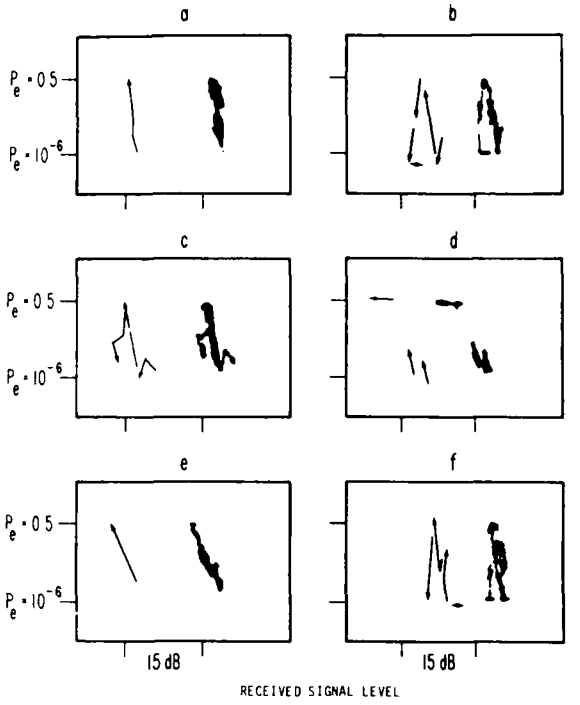

Figure 5. Storage oscilloscope displays of the BER performance vs the received signal level for the 400 Mb/s digital transmission tests described in [39]. Signal power increases to the right. Development of each 4 minute sample is illustrated by the arrows at the left of each display.

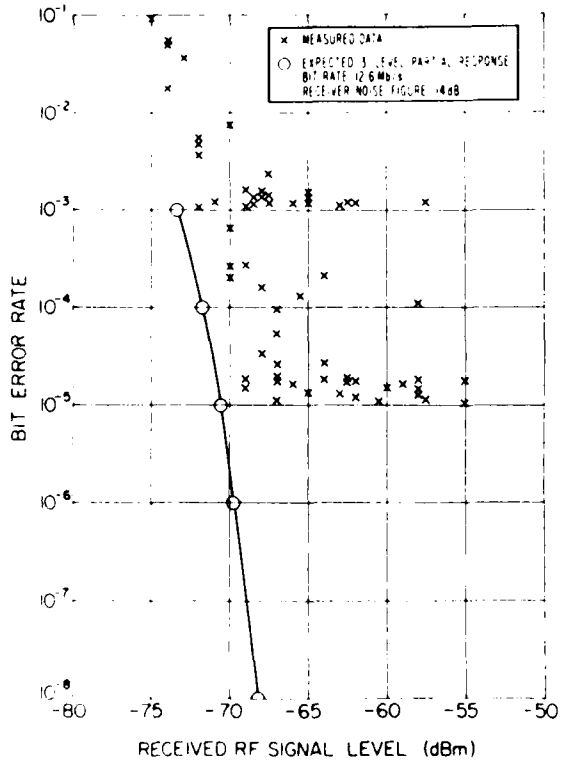

Figure 6. Digital BER performance measured over a line-of-sight path in eastern Colorado at 11 GHz. Each data point is for a five-minute sample (22 March, 1975; 0100-0730 MDT). The tests are described in [40].

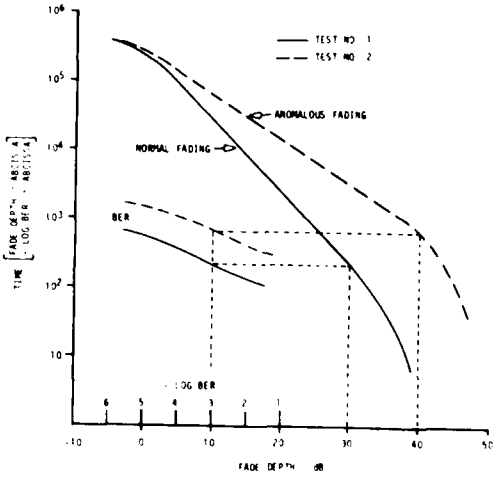

Figure 7. An illustration of the test results for the digital LOS system described in [43]. The effective fade margin for test no. 2 corresponds to 40 dB, however, the system outage time is greater than that for test no. 1 due to the anomalous multipath fading during test no. 2.

[51] Sasaki, O., and T. Akiyama, "Multipath delay characteristics on line-of-sight microwave radio system," IEEE Trans. on Comm., Vol. COM-27, No. 12, 1979, pp. 1876-1886.

[52] Dougherty, H.T., and E.J. Dutton, "The role of elevated ducting for radio service and interference fields," NTIA Report 81-69, U.S. Department of Commerce, Boulder, CO 80303, March 1981.

[53] Dutton, E.J., D.C. Hyovalti, C.E. Lewis, and F.K. Steele, "Elevated duct data-base improvement," NTIA Report 81-89, U.S. Department of Commerce, Boulder, CO 80303, December 1981.

[54] Chadwick, R.B., and E.E. Gossard, "Radar remote sensing of the clear atmosphere-review and applications," Proc. of the IEEE, Vol. 71, No. 6, 1983, pp. 738-753.

[55] Sorovacu, N.J., and W.J. Cybrowski, "Performance analysis of four digital troposcatter links in the European DCS," Defense Comm. Engineering Center, Tech. Report xx-84, 1984, to be published.

[56] Ural, A.T., "Multipath measurements over two Ace High troposcatter links," SHAPE Technical Center, Consultant Report STC CR-NICS-64, January 1982.

[57] Pusone, E., "A channel model for the prediction of delay and Doppler power spectra and frequency correlation function for troposcatter communication links," Proc. of International Seminar on Digital Communication, Zurich, Switzerland, March 1980.

[58] Violette, E.J., R.H. Espeland, and K.C. Allen, "A diagnostic probe to investigate propagation at millimeter wavelengths," NTIA Report 83-128, U.S. Department of Commerce, Boulder, CO 80303, August 1983.

[59] Hubbard, R.W., "Error distribution analysis of a 45 Mb/s 8 PSK system in a LOS multipath channel," NTIA Report to be published.

[60] Hoffmeyer, J.A., "LOS channel simulation - a survey of models, realizations and new concepts," Paper no. 22, this symposium.

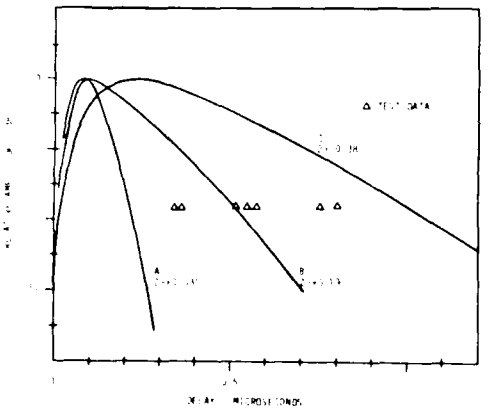

Figure 1. Average multipath power profiles developed for typical troposcatter transmission paths. The data points are the 98% cumulative values measured over selected test paths in southern Arizona.

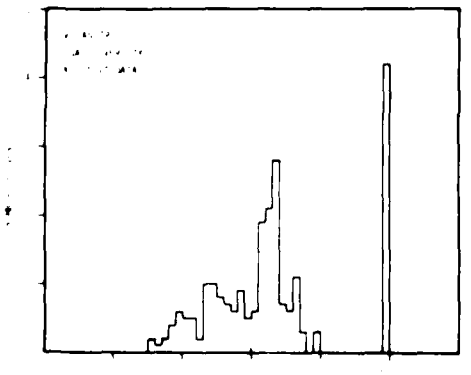

Figure 3. Distribution of digital performance data relative to specification for multipath profile A in Figure 1. The data are from digital troposcatter tests conducted in southern Arizona.

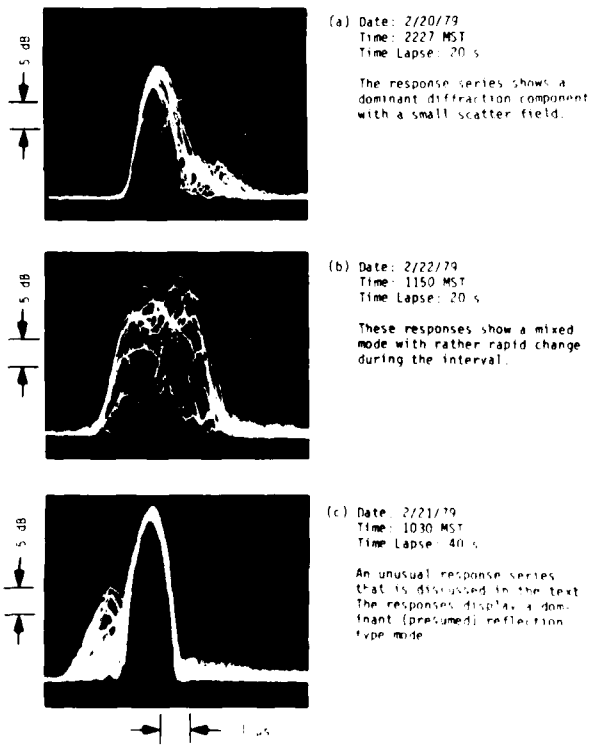

Figure 2. Power impulse response functions measured over a 61km (38mi) troposcatter path in southern Arizona.

[26] Hubbard, R.W., "Investigation of digital microwave communications in a strong meteorological ducting environment," NTIA Report 79-24, U.S. Department of Commerce, Boulder, CO 80303, August 1979.

[27] Hubbard, R.W. "Digital microwave transmission tests at the Pacific Missile Test Center, Pt. Mugu, California," NTIA Report 83-126, U.S. Department of Commerce, Boulder, CO 80303, June 1983.

[28] Surenian, D., "Experimental results of angle diversity tests," IEEE Trans. on Comm. Technology, Vol. COM-13, 1965, pp. 208-219.

[29] Bell Telephone Laboratories, "Feasibility trial of the forward acting linear combiner and angle diversity reception on the DYE 4-DYE 5 troposcatter radio link," Final Report to AF Systems Command, Hanscom AFB, MA, November 1968.

[30] Raytheon Co., "Multiple diversity troposcatter tests using the PDC-4 predetection combiner," Raytheon Technical Report CDP-TR-19, July 1968.

[31] IEEE Conference Record, "Intertnational Conference on Communications," Session 26, Angle diversity systems for scatter applications, Montreal, Canada, June 1971.

[32] Bello, P.A., "A troposcatter channel model," IEEE Trans. Comm. Technology, Vol. COM-17, No. 4, 1969, pp. 130-137.

[33] Bello, P.A. L. Ehrman, and D.S. Arnstein, "Modeling and data analysis - short and medium range digital troposcatter tests," Technical Report RADC-TR-233, October 1969.

[34] Sherwood, A., and L. Suyemoto, "Multipath measurements over troposcatter paths," The MITRE Corp., Report MTP-170, April 1976.

[35] JTCO, "Development test and evaluation of troposcatter radio AN/TRC-170," Final Report, JTCO, Fort Huachuca, AZ (distribution limited), November 1980.

[36] Defense Communications Engineering Center, "Application of digital troposcatter to the DCS," DCEC Tech. Report 10-80, September 1980.

[37] Dougherty, H.T., "Survey of microwave fading mechanisms, remedies, and applications," ESSA Technical Report ERL 69-WPL 4, (NTIS Access No. COM-71-50288). March 1969.

[38] McGavin, R.E., H.T. Dougherty, and C.B. Emmanuel, "Microwave space and frequency diversity performance under adverse conditions," IEEE Trans. on Comm., Vol. COM-18, 1970, pp. 261-263.

[39] Dougherty, H.T., and W.J. Hartman, "Performance of a 400 Mbit/s system over a line of sight path," IEEE Trans. on Comm., Vol. COM-25, No. 4, 1977, pp. 427-432.

[40] Samson, C.A., A.P. Barsis, and D. Smith, "Perofrmance measurements over long line-of-sight microwave links in Colorado," OT Report 76-92, U.S. Department of Commerce, Boulder, CO 80303, June 1976.

[41] IEEE Conference Record, "International Conference on Communications," Toronto, Canada, June 1978.

[42] Barnett, W.T. "Multipath fading effects on digital radio," IEEE Trans. on Comm., Vol. COM-27, No. 12, 1979, pp. 1842-1848.

[43] Anderson, C.W., S.G. Barber, and R.N. Patel, "The effect of selective fading on digital radio," IEEE Trans. on Comm., Vol. COM-27, No. 12, 1979, pp. 1870-1875.

[44] Komaki, S., I. Horikawa, K. Morita, and Y. Okamoto, "Characteristics of high capacity 16 QAM digital radio system in multipath fading," IEEE Trans. on Comm., Vol. COM-27, No. 12, 1979, pp. 1854-1861.

[45] Morais, D.H., A. Sewerinson, and K. Feher, "The effects of the amplitude and delay slope components of frequency selective fading on QPSK, Offset QPSK and 8 PSK systems," IEEE Trans. on Comm., Vol. COM-27, No. 12, 1979, pp. 1849-1853.

[46] Rummler, W.D., "A new selective fading model: application to propagation data," BSTJ, Vol. 58, 1979, pp. 1037-1071.

[47] Lundgren, C.W., and W.D. Rummler, "Digital radio outage due to selective fading - observation vs. prediction from laboratory simulation," BSTJ, Vol. 58, 1979, pp. 1073-1100.

[48] Lakes, W.C., Jr., "An appropriate method to estimate an upper bound on the effect of multipath delay distortion on digital transmission," IEEE Trans. on Comm., Vol. COM-27, No. 1, 1979, pp. 76-81.

[49] Greenstein, L.J., and V.K. Prabhu, "Analysis of mutlipath outage with applications to 90 Mb/s PSK systems at 6 and 11 GHz," IEEE Trans. on Comm., Vol. COM-27, No. 1, 1979, pp. 68-75.

[50] Ruthroff, C.L., "Multiple-path fading on line-of-sight microwave radio systems as a function of path length and frequency," BSTJ, Vol. 50, 1971, pp. 2375-2398.

7. REFERENCES

[1] Zadeh, L.A., "Frequency analysis of variable networks," Proc. IRE, Vol. 38, 1950, pp. 291-299.

[2] Hubbard, R.W., "Characterization of multiplicative noise in propagating systems," IEEE Electromagnetic Compatibility Conference Record, Tucson, AZ, 1971, pp. 141-154.

[3] Linfield, R.F., R.W. Hubbard, and L.E. Pratt, "Transmission channel characterization by impulse response measurements," OT Report 76-96, U.S. Department of Commerce, Boulder, CO 80303, August 1976.

[4] Hubbard, R.W., R.F. Linfield, and W.T. Hartman "Measuring characteristics of microwave mobile channels," NTIA Report 78-5, U.S. Department of Commerce, Boulder, CO 80303, June 1978.

[5] Crawford, A.B., and W.C. Jakes, Jr., "Selective fading of microwaves," BSTJ, Vol. 31, 1952, pp. 68-90.

[6] DeLange, O.E., "Propagation studies at microwave frequencies by means of very short pulses," BSTJ, Vol. 31, 1952, pp. 91-103.

[7] Kaylor, R.L., "A statistical study of fading of super high frequency radio signals," BSTJ, Vol. 32, 1953, pp. 1187-1202.

[8] Beach, C.D., and J.M. Frecker, "A method for predicting interchannel modulation due to multipath propagation in FM and PM tropospheric radio systems," BSTJ, Vol. 42, 1963, pp. 1-36.

[9] Sunde, E.D., "Intermodualtion distortion in analog troposcatter systems," BSTJ, Vol. 43, 1964, pp. 399-535.

[10] Norton, K.A., G.A. Hufford, H.T. Dougherty, and R.L. Wilkerson, "Diversity design for within-the-horizon radio relay systems," NBS Report 8787, U.S. Department of Commerce, Boulder, CO 80303, April 1965.

[11] Makino, H., and K. Morita, "Design of space diversity receiving links," IEEE Trans. on Comm., Vol. COM-15, No. 4, 1967, pp. 603-641.

[12] Nomura, T., and T. Akiyama, "Characteristics of multipath propagation due to radio ducts," IECE, International Conference on Microwaves, Circuit Theory and Information (ICMCI), Tokyo, Japan, 1964.

[13] Turner, J., B.T. Easterbrook, and J.E. Golding, "Experimental investigation into radio propagation at 11.0-11.5 Gc/s," Proc. IEE, Vol. 113, No. 9, 1966.

[14] Sperjmeo, R.E., "Data results on nanosecond pulse propagation measurements over line-of-sight paths, OT Telecomm. Research and Engineering Report, TRER 37, November 1972.

[15] Meadow, R.W., R.E. Lingren, and J.C. Samuel, "Measurements of multipath propagation over a line-of-sight radio link of 4 Gc/s using frequency sweep technique," Proc. IEE, Vol. 113, 1966, pp. 41-48.

[16] Nomura, T., S. Morimoto, K. Morita, and T. Amekura, "Distortion due to fading in high-capacity FDM-FM transmission," Journal of IECE Japan, Vol. 50, 1967, pp. 983-989.

[17] Vogler, L.E., "Tropospheric pulse propagation," ESSA Technical Report ERL 125-ITS 88, Department of Commerce, July 1969.

[18] Barnett, W.T., "Multipath propagation at 4, 6, and 11 GHz," BSTJ, Vol. 51, No. 2, 1972, pp. 321-361.

[19] Bahler, G.M., "A study of frequency selective fading for a microwave line-of-sight narrowband radio channel," BSTJ, Vol. 51, No. 3, 1972, pp. 731-757.

[20] Bahler, G.M., "Selectively faded nondiversity and space diversity narrowband microwave radio channels," BSTJ, Vol. 52, No. 2 1973, pp. 239-261.

[21] Vigants, A., "Number and duration of fades at 6 and 4 GHz," BSTJ, Vol. 50, No. 3, 1971, pp. 815-841.

[22] Price, R., and P.E. Green, Jr., "A communication technique for multipath channels," Proc. IRE, Vol. 46, No. 3, 1958, pp. 555-570.

[23] Barrow, B.B., D.L. Abraham, W.W. Rowan, and E.M. Gallant, "The RAKE tropospheric scatter technique," International Scientific Radio Union (URSI), Fall Meeting, Boston, MA, September 1968.

[24] Phillips, G.J., "Characterization of tropospheric scatter channels by impulse response measurement," NATO AGARD Symposium on Tropospheric Radio Wave Propagation, Dusseldorf, West Germany, September 1970.

[25] Hubbard, R.W., "Measurements in microwave telecommunication systems using a pseudo-random noise (PN) probe," Proc. of the International Symposium on Measurements in Telecommunications, CNET, Lannion, France, October 1977.

that they can be fairly rapid. Delay changes have been observed on the order of a few ns/s. A rate of 1 ns/s would result in the 59 nulls (in our example) passing through the signal spectrum in approximately 4 s. The resulting dispersion could be serious, and it seems reasonable to speculate that it could result in short-term error bursts as those noted above.

Channel probe measurements may be the best available technique to develop the short-term statistics for existing meteorological conditions. The propagation in the LOS channel is influenced by the meteorology over the entire path, and a direct characterization beyond that suggested in Section 5 may be an impossible task. The data being developed from the probe measurements today include the rates of change of all factors listed in Table 3. We anticipate that these data will begin to answer the need for the short-term statistical characterization. They should provide the dynamic features for the model given in (3) that will represent more realistic conditions than the analytically tractable situation of a fixed delay. Specifically, we expect these statistics to play an important roll in implementing a channel simulator that is the subject of a companion paper at this symposium [60].

Table 1. Multipath Characteristics of Troposcatter Transmission

Important Parameters and Features:

- Standard deviation of delay-power spectrum (σ) used to characterize dispersion property
- Dispersion measurements reported in 2σ values
- Delay power spectrum modeled by a gamma function; greatest power from lower portion of common volume
- Digital performance dependent on $2\sigma/T$, where T is symbol length in transmission
- Intersymbol interference increases with increase in $2\sigma/T$
- Path length/propagation mode; ratio of specular to scatter power
- Effective vs potential common volume

Data Summary:

- 2σ measured over limited number of paths; range 0.03 to 0.38 us over paths 138 to 270 km (86 to 168 mi)
- Larger delay spread observed in mixed-mode propagation (diffraction/scatter)
- Seasonal variation in 2σ not significant
- Diurnal trend: 2σ larger during winter morning than afternoon
  2σ smaller during summer morning than afternoon
- Large volume of data available for path loss models; provides fairly reliable predictions
- Very small volume of 2σ data; no comparable prediction reliability
- Mixed mode propagation shows added dependence on differential delay; specular vs scatter components

Correlation Properties:

2σ vs L_p, 2σ vs N_s, 2σ vs k — Not significant over long samples

2σ vs N_s — Moderate (0.5 - 0.6) for longer sample

L_p vs N_s — High, on order 0.9

Legend:

L_p = path loss
N_s = surface refractivity
k = earth radius factor

Unknowns or Uncertainties:

- Maximum delay-spread values
- 2σ for longer paths
- 2σ variation with frequency
- 2σ vs effective/potential common volume
- Antenna foreground effects
- Common volume size; effective vs potential
- Meteorological values and variances; C_N^2 (scale of turbulence, temp., pressure, humidity)

Table 2. Summary of System Performance in LOS Channels

Author Organization Reference	Description of Tests and Test Parameters	Measured Parameters	Significant Results (IF = Improvement Factor)	Author Comments
1. Barnett Bell Telephone Laboratories [56]	8 PSK 76 Mb/s 6 GHz 42.5 km (26.4 mi) link Nondiversity (28 days) Space diversity (41 days) phase IF combiner Flat fade margin 46.3 dB for BER 10^{-3} BW = 30 MHz	BER in 1 s Spectrum sampling 1.1 MHz spacing Peak-to-peak amplitude dispersion in rec. spectrum	Digital radio "fragile" to multipath Modest in-band dispersion 0.2 dB/MHz sufficient to cause BER>10^{-3} at average power fade of 20 dB Nondiversity missed objective by factor of 9 Estimated diversity IF = 6 Introduced "effective fade margin" Ave. power fade poor indicator of performance	Engineering will require careful tradeoffs with: - path length - space diversity/antenna spacing - adaptive equalizers - sensitivity to selective fading For in-phase IF combining, if one signal is dispersive, the combiner output is likely to be dispersive
Ad[illegible] et al Bell N[illegible] Research [11]	8PSK 91 Mb/s 8 GHz 71 km (31.7 mi) link Nondiversity and space div. phase IF combiner Performance objective Prob. of outage 1.13×10^{-6} Flat fade margin 48 dB BW = 40 MHz	BER simultaneously in horn reflector, space div. parab., combined Spectrum sampling at 5 freq in 30 MHz	Multipath outage much higher than predicted from flat fade margin Nondiversity performance a factor of 700 from objective Primary cause of outage was in-band distortion from freq. selective fading Phase adaptive diversity combing very effective (IF = 38) Diversity combining with adaptive equalizer more effective (IF>20) Adaptive equalizer alone provided IF = 2	High degree of correlation between outage and amplitude slope dispersion No similar correlation with quadratic distortion Linear amplitude distortion dominates, delay distortion small Suggests linear slope equalizer
[illegible] et al Bell Northern Research and Telephone [12]	16 QAM 200 Mb/s 5 GHz Depolarization tests 3.8 ns 43 km (26.7 mi) link Nondiversity and space div. in-phase rf combiner Flat fade margin 39.7 dB for BER 10^{-6} BW = 40 MHz Channel slope and delay equalizer	BER @ 50 Mb/s Spectrum sampling at 3 frequencies BER simultaneously in nondiversity and space div.	In band dispersion of 4 dB (0.1 dB/MHz) causes outage of BER 10^{-3} Results for in band dispersion insensitive to value of delay for both diversity and nondiversity Outage probability in field tests corresponds to 5 dB in-band dispersion	Linear amplitude dispersion dominates Linear dispersion order of magnitude greater than quadratic Pointed out the worst-time phase condition in multipath
[illegible] et al Carleton Canada Univ. of Ottawa [57]	Computer simulated tests of BPSK, QPSK and 8 PSK System test of 45 Mb/s QPSK in laboratory Outage criteria BER 10^{-3}	S/N degradation due to amplitude and delay distortion	For equal signal spectrum: - QPSK least degraded/amp. dist. - OQPSK least degraded/delay dist. For equal bit rates: - QPSK least degraded/amp. dist. - OQPSK least degraded/delay dist.	Measured and simulated results for 45 Mb/s QPSK system compare favorably

Experiments to better characterize the LOS channel are in progress, along with system performance tests. The channel probe measurements at microwave frequencies are continuing, and are being extended to the millimeter range by the ITS and the Air Force [58, private communication]. We are also aware of similar work under way in the United Kingdom [private communication].

The most important unknown characteristic of the LOS channel appears to be its short-term dynamic nature. In Section 4, we discussed two examples of anamolous conditions that were reported in system performance tests. Recent measurements made by the ITS have also revealed a potential source of digital error that has not been previously reported. In these tests, a special burst-error analyzer was used to measure the performance of a 45 Mb/s 8 PSK system in a channel with very dynamic multipath features [26,27]. The test instrumentation and data acquisition methods are given in [27], but the results of these tests have not been published. We anticipate a report prior to the end of 1984 [59]. The interesting result from these tests is a disproportionately large number of error bursts that occur in very short intervals of time. Roughly, these bursts of error show 50% of the received bits to be in error when compared with the length of the burst (both parameters are measured). We do not know at this time how these short bursts of error are distributed with respect to each other. The analyses to date only show the density distributions of number of errors, and the length of the bursts in bits. The distributions do not shift significantly as the analysis period is changed over several hours. This suggests that the process may be stationary, but its cause is currently unknown. The data are being scrutinized with respect to the dynamic factors that can be identified from the measured impulse response data.

Our study of measured impulse response data from LOS circuits has shown that there are four important dynamic factors. These are listed in Table 3.

Table 3. The Dynamic Factors of Multipath

1. Change in relative magnitudes between direct and delayed components.
2. Change in relative phase between components.
3. Change in delay time between components.
4. Sudden development or collapse of a multipath component.

Factors 1 and 2 in Table 3 may appear to be redundant. However, we list them separately because 2 is a special case of 1 that can produce a rapid loss of synchronization in the data stream. To facilitate our discussion of the various effects, we present a simplified model of a two-path transmission channel in Figure 11. The magnitude of the theoretical frequency transfer functions for two different values of delay are sketched in this figure, based on the assumption of nearly equal magnitudes for the multipath signals. In addition, the function for a 10 ns delay is sketched for both an in-phase and phase-opposing condition. The spacing between adjacent frequency nulls (Δf_n) is given by

$$\Delta f_n = \frac{1}{\tau} , \tag{10}$$

where τ is the delay time between the multipath signals. The location of the nulls on the frequency axis is found from

$$f_n = \frac{n}{2\tau} , \tag{11}$$

where n is a series of either even or odd integers depending on the relative phase of the multipath components. If the components are out of phase, the series is even. For in-phase conditions, the series is odd. The factor n is thus equivalent to the $\frac{1}{2}$ Fresnel zones in reflective multipath, where λ is the wavelength of the carrier frequency. The value of n for the situations sketched in Figure 11 is indicated on the figure. For illustrative purposes, we have sketched a 20 MHz signal bandwidth centered on a carrier frequency of 7.35 GHz. Frequency selective fades due to a 10 ns delay and a 14 ns delay are seen to fall within this signal spectrum.

The first factor of Table 3 is very straightforward. As the relative magnitude of the components changes, the depth of the frequency selective fade changes. The second factor is illustrated with the two delay functions; an in-phase relationship places a null directly in the center of the signal pass band, and a phase-opposing condition has no appreciable effect.

It is sometimes helpful to consider the transfer function as a rubber band--one that retains its general shape in magnitude, but changes its null-to-null spacing and/or position along the frequency axis. In the case of a relative phase change, the function retains the null-to-null spacing, but the entire function moves along the frequency axis. When this occurs, it is obvious that one (or more) frequency nulls are likely to impinge on the signal pass band. This is a common occurrence in atmospheric multipath. As the time delay changes, the selective nulls also move along the axis. In this case, however, the "rubber band" function is anchored at zero frequency and it stretches or contracts as the delay time changes.

The latter case has an inherent characteristic that has been essentially overlooked in most studies reported in this paper. It is a potentially serious problem with respect to digital performance, and perhaps the most dynamic factor of those listed in Table 3. To illustrate this, we consider the two frequency selective fades illustrated in Figure 11 that are within the signal pass band. One of these is a result of a 10 ns in-phase delayed component, where n = 147. The second would result from a 14 ns in-phase reflected delay component where n = 206. In a multipath environment where the delayed component changes in delay with time, a number of the transfer function nulls will move through the signal spectrum. In the example we have chosen, we can assume that the delay time changes from 10 to 14 ns (or the reverse direction). From the values of n noted in Figure 11, one concludes that up to 59 null frequencies traverse the signal spectrum during the period in which the component delay changes take place. The effects of these are not well documented at present, but based on impulse response data we conclude

$$\ell_n = \left[\frac{2\Delta p\, d_1\, d_2 \times 10^3}{D}\right]^{1/2} = \left[\frac{0.6\tau\, d_1\, d_2}{D} \times 10^3\right]^{1/2}, \text{ (km)} \qquad (9)$$

where ℓ_n is the vertical distance from the straight-line path between antennas to the ellipse, d_1 and d_2 are the distances from each terminal to the point of calculation ($D = d_1 + d_2$), τ is the mean delay value, and Δp is the path length difference for the value of τ. Distances are in km, τ in ns, and Δp in meters. This method is much simpler than ray tracing, and it allows for nonuniform layer conditions.

The discussion above outlines the application of meteorological data, first in a statistical sense, and secondly in a discrete sense for specific conditions. In order to provide a complete model that includes the meteorology for prediction purposes, there is not sufficient data available. Before installing any given system over any path, one would like to predict its performance. With the present models illustrated by Figure 9, we can only estimate the upper bound, and then only with some uncertainty. However, if one had a statistical model such as that presented in Eq. (7) that was accurate for the particular location of the path, one could predict the performance of a system with fair accuracy. Knowing the true distribution of τ_m over the performance interval of interest (hour, day, month, etc.), coupled with a confident prediction that this condition will exist, one can forecast the long-term performance. To carry this proposition to any region of interest would be a monumental task. There are, however, data available that permit some gross modeling of this type.

Two recent studies by the ITS address the regional aspects of the meteorological data base. Reference [52] presents a statistical compilation of data to predict the likelihood of key parameters associated with ducting, as well as the annual and worst-month occurrences of elevated ducting. The data were taken from 107 observing stations spread throughout the United States, and consists of approximately 5 years of radiosonde recordings. Humidity measuring elements in a radiosonde are known to be slow in response. Thus, reference [53] develops a correction factor for the radiosonde data. Applying the correction to 5 years of data from Washington, D.C., a 25% increase in the annual occurrence of elevated ducts was predicted over the earlier uncorrected data. This one example exhibits the high degree of uncertainty in predicting elevated ducting in a given region, if indeed any applicable summary of data exists. The regional data in [52] is a good starting point.

Finer grain distributions are needed, like those in [51], for many paths where the path delays are measured. We desire probability distributions that are applicable in a given location along with estimates of the probability that certain multipath conditions will exist on a regional basis. These prediction techniques must eventually be focused on specific time periods. In this discussion, and that in Section 4, we have referred to the prevalent concept of the "worst fading month." This period of time is perhaps more appropriate for the analog channels than it is to the new era of digital communications. Cases where anamolous conditions effect the digital channel over shorter periods of time are more pronounced, and require a finer scale of resolution than monthly statistics. This subject is discussed further in Section 6.

6. PROGRESS FOR THE 1980's

Previous sections have presented a review of the multipath problem and its impact on digital communication systems up to the beginning of the 1980's. This section discusses what we feel is lacking in our knowledge. The section concludes with an outline of current investigations that should provide new data and insight.

Multipath measurements in the time domain are continuing to be made by the Air Force, the ITS, and others. Some of these efforts are in association with system performance measurements and are supported with meteorological data. The experiments for the troposcatter channel are primarily under the auspices of the Air Force JTCO, and are scheduled to continue for several years. The multipath statistics are generally better known for this channel than they are for the LOS channels. However, the early troposcatter characterization (summarized in Section 4) underestimated the delay spreads, and the measurements did not provide the dynamic data necessary for future developments. In addition, no meteorological data were taken. Current study and experimental programs devoted to the short tactical troposcatter channel are treating these deficiencies. New and improved probing techniques are being applied to channel measurements in the tactical test program, and meteorological data are being acquired.

The troposcatter channel should be more amenable to meteorological measurements for fine scale structure, since (presumably) the common volume is the most important area and can be defined fairly readily in the atmosphere. Its height above the surface may be the restricting factor for conventional measurements. However, a program is under way by the AFGL to provide airborne measurements using refractometers in the region of the common volumes. Recent work performed by the National Oceanic and Atmospheric Administration (NOAA) has shown promise in remote sensing of the common volume, using FM-CW and acoustic radar [54]. Correlations between these measurements and probe or RAKE data should be forthcoming. There does appear to be a serious lack of information concerning the delay-spread values for longer strategic scatter channels. Link upgrade analyses performed recently [55] for many of these links have included only estimated delay-spread parameters, from computer models that by themselves have not been verified. Delay-spread measurements have been made recently on two European links where diffraction components were found to change the expected values [56]. We would recommend that more measurements be made to provide impulse response data for these channels, prior to their conversion from analog to digital transmission. Models of the troposcatter channel have improved [DCA private communication, 57], and they provide more realistic estimates of the delay spread. However, more verification of these models is needed, and meteorological parameters are required to facilitate and confirm the latest model given in [57].

[illegible] and consideration of the launch angle for rays penetrating the layer, a "cap" may be placed on the estimate for maximum delay. It follows that the f^2 dependence is limited to approximately [illegible] or less in path length, and a linear dependence is applicable to longer paths. This result helps to confirm the conclusion reached above, and the relevance of the boundaries shown in Figure 8.

[illegible] paper [25] also develops a probability distribution of path-length difference for multipath fading conditions, based on a two-ray multipath model given in [26]. It is shown to compare [illegible] with measured distributions on two paths in Japan, but the confidence of the fit is not presented. The reference data were taken from four different years between 1956 and 1963. The probability [illegible] is given as a normalized function,

$$P(\tau p) = \frac{11.3\ P_R(4\ \text{GHz})}{P_R}\ \tau p^{-2.4}\ , \tag{7}$$

[illegible]

$$P_R = Q\ (\frac{f}{4})^{1.\cdot}\ \bar{h}^{3.5}\ , \tag{8}$$

[illegible], and P_R (4 GHz) is the value of Eq. (8) at f = 4 GHz. The factor Q is a constant that is [illegible] appropriate path terrain conditions: 2.0×10^{-6} for mountains, 5.1×10^{-7} for smooth terrain, and [illegible] $\times 10^{-}$ for an overwater path. In the last expression, $\bar{h}$ is an average path height for the [illegible] path. This form of distribution for multipath delays is a statistic that is essential to [illegible] model and predict the LOS channel. The data sample used to derive this model statistic is [illegible] adequate in length, but it does not contain the path variability necessary to provide confidence [illegible] other regions. Similar data must be developed to extend this or similar models to other regions of the world.

Both the channel and meteorological models noted above are based on ray-tracing theory. The calculations for specific conditions over a path are tedious, unless a computer program is available. The computer methods are generally not adequate because of limitations on the refractive data they can accommodate. For example, those known to this author are restricted to a single profile, and it must be assumed that the refractive structure is uniform over the path. This is frequently not the case, as we see in the following discussion.

In [26,27] we have shown that the measured values of delay from atmospheric multipath correspond with graphical analyses of the link profile and the refractive structure. An example of this is shown in Figure 10. Figure 10(a) shows the refractive index profiles measured by radiosonde at the terminals of a test link in southern California. Two digital radios were under test at this time. Their performance was good during the morning hours, when the refractive layer was at a higher elevation. The layer was moving downward at that time. The performance of both radios began to degrade noticeably around 1800 Z on this date. The refractive profiles measured at both terminals between 1600 and 2000 Z show that the base of the inversion had lowered to an elevation between 600 and 800 m, and it was approximately 200 m lower at the San Nicolas Island (SNI) terminal. In addition, both afternoon profiles show a subrefractive gradient near the surface. A near standard gradient is seen from the base of the layer down to approximately 150 m to 250 m. The elevations of the radio terminals at Laguna Peak (LP) and SNI are shown on the ordinate.

A probability density of the delays measured with the PRBS probe during the afternoon hours showed peaks at delay values of 5 and 14 ns; the highest density and component magntiude was observed at 14 ns. These data can be directly compared with the channel conditions where the refractive structure is known. Figure 10(b) illustrates the above path conditions. The superrefractive layer is shown in the shaded area, plotted on the basis of a 4/3 (standard refractivity) earth radius, which also applies to the solid-line surface profile. The radio terminals are within the standard refractivity region, and the direct-path radio rays are plotted as straight lines. For the measured delay-spread values of 5 and 14 ns, two loci (half-ellipse for each) have been plotted on the figure. These Fresnel ellipsoids define the locus of all points from which multipath signals could emanate with the given delay value, if the signals were reflected. Note that the 14 ns ellipse is tangential to the refractive layer, a clear indication that the layer is the source of the multipath with that delay value.

The source of the shorter 5 ns delay is not as well defined. We note that this ellipse does not correspond to any meteorological feature, and it is not tangential to the 4/3 earth profile. The subrefractive gradients at the lower elevation in the radiosonde data become important in this case. Both [illegible] soundings show a significant, positive gradient that will affect the propagation near the [illegible] surface. A method of analyzing the subrefractive region is included in Figure 10. First, the boundary between the k = 4/3 region and the subrefractive regions has been sketched near the elevation of 300 meters. Second, we sketched the half-power beamwidths of the antennas (lower bounds) within the [illegible] of the figure. The intersection of these lines with the boundary for the subrefractive [illegible] defines a new propagation path. Radio rays from the terminals would follow straight [illegible] within the standard refractive region. At the intersection with the subrefractive re[illegible] would [illegible] the top of the lower atmosphere before rising again to the antennas. At these points, [illegible] a secondary propagation path. The new path would exist only within the subrefractive [illegible] refractive profile may be computed. Note that the secondary path is roughly [illegible] the true path, and for this reason the effective earth profile will be considerably [illegible] the actual profile. The modified earth-surface profile for the subrefractive path is [illegible], plotted for a k = 1 (typical of moderate subrefractivity), [illegible] the two solar loci correspond to the modified surface. The important result [illegible] that this graphical approach can be effectively used to find at least a cross correlation between multipath delays and the atmospheric/surface profiles. Other examples may be found [illegible], including a condition where the link terminals are within a strong ducting layer. The [illegible] to this graphical method can be plotted directly on the modified profile plot to aid in

$$\tau_m = 3.7 \left(\frac{D}{20}\right)^3 \text{ ns}, \qquad (4)$$

where D is the path length in miles. This expression was combined with Eq. (3) in [48] to derive a bound for the "breaking point" of several digital systems. The breaking point was defined as that condition where the multipath delay distortion would cause a BER $\geq 10^{-3}$. This condition was established in the laboratory for a ratio of τ/τ_s as a function of fade depth, where τ_s is the symbol duration of the system tested. Carrying the development further, an estimate for the upper bound for system failure in the "worst fading month" was derived. The work in [49] presents similar curves for a yearly estimate, assuming multipath fading in the three summer months, and none for the balance of the year.

The striking conclusion from this modeling is that the length of an unprotected channel for the common carrier network would be limited to the order of 24 km (15 mi) or less to meet the so called "short-haul objectives." This is a very restrictive result, imposed entirely by multipath fading. However, each author has indicated the lack of adequate data to accurately characterize the multipath fading statistics. Imperical data are essential to verify the model and to provide the foundation for the design of adaptive techniques that are capable of improving the performance.

The ITS has been conducting measurements of multipath in LOS circuits for several years, using the PRBS channel probe mentioned previously. This work is summarized in Section 6. However, before leaving this discussion, we will present some results that are relevant to this model, and that pertain to the outage predictions given in [48,49].

The multipath delays to be expected in a LOS link as a function of path length have been of concern for some time. The value given by Eq. (4) was developed in a comprehensive treatment in [50], based on a meteorological model that gives an accurate description of the physical basis of the multipath problem. It treats the problem analytically, by considering an elevated ducting layer in the path that causes multipath signals by refraction. The ITS probe measurements were made over a number of paths in Europe and in the United States, each of which were known to have multipath generated by such elevated layers. The probe impulse response data were analyzed for statistical distributions of the measured delays. From these, we have compiled the maximum delay and the median delay values for each distribution. A plot of these data as a function of path length departs from the theoretical delay boundary computed from Eq. (4). This is illustrated for the measured maximum values in Figure 8.

The boundary lines plotted in Figure 8 are based on a simplified geometry. For example, a heuristic argument can be made that any multipath component (of significant magnitude) will have an angle of arrival within the half-power beamwidths of the antennas. Therefore, for any uniform refractivity that is not substandard, a pseudo-maximum path-length difference between a direct and multipath ray can be calculated from

$$\Delta p = \frac{D \times 10^3}{2} \tan^2 \frac{\theta}{2} \text{ (meters)}, \qquad (5)$$

where θ is the half-power beamwidth in degrees, and D is the path length in km. The geometry assumes that the intersection of the antenna beams is at midpath, or D/2. Delay time is approximately 3.3 ns/m, so that the path delay for Eq. (5) may be written as

$$\tau_m = 1668\, D \tan^2 \frac{\theta}{2} \text{ (ns)}. \qquad (6)$$

We note that the delay depends linearly on D, in contrast to the D^3 dependence in Eq. (4). The data plotted in Figure 8 are the maxima for the data base. Some measurements were made using 1.2 m (4 ft) parabolic antennas, and others with 2 m (10 ft) paraboloids. These data points are distinguished in the figure, and half-power locii based on Eq. (6) for each set of data are shown. There is an empirical division between the two sets of data at approximately D = 100 km.

The measured values of delay shown in Figure 8 suggest that a delay boundary given by Eq. (6) is much more practical than that of Eq. (4), particularly for paths longer than about 20 km. We have used this boundary for one of the system outage functions given in [48], to test the impact that the linear D dependence would have on the performance predictions. The results are plotted in Figure 9. The modified curve shows that if the linear path length dependence is realistic, the maximum path length imposed by the performance objective would be almost doubled. More important, however, are the nearly two orders of magnitude improvement in the prediction of outage for longer LOS paths.

Carrying this comparison one step further, we apply a diversity improvement factor of 20 (an arbitrary value between those reported in Table 2) to the nondiversity prediction. This result is also plotted in Figure 9, showing another significant increase in the maximum path length, and another order of magnitude decrease in outage time for the longer paths. There remains a considerable uncertainty about these results, ranging from the analytical assumptions made in [48,49] to the statistical significance of the improvement factor used. It is considerably larger than that reported in the BTL tests, and smaller than that reported by Bell-Northern. These speculative results have been found to have more basis in fact with respect to path length in recent meteorological modeling. We discuss this in the following.

In the summary for this paper, we stated that the morphology of the multipath phenomenon must include the meteorological aspect. The most important feature is that of the elevated layer in the atmosphere that is responsible for the multipath signal, as shown in [50]. A considerable amount of work has been devoted to this atmospheric feature with respect to radio propagation. Time and space do not permit us to provide any comprehensive review of this subject. We do wish to include enough information to illustrate the important parameters and the need for additional investigations. A paper that illustrates basic requirements for meteorological data also appeared in the IEEE special issue on digital radio [51]. Using ray tracing methods, the authors first developed estimates of path length differences in LOS links in relation to ducting layers in the atmosphere. Surface gradients and the gradient intensity of the layers are parameters for the estimates given as functions of path length. The cubic dependence on D is noted in the development, as discussed earlier in this section. However, with finite

2.0 ELECTROMAGNETIC MODELING OF FORESTS

The electromagnetic modeling of forests can proceed from two fundamental points of view: the first describes the forest medium by a (possibly time-variant and/or anisotropic) stochastic permittivity which is spatially continuous; the second describes it by a (possibly time-variant and/or anisotropic) stochastic permittivity which is spatially discrete (localized). Theories based upon the former usually prove considerably more tractable analytically and have been applied successfully in studies of radiowave propagation through turbulent and randomly inhomogeneous atmospheres. Theories based upon the latter have been applied with similar success in studies of radiowave propagation through atmospheric hydrometeors and particulates. However, because the characterization of a spatially stochastic medium as continuous or discrete is clearly only one of resolution or scale, and because theories based upon a spatially continuous distribution of permittivity have proven more tractable, radiowave propagation through discrete random media is more often studied as though the media were continuous.

Electromagnetic modeling of forests has been studied from both points of view. In fact, the earlier HF/VHF radiowave propagation models [3,7] were predicated upon an assumed lossy, dielectric forest continuum and experimental studies were conducted to determine appropriate values for the dielectric constant and conductivity of the assumed continuum. Unfortunately, although these earlier models were undeniably successful in describing the behavior of the propagating radiowaves, they were unable to relate the dielectric constant and conductivity of the assumed continuum to directly measurable biophysical parameters of the forest (e.g., tree trunk number density, tree trunk diameter) in more than a qualitative way. Further, in the UHF band, where incoherent scattering can be significant, it becomes necessary to statistically characterize the spatial fluctuations of the forest's permittivity. Because such a characterization for an assumed forest continuum would be heuristic at best and also suffer from an inability to be related to directly measurable biophysical parameters, the electromagnetic model described in this paper is based upon a description of the forest as a discrete random medium.

2.1 SCATTERING IN DISCRETE RANDOM MEDIA

The scattering of electromagnetic waves in discrete random (dielectric) media can be studied using two fundamental approaches: the first, exemplified by Twersky's theory [2], is based upon Maxwell's equations and so is mathematically rigorous in the sense that, in principle, all multiple scattering, diffraction, and interference effects can be included; the second, exemplified by the radiative transport theory [20], is based upon the conservation of energy but is heuristic, accounting for multiple scattering but not for diffraction and interference effects. Because of the intrinsic complexity of multiple scattering, these two distinct approaches should not be considered competitive, but rather complementary.

The theoretical approach employed in this paper is that of Twersky which proves fairly tractable in relating first-order statistics of the propagating radiowave to the biophysical parameters of the forest. Second-order statistics prove considerably more difficult to derive and, for these, attention is focussed on scattering behavior in the Rayleigh (low frequency) regime. Complementary results, not described here, have been obtained using radiative transfer theory.

2.1.1 TWERSKY'S SCATTERING MODEL [2]

According to Maxwell's equations

$$\nabla \times \underline{E}(\underline{x}) = -j\omega\mu \underline{H}(\underline{x}) \tag{1}$$

$$\nabla \times \underline{H}(\underline{x}) = j\omega \varepsilon(\underline{x}) \underline{E}(\underline{x}) + \underline{J}(\underline{x}) \tag{2}$$

where $\underline{E}(\underline{x})$ and $\underline{H}(\underline{x})$ represent, respectively, the electric and magnetic fields within the scattering region, $\underline{J}(\underline{x})$ represents the impressed current distribution of the transmitting antenna, and $\varepsilon(\underline{x})$ represents the relative (complex) permittivity of the unbounded scattering medium all as a function of the position vector x. In writing Eqs. (1) and (2) a complex harmonic time dependence $\exp(j\omega t)$ has been assumed and suppressed. In order to account for the discrete character of ,say, N scatterers, let

$$\varepsilon(\underline{x}) = 1 + \varepsilon_0 + \sum_i \varepsilon_i(\underline{x}) \tag{3}$$

where ε_0 is the susceptibility of the surrounding medium (which for air is about 0.0003),and $\varepsilon_i(x)$ is the susceptibility of the i-th scatterer, so defined that

$$\varepsilon_i(\underline{x}) \begin{cases} \varepsilon_i & \text{within the i-th scatterer} \\ 0 & \text{outside the i-th scatterer} \end{cases} \tag{4}$$

Note that the shape and orientation of each scatterer is implicitly defined through $\varepsilon_i(x)$.

From Maxwell's equations, the wave equation for the electric field within the unbounded medium of discrete scatterers can be shown to be

$$\nabla\times(\nabla\times\underline{E}(\underline{x})) - k_o^2\varepsilon_a\underline{E}(\underline{x}) - \sum k_o^2\chi_i(\underline{x})\underline{E}(\underline{x}) = -j\omega\mu_o\underline{J}(\underline{x}) \tag{5}$$

where

$$\varepsilon_a = 1 + \chi_a \tag{6}$$

is the relative (complex) permittivity of the surrounding medium and k_o is the free-space wave-number (ω/c).

Consider, now, the electric field within the unbounded medium to consist of two components: the electric field $\underline{E}_i(\underline{x})$ which would exist in the absence of all scatterers due to the impressed current $\underline{J}$, and the residual scattered electric field $\underline{E}_s(\underline{x})$. The total electric field $\underline{E}(\underline{x})$ could then be written as

$$\underline{E}(\underline{x}) = \underline{E}_i(\underline{x}) + \underline{E}_s(\underline{x}) \tag{7}$$

Substitution of Eq. (7) into Eq. (5) suggests that

$$\nabla\times(\nabla\times\underline{E}_i(\underline{x})) - k_o^2\varepsilon_a\underline{E}_i(\underline{x}) = -j\omega\mu_o\underline{J}(\underline{x}) \tag{8}$$

and

$$\nabla\times(\nabla\times\underline{E}_s(\underline{x})) - k_o^2\varepsilon_a\underline{E}_s(\underline{x}) = -j\omega\mu_o\sum\underline{J}^i(\underline{x}) \tag{9}$$

where the current induced in the i-th scatterer

$$\underline{J}^i(\underline{x}) = j\omega\chi_i(\underline{x})\underline{E}(\underline{x}) \tag{10}$$

is found to depend upon the total electric field $\underline{E}(\underline{x})$. Now if the scattered field attributable to the i-th scatterer alone does not by itself contribute significantly to the currents induced in any one of the other (N-1) scatterers (the so-called independent scattering approximation), then the current induced within the i-th scatterer can be related to the electric field $\underline{E}(\underline{x})$ incident upon it by the alternate relation

$$\underline{J}^i(\underline{x}) = (j/\omega\mu_o)\int d\underline{x}'t_i(\underline{x},\underline{x}')\underline{E}_i(\underline{x}') \tag{11}$$

where $t(\underline{x},\underline{x}')$ is the so-called dyadic transition kernel of the i-th scatterer, and Eq. (11) defines $t(\underline{x},\underline{x}')$ implicitly.

Substitution of Eq. (11) into Eq. (9) reveals, in consonance with Eqs. (7) and (8), that the total electric field within the unbounded medium of discrete scatterers satisfies the wave equation

$$\nabla\times(\nabla\times\underline{E}(\underline{x})) - k_o^2\varepsilon_a\underline{E}(\underline{x}) - \sum\int d\underline{x}'t_i(\underline{x},\underline{x}')\underline{E}_i(\underline{x}') = -j\omega\mu_o\underline{J}(\underline{x}) \tag{12}$$

Because the dyadic transition kernel $t(\underline{x},\underline{x})$ depends upon the orientation and position of the i-th scatterer the electric field $\underline{E}(\underline{x})$ is a random variable.

2.1.2 THE COHERENT (MEAN) FIELD

The mean electric field $\langle\underline{E}(\underline{x})\rangle$ may be determined by averaging Eq. (12) over an ensemble of scatterers having prescribed orientation and position statistics. The mean electric field thus satisfies the wave equation

$$\nabla\times(\nabla\times\langle\underline{E}(\underline{x})\rangle) - k_o^2\varepsilon_a\langle\underline{E}(\underline{x})\rangle - \sum\int d\underline{x}'\langle t_i(\underline{x},\underline{x}')\underline{E}_i(\underline{x}')\rangle = -j\omega\mu_o\underline{J}(\underline{x}) \tag{13}$$

where the angular brackets $\langle\ \rangle$ denote ensemble averaging over the 6N-dimensional joint probability density function for the orientation (3 degrees of freedom per scatterer) and position(3 degrees of freedom per scatterer) of all N scatterers. This averaging is significantly simplified by introducing the Foldy approximation

$$\underline{E}_i(\underline{x}) \approx \langle\underline{E}(\underline{x})\rangle \tag{14}$$

so that

$$\langle t_i(\underline{x},\underline{x}')\underline{E}_i(\underline{x}')\rangle \approx \langle t_i(\underline{x},\underline{x}')\rangle\langle\underline{E}(\underline{x}')\rangle \tag{15}$$

and by assuming that the orientation and position of each scatterer is independent of all others. In this case,

$$\int d\underline{x}'\langle t_i(\underline{x},\underline{x}')\underline{E}_i(\underline{x}')\rangle = \int d\underline{x}'\int\int p_i(\underline{\xi}_i,\underline{\Omega}_i)t_i(\underline{x},\underline{x}')\langle\underline{E}(\underline{x}')\rangle \tag{16}$$

where $p_i(\underline{\xi}_i,\underline{\Omega}_i)$ is the joint probability density function for the position ($\underline{\xi}_i$) and orientation ($\underline{\Omega}_i$) of the i-th scatterer. If the orientation and position are statistically independent so that

$$p_i(\underline{\xi}_i,\underline{\Omega}_i) = p_i(\underline{\xi}_i)p_i(\underline{\Omega}_i) \tag{17}$$

then the dyadic transition kernel $t_i(\underline{x},\underline{x}')$ can be averaged with respect to orientation (thence denoted by $t_i(\underline{x},\underline{x}')$) and translated with respect to position so that (with a slight abuse of notation)

$$\int d\underline{x}'\langle t_i(\underline{x},\underline{x}')\underline{E}(\underline{x}')\rangle = \int d\underline{\xi}_i\int d\underline{x}'t_i(\underline{x}-\underline{\xi}_i,\underline{x}'-\underline{\xi}_i)\langle\underline{E}(\underline{x}')\rangle \tag{18}$$

If all N scatterers are identical, then

$$t_i(\underline{x},\underline{x}') = t(\underline{x},\underline{x}') \tag{19}$$

and the substitution of Eqs.(18) and (19) into Eq. (13) yields

$$\nabla\times(\nabla\times\underline{E}(\underline{x})) - k_0^2\,\varepsilon_a\underline{E}(\underline{x}) = -\int ds\,\rho(\underline{s})\int d\underline{x}'\,\bar{t}(\underline{x}-\underline{s},\underline{x}'-\underline{s})\cdot\underline{E}(\underline{x}') = -j\omega\mu\,\underline{J}(\underline{x}) \tag{20}$$

where

$$\rho(\underline{s}) = Np(\underline{s}) \tag{21}$$

is the number density of the scatterers as a function of position $\underline{s}$.

Inasmuch as the scatter region is assumed unbounded and statistically homogeneous, the mean wave equation (Eq. (20)) may be Fourier transformed to obtain

$$\nabla\times(\nabla\underline{E}(\underline{\cdot})) + k^2[\varepsilon_a I + [(2\pi)^3\rho/k_0^2]\tilde{t}(\underline{\cdot},\underline{\cdot})]\cdot\underline{E}(\underline{\cdot}) = 0 \tag{22}$$

where I is the unit dyadic and $\tilde{t}(\underline{\cdot},\underline{\cdot})$ is the double Fourier transformation of $t(\underline{x},\underline{x}')$ so defined that

$$\tilde{t}(\underline{\cdot},\underline{\cdot}') = \int t(\underline{x},\underline{x}')\exp[j(\underline{\cdot}\cdot\underline{x}+\underline{\cdot}'\cdot\underline{x}')]d\underline{x}d\underline{x}' \tag{23}$$

Through a comparison of Eq. (22) with the corresponding equation for a continuous, homogeneous medium (set $\rho=0$ in Eq. (22)), it is apparent that so far as the mean wave is concerned, the unbounded medium of discrete scatterers behaves as a continuous homogeneous medium with an effective dyadic permittivity of

$$\varepsilon = \varepsilon_a I + [(2\pi)^3\rho/k_0^2]\tilde{t}(\underline{\cdot},\underline{\cdot}) \tag{24}$$

Note that, in general, the equivalent continuous medium is anisotropic and spatially dispersive. The effective dyadic susceptibility attributable to the scatterers is

$$\underline{\chi} = [(2\pi)^3\rho/k_0^2]\tilde{t}(\underline{\cdot},\underline{\cdot}) \tag{25}$$

and is directly proportional to the number density of the scatterers.

Eq. (22) can also be used to establish a dispersion relation. If the equivalent medium is uniaxially anisotropic so that

$$\varepsilon = \varepsilon_t(\underline{x}'\underline{x}'' + \underline{y}'\underline{y}'') + \varepsilon_z\underline{z}'\underline{z}' \tag{26}$$

then for a vertically-polarized (z-polarized) electric field propagating in a direction parallel to the x-y plane ($\underline{\cdot}_z = 0$) the propagation constant is

$$\kappa_v = k_0\sqrt{\varepsilon_z} \tag{27}$$

For a horizontally polarized electric field propagating in a direction parallel to the x-y plane ($\underline{\cdot}_z=0$) the propagation constant is

$$\kappa_h = k_0\sqrt{\varepsilon_t} \tag{28}$$

If $|\chi| \ll 1$, the specific attenuation of the mean wave attributable to the scatterers is

$$\alpha_v = (8.686)[(2\pi)^3\rho/2k_0]\tilde{t}''(k_0\underline{\kappa}_t^0, k_0\underline{\kappa}_t^0) \tag{29}$$

for vertical polarization, and for horizontal polarization

$$\alpha_h = (8.686)[(2\pi)^3\rho/2k_0]\tilde{t}''(k_0\underline{\kappa}_t^0, k_0\underline{\kappa}_t^0) \tag{30}$$

where $\underline{\kappa}_t^0$ is a unit vector in the direction of propagation and the double prime denotes the imaginary part.

2.1.3 THE INCOHERENT (FLUCTUANT) COMPONENT

It has been noted previously that the electric field E(x) is a random variable. As such, it can be represented as the sum of its mean $\langle E(x)\rangle$ and residual, zero mean, fluctuating component $\tilde{E}(x)$, i.e.

$$\underline{E}(\underline{x}) = \langle\underline{E}(\underline{x})\rangle + \tilde{\underline{E}}(\underline{x}) \tag{31}$$

When the number of independent, randomly-positioned scatterers contributing to the resultant electric field E(x) is large, it may be surmised as a consequence of the central limit theorem that the zero-mean, fluctuating component $\tilde{E}(x)$ is representative of a gaussian random process. Under this hypothesis, $\tilde{E}(x)$ can be completely characterized, at least for time-invariant scattering configurations, by its joint space-frequency correlation function. It is this function which provides information on the effective bandwidth, the delay spread, and the coherence bandwidth of the channel.

The mean power associated with the total electric field is usually characterized by the electric field intensity

$$I = \langle\underline{E}(\underline{x})\cdot\underline{E}^*(\underline{x})\rangle \tag{32}$$

which, as a consequence of Eq. (31), may be written in the form

$$I = \langle\underline{E}(\underline{x})\rangle\cdot\langle\underline{E}^*(\underline{x})\rangle + \langle\tilde{\underline{E}}(\underline{x})\cdot\tilde{\underline{E}}^*(\underline{x})\rangle \tag{33}$$

The intensity associated with the mean (coherent) field component

$$I_c = \langle\underline{E}(\underline{x})\rangle\cdot\langle\underline{E}^*(\underline{x})\rangle \tag{34}$$

can be determined from Eq. (20). Determination of the intensity associated with the

fluctuating (incoherent) field component

$$I_i = \langle \tilde{\underline{E}}(\underline{x}) \cdot \tilde{\underline{E}}^*(\underline{x}) \rangle \tag{35}$$

requires an equation analogous to Eq. (20). For example, in a two-dimensional, unbounded medium of parallel circular cylinders of radius a and relative permittivity ϵ_r, the total field intensity in the Rayleigh (low frequency) regime due to a parallel line source satisfies the equation

$$I(\underline{x}_t) = I_c(\underline{x}_t) - \gamma \int d\underline{s}_t |G(\underline{x}_t - \underline{s}_t)|^2 I(\underline{s}_t) \tag{36}$$

where,

$$I_c(\underline{x}_t) = \omega^2 \mu_0^2 J_z^2 |G(\underline{x}_t)|^2 \tag{37}$$

$$\gamma = \pi^2 (ka)^4 |\epsilon_r - 1|^2 \tag{38}$$

$$G(\underline{x}_t) = -(j/4) H_0^{(1)}(k \underline{x}_t) \tag{39}$$

$$k = k_0 \sqrt{1 + \pi^2 a^2 (\epsilon_r - 1)} \tag{40}$$

The normalized intensity

$$I_n(\underline{x}_t) = I(\underline{x}_t)/I_c(\underline{x}_t) \tag{41}$$

is plotted in Fig. 1. The ratio of the incoherent intensity to the coherent intensity

$$\gamma^2 = I_c(\underline{x}_t)/I_i(\underline{x}_t) \tag{42}$$

is an important parameter which, under the gaussian hypothesis, completely describes the statistical distribution of the total electric field $\underline{E}(\underline{x})$.

2.2 UNBOUNDED FOREST MODELS

The scattering theory for discrete random media which is described in Section 2.1 has been applied to radiowave propagation through forests. In applying this theory, the forest is considered initially as an unbounded medium of randomly-oriented and -positioned canonical scatterers representative of various vegetative components. For the unbounded case, a simple plane-wave solution to the mean wave equation (Eq. 20) can be found. This allows direct and explicit calculation of propagation parameters and attenuation rates without introducing the complicating features of sources and boundaries.

2.2.1 CANONICAL FOREST SCATTERERS

The scattering theory for discrete random media described in Section 2.1 has been applied to radiowave propagation through an unbounded medium of canonical scatterers representative of various vegetative components. Tree trunks are modeled as infinitely-long, parallel, circular, dielectric cylinders; branches as finitely long, circular, dielectric cylinders; and leaves as flat, circular, dielectric discs. For each of these canonical scatterers, an expression has been found which relates the dielectric constant, size, shape, and orientation of the scatterer to its dyadic scattering amplitude $\underline{f}(\underline{o},\underline{i})$. The dyadic scattering amplitude is defined implicitly by the relation

$$\underline{e}_s(\underline{x}) = \underline{f}(\underline{o},\underline{i}) \cdot \underline{q}^i \exp[-jk_0(\underline{o}\cdot\underline{x})]/|\underline{x}| \tag{43}$$

where $\underline{e}_s(x)$ is the field scattered in direction $\underline{o}$ due to an incident plane wave of unit amplitude and polarization $\underline{q}^i$ travelling in direction $\underline{i}$. The dyadic scattering amplitudes have been related to the double Fourier transform of the transition operator kernel using the relation

$$\underline{f}(\underline{o},\underline{i}) = 2\pi^2 (\underline{I} - \underline{o}\underline{o}) \cdot \tilde{\underline{t}}(k_0\underline{o}, k_0\underline{i}) \cdot (\underline{I} - \underline{i}\underline{i}) \tag{44}$$

The Fourier transform $\underline{t}(\cdot,\cdot)$ is then used in Eq. 24 to determine (for the coherent field) the effective dyadic permittivity of an equivalent, continuous, unbounded medium which is subsequently employed in Section 2.3 to establish constitutive relations for the coherent field of a radiowave propagating within a stratified forest. Explicit expressions for the dyadic scattering amplitudes of the canonical scatterers representing trunks, branches, and leaves can be found, respectively, in Eqs. (3-1-1), (3-2-16), and (3-3-30) of [1].

2.2.2 PERMITTIVITY OF WOOD AND LEAVES

The electrical properties of green wood and leaves can be specified in terms of their relative permittivity ϵ_ℓ and permeability μ_ℓ. As with most biological materials, the relative permeability μ_ℓ can be set equal to unity. The relative permittivity ϵ_ℓ is complex and, for the complex exponential time dependence $\exp(j\omega t)$, can be written in the form

$$\epsilon_\ell = \epsilon'_\ell - j\epsilon''_\ell \tag{45}$$

where ϵ'_ℓ and ϵ''_ℓ represent, respectively, the real and imaginary parts of the permittivity ϵ_ℓ. The imaginary part is proportional to the conductivity σ through the relation

$$\epsilon''_\ell = \sigma/\omega\epsilon_0 \tag{46}$$

where ϵ_0 is the permittivity of free space. The real part ϵ'_ℓ is often called the dielectric constant: the imaginary part ϵ''_ℓ, the loss factor.

Although the electrical properties of wood has been the subject of numerous studies, relatively few measured data pertain to green wood and leaves, and fewer still to frequencies above 100 MHz. The most appropriate appear to be those of Broadhurst [14]. These studies suggest that, firstly, the permittivity of green wood is not strongly species-dependent, although, taken as a class, coniferous (needle-bearing) trees appear to have somewhat smaller permittivities than those of deciduous (leaf-bearing) trees. Secondly, although the importance of intrinsic water content upon the relative permittivity of wood has been substantiated by many studies, because green wood nearly always has a high intrinsic water content (approximately 75% by volume), the permittivity of green wood is relatively independent of water content. Thirdly, Broadhurst's measurements on tulip and balsa suggest very little difference between the permittivity of green wood and leaves.

Broadhurst's data for tulip and maple suggest that above 10 MHz the dielectric constant is only weakly dependent upon frequency and that over the UHF frequency band ϵ'_ℓ is approximately equal to 40. For frequencies below 1000 MHz, the imaginary part ϵ''_ℓ appears to be inversely proportional to losses and so decreases linearly with increasing frequency. Above 1000 MHz, however, relaxation losses associated with molecular polarization begin to predominate and, in this frequency regime, ϵ''_ℓ begins to increase with increasing frequency. Accordingly, in this study of UHF radiowave propagation through forests, the relative complex permittivity of green wood and leaves has been modeled using the relation

$$\epsilon_\ell = [40 + 20/f_{GHz}] + 2f_{GHz}/[1+(f_{GHz}/20)^2]\cdot \tag{47}$$

where f_{GHz} is the radiowave frequency expressed in GHz. This relation is plotted in Fig. 3.

2.3 BIOPHYSICAL FOREST DESCRIPTION

The application of these electromagnetic models in characterizing radiowave propagation through forests requires a representation of the forest in terms of select biophysical parameters. Trunk-related parameters include the tree-trunk number density, the probability density of the tree trunk diameters, the forest height, and the fractional ground area occupied by the canopy. Branch-related parameters include the branch number density, and the probability density functions for branch length, diameter, and angular orientation. Leaf-related parameters include the leaf number density, leaf diameter, and thickness (or, equivalently, at least in the UHF frequency band, the fractional volume occupied by the leaves), and the probability density function for leaf orientation. Terrain characterization is also required: the dielectric constant and conductivity of the ground, and the terrain irregularity (although the latter is not now employed in the model).

Such a detailed description of biophysical forest parameters as summarized above is virtually unattainable at present for any but a few of the world's forested regions and a requirement for the same would clearly preclude the model from any practical engineering application. There is, therefore, a clear requirement to (1) exercise the model, (2) assess its sensitivity to various biophysical parameters, (3) identify the most salient biophysical parameters, and (4) seek alternate means for deriving the most salient biophysical parameters from available forest data.

The largest forest data base available - broadest in both geographical coverage and in parameters considered - appears to be "World Forest Biomass and Primary Production Data" by M.G.R. Cannell [15]. The data for various forests available in this compilation include species-composition and, for each species, age (if an even-aged stand), tree-trunk number density, average forest height, fractional basal-area, leaf-area index, and biomass. From this data many of the above-mentioned parameters can be determined directly or inferred. For example, if the forest is even-aged, the trunk diameter probability density function is likely to be gaussian (Fig. 3a); if uneven-aged, it is likely to be exponential (Fig. 3b). The parameters describing these distributions (the mean trunk diameter and, perhaps, its variance) can often be inferred from the fractional basal-area, species-composition, and forest age.

2.2.4 THE EQUIVALENT FOREST CONTINUUM

The effective dyadic susceptibility ( ) and specific attenuation ( ) have been found for unbounded forests consisting of one type of canonical scatterer. Eqs. (25),(29) and (30) have been used to relate and to the dyadic kernel of the transition operator and Eq. (44) used to relate t(,) to the scattering amplitude. The scattering amplitude f(o,i) has been found for each type of canonical scatterer. In finding and , t(,) and f(o,i) have been appropriately averaged statistically to account for any prescribed orientation statistics of the canonical scatterers. In effecting these averages, it has been assumed that the azimuthal orientation of all canonical scatterers is uniform about the vertical. As a consequence, the equivalent continuous media are all uniaxially anisotropic (refer to Eq. (26)).

For describing the equivalent continuous forest media, the effective dyadic susceptibility appears to be preferable to the effective dyadic permittivity because is directly proportional to the number density of the scatterers (refer to Eq. (25)). Note also that, in contradistinction to early forest propagation models which simply postulated an effective (or), the model described here actually permits the calculation of (or) from measurable biophysical forest parameters (eg., tree trunk diameter, leaf size, etc.)

The effective dyadic susceptibility of tree trunks is exemplified in Fig. 4 for the case of a radiowave propagating parallel to the forest floor. These calculations for an uneven-aged forest are based upon a mean tree trunk diameter of 6.35 centimeters and a trunk number density of 1000 trunks per hectare. Although the resonant response for individual tree trunks is not apparent in this figure, it is, nevertheless clear from this figure that resonance plays a major role in the frequency band of interest. In this frequency band, the real parts of the dyadic susceptibility decrease as roughly the square of the frequency; the imaginary part of the transverse component decreases roughly as the two-thirds power of the frequency; and the imaginary part of the longitudinal component decreases roughly as the five-thirds power of the frequency.

The effective dyadic susceptibility of leaves is exemplified in Fig. 5 for the case of a radiowave propagating parallel to the forest floor. These calculations are based upon a set of values typical of temperate latitude forests: a leaf radius of 5 centimeters, a leaf thickness of 1 millimeter, and a leaf number density of 133 leaves per cubic meter (or, equivalently, a fractional volume for leaf occupancy equal to 0.1 percent). The random orientation of the leaves is described by a probability density function assumed to be uniform in azimuth and uniform in elevation angle over the range 0-30 degrees (ie. the leaves tend to be horizontal). Note that the effective dyadic susceptibility of the leaves exhibits the same frequency response as the susceptibility of individual leaves (refer to Fig. 2).

A comparision of Figs. 4 and 5 reveals that for tree trunks the longitudinal components of the susceptibility dominate the transverse ones; for leaves, the opposite is true with transverse components dominating the longitudinal ones. This reflects the fact that tree trunks tend to be oriented vertically, whereas the leaves tend to be predominately horizontal. As a consequence, horizontally polarized radiowaves tend to be more affected by the leaves whereas vertically polarized radiowaves tend to be more affected by the trunks. Further, for trunks, susceptibility is intimately related to resonant scattering; for leaves, Rayleigh scattering applies and the frequency behavior of the effective dyadic susceptibility reflects that of the susceptibility of individual leaves (refer to Fig. 2).

The specific attenuation attributable to tree trunks is exemplified in Fig. 6 for the case of a radiowave propagating parallel to the forest floor. These calculations for an uneven-aged forest are also based upon a mean tree trunk diameter of 6.35 centimeters and a trunk number density of 1000 trunks per hectare. It is apparent from this figure that vertically polarized radiowaves are attenuated more severely than are horizontally polarized ones, although the differential specific attenuation between polarizations tends to decrease with increasing frequency. Although the resonant response for individual tree trunks is not apparent in this figure, resonance has been found to play a major role. Note that these results agree reasonably well with experimental data of Saxton and Lane which is reproduced in Fig. 7.

The specific attenuation attributable to leaves is exemplified in Fig. 8. These curves are based upon the same leaf parameters described above. For both curves

$$\alpha = (\text{FV})\,\omega\,\mathrm{Im}(\chi_{\ell}) \qquad (48)$$

where is the leaf number density, a is the leaf radius, t is the leaf thickness, and " is the imaginary part of the susceptibility of a single leaf (refer to Fig. 2). Note that this factor within parentheses constitutes the fractional volume (FV) occupied by the leaves; the frequency dependence is determined solely by ". Note also that the specific attenuation due to leaves increases with increasing frequency. The relatively poor agreement with Saxton and Lane's experimental data(Fig. 7) may simply reflect the fact that tree trunks, rather than leaves, tended to dominate the transmission paths in their measurements. This would certainly be the case for short paths of, say, less than 100 meters, and low antenna heights.

A comparison of Figs. 6 and 7 reveals that for propagation through tree trunks, vertically-polarized radiowaves are attenuated more than horizontally-polarized ones; through leaves, the opposite is true. Further, at lower frequencies tree trunks will tend to dominate the excess attenuation attributable to the forest; at higher frequencies, leaves will.

2.3 STRATIFIED FOREST MODELS

In the previous section, the forest was considered as an unbounded medium of discrete scatterers. It was shown, however, that so far as the mean field $\langle \underline{E}(\underline{x}) \rangle$ is concerned, this unbounded medium of discrete scatterers behaves as a continuous, homogeneous, anisotropic medium with an effective dyadic permittivity . This observation suggests that a more realistic, albeit heuristic, model for the forest can be developed by considering the forest as a stratified, continuous medium wherein each stratum might represent the air, the forest, and the ground. Anticipating, on the basis of experiment, a major contribution to $\langle E(x) \rangle$ from a lateral wave propagating along the air-forest interface, the simplest of these stratified forest models would, as a first approximation, ignore the effects of the ground. Such a half-space model is illustrated in Fig. 9a. The resultant field $\langle \underline{E}(\underline{x}) \rangle$ arises as a consequence of a direct ray, a reflected ray, and the lateral wave. The corresponding variation of the effective dyadic permittivity with height (h) is also shown. The scalar permittivity of the air is denoted by . The ground is introduced in the slab model of Fig. 9b as is a single ground-reflected ray. Multiple reflected rays between the ground and the air are not shown. The scalar permittivity of the ground is denoted by . In both the half-space and slab models, the effective dyadic susceptibilities attributable to the tree trunks, branches, and leaves are simply added to find the complete susceptibility of the forest. Recognizing, however, that the branches and leaves tend to be located primarily within the canopy, a further extension of the model might concentrate branches and leaves in one forest layer and trunks in another. This model is illustrated in Fig. 9c where the effective dyadic susceptibility of the leaves and branches is denoted by and . The inhomogeneous model shown in Fig. 9d recognizes that the tree trunk diameters vary with height above the forest floor as does the number density of the leaves and branches.

2.3.1 HALF-SPACE MODELS

The source, a vertical electric (Hertzian) dipole antenna at T (refer to Fig. 9a) is assumed to have a time-harmonic current moment Idl·exp(j t) and to be situated a distance d below the air-forest interface. The air is characterized by permittivity and permeability , where and are the corresponding free-space values. The electrically anisotropic forest is characterized by the effective dyadic permittivity and free-space permeability . Because the forest is assumed to be uniaxially anisotropic (refer to Section 2.1.2) with

$$\underline{\underline{\epsilon}} = \epsilon_x(\underline{x}\,\underline{x} + \underline{y}\,\underline{y}) + \epsilon_z \underline{z}\,\underline{z} \tag{49}$$

the corresponding inhomogeneous vector wave equation for the anisotropic forest can be re-cast into an inhomogeneous vector wave equation for an equivalent isotropic medium by introducing the Clemmow transformation

$$z' = \sqrt{\epsilon_x/\epsilon_z}\, z \tag{50}$$

Under this transformation, the boundary value problem suggested by the geometry of Fig. 9a reduces to the classic Sommerfeld problem with the result that the mean electric field at R, $\langle E(X) \rangle$, can be derived from the relation

$$\langle \underline{E}(\underline{x}) \rangle = -k_o^2 \underline{A} + \nabla(\nabla \cdot \underline{A}) \tag{51}$$

where A is the vector potential whose only non-zero component is

$$A_z(\rho, z) = \frac{-I\,dl}{8\pi^2 \epsilon_z} \int \left[\frac{\exp(-j\gamma_1 |z+d|)}{\gamma_1} + \left(\frac{\gamma_1 - \gamma_2}{\gamma_1 + \gamma_2} \right) \frac{\exp(-j\gamma_1 (z-d))}{\gamma_1} \right] \times \exp(-j\underline{\rho}_t \cdot \underline{r}) d\underline{\rho}_t \tag{52}$$

where

$$\gamma_1 = (k_o^2 - \rho_t^2)^{1/2} \tag{53}$$

$$\gamma_2 = (k_o^2 - \rho_t^2)^{1/2} \tag{54}$$

Following Sommerfeld, the integral appearing in Eq. (52) may be evaluated asymptotically to reveal that $\langle E(X) \rangle$ consists of three principal components: the direct wave

$$E_1 = \text{[illegible]} \sin^2\theta \exp(-jk R_1)/R_1 \tag{55}$$

the reflected wave

$$E_2 = \text{[illegible]} \sin^2(\theta_2) \exp(-jk R_2)/R_2 \tag{56}$$

and the lateral wave

$$E_3 = \text{[illegible]} \exp(-\rho [r + a(z-1)]) \tag{57}$$

where

$$R_1 = [r^2 + a^2(z+d)^2]^{1/2} \tag{58}$$

$$R_2 = [r^2 + a^2(z-d)^2]^{1/2} \tag{59}$$

$$\theta_1 = \arctan[r/a(z+d)] \tag{60}$$

$$\theta_2 = \arctan[r/a(z-d)] \tag{61}$$

and $$\Gamma(\theta_r) = [\cos\theta_r - \sqrt{\varepsilon_t}(1-\varepsilon_z\sin^2\theta_r)^{\frac{1}{2}}]/[\cos\theta_r + \sqrt{\varepsilon_t}(1-\varepsilon_z\sin^2\theta_r)^{\frac{1}{2}}] \quad (62)$$

$\Gamma(\theta_r)$ may be recognized as the Fresnel reflection coefficient at the air-forest interface. The behavior of $\Gamma(\theta_r)$ as a function of a (real) incidence angle θ_r is shown in Fig. 13.

2.3.2 SLAB MODELS

A completely analogous development can be carried out for the configuration of Fig. 9b to show that, for a vertical electric dipole situated at a distance z above the forest floor, the only non-zero component of vector potential is now * interchanged.

$$A_z(\underline{r},z) = \frac{-Id\ell}{8\pi^2\omega\varepsilon_o\varepsilon_z}\int\frac{[1+R_g\exp\{-j2\tau_2 z_o\}][1+R_a\exp\{-j2\tau_2(H-z)\}]}{[1-R_aR_g\exp\{-j2\tau_2 H\}]} \quad (63)$$
$$X(1/\tau_2)\exp\{-j(\underline{\beta}_t\cdot\underline{r}+\tau_2|z-z_o|)\}d\beta_t$$

where, in addition to the parameters previously defined in Section 2.3.1,

$$R_a = [\tau_2-\tau_3\varepsilon_t]/[\tau_2+\tau_3\varepsilon_t] \quad (64)$$

$$R_g = [\tau_2\varepsilon_g-\tau_3\varepsilon_t]/[\tau_2\varepsilon_g+\tau_3\varepsilon_t] \quad (65)$$

$$\tau_3 = (k_o\varepsilon_g - \beta^2)^{\frac{1}{2}} \quad (66)$$

Asymptotic evaluation of Eq. (63) reveals not only the rays shown in Fig. 9b (direct, ground-reflected, air-reflected, and lateral), but also intra-forest multipath (refer to Fig. 10) and ground-reflected lateral waves [18]. The relative strength of single-, double-, triple-, etc. reflected rays can be assessed by considering the behavior of the Fresnel reflection coefficients at the air-forest and forest-ground interfaces. The forest-ground Fresnel reflection coefficient for the case of moist earth is plotted in Fig. 11 as a function of glancing angle. At the pseudo-Brewster angle of about 10 degrees, the magnitude of the forest-ground Fresnel reflection coefficient exhibits a deep minimum and its phase changes by about 180 degrees. The air-forest Fresnel reflection coefficient associated with a forest of lossy leaves is plotted in Fig. 12. In this case, the radiowave is directed from the denser medium (the forest) toward the rarer medium (the air) and experiences, for glancing angles shallower than the critical angle, so-called internal reflection. If the leaves were lossless, the internal reflection would be total (ie. $R = -1$). Note that for glancing angles greater than critical, the magnitude of the air-forest reflection coefficient is nearly zero.

The relative strength of the intra-forest multipath can be estimated by considering the relative magnitudes of the composite forest reflection coefficients(viz., $R_a, R_g, R_aR_g, R_gR_a, R_aR_gR_a, R_gR_aR_g$) which can be associated with intra-forest rays reflected only once from each interface or multiple times between interfaces (Refer to Fig. 10). The magnitude (in dB) of the composite Fresnel reflection coefficients have been plotted in Fig. 13 for a forest of leaves having a fractional volume of 0.1 percent as a function of path length (which is geometrically related to the glancing angle). It is apparent from this figure that the ray reflected only once from the air-forest interface is important at all distances in excess of about 300 meters. The ray reflected once from the ground is important not only at distances in excess of 300 meters, but also at very short distances as well. The double reflection (R_aR_g and R_gR_a) contributions become important only at ranges exceeding about 600 meters; and the triple reflection ($R_gR_aR_g$ and $R_aR_gR_a$) contributions can probably be neglected altogether. It should be mentioned, in passing, that Fig. 13 does not account for multipath discrimination due to antenna pattern directivity.

3. CHANNEL CHARACTERIZATION OF FORESTS

The electromagnetic models described in Section 2 can be employed to estimate or predict the performance of communications systems operating within forested environments. However, in order to characterize the forest radio channel suitably, it is first necessary to identify those electromagnetic forest channel characteristics which affect system performance. Perhaps the most basic and fundamental parameter affecting system performance is transmission loss. For fixed equipment parameters (e.g. transmitter power, antenna gains, noise figure) the bit-error-rate (BER) or, indeed, any measure of quality, depends primarily upon the received-signal-level (RSL) which depends, in turn, upon the transmission loss experienced by the propagating radiowaves.

It has long been recognized, however, that transmission loss is not the only radio channel characteristic affecting radio system performance. Others include frequency dispersion and fading. Frequency dispersion in tropospheric radio channels (e.g., terrestrial line-of-sight, troposcatter, and intra-forest paths) is primarily a consequence of multipath; fading is primarily a consequence of time-variant multipath and/or terminal antenna motion. The effects of fading on the relatively short, fixed-terminal intra-forest paths considered here are generally small and

*Eq. (63) tacitly assumes that $z>z_o$. If $z<z_o$, then the roles of z and z_o must be

will be assumed negligible. The effects of frequency dispersion, however, are significant and affect both the coherent (mean) and incoherent (fluctuant) components of the electric field E(x) . Frequency dispersion in the coherent component is perhaps best characterized by determining the response of the forest channel to a prescribed input pulse (forest pulse response); this is considered in Section 3.2. Because the central limit theorem suggests that the incoherent component is a sample function from a Gaussian random process, frequency dispersion in the incoherent component is perhaps best characterized by its two-frequency correlation function; this is considered in Section 3.3.

3.1 BASIC TRANSMISSION LOSS

The most important parameter characterizing radiowave propagation channels is transmission loss. Loosely defined, transmission loss is the ratio of transmitted power to received power (or its inverse). Basic transmission loss, however, is a quantity specifically defined as the ratio of the power transmitted to the power received between isotropic, lossless, co-polarized antennas. In free-space, the basic transmission loss can be calculated (in decibels) from the well-known expression

$$L_{fs} = 92.4 + 20 \log_{10} d_{km} + 20 \log_{10} f_{GHz} \tag{67}$$

where d_{km} is the distance between the antennas in kilometers and f_{GHz} is the radiowave frequency in Megahertz.

In calculating the basic transmission loss associated with the stratified forest models described previously in Section 2.3, it is important to recognize that postulated for those models was a vertically-polarized electric dipole antenna. Such an antenna is not isotropic. Nevertheless, the basic transmission loss can still be determined by noting that (1) in free-space, the vertically-polarized electric field can be determined from Eq. (55) by setting $\gamma_t = \gamma_z = 1$ so that

$$E_{fs} = (\omega\mu_o/4\pi) Idl \cdot \sin^2\theta_d \cdot \exp\{-jk_o\sqrt{\varepsilon_z} R_d\}/R_d \tag{68}$$

and (2) the power received will be directly proportional to the field intensity

$$I(\underline{x}) = \underline{E}(\underline{x}) \cdot \underline{E}^*(\underline{x}) \tag{69}$$

Thus, for the stratified forest models, the basic transmission loss can be expressed by

$$L_b = L_{fs} + 20 \log_{10} |E_{fs}/E_{d,r,\ell}| \tag{70}$$

The basic transmission loss between two isotropic, lossless, vertically-polarized antennas has been determined for two types of forest: a leaf-dominated forest characterized by a fractional volume (FV) of 0.1 percent (5 cm leaf radius, 1 mm leaf thickness, 133 leaves per cubic meter); and an uneven-aged, trunk-dominated forest characterized by a mean tree trunk diameter of 6.35 cm. Within both forests, the vertically-polarized transmitting and receiving antennas have been situated 2.5 meters below the air-forest interface and separated laterally from each other by 1000 m. The basic transmission loss for the leaf-dominated forest is shown in Fig. 15. The basic transmission losses associated with the direct and reflected waves are virtually indistinguishable and for frequencies less than about 500 MHz increase by about 6dB/octave of frequency. The direct and reflected waves destructively interfere so that their resultant is nearly 20 dB below either of them. Particularly strong destructive interference is apparent near 550 MHz. The basic transmission loss of the total is clearly dominated by that of the lateral wave which increases by about 12 dB/octave of frequency. Note that, in general, a leaf-dominated forest behaves as a low-pass filter for vertically-polarized radiowaves.

The basic transmission loss for the trunk-dominated forest is shown in Fig. 16. As for the leaf-dominated forest, the basic transmission losses associated with the direct and reflected waves are virtually indistinguishable and they destructively interfere so that their resultant lies 10-15 dB below either of them. The basic transmission loss of the total is clearly dominated by that of the lateral wave (they are indistinguishable) which increases approximately 12 dB/octave of frequency.

3.2 FOREST PULSE RESPONSE

The anisotropic half-space model described in Section 2.3.1 is a time-harmonic model. The transmitting antenna was assumed to be a vertical electric dipole having a time-harmonic current moment $Idl \cdot \exp(j\omega t)$. However, because the effective dyadic permittivity characterizing the equivalent continuous medium of the mean wave is linear, the model can be extended using linear system theory to accommodate the transmission of modulated waveforms. The dynamic variable representing the input [x(t)] to this system is the electric current moment Idl; the dynamic variable representing the output [y(t)] of this system is the vertically-polarized component of the coherent (mean) electric field $\langle E(x) \rangle$ at the location of the receiving antenna. System input and output can be related to each other by

$$y(t) = \int X(f) F(f,t) \exp\{j2\pi ft\}\, df \tag{71}$$

which implicitly defines the (possibly) time-variant forest transfer function F(f,t).

Inasmuch as the transmitting antenna of the anisotropic half-space model was taken to be a vertical electric dipole having a time-harmonic current moment Idl· exp(j t), the vertically-polarized component of the coherent (mean) electric field arising in response to that current moment (Eqs.55,56,57) may be considered the mean forest transfer function F(f,t) following normalization by Idl. Further, in consonance with Eqs.(55,56, and 57) the mean forest transfer function F(f,t) may be considered to consist of three components: the direct wave [$F_d(f,t)$], the reflected wave [$F_r(f,t)$], and the lateral wave [$F_l(f,t)$].

The mean forest pulse response has been determined for a 600-MHz carrier frequency and a 5-nanosecond rectangular pulse which has been passed through an ideal bandpass filter. Two forests have been considered: a leaf-dominated forest characterized by a fractional volume (FV) of 0.1 percent (5 cm leaf radius, 1 mm leaf thickness, 133 leaves per cubic meter); and an uneven-aged, trunk-dominated forest characterized by a mean tree trunk diameter of 6.35 cm. Within both forests, the vertically-polarized transmitting and receiving antennas have been situated 2.5 meters below the air-forest interface and separated laterally from each other by 1000m. The forest pulse response for the leaf-dominated forest is shown in Fig. 17. The forest pulse response associated with radiowave propagation along the direct path is shown uppermost in this figure. The propagation delay along the direct path can also be estimated from the approximation

$$t_d \approx (R_d/c)\,\epsilon_z' \tag{72}$$

where ϵ_z' is the real part of the longitudinal component of the effective dyadic susceptibility (refer to Fig. 5). For this example, R =1000m, ϵ_z'=1.0004265 , and c=3X10^8 m/sec. The companion pulse response for the reflected pulse shown next in Fig. 17 exhibits essentially the same delay. The rather shallow glancing angle at the air-forest interface associated with this particular geometric configuration (about 0.14 degrees) ensures a relatively strong reflected pulse (at 600 MHz the reflection coefficient is 0.9942), although essentially in antiphase with the direct pulse. As shown in the figure, the direct and reflected pulses virtually cancel each other and, as a consequence, the contribution of the lateral wave dominatees the resultant. The propagation delay associated with the lateral wave is essentially that of free space.

The forest pulse response for the trunk-dominated forest is shown in Fig. 18. In this case, the pulse response associated with the direct wave arrives prior to the pulse response associated with the lateral wave. This is a consequence of the fact that the longitudinal component of the effective dyadic susceptibility is negative. Eq. (72) can still be used to estimate the arrival time of the direct pulse, although for this example, because ϵ_z' =0.99903 the velocity of pulse propagation appears to exceed that of light in a vacuum. A more exact expression for pulse delay time and the Kramers-Konig relation can be employed to refute this contention in general; the apparent paradox that Fig. 18 supports this contention can be resolved by noting that the strictly band-limited transmitted pulse cannot be localized in time. The small, rapid oscillations may be the so-called Somerfeld precursor. In any case, the high specific attenuation associated with the propagation of a vertically-polarized wave through a trunk-dominated forest (refer to Fig. 6) severely attenuates all but the lateral wave which, as is apparent from Fig. 18 dominates the resultant pulse response.

3.3 TWO-FREQUENCY CORRELATION FUNCTION

The two-frequency correlation function of the vertical electric field $E_z(\underline{x})$ is defined as

$$R_{zz}(\underline{x};f_1,f_2) = \langle E_z(\underline{x},f_1)E_z^*(\underline{x},f_2)\rangle \tag{73}$$

where the frequency dependence of the vertical electric field on frequency is clearly indicated and the brackets < > denote a statistical average over an ensemble of forest configurations. As a consequence of Eq. (31), the two-frequency correlation function may be written as

$$R_{zz}(\underline{x};f_1,f_2) = R^c_{zz}(\underline{x};f_1,f_2) + R^i_{zz}(\underline{x};f_1,f_2) \tag{74}$$

where the two-frequency correlation function associated with the coherent field <E(x)> component is

$$R^c_{zz}(\underline{x};f_1,f_2) = \langle E_z(\underline{x},f_1)\rangle\langle E_z^*(\underline{x},f_2)\rangle \tag{75}$$

and the two-frequency correlation function associated with the incoherent field $\tilde{E}_z(x)$ is

$$R^i_{zz}(\underline{x};f_1,f_2) = \langle \tilde{E}_z(\underline{x},f_1)\tilde{E}_z^*(\underline{x},f_2)\rangle \tag{76}$$

However, because the coherent component <E(x)> is deterministic, its two-frequency correlation function is of little interest. Conversely, because the incoherent component E(x) is a sample function from a (perhaps Gaussian) random process, its two-frequency correlation function is of major interest.

The two-frequency correlation function can be derived from Eq. (12) through appropriate ensemble averaging in the same manner that Eq. (20) was developed for the coherent (mean) field. For example, in a two-dimensional, unbounded medium of parallel circular cylinders of radius a and relative permittivity , the two-frequency correlation function of the incoherent electric field E (x) due to a parallel line-current is, in the

Rayleigh (low frequency) regime, given by

$$R_{zz}(\underline{x};t_1,t_2) = j\,a_2 a_1 H^*(j\sqrt{a_1^2-a^2}\,x_t) - j a_1^2 a_4 \int dp\; H^*(j\sqrt{p^2+a_1^2}\,x_t)/(p^2+a^2) \qquad (77)$$

where

$$a_1 = j(t_1 - t_2) \qquad (78)$$

$$a_2 = (k_1 k_2)^{3/2} \gamma_0(f_1)\gamma_0^*(f_2)[\pi a^2]^2/4 \qquad (79)$$

$$a_4 = [8\pi\sqrt{k_1 k_2}]^{-1} \qquad (80)$$

and all other parameters have been defined previously in Section 2.1. Both the real and imaginary parts of the two-frequency correlation function have been plotted in Figs. 19 and 20 for path lengths of 200 and 500 meters, respectively. It is apparent from the figures that although the frequency of the rapid oscillations is proportional to the path length, the envelope of these oscillations remains nearly invariant with distance and, as a consequence, the correlation (1/e) bandwidth is about 500 KHz in both cases.

4. FUTURE PLANS

Plans for model improvement are already proceeding. Specifically, the model has already been extended to account for ground effects (Fig. 9b). Further, an expression for the dyadic scattering amplitude of a finite cylinder has already been derived which, in consonance with the earlier derived analagous expression for leaves, will permit, when averaged over branch and leaf orientation angles, the calculation of the effective dyadic susceptibility and specific attenuation for an unbounded forest of branches and leaves. Subsequently, this will lead to the development of the stratified canopied forest model shown in Fig. 9c . The stratified forest model will also be extended to accommodate arbitrary antenna directivity and polarization.

An expression for the frequency-spatial correlation function has already been derived for a line source immersed in a trunk-dominated forest. This expression, although incorporating Eq. (77) as a special case, is considered more general because it is not restricted to Rayleigh(low frequency) scatterers. Analogous results for dipole excitation, and branch- and leaf-dominated forests will be derived subsequently as will their Fourier transforms, the coherence matrix, and the delay-spread function. These latter functions will prove especially important in ascertaining the effects of antenna directivity and coherence bandwidth upon communications system performance.

The theoretical development reported herein is only a portion of a large effort to improve the scientific community's understanding of the behavior of UHF communications systems in ground-to-ground applications. Planning is already well underway for the next step; a comprehensive series of channel characterization experiments. These experiments will utilize a wideband channel probe designed to make impulse response measurements of forested channels in the UHF band. The automated measurement system is now being completed, and will soon be installed in vehicles to begin a measurement effort expected to last at least two years.

Design of the measurement system is based on a similar system described in [12]. The basic configuration of the channel probe is a dual-channel transmitter/receiver in which a transmit power of 100 watts is provided over the entire measurement band. These power levels provide a sufficiently high signal-to-noise ratio to permit propagation channel data to be collected over paths with losses of 145 dB at frequencies up to 900 MHz and losses of 155 dB at higher frequencies when directional antennae are used. In order to determine the impulse response of the communications channel, the system uses a sliding correlator technique and a parallel receiver structure to process the wide bandwidth pulse modulated probe signal. Multiple operating modes are provided to achieve a range of measurement resolutions (i.e. transmitted bandwidths), maximum multipath delay spread windows, effective impulse response sampling rates, and maximum doppler spreads. Maximum spread characterization bandwidth is 250 MHz and maximum multipath delay spread is approximately 10 microseconds. Tradeoffs between the two dimensions may be made under operator control.

In order to improve the efficiency of an extremely complicated data acquisition process microcomputers play an important role. A microprocessor-based data acquisition system records both in-phase and quadrature components of the received signal from each of two receiver channels, and produces a complex representation of the channel's impulse response. From this function, an array processor is used to compute the frequency-dependent modulation function, and a variety of peripheral power meters and spectrum analyzers, all under HPIB control,is used to obtain calibrated measurements of received signal level. System outputs include real-time display of the time varying impulse response or operator-selected processed data. The system provides hard copy or data storage on either hard disk or 1600 bits per inch magnetic tape.

These experiments will provide a unique opportunity to examine the structure of the scattered components through the various parts of the forest and to verify assumptions and intermediate results of the theory presented above. For example, Twersky's theory and Maxwell's equations permitted the representation of the scattered electromagnetic field in terms of two components, the mean component and the zero-mean random fluctuating component. The ratio of power attributable to each of these is called the coherence ratio. This fundamental parameter is not only important to the physical understanding of the forest channel, but also to the prediction of the effects of the forest on

communications signals. The impulse response measurement capability of the wideband channel probe will lead directly to the computation of the channel's transfer function as derived above, and will enable a characterization of the statistics of this complex quantity. It will enable measurement of amplitude and phase statistics of both the mean and random scattered signals as a function of frequency, path geometry, and forest characteristics. The improved resolution of the measurement system will enable discrimination between signals arriving over direct, reflected, and lateral wave paths, and will provide a heretofore unavailable view of forest propagation at UHF frequencies.

5. REFERENCES

1. R. H. Ling, A. Schneider, S. Seker, and F. J. Altman, "UHF Radiowave Propagation Through Forests", CyberCom Technical Report CTR-108-01 (September 1982).

2. V. Twersky, "Multiple Scattering of Electromagnetic Waves by Arbitrary Configurations," J. Math. Phys., Vol. 8, No. 3, pp 589-610 (1967).

3. D. L. Sachs and P. J. Wyatt, "A Conducting-Slab Model for Electromagnetic Propagation within a Jungle Medium," Radio Science, Vol. 3, No. 2, pp 125-134 (February, 1968).

4. R. A. Nelson, "UHF Propagation in Vegetative Media," SRI Int., Menlo Park, CA, for U.S. Army CORADCOM, Ft. Monmouth, NJ, Final Rep., contract DAAG29-76-D-0100, (April, 1980).

5. B. Trevor, "UHF Propagation Through Woods and Underbrush," RCA Rev., Vol. 5, No. 1, pp 97-100, (July, 1940).

6. J. A. Saxton and J. A. Lane, "VHF and UHF reception: Effects of trees and other obstacles," Wireless World, Vol. 61, No. 5, pp. 229-232, (May, 1955).

7. A. H. Lagrone, P. E. Martin, and C. W. Chapman, "Frequency characteristics of radio propagation over a grove of trees in full leaf," Rep. No. 644, Univ. Texas EE Res. Lab, Austin, TX, for U.S. AFCRL, contract AF196048038, (January, 1962) (AD 272 042).

8. M. A. Weissberger, "An initial critical summary of models for predicting the attenuation of radiowaves by trees," IIT Res. Inst. for Dept. Defense Electromagn. Compat. Analysis Center, Final Rep. ESD-TR-81-101, (July, 1982).

9. T. Tamir, "Radio wave propagation along mixed paths in forest environments," IEEE Trans. Antennas Propagation, Vol. AP-25, No. 4, pp. 471-477 (July, 1977).

10. Jansky & Bailey Engineering Dept., "Tropical Propagation Research," Vol. 1, Atlantic Research Corp., Alexandria, VA, for U.S. Army Electron. Command, Advanced Res. Proj. Agency, contract DA36-039-SC-90889, ARPA order 371, 1966, Final Rep., (AD 660 318).

11. H. Head, "The influence of trees on television field strengths at UHF," Proc. IRE, Vol. 48, No. 6 pp. 1016-1020 (June, 1960).

12. R. F. Linfield, R. W. Hubbard, and L. E. Pratt, "Transmission channel characterization by impulse response measurements," U.S. Dept. Commerce, Office Telecommunications (OT) Rep. 76-96 (August, 1976).

13. L. O. Foldy, "The Multiple Scattering of Waves," Phys. Rev., Vol. 67, No. 3, pp 107-119 (March, 1945).

14. M. G. Broadhurst, "Complex Dielectric Constant and Dissipation Factor of Foliage," National Bureau of Standards Report 9592 (October, 1970).

15. M. G. Cannell, World Forest Biomass and Primary Production Data, New York: Academic (1982).

16. P. C. Clemmow, "The Theory of Electromagnetic Waves in a Simple Anisotropic Medium," Proc. IEE, Vol. 110, No. 1, pp 101-106 (January, 1963).

17. L. M. Brekhovskikh, Waves in Layered Media, New York: Academic (1960).

18. D. Dence and T. Tamir, "Radio Loss of Lateral Waves in Forest Environments," Radio Science, Vol. 4, No. 4, pp 307-318 (April, 1969).

19. J. D. Jackson, Classical Electrodynamics, New York: Wiley (1975).

20. S. Chandrasekhar, Radiative Transfer, New York: Dover (1960).

6. ACKNOWLEDGMENTS

The author is pleased to acknowledge the substantive contributions to the development of this model by Professor Roger H. Lang of the George Washington University, Washington, D.C., Professor Selim Seker of Bogazici University, Istanbul; and Frederick J. Altman of CyberCom Corporation.

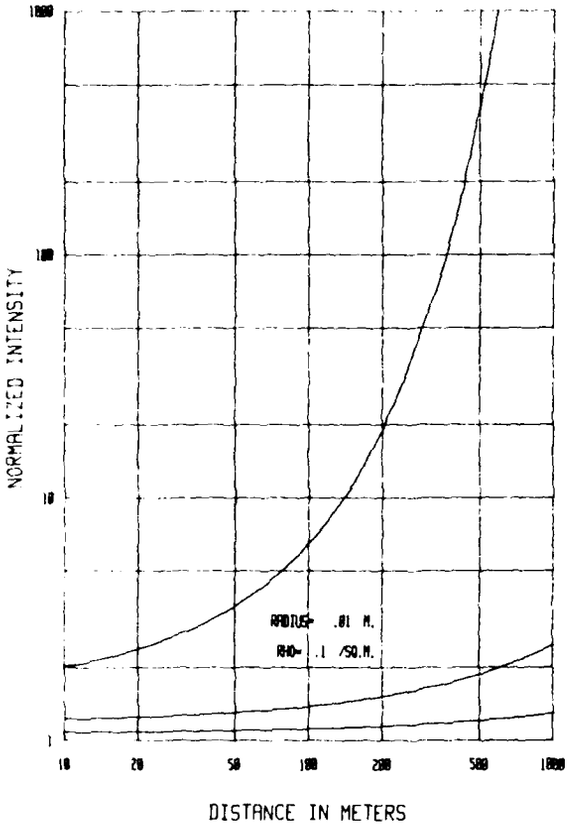

Fig. 1 Coherent/Incoherent power ratio.

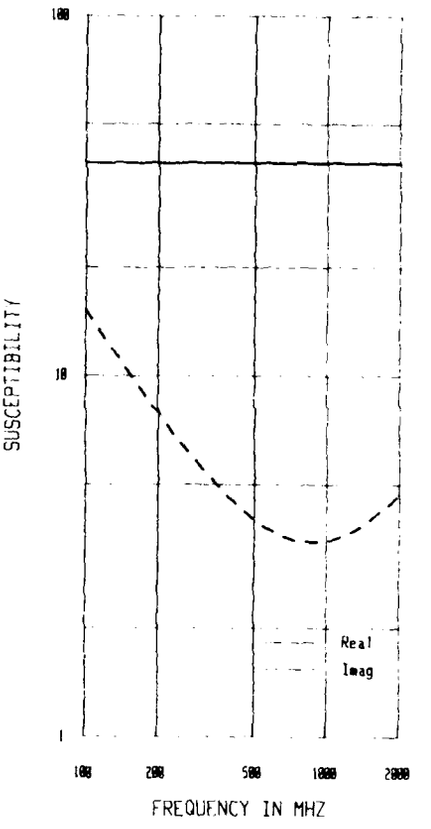

Fig. 2 Susceptibility of wood and leaves ($\chi = \epsilon - 1$).

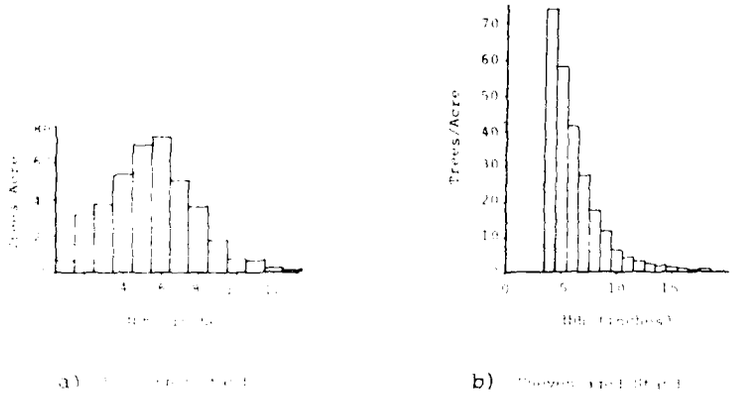

a) b)

Fig. 3 Trunk diameter probability density functions.

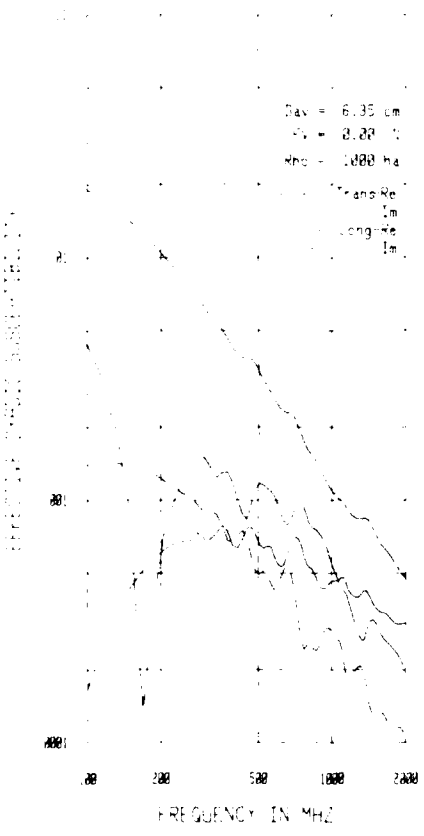

Fig. 4 Effective dyadic susceptibility (trunks).

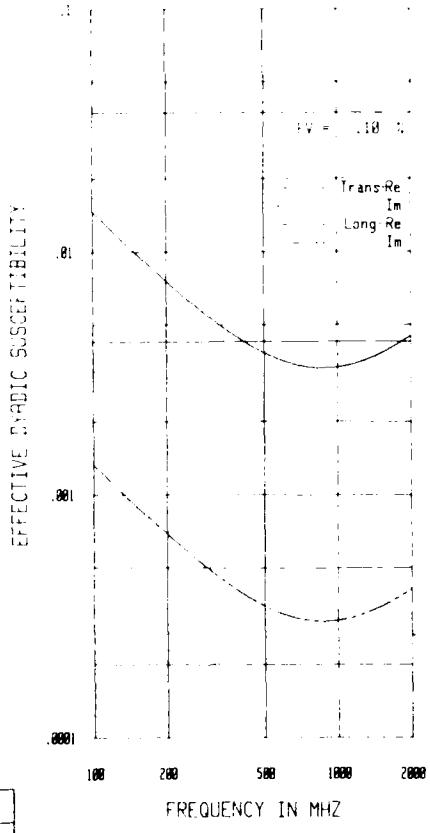

Fig. 5 Effective dyadic susceptibility (leaves).

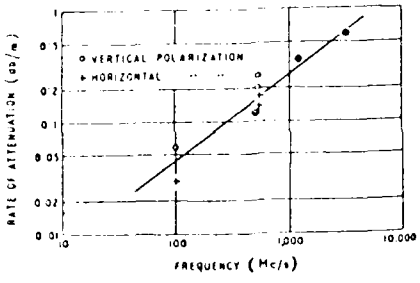

Fig. 7 Attenuation rate in woods with trees in leaf.

Fig. 6 Specific attenuation (trunks).

Fig. 8 Specific attenuation (leaves).

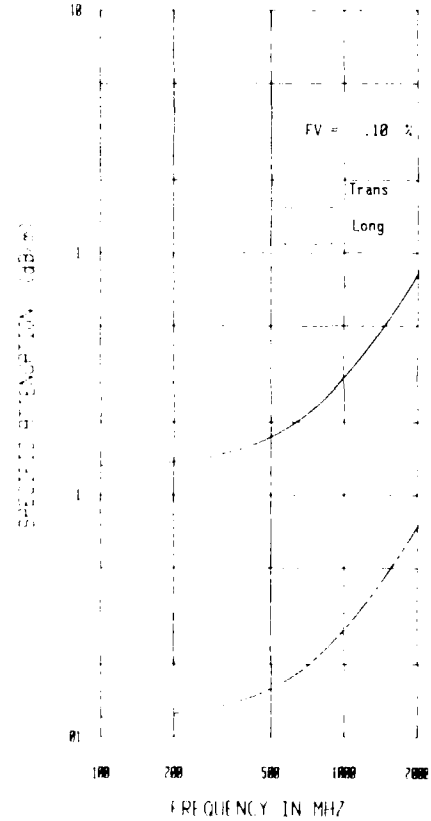

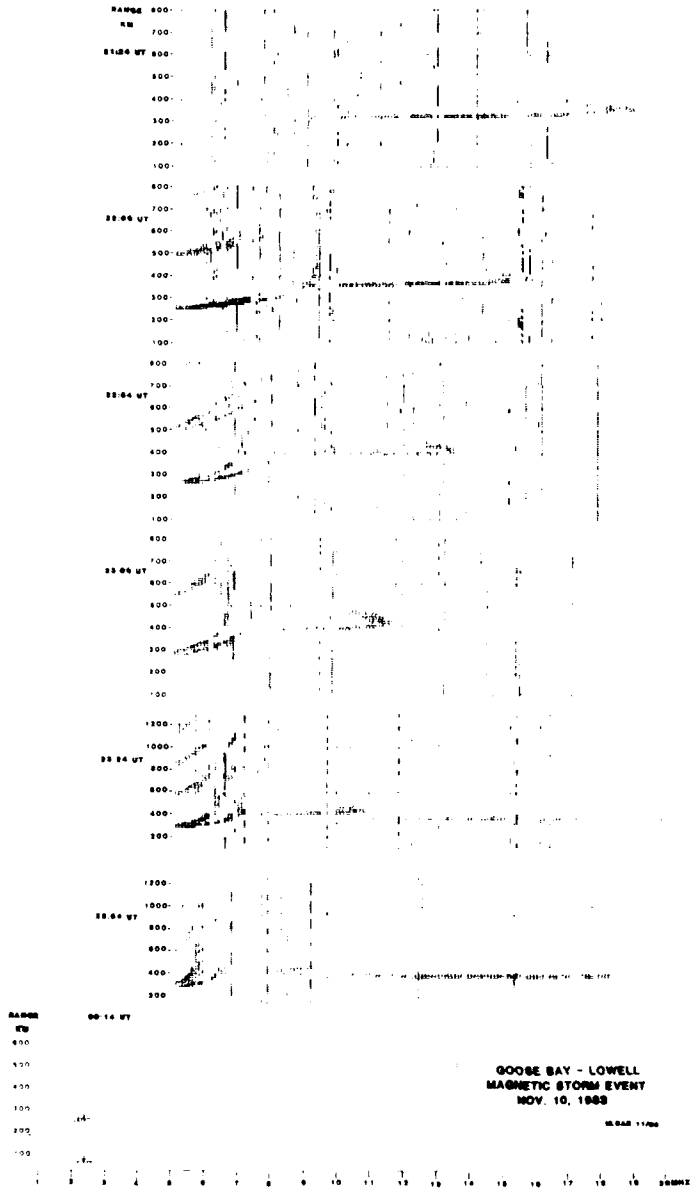

FIGURE 9

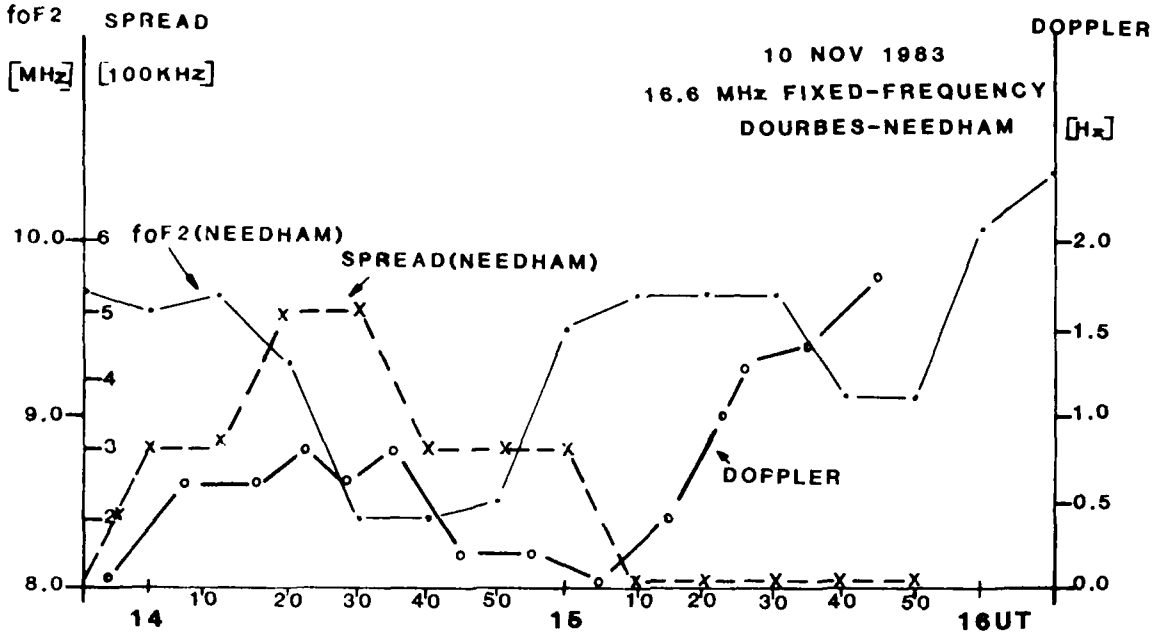

DOPPLER VARIATION FOR 3F PROPAGATION

FIGURE 7

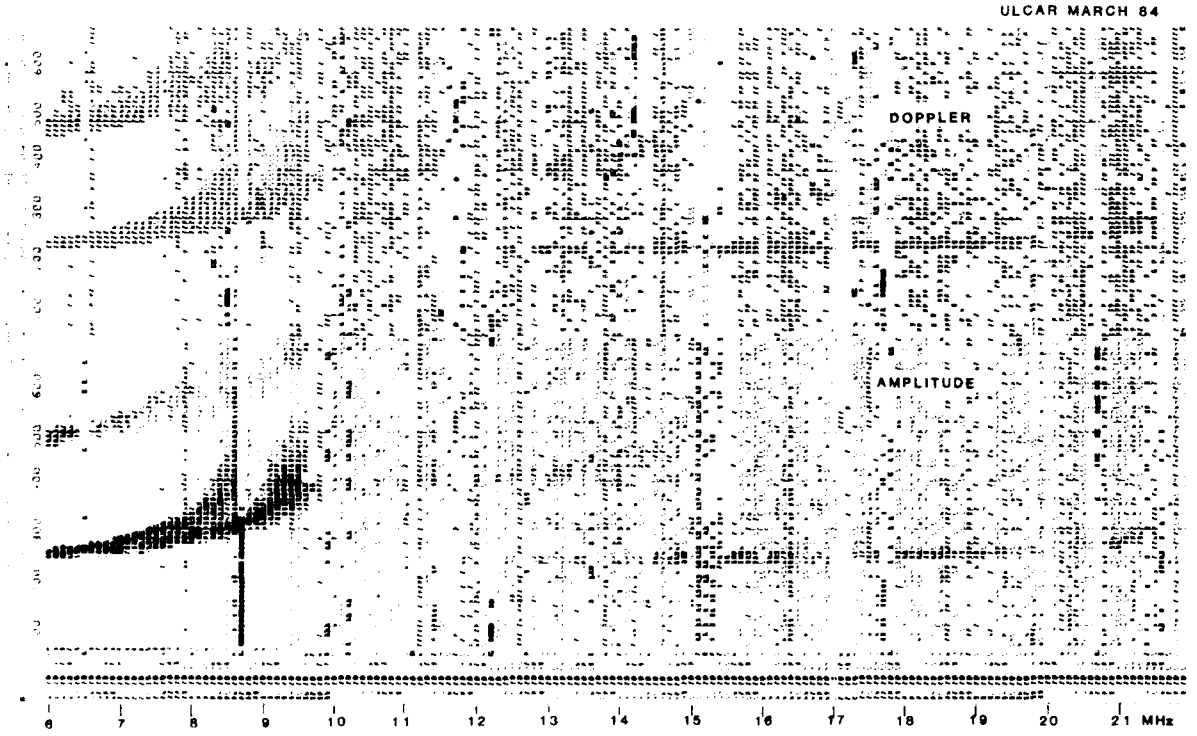

VERTICAL + OBLIQUE IONOGRAM DOURBES-NEEDHAM 10 NOV 1983 1430UT

FIGURE 8

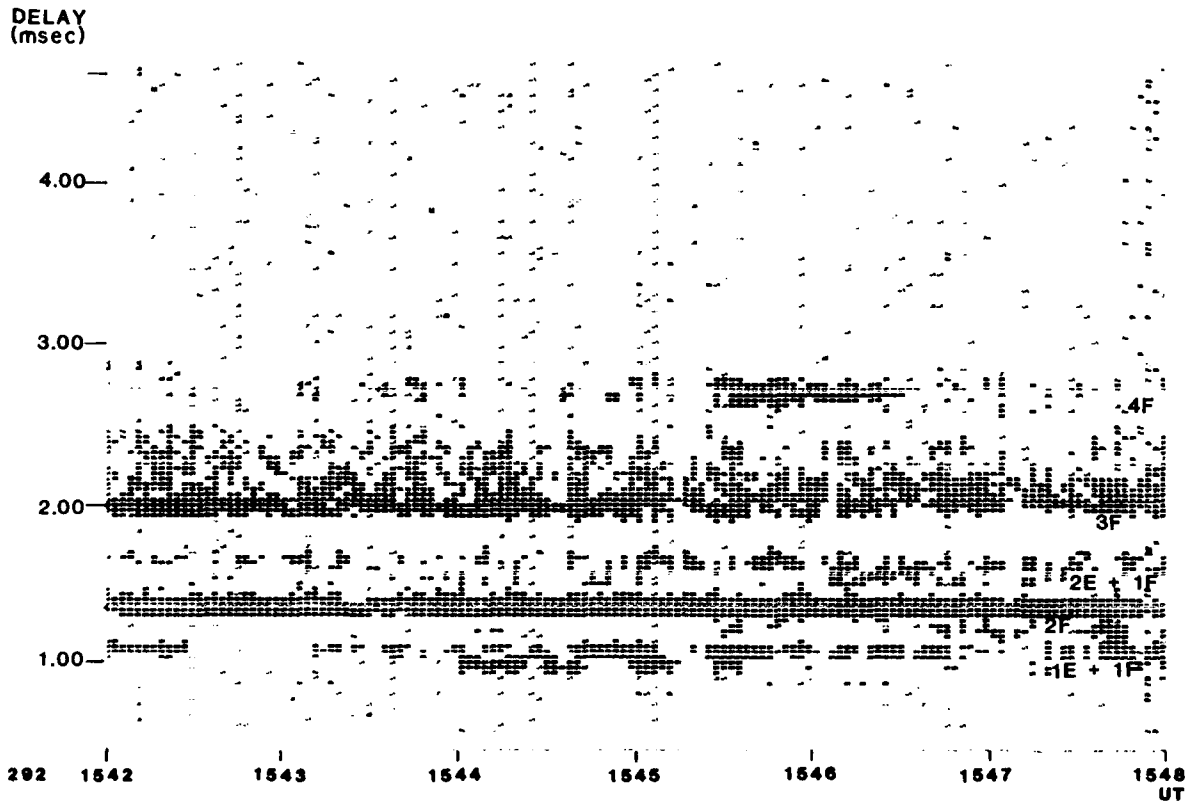

16.63 MHZ 2.5 SECONDS INTEGRATION DOPPLER 0.4 HZ/NUMBER

DOURBES-NEEDHAM OBLIQUE SOUNDING 18 OCT,1983

FIGURE 5

ULCAR 11/83

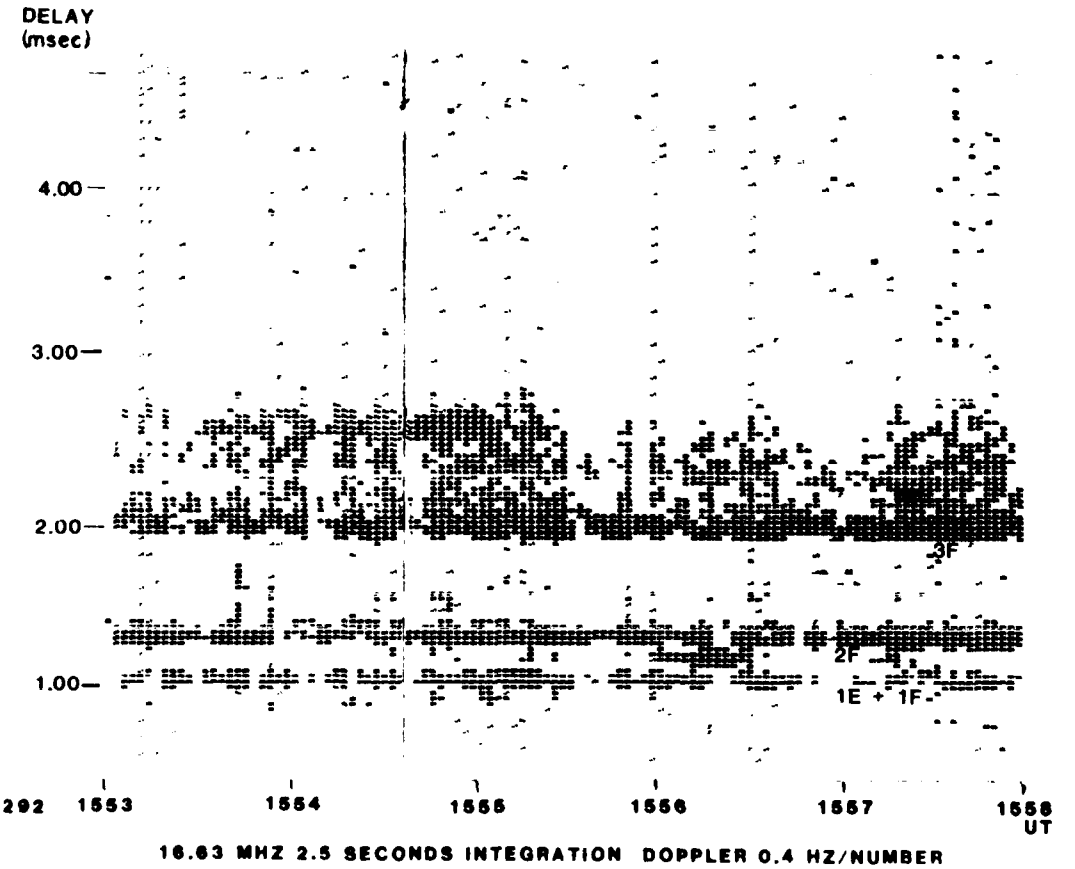

16.63 MHZ 2.5 SECONDS INTEGRATION DOPPLER 0.4 HZ/NUMBER

DOURBES-NEEDHAM OBLIQUE SOUNDING 18 OCT,1983

FIGURE 6

ULCAR 11/83

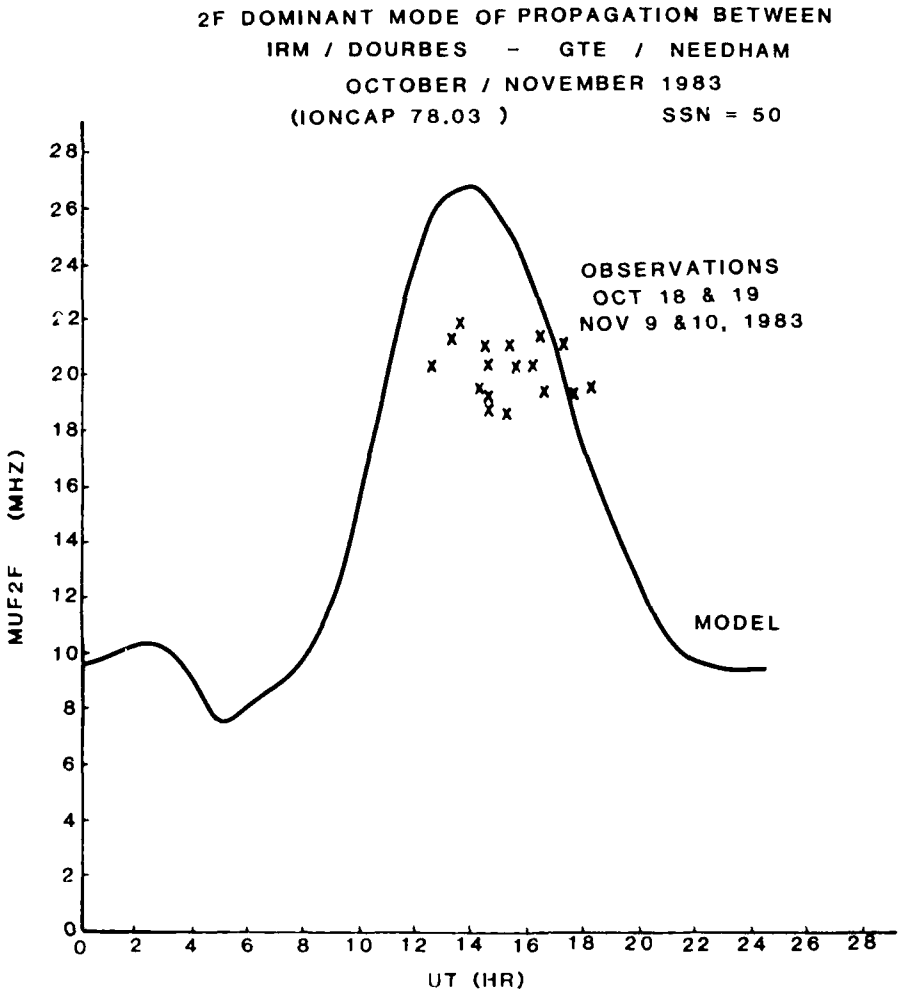

COMPARISON OF THE PREDICTED MUF'S OBTAINED USING THE IONCAP PROPAGATION MODEL PREDICTIONS WITH OBSERVATION DURING OCTOBER AND NOVEMBER 1983

FIGURE 4

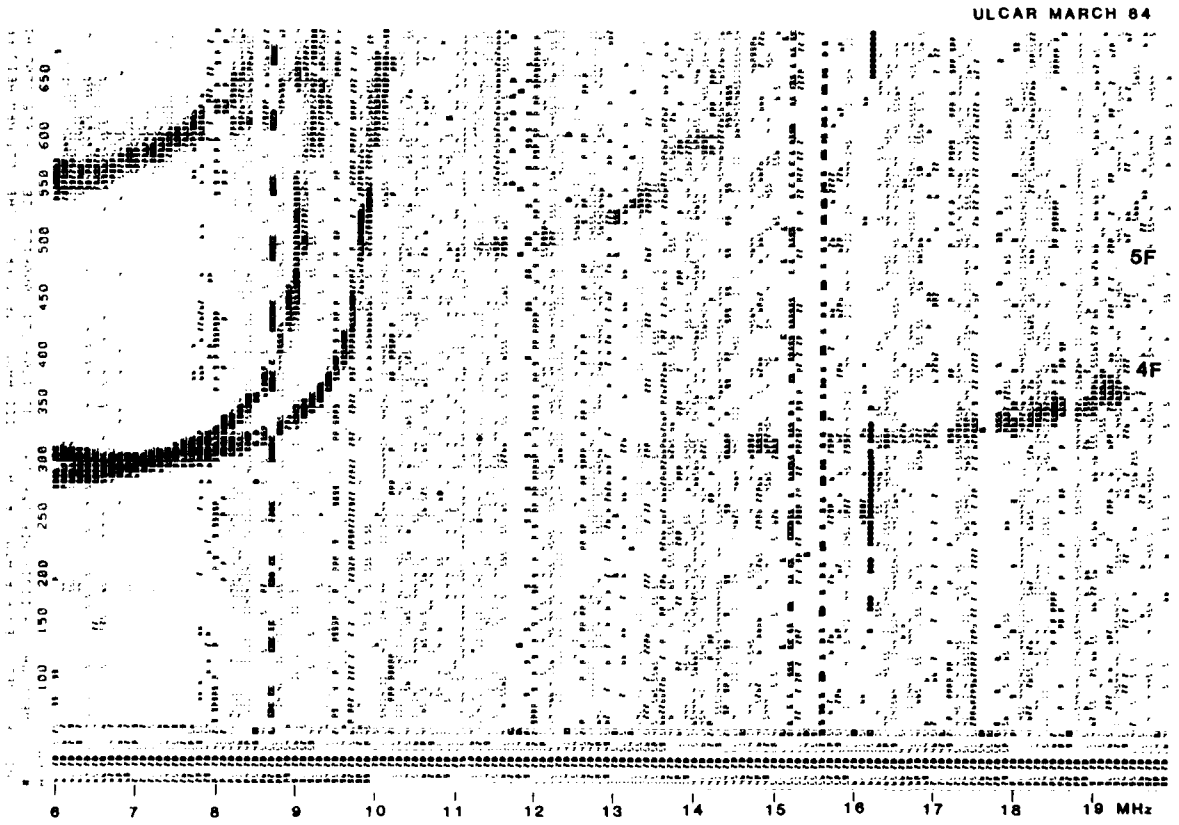

VERTICAL + OBLIQUE IONOGRAM DOURBES-NEEDHAM 8 NOV 1983 1709UT
FIGURE 2

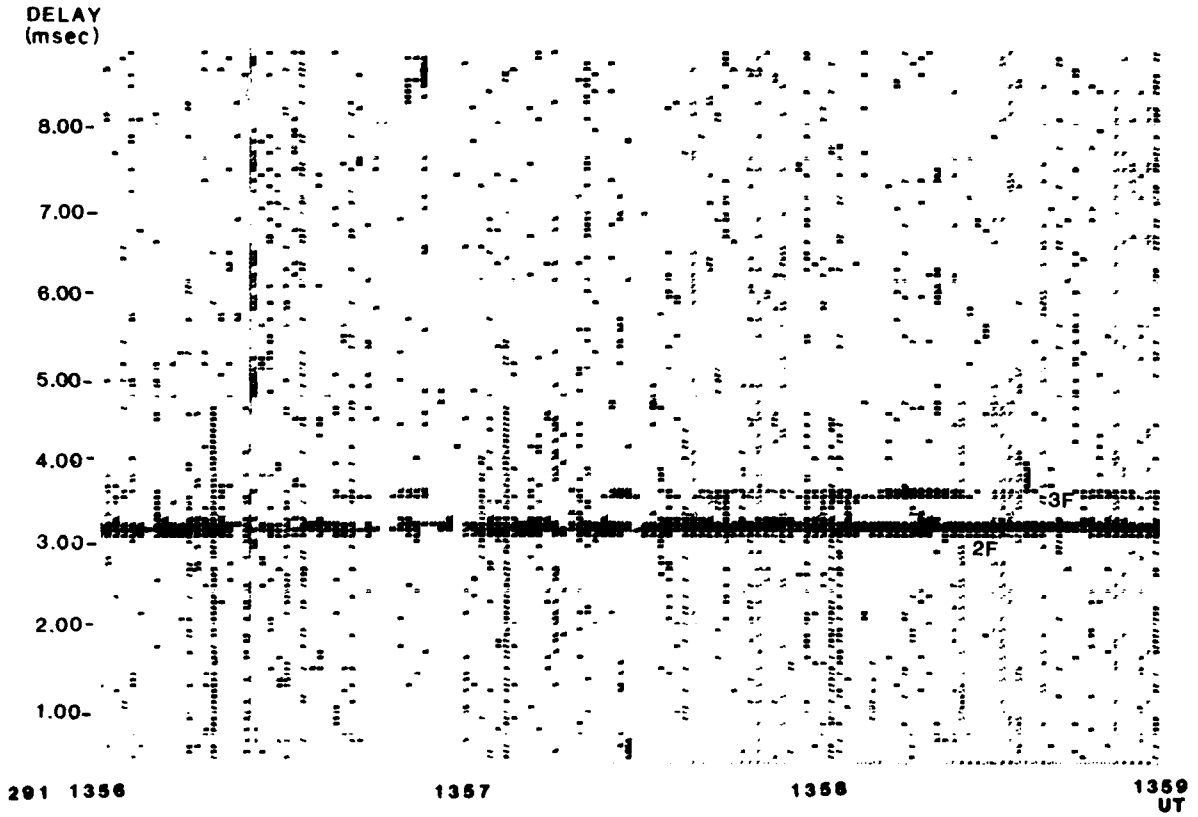

16.63 MHZ 1.2 SECONDS INTEGRATION AMPLITUDES IN 2DB/STEP

DOURBES - NEEDHAM OBLIQUE SOUNDING 18 OCT, 1983

ULCAR 11/83

FIGURE 3

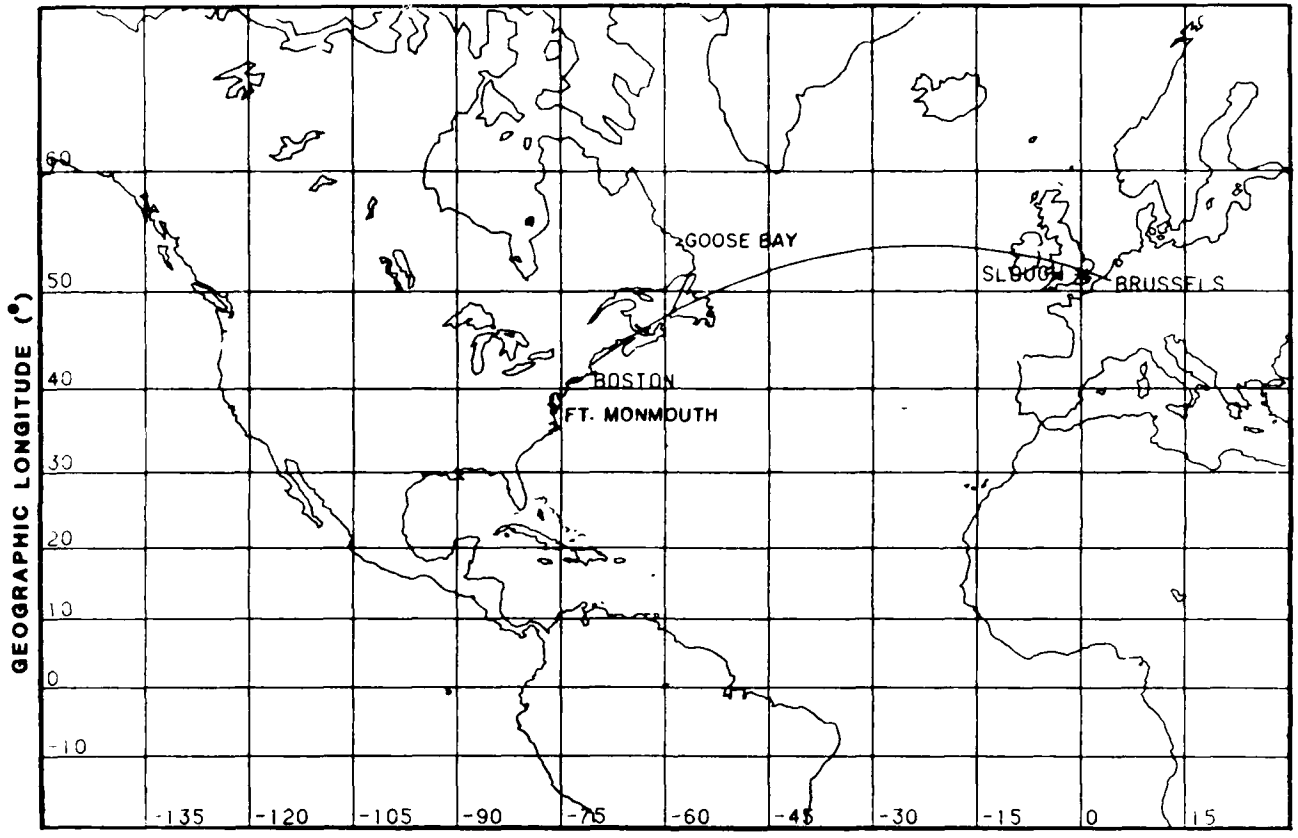

HIGH, MIDDLE AND LOW LATITUDE PROPAGATION PATHS BETWEEN CONUS - EUROPE

FIGURE 1

than the measured frequency, while there is fair agreement at 17 UT.

Figures 5 and 6 show Doppler recordings for the fixed-frequency observation. The integration time was 2.56 sec for each measurement and the Doppler resolution is 0.4 Hz. If we assume the vertical velocities of the reflecting ionosphere to be smaller or equal to 25 m/s then the Doppler shift for a 6 MHz vertically reflected signal is $d_v \leq 1.0$ Hz. The same Doppler shift is expected for oblique signals reflected at the same level (Pickering, 1975), because the sec ϕ (ϕ is the ionospheric incidence angle) increases the operating frequency by the same factor it decreases the radial velocity component:

$$d_{obl} = f_{obl}\,(d_v/\sec\phi) = (f_v \sec\phi)\cdot(d_v/\sec\phi) = d_v.$$

For an n-hop propagation path the total Doppler is the sum of the individual Doppler shifts. If all n reflection points are moving in the same direction the total Doppler will increase, if they move in different directions the Doppler will become smaller or zero. On 18 October 1983 from 1542 to 1548 UT (Figure 5) the modes at 1.0 and 1.3 msec have identical Doppler of about +0.2 Hz. No significance is placed on this value since the two 16 MHz oscillators at Dourbes and Needham had not been adjusted to this accuracy. (If both stations were transmitting and receiving the oscillators offset would manifest itself as the difference in the measured apparent Dopplers for identical propagation paths.) The Doppler shift of the higher order mode at 2.0 msec is 0.4 Hz higher until 1546 UT. At 1548 it is about 0.4 Hz smaller and then it levels into the same value as the 1.3 ms mode. The signal at 2.7 msec (longest delay) in Figure 6 (the origin of the delay time scale is arbitrary) has again a 0.4 Hz lower Doppler compared to the 2.0 ms mode. It is interesting to notice that the 3F mode has the largest time spread but not the largest Doppler variation.

Significant changes in the ionosphere observed along the Dourbes-Needham transatlantic link during moderately stressed propagation conditions, such as during November 10, 1983 (local K ~4 from "Preliminary Reports of Solar Geophysical Data") are illustrated in Figure 7. The foF2 (scaled from the vertical F echoes) at Needham is about 9.5 MHz until 1415 UT; the frequency spread of 0.5 MHz peaks later at 1430 UT as observed in Figure 8. The Doppler shift of the 3F fixed frequency signal from Dourbes also peaked around this time at 0.8 Hz. At 1510 UT, both the spread on the vertical echoes and the Doppler shift on the oblique signal disappear. The Doppler shift starts to increase again reaching 1.8 Hz at 1545 UT, while no new spread develops.

During these early stages of the experiments, the power transmitted and the gain of the antenna used at Dourbes were apparently not high enough to maintain the connectivity of the transatlantic link during the evening and night hours for monitoring the development of the auroral/magnetic storm. However, the stressed propagation effects near Needham and along the western end of the transatlantic link were monitored by activating the medium range (1500 km) Digisonde link between Goose Bay, Canada, to Lowell, Massachusetts. Figure 9, a composite of seven recordings made at the University of Lowell illustrates the evolution in the vertical ionospheric structure over Lowell and along the oblique path from Goose Bay during the course of the auroral/magnetic storm. Starting at 2249 UT the foF2 is decaying rapidly from a peak value of 9 MHz to 2.5 MHz at 0014 UT, while the 1F MUF decreases from 15 MHz at 2249 UT to 9 MHz at 2354 UT. An Es mode exists from 2324 to 2354 UT. Absorption wipes out the oblique propagation signal at 0014. For comparison, Figure 10 shows a daytime (15:45 LMT) oblique ionogram for a magnetically quiet day. The 1F hop trace is well developed with both low and high angle rays present; the 2F and 3F hops show the low angle rays.

4. REFERENCES

Bibl, K., B. W. Reinisch and D. F. Kitrosser, "Digisonde 256 - General Description of the Compact Digital Ionospheric Sounder," First Edition, University of Lowell Center for Atmospheric Research, December 1981.

Bradley, P. A., "Focussing of radio waves reflected from the ionosphere at low angles of elevation," Electronic Letters, 6, 457-458, 1970.

Lloyd, J. L., G. W. Haydon, D. L. Lucas and L. R. Taters, "Estimating the performance of telecommunication systems using the ionospheric transmission channel," Draft Report, Institute for Telecommunication Sciences, Boulder, Colorado, 1978.

Patenaude, J., K. Bibl and B. W. Reinisch, "Direct Digital Graphics," American Laboratory, pp. 95-101, September 1973.

Pickering, L. W., "The Calculation of Ionospheric Doppler Spread on HF Communication Channels," IEEE Trans. Commun. COM-23, 5, 526, 1975.

Reinisch, B. W., P. P. Gamache and J. S. Tang, "Automatic Electron Density Profiles from Digital Ionograms," AGARD Conference Proceedings No. 345, pp. 16-1 to 16-11, 1983.

2. CURRENT STATUS OF THE DIGISONDE 256 NETWORK

In fall of 1983, two Digisonde 256 systems were operating along the transatlantic link with nodes at Dourbes and Needham, using horizontally radiating antennas. GTE Sylvania at Needham had set up a horizontally polarized rotatable log-periodic antenna on a 24 m tower, operating in the frequency range from 4 to 30 MHz. The maximum gain is 10 dBi at an elevation angle of 12° for 15 MHz, and at 6° for 30 MHz. In Dourbes a horizontal 3-wire rhombic antenna (80 m long, 34 m wide) was installed 15 m above ground. At 15 MHz the radiation maximum occurs at an elevation angle of 21° where the gain is 16 dBi; for 30 MHz the radiation maximum occurs at 10° with 22 dBi. The great circle range between Dourbes (50.1°N, 4.6°E) and Needham (42.4°N, 71.3°W) is D = 5600 km. Table 1 shows the expected elevation angles for 2, 3, 4 and 5 hop F2 propagation paths for a virtual height of h'F = 320 km. A horizontal rhombic antenna identical to the one in Dourbes will be erected in Slough in summer 1984. Fort Monmouth will start operating the Digisonde 256 using a horizontal antenna in fall of 1984.

Elevation Angles for Dourbes-Needham Propagation Assuming h'F = 320 km

Table 1

Path	2xF2	3xF2	4xF2	5xF2
Elevation	6°	10°	16°	22°
Prop. Time [ms]	19.6	20.2	20.9	21.9

Oblique propagation experiments between Dourbes (south of Brussels) and Needham (west of Boston) were started on October 14, 1983. The oblique transatlantic signals transmitted from Dourbes are continuously recorded at Needham. The Needham sounder uses the same log-periodic antenna for both transmission and reception. Presently, the Dourbes sounder is operating only in the transmit mode and future modifications will enable simultaneous transmission and reception.

To probe the propagation channel, ionograms were recorded every ten minutes with interspersed fixed frequency measurements. The ionograms were stepping in 100 kHz increments from 4 to 22 MHz as shown in Figure 2. This daytime ionogram recorded in Needham at 1709 UT on 6 November 1983 shows the 4F and 5F modes. The vertical echoes of the Needham transmission seen on the left side, indicate a critical frequency of 9.1 MHz. It should be mentioned that the ionogram display is composed of small numbers (2 dB amplitude increments in this ionogram) using an optically weighted font (Patenaude et al, 1978). The same method of presentation is used for the fixed-frequency observations (Figure 3) on 15.63 MHz. Data are digitally integrated for 1.28 seconds corresponding to 128 pulses at a repetition rate of 100 Hz. After each transmitted pulse, 128 digital quadrature samples are taken at time increments of 33-1/3 μsec, resulting in 128 range bins (or pixels). Hardware limitations constrain the Doppler calculations to sixteen spectral lines in the ionogram mode. However, if the number of ranges is limited to four, which is the so-called "drift mode" of operation, all 128 spectral lines are calculated. This mode of operation has not yet been used in the Dourbes-Needham link.

3. PRELIMINARY EXPERIMENTAL RESULTS

The results of preliminary analyses of the first month (mid-October to mid-November 1983) of oblique HF transatlantic soundings are reported here.

By means of an examination of several swept frequency ionograms, a frequency with relatively low interference level (and usually beyond the frequency range of direct path, auroral and backscatter echoes) is selected for the fixed frequency transmission. The fixed-frequency measurements (Figure 3) are well suited for determining the fading period and depth for different propagation modes. The observed fading periods for the 15.63 MHz signal vary in general from 10 to 60 sec with fading depths of 10 to 20 dB. It is likely that this fading is caused by focussing in the reflecting F-layer (Bradley, 1978). It appears that the fading patterns for the different propagation modes are often different. Extensive analyses underway will lead to a deeper understanding of the phenomenon.

Figure 4 shows the observed MUF values for 18/19 October and 9/10 November 1983 together with the ICEPAC (Lloyd et al, 1978) prediction curve for a sunspot number of 50. For the available antennas and the peak power of 10 kW, link connectivity was generally maintained only from 12 to 18 UT. The data points in Figure 4 show less of a diurnal variation than predicted by ICEPAC. At 14 UT the predicted MUF is 25% higher

MULTIPATH AND DOPPLER OBSERVATIONS DURING TRANSATLANTIC DIGITAL HF PROPAGATION EXPERIMENTS

Bodo W. Reinisch and Klaus Bibl
University of Lowell Center for Atmospheric Research
Lowell, MA 01854

Mukhtar Ahmed
GTE Products Corporation
Needham Heights, MA 02194

Haim Soicher and Frank Gorman
USACECOM
Fort Monmouth, NJ 07703

Jean Claude Jodogne
Institut Royal Météorologique
Brussels, Belgium

SUMMARY

Digital HF transatlantic propagation experiments between two nodes at Dourbes, Belgium, and Needham, MA, USA, using identical Digisonde 256 systems became operational in October 1983. Additional nodes at Slough, England, and Fort Monmouth, NJ, using identical instrumentation are expected to become operational in summer 1984 forming a four node transatlantic network. Adaptive two way sounding and real time channel evaluation studies will be conducted among the network's four nodes. Presently, the Dourbes station is transmitting 10 kW pulses using a horizontal rhombic antenna while the Needham station uses a log-periodic antenna for both transmission and reception. Measurements of amplitude and Doppler shifts of different multipath modes during magnetically quiescent and disturbed periods for the first month of operation are reported.

The pulse modulation (130 μsec at 100 Hz pulse repetition rate) enables clear separation and identification of the multihop paths. Real time discrete Fourier transforms determine the Doppler shifts imposed by height changes of the reflecting ionospheric layers. A comparison of the observed MUF's of the dominant 2F mode with the MUF's predicted by the IONCAP model show the latter to be about 20-30% higher. Significant changes in the ionospheric structure and dynamics along a medium range link from Goose Bay, Canada, to Lowell, USA, were observed during a moderately stressed event on November 10, 1983.

1. INTRODUCTION

The availability of Digisonde 256 systems at a number of widely dispersed stations suggested their use for digital HF propagation studies. In summer 1983, a Digisonde users group was formed with the goal of conducting joint oblique propagation experiments. The members of the group are GTE Sylvania in Needham, Massachusetts, USACECOM in Fort Monmouth, New Jersey, the Institut Royal Météorologique in Brussels, Belgium, the Rutherford-Appleton Laboratory in Slough, England, and the University of Lowell in Massachusetts (Figure 1). The Digisonde 256 is well equipped to measure important propagation parameters with high digital resolution (Bibl et al, 1981):

Amplitude	1/4 dB
Phase	24 mrad
Doppler	0.2 Hz (16 spectral frequencies in ionogram)
	0.01 Hz (256 spectral frequencies in drift mode).

The resolution of the angle of arrival measurements depends on the dimensions of the receiving antenna array. For vertical sounding, the Digisonde generally uses a receiving array of seven crossed-loop antennas to determine the angle of incidence of the ionospheric echoes and to separate the O and X-polarization echoes (Reinisch et al, 1983).

Adequate frequency stability and time synchronization are necessary for any bistatic link. In the Digisonde all signals are derived from a heated 16 MHz quartz oscillator with a stability of one part in 10^8 per day. The system's clock is software controlled and synchronized with a one second pulse derived from the quartz. Therefore, the transmission schedule, the transmitter pulses, the transmitted high frequency and the digitizing pulses are all phase coherent allowing the calculation of the complex Fourier spectrum for the received echoes.

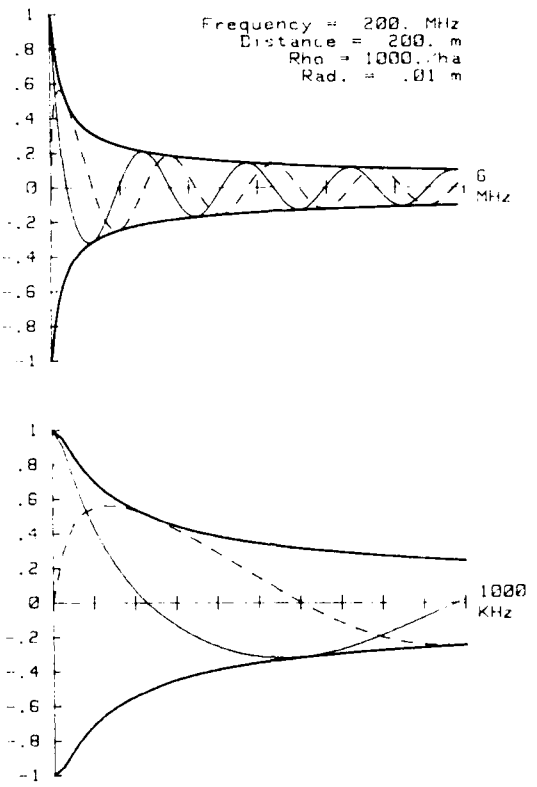

Fig. 19 Two-frequency correlation function (200 m path)

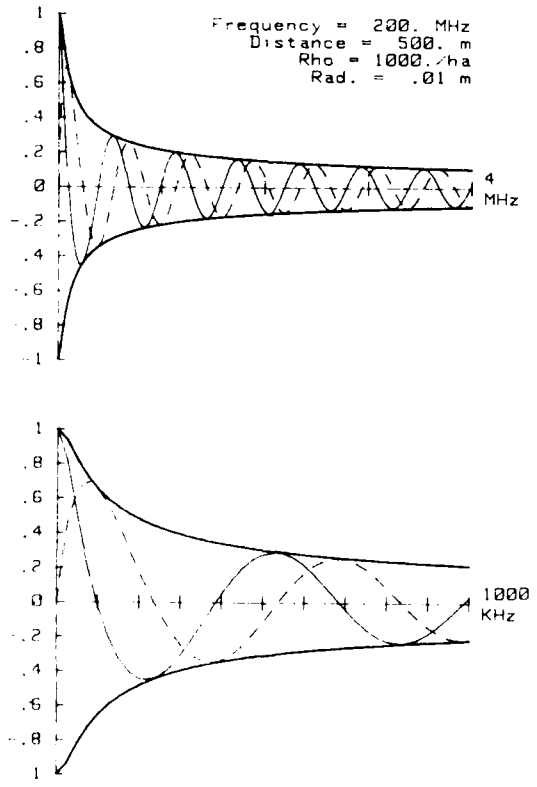

Fig. 20 Two-frequency correlation function (500 m path).

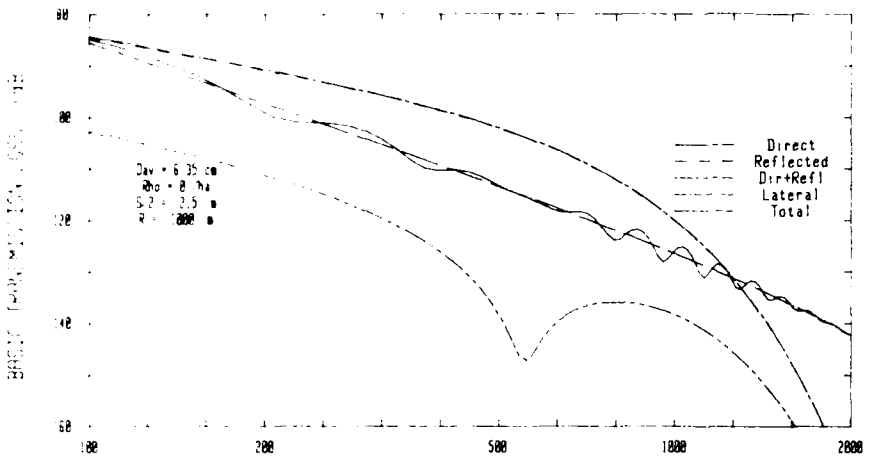

Fig. 15 Basic transmission loss (leaves).

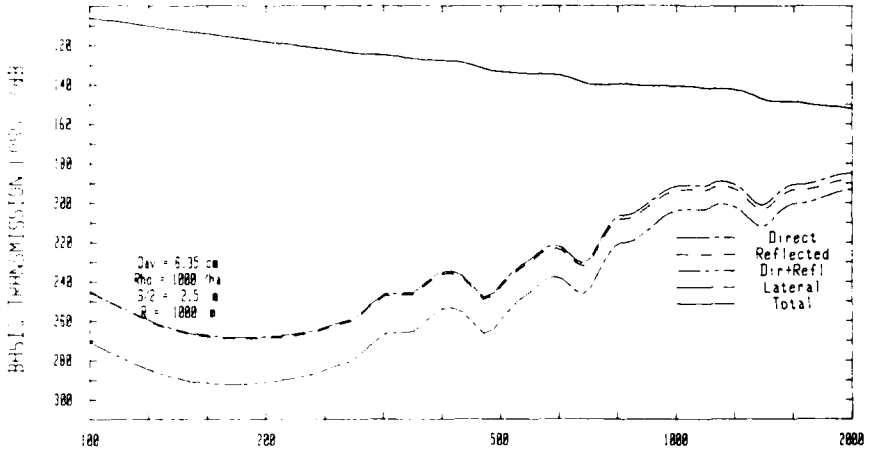

Fig. 16 Basic transmission loss (trunks).

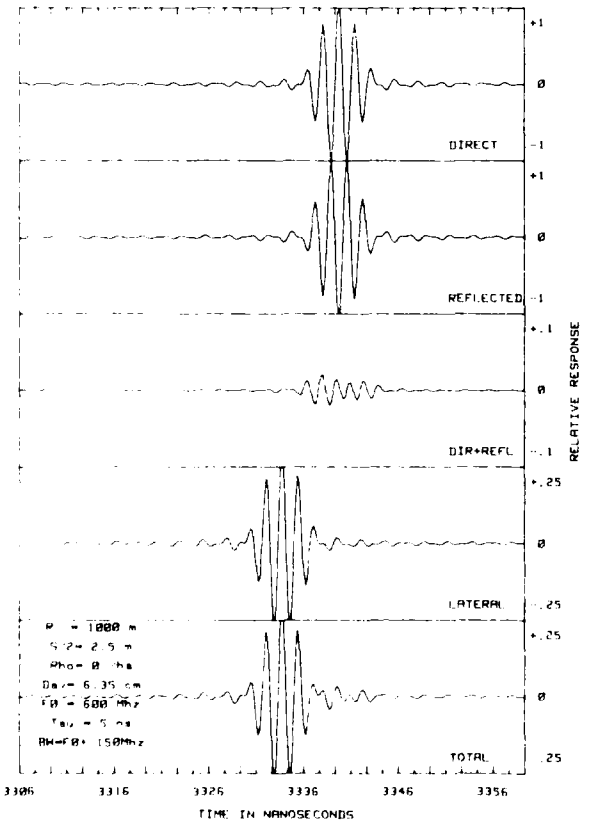

Fig. 17 Mean forest pulse response (leaves).

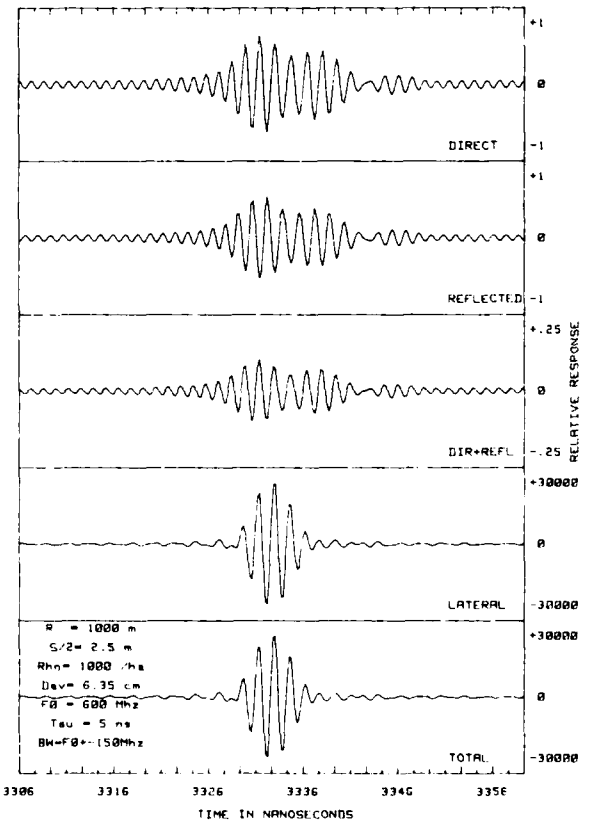

Fig. 18 Mean forest pulse response (trunks).

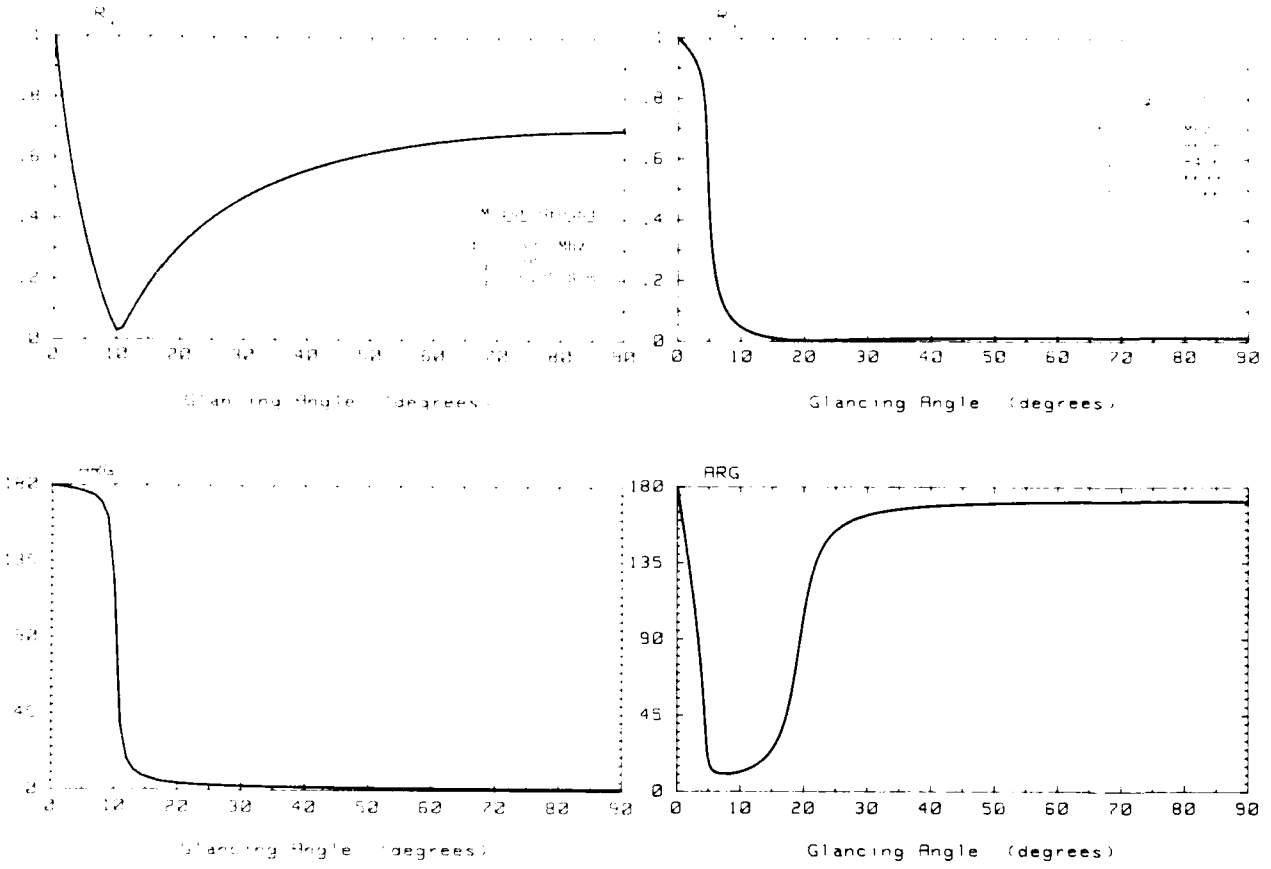

Fig. 11 Fresnel reflection coefficient (moist ground).

Fig. 12 Fresnel reflection coefficient (lossy leaves).

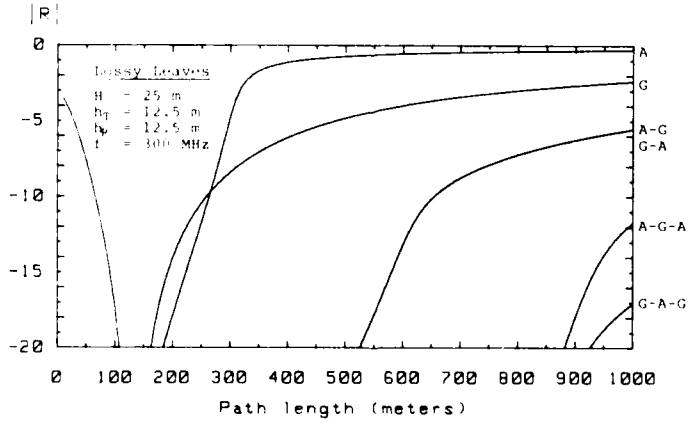

Fig. 13 Composite forest reflection coefficient.

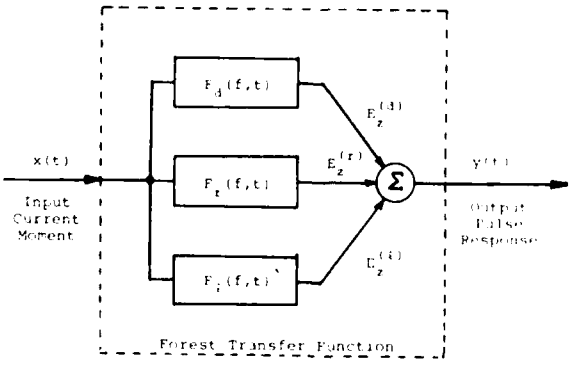

Fig. 14 Forest channel model.

a)

b)

c)

d)

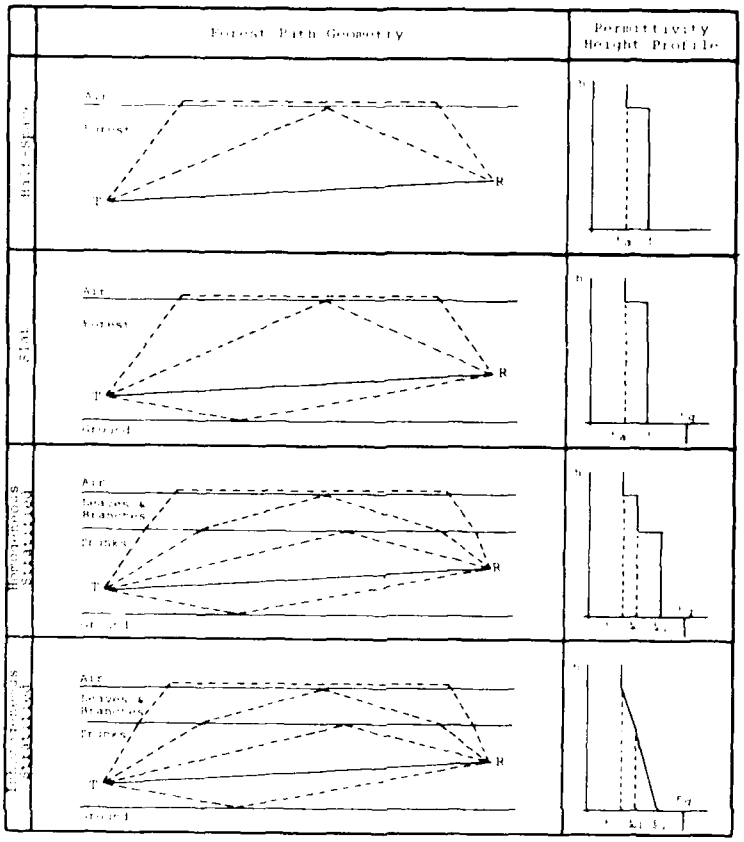

Fig. 9 Stratified forest models.

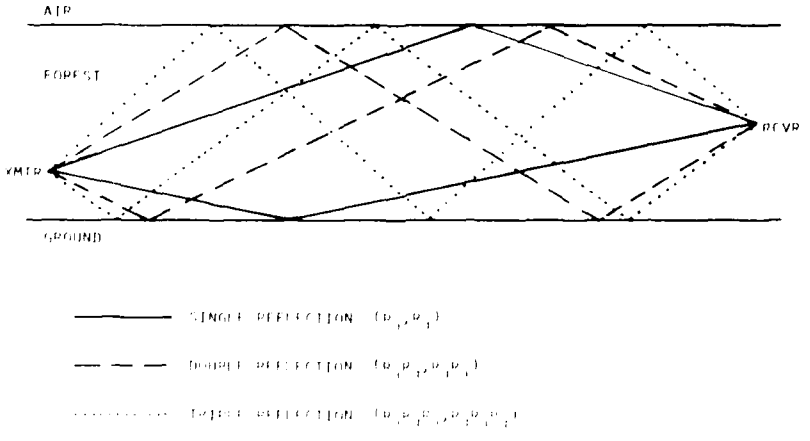

Fig. 10 Forest Multipath.

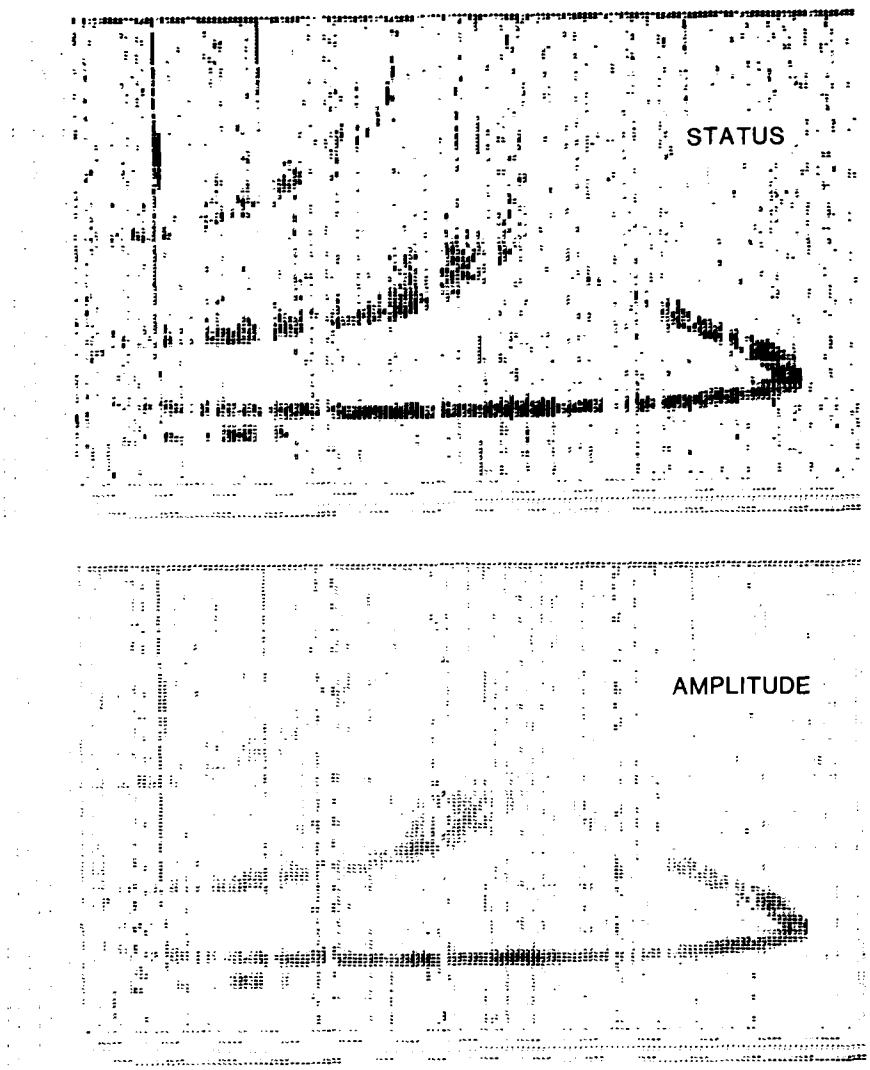

OBLIQUE PROPAGATION
GOOSE BAY - LOWELL
03 FEB 1983

FIGURE 10

DISCUSSION

P.A.Bradley, UK

You show a comparison between maximum observed frequencies and monthly median MUF's predicted by the Ioncap procedure (Fig.4). Measured values are less than those predicted, which is in the reverse sense to that normally found for other paths (see CCIR documents). This result may well be true, but I would be reluctant to form a conclusion on the basis of only 4 days measurements, especially when day-to-day variability is so great that the decile range is at least 40% of the median value. I would recommend further comparisons with the new prediction maps produced at the Institute for Telecommunication Sciences, USA (Rush, Anderson et al.). These maps are believed to be more accurate over the oceans, particularly in the area pertinent to your experiment, than the maps inherent in Ioncap.

Can you measure the azimuth of arrival of oblique-path signals with your equipment?

Author's Reply

The observations on four days can certainly not be generalized. The digisonde 256 is well equipped to measure the incidence angle if an adequate receiving antenna array of either 4 or 7 antennas is available.

C.Goutelard, Fr

Comment: Il est intéressant d'effectuer des mesures d'angles de site mais ces mesures sont délicates pour deux autres raisons: Le fading qui affecte les signaux et le bruit a un role important sur la précision de mesures.

Question: Le parcours sur lequel vous avez fait vos mesures est au quasi totalité maritime. Le doppler que vous mesurez dépend de l'ionosphère et de l'état de la mer. Avez-vous étudié une méthode qui permettrait de décorréler ces deux effets?

Author's Reply

We have not tried to separate the ionospheric and ocean state doppler. Frankly, I do not know how to do it. We had used the Digisonde in the past to determine the Bragg scatter lines from direct sea reflections, but then the ionosphere is not involved.

AN IONOSPHERIC MODE DETECTION SYSTEM FOR HF COMMUNICATIONS APPLICATION

T.B. Jones and P.L. Hayhurst
Physics Department
University of Leicester
Leicester, LE1 7RH, England

1. INTRODUCTION

A major problem experienced in HF data communications is that of multipath interference. When this situation occurs, components of a transmitted signal arrive at a receiving station over different propagation paths. If these components are of comparable signal strength, their mixing can lead to serious destructive interference fading and therefore loss of data. Another result of multipath interference is that the delay between the signal components imposes an upper limit on the transmission rate since data bits transmitted at different times can arrive at the receiver at the same instant, thus leading to confusion in the decoding system.

Since these errors are caused by multipath radio propagation it is important to identify the paths over which the signal components have travelled and by what time delays they are separated. This is best achieved using one of the many available oblique ionospheric sounding techniques. Examples of such techniques are Oblique pulse sounding (1) (2), Chirp sounding (3) and Backscatter sounding (4). Examples of other sounding techniques more directly related to communications are described by Fenwick (5), Probst (6), Stevens (7), Betts (8) and Filter (9).

These techniques in general either require costly and bulky ground based equipment combined with large antenna arrays, or do not provide an unambiguous picture of the multipath structure of the radio signal. The technique described in this paper, however, enables the longer time delay multipath structure of the communications channel to be readily monitored with a minimum of expensive specialised radio equipment.

Once the mode content information has been measured from the sounding technique it is possible to use this information to calculate the error rate one could expect on a given data link. This prediction could in turn be used to improve the system performance by initiating a change in transmitter frequency, a reduction in the data rate or an increase in the level of any error protection encoding.

2. A TECHNIQUE FOR MODE CONTENT EVALUATION

The technique for mode detection chosen in this investigation is that of injecting sounding pulses into the communications channel. The format of the pulse sounding signal is reproduced in Fig.1A. It consists of a sounding pulse Ø.7ms long in the centre of a break in the carrier of 21.8ms. The entire sequence is repeated every 9Øms. The pulse length is chosen so that it can be contained within a normal voice communications channel (3KHz) bandwidth. The sounding pulse is made as short as possible to facilitate the resolution of the modes by measuring the times of flight of each mode. If the pulse was shorter it would spread over a greater bandwidth or it would be filtered out by normal communications equipment. The exact length of the pulse results from the availability of a commercial crystal whose frequency was a convenient multiple of that required. The duration of the gap surrounding the sounding pulse corresponds to the original estimate of the maximum possible observable delays between modes in a multimode situation (ie a difference of 11ms between the longest and shortest time of flight). The 11ms gap ensures that the sounding pulses are not confused with the large blocks of carrier. The blocks of carrier are sufficiently long to activate the automatic gain control (AGC) of a standard radio receiver so the sounding pulses are clearly visible and the receiver does not limit. The exact lengths of both the gap and the carrier block are again selected for convenience, being 31 and 97 times the length of the sounding pulse respectively (31+97=128).

When the sounding signal is transmitted via the ionosphere more than one propagation path is usually possible. These will result in the sounding signal arriving at the receiver at different times and with different amplitudes and phases (Fig.1B and 1C). With a normal omnidirectional antenna these two waveforms would add vectorially to give the waveform reproduced in Fig.1D which contains sounding pulses from both modes. In this instance the two blocks of carrier add constructively but this is not always the case and cancellation could equally well occur. One of the main aims of this research project is to detect and resolve this combined signal automatically.

As indicated in the illustration, the transmitted pulse is dispersed during its propagation through the ionosphere and probably to an even greater extent by the transmitting and receiving equipment. This process leads to a deterioration in the ability to resolve pulses with closely similar times of flight.

To obtain a qualitative assessment of the relationship between the pulse sounding result and the measured data error rate a test data sequence was developed. This sequence consists of 1125 bits of on/off keying, a 33 bit Barker code for synchronisation and finally a 1Ø23 bit pseudo random sequence (PRS) over which the error rate is measured.

By employing a micro-computer to produce the PRS, different data rates could easily be generated. Of these the most common were 5Ø, 75 and 6ØØ baud. The 1125 bit on/off keying at the start of the test sequence was used for bit synchronisation. The 33 bit Barker code was made up of three 11 bit Barker sequences, and is taken to define the start of the data. The test data itself consists of a 1Ø23 bit PRS produced from a ten bit shift register with feedback taken from elements 5 and 1Ø fed through an exclusive OR to generate the new first element. The message is sent as non return to zero (NRZ) and is continuous.

The experimental transmissions were constructed from a combination on the pulse sounding and the test data sequences so that both could be evaluated under similar conditions.

3. EXPERIMENTAL TECHNIQUE

The experimental hardware consists of a transmitting and a receiving station and is summarised in Fig.2.

The transmitting equipment was required to operate unattended for long periods and was therefore automated to a large extent. The control system was a Motorola 68ØØ based micro-computer with its program stored in EPROM and an automatic restart facility to protect against power failure at remote sites. Different sounding sequences and data rates described in the previous section were selected via a thumbwheel switch which was read on restart. This computer then keyed a Heathkit DX6ØB radio transmitter to produce about 2ØW on the allocated frequency of 4.7925MHz. The output of the DX6ØB was fed into a Dentron GA4Ø6 linear amplifier producing a CW power of 4ØØW. To protect the transmitter a novel device was installed which measured the standing wave ratio onto the antenna and cut the power to the amplifier if this deteriorated seriously.

The computer controlled receiving station automatically detects the sounding signal and records its parameters in digital form. Data analysis can be carried out on line or alternatively by the campus mainframe computer. The sounding signals transmitted via the ionosphere were detected by a computer controlled receiver. This was a Racal RA117 slave, tuned by generating the first and second VFOs from external computer controlled Adret synthesisers. The receiver bandwidth was variable from 1ØØHz to 12KHz and the gain could be controlled either manually or by means of the automatic gain control (AGC). Output from the receiver was taken at the 1ØØKHz IF. In order to test the receiving station the 1ØØKHz pulsed signal could be generated locally by a small electronic simulator.

The amplitude and phase of the incoming signal were detected and converted to digital values for processing by the computer. A sample rate of once every 9Øμs was chosen so as to give adequate time resolution without overburdening the computer with too much processing.

The project computer was another Motorola 68ØØ based unit. It was constructed around the popular S5Ø bus to enable easy expansion and testing. Memory on the computer is provided by EPROM for program storage, RAM for workspace, and floppy disc for temporary storage of collected digitised pulse information. An internal clock was incorporated with the computer to add time of day information to the data files. After an experimental run the digitised sounder information was transferred directly or via nine track magnetic tape to the CDC Cyber 73 University mainframe computer for long term storage and more detailed analysis.

4. DATA ANALYSIS

The first stage in identifying the mode content of the received signal was to automatically measure the amplitudes and relative times of arrival of the sounding pulses. In order to do this under conditions of moderate to severe noise the following averaging technique was employed and is illustrated in Fig.3.

The computer first looks for a transition from a long block of carrier on, to carrier off (A in Fig.3). To confirm its decision it then checks to ensure the following period of carrier on and off occur at the correct times (B). If these agree, then synchronisation has been achieved and the computer stores the digitised pulse signatures of the following eight returned soundings (C). Eight pulses were found to be sufficient to greatly reduce the probability of mistaking a noise spike for a pulse echo without causing too great a computer overhead.

Once the captured echoes had been combined to give one average pulse return (D) the computer scanned this looking for significant echoes. A pulse is said to exist if the signal rises above a threshold level for more than two consecutive samples. The amplitude is taken as the highest signal level during the period of the pulse. The relative time of arrival is arbitrarily taken as being from the start of the sample window to halfway between the sides of the chosen pulse echo. The sides of the pulse were chosen since they are less susceptible to noise than the actual peak.

In order to convert the amplitude to a prediction of the signal mode content a simple ionospheric model was employed (Fig.4). The model allowed flight times to be determined from geometrical considerations given the ground range of the transmitter and receiver values for the height of the E and F layers of the ionosphere. The mode

amplitudes were estimated by allowing for a certain percentage absorption loss during passage through the lower ionosphere. Although the curvature of the Earth was not taken into account while calculating the time of flight, allowance was made for the E region falling below the horizon for paths in excess of 21ØØKm for certain portions of the day. Finally the model allowed for the possibility of blanketing sporadic E (Es) where the E region critical frequency rises above that of the F and so blankets out the F layer reflection.

The actual mode content evaluation was made as follows. From the simple model considerations above, the mode likely to have the greatest amplitude is identified. Next the first two pulses received are examined and the larger of the two is ascribed to the largest expected mode. The other pulses in the received signal are then compared with the predicted time delays and the level of agreement is indicated by a four point probability scale. In the case of a short path where ground wave is possible this is forced to be identified as the first received pulse.

In addition to the mode content evaluation, the software generates information on the average pulse length, the number of significant modes and the resultant likelihood of multipath interference. As a guide to the noise content of the channel, the average signal level and the signal to noise ratio are also calculated.

The next objective is to read the 1Ø23 bit PRS and thus measure the error rate. This requires that the exact starting time is determined and is achieved in two separate operations. Firstly the on/off keying. A transition from a "1" (signal on) to a "Ø" (signal off) is detected and taken to be the start of a bit of information. The next eight bits of information are then read. If these bits form the word (Ø1Ø1Ø1Ø1) then bit synchronisation has been achieved. If, however, at any point in this sequence an error is found, the program returns to the start.

The second operation is to identify the Barker sequence. After bit synchronisation the incoming signals from the ADC are converted to "1" or "Ø" data bits which are fed into the software equivalent of a shift register, (actually a continuous loop of memory). After the latest bit has been added to this loop by clocking the shift register, the contents are compared with the known values of the Barker sequence. If the sequence has been received correctly the result will be 33, one for each correct bit. For signals received over an ionospheric path errors are likely, hence a threshold of 25 is set and for values greater than this the Barker code is said to have been recognised. If the result of the comparison yields a value of less than 25 the Barker code has not been found and therefore the next bit of data is clocked into the shift register and the test is repeated. The implementation of this routine is the most difficult part of the entire process involving 33 comparisons plus the associated instructions to set up addresses and collect the data bit taking place within 1.6ms (1 bit at 6ØØ baud). Once the Barker code has been recognised the program reads the 1Ø23 bit PRS into main memory. When this has finished the contents of memory are compared bit by bit with the known composition of the data sequence which is stored in EPROM. The number of bit errors is then displayed on the VDU connected to the project computer.

5. RESULTS OBTAINED FOR VARIOUS PROPAGATION PATHS

During the course of the project experiments were performed over paths of different lengths, details of which are shown below.

Path	Length (km)	Data sets
Oadby - Leicester	4	12
Durham - Leicester	241	22
Elgin - Leicester	578	144
Tromsø/Bodo - Leicester	2156	75/23

A typical set of data from the Oadby transmitter is reproduced in Fig.5A. The first feature to note is the very low noise level even though on several occasions the signal is limiting. In the sounding records, three pulses can clearly be seen with relative arrival times (ie the arrival times relative to the first pulse received) of 1.6ms and 3.2ms respectively. Comparison with the model suggests that the three propagation modes present correspond to ground wave, 1 hop F and 2 hop F. A second feature of the Oadby data is the ease with which sporadic E or Es modes can be recognised. Fig.5b presents data received from Oadby during a 5.7 second period which contains two obvious propagation modes separated by Ø.7ms. The first of the two pulses must be the ground wave, consequently the second must be reflected from the ionosphere at a height of about 1Ø5km, which is consistent with an E layer path. This Es blankets out all the F layer propagation paths which would have otherwise been received with longer time delays.

The path from Durham to Leicester is considerably longer with a ground range of 241Km. An example of results obtained over this path is given as Fig.5C. This plot contains two modes separated by approximately Ø.7ms, and reference to the model suggests that they correspond to E and F layer propagation. This example shows particularly well

the fadeout in the signal where the dominant mode changes from E to F layer propagation.

The third path over which tests were conducted was from Elgin in Scotland to Leicester (578Km). It was over this path that most of the pulse sounding/data comparison experiments were conducted. An example of the results obtained is given as Fig.5D. This shows two pulses separated by about 1.6ms. Comparison with the predictions suggests E and 2 hop F propagation, but no 1F due to E layer screening. More typically, however, the pulse structure was partially obscured by noise or interference and required averaging over many echoes to clarify the picture.

The longest paths considered are those from Norway to Leicester and an example of this data set is reproduced as Fig.5E. On this plot two pulses separated by about Ø.5ms are present. The predictions indicate that this could be either a 1 hop E or 1 hop F, together with 2 hop F. 1 hop F appears to be more likely than 1 hop E for the day when the measurements were made. The E layer signal would be quite heavily attenuated and it is also possible that for non-average conditions (ie lower E layer reflection height) the Tromsø Leicester path would be longer than the maximum range of an E layer reflection (2365Km for a reflection height of 11ØKm).

A noteworthy feature of the data received from Tromsø and Bodo in Norway is that large differences in arrival times of the sounding pulses were recorded for about 1Ø% of the observing period. Fig.5F presents a very clear example of this phenomenon, where there are two pulse returns present separated by about 1.8ms. Comparison with the propagation mode predictions reveals that none of the normal modes can have such large differences in propagation times. From these and other examples, it became clear that the long-delayed pulses must be received over none great circle paths (NGC). Previous work (1Ø)(11) has connected this type of propagation with reflections from the edge of the auroral zone. For the path in question the average position of the southern edge of the auroral zone has been displayed as a function of the time of day (Fig.6). From this map and assuming an auroral reflection height of 25ØKm, propagation times of between 12 and 8ms at 1ØØØ and 18ØØ hrs respectively were predicted. This would give relative times of flight of between 5 and 1ms when compared with a normal great circle 1F reflection.

The recorded time delays were, however, consistently shorter than those predicted from the map geometry. Moreover, the reflections were sharp rather than spread as might be expected from a diffuse auroral scattering process. For these reasons it is suggested that the origin of the NGC modes is the poleward wall of the mid-latitude trough (MLT). The MLT usually lies several hundred kilometers south of the edge of the auroral oval thus explaining the differences between the measured and predicted propagation times. The MLT is generally considered to be a night time phenomenon but there is evidence (12) that it can be observed from 14ØØ to Ø7ØØ local time which would confirm the present observations.

6. THE RELATIONSHIP BETWEEN ERROR RATES AND SOUNDING RESULTS

It is of considerable practical importance to investigate the relationship between the pulse sounding results and the error rates measured in the test data sequence. The format of the transmitted sequence has already been discussed. This section presents comparative results for both the pulse sounding and the data sequence.

Fig.7 is a sample plot of four pulse sequences and their associated error rates. For each of the pulse sequences the following procedure was followed: First the eight pulse returns are averaged to reduce the effect of random noise. Then the computer analyses the pulse signature as described in section 4 to produce figures for the number and size of the modes present and the signal to noise level. For each block of pulse sounding, two blocks of data are sent. These are received, decoded and stored as previously described. Once the data is in memory it is compared with the original format and the errors counted and printed at the bottom of the plot. The error analysis, however, extends this procedure. First the data stream is searched for bursts of errors of a particular type. A burst of high errors (a '1' where a 'Ø' was expected) usually indicates that a channel is being shared with a second interfering transmitter. A burst of low errors (a 'Ø' where a '1' was expected) suggests that the signal is suffering from destructive modal interference. Finally the totals of these error bursts are printed out on a line printer log, along with a qualitative evaluation of the condition of the communications channel.

Fig.7 clearly demonstrates that the higher noise levels recorded in block 3.4 are associated with an increase in the error rate as would be expected. This figure also demonstrates how rapidly the noise environment of the system can change. Between blocks 3.3 and 3.4 a sudden increase in the general noise level has occurred. This suggests the presence of man-made local electrical interference as might be caused by an electric motor.

The effects of noise on the data are summarised in Fig.8. This displays the entire data set upon which this analysis is based and indicates the received error probability against the ratio (S/N) for each PRS data set. The points follow a general trend from the bottom right hand corner to the top left hand corner of the graph. This is expected, since the greater the noise level the more errors would be present.

The points running up the vertical axis are caused by a measured (S/S+N) of zero which implies that the program was unable to recognise the pulse sounding signal and therefore could not find a value for S. The points running along the top of the graph

represent error rates of approximately 5Ø% and hence no correlation with the PRS. This situation is caused by a failure of the program to identify the Barker sequence. Both of these events indicate a system failure due to a rapid change in the propagation conditions between the reception of the pulse sounding and the PRS data (ie within 25 sec). This partially explains the wide spread of points around the general trend. It should also be noted that multipath fading will also cause some spread in the data points.

In order to predict these errors, the incoming data stream was reconstructed from the results of the pulse sounding. Waveforms representing different modal components were added together vectorially within the computer so that the resulting vector sum would enable the simulation to take account of fading effects. Next a normal noise distribution is added, centered on the mean level from the S/N ratio. Part of the noise energy is added in the form of short pulses to simulate local electrical noise at the receiving site. A simple running mean filter was then applied to the data to simulate the bandwidth limits of the radio system. An example of the above process applied to both the pulse waveform and the data stream is given in Fig.9. The solid line drawn through the data represents the threshold level between a '1' and a 'Ø' data bit. With this level the data was decoded and the number of errors calculated.

By means of this process the error rates can be predicted. Furthermore, the effect on error rate of various changes in the channel environment (eg data rate, fading rate, fading depth, noise level and radio bandwidth) can be evaluated.

The validity of this procedure can be judged by plotting out the predicted errors against the actual received errors (Fig.1Ø). This graph indicates that in general a low predicted error rate corresponds to a low measured error rate. A similar correlation exists for very high error rates as indicated by the worst possible case of the 5Ø% error rate. The expected wide spread of points due to the variability of ionospheric and local noise characteristics is apparent over the middle section of the graph. The most serious area of disagreement, however, is the line of errors in the bottom right hand corner of the plot, caused by the program failing to recognise the sounding pulses.

If the pulse sounding signals are employed in real time under operational conditions, rather than being stored for later analysis as in this investigation, this problem would not arise. Under operational conditions the program would restart and try again if it failed to recognise the pulse sounding sequence, rather than simply reporting the failure as in the situation represented in Fig.1Ø. The resultant potential accuracy of the system can now be displayed as indicated in Fig.11. This illustrates the true error (ie the difference between the measured and the predicted values) associated with a particular error prediction. Thus for a 2Ø% predicted error rate, the measured errors will on average be within 15% of the value. It must be noted that such predictions only apply to this particular data transmission format. The longer the time separation between the pulse sounding and the data stream, the less accurate the predictions become.

7. CONCLUSION

The principal objective of this study was to provide a low cost ionospheric sounder for determining the mode content of the received signal with a view to improving system performance. The investigations have shown that the pulse sounding procedure can reliably recognise propagation modes within the following limits.

The maximum time resolution of the system is approximately Ø.5ms between arriving pulses. Thus modes with nearly equal times of flight (eg 1E and 1F on paths longer than 5ØØKm) are not easily resolved. However, the major limitations of the system are the twin evils of noise and interference. To achieve the best time resolution, a receiver bandwidth of at least 3KHz is required, which under normal circumstances, allows a significant amount of noise to enter the system. The compromise solution was to adopt a bandwidth of 12ØØHz which reduced the noise by 5Ø% and degraded the time resolution to about Ø.7ms. This bandwidth was adequate for most of the experiments undertaken. It was not, however, possible to overcome co-channel interference within the 12ØØHz pass band and this proved to be one of the system's major operational limitations. Under these conditions recourse must be made to predictions, or a new frequency selected.

If the sounding system is to be employed as an aid to data communications, it is important to establish the dependence of the error rate over the link on the mode content as determined from the sounding pulses. An attempt was made to identify the causes of the errors in the particular data test sequence employed, so that the error rates could be predicted from observations of the mode content.

In general the error rate increases with the number of modes present and the expected error rates could be predicted from this mode structure. The reliability of these predictions varied with the actual error rate and the confidence factors discussed in the previous section must be applied. The low confidence values sometimes noted are thought to be due to rapid changes in ionospheric conditions in the interval between the pulse sounding and the data test sequence. For accurate error predictions the pulse sounding must therefore be closely integrated within the data stream. A possible scheme would involve 1Ø cycles of sounding every 1ØØ characters, which would provide real time sounding once every 1Ø seconds, compared with every two minutes during the present study. This improvement in predictions would be at the expense of a 12% reduction in the overall data rate (at 75 baud). Even more accuracy would be gained by interleaving the transmitted data within the carrier block portion of the pulse sounding signal. This would, however, involve major alterations to existing communications equipment and can therefore be

rejected as impractical.

The majority of errors recorded during the experiment were due to random noise. These could be minimised by reducing the receiver bandwidth but this is detrimental to the pulse sounding. This highlights a major problem encountered when mixing sounding and data transmissions. The optimum available bandwidth for 75 baud data is 3ØØHz, whereas for pulse sounding it is at least 12ØØHz. For future experiments of this type it would be advantageous to have a variable pass band receiver which could be changed by the control computer to suit the type of signal being monitored at any instant.

The pulse sounding system is a low cost aid to HF communications which enables the structure of signals received via multiple propagation paths to be evaluated. From this information an estimate of the expected fading induced error rate is obtained by comparing the relative amplitudes of the active modes. The measured relative time delays between modes provide an indication of the maximum data transmission rate possible before bit errors occur due to multipath propagation. Moreover, the pulse sounding signal can provide the (S/N) ratio for a given channel from which error rate estimates can be based. Finally, the presence of unpredicted modes such as sporadic E and Auroral zone reflections can be indicated, thus enabling the operator to make more efficient use of the prevailing propagation conditions.

8. ACKNOWLEDGEMENT

The authors wish to thank their colleagues at RAE Farnborough for supporting the project and for many helpful discussions. Peter Hayhurst acknowledges the receipt of an SERC "CASE" award.

9. REFERENCES

1. Hatton, W.L. (1961) IRE, Trans. Comm. Sys., CS9, 3, p 275.

2. Egan, R.D. and Pratt, D.S. (1963). Granger Associates, Palo Alto, California.

3. Fenwick, R.B. and Barry, G.H. (1967). Conf. Ground Based Rad. Wave Studies of the Lower Ionosphere, Ottawa, p 532.

4. Shearman, E.D.R. and Martin, L.T.J. (1956). Wireless Eng., p 19Ø.

5. Fenwick, R.B. and Woodhouse, T.J. (1979). AGARD Conf., CP263, p 5-1.

6. Probst, S.E. (1968). Ionospheric Radio Communication, Plenum, New York, p 37Ø.

7. Stevens, E.E. (1968). Ionospheric Radio Communication, Plenum, New York, p 359.

8. Betts, J.A. and Darnell, M. (1975). AGARD Conf., CP173, p 18-1.

9. Filter, J.H.J., Arazi, B. and Thomson, R.G.W. (1978). IEEE, Trans. Comm., COM26, p 913.

10. Wagner, R.A. and Pike, C.P. (1971). AGARD Conf., CP97, p 4-1.

11. Bates, H.F., Albee, P.R. and Hunsucker, R.D. (1966). J. Geophys. Res., 71, 5, p 1413.

12. Muldrew, D.B. (1965). J.Geophys. Res., 7Ø, 11, p 2635.

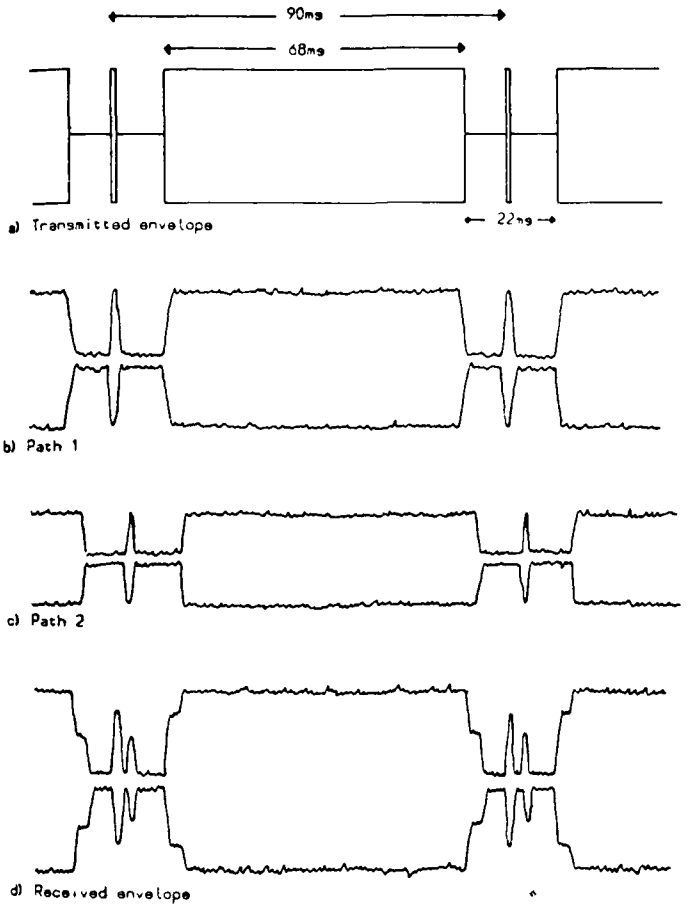

Fig. 1 Pulse sounding envelopes. (a) Transmitted sequence, (b) and (c) Signals received over two propagation modes, (d) Total received sequence

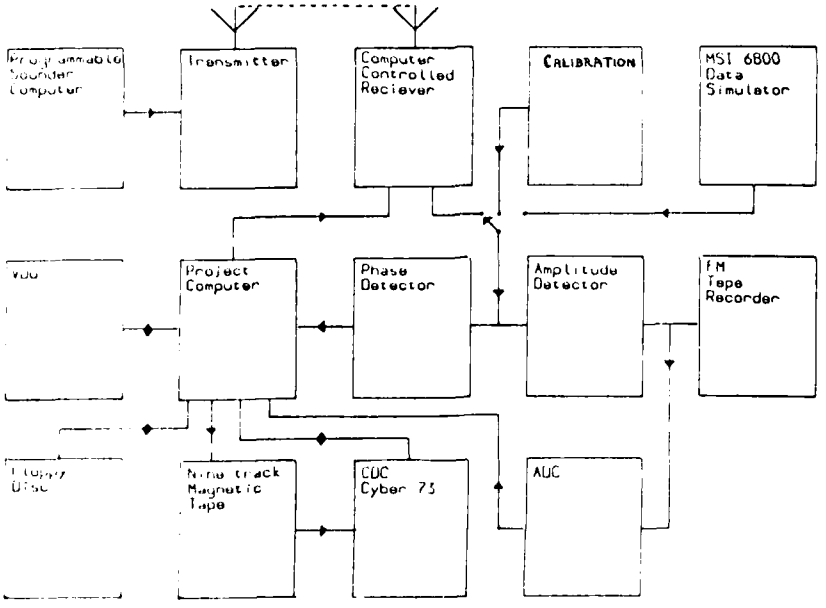

Fig. 2 Block diagram of mode detection sounder

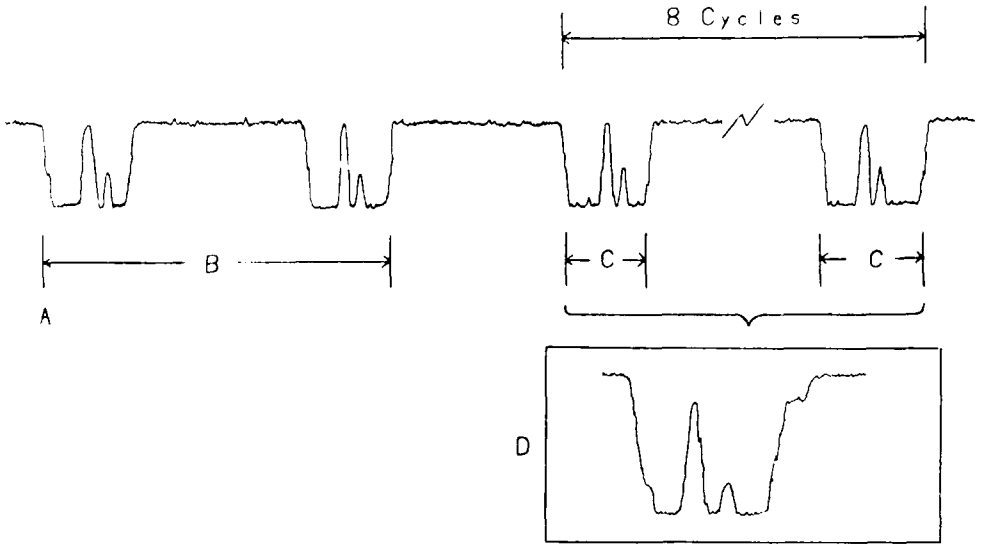

Fig. 3 Procedure for capture and analysis of the pulse echoes (see text for details)

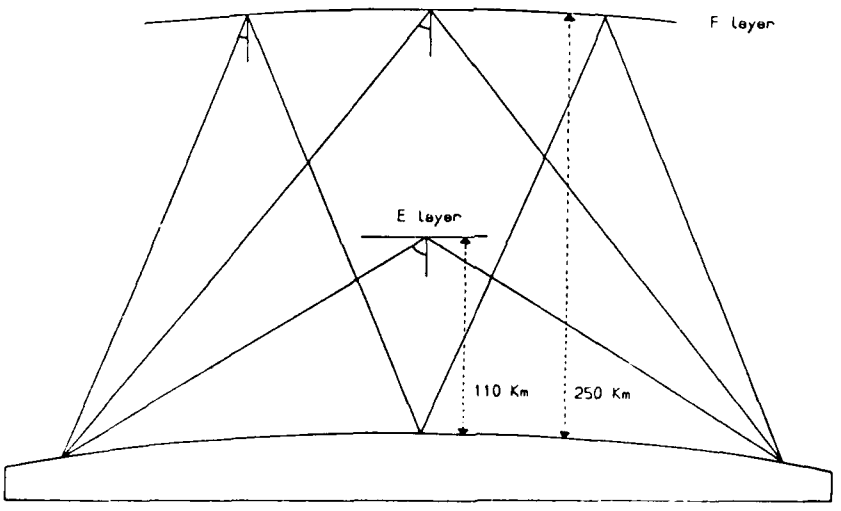

Fig. 4 Typical ionospheric propagation modes employed in prediction model

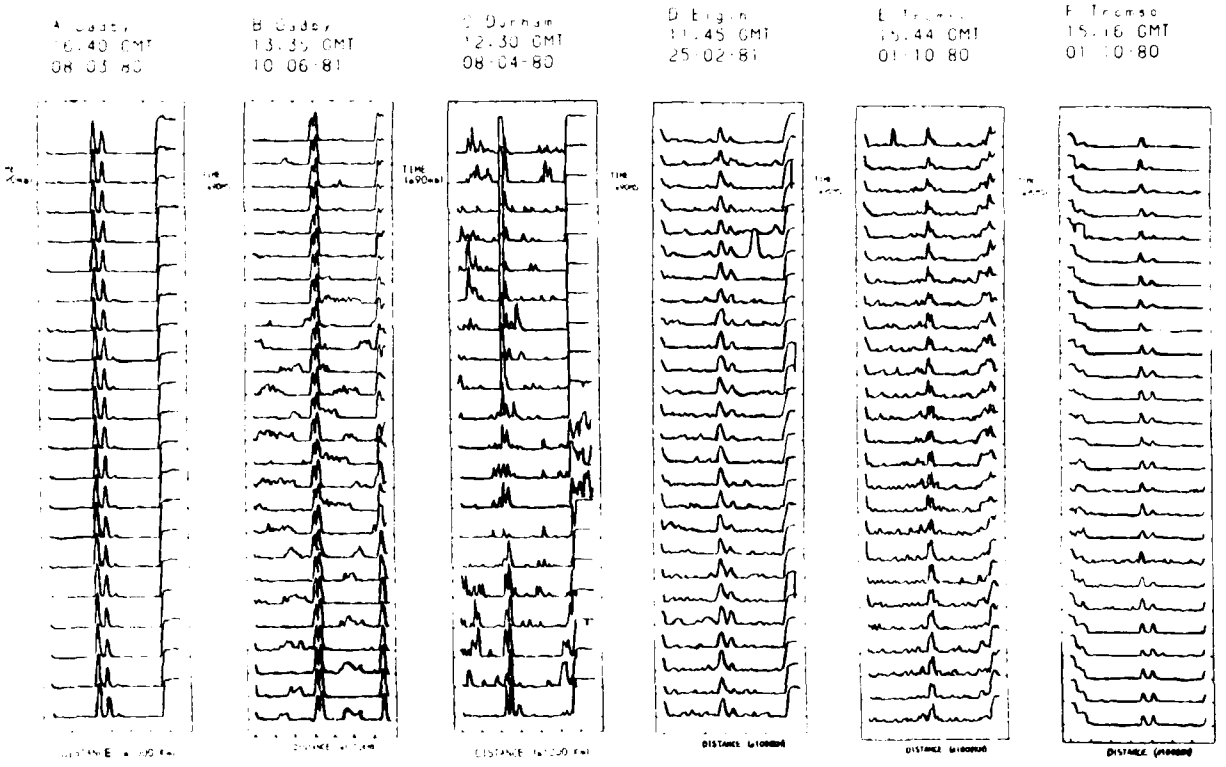

Fig. 5 Examples of pulse sequences received over various propagation paths. Path lengths range from 4 to 2156 km

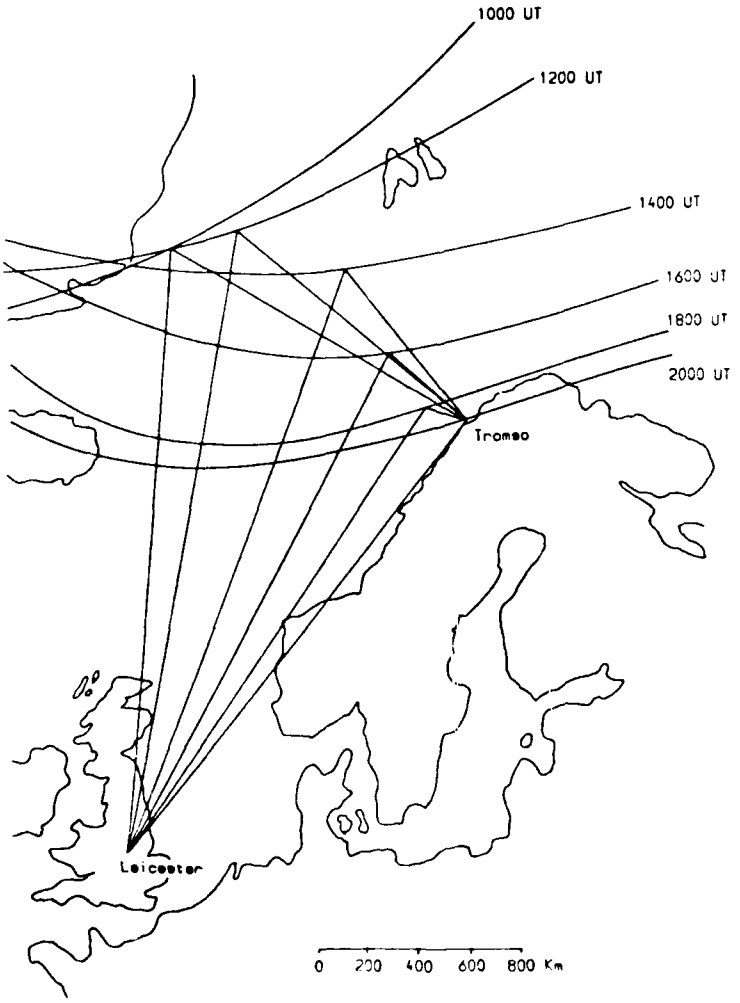

Fig. 6 Possible path geometry to account for long delayed echoes received from the auroral zone

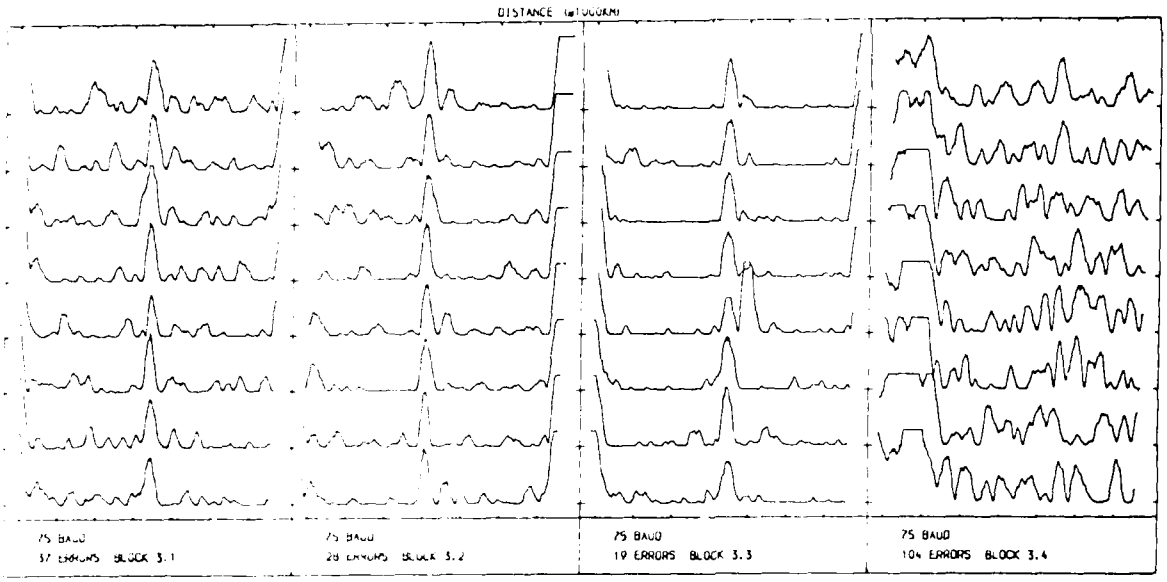
DISTANCE (x100KM)
75 BAUD
57 ERRORS BLOCK 3.1
75 BAUD
28 ERRORS BLOCK 3.2
75 BAUD
19 ERRORS BLOCK 3.3
75 BAUD
104 ERRORS BLOCK 3.4
ELGIN 14.27 GMT 29.05.81 4.792500 MHZ SUNDAY

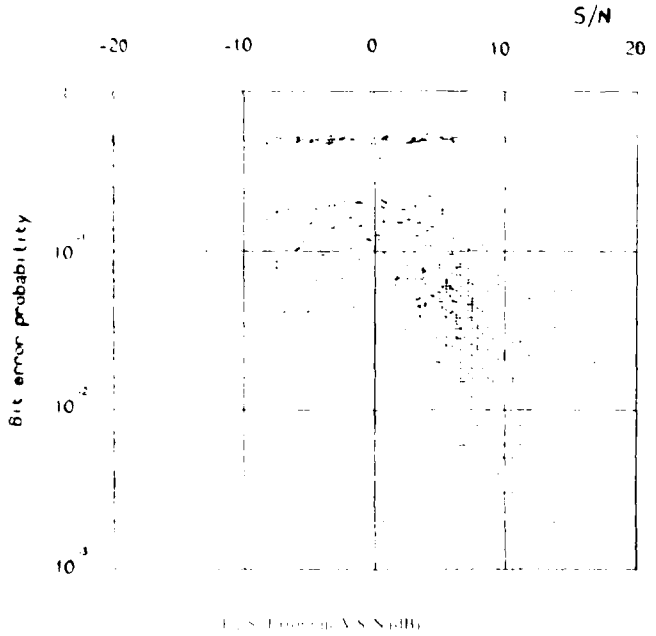
S/N
-20
-10
0
10
20
Bit error probability
10^{-1}
10^{-2}
10^{-3}

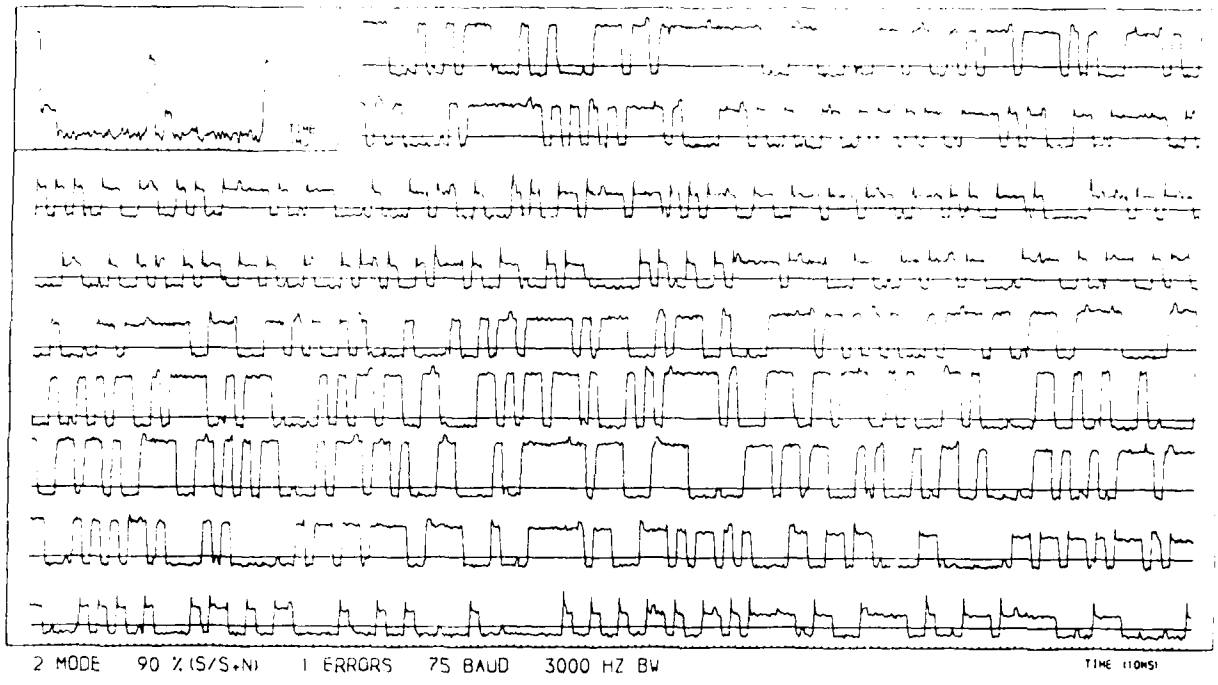

Fig. 9 Simulated data set. Plot sequence is shown with noise added. Horizontal line represents threshold between 0 and 1. Insert illustrates the two mode signal modelled

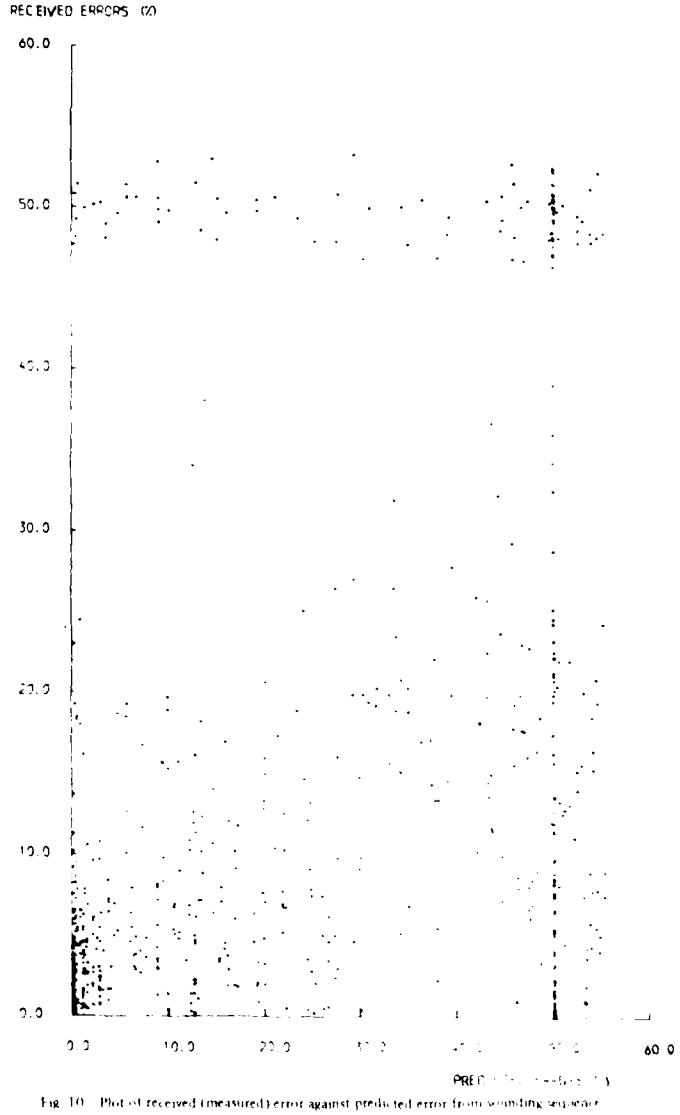

Fig. 10 Plot of received (measured) error against predicted error from sounding sequence

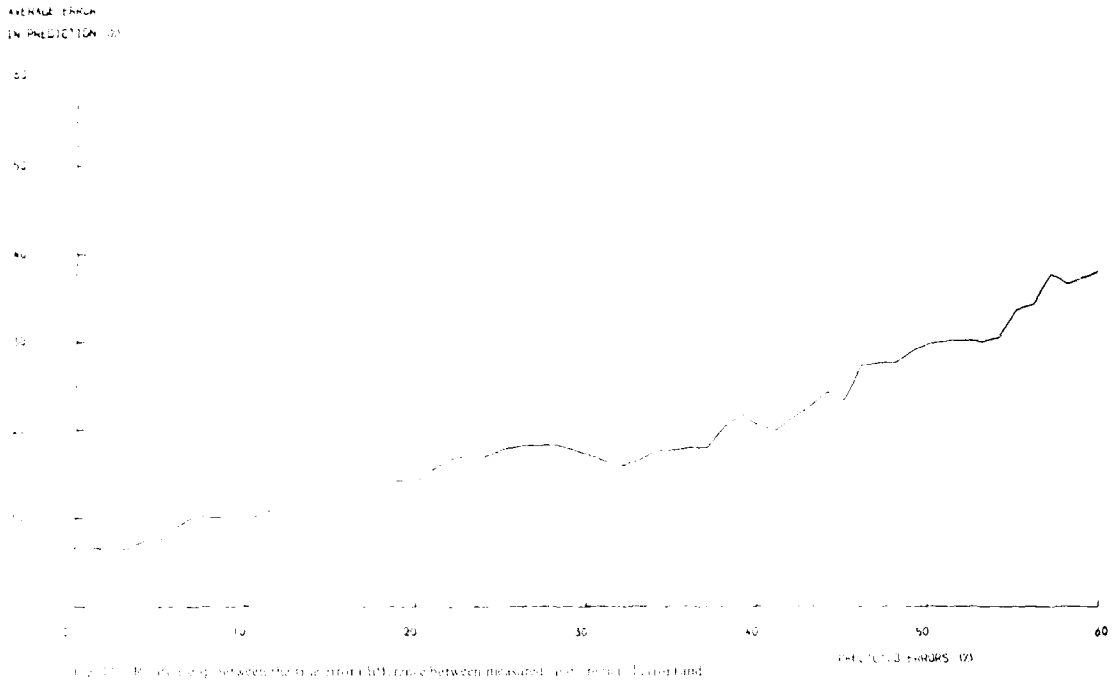

DISCUSSION

R.W.Jenkins, Ca

I would like to concur with the authors' observations of reflections from the poleward edge of the trough. Seven years ago at the Communications Research Centre in Ottawa, we used a large Mills Cross array to make directions and Doppler measurements on signals transmitted from a USAF Geophysics Laboratory aircraft, from which we were able to clearly identify well-behaved reflections from the poleward edge of the trough. These results were repeated on several flights, so it appears, from our small sample, to be a regularly occurring phenomenon. This work was reported in a paper entitled "Direction and Doppler Characteristics of Medium and Long Path HF Signals within the Night-time Sub-auroral Region" by Hagg, Montbriand and myself and was presented at the AGARD Conference, "Special Topics in HF Propagation", held in Lisbon in May-June 1979.

B.W.Reinisch, US

The auroral oval should not be considered as a possible explanation for the propagation delays as you have done. The oval is an F-region phenomenon, with generally low F-region ionization. The mid-latitude F-region trough is of course a likely candidate. However, it will be difficult to identify or specify whether it is the poleward or equatorward wall of the trough. Since the poleward wall is generally less well defined, it may be the irregularities in the equatorward wall that caused the sideways reflections.

Author's Reply

The long duration propagation delay are associated with well defined reflections and not scattered signals from an irregular region. This seems to fit well with the observations of Jenkins et al. given in the previous question.

AD-A154 031 PROPAGATION INFLUENCES ON DIGITAL TRANSMISSION SYSTEMS: 3/6
PROBLEMS AND SOLU.. (U) ADVISORY GROUP FOR AEROSPACE
RESEARCH AND DEVELOPMENT NEUILLY.. J H BLYTHE
UNCLASSIFIED 08 JUN 84 AGARD-CP-363 F/G 17/2 NL

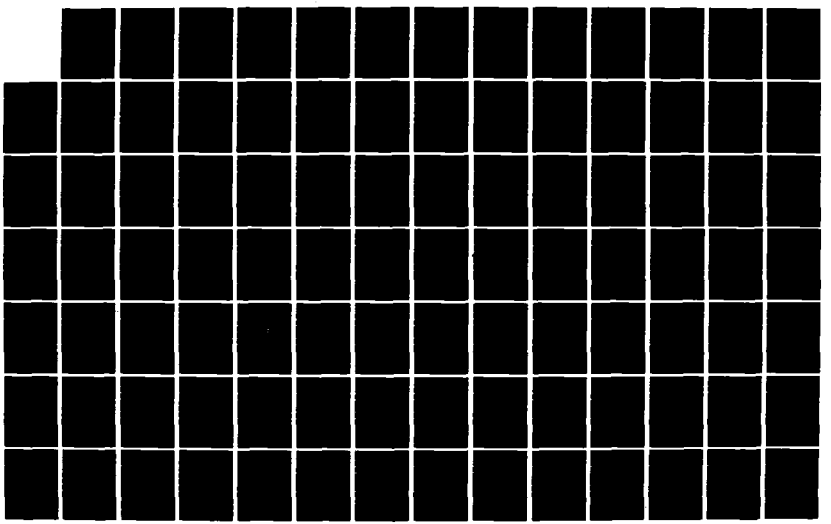

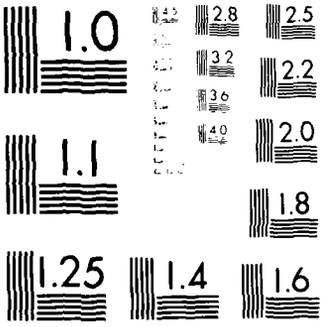

MICROCOPY RESOLUTION TEST CHART

WIDEBAND LINE-OF-SIGHT CHANNEL MEASUREMENTS AND SIMULATION: APPLICATION TO DIGITAL RADIO LINKS

R. Valentin, K. Metzger

Research Institute of the Deutsche Bundespost at the FTZ,
Am Kavalleriesand 3, 6100 Darmstadt, Fed. Rep. of Germany

SUMMARY

The performance of high-capacity digital radio links is impaired by frequency-selective fading during multipath propagation, even if the signal-to-noise ratio is adequate. In order to assess this degradation, measurements of the amplitude and group-delay distortions were carried out in a 40-MHz bandwidth at 4 GHz on a line-of-sight path. The results showed that the complex transfer function $H(\omega)$ of the propagation channel can be well approximated by a two-ray model. The influence of two-path fading can be estimated if the dependence of the notch depth versus the deviation between the notch frequency and the carrier frequency f_c for a fixed bit-error rate is known. This characteristic m-shaped curve (signature) was measured and calculated for a 140-Mbit/s 16-QAM system for different values of the delay time τ. For the calculations, perfect Nyquist pulse shaping was assumed and the effects of timing and carrier recovery circuits during two-path propagation were taken into account. The comparison with the measured signature showed a small degradation which can be attributed to modem imperfections. From the statistical distribution of the propagation parameters and the corresponding signature the outage time of the 16-QAM radio system due to selective fading was estimated at 0.024 % of the time in the worst month in 1982.

For testing modems, adaptive equalizers and/or diversity techniques which diminish the system sensitivity against selective fading, it is desirable to simulate the fading process in the laboratory. For this purpose a two-channel simulator for two-path fading has been developed, where the indirect wave which was delayed by τ = 6.3 ns relative to the direct wave was Rayleigh-distributed. By variation of the parameter K which describes the power ratio between the indirect and the direct wave, it is possible to simulate different fading processes. The simulator operates in the 4-GHz band and allows the correlation between the two channels to be adjusted.

The use of the simulator was demonstrated by means of measurements carried out on a 34-Mbit/s QPSK and a 140-Mbit/s 16-QAM radio system. Here the bit-error rate was determined as a function of the signal-to-noise ratio for different parameters K. Moreover, the improvement by the use of an inphase diversity combiner was investigated for different values of the correlation coefficient between the two channels.

1. INTRODUCTION

In radio-relay systems with digital modulation, frequency-selective fading occurring in multi-path propagation impairs the transmission quality. The signal-to-noise ratio is then no longer decisive for the system performance. In order to assess the outage time of the digital radio system, the propagation channel has to be described and modelled, and the statistical distribution of the parameters included in the model has to be determined. Therefore, the first part of this paper gives the results of propagation measurements (amplitude and group delay distortions in a 40-MHz bandwidth). They allow the evaluation of the outage time for a 140-Mbit/s 16-QAM radio-relay system using measured and calculated signatures.

On the basis of the propagation measurements a fading simulator was developed, which will be described in the second part of the paper. This fading simulator can be used in laboratory measurements to determine the improvement achieved by diversity operation in the performance of radio-relay links. Since

with some diversity methods, the combination of the received signals obtained via different receiving antennas (space diversity) or carrier frequencies (frequency diversity) takes place already in the RF range, it is furthermore necessary to simulate two fading processes with adjustable correlation in the RF range. The use of the simulator is demonstrated by determining the diversity gain using an inphase-diversity combiner for a 34-Mbit/s QPSK and a 140-Mbit/s 16-QAM radio system.

2. PROPAGATION MEASUREMENTS AND DESCRIPTION BY AN EFFECTIVE TWO-PATH MODEL

The radio link has a length of 43 km, which is a typical distance for the radio-relay network. The first Fresnel-zone of the hop is free for k = 4/3. The measurements were carried out in a frequency band of ± 20 MHz. The amplitude- and group delay distortions in the worst month (23-08 - 23-09-83) of the investigation period were evaluated, where only events with a maximum group delay distortion $\tau_g \geq 9$ ns were taken into account.

For the statistical description of the transmission distortions, it is of advantage to use a simple two-path model. Here it is assumed that besides a direct wave a reflected one with the delay τ arrives at the receiving antenna. The transfer function of such a radio channel is given by [1,2]

$$H(\omega) = a\left[1 - b\,\exp(-j(\omega-\omega_0)\tau)\right] \qquad (1)$$

with a = frequency-independent attenuation

b = relative amplitude of reflected wave

$f_0 = \omega_0/2\pi$ frequency of attenuation maximum (notch frequency)

τ = delay of reflected wave.

From the transfer function $H(\omega)$ we can calculate the amplitude and group delay distortion in the investigated frequency band. The parameters a, b, ω_0, and τ were for each fading event fitted to the measured curve by least squares minimization. The group delay τ_g has a minimum for the cases b < 1 and a maximum at the notch frequency f_0 for b > 1.

As an example, Figs. 1 and 2 show the attenuation and group delay distortion of an event with b = 1.44 and τ = 12.7 ns together with the theoretical curves according to Eq. (1). Maxima of the group delay corresponding to b > 1 as shown in Fig. 2 occurred in 5.9 % of the cases of frequency-selective fading. The fit of the theoretical to the measured curves was, similar to this example, possible in all cases of frequency-selective fading. This does not mean that two-path propagation existed really in all events. An agreement of the curves in the narrow frequency band investigated indicates only that the transmission characteristics of the radio-relay link within the transmission bandwidth can be described by an effective two-path model with the fitted parameters.

The parameters b and τ which are decisive for the distortions are correlated with each other. Fig. 3 shows the mean values of the fading depth (1-b) of the transfer function plotted versus the delay τ. Shorter delay times correspond with large values of b and vice versa. In the physical model of two-path propagation, short delays correspond to a small angle of incidence of the reflected wave on the reflecting layer, the associated reflection coefficients have here higher values than with steep incidence.

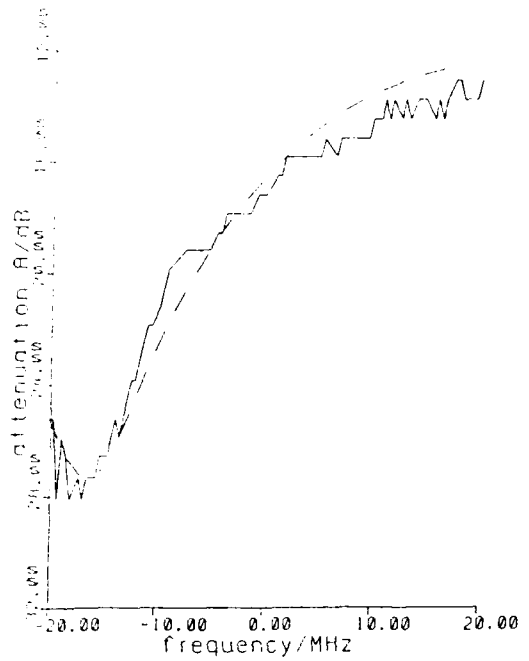

Fig. 1: Attenuation distortion of an event with b = 1.44 and τ = 12.7 ns
..... calculated
_____ measured

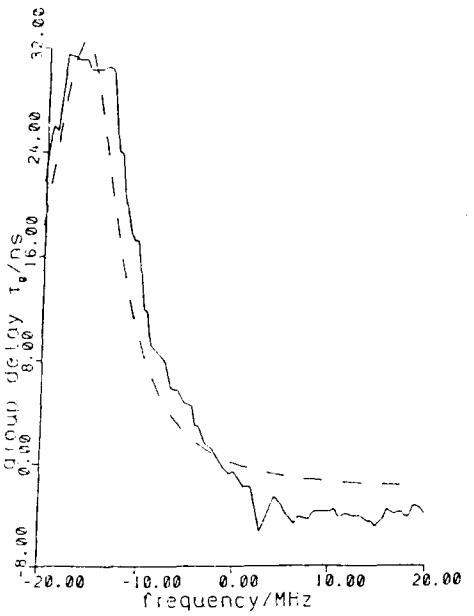

Fig. 2: Group delay distortion of an event according to Fig. 1
..... calculated
_____ measured

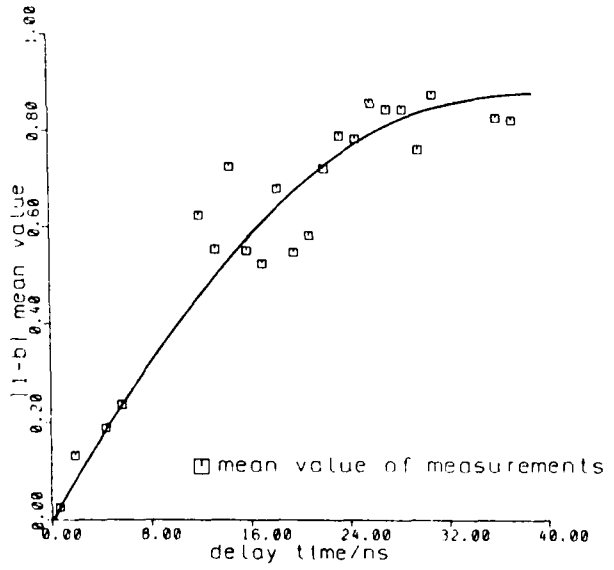

Fig. 3: Mean value of fading depths /1-b/ as a function of τ

3. EFFECTS ON A 16-QAM 140-Mbit/s RADIO-RELAY SYSTEM

If the statistical distribution of the parameters b and τ of the measured fading events is known, the influence of two-path propagation on the digital radio-relay system can be evaluated quantitatively. To this end, the so-called signature was introduced in /3/. Fig. 4 shows for different values of τ over the offset between the notch and carrier frequencies that value of the notch depth /1-b/ at which a bit error rate of 10^{-3} is reached. The critical notch depth 20 lg /1-b/ decreases with increasing τ. Therefore, the sensitivity of a radio-relay system to frequency-selective fading will increase with the height of its signature. The dashed curves were measured on a commercial 16-QAM 140-Mbit/s radio-relay equipment. To be able to obtain information quickly for other delay times and to keep the results free from the influence of modem imperfections, the signature calculations were carried out with an idealized model. In this connection, it was assumed that the transfer function for the total system in

periods free of fading are band-limited according to the Nyquist criteria, i.e. the overall transfer function has the raised cosine frequency characteristic so that there is no intersymbol interference at the sampling instants. The timing and carrier recovery circuits were modelled thus taking into account the effects of timing and phase offsets during two-path propagation. In Fig. 4 good agreement between calculated and measured results can be recognized.

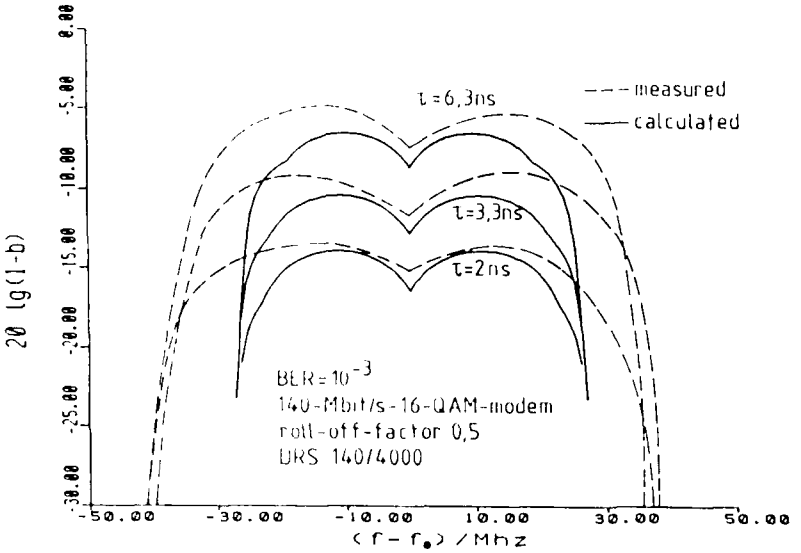

Fig. 4: Signatures of a 16-QAM 140-Mbit/s radio-relay system for different delays

with increasing τ, the signature moves upwards and by that indicates that the outage already occurs at smaller notch depths. To determine the outage time of the radio-relay system, the worst value of b which leads to a BER = 10^{-3} corresponding to the highest point of the signature was plotted in Fig. 5. Here the curves b = 1 and b = 1, which result in different signatures, are described by one branch each of the curve b = τ.

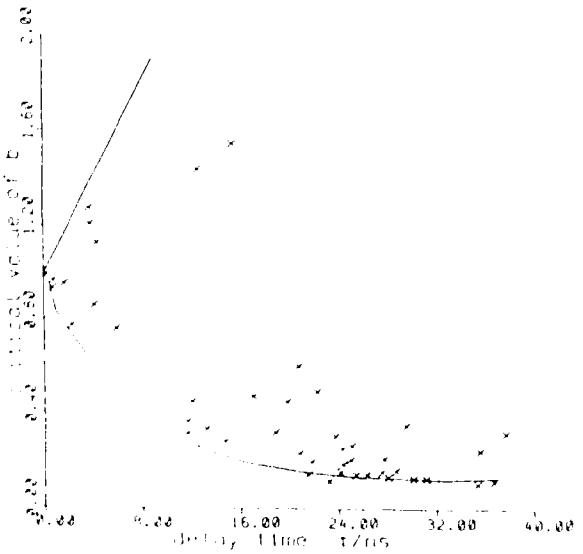

Fig. 5: Critical value of reflection coefficient as a function of τ.
x: fading events with associated parameters b and τ.
-: highest value of signature $20\,^{10}\log\,1\text{-}b$ as a function of τ

The [illegible] of the critical reflection coefficient b [illegible] b = 1 or second b = 1 [illegible] τ corresponds to the outage probability of the radio-relay system in case of longer [illegible] delay. The [illegible] between the critical curve and the [illegible] line [illegible] the failure. In the worst [illegible] the total outage time, in consideration of the [illegible] of the [illegible], would [illegible] [illegible] i.e. 5.10⁻⁴ of the time.

4. TWO-PATH MODEL FOR DIVERSITY OPERATION

The possibility of describing all fading events by an effective two-path model points also to a simple way of simulating them in the laboratory. However, since the test of diversity methods requires the generation of two propagation channels with defined (adjustable) correlation, it is necessary to extend the two-path model to these two propagation channels.

Let the transfer function $H_1(\omega,t)$ of a propagation channel 1 be given by

$$H_1(\omega,t) = a_1 - h_1(t)\,\exp(-j(\omega-\omega_1(t))\tau_1) \qquad (2)$$

In a twofold diversity arrangement there is a second propagation channel with

$$H_2(\omega,t) = a_2 - h_2(t)\,\exp(-j(\omega-\omega_2(t))\tau_2) \qquad (3)$$

From the transfer function we can calculate the amplitude and group delay distortion /1/.

The delays τ_1 and τ_2 are assumed to be constant as an equipment realization of different varying delay times would have been difficult. In accordance with the propagation measurements /2/ we set $\tau_1 = \tau_2 = \tau = 6$ ns. The measurements of the amplitude and group delay distortions in a wider frequency band described in Section 2 showed, however, that an effective two-path model with variable delay time allowed a better description of the experiments.

For the wave arriving at the receiving antenna with a delay it is assumed that its amplitude is Rayleigh-distributed and the phase relative to the main wave is uniformly distributed in the interval 0 to 2π. This means that at a fixed frequency $\omega = \omega_c$ in the relations

$$\begin{aligned} h_1(t)\,\exp(-j(\omega_c-\omega_1(t))\tau) &= x_1(t) + j\,y_1(t) \\ h_2(t)\,\exp(-j(\omega_c-\omega_2(t))\tau) &= x_2(t) + j\,y_2(t) \end{aligned} \qquad (4)$$

the quantities x_1, y_1, x_2 and y_2 have a Gaussian or normal distribution with the mean value 0 and the variance σ^2. Furthermore the following condition

$\langle x_1 y_1 \rangle = \langle x_2 y_2 \rangle = 0$

has to apply, i.e. the inphase and quadrature components of the Gaussian processes producing the fading shall be uncorrelated. Additionally there be

$\langle x_1 y_2 \rangle = \langle x_2 y_1 \rangle = 0$

Correlation between the transfer functions for the two diversity branches is determined by

$$\varrho_0 = \langle x_1 x_2 \rangle = \langle y_1 y_2 \rangle \qquad (5)$$

On the preceding assumptions the joint probability density is

$p(x_1, x_2, y_1, y_2) = p(x_1, x_2)\,p(y_1, y_2)$ with

$$p(x_1,x_2) = \frac{1}{2\pi\sigma^2\sqrt{1-\varrho_0^2}}\,\exp\left\{-\frac{1}{(1-\varrho_0^2)2\sigma^2}\,(x_1^2 - 2\varrho_0 x_1 x_2 + x_2^2)\right\}. \qquad (6)$$

An analogous expression results for $p(y_1,y_2)$ / 4 /.

With these assumptions the statistical characteristics of the two transfer functions $H_1(\omega,t)$ and $H_2(\omega,t)$ have been defined. The complex spectral densities of the received signals $R_1(\omega,t)$ and $R_2(\omega,t)$ can then be obtained as follows

$R_1(\omega,t) = H_1(\omega,t)\,S(\omega)$

$R_2(\omega,t) = H_2(\omega,t)\,S(\omega)$

where $S(\omega)$ denotes the spectral density of the transmitted signal.

[illegible] specification for very narrow-band transmitted signal at the carrier frequency f_c [illegible] Fourier transform of $R_{1,2}(\omega,t)$ is given by

$$V_{1,2}(t) = \frac{1}{2\pi}\int_{-\infty}^{+\infty} H_{1,2}(\omega,t)\, V_0\, \delta(\omega-\omega_c)\, \exp(j\omega t)\, d\omega$$

$$= \frac{1}{2\pi} H_{1,2}(\omega_c)\, V_0 \exp(j\omega_c t)\ ,$$

[illegible] the absolute values of the receiving voltages, normalized to V_0 are

$$A_{1,2} = |H_{1,2}(\omega_c,t)| = \sqrt{(x_{1,2}+a_{1,2})^2 + y_{1,2}^2} \qquad (7)$$

[illegible] joint probability density $p(A_1, A_2)$ cannot be given in closed form. However, since the process [illegible] of the superposition of a Rayleigh-distributed component on a direct one, the marginal distribu-[illegible]

$$p(A_1) = \int_0^\infty p(A_1,A_2)\, dA_2 \ ; \qquad p(A_2) = \int_0^\infty p(A_1,A_2)\, dA_1$$

[illegible] to Rice-distribution

$$p(A_{1,2}) = \frac{A_{1,2}}{\sigma^2} \exp\left\{-\frac{A_{1,2}^2+a_{1,2}^2}{2\sigma^2}\right\} I_0\left(\frac{A_{1,2}a_{1,2}}{\sigma^2}\right) \qquad (8)$$

[illegible] modified Bessel function of the 0th order.

[illegible] appropriately normalized to the direct component $a_{1,2}$ with

$$r_{1,2} = A_{1,2}/a_{1,2} \quad \text{and} \quad k_{1,2}^2 = 2\sigma^2/a_{1,2}^2 \ . \qquad (9)$$

The parameter k describes the ratio of the mean power of the delayed component to the power of the direct component. The probability density relative to $r_{1,2}$ is then given by

$$p(r_{1,2}) = \frac{2\, r_{1,2}}{k_{1,2}^2} \exp\left(-\frac{1+r_{1,2}^2}{k_{1,2}^2}\right) I_0\left(\frac{2r_{1,2}}{k_{1,2}^2}\right) \qquad (10)$$

For the joint probability density $p(A_1, A_2)$ or $p(r_1, r_2)$ we obtain a closed expression only in the event of pure Rayleigh fading (see for instance / 5 /).

The correlation coefficient for the absolute values of the receiving voltages A_1 and A_2 as well as r_1 and r_2, which can easily be determined by measurement on the fading simulator can be calculated approximately if the statistical definition of the moments / 4 / is introduced with

$$m_{k,l} = \langle r_1^{\,k}\, r_2^{\,l} \rangle = \int_0^\infty\int_0^\infty r_1^{\,k}\, r_2^{\,l}\, p(r_1, r_2)\, dr_1\, dr_2 \qquad (11)$$

or the central moment

$$m_{k,l}^* = \langle (r_1 - m_{10})^k\, (r_2 - m_{01})^l \rangle \qquad (12)$$

The correlation coefficient ϱ_A of the receiving voltages is then supplied by

$$\varrho_A = \frac{m_{11}^*}{\sqrt{m_{20}^*\, m_{02}^*}} \qquad (13)$$

Although for the case that the two diversity channels exhibit pure Rayleigh fading, the integrals in Eq. (13) do not allow a closed evaluation, the numerical evaluation yields here approximately

$$\varrho_A = \varrho_r \approx \varrho_G^2 \ . \qquad (14)$$

For the case of Rice fading, existing in our cases, Eq. (13) was evaluated numerically for different values of k.

For a complete characterization of two-path fading, it is essential to know, in addition to the statistical distribution of the parameters in Eqs (2) and (3), also the rate of change of the fading event. The power density spectrum of the fading event (Doppler power density spectrum) is obtained via the Fourier transformation from the autocorrelation function (ACF) of the inphase or quadrature component. As the measured ACF's often have a bell-shaped curve, an approximation by a Gaussian function is possible to :

$$\langle x_1(t)\ x_1(t+\tau')\rangle = \langle y_1(t)\ y_1(t+\tau')\rangle = \exp(-\tau'^2/\tau_0'^2) \qquad (15)$$

The Doppler spectrum then becomes

$$P(f) = 2\sqrt{\pi}\,\tau_0'\exp(-f^2/f_0^2) \qquad \text{with} \qquad (16)$$

$$f_0 = 1/(\sqrt{\pi}\,\tau_0')$$

The width of the Doppler spectrum which is defined as the root of the second central moment relative to P(f) leads to the mean fading frequency f_D. Substituting it into (15) we obtain /6/

$$f_D = f_0/\sqrt{2}$$

5. LAYOUT OF FADING SIMULATOR

The fading process with the previously defined mathematical characteristics was realized as shown in the block diagram in Fig. 6. The transmitted signal is first distributed to the two channels. In each channel it is then further split up into the direct component and the component delayed by τ. The delayed component is Rayleigh-modulated as has already been described in /7/ and /8/. Since the ring modulators used as voltage-controlled attenuators have to be operated with one very large signal switching the mixer diodes on and off, they represent a non-linear component.

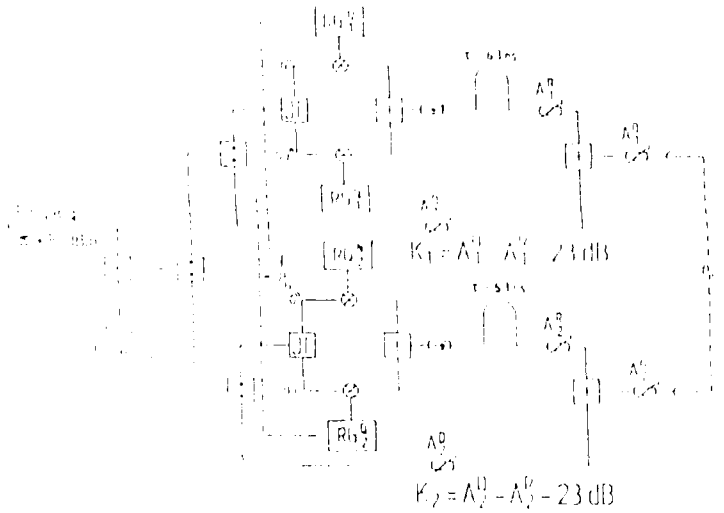

Fig. 6: Block diagram of fading simulator
x_1, y_1: inphase and quadrature components
x_2, y_2: direct and delayed components

The ... simulation methods with amplitude shift keying ... for 2PSK lead ... measurement result. To achieve the required ... the frequency f_D was applied to the input. ... the mixer diodes are switched on and off. The frequency ... the transmission band of the ...

The ratio of the mean power of the delayed component to that of the direct component and by that the parameter k (Eq.9) can be adjusted separately for both channels with two attenuators A_D and A_R.

The mixers are driven by the noise generators RG_1^I, RG_1^Q, RG_2^I and RG_2^Q. These noise generators produce a Gaussian distributed voltage with the mean value 0 and the variance σ. They consist of feedback shift registers. Summing up of the individual taps of the shift register yields, according to the central limit theorem, a Gaussian probability density for the sum amplitude.

To obtain the correlation between the corresponding noise generators required according to Eq. (5), two uncorrelated noise signals can be weighted according to the desired degree of correlation and summed up (8). For the equipment built up in our laboratory a different solution was chosen. Since the noise generators have an ACF according to Eq. (15), it is possible to determine the cross-correlation between two identical generators from Eq. (15), which are, however, delayed in their clock time by n Δ t.

A computer simulation supplied the following values for a delay of

Δt : ρ_{xx} = 0.97
$2\Delta t$: ρ_{xx} = 0.90
$3\Delta t$: ρ_{xx} = 0.79
$4\Delta t$: ρ_{xx} = 0.66
$5\Delta t$: ρ_{xx} = 0.52
$6\Delta t$: ρ_{xx} = $3.2 \cdot 10^{-5}$

A comparison of the calculated values with those measured on the generators showed good agreement.

The fading simulator was tested by first separating the noise generators and by checking at fixed dc voltages on the ring modulators whether the transfer function for the two-path model was simulated. Good agreement was obtained. The Rice-distribution of the output amplitude required when driving the ring modulators with the noise generators and a fixed rf frequency was tested as well. A typical result of the comparison is shown in Fig. 7.

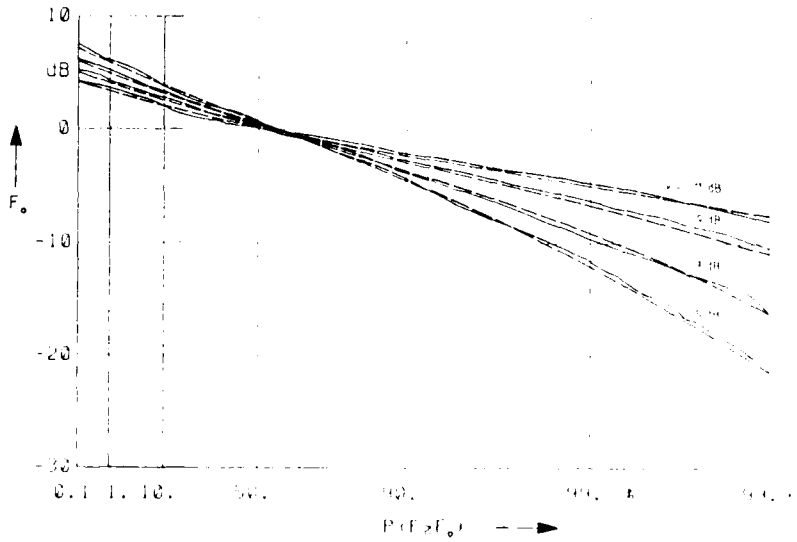

Fig. 7: Measured ——— and calculated --- distribution of output amplitude for different K values at a fixed frequency f_0 = 3.95 GHz

If the frequency is altered, the distribution should change as little as possible. Measurements of the distribution in the frequency range between 3.85 and 4.05 GHz show a variation of about 3 dB for the 99 % value, i.e. the corresponding value for the parameter K = 20 lg k is adjusted with an accuracy of about ± 1 dB.

The statistical correlation between the output voltages of the two channels was also examined. According to Eq. (13) this correlation is dependent on the correlation ϱ_G of the noise generators and the k-value, i.e. the ratio of the mean power of the delayed component to the power of the direct component. Fig. 8 shows the correlation coefficient between the output voltages as a function of $K_1 = K_2 = K = 20$ lg k for $\varrho_G = 0.66$. The solid curve was calculated from Eq. (13), the moments of the distribution being determined by numerical integration. The plotted dots indicate the mean value, the error limits the standard deviation of the measured results. There is good agreement with the calculated results. We can recognize that for K < -5 dB there holds $\varrho_A \approx \varrho_G$ in good approximation, i.e. for the values of K which have to be adjusted for the test of digital radio-relay systems the correlation between the output voltages is equal to that between the Gaussian processes.

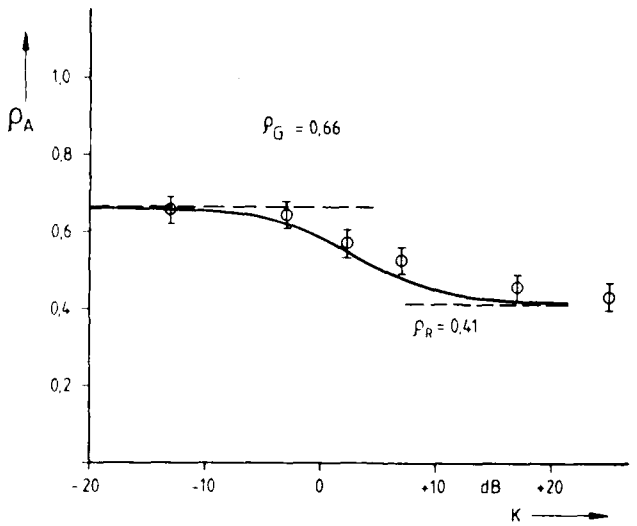

Fig. 8: Calculated (—) and measured (Φ) correlation coefficient of the output voltage of the two channels with a correlation of the Gaussian generators of $\varrho_G = 0.66$ as a function of K

6. DETERMINATION OF DIVERSITY IMPROVEMENT

After having tested the function of the fading simulator and the statistical distribution of the parameters resulting from the model, we carried out measurements on two different systems, namely a 140-Mbit/s 16-QAM and a 90PSK system. It was possible to determine the improvement resulting for both systems from the use of an inphase diversity combiner.

Fig. 9 shows the block diagram of the test set-up. The inphase combiner consists of a phase shifter which adjusts the phase of the signal in the diversity path in cophase to the signal in the main path. For the purpose of generating a phase control signal, the phase of the diversity antenna signal is modulated sinusoidally, which results in a AM-modulation of the combined signal power. The fundamental modulation component of the combined signal is detected and used in a feedback arrangement to control the phase-shifter value. It can be shown [9] that the condition of the vanishing AM-component of the combined signal results in maximum power combining of the two diversity branches. Simultaneously, maximum power combining will to some extent reduce inband amplitude and group delay distortions caused by selective fading: for instance, if one or both diversity branches experience fade notches well within the channel bandwidth, the distortions in the combined signal will be less severe. There are channel conditions, however, where both diversity signals are affected by linear amplitude distortion of the same slope in the channel bandwidth. The combined signal will then experience about the same linear amplitude distortion.

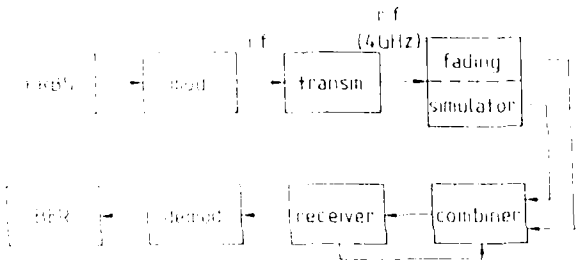

Fig. 9: Block diagram of the test set-up.

For diversity gain under two-path fading conditions can now be demonstrated in the results of measurements on a 34-Mbit/s QPSK and a 140-Mbit/s 16-QAM-system (Figs. 10 and 11). In both figures the bit error rate is plotted versus the averaged input power of the main signal for the same simulated fading scenario with $K_1 = K_2 = K = -10$ dB in both channels. The straight lines denoted by $K = -\infty$ dB refer to the system only stressed by thermal noise.

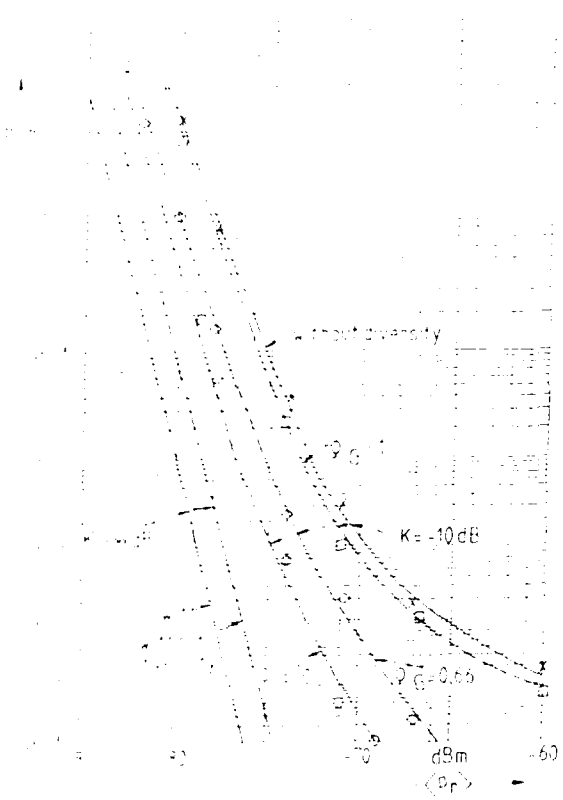

Fig. 10: Averaged BER vs. averaged input power on single branch for a 34-Mbit/s QPSK system with and without diversity

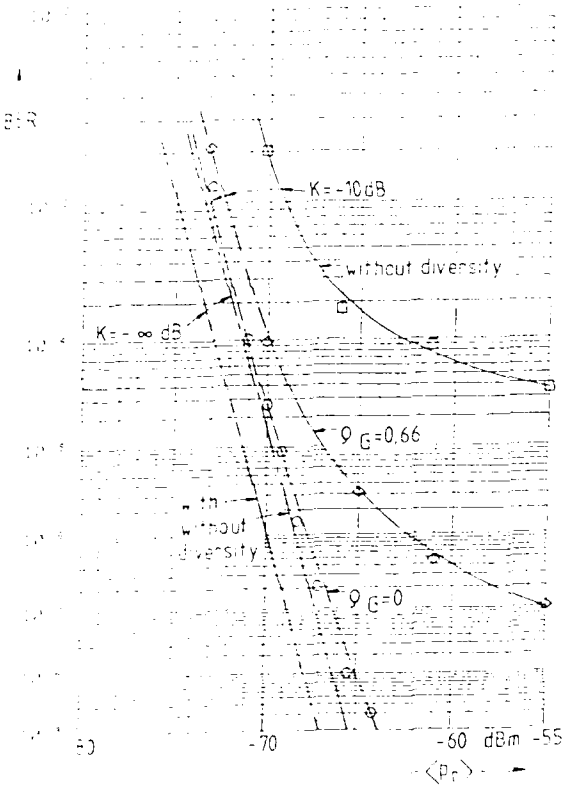

Fig. 11: Averaged BER vs. averaged input power on single branch for a 140-Mbit/s 16-QAM system with and without diversity

The performance of the 16-QAM system without diversity is much poorer compared with that of the QPSK system. With both systems remarkable improvement can be observed if the diversity combiner is switched on. If the diversity channels are totally uncorrelated, the curves of BER versus averaged input power are shifted to the respective system without diversity stressed only by thermal noise. The gain which can be defined as the ratio of the input power without diversity to that with diversity at a given BER is equal to 3 dB for the QPSK-system and

is more than 8 dB for the 16-QAM system. This can be explained by the fact that the combiner reduces the equivalent distortions of the channels to some extent. Therefore the performance of the 16-QAM system, which is more sensitive to selective fading, is on the other hand more improved if diversity and maximum power combining are used. Further measurements of the diversity gain using different diversity combining methods are in progress.

7. REFERENCES

1. Fel'Huber, L.: Verfahren zur Berechnung der Bitfehlerhäufigkeit von Richtfunkstrecken mit digitaler Modulation, Techn. Ber. 67, FI der DBP, A 455 TBr 27, 1970.

2. Rummler, W.D.: A Simplified Method for the Laboratory Determination of Multipath Outage of Digital Radios in the Presence of Thermal Noise, IEEE Transact. COM-30 (1982) pp 487-494.

3. Emshoeller, M.: Characterization on the Performance of PSK Digital Radio Transmission in the Presence of Multipath Fading, Int. Conf. Commun. (1978), Toronto, Canada, 47.3

4. Kreyszig, E.: Statistische Methoden und ihre Anwendungen, Vandenhoeck & Ruprecht, Göttingen 1973.

   Schwartz, M., Bennett, W.R., Stein, S.: Communication Systems and Techniques, McGraw-Hill, New-York, 1966.

5. Gerthsen, Kopf, L.: Wellenausbreitung, Bibliographisches Institut, Mannheim, 1970.

6. [illegible], R.W., Pabl, M.: Geräte zur Simulation der Feldstärkenschwankungen von Funkstrecken zwischen einer ortsfesten und einer bewegten Station, Techn. Bericht, FI der DBP, 44 TBr 86, 1981.

7. [illegible], C.: Simulator für Mehrwegeschwund in Richtstrahlverbindungen, Techn. Mitteilungen der Schweizer PTT (2) 1981, pp 466-473

8. [illegible], Y., [illegible]: Simulation and Measured Performance of a Space Diversity Combiner for 6 GHz Digital [illegible], IEEE Trans. COM-27, (1979) pp 1896-1907.

ACKNOWLEDGEMENT

We would like to thank Mr. R. Schneckenburger for implementing the fading simulator and performing most of the measurements.

DISCUSSION

R.W. Hubbard, US

Would you please explain the manner in which you control the correlation between the two channels of your simulator.

Author's Reply

The correlation is controlled by the correlation of the Gaussian generators. They consist of feedback-shift registers. The cross correlation between two identical shift registers can be changed if one of them is delayed relative to the other by $n \cdot \Delta t$, where $\Delta t = 1/f_c$, with f_c = clock frequency of the shift registers.

Thus it is possible to change the correlation of the generators in discrete steps, in our case by $\zeta = 1, 0.97, 0.9, 0.79, 0.66$ etc.

DESIGN CRITERIA FOR LIMITED SCAN ANTENNAS AT DIGITAL MICROWAVE LINE OF SIGHT LINKS

by
ir. L.P. Ligthart
Delft University of Technology
Dept. of Electrical Engineering
Microwave Laboratory
P.O. Box 5031
2600 GA Delft
The Netherlands

SUMMARY

In 4 and 6 GHz digital radio links the Bit Error Ratio (BER) increases strongly during deep multipath fading.

This paper deals with the so-called "angle diversity technique" for multipath fading reduction where use is made of limited scan antennas. Antenna design criteria for this purpose are investigated under the assumption that only group delay requirements instead of fading depth are the determining factors to fulfill BER specifications.

In a two-way fading model the maximum group delay time difference is in first approximation equal to the ratio between the minimum received signal strength and the path delay time difference. From simulation measurements it is known that group delay time differences are dependent on the worst BER and the modulation system. Quantitative information is given for 34 Mb/s, 8 PSK and for 140 Mb/s, 16 QAM.

The path delay time difference and the angles of arrival are calculated in a spherical propagation model. To come to a design procedure independent of refractive index profiles it is assumed that each ray is influenced along its path by a constant refractive index gradient. This means that for given link geometries generalized graphs characterizing the propagation of each ray will be shown.

Combining the results from the spherical propagation model and the group delay measurements allows the computation of the maximum fading depth for given angles of arrival. In this way the pattern envelope of limited scan antennas around the angles of interest can be derived under the assumption that infinite deep fading occurs if no diversity technique is used.

1. INTRODUCTION

In 1980 a number of European countries (Belgium, Federal Republic of Germany, France, Finland, Italy, The Netherlands, Sweden, United Kingdom) and the European Space Agency started a project in the field of phased array techniques and technology. This project is being carried out within the framework of COST (European Co-operation in the field of Scientific and Technical Research) and is entitled COST-204 project: "Phased Array Antennas and their Novel Applications". One area of interest within COST-204 is limited scan hybrid reflector antennas for the reduction of multipath fading. These interests form the main contribution in COST-204 of the Federal Republic of Germany and The Netherlands (Ref. 1).

To fulfill the CCIR requirements on digital radio links for frequencies up to 15 GHz measures such as frequency diversity, height diversity, angle diversity, adaptive equalizers or adaptive modulation/demodulation are proposed, in order to suppress frequency selective fading.

In the Netherlands the Dr Neher Lab (PTT) and the Delft University of Technology in a joint project are studying the feasibility of "angle diversity" techniques for fading reduction at the receiver side of a 4 GHz digital microwave line of sight link. Two limited scan possibilities are considered:

However, we find that elaborate measures to further improve the prediction ability are hardly justifiable for most operational purposes.

The emphasis should be put on assessing overall performance and probability of mission success at the planning stage, rather than trying to calculate detailed terminal locations and performance of individual links. Skilled operators with knowledge of the expected magnitude of local variations and possible special propagation situations will allow a flexible siting policy.

Further propagation measurements will therefore be made to gather data for calibrating our model, and especially to obtain data on signal variability in various terrain.

References

1. [illegible], et al. 1967: "Transmission Loss Predictions for Tropospheric Communication Circuits", Vol I and II, NBS Technical Note 101.

2. [illegible] 1983: "NDRE Transmission Simulation Program, Users Reference Guide".

3. [illegible] 1983: "The Prediction of Field Strengths in the Frequency Range 30 - 1000 MHz", AGARD [illegible].

4. [illegible] and Tandell 1974: "Prediction and Calculation of Transmission Loss in Different Types of Terrain", AGARD-CP-144.

Acknowledgements

The authors would like to thank Tore Lund-Hanssen who was responsible for the computer transmission simulations, and [illegible] for assistance during the field measurements.

The type of distribution of values within a small area has not been verified.

Even with conservative assumptions about the accuracy and statistical properties of the field measurement data, some important observations may be made from figure 4 and 5.

It is noted that the measured signal levels at 34,5 MHz are consistently below the predicted values. At UHF (900 MHz) the reverse is true, the predictions being on the pessimistic side.

Ignoring this "scaling error" and fitting a simple $1/R^4$ propagation curve to the set of predicted values, it is evident that the computer predictions are limited to excursions of about ± [illegible] dB from this curve.

Other work [4] supports this observation, indicating that the use of correction factors obtained from 50 may be insufficient for use in rugged areas.

The absolute values of the difference between the predicted and measured signal [illegible] are [illegible] according to normalized number of occurences, see figure 6.

Using this diagram, the median error is found to be 20 dB at 34,5 MHz and 14 dB at [illegible] MHz.

The large errors at 34,5 MHz may be explained by wrong estimates of ground parameters, [illegible] smoothing effects in the topographic data, giving rise to diffraction edges in otherwise [illegible].

A detailed investigation of the material substantiates the presence of "[illegible]" and diffraction paths. The measurements on 390 MHz are of particular interest, since the observed field strength consistently exceeds the predictions by 10 - 30 dB.

On some paths the low propagation loss cannot be explained by LOS-segments only, and reflections from horizontal obstacles along the line of propagation were suspected.

Inspection of the map from the LYGNE test area, figure 2, reveals that this very well may be the case.

4 DISCUSSION OF PREDICTION ACCURACY AND POSSIBLE IMPROVEMENTS IN A TACTICAL CONTEXT

Focusing the attention again on the general problem of deterministic propagation calculations in rugged terrain, we perceive a confusing picture of diffraction, local scattering, horizontal multipath, non-homogenous ground conditions and a variety of other phenomena. This is illustrated in figure 7.

Large-scale topographic features influencing VHF/UHF propagation may be modelled with reasonable accuracy. This includes horizontal scattering from mountain walls etc. To improve our prediction ability, ground conductivity and permittivity data must be mapped. Furthermore, vegetation effects must be included. If this can be done for each resolution cell of the data base, eg. 30 by 30 metres, the possibility of predicting path loss between sites unobstructed by local scatterers should be fairly good.

In a tactical situation this procedure may become grossly inaccurate, since a tactical communicator must live with:

- obstructed or even concealed antenna emplacements
- a navigational uncertainty of 100 metres (CEP)
- only rough estimates of ground and vegetation parameters along a given path.

Adding the requirements for militarily sound deployment and considering the establishing of radio networks, optimizing each communication link by detailed propagation modelling seems rather unrealistic.

By calibrating a computer model using data from actual measurements in various terrain, we believe that the median signal level at a given spot may be estimated to within ± 10 dB with better than 75 % confidence.

This alone is sufficient to avoid clearly hopeless locations for communication or electronic warfare resources.

An accuracy of ± 10 dB would also be helpful for emission (power) control purposes.

Presence of possible horizontal reflections may cause severe multipath problems in transmissions systems, and could possibly be revealed by ray-tracing in the propagation model. By alerting operators to these situations, location of relays and network nodes may be optimized with such factors in mind.

By providing the communications officer with estimates of the expected variability in propagation conditions, the probability of mission success can be objectively assessed at the planning stage.

5 CONCLUDING REMARKS

Optimization of tactical communication network deployment and of emission control strategies depends heavily on the ability to predict link transmission parameters.

Preliminary measurements indicate that the probability of predicting loss within 15 dB at UHF and 20 dB at VHF is rather poor if we rely solely on a ray-optical Fock model for our test area. This can be improved by using [illegible] experiments to calibrate the model.

... to the problem of statistical significance. One faces a paradoxal ... with a deterministic propagation model. A tactical communicator using such a ... "probability of success" in several one-shot predictions, i.e. the user ... must be has chosen a particular position and instant of time to ...

... statistical simulation, where overall performance is evaluated on a basis of a large ... stochastic process.

... tried to be been to make spot measurements on several independent paths, and trying to ... within a radius of a few wavelengths, rather than being concerned with site ... time averages.

... measurements have been made in a moderately rugged area at the south coast near Kristian-sand. However, measurements in mountainous terrain in North-Norway are being planned.

An important aspect of the preliminary measurements was to obtain experience with equipment and procedures in preparation for a larger and more ambitious data collecting campaign at a later date.

Existing broadcasting, mobile subscriber telephone etc transmitters were proposed as emitters for the field strength measurements. In view of the small number of such transmitters in rural parts of Norway, the rather tedious problem of obtaining accurate siting and ERP-data, and the limited coverage thus obtainable in the interesting tactical band from 30 to 80 MHz, it was decided to employ dedicated transmitters.

A laboratory type signal generator and power amplifiers were used in conjunction with suitable broadband antennas.

Ideally measurements should be taken at different ranges along a straight radial line from the transmitter. However, this proved difficult due to limited accessibility, and different paths had to be used for each transmitter to receiver range.

A typical situation is depicted in figure 2.

The transmitter power was 10 watts, feeding a 3 dB_i vertically polarized, omnidirectional antenna on a ... mast.

The error budget includes contributions from the following sources:

- Navigational accuracy. The CEP is estimated to approximately 100 meters.
- Instrument calibration errors. Field strength meter specifications guarantees ± 2 dB.
- Receiver antenna gain and height errors. The antenna gain is 3 dB_i, and the combined estimated errors due to mismatch, local reflections, proximity to the mast and cable, height variations etc. is ± 1,5 dB.
- Variations in effective radiated power from the emitter. Including the same factors as above, this contribution should be less than ± 1,5 dB.

... therefore reasonably assume that combined instrument accuracy is better than the observed limiting ± ... dB uncertainty in field strength measurements (3).

... navigational errors were found to be larger than one resolution cell in the digitized map, and may ... problems if measurements are taken close to distinct terrain features.

COMPARISON, MEASURED AND PREDICTED DATA

... knife-edge prediction method is based on a calculated index of terrain roughness, $\Delta h(r)$, being ... of the interdecile heights above and below a straight line fitted to the contour of elevations ... As the distance, r, increases, $\Delta h(r)$ approaches an asymptotic value of Δh according to ...

... (3.1)

... NAM simulation model are path profiles derived from a digitized map data base with ... size of 1 by 1 seconds of arc (DMA level II).

... is given in figure 3, corresponding to the path L1 to L4 in figure 2.

... were performed at 34,7 MHz and 390 MHz were carried out for 18 paths.

... of received signal in dBμV plotted versus range is given in figure 4 ...

... has been carried out on short paths, being representative for tactical radio ... Under these circumstances, a quasi-homogenous path consisting of line-of-sight and diffraction ... is to be expected. Furthermore, the measurements at 390 MHz showed presence of multipath components, ... spatial nulls.

A COMPARISON BETWEEN PREDICTED AND MEASURED PROPAGATION LOSS IN THE VHF UHF RANGE IN RUGGED TERRAIN.

by

K Besserudhagen, N Klippenberg and M Norland

Norwegian Defence Research Establishment
N-2007 Kjeller
Norway

SUMMARY

Increasing utilization of sophisticated propagation models using digitized terrain and vegetation data bases leads to the question: Is the accuracy of propagation predictions sufficient for meaningful calculation of transmission parameters on individual tactical links?

This paper compares data from field measurements with predictions based on the Longley-Rice model applied to individual path profiles. The propagation model was regarded as a black box, i.e. no detailed analysis or improvement of the model itself was contemplated. The field experiments were designed to reflect the communications deployment situation experienced by ground forces.

Predictions and measurements were carried out at frequencies in the important military bands 30 - 80 MHz and 225 - 400 MHz.

Preliminary results indicate that the value of "accurate" transmission loss calculations is doubtful, particularly in rugged terrain. Strong local variations introduce significant spread in the observed field strength at a given location. The median prediction error was 13 dB at 390 MHz and 20 dB at 54,5 MHz in a moderately rugged area.

Reflections from objects in the horizontal plane are belived to be an important contributing factor in reducing prediction reliability at VHF and UHF. The possibility of modelling such phenomena is discussed in a context of tactical applications.

1 INTRODUCTION

Propagation modelling is a valuable tool in communications and electronic warfare systems' simulation and network planning.

Conclusions intended as engineering guidelines and for establishing doctrines will in most circumstances be based on the statistical properties of the parameters involved.

However, increasing availability of sophisticated propagation models utilizing digitized terrain and vegetation databases may justify the following question:

Is the accuracy of modern propagation prediction methods sufficient for meaningful calculation of transmission loss on an individual link basis?

If an affirmative answer can be given, such models may potentially offer detailed, on-line information to field commanders facing the task of establishing communication networks or deploying electronic warfare assets in difficult terrain.

This interaction between propagation factors and equipment deployment is illustrated in figure 1.

In order to answer the question above, and as a next, lower, level of ambition to verify that the behaviour of a given deterministic propagation model corresponds to actual (observed) field strength distributions, measurements must be carried out.

This paper addresses the problem of collecting and comparing data from field measurements with predictions given by a computer program derived from the Longley and Rice model (1).

The model, at hand, being a part of a larger transmission simulation package developed for the NDRE by Boeing Aerospace Company, accounts for terrain loss in an individual path profile mode and in an area mode.

Antenna structure parameters, ground conductivity, vegetation and atmospheric conditions are incorporated (2).

Our interest is focused on applications in the tactical VHF and UHF bands (30 - 80 MHz and 225 - 400 MHz), thus all observations and conclusions in this report apply to these frequencies only.

2 MEASUREMENTS

Our aim has been to devise a measurement procedure that most closely reflects the situation experienced in a tactical environment and that later may be reproduced by service personnel.

SUMMARY OF SESSION IIB

RECENT PROGRESS IN PROPAGATION MEASUREMENTS AND PROPAGATION MODELS

by

Dr B.Burgess
Session Chairman

This session covered experimental results and comparisons with predictions over all the bands from HF to microwave. A comprehensive system to measure ionospheric characteristics which would be of use to the communications engineer was presented by Le Roux et al. (France); measurements applicable to Army VHF/UHF tactical communications were given by Besserudhagen (Norway); Cellular radio applications (900 MHz) were covered by Havel and Maloberti (France); Larsen (UK) presented work covering troposcatter links (4.5 GHz), while Fabbri (Italy) was concerned in combatting propagation distortion on 7 and 11 GHz 140 Mbit/s line-of-sight links.

Besserudhagen et al. presented work on the application of the Langley-Rice propagation model to realistic field ratio tactical communications in the rugged environment of Norway. These predicted values for particular paths were compared with measured values as would be experienced by the actual military users. Over path lengths of the order of 10 km, the median prediction error was 13 dB at 390 MHz and 20 dB at 34.5 MHz. In discussion the point was made that predictions of signal levels by computer modelling should be readily achievable, but detailed modelling of the physical path would have to be made. However, even this may not be worthwhile for operational purposes in this sort of terrain.

Fabbri's paper addressed the problem of achieving a more economic solution to protecting high bit rate line-of-sight communication links (7 and 11 GHz) over long paths (40 to 200 km) due to considerable expense of using space diversity. In order to combat multipath and ground reflections at these frequencies a number of protection techniques were examined viz., IF equalisation, baseband equalisation, frequency diversity with hitless baseband switching and space diversity with an IF combiner. Field trials were performed over several paths (46, 60 and 240 km) and results have shown that adaptive equalisation will make substantial improvements to link performance; however, other techniques will have to be used to ensure full performance. Frequency diversity with hitless baseband switching was shown to be very effective against multipath, but antennas need to be developed to reduce the multipath effects of cross polarisation.

Prof. Bertel presented a paper on a new system to measure the ionospheric channel characteristics that are of importance to the effective transmission of digital data over HF skywave communications links, especially in the design of modems. The goal of such work was to improve the quality of high data rates (2.4 kb/s) over HF paths of 300 — 3000 km in length with the use of bandwidths of 3 to 10 kHz. The information would also be used in simulation where not only the modularized characteristics of the ionosphere would be employed, but also antenna characteristics, jamming and non-stationary events. Initial results on the use of the equipment during an experiment at vertical incidence were given.

Havel and Maloberti's paper concerned measurements on the VHF band pertinent to cellular radio in the urban environment of Paris. A series of measurements showed that a simple law in the form $A(dB) = 10\alpha \log D + \beta$ gave a very good description of the measurements and tied up well with the model of Hata-Okumura. Characteristics of fading statistics were also given.

The final paper of the session concerned the measurement and prediction of multipath dispersion of troposcatter links, the measurements referring to several 4.5 GHz paths in the United Kingdom. In general it was found that dispersion and signal level were weakly correlated but that dispersion measured on two space diversity antennas were well correlated. For angle diversity, measurements on the elevated beam showed larger and more variable dispersion than that measured on the lower beam. A comprehensive comparison of these and other measurements was made with the prediction methods of Bello and Pusone. Both methods tended to underestimate the dispersion, but allowance for beam broadening in the Pusone method improved significantly the prediction. The paper gives an excellent critique of the current status of this topic.

Overall, the papers gave an interesting snapshot of the session topic across the frequency bands as of this time.

system for voice or data, but they all contribute to the bit error rate. So it is these matters that we see in terms of the actual performance of digital systems that I think relate to the time statistics of the impulse data.

Dr Blythe

Do you think that the bursts of errors are related to the equipment or are they more fundamentally related to some behaviour of the propagation medium?

Dr Hubbard

I think that they are not equipment related because we have seen the same phenomena in this burst error activity happening over different periods of the test when we have had multipath. What I have been trying to do and it is not an easy task because we do not have a direct correlation path that I am aware of, is to correlate this burst activity with what I implied is the rapid "flyby" of the selective notches that can occur as the time delay changes slowly. For this we have tried to look at the rate of change that we see in the time delay and our measurements to date have been rather crude. We have not done it in any statistical sense, we have looked at the time variation in the width of our impulse response data, and we find slopes or rates of change on the order of 1 to 2 nanoseconds per second, and if you relate these to the burst error data one can conclude with tongue in cheek that perhaps we have found the elusive millisecond fade in LOS.

DISCUSSION OF SESSION II A

Audience member

Dr Schneider, in Paper 11 you introduced a model of forested regions. Can you tell us more about the area of application of this model. For example, is it applicable to mobile communication in the 900 MHz band, which will be used in Europe for digital communications in the new future. As presently configured, the model is suitable only for transmitter and receiver immersed within the forest, so that the model would have to be extended for a well-sited base station that is not within the forest.

Dr Schneider

In order to assure ourselves that the model is valid we need additional information on the electromagnetic characteristics of vegetation. We have found very few measurements on the permittivity of green wood; in fact the only ones we feel are suitable were made several years ago by Dr Broadhurst at the Institute for Telecommunication Sciences. If anyone could advise us of other measurements of the permittivity of green wood I would be very grateful. Furthermore we are very interested in calibrating or verifying our model by field trials. We would prefer to make these measurements over rather flat terrain where the forest is dominated by tree trunks rather than by deciduous leaves and branches. If there are any particular locations in your respective countries that you feel would be particularly suitable for validating this particular model we would be very interested to hear about them.

Dr Albrecht

The subject is quite old; it has been worked on for a few decades now, particularly in the NATO Central Region. We find that the variability in certain parameters is perhaps the more problematic question. That is to say seasonal changes, the foliage problem, snow cover on the trees, icy covers, etc. I understand also that your model did not take into account any terrain irregularities. Now in the Central Region there is not too much flat ground with forest on it. In the northern part perhaps, but in the southern part there is nothing which cannot be called irregular. Are you planning to make tests using digital terrain data available for instance from the US Defence Mapping Agency, where you could perhaps find a number of representative paths on which you could try your particular model. In any case I do agree with you that more measurements are required, and it is very difficult on account of the very large number of variable factors.

Dr Schneider

The comments about the effects of snow and moisture on leaves, and of irregular terrain, are certainly valid, and these effects must be included in the ultimate development of the model. However, at this stage we feel it would be premature to try to develop a very detailed model that takes into account these and certain other parameters for which ground truth may be very difficult to acquire. Our preliminary concern is to constrain the testing to a forest that is rather easily described and for which ground truth can easily be acquired.

Dr Belrose

There is one further requirement for Dr Schneider's ground truth measurements, which is that the wind is not blowing. We have measured VHF and UHF signal strength in forests, and the wind puts a good strong fade on the signal.

Dr Schneider

This is one of the reasons we wish to identify trunk-dominated forests at this time, and these would probably be coniferous. We want to simplify the model and address some of the more fundamental issues associated with the scattering. You are quite right, we would like to take measurements when the effects of the wind are negligible.

Dr Neessen, Session Chairman

Now I would like to go to another topic, which has been discussed by Dr Hubbard, and it would be interesting to me to hear more about it. It is common practice to evaluate the sensitivity of particular radio equipments to frequency selective fading by system signatures. In that case we assume that the parameters of the transfer function of the multipath channel do not vary with time. Can you, Dr Hubbard, comment on the statement that, for instance, modulation schemes which apply coherent detection are sensitive to the dynamic behaviour of the multipath channel, and this sensitivity may not be evaluated by the use of the system signature concept. Is there anything right in that statement?

Dr Hubbard

We have been conducting some performance tests in Southern California on the different digital radios, and in these measurements we are attempting to correlate what we see in the time domain, in the impulse response data, with actual performance parameters. Viewing these data has convinced me that there is a very growing need for the dynamic characterisation of the impulse response with these data. We have observed errors in short bursts, distributed on the order of 20 errors per burst, in length of roughly twice that value, which suggests a 50% error rate in a very short interval of time. It is hard to say what would be the effect of these error bursts on performance if we were using the

limited scan reflector antennas have to meet.

CONCLUSIONS

Design criteria for limited scan antennas at digital microwave line of sight links have been derived. The antenna pattern specifications result in minimum pattern evelopes of a limited scan antenna. The specifications are given in a limited angle interval of ± 0.5 degrees around the angle of arrival during standard atmospheric conditions. The specifications are dependent on the modulation system and the link geometry. For 140 Mb/s, 16 QAM the minimum pattern envelopes are very steep when compared to 34 Mb/s, 8 PSK. This means that the 140 Mb/s, 16 QAM modulation system with angle diversity is much more sensitive to multipath fading than the 34 Mb/s, 8 PSK. The strong negative refractive index gradients with large positive angles of arrival require the most stringent antenna specifications. Consequently, the CCIR quality requirements for a digital radio link with angle diversity is strongly dependent on the refractive index gradients.

ACKNOWLEDGEMENTS

Many thanks are due to the Dutch Post Office, Dr. Neher Laboratory, for having made this study possible.

REFERENCES

1. L.P. Ligthart, K.P. Dombek, G. Doro, V. Santomaa: "COST-204 Review of Limited Scan Arrays", ESA SP-204, June 1983, pp. 15-19

2. W.C. Jakes, Jr.: "An approximate method to estimate an upper bound on the effect of multipath delay distortion on digital transmission", IEEE COM-27, No. 1, January 1979, pp. 76-81

$\alpha_d - \alpha_i$ than when negative angles of arrival are considered. Therefore, the most stringent antenna specifications are derived for positive angles α_d and α_i. For a specific digital modulation system and given $\Delta\tau = \tau_d - \tau_i$ the maximum amplitude ratio

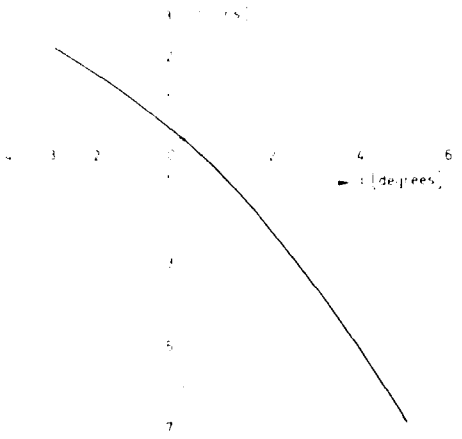

Figure 3. Angle of arrival α as a function of delay time difference τ for linear refractive index profiles.
Antenna heights = 80 m
Radio link distance = 40 km

r = 1 between the two rays are calculated. By using Eq. (6) r becomes:

$$r = 1 - \frac{\Delta\tau}{\tau_s} \tag{7}$$

where:

τ_s = 28.6 ns for 140 Mb/s, 16 QAM
= 88.2 ns for 34 Mb/s, 8 PSK

If infinite deep fading is assumed for angles of arrival α_d and α_i near the maximum of the main lobe pattern of the antenna without fading reduction, according to Eq. (7) and the $\alpha - \tau$ relationship the amplitude ratio r of the pattern of the antenna with fading reduction can be computed. Figures 4 and 5 demonstrate for a 40 km radio link the minimum antenna specifications (pattern envelope of the limited scan antenna) which

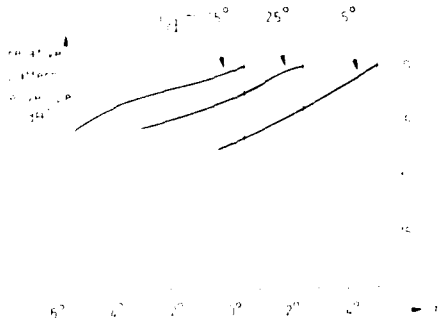

Figure 4. Minimum specifications of limited scan antennas for fading reduction in the case of 34 Mb/s, 8 PSK

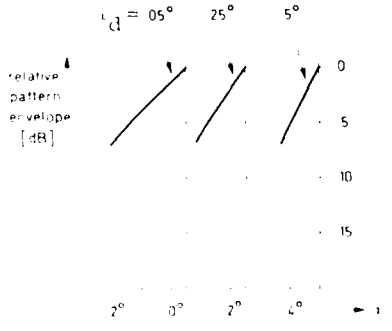

Figure 5. Minimum specifications of limited scan antennas for fading reduction in the case of 140 Mb/s, 16 QAM

The τ/τ_s curve for 8 PSK is approximated by a linear relationship between this critical delay time difference $\tau = \tau_c$ and the corresponding amplitude (1-r) at the receiver. To fulfill the CCIR quality requirements for 8 PSK and 16 QAM this relationship becomes (Ref. 2):

$$\tau_c/\tau_s \approx 0.25\ (1-r) \qquad (6)$$

In Table II τ_c values are given for 34 Mb/s, 8 PSK and 140 Mb/s, 16 QAM and for fading depths of 10, 15, 20, 30 and 40 dB. The fading depths are defined here relative to the remaining amplitude of the direct ray, which means that amplitude reduction of the direct ray due to beam steering does not have to be considered.

FD [dB]	τ_c [ns] 34 Mb/s, 8 PSK	τ_c [ns] 140 Mb/s, 16 QAM
10	6.98	2.26
15	3.92	1.27
20	2.21	0.71
30	0.70	0.23
40	0.22	0.07

Table II: Computational results for critical delay time differences τ_c as a function of fading depth. The modulation systems are 34 Mb/s, 8 PSK and 140 Mb/s, 16 QAM and the BER = 10^{-3}

From Table II it is concluded that for delay time differences <2 ns 34 Mb/s, 8 PSK digital radio links need only angle diversity if the fading depths are below 20 dB. For 140 Mb/s, 16 QAM the demands on fading reduction are harder to meet.

To investigate the possible fading reduction by means of limited scan antennas, information about the angles of arrival is needed. This information in combination with the path delay time difference is given in Section 3.

3. PROPAGATION CHARACTERISTICS

To come to a generalized design procedure of limited scan reflector antennas to be used for fading reduction it is assumed that the propagation phenomena are described in a two-way propagation model as far as angles of arrival and delay time differences are concerned. Each ray is influenced along its path by a constant refractive index gradient. For a given link geometry (antenna heights, distance between antennas) a unique relationship is found in this way between the angle of arrival α and delay time difference τ. The delay time computations are done in such a way that $\tau = 0$ for $\alpha = 0$. The results of the spherical propagation model are shown in Figure 3.

A specific refractive index gradient is implicitly needed to get a specific point on the curve of the $\alpha - \tau$ relation. This means that a general procedure is applied for the most frequently occurring refractive index gradients.

4. LIMITED SCAN ANTENNA SPECIFICATIONS FOR FADING REDUCTION

The $\alpha - \tau$ relationship is used to derive the antenna specifications during deep fades. One direct ray with angle of arrival α_d and delay time difference τ_d is compared with one selected from a large number of indirect rays with angle of arrival α_i and delay time difference τ_i. From Figure 3 it is concluded that for positive angles of arrival $|\tau_d - \tau_i|$ reaches the delay time τ_c of a given modulation system for smaller

τ [ns]	Δf [MHz] for FD = 5 dB	Δf [MHz] for FD = 20 dB	Δf [MHz] for FD = 40 dB	$f_{c_2} - f_{c_1}$ [MHz]
0.4			56.3	
0.8			28.1	
1.2		59.3	18.8	
1.6		44.5	14.1	
2.0	84.4	35.6	11.3	500
2.4	70.3	29.7	9.4	416.7
2.8	60.3	25.4	8.0	357.1
3.2	52.7	22.2	7.0	312.5
3.6	46.9	19.8	6.3	277.8
4.0	42.2	17.8	5.6	250
4.4	38.4	16.2	5.1	227.3
4.8	35.2	14.8	4.7	208.3
5.2	32.5	13.7	4.3	192.3
5.6	30.1	12.7	4.0	178.6
6.0	28.1	11.9	3.8	166.7

Table I: Computational results for Δf and $f_{c_2} - f_{c_1}$ as a function of delay time difference τ in a two-way propagation model

into account by assuming that the BER becomes excessively large, for $\max(\Delta\tau_g)$ lies in the vicinity of the symbol time τ_s. The relationship between BER and $\max(\Delta\tau_g)$, not computed here, is taken from simulation measurements of two ray fading described in (Ref. 2). Figure 2 shows measured τ/τ_s data as a function of fading depth for different modulation systems and with BER = 10^{-2}. Although for 16 QAM no simulation measurements have been performed it is assumed that it has the same sensitivity to multipath fading as 8 PSK.

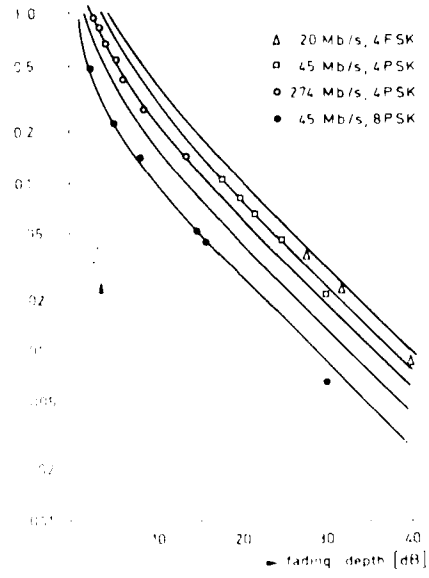

Figure 2: Value of τ/τ_s and fade depth needed to cause failure assuming 2-ray fade with its minimum at the band edge of a radio channel (Ref. 2)

2. TWO-RAY FADING WITHIN A RADIO CHANNEL

The frequency selective effects on a radio channel with bandwidth B ≤ 40 MHz are described by two incoming rays at the receiving antenna. The received field strength at radial frequency ω becomes:

$$R \exp(j\phi) = 1 + r \exp(j\omega\tau) \tag{1}$$

where r is the amplitude ratio between the indirect ray and the direct ray and τ is their delay time difference.
The group delay time $\tau_g = d\phi/d\omega$ delivers:

$$\tau_g = 2\tau \frac{r+\cos\omega\tau}{1+2r\cos\omega\tau+r^2} \tag{2}$$

In Figure 1 τ_g/τ is given for fading depths of 5 dB and 20 dB.

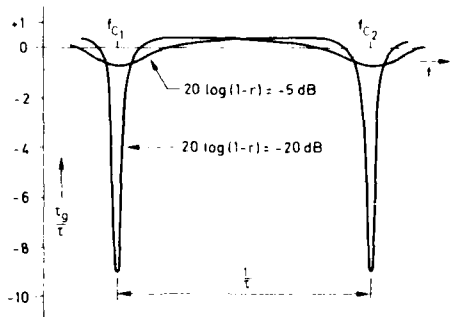

Figure 1. Group delay time for two-ray fading with fading depths of 5 dB and 20 dB

From this figure it can be seen that for deep fades (r ≈ 1) the maximum variation $\max(\Delta\tau_g/\tau)$ can be approximated by taking the difference between the minimum τ_g/τ value and $\tau_g/\tau = 0$. This maximum variation becomes:

$$\max(\Delta\tau_g/\tau) \approx \frac{r}{1-r} = 0.8 \text{ for fading depth } = 5 \text{ dB}$$

$$= 9 \quad " \quad " \quad " = 20 \text{ dB}$$

$$= 99 \quad " \quad " \quad " = 40 \text{ dB} \tag{3}$$

From Eq. (2) it is found that:

$$\text{minimum } \tau_g/\tau \qquad \text{for } \cos\omega_1\tau = -1 \Rightarrow \omega_1\tau = \pi(2n-1), \quad n = \text{integer} \tag{4}$$

$$\tau_g/\tau = 0 \qquad \text{for } \cos\omega_2\tau = -r \Rightarrow (\omega_2-\omega_1)\tau \approx \sqrt{2(1-r)} \tag{5}$$

In Table I $(f_{c_2}-f_{c_1})$ and $\Delta f = (\omega_2-\omega_1)/2\pi$ are given for fading depths FD = 5, 20 and 40 dB. From this table it is concluded that for deep fades ≥ 20 dB and delay time difference ≤ 2 ns frequency and/or space diversity combined with angle diversity is very effective because $\max(\Delta\tau_g/\tau)$ can be limited to a single radio channel. The approach outlined here is different, for it makes use of angle diversity to reduce the fading depth below 20 dB. In that case the angle diversity technique is based on the principle of reducing $\max(\Delta\tau_g/\tau)$ within a radio channel with frequency selective fading. At the same time the beam steering results in flat fading for the other radio channels.

The modulation system in the radio channel with frequency selective fading is taken

- electronic steering of beam elevation
- electronic change of the main lobe pattern

both methods have in common that interference signals can be weakened relative to the desired direct signal to reduce the effective fade depth. However, the quality and the availability of digital microwave radio links are not determined by fading depth but by degradations in Bit Error Ratios (BER) during given time intervals. According to CCIR documents 556 and 557 the 2500 km Hypothetical Digital Reference Path (HDRP) is considered not available if BER $> 10^{-3}$ during a time interval of 10 seconds. The long-term availability has to be larger than 99.7% of time. During this 99.7% of time the quality specification of the HDRP is given by BER $> 10^{-3}$ during maximally 0.05% of time in an arbitrary month.

The duration of deep frequency selective fading is mostly shorter than 10 seconds. This means that multipath fading influences the quality of the link mainly as long as the combination of frequency selective and "flat" fading does not have to be taken into account. Under this assumption the effects of a receiver antenna with fading reduction capability can be investigated by determining the fraction of time (FT) that BER $> 10^{-3}$. According to the quality specification is FT $< 5.10^{-4}$ for the HDRP.

If the HDRP is built up in 50 digital radio links at equal distances of 50 km and it is assumed that no simultaneous multipath fading occurs at more than one link, then:

$$FT < 10^{-5}, \text{ for a 50 km path.}$$

In the Netherlands the 4GHz band might be used at first for digital radio links with a large capacity. Two modulation techniques are being considered at the moment:
- 34 Mb/s, 8 Phase Shift Keying (8 PSK)
- 140 Mb/s, 16 Quadrature Amplitude Modulation (16 QAM)

Initially introducing digital radio links the arrangements within existing radio relay chains have to be maintained and the antenna concepts have to be based on existing parabolic antennas on the radio towers. Therefore, the discussion in this paper is restricted to a digital radio link characterized by:

- center frequency	4 GHz (3.8 - 4.2 GHz)
- modulation	34 Mb/s, 8 PSK
	140 Mb/s, 16 QAM
- path length	40 km
- antenna heights	80 m
- reflector	3 m parabolic dish with F/D = 0.25

The description of the radio path by a two-ray fading model is given in Section 2. In addition, BER measurements, given in (Ref. 2) and based on this model, are used to determine a simplified relationship between the model and the modulation characteristics. Section 2 concludes with specifications for a given modulation system with respect to the maximum allowable fading depth in relation to the path delay time difference between the two rays.

Path delays and angles of arrival are fully determined by the radio path itself. The fading depth is dependent on the amplitudes of the incoming rays and on the main lobe pattern of the receiver antenna.

In Section 3 the propagation characteristics of the two radio paths are derived by assuming that each ray is influenced by an artificial constant refractive index gradient as a function of height above a spherical earth. To avoid caustic problems in amplitude considerations, the path delay times and angles of arrival are used as input for the antenna specifications of antennas for fading reduction. The specifications, derived in Section 4, assume infinite deep fading if no diversity techniques are used. In this case a theoretical design procedure can be proposed because of the unique relationships between the maximum allowable fading depth, path delay time difference and angles of arrival.

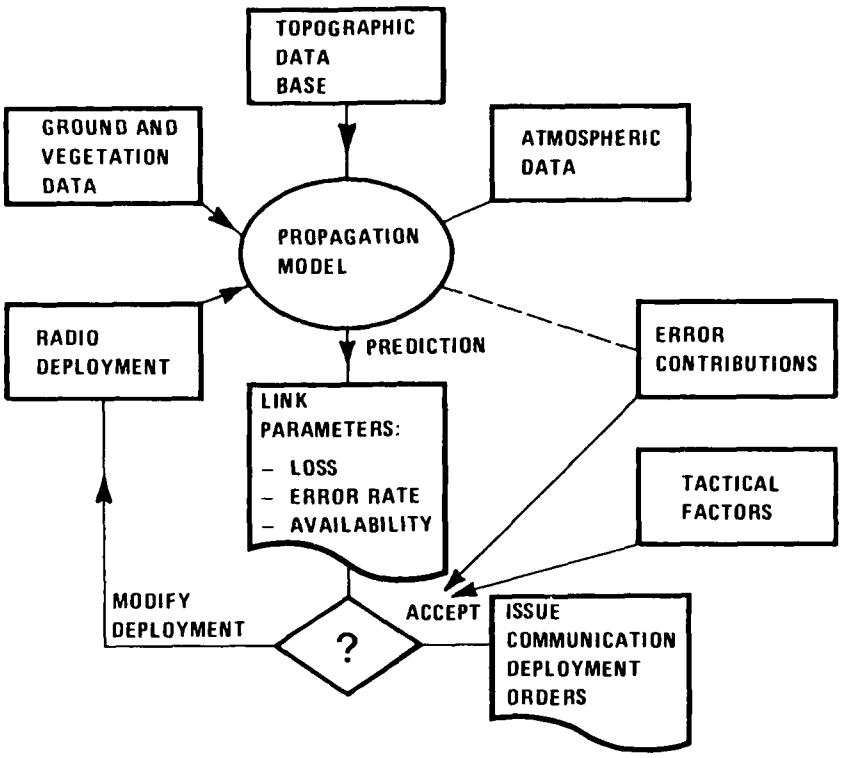

Figure 1 The interaction between propagation modelling and deployment of radio communication equipment

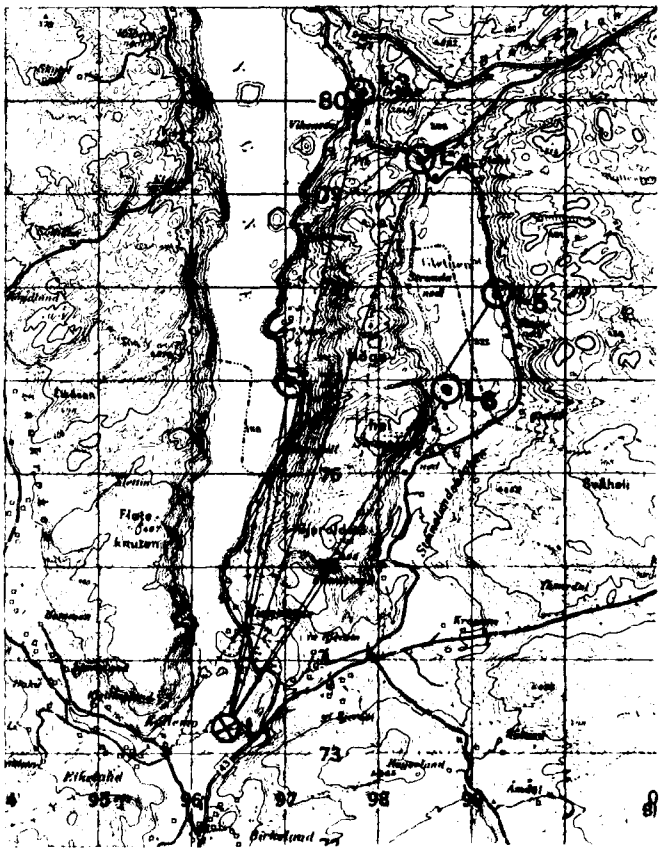

Figure 2 Typical lay-out of the transmission measurements. TYGNE test area shown. Transmitter at point L1

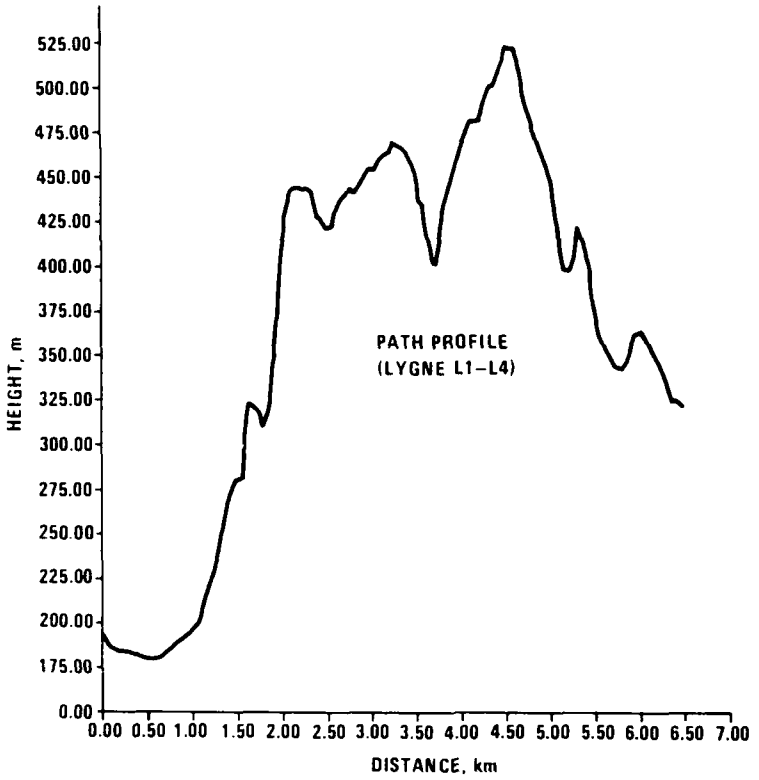

Figure 3 Example of path profile derived from the topographic data base. The L1 to L4 path in figure 2 is shown

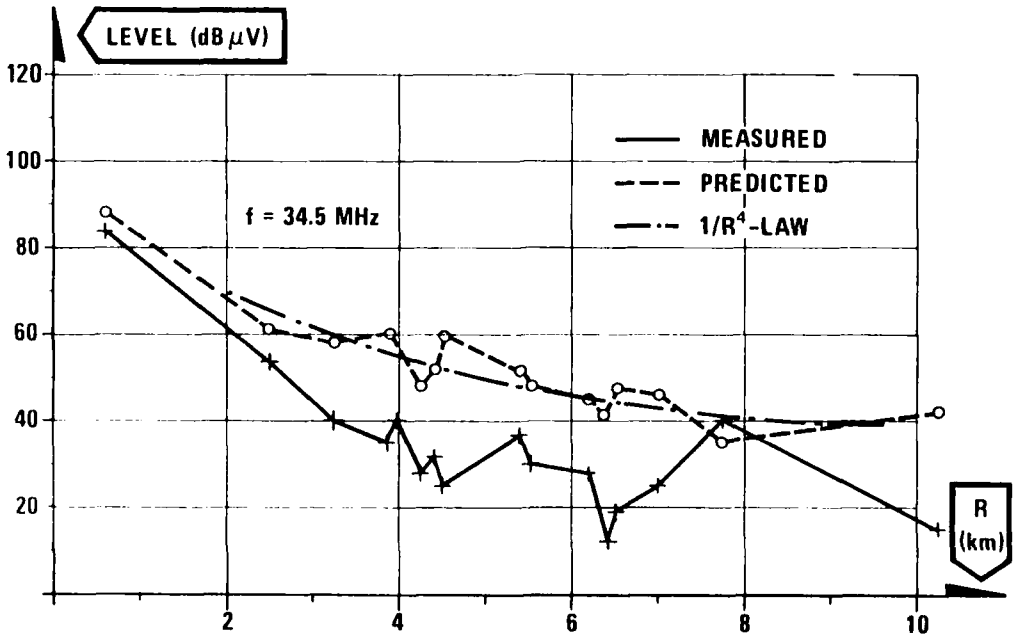

Figure 4 Predicted and measured level at 34,5 MHz versus range

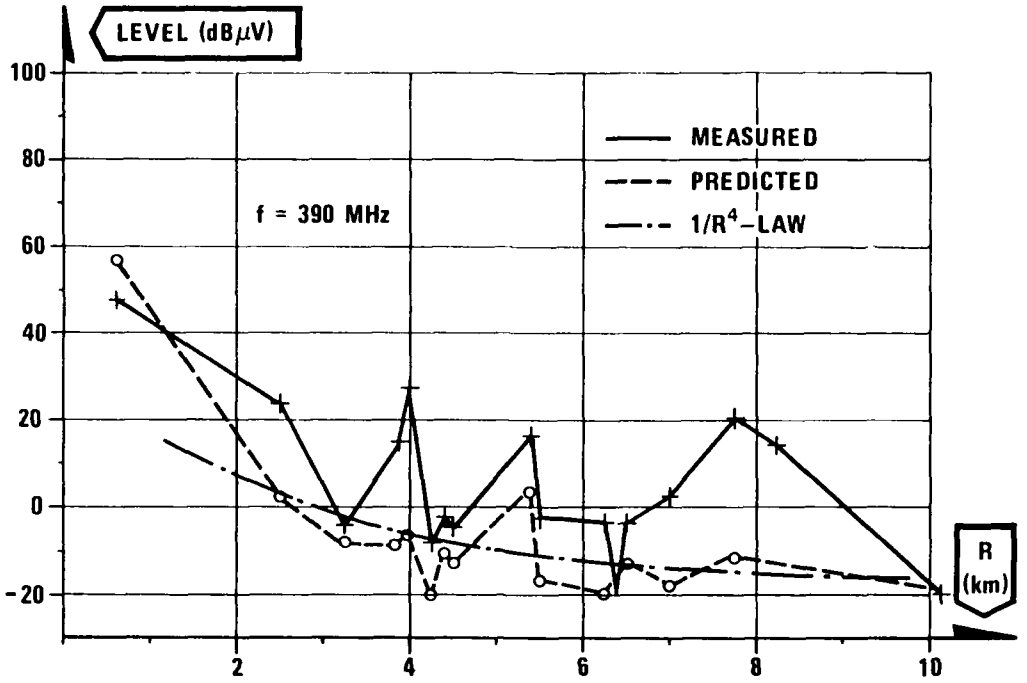

Figure 5 Predicted and measured level at 390 MHz versus range

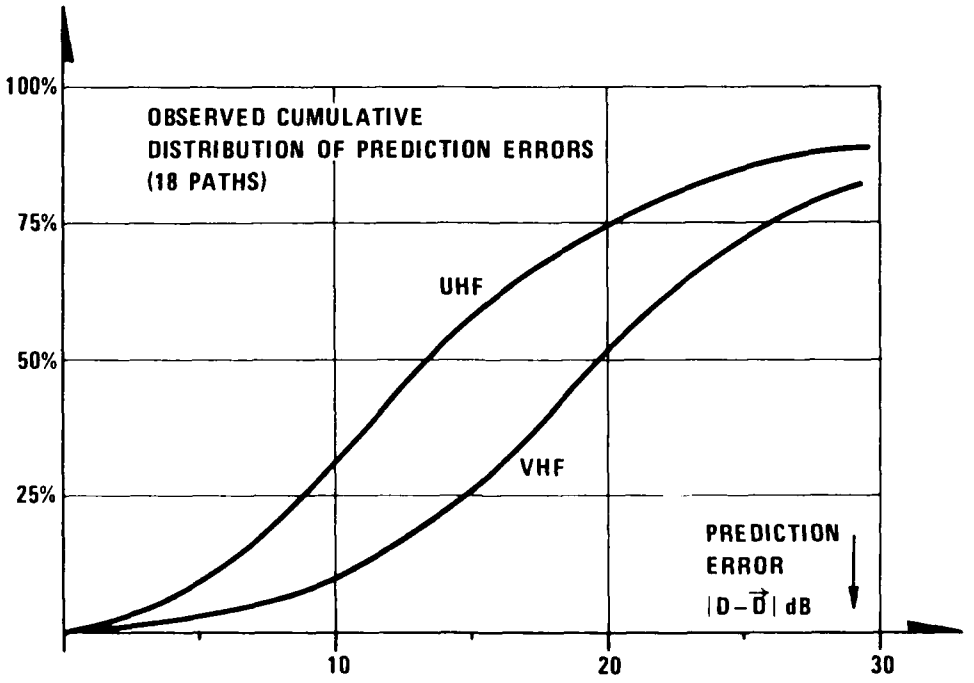

Figure 6 Observed cumulative distribution of prediction errors (data from 18 paths)

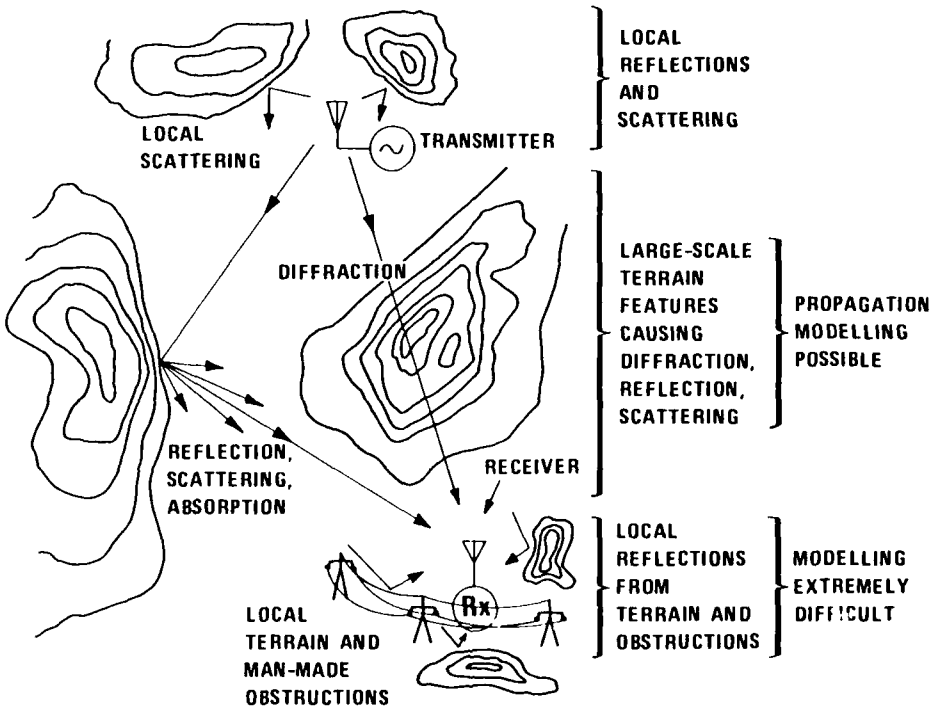

Figure 7 Illustration of the complex propagation environment created by terrain features and obstructions.

DISCUSSION

J.S.Belrose, Ca

(1) You mentioned the transmitter antenna, and its gain (– dBi), but you did not tell us what receiver antenna was used. Was it a military man-pack type?

Author's Reply

A half-wave vertical dipole antenna was employed at the receiver. A mast was used to elevate the feed-point to approx. 3 metres.

J.S.Belrose, Ca

(2) Okay. The point I wished to make is that for the tactical communicator, an apparent difference between predicted and measured signal strengths between VHF and UHF (of 10 dB or more) can easily be explained as due to antenna performance. The tactical military communicator usually uses a quarter wave or shortened quarter wave antenna. This antenna has to be operated against a ground plane. The chassis of a man-pack radio makes a very inadequate "ground plane" that is less effective at low VHF frequencies than at UHF. A man-pack radio should ideally employ an end fed half wave, which does not need a ground plane.

L.Boithias, Fr

Comme votre exposé semble concerner des liaisons militaires, quels sont les conditions qui résultent de ce fait, en particulier:—

(1) De quel temps dispose t'on pour faire les prévisions (quelques minutes ou plusieurs heures)?

(2) Peut-on envisager de faire le calcul pour plusieurs points de récepteurs, afin de choisir le meilleur?

Author's Reply

(1) The available time for on-line tactical radio network performance predictions will be different at different levels of command, e.g. at battalion level, one will in most cases have a few hours available for planning.

(2) To predict propagation for alternative positions would be consistent with normal military practice, and may of course be done. The communicator must then chose the site that represents the best compromise between tactical and electromagnetic factors.

E.Lintz Christensen, De

Your explanation of the extraordinary high level at 8 km distance in the VHF measurement, bringing the measured level to correspond to the predicted, was that a line of sight situation occurred. However, at UHF the measured level at the same site is 18 dB above the predicted. Is the reason local phenomena, or possibly the lack of inclusion of LOS in the model?

Author's Reply

The measured values at UHF were consistently above the predictions, whereas the reverse was true at VHF. Speculations on reasons for particular values at certain sites are not very meaningful, and no clear answer can be given.

A.Schneider, US

How would you characterise the vegetation on your path; and what is your vegetative data base?

Author's Reply

The vegetation in the terrain involved is light pine woods, and it was relatively dry during the experiments. The vegetation data base was approximated by the use of standard values, without using digitised map data.

E.H.Palmer, Ca

Based on the experience I have had in the development of VHF–UHF propagation models, I would suggest that point-to-point prediction models are capable of higher accuracy than you seem to suggest. In order to obtain higher accuracies however, one needs to take into account multiple diffracting obstacles, and radii of curvature of their crests, the effects of Fresnel zone obstruction by obstacles below line-of-sight, and so on. This requires considerable computing power, but with the rapid increases in computing speed and decreases in physical size that we are witnessing in portable computers at the present time, I think that we should not be deterred from applying these techniques to the tactical scenario because of present computer hardware limitations.

SOME PROPAGATION EXPERIMENTAL RESULTS ON PROTECTION TECHNIQUES FOR LINE-OF-SIGHT DIGITAL SYSTEMS

by
F. Fabbri
TELETTRA S.p.A
30, Via Trento
Vimercate (MI)
20059
Italy

SUMMARY

It is known that with respect to the analog systems the high capacity digital microwave systems are more sensitive to propagation distortion caused by selective fading and that in fact their performance would be very far from the CCIR objectives without adequate protective actions.

Some field trials over a 100 km path at 7 and 11 GHz on a 140 Mbit/s 16QAM system are being performed by Teletra in order to evaluate the performance and behaviour of some protection devices as baseband and IF equalizers, space diversity with IF and RF combiners, frequency diversity with hitless switching and special antennas purposely designed to reduce the multipath distortion. The object of these recent researches, still in progress, is to perfect protection systems and prevision methods so as to minimize space diversity, economically with its considerable expenses of infrastructures and apparatus, thus reducing the actually present economical difference between digital and analog radio links systems.

INTRODUCTION

In the last few years many studies, researches and experiments on digital propagation have been carried out. The reason is that a fast conversion of the transmission systems from analog to digital is in progress in the telecommunication networks and that high capacity digital systems are known to be more sensitive to propagation distortion caused by the multipath than analog systems. The objective is to be able to effect the above conversion in the most economical way by making use of existing infrastructures and to adopt adequate protections against the most distorting actions of the propagation.

In this paper examines the main causes of distortion produced by propagation on digital links, the protection systems generally adopted in order to reduce the outage time and more in detail by Teletra, for the realization of the digital test system. In addition it presents the most significant results obtained from some experimental tests carried out in order to evaluate the efficiency of the protection systems, and finally it gives some considerations on the correct possibilities of high capacity digital radio links which can be drawn on the basis of theoretical and experimental results.

1. ATMOSPHERIC MULTIPATH

In clear air conditions, the analog and high capacity digital signals behave differently. In fact, the attenuation introduced by the propagation medium is flat, while the distortion is selective. Selective fading is produced by the interference between the direct signal and one or more echoes. In practice we can expect values of atmospheric multipath which are very small. But fading may be considerably increased in extension and depth in the presence of layers of the type, by attenuation due to rain and by reflection from the ground and the sea.

The above explains why with respect to analog systems, digital systems are more sensitive to fading. For example, the CCIR recommends with reference to a 2500 km hypothetical connection with different numbers of hops, that in the worst month, besides the useful new, the unavailability time due to fading, for analog systems, should not exceed 0.3%, while experiments with digital techniques show that the

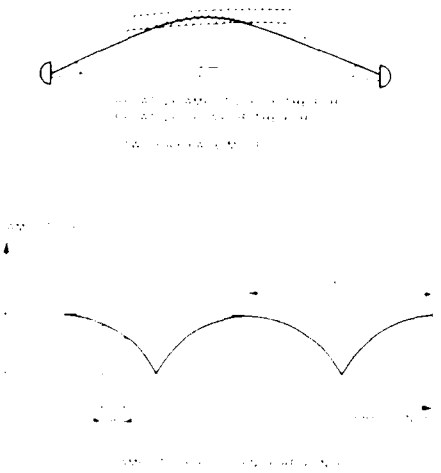

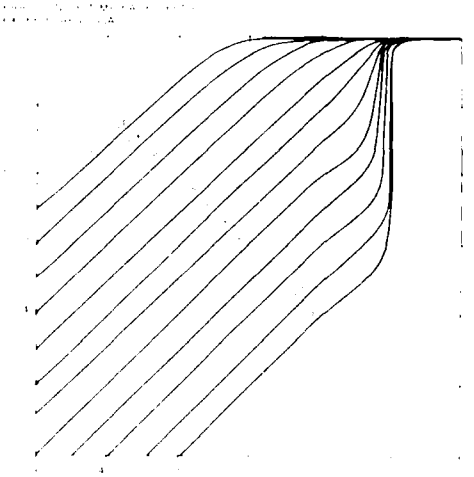

1. GROUND REFLECTION

[illegible] In the first case distortion is negligible but for the analog and for the digital systems of high capacity; in the second case, it may become unacceptable even if the [illegible] space diversity. In these extreme cases the problem can be solved only by reducing the cause of distortion rather than by acting on the distortion produced.

The reflected ray may be attenuated by:
- the ray path geometry;
- the reflecting surface;
- the divergency due to the earth's sphericity;
- the directivity of the antennas.

The contribution of the first two is frequently negligible. The divergency due to the earth's sphericity introduces an attenuation of a few dB into typical hops having a clearance in the order of the first Fresnel zone. In extreme cases of very large clearance this attenuation reaches maximum values of 4-6 dB.

The reflecting attenuation due to the divergency is practically reduced to zero in case with a large visibility margin. This situation is most dangerous, because it is associated with a noticeable echo delay and consequently because of the high distortion introduced into the analog and digital signals. Often the use of space diversity is ineffective. In these cases, the profiles of which are characterized by angles between direct and reflected rays ranging from half degree to a few degrees, Telettra implements a particular antenna device, the so-called antireflecting system /3/.

It is constituted of two antennas spaced vertically and placed on a plane perpendicular to the propagation axis (see Fig. 3). The signals received by the two antennas are combined by a hybrid after travelling along two feeders of equal length. The vertical distance d between the middle of the two antennas is calculated in such a way that the reflected ray entering into the upper antenna is delayed by half wavelength with respect to the ray entering into the lower antenna. So, whereas the two main signals are [illegible] combined, the reflected signals are in phase opposition and annul each other. The radiation pattern of the array can be made as directive as we want (Fig. 4). In consideration of all variability present, in practice it is possible to obtain, for 80% of time, reflected ray attenuations of approx 20 dB per terminal.

In every digital system, for each value of the echo delay there is a "minimum attenuation" value the echo must have in order to assure the transmission is free of errors. The [illegible] curve between the echo relative delay and the minimum attenuation [illegible] can be easily obtained in the laboratory by measuring on the digital [illegible] facility [illegible] signatures, for different values of echo delay and for a fixed BER, which [illegible] almost practically free of errors. For very large delays this curve [illegible] asymptotically to a constant value of attenuation coinciding with the attenuation that must be [illegible] in interference channel and consequently also to a very much [illegible] BER. This measurement too is performed in the laboratory. [illegible] typical signatures for different values of relative [illegible] 34 Mbit/s DJAM system. Fig. 6 shows the "minimum [illegible] to accept the BER less than 10^{-7} in function of the relative [illegible] 34 Mbit/s DJAM system. The required attenuations can be obtained [illegible] the directivity of the antennas, by the directivity of conventional [illegible] by using the antireflecting system.

C. BEHAVIOUR DIFFERENCES BETWEEN DIGITAL AND ANALOG PROPAGATION

[illegible] differences between digital and analog transmission [illegible] such as the [illegible] small echoes. [illegible] delayed echoes may accidentally [illegible]

[illegible]

[illegible] 34 Mbit/s DJAM system [illegible]

Summarizing we may say that the propagation problems related to the digital radio-relay links with ground reflection can be overcome in all practical cases with the use of protection systems of the diversity type, mainly effective for rare, severe fades, while the problems arising from the frequent multipath are more typical of the clearly regular optical profiles.

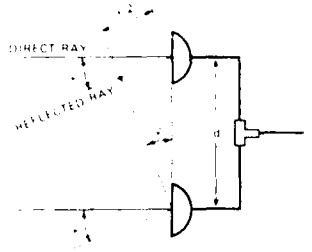

Fig.3 - Antireflecting system

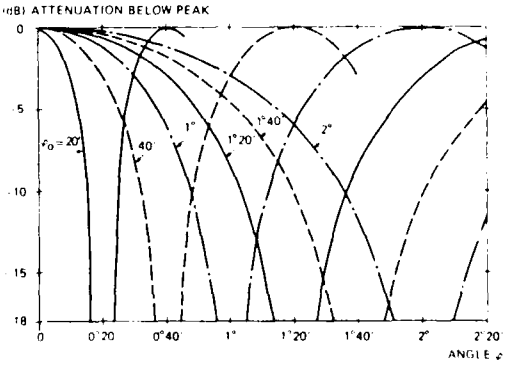

Fig.4 - Vertical radiation pattern of the antireflecting system for some values of φ_o (φ_o=angle corresponding to the first zero of the antenna system)

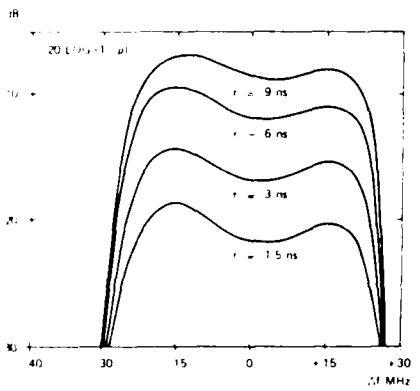

Fig.5 - Typical signatures for different values of τ and for BER 10^{-7} (140 Mbit/s 16 QAM)

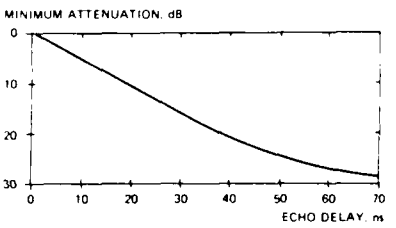

Fig.6 - Minimum attenuation of the echo vs echo delay for avoiding errors. (140 Mbit/s 16 QAM)

4. UNAVAILABILITY OF AN UNPROTECTED DIGITAL SYSTEM

[illegible] is the main cause of system unavailability in high capacity digital [illegible] in many cases, it is not possible to neglect the contribution [illegible], especially for links having a low fade margin. A reasonable [illegible] unavailability is given by:

$$U = U_{FLAT} + U_{SEL} \qquad (3)$$

[illegible] flat fade U_{FLAT} is given by Eq. 1:

$$U_{FLAT} = 10^{-(A-1)/10} \qquad (4)$$

[illegible]

[illegible] evaluating the unavailability due to selective fading [illegible] the signature of the system and the [illegible] may be [illegible]:

$$U_{SEL} = \eta \cdot K\left(\frac{\tau_m}{\tau_0}\right) \qquad (5)$$

where η [illegible] is the probability of [illegible] affected by multipath fading [illegible] probability [illegible], obtained from the measurements on the operating 6 GHz [illegible] 140 Mbit/s D.A.M. system with no equalizer in multipath conditions;

τ_m = mean relative delay
τ_{rms} = rms delay spread;
L = hop length, km;
T_s = symbol time.

Derived from the above expression, Fig. 7 shows unavailability graphics of an unprotected digital system (without equalizing) vs hop length for different values of the climatic and terrain factor, the extreme values and two intermediate values are interpolated. The dotted line represents the CCIR objective. It is clear that in most cases it is impossible to comply with the CCIR limits without applying more or less powerful protective actions.

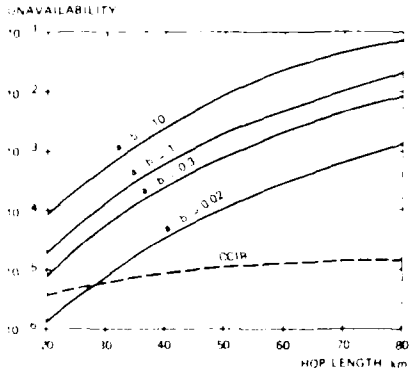

Fig. 7 - Unavailability of an unprotected digital system operating at 140 Mbit/s in 64 QAM, 7 GHz frequency band

5. PROTECTIONS

In sequence of their efficiency the most important protections are:
- IF equalization;
- baseband equalization;
- frequency diversity with hitless BB switching;
- space diversity with IF combiner.

Slope and bump IF equalizer

It acts in the frequency domain to produce a distortion complementary to that occurring in the channel so as to bring the overall characteristics back to an ideally flat amplitude-frequency response. Due to practical implementation, equalization takes place at IF and is limited to correcting the amplitude-frequency response only. In fact, group delay measurement and correction in BB would require rather complex circuits.

Baseband equalization

In digital systems, time domain signal processing can be considered to be the most effective equalization technique, since it directly combats intersymbol interference. The correction is derived by correlating the interference that appears at the sampling instant with the various adjacent symbols producing it. Equalization is achieved by means of tapped delay line networks to provide appropriate cancellation signals. Automatic equalization is always included in the demodulator.

Frequency diversity with hitless BB switching

In this case, two high capacity digital radio channels are arranged in 1+1 or n+1 configuration with hitless BB switching in order to have the apparatus protected against fading. In fact a certain amount of frequency diversity is always present and may represent a tolerable and inexpensive protection against multipath distortion.

The hitless BB switching system is of the self-synchronizing type and is basically based on the compensation of the transit time differences between the two switching paths, variable by propagation. It does not add errors to the digital signal, while the non hitless switching may produce errors or even loss, depending on the relative delay of the two paths.

Space diversity with IF combiner

[illegible]

6. DIVERSITY IMPROVEMENT

[illegible] Vigants [illegible]

$$I' = \frac{I}{\eta}$$

[illegible]
I' = unavailability of the diversity channel
I = unavailability of the non-diversity channel
η = correlation coefficient

[illegible]

$$I'_{FLAT} = \frac{I_{FLAT}}{\eta_{FLAT}} \qquad I'_{SEL} = \frac{I_{SEL}}{\eta_{SEL}}$$

$$I'_{TOT} = I'_{FLAT} + I'_{SEL}$$

[illegible]

$$\eta = \eta_0 (1-\rho) \qquad \text{where } \eta_0 \text{ multipath probability} = 0.18\, f_0^{0.7}$$
f_0 multipath occurrence factor (see (2))
ρ correlation coefficient

$\rho^2_{SD} = e^{-4.10^{-6}\left(\frac{s}{\lambda}\right)^2}$ for space diversity

$\rho^2_{FD} = e^{-2.5\left(\frac{\Delta f}{f}\right)}$ for frequency diversity

$\rho^2_{(SD+FD)} = \rho^2_{SD} \cdot \rho^2_{FD}$ for space plus frequency diversity

[illegible]
λ = wavelength
Δf = [illegible]
s = [illegible]

7. FIELD TRIALS ON DIGITAL RADIO SYSTEMS

[illegible]

[illegible]

[illegible]

[illegible]

8. RESULTS ACHIEVED ON THE MOZZECANE-VIMERCATE LINK

8.1. Fade statistics

8.2. Cross-polarization discrimination (XPD)

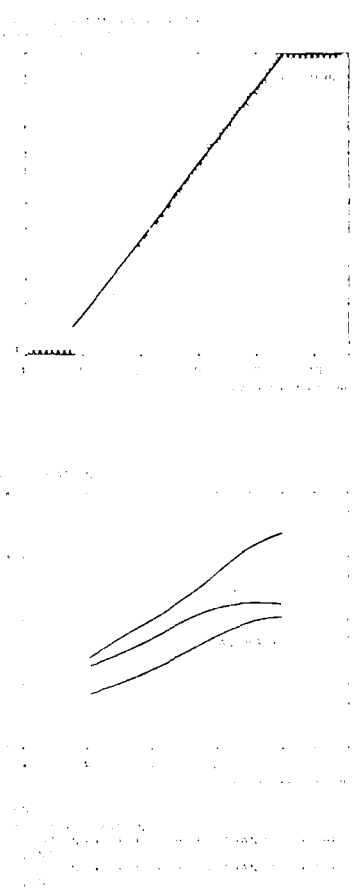

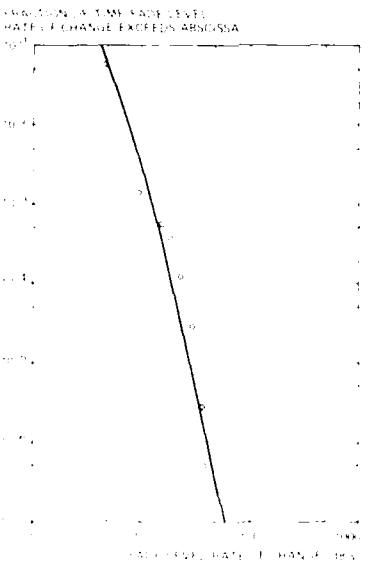

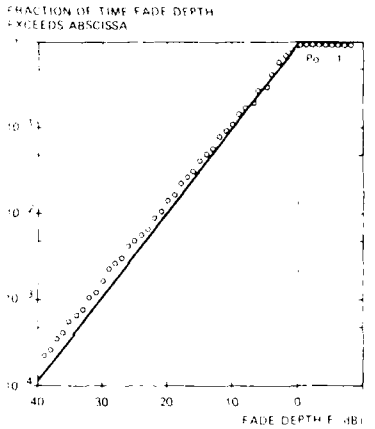
FRACTION OF TIME FADE DEPTH
EXCEEDS ABSCISSA
P_0 1
10^{-1}
10^{-2}
10^{-3}
10^{-4}
40
30
20
10
0
FADE DEPTH F (dB)

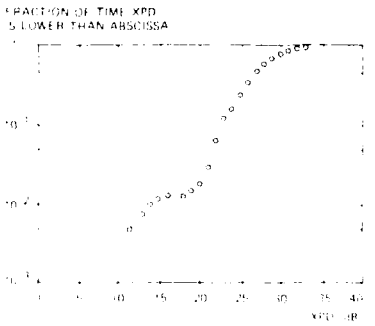
FRACTION OF TIME XPD
S LOWER THAN ABSCISSA

... organigramme de ces deux niveaux de traitement est fourni par la figure ...

... premier niveau de traitement est appliqué à l'issue d'une détection quadratique du signal ... premier étage de traitement. Le rôle des algorithmes de discrimination est de déterminer ... pics du signal détecté, repérant l'instant d'apparition des échos reçus. Les seuls pics retenus ... sont ceux qui émergent d'un seuil établi sur un compromis entre les probabilités de détection et de ... fausse alarme. Les algorithmes de discrimination effectuent également une estimation de l'amplitude ... signaux utiles reçus et du niveau de bruit moyen présent dans la bande d'analyse.

Le premier algorithme de discrimination s'effectue à un rythme égal à la période de répétition ... séquences d'émission et fournit l'estimation à court terme (quelques dizaines de ms) des paramètres ... canal. Un deuxième algorithme s'effectue à l'issue d'une intégration post-détection, dont le but ... est d'améliorer le rapport signal à bruit et donc les probabilités de détection et de fausse alarme. Il en résulte une estimation à moyen terme (quelques secondes) des paramètres du canal.

Le deuxième niveau de traitement effectue le stockage en mémoire des signaux en quadrature directement issus du premier étage de traitement. Ces signaux contiennent les informations sur la phase instantanée des échos reçus. La mémoire est relue à l'issue de chaque discrimination post-détection, aux seules adresses utiles repérées par ces discriminations. On dispose ainsi de la phase instantanée à court terme (quelques dizaines de ms) de chaque mode ou chaque trajet. Une analyse spectrale par maximum d'entropie fournit alors les décalages Doppler à moyen terme (quelques secondes) de chaque mode ou chaque trajet. La technique du maximum d'entropie [Haykin et al. 1979] a été retenue car elle autorise une meilleure résolution spectrale sur des durées d'analyse plus courtes que la FFT. Un inconvénient de cette méthode est sa sensibilité au bruit. Cependant, compte tenu du principe d'estimation ... phases instantanées qui est décrit ici, et qui tend à limiter l'influence du bruit, le bon comportement ... maximum d'entropie a été mis en évidence.

III.3 - Système de surveillance du canal

III.3.1 - Présentation du système

Le système de surveillance représenté figure ... a été construit à partir d'éléments pratiquement ... spécifiés au tableau ... L'objectif essentiel était de rendre ce dispositif rapidement modifiable ... et entièrement automatique de façon à pouvoir l'utiliser à des fins d'analyses statistiques ... L'ensemble est piloté par un calculateur en utilisant le bus IEEE-488.

... ont été réalisés avec un système composé :

- d'un ensemble émission réception ... associé à un amplificateur large bande. Les signaux émis sont ... d'impulsions à la fréquence f_0, de période de répétition T_r et de durée τ. A la sortie ... récepteur, les signaux sont transposés à la fréquence intermédiaire f_i ... et affectés d'un effet ... Δf_i. Par mélange avec un signal provenant d'un synthétiseur à la fréquence f_i + 10 kHz le ... signal utile est ramené à 10 kHz ± Δf_i. Le choix de cette dernière fréquence intermédiaire de 10 kHz ... ... la fréquence d'échantillonnage de l'oscilloscope (extérieur 7854 (102,4 kHz pour la base ... temps utilisée).
- ... de type delta (polarisation linéaire)
- ... de signal comprenant :
  - ... permettant la détermination du temps de groupe t_g en l'absence ...
  - ... Hewlett Packard donnant le spectre du signal à 10kHz f_i ... ... de fréquence de ... à 2,5 Hz (durée d'intégration : 50s) autour de 10 kHz. Les ... ... ou ...
  - ... type 4052 A pilotant l'ensemble de l'expérience et permettant ... ... cassette de 500 k octets.
  - ... programmable. Le système peut alors travailler avec ... fréquences différentes. Ainsi défini le système détermine spectre Doppler et ... ... et assure ... des ...

en fréquence sont également possibles.

III.1.2 - Réception

Des filtres de gabarits divers peuvent être insérés dans l'étage de sortie du récepteur de façon à pouvoir travailler avec des signaux d'encombrements spectraux différents ; ceci est en accord avec les possibilités d'émission. Une modification des retards et des durées d'ouverture du récepteur autorise l'analyse de tranches d'ionosphère d'épaisseurs quelconques.

III.1.3 - Modes de fonctionnement

L'étude des bruits et brouilleurs en alternance avec celle du milieu s'opère en coupant l'émission tout en maintenant la réception. En mode de fonctionnement réception pendant l'émission, un atténuateur est commuté automatiquement de façon à protéger le récepteur en limitant le niveau du signal à son entrée. Grâce à cette fonction, un étalonnage de la chaîne complète d'émission réception peut être effectué à tout moment. Une discrimination entre les déformations du signal, dues au système lui-même ou à l'ionosphère est donc possible.

III.2 Le traitement de l'information

Le mode de fonctionnement choisi pour les expérimentations sous incidence verticale est représenté schématiquement par la figure 5. Il se compose de l'émission - réception - acquisition de séquences de 2, 4, 6 ou 8 impulsions codées en phase. Les signaux provenant de la réception de chaque séquence sont stockés temporairement dans une mémoire tampon. A l'issue de la réception d'une séquence, le contenu de la mémoire est transféré sur un enregistreur de bandes magnétiques. Une fois le transfert achevé, l'émission d'une deuxième séquence peut débuter. Chaque doublet d'impulsions entrant dans la composition d'une séquence est formé de deux codes complémentaires [Isenq et al. 1972].

Les bandes magnétiques contiennent donc des signaux bruts, réfractés par l'ionosphère. De façon à en extraire les informations utiles sur le canal, un traitement est actuellement effectué en temps différé, sur ordinateur. Une première étape est constituée de la démodulation et du filtrage adapté des signaux, afin d'optimiser le rapport signal à bruit. La deuxième étape concerne l'extraction des paramètres utiles du canal : temps de propagation, atténuations, phases instantanées, décalages Doppler et niveaux de bruit.

III.2.1 Démodulation et filtrage adapté

Le signal à la fréquence intermédiaire f_i est tout d'abord ramené en bande de base sur deux voies en quadrature de façon à conserver la possibilité d'identifier par la suite le sens positif ou négatif des décalages Doppler.

Le filtrage adapté s'effectue par intercorrélation du signal reçu avec une référence correspondant au signal émis, compte-tenu des déformations propres à la chaîne d'émission - réception. Un étalonnage de celle ci doit donc préalablement avoir lieu pour définir la référence d'intercorrélation, grâce au mode de fonctionnement prévu à cet effet. Une sommation cohérente sur chaque voie en quadrature met en application la complémentarité des codages, de façon à disposer d'un bon diagramme d'ambiguité en temps. Il faut toutefois noter qu'une hypothèse de stationnarité doit être faite sur le canal pour que la propriété de complémentarité des codes émis se conserve à la réception. La durée entre la réception des deux codes étant au maximum d'environ 10 ms, cette hypothèse est tout à fait licite aux moyennes latitudes et sous incidence verticale.

III.2.2 Extraction des paramètres principaux de la fonction de transfert du canal

L'extraction des paramètres du canal s'effectue parallèlement sur deux niveaux. Le premier niveau permet d'accéder aux temps de propagation et aux atténuations des différents modes et trajets, ainsi qu'au niveau des bruits présents dans la bande d'analyse. Le deuxième niveau concerne la mesure de la phase instantanée de chacun des modes et trajets, de même que l'estimation des décalages Doppler

... de tous les signaux correspondant aux differents multi-modes et multi-trajets. Compte ... de liaisons etudiees, une duree maximum d'ouverture de 10 ms a ete jugée suffisante.

... Le choix de la frequence d'echantillonnage (f_e) depend de l'encombrement spectral du ... mais est limité par un compromis quantité/qualité de l'information. Pratiquement, ... trois la bande utile du signal.

... La periode de reactualisation (T_R) des mesures depend de l'ordre de grandeur des vitesses ... des conditions de propagation. Cette vitesse est liée aux decalages Doppler maxima attendus: ... mn. ... ms. D'autre part, la vitesse de transfert de l'information sur les unités ... impose une limite inferieure à T_R. Si l'organe d'acquisition est capable de stocker N ... la limite inferieure de T_R sera : $T_R \geq (1/N).T_o.f_e$.

... La largeur de bande d'analyse (B) doit être la plus grande possible pour obtenir une meilleure ... de resolution sur les multi-modes et multi-trajets [Le Roux et al. 1983]. Elle est cependant ... par la nature dispersive du milieu. On peut retenir la condition empirique de non distorsion [Saitors et al. 1977] :

$$B < \frac{2\pi}{\sqrt{(\partial\varphi/\partial\omega)_{f_o}}}$$

où $(\partial\varphi/\partial\omega)_{f_o}$ est la pente de l'isochronisme à la frequence f_o.

... Pour optimiser la dynamique du recepteur, la dynamique de conversion est liée à l'écart maximum I_m ... entre les modes et trajets que l'on souhaite détecter. Pour I_m de l'ordre de ... codage sur 8 bits (plus le bit de signe) ; la dynamique est alors legèrement ...

... caractériser le canal HF, on ne doit pas se limiter aux périodes de relative ... Ainsi, les evolutions du milieu aux transitions jour - nuit et nuit - ... le développement de perturbations de moyenne échelle (ondes de gravité) et de grande ... ionosphériques sont à étudier [Goutelard 1979].

... notre envisage d'analyser l'incidence de la geométrie des liaisons sur les communi... ... les effets de polarisation qui peuvent plus ou moins être mis en evidence suivant ... et d'antenne utilisé [Compton 1981].

II. LE SYSTEME DE MESURE DU CANAL HF

II.1. L'analyseur de liaison

... la version "utilisation zenithale" qui est presentée ici, l'analyseur de liaison se présente ... ... système d'emission - reception microprogrammable, couplé à un module d'acquisition ... ... traitements retenus par l'ionosphère. Toute la partie traitement de l'information est actuellement ... ... temps différé, sur ordinateur. Sa realisation en temps réel s'intégrera à la version "utili... ... La figure 1 présente un synoptique du système et le tableau I récapitule ... les differents modes d'emission, de reception et de fonctionnement.

II.2. Mesures

... La qualité de la mesure Doppler et le pouvoir séparateur en temps recherché sur les mesures, ... sont liés. Ce dernier peut être modifié en jouant notamment sur les codages de phase ... ... la durée de l'impulsion émise constante. L'energie des signaux emis peut être ajustée ... ... à la reception. Il suffit pour cela d'augmenter la durée ... ... Il convient toutefois de noter que la durée de l'impulsion d'emission condi... ... ... l'altitude maximale à laquelle l'analyse de l'ionosphère pourra être effectuée. Des balayages

donne : l'analyse spectrale permettant d'accéder aux décalages Doppler se fait en effet le plus souvent globalement. Il en résulte un spectre composite, représentatif de l'ensemble des multi-modes ou multi-trajets. [Martin 1982].

D'autre part, bien que représentant une étape importante pour la simulation de la propagation décamétrique, les modèles statistiques résultant de l'analyse de ces mesures sont volontairement trop simplifiés pour des raisons d'implantation en temps réel [Ehrman et al. 1982]. Ils ne représentent ainsi que le canal HF, que dans des configurations de comportement moyen et stationnaire [Watterson et al. 1969].

Compte tenu de ces problèmes, nous nous proposons ici de contribuer à améliorer la connaissance de la fonction de transfert du canal HF.

II.2 - Les caractéristiques principales du canal HF

Le canal HF peut, en bonne approximation, être considéré comme linéaire. Il se prête donc à une caractérisation en terme de fonction de transfert. Le signal reçu à l'extrémité d'une liaison est ainsi une fonction de plusieurs variables associées au signal émis et modifiées par le canal de transmission. Parmi les principales, citons l'amplitude, le temps, la fréquence et la polarisation. D'autres paramètres, sources de distorsions du signal, peuvent également être pris en compte, comme la dispersion en fréquence suivant la largeur de bande utilisée, de même que les caractéristiques d'antennes et la géométrie de la liaison [Moorat et al. 1968] [Whitehead et al. 1983].

Pour des liaisons à un bond aux moyennes latitudes, la propagation se fait généralement par les couches E, F et F_2. Dans ce cas, l'ordre de grandeur des paramètres de la fonction de transfert est le suivant (CCIR 1978) :

. Etalement du temps de propagation : $3\ ms \leq \Delta\tau \leq 6\ ms$

. Temps de propagation du premier mode $> 650\ \mu s$ (incidence verticale)

. Décalage Doppler moyen : $-5\ Hz \leq f_d \leq 5\ Hz$

. Elargissement du spectre Doppler d'un mode ou trajet : il dépend de la durée d'intégration de la mesure. Pour des durées de l'ordre de 5 mn, on peut retenir : $\Delta f_d \leq 5\ Hz$.

. Atténuation : environ 40dB d'écart entre le plus fort et le plus faible niveau des principaux trajets.

Tous ces paramètres se combinent et induisent des phénomènes d'évanouissement sur le signal reçu. Il convient alors d'interpréter ces évanouissements en terme de fonction de transfert du canal. Dans le cas envisagé ici, les valeurs extrêmes retenues pour les évanouissements sont les suivantes : [CCIR 1978] :

. Durée d'un évanouissement : 0,05 s à 1,5 s

. Taux d'évanouissement : 5 à 40 par mn

. Largeur de spectre d'un évanouissement : 0.1 kHz à 1 kHz

. Vitesse à laquelle un évanouissement traverse le spectre : 0,5 kHz/s à 2 kHz/s

En plus de ces phénomènes perturbateurs d'une transmission HF, il convient de noter la présence de brouilleurs de forts niveaux qui sont essentiellement dûs à la télégraphie (spectre étroit) et aux liaisons BLU (spectre large). De façon évidente, les liaisons numériques se comportent elles aussi comme des brouilleurs les unes vis à vis des autres.

Pour pouvoir mesurer, analyser et modéliser la fonction de transfert du canal à des fins de simulation en laboratoire, il est nécessaire de concevoir un système spécifique. La mise en oeuvre de ce système est conditionnée par les caractéristiques du canal, qui viennent d'être citées.

II.3 - Contraintes liées aux variations des caractéristiques du canal

. La durée d'ouverture (T_o) des récepteurs doit être suffisamment importante pour permettre

Dans sa version finale, l'analyseur de liaison fonctionnera en mode oblique : il effectuera simultanement la mesure de la fonction de transfert globale du canal HF et celle de ses principaux parametres caracteristiques : temps de propagation, attenuations et decalages frequence Doppler. Il permettra en outre l'etude des bruits et des brouilleurs presents dans la bande. La période minimale de reactualisation des mesures de la fonction de transfert sera de l'ordre de 10 ms. La grande quantite d'information acquise à un tel rythme limite nécessairement la durée des expérimentations, pour des raisons de stockage et d'exploitation des résultats.

Nous décrivons ici une première version de ce système qui permet de mesurer les principaux parametres de propagation du canal de transmission HF. La durée des acquisitions est limitée à quelques dizaines de minutes. C'est pourquoi il a été jugé utile de pouvoir disposer d'un système complémentaire, permettant de surveiller parallèlement le comportement du canal sur des échelles de temps plus grandes (quelques dizaines d'heures). Ce deuxième système se limite à la mesure du décalage Doppler (intégré sur une minute) [Bertel et al. 1983] et à celle du temps de propagation du premier mode ou trajet reçu. Pour des raisons de commodités de mise en oeuvre, l'analyseur de liaison a tout d'abord été testé sous incidence verticale.

Apres avoir rappelé les contraintes essentielles apportées par les caractéristiques du canal HF sur sa mesure, nous décrivons donc dans la suite, un prototype du système d'analyse de liaison dont le fonctionnement est actuellement limité à l'incidence verticale [Le Roux et al. 1983]. Pour terminer, nous présentons des résultats de mesures obtenues dans ces conditions. Ce type d'expérimentation est destiné à valider les principes de fonctionnement et de traitement de l'information qui ont été retenus pour la realisation à venir de la version oblique bistatique de l'analyseur de liaison.

II - LES CARACTERISTIQUES DU CANAL ET LEURS MESURES

II.1 - Données actuelles

Des etudes portant sur l'amélioration de la connaissance du milieu de propagation ionosphérique sont en cours depuis plusieurs décennies. Elles ont pour but l'interprétation physique et/ou statistique de mesures effectuées, soit en routine par les stations de sondages zénithaux réparties sur tout le globe, soit à l'occasion de campagnes d'expérimentation plus spécifiques, mises en oeuvre sous incidence oblique.

Les ionogrammes obtenus par les stations de sondage verticaux fournissent une représentation d'ensemble des hauteurs virtuelles de réfraction des différentes couches ionosphériques en un lieu donné. Ils permettent de disposer d'une surveillance quasi continue du milieu. Les données issues du dépouillement des ionogrammes servent de base à l'établissement des méthodes de prévisions à moyen et long terme de certaines caractéristiques ionosphériques [Le Roux 1980] [Jones et al. 1962] ; cependant, le degré de précision insuffisant et la trop grande période de réactualisation de ces mesures (15 mn en moyenne), ainsi que la limitation du nombre de paramètres caractéristiques qu'elles concernent, rendent impossible leur application directe aux problèmes des transmissions à plusieurs kb/s.

Le deuxième type de mesures, effectué sous incidence oblique, en mode monostatique par la technique de rétrodiffusion [Goutelard et al. 1977] ; [Shearman et al. 1980], ou en mode bistatique (liaisons expérimentales) [Chavand et al. 1982] [Watterson et al. 1969] ; [Lockwood et al. 1980], est beaucoup plus proche des préoccupations d'augmentation des débits de transmission par voie HF. Dans ce cas, les objectifs sont de deux natures : ils concernent l'analyse des mécanismes de la propagation dans la gamme décamétrique ainsi que la modélisation du canal HF, en vue de sa simulation en temps réel en laboratoire [Sailors et al. 1976], [Goldberg et al. 1965].

Dans ces circonstances, les paramètres étudiés sont généralement les temps de propagation, les atténuations et les décalages de fréquence Doppler des différents multi-modes et multi-trajets. Mais, les techniques utilisées, notamment pour l'estimation des décalages Doppler (par FFT), peuvent parfois entraîner une trop grande intégration dans le temps des mesures et rendre impossible le suivi d'évolution du canal au niveau de ses fluctuations à très court terme. De plus, dans la plupart des cas, on n'identifie pas les décalages Doppler et les atténuations correspondant à un mode ou trajet

SYSTEME DE MESURE DES CARACTERISTIQUES DU CANAL IONOSPHERIQUE POUR LES TRANSMISSIONS NUMERIQUES

Y.M. Le Roux, L. Bertel, J.P. Jolivet, P. Lassudrie-Duchesne, H. Rouault

Centre National d'Etudes des Télécommunications
Centre Lannion B - Département MER/GER
BP 40 - Route de Trégastel - 22301 LANNION

ABSTRACT

Numerous industrial laboratories are currently working on increasing the rate of digital transmissions in the decametric range, by means of adaptative modems. To contribute to this work, one must define more closely the ionospheric channel, not only concerning its rapid fluctuations, but also its slower time evolutions. The measuring system described in this paper has been drawn up with this in mind. It is therefore designed to provide for two types of ionospheric medium investigation. The first concerns the estimation of the main parameters of the channel transfer function, with an up-dating process in the order of ten milliseconds. With such a cyclic-rate analysis, constraints of data recording restrict the length of the observations. This system then also gives information about the channel time-varying characteristics over intervals of a few tens of seconds, and thus allows a survey of the average behavior of the channel in a quasi-continuous manner. Here we comment on the first results obtained during an experiment at vertical incidence with the aim of validating equipment and measurement technique.

I - INTRODUCTION

Il est bien connu que l'ionosphère réfracte les ondes électromagnétiques de la gamme décamétrique. Cette propriété est très largement utilisée pour établir des liaisons de communication transhorizon. Mais, l'ionosphère est également un milieu anisotrope, dispersif en temps et en fréquence, inhomogène et non stationnaire dans le temps. Ces caractéristiques sont sources de divers types d'évanouissements sévères qui affectent les transmissions HF et en dégradent singulièrement la qualité. A cet inconvénient, s'ajoute celui de l'encombrement spectral de la gamme décamétrique. Il se traduit souvent par un fort brouillage de toute communication par voie ionosphérique.

Malgré ces problèmes, les utilisateurs de systèmes de transmission HF ont le désir d'augmenter les débits et la fiabilité de leurs communications. De telles améliorations passent par une meilleure caractérisation quantitative et qualitative du canal HF et notamment de ses fluctuations à très court terme [Watson et al. 1982]. En effet, les progrès constants de la technique aidant, les laboratoires chargés de concevoir les équipements de transmissions dans la gamme 2-30 MHz, peuvent actuellement réaliser des systèmes de modulation et de démodulation basés sur des algorithmes de plus en plus performants. Il est toutefois nécessaire de bien adapter ces derniers aux réalités de comportement du canal utilisé.

Les laboratoires chargés des études de transmission par voie ionosphérique ont ainsi besoin de connaître la fonction de transfert du canal HF, de même que son évolution dans le temps. Il est donc important de savoir mesurer et modéliser celle-ci. Les résultats de mesure et d'analyse de la fonction de transfert sont destinés à orienter la conception des modems vers une meilleure adaptation aux conditions de propagation dans l'ionosphère. La modélisation de la fonction de transfert doit permettre la simulation en laboratoire du canal HF ; elle est utile de mettre au point et de tester les prototypes de modems, soit préalablement à leur réalisation, soit lors de phases d'études comparatives des performances de différents types de modems [Brook et al.1981] [Watterson 1981].

Dans le présent article, la première étape d'une étude dont l'objectif final est de mesurer la fonction de transfert du canal de transmission ionosphérique, à l'aide d'un analyseur de liaison, l'application visée est la simulation en temps réel et en laboratoire de ce canal de transmission. On s'intéresse à des liaisons HF de 500 à 3000 km. Les largeurs de bande envisagées sont de 3 kHz à 10 kHz, pour des vitesses de transmission de l'ordre de 2,4 kb/s.

REFERENCES

1. K. Morita - Prediction of Rayleigh fading occurrence probability in line-of-sight microwave links. Rev. Elec. Comm. Labs - Vol. 18, 1970, pages 11-12.
2. CCIR, Geneva 1982, Vol. V, Rep. 338, page 286.
3. S. Fatteri - Antiinterfering system for 2 GHz overseas radio links. Alta Frequenza - No. Vol. XLII - 1973, pages 393-397.
4. I. Majoli, C. Mengali - Propagation in line-of-sight radio links. Supplement to Telettra Review no. 34 - Special Edition, 1984, pages 74 to 77, pages 94 to 110.
5. I. Majoli - Selective Fading on a 2 GHz hop. Telettra Internal Report ES 1033 - December 1977.
6. I. Majoli - Final Report on FMV hop measurements. Telettra Internal Report I. 1956 - March 1981.
7. CCIR, Geneva 1982, Vol. IX, Rec. 594, pages 93-94, Rec. 557, pages 73-74.
8. C. Cairoghi, N. Calia - Digital field trial link Ferrara-Bologna, 7 GHz, 70 Mbit/s, 16-QAM - Period 28th July to 25th August 1983 - Telettra Internal Report MS 1057 - September 1983.
9. C. Cairoghi, N. Calia - Digital field trial link Arzentario - Limbara, 4 GHz, 34 Mbit/s 4PSK - Period 27th January to 7th February 1984 - Telettra Internal Report MS 1 - - March 1984.

DISCUSSION

J.F.Patricio, Po

L'etude est basee sur la fréquence de 7 GHz, je le crois. Peut-on conclure que les résultats seront les mêmes e autre fréquence de la bande des ondes centimétriques?

Author's Reply

From the expressions of paragraphs 4 and 1:

(a) The flat fading unavailability increases linearly with the radio frequency f ($U_{FLAT} = f$)

(b) The selective fading unavailability increases with f according to the law:

$$U_{SEL} \; f^{n}$$

G.Argyropoulos, Gr

(1) In table 3, on page 17-15, standard space diversity of 10 m is given as one of the system characteristics. Is this distance between the two antennas the optimum?

(2) Is there any formula to calculate the optimum space diversity for digital radio-relay systems using data as (a function of) the distance and the frequency? What do you foresee at this point?

Author's Reply

(1) A space of 10 m between the diversity antennas has been chosen as a typical value generally adopted in high capacity line-of-sight links.

(2) The formulae given in paragraph 6 for calculating the correlation coefficient k for space diversity have been derived from propagation experiments on analogue systems over many years.

The very last experimental results obtained from digital systems seem not to confirm the supposition that the digital diversity behaves as the analogue one. Theoretical and experimental research is in progress in order to clarify the problem.

however, it is very expensive in that it requires two times the number of antennas, towers and transmitters as well as affecting the cost of antenna support towers.

Hence, for limiting the use of space diversity as much as possible, the possibility of using other methods have been investigated and tested. Thanks to the excellent results fully listed, adaptive equalizer has permitted to improve the value of the digital links, far above it is able to protect only a part of the events with a probability. In many cases frequency diversity with digital techniques has been tested to be an inexpensive and effective protection against multipath fading. However, its proper fully exploitation it is necessary to have a network able to switch the bandwidth of RF line to multipath. Also the first results obtained by using very directive antennas, whose half lobe is far as the multipath, which is responsible for the outages, is the latter advance the radio relaying will have a great boost that in the near future the distinction between digital and analog transmission will be more and more evident.

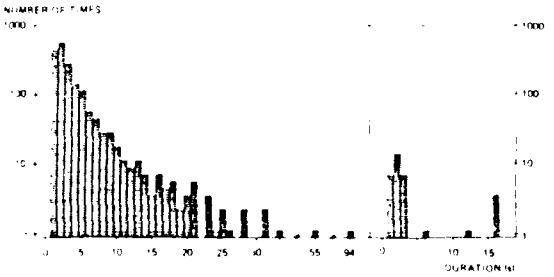

a) b)

Fig.32 - Histogram of the number of times with BER 10^{-7} versus duration of such events.
27th Jan.to 7th Feb.1984, 34 Mbit/s
4 PSK, 4 GHz, 240 Km.
a) before switching
b) after switching

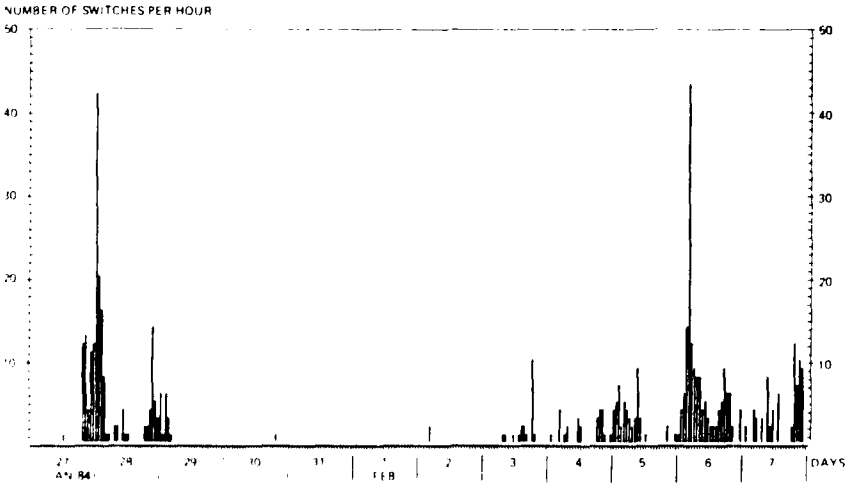

[illegible] switches in the last period days

ACKNOWLEDGEMENTS

[illegible]

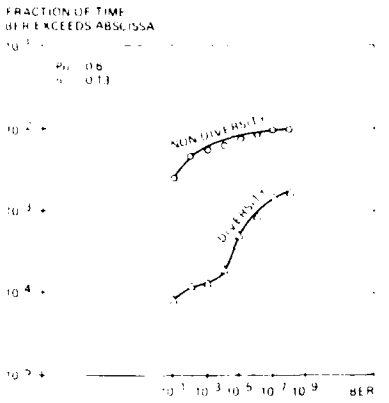

[illegible] BER statistics [illegible] frequency and diversity [illegible].

[illegible] Maximum hop length (km) within 99.9% objectives of typical digital systems for a few configurations and fade factors.

[illegible]	SYSTEM CONFIGURATION	Climatic and terrain factor [illegible]			
		[illegible]	[illegible]	1	1
	NON-DIVERSITY	4	<20	<20	<20
	BASIC SYSTEM (no diversity) Quasi-adaptive equalizer	20	14	10	<10
1+1	BASIC SYSTEM with freq diversity	5	43	32	42
	BASIC SYSTEM with space diversity	11	84	61	80
	BASIC SYSTEM	44	92	73	<20
1+1	BASIC SYSTEM with freq diversity	70	54	48	46
	BASIC SYSTEM with space diversity	45	78	66	74

System characteristics

140 MBIT/S QUADRATURE PSK, f = 4 GHz, SPACE DIVERSITY = 10 m, FREQUENCY DIVERSITY = 40 MHz, FADE MARGIN REFERRED TO THE [illegible] RECEIVER THRESHOLD = 40 dB, "FOR" BIT ERROR RATE = FOR LESS THAN 0.025% OF ANY MONTH.

[illegible] statistics from the [illegible] expressions reported in paragraphs 1, 4 and 6, [illegible] have been obtained through field trial tests and from the modem signatures [illegible] by the [illegible] BER. In order to evaluate the improvement introduced by [illegible] frequency and space diversity we consider the unprotected channel with included [illegible] a performance. In high capacity digital systems, the frequency [illegible] always present. For the sake of simplicity, the 1+1 configuration [illegible] MHz has been considered. As far as the climatic factor is [illegible], two extreme situations and two intermediate conditions have been considered [illegible] the worst month, while a·b = 0.3 is the value [illegible] Barnett-Vigants type. Calculations have been made for two conditions [illegible].

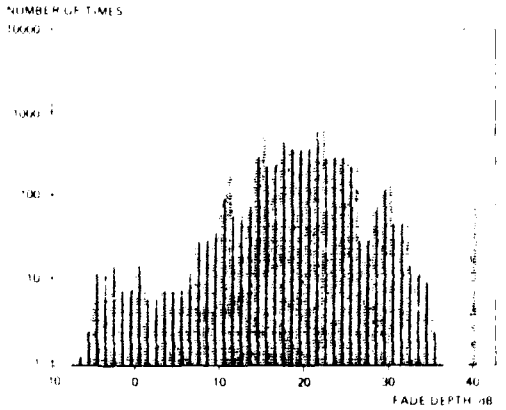

[illegible] correspondence between number of times with BER [illegible] and fade depth. [illegible] 7th Jan. to 7th Feb. 1984, 64 Mbit/s, 4 PSK, 4 GHz, 4 Km.

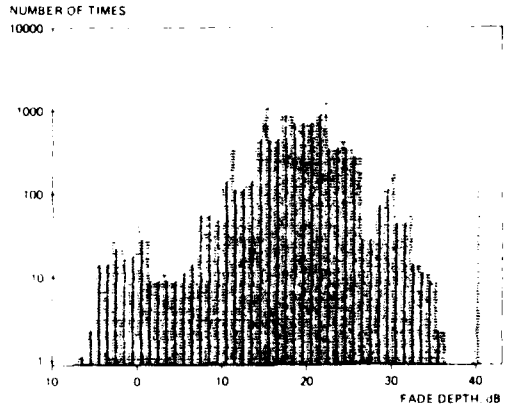

[illegible] correspondence between number of times with BER 10^{-7} and fade depth. 7th Jan. to 7th Feb. 1984, 64 Mbit/s, 4 PSK, 4 GHz, 340 Km.

CONCLUSIONS

[illegible] to verify the transmission of high capacity digital signals over radio links [illegible] to be much more expensive than the transmission of analog signals. In fact, it was necessary to adopt [illegible] space diversity on almost all the hops. Space diversity with [illegible] the most efficient protection system against multipath distortion.

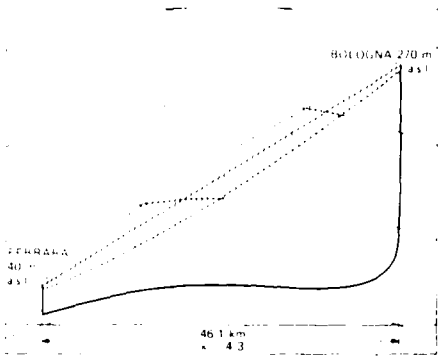

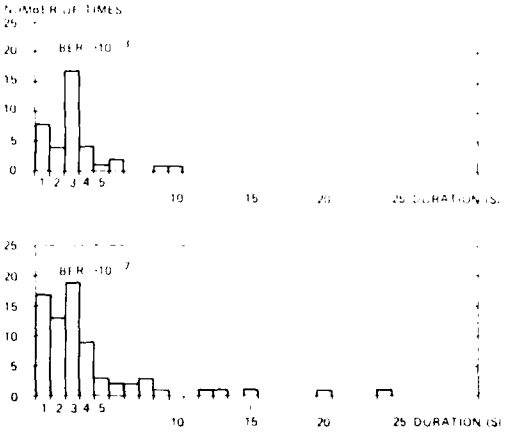

Fig.26 - Histogram of the number of times with BER 10^{-3} and 10^{-7} versus duration of such events. August 1984

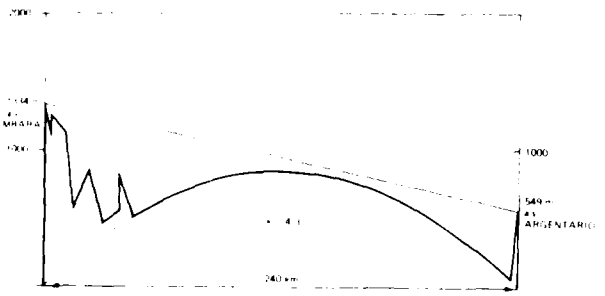

Fig.27 - Argentario-Elmbara path profile

11. PRESENT POSSIBILITIES OF THE HIGH CAPACITY DIGITAL LINKS

Concerning space diversity experiments, two types of combiners have been tested: the IF combiner and the IF combiner. They are both of the maximum-power type and combine the received signals in order to maximize the resultant signal level. With respect to the RF type, the IF combiner has the drawback of progressively excluding the worst signal. The most recent experimentation of the RF combined space diversity in a period of 2,592,000 seconds [ ] has shown that the RF combiner. The antenna spacing was 17 m and the frequency 7 GHz. Subjectively, the IF combiner has an improvement greater than 100.

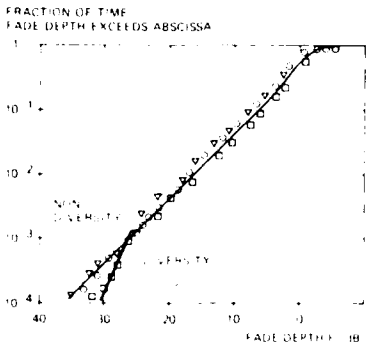

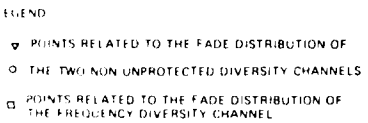

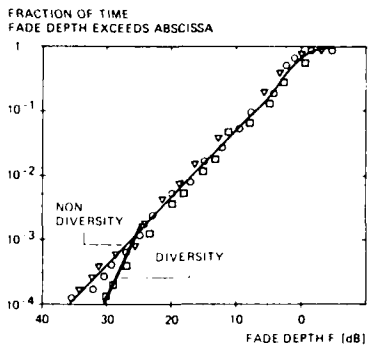

Fig.21 – Frequency diversity, Δf = 10 MHz

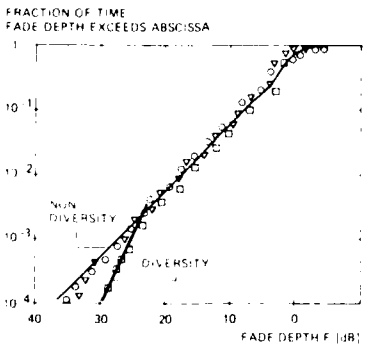

Fig.22 – Frequency diversity, Δf = 15 MHz

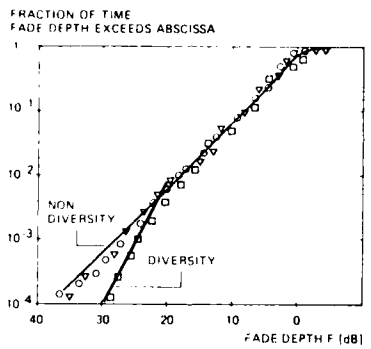

Fig.23 – Frequency diversity, Δf = 20 MHz

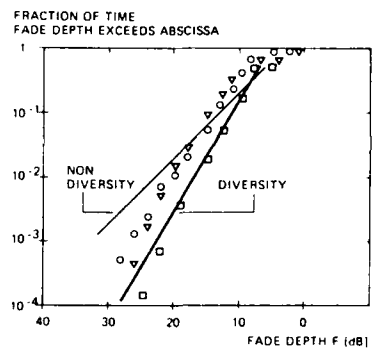

Fig.24 – Cross-band diversity, Δf=4634 MHz

9. PERFORMANCE OF FERRARA-BOLOGNA HOP

Fig. 25 shows the Ferrara-Bologna field trial path profile. The link crosses the Po Grande Valley. A single frequency of 7177 MHz, modulated by a 16QAM 70 Mbit/s digital signal, is transmitted. The baseband equalization is included in the demodulator. We limit to report the main results achieved in August 1983 [8] which was one of the worst months of the year. Table I reports the BER statistics relevant to a period of 9570 seconds (B= 1.1, η = 0.19).

The quality for BER 10^{-7} largely met the CCIR objective (Rec 594), while the quality for BER 10^{-3} was about 10 time worse than CCIR limits. The adoption of frequency diversity was considered sufficient for having the quality comply with the above mentioned limits. The measured quality is practically coincident with the foreseen value.

Fig. 26 reports the histogram relative the number of times the BER exceeds 10^{-6} and 10^{-3} in the worst month observed.

10. RESULTS ON THE FIELD TRIAL LINK ARGENTARIO-LIMBARA

Argentario-Limbara is a line-of-sight trial link of 240 km over the Tyrrhenian Sea (Fig. 27). Here a 3970 MHz frequency is modulated by a 34 Mbit/s 4PSK digital signal and

[illegible] the [illegible] part [illegible] the [illegible]. The first [illegible] [illegible] the [illegible] [illegible] [illegible]

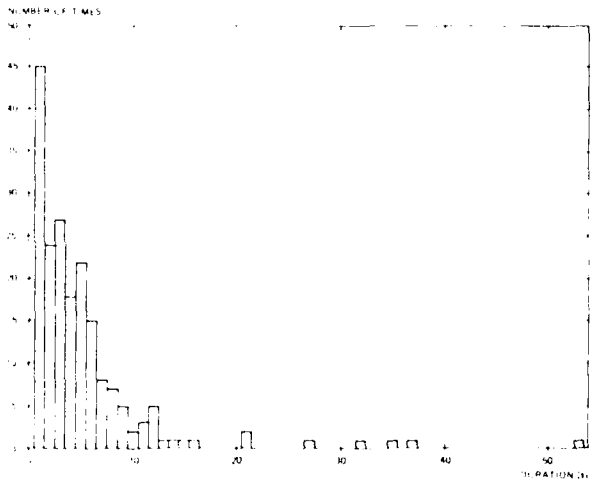

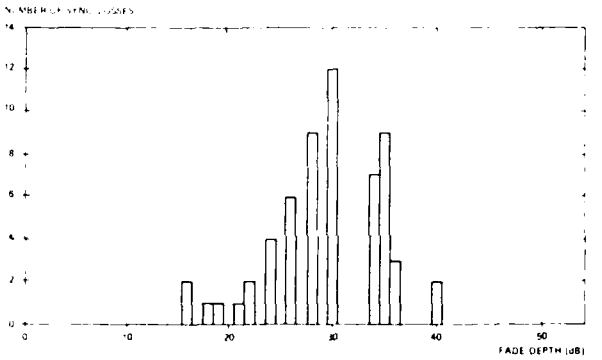

Fig.17 - Correspondence between number of sync losses and fade depth, 140 Mbit/s, 7GHz, October 1982

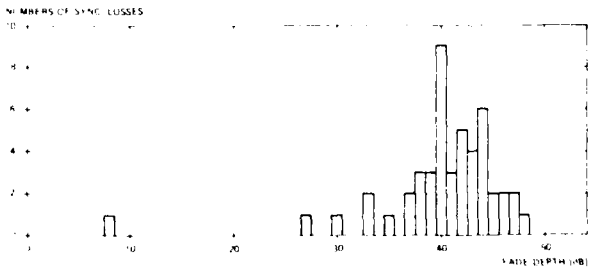

8.4. Minimum phase and non minimum phase probability

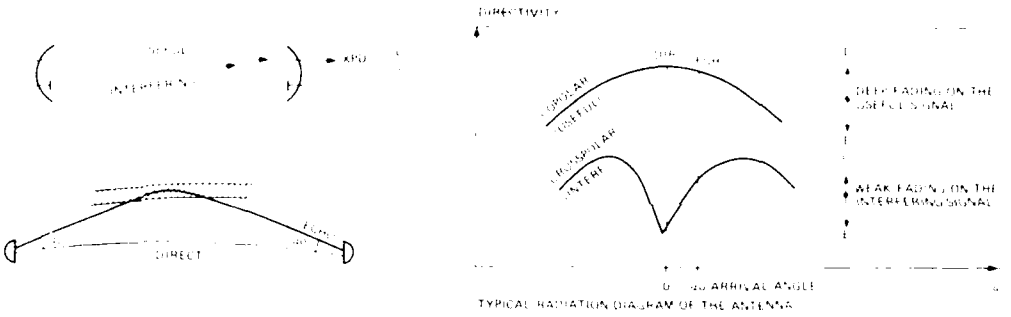

TYPICAL RADIATION DIAGRAM OF THE ANTENNA

8.3. Performance of the 140 Mbit/s unprotected channel

III.2.2 - Mode de fonctionnement

Un nombre de fréquences est d'abord choisi en fonction des objectifs de l'expérience [Bertel et al, 1984] ; le système explore ensuite séquentiellement les fréquences préréglées.

Au début de l'expérience le zéro doppler est calibré de façon à éviter toute erreur d'interprétation ultérieure. A cette fin la raie parasite liée au couplage émetteur-récepteur a été utilisée. Cette raie, comme on le verra par la suite, perturbera parfois les spectres présentant des décalages doppler voisins de zéro.

Pendant une minute, pour chacune des fréquences, les opérations suivantes sont effectuées :

- acquisition du signal sur l'analyseur de spectre en vue de déterminer le spectre doppler ; la durée d'acquisition a été choisie égale à 50 secondes ce qui conduit à un pouvoir séparateur théorique de 0,02 Hz ;
- pendant le temps d'acquisition sur l'analyseur de spectre le calculateur de l'oscilloscope Tektronix 7854 détermine par une procédure simple l'enveloppe des impulsions reçues (en l'absence de brouilleurs). Les deux courbes sont ensuite stockées sur la cassette du calculateur.

III.2.3 - Traitement des résultats

La figure 5 représente un exemple de courbes observées avec le système. Afin de limiter le nombre de données, seules les valeurs supérieures à celles fixées par un seuil ont été enregistrées ; ceci explique l'allure "tronquées vers le bas" des courbes.

Dans la plupart des cas, les spectres présentent au moins deux raies correspondant aux modes ordinaire et extraordinaire. Lorsqu'on observe des échos multiples, des décalages doppler peuvent être au double ou au triple de celui du premier écho apparaissant sur le spectre. Ce n'est toutefois pas toujours le cas.

Le système de surveillance ainsi mis en oeuvre est toutefois limité dans ses applications :

- il ne permet que la détermination d'un seul temps de groupe (celui du premier écho) en absence de brouilleurs ;
- la raie parasite utile pour la calibration perturbe toute mesure au voisinage du zéro doppler.

IV - RESULTATS D'EXPERIMENTATION

Nous présentons ici deux types de résultats obtenus à Lannion, sous incidence verticale. Les premiers sont destinés à illustrer les performances de chacun des deux systèmes de l'outil d'analyse de canal qui vient d'être présenté. Les résultats suivants ont pour but de confronter les mesures des deux systèmes, au cours d'expérimentation en fonctionnement simultané.

IV.1 - Exemples de mesures fournies par l'analyseur de liaison

La figure 6 correspond à une expérimentation qui a eu lieu le 7.11.83, entre 8 h 35' et 10 h 20' T.U., à la fréquence de 7,75 MHz, c'est-à-dire au niveau de la séparation des modes ordinaire et extraordinaire de la couche F_2.

Les mesures sont issues de la discrimination post-intégration (cf. figure 2). Elles sont intégrées sur environ 12 s et sont réactualisées toutes les 5 mn. Les codes complémentaires d'émission sont de longueur 16, pour une durée de l'état élémentaire de 40 µs, soit une durée d'impulsion de 640 µs. Les échos doubles correspondant à une réflexion au sol étaient présents dans la fenêtre d'analyse. Bien qu'en parfait accord avec les caractéristiques des échos simples, ils n'ont pas

etc représentés pour des raisons de clarté de figure.

On peut constater des variations importantes des hauteurs virtuelles de réfraction des deux modes, dues à un mouvement d'ensemble de la couche, sans modifications importantes du profil de densité. Ce mouvement d'ensemble est confirmé par la corrélation des évolutions des décalages doppler de chacun des deux modes.

La portion d'ionogramme correspondant à la fréquence d'analyse est schématisée en bas de figure et donne une vue d'ensemble des mouvements constatés.

La figure 7 correspond à une expérimentation qui a eu lieu le 22/2/83, entre 15 h 12' et 15 h 23' (au voisinage du coucher de soleil), à la fréquence de 9 MHz où les modes ordinaire et extraordinaire de la couche F_2 sont bien séparés. Les mesures issues de la discrimination post-intégration sont intégrées sur 12 s environ et sont réactualisées 4 fois consécutives. Chacune de ces expérimentations de 48 s est reprise toutes les 2 mn. Les conditions d'émission sont celles de la figure 3.

Ces résultats illustrent une situation où les évolutions des caractéristiques des deux modes réfractés sont opposées. La cause de ceci peut être due cette fois à une modification du profil de densité électronique [Bertel et al. 1984].

IV.2 - Exemple de mesures du système de surveillance

Le système de surveillance fournit des spectres dont l'échelle de fréquence est inversée. Le signe des décalages Doppler qui y sont représentés est donc positif lorsque la vitesse apparente des couches ionisées est dirigée vers le haut.

La figure 5 a, présente un spectre de trois raies, dont deux sont centrées sur 0,12 Hz et -0,20 Hz. La troisième est la raie parasite centrée sur le zéro de fréquence. Le seuil de détection est visualisé par un trait horizontal.

La figure 5 b, montre l'enveloppe du signal reçu, correspondant au premier écho dont le niveau franchit le seuil de détection matérialisé par le trait horizontal. Les impulsions d'émission correspondantes avaient une durée de 600 µs pour une période de répétion de 11,36 ms. Le spectre fournit est intégré sur 50 s et l'enveloppe du signal est définie par 128 points.

IV - 3 - Résultats en fonctionnement simultané

Nous proposons dans ce qui suit deux séries de résultats communs obtenus par les deux systèmes travaillant parallèlement, mais décalés en fréquence d'émission, d'environ 50 kHz. Le système de surveillance à moyen terme ne permettant d'avoir accès qu'aux décalages Doppler, aux amplitudes des raies spectrales et au premier temps de groupe, on se limite à la comparaison de ces seuls paramètres. Les signes des décalages Doppler fournis par l'analyseur de liaison ont été inversés de façon à les rendre compatibles avec les spectres issus du système de surveillance.

La figure 8 montre un spectre Doppler intégré sur 50 s, obtenus par ce système de surveillance ainsi que les quatre spectres obtenus pendant ce laps de temps à l'aide de l'analyseur de liaison. Mis à part la raie centrale parasite du spectre global, on peut noter le bon accord entre les amplitudes et les décalages fréquences obtenus par les deux méthodes. Il faut toutefois remarquer que cette concordance des résultats n'est pas générale, notamment lors d'évolutions très rapides de l'ionosphère où les effets d'intégration deviennent plus sensibles. Néanmoins, la complémentarité des échelles de temps des mesures du système de surveillance vis-à-vis de celles de l'analyseur de liaison, doit permettre de mieux appréhender les processus physiques mis en évidence par ce dernier.

La figure 9 se réfère à une durée d'analyse beaucoup plus grande : 18 mn. On y trouve représentés 18 spectres consécutifs intégrés sur 50 s et obtenus par le système de surveillance, de même que ceux intégrés sur environ 13 s, obtenus par l'analyseur de liaison. L'emplacement des raies spectrales obtenues par l'analyseur de liaison est représenté par des points et correspond à un écho dont le temps de propagation est d'environ 1840 µs. Les croix matérialisent l'emplacement des raies Doppler de l'écho double, dont le temps de propagation n'est fourni que par l'analyseur de liaison et qui est dû à une réflexion au sol. Son écart de retournement plus faible que celui de l'écho simple,

Comme précédemment, à part la présence de certaines raies parasites pouvant être dues à des brouilleurs, on constate que les évolutions générales des raies spectrales sont voisines. On peut également noter que les évolutions à court terme du Doppler matérialisé par les points se traduisent par un élargissement de la raie correspondante du spectre donné par le système de surveillance.

V - CONCLUSION

Le système de mesure présenté dans cet article a été conçu dans le cadre d'une étude dont les buts sont l'analyse et la simulation en laboratoire du canal H.F. Il est constitué d'un analyseur de liaison associé à un système de surveillance permettant la mesure à court terme de la fonction de transfert du canal et de ses principaux paramètres caractéristiques. La période minimale de réactualisation des mesures est d'environ 10 ms et la durée maximale de surveillance automatique atteint 24 h. Il autorise un contrôle quasi-continu du comportement moyen du milieu ionosphérique, en le ponctuant de périodes d'analyse de ses évolutions plus rapides.

Des résultats acquis sous incidence verticale ont été présentés en se limitant aux seuls temps de propagation, amplitudes et décalages fréquences ; ils illustrent les possibilités de l'outil de mesure et l'intérêt que présente cette étude qui se développe actuellement sous incidence oblique.

BIBLIOGRAPHIE

AARONS J., GROSSI M.D. : HF propagation factors affecting the design and operation of real time, channel evaluation, adaptative systems. AGARD May 1982.

BERTEL L., GUYADER P., LASSUDRIE P. : Etude de l'effet Doppler ionosphérique par sondages multi-fréquentiels. Note technique NT/LAB/MER/59 - Juin 1983.

BERTEL L., GUYADER P., LASSUDRIE P. : Multiple-frequency Doppler sounding of the ionosphere : Theory and experimental comparison with incoherent scatter results. Radio Science vol. 19 - N°3 - May-June 1984 (to be published).

C.C.I.R. : Utilisation de simulateurs de voies ionosphériques en ondes décamétriques. Simulateurs de voies ionosphériques en ondes décamétriques. Rapports 549-1 et Avis 520 - 1978.

CHAVAND E., GOUTELARD C., HARARI S. : Système de protection contre les erreurs pour liaison ionosphérique. Ann. Télécom. 37 N° 5-6, pp. 272-284, 1982.

CLARK A.P., Mc VERRY F. : Performance of 2400 bit/s serial and parallel modems over an H.F. channel simulator - IERE Conf. Proc. Loughborough - 1981.

COMPTON R.T. : The tripole antenna : an adaptative array with full polarisation flexibility. IEEE Trans. on Antennas and Propagation. Vol. AP 29 - N°6 - Nov. 1981.

FORMAN E., BATES E.B., ESCHLE J.E., KATES J.M. : Real time software simulation of the H.F. radio channel. IEEE Trans. on Comm. Vol. 30 - N° 5 - Aug. 1982.

GOLDBERG B., HEAD R.E., POMERSKI D. : Stored ionosphere. IEEE Annual Comm. Conv. June 1965.

GOUTELARD C. : Caractérisation du canal ionosphérique dans les transmissions numériques hautes fréquences. Revue du CETHEDEC - NS 72/2 - 1979.

HAYKIN S. et al. : Nonlinear methods of spectral analysis Topics in applied physics. Vol. 34 - Springer - Verlag 1979.

JONES W.B., GALLET R.M. : Representation of ionospheric and propagation variations of ionospheric data by numerical methods. J. Res. NBS sec. D, 4, 419-438, 1962.

LE ROUX Y.M. : Prévisions ionosphériques à court terme par modélisation mathématique prédictive. Annales de géophysique - Tome 36 - 1980.

LE ROUX Y.M., JOLIVET J.P., ROUAULT H., MADANI A. : Rappels sur les méthodes modernes de traitement du signal radar. Présentation d'un système radar décamétrique d'acquisition. Rapport technique LAB/MER/GER/76 - Janvier 1983.

LOCKWOOD M., MITCHELL V.B. : Oblique H.F. radiowave propagation in the main trough region of the ionosphere. The radio and Electronic Engineers - Vol. 50 - N° 11-12 - pp. 559-566 - Nov. 1980.

MASLIN N.M. : High data rate transmissions over H.F. links. The radio and electronic engineers - Vol. 52 - N°2 - pp. 75-87 - Feb. 1982.

MOORAT A.J.G., BRADLEY P.A., BRAMLEY E.N. : Wave polarization and its influence on the power available from a radio signal propagated through the ionosphere. Proc. IEE - Vol. 115 - N°6 - June 1968.

SAILORS D.B., HILL J.R. : Simulation and measurement of H.F. ionospheric channels. Technical Report III NOSC - San Diego 1976.

SHARMALI D.R., OBISAL R.R. : Compatibility of high-frequency radar remote sensing with communications. IEE Conf. Pub. - N°188 - pp. 103-107 - London - July 1980.

TSENG C.C., LIU C.L. : Complementary set of sequences. IEEE Trans. on Inf. Theory - Vol. IT 18 - N°5 - Sept. 1972.

WATTERSON C.C., JUROSEK J.R., BENSEMA W.D. : Experimental verification of an ionospheric channel model. Technical Report ESSA - Boulder 1969.

WATTERSON C.J. : HF channel measurements on the KY-879/PESK burst - communication modem - Set 2 NTIA - CR - 82 - 28 1983.

WHITEHEAD J.D., FROM W.R., JONES K.J., MONRO P.E. : Measurements of movements in the ionosphere using radio reflections. J.A.T.P. - Vol. 45 - N° 5 - pp. 345-351 - 1983.

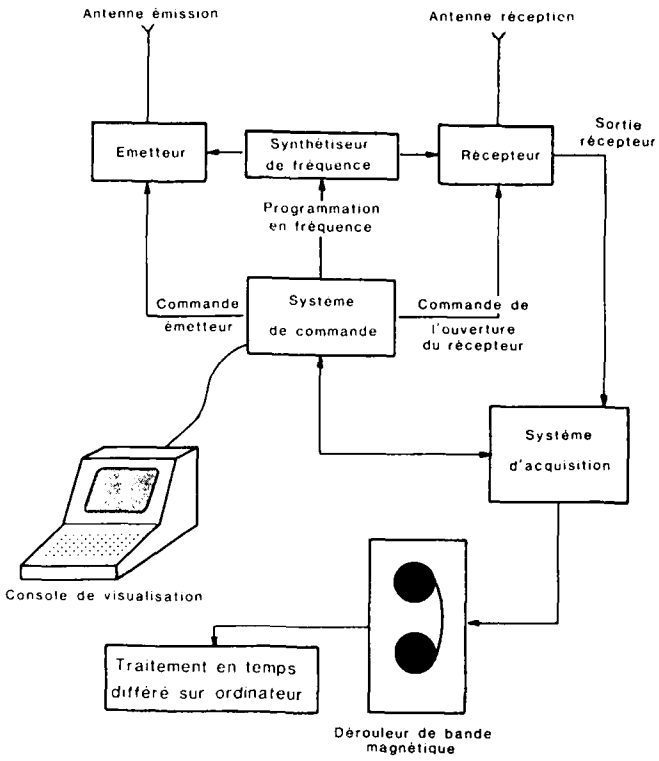

Figure 1 : Schéma de principe de l'analyseur de liaison (version incidence verticale)

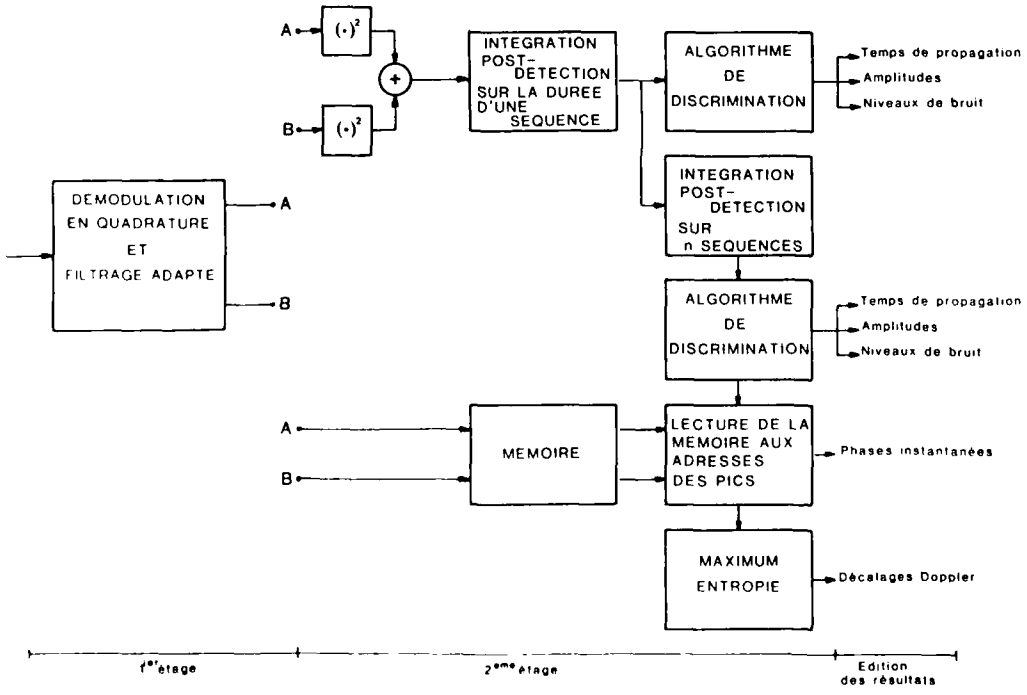

Figure 2 : Schéma bloc du traitement de l'information de l'analyseur de liaison, version incidence verticale

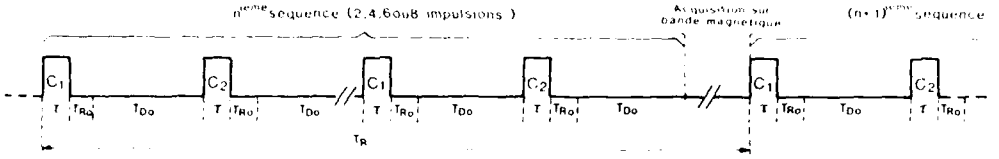

figure 5 : Mode de fonctionnement émission - réception - acquisition de l'analyseur de liaison en incidence verticale.

τ : durée des impulsions d'émission - TRo : Retard à l'ouverture du récepteur - TDo : Durée d'ouverture du récepteur - TR : Période de réactualisation des mesures - C1 et C2 : Codes complémentaires à deux états de phase.

CARACTERISTIQUES D'EMISSION

. Puissance crête : 400 W

. Durées d'impulsions (µs) : 80 ; 160 ; 320 ; 640 ou 1280.

. Types de modulation :

Deux états de phase 0 - π

- Phase : Durée d'un état : 40 µs.
  9 codes préprogrammables pouvant être sélectionnés arbitrairement.

- Amplitude : 4 enveloppes preprogrammables definies par 1 point/200 ns, sur 2048 points maximum.

- Possibilite de combiner les modulations en phase et en amplitude.

. Emission-reception de sequences d'impulsion avant enregistrement sur bande magnétique.
Chaque sequence est composée de 1, 2, 4 ou 8 impulsions.

. Fréquence d'emission d'une séquence : programmable avec incrémentation automatique en cours de fonctionnement. L'incrémentation est programmable de 0 (fonctionnement à fréquence fixe), à 1 MHz, par pas de 500 Hz.

. Nombre de sequences d'emission-reception : programmable de 1 au fonctionnement en continu, par pas de 1.

CARACTERISTIQUES DE RECEPTION

. Reception synchrone de l'emission

. Fréquences centrales en sortie de recepteur : Bande de base ; 25 kHz ou 100 kHz

. Largeurs des filtres du dernier etage du recepteur :

- En bande de base : bande passante à 3 dB : 22 kHz
  bande passante à 40 dB : 40 kHz
  ondulations dans la bande : 0,1 dB

A 25 kHz : bande passante à 3 dB : 15 kHz ;
ondulations dans la bande : 0.5 dB

A 100 kHz : bande passante à 3 dB : 15 kHz, 30 kHz ou 60 kHz
ondulations dans la bande : 0.5 dB

. Conversion analogique digital : 8 bits significatif plus le bit de signe
cadence d'echantillonnage (µs) : 2.5 ; 5 ; 10 ou 20

. Retard à l'ouverture du recepteur (µs) : 0 (reception pendant l'emission avec attenuation), 720 ; 800 ; 960 ; 1280 ; 1720 ; 3200 ; 5760 ou 10880.

. Durée d'ouverture du recepteur (µs) : 1280 ; 2560 ; 3840 ; 5120 ou 30720.

MODES DE FONCTIONNEMENT

. Mode normal : repetition de sequences d'emission-reception, chacune suivie d'un enregistrement

. Reception pendant l'emission de la premiere impulsion d'une sequence pour l'etalonnage de la chaine complete d'emission-reception

. Emission de l'emission et suppression de la reception : une impulsion sur deux pour l'analyse des bruits et brouillages et l'adaptation des seuils de detection.

. Pilotage du système : manuel
- automatique avec programmation de l'heure, minute et seconde du début d'expérimentations. Programmation du nombre de séquences d'émission-réception, du nombre d'impulsions les composant et de l'intervalle de temps entre deux expérimentations consécutives.

tableau 1 : Caractéristiques d'émission, de réception et de fonctionnement de l'analyseur de liaison, version incidence verticale

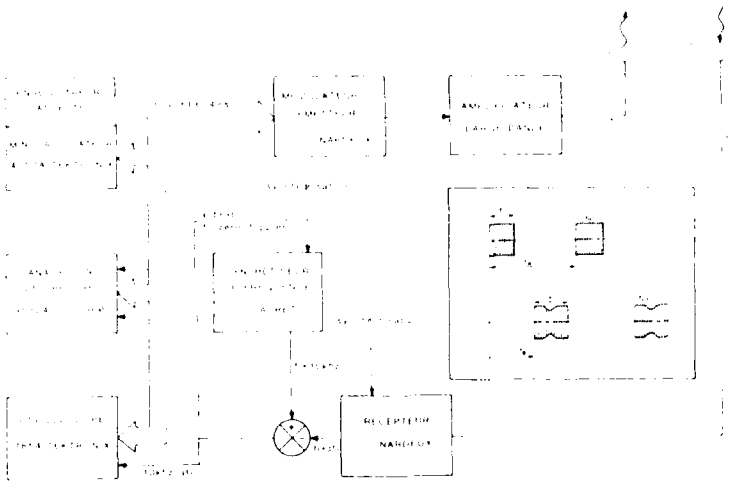

Figure 4 : Schéma de principe du système de surveillance - version interférométrique verticale

Modulateur émetteur (HARDEUX)	Générateur d'impulsions	- impulsion de durée variable de 10 à 999 µs - fréquence de répétition variable
	Système générateur de la fréquence fo	- fréquence variable de 0,5 à 30 MHz par pas de 10 Hz
	Système de commande de la fréquence d'émission par bus IEE-488 (système mis au point au département)	- 8 fréquences préréglées peuvent être programmées
Recepteur (HARDEUX)	Synchrone du système d'émission sortie vidéo à 100 kHz puis mélange avec un signal 110 kHz → sortie à 10 kHz de f_i	sensibilité : 1 µV/50Ω pour $\frac{S+B}{B} \geq 10$ dB

Tableau 2 : Caractéristiques principales de l'ensemble Emission-Réception du système de surveillance.

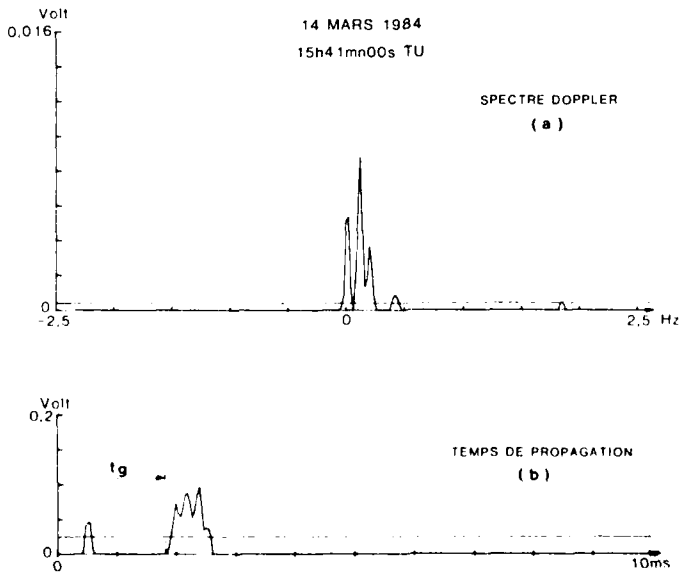

Figure 5 : Exemple de mesure du système de surveillance - Lannion 14,P3,84°, fo = 6,61 MHz. Le signe des décalages Doppler est inversé.

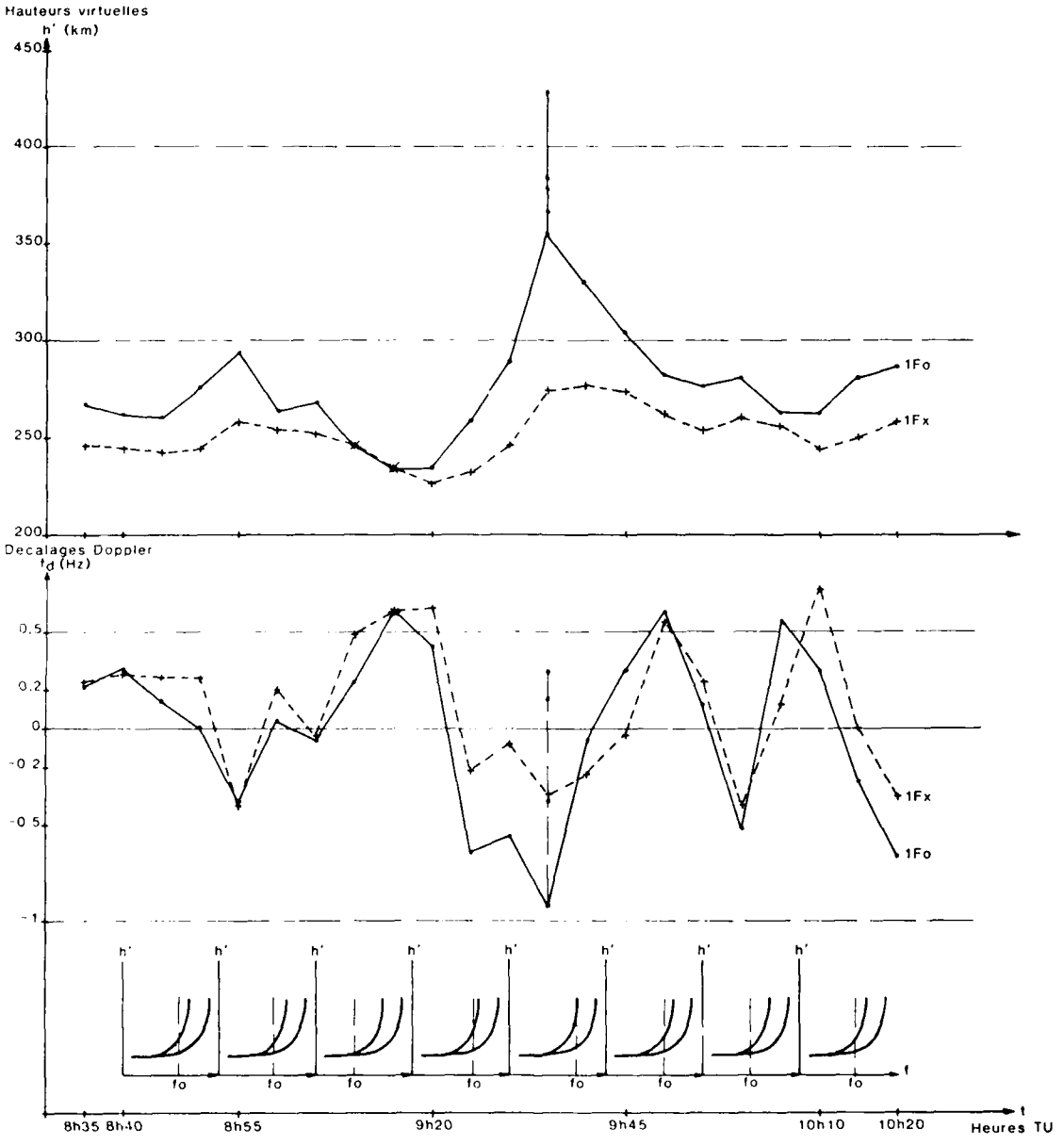

Figure 6 : Résultats de mesures de l'analyseur de liaison (avion 7.11.83 , fo = 7,75 MHz

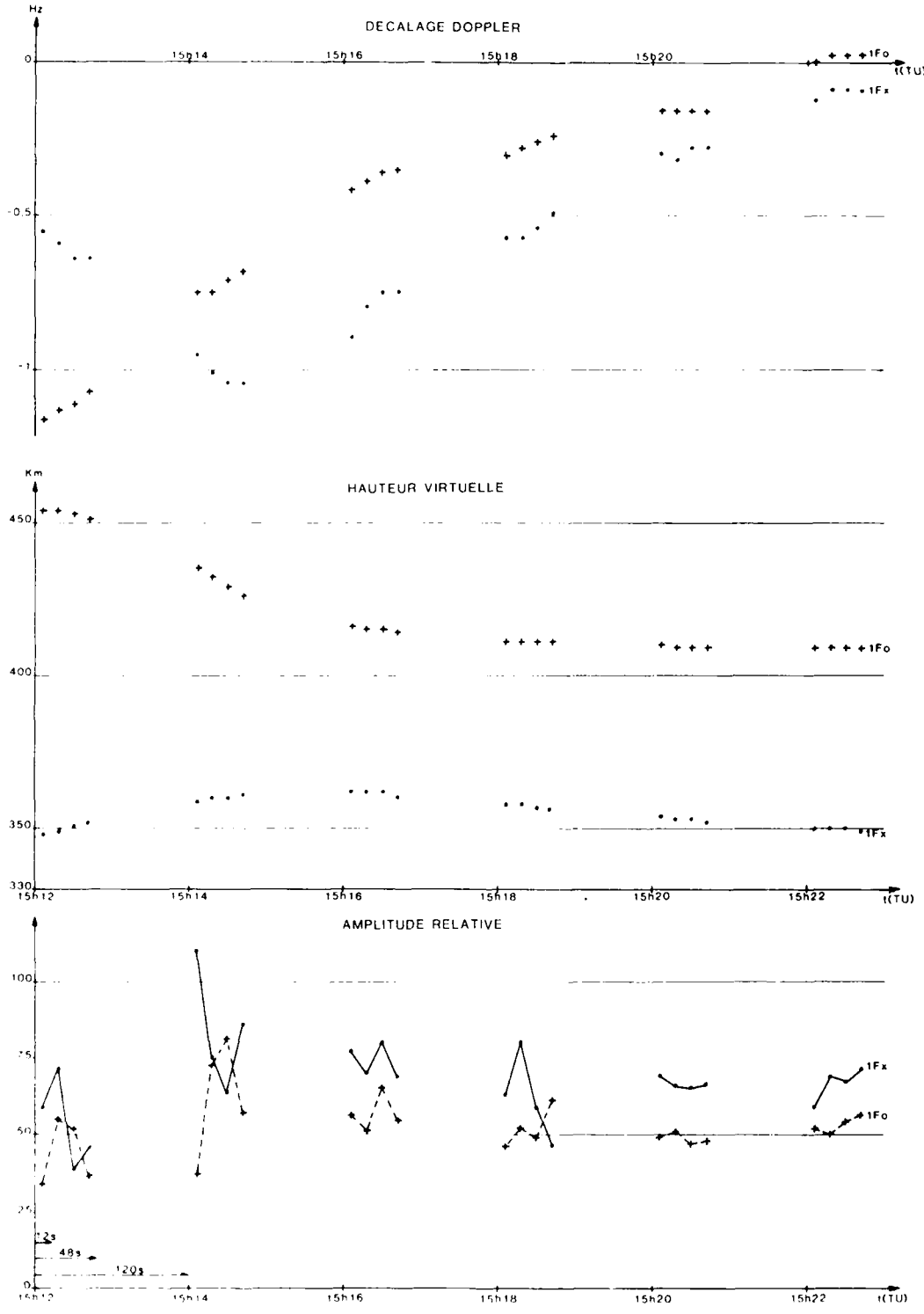

Figure 7 : Résultats de mesures de l'analyseur de Dourbes - Lannion 2.02.83 - fo = 9 MHz

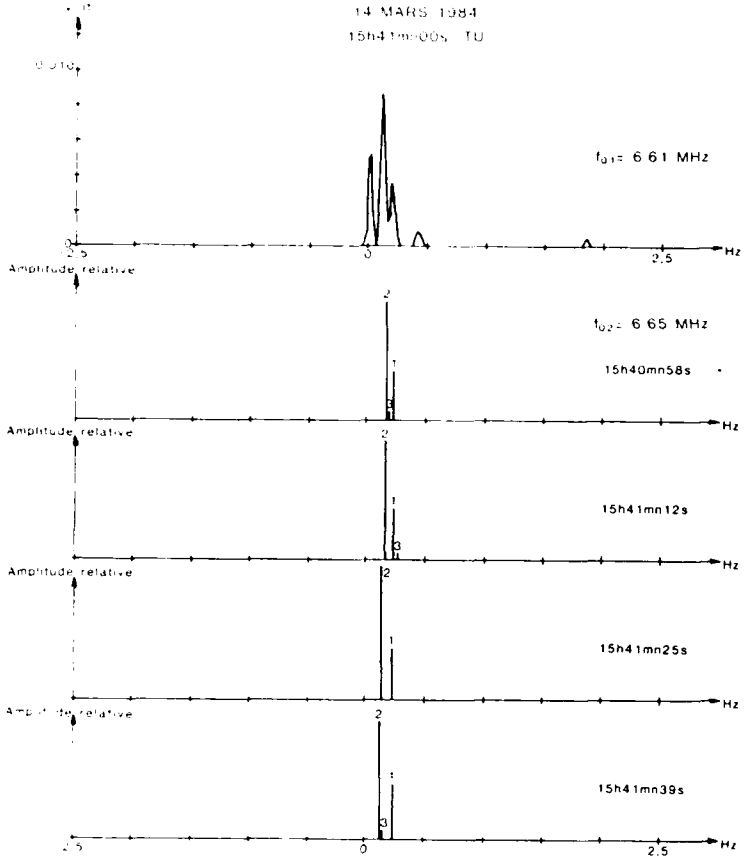

Figure 8 :

Résultats du système de mesure en fonctionnement simultané (annion 14.03.84)
Système de surveillance : fo1 = 6,61 MHz ; Analyseur de liaison : fo2 = 6.65 MHz
Durée de l'expérimentation : 50 s. Temps de propagation : 1 : 1Fx = 1980 µs ;
2 : 1Fo = 2170 µs ; 3 : 2Fo = 4340 µs. Signes des décalages Doppler inversés.

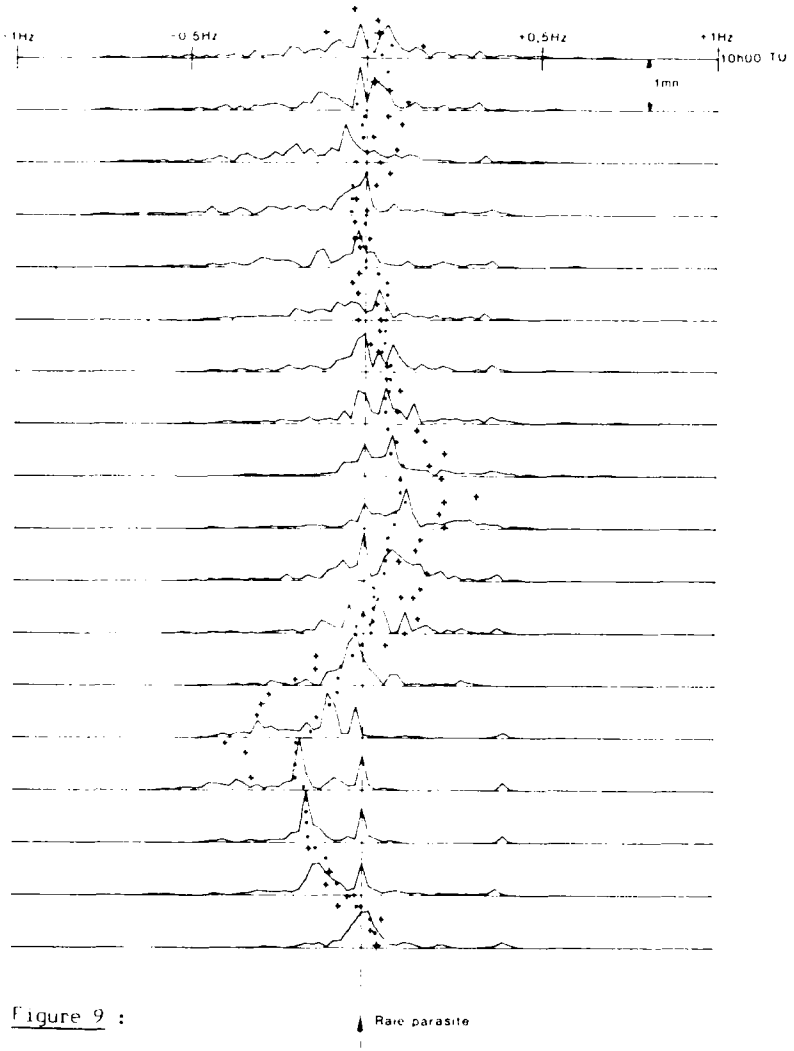

Figure 9 :

Résultats du système de mesure en fonctionnement simultané (annion 20.03.84).
Système de surveillance : fo1 = 5,5 MHz ; Analyseur de liaison : fo2 = 5,55 MHz
Durée d'expérimentation : 18 mn. Signes des décalages Doppler inversés.

DISCUSSION

P.A.Bradley, UK

(1) What paths and periods of measurement are you planning to adopt for future trials?

(2) How do you choose the recording frequency?

(3) Have you gained information from measurements so far indicating the fraction of time 2.4 kbit/s transmissions are possible with acceptable error rates?

Réponse d'Auteur

(1) Dans un premier temps, l'analyseur de liaison sera mis en oeuvre sur la liaison St. Santin-Lannion. Par la suite, d'autre geometries (distances, orientation, etc...) seront utilisées. Les premières campagnes de mesures se feront à des periodes de la journée, du mois ou de l'année pendant lesquelles l'ionosphère a un comportement caracteristique de certaines conditions de propagation influant plus particulièrement sur la qualité des transmissions HF. Il serait intéressant de faire fonctionner par la suite l'analyseur de liaison sur alertes à partir de criteres (à déterminer), fournis par le système de surveillance en fonctionnement quasi-continu.

(2) Deux gammes de fréquences on été retenues dans un premier temps, en relation avec les prévisions ionosphériques: une pour les expérimentations de jour, l'autre pour celles de nuit. L'interprétation des ionogrammes du sondeur de Poitiers, point quasi sub-ionosphérique de la liaison St. Santin-Lannion, sera mise à profit pour mieux situer l'état de l'ionosphère au moment des mesures effectuées par l'analyseur de liaison.

(3) C'est en particulier à cette question que vise précisément de répondre l'étude en cours. Les résultats obtenus sous incidence verticale ne permettent actuellement pas d'apporter des éléments de réponse significatifs.

MESURES DE PROPAGATION EN ZONE URBAINE A 900 MHZ POUR L'ETABLISSEMENT D'UN SYSTEME RADIOMOBILE NUMERIQUE

Christophe HAVEL
Alain MALOBERTI
Ingénieurs

CNET PAB/ETR
38-40 rue du Général Leclerc
92131 ISSY LES MOULINEAUX
FRANCE

Le CNET (Centre National d'Etudes des Télécommunications) a effectué des expériences de propagation dans la bande UHF (900 MHz) en zone urbaine (Paris et banlieue); ces expériences, consistant en des mesures de champ en porteuse pure, seront utilisées pour l'ingénierie d'un système cellulaire de communication avec des mobiles fonctionnant en numérique.
Dans une première partie une analyse de la propagation radio avec les mobiles est présentée ainsi que la définition des besoins en mesures. Celles-ci sont décrites en deuxième partie, ainsi qu'une comparaison des résultats obtenus avec des modèles déjà proposés dans la littérature. La décroissance du champ suit une loi en $D^{-\alpha}$ avec $\alpha = 3.5$, et une bonne corrélation a pu être établie avec une loi log-normale d'écart type 8 dB pour les "effets de masques" et une loi de Rice pour les évanouissements rapides. En guise de conclusion nous présentons deux types d'applications de ces mesures effectuées au CNET.

1 - INTRODUCTION

Le CNET (Centre National d'Etudes des Télécommunications) met actuellement en oeuvre un programme de recherche qui a pour but d'établir les caractéristiques d'un système cellulaire de radiotéléphonie avec les mobiles, à transmission numérique. Pour ce faire il a été décidé de lancer des campagnes de mesures dans la région parisienne afin de connaître les caractéristiques de propagation en milieu urbain, dense et moins dense, et ses conséquences sur une transmission numérique. Cette campagne de mesure, découpée en plusieurs phases a débuté en juillet 1983 et devrait se poursuivre jusqu'au début de 1985. Nous présentons ici une description de la campagne de mesure effectuée ainsi que les premiers résultats recueillis, portant essentiellement sur des mesures en bande étroite. Nous esquisserons ensuite les développements ultérieurs, que ce soit en ce qui concerne les mesures qui seront effectuées, ou en ce qui concerne l'utilisation des résultats obtenus.

Dans une première partie nous analysons d'un point de vue théorique la propagation radio en milieu urbain dans le but de déterminer les paramètres les plus importants et les mesures à effectuer.

2 - ANALYSE DE LA PROPAGATION RADIO POUR UN SYSTEME NUMERIQUE CELLULAIRE

Pour un service et une qualité donnés deux questions sont fondamentales lorsqu'il s'agit de concevoir un système cellulaire numérique de radiotéléphonie avec les mobiles :

- 1ère question : S'agissant d'une transmission numérique, quel est le débit maximal que l'on peut transmettre pour assurer une qualité donnée ? Ce point est particulièrement important pour choisir le mode d'accès radio : bande large (type AMRT) ou bande étroite (type AMRF) et éventuellement obligation de rajouter des traitements complémentaires (égalisation) pour assurer une qualité déterminée.

- 2ème question : S'agissant d'un système cellulaire, quel va être le niveau de brouillage intrinsèque (sur un même canal de fréquence) suivant la taille des motifs ? Il est bien connu que, la bande de fréquence à utiliser étant déterminée, l'efficacité spectrale (nombre de communications par hertz) sera plus importante si les motifs ont peu de cellules ; mais dans ce cas, les cellules utilisant les mêmes fréquences étant rapprochées, le brouillage sera plus important. Un compromis devra donc être trouvé entre l'occupation la plus économique de la bande de fréquence, et un niveau de brouillage compatible avec la qualité souhaitée.

La réponse à ces deux questions ne peut passer que par une connaissance précise du canal radioélectrique ; nous allons brièvement examiner quels sont les paramètres les plus importants qu'il faudra déterminer par des mesures adéquates.

2.1 - Etude locale : les trajets multiples

Une des particularités de la transmission avec un mobile est la position de celui-ci au milieu d'immeubles ou autres objets réfléchissants ; l'onde incidente va donc être réfléchie ou diffractée sur ces objets pour être finalement décomposée en une somme d'ondes arrivant sur le mobile selon des angles très divers ; ces ondes parcourant alors toutes un chemin différent vont avoir des temps de trajet légèrement différents eux aussi.

Supposons qu'on ait envoyé : $s(t) = Re\left(a(t)e^{2i\pi f t}\right)$

le signal reçu sera alors : $r(t) = Re\left(\left(\sum_{n=1}^{N} a_n e^{i\theta_n}\, a(t-t_n)\right) e^{2i\pi f t}\right)$

où l'indice n représente chaque trajet et les a_n, θ_n , t_n, respectivement leur amplitude, leur phase et leur retard.

La connaissance des caractéristiques du canal radioélectrique nécessite donc la connaissance de la statistique des a_n, t_n , θ_n . Cette représentation est particulièrement importante en modulation numérique ; en effet :

- supposons la rapidité de modulation petite devant l'inverse de t_N (retard maximal). A ce moment là tous les trajets réfléchis vont arriver pendant une fraction de la durée du symbole ; on pourra donc, relativement à la modulation, supposer $t_n = t_1$ et on aura donc :

$$r(t) = Re\left(a(t-t_1)\left(\sum_{n=1}^{N} a_n e^{i\theta_n}\right) e^{2i\pi f t}\right) = Re\left(\rho e^{i\theta} a(t-t_1) e^{2i\pi f t}\right)$$

On pourra appeler ce modèle, le modèle "faible débit". Si on suppose que l'onde incidente se décompose en un trajet direct (plus ou moins atténué) et un grand nombre de trajets réfléchis (dont les composantes en phase et en quadrature peuvent donc être considérées comme gaussiennes), la théorie montre que ρ suit une loi de Rice et θ est réparti uniformément sur $[0, 2\pi]$ ([1]) .

- Si la durée d'un symbole n'est plus grande comparée aux différents retards, chaque symbole va déborder sur le symbole suivant de façon importante et provoquer une interférence intersymboles élevée. Dans ce cas le modèle complet sera nécessaire pour étudier les performances d'une modulation donnée, performances qui n'auront de chances d'être acceptables que si les dégradations apportées sont compensées au préalable par une égalisation.

Ce problème est fondamental pour l'élaboration d'un système de radiocommunications avec les mobiles; en effet les deux types de rapidité de modulation vont correspondre à deux techniques d'accès différentes. Si on suppose que la durée maximale des retards se situe entre 3 et 5 μs on peut supposer que le débit charnière va se situer vers 50 kbit/s. Dans ce cas le modèle "faible débit " sera adapté à une technique d'accès AMRF alors que la technique AMRT, nécessitant des débits de l'ordre du mégabit par seconde ne pourra être étudiée que dans le deuxième cas. Les mesures nécessaires pour l'établissement de ce modèle feront l'objet d'une prochaine campagne de mesures au CNET, elles sont du type par impulsions.

2-2 - Etude globale

Indépendamment des phénomènes locaux de trajets multiples d'autres perturbations vont se manifester sur le trajet radioélectrique. En effet dans une transmission radio en milieu urbain, la hauteur des antennes est telle (environ 30 m pour la base et 2 m pour le mobile) que l'ellipsoïde de Fresnel n'est pratiquement jamais dégagé et que, en plus de l'atténuation dépendant de la distance, le signal va subir une diffraction dépendant du relief, phénomène connu sous le nom d'"effet de masques". Si on considère uniquement les variations à grande et moyenne échelle on peut donc considérer que la puissance moyenne reçue peut se mettre sous la forme : $P_r = P_d \cdot P_m$, où :

- P_d : est la moyenne de la puissance, dépendant de la distance. Le modèle retenu par le CCIR [2] a été proposé par Hata [3] à partir des mesures d'Okumura [4] et donne une valeur de l'affaiblissement, qui s'écrit :

$$A(dB) = 69{,}55 + 26{,}16 \log f - 13{,}82 \log h_b - a(h_m) + (44{,}9 - 6{,}55 \log h_b) \log d$$

où : d : distance entre émetteur et récepteur (en km)
h_b : hauteur d'antenne de base (en m)
h_m : hauteur d'antenne du mobile (en m)
f : fréquence (en MHz)

- P_m : variable aléatoire, de moyenne 1, rendant compte des effets de masques. On reconnaît en général que P_m suit une loi lognormale de variance σ comprise entre 2 et 12 dB.

Les résultats de propagation seront ici donnés par des mesures d'atténuation du signal, en porteuse pure ; les mesures nécessaires sont décrites en 3) ; les résultats obtenus seront utilisés pour :

- l'étude de la modulation bas débit (cas AMRF) en y rajoutant un terme P_f représentant les évanouissements de Rice (ou Rayleigh) tels qu'ils seront déterminés dans les mesures par impulsions dans le cadre du modèle "faible débit"

- l'étude de la géométrie des motifs de cellules par calcul du niveau de brouillage intrinsèque résultant de l'interférence co-canal

- l'étude de la position et des caractéristiques des stations de base, à géométrie de motif fixée, par établissement d'un modèle de prédiction.

3 - PRINCIPE DES MESURES

Le but de ces mesures est d'acquérir une base de données portant sur les trois paramètres de la propagation définis précédemment : éloignement, effets de masques et trajets multiples. Ces trois

phénomènes se produisant à des échelles de distance différentes, deux types de système de mesures sont définis :

- système dit à grande échelle pour les mesures des effets de distance et de masques
- système dit à petite échelle pour les mesures sur les trajets multiples.

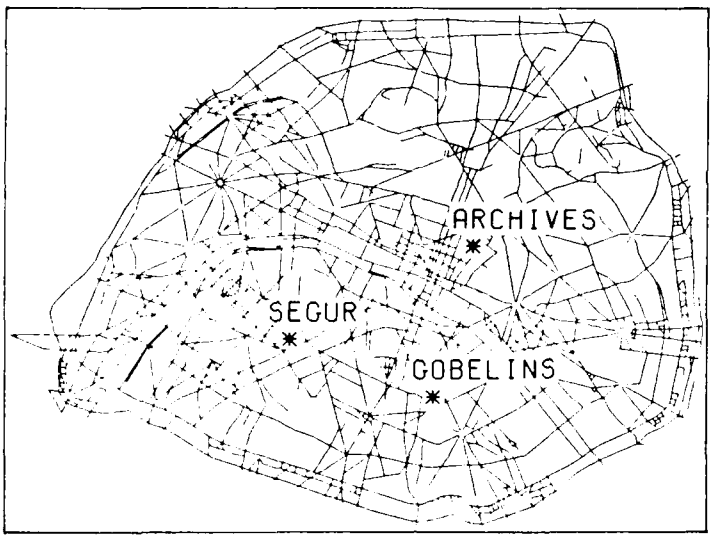

figure 3.1:Implantation des sites d'émission

L'ensemble de ces mesures est effectué en porteuse pure, à partir de trois stations d'émission fixes situées dans Paris intra-muros (cf fig. 3.1). Une quatrième station est installée à 15 km à l'ouest de Paris (Chennevières) et est utilisée pour aborder les problèmes de réutilisation de fréquence et de propagation en zone suburbaine. Ces quatre stations sont implantées dans des zones d'urbanisme différent, avec des caractéristiques d'émission différentes décrites dans le tableau de la fig. 3.2.

NOM DU SITE	URBANISME	HAUTEUR D'EMISSION	ANTENNE	P.I.R.E.	FREQUENCE
ARCHIVES	dense - rues étroites	40 m	perche 7 dBi	250 W	855,5 MHz
GOBELINS	moyennement dense	31 m	perche 11 dBi	250 W	854,65 MHz
SEGUR	peu dense - larges avenues	24 m	perche 7 dBi	140 W	855,0 MHz
CHENNEVIERES	suburbain	80 m	dièdre 120°	250 W	860,0 MHz

Figure 3.2 : Caractéristiques des sites d'émission

La station de réception est installée dans un camion laboratoire spécialement aménagé. D'une manière générale, le système de mesure se compose de :

- une antenne étalonnée
- un récepteur programmable par bus IEEE 488
- un dispositif de mesure de la distance parcourue et de la vitesse du véhicule
- un microcalculateur avec mémoire de masse.

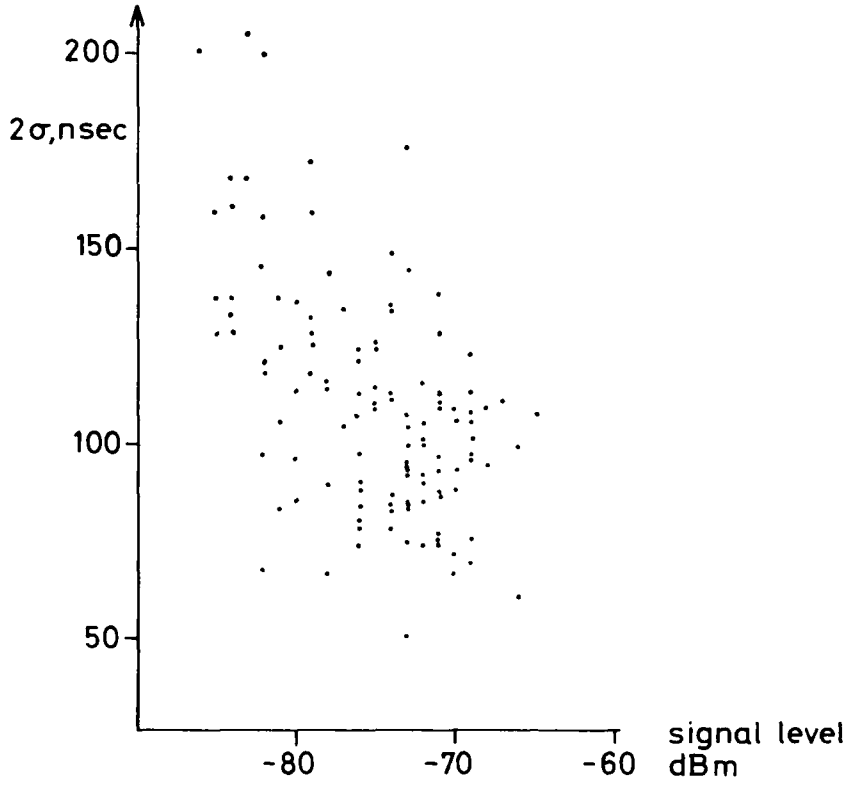

FIG. 5. DISPERSION V. SIGNAL FOR LOWER BEAM. PATH 2. 1.9^{0} TX.

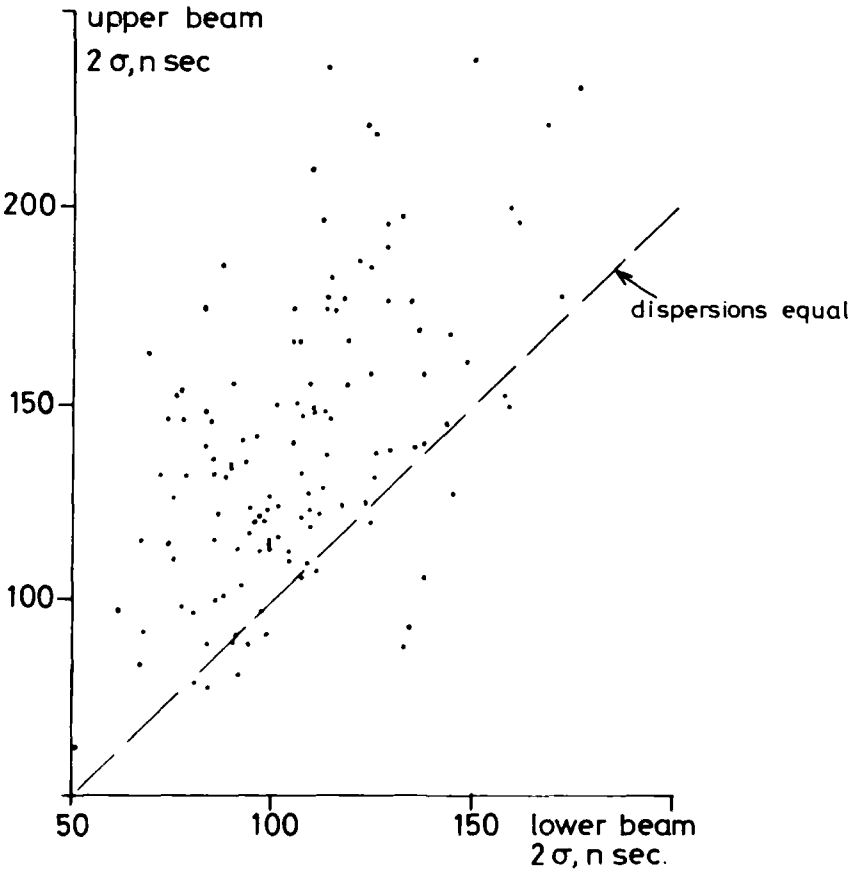

FIG. 6. DISPERSION OF UPPER AND LOWER BEAMS. PATH 2. 1.9^{0} TX.

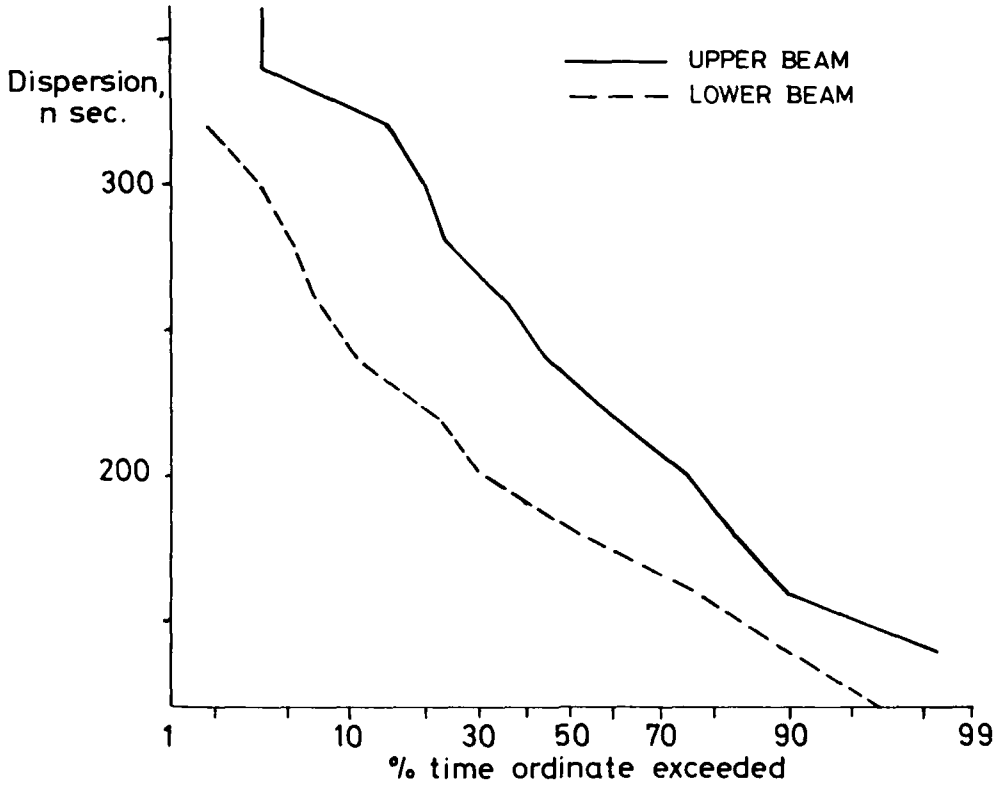

FIG. 3. DISTRIBUTION OF MULTIPATH DELAY SPREAD FOR PATH 3.

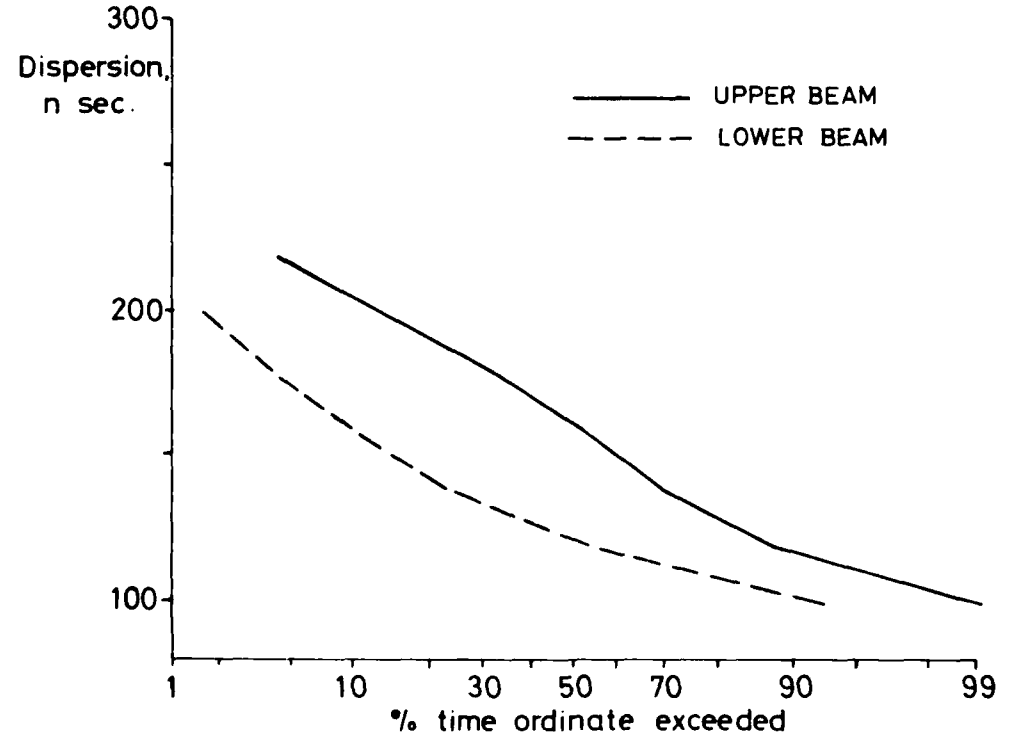

FIG. 4. DISTRIBUTION OF MULTIPATH DELAY SPREAD FOR PATH 4.

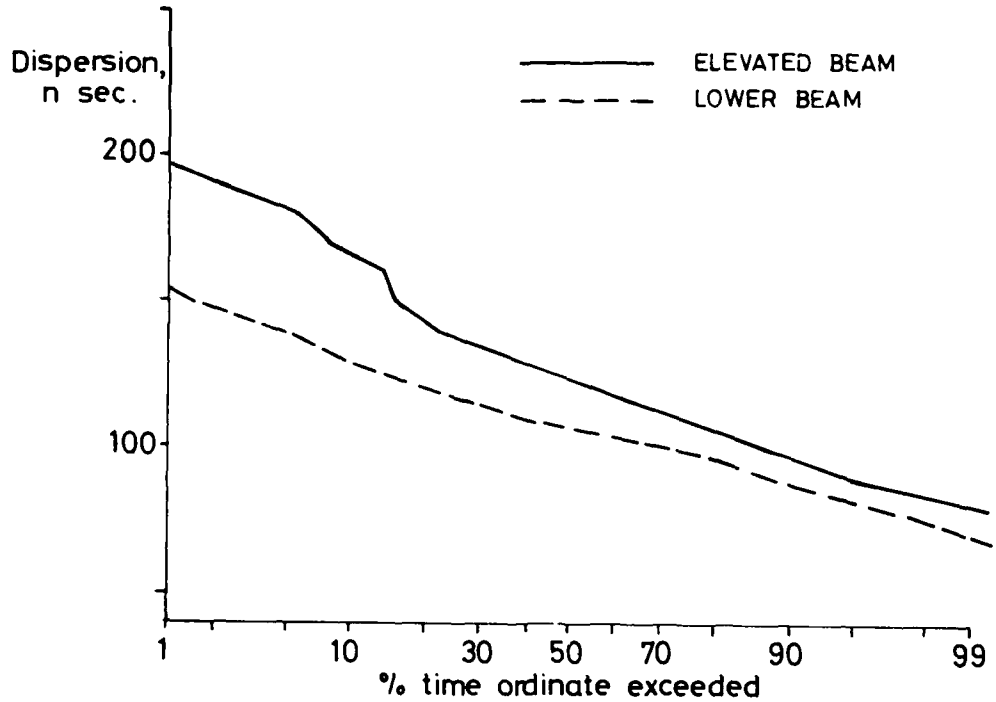

FIG. 1. DISTRIBUTION OF MULTIPATH DELAY SPREAD FOR PATH 2. 1^{0} TX.

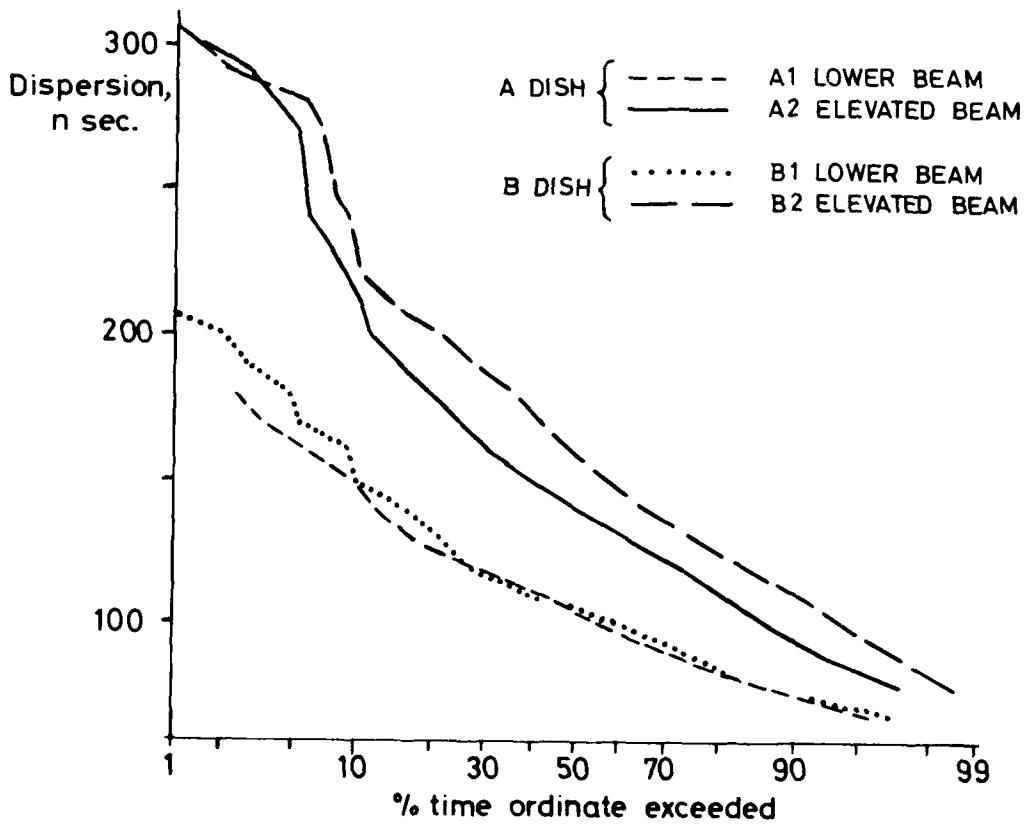

FIG. 2. DISTRIBUTION OF MULTIPATH DELAY SPREAD FOR PATH 2. 1.9^{0} TX.

TABLE 1

EQUIPMENT PARAMETERS FOR UNITED KINGDOM MEASUREMENTS

Path	Path Length (km)	Minimum Scatter Angle, mr	Horizon θ_t	Elevation, mr θ_r	Asymmetry Factor S
2	124	22.0	-3.4	10.8	0.217
3	187	38.9	1.3	15.1	0.491
4	189	24.1	-2.2	4.1	0.588

For all paths:-

Frequency	4.58 GHz (λ = 65.5 mm)	Beamwidth	1° (18 mrad)
Polarisation	Vertical	Gain	44.3 dBi
Rx Antenna	4.5 m Diameter	Vertical Separation of Angle Beams	1.3°

TABLE 2

COMPARISON OF DISPERSION MEASUREMENTS WITH PREDICTIONS

	Path (Reference)	F GHz	d km	θ mrad	β_t, β_R mrad	Measured 2σ, nsec	Predicted 2σ, nsec Bello	Pusone	Modified
1.	Path 2	4.6	124	22	18, 18	107	25	51	74
	" elevated beam	4.6	124	22	18, 18	124	50	81	101
2.	Path 2	4.6	124	22	33, 18	104	32	86	112
	" elevated beam	4.6	124	22	33, 18	150	65	134	151
3.	Path 3	4.6	187	39	18, 18	182	89	119	165
	" elevated beam	4.6	187	39	18, 18	232	148	171	226
4.	Path 4	4.6	189	24	18, 18	127	48	80	98
	" elevated beam	4.6	189	24	18, 18	162	103	136	153
5.	Youngstown - Verona	4.8	270	41	9, 9	160	57	66	130
6.	Ontario - Verona (20)	4.8	138	42	33, 33	170	90	144	163
7.	Ontario - Verona (20)	4.8	138	42	17, 17	110	53	71	110
8.	Ontario - Verona (20)	4.8	138	42	33, 17	130	71	107	137
9.	Tobyhanna (20) Fort Monmouth	4.8	150	12	24, 24	82	17	60	63
10.	Model City - (20) Ontario	4.6	140	15	26, 26	110	18	54	58
11.	Model City - (20) Whitford	4.6	199	39	26, 26	190	96	142	184
12.	Model City - (20) Pt. Petre	4.6	163	18	26, 26	100	28	69	74
13.	Model City - (20) Pt. Byron	4.6	190	23	26, 26	140	47	94	103
14.	Tetcott/Beam - (2) Worthington	4.5	278	41	46, 46	325	260	380	412
	" elevated beam	4.5	278	41	46, 46	500	560	554	594
15.	Tetcott/Beam (2) Worthington	4.5	278	41	9, 9	220	87	97	170
	" elevated beam	4.5	278	41	9, 9	275	133	138	236

Where F is Frequency, β_t, β_R - 3dB Beamwidths of Transmitting, Receiving Antennas
d - Path Length, σ - rms Multipath Delay
θ - Minimum scatter angle

5. ACKNOWLEDGEMENT

The measurements of multipath dispersion described in Section 2 of this Paper were made with a RAKE analyser kindly loaned by SHAPE Technical Centre.

REFERENCES

(1) J.B.S. Cairns, A Review of Digital Troposcatter Links, Telecom 79-3rd World Telecommunications Forum, Geneva, September 1979, pp. 2.3.10.1-2.3.10.10.

(2) J.L. Osterholz, Design Considerations for Digital Troposcatter Communications Systems, AGARD CP244, Massachusetts, October 1977, pp. 22.1-22.15.

(3) F.D. Sunde, Digital Troposcatter Transmission and Modulation Theory, Bell System Technical Journal, Vol. 43, January 1984, pp. 143-214.

(4) S.O. Rice, Statistical Fluctuations of Radio Field Strength Far Beyond the Horizon, Proc. IRE, Vol. 41, February 1953, pp. 274-281.

(5) P.A. Bello, A Troposcatter Channel Model, IEEE Trans. Comm. Tech., Vol. COM-17 No. 2, April 1969, pp. 130-137.

(6) C. Collin, Selectivity Predictions for Troposcatter Links, Military Microwaves 80, London, 1980, pp. 135-140.

(7) F. Pusone, A Troposcatter Prediction Model of Long-term Statistics of Multipath Dispersion and Doppler Spread Based on Atmospheric Parameters, IEE Colloquium Troposcatter Communications - Digital Developments, Digest No. 1981/66, London, October 1981, pp. 2/1-2/10.

(8) J.D. Rogers, M. Stears and D.W. Baker, Introduction to Digital Troposcatter for Military Tactical Communication, Communication and Broadcasting, Vol. 6, No. 3, June 1981, and Vol. 7, No. 1, September 1981.

(9) D.R. Bitzer et al, A RAKE System for Troposcatter, IEEE Trans. Comm. Tech., Vol. COM-14, No. 4, August 1966, pp. 499-506.

(10) D.T. Gjessing, Atmospheric Structure Deduced from Forward-Scatter-Wave Propagation Experiments, Radio Science, Vol. 4, No. 12, December 1969, pp. 1195-1210.

(11) C.D. Beach and J.M. Trecker, A Method for Predicting Interchannel Modulation due to Multipath Propagation in FM and PM Tropospheric Radio Systems, Bell System Technical Journal, Vol. 42, No. 1, January 1963, pp. 1-36.

(12) H.S. Merrill, A Power Impulse Response Model for Troposcatter Channels, IEEE Conference on Communications, Montreal, June 1971, pp. 26.13-26.18.

(13) H.G. Booker and W.E. Gordon, A Theory of Radio Scattering in the Troposphere, Proc. IRE, Vol. 38, April 1950, pp. 401-412.

(14) L.D. Daniel and R.A. Reinman, Performance Prediction for Short Range Troposcatter Links, IEEE Trans. Communications, Vol. COM-24, June 1976, pp. 670-672.

(15) M.P.M. Hall, Statistics of High-level Beyond Horizon Signals at 2.2 GHz and 2.6 GHz and Measurements of the Variation of the Arrival Angle Structure, AGARD CP127, Rome 1973, pp. 17.1-17.10.

(16) D.C. Cox and A.T. Waterman, Phase and Amplitude Measurements of Transhorizon Microwaves with a Multi-Data-Gathering Antenna Array, AGARD CP 37, August 1968, pp. 18.1-18.16.

(17) M. Hirai et al, Transmission Loss In VHF and UHF Overland Propagation Beyond the Horizon, Journal of the Radio Research Laboratories, MPT Tokyo, September 1963, pp. 357-422.

(18) M.W. Gough and G.C. Rider, Angle Diversity in Troposcatter Communications, Proc. IEE, Vol. 122, No. 7, July 1975, pp. 713-719.

(19) R. Larsen, Space Polarisation Diversity in Troposcatter Systems, IEE/IEEE and AFCEA Conference on 'Digital Troposcatter Systems', Brussels, 1980.

(20) A. Sherwood and L. Suyemoto, Multipath Measurements over Troposcatter Paths, Mitre Corporation, ADA 046611, November 1977.

the phenomenon of antenna gain degradation, or coupling loss. The important point to observe is that coupling loss (and hence beam broadening) is small for low gain (i.e. wide beam) antennas, but coupling loss and beam broadening effect are large for high gain antennas with narrow beams. It is found that the dispersion predictions are strongly influenced by the size of the common volume over which the formulae are integrated. This leads to the expectation that predictions of dispersion for broad beam antennas will be little changed by the inclusion of a beam broadening factor, while those for narrow beam antennas are likely to be significantly increased. These are the type of changes required to minimise the prediction errors of the Bello and Pusone models.

The concept of using an effective beamwidth instead of the plane wave beamwidth for dispersion predictions is not new. Sunde (3) discussed the problem, but did not give specific formulae. In Collin's method all the antenna effects are incorporated in a single term, the antenna gain degradation, so that beam broadening is implicitly included. For the present study, the Pusone simplified model was modified to include the beam broadening effect, using results due to Hirai (17). The Hirai theoretical framework has provided a fruitful approach to a number of previous studies in troposcatter modelling (e.g. (18), (19)), which provide some support for its use in the present context. The beam broadening factor depends on atmospheric parameters, path geometry and beamwidth in a rather complicated fashion, and the evaluation requires the interpolation of some numerical results which do not fall easily into an analytic form; however, the task is readily accomplished by computer, and the details are given in (17). The predictions given by the simplified Pusone model with beam broadening included are shown in the final column of Table 2.

3.3 Predictions of Modified Pusone Model

In the majority of paths listed in Table 2, it can be seen that the inclusion of beam broadening has led to a useful improvement in prediction accuracy. In two cases (the upper and lower beams of Leiselheim-Werthhoven UHF Link) the standard Pusone predictions were slightly larger than the measured values, and additional beam broadening for these cases makes the prediction error larger. For some paths the beam broadened predictions are still well below the measured values of multipath delay spread.

When considering the agreement between measurements and predictions in Table 2 there are several points of importance concerning the validity of both the measurements and the predictions. For the majority of paths the dispersion measurements were made using a RAKE analyser with a delay tap spacing of 100 nsec (on Paths 9-13 the basic measurements were of correlation bandwidth, from which the multipath delay spreads were inferred). The tap spacing effectively sets the resolution of the dispersion measurements, and if the delay spread of the path is comparable with or less than 100 nsec, the RAKE measurements may be unreliable. A further point concerning the measurements involves the setting of a threshold to exclude delay taps which contain only noise from the calculation of delay spread. The threshold must be set high enough to exclude all the noise terms, but not so high that parts of the true delay power spectrum are cut off. It was found in practice that often the calculated value of dispersion was quite sensitive to the value of noise threshold used. Different practices among the various experimenters may mean that the measured results in Table 2 were not all evaluated on the same basis.

A final point concerns the input data for the dispersion prediction methods. In the preparation of these predictions it was found that the results were quite sensitive to the elevation of the beam axes relative to the radio horizon. Unfortunately this is a parameter which is difficult to measure accurately, and is often not quoted. For the data taken from (20) it appeared that in most cases the beam axis was directed at the radio horizon. For the remaining paths it was assumed that the beam elevations were adjusted for optimum signal. The theory of (17) permits the optimum elevations to be calculated, and these values were used in the prediction of dispersion. However, different assumptions about the elevations might significantly alter the values in Table 2.

4. CONCLUSIONS

A programme of measurements of multipath dispersion has been completed on several 4.5 GHz links in the United Kingdom. Distributions of delay spread are presented for both lower and elevated beams of the dual angle receiving system, and the influence of beamwidth and scatter angle on the results is illustrated. A relatively weak negative correlation between dispersion and signal level was observed. Dispersion measured on two space diversity antennas was found to be well correlated, while for angle diversity the dispersion on the elevated beam was usually larger and more variable than that on the lower beam.

These measurements and other data from the literature were compared with predictions of median delay spread by the Bello and Pusone methods. Both methods generally gave predicted dispersions that were less than the measured values, but the Pusone method gave the closer agreement. When the Pusone model was modified by the inclusion of a beam broadening factor due to Hirai, the overall agreement was very much improved. However, the results were quite sensitive to the beam elevation angles, which are difficult to determine accurately.

3. PREDICTIONS OF MULTIPATH DISPERSION

3.1 Prediction Methods

Many authors have proposed methods for the prediction of multipath dispersion on troposcatter links, including Sunde, (3), Rice (4) Bello (5), Gjessing (10), Beach and Trecker (11), Merrill (12), Collin (6) and Pusone (7). The approaches range from elementary geometrical treatments of path and beam geometry, through the fitting of empirical functions to available mesurements, to models involving physical description of scattering or reflection from refractivity structures in the troposphere. Sunde's model is an example of a simple geometrical approach. He assumed that the signal power arrived at time delays uniformly distributed about the mean time delay, giving rise to a rectangular delay power spectrum. The width of the rectangle (i.e. range of time delays to be expected) is determined from the path geometry and the antenna beamwidths, but involved no atmospheric parameters beyond an effective radius factor to account for average refraction. Rice's model was a very early attempt which represented the troposphere as an assembly of scattering elements with a three dimensional Gaussian density distribution about the centre of the common volume.

A model which has been much quoted in the literature is that due to Bello (5), which uses the turbulent scattering theory of Booker and Gordon (13). It assumes a well mixed atmosphere in which the mean squared value of dielectric constant fluctuations decreases inversely with height above the surface of the earth. Various workers have noted that the model appears to give predictions which agree reasonably well with measurements on long paths (longer than about 250 km), but may seriously underestimate multipath dispersion on shorter paths. Attempts have been made to modify the Bello model to improve its accuracy for shorter paths. One due to Daniel and Reinman (14) proposed that the scattering cross-section dependence on scatter angle should itself be a function of distance. This modification was an empirical correction based on a limited number of observations, and it is difficult to find any physicial justification for it.

More recently a method for the prediction of multipath dispersion has been proposed by Collin(6). This is an empirical formulation based on the analysis of measurements from a number of paths, which results in an expression for multipath delay spread that involves frequency, path length, scattering angle and antenna coupling loss. Expressions are also given which allow multipath dispersion and correlation bandwidth to be calculated for time percentages other than the median. However, as the method does not appear to embody any physical model of the propagation process, it is not clear to what extent it may apply to paths other than those used to generate it.

A more fundamental approach to multipath dispersion modelling has been attempted by Pusone (7). This again employs the Booker-Gordon formulation for scattering cross-section, but developes a physical model of the atmosphere to derive turbulance correlation distance and mean square dielectric fluctuations from radiosonde measurements of temperature, pressure, humidity and wind velocity. The objective of this work was to derive distributions of multipath dispersion, and in particular the values exceeded for small time percentages, from distributions of observed meteorological parameters. The predictions were found to be in good agreement with measurements over a path operating at 900 MHz, but much poorer for the same path at 4.5 GHz. The principle drawback of the method is that a considerable amount of meteorological data is required to compute the atmospheric parameters.

3.2 Influence of Beamwidth

In order to discover what sort of prediction accuracies might be achieved in practice, the measurements of dispersion that have been published in the literature were used to test two prediction methods, Bello and Pusone. The Pusone model used was a simplified method derived from his early development of the atmospheric model, and required only surface meterological parameters as input data.

A summary of the principal path parameters, and the measured and predicted values of median dispersion are given in Table 2. The results will be considered in greater detail below, but several points are readily apparent:-

(1) Both Bello and Pusone models underestimate dispersion in almost all cases.

(2) The Bello prediction is less than the Pusone prediction in almost all cases, sometimes by a large amount.

(3) The discrepancy between measurement and prediction tends to be least for broad beams and greatest for narrow beams.

This last point is interesting, and raised the suggestion that an effective beamwidth might be more appropriate for the calculations than the true beamwidth. The concept of broadening of a beam beyond the normal free space pattern when high gain antennas are used for troposcatter communications has long been recognised. Beam scanning experiments using high gain narrow beam antennas have demonstrated how the effective beam pattern may be subject to large variations (15, 16). The use of an effective beamwidth larger than the free space beamwidth is also one way to interpret

The dispersion measurements were part of a larger programme which also included measurement of signal level and system performance. Since it was necessary to interrupt the signal measurements in order to measure dispersion, the dispersion measurements were made on a sampling basis, the objective being to make one measurement of each diversity channel in each hour. This represented a compromise between making detailed studies of the behaviour of dispersion, and minimising interruptions to the signal data logging.

The measurements of multipath dispersion were accomplished using a conventional RAKE multipath analyser (9). The RAKE transmit unit generated a 70 MHz IF signal modulated by a 255 bit pseudo-random code sequence. Using a clock rate of 10 MHz gave a time resolution at the receiver of 100 nanoseconds. The receiving unit had correlators for 16 delay steps, allowing a maximum delay spread of 1.5 μsec to be observed. The integration time of the correlators was 10 msec, and one complete RAKE measurement (known as a frame of data) was obtained in 92 seconds of real time.

2.2 Results of Measurements

Each frame of data was analysed to extract amongst other things, the normalised delay power spectrum, the mean time delay and r.m.s. time delay, σ. The results are mainly presented in terms of the multipath delay spread, 2σ, each datum being an average over the 1½ minutes of a RAKE frame.

Figures 1 and 2 give the cumulative distributions of delay spread (2σ) for two cases (a) Figure 1 is for Path 2 using dual angle diversity reception with 1° transmitter beamwidth, and (b) Figure 2 is for Path 2 using dual angle/dual space diversity reception with 1.9° transmitter beamwidth. In both cases the elevated beam has rather more dispersion than the lower beam, as is expected from consideration of the geometry of the common volumes. During quadruple diversity operation (Figure 2) the two lower beams had very similar dispersions, while the two elevated beams differed somewhat. It is thought that these differences are probably attributable to slight differences in beam alignment. For small percentages of time the elevated beams of the quadruple diversity system suffered very large values of delay spread (2σ exceeding 250 nsec); some of these cases were most likely due to aircraft entering the common volumes of the elevated beams. Comparison of Figures 1 and 2 shows that the change of transmitter beamwidth (from 1° to 1.9°) has had almost no effect on the median value of dispersion for the lower beams (delay spreads between 105 and 110 nsec in all cases). However, the slopes of the distributions, or range of values measured, are significantly larger for the wider transmitter beamwidth. It is possible that these differences may have been due to a change in the meteorological conditions between the two measuring periods, but the change in beam geometry provides the more likely explanation. Under normal well-mixed atmospheric conditions the lower part of the common volume (defined by the intersection of the rays that graze the radio horizons) contributes the major part of the received power; increasing the maximum height of the common volume by increasing the beamwidth will have a relatively small effect on the dispersion. However, the difference in size of common volume may be much more noticeable for the small percentage of time that one or more elevated layers are present in the atmosphere, as these will be illuminated more readily by the broad beam than by the narrow one.

Figures 3 and 4 show the cumulative distributions of multipath delay spread for Paths 3 and 4 respectively. These two form an interesting comparison as they are almost the same length, but Path 3 has the larger scatter angle (39 mrad for Path 3, 24 mrad for Path 4). It is noticeable that the path with the larger scatter angle has the larger median values of dispersion for both upper and lower beams, and also has larger variability of dispersion (e.g. a larger difference between 5% and 50% values). In this comparison, as previously, the two sets of measurements were carried out at different times, so that gross changes of atmospheric structure cannot be ruled out, but once again the more likely explanation of the results lies in considerations of path geometry.

Figure 5 is a scatter diagram showing the variations of multipath delay spread with signal level; this example is for one of the lower beams of Path 2 using the 1.9° transmission. It can be seen that there is a tendency for large values of dispersion to occur at the lower signal levels, although the trend is not very strongly marked. Broadly similar results were found on other beams and on other paths in these trials, with correlation between minute mean signal and 92-second mean dispersion generally in the region of -0.3 to -0.4.

Figure 6 illustrates the relationship between dispersion measured on the lower beam and that measured on the upper beam for Path 2. Dispersion for the elevated beam almost always exceeded that for the lower beam, and sometimes by a large margin, but there were occasional exceptions. When the delay spreads for the two lower beams of the space diversity system were compared, it was found that the measurements were very well correlated. This is as expected from the fact that two space diversity antennas illuminate very nearly the same common volume.

MEASUREMENTS AND PREDICTIONS OF MULTIPATH DISPERSION FOR TROPOSCATTER LINKS

R. Larsen,

Communications Research Laboratory,
Marconi Research Centre,
Great Baddow,
Chelmsford,
Essex, CM2 8HN,
United Kingdom.

SUMMARY

Multipath dispersion measurements made on several 4.5 GHz paths in the United Kingdom are presented. Beamwidth and scatter angle dependence and several features of dispersion in angle and space diversity are discussed. These measurements and others from the literature are compared with predictions of dispersion. The predictions considerably underestimated the measured dispersion, but the inclusion of a beam broadening factor in the calculations gave a significant improvement in accuracy.

1. INTRODUCTION

The work described in this paper was carried out as part of a programme to develop a 4.5 GHz troposcatter communications system. The forward scatter mode of propagation is characterised by large and time-varying path losses, and multipath dispersion which may also be very variable. Both the path loss and the dispersion have an important influence on the performance of a digital system as measured in terms of bit error rate or system availability (e.g. (1), (2)).

A number of workers have proposed methods for the prediction of multipath dispersion on troposcatter links. (see e.g. (3), (4), (5), (6) and (7)). However, there is little consensus between the various approaches, and furthermore there is only a limited amount of data available from published measurements of dispersion. The programme of measurements described here was undertaken to expand the existing database of dispersion measurements, and also to investigate various aspects of system performance under dispersive conditions.

The dispersion measurements on three paths in the United Kingdom are described, and a number of interesting features of the results are discussed. The multipath delay spreads are also compared with the predictions of two published methods, and it is shown that in general the predictions underestimate the amount of dispersion encountered in practice. The comparison of measurements and predictions was extended to embrace other published data, and large prediction errors were again encountered in some cases. However, a consideration of the results suggested a modification to one of the methods, and the results of this amended prediction have also been compared with the measured data. The revised prediction method was found to give a useful improvement in prediction accuracy in many cases.

Section 2 of the paper describes the United Kingdom measurements of multipath dispersion and discusses various features of the results. Section 3 compares predictions of dispersion by several methods with the available measurements. It also outlines the reasoning behind the modified prediction method and compares its predictions with the measured data.

2. UNITED KINGDOM MEASUREMENTS OF MULTIPATH DISPERSION

2.1 Measurement Programme

A programme of measurements using Marconi Communication Systems equipment (8) was carried out on three paths in the United Kingdom. Measurements on each path lasted for several weeks, and the total measurement period ran from January/March for Path 2 to May/June for Path 4. Basic parameters of the path geometry and the equipment used are summarised in Table 1. The antennas used for most of the tests were 4.5 metre diameter, giving approximately 1° beamwidth at 4.5 GHz; dual angle diversity reception was used in all cases. Path 2 was operated in two different configurations,

(a) with dual angle diversity reception from a transmission of 1° beamwidth (i.e. as for Paths 3 and 4) and

(b) using dual angle/dual space diversity reception of a transmission with 1.9° beamwidth.

l'enveloppe de ce signal suit alors une loi de Rayleigh si b_1 et b_2 sont gaussiens et indépendants.

- Affaiblissement lognormal : il est produit simplement par un atténuateur en dB commandé par une tension suivant une loi normale, filtrée passe-bas.

Les différents filtres nécessaires pour contrôler la vitesse de variation des phénomènes ont été déterminés par les mesures effectuées, décrites en 3.

Références

[1] Schwartz, Bennet & Stein: Communication systems and techniques
Mc Graw-Hill (1966) ; par.1-4,pp.20-26

[2] CCIR Avis 529 ,R 567-2:Méthodes et statistiques permettant d'évaluer le champ pour les services mobiles terrestres fonctionnant dans les bandes de fréquences comprises entre 30 MHz et 1 GHz.

[3] Hata M.:Empirical formula for propagation loss in Land Mobile Radio services.
IEEE Trans.VT 29 n°3, août 1980, pp.317-325

[4] Okumura et al.: Field strength and its variability in UHF and VHF land-mobile radio service.
Rev.of the Electr.Comm.Lab. (Jap.) volume 16,n°9-10 (sept.-oct. 1968) pp.825-873

DISCUSSION

J.S.Belrose, Ca

I wish to make a comment relating to your paper, which I found very interesting, because we in Canada, of the Communications Research Centre, Ottawa, have been studying the land mobile radio environment at 860 MHz (as well as at lower frequencies 150 and 450 MHz traditionally used for mobile radio). We have been measuring the coherence bandwidth by two quite different techniques (Bultitude and Melanson, private communications), and the signal and noise environments. We have also been measuring BERs, and their correlation with these parameters. I had hoped to present some of these results at this meeting, but the work is still on-going and has not reached the stage where I could present an overview on it.

However, the purpose of my comment concerns the performance of mobile antennas in a multi-path/clutter environment. At 860 MHz we employed two quite different "gain" antennas. One was a conventional colinear whip, and the other two orthogonal ground plane half-twin-delta loops fed in quadrature to provide omnidirectional gain. In rural areas, and on streets running approximately radially from the base station transmitter, both exhibited the same gain (~ 4 dB w.r.t. a quarter wave). But on orthogonal streets, where the signal received was entirely a scatter signal, these antennas exhibited −2 to 0 dB gain. The delta loop antenna array, which depended for its gain on signal coherence in the horizontal plane, suffered the greatest gain degradation. Clearly, the received signal is so incoherent over distances as small as the dimensions of these modest antennas, that "gain" is not achieved (ref. Belrose, IEEE Vehicular Technology Conference, Toronto, May, 1983 and AGARD LS 131, 1983).

This fact, along with azimuthal nulls associated with the positioning of the mobile antenna on the vehicle, contributes to the observed fading.

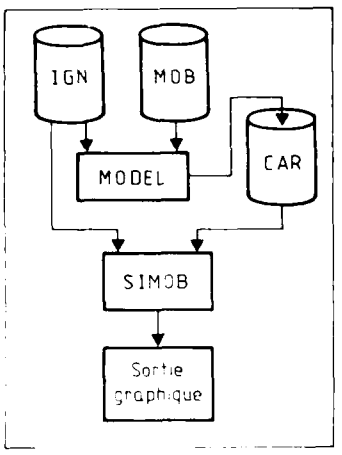

Fig 5.1 Principe du modèle prévisionnel de couverture

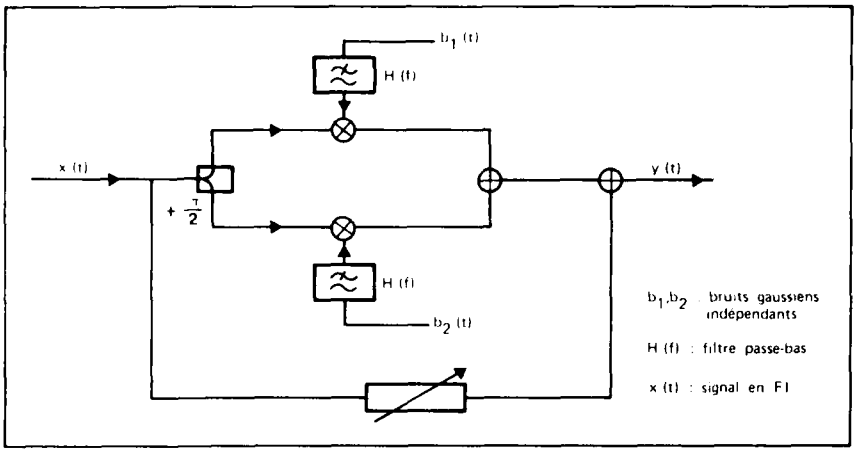

figure 5.2 : "Module Rice" du simulateur de canal

5.2 - Simulateur matériel de canal

Le but de ce simulateur est de permettre une évaluation et une comparaison en laboratoire de modems numériques à petit débit destinés à un accès en AMRF sur le réseau de communication avec les mobiles. Ce simulateur devra donc figurer le modèle "faible débit" qui a été décrit en 2) et donc pouvoir effectuer :

- un affaiblissement variable (représentant l'affaiblissement en fonction de la distance)
- un affaiblissement lognormal de moyenne 0 dB (représentant les masques)
- un affaiblissement de Rice, de moyenne 1 (représentant les trajets multiples).

Un synoptique général est donné figure 5.3. Ces différents affaiblissements sont produits de la façon suivante :

- Affaiblissement de Rice : on fait la somme du signal d'entrée plus ou moins atténué et du même signal affecté d'une statistique de Rayleigh produite par une multiplication de ses composantes en phase et en quadrature par deux bruits gaussiens filtrés (fig. 5.2).

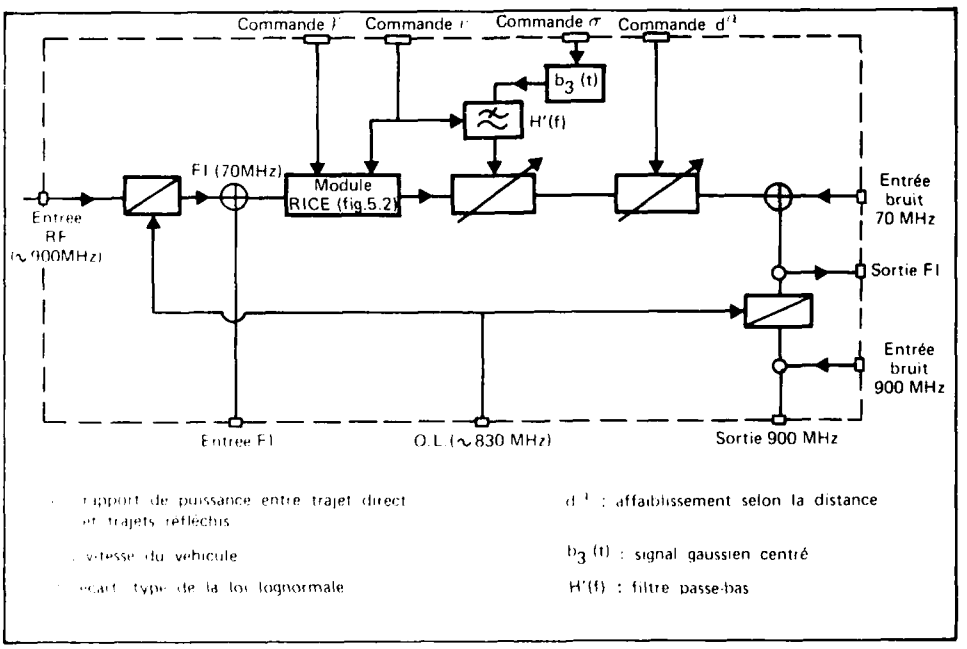

figure 5.3 : Simulateur de canal radiomobile

Si x(t) est le signal entrant, il est décomposé, en phase et en quadrature, en deux signaux $A(t)\cos\omega t$ et $-B(t)\sin\omega t$; le signal de sortie est alors égal à :

$$y(t) = b_1(t)A(t)\cos\omega t - b_2(t)B(t)\sin\omega t$$

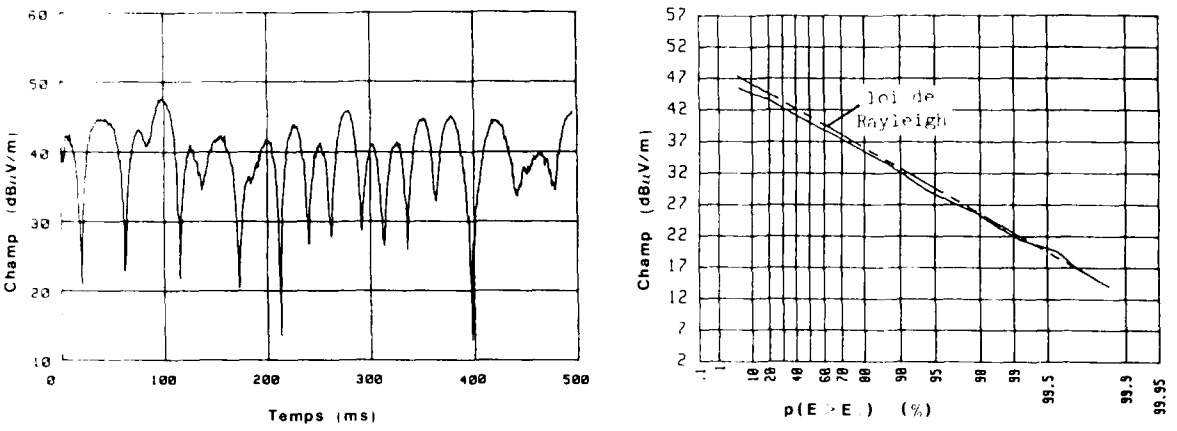

Cas a) : Absence de trajet privilégié

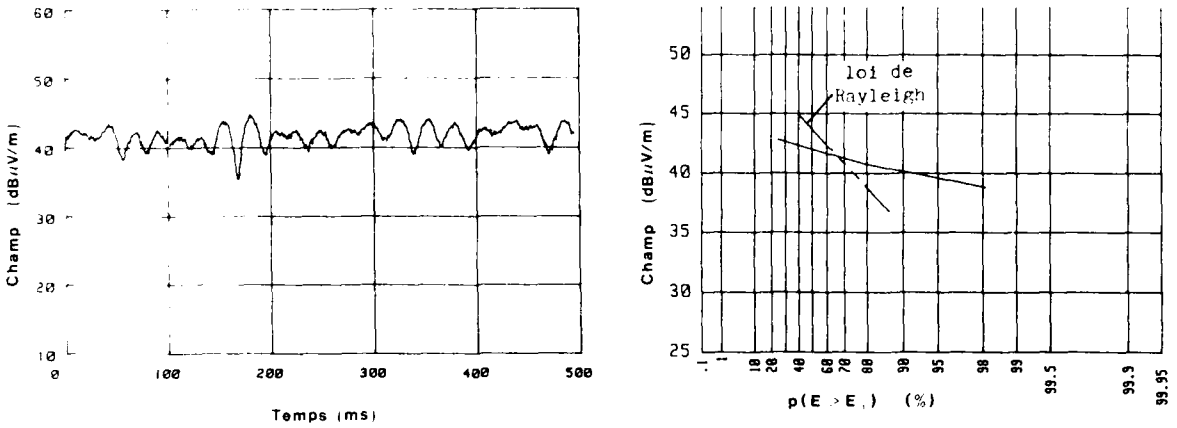

Cas b) : Existence d'un trajet privilégié

figure 4.2 : Mise en évidence des trajets multiples
et comparaison avec la loi de Rayleigh

5 - UTILISATIONS

5.1 - Modèle prévisionnel de couverture

Le but de ce modèle est de permettre d'établir, à partir d'une position d'émission donnée, une carte des niveaux de champ reçus en tous points de l'environnement proche, soit par tracé des courbes d'isochamp, soit par tracé des coupes de terrain sur des axes particuliers.

Pour ce faire, le centre de calcul dispose d'un fichier de données altimétrique (IGN) de l'ensemble de la région parisienne réalisé avec un maillage carré de 1 km de côté. Chacune de ces mailles contient des informations sur l'altitude du sol et du sur-sol (bâtiments, bois) en différents points caractéristiques. Certaines parties de la zone numérisée peuvent être affinées avec des mailles de 200 m ou de 25 m.

Dans un premier temps, ce fichier permet d'établir des corrélations entre les variations locales du niveau de champ et l'environnement, afin d'en tirer un certain nombre de lois empiriques tenant compte de ces phénomènes (densité urbaine, orientation de rues, ...).

Une fois le modèle établi, ce même fichier en permettra l'exploitation, c'est à dire l'édition de cartes de couverture de champ à partir du programme SIMOB (fig. 5.1).

Dans le cadre de l'établissement d'un réseau cellulaire, l'exploitation d'un tel modèle est intéressante de plusieurs manières :

- à partir d'un site d'émission aux caractéristiques connues (position et hauteur d'antenne, puissance d'émission), détermination de la zone de couverture à différents niveaux de champ

- réciproquement, à partir d'une certaine zone à couvrir, détermination des caractéristiques d'émission (puissance, hauteur d'antenne,...)

- détermination des niveaux à grande distance pour permettre la réutilisation des fréquences.

récepteur utilisé étant un analyseur de spectre à mémoire numérique. L'interface du capteur de distance déclenche les acquisitions et fournit l'information de vitesse du véhicule permettant de passer de l'échelle temporelle à l'échelle spatiale.

Scénario

Le véhicule étant placé dans différentes configurations urbaines (zones fortement masquées, zones dégagées,...) avec des niveaux de champ moyen divers, une acquisition est lancée pendant une durée de 500 ms, au cours de laquelle sont prélevés 1000 échantillons sur l'analyseur de spectre, qui sont ensuite transférés vers le calculateur de bord et stockés sur disquette. Ces mesures sont répétées pour diverses vitesses du véhicule.

4 - RESULTATS OBTENUS

4.1 - Mesures à grande échelle

Les traitements effectués sur les mesures à grande échelle visent d'une part à définir une loi de l'affaiblissement en fonction de l'éloignement de l'émetteur et du récepteur, d'autre part à étudier le phénomène de variation du champ due aux masques.

La loi de l'affaiblissement en fonction de la distance se présente sous la forme $A(dB)=10\,\alpha\,\log D + \beta$. D'après les résultats obtenus jusqu'à présent, la valeur de α converge vers 3,5 pour Paris intra-muros (fig. 4.1). La comparaison avec le modèle d'Okumura-Hata, décrit au chapitre 2, est très satisfaisante, du moins dans la zone urbaine de la région parisienne. Cependant des mesures effectuées sur des radiales s'éloignant du centre de Paris vers la banlieue mettent en évidence les remontées du champ sur les collines situées à la périphérie, où l'on se rapproche de la propagation en espace libre, puis le retour à une propagation par diffraction .

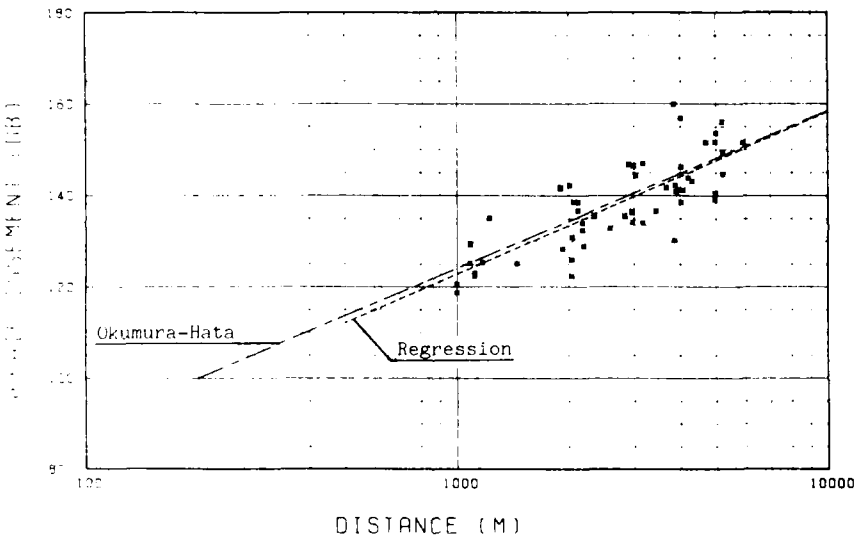

figure 4.1 : Relevé des moyennes sur l'émetteur ARCHIVES

Deux approches sont envisagées pour le traitement des variations locales du champ en fonction des masques. L'une, à caractère déterministe, est décrite au chapitre 5.1. L'autre approche, de type statistique, consiste à considérer que le phénomène suit une loi log-normale centrée d'écart-type σ, qu'il s'agit de déterminer. Les calculs de corrélation avec cette loi, effectués sur un certain nombre de fichiers, confirment l'hypothèse du type de loi, avec un écart type voisin de 8 dB. Ce résultat est utilisé pour la détermination d'algorithmes de contrôle automatique de puissance sur les liaisons bases-mobiles.

4.2 - Mesures à petite échelle

Un programme réalisé sur microcalculateur permet de vérifier la validité de la loi de Rayleigh sur les enregistrements effectués. Dans de nombreux cas, où la propagation s'effectue en absence de trajet direct ou privilégié (zones de non visibilité), cette loi donne un résultat très satisfaisant (cf fig. 4.2-a). Lorsqu'il existe un axe de propagation privilégié, alors le résultat des mesures s'écarte assez sensiblement de cette loi (cf fig. 4.2-b).

3.1 - Mesures à grande échelle

Système de réception

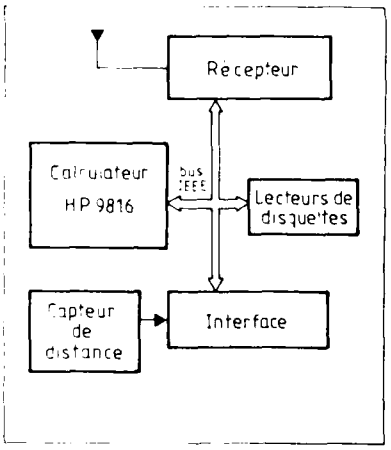

Fig 3.3 Synoptique du système de réception

Le synoptique du système de réception est donné à la figure 3.3. Le récepteur utilisé permet l'acquisition d'échantillons du champ local par l'intermédiaire d'un bus IEEE 488. L'interface entre le capteur de distance et le calculateur fournit à ce dernier, outre la valeur de la distance parcourue, les signaux de déclenchement permettant la mesure du champ local.

Définition des trajets

Trois principes sont utilisés :

- mesures sur des cercles concentriques des émetteurs, par pas de 1 km. On obtient alors, pour une distance donnée (rayon du cercle), un nuage de points (fig. 3.4-a)

- mesures sur des radiales passant par les émetteurs. On obtient alors, pour un ensemble de distances à l'émetteur, une valeur de champ par distance (fig. 3.4-b)

- mesures à l'intérieur de carrés de section 500 m. On obtient alors un nuage de points répartis dans une tranche de distance (fig. 3.4-c).

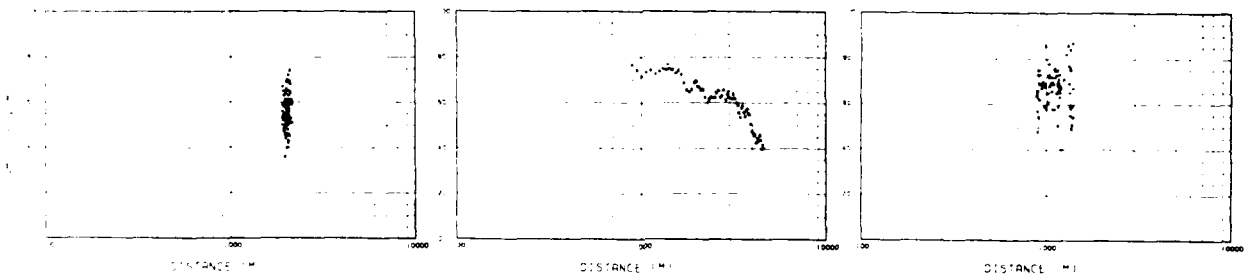

a) cercle b) radiale c) carré

fig. 3.4 : Résultats suivant le type de trajet

Scénario

Un trajet étant déterminé selon l'un des trois principes précédents, le véhicule effectue le parcours en enregistrant les échantillons du champ et la distance parcourue pour chaque intervalle de distance programmé. Deux fréquences d'échantillonnage sont utilisées :

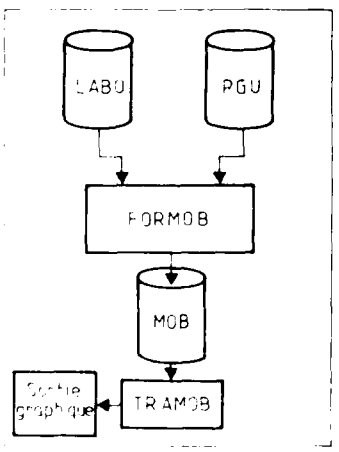

Fig 3.5 Numérisation et traitement des mesures

- acquisition sur un seul émetteur, avec un relevé par mètre

- acquisition simultanée sur trois émetteurs, avec un relevé tous les 5 mètres.

En des points privilégiés du parcours (carrefours, ponts,...) et prévus à l'avance l'opérateur valide son passage au moyen d'une touche de fonction du calculateur, ce qui permettra, lors du traitement en laboratoire, de se recaler sur le trajet numérisé. En fin de parcours les données enregistrées sont stockées sur disquette afin d'être transmises ultérieurement vers le centre de calcul graphique.

Traitement en laboratoire

Les fichiers de données acquises sur le terrain sont transmis vers le centre de calcul par l'intermédiaire d'une liaison série et stockés dans le fichier global LABO (fig. 3.5). Ce centre de calcul dispose d'une base de données topographiques (fichier RGU) contenant un répertoire des rues de PARIS avec leur position géographique et leur largeur entre immeubles. Le programme FORMOB permet, à partir des deux fichiers précédent, la numérisation du parcours et l'élaboration du fichier global MOB qui contient, pour chaque valeur de champ mesurée, sa position géographique et sa distance à l'émetteur.

3.2 - Mesures à petite échelle

Système de réception

Le principe du système de réception est le même que pour les mesures à grande échelle, le

DISCUSSION

P.Monsen, US

A theory to explain the larger multipath spread involves the effect of the foreground on the antenna. Could you comment on this theory and on the foreground used in your tests?

Author's Reply

If foreground was a factor, the broader beams would have a larger error but results are opposite to this. Foreground for tests was not especially favourable.

L.Boithias, Fr

Quels sont les paramètres radiométéorologiques utilisés dans les méthodes de prévision de Bello et Pusone?
L'utilisation de N_s n'est certainement pas la meilleure solution — l'influence du gradient de l'indice de réfracteur dans le volume a-t-elle été étudiée (car c'est le paramètre essentiel pour la prévision des atténuations).

Author's Reply

Surface refractivity does not enter either the Bello or Pusone models. Refractivity gradients near the surface are implicit in the use of an effective earth radius factor to define the path geometry and scatter angles. Refractivity gradients in the common scattering volume are implicit in atmospheric models embodied in both prediction methods.

E.Lintz Christensen, De

Printouts of the delay spread show samples every 0.64 sec. and there seems to be little correlation between subsequent samples. Do you know the correlation time (e.g. the sampling time which will give almost identical response)? In other words — how fast does the shape change?

Author's Reply

We have not looked specifically at the autocorrelation times of changes in shape of the delay power spectrum. Variation of power summed over all delay taps gives a measure of the effective flat fading rate. Values of this parameter averaged about 3 Hz, with values of about 6.5 Hz exceeded for 1% time.

A.Schneider, US

Does the optimum beam elevation depend on the time of year, or on the effective earth's radius?

Author's Reply

In principle the calculated optimum beam elevation angles involve the scatter angle, which is calculated using an effective earth's radius which changes with season, so that optimum beam elevation angles do depend on season. I have not looked at the sums explicitly, but I would say that it is a second order effect. I would not imagine that you would be advised to go about changing the beam elevation angles with season.

DISCUSSION OF SESSION IIB

Dr Burgess, Session Chairman

During the afternoon we have covered frequencies from HF, 2—30 MHz, though VHF–HF in Paper 16, 900 MHz for cellular radio, 4 GHz for troposcatter, and we have looked at 7 GHz. Dr Palmer indicated that there are a number of prediction programmes that could be used; have we got any comments on what we should do these days bearing in mind the availability of small powerful computers which could be used to implement many of these programmes?

Dr Boithias

To have very powerful computers is a very useful and necessary condition, but it is not sufficient because we have to know what to put into the computer. If the input data is not known, the most beautiful computer will not give anything of value. The problems of prediction programmes are that we do not know the starting parameters.

Dr Palmer

I guess my views differ somewhat there. I agree that garbage in – garbage out, but I think that enough of the input requirements are known that one can do a reasonable modelling job given a sufficiently good basic model to put into the computer. I mean that one can model diffraction losses over multiple obstacles taking account of the shape or at least the radii of curvature of these obstacles. One can study the effect of obstructed Fresnel zones below the line of sight, one can develop techniques for summing the losses from these various obstacles which is one of the most difficult problems. These are computationally intensive problems which can be attacked with modern computing methods. However, one still needs a suitable set of measurements with which to compare the results of the modelling. In the work that I was associated with one of the difficulties was in fact getting data, we carried out some field measurements of our own, because when you look through published records you find that almost invariably there is something missing. There may be a measurement of path loss, but there may be no explicit description of the foreground, clutter or trees, tree density, whatever, and you find that you need to know that. So I would say that my belief is that you can do a better job than is commonly done. Obviously it is an exponential type of activity to try and get these last few dBs; they cost you more and more computing power, and you get to a point where no model can do any better; simply you cannot take every small detail into account. But I believe that it is in the order of 6 or 10 dB standard deviation rather than 20 to 30 dB. Incidentally, I would just like to point out a common error that is made concerning line of sight systems, which is to assume that if a path has optical line of sight it is free space. Tactical situations at VHF are such that it is very rare to find a free space path because the Fresnel zones are almost invariably obstructed. In such cases it is necessary to do a small amount of modelling which will certainly improve the results.

SUMMARY OF SESSION III

CHANNEL SIMULATION

by

M.Darnell
Session Chairman

The five papers included in Session III described a wide range of channel simulation activities.

Paper 12 by Holtzman and Shanmugan presented an overview of digital simulation techniques for communications channels. The authors described, in general terms, the rationale for channel simulation and widely applicable channel models; modelling of frequency-selective fading and wideband/spread-spectrum paths was stressed. Finally an example of the application of simulation to an EHF communication system was discussed.

Paper 22 by Hoffmeyer and Hartman surveyed models, realisations and new concepts for the simulation of line-of-sight microwave channels. The emphasis in this paper was on the use of an RF path simulation for the comparative testing of complete radio systems already implemented in hardware form.

In paper 23 by Klinker and Pietersen, the authors considered the use of simulation in the evaluation of the performance of one particular element of an electromagnetic system, namely adaptive antenna systems for reception of Navstar GPS transmissions. The performance of the antennas was examined under simulated battlefield conditions with specified ECM threat levels.

The topic of HF path simulation for RTCE-based systems was discussed by Dawson in Paper 24. In particular, the requirements for a realistic simulation of the effects of co-channel interfering signals was identified. In practice, in certain operational zones, it is interference rather than propagation which limits HF system performance.

Paper 25 by Bouidène and Vandamme returned to the topic of line-of-sight digital radio channel simulation. The simulator described effectively reproduced conditions measured and recorded from a real LOS link. Again, emphasis was placed upon the need to simulate selectively-fading wideband channels.

The major discussion topics raised during Session III were:

(i) the merits of mathematical and physical channel models and, in particular, the advantages and disadvantages of the Rummler model;

(ii) roles for channel simulators; whilst the session papers concentrated upon the use of simulators as system design aids and for equipment evaluation, a requirement for simulation as a form of operation training was also identified.

It would appear that the development of simulators for specific channel types is relatively far advanced. However, there are several aspects of electromagnetic system design, having a significant influence on overall performance, which are not yet simulated adequately; these include:

- network operation
- the effects of ECM activity
- ECM constraints (particularly for mobile platforms)
- the effects of non-linearity
- the effects of co-channel interference (most important in HF systems).

DIGITAL SIMULATION OF COMMUNICATIONS CHANNELS
AN OVERVIEW

by
J. C. Holtzman
K. Sam Shanmugan
Telecommunications and Information Systems Laboratory
University of Kansas Center for Research, Inc.
2291 Irving Hill Road
Lawrence, Kansas 66045

SUMMARY

Improved characterization of the propagation channel is required in the simulation of wideband communication systems. In this paper, we review some of the popular channel models that are currently in use and discuss their capabilities and limitations. One major shortcoming of these models is the way in which they are most often used to calculate transmission losses at a single frequency; neglecting the frequency and time dependency of the various propagation phenomena. We propose a tapped delay line model with time varying tap gains as the generic simulation model for propagation channels and show how this model can be used to analyze the effects of gaseous absorption and dispersive refraction of moist air at microwave frequencies.

INTRODUCTION

Simulation of communication systems has been widely employed for many years. For the most part, specific models were generated for each application or system. With the advent of satellite systems, several powerful generic models were created that could be made system specific in a user/interactive mode. More recently, these generic simulation systems have been developed to predict performance for terrestial (both fixed point to point and mobile) and airborne systems. With the increased emphasis on wide band systems, attention has been focused on the adequacy of the channel model. We will first, very briefly examine some of the uses of the simulation systems, to gain an understanding of the complexity of the problem. We then review some of the most popular of the current channel models. Finally we examine a few of the wideband models which include the frequency dependence of the amplitude and phase of the channel transfer function and present some new results for an EHF channel.

Simulation of communication systems is receiving increased attention as a viable and reliable method of predicting performance for complex systems. Moreover, many of the processes involved in the analysis and prediction of performance of communication systems cannot be described in an analytic form. For example, nonlinear channels or receivers can only be evaluated by simulation employing stochastic modeling. Simulation is not a new tool to communication engineering. In fact, the prediction models used to determine siting, fading, and diversity effects are examples of very specific simulation models. As satellite channels became more sophisticated, so did the simulation systems [1], [2], [3], [4]. These simulation systems are generally characterized by a reconfigurable block diagram approach. That is, with varying degrees of user-friendly interactive sessions, a communication system is specified block by functional block. The user defines modulation types, filters, channel models, receivers, etc. Usually a random signal is generated as the data stream, with various outputs generated in the time and frequency domain, to describe the system performance.

Simulation systems as noted above, have found wide acceptance in increasingly more sophisticated environments. For example, the Kansas Interference Prediction System (KIPS) [4] is planned for use in spectrum management and network performance evaluations by the U.S. Army. The U.S. Air Force purchased a system known as Interactive Communications Simulation System (ICSSM) [3] to aid in the evaluation of Air Force Systems. SYSTID, designed and implemented by Hughes Aircraft Co., has been used by Hughes, Bell Laboratories and others to evaluate satellite links and to evaluate the performance of new modems. Lee and Smith [5], report on a simulation model which incorporates, among other features, a statistical deployment of transmitters and receivers. They list three objectives of simulation models which are repeated here to set the stage for the discussion of channel models. "...1) to obtain design decisions from statistical data; 2) to demonstrate the feasibility and [practicality] of complex systems in a simulated "real world" environment; 3) to allow comparative evaluations of alternative design approaches even when absolute data are not available." Clearly, the accurate representation of each block is critical to the overall accuracy of the simulation system.

Each of the referenced simulation systems, has been applied to spread spectrum systems as well as other wideband modulation systems with relatively good success. However, as the environments have become more complex, researchers have begun to focus attention on the adequacy of the channel model. The early applications of the various simulation systems were mostly concerned with relatively narrow band systems where the frequency selectivity of the channel could be safely ignored. Hence, the channel model essentially consisted of a single point calculation of path attenuation (fading margin) caused by absorption, refraction, multipath, reflection as well as just the free space path loss. Giger and Barnett [6], have stated that "it is meaningless to speak of the traditional flat fade margin in digital radio systems." They, Bloomquist and Norbury [7], Rummler [8] among others have observed that the frequency selectivity of the channel results in severely degraded performance due to intersymbol interference, a degradation in excess of that predicted by simple single point attenuation calculations. Bougusch, Guigliano and Knepp [9] have performed an extensive analysis of direct sequence PN systems, noting the effect of frequency selective scintillation on carrier and code tracking. A major effort is required to improve the channel modeling in simulation systems if they are to be an accurate representation of the communications environment, producing reliable and useful predictions.

BACKGROUND OF CHANNEL MODELING FOR SIMULATION

Proakis [10] has an excellent overview of the channel modeling problem. He defines a statistical representation of the time varying multipath channel in terms of an impulse response and transfer function as

$$h(\tau,t) \overset{F}{\leftrightarrow} H(f,t) \tag{1}$$

where

t is the observation time
τ is the delay time and is a random variable
f is the frequency variable with respect to τ and is a random variable
F is the Fourier Transform

Several correlations functions are then derived. Making use of the fact that for uncorrelated scattering channels, the correlation functions of the impulse response depend only on the time difference Δt and the correlation function for the transfer function depend only on the frequency difference Δf, the respective correlation functions are

$$\phi_h(\tau,\Delta t) = \text{"average power out as function of delay and time difference"} \tag{2}$$

$$\phi_h(\tau) = \phi_h(\tau,\Delta t=0) \tag{3}$$

$$= \text{"delay power spectrum"}$$

$$\phi_H(\Delta f,\Delta t) = \text{"spaced-frequency spaced time correlation function of channel} \tag{4}$$

$$\phi_H(\Delta f) = \phi_H(\Delta f,\ \Delta t = 0) \tag{5}$$

$$= F\{\phi_h(\tau)\} \tag{6}$$

where $\phi_h(\ \ )$ is the correlation function of statistical channel impulse response or $\phi_H(\ \ )$ is correlation function of the statistical channel transfer function. The observation in Eq.(6) permits a duality relationship to be expressed as

$$\Delta f_c = 1/T_m \tag{7}$$

where

Δf_c = "coherence bandwidth of channel"

T_m = effective duration of delay power spectrum, i.e., length of non-zero cross correlation of received pulse with itself

Now the observation time dependence, that is the time dependence of the multipath channel causes effectively a Doppler broadening due to the changing delay on a single path for a single frequency. This permits the definition of the Fourier Transform of the spaced frequency space time correlation function to be interpreted as follows:

$$S_H(\Delta f,\lambda) = F\{\phi_H(\Delta f,\Delta t)\} \tag{8}$$

$$S_H(\lambda) = S_H(\Delta f=0,\lambda) \tag{9}$$

$$= F\{\phi_H(\Delta t)\}$$

$$= \text{"Doppler power spectrum of channel"}$$

Again we can make use of the inverse Fourier Transform relationship to obtain a duration-bandwidth spread as

$$\Delta t_c = 1/B_d \tag{10}$$

where

Δt_c = coherence time of the channel

B_d = effective bandwidth of Doppler spread of channel

Proakis goes on to define a two dimensional Fourier Transform of the spaced frequency space time correlation function as the "scattering function of the channel" which presents a good graphical interpretation of the time varying channel. However, we have at this time all the necessary concepts and parameters to establish the frequency selective and time varying properties of the multipath propagation medium.

If the information signal has a symbol or signaling rate less than the coherence time of the channel, then we have effectively a single attenuation per symbol or slow fading. If the information signal bandwidth is less than the coherence bandwidth of the channel, then we are faced with a non-frequency selective channel that may be slow or fast fading. On the other hand, if the signal bandwidth exceeds the coherence bandwidth as is the case in most digital signaling schemes and, of course, spread spectrum systems, then we have a frequency selective channel with either slow or fast fading. Without

much difficulty many authors have shown that the frequency selective channel can be modeled as a tapped delay line with time varying tap gains [11]. We shall explore this in a later section.

CHANNEL MODELS FOR NON-FREQUENCE SELECTIVE SLOW FADING CHANNELS

Crane [12], gives a good overview of the various propagation effects causing signal degradation. He discusses such phenomena as molecular absorption, refraction by the variable index of refraction of the atmosphere, scattering by particles such as rain, snow, ice, etc., scattering by turbulence, and multipath. Each of the phenomena is treated from a point of view of non-frequency selective, slow fading, although fast scintillation and some frequency dependence is indicated.

The most basic of the channel model calculations is simply the free space path loss caused by the beam spreading and receiving aperture. The fundamental relationship for the path loss is

$$L_{FS} = (4\pi R/\lambda)^2 \tag{11}$$

which can be put in a more convenient form for link calculations as

$$L_{LS}(db) = 92.44 + 20 \log R_{km} + \log f_{GHz} \tag{12}$$

This can be randomized to account for variable placement, but it is usually not worth the effort. In a strictly additive channel and linear receiver, the free space path loss is usually omitted as only the S/N ratio at the input to the receiver is of importance. If the receiver front-end is nonlinear, then it should be included. The excess attenuation caused by the phenomena described by Crane and others are then calculated to determine the flat fade margin and should be included in accurate simulation modeling.

Probably the most familiar propagation prediction is that for rain attenuation. Much research has gone into the problem of calculating fading statistics for rain attenuation based on rainfall rates drop size, etc. One of the most popular models is described by Olsen, Rogers and Hodge [13]. The relationship

$$A = aR^b \tag{13}$$

gives the attenuation per unit distance. The parameters a and b are tabulated as regressions from extensive sets of experimental data as well as theoretical scattering models and are in turn parameterized by frequency, drop size and rain temperature. The later two parameters are found from average meteorological data usually in three months cycles for various areas. For polarization re-use or diversity channels, Eq.(13) should be modified as suggested by numerous researchers and reported in [14]. Horizontal polarization suffers a higher loss than does vertical polarization, an effect which increases with frequency.

For transmission in the "atmospheric windows," most channel models omit any calculation of excess loss due to absorption. However, certain systems are predicated upon operation in or near absorption bands. For narrow band transmissions, that is when the signal bandwidth is less than the channel coherence bandwidth (rarely the case for digital transmissions in or near the absorption bands), attenuation modifications to the originally published data have been suggested but, as will be discussed in a later section, the phenomena is almost assuredly frequency selective and thus refinements to the basic calculation are not warranted for simulation of communication systems.

The most important of the degradation effects are those attributed to multipath. Currently, the most used "total" or inclusive model is the Irregular Terrain Model (ITM) better known as the Longley-Rice model. Chamberlin and Luebbers [15,16] give a good summary of that model while proposing a supplemental model, the Geometric Theory of Diffraction (GTD) model. The ITM model has many extensions, however, it basically calculates attenuation for a path provided either directly by the user or from profiles calculated from a digital terrain data base. The model assumes only gross characteristics about the terrain, that is, three or so classes of terrain irregularity (roughness), and complex terrain reflectivity. The ITM considers three basic cases, line of sight, diffraction, that is blockage exists but the "shadow is not deep, and scattering, when the antennas are physically deeply obscured but are electrically visible to each other by virtue of forward scatter. A single multipath is calculated in the line of sight mode based on the geometry of antenna heights and the path profile. The model is reasonably accurate, is fairly computationally efficient and has been widely used with satisfactory results.

When a good description of the terrain is available, Chamberlin and Luebbers [15] have proposed a much more precise model based on the geometrical theory of diffraction. Fourteen classes of multipath rays are calculated for various combinations of diffraction and reflection. However, since the GTD model is also non-frequency selective it would seem to have margiral value for the more sophisticated digital and spread spectrum systems.

FREQUENCY SELECTIVE MODELS

As was mentioned earlier and noted by many authors in the past several years, the purely fading, non-frequency selective channel model is not adequate to characterize the channel for most digital signaling and especially for spread spectrum systems. Giger and Barnett [6] noted that at a received signal level (RSL) of only some 19dB below nominal, the bit error rate (BER) exceeded the threshold of in-operability defined as (10^{-3}) for a given link. The nominal fade margin had been calculated as -41dB for the same threshhold. Intersymbol interference caused by the frequency selective behavior of the channel is the culprit, which is in turn caused by the frequency dependent behavior of the various delays in a multipath situation. Boumsch, et al. [9], studied the effects of Ionospheric irregularities, resulting in frequency selective scintillation for satellite links. Pickering and Bello [16] constructed

an elaborate theory for frequency dependent multipath caused by steep changes in the refractive index of the atmosphere. We will restrict the discussion in this paper to three studies which have resulted in models that are readily implemented in a simulation environment.

For reasons such as increased bandwidth, security, spectrum crowding at lower frequencies, etc., interest in EHF (30-30 GHz) channels has resulted in more detailed studies of the frequency selective behavior of the absorption phenomena. Liebe [17,18] has developed a most useful model which was implemented at the Telecommunications and Information Sciences Laboratory at the University of Kansas. Results are reported in section V. The model proposed by Liebe is relatively straightforward, at least in form and is given below.

$$H(f) = H_o \exp[j\ 0.02096\ f\ (10^6 + N)L] \tag{14}$$

$$N = N_o + D(f) + jN''(f) \tag{15}$$

where

$H(f)$ = channel transfer function
H_o = constant determined from table look up
N = complex refractivity in parts per million
N_o = frequency independent refractivity
$D(f)$ = refractive absorption
$N''(f)$ = absorption
L = distance in Km

The values of the parameters have been determined from a wealth of theoretical studies and experimental data, and tables of these parameters are given in [17]. The tables are generated from two computer programs which compute the parameters from inputs such as the pertinent resonance lines, the pressure, temperature and humidity and the altitude. The physical explanation of the process is fairly complex. Essentially, the frequency dependence arises from an overlapping of the spectral lines far from the peak absorption of a given line, thus forming a complex overlapping spectra. While not without its detractors, the Liebe model has been noted to give results in close agreement with actual observations and thus serves as a good state of the art channel model for simulation today. For earth to satellite paths, Hoppen [20] gives an empirically derived equation for N, the complex refractivity. To our knowledge, this model has not been extensively validated.

Rummler [8] has taken a different approach to modeling the frequency selective behavior of multipath. Without specifying the source of the reflections of the multipaths, he has used a sophisticated s-plane analysis of the pole and zero location of the transfer function, coupled with a statistical approach to the location of the poles in one event period to arrive at the frequency transfer function given below.

$$H(f) = a\ [1 - b \exp(\pm\ j\ 2\ \pi\ (f-f_c)^2)] \tag{16}$$

where

a = scale factor
b = shape factor
f_o = frequency of fade minimum
τ = constant determined from experimental data

He stresses that no physical significance can be attributed to τ. In [21], Rummler gives a statistical approach to determine a, b, and f_o for given channels. The model has been applied to several links where a great amount of statistical propagation data is available. Predicted results agree very well with the observed BER. Geiger and Barnett [6] have used the validated model to predict outages on digital links due to the excess intersymbol interference, developing a modified figure of merit. They also propose a method, based on the Rummler model for establishing an equipment signature. However, at this time, unless a significant amount of statistical propagation data is available to estimate a, b, and τ, this model would seem to have limited utility in simulation systems although its analytical simplicity suggests it be further explored.

The third approach to frequency selective channel modeling we will discuss, possibly holds the greatest promise for simulation systems. Sass [22] reports on a measurement program undertaken by the U.S. Army. The problem of mobile communications with spread spectrum systems in vegetated terrain, with transmitters and receivers in motion, with antennas in less than ideal locations is indeed complex. Wideband instantaneous measurements clearly show that the flat fading, that is non-frequency selective model, is a very inadequate representation of the channel model. This measurement program should generate a rich data base of statistical channel impulse response functions. As noted earlier, the frequency selective channel can readily be modeled as a tapped delay line, with tap gains modeled as stationary random processes for fast fading channels and constants for snapshots, that is, intervals of slow fading statistics.

Although it is not clear at this time how each of the several frequency selective models should be combined when more than one process is at work, it should be possible to use the tapped delay line model to implement the Rummler model when the channel and receiver are both linear since absolute power levels are not important. There is enough propagation data to estimate the tap gains both for fast and slow fading. One approach would seem to be the use the ITM model to predict the extremes of the absolute CW fades for a given terrain to determine the transfer function constant and then use the general shape of the Rummler model or an average impulse response from the data Sass reports. Clearly, this is an area of active research needed for simulation.

For purposes of simulation, the frequency selective and time varying effects of the propagation channel can be represented by a tapped delay line filter shown in Figure 1 [23]. The output of the filter is related to the input by

$$y(t) = C_{-M}x(t+MT_s) + ... + C_o x(t) + ... + C_M x(t-MT_s) \quad (17)$$

where T_s is the sampling time and C_j's are the tap gains. The transfer function of the filter, which approximates the channel transfer function, can be obtained as

$$H(f) = Ex(-j2fMT_s) \left[\sum_{m=-M}^{M} C_m \, Exp(-2\pi jfmT_s) \right] \quad (18)$$

Eq.(18) shows that the tap gains of the filter can be obtained from the Fourier series representation (or from the FFT) of the channel transfer function. By allowing the tap gains to vary as a function of time, the time variations of the channel response can be easily simulated.

EXAMPLE: SIMULATION OF FREQUENCY SELECTIVE ABSORPTION

In 1981 Liebe proposed a model for calculating the attenuation and phase of radio waves propagating through moist air. In this model (given in Eqs.(14 and 15)), the complex refractivity of moist air is characterized by a frequency dependent component which leads to dispersion. When a wideband digital signal is transmitted over this channel, the dispersion introduces intersymbol interference (ISI) resulting in a degradation in the system performance. We have evaluated the extent of this degradation for a QPSK system using digital simulation of the signals and the channel.

In our simulation, a QPSK signal with a carrier frequency in the range of 30-50 GHz is bandpass filtered and transmitted over an atmospheric channel. The transfer function of the channel, as given by the Liebe model, is implemented by a tapped delay line filter whose tap gains are obtained from the FFT of the sampled values of the transfer function. Assuming that the receiver input consists of the channel output plus additive Gaussian noise, the system performance as measured by the bit error probability is computed analytically [23] using the signal plus ISI values generated during the simulation. In order to obtain a statistically accurate ISI distribution, a long sequence of random binary digits is used as the input to the system. The sequence length is chosen to ensure that the estimate of the ISI distribution has a small variance.

Results of the simulation showing the performance degradation due to the frequency selective nature of the channel are shown in Figures 2 to 4. The attenuation and dispersion of the channel is shown in Figure 2, followed by an eye diagram showing the ISI generated by the channel in Figure 3 and the performance degradation as a function of carrier frequency, bandwidth, and link length in Figure 4. The losses shown in Figure 4 will have to be added to the link budget in order to account for the dispersive nature of the channel.

Simulation results shown in Figure 4 indicate that for short EHF links (<1km), the degradation is relatively constant till the carrier frequency exceeds 45 GHz. Beyond 45 GHz, the refractive dispersion increases rapidly due to absorption line in the viscinity of 60 GHz. There are some systems being considered for covert operations in the frequency range near 50 GHz and our simulations indicate that the increase in transmitted power required to overcome the dispersion in the channel is significant in the frequency range near 50 GHz.

SUMMARY AND CONCLUSIONS

Simulation plays a very important role in the analysis and design of communication systems. The accuracy and usefulness of simulation results depend, to a large extent, on the accuracy with which the various functional blocks in the communication system including the propagation channel are characterized. In this paper we reviewed the propagation models that are currently in use and point out their usefulness and limitations. We discussed the need for more accurate characterization of the frequency selective and time varying nature of the propagation effects. An example of how to model an atmospheric channel at EHF channel was presented and simulation results using the model were also given.

As we attempt to design very wideband systems for operation in complex environments it has become clear that adequate models and data do not exist for accurate characterization of the frequency dependent propagation effects at these frequencies. This is an area in which a significant amount of theoretical as well as experimental work will be needed over the next decade.

REFERENCES

1. "Computer-aided Design, Modeling, and Simulation of Communication Systems,", January 1984 issue of the IEEE Journal on Selected Topics in Communications, P. Balaban, K.S. Shanmugan, and B.W. Stuck, Co-editors.

2. Fashano, M. and A.L. Strodtbeck, "Communication System Simulation and Analysis with SYSTID," i.b.i.d.

3. Wade, W. D., et al., "Interactive Communication Systems Simulation Model - ICSSM," i.b.i.d.

4. J. C. Holtzman, et al., "Prediction of the Interference of Spread Spectrum Systems on Non-spread Spectrum Systems," University of Kansas Telecommunications Laboratory, TISL TR-588, August, 1983.

5. Lee, William, and Smith, Herbert, "Computer Simulation Model for the Evaluation of Mobile Radio Systems in the Military Tactical Environment," IEEE Transactions on Vehicular Technology, Vol. 32, No. 2, May 1983, pp. 177-190.

6. Giger, Adolf and Barnett, William, "Effects of Multipath Propagation on Digital Radio," IEEE Transaction on Communications, Vol. Com-29, No. 9, Sept. 1981, pp. 1345-1352.

7. Bloomquist, A. and Norbury, J.R., "Multipath Effects on a Terrestrial Path," Alta Frequenza, Vol. XLVIII, No. 4, April 1979, pp. 191-200.

8. Rummler, W.D., "Time- and Frequency-Domain Representation of Multipath Fading on Line-of-Sight Microwave Paths," Bell System Tech. Journal, Vol. 59, No. 5, May-June 1980, pp. 763-797.

9. Bougusch, R.L., Guiqliana, F.W. and Knepp, D.L., "Frequency-Selective Scintillation Effects and Decision Feedback Equalization in High Data-Rate Satellite Links," Proceedings of the IEEE, Vol. 71, No. 6, June 1983, pp. 754-767.

10. Proakis, John G., Digital Communications, McGraw Hill, 1983, pp. 454-477.

11. Modestino, et al., "Design and Implementation of the Interactive Communications Simulator," RADC Technical Report, TR-81-37, April 1981.

12. Crane, R.K., "Fundamental Limitations Caused by RF Propagation," Proceedings of the IEEE, Vol. 69, No. 2, Feb. 1981, pp. 196-209.

13. Olsen, R.L., Rogers, D.V., and Hodge, D.B., "The aR^b Relation in the Calculation of Rain Attenuation," IEEE Transactions on Antennas and Propagation, Vol. AP-26, No. 2, March 1978, pp. 318-329.

14. "Recommendations and Reports of the CCIR," 1982, Vol. V, paper #721-1, International Telecommunications Union-CCIR.

15. Longley, A.G., and Rice, P.L., "Prediction of Tropospheric Radio Transmission Loss Over Irregular Terrain - A Computer Method," U.S. Department of Commerce, ESSA Report ERL-79-ITS-67, 1968.

16. Chamberlin, K.A. and Leubbers, R.J., "An Evaluation of Longley-Rice and GTD Propagation Models," IEEE Transactions on Antennas and Propagation, Vol., AP-30, No. 6, Nov. 1982, pp. 1093-1098.

17. Pickering, L.W. and Bello, P.A., "Refractive Multipath on Microwave Links," Proceedings of NTC, 1977, 38:2, 1-7.

18. Liebe, H.J., "Modeling Attenuation and Phase of Radio Waves in Air at Frequencies Below 1000 GHz," Radio Science, Vol. 16, No. 6, Nov.-Dec. 1981, pp. 1183-1199.

19. Liebe, H.J., "Atmospheric Window Transparencies Near 35, 90, 140 and 220 GHz," IEEE Transactions on Antennas and Propagation, Vol. AP-31, No. 1, Jan. 1983, pp. 127-223.

20. Hoppen, J.D., "Simulation of EHF Propagation Through the Atmosphere," AGARD Conference Proceedings, AGARD-CP-284, 1981, 6/1-6/11.

21. Rummler, W.D., "A New Selective Fading Model: Application to Propagation Data," Bell System Tech. Journal, Vol. 58, No. 5, May-June 1979, pp. 1037-1071.

22. Sass, P.F., "Propagation Measurements for UHF Spread Spectrum Mobile Communications," IEEE Transactions on Vehicular Technology, Vol. VT-32, No. 2, May 1983, pp. 168-176.

23. Shanmugan, K.S., Digital and Analog Communication Systems, John Wiley and Sons, 1979.

ACKNOWLEDGEMENT

This work was supported in part by RADC/USAF under contract no. F30602-81-C-0205.

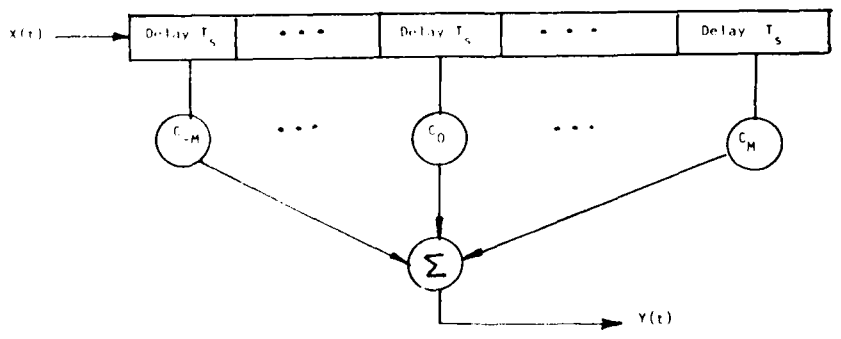

Figure 1 Tapped Delay Line Filter

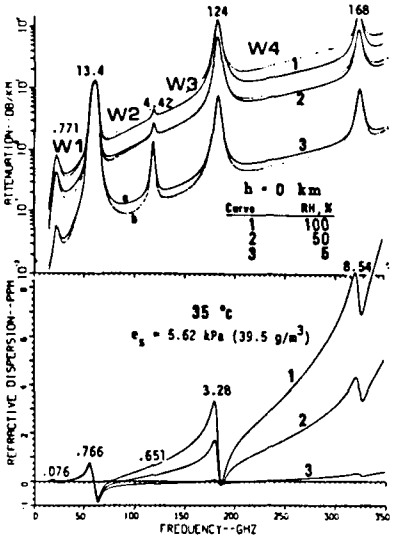

Figure ... Examples of attenuation and dispersion in the millimeter wavelength region.

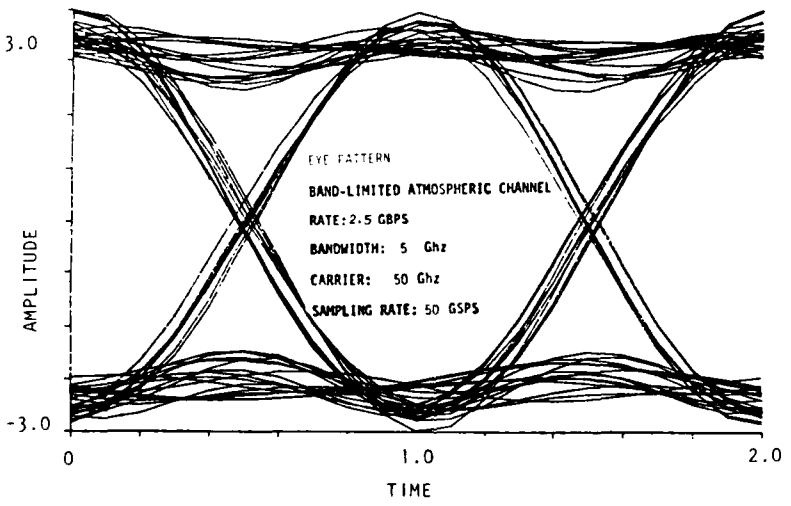

Figure 3. Eye Diagram.

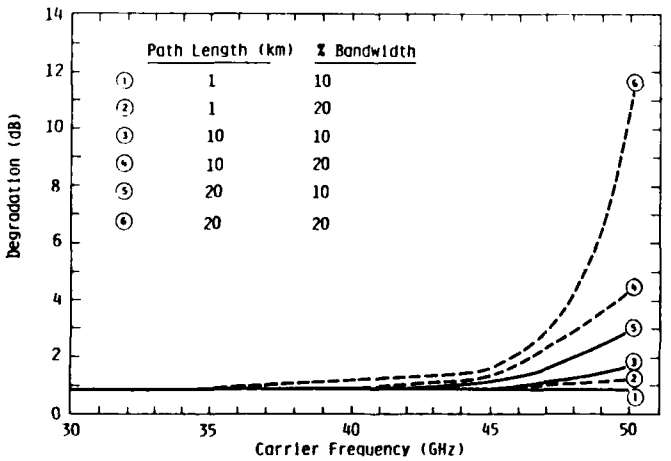

Figure 4. Degradation in QPSK System Performance Due to Refractive Dispersion of Moist Air

DISCUSSION

J.Aarons, US

What account is taken of ionospheric irregularities in your model?

Author's Reply

In the paper we discuss some of the models for ionospheric irregularities, but we did not use them in any of the simulation; since discussions about their acceptability are still taking place it would have been premature.

W.F.Utlaut, US

The results given for 50 GHz simulation were based upon the Liebe model which does not include multipath. Therefore, the results show the inherent limitations imposed by the atmospheric water vapour and oxygen line fine structure and multipath could degradate performance even further. Is that correct?

Author's Reply

Quite correct; in terrestrial application, frequency selective multipath would, our preliminary studies show, produce significant additional degradation.

L.Boithias, Fr

(Editor's translation)

Who is the client for your model? In order to make a model it is necessary to decide on the nature of the link, e.g. terrestrial or satellite, on the percentage of time of interest, e.g. 50%, 80% or 99.99%, and on the frequency. For terrestrial links multipath is a very important factor, but is not included in your model.

Author's Reply

The models we worked on at Kansas are generic models that can be used in a variety of situations, including ground-ground and air-ground by selecting the appropriate modules from the library. The work was sponsored by the USAF at Rome Air Development Centre. The reason we did not look at multipath beyond using the ITM model is that as yet we don't have the proper data to implement a Rummler type of model.

LOS MICROWAVE CHANNEL SIMULATION - A SURVEY OF MODELS, REALIZATIONS AND NEW CONCEPTS

by
James A. Hoffmeyer and William J. Hartman
United States Department of Commerce
National Telecommunications and Information Administration
Institute for Telecommunication Sciences
Boulder, Colorado 80303
United States of America

SUMMARY

The need for channel simulation becomes apparent when one considers the complexity of analytically evaluating digital radio performance or the difficulty and expense in field testing digital radios. For digital radios designed for military use, one must consider the radio performance not only in a channel that is subject to frequency selective fading but also one which may be corrupted by intentional jamming as well. Digital radio performance is dependent upon numerous factors such as the radio parameters and the channel fading characteristics. Although many papers may be found in the literature that report a specific radio's performance during fading conditions, it is difficult to generalize on these results so that the performance of some other radio operating under some other fading conditions can be predicted. It would be time consuming and prohibitively expensive to exhaustively field test a large variety of different radio configurations, i.e., different modulations, different types of adaptive equalizers, different types of space diversity combiners or switching algorithms, etc. Therefore, the use of a channel simulator is a logical approach for the performance evaluation of digital radios.

It is the purpose of this paper to review channel simulation concepts and to summarize recent work in LOS channel modeling and the hardware realizations of these models in a channel simulator. The paper also describes a new approach in which the channel simulator is realized at rf rather than at IF.

The paper briefly discusses the need for a standard performance measure for digital radios. Although bit-error rate (BER) is frequently used, this measure does not facilitate comparisons between tests conducted by different researchers because of differences in the ways that BER statistics are accumulated. The use of the synchronous error second (SES) and other performance measures are addressed in the paper.

1. THE NEED FOR CHANNEL SIMULATION

The concept of channel simulation has been investigated by many people for at least twenty years. Many simulation systems have been designed and constructed during this period of time. Most of these devices were designed to simulate specific types of channels or frequency bands. For example the pioneering work of Watterson in HF channel simulation (see ref. 1 through 4 for example) and Bello in troposcatter and line-of-sight (LOS) channel simulation (see ref. 5, 6, and 7 for example) is well-known. Despite these inroads the potential for the use of channel simulation has not been fully tapped as of this date. One needs only to casually peruse papers presented at recent conferences and journals in the field of communications to conclude that a significant amount of field testing of digital radios is still taking place. As a specific example, the performance evaluation of the digital radio to be used in the Digital European Backbone (a U.S. owned and operated transmission network) is being accomplished through a lengthy, and expensive, field testing program. Because the potential for the performance evaluation of radios using channel simulators has not been fully exploited it is worthwhile to reexamine this issue and to summarize the recent advances in this technology.

To start, one should recognize that channel simulators are in reality test instruments. These devices are not an end objective in themselves, but rather a means to an end, namely, the performance evaluation of a radio set. These devices might be more appropriately named radio test sets. The focus needs to be on their capability for the performance evaluation of radios. This helps to justify the cost of their design and construction. Examples will be given later in which signature curves are used for comparison of digital radio performance. These signatures may be generated through the use of a simulator.

The emphasis in this paper is on simulator's to be used in the performance evaluation of digital radios. The effect of fading on analog radios is well understood. It is more difficult to predict the effect of fading on digital radio performance or to design and evaluate various countermeasures to this phenomenon. The multiplicative nature of frequency selective fading precludes the use of additional transmitted power as a solution to the problem. Many approaches to minimizing the effect of frequency selective fading have been proposed and implemented. A discussion of these techniques is outside the scope of this paper. Of interest here is the use of channel simulators for the comparative evaluation of these techniques.

In general radio performance can be estimated using any of the following techniques:

1) theoretical performance evaluation,
2) performance measurements in the field made on representative links, and
3) performance evaluation in the laboratory using a channel simulator.

Theoretical performance evaluation is not tractable for realistic channel conditions. In many cases, the theoretical evaluation is restricted to the additive white gaussian noise (AWGN) situation. On

the other hand, actual digital radio performance measurements can be made through the use of field testing. This, however, tends to be expensive and time-consuming. Typically the radio must be tested under a variety of configurations such as with and without an adaptive equalizer, with and without space diversity, combination of equalization and diversity, different modulations, etc. Field testing therefore tends to be costly. Because of this expense, the field tests tend to be limited in duration which may give an incomplete picture of the radio performance in a variety of conditions. Limited testing also tends to preclude meaningful comparisons of performance for different radio configurations due to the random behavior of the transmission media.

Watterson[3] has described the advantages of simulation. They are accuracy, repeatability, stationarity, availability, range, and cost. A statistically stationary channel simulator imposes no time limitation on the experiment, while field testing tends to be less complete because the media is time-variant and not controllable. Thus experiments can be easily repeated using a channel simulator, but not precisely repeated for field tests. Channel conditions in a simulator can be selected at will (availability), permitting controlled experiments that are impossible in field-testing. Channel conditions in a simulator can cover wide ranges of values, the extremes of which may occur rarely for actual channels.

In-the-field measurements of error performance have been conducted for evaluation purposes. However, under these circumstances the channel and noise characteristics are often changing with time, results are not repeatable, and confidence limits unacceptable. Meaningful comparisons between competing systems require simultaneous measurements over the same path. It is better to perform such comparative measurements in the laboratory under a controlled environment.

The limitations and disadvantages of both theoretical evaluation and field testing have motivated researchers in the field of digital communications to develop channel simulators. Such simulators have been utilized, for example, by Bell Laboratories for the laboratory performance evaluation of digital radios to be utilized in the Bell System. Such simulators should be utilized for the evaluation of radio systems to be employed in military networks as well. The simulators to be used for evaluating military radios have the additional requirement for simulation of intentional jamming interference as well as channel propagation simulation.

2. SIMULATION CONCEPTS

There are several ways to classify channel simulators. Bello[7] describes two basic types, the playback and the synthetic channel simulators. Linfield[8] and Bagdady[9] describe three simulation concepts: dynamic analogies, electronic or electromechanical, and the stored channel. Dynamic analogy simulators are those whereby channel effects of electromagnetic wave propagation are reproduced by some other physical wave phenomena such as an acoustic wave in a turbulent tank of water. Electronic simulation of a channel includes both analog, digital, or hybrid systems. Both the dynamic analogy and electronic simulators come under the synthetic simulator classification used by Bello. Simulators also may be classified as being either real-time or non-real-time. Simulators used for testing radio sets operate in real time. Theoretical calculations of digital radio performance can be performed on a digital computer in non-real-time and are also sometimes called simulators.

The stored channel terminology used by Linfield is conceptually the same as the playback terminology used by Bello. Stored channel simulation is a two-stage process. Channel parameters are first measured and recorded over a suitable period of time. These data are then played back for the purpose of controlling some parameter within the simulator. Bello[7] used a pseudo-random binary phase-shift-key (PSK) transmission signal. The received signal was correlated with delayed replicas of the pseudo-random signal to produce complex estimates of the time-variant impulse response of the channel. This response was digitized and recorded on magnetic tape. These data can then be played back into the simulator to drive the analog complex modulators of an analog tapped delay line model of the channel. In synthetic simulation of the propagation channel, tapped delay lines may also be used, but now the complex tap gains must be generated synthetically.

One drawback of the playback approach is that it may involve considerable time and expense to record sufficient data. However it has an advantage over actual field testing of the radio itself because the data are available for the comparative performance evaluation of several radios or one radio in several configurations.

In the remainder of this paper we shall restrict our discussion to synthetic channel simulation. Before providing specific examples of channel simulators it is necessary to first discuss the signal model and channel filter model concepts of simulation.

The early work of channel simulators was nearly always based upon the concept of the signal-distorting randomly time-variant linear filter. The realization of this model was usually based upon tapped delay line forms. Some of the early work that describes this time-variant channel analytically was performed by Kailath[10]. The received signal $y(t)$ can be represented by the convolution of the input signal $x(t)$ with some transfer function of the channel. Thus

$$y(t) = h(\cdot,t) * x(t) + n(t) \tag{1}$$

where $*$ denotes convolution, $h(\cdot,t)$ is the impulse response function of the channel, and $n(t)$ is the additive noise. The hardware implementation of this model is shown in Figure 1. Two of the most critical features necessary for the model to simulate any time-variant channel properly are the tap spacing and the time-variant tap-gain control signals. The first is critical to the overall bandwidth, and the latter completely controls the time-variant aspects of the filter. It should be noted that these control signals are usually both complex and statistical in nature, and the correlation properties between adjacent tap-gain functions are important. As discussed earlier, the tap-gain

controls can be either generated synthetically or they can be provided by play-back of data recorded on an actual channel. Several simulators at various frequencies have been built based upon the tap-delay-line channel model. An example will be given in a later section of this paper.

As discussed by Linfield[8], the signal model can be represented by the linear combination of signal components propagating by different, but distinguishable, time-variant paths. Thus

$$y(t) = \sum_{n=1}^{\infty} a_n(t)x(t - \tau_n) + n(t). \qquad (2)$$

Here $a_n(t)$ is the time-varying amplitude of the nth path delayed by an amount τ_n relative to the direct path (shortest delay) and n(t) is the additive noise as before. Figure 2, after Linfield[8], is a block diagram of the hardware implementation of this generic model.

Although most of the early work in channel simulators was based upon the tap-delay-line model (including the HF simulator used at the Institute for Telecommunication Sciences) there has been much interest in recent years in simulators based upon the signal model. Examples of both types will be provided in the following sections.

Most of the foregoing discussion is relevant to the simulation of a variety of media (HF, tropo-scatter, or LOS microwave). In the remainder of this paper we shall focus on LOS microwave models and their hardware implementations.

3. MODELS USED IN THEORETICAL CALCULATIONS

Although the emphasis in this paper is on LOS channel models that have been implemented in hardware for the purpose of real-time channel simulation, it is worthwhile to make note of models that have been developed that have resulted in theoretical evaluation of digital radio performance.

Jakes[11] provides the following model for the envelope delay distortion:

$$T(\omega) = r\tau \frac{r + \cos \omega\tau}{1 + 2r \cos \omega\tau + r^2}. \qquad (3)$$

In this two path model, the direct ray has unity amplitude, and the secondary ray has amplitude r (<1) and a propagation delay of τ relative to the direct ray. Jakes stated that in most cases a two-ray model can serve as a good approximation for the relatively narrow (20-40 MHz) channel bandwidths of interest. He used this model along with a number of simplifying assumptions to predict system outage for several types of systems. The system outage was taken to be the time during which the digital radio system "breaks" completely because of excessive delay distortion. "Breaking" in this case means error rates of 10^{-2} or greater; no attempt was made to associate BER quantitatively with envelope delay distortion before the break point is reached.

Greenstein and Czekaj[12,13,14] assume a first-order complex polynomial to model multipath fading. The transfer function, $H(\omega)$, for this model is given by:

$$H(\omega) = A_0 - \omega B_1 + j\omega A_1 \qquad (4)$$

where ω is measured from the center of the channel and A_0, A_1 and B_1 are slowly varying random coefficients. The model applies to channel bandwidths of 40 MHz or less. Greenstein's model includes the joint probability density function (pdf) of the three coefficients. The radio is considered to be vulnerable whenever A_0, A_1, and B_1 are such that receiver eye pattern is closed. A given system design can be evaluated by a) identifying the region of the parameter space (A_0, A_1, B_1) over which the eye closes, and b) integrating the joint pdf of A_0, A_1, and B_1 over that region. The outcome of this computation is the probability of eye closure given that multipath fading is occurring. The objective of Greenstein was not to obtain absolute performance measures such as outage probability but to obtain comparisons and relative rankings for a number of different digital radios. Comparisons can be made between radios having different modulations or different types of adaptive equalizers using Greenstein's techniques.

Greenstein's model has been validated using the same data base used to verify the model developed by Rummler (discussed in the next section). The data base consists of 25000 recorded measurements of received power vs. frequency in a 25.3 MHz band at 6 GHz over a 26.4-mile path in Georgia in June of 1977. Greenstein and Czekaj[13] note that the validity of the model for other paths, frequencies, seasons, etc., is unknown.

There are limitations on the use of the models formulated by Jakes and by Greenstein. Neither results in calculated bit error rate probabilities. Jakes' work resulted in an upper bound on the outage probability, while Greenstein's work resulted not in outage probability, but in the probability of eye closure. Normally link specifications are given in terms of outage probability specified in terms of BER. For example, the Defense Communications System (DCS) specification for the Digital European Backbone (DEB)[15] is based upon system unavailability where unavailability is defined as follows:

a) loss of path continuity for a period in excess of 1 minute,

b) error rate worse than 10^{-6} for a period in excess of 1 minute, and

c) fade outage greater than 5 per minute for a period in excess of 1 minute.

Each DEB LOS microwave link will be designed to achieve a minimum availability of 0.99994. Thus, it is imperative to be able to quantitatively evaluate radio performance in terms of the parameters

AD-A154 031 PROPAGATION INFLUENCES ON DIGITAL TRANSMISSION SYSTEMS: 4/6
PROBLEMS AND SOLU.. (U) ADVISORY GROUP FOR AEROSPACE
RESEARCH AND DEVELOPMENT NEUILLY.. J H BLYTHE
UNCLASSIFIED 08 JUN 84 AGARD-CP-363 F/G 17/2 NL

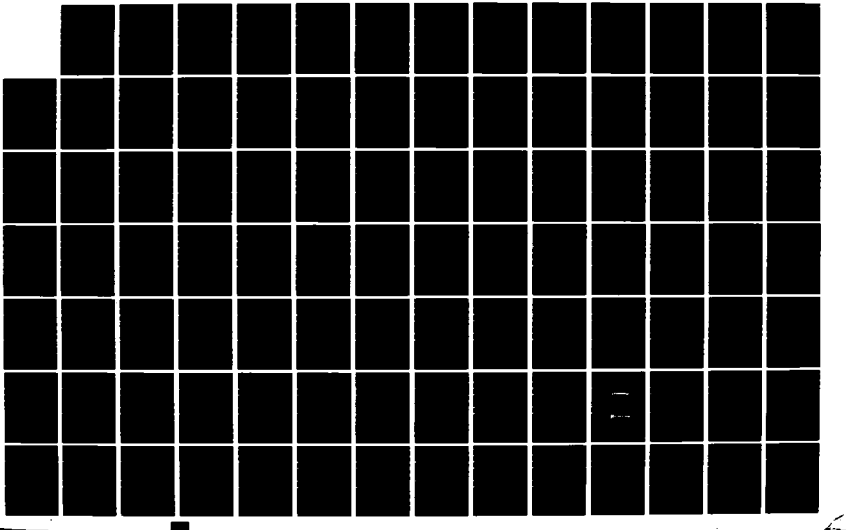

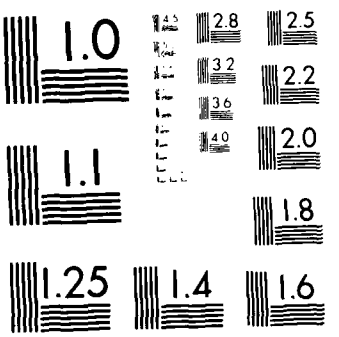

MICROCOPY RESOLUTION TEST CHART

specified for the system. The theoretical approaches formulated by Jakes and by Greenstein do not attain this objective. More will be said later about the need for a performance measure other than BER.

Another limitation on the results of both Jakes and Greenstein is that both assume an exponential distribution of the time delay. As noted by Jakes[11] very little is known about how often particular delays can occur, i.e., the statistical distribution of the delay differences. This is an important point that applies equally well to the use of either a theoretical approach or a simulation approach to digital radio performance evaluation. It is not sufficient to merely know the range of the fading parameters; knowledge of their probabilistic distribution is essential for the determination of outage probabilities. Consider delay time for example. Ruthroff[16] gives the maximum value of the delay difference as:

$$\tau_{max} = 3.7 \left(\frac{D}{20}\right)^3 \text{ ns} \qquad (5)$$

where D is the path length in miles. However, knowledge of τ_{max} is not sufficient. Knowledge of the statistical distribution of τ is also required.

4. RUMMLER'S SIGNAL MODEL

One signal model used in LOS channel simulation that has been widely discussed in the literature is that formulated by Rummler (see reference 17-25). Rummler as well as other researchers have implemented this model in hardware and software for the comparative performance evaluation of digital radios. Matsuura[26] has used a simulator based on this model for limited performance evaluation of the digital radio to be used in the Digital European Backbone. Chao and Lui[27] have used a simulator based on Rummler's model to compare the performance of two types of adaptive equalizers. Wang[28] used the model as part of software calculations for the performance of both a space diversity combiner and an adaptive equalizer. Foschini and Salz[29] have also used Rummler's model as part of a computer program designed to evaluate the upper bound on efficiency indices for various communications techniques (such as modulation schemes, and adaptive equalizers). Greenstein and Prabhu[30] use Rummler's channel model as part of an analytical study to predict multipath fading outages in terrestrial digital radio systems. Because of this apparent widespread acceptance of Rummler's model, it is deemed worthwhile to examine its salient characteristics in some detail.

Rummler's model is given by:

$$H(\omega) = a\,[1 - be^{\pm j(\omega - \omega_0)\tau}]. \qquad (6)$$

The plus and minus signs in the exponent correspond, respectively, with nonminimum and minimum phase states of the channel. Although a physical interpretation is difficult, some insight into the parameters a, b, and τ can be gained through the examination of Figure 3 which is due to Rummler[17]. This is a phasor diagram of the complex voltage transfer function, $H(\omega)$. A three-path model is depicted in Figure 3(a). The direct path has a normalized received amplitude of unity while the remaining paths have amplitudes a_1 and a_2. The second and third rays are delayed with respect to the first by τ_1 and τ_2 seconds, respectively where $\tau_2 > \tau_1$. $H(\omega_2)$ is superimposed on the diagram with $H(\omega_1)$. Here, ω_2 and ω_1 are the highest and lowest radian frequencies in the band. Because Rummler assumed $(\omega_2 - \omega_1)\tau_1 << 1$ (i.e., the delay differential between the first two paths is required to be small), the vector sum of the first two rays is the same for ω_1 and ω_2. This vector sum is designated as "a" and the angle of the sum is designated by $\psi = \omega_0\tau - \pi$ where τ is equal to τ_2, the delay difference in the channel. Figure 3(b) is the resulting simplified phasor diagram for Eq. (6) in which a_2 is set equal to ab (i.e., b is the ratio of the amplitude of the second delay path and the vector sum of the first two ray paths). The model function of (6) may be interpreted as the response of a channel which provides a direct transmission path with amplitude "a", and a second path with a relative amplitude "b" at a delay of τ ns and with a phase of $\omega_0\tau$ + - (independently controllable) at the center frequency of the channel.

Figures 4 through 6 provide additional insight into the model by showing the effect on the magnitude of $H(\omega)$ resulting from variation of the parameters a, b, τ, and f_0. As can be seen "a" affects the depth of the fade notch, "b" affects the shape and the depth of the notch, and "f_0" affects the location of the notch within the receiver passband. The parameter "τ" determines the frequency interval between notches, and also affects the shape of the notch.

Rummler[17] argues that the simple three-path model cannot be used for a channel model because the path parameters lack uniqueness, and that it is impossible to distinguish between such fades unless one of the four parameters (a, b, f_0, and τ) is fixed. He then demonstrates that the parameter τ should have a fixed value of 6.31 ns and that the model provides a good fit for a data base of 25,000 data points. These data were collected over a period of 41 days over a 26.4-mile (42.2 km) link from Atlanta to Palmetto, Georgia. From these data statistical distributions of the parameters a, b, and f_0 were obtained[17]. As a result of fixing the delay at 6.31 ns, the model no longer has a physical interpretation.

The statistics of the parameters of the fixed delay model provide the means for statistically generating all of the channel conditions. The model as represented by (6) can be implemented in hardware. By varying hardware controls in conformance with the statistical distribution of the parameters a, b, and f_0, one can calculate the time during a heavy fading month that the error rate will equal the critical error rate defined as an outage.

Several hardware implementations of (6) have been effected at intermediate frequency (IF) by different researchers[18, 26, 27, 31]. The choice of an IF simulator was based primarily on considerations of signal and noise levels, and the repeatability of adjustments[18]. However, there are some disadvantages to simulation at IF rather than radio frequency (rf) as will be discussed later.

Figure 7 depicts a typical test configuration for evaluating the performance of a digital radio using an LOS channel simulator implemented at IF. Figure 8 depicts an implementation of Rummler's model. Both figures are representative of testing reported both by Rummler[18] and by Matsuura[26] whose work was based on Rummler's model. In Figure 8, the time-delay parameter τ is fixed, and the variable parameters are the magnitude and phase of the individual signal paths. Matsuura's work differed from that of Rummler in that the former allowed τ to be variable. Matsuura used the simulator for some initial testing of the DRAMA (Digital Radio and Multiplexer Acquisition) radio.

Both Matsuura[26] and Giger and Barnett[25] generated so-called "m-curves" for characterization of a digital radio's performance. Typical m-curves are shown in Figure 9 for two different digital radios. The curves are the locus of data points for a specified BER threshold (e.g. 10^{-3}) and for $a = 1$ in (6). The parameters b and ω_0 in (6) are varied (through simulation) to obtain this locus of data points. The curves for different radio configurations can be compared. For the hypothetical example of Figure 9, the System II m-curve might be for a digital radio with an adaptive equalizer and the System I curve might be for the same radio without an adaptive equalizer. The m-curve is sometimes called the "signature" of a radio. Emshwiller[32] used the concept of the radio signature in his early work in the area of modelling and simulation. Giger and Barnett[25] provide comparative m-curves for several actual digital radios. Fenderson, et al.[31] provide m-curves for the DR-6 digital radio with and without an adaptive transversal equalizer.

Using a simulator based on Rummler's model Fenderson, et al.[31] report an outage time improvement factor of the order of 20 for the DR-6 radio with both slope and transversal equalizers in comparison with a DR-6 radio having only a slope equalizer. By way of contrast, they found, using field testing, an improvement of the order of only 3 for the same two radios. This difference in the performance evaluation using simulation in comparison to performance evaluation using field tests is a matter of some concern because the value of channel simulators purportedly is that they can be used in the cost-effective and accurate performance evaluation of radios. Fenderson, et al., explain that the difference between simulation and field test results stems from the fact that the equipment signature obtained using the simulator is a measure of static performance in a noise-free condition and thus does not reflect the effects of multipath fading dynamics or combined dispersive and flat fading. This would seem to present an argument for an improvement in the simulator, because these devices are valuable only if they can be used to accurately characterize a system's performance. If the results obtained through the use of simulation are not compatible with those that would have been obtained in the field, then the value of channel simulation is greatly diminished.

There may be other explanations for the differences in Fenderson's improvement factor determined through simulation and that obtained through field testing. His laboratory evaluation may have been based on pdf's for a, b, and ϕ described by Lundgren and Rummler[18] which was based solely on one path. Conceivably these distributions may not accurately represent the path Fenderson used as a test link. Another factor that may have had an impact was that the phase-locked loop (PLL) is not part of the simulator when the simulation is implemented at IF. Frequency selective fading can have an impact on the performance of PLL's. Thus a channel simulator implemented at IF could result in higher performance estimates than actually obtained in the field.

Typically there are two objectives in using a real-time simulator: 1) to compare the relative performance of two radios, and 2) to determine whether the radio having the best relative performance meets the established outage standards for a link. The first objective can be met by comparing the m-curves for each of the candidate radios being evaluated. In general, if one signature falls entirely below another signature it can be said that the performance of the first radio is better than that of the second. If the signatures cross-over, evaluation of the estimated outage time may be required for more than one radio. The second objective can be achieved only if path statistics (which may be thought of as the channel signature) are well known.

This second objective of simulation, estimation of the probability of outage and comparison to link standards, may be achieved by a procedure for the integration of the area under the m-curve. Emshwiller, who performed pioneering work in use of equipment signatures or m-curves, developed this integration approach for converting these curves into an estimate of outage probability. This approach was refined by Lundgren and Rummler[18], and has been adopted by other researchers such as Matsuura[26]. The probability of outage caused by multipath, P_{OM}, is estimated from the following:

$$P(b, \omega_0) = \iint p(b, \omega_0)\, db\, d\omega_0 \qquad (7)$$

where $p(b, \omega_0)$ is the joint probability density function of the parameters b, ω_0 in (6) and the limit of integration in (7) is the critical region defined by the m-curve since the area under this curve is the b/ω_0 space for which the BER is less than the specified value. Unfortunately this procedure requires a knowledge of the statistics for the parameters used in the voltage transfer function given in (6). Although Rummler[17,18] provides statistics for these parameters, validation is required[26,29].

5. FILTER MODELS

Filter function models are typically implemented with tap delay lines. Tap-delay line simulators are based upon the concept depicted earlier in Figure 1. Much research has focused on the use of tap-delay line simulators for LOS simulation[6,7,33], troposcatter simulation[5,32] and HF simulation[1-4].

The key to the successful use of the tap delay line concept of simulation is in the generation of the tap gain control. In dynamic channel simulation these control parameters must fluctuate so that the simulator can reproduce the time dependent amplitude and phase variations in multipath which account for the dynamics of fading. In practical designs, the amplitude and phase are controlled through the use of complex control signals. These signals may be either of the synthetically generated variety or the stored channel variety.

Bello[6,7] has reported on extensive research in the investigation of a LOS tap-delay line simulator designed to simulate ground-ground (GG), ground-aircraft (GA), aircraft-aircraft (AA), and aircraft-satellite (AS) line-of-sight links. Although the simulator is implemented at IF, it effectively simulates both multipath and Doppler spread that would be observed at UHF and microwave frequencies. The simulator models three propagation modes: refractive multipath, surface multipath and ionospheric scintillation (AS links only). The tap-gain controls may be either synthetically generated or stored channel. The interested reader is referred to references [6] and [7] for a detailed explanation of the mathematical formulation of the synthetic complex tap gains for both refractive and surface multipath and for the channel prober/analyzer equipment used in the recording of channel parameters used in the stored program mode of tap-delay line gain control.

Because the simulator has both modes of tap-gain control, it is able to overcome the disadvantages inherent in either approach alone. The advantage of the playback mode is that it makes no assumptions about the characteristics of the channel, but it has the disadvantage of the time and expense in the field recording of channel parameters. The synthetic channel mode has the disadvantage that it is based upon certain assumptions about the channel, but has the advantage of being able to simulate ranges of propagation conditions at will, in particular conditions which rarely occur and thereby are difficult to capture in the stored channel approach.

The simulator reported by Bello has the capability for the simulation of jamming as well as for simulation of multipath fading.

Another channel simulator that is based on the tap delay line principle is one built for the Defense Communications Engineering Center[34,35]. This is a hybrid (digital and analog) device which is used to simulate a microwave radio as well as the LOS channel. A hybrid computer is used for the radio portion of the simulator (the radio is scaled down in frequency) while the tap-delay line simulates the LOS channel. The mathematical model used in this simulator is based upon the following assumptions: 1) the LOS channel comprises a "direct" component and a "delayed", time dispersive component, 2) the direct component exhibits a slow variation in intensity over a 30-40 dB dynamic range, 3) the differential time delay between the specular and time dispersive components is dependent upon both antenna and meteorological parameters, and 4) the temporal width of the time dispersive component is related to the number of layers of the refractive region and their dimensions. Based upon these assumptions, Smith and Osterholz[34,35] derive an equation for the differential delay, τ, between the direct component and the first arrival of the refracted component. The complex tap weights for the refracted path are generated synthetically.

The block diagram of the hybrid system for simulating both the radios and the LOS channel is provided in Figure 10. The space diversity version of the DRAMA radio has been simulated using this facility. The system has the capability for simulating both of the modulations used in the DRAMA radio (quadrature partial response and quadrature phase shift key) bit-stream generation, partial response filters, transmitter signal processing, IF filter, automatic gain control, baseband equalizer, bit timing recovery, data regeneration diversity combiner and signal quality monitor. The hybrid computer simulation of the AN/FRC-170(V) radio provides an interactive scale model which can be changed programmatically by the simulation user to evaluate the resulting performance of product improvements and design changes. This simulation has been implemented by frequency scaling hybrid computer models of the prototype modem circuits and implementing these models with analog digital computing elements. The two time scales selectable in the simulator are unity and one-tenth. Radio frequencies are scaled down to values that fit within the hybrid computer bandwidth. In the normal time scale mode, IF, bit stream, and baseband frequencies of 70 MHz, 26.112 Mbs, and 13.065 MHz are scaled down to 2.688 kHz, 1 kb/s, and 500 Hz, respectively.

This hybrid simulator has been used for the evaluation of an improved dual-diversity combiner, an improved signal quality monitor, and an improved slope adaptive equalizer for the DRAMA radio. It is currently being used to evaluate a decision feedback equalizer for the DRAMA radio.

6. A PROPOSED NEW CONCEPT FOR AN LOS CHANNEL SIMULATOR

The device that is described in this section is not a simulator in the sense that parameters in the device are varied dynamically in order to simulate the random fluctuations of a real-world LOS microwave channel. Rather it is a device that uses static rather than random variation of device parameters in order to obtain equipment signatures. These signatures can then be used for the comparative evaluation of digital radios.

One of the key differences between the concept of an LOS channel simulator presented in this section and those discussed in the literature is that in the proposed device, the simulation is implemented at rf rather than at IF. Simulation at IF has the disadvantage that some of the critical components of the signal path are left out. These components include the phase locked loop (PLL) and automatic gain control (AGC) systems as well as circuitry that limits the rf bandwidth.

One of the key radio components that is not included when testing radios using an IF simulator is the phase locked loop circuitry. Biswas, et al.[36] note there has been little work on the acquisition behavior of PLL's in an environment that has been corrupted by time varying channel disturbances (such as frequency selective fading) in addition to additive white Gaussian noise (AWGN). Some early work was

done by Weber[37] for analyzing performance of PLL's in lognormal, Rician, and Rayleigh fading channels. Weber calculates the variance of ϕ, the phase error, as a measure of tracking performance of the PLL. For a phase shift key (PSK) system, he shows the degradation of the probability of error (P_E) as a function of the variance σ_ϕ. His results show a large degradation in P_E for a specified E_b/No (bit energy to noise ratio) as σ_ϕ increases in a fading channel. His results are indicative of the need to include the rf sections in the evaluation of digital radio performance using a channel simulator.

Another component that is not included in testing a radio at IF is the AGC circuity which is designed primarily to compensate for flat fading. Just how well the AGC is able to respond to notches within the receiver passband due to frequency selective fading and how the performance of a digital radio is affected are unclear.

For the above reasons the approach we are taking is to implement the simulator at rf rather than at IF. The model on which the simulator is to be based is a two path model and may be classified as a signal model rather than as a filter model. Although simulators have been built using a tap-delay line implementation of a filter model, there are some disadvantages in doing so. Two disadvantages are:

1) The tap-gain functions are complex. They generally are not Gaussian in nature, yet most of the tap delay-line applications treat them as such.
2) The tap-gain functions are not independent of each other, thus making it very difficult to establish proper control for simulating a variety of channels.

The difficulty of synthetically generating the tap gain-controls can be overcome through the use of the playback approach, but this approach also has disadvantages as discussed earlier.

For the reasons given above we have elected to develop a simulator based on the signal model concept, and to implement this concept at rf. We shall now discuss the specifics of this implementation.

The block diagram of the proposed rf simulator is shown in Figure 11. It is based on the simple two-path mathematical model. The most important component is the block labeled as the switch section. This in essence is the delay element for the multipath signal, which follows the upper portion of the diagram. The lower path is the route for the direct path signal. At first glance, this figure implies that the control of the parameters (time delay and phase) is going to require critical adjustments in order to precisely set the position of frequency-selective notches at desired positions (particularly difficult at the rf). This is not the case however, as the control function does not follow this basic approach. In other words, the objective is not to precisely adjust the system for notch position, but to provide a control method that places a great many notches in positions that are both measurable and predictable. This method should alleviate a great deal of concern and implementation problems that others have experienced even at IF.

The signal leveler in Figure 11 serves the purpose of maintaining a nearly constant signal level for the delayed signal path regardless of the amount of delay switched into the path. In other words, it compensates for the insertion loss of the delay elements. The line stretcher has the function of providing very small relative delays between the direct path and the delay path.

Before presenting the proposed control method, we shall briefly describe the function of the switch section block in Figure 11. This is the basic delay line for the multipath signal. It should be noted that it is not a tapped delay line, but one that is composed of a number of elemental delays in a sequence arrangement, each one associated with a switch network. The configuration for each element of the line is shown in Figure 12. In this figure, F is a fixed-delay value common to all switch sections, and d_i is an incremental value of delay. Both sections of the switch operate together, so that in the position shown, the delay of the output signal with respect to the input is given by F. When the switch changes state, this relative delay is incremented by the small amount d_i, and becomes $F + d_i$. The amount of incremental delay increases by powers of 2 for each successive switch section. Thus the delay for the i_{th} section is given by:

$$d_i = 2^i d', \tag{8}$$

where d' is the smallest incremental delay when both switches in Figure 12 are activated. The total delay is the sum of the delays from the individual switch sections. As an illustrative example, let the switch be composed of 8 sections where i = 0, 1, 2 . . . 7. Also assume a value for d' = 0.1 ns. For this arrangement the number (N) of independent incremental delays is given by

$$N = (2^8 - 1) = 255, \tag{9}$$

and we see that the switched-control delay line functions in a binary manner. The range of possible delays thus becomes 0.1 to 25.5 ns when d' = 0.1 ns, in steps of 0.1 ns. These values are for illustration only. The actual incremental values that will be used in the design will depend on a more detailed mathematical development of the binary chain, with respect to other parameter values that will have an effect. Some of these will necessarily have to be derived on an experimental basis, and cannot be quantified at this time. As an example, in Figure 12 we have included a delay value attributed to the switch itself, which is labeled S. This must be minimized by testing and selection of the switch, and also compensated for by adjustments in the value of i and/or the selection of d'.

It is anticipated that the realization of the simulator will permit operation over a frequency range on the order of 1 to 10 GHz. The design will be optimized at one frequency (probably 8 GHz) and calibration procedures will be developed for other operating frequencies. The elemental delay lines will be fabricated from miniature semirigid coaxial lines useful at these frequencies. When, during

the development, a precise measure of the incremental delay is established, and the tolerances due to parameters such as S are determined, then a calculation can be performed that will describe the multipath structure in the frequency domain for each of the (say) 255 switch settings. From this analysis, a number of subset conditions can be determined that will describe the position of a certain notch within a subrange of the signal spectrum, and also provide a predictable count of the number of times during a test run (for any given number of settings) that the notch fell within any particular subrange. It is this process that permits us to elude the problem of trying initially to position a given notch at any particular position within the spectrum. In a sense, the performance evaluation technique becomes a statistical process, but with predictable features that will permit static performance data to be derived.

Since the switched delay line functions as a binary chain, the possibilities of both manual operation and external control are easily seen. A BER measurement made over an interval of 1 s should be adequate for a test of a system having a digital bit rate of the order of ten Mb/s since our interest is in outages due to BER of the order of 10^{-6}. By placing the switched line under control of a simple clock (1 s intervals) a complete set of 255 measurements (the full range of an 8-section line) can be performed automatically in as many seconds (less than 5 min.). Each of these sets would be developed for a fixed ratio between the direct path and multipath magnitudes. This ratio is controlled by the programmable attenuator in the multipath signal line of Figure 11. The overall signal level at the output (input to system under test) is controlled by a similar attenuator following the two-signal summing junction. These attenuators are also binary switched units, and can be controlled in the same or similar fashion as that applied to the delay-line unit.

The development of this simulator is planned in phases. The first task is to prove the basic concept of an rf, two-path, LOS simulator. Detailed design of the simulator depicted in Figure 11 will be accomplished. All necessary hardware for the basic simulator will be acquired and assembled. The simulator control will be accomplished through the use of a simple clock. Testing and calibration of the simulator will be performed in order to verify that the simulator output is representative of LOS fading. This testing will consist of using the clock control to step sequentially through the 8 switch sections thereby stepping through the full range of delays of the multipath signal. This procedure will be repeated for a variety of attenuator settings. The output of the simulator will be monitored on a spectrum analyzer to verify that the notch is being correctly placed within the spectrum.

The objective of the next task is to refine the capabilities of the simulator by using a microcomputer to control the setting of the switches and attenuators. The microcomputer will also be utilized to collect and analyze bit-error-rate (BER) or synchronous-error-second (SES) data. Figure 13 depicts the test configuration. A data bit stream generator will be fed into the transmitter portion of the radio under test. The input signal to the simulator will come from the rf section of the transmitter preceding the TWT, and the output will go to the rf input of the receiver. The output from the receiver will be fed into an error analyzer. Information on the BER or SES will be recorded on magnetic tape or other mass storage under control of the microcomputer. The software for performing the control, recording, and data analysis functions will be developed under this task. A microcomputer, a magnetic tape drive (or other storage device), and the equipment to provide data bit stream generator and error analysis will be procured under this task. A second channel will be added to the simulator in order to provide the capability for evaluation of space diversity radios.

The simulator will be utilized to analyze the performance of a DRAMA radio. The testing will be performed on a DRAMA radio in a configuration for which field test data are available. The DRAMA radio is currently undergoing testing at Pt. Mugu, California on a 65-mile (104-km), over-water path. The radio is being tested using various configurations of adaptive equalization and space diversity combining. The simulator will be utilized to evaluate the DRAMA radio in the same configuration as that used in the Pt. Mugu tests. This will lend credibility to use of the simulator for radio performance evaluation assuming that the laboratory results are compatible with the results obtained in the prior field testing of the DRAMA radio.

A typical set of measurements for a given radio configuration will consist of stepping through each of the possible delays (say 255) for a given attenuation setting. This is then repeated for additional attenuation settings, i.e., differences in amplitude between the direct path and the delay path. For each delay switch and attenuator setting, the BER and/or SES data will be recorded on the floppy disk. This will permit the generation of plots similar to "m-curves" for different radio configurations. Here the plots will be attenuation vs. delay for fixed BER or percent SES as opposed to the plot of fade depth vs. notch frequency for a fixed BER as depicted previously for the m-curves of Figure 9. The use of these curves for comparing the performance of different radios tends to be somewhat subjective if the curves cross each other at some point. A quantitative comparison can be obtained by using the numerical integration of the area under the curves as suggested by Easwaller[32].

A jamming signal simulator will be added at a later date to the hardware depicted previously in Figure 11. The capability to simulate the jamming threat as well as the multipath fading phenomenon is particularly needed for the development and testing of electronic counter-counter measure techniques that are expected to be employed in the next generation digital microwave radios to be used in the Defense Communications System.

5. DIGITAL RADIO PERFORMANCE EVALUATION MEASURES

Channel simulators should be viewed as tools for the performance evaluation of radios. Typically their use is in the comparative performance evaluation of one radio against another or the comparative evaluation of different configurations of a sigle radio (e.g., with and without an adaptive equalizer). In order to perform this evaluation some performance measure is required. In field testing the measure usually reported is BER. In recent simulation work, the measure frequently used is the equipment signature or m-curve. The m-curve is the locus of points for a fixed BER and is a plot of fade depth vs. notch position. Thus BER is the first performance measure one usually thinks of in connection with digital radio performance evaluation.

Unfortunately BER is an ambiguous measure unless the length of time over which the BER is measured is specified and becomes uniform in application. This is the only way that the data from different experiments can be compared. By nature, the errors caused by multipath propagation develop in bursts of various lengths. For a given error burst, the longer the duration of the measurement interval, the lower the BER becomes, if no more errors occur. For this reason two values of BER when compared may give a completely false conclusion if they were not measured over a comparable period of time.

Another performance measure that is frequently encountered is system outage. This measure is usually based on some threshold of BER activity either with or without a specified unit of time. An outage is declared when the BER exceeds the established threshold. Frequently reports in the literature do not specify the length of time over which the BER is measured, the length of time the condition must last before an outage is declared, or the length of time error-free conditions are resumed before the end of outage is declared.

Another problem with the measurement criteria is in regard to the system mission. It is generally recognized that the level of performance for data transmission must be better (in terms of BER) by several orders of magnitude than for voice transmission. The absolute requirements for each are not well specified.

Because of the problems noted above, it appears desirable for some performance measure to be utilized. The CCITT[38,39] has adopted the following conventions for an international digital connection at 64 kb/s:

1) at least 90 percent of 1-minute intervals with error rate of 10^{-6} or less averaged over that minute, and
2) at least 92% of 1-second intervals to be error-free (i.e., to have zero error rate).

The first criterion was chosen for voice telephone calls, while the second was chosen for data transmission. Recent proposals have suggested the use of an interval of 0.1 s instead of 1 s[38].

There has also been a proposed new definition for the failure of a digital system so that outage is defined without ambiguity. Complete failure has been tentatively defined as beginning when ten consecutive seconds each have an error rate of 10^{-3} or worse and ending when ten consecutive seconds each have an error rate of better than 10^{-3}.

Another measure that is sometimes used is the synchronous error second (SES) measure. Here the second of time always starts synchronously with the first error. Variations in performance criteria based on SES have been proposed, such as defining outage as a specified number of continuous SES's with a BER specified for each.

The U.S. National Telecommunications and Information Administration has submitted a contribution[41] to the CCITT Study Group XVIII in which it is demonstrated that there is a need for at least two parameters to characterize transmission system accuracy. It is stated in this contribution that "a system with independent errors can appear to be more accurate than a system with clustered errors if the specification is based on Bit Error Probability, but less accurate if the specification is based on Error Free Seconds." It is suggested in the contribution that two parameters (e.g. bit error probability and a time-based error ratio such as percent error free seconds) may be satisfactory for the digital performance evaluation standard.

Obviously, there is still work to be done in the standardization of measurement parameters. Until such standardization is accomplished it will be difficult to compare digital performance results (obtained either in the field or in the laboratory with a simulator) reported by different researchers.

8. CONCLUSIONS

Table 1 provides a summary of models discussed in this paper that have been implemented in hardware. Table 2 lists models that have been used in theoretical calculations of radio performance (sometimes called software simulators). Some models, such as Rummler's model, have been used both in hardware simulators and in theoretical calculations of digital radio performance. For the theoretical calculation category, the results are typically upper bounds on digital radio performance, involve approximations in the calculation process, and are based on a number of assumptions. While such calculations serve a useful purpose for establishing the baseline for systems performance, we conclude that simulation is needed for a more precise comparison of different digital radios against each other and against the performance standard defined for the network.

ACKNOWLEDGMENT

The authors wish to acknowledge the suggestions of Mr. R. Linfield whose encouragement made this paper possible.

REFERENCES

[1] Watterson, C.C., and R.M. Coon, "Recommended Specifications for Ionospheric and Atmospheric Noise Simulators," Report ERL 112-ITS-89, U.S. Department of Commerce, Boulder, Co 80303, September 1969.

[2] CCIR, "HF Ionospheric Simulators," CCIR Rept. 549, XIIIth Plenary Assembly, Geneva, 1975, pp. 66-72.

[3] Watterson, C.C., "HF Channel-simulator Measurements on the KY-870/P FSK Burst-communication Modem - Set 1," NTIA Rept. CR-81-13, U.S. Department of Commerce, Boulder, CO 80303, August 1981.

[4] Watterson, C.C., "HF Channel-simulator Measurements on the KY-879/P FSK Burst-communication Modem - Set 2," NTIA Rept. CR-82-20, U.S. Department of Commerce, Boulder, CO 80303, December 1982.

[5] Bello, P.A., and L. Ehrman, "Troposcatter Modem Performance Prediction with Complex Gaussian Troposcatter Channel Simulator," Int. Conf. on Comm., 1969.

[6] Bello, P.A. "Wideband Line-of-Sight Channel Simulation System," AGARD Conf. Proc. No. 244, pp. 12-1 to 12-14, October 1977.

[7] Bello, P.A., "Wideband Line-of-Sight Channel Simulator," RADC-TR-78-118, Rome Air Development Center, Griffiss AFB, NY 13441, June 1978.

[8] Private communications: Unpublished report by R.F. Linfield, "Simulation of Avionics Line-of-Signt Radio Transmission Channels," OT Tech. Memo 75-204, U.S. Department of Commerce, Boulder, CO 80303, July 1975.

[9] Bagdady, E.J., "Principles of Simulation of Randomly Time-variant Multipath Propagation," Int. Conf. on Comm., 1969.

[10] Bagdady, E.J., Editor, "Lectures on Communication System Theory," McGraw-Hill, NY, NY, Chapter 6 (T. Kailath), pp. 95-123, 1961.

[11] Jakes, W.C., "An Approximate Method to Estimate an Upper Bound on the Effect of Multipath Delay Distortion on Digital Transmission," IEEE Trans. on Comm., COM-27, No. 1, January 1979, pp. 76-81.

[12] Greenstein, L.J., "A Multipath Fading Channel Model for Terrestrial Digital Radio," IEEE Trans. on Comm., COM-26, No. 8, August 1978, pp. 1247-1250.

[13] Greenstein, L.J., and B.A. Czekaj, "Performance Comparisons Among Digital Radio Techniques subjected to Multiapth Fading," Int. Conf. on Comm., (ICC-81) Denver, CO, June 1981.

[14] Greenstein, L.J., and B.A. Czekaj, "A Polynominal Model for Multipath Fading Channel Responses," BSTJ, Vol. 59, No. 7, September 1980, pp. 1197-1225.

[15] Defense Communications Agency, Management/Engineering Plan for the Digital European Backbone, December 1980.

[16] Ruthroff, C.L., "Multiple-path Fading on Line-of-Sight Microwave Radio Systems as a Function of Path Length and Frequency," Bell Syst. Tech. J., September 1971, pp. 2375-2398.

[17] Rummler, W.D., "A New Selective Fading Model: Application to Propagation Data," Bell Syst. Tech. J., 58, No. 5, May-June 1979, pp. 1037-1071.

[18] Lundgren, W.C., and W.D. Rummler, "Digital Radio Outage Due to Selective Fading - Observation vs. Prediction From Laboratory Simulation," Bell Syst. Tech. J., 58, No. 5, May-June 1979, pp. 1073-1100.

[19] Rummler, W.D., "Time and Frequency Domain Representation of Multipath Fading on Line-of-Sight Microwave Paths," Bell Syst. Tech. J., 59, No. 5, May-June 1980, pp. 763-796.

[20] Rummler, W.D., "More on the Multipath Fading Channel Model," IEEE Trans. on Comm., COM-29, No. 3, March 1981, pp. 346-351.

[21] Rummler, W.D., "A Simplified Method for the Laboratory Determination of Multipath Outage of Digital Radios in the Presence of Thermal Noise," IEEE Trans. on Comm., COM-30, No. 3, March 1982, pp. 487-494.

[22] Rummler, W.D., "A statistical Model of Multipath Fading on a Space Diversity Radio Channel," Int. Conf. on Comm. (ICC-82), Philadelphia, PA., June 1982, pp. 3B.4.1-3B.4.6.

[23] Rummler, W.D., "A Statistical Model of Multipath Fading on a Space Diversity Radio Channel," Bell Syst. Tech. J., 61, No. 9, November 1982, pp. 2185-2219.

[24] Rummler, W.D., "A Comparison of Calculated and Observed Performance of Digital Radio in the Presence of Interference," IEEE Trans. on Comm., COM-30, No. 7, July 1982, pp. 1693-1700.

[25] Giger, A.J., and W.T. Barnett, "Effects of Multipath Propagation on Digital Radio", IEEE Trans. on Comm., COM-29, No. 9, September 1981, pp. 1345-1352.

[26] Matsuura, S.T., "Estimated Performance of a OPRS Radio in the Presence of Frequency Selective Fading," U.S. Army Communications - Electronics Engineering Installation Agency, Tech Rept. EMEO-PED-81-8, Fort Huachuca, AZ 85613, June 1981.

[27] Chao, C.L., and G.L. Lui, "A Comparative Performance Evaluation of Slope Equalizers and Decision Directed Weight Control Equalizers," TRW Rept. CS-009, March 1982.

[28] Wang, Y.Y., "Simulation Performance of a Space Diversity Combiner for 6 GHz Digtal Radio," IEEE Trans. on Comm., COM-27, No. 12, December 1979, pp. 1896-1907.

[29] Foschini, G.J., and J. Salz, "Digital Communications over Fading Radio Cahnnels," Bell Syst. Tech. J., Vol. 62, No. 2, February 1983, pp. 429-456.

[30] Greenstein, L.J., and V.K. Prabhu, "Analysis of Multipath Outage with Applications to 90 Mb/s PSK Systems at 6 and 11 GHz," IEEE Trans. on Comm., COM-27, No. 1, January 1979, pp. 68-75.

[31] Fenderson, G.L., S.R. Shepard, and M.A. Skinner, "Adaptive Transversal Equalizer for 90 mb/s 16-QAM Systems in the Presence of Multipath Propagation," Int. Conf. on Comm., (ICC-83) June 1983, Boston, pp. C8.7.1-C8.7.6.

[32] Emshwiller, M., "Characterization of the Performance of PSK Digital Radio Transmission in the Presence of Multipath Fading," Intl. Conf. on Comm. (ICC-78), Toronto 1978, pp. 47.31-47.3.6.

[33] Bussgang, J.J., B. Goldberg, and E.H. Getchell, "Simulation and Probing of Radio Channels," Telecommunications, January 1974, pp. 17-21.

[34] Smith, D.R., and J.L. Osterholz, "Assessment of Frequency Selective Fading on DCS Transmission System Performance," (report no. 1), Defense Communications Engineering Center Report EP-5-79, August 1979.

[35] Klukis, M.K., J.J. Viviano, and R.B. Wavell, "LOS Selective Fading and AN/FRC-170(V) Radio Hybrid Computer Simulation," Martin-Marietta Aerospace report produced under contract DCA 100-81-C-0016, Defense Communications Engineering Center, September 1982.

[36] Biswas, B.N., S.K. Ray, and A.K. Bhattacharza, "Phase locked Loop Acquisition for a Fading Signal in a Noisy Environment," IEEE Trans. on Comm., COM-27, No. 1, January 1979, pp. 170-176.

[37] Weber, W.J., "Performance of Phased-locked Loops in the Presence of Fading Communications Channels," IEEE Trans. on Comm., COM-24, No. 5, May 1976, pp. 487-499.

[38] Johannes, V.I., "Performance Parameters for Digital Communications," Proceedings of the IEEE, Vol. 71, No. 4, April 1983. p. 539.

[39] International Telephone and Telegraph Consultative Committee (CCITT), "Error Performance of an International Digital Connection Forming Part of an Integrated Services Digital Network," Rec. G.821, in VIIth Plenary Assembly Yellow Book, Vol. III, Geneva, Switzerland: CCITT, 1980.

[40] Private communications: Unpublished report by C.L. Chao and G.L. Lui, "An Improved technique for Calculating Outage Time Due to Multipath Fading Effect".

[41] CCITT Study Group XVIII Contribution No. 172-E, "Effect of Clustering on the Selection of Error Probability Parameters", Question 9/XVIII, April 1983.

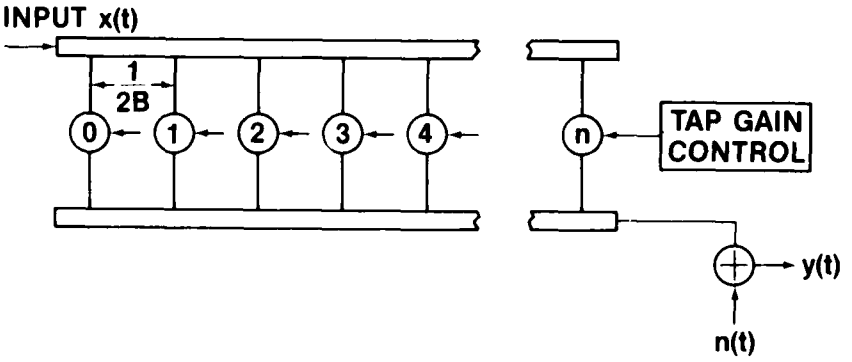

Figure 1. Block diagram of a basic tap delay-line simulator.

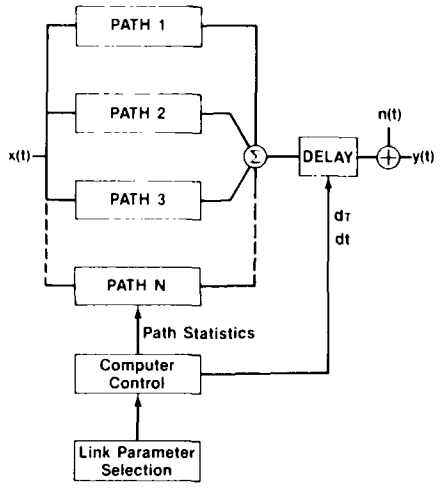

Figure 2. General block diagram of a simulator based on the signal model.

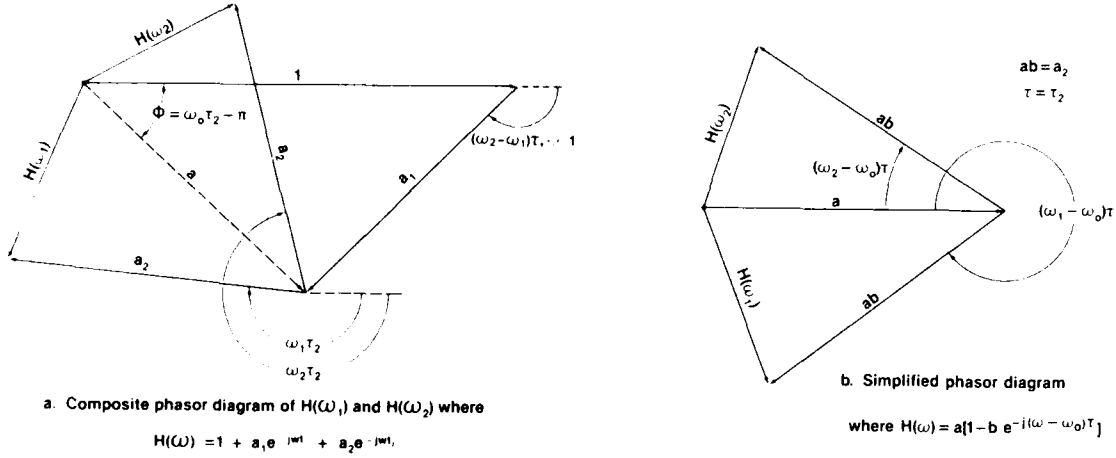

a. Composite phasor diagram of $H(\omega_1)$ and $H(\omega_2)$ where

$H(\omega) = 1 + a_1 e^{j\omega\tau_1} + a_2 e^{-j\omega\tau_2}$

b. Simplified phasor diagram

where $H(\omega) = a[1 - b\, e^{-j(\omega - \omega_0)\tau}]$

Figure 3. Phasor diagrams (after Rummler [17]).

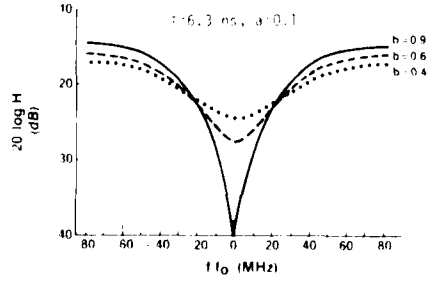

Figure 4. Rummler's channel model showing the effect of varying the parameter b.

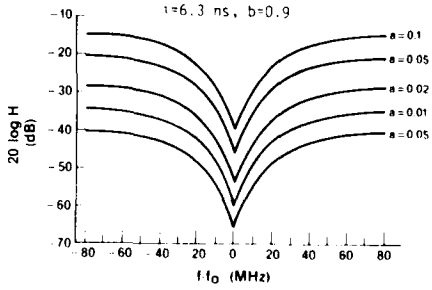

Figure 5. Rummler's channel model showing the effect of varying the parameter a.

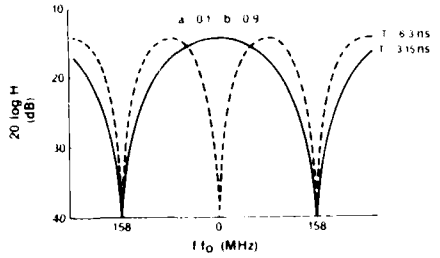

Figure 6. Rummler's channel model showing the effect of varying the parameter τ.

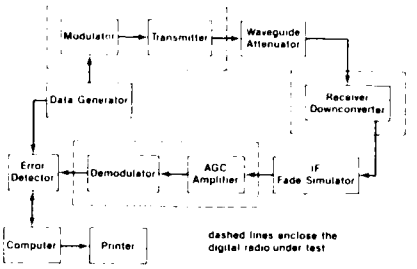

Figure 7. Typical channel simulator test configuration for IF.

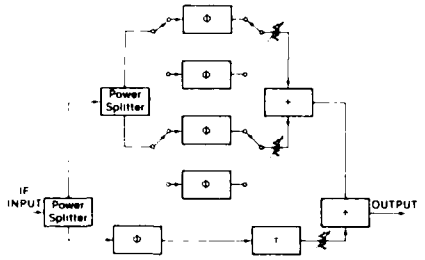

Figure 8. A block diagram for a simple three-ray simulation process.

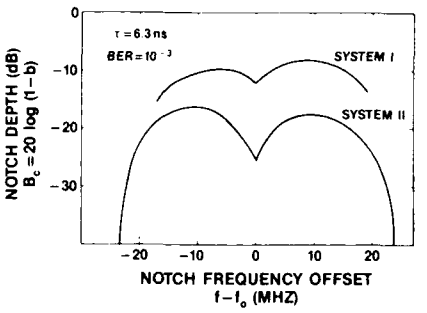

Figure 9. Typical "m-curves" for two digital radio systems.

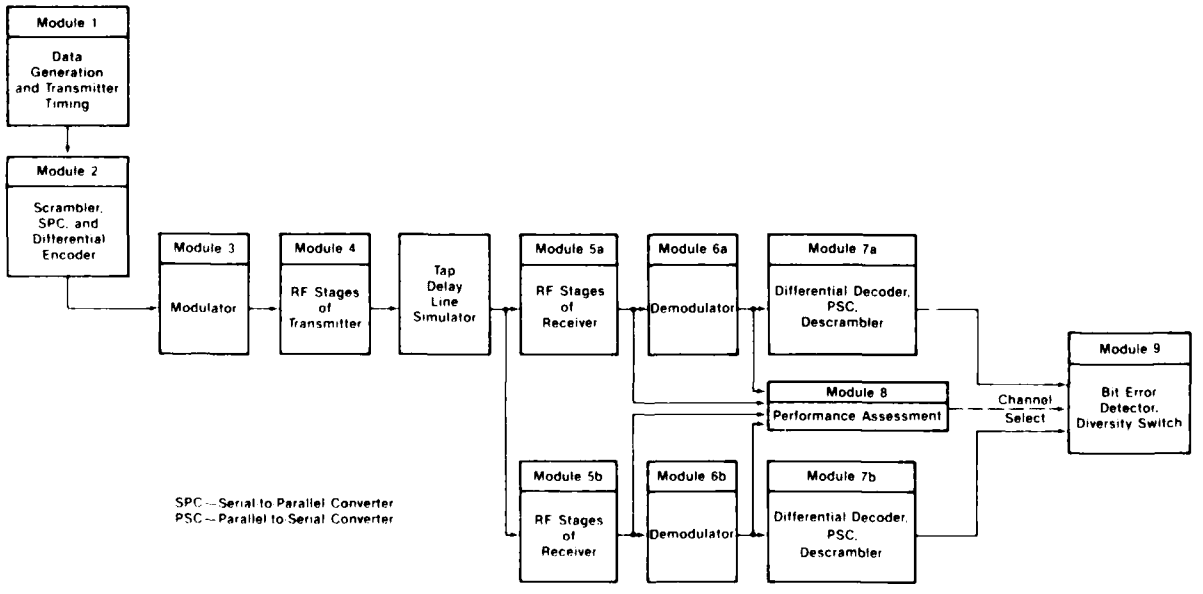

Figure 10. Hybrid dual diversity simulator developed for Defense Communications Engineering Center.

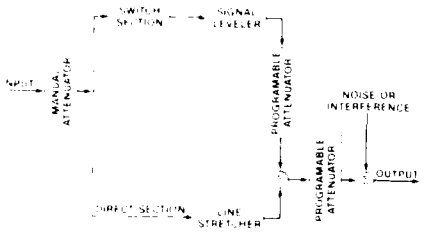

Figure 11. Block diagram of the proposed rf simulator.

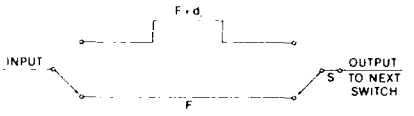

Figure 12. An illustration of a single delay element of the switch section in Figure 11.

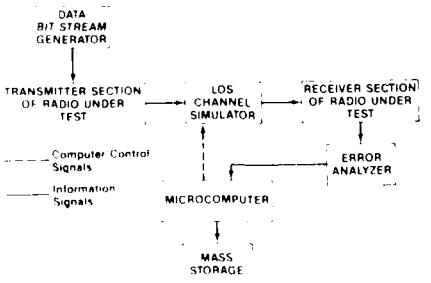

Figure 13. Radio test configuration.

Table 1. Summary of LOS Channel Models and Hardware Simulator Information

Author/Organization	Model Type	Model	Reference	Comments
[illegible]	Tap delay-line filter model	$y(t) = n_0 t, \}*x(t) + n(t)$	6,7	This simulator is implemented at IF, i.e., it simulates ground-air, air-air-ground, air-air-satellite, and ground-ground paths. It simulates refractive multipath, surface multipath, and ionospheric scintillation. Simulated fading signals can be input into the device. The multiplex tap gains can be either synthetically generated or played back.
[illegible] Systems Research Laboratories Engineering Computer	Tap delay-line filter model	$y(t) = n_0 t, \}*x(t) + n(t)$	34,35	Hybrid computer is used to simulate the entire radio system as well as the LOS microchannel. The analog frequency in order to fit within the hybrid computer's bandwidth. The simulator has been used to evaluate adaptive equalizers for the DRAMA radio.
Rummler, et al (Bell Laboratories)	Pseudo 3-path signal model	$H(\omega) = a[1 - be^{-j(\omega - \omega_0)\tau}]$	17-24	This mode has a nonphysical interpretation. It was formulated to fit a data base of 25,000 data points collected on a 26.4 mile path in Georgia. The model has been used widely for both theoretical calculations and as the basis for a simulator. It is implemented at IF. The model has been extended to a space diversity version.
Geiger and Barnett	Rummler's model	Rummler's model	25	Geiger and Barnett report the use of a simulator based on Rummler's model to obtain equipment signatures for several different radios.
Fenderson, et al. Bell Laboratories)	Rummler's model	Rummler's model	31	Fenderson, et al, use a simulator implementation of Rummler's model to compare a DR-6 radio with and without a transversal equalizer. Both configurations had a slope equalizer. The improvement factor for the radio with a transversal equalizer was approximately 20 using a simulator for testing and approximately 3 in field testing.
Matsuura (U.S. Army Comm.-Elect. Engr. Installation Agency)	Rummler's model	$H(\omega) = a[1 + be^{-j(\omega\tau + \phi)}]$	26	Matsuura used a simulator based on Rummler's model and Jakes'[11] method for calculating outage to estimate the performance of the DRAMA radio with both space diversity and adaptive equalization. The simulator implemented at IF.
Cao and Lui (TRW)	Rummler's model		27	This simulator was used in the comparative evaluation of different types of adaptive equalizers.
Proposed simulator (ITS)	Two-path signal model	$H(\omega) = a[1 + re^{j\omega\tau}]$	--	This simulator is unique in that it is being implemented at rf. A baseline version of the simulator is currently being built in order to prove the concept.

AN H.F. SIMULATOR FOR USE WITH REAL TIME CHANNEL EVALUATION SYSTEMS

by

J. Dawson
University of York
Heslington
York YO1 5DD
U.K.

SUMMARY

There is a growing interest in the use of RTCE (Real time channel evaluation) to improve the performance of HF communication systems. This implies the need for a method of comparative testing between different systems in a repeatable environment. An ability to conduct such tests in real time would also be advantageous, since the performance of a channel evaluation system depends not only on its ability to select the best available channel, but also the time it takes to do so.

The paper describes an HF simulator constructed at York University as an off-air test bed for an HF radio link using real time channel evaluation aided frequency selection. The simulator implements the basic channel model proposed by Watterson et al [Watterson 69a] with the addition of several novel features applicable to real time channel evaluation systems.

a) Rapid selection of channel parameters from stored sets
This enables an RTCE based system to control the simulator as a direct replacement for a real HF station selection one out of n available channels.

b) A realistic and repeatable interference simulation
Previously two methods of introducing interference into a simulation have been used, either recorded interference or locally generated noise (usually gaussian white noise). Neither of these is particularly attractive as the former is difficult to repeat at different sites and the latter is unrepresentative of real interference. The York simulator aims to incorporate a realistic but repeatable interference simulation with variable spectrum shape and fade rate.

c) Time variable channel statistics
Stationary channel statistics are ideal for error rate measurements on modems, allowing measurements to take place over an extended period of time. However a real time channel evaluation scheme must react to changing conditions, making time variable statistics a desirable feature.

The paper is mainly concerned with the novel aspects of the simulator rather than detailed design. A brief resume of channel modelling and atmospheric noise is given for completeness.

1. INTRODUCTION

The University of York is currently conducting research into the application of real time channel evaluation (RTCE) to H.F. communication in collaboration with the University of Kent at Canterbury (UK). For the purpose of this research an H.F. link is being established between the two sites. The equipment being used has several novel features that are intended to allow its use as a research tool for RTCE, whilst at the same time costing little more than a simple low power (200W) H.F. station:

1) Fast tuning digitally controlled transmitter, receivers and aerial tuning unit (ATU). (approx. 100ms channel change time)

2) Programmable digital signal processor instead of a hard wired modem

The aim of the research programme is not only to examine RTCE techniques but also to produce an RTCE sytem which can be integrated into the design of an H.F. station without the expense of separate sounding equipment , or the requirement for a skilled operator to interpret its results. Fig. 1 shows The equipment configuration at York illustating the incorporation of the H.F. simulator into the system.

Although the York - Canterbury link will provide a useful, real and reasonably difficult path over which to work , it was decided that an H.F. channel simulator would be a very useful tool during system development. The advantages of using a simulator instead of a real link are summarised below.

a) Repeatability
This has been found useful for comparative testing of modulation and coding schemes and modem performance. Similarly repeatability is highly desirable when assessing the performance of an RTCE technique.

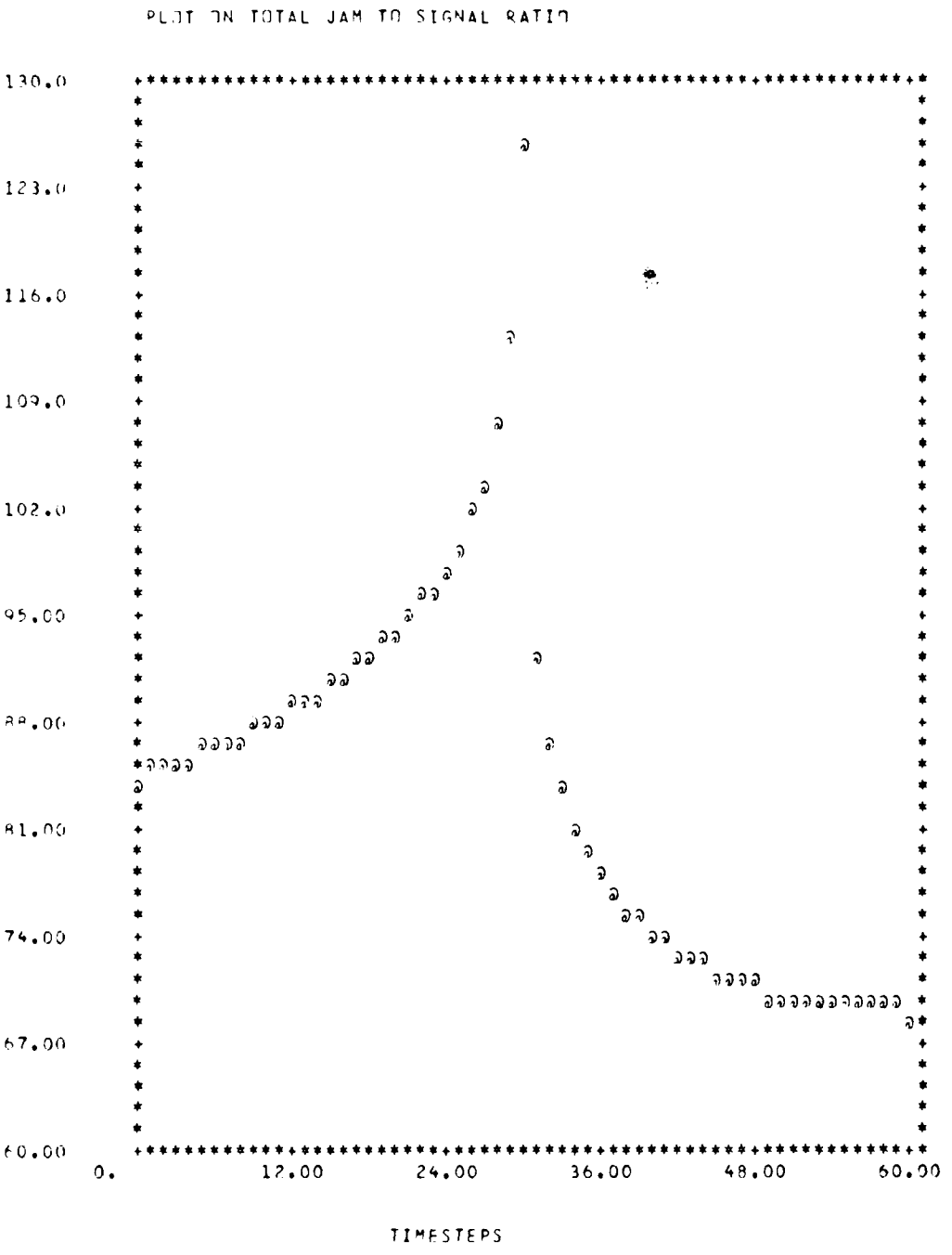

Fig. 6 Example of output (diagram)

VEHICLE INFORMATION :

TIME STEP	ACTUAL TIME	POSITIONS X	Y (METERS)	HEIGHT	ATTITUDES ROLL	PITCH (DEGREES)	HEADING	SATELLITE ASPECT ANGLES THETA (DEGREES)	PHI	DYN. SEQ.	TOTAL JAM TO SIGNAL RATIO (DB)	RECEIVED SAT. POWER (DBW)
0	00.20.00	200000.0	.0	1666.7	.0	.0	270.0	170.6	180.0	L	84.4	-194.7
1	00.20.20	198333.3	.0	1677.8	.0	.0	270.0	170.6	180.0	L	84.7	-194.7
2	00.20.40	196666.7	.0	1688.9	.0	.0	270.0	170.6	180.0	L	85.0	-194.7
3	00.21.00	195000.0	.0	1700.0	.0	.0	270.0	170.6	180.0	L	85.3	-194.7
4	00.21.20	193333.3	.0	1711.1	.0	.0	270.0	170.5	180.0	L	85.6	-194.7
5	00.21.40	191666.7	.0	1722.2	.0	.0	270.0	170.5	180.0	L	86.0	-194.7
6	00.22.00	190000.0	.0	1733.3	.0	.0	270.0	170.5	180.0	L	86.3	-194.7
7	00.22.20	188333.3	.0	1744.4	.0	.0	270.0	170.5	180.0	L	86.7	-194.7
8	00.22.40	186666.7	.0	1755.6	.0	.0	270.0	170.5	180.0	L	87.1	-194.7
9	00.23.00	185000.0	.0	1766.7	.0	.0	270.0	170.5	180.0	L	87.5	-194.7
10	00.23.20	183333.3	.0	1777.8	.0	.0	270.0	170.5	180.0	L	87.9	-194.7
11	00.23.40	181666.7	.0	1788.9	.0	.0	270.0	170.5	180.0	L	88.3	-194.7
12	00.24.00	180000.0	.0	1800.0	.0	.0	270.0	170.5	180.0	L	88.8	-194.7
13	00.24.20	178333.3	.0	1811.1	.0	.0	270.0	170.5	180.0	L	89.3	-194.7
14	00.24.40	176666.7	.0	1822.2	.0	.0	270.0	170.5	180.0	L	89.8	-194.7
15	00.25.00	175000.0	.0	1833.3	.0	.0	270.0	170.5	180.0	L	90.4	-194.7
16	00.25.20	173333.3	.0	1844.4	.0	.0	270.0	170.5	180.0	L	90.9	-194.7
17	00.25.40	171666.7	.0	1855.6	.0	.0	270.0	170.5	180.0	L	91.6	-194.7
18	00.26.00	170000.0	.0	1866.7	.0	.0	270.0	170.5	180.0	L	92.3	-194.7
19	00.26.20	168333.3	.0	1877.8	.0	.0	270.0	170.5	180.0	L	93.0	-194.7
20	00.26.40	166666.7	.0	1888.9	.0	.0	270.0	170.5	180.0	L	93.8	-194.7
21	00.27.00	165000.0	.0	1900.0	.0	.0	270.0	170.5	180.0	L	94.8	-194.7
22	00.27.20	163333.3	.0	1911.1	.0	.0	270.0	170.5	180.0	L	95.8	-194.7
23	00.27.40	161666.7	.0	1922.2	.0	.0	270.0	170.5	180.0	L	96.9	-194.7
24	00.28.00	160000.0	.0	1933.3	.0	.0	270.0	170.5	180.0	L	98.2	-194.7
25	00.28.20	158333.3	.0	1944.4	.0	.0	270.0	170.4	180.0	L	99.8	-194.7
26	00.28.40	156666.7	.0	1955.6	.0	.0	270.0	170.4	180.0	L	101.6	-194.7
27	00.29.00	155000.0	.0	1966.7	.0	.0	270.0	170.4	180.0	L	104.0	-194.7
28	00.29.20	153333.3	.0	1977.8	.0	.0	270.0	170.4	180.0	L	107.3	-194.7
29	00.29.40	151666.7	.0	1988.9	.0	.0	270.0	170.4	180.0	L	113.3	-194.7
30	00.30.00	150000.0	.0	2000.0	.0	.0	270.0	170.4	180.0	L	125.3	-194.7
31	00.30.20	148333.3	.0	2011.1	.0	.0	270.0	170.4	180.0	L	92.5	-194.7
32	00.30.40	146666.7	.0	2022.2	.0	.0	270.0	170.4	180.0	L	86.8	-194.7
33	00.31.00	145000.0	.0	2033.3	.0	.0	270.0	170.4	180.0	L	83.4	-194.7
34	00.31.20	143333.3	.0	2044.4	.0	.0	270.0	170.4	180.0	L	81.0	-194.7
35	00.31.40	141666.7	.0	2055.6	.0	.0	270.0	170.4	180.0	L	79.2	-194.7
36	00.32.00	140000.0	.0	2066.7	.0	.0	270.0	170.4	180.0	L	77.7	-194.7
37	00.32.20	138333.3	.0	2077.8	.0	.0	270.0	170.4	180.0	L	76.5	-194.7
38	00.32.40	136666.7	.0	2088.9	.0	.0	270.0	170.4	180.0	L	75.6	-194.7
39	00.33.00	135000.0	.0	2100.0	.0	.0	270.0	170.4	180.0	L	74.7	-194.7
40	00.33.20	133333.3	.0	2111.1	.0	.0	270.0	170.4	180.0	L	74.0	-194.7
41	00.33.40	131666.7	.0	2122.2	.0	.0	270.0	170.4	180.0	L	73.4	-194.7
42	00.34.00	130000.0	.0	2133.3	.0	.0	270.0	170.4	180.0	L	72.8	-194.7
43	00.34.20	128333.3	.0	2144.4	.0	.0	270.0	170.4	180.0	L	72.4	-194.7
44	00.34.40	126666.7	.0	2155.6	.0	.0	270.0	170.4	180.0	L	72.0	-194.7
45	00.35.00	125000.0	.0	2166.7	.0	.0	270.0	170.4	180.0	L	71.6	-194.7
46	00.35.20	123333.3	.0	2177.8	.0	.0	270.0	170.3	180.0	L	71.3	-194.7
47	00.35.40	121666.7	.0	2188.9	.0	.0	270.0	170.3	180.0	L	71.0	-194.7
48	00.36.00	120000.0	.0	2200.0	.0	.0	270.0	170.3	180.0	L	70.7	-194.7
49	00.36.20	118333.3	.0	2211.1	.0	.0	270.0	170.3	180.0	L	70.5	-194.7

Fig. 5 Example of output (table)

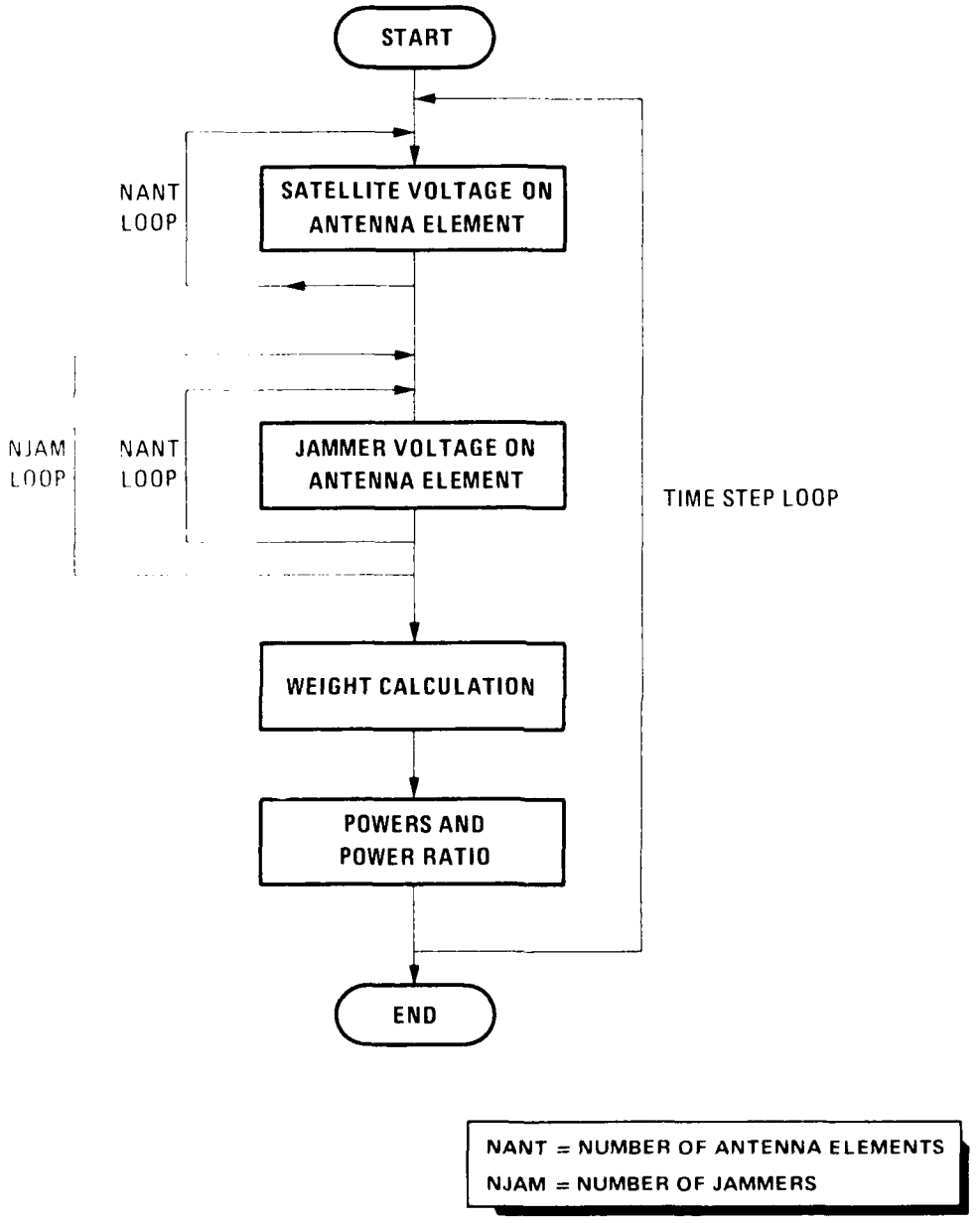

Fig. 1 Overall flow diagram

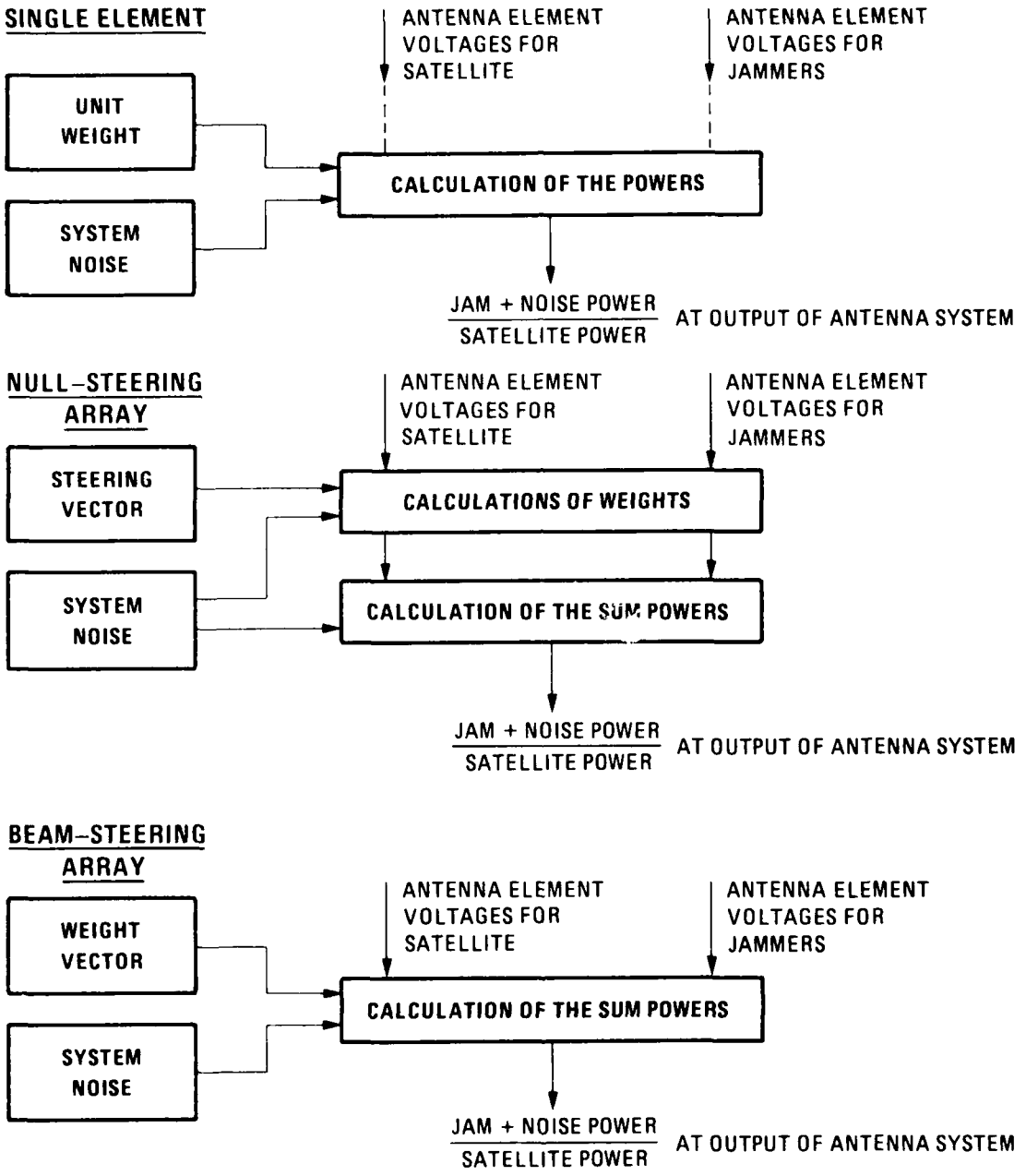

owing the processing of antenna element voltages for the various antenna systems

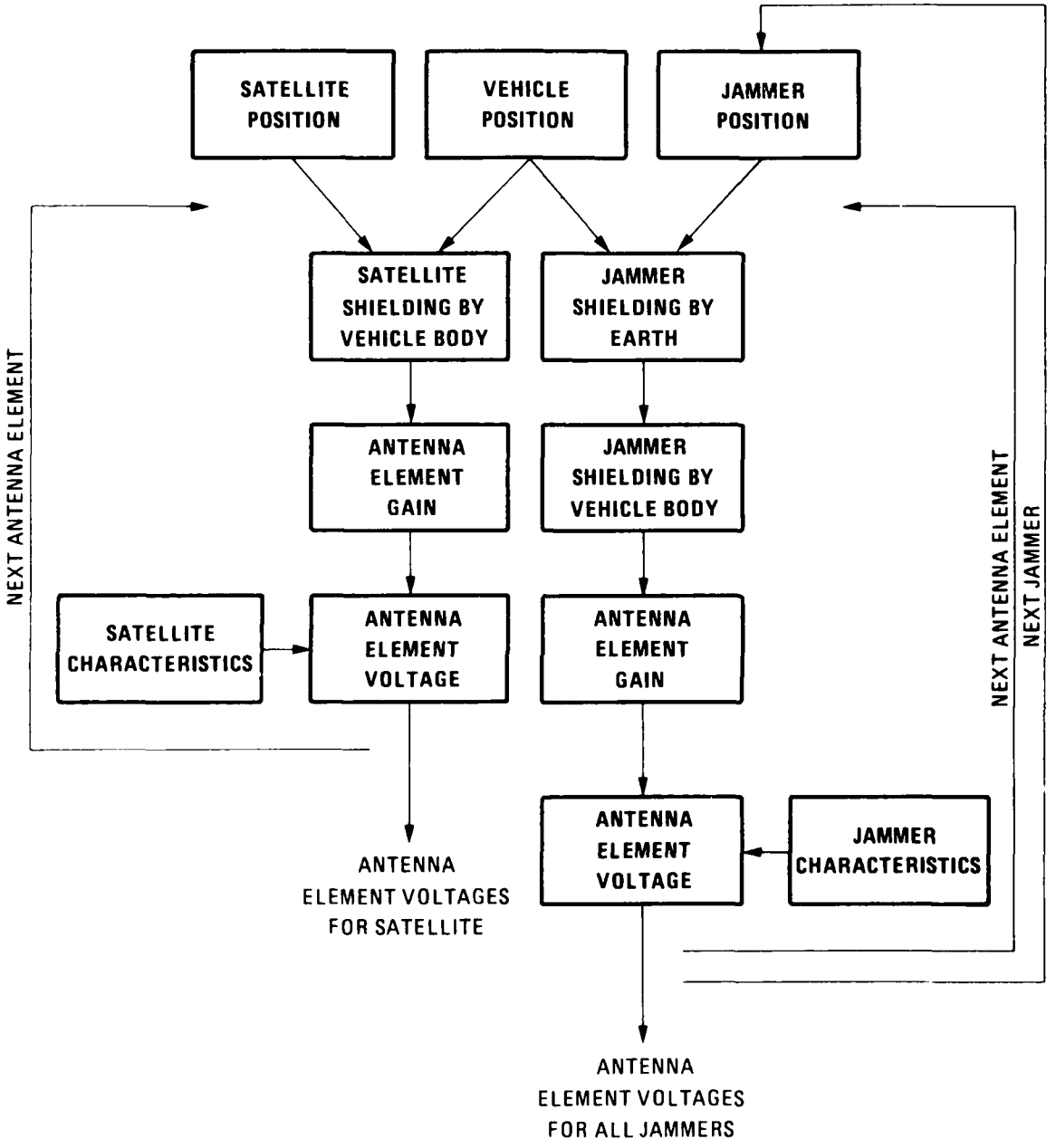

Fig. 2 Block diagram of the computation of the antenna element voltages

TABLE 1

Storage of antenna element voltages

For each antenna element: - satellite voltage
- noise voltage
- jammer voltage

are calculated.
Storage:

Antenna element	jammer 1	jammer 2	-	jammer NJAM	NOISE	SATELLITE
Antel 1	$V_{1,1}$	$V_{1,2}$	-	$V_{1,NJAM}$	$V_{1,NJAM+1}$	$V_{1,NJAM+2}$
2			-			
3			-			
⋮	⋮	⋮	-	⋮	⋮	⋮
NANT	$V_{NANT,1}$	$V_{NANT,2}$	-	$V_{NANT,NJAM}$	$V_{NANT,NJAM+1}$	$V_{NANT,NJAM+2}$

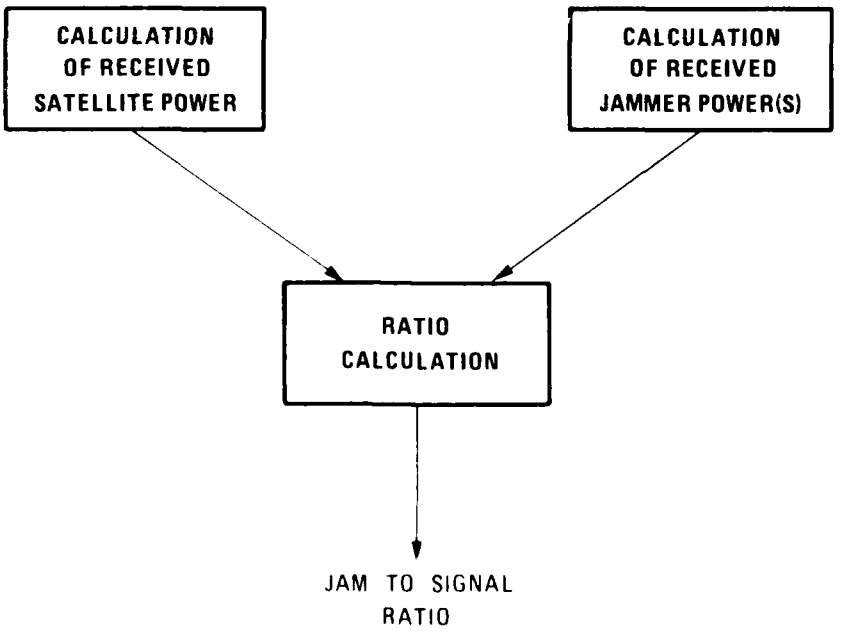

Fig. [illegible] Diagram showing the main activities of the computer program

The simulation is carried out in the batch mode and it results in output in the form of tables and diagrams on the line printer, such as:

- * Vehicle and jammer positions
  * Vehicle attitude angles
  * Jam-to-signal ratios

  } Versus time (in table)

- * Received satellite power
  * Received jamming power
  * Aspect angles to satellite and jammers
  * Calculated weight vectors

  } Versus time (in table)

- * Horizontal Y vs X position of vehicle and jammers
  * Height of vehicle vs time
  * Aspect angles to jammers vs time
  * Jam-to-Signal ratios vs time

  } (in diagrams)

Examples of output in the form of tables and diagrams are shown in figure 5 and 6 respectively.

4. VERIFICATION, LIMITATIONS AND FUTURE DEVELOPMENTS

To enhance the confidence in the simulations carried out with the ANABASIS program it is planned to verify it with the results of actual measurements. These measurements will be carried out to investigate the operation of Navstar receivers and adaptive antennas on board of an aircraft in a jamming environment.

This computer program is no exception to the rule that nothing is perfect and the obvious limitations are: i) the use of only one (stationary) satellite, ii) the lack of a time domain model of the adaptive antenna system, iii) there is no model to account for the scattering of signals by the vehicle and iv) the lack of a model of the operation of the Navstar receiver in a jamming environment. However, the main objective of the program is to determine if a nulling antenna is required anyhow and then compare the realtive performance of various antenna element configurations. Thus the effects of the limitations apply to all the configurations in the same way and are therefore considered less important.

The use of the program for a number of scenarios has brought about some points which should be added: i) extension of the program so that the received satellite signal and the jam-to-signal ratio for all visible Navstar satellites are calculated in one run, ii) determination of the influence of the finite accuracy of the weights, iii) include limits for proper Navstar receiver operation in terms of received satellite power and jam-to-signal ratio, iv) an indication of the accuracy of the vehicle position obtained from the Navstar system in case of a jamming environment.

5. CONCLUSIONS

A computer program developed for the simulation of the performance of adaptively controlled Navstar antennas in battlefield scenarios has been described. The program is used to determine if a null-steering antenna is required. If so, then the relative performance of various antenna element configurations can be compared. The program will be verified with the results of actual measurements.

6. REFERENCES

Hudson, J.E. Adaptive array principles, Stevenage U.K., Peter Peregrinus Ltd., 1981, Chapter 3.

Pietersen, O.B.M. and Klinker, F., Theoretical and computational aspects of adaptively controlled Navstar antennas, National Aerospace Laboratory NLR, 1984, NLR - TR 84004 U.

Siegel, M.D. Aircraft antenna - coupled interference analysis, Electromagnetic Compatibility Symposium Record, IEEE 69C3-EMCC, 1969.

- jammer J $$P_{JO} = \frac{1}{NANT} \sum_{i=1}^{NANT} (V_{i,J} W_i)^2 \qquad (14)$$

- all jammers $$P_{JOT} = \sum_{J=1}^{NJAM} P_{JO} \qquad (15)$$

The jam + noise-to-signal ratio at the antenna output is again:

$$\frac{J+N}{S} = \frac{P_{JOT} + P_{NO}}{P_{SO}} \qquad (5)$$

where the contributions are now defined by Eq.'s (12) to (15).
The division by the number of antenna elements NANT in Eq.'s (12) to (14) is required because it is assumed that the signals, after weighting, are summed in a matched power combiner.

The weights obtained by the direct matrix inversion method give optimum null-steering behaviour of the antenna. However, in practice, the finite accuracy of the weight setting, the time delays in iterative systems and the finite number of samples of input and output voltages used in the calculation of the weights all contribute to a non-optimum antenna performance. To account for this a null-depth limitation has been built into the program. It operates in the following way:
The user specifies the null-depth (in fact the maximum suppression as compared with a single antenna element), say δ dB, as an input to the program. Then, during the calculation, a comparison is made between the individual jammer power P_{JO} given by Eq. (14) and the power P_{JOR} that would be received by antenna element 1 with weight equal to 1 from that jammer:

$$P_{JOR} = V_{1,J}^2 \qquad (16)$$

If P_{JOR} and P_{JO} are expressed in dBW the difference between them is the suppression of the jammer by the null-steering array.
If this suppression exceeds the specified null-depth δ, then P_{JO} is increased according to:

$$P_{JO} = P_{JOR} - \delta \text{ (dBW)} \qquad (17)$$

otherwise P_{JO} is given by Eq. (14).

When a beam-steering array is used the equations (5) and (12) to (15) can be applied to calculate the various output powers and the antenna performance.
The difference with the null-steering array is the fact that the weights W are not calculated in the program but are specified by the user at the start of the simulation. During the simulation the weights are not changed.

In figure 4 the overall flow diagram for the calculation model is shown. The complete set of calculations is executed for each time step. The received satellite signal is calculated for each antenna element, as is the signal received from each jammer. The weight calculation, which depends on the array type (single element, null-steering or beam-steering array), the calculation of the antenna output powers and the power ratio are the last part of the sequence.

3. INPUT / OUTPUT DESCRIPTION

To operate the program a certain amount of input data is required. This data is prepared in an interactive way and it can be classified to the following categories:

- scenario data : title
  : time duration (min. 60 s)
  : mode (single element, null-steering, beam-steering)
- vehicle data : model (block, cylinder, flat plate)
  : dimensions
  : dynamics (i.e. attitude variations)
  : trajectory
- antenna array data : position and orientation of the elements (max. 19)
  : type of elements: blade, helix, microstrip patch, omni
  : steering/ weight vector
- jammer(s) data (max.30): trajectory (fixed or moving)
  : frequency
  : power
- satellite data : position
  : frequency
  : power

These definitions imply that jammer signals, the satellite signal and the noise are uncorrelated. The jam + noise -to-signal ratio at the antenna output equals:

$$\frac{J+N}{S} = \frac{P_{JOT} + P_{NO}}{P_{SO}} \tag{5}$$

which can be calculated using Eq.'s (1) to (4).

In the case of a null-steering array NANT antenna elements are in use (NANT ≥2) and the weights are calculated in such a way that jammer signals are more or less suppressed. The calculation procedure for the weights is based on the direct matrix inversion method. The reasons for this choice are:
- optimum weights are obtained directly, which are attained anyhow after enough iterations in the steepest descent or weight perturbation technique,
- no waste of computer time as compared with methods based on iterative solutions,
- imperfections of practical systems can be accounted for by specifying a maximum null-depth.

First the covariance matrix M is determined:

$$M = \begin{bmatrix} m_{11} & m_{12} & \cdots & m_{1NANT} \\ m_{21} & & & \vdots \\ \vdots & & & \vdots \\ m_{NANT1} & \cdots & \cdots & m_{NANT\ NANT} \end{bmatrix} \tag{6}$$

where, for example, m_{11} equals:

$$m_{11} = V_1^* V_1 = (V_{1,1} + V_{1,2} + \cdots V_{1,NJAM} + V_{1,NJAM+1} + V_{1,NJAM+2}) \times$$
$$(V_{1,1}^* + V_{1,2} \cdots V_{1,NJAM}^* + V_{1,NJAM+1}^* + V_{1,NJAM+2}) \tag{7}$$

In this expression is V_1 the sum of the voltages on antenna element 1, and * denotes the complex conjugate. For the remaining elments of the convariance matrix similar expressions as Eq. (7) can be developed. If it is assumed that the satellite signal $V_{...,NJAM+2}$ is negligible as compared with the noise and that the jammer signals are not correlated then Eq. (7) reduces to:

$$m_{11} = V_{1,1}^* V_{1,1} + V_{1,2}^* V_{1,2} + \cdots V_{1,NJAM}^* V_{1,NJAM} + V_{1,NOISE}^* V_{1,NOISE} \tag{8}$$

where $V_{1,NOISE} = V_{1,NJAM+1}$

A non-diagonal element of M, e.g. m_{12}, can be written as:

$$m_{12} = V_1^* V_2 = V_{1,1}^* V_{2,1} + V_{1,2}^* V_{2,2} + \cdots V_{1,NJAM}^* V_{2,NJAM} \tag{9}$$

because the noise voltages on the individual antenna elements are not correlated. In the same way as given by the Eq.'s (8) and (9) the remaining elements of M can be determined. The next step is the inversion of the complex matrix M, and finally, the weights are calculated according to:

$$[W] = \alpha [M]^{-1} [S]^* \tag{10}$$

where S represents the steering vector. The factor α is a normalizing constant which is used to bring the weight with the greatest modulus to 1. The phase is not changed. Thus:

$$\alpha = \frac{1}{|W_i|_{max}} \tag{11}$$

It is now possible to calculate the antenna output power. The assumption made is that the weights are preceeded by the low-noise amplifiers. This assumption and the fact that one of the absolute values of the weights is always 1 means that the antenna output noise is completely determined by the noise at the pre-amplifier input (i.e. $V_{...,NJAM+1}$).

The respective antenna output powers are:

- satellite $$P_{SO} = \left| \frac{1}{\sqrt{NANT}} \sum_{i=1}^{NANT} (V_{i,NJAM+2} W_i) \right|^2 \tag{12}$$

- noise $$P_{NO} = \frac{1}{NANT} \sum_{i=1}^{NANT} (V_{i,NJAM+1} W_i)^2 \tag{13}$$

2. THE ANABASIS COMPUTER PROGRAM

2.1. General

Anabasis is an acronym formed from Adaptive Nulling Antennas in Battlefield Simulations. The function of the program is to support the determination of the performance of various receiving antenna systems in electronic warfare conditions. To that end the program contains the following calculation model:
A vehicle equipped with a specified receiving antenna system (e.g. a single element, a beam-steering array or an adaptive nulling array) moves in a fixed, topocentric coordinate system. This coordinate system is also used to describe the position of a stationary satellite, which transmits the desired signal and of a number of stationary and/or moving jammers which transmit interfering signals. The received signal power at the output of the vehicle's antenna system, due to satellite and jammer(s) is calculated and together with the system noise, the resulting interference-to-signal ratio is obtained. This ratio is the main discriminant in judging antenna performance. In case of a single element, the calculations are straight forward. With a beam-steering array the steering information has to be supplied as an input to the program. In case of an adaptive nulling array a weight vector is calculated in the program, according to the method of direct matrix inversion (Hudson, 1981). The reasons for this choice are described elsewhere (Pietersen, 1984) and also summarised in section 2.2. The program is a time-stepping one, that is to say, for each new step the position of the vehicle and jammers can be changed and the calculations are carried out again. When using Anabasis two stages can be distinguished, viz. the scenario handling and data preparation which is carried out in the interactive mode and the simulation processing which is carried out in the batch mode.

2.2. The calculation model

The main activities in the computer program are the calculation of the power of the satellite signal and of the jammer signal(s) at the output of the receiving antenna system. The ratio of these powers (jam-to-signal ratio) is a measure of the antenna performance. Figure 1 shows the block diagram for these activities. Since the antenna output power is the sum of the weighted contributions of the individual antenna element voltages, the latter are to be calculated first. This is shown in figure 2 for both the satellite and the jammer signal(s). The antenna is located on the vehicle and it can occur that the view from the antenna element to the satellite or jammer is blocked by the vehicle structure. In two cases, viz. the cylinder and the flat plate used for the description of the vehicle, models are incorporated in the program accounting for the additional losses due to the shielding. The cylinder shielding model (Siegel, 1969) is based on the properties of wave propagation around a cylinder, the flat plate shielding model assumes simply a fixed amount of attenuation if the path between the antenna element and jammer or satellite is blocked by the vehicle. To facilitate the calculations three coordinate systems have been used:

- The fixed coordinate system (FCS), a topocentric coordinate system in which the position of satellite, jammer(s) and vehicle are defined.
- The vehicle coordinate system (VCS) which is used to define the dimensions of the vehicle and the position of the antenna elements. Together with the FCS, the VCS also provides for the definition of the vehicle's attitude.
- The antenna coordinate system (ACS) which is a reference system to describe the antenna element gain as a function of angular directions. Together with the VCS, the ACS also provides for the definition of antenna element orientation on the vehicle.

The antenna element voltages corresponding to the jammer signals, the satellite signal and the system noise are stored in an array with dimensions equal to (the number of antenna elements) x (the number of jammers + 2). This array is the data base used for the calculation of the antenna output power. It is shown in figure 3. With the element voltages known it is possible to calculate the power and the jam-to-signal ratio at the output of the antenna system. Depending on the type of antenna system, i.e. a single element, a null-steering array or a beam-steering array, different expressions are obtained. The processing of the antenna element voltages is in all cases a weighted summing but the details of the process depend on the antenna system. For a single element the weighting factor is 1 and the determination of the output powers is straight forward. In the case of a null-steering array the weights are to be calculated before the output powers can be obtained. When a beam-steering array is used the weights are input at the start of the simulations and then used as constants in the summation procedure during the whole simulation run. The processing of the antenna element voltages is shown schematically in figure 3 and is more detailed described below.

In the program the use of a single element is called the requirements mode. This is a practical mode because it is possible to probe the jam-to-signal ratio during the mission if no special antenna facilities are used, and, by considering the properties of the receiving system, define the required [illegible] protection. Since, by definition in the program, antenna element 1 is used for this requirements mode and the weight vector is 1, the respective antenna output powers are (using the nomenclature of Tab. 1):

$$[illegible] = [illegible]_{1,1}[illegible]^2 \quad (1)$$

$$[illegible] = [illegible]_{1,1}[illegible]^2 \quad (2)$$

$$[illegible] = [illegible]_{1,1} \quad (3)$$

$$[illegible] = [illegible]_{1,1} \quad (4)$$

SIMULATION OF THE PERFORMANCE OF ADAPTIVELY CONTROLLED NAVSTAR ANTENNAS IN BATTLEFIELD SCENARIOS

by
F. Klinker and O.B.M. Pietersen
National Aerospace Laboratory NLR
P.O. Box 90502
NL-1006 BM AMSTERDAM
The Netherlands

SUMMARY

The Navstar Global Positioning System, GPS, is a navigation system developed by the US Department of Defense. Its main purpose is to provide highly accurate positioning and timing data to military users. Although the use of the spread spectrum technique in GPS provides for a reasonable protection against jamming or other interference signals, one can increase the immunity to a great extent by using adaptive antennas. It depends on the expected scenarios, including jammers, if any suppression by antennas is necessary .

As the tool for the determination of the requirements for threat suppression and the performance of adaptively controlled antennas in electronic warfare conditions, the ANABASIS computer program was developed. The paper will address among others the signal propagation model and the weight vector calculation. Some examples of simulation results will be presented.

1. INTRODUCTION

The Navstar Global Positioning System, GPS, is a navigation system developed by the US Department of Defense. Its main purpose is to provide highly accurate positioning and timing data to military users. In principle, each user has a receiver with which he determines, in real time, his distance to a number of non-geostationary satellites. From these data he computes its actual position and velocity. Use is being made of spread spectrum signals radiated by the satellites having a unique code for each satellite. Only two frequencies are being used, 1575.42 MHz and 1227.60 MHz.
Although the spread spectrum technique provides for a reasonable protection against jamming or other interference signals, one can increase the immunity to a great extent by using antennas which can adapt their pattern in such a way that jamming signals are suppressed and/or satellite signals are enhanced.

ADAPTIVELY CONTROLLED ANTENNAS are defined here as array-antennas which are able to control their power pattern automatically in such a way that wanted signals are favoured and/or not-wanted signals are suppressed. From this definition, the following general classes of adaptive antennas can be defined:
- BEAM-STEERING antennas; using the wanted signal itself, or knowledge about the instantaneous direction to the signal source, the amplitude and phase of the signals, received by each antenna element of an array, are changed in such a way that maximum gain is obtained towards the signal source. The gain in other directions is low.
- NULL-STEERING antennas; using the not-wanted signals themselves, or knowledge about the instantaneous directions towards these interfering or jamming sources, the amplitude and phase of the signals received by each antenna element, are controlled in such a way that a very low gain, a NULL, is placed in the direction towards each jammer.

An important observation in the evaluation of the pros and cons of beam-steering and null-steering is that for the same physical size of an array-antenna, the difference in gain to the wanted signal and to the jammer signal can be much larger for null-steering than for beam-steering.
In case of the Navstar system, other aspects have to be considered:
- because the satellite signals are far below the noise level, no wanted signals are readily available for use in adaptive beam-steering. Weights should have to be computed, going out from known positions of satellites and the vehicle, and the attitude of the vehicle. Especially this last parameter is often not known. Also the required speed of computation of weights in case of attitude changes will pose a serious problem.
- in Navstar one needs the signals of four satellites. Creating four beams simultaneously requires at least five elements; otherwise the satellites have to be polled, creating a loss in average satellite power. In case of null-steering, one needs n+1 elements, where n is the expected number of simultaneously visible and transmitting jammers. If the jammers are in about the same direction, they can be counted for one if no extreme nulling is required.
- because the Navstar signals are below the noise level, there exists a very simple criterium for null-steering: all signals above noise (or a defined power level above noise), within the Navstar bandwidth, are jamming signals which have to be suppressed.

Taking into account all the observations above, it is clear that in most applications the choice will be for automatic null-steering.

It depends on the expected scenarios, including jammers, if any suppression by antennas is necessary. How much suppression eventually can be effectuated depends on the antenna geometry and the algorithms used in the control electronics. As the tool for the determination of the requirements for threat suppression and the performance of adaptively controlled antennas in electronic warfare conditions, the ANABASIS computer program was developed. The computer program is described in chapter 2 and some of the reasoning which went into the program is presented there. Chapter 3 gives a description of the required input data and the corresponding output, while chapter 4 contains a discussion on the verification, the limitations and future development of the program. The conclusions are contained in chapter 5.

DISCUSSION

F.Lintz Christensen, De

We have implemented an RF simulator similar to the one proposed in Figure 11 for testing of a 12 GHz 400 Mb/s QPSK system. Isolation of the power splitter and power combiner, and the reflection coefficients, proved to be very critical to avoid multiple reflections giving additional signal components with high delay. Have you calculated the requirements to the system components needed to obtain a faithful broadband realization of the wanted channel transfer function?

Author's Reply

Our simulator is currently in the detailed design phase. We have not as of this time given consideration to the problems caused by multiple reflections which give additional signal components. This is an excellent question because it emphasizes the care one must use in the actual hardware implementation of such simulation devices. In the final design and construction of the simulator we shall use isolators for the purpose of minimizing unwanted signal components.

P.Monsen, US

Analysis (paper by Dr Steen Parl) has shown that the number of rays in single layer multipath fading has to be odd. Therefore, 3 rays is the first and probably most interesting case of multipath fading. Why was the Rummler 2-ray model emphasized in your work?

Author's Reply

The question of a 2-path vs 3-path model has been under consideration for some time. Other researchers (e.g. Emshwiller, ICC 1978) state that a 2-path model permits a good approximation of most frequency selective fading. We chose a 2-path model because of the simplicity of its implementation while at the same time providing a reasonably good fit to the actual channel.

L.Boithias, Fr

Is the model proposed by Rummler as general as it is said? This model has been set up from measurements on a single link at a given frequency and in a given climate. What has to be modified if the distance or the climate are changed? Does a flat fading always exist in addition to a selective fading? You use a slightly different model. For what reason?

Author's Reply

It is true that Rummler's model has been validated only for a single path, namely a 26.4 mile link in Georgia. Additional channel measurements which could be used to verify the statistical distributions Rummler developed for the parameters a, b, and ω_0 would be quite useful. Flat fading may or may not be present with frequency selective fading. As is well known, digital radio performance may be greatly degraded at relatively shallow fade depths when the fading is frequently selective. The ITS model is postulated as being more representative of the actual physical situation.

J.S.Belrose, Ca

I would like to tell you that the Communications Research Centre, Ottawa is sponsoring the industrial development of two mobile radio channel simulators: one for satellite relay systems (M-SAT), and one for terrestrial mobile radio systems. Let me describe the latter in a little detail.

The simulator is designed to evaluate the performance of digital and analogue mobile radio systems, and hence the frequency bands for which the simulator is usable are: 138 - 174 MHz, 406—470 MHz and 806—890 MHz, and 63 - 75 MHz for modem testing.

The input signal is split into two components, representing direct and multipath propagation. Each component can be Doppler shifted. The multipath component is further shifted into "prompt" and "delayed" components. Both prompt and delayed components are split into in-phase and quadrature components, which are multiplied by independent low pass Gaussian signals. By a selectable combination of the various signal components, the land mobile channel simulator simulates the following propagation effects: Rayleigh fading, Rice fading, multipath delay, Doppler shifts, shadowing and additive noise. The parameters are selectable from manual front panel controls and via an IEEE-488 general purpose interface bus, for computer control and graphics. Delivery of these simulators is expected by March of next year.

Table 2. Summary of Two (Channel) Models Used in Theoretical Calculations (Software Simulation

Investigator	Model Type	Model	Reference	Comments
Ehrenwiller (Bell Laboratories)	Two-path signal model	$Le^{j\theta}$ $1 + Re^{j\theta}$	32	Ehrenwiller presents a method for calculating the fraction of time that the transmission performance over a single hop would be unacceptable due to multipath fading. It requires knowledge of equipment signatures.
Jakes (Bell Laboratories)	Two-path signal model	$\tau(\ ) = r\frac{r+\cos\ldots}{1+2r\cos\ldots+r^2}$ = envelop delay $H(\ ) = 1 + re^{-j\ldots}$ channel transfer function	11	Jakes presents a method for estimating the upper bound on the outage time of a digital system due to multipath fading. A number of assumptions were made concerning the fading statistics.
Chao and Liu (TRW)	Two-path signal model	Same as Jakes	40	Extended the theoretical evaluation technique formulated by Jakes
Greenstein and Czekaj (Bell Laboratories)	Channel response (filter) model	$H(\ ) = A_0 - \ldots B_1 + j\ldots A_1$	12-14	This model is based on the same data base that Rummler's model is based on. It is used to compute the expected fraction of time that the eye pattern at the receiver detector is closed.
Greenstein and Prabhu (Bell Laboratories)	Pseudo three-path signal model	$H(f) = a[1+ke^{-j(2\pi f\ldots+\ldots)}]$ (Same as Rummler's model)	30	The model formulated by Rummler is used along with models of the transmitter and receiver in the calculation of the probability of link outage due to multipath.
Wang (Bell) Laboratories)	Pseudo Three-path signal model	Rummler's model	28	Rummler's model is used along with a model of a space diversity combiner to calculate the performance improvement of space diversity over an unprotected link.
Foschini and Salz (Bell Laboratories	Pseudo Three-path signal model	Rummler's model	29	A computer program is used that uses Rummler's model for the fading channel and models of modems and equalizers in order to calculate channel capacity and an efficiency index figure of merit.

b) Stationarity
The fact that a simulated channel may have stationary (time invariant) statistics means that long periods of measurement may be used to increase measurement accuracy. This is useful for modem tests at low error rates. For RTCE systems stationarity, is also useful to allow measurement noise and errors during the channel evaluation process to be observed. It should be noted that the York simulator can produce stationary or non-stationary channel characteristics, since to produce a realistic environment for a RTCE system non-stationary channel characteristics are essential.

c) Accuracy
Channel conditions can be mathematically described and hence are complementary to theoretical studies.

d) Range of variation
Using a simulator, channel conditions can be reproduced which exceed the range which can normally be expected from a real link. This allows system performance to be assesed at its limits.

e) Availability
Any conditions can be selected at will. To experience the full range of conditions possible on a real H.F. link measurements over many 11 year sunspot cycles would be necessary.

f) Convenience
The research being undertaken at York involves the writing of much software for link control and signal processing. The problems associated with testing and debugging software are greatly reduced when operations take place at a single site under the controlled conditions found with a simulator. This advantage is likely to be found wherever complex, software or hardware systems are being developed.

2. REQUIREMENTS FOR AN H.F. SIMULATOR FOR USE IN AN RTCE ENVIRONMENT

Many H.F. simulators have been built [Watterson 69b, O'Reilly 82, Cole 69, Ralphs & Sladen, Matley 1975] for the purpose of evaluating modem performance. As far as the author is aware, no other H.F. simulator has been built with RTCE systems in mind. This section outlines the specification of earlier simulators and considers changes and additions neccessary for the RTCE environment.

Table 2.1 below summarises the specification of a typical H.F. channel simulator of the type used for modem testing.

Table 2.1
Typical H.F. Channel Simulator Specifications

a) Propagation Model
Single channel setting manually controlled
i) multipath delay : 2-10 components over range of 0-20ms 20uS steps
ii) Fading : variable fade rate on each channel 0.1-50Cz , Rayleigh fading
iii) Doppler shift : 0.1 - 500Hz switched in 1,2,5 sequence

b) Noise model
i) Gaussian White noise variable amplitude
ii) Impulsive noise : Variable pulse rates & amplitude

Several extra features are required for an H.F. simulator to be useful in an RTCE environment:

a) An interference model
It has been shown that interference is often the limiting factor in an H.F. environment. Any RTCE system must therefore consider and be operated in interference. Thus any H.F. smulator for use with RTCE must be capable of simulating interference to some degree. It should also be noted that any realistic test of modem performance would also require the effects of interference to be taken into account.

b) Multiple channel models
The prime object of RTCE is to allow the selection of the optimum channel for transmission from a set of available channels, with least disruption to normal communication. To observe this in real time it is neccesary to have a simulator which can store multiple sets of channel parameters, any one set being selected at a given time by the RTCE system.

) Time variant channel parameters
Whilst considering modem testing the stationarity of previous H.F. simulators is very useful, allowing measurements to be made over an extended period of time, enhancing accuracy. RTCE system performance is however dependant upon its ability to react to changing conditions. It is therefore neccessary to have a simulation which

produces some repeatable time variation of channel parameters to allow useful comparisons between different techniques.

The following subsections discuss the individual models used, or to be used in the York H.F. simulator in more detail.

2.1 The Watterson H.F. Channel Model

Watterson [Watterson 69a, 70] suggested a model for H.F. propagation which has become widely accepted for use in modern H.F. simulators. The model is based on the use of a tapped delay line to produce the differential time delays associated with multipath effects (Fig. 2). Rayleigh Fading effects for each multipath component are achieved by multiplying the signal from each delay line tap by a complex tap gain function Gn(t) with a bi-variate Gaussian amplitude probability density function and Gaussian spectrum. The tap gain function produces a signal from each tap with the Rayleigh amplitude and uniform phase probability density functions associated with Rayleigh fading. The fading rate (doppler spread) is determined by the bandwidth of the tap gain spectrum. The relative amplitudes of each of the multipath components are represented by the amplitudes of the tap gain functions. An offset may also be added to the tap gain function spectrum to repesent frequencey offsets (doppler shift) due to changes in ionospheric layer height.

The Watterson channel model is used in the York H.F. simulator as it represents the best defined model available. Also its widespread use makes it a de facto standard.

2.2 Noise Models

Noise at H.F. can be considered under several categories :

a) Galactic noise
b) Receiver noise
c) Atmospheric noise
d) Unintentional man made noise (Electric motors, Electronic equipment etc.)
e) Interference (Other radio transmissions)

Galactic and receiver noise can be considered Gaussian and white within the bandwidth of an H.F. receiver. For many H.F. simulators this is the only noise source available. However the levels experienced in a modern H.F. system are considerably lower than the other categories mentioned above. Atmospheric noise is mostly caused by electrical storms (Bolton 71, Merkel) and tends to consist of bursts of short pulses associated with an electrical discharge, separated by quiet intervals of random length. This has been simulated by Bolton (Bolton 71) using combinations of various pseudo random sequences and groups of asychronous osciilators generating random pulse trains of varying amplitude. Other simulators have used recordings of noise found on a real H.F. link. Matley [Matley 75] suggests that the pulses are usually of sufficient amplitude to cause clipping within receiver circiuts and as such recommends the use of a single level impulse with inter pulse intervals having an inverse exponential distribution. Currently no atmospheric noise simulation is implemented on the York H.F. simulator. This may be added in the near future.

2.3 Interference

2.3.1 The importance of interference to H.F. communications

The characteristics of interference at H.F. have been considered by several workers [Gott, Wilkinson, Cotterel], the main conclusion that can be drawn from this work is that interference is generally dominant over other sources of noise. Some typical spectrograms of activity across the H.F. bands are shown in Fig. 3, a probability density function for unoccupied areas of the H.F. spectrum derived from these spectrograms is also shown (an occupied part of the spectrum is considered to be where a signal is present which exceeds the slicing level specified). The following conclusions can be drawn from Fig. 3:

a) Interference levels are generally 10db or greater above the noise floor shown on the spectra.
b) The probability of finding a 3kHz wide channel free of interference is very small.

A change in signal to noise ratio of 10db can produce changes in modem error rates of an order of magnitude [Watterson 75]. Therefore it must be concluded that the presence of interference is a very important factor limiting the performance of H.F. communications systems. Thus any realistic simulation of an H.F. channel must include an interference model.

2.3.2 Characteristics of interference at H.F.

For the purpose of modelling in an H.F. simulator interference characteristics are best split into two distinct areas :

a) Detailed model for use within a single channel (spectral shape, time variability etc.)
a) Broad model for use across entire H.F. spectrum (ie average density of interference in channels)(N.B. only applicable to simulators dealing with multiple sets of stored channels)

The detailed model of interference to be used in an H.F. simulator is possibly the easiest of the two to specify since much interference is likely to emanate from transmissions of a digital nature using a single or multiple sub-carrier FSK or PSK modem; other sources being speech, or music from broadcast stations. The time variability of the interference depends on three factors :

a) Fading
An interfering signal may come from one or more sources each of which will be subject to fading effects.
b) Transmission duty cycle of interfering stations
The interference may be continuous (broadcast music) or come in short bursts (comms. speech) or may be a mixture of various types.
c) Frequency changes
The interfering staion may change its operating frequency at dusk or dawn (relative to interfering signal ; not local), or for some other reason

The problem of considering the broad characteristics of interference across the H.F. band for aplication to an H.F. simulator is much the same as considering what settings of channel characteristics constitute a realistic channel. Interference across the H.F. bands has been examined by various workers [Gott , Wilkinson , Cotterel] which give some indication of the probabilities of interference occuring at various levels and within various bandwidths (see also fig.3). Dutta has shown [Dutta 82] that the probability of occurence of interference is independent for frequencies separated by more than about 1kHz and bases his measurements on the concept of congestion Q for a particular band .

Q = Probability of finding inteference above a threshold level in a 100Hz bandwidth

It may be possible to use use a figure for Q as a parameter when setting up a simulator for RTCE measurements. The simulator would then use some pseudo-random means of adding interference which would satisfy this model across a set of channels. However it is felt that to a large extent interference should be hand tuned to investigate the sucseptibility of systems to interfernce (as are other simulator settings) .This is the method currently used in the York H.F. simulator although some automatic means for setting interference levels may be implemented at a later date.

2.3.3 Requirements for an inteference simulation
From the above discussion the main requirements for an interference simulation can be summarised :-

a) Variable interference spectrum shape capable of simulating one or more H.F. modems interfering at different levels or speech/music spectra
b) Control of overall amplitude of interference
c) Time variability of interference (Fading)
d) Time variability of spectrum (changing interference pattern)

2.3.4. Proposed interference model

In order to fulfil as many of the above requirements as possible whilst still producing a model which can be constructed in hardware with reasonable simplicity the following system is suggested. Fig. 4 shows a block diagram of the proposed interference simulation. Fifteen sinusoidal generators are used each with a center frequency at one of the CCIR recommended sub channel frequencies for H.F. modems [CCIR]. The amplitude of each carrier can be individually controlled and each may be individually modulated in amplitude and/or phase (+/- 180 degrees) ; a short pseudorandom sequence is suggested. A modulation rate of 42.5 Hz would give each component a spectrum whose main lobe is within its own particular sub channel. Adjustment of individal amplitude levels of each sub channel would allow interference with an arbitrary spectrum (ie. speech) to be simulated whilst other modulation rates would simulate the various types of modem found in use at H.F.. The final interfering signal is then subjected to Rayleigh fading before mixing with the output from the propagation model of the simulator.

3.0 THE YORK H.F. SIMULATOR

Fig 5 shows a simplified block diagram of the York H.F. channel simulator. Rapid parameter changes are made possible by bringing the whole system under the control of an 8085 microprocessor. Sets of channel parameters can be loaded into RAM and recalled at will with a single command over a serial line. The multipath delay for each path is achieved using a separate 512 stage CCD delay line. The clock rate for each delay line is generated from the 8085 system clock via a programmable divider. After the delay line the overall gain of each channel is set using a multiplying D-A converter as a digitally controlled attenuator. Rayleigh fading (multiplicative noise) on each channel is achieved using a further pair of multiplying D-A converters. The signal is split into two components, each component being multiplied by an independent Gaussian noise source. One of the components is modulates an intermediate frequency sine carrier whilst the second modulates a cosine carrier. The nett result being a double sideband I.F. with a random phase and Rayleigh amplitude probability density functions. Each of the Gaussian noise components is generated by the 8085 cpu by digitally filtering a maximal length pseudo-random binary sequence. The fading rate is determined by the sequence clock rate. Doppler

shift is incorporated by varying the frequency of the I.F. carrier for each channel. To produce an SSB signal the first I.F. signals from each channel are combined and up converted to 452 kHz where they are passed though a crystal upper sideband filter. Synchronous detection is used to convert the SSB signal back to baseband, where inteference and additive noise can be added. Table 3.1 summarises the simulator specification.

Table 3.1

The York H.F. Simulator Specification

number of multipath components	:	2 (Expandable)
Multpath delay range	:	0.5-15 ms
Channel attenuation	:	0 - 48db linear steps
Fade rate	:	> 20 to < 2X10^3 Fades/s
Doppler shift	:	+/-100Hz
Channel bandwidth	:	6 kHz (depends on SSB filter used max=6kHz)
Number of stored channels	:	Greater than 50 Max = 255 with memory expansion
Inteference model	:	Fading, Variable spectrum; modem type interference

3.1 Hardware Implemntation of the Interference model

An outline circuit diagram of the interference simulator used in the York H.F. simulator is given in Fig. 6.The implemetation was chosen to use minimum hardware whilst still maintaining maximum flexibility. Two ROM memories store delta modulation coefficients for 15 sinewave components at the CCIR recommended sub channel frequencies [CCIR] and are all multiples of 85Hz. A 12 bit binary counter is connected to the ROM address lines and cycles through the full address range at a rate of 85Hz. Each data line of the ROM outputs in integral number of cycles of a particular sub-carrier for each cycle of the counter (5 cycles at 425Hz to 33 cycles at 2805Hz). A single R-C filter is used to decode the delta modulated output of each ROM data line. Two multiplying digital to analogue converters contol the amplitude and phase of all 16 sub-carriers; each controlling 8 sub-carriers *in a time division multiplexed mode. coefficients for the* d-a converters are stored in a dual port RAM. The top three ram address lines are connected to a fast counter and an eight input multiplexer for each d-a converter. As each sub-carrier is connected to the d-a converter via the multiplexer its current amplitude is read from the current block of coefficients selected by the lower ram address lines. The 2048 x 16 Ram used in the York simulator allows a sequence of 256 coefficients for each sub carrier to be stored. A counter clocked at the required modulation rate is connected to the remaining ram address lines and steps through the coefficients allowing modulation by pseudo random and other sequences to be used individually for each sub-carrier. A modulation bit rate of 42.5Hz could be used, which would limit the main lobe of the sinx/x spectrum to a single sub channel with sidelobes spreading into adjacent sub channels. Although this limits the control of the overall spectrum shape it is representitive of real interference which is likely to have been generated by a similar mechanism. Modulation bit rates of 50, 75, 110 etc. could also be used to simulate interference from common digital transmissions.

The possibility of storing other sets of waveforms in ROM, such as a truncated sinc pulse giving a restricted spectrum mostly within a single sub channel is also open.

4.0 CONCLUSION

The York H.F. simulator has not yet been tested in a full RTCE system, so little practical evidence of its usefulness exists. It is hoped that it will be possible to present such results in the near future.

It is felt that the simulator described will be an invaluable tool for work with real time channel evaluation systems, allowing quantitative comparisons between different techniques to be performed in a well defined and repeatable environment. Also much greater insight can be gained into the weaknesses and strengths of particular channel

evaluation and/or selection technique when using a simulation; because of the ability to isolate the effect of a particular channel parameter. This has of course already been the case when conducting modem tests with previous H.F. simulators.

The inclusion of an interference simulation in H.F. simulators is essential if a realistic environment is to be recreated for H.F. systems testing whether it be for modem, RTCE or other types of equipment. The white and impulsive noise models used in previous simulators whilst giving useful comparative performance figures cannot provide adequate information on system performance in the prescence of narrow band interference such as often found in the H.F. bands. This is particularly important when assesing the performance of RTCE systems.

The stationary statistics model for H.F. propagation used in many previous H.F. simulator designs, whilst advantageous for modem testing, must be replaced by a model with time varying statistics if RTCE systems are to be tested. This is because the performance of such a system is highly dependant on its reaction to changing propagation conditions. Also the type of time variance needs more consideration although a simple linear time variance is proposed as an initial starting point, with some channels deteriorating and some improving all at different rates.

An ability to store and rapidly switch between different sets of channel conditions is highly desireable if an H.F. simulator is to be used to test the performance of a real time channel evaluation system.

More work is needed to determine a realistic set of channel conditions to use for comparative testing of RTCE systems. Factors such as interference levels and density across a set of channels and the spread of channel characteristics representing a realistic link should be considered to provide a small set of standard atmospheres.

References

Bolton E. 1971
Simulating Atmospheric Radio Noise from Low Frequency through High Frequency
The Review of Scientific Instruments, Vol 42, No. 5, 574-577, May 1971

CCIR
XII Plenary Assembly Document Vol 3

Cole R., Jewett W.M.
A Programmable Real Time H.F. Channel Simulator

Coon R.M., Bolton E.C., Bensema W.D. 1969
A Simulator for H.F. Atmospheric radio noise
ESSA Tech. Rept. ERL 128 ITS 90

Cotterel R.A. 1979
An Automatic H.F. Channel Monitoring System
IEE conf. "Recent Advances in H.F. Communication Systems & Techniques"

Darnell M. 1977
New H.F. Data Transmission Techniques
NATO Advanced Study Institute on Communication Systems and Random Process Theory 1977

Dutta s. , Gott G.F.
H.F. Spectral Occupancy
IEE second conf. "H.F. Communication Systems & Techniques"
Feb 1982

Gott G.F. 78
Characteristics of Interfering Signals in Aeronautical H.F. Voice Channels
Proc. IEE Vol. 125 No 11, Nov 78

O'Reilly E.P. 1982
A Real Time H.F. Channel Simulator
IEE second conf. "H.F. Communication Systems & Techniques"
Feb. 1982

R.S.G.B. 1976,77,82
Radio Communication Handbook Fifth Edition
Radio Society of Great Britain, 35 Doughty St. London
ISBN 0 900612 58 4

Watterson C.C., Juroshek J.R., Bensema W.D. 1969
U.S. Dept of Commerce
Experimental Verification of an Ionospheric Channel Model
ESSA Technical Report ERL 112-ITS 80

Watterson C.C., Ax G.G., Demmer L.J., Johnson C.H. 1969
An Ionospheric Channel Simulator
ESSA Tech. Memorandum ERLTM-ITS 198

Watterson C.C. and Coon R.M. 1969
Recommended Specifications for Ionospheric Channel and Atmospheric Noise Simulators
ESSA Tech. Rept. ERL 127-ITS 89

Watterson C.C., Juroshek J.R., Bensema W.D. 1970
U.S. Dept of Commerce
Experimental Confirmation of an Ionospheric Channel Model
IEEE Trans on Comm. Technology Vol Com-18 Dec. 1970

Watterson C.C. 1975
A Review of Channel Simulation Techniques at the Institute for Telecomunicaton Sciences

Wilkinson R.G. 1982
A Statistical Analysis of H.F. Radio Interference and its Application to Communication Systems
IEE second conf. "H.F. Communication Systems & Techniques"
Feb 1982

ACKNOWLEDGEMENTS

I wish to thank the Science and Engineering Research Council for funding the research program under which the York H.F. Simulator was constructed and also Dr G Gott and A. Ray of UMIST for providing the H.F. occupancy spectrograms and an analysis of interference free gap sizes.

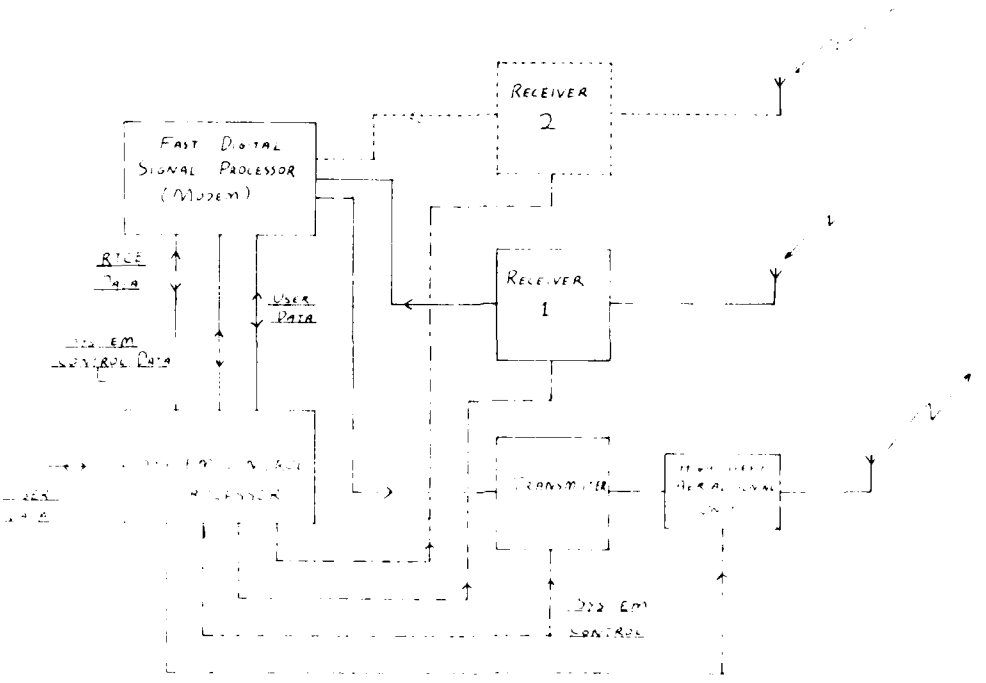

Fig. 1a The H.F. communication system at York

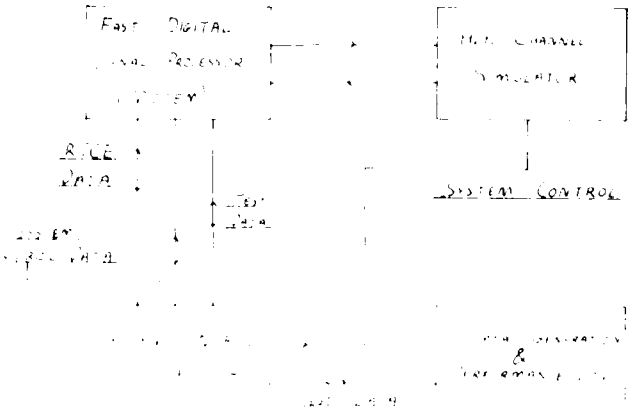

Fig. 1b The York H.F. simulator replaces the transmitter and receiver for simulator trials

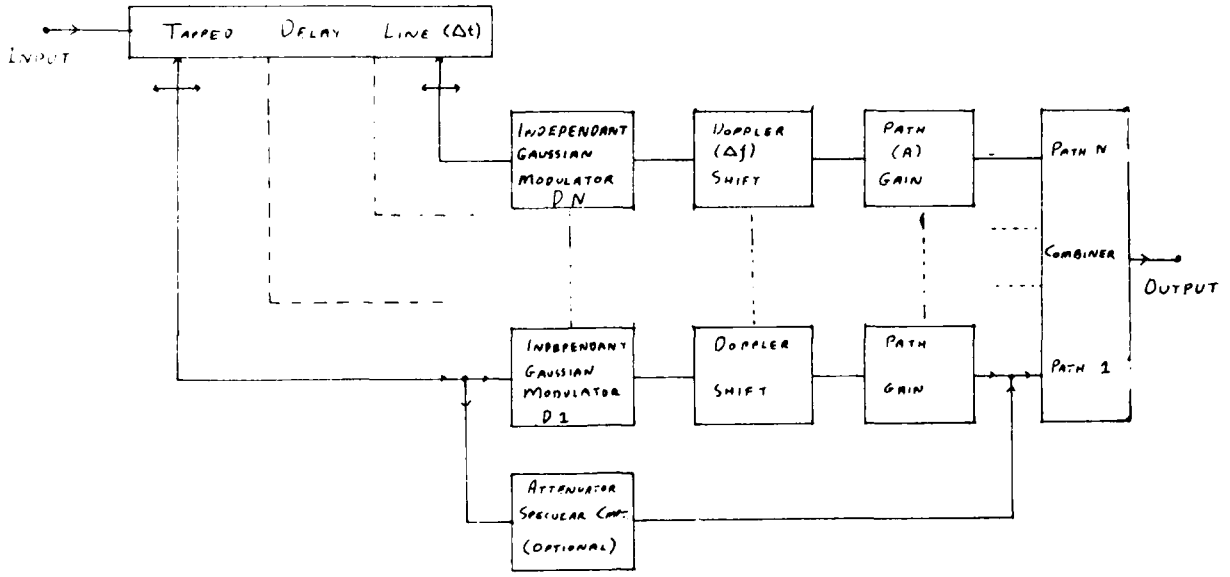

Fig. 2a The Watterson channel model

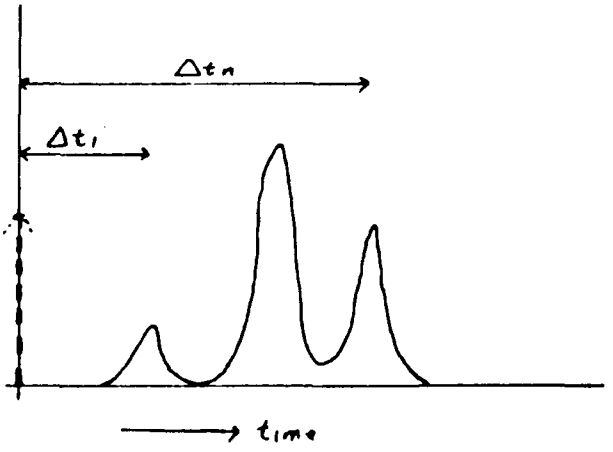

Fig. 2b Impulse response of the Watterson channel

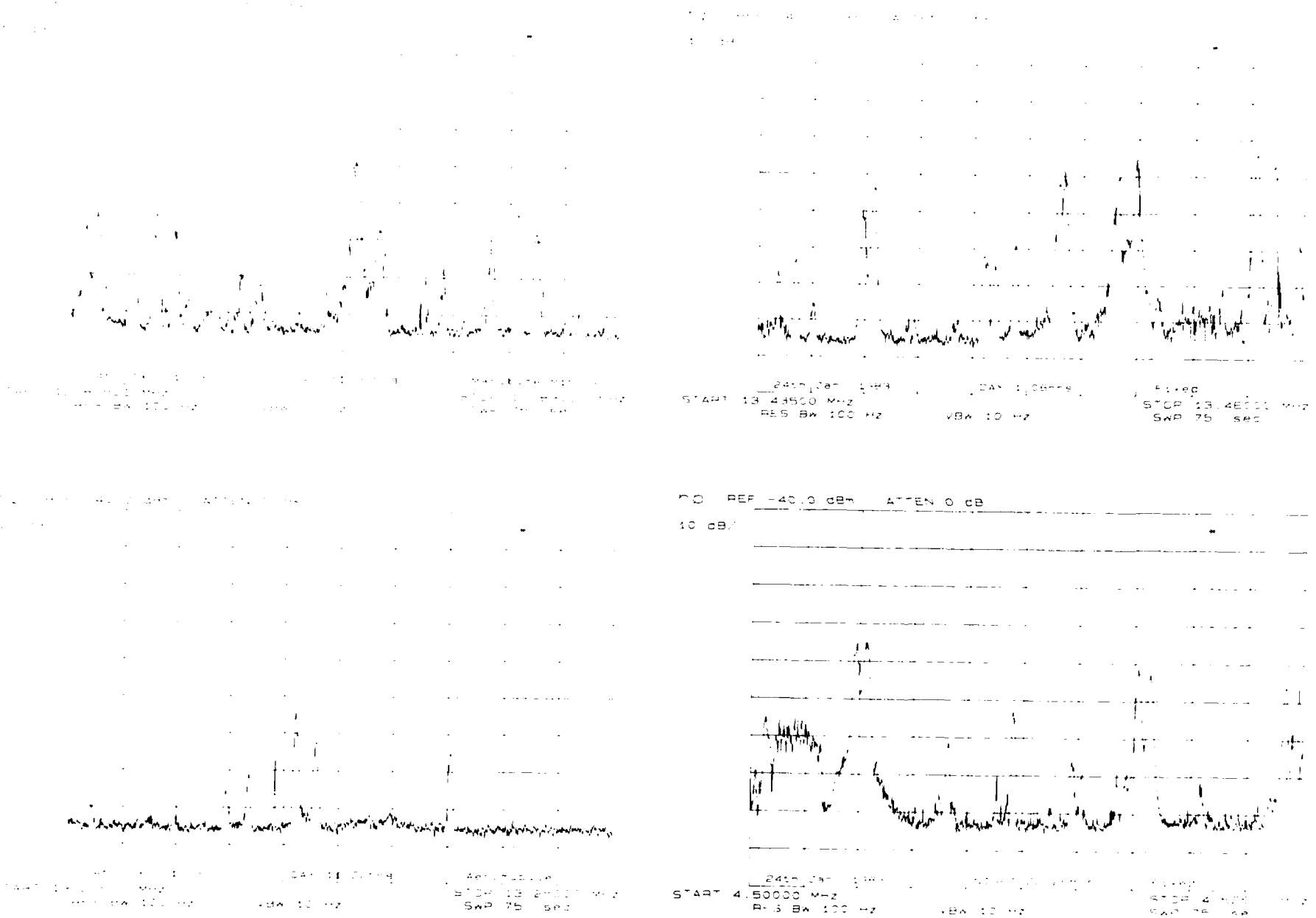

Fig. 3 Spectra of some typical H.F. bands and their distribution of interference free gaps

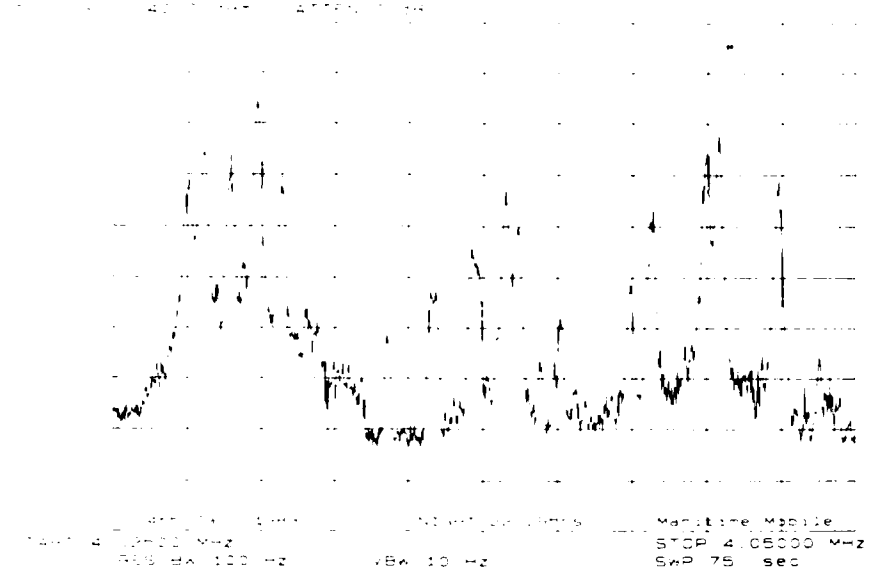

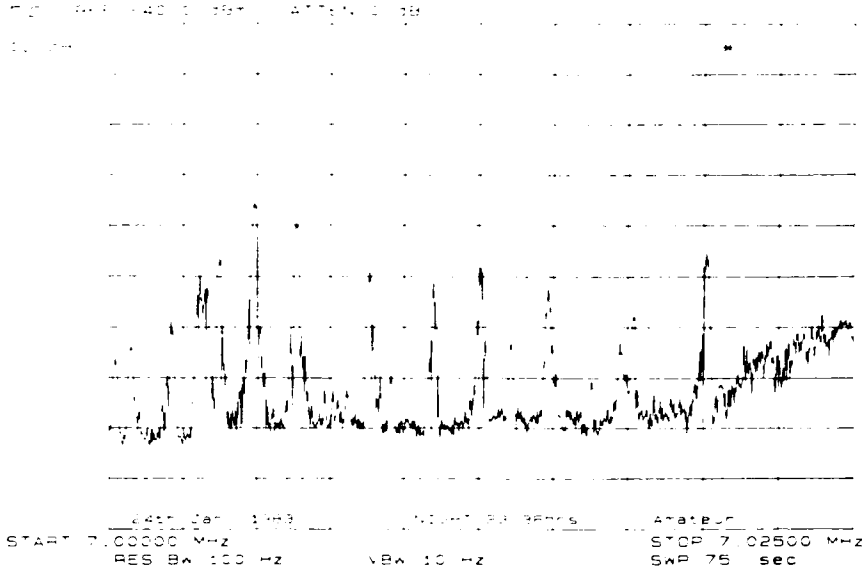

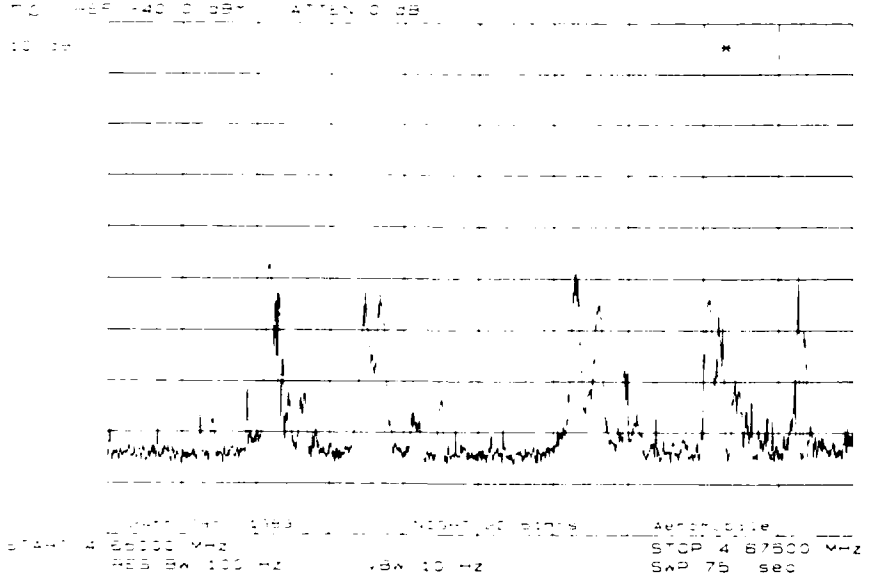

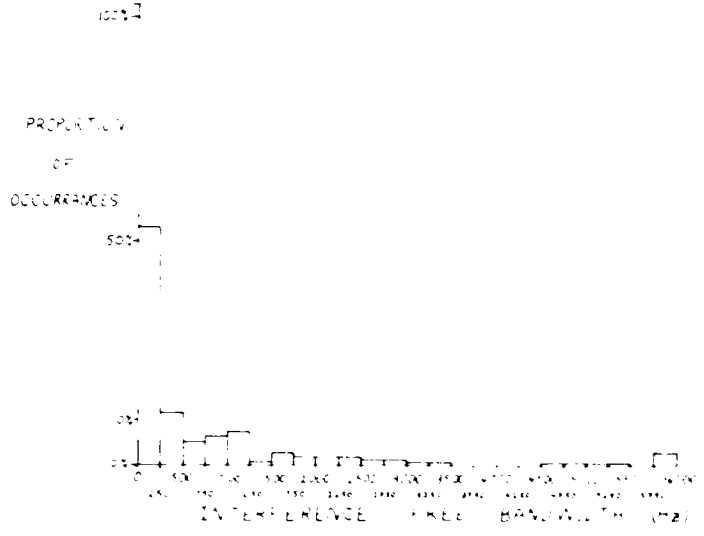

Fig. 3 cont. Spectra of some typical H.F. bands and their distribution of interference free gaps

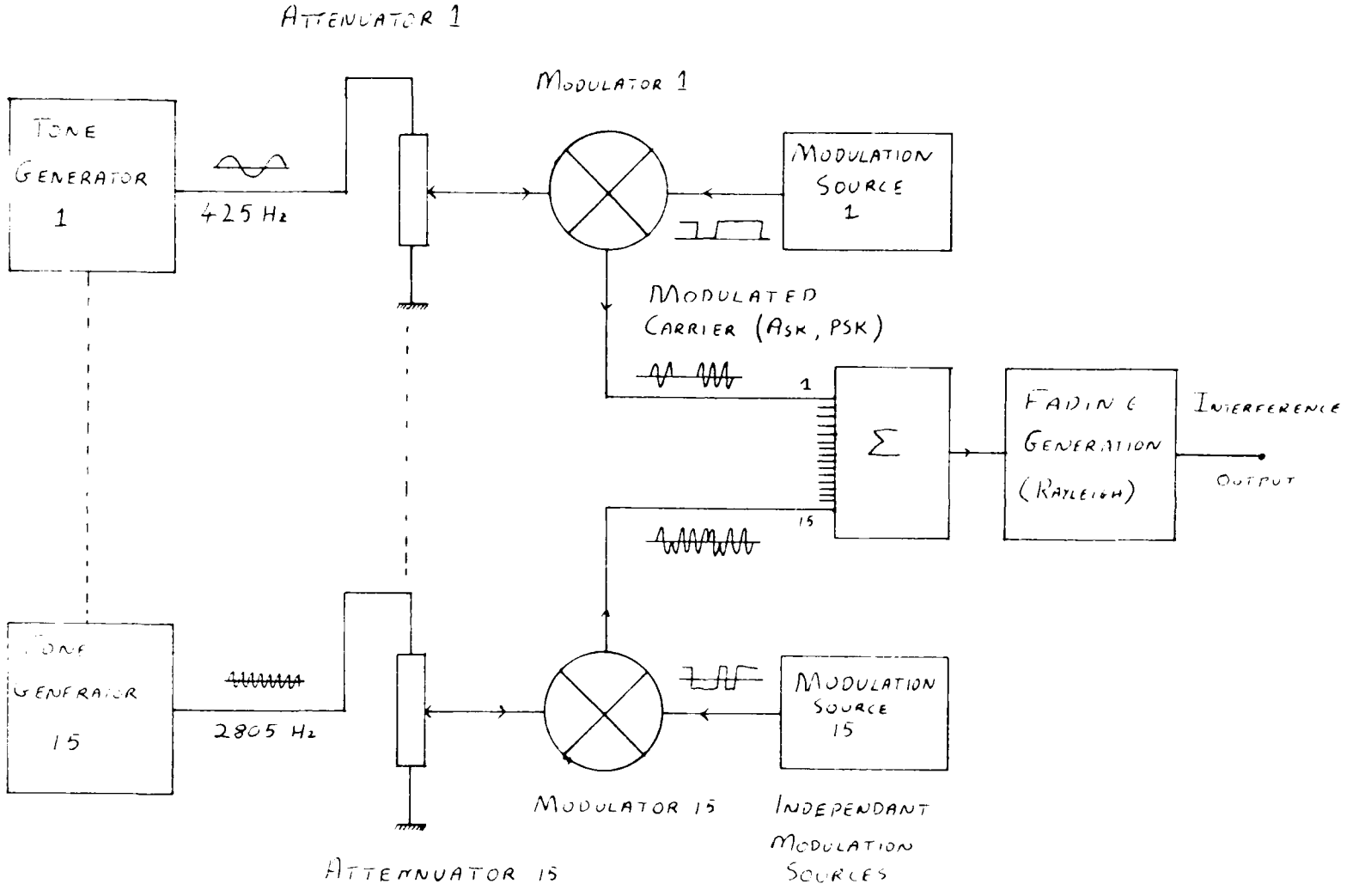

Fig. 4 Interference simulation block diagram

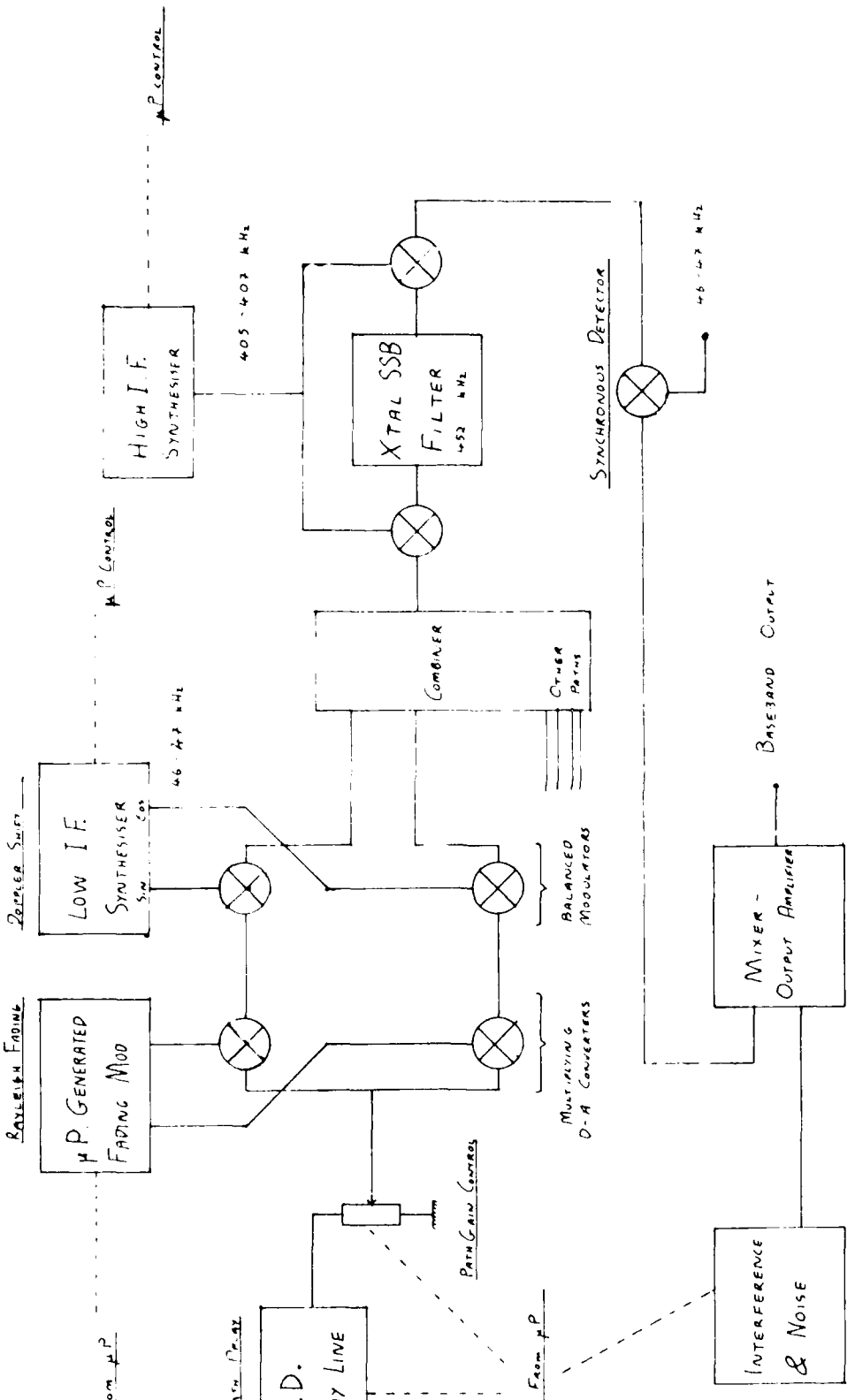

Fig. 5 The York H.F. channel simulator (one path shown)

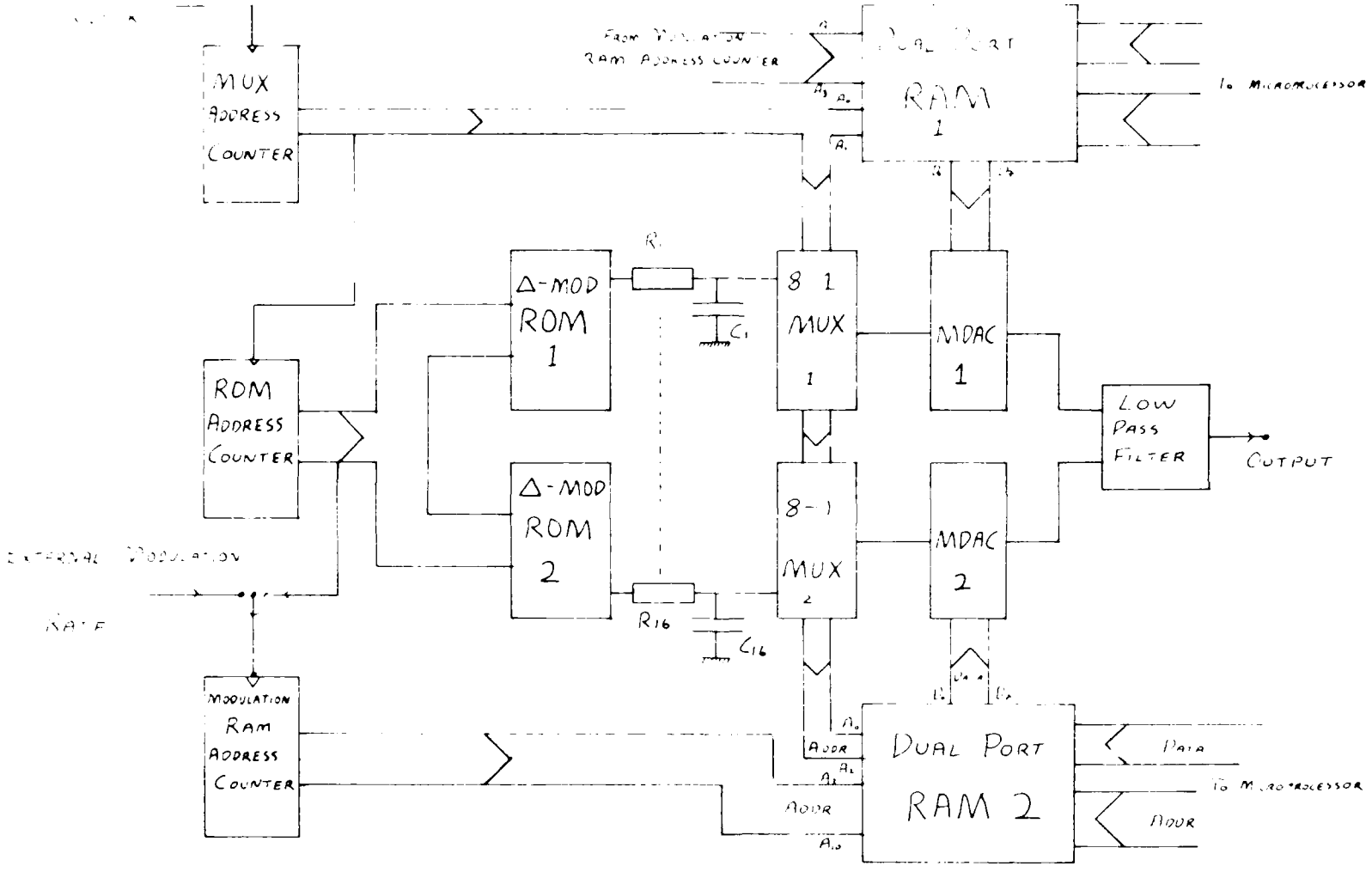

Fig. 6 Hardware implementation of the interference simulator

DISCUSSION

P.A.Bradley, UK

You state 'interference levels are generally 10 dB or greater above the noise floor shown on the spectra'. There must be other interference bursts only just exceeding the noise. Also with a sweep of 75 sec given in the examples of Figure 3 some of the spikes may result from wideband atmospherics not present at other sweep instants. How can you tell, for example, with the fifth sample (maritime mobile) whether there are any clear channels? What is the definition of a clear channel? Should it be related to the lowest measured power spectral density or to reference CCIR noise data?

Author's Reply

(1) The spectra shown are the result of averaging several sweeps so as to minimise the effect of short bursts of noise, atmospheric or otherwise.

(2) For the purpose of the histogram shown (Figure 3) the results were obtained by measuring widths of gaps between spectral peaks exceeding a threshold of −108 dBm.

The histogram shows the proportion of gaps in a particular size range, i.e. 0– 249 Hz, 250 – 499 Hz etc.

(3) For a particular system the question of whether or not a channel can be considered clear of interference depends very much on the characteristics of that particular system, i.e. received signal levels relative to the interference, fine structure of the interference and signal spectra.

R.W.Jenkins, Ca

In Figure 4 of your paper, the fading generator for the interference simulation block occurs after the various tones are summed. This implies that the fading will occur equally on all tones, and that for the present system, frequency-selective fading of the interference will not be simulated. Is this interpretation correct, and, if so, do you envisage extending the simulator in the future to cover frequency-selective fading of interference?

Author's Reply

Your interpretation of Figure 4 is correct. Frequency selective fading of the interference is not possible with the current simulator design, although frequency selective fading could be simulated in a limited manner by variation of individual tone amplitudes using the attenuators. The inclusion of frequency selective fading in the future will depend on whether or not it appears a necessity, based on comparisons with the HF Link being set up at York.

DISCUSSION OF SESSION III

M. Boithias

Could we discuss the use of Rummler model. To what extent does Rummler model fading simulate real fading?

Dr Hoffmeyer

I really have no further comments on the Rummler model beyond those in my paper. It does seem to be a model that has been picked up by a variety of people in the field, both inside and outside Bell Labs. I think that there is a definite distinction between the Rummler model approach as opposed to earlier approaches using a tapped delay line model as described for example by Bello (in AGARD Conference Proceedings No.244, October 1977 pp 12-1 to 12-14).

Dr Belrose

It is very important that the simulated radio transmission channel bears some resemblance to the real world and I guess none of the speakers this morning addressed that subject particularly. We intend to try to assure that our channel simulator is simulating the land mobile channel (both terrestrial links and satellite-to-ground links) by the following means. We have a mobile van in which we can drive around inside cities and in the suburbs and countryside and measure various parameters of the signal — multipath parameters as well as detailed signal fading. We will also be making measurements of bit error rate for particular data rates and modems. We will then test these same equipments in the laboratory under channel simulation and try to get the same kind of answers and try to make our simulated signals like those that were actually recorded in the field. It is a very important matter that must be addressed in detail by all those who simulate channels.

Dr Darnell, Session Chairman

You illustrate a general point, the match between the simulated environment and the real environment. How far do we need to take it? I think, from what we have heard this morning, that the state of that simulation is relatively advanced. Perhaps what are not yet adequately simulated are things like network operations, the true ECM threat, and interference in the case of HF. In the case of mobiles, particularly ships and aircraft, there is a real need to simulate EMC constraints. Further, the simulations that we have heard about tend to confine themselves to linear models. How important is it that we take account of non-linearity? So I think *there are a number of factors that could potentially* be brought into simulation models and I wonder whether anyone has any comments on how significant these factors are, or whether the simulation techniques that we use at present are in fact adequate.

We heard also about two roles for simulators: in the system design phase; and for testing equipment which already exists. Are there other valid roles for simulators that we ought to be thinking about?

Dr Jenkins

During the coffee break an additional role came up which seems to be quite useful, especially for the hardware type of simulator on which you can test equipment. Such simulators could be a reasonable way of training operators, because we could use them to create, in a relatively short time, all the kinds of conditions that an operator would encounter in the field.

Mr George

I wonder whether I could turn the question back to you, Dr Darnell. Do you consider that 2.4 kbps data transmission at HF is adequately simulated and modelled, bearing in mind that things are happening very quickly and an attempt to make real measurements on an ionospheric path at 2.4 kbps using even Fast Fourier techniques necessarily takes many seconds to do the analysis, during which time things have changed.

Dr Darnell

I think the *feasibility of 2.4 kbps at HF really depends where in the world you are located at the time. In the United* States it probably looks a fairly feasible proposition. In Central Europe it perhaps doesn't look quite so bright. I think *what is needed is a systematic programme of measurements to characterise interference more accurately, and these* have to be done in a uniform way at several sites on a global basis, to take into account the different environments that are experienced. In short my answer to that particular point is that it is not characterised adequately. It is probably characterised adequately from a propagation viewpoint but not from an interference viewpoint.

M. Boithias

I think that the question raised earlier about the purpose of simulators is a very important one. There is perhaps some confusion in the minds of a certain number of people concerning link performance prediction. They imagine perhaps that simulators will tell us about the performance of, for example, a digital link, and they are often rather disappointed. In fact those who seek to make a prediction of link performance are dealing with a statistical problem. That is to say they wish to know for what percentage of time does the link provide a certain quality of performance, without being too

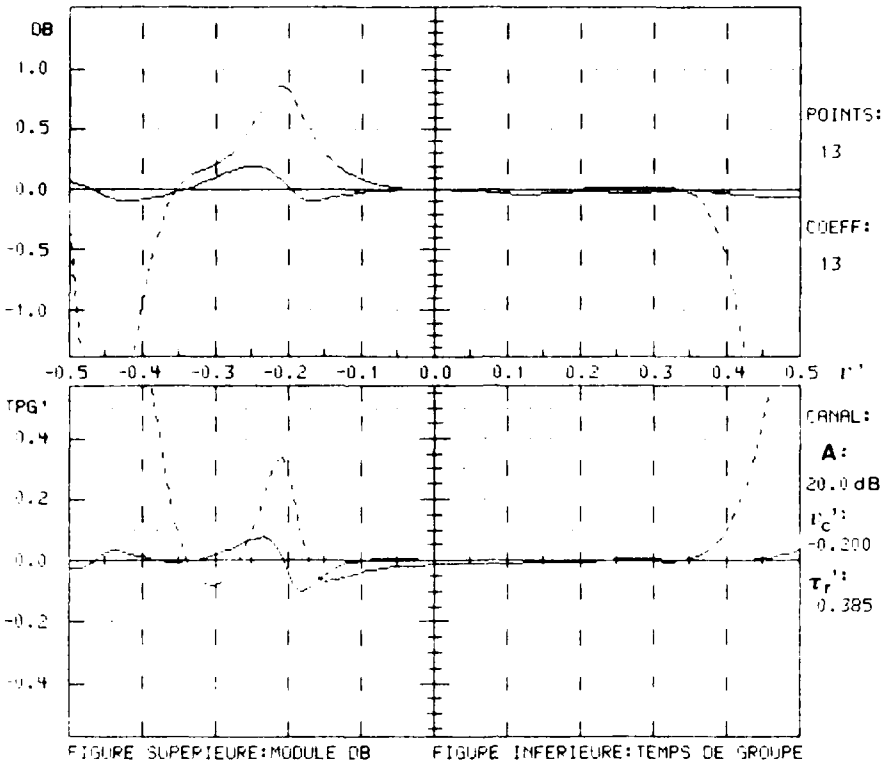

Figure 8 : Exemple de distorsions parasites
pour une précision sur les retards de 1 % (crête à crête)

En trait plein : Distorsions liées seulement à la précision

En trait pointillé : Distorsions globales

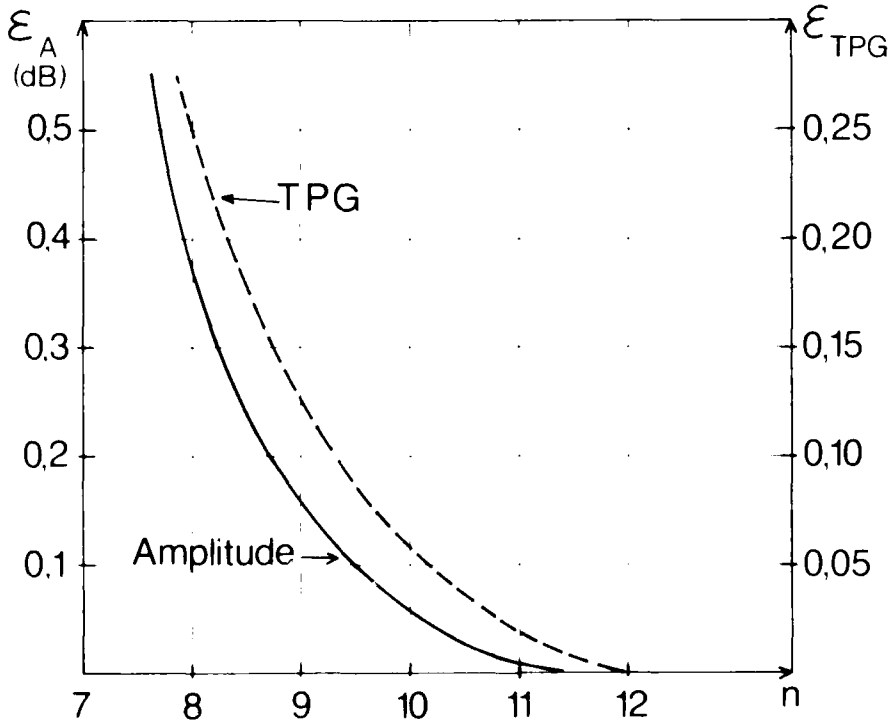

Figure 9 : Ondulations en bande utile introduites par la quantification des coefficients, en fonction du nombre n de niveaux

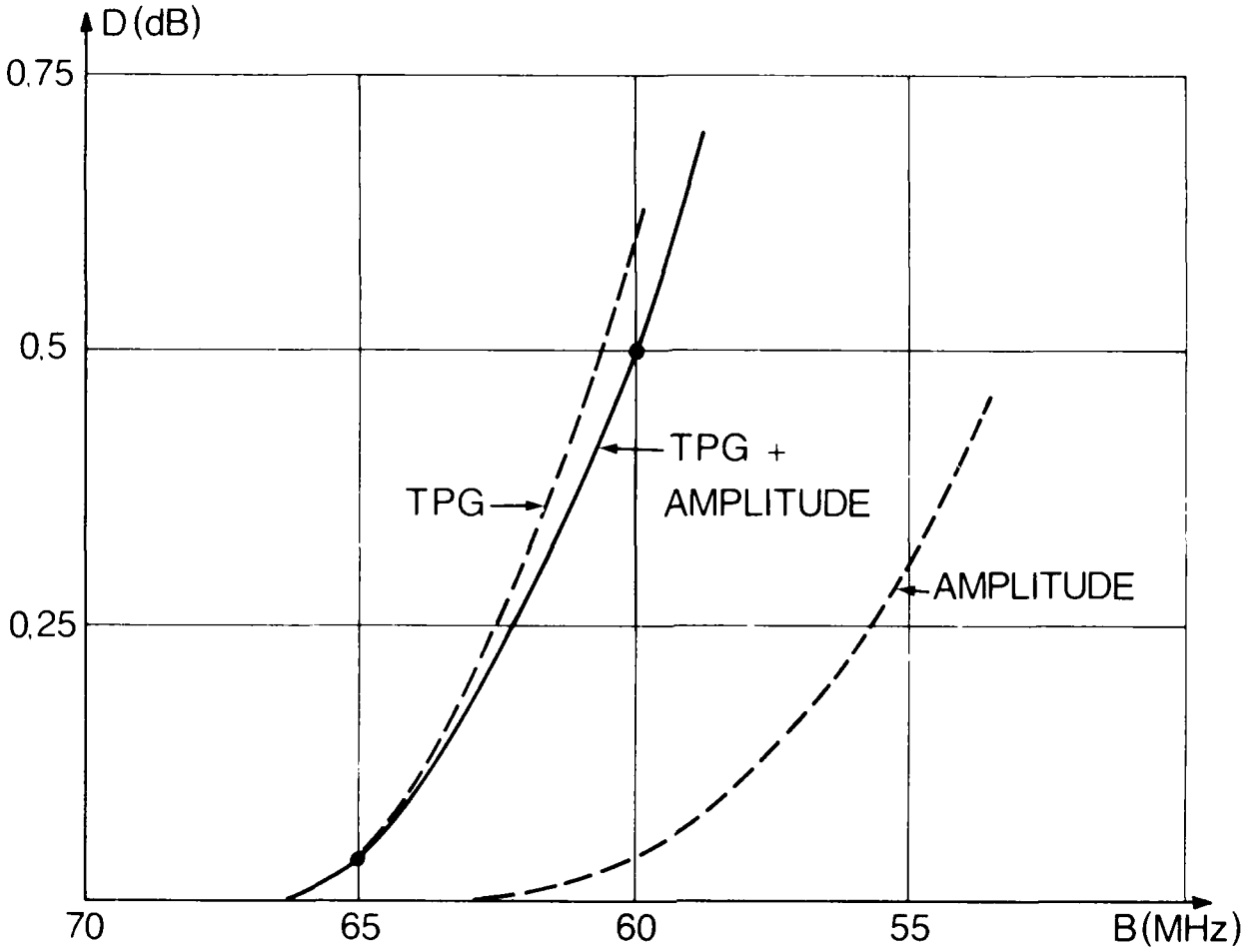

Figure 6 : Dégradation en fonction de la période B du filtre
(modulation MAQ 16 , P_e = 10^{-6})

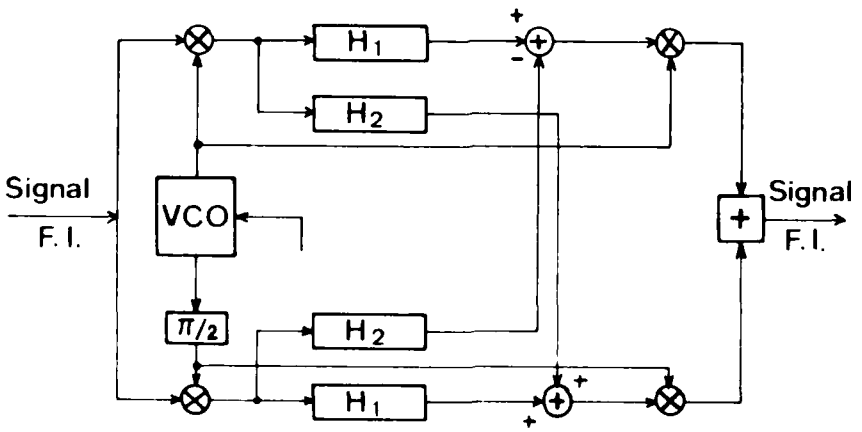

Figure 7 : Schéma du filtre en bande de base

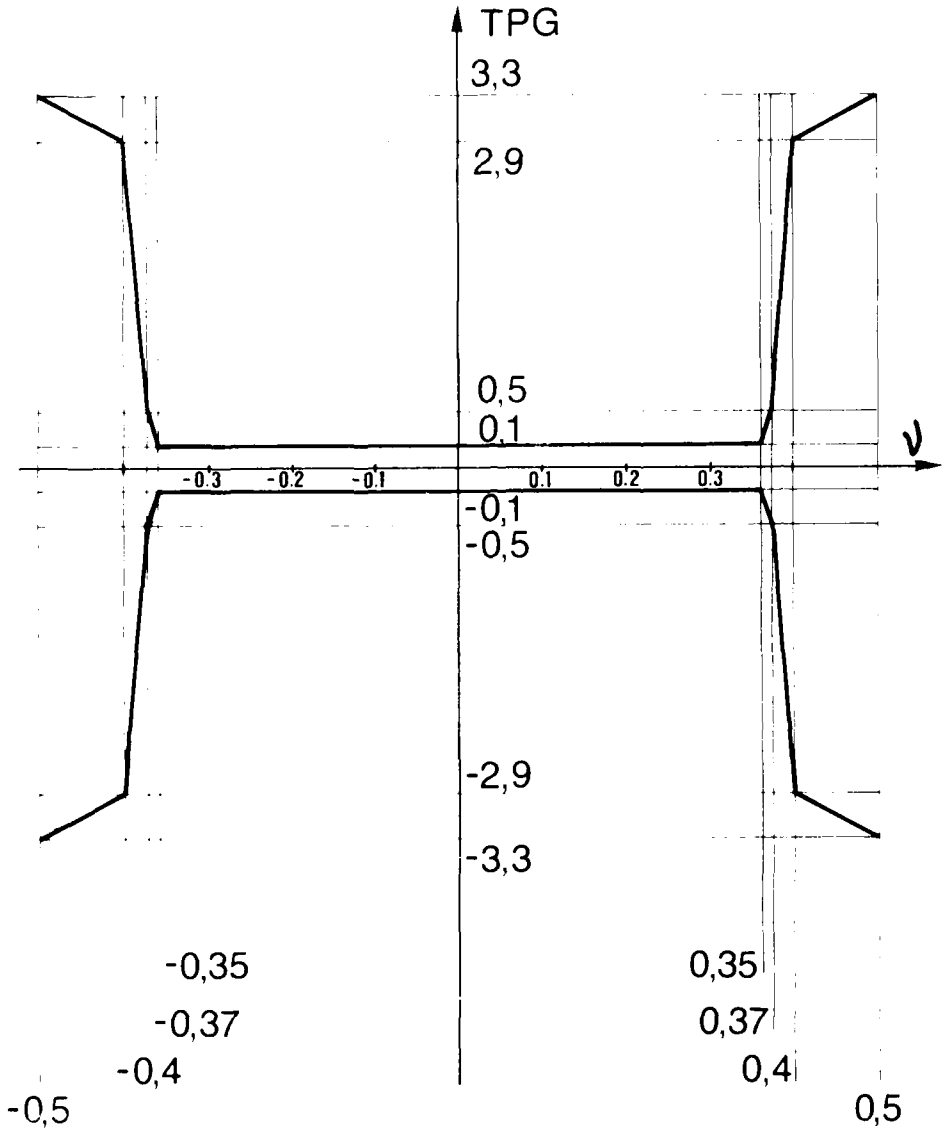

Figure 5.b : Gabarit du TPG

Figure 5 : Gabarit des distorsions pour 13 coefficients et τ_{rmax} 0,385
(à l'exclusion du défaut de poursuite)

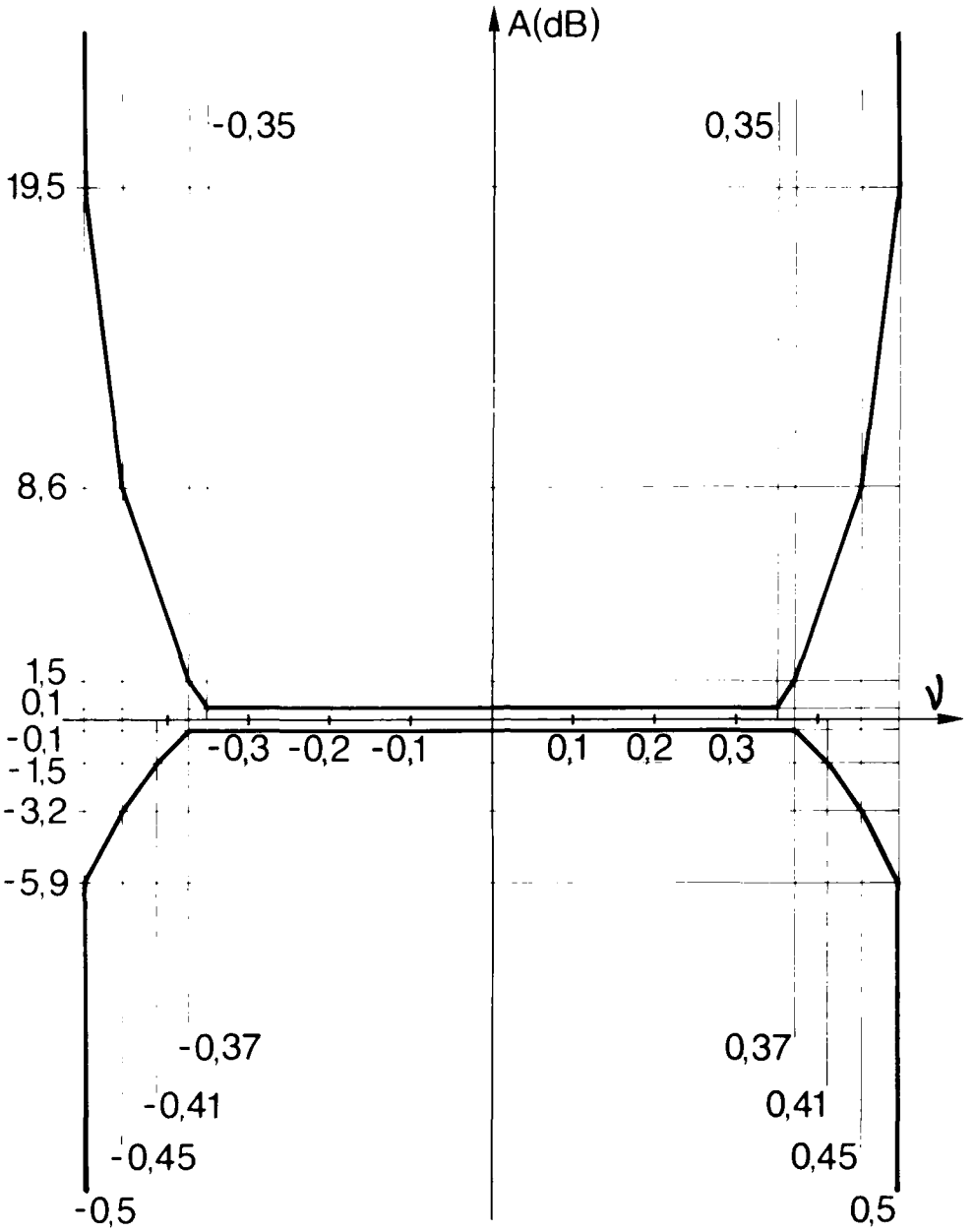

Figure 5.a : Gabarit du module

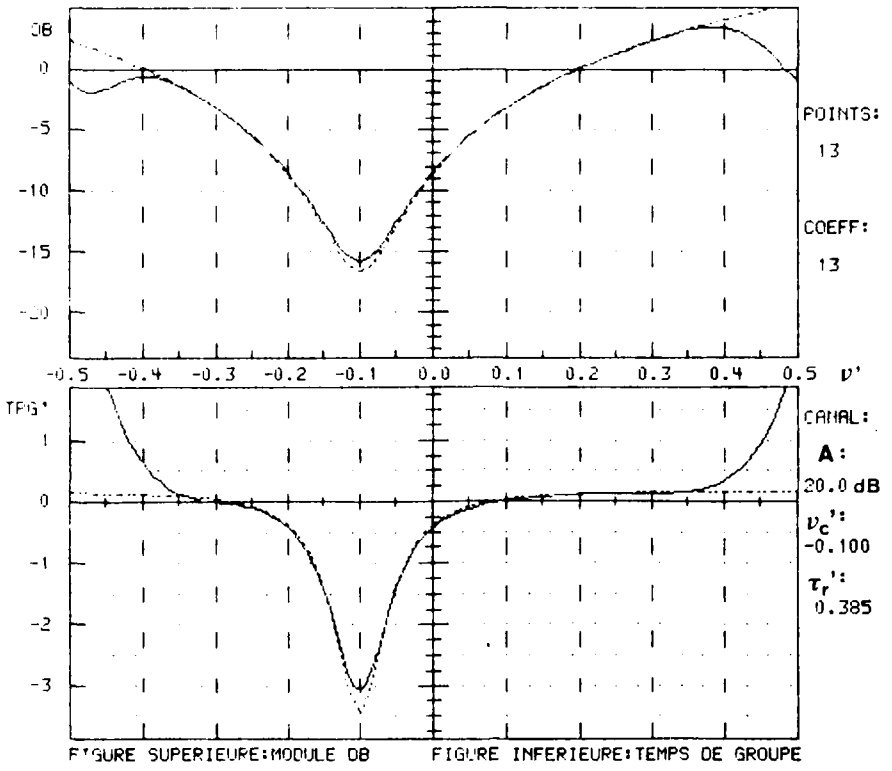

Figure 3 : Comparaison des fonctions de transfert
En trait plein : fonction de transfert simulée
En trait pointillé : fonction de transfert donnée (modèle à 3 rayons simplifié)

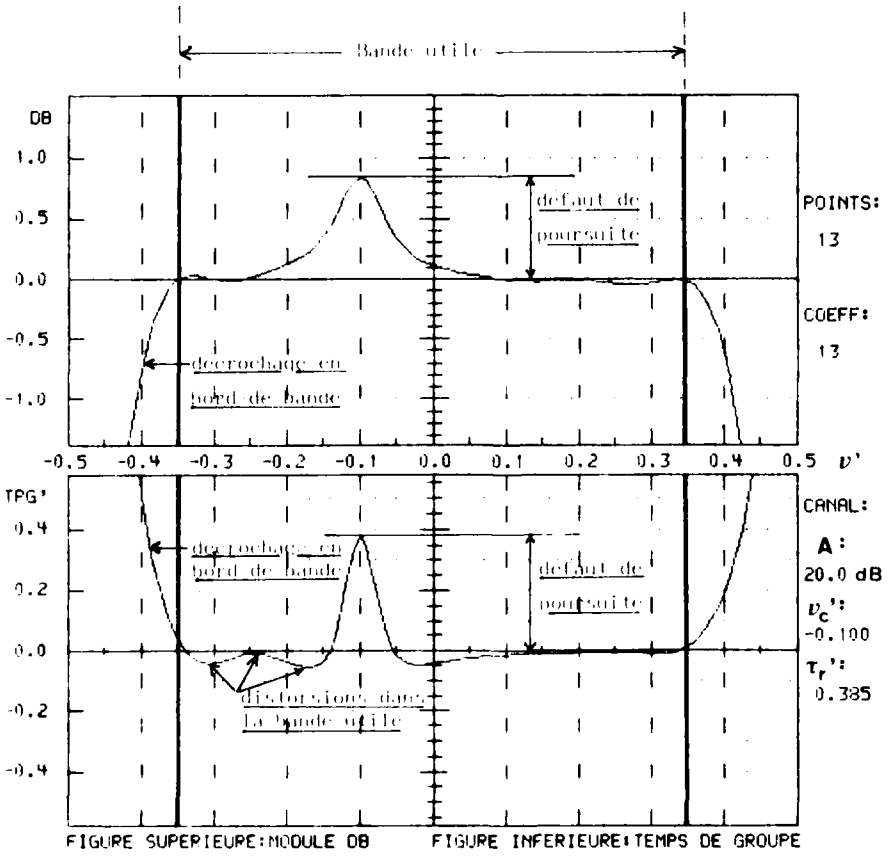

Figure 4 : Distorsions parasites

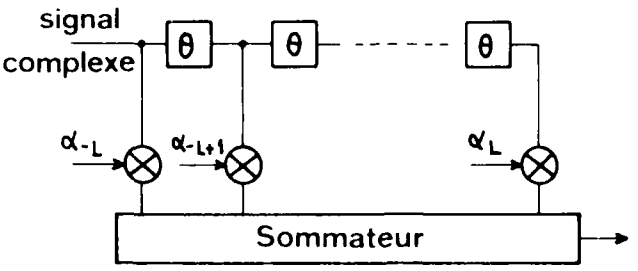

Figure 1 : Filtre linéaire transversal

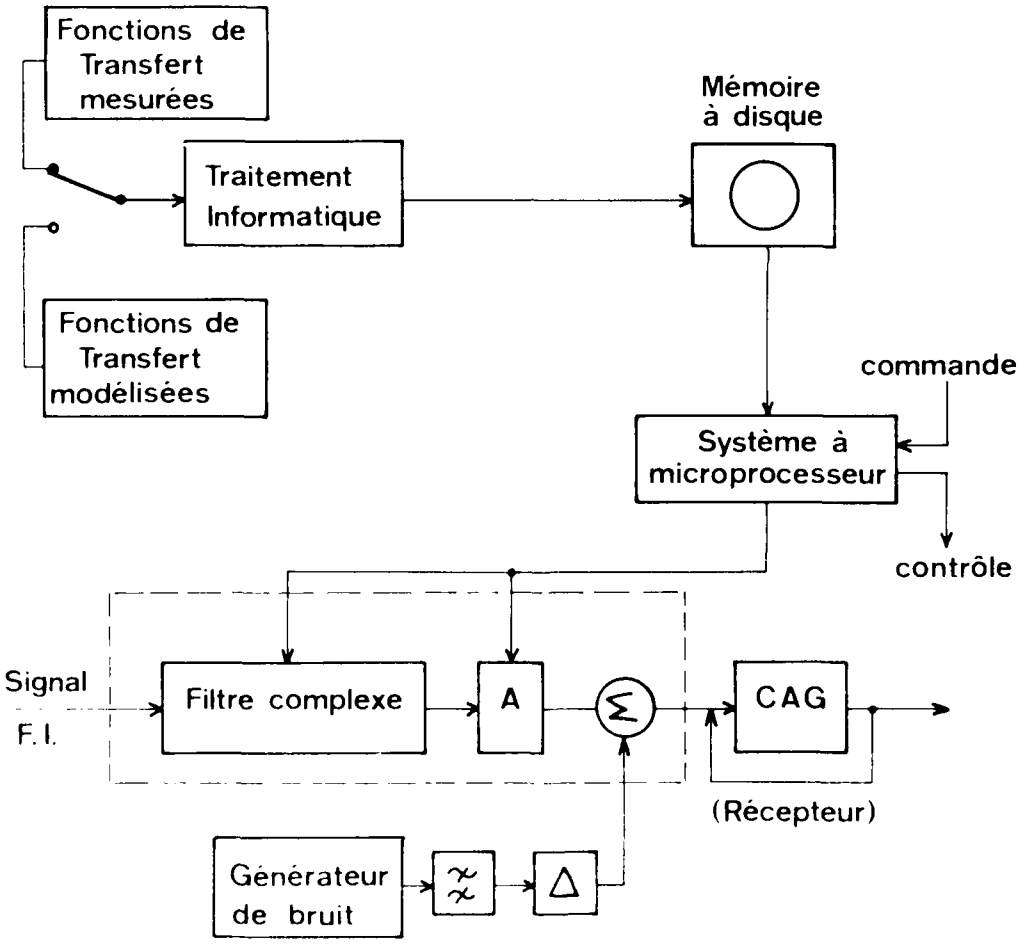

Les valeurs citées des distorsions parasites dans la bande utile sont données à la figure 9 en fonction de n. On constate que la dégradation de la qualité devient importante lorsque n est inférieur ou égal à 8 et est négligeable pour n supérieur ou égal à 11.

5 - CONCLUSION

Cette étude a déterminé les paramètres principaux d'un filtre linéaire transversal à coefficients complexes utilisé pour reproduire les fonctions de transfert mesurées du canal hertzien . Afin d'assurer une bonne qualité de reproduction, un nombre minimal de treize coefficients complexes est nécessaire. Ceci oblige à un effort technologique important quant à la réalisation pratique du filtre, étant donné le risque d'accumulation des défauts le long de la chaine de treize cellules. Le filtre est en cours de réalisation à la Société Anonyme des Télécommunications (SAT) - FRANCE.

Ce type de simulateur permettra une analyse beaucoup plus fine des performances des systèmes hertziens en présence d'évanouissements sélectifs. Plus particulièrement, les systèmes de synchronisation et d'égalisation auto-adaptative pourront être étudiés de manière dynamique en laboratoire, sur des évènements réels. Ceci devrait permettre de caractériser les équipements non plus seulement par leur signature, mais aussi par des critères prenant en compte la vitesse d'évolution du canal de transmission.

BIBLIOGRAPHIE

[1] L. MARTIN, "Etude de la sélectivité des évanouissements dus aux trajets multiples", Annales des Télécommunications, Tome 35, n° 11-12, pp. 482-487, Novembre - Décembre 1980.

[2] L.R. RABINER et B. GOLD, "Theory and application of digital signal processing," Prentice Hall, INC, New Jersey, 1975.

[3] L. MARTIN, "Statistical results on selective fadings", ICC'82, Philadelphia, pp. 7B.5.1 - 7B.5.5., Juin 1982.

Un nombre important de simulations sur ordinateur a permis de déterminer le nombre minimal de coefficients en fonction des plages de variation des paramètres de propagation. Le retard a une valeur maximale prise égale à $0,385\,\theta$, ce qui correspond à 5,5 ns pour B = 70 MHz.

Le nombre minimal retenu est de treize coefficients. Il conduit à une bande utile de l'ordre de 70 et des distorsions crête maximales dans cette bande de 0,1 dB en amplitude et $0,1\,\theta$ en TPG. Le défaut de poursuite est inférieur à 0,9 dB en amplitude et $0,4\,\theta$ en TPG.

La figure 5 donne les gabarits définissant les régions dans lesquelles se situent l'ensemble des distorsions parasites calculées, (exception faite des défauts de poursuite).

La valeur du retard élémentaire est choisie en fonction des dégradations dues aux défauts en bord de bande. La figure 6 donne la valeur des dégradations obtenues pour une probabilité d'erreur de 10^{-6} en fonction de la période du filtre. Les distorsions utilisées dans ce cas correspondent aux distorsions paraboliques maximales compte tenu des gabarits obtenus précédemment. Le retard élémentaire retenu est de 14,29 ns, soit une période B = 70 MHz.

4 - ASPECTS TECHNOLOGIQUES

L'implantation du filtre décrit au paragraphe précédent peut être effectuée soit en FI, soit en bande de base. Bien que la solution en FI présente de nombreux avantages (structure deux fois moins complexe et directement adaptée à l'insertion dans la partie FI du récepteur), elle nécessite une précision sur les valeurs des retards difficilement compatibles avec la technologie actuelle. Contrairement aux systèmes auto-adaptatifs, la précision requise sur les retards est directement liée à la précision imposée sur les coefficients. Pour cette raison, la solution en bande de base a été retenue. Sa structure générale est donnée à la figure 7.

Les défauts liés à l'implantation du filtre sont principalement dus à la précision sur les retards et à la quantification des coefficients. Leur influence sur la qualité des fonctions de transfert reproduites est analysée par simulation sur ordinateur.

4.1 Précision des retards

Les distorsions parasites dues à une imprécision sur les retards sont analysées de la manière suivante. Chaque retard est considéré comme une variable aléatoire équirépartie sur $\left[\theta(1-p/200),\theta(1+p/200)\right]$ où p représente en pourcent la précision relative pour l'ensemble des coefficients. Pour des valeurs des paramètres de propagation fixées, les distorsions parasites sont calculées pour différentes valeurs des variables aléatoires. Un exemple de distorsions particulièrement fortes parmi tous les cas qui ont été étudiés est donné à la figure 8. Les distorsions parasites sont tracées pour p=1, A_{max}=20 dB, τ_r = 5,5ns et r_c =-0,2. Le défaut de poursuite est très peu affecté par la précision des retards tant que p reste inférieur à 2 , l'effet principal portant sur les distorsions dans la bande utile. L'ensemble des simulations permet d'obtenir la valeur crête des distorsions parasites maximales dans la bande utile. Pour p=1, on a obtenu des valeurs crêtes de 0,2 dB en amplitude et 0,1 en TPG. Une précision relative de 1 représente l'objectif minimal à respecter lors de l'implantation.

4.2 Quantification des coefficients

Après calcul par le sous-ensemble traitement des données, les coefficients sont stockés sous la forme de mots de n éléments binaires (dont un élément binaire pour le signe). L'analyse de l'effet de la quantification est faite en déterminant d'une part la longueur n des mots, d'autre part la dynamique requise sur les résultats intermédiaires utilisés pour les opérations de multiplication.

$$\left.\begin{array}{l} 0 \leqslant \tau_r \leqslant 5{,}5\,\text{ns} \\ 0 \leqslant A_{max} \leqslant 20\,\text{dB} \end{array}\right\} \qquad (10)$$

Les enregistrements effectués pendant un mois particulièrement défavorable montrent que la valeur de 5,5ns n'a été dépassée que pour 1 % des cas et que sa fonction de répartition est indépendante de la profondeur d'évanouissement [3]. Cette valeur, associée à la limitation de A_{max} à 20 dB conduit à une prise en compte de 90 % des cas où la marge nette mesurée de la liaison a été dépassée.

3.2 Objectifs et critères de qualité

La sensibilité des systèmes hertziens aux évanouissements sélectifs est mesurée par la dégradation de la probabilité d'erreur pour un rapport signal à bruit (SNR) donné. Cette dégradation est souvent exprimée en décibel, et correspond alors à l'accroissement nécessaire du SNR pour maintenir la probabilité d'erreur à sa valeur en l'absence de défauts de propagation.

Un objectif majeur dans le choix des paramètres du filtre est de rendre l'effet sur la probabilité d'erreur des distorsions parasites dues aux défauts de reproduction des fonctions de transfert négligeable par rapport à la dégradation due à l'évanouissement sélectif même. On peut classer ces distorsions parasites en trois catégories :

1 - Défaut de poursuite : il correspond à l'écart entre la fonction de transfert mesurée et reproduite à la fréquence du creux de l'évanouissement. Ne changeant pas fondamentalement la nature des distorsions mais simplement la profondeur de l'évanouissement, il est considéré comme peu critique.

2 - Décrochages en bord de bande : la fonction de transfert donnée par l'équation (1) étant périodique et continue, la qualité de reproduction sera nécessairement médiocre en bord de bande. On est ainsi amené à définir la bande utile du filtre (exprimée en pourcentage de la bande totale B) qui représente la bande de fréquence maximale dans laquelle les effets de bords n'ont pas d'incidence sur la qualité de la reproduction.

3 - Distorsions dans la bande utile : ces distorsions dues au nombre limité de coefficients du filtre sont généralement moins marquées que les précédentes. Elles doivent toutefois être maintenues dans des gabarits tels que leur influence soit négligeable sur la dégradation de la probabilité d'erreur.

La figure 3 où sont tracées les fonctions de transfert en amplitude et TPG met en évidence ces différents défauts pour L=6, A_{max} = 20 dB, τ_r = 0,385 et r_c =-0,1. De même la figure 4 montre les distorsions parasites obtenues par différence des fonctions de transfert mesurée et simulée pour les mêmes valeurs des paramètres.

3.3 Choix des paramètres

La bande utile minimale requise ainsi que les gabarits des distorsions acceptables dans cette bande sont directement fonction des caractéristiques du système de transmission (débit, modulation). Le simulateur est conçu pour tester les sytèmes à 140 Mb/s et utilisant une modulation MAQ 16 en cours de développement pour le réseau français dans la bande supérieure des 6 GHz.

$$Q_{ech}^{opt} = \sum_{n=-N}^{N} P_n |S_n|^2 - (\underset{\sim}{\alpha}^{opt})^T \underset{\sim}{g} \qquad (5)$$

Différentes fonctions de pondération ont été analysées au cours de cette étude. Il est apparu que les allures extrêmement variables des fonctions de transfert à reproduire ne permettaient pas de définir une stratégie globale pour le choix de cette fonction. D'autre part, les améliorations obtenues étaient faibles comparées au cas sans pondération. Ceci nous a conduit à prendre :

$$P(\tau) = 1 \quad , \quad \text{pour} \quad |\tau| \leq 1/2 \qquad (6)$$

Dans ce cas, l'analyse de l'équation (4) montre que le vecteur $\underset{\sim}{\alpha}^{opt}$ de dimension 2L+1 est la transformée de Fourier discrète du vecteur S_n de dimension 2N+1. On en déduit que l'erreur quadratique est nulle lorsque la condition N=L est satisfaite, et que cette condition conduit aux oscillations minimales entre les points de test pour un nombre de points N donné. Le vecteur $\underset{\sim}{\alpha}^{opt}$ représente alors les coefficients de la série de Fourier, tronqués à 2L+1 élément de $S(\tau)$ périodifiée (de période B).

Afin de réduire les effets de la troncature, $\underset{\sim}{\alpha}^{opt}$ est pondéré par application d'une fenêtre temporelle. Nous avons retenu la fenêtre de Kaiser-Bessel [2] dont l'échantillon de rang k est donné par :

$$f_k = \frac{I_0\left[\beta\sqrt{1-(k/L)^2}\right]}{I_0[\beta]} \quad , \quad k = -L, L \qquad (7)$$

où $I_0(\alpha)$ est la fonction de Bessel modifiée de première espèce d'ordre zéro. β a été choisi égal à 6.

3 - PERFORMANCES DU FILTRE

3.1 Modèle de test

Afin de prévoir les performances du filtre sur un maximum de cas et avec simplicité, un modèle analytique du canal a été retenu dans un premier temps. C'est le modèle à trois rayons simplifié dont la fonction de transfert en bande de base est donnée par :

$$S(\tau) = a\left[1 - be^{-j2\pi(\tau-\tau_c)\frac{\tau_r}{B}}\right] \qquad (8)$$

où a représente la composante apériodique de l'évanouissement, b l'amplitude et τ_r le retard (non normalisé) du rayon réfléchi, τ_c le décentrage de l'évanouissement par rapport à la fréquence centrale du canal. Le signe de τ_r détermine le caractère minimum ou non minimum de phase de l'évanouissement. La profondeur de l'évanouissement est reliée à b par la relation :

$$A_{max}\ (dB) = -20\log_{10}(1-b) \quad , \quad b \leq 1 \qquad (9)$$

Le paramètre a est choisi égal à 1 pour l'ensemble des simulations effectuées, seules les distorsions étant approximées par le filtre (voir paragraphe 2.1). Les plages de variation des paramètres A_{max} et τ_r ont été choisis en fonction des mesures effectuées sur la liaison où ont été enregistrées les fonctions de transfert. Les valeurs retenues sont :

2.2 Méthode de calcul du filtre

La fonction de transfert d'un filtre complexe est donnée par

$$H(\nu) \quad \sum_{k=-L}^{L} \alpha_k e^{-j 2\pi \nu k \theta} \tag{1}$$

où (2L+1) est le nombre de coefficients (α_0 représentant le coefficient de référence), θ le retard élémentaire du filtre et α_k le coefficient d'ordre k. La fonction de transfert est périodique de période $B=1/\theta$. Dans la suite, fréquences et temps sont normalisés respectivement à B et θ .

Le critère retenu pour le calcul des coefficients est le critère de l'erreur quadratique minimale qui s'exprime par :

$$\min_{\{\alpha_k\}} Q = \int_{-1/2}^{1/2} P(\nu) \left| S(\nu) - H(\nu) \right|^2 d\nu \tag{2}$$

où $S(\nu)$ est l'équivalent en bande de base de la fonction de transfert à approximer et $P(\nu)$ une fonction de pondération permettant de privilégier certaines composantes spectrales. Rappelons que le critère tient compte à la fois de l'erreur sur l'amplitude et la phase.

Disposant de $S(\nu)$ sous forme échantillonnée, la version discrète de (2) que nous utiliserons s'écrit :

$$\min_{\{\alpha_k\}} Q_{ech} = \sum_{n=-N}^{N} P_n \left| S_n - H_n \right|^2 \tag{3}$$

où (2N+1) est le nombre de points pris en compte par le critère et P_n (respectivement S_n et H_n) est la valeur de $P(\nu)$ (respectivement $S(\nu)$ et $H(\nu)$) pour $\nu = n/(2N+1)$.

Les coefficients optimaux sont alors donnés par :

$$\underset{\sim}{\alpha}^{opt} = \tilde{E}^{*-1} \underset{\sim}{g}^{*} \tag{4}$$

avec :

$$\underset{\sim}{\alpha}^{T} = \{ \alpha_{-L}, \ldots, \alpha_0, \ldots \alpha_L \}$$

$\tilde{E} = \{ E_{mn} \}$, matrice carrée d'élément générique $E_{mn} = \sum_{k=-N}^{N} P_k e^{j 2\pi k \frac{i-n}{2N+1}}$

$\underset{\sim}{g}^{T} = \{ g_{-L}, \ldots, g_0, \ldots, g_L \}$, où $g_i = \sum_{k=-N}^{N} P_k S_k^{*} e^{j \frac{2\pi k i}{2N+1}}$

($*$ désigne la conjugaison complexe).

L'erreur quadratique minimale est :

(iii) l'absence de données dynamiques associées à ce modèle, ce qui rend impossible la simulation d'une séquence d'évanouissements en temps réel qui soit significative. Ce dernier point est particulièrement important pour l'analyse du comportement de sous-ensembles auto-adaptatifs du récepteur, par exemple sous-ensembles de synchronisation et d'égalisation.

Cet article présente l'étude d'un nouveau simulateur basé sur la reproduction de fonctions de transfert mesurées sur le site. Depuis plusieurs années, les études de propagation menées au CNET LAB ont donné lieu à l'enregistrement de fonctions de transfert en amplitude et temps de propagation de groupe sur une liaison expérimentale de 50 km de long fonctionnant à 11 GHz. La bande d'analyse est de 400 MHz et les fonctions de transfert mesurées tous les 1/18ème de seconde [1]. Le simulateur étudié utilise la banque de données ainsi constituée et permet de reproduire les distorsions enregistrées dans une bande utile de 50 MHz.

Le principe général du simulateur ainsi que la méthode retenue pour le traitement des données sont présentés au paragraphe 2. Les caractéristiques du filtrage et les performances théoriques sont détaillées au paragraphe 3. Enfin le paragraphe 4 analyse les problèmes technologiques liés à la réalisation de ce type de simulateur.

2 - PRINCIPE ET METHODE DE CALCUL

2.1 Principe du simulateur

Le principe retenu dans cette étude est de reproduire la fonction de transfert mesurée par l'intermédiaire d'un filtre transversal linéaire (Figure 1). L'absence de condition de symétrie hermitienne implique la nécessité d'utiliser un filtre à coefficients complexes. Le schéma général du simulateur est donné à la figure 2. On distingue trois sous-ensembles :

(i) Sous-ensemble de données

Cette partie assure le calcul des coefficients complexes du filtre pour chaque fonction de transfert à reproduire. Ce traitement peut être effectué en différé. Il convertit la banque de données initiale en une autre banque de données directement exploitable par le simulateur. Notons qu'il est également possible de simuler n'importe quel type de fonctions de transfert obtenues par modélisation analytique du canal de transmission. Ce principe retenu pour le stockage des données après traitement permet de reproduire un évènement d'une durée maximale d'une minute, ceci sans interruption.

(ii) Sous-ensemble de commande

La partie commande et contrôle est organisée autour d'un microprocesseur 16 bits. Elle assure le transfert des données vers le filtre et controle le déroulement de l'expérimentation en temps réel. La souplesse d'un tel système permet de reproduire un évènement à une cadence choisie par l'opérateur, du défilement à vitesse réelle jusqu'au bloquage du filtre dans une configuration déterminée.

(iii) Sous-ensemble de filtrage

Le filtre proprement dit s'insère dans la partie en fréquence intermédiaire du récepteur. Un atténuateur commandé (ii) est associé afin de séparer les fonctions de reproduction des distorsions et de l'atténuation du canal. Cette separation est particulièrement utile pour diminuer la précision absolue requise pour les coefficients du filtre, les évanouissements sélectifs étant accompagnés d'une atténuation apériodique [1]. Un banc de bruit couplé en sortie de l'atténuateur facilite la mesure de taux d'erreur.

ETUDE THEORIQUE D'UN SIMULATEUR DYNAMIQUE D'EVANOUISSEMENTS SELECTIFS POUR FAISCEAUX HERTZIENS NUMERIQUES

A. Bouidène, P. Vandamme

Centre National d'Etudes des Télécommunications
Centre Lannion B
Département MER/TSF
BP 40 - Route de Trégastel
22301 LANNION

ABSTRACT

This paper presents the theoretical study of a new type of channel simulator for line-of-sight digital radio systems. The basic principle is to reproduce channel transfer functions measured in the field during multipath propagation activity, by driving a complex linear transversal filter with precomputed data. The criterion used for calculating the values of the filter taps for each transfer function is the minimum mean square error criterion. It is shown that a thirteen-taps complex transversal filter with a period of 70 MHz in the frequency domain leads to accurate simulations of selective fading transfer functions in a 50 MHz bandwidth. Finally, technological features are investigated. Effects of the accuracy in the delays implementation and of the tap-weight quantification are particularly analyzed.

1 - INTRODUCTION

La qualité des faisceaux hertziens numériques à moyenne et grande capacités est principalement affectée par les phénomènes de propagation par trajets multiples. Ces périodes de propagation anormale sont responsables de l'apparition d'évanouissements sélectifs se traduisant par des distorsions à la fois d'amplitude et de temps de propagation de groupe (TPG) dans la fonction de transfert du canal. Afin de prémunir les systèmes de transmission par voie hertzienne contre des temps de coupure inacceptables dus à la propagation, des dispositifs correcteurs sont généralement associés au récepteur de structure classique. Parmi ceux-ci, les égaliseurs auto-adaptatifs commandés en bande de base représentent le moyen de compensation le plus puissant.

La nécessité de prévoir le temps de coupure d'une liaison amène à caractériser les performances du système en présence de propagation par trajets multiples, donc à pouvoir disposer en laboratoire d'un simulateur d'évanouissements sélectifs. Les simulateurs classiquement employés sont réalisés selon un modèle simple du canal hertzien : modèle à deux rayons dont l'un est retardé de manière fixée, avec commande de la fréquence du creux de l'évanouissement et de sa profondeur. Réalisés en hyperfréquence ou en fréquence intermédiaire (FI), ils représentent un outil simple permettant la caractérisation du système de manière statique, par exemple par relevés de signatures. Toutefois, l'efficacité de tels simulateurs est limitée par :

(i) Une reproduction de fonction de transfert selon un modèle figé qui est loin de correspondre avec précision à l'ensemble des cas effectivement observés. Entr'autres, la caractéristique en phase de la fonction de transfert simulée est déterminée de manière unique une fois la caractéristique en amplitude donnée. D'autre part, ce modèle n'autorise qu'un seul type de transition entre évanouissements à minimum et non minimum de phase.

concerned if the bad performance comes from such or such a type of fading. Perhaps those who construct models are not sufficiently interested in the notion of percentage of time. They are satisfied when they have simulated a real type of fade properly, without being sufficiently aware of whether the type of fade occurs for 1% of the time or .001% of time. From a practical point of view there is a very real difference.

Dr Hoffmeyer

Yes, I agree that the statistical distributions of parameters on the link are extremely important. It is important to validate the distributions given by Rummler for example for the parameters a, b and τ_{rr}.

Audience member

There has been some mention of the problems of ECM, in particular of the simulation of jamming. Is is possible to describe the different kinds of jamming presently used or envisaged, and systems used to overcome this jamming. We have spoken about antenna arrays, are other solutions envisaged?

Mr Klinker

The types of jamming we consider in our programme are CW jammers and noise jammers, and the only counter measure we consider is the null steering array.

SUMMARY OF SESSION IV

SIGNAL PROCESSING TECHNOLOGY

by
Vincent J.Coyne
Session Chairman

The papers presented in this session were all oriented toward the common goal of improved communications by reducing the deleterious effects of fading, multipath, and interference through the use of advanced signal processing schemes. Non-adaptive as well as adaptive techniques were discussed and it is apparent that the approach one might select is dependent upon the requirement, the operational environment and the funding available. The most complex scheme presented combined time filtering techniques with spatial filtering techniques to suggest the possibility for a dramatic improvement in the ability to provide reliable communications in a hostile environment. Although complex approaches such as this combination of spread spectrum technology and adaptive antenna technology have been postulated and simulated they have yet to be evaluated through field demonstration. Perhaps a more detailed treatment of this area, adaptive antenna and signal processing techniques, would be appropriate through a specialists meeting in the future.

The papers presented by Olaisen (paper 27), and Schilliger (paper 32), dealt with non-adaptive signal processing using wide bandwidths and state-of-the-art surface acoustic wave (SAW) matched filters to provide the high throughput, rapid synchronization, required for "push-to-talk" systems in the presence of interference. It is clearly emphasized that although digital processing infers increased speed, analog SAW devices might out-perform digital approaches in circumstances where high data rates and high processing gains (ECM considerations dictate about 1000) are required. Simulations demonstrate that a 20 microsecond synchronization time can be achieved and detection accomplished at jammer to signal ratios greater than 30 dB. Field tests are required for full evaluation of the concept. Lorenzoni (paper 28) also describes the advantage of a wideband concept using modulation and coding techniques in a satellite to ground digital transmission system as a method of reducing multipath effects.

The remaining three papers of the session dealt with the more complex approaches to signal processing associated with adaptive techniques. Peter Monsen (paper 26) provided an excellent tutorial of adaptive processing techniques currently available. He evaluated the concepts and described the drawbacks and advantages of each approach and concluded with a good example of the attributes of the Kalman-Godard algorithm in a General Decision Feedback Equalizer. Although this may represent an optimal approach, it does not necessarily represent the most economical approach and it behooves one to carefully evaluate requirements prior to selecting an approach.

Luvera (paper 31) provided an overview of US Air Force adaptive antenna developments being conducted at Rome Air Development Center which are oriented toward advancing the state-of-the-art. Developments covered were small adaptive loop modules, a system architecture for combining an adaptive array with a frequency hopping spread spectrum modem, and a new test bed for the evaluation of various adaptive spatial processing algorithms and architectures. The test bed utilizes a high speed digital, programmable array processor to implement a wide variety of adaptive algorithms and has the capability to implement either analog or full digital modes as well. It promises the ability to provide real-time, comparative analysis and evaluations of different processing techniques and should be an excellent tool for the development of new adaptive processing technology. His discussion of digital beamforming null steering systems provided a sense of the high computation rates required and emphasized the need for the utilization of very large scale integrated circuits (VLSI), optical processing and systolic arrays to make such systems feasible in the future.

Smith (paper 30) described how combining time processing techniques such as spread spectrum and adaptive equalization technology with spatial processing methods such as adaptive arrays could provide a formidable combination that holds promise for providing highly interference resistant communication systems with high data throughput. Computer simulations of combined time and space spectral whitening have been developed but hardware demonstrations are not described.

ADAPTIVE SIGNAL PROCESSING FOR RADIO COMMUNICATIONS

P. Monsen ScD
SIGNATRON, Inc.
12 Hartwell Avenue
Lexington, MA 02173

SUMMARY

A tutorial examination of adaptive processors for radio communication applications is presented. The general form of adaptive equalizers and Maximum Likelihood Sequence Estimators is discussed. The method of determining the performance of an adaptive equalizer in a fading channel environment is summarized. A simple example illustrates how "implicit" diversity is realized by channel adaptation. Methods of adaptation including Kalman filter techniques are presented along with performance results of practical fast adapting systems. The use of channel adaptation with error correction coding is also examined and practical results presented. These results show that most of the fading effect can be eliminated when there is no restriction on channel time delay. Multiple channel adaptive processors which eliminate correlated interference are also discussed. Performance results for a tropospheric scatter application are predicted and compared with laboratory measurements on a real system. Methods of fast adaptation of these multi-channel processors are discussed.

1. INTRODUCTION

Radio communication channels may suffer from a fading received signal level, multiple transmission paths with different time delays, and in-band or adjacent channel interference. Examples of these channels include tropospheric scatter communication in the 0.5 to 5.0 GHz frequency range, high frequency radio transmissions at 3 to 30 MHz utilizing ionospheric reflections, and line-of-sight radio communications at microwave frequencies. In many applications, the information bandwidth of the communication system is much larger than the rate of change of the radio channel. Under this condition, it is possible for the radio receiver to "learn" the channel characteristics and compensate for their deleterious effects. The channel characteristics include the gain, phase, and delay of individual transmission paths and the noise and/or interference statistics in both the frequency and spatial, i.e., antenna arrival angle, domains. This learning and compensation process is more conveniently accomplished when the transmission content is digital. With digital transmission, known reference signals such as Pseudo-Noise sequences can be time division multiplexed into the information stream. Correlation operations at the receiver between the known sequence and the received signals provide estimates of the channel characteristics. Alternatively, one can omit transmitting the reference signal and assume that the receiver decisions are correct for these correlation operations.

These adaptive processor techniques have been successfully applied in radio communications to significantly increase the information data rate capacity. In this tutorial paper we review some of the major features of these adaptive processors and present performance characteristics. We begin the presentation with a discussion of single channel adaptive processors in Section 2. Separate discussions are given for the adaptive equalizer and the maximum likelihood sequence estimator. Because of the wider application of equalizers and the limited scope of this paper, the remainder of the paper focuses on adaptive equalizer technology. In Section 3 we summarize the analysis for evaluating the performance of these adaptive systems in fading radio channel applications. The problem of adaptation is addressed in Section 4. The fastest known adaptation technique, the Kalman filter, is described and compared with the widely used Least Mean Squares (LMS) adaptation algorithms. Performance results for fast tracking algorithms in an HF radio application are presented. In Section 5 the role of error correction coding in the fading channel application is discussed. The condition under which channel adaptation can be used with coding is presented. Results from practical "adaptive channel" coding techniques are used to show that most of the fading effects can be eliminated when sufficient channel delay is introduced. Finally, in Section 6, we consider adaptation to multiple received signals particularly in the presence of correlated interference. We show how the performance of the single channel adaptive processor is extended and we present performance results for an example of adjacent channel interference. This section concludes with an examination of two fast adaptation schemes in this multi-channel application.

2. SINGLE CHANNEL ADAPTIVE PROCESSORS

Two adaptive processors for radio communication are the equalizer and the Maximum Likelihood Sequence Estimator (MLSE). The equalizer attempts to compensate for the channel imperfections by inserting filter components at the receiver which convert the tandem channel and equalizer combination into a quality communications medium. The MLSE works on the received sequence to produce an estimate of the most likely transmitted digital sequence. Other techniques used in fading channel applications concentrate on specific elimination of multipath induced intersymbol interference or burst noise phenomena. We examine here only the broad equalizer and MLSE generic systems.

2.1 EQUALIZERS

An adaptive equalizer performs filtering of one of more signal inputs in a manner which minimizes an error functional related to communications quality. The two most common error functionals are intersymbol interference (ISI) distortion and mean-square error where the error is defined as the difference between the decision sample variate and the correct decision. Minimization of ISI distortion ignores additive noise effects and is more often applied in large signal to noise ratio environments such as the telephone channel. The Minimum Mean-Error-Square (MMSE) criterion simultaneously copes with the effects of both ISI and additive noise. When the noise is small, the equalizer acts similar to an ISI distortion equalizer and when the noise is large, the equalizer has more of a matched filter structure. Because noise effects are just as important as ISI for radio channels, the MMSE criterion is more appropriate for this application. Note that the MMSE criterion is not optimum in that a one-to-one correspondence between bit error probability and MMSE does not exist. However, the MMSE criterion is clearly a "good" criterion since a clean decision sample variate is vital to producing small bit error probabilities. In a comparison study [1], the MMSE criterion was found to be inferior only when the SNR was very large and the ISI distortion after equalization nearly closed the data eye. Under more typical operating conditions, the criteria gave identical results. In the next subsection we discuss adaptive processors which minimize the sequence bit error probability rather than the mean-square error.

The linear equalizer (LE) is an adaptive filter which uses the received signal from the channel as an input. It has been long recognized that if the bit error probability is small, detector decisions could also be filtered and used to eliminate ISI effects. This concept leads to the Decision-Feedback Equalizer (DFE) which is composed of a forward filter with the received signal as an input and a backward filter with the reconstructed receiver decisions as an input. The MMSE DFE has been shown [2] to be theoretically superior to the MMSE Linear Equalizer in the absence of decision errors. The error propagation phenomenon resulting from decision errors in the DFE can be modeled as a Markov process and the increase in bit error probability calculated. These calculations [3] show only a small increase in the bit error rate for ISI typical of the radio channel applications. These results are consistent with error propagation bounds developed by Duttweiler, Mazo, and Messerschmitt [4].

A general Decision-Feedback Equalizer receiver is shown in Figure 1. The first two filters, the noise and matched filters, correspond to a small ISI receiver. The noise filter reduces correlated noise effects and the matched filter coherently combines the multipath returns. The forward filter minimizes the effect of ISI due to future pulses, i.e., pulses which at that instant have not been used to form receiver decisions. After detection, receiver decisions are filtered by a backward filter to eliminate intersymbol interference from previous i.e., past, pulses. Because the backward filter compensates for this "past" ISI, the forward filter need only compensate for "future" ISI.

A significant problem in the use of adaptive equalizers in certain radio HF channel applications is the requirement for rapid tracking of the adaptive equalizer weights. Simple estimated gradient techniques sometimes called Least Mean Squares algorithms, are not necessarily fast enough because of the correlation between signals on the equalizer taps. Because of this correlation, when the algorithm attempts to adjust one tap, noise fluctuations result in other taps. This problem will be discussed in a later section.

2.2 MAXIMUM LIKELIHOOD SEQUENCE ESTIMATOR

Since the DFE minimizes an analog detector voltage, it is not optimum for all channels with respect to bit error probability. By considering intersymbol interference as a convolutional code defined on the real line (or complex line for bandpass channels), maximum likelihood sequence estimation algorithms have been derived [5,6]. These algorithms provide a decoding procedure for receiver decisions which minimize the probability of sequence error. A Maximum Likelihood Sequence Estimator (MLSE) receiver in general requires a noise filter and matched filter although these functions can be imbedded in the estimator structure. Figure 2 illustrates the filtering and sampling functions which precede the MLSE. The estimation techniques used to derive the noise

and matched filter parameters also provide an estimate of the discrete sample response used by the MLSE decoder to resolve the intersymbol interference. An implementation of an MLSE receiver has been described by Crozier, et., al [7].

The MLSE algorithm works by assigning a state for each intersymbol interference combination. Because of the one-to-one correspondence between the states and the ISI, the maximum likelihood source sequence can be found by determing the trajectory of states.

If some intermediate state is known to be on the optimum path, then the maximum likelihood path originating from that state and ending in the final state will be identical to the optimal path. If at time n, each of the states has associated with it a maximum likelihood path ending in that state, it follows that sufficiently far in the past the path history will not depend on the specific final state to which it belongs. The common path history is the maximum likelihood state trajectory [5].

Since the number of ISI combinations and thus the number of states is an exponential function of the multipath spread, the MLSE algorithm has complexity which grows exponentially with multipath spread. The equalizer structure exhibits a linear growth with multipath spread. In return for this additional complexity, the MLSE receiver results in smaller (sometimes zero) intersymbol interference penalty for channels with isolated and deep frequency selective fades.

This additional complexity of the MLSE receiver has been the significant factor in the selection of adaptive equalizers for most practical applications. For this reason, the remainder of this paper will focus on adaptive equalizers. We now turn our attention to the achievable performance in fading channel applications.

3. FADING CHANNEL PERFORMANCE

The Decision-Feedback Equalizer has been developed for both troposcatter and HF radio communication applications. The performance of the DFE on a fading channel is a function of the radio/modem filters, the multipath profile of the channel, and the additive noise statistics. We consider a radio system as depicted in Figure 3. Here a modulator is used to convert a series of information digits to a continuous waveform s(t). For purposes of presentation we consider 4PSK because of its spectral and detection efficiency. In complex notation the modulating waveform for a $2/T$ bit rate is

$$s(t) = \sum_{k=-\infty}^{\infty} s_k f(t-kT), \quad \{s_k\} = \{\pm 1 \pm j\} \tag{1}$$

The transmit and receive filters are defined with impulse responses $f_1(t)$ and $f_2(t)$, respectively. The combined filter response is defined as

$$f(t) = \int_0^{\infty} f_1(\tau) f_2(t-\tau) d\tau \tag{2}$$

Either a discrete or continuous echo model of the radio channel can be used for the multipath profile. For the discrete model, the multipath profile has the form:

$$Q(\tau) = \sum_{i=1}^{I} q_i \delta(\tau - \tau_i) \tag{3}$$

where q_i is the average power in the i^{th} echo with τ_i as the multipath delay.

The structure of the DFE in a fading channel application is illustrated in Figure 4. Two comparators compare the analog voltages at the symbol sample time to zero and generate ± 1 outputs on each of the I and Q channels in Figure 4. These 4PSK decisions are fed back through the backward filter for cancellation of past intersymbol interference. Because of the discrete nature of the detected symbols the backward filter is a tapped delay line filter with complex tap weights, i.e.,

$$b(t) = \sum_{i=1}^{B} b_i \delta(t-iT), \quad b_i \text{ complex} \tag{4}$$

The forward filter must combine matched filtering of the channel with ISI removal. This suggests the use of a tapped delay line filter with complex tap weights but with less than one 4PSK symbol duration separation, i.e.,

$$w(t) = \sum_{k=1}^{K} w_k \delta(t-t_k), \quad w_k \text{ complex}, \quad t_k < T \ . \tag{5}$$

The performance of the DFE under ideal tracking conditions of the fading channel is summarized as follows [8]. Enough backward filter taps are assumed to cancel the past intersymbol interference. The DFE performance then only depends on the number and location (t_k values) of the forward filter taps. Under perfect tracking conditions, the equalizer performance is defined by a matrix signal-to-noise ratio S which is of rank K equal to the number of forward filter weights. The equalizer SNR which includes the fading effect is given by

$$S = A^{-1}C, \quad S \text{ is KxK, } K = \text{Number of Forward Filter Taps} \tag{6}$$

where A is the equalizer noise matrix and C is the equalizer signal matrix. For a sampling time t_0, the signal matrix is given by

$$C_{ij}(t_0) = \int_{-\infty}^{\infty} f(t-t_i)f(t-t_j)Q(t+t_0)dt, \quad i,j = 1,2,\ldots K \tag{7}$$

The noise matrix includes both an additive noise component and ISI component. The latter is an approximation by a Guassian noise effect and requires a scale factor γ which improves the approximation. We have for the noise matrix

$$A_{ij} = N_0\Phi_2(t_i-t_j) + \gamma \sum_{j=1}^{J} C_{ij}(t_0-jT) \tag{8}$$

where J future ISI interferers have been considered. When the ISI term is omitted in Eq. (8), the SNR matrix defines the no intersymbol interference bound on the DFE performance. The difference between realized performance and this bound is the intersymbol interference penalty.

The eigenvalues of the SNR matrix S are independent implicit diversity signal strengths normalized by the additive noise spectral density. Once the eigenvalues λ_k are found, the computation of bit error rate statistics proceeds as for any K^{th} order independent diversity system.

As a simple example, consider the single echo multipath channel which has an equal power echo delayed exactly one 4PSK symbol interval. If only a two tap forward filter is employed, one finds that the SNR matrix is given by

$$S = \frac{2\bar{E}_b}{3N_0}\begin{bmatrix} 1/4 & 0 \\ 1/4 & 3/4 \end{bmatrix} \tag{9}$$

where $\bar{E}_b/N_0$ is the ratio of average bit energy to noise spectral density.

The system is equivalent to a dual diversity channel with independent diversity strengths $\bar{E}_b/2N_0$ and $\bar{E}_b/6N_0$. Note that with a finite DFE structure, it is not possible to collect all of the available signal energy, i.e., the sum of the implicit diversity strengths does not equal $\bar{E}_b/N_0$. Even in this simple example, however, the potential implicit diversity gain is evident. A flat fading channel has an average bit error rate which varies as

$$\text{BER} = 1/2\,(\bar{E}_b/N_0)^{-1}, \qquad \bar{E}_b/N_0 >> 1$$

whereas the DFE in this example will give performance lower bounded by

$$\text{BER} = \frac{1}{2}\cdot\frac{1}{12}(\bar{E}_b/N_0)^{-2}, \qquad \bar{E}_b/N_0 >> 1 .$$

At an average BER of 10^{-5} this represents a gain of 29 dB.

4. EQUALIZER ADAPTATION

The equalizer adaptation problem can be viewed as the least mean square estimation of a tapped delay line weight vector given the sequence of equalizer inputs and of desired outputs. Using this formulation, D. Godard [9] developed a Kalman estimation algorithm for the equalizer tap coefficients. Since a Kalman algorithm minimizes the mean square error at every iteration, there is reason to believe that this algorithm is the fastest MMSE adaptation procedure. This assertion is supported by an interpretation of the Kalman/Godard algorithm as an ideal self-orthogonalizing algorithm [10] and by telephone channel simulation results reported in [9] and [10].

4.1 KALMAN FILTER ADAPTATION

The potential gain from an adaptive processing scheme can only be realized if the channel time variations can be closely tracked by the adaptation algorithm. The use of the Kalman approach or an approximation with many of its features promises the best chance of realizing this gain. One can also show that the tracking modes of a conventional least mean square (LMS) algorithm are too slow for some radio channel applications. For these reasons we review the Kalman approach to adaptive equalization.

A partitioned vector $\underline{h}_k$ can be used to describe the input processes for the forward and backward filters. The tap gains of the forward and backward filters can be similarly partitioned; let

$$\underline{c}_k = \begin{bmatrix} \underline{w}(k) \\ \hline \underline{\beta}(k) \end{bmatrix} \tag{10}$$

where $\underline{w}(k)$ is the forward filter weight vector at iteration time k and $\underline{\beta}(k)$ is the corresponding backward filter weight vector. The error sample is then given by

$$e_k = \underline{h}_k' \underline{c}_k - s_k, \quad \{s_k\} = \{\pm 1 \pm j\} \tag{11}$$

The conventional LMS algorithm has the form

$$\underline{c}_{k+1} = \underline{c}_k - \Delta \underline{h}_k e_k \, . \tag{12}$$

The Kalman estimation algorithm is derived from the state vector representation of $\underline{c}_k$. It updates a mean square estiamte c_{k-1} of the state using the latest measurement information s_k.

To utilize the Kalman equations in the equalizer adaptation problem, let $\underline{c}_{opt}$ be a fixed state variable, i.e., the state trajectory is a constant. We wish to find an estimate $\underline{c}_k$ of $\underline{c}_{opt}$.

Let the measurement equation express the relationship between the transmitted source digit s_k and the optimum error sample $e_{k,opt}$, i.e.,

$$s_k = \underline{h}_k' \underline{c}_{opt} + e_{k,opt} \, . \tag{13}$$

The Kalman equations [9] use the predicted source digit as the equalizer output

$$\hat{s}_k = \underline{h}_k' \underline{c}_k \tag{14}$$

and the Kalman algorithm for updating the state estimate (equalizer tap gains) is

$$\begin{aligned} \underline{c}_k &= \underline{c}_{k-1} + \underline{k}_k (s_k - \hat{s}_k) \\ &= \underline{c}_{k-1} - \underline{k}_k e_k \end{aligned} \tag{15}$$

where the Kalman gain vector is computed to be

$$\underline{k}_k = P_{k-1} \underline{h}_k (\underline{h}_k' P_{k-1} \underline{h}_k + \delta) \tag{16}$$

and the Kalman matrix is

$$P_k = P_{k-1} + \underline{k}_k \underline{h}_k' P_{k-1} \tag{17}$$

Inaccuracies in estimating the mean square measurement noise δ have negligible effect on the final results [9].

For the LMS algorithm, the Kalman vector, $\underline{k}_k$, in (15) is replaced by a constant times $\underline{h}_k$. The Kalman algorithm is significantly more complex as every iteration requires N^2 multiplications to obtain $P_{k-1}\underline{h}_k$ and N more to obtain the quadratic form. The LMS algorithm has N+1 multiplications per iteration. The computational burden of the Kalman algorithm, as measured by the number of required multiplications per iteration, is N+1 times larger than the LMS algorithm.

As an example of a practical application where channel tracking is a problem, consider the transmission of serial data over the HF radio channel. In HF transmission the ratio of the modulation symbol rate to the fastest channel rate fluctuations is not all that large as information rates of a few kilobit/second must allow for tracking channel rates on the order of a few Hertz. The classic Least-Mean-Square (LMS) algorithm widely used in telephone and microwave radio equalizer applications fails to track under these conditions.

The tracking failure of the LMS gradiant algorithm is due to the slow convergence caused by the smaller eigenvalues of the correlation matrix of the tap signals in the equalizer. Tracking convergence can be speeded up by modifying this correlation matrix by a transformation that generates equal eigenvalues. One tracking solution which achieves this result is the Kalman filter algorithm defined in Eqs. (15-17). The performance of the LMS and Kalman tracking systems under typical HF radio frequency selective fading conditions has been simulated to determine the improvement provided by the Kalman approach. An example is provided in Figure 5 for a 2400 bps data rate application over a 3 kHz HF radio channel. The irreducible error rate of the LMS system is due to slow tracking modes which can not keep up wit. the channel fluctuations.

4.2 SUBOPTIMUM FAST ADAPTIVE PROCESSORS

Although the Kalman filter offers the fastest tracking capability, its complexity grows as the square of the number of equalizer taps rather than linearly as with slower LMS equalizers. As a result there have been developed suboptimum tracking techniques which have almost the same tracking speed of the Kalman filter but considerably less complexity. Because of the proprietary nature of these algorithms, it is not possible to report on the details of the tracking method. However, performance results are available for modem implementations of these techniques. The application of most interest is adaptive equalization of the HF radio channel for data transmission at rates of 2400 bps or higher.

A series of tests on parallel tone modems by Watterson [12], and on two serial tone modems provide a basis for modem performance comparison for a high data rate HF channel application.

The parallel tone modems divide the data into low rate parallel sub-channels so that nonadaptive techniques can be used and ISI effects can be avoided. The serial tone approaches use PSK transmissions and some form of decision feedback equalization in an adaptive receiver structure.

There is considerable performance data available for the flat fading (single path) and the dual fading path suggested by Watterson [11]. This latter channel has two "skywave" returns which are spaced by 1 millisecond and they each fade with a 2σ Doppler spread of 1.0 Hz. In general the more echoes, the easier it is for the equalizer to track because it is less likely that all echoes will simultaneously become small. The Watterson two path channel has thus become a good standardized test case. Watterson tested conventional parallel tone modems on this channel and the results are given in his report [11]. This channel was also used in an evaluation of a Harris Corporation modem and a SIGNATRON modem. The results from these tests [12] provide a comparison of present day serial tone modem technology with the parallel tone modem approaches tested by Watterson.

All of the modems in this comparison are uncoded except for the parallel tone MX-190 modem which used a rate 16/25 block code. Although the simulators used on some of the tests were not exactly the same, no appreciable performance difference is anticipated from this factor. The fairest comparison is on a peak power basis because HF radios are peak power limited. For this reason we use peak bit energy E_{pb} rather than average bit energy E_b. The peak-to-average ratios assumed for the modem comparison were

SIGNATRON (SIG) Modem:	1 dB	SERIAL TONE
Harris (HRS) Modem:	1 dB	SERIAL TONE
USC-10:	7 dB	PARALLEL TONE
ACO-6:	7 dB	PARALLEL TONE
MX-190:	7 dB	PARALLEL TONE

Frequency selective fading results are shown in Figure 6. In these tests the Harris and SIGNATRON modem realize almost exactly the same implicit diversity when the fading is slow. The performance advantage of these modems over the parallel tone modems is very large under these conditions.

In comparison with parallel tone modems under the faster fading conditions, both the SIGNATRON and Harris modem still have a significant performance gain even over the coded MX-190 system. Both the Harris and SIGNATRON modems have not included error correction coding, which is the subject of our next section.

5. ADAPTIVE ERROR CORRECTION CODING

Coding gains for error correction coding techniques on radio channels must be examined relative to a delay constraint which allows or precludes interleaving over the fading epochs. These fading epochs are typically on the order of 1 second. The delay constraint determines whether adaptive techniques coupled with error correction coding will be effective or not.

5.1 DELAY CONSTRAINT PRESENT

Speech and certain digital data communication systems fall into this class. Under this constraint, error correction coding and modest interleaving will protect against burst noise. However no significant coding gain against fading is realizable under an average probability of error criterion. Under an outage probability criterion* the coding gain is exactly the coding gain realized on a nonfading channel at the Bit Error Rate (BER) threshold where the outage is determined. An off the shelf 1/2 rate convolutional decoder [13] with constraint length 7 gives a coding gain of 4.6 dB at a threshold BER of 10^{-4}. This coding gain drops to 3.8 dB at the BER threshold of 10^{-3}. Concatenated codes [14] which use a convolutional code for the inner code and a Reed-Solomon code for the outer code can do significantly better. This delay constraint condition reduces to an evaluation of coding gain on the non-fading channel. Adaptation to the channel in this case does not lead to any performance advantage.

5.2 NO DELAY CONSTRAINT

One can show that theoretical performance on the fading channel can come within 1 to 3dB of the non-fading channel [15] if we de-interleave the channel state information as well as the soft decision outputs from the modem. This implies that the receiver must adaptively learn the channel state information in a fading channel environment. It is of interest to examine practical adaptive coding schemes to determine realistic coding gains with this approach. Hagenauer [16] has computed the performance of a rate 1/2, constraint length 7, convolutional code for different quantitization levels of channel state information and decision values. The following nomenclature is used in the comparison.

Unquantized Decision = Y SOFT (YS)
1 bit quantized Decision = Y HARD (YH)
Unquantized Channel State = A SOFT (AS)
1 bit quantized Channel State = A HARD (AH)
No Channel State Information = A NO (AN)

The result of his calculations are reproduced in Figure 7.

This code has a 4.6 dB gain at a BER of 10^{-4} on the non-fading channel. It requires an E_b/N_0 of about 7.4 dB under fading conditions when both decisions and channel state are unquantized. This represents a coding gain over the non-fading channel of about 1.2 dB. The loss due to the fading is then only 3.4 dB. This small loss can be better appreciated by comparing the coded performance with dual diversity in Figure 7. It is also of interest to note that one bit quantization on the decisions and channel state does as well as unquantized decisions alone.

6. MULTI-CHANNEL ADAPTIVE PROCESSORS

In the previous sections we have been examining single channel adaptive processors, in particular, adaptation using a least mean-squares error criterion. This concept was first extended [17] to include parallel channels channels in a troposcatter application. The equalizer in this application not only removed intersymbol interference but also performed channel Doppler compensation and maximal ratio diversity combining. An improved performance capability was realized when the multi-channel linear equalizer was augmented with decision-feedback [2] for cancellation of previous receiver decisions. The application emphasis for these MMSE multi-channel processors has centered on intersymbol interference removal and the provision of additional implicit diversity through coherent recombining of multipath returns [8]. Although it has been historically recognized that these processors could also cancel correlated interference, this feature has not been exploited for the following reasons:

---

* The fraction of time that the error rate is greater than a selected threshold.

1. Cancellation of correlated interference signals results in loss of signal diversity which was needed for fading protection. System design typically provided enough diversity for signal fading with the premise or hope that interference would not be a problem.

2. The cancellation of large interferers such as jammers presents a tracking problem to the processor because the signal component is "hidden" in the interference signal.

3. In many communication applications such as LOS microwave radio, the use of multiple antenna aperture (space diversity) channels, which are required for interference cancellation, has only recently become popular.

Diversity concepts such as angle diversity [19] in troposcatter and LOS radio systems* and polarization diversity in HF systems can be used to augment existing diversity techniques to compensate for the diversity loss inherent in interference cancellation. Also the diversity loss associated with interference cancellation is ameliorated by the multipath or implicit diversity. The tracking problem can be solved by a pre-processor which adaptively orthogonalizes the channel outputs thus separating the large interference from the signal component. This pre-processor concept has been used in null steering applications for interference cancellation.

Evaluation of the performance of a MMSE processor is complicated by the presence of fading signals and intersymbol interference. In a recent paper [20] an approach to determine this performance has been developed.

This analysis converts the general correlated diversity, correlated noise (or interference) problem to which equalization is applied to an uncorrelated diversity, uncorrelated noise problem of the form shown in Figure 8.

The equalizer output then has the simple form

$$\tilde{s}_k = s_k \underline{w}'\underline{g} + \underline{w}'\underline{y}_k$$

where $\underline{y}_k$ is a white noise process and the random channel vector $\underline{g}$ has uncorrelated components.

Since $\underline{y}_k$ is a white noise process, the optimum solution to the minimization problem is the matched filter [21],

$$\underline{w}_0 = c\underline{g} \ .$$

Since the constant c multiplies both signal and noise, its value is of no importance. In this equivalent system, performance is completely determined by the set of d explicit/implicit diversity gains λ_i, i=1,2,...d and the average bit energy to noise power ratio.

6.1 PERFORMANCE RESULTS, AN EXAMPLE

The potential for interference reduction in a high speed digital troposcatter system is illustrated by computing the outage probability for a typical diversity configuration and a range of interference conditions.

For our example we assume a fourth order diversity system composed of two antennas (dual space) and two frequencies (dual frequency). This diversity configuration is denoted 2S/2F. The MMSE processor considered is a decision-feedback equalizer with a Tapped-Delay Line (TDL) filter on each of the four diversity branches. The TDL filter consists of 3 taps spaced at approximately a reciprocal bandwidth. The modem which utilizes this adaptive processor system is described in [18].

The model has been used to predict performance when the interference is out of band, i.e., adjacent channel interference. Performance is shown in Figure 9 (solid lines) when the interference is another QPSK signal but offset by two channel allocations (21 MHz). Here the degradations are not as large as an in band interference problem because of receiver filtering of some of the adjacent channel interference. The receiver filtering provides about 50 dB of rejection in this example. Note that even with 50 dB of filter rejection, the resulting interference to signal level is still 0 dB

---

* Although existing LOS systems do not use angle diversity, recent propagation analysis shows promise for this technique in this application.

for the top curves in Figure 9. There is no irreducible error probability due to this interference however because of the adaptive cancellation provided by the multi-channel equalizer. The dashed lines indicate experimental results on a troposcatter modem [22] under the adjacent channel conditions defined in here. A troposcatter simulator was used to synthesize the quadruple diversity fading channel. Good agreement between predicted and measured results was obtained.

6.2 ADAPTATION OF MULTI-CHANNEL PROCESSORS

Basic approaches to this problem can be divided into closed loop adaptive systems such as the LMS algorithm and open loop systems such as Direct Matrix Inversion. Regardless of the adaptation technique, the adaptive processing configuration can be further divided into two generic types. Here we briefly discuss these two generic adaptive antenna processor systems. These systems, shown in Figure 10(a) and (b), will be referred to as the Beam Steerer/Nuller Steerer (BN/NS) and the Gram-Schmidt Orthogonalizer/Combiner. The Beam Steerer/Null Steerer is so named because the beam steering function attempts to adaptively align an antenna system in the direction of the signal in order that effective antenna nulls can be formed on the aligned signals by the null steering system. In the GSO/Combiner, the GSO orthogonalizes the input signals and the combiner is a least mean square equalizer which seeks to maximize the output signal-to-noise ratio.

To compare the two adaptive processors let us assume that there is one mainbeam interferer $j(t)$ of power J and that a two port antenna system is to be used to adaptively reduce the interference effect. The outputs from these two antenna ports in this illustrative example are

$$x_1(t) = s(t) + j(t) + n_1(t)$$

$$x_2(t) = 0.1s(t) + 0.5j(t) + n_2(t)$$

where $s(t)$ is the desired singal of power S, and $n_1(t)$ and $n_2(t)$ are independent noise processes each of power N. We assume that $J >> S >> N$.

The BS/NS processor first performs a beam-steering operation on the antenna outputs x_1 and x_2 with the objective of driving the signal component in x_2' to zero, c.f. Figure 10(a). For the example, the optimum BS weights are $v_1 = -0.1$ and $v_2 = 0$, which yield the following beam steered signals:

$$x_1' = s + j + n_1$$

$$x_2' = 0.4j + n_2 - 0.1n_1$$

where we have for notational convenience suppressed the time dependence. The null-steering portion of the processor weights x_2' and adds the result to x_1 so as to minimize the total output power. For the assumed $J >> N$, the optimum NS weight is $w = -2.5$, which yields an output free of interference

$$y = s + 1.25n_1 - 2.5n_2 \quad . \tag{18}$$

We pause here to address the noise enhancement aspect of jamming suppression. For the example, the output noise power is $7.8N$, which is nearly 9 dB larger than that at the output of antenna port 1. This is purely a consequence of the fact that there is amplification in order to cancel the interference thus raising the noise level. The amount of noise enhancement goes up as the arrival angle between interference and signal decreases.

A disadvantage of the BS/NS system is that the BS is slow in the presence of strong jamming because long averaging times are required to extract the signal from the interfering noise in the beam steering function. As a result the BS could fail to keep up with rapid signal changes, possibly creating a situation where the electronic antenna boresight is pointed more towards the interference than the signal source. Null forming would induce large noise enhancement which may be sufficiently severe to cause communication outages.

The GSO/Combiner processor performs the beam-steering and null-steering operations in the reverse order in order to speed up the LMS tracking loops. More specifically, the GSO performs a linear transformation on x_1 and x_2 to produce two orthogonal signals:

$$x_1' = x_1$$

$$x_2' = x_2 - v\,x_1$$

where $v = E\{x_2 x_1^*\} / E\{|x_1|^2\}$. The GSO outputs are gain-equalized and then optimally combined by the adaptive LMS combiner. We note that the GSO does the null-steering while the LMS combiner performs the beam-steering to separate the signal from the interference.

To see how the GSO helps to speed up the LMS combiner, we note that for the example, the GSO weight is approximately $v = 0.5$. It follows that the GSO outputs are

$$x_1' = s + j + n_1$$

$$x_2' = -0.4s + n_2 - 0.5n_1 \quad .$$

These signals are then gain-equalized and then fed to the LMS combiner. Since x_1' is mainly interference and x_2' is mainly signal, the effective signal to interference ratio after gain equalization is 0 dB. At this SNR, the combiner can quickly track the signal, i.e., a shorter averaging time is required to arrive at the correct weights. If the combiner were to operate on the signals x_1 and x_2 instead, as in the case of the beam-steerer in the BS/NS processor, a much longer averaging would be required to extract the signal from the jamming noise.

Note that the optimum LMS combiner weights for this example are $w_1 = 0$, $w_2 = -2.5$, which yields the output y in Equation (18). The two adaptive processors yield the same output in the steady-state. The difference in performance lies in the tracking, or, transient, behavior of the two processors, i.e., the averaging times required to reach steady state.

The GSO can be realized using LMS adaptation, direct matrix inversion, or by computation in an off-line processor using digitized versions of the signals.

REFERENCES

[1] P. Monsen, Linear Equalization for Digital Transmission Over Noisy Dispersive Channels, SCD Thesis, Columbia U., New York NY, June 1970, P. 150.

[2] P. Monsen, "Feedback Equalization for Fading Dispersive Channels", IEEE Trans. on Information Theory, Vol. IT-17, No. 1, January 1971, pp. 56-64.

[3] P. Monsen,"Adaptive Equalization of the Slow Fading Channel", IEEE Trans. on Communications, Vol. COM-22, August 1974, pp. 1064-1075.

[4] D.L. Duttweiler, J.E. Mazo, D.G. Messerschmitt, "An Upper Bound on the Error Probability in Decision-Feedback Equalization", IEEE Trans. on Information Theory, Vol. IT-20, July 1974, pp. 490-496.

[5] G.D. Forney, Jr., "Maximum likelihood sequence estimation of digital sequences in the presence of intersymbol interference", IEEE Trans. on Information Theory, May 1972, pp. 363-377.

[6] G. Ungerboeck, "Adaptive maximum-likelihood receiver for carrier-modulated data transmission systems", IEEE Trans. on Communications, Vol. COM-22, No. 5, May 1974, pp. 624-636.

[7] S. Crozier, et al., "An adaptive maximum likelihood sequence estimation technique for wideband HF communications", MILCOM '82, Conference Record, Vol. 2, pp. 29.3, October 1982.

[8] P. Monsen, "Theoretical and measured performance of a DFE modem on a fading multipath channel", IEEE Trans. on Communications, Vol. COM-25, No. 10, October 1977, pp. 1144-1152.

[9] D. Godard, "Channel Equalization Using a Kalman Filter for Fast Data Transmission", IBM Journal of Research and Development, May 1974, pp. 267-273.

[10] R.D. Gitlin and F.R. Magee Jr., "Self-Orthogonalizing Adaptive Equalization Algorithms", IEEE Trans. on Comm., Vol. COM-25, No. 7, July 1977, pp. 666-673.

[11] C.C. Watterson, C.M. Minister, HF Channel-Simulator Measurements and Performance Analyses on the DSC-10, ACO-6, and MX-190 PSK Modems, Office of Telecommunications, Boulder, Colorado, Report No. OTR 75-56, July 1975.

[12] L.K. Cosell, S.R. Kolek, P. Monsen, and L.C. Perry, "HF Modem Test and Evaluation", RADC-TR-83-19, Final Technical Report, Distribution Unlimited, January 1983.

[13] Linkabit Corporation, LV7026 CODEC brochure, San Diego, CA.

[14] G.C. Forney, Concatenated Codes, MIT Press, Cambridge, MA, 1966.

[15] P. Monsen, "Modem HF Communications, Modulation and Coding", AGARD Lecture Series, No. 127, May 1983, pp. 8-1 to 8-13.

[16] J. Hagenauer, "Viterbi-decoding of convolutional codes for fading and burst channels", Proc 1980 International Zurich Seminar on Digital Communications, G2.1 - G2.7.

[17] D.M. Brady, "An adaptive coherent diversity receiver for data transmission through dispersive media", IEEE Internat. Communications Conf. Rec. (San Francisco, CA), June 1970.

[18] D.R. Kern and P. Monsen, "Megabit Digital Troposcatter Subsystem (MDTS)", GTE Sylvania, Needham, MA and SIGNATRON, Lexington, MA, Final Report, Distribution Unlimited, ECOM-74-0040-F.

[19] G. Krause and P. Monsen, "Results of an angle diversity field test experiment", NTC Conference Record, 1978.

[20] P. Monsen, "MMSE equalization of interference on fading diversity channels", to be published in the IEEE Trans. of Communication.

[21] L.A. Wainstein, V.D. Zubakov, Extraction of Signals from Noise, Prentice-Hall, Inc., 1962.

[22] John Gadoury, Error Performance Characterization Study of a Digital Troposcatter Modem (MD-918/GRC), Final Report, Distribution Unlimited, for Defense Communications Engineering Center, Reston, VA, prepared by GTE Sylvania, Needham, MA, July 1983.

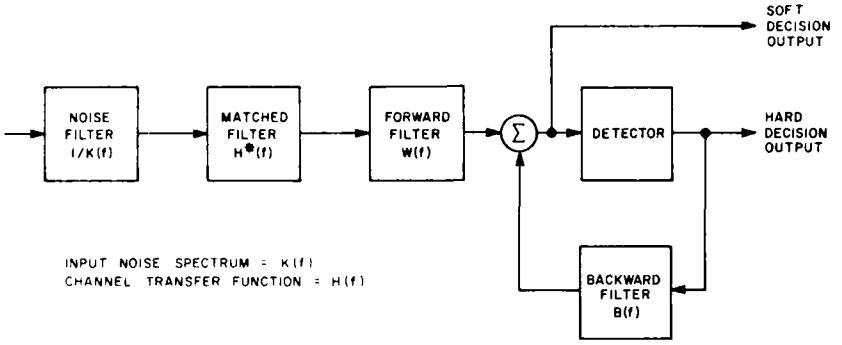
SOFT
DECISION
OUTPUT
NOISE
FILTER
1/K(f)
MATCHED
FILTER
H*(f)
FORWARD
FILTER
W(f)
Σ
DETECTOR
HARD
DECISION
OUTPUT
BACKWARD
FILTER
B(f)
INPUT NOISE SPECTRUM = K(f)
CHANNEL TRANSFER FUNCTION = H(f)

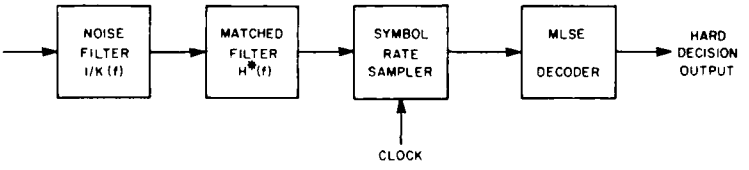
NOISE
FILTER
1/K(f)
MATCHED
FILTER
H*(f)
SYMBOL
RATE
SAMPLER
MLSE
DECODER
HARD
DECISION
OUTPUT
CLOCK

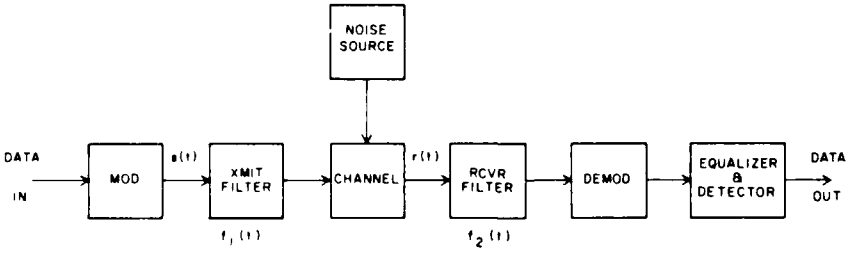
NOISE
SOURCE
DATA
IN
MOD
s(t)
XMIT
FILTER
CHANNEL
r(t)
RCVR
FILTER
DEMOD
EQUALIZER
&
DETECTOR
DATA
OUT
f1(t)
f2(t)

transfer function, that are spaced, in frequency, of $1/\tau$.
So, for a given τ, it is possible to design an integrate coding/modulation structure, with bandwidth $1/\tau$, that allows to minimize the losses.
In particular an efficient technique consist in the mapping of codewords into channel waveforms, by means of multiple frequency shift keying (MFSK), and with a frequency shift between the symbols equal to $1/L\tau$, if L is the number of tones of the modulation (L = 8 for example).
For a given geometrical situation a value of bandwidth B is required to enable the efficient transmission of a particular word not only over a minima of $|H(w)|$ but also over a maxima.
Fig. 2 shows the bandwidth required, with several aircraft - satellite geometries, to obtain the transmission of a codeword over a whole period of the transfer function $|H(w)|$.
Fig. 3 simply, shows, a typical function $|H(w)|$ and fig. 4 represent the possible allocations of the eight frequency slots of two signals arriving from the satellite repeater; the frequency slots of the signals are multiplexed, staggering the frequencies of a quantity equal to the symbol rate, so that the transponder bandwidth can be more efficiently utilized.
Fig. 2 shows that the bandwidth requirements does vary with the aircraft height and that the more demanding situations are the ones relative to low aircraft heights.
A bandwidth of about 200 KHz con be suitable for heights above 1 Km.
If the reflection is diffuse rather than specular, the multipath signal is the sum of rays scattered from several points of the earth's surface. The channel tranfer function might take the form:

$$H(\omega) = 1 + \sum_{K} \gamma_K e^{-j(\omega\tau_K - \varphi_K)}$$

where K refers to an infinitesimal scattering area that contributes to the multipath with a delay τ_K and with a reflection coefficient $\gamma_K e^{j\varphi_K}$.
We have:

$$|H(\omega)|^2 = 1 + 2\sum_{K}\gamma_K\cos(\omega\tau_K - \varphi_K) + \sum_{ij}\gamma_i\gamma_j\cos[\omega(\tau_i - \tau_j) + \varphi_j - \varphi_i]$$

and, neglecting the infinitesimal term's of second order, is:

$$|H(\omega)| = \left[1 + 2\sum_{K}\gamma_K\cos(\omega\tau_K - \varphi_K)\right]^{1/2}$$

The delays τ_k are all greater than the one, τ_{min}, that would be produced by a 2 ray multipath.
Also in this case the bandwidth, required to have the transmission of a codeword over a whole period of $|H(w)|$ is equal to $1/\tau_{min}$. So the fig. 2 represents the demand of bandwidth also fo a diffuse multipath.

4. RECEIVER FUNCTIONAL DESCRIPTION

The detection of energy associated to each codeword can be easily performed through a FFT digital filter bank. A simplified scheme of the frequency characteristic of the bank is shown in fig. 5.
We can think of the DFT as a bank o matched filters, where each filter is matched to only one of the complex sinusoidal sequences of the basis set, Ref.(1), and is insensitive to the others.
In other words the q-th DFT filter is matched to a sequence of samples, taken each T seconds, of the form

$$f_q(nT) = A\, e^{j\omega_q nT} \qquad , \quad q = 0, 1, \ldots, N-1$$

where $\omega_q = 2\frac{\pi q}{NT}$, NT is the observation interval.
Moreover the N complex sequences are orthogonal, meaning that the sum $\sum_{n=1}^{N} f_v(nT) f_l^*(nT)$ is zero whenever $v \neq l$; and the l-th matched filter output, u_l is:

$$u_l = \sum_{n=1}^{N} f_v(nT)\, e^{-j\omega_l nT}$$

and is zero when $v \neq l$.
However the problem of the filter sidelobes contribution must be carefully considered, especially in presence of frequency mismatching due to Doppler shifts or to oscillator unstabilities.
A possible implementation of the demodulator/decoder is represented in fig. 6.
The satellite received signal is converted from IF analog form into digital complex samples carrying frequency and amplitude information. Two parallel IF to baseband converters operate in quadrature each followed by A/D converters.
A 64 point FFT performs the square-law envelope detection of the channel symbols. The maximum likelihood of each of 64 codewords of a Reed Solomon 8-ary code is computed and a soft decision is carried out.
In fact the decoder,that achieves the smallest possible probability of error in chosing the correct codeword based upon the received waveform, computes the 64 decision variables (log - likelihood quantities):

$$x_i = \sum_{K=1}^{7} |u_{W_{iK}}|^2 \qquad i = 1, 2, \ldots, 64$$

where $|U_W|^2$ denotes the w-t FFT matched filter output, for W = 1, ..., 8 and W_{ik} is the Kth element of the ith codeword.
The above described operation requires that the FFT is matched to the received signal. To this purpose a Doppler Tracking Loop (DTL) has to be implemented wich sets the converted tones exactly at the center of each filter.
Also, an AGC system normalizes the average output of the detector to avoid gain variation (and instabilities) in the DTL.
The Doppler shift sensing is obtained through comparison of the outputs of two contiguous filters. Fig. 7 represents, conceptually, how the measure can be performed.

5. PERFORMANCE RESULTS

A model of the digital communication system that we have considered is shown in fig. 8. The transmitter employs a combined encoder/modulator to generate the waveforms from the input data bits. In ref. (2) the performances of a M-ary non coherent multichannel communication system, using orthogonal codewords are derived.
A multipath model, considered there, is the Rayleigh channel that is a useful theoretical reference model, for the performance of the assumed system.
Moreover we assume that the codeword, chosen for transmission, is selected from a set of 64 equiprobable words and that each codeword is sent to the receiver with a constant energy waveform composed of a sequence of M sinusoidal symbols at different frequencies. Assuming for M the values 7, 8, 9 the curves of fig. 9 can be obtained.
The same figure represents the performance of the FSK uncoded system over a Rayleigh channel.
The curves of fig. 9 take into account the supplementary energy required for the word syncronization and Doppler compensation. In the hypothesis of M = 7 a total of 8 symbol are assumed to be transmitted for each codeword.

A TECHNICAL SOLUTION TO FADINGS IN TACTICAL SATELLITE DIGITAL TRANSMISSIONS

by

Giacinto Losquadro
Selenia Spazio
Via Tiburtina Km. 12,400, Roma
00100
Italy

Lt. Col. Andrea Lorenzoni
Centro Consultivo studi e Ricerche dell'Aeronautica Militare,
Aereoporto di Pratica di Mare, Roma
00140
Italy

SUMMARY

Tactical satellite communication systems may provide service to high performance aircrafts employing antennas with relatively wide beamwidths.
Unfortunately, the fadings and multipath phenomena could strongly influence the capability of point to point data transmission.
In order to overcome the problem of the design of a coding/mo-demodulation structure, and to determine the actual link margin, an analysis and a simulation of a multipath channel has been performed.
The performance gains that are achieved with the use of a suitably wide bandwidth modulation and with three different theoretical fading models are shown.
The problem of the bandwidth spreading has been related to the aircraft height and to the geometry of the multipath model.
A solution to the problem of multiplexing of several wideband signals, over a repeater bandwidth, has been proposed and the performances of a receiver, based on a FFT spectra analyzer, are illustrated.
The simulation results confirm that, the FFT based receiver allows the soft decision demodulation of one or several simultaneous channels, with performances that are very close to the ones given by the optimal receiver for ortogonal codewords; moreover, the FFT solves, elegantly, the problem of Doppler shifts even in presence of fadings and with the capability to track the satellite signal even for manouvering aircraft.

1. INTRODUCTION

Purpose of this work has been to study the improvement offered by the FFT processing of the signal transmitted by a fixed station to a satellite, and then received by an aircraft in level flight or manoeuvering.
The FFT processing, useful for the non-coherent detection of a MFSK signal, could be used also for Doppler compensation and code word synchronization in a multipath environment.

2. GEOMETRY FOR MULTIPATH AERONAUTICAL CHANNELS

The signal arriving at the aircraft antenna is the sum of a direct ray and a (potentially) indirect ray resulting from reflection of the satellite signal from the earth surface and received by the aircraft user.
The user antenna is assumed to be almost omnidirectional so that a multiplicity of indirect signals arrives to the user delayed with respect to the direct path.
Being: h the height of the aircraft with respect to the earth surface; θ the angle between the two segments, aircraft center of the earth, and satellite - center of the earth; d the distance between satellite and the surface point directly below the aircraft, we have:

$$\tau_{min} \approx \frac{2h}{d}\left(6.6\cos\theta - 1\right)\frac{R}{c}$$

where τ min is the minimum delay between direct and indirect path, R is the earth radius and c is the speed of light.
The delay of the indirect ray w.r.t. the direct one is shown in fig. 1 for different aircraft heights and different angles.
The minimum delay occurs when the aircraft is at low altitude or when the elevation angle of the satellite, with respect to the earth surface, is low.

3. DIVERSITY RECEPTION AND BANDWITH REQUIREMENT

As shown in fig. 1, the differential delay, that characterizes the aeronautical channel, assumes values ranging from 0 to several μsec.
Moreover the reflected ray, combining with the direct one, results in additive or destructive interference causing a "reinforcement" or a "weakening" of the signal.
In case of specular reflection (in flat sea state) the transfer function of the channel can be represented as:

$$H(\omega) = 1 + \gamma e^{-j(\omega\tau - \varphi)}$$

where $\gamma e^{j\varphi}$ is the reflection coefficient of modulus γ and phase φ and ω is the actual radian frequency of the signal.
We have:

$$|H(\omega)| = \left[\left(1+\gamma^2\right) + 2\gamma\cos\left(\omega\tau - \varphi\right)\right]^{1/2}$$

That reveals a minimum if:

$$\omega\tau - \varphi = \left(2K+1\right)\pi \qquad K = 0, 1, \ldots$$

or, in the hypothesis of a radian frequency shift $\Delta\omega$, if:

$$(\omega + \Delta\omega)\tau - \varphi = (2K+1)\pi$$

So, when $\Delta\omega\tau$ is equal to a integer multiple of 2π, we have a second minimal condition.
In other words, the two ray fading, in the hypothesis of an unchanged reflection coefficient (which is reasonable for a very small frequency shift, of the order of 1‰ of the signal center frequency) causes a set of minime, of the channel

DISCUSSION

E.W.Lampert, Gc

For detection of a spread spectrum signal with convolvers you have to invert the reference code with respect to the transmitted. When you are using a code which is many bits long, have you to know in advance the time structure of the code, i.e. bit structure and periodicity?

Author's Reply

The appropriate reference signal must be known at the moment the incoming signal is entering convolver. If the reversing of the codes is performed in shift registers, by first loading the register with code and then shifting in reverse, the code has to be known at a time equal to the length of the convolver before TOA.

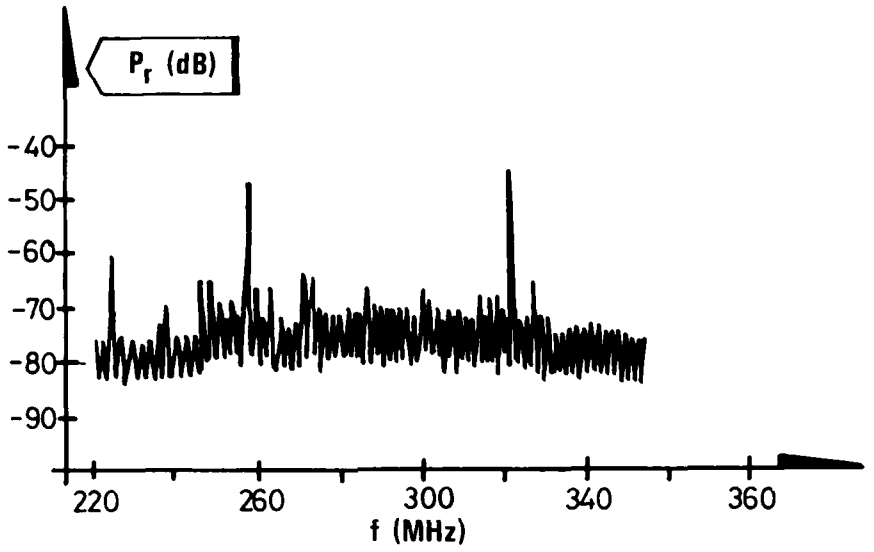

FIGURE 8. SIGNAL SPECTRUM DURING SPREAD SPECTRUM RECEPTION

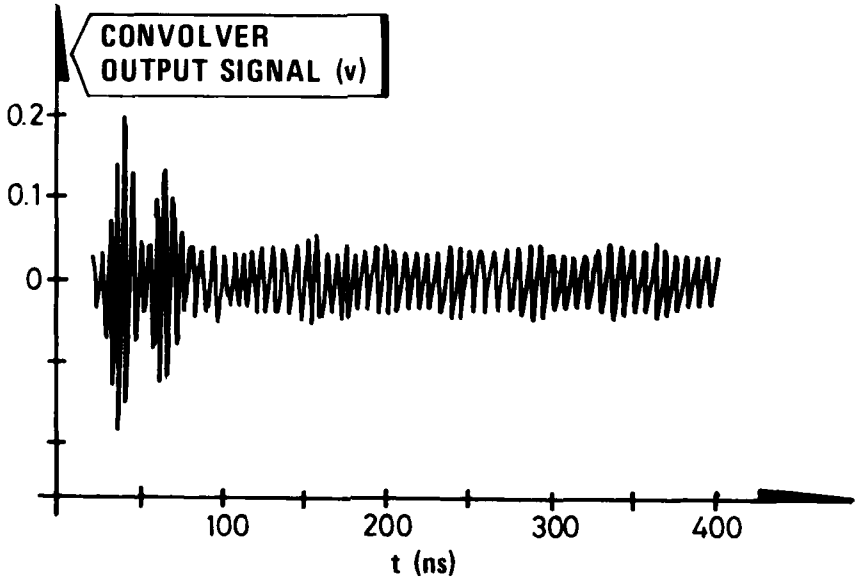

FIGURE 9. CONVOLVER OUTPUT SIGNAL FOR INPUT SPECTRUM SHOWN IN FIGURE 8

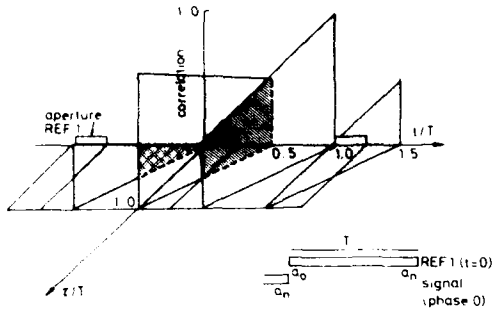

t/T is the time axis and τ/T represents the phase of the received signal

FIGURE 4. CORRELATION FUNCTION FOR REFERENCE 1 AND RECEIVED SIGNAL

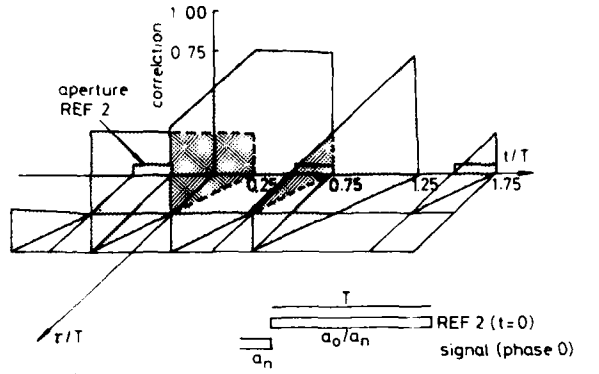

t/T is the time axis and τ/T represents the phase of the received signal

FIGURE 5. CORRELATION FUNCTION FOR REFERENCE 2 AND RECEIVED SIGNAL

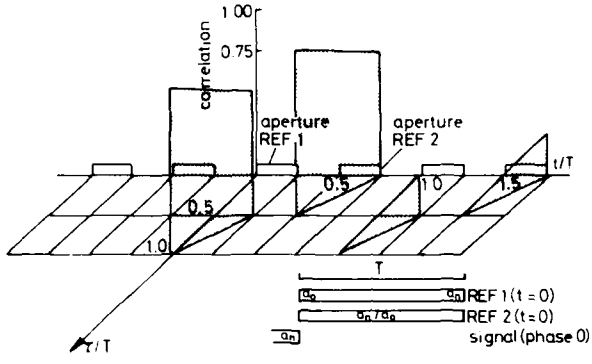

t/T is the time axis and τ/T represents the phase of the received signal

FIGURE 6. CORRELATION FUNCTION FOR RANDOM ARRIVING PREAMBLE AS SEEN THROUGH THE APERTURE WINDOWS OF CONVOLVER 1 AND CONVOLVER 2

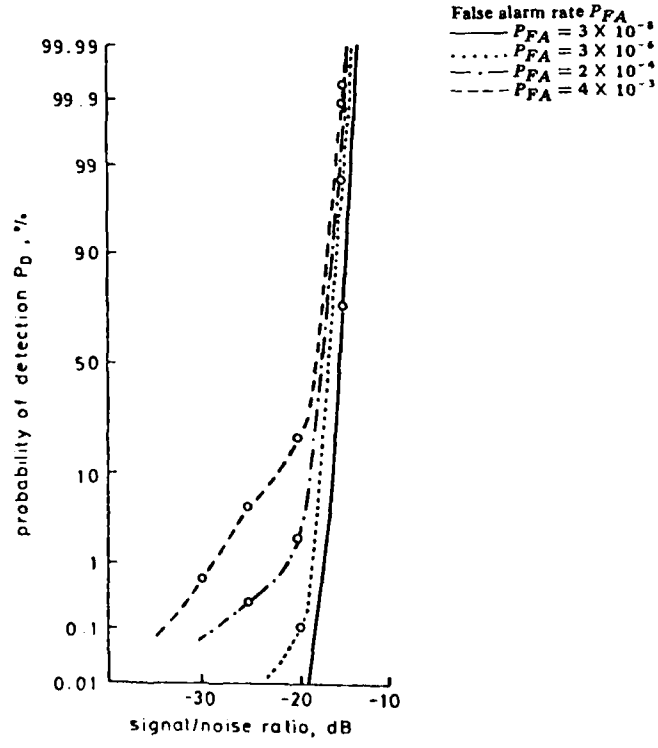

FIGURE 7. EXPERIMENTAL PERFORMANCE OF SYNCHRONIZED MODEM WITH WHITE GAUSSIAN JAMMER

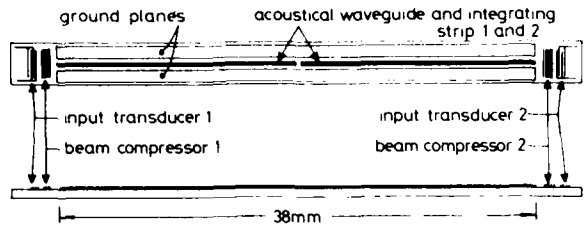

FIGURE 1. REPORTED CONVOLVER

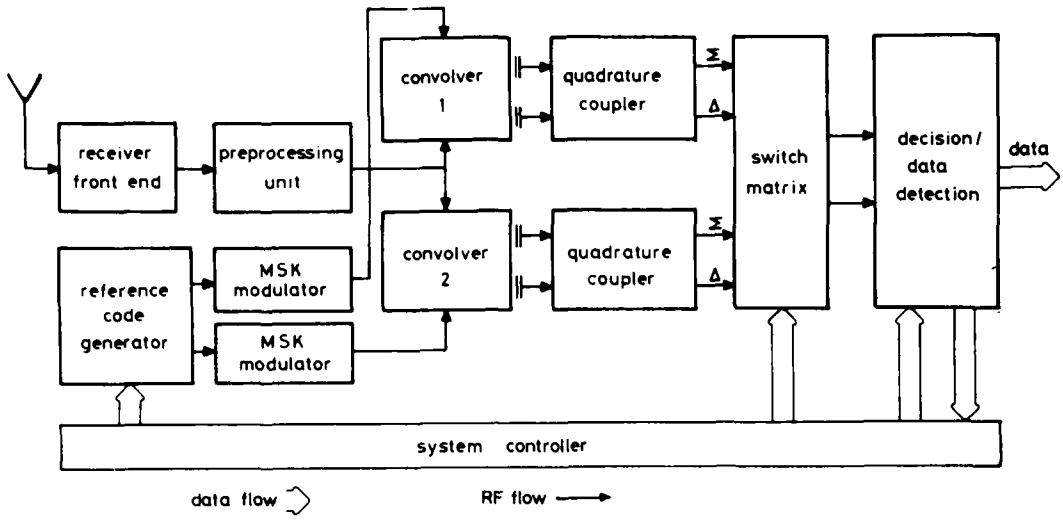

FIGURE 2. DEMODULATOR/RECEIVER

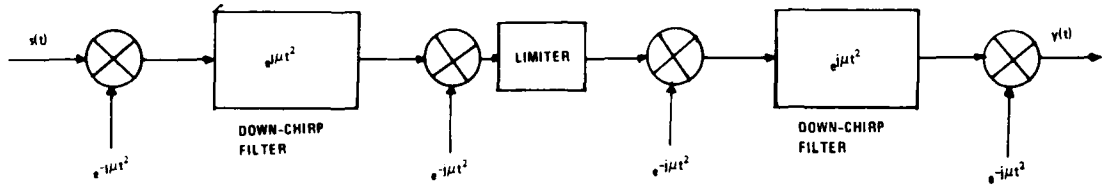

FIGURE 3. FOURIER TRANSFORM PROCESS FOR INTERFERENCE SUPRESSION

Experiments have verified that correct operation is attainable to -28 dB SNR. The degradation from 30 to 28 dB is due to internal reflections within the convolver, where the coded signal beats with its time-symmetrical image and raises the overall peak sidelobe level by 2 dB.

Experiments have also verified that pulsed CW jamming gives no further degradation relative to continuous jamming even if the pulse frequency is phased to the code chip frequency.

If wideband white-noise jamming is applied, the obtainable jammer spectral intensity will generally be much lower. The threshold setting of the correlation peak detection circuit will have to be adapted to a maximum allowable false alarm rate. This is the same situation as in pulsed radar systems, where a target (correlation) is to be detected in the presence of clutter (noise), and the same theory applies.

It is important to note that, owing to the expected stochastic noise in a practical system the probability of detection will never equal unity because a high probability of detection corresponds to a high rate of false alarms.

The performance of the system with respect to wideband Gaussian noise has been measured to a precision of 10^{-6} (10^{8} samples). Figure 7 shows the probability of detection against signal/noise ratio, with the false alarm probability (threshold setting) as the parameter. These curves give the basic performance of the system. They are within the significance of the measurements in accordance with theory. As can be seen from the curves, the probability of detection exceeds 99.99% for signal/noise ratios greater than -13 dB at false alarm rates of less than 10^{-8}.

At the 99% level of detection, which is a reasonable point of operation during transmission, the necessary input level varies by less than 2 dB for false alarm rates between 10^{-3}-10^{-8}.

The conclusion of the performance evaluation is that the modem performs according to expectations. The protection given by the spreading code is maintained, even during severe jamming conditions.

5 PROPAGATION TEST

So far only preliminary field trials have been carried out due to the fact that appropriate test equipment is still under development. The purpose of the performed tests have therefore been to verify laboratory tests and to demonstrate the modem. For the same purpose the modem is used to transmitt 5 delta-modulated voice channels. For simplicity the 300 MHz IF was transmitted directly without heterodyning. The antennas used was disc cones with a gain of 2 dBi, the transmitter and receiver antenna heigths were 3 respectively 12 m. For line of sight communications across a distance of 25 km, 140 mW radiated power was sufficient to attain accepable voice quality when little interference was present. This corresponds to a power density of only 1 µW/KHz and shows the potensial for concealed communications.

Figure 8 shows a situation where two strong and unwanted signals and several unwanted weak signals are present within the spread spectrum bandwidth. The spread spectrum signal is barely recognized in the noise as a slight curvation of the noise floor inside the bandpass filter of the receiver.

For this test the distanse is 7 km and the terrain roughness parameter Δh is 20 m. Figure 9 shows the corresponding convolver output signal. The two correlation peaks exhibit conditions of multipath. Due to the timecompression in the convolver the delay of the reflected signals is twice the time between the peaks. The presence of multipath was also seen as distortion of the spectrum of the received signal when full power was transmitted.

The two narrowband signals are apprently removed.

The preliminary field trials have clearly demonstrated the LPI potensial of the modem and indicated that performance in all respects are according to theory.

When the new test equipment is available a complete test program will be conducted. The data analyzer/logger under development is based on a Z 80 µP and are very flexible. It will measure and record bit error rates and probability of synchronization.

A special part of the test program will investigate the influence of a DS spread spectrum system on conventional communication systems both analog and digital and vice versa. This part of the program is carried out in co-operation with the Norwegian Telecommunication Administration.

References

(1) Engan H, Ingebrigtsen K A, Rønnekleiv A: "Design of SAW convolver for processing MSK modulated waveforms", Electron Lett, 1980, 16, (24), pp 908-909

(2) Brodtkorb D, Layton J E: "Fast Synchronization in a spread spectrum System based on acoustoelectric convolver" Proceedings of IEEE ultrasonic symposium 1978, pp 561-566

The detection concept presupposes random arrival time of the message signal. Coarse synchronization of convolver reference signal and received signal under these conditions introduces special and significant problems related to correlation ambiguities. The convolver differs from a usual matched filter in the sense that the reference is not merely stored but rather recirculated. Thus the received signal and the reference may not only produce one correlation peak at the output for each databit period but multiple peaks. The peaks do however differ considerably in magnitude and it is not unimportant to choose the largest possible. The problem is however that at the point in time when one correlation peak is detected the receiver do not out of hand have any information on whether a larger peak will arrive later or if the largest peak has been missed. This situation is a result of the random phase of the recirculating code reference when the signal arrived.

For the reported design the two DPSK convolvers are linked to a pair of code generators recirculating code-references which are time-reversed images of the expected transmitted preamble. The two references are identical but are time displaced by one bit time (= 1 data bit). The references and the received signal propagate in opposite directions in the convolvers so that they have an apparent relative speed twice the actual speed of either. It takes four bit times for a received preamble to pass completely through the convolver, and thus four partial-correlation peaks, spaced one bit time apart, will result at the output of each convolver. This is shown in figures 4 and 5.

These multiple partial correlations introduce ambiguities and detection methods are required that can guarantee that only the largest peak produces a synchronization. Some systems (2) use coincidence detection and logic gating to remove the ambiguities and guarantee correct synchronization. This method usually requires storing and delay of the output from one of the convolvers until there is a decisive output from the second convolver. The practical realization of delay and store is considered nontrivial, and the coincidence method may also require a nonprocessed or dummy bit in the message preamble to align local reference and received signal which increases the time to synchronize. These problems are avoided in this system using a specially designed scheme of time-displaced references and aperture signals.

The synchronized aperture signals are simple aperture window functions defining what may be said to be useful regions of correlation. There are two window functions, one for each of the DPSK convolvers, and they open at time intervals displaced by half a bit time. The functions are traced in figures 4 and 5. They remain open for half a bit time every two bit times. With a 25% duty cycle for each aperture window and the use of two convolvers recirculating the same, but time-displaced, sequence, the received signal is observed half the time. This is, however, acceptable because of the time compression due to counterpropagating references and received signal. The time-bandwidth product of input and output signals remains the same, and no significant information is removed.

The correlation at any instant is defined as

$$CORR = (S_\ell) \cap (A^j) \qquad \begin{matrix} 0 < \ell < p-1 \\ j = 1,2 \end{matrix}$$

where S is the received sequence of elemnts a_0, a_1, a_2,..., a_{2046}, and $A^j = \overline{S}$ is the time-displaced reference, the overbar denoting time reversal. The parameter ℓ describes the distance from the edge of the output transducer to the position of the received signal.

Figure 6 shows the phase-time-correlation function for a randomly arriving message as seen through the aperture windows of convolvers 1 and 2. As the figure points out, the largest partial-correlation peak is seen first, either by convolver 1 or by convolver 2. Thus there is no need for storing, delaying and logic gating to determine the received-signal arrival time. To bring the received signal and references in bit alignment for full correlation, the receiver uses counters that keep track of the recirculating references. The use of time-displaced references and two aperture window functions ensures that the largest partial-correlation peak is detected within an epoch of two time bits from the appearance of a message. This is important because, after the two time bits of the preamble, the next bit in the message will enter the convolver, and, in order to perform demodulation, the references must also start to enter the convolvers at this point in time. Thus the signal processing used avoids the need for nonprocessed or dummy bits in the message, and the system achieves synchronization after 20 μsec.

If the peak is detected before two time bits have elapsed, the code generators are stopped, loaded with their starting vector and then restarted on information from the counters. The counters keep track of the reference time base and determine by how much it must be shifted to achieve perfect alginment. This removes any loss due to misalignment.

4 ECM TESTS ON MODEM

Measurements have been performed to evaluate the modem performance in wideband and narrowband jammer environments.

The processing gain offered by the spreading code will, in principle, give equal protection against wideband and narrowband jammers of equal energy within the processed frequency band. This system with a spreading code chip rate/data bit rate of ~ 1000 should thus allow for jammer energy to exceed signal energy by up to 30 dB before detection becomes impossible.

Extensive tests have been performed with CW jamming of the transmissions. The frequency spectrum of the transmitted code consists of lines separated by the inverse of the code length, and the energy in each line is given by the MSK power distribution. A CW jammer will beat with each of these lines, and the sum of all these beats will be seen as sidelobes in the correlator output signal. The sidelobe pattern will have a rapid frequency dependence as the beat frequencies change, but the envelope will remain constant. The detectability of the spread-spectrum signal should thus be unaffected by the jammer down to a 30 dB negative signal/jammer-level ratio, where the sidelobe level approaches that of the correlation peak.

2 THE SURFACE ACOUSTIC WAVE CONVOLVER AND RF SUBSYSTEM

The basic concept of surface acoustic convolvers is to launch acoustical waves on opposite ends of a piezoelectric crystal with sufficient acoustical amplitude to activate nonlinear effects in the crystal. As the two waves overlap, they will interact through the nonlinearities to induce a potential on the surface of the crystal which is proportional to the product of their amplitudes. If this potential is integrated along the surface, the total voltage is proportional to the convolution between the signals leaving the two transducers. It is, however, necessary for one of the input signals to be time inverted in order to compensate for the effect of wave propagation in opposite directions.

If the two acoustic waves with wave vectors k_1, k_2 and frequencies f_1, f_2 are launched in opposite direction ($k_1 = -k_2$) and with the same frequencies ($f_1 = f_2$), the resultant product wave will have wave vector $k = k_1 + k_2 = 0$ and frequency $f_1 + f_2 = 2f_1$. The convolver is then said to be degenerate, and the product wave can be picked up by integrating the potential along the convolver the integral expressing the correlation between the two signals. If k were nonzero, an interdigital transducer would be needed to couple out the convolved signal.

Transmitter and receiver modems for spread spectrum signals based on acoustoelectric convolvers as programmable matched filters has been developed at NDRE. The modems offer fast synchronization and may handle burst formatted messages or digitized speech. With a bandwidth of 100 MHz and an IF center frequency of 300 MHz the time between clock cycles is short and efficient algorithms have been developed to synchronize the received signal and the reference in the convolver. The system is developed for MSK spreading modulation and DPSK data modulation with a Processing gain of 30 dB during data transfer and 33 dB during synchronization.

A convolver design specifically adapted to process MSK-modulated waveforms was reported in 1980 by Engan, Ingebrigtsen and Rønnekleiv (1). In this system the convolver frequency response and phase characteristics are matched to the spread-spectrum signal (with timebandwidth product of ~ 1000) in order to optimise the dynamic range of the signal processing unit.

The DPSK data modulation requires the convolver to have a length of 2 data bits and separate convolver plating for each data bit as depicted in figure 1.

Choice of RF-modulation scheme is crucial to system performance. Military tactical communication requires maximal spectral flatness and constant envelope waveforms in order to minimize jamming and intercept susceptibility. Phase or frequency shift keying give the required constat envelope, but out of band energy is high due to the sharp transitions in the RF waveform. Minimum frequency shift keying (MSK), as used in this system, is advantageous compared to PSK or FSK because fractional out of band power is less and the signal waveform has a continuous first derivative. The block diagram of the receiver is shown in figure 2. From the RF-front end the signal is entering an IF-preprocessing unit at the intermediate 300 MHz frequency. This unit is critical to system performance because of the very broad bandwidth of the system. Ideally, the signal entering the convolvers should have a uniform spectrum and be free from narrowband interference. Research is presently going on at NDRE to achieve increased ECM performance through limiting in the frequency domain by means of Fourier transform processors. The system is implemented using linear FM sweep signals and chirp filters implemented in SAW-technology. The transformation of the total received signal to a representation in frequency, "spreads" the different interference out in time and a limiter can in its simplest form be used to reduce interference "peaks". The system is shown schematic in figure 3. A conventional configuration do however consist of bandpass filtering and automatic gain control.

The reference sequence is MSK modulated onto a carrier in the same way as in the modulator and convolved with the incoming IF-signal.

Generally MSK modulation is achieved by converting the code bit stream to a RF waveform by hopping between two frequencies separated by half the bitrate. By switching frequency at the top of the waveform, the first derivative will be continuous and out of band power and spectral roll off is at optimum. For this system MSK modulation is implemented by passing a PSK modulated carrier of frequency f_1 through a bandpass filter with a sinx x transfer function centered at f_2 and with a null to null bandwidth equal to that of the PSK signal. The filter is implemented in SAW technology.

Because each convolver operates at 50 % duty cycle due to the DPSK data coding, two convolvers are operated in a bit-staggered fashion. A receiver control and reference generator unit feeds the convolvers with the appropriate sequences while selecting the required outputs from quadrature hybrids. The hybrids detect the relative phase between the convolvution output of each half of each convolver and dependent on the data content the correlation peak will appear on either the Σ or Δ port of the hybrid.

3 DETECTION CONCEPT

To avoid repeating codes and their vulnerability to jamming spectal emphasis must be put on spreading code design. In the test system the spreading codes used during datatransmission will however be segments from a long code. This makes it possible to transmit on the order of one thousand data bits each using consecutive and different segments of the long sequence. However message synchronization to a precision of one spreading code bit must, as in all spread spectrum systems, be performed before any fine synchronization and data demodulation takes place. This requires a suitable preamble. In the test system the choice is a maximal-length sequence with good autocorrelation properties and a duration equivalent t two data-bits.

FAST SYNCHRONIZATION MODEM FOR UHF SPREAD-SPECTRUM COMMUNICATION SYSTEM

Reidar Skaug/Hermund Olaisen
Norwegian Defence Research Establishment
P O Box 25
N-2007 Kjeller
Norway

ABSTRACT

Communication systems employing wideband digital techniques and special modulation methods are presently being developed to support the requirements for speed and volume as well as survivability and efficiency in tactical battlefield data distribution.

The transport of information in a battlefield scenario presents considerable problems where both the laws of physics and, enemy and own actions are limiting factors. Introduction of spread spectrum equipment able to withstand the electronic warfare threat has often been impracticable in tactical systems with "push-to-talk" signalling One of the reasons has been synchronization difficulties. Rapid and effective synchronization of spread spectrum systems often requires matched filter processing in the receiver. The realization of such filters presents technological problems for high data speeds. Surface acoustic wave (SAW) technology has however been very promising in this connection.

The paper will present a spread spectrum modem utilizing state of the art SAW technology to process the communication signals. The system operating at UHF is optimized for "push-to-talk" operation with a synchronization time of 20 µsec and offers data speeds up to 100 kbit/sec. With a processing gain of approximately 30 dB, the radio modem is also able to resolve and reject multipaths on the order of 10 nsec. It is thus expected to avoid certain selective effects due to multipath which are usually encountered in narrowband communication systems.

1 INTRODUCTION

The recent rapid advance within computer technology has made cheap processing power available for military command, control and communication systems. Computers able to handle and classify received data no longer represent any major technological challenge. On the other hand, transport of tactical information within the areas of battle do represent significant problems where both the laws of physics and own and hostile electromagnetic activity represents degrading factors. The need for updated and to the greatest possible extent correct scenarios make it necessary in certain situations for the radios to handle high signalling speeds.

For appropriate functioning in the anticipated electronic warfare (EW) scenarios new radio systems are expected to apply various measures. The most noted of these measures are:

- Direct sequence spread spectrum
- Frequency hopping
- Antenna nullsteering
- Adaptive frequency, filtering
- Adaptive power control
- Automatic, adaptive traffic routing

Communication systems employing wideband digital techniques and special modulation methods, such as direct sequence spread spectrum are presently being developed to support these requirements for speed and volume as well as survivability and efficiency in tactical battlefield data distribution.

Introduction of spread spectrum equipment able to withstand the electronic warfare threat has often been impractical in tactical systems with "push to talk" signalling. One of the reasons has been synchronization difficulties. Rapid and effective synchronization of spread spectrum systems may require matched filter processing in the receiver. These matched filters are usually implemented as correlators.

State of the art digital gates and advanced LSI design are presently only able to handle spread spectrum datarates of a few kbit/sec if a reasonable EW protection is to be built into the system. And the demands on the processor are not modest. If for example the datarate required is close to 100 kbit/sec and EW considerations demands a processing gain on the order of 1000, the processor in the receiver must be able to carry out one thousand multiplications and summations in a time period of 10 nsec, or in other words 100 billion (10^{11}) multiplications and summations in one second. Digital signal processing is usually associated with increased speed but for these wideband systems analog processing may outperform digital processing due to the natural speed in the physical process in analogue matched filters. In this respect Surface Acoustic Wave devices seem optimal for high speed systems.

These devices are basically analog delay lines with a propagation delay of a few microseconds per centimetre and an operating frequency in the range of 1-1000 MHz and fractional bandwidths up to 100%.

When used as a processing device in direct-sequence spread spectrum communication, the usefulness of fixed-function matched filters is limited because repeated use of the same spreading code makes the system increasingly vulnerable to eavesdropping and intelligent jamming. Thus processing of effectively coded direct sequence spread spectrum signals requires correlation/convolution of signals against a variable reference signal as is attainable in programmable matched filters.

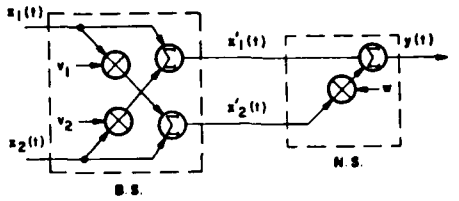

Figure 10a. Beam Steerer Null Coarser (BS Nul Processor

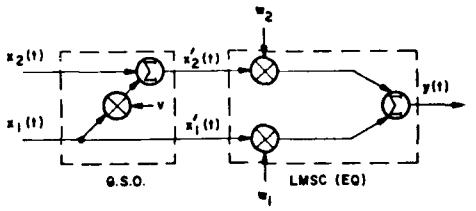

Figure 10b. GSO/Combiner Processor

DISCUSSION

J.S.Belrose, Ca

I would like to ask two questions relating to the practical application of the sophisticated signal processing techniques that you have described at HF and for the more typically employed baud rates (say 75 and 300 baud).

(1) You mentioned that for these adaptive techniques to work, you need to have a large number of bits in each fading cycle. Will these techniques therefore work for signalling rates significantly slower than those you have used in your simulation tests? and

(2) Have your techniques been hardware implemented, and used at signalling rates of 2400 and 2900 baud in practical HF links? If so, where and for what links (path lengths and latitudes)?

Author's Reply

(1) These adaptive coding systems should be easier to implement for low data rates because less memory is required to store the bits over multiple fading epochs. The equalization techniques do not require delays on the order of the fading epochs.

(2) Signatron is presently developing an HF modem using the principles presented in my paper.

B.Burgess, UK

Thank you for an excellent review paper, which was comprehensive and will need reading many times. I have a question relating to comparison of modems as illustrated in your Figure 4. In NATO on this side of the Atlantic we have been exposed to the merits of the ANDVT (Advanced Adaptive? Narrowband Digital Voice Terminal) which incorporates a modem pioneered at NRL and is I believe the CODEM as described by Chase. Can you give any comments on the performance of this 2.4 kb/s system compared with those given in your Figure 4.

Author's Reply

The AN-DVT uses a parallel tone modem approach and has a peak-to-average ratio of about 8 dB. Hence its performance is similar to the parallel tone modems shown in my Figure 4. Final transmission using adaptive equalization and error correction coding has the potential to perform many dB better.

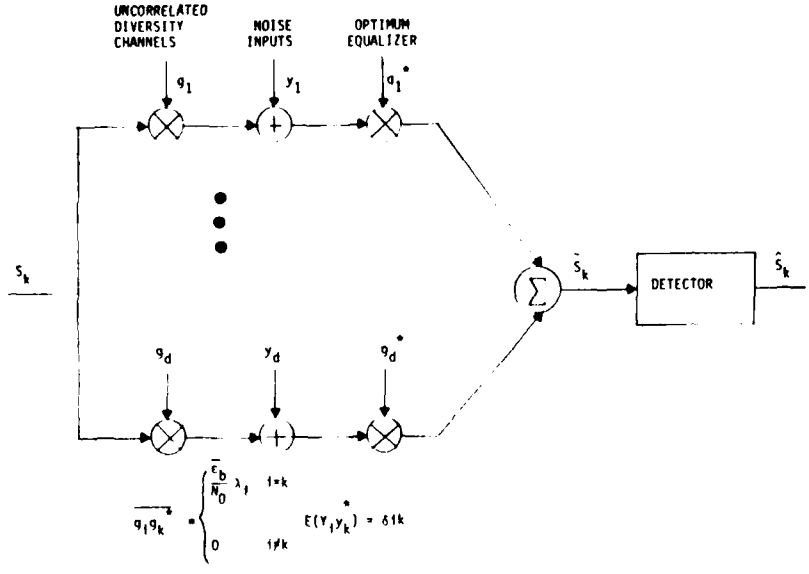

Figure 8 Uncorrelated Diversity Equivalent System

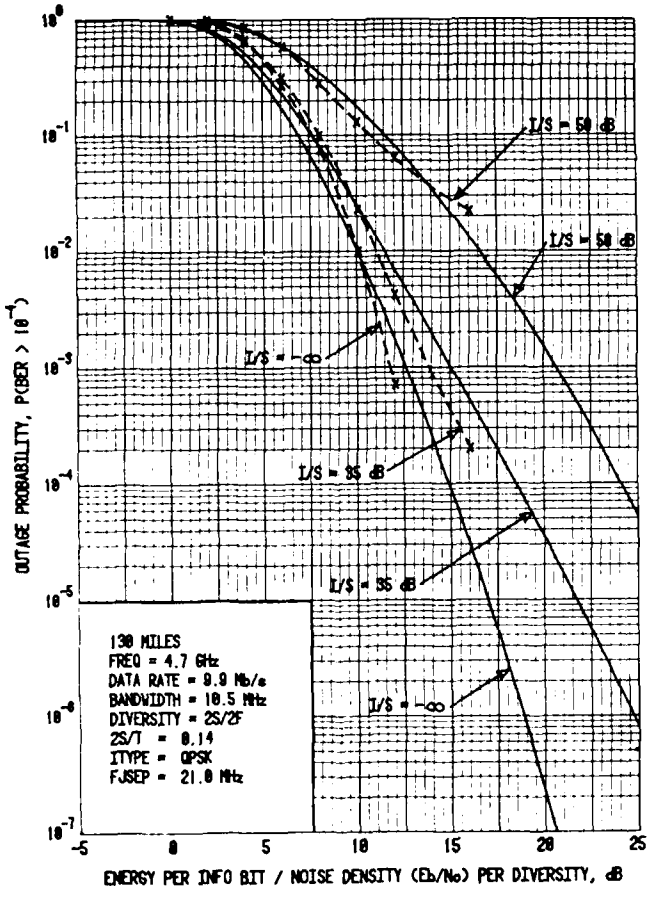

Figure 9 Predicted MMSE Performance with Out-of-Band Interference

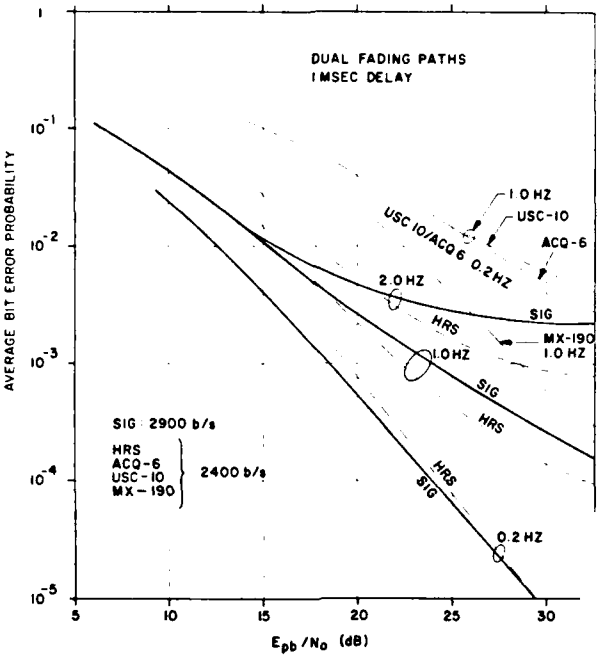

Figure 6 Waveform Test Bands

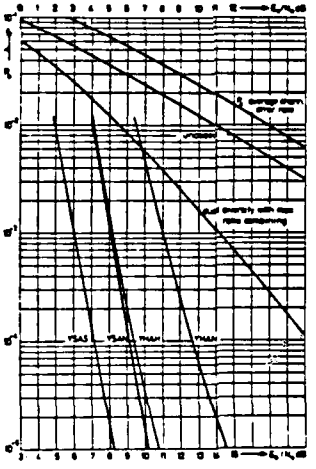

From Hagenauer [16].

[illegible]

[illegible]

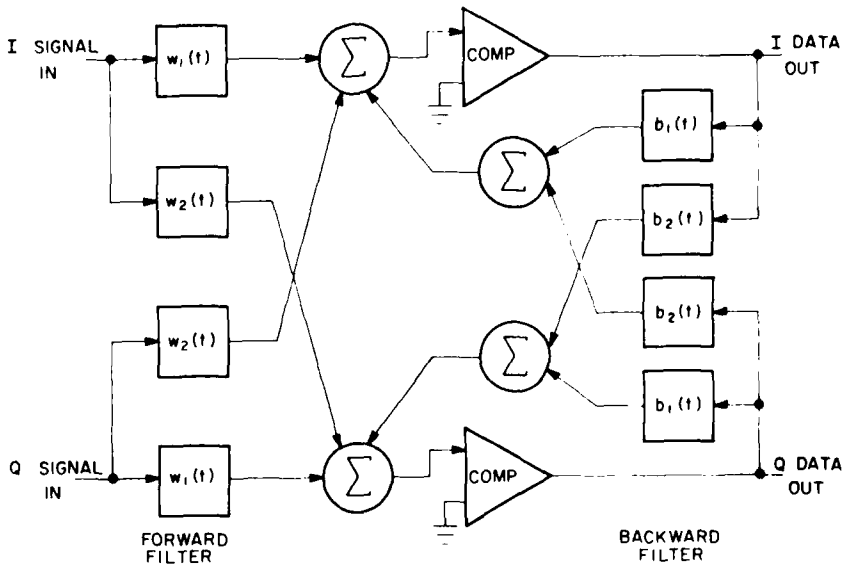

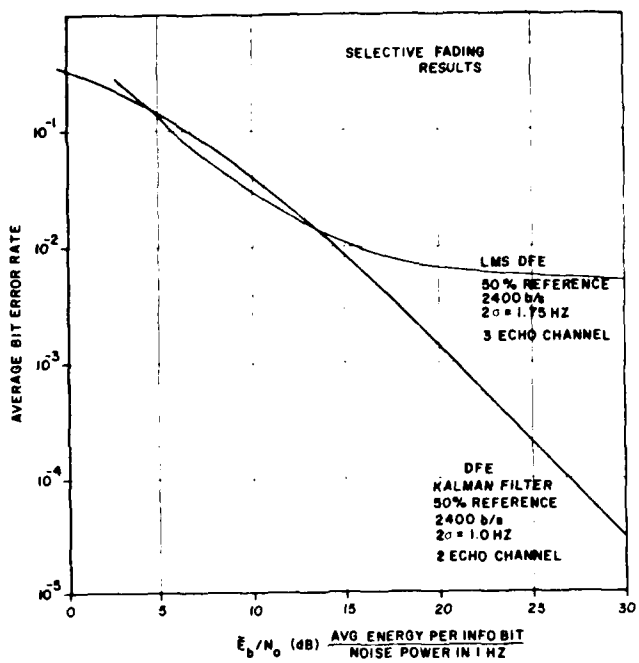

Figure 5 LMS and Kalman Filter Equalizer Performance

A simulation has been performed in order to evaluate the receiver capabilities in terms of bit error rate with respect to the bit energy/noise power density. Fig. 10 represents the simulation results of the described receiver in absence of fadings and for gaussian noise only.
The figs. 11, 12, 13 represent the simulation results in presence of multipath. Fig. 11 points out the difference between the theoretical performances, i.e. 64 exactly orthogonal codewords employing 7 symbols each, over a Rayleigh channel, and the system with 64 Reed Solomon codewords employing 7 symbol of a 8-ary alphabet.
The degradation of the performances, in the second case, are due to the imperfect orthogonality of the words.
Fig. 12 represents the performances in case of a 2 ray channel, with reflection coefficient γ = 0.5 and random phase angle.
A FFT processed bandwidth of 204.8 KHz and a spacing of 25.6 KHz between the 8 FSK tones has been considered.
The case with differential delay τ = 5.6 μs clearly shows the improvement of the frequency diversity.
The improvement is high at low Eb/No and becomes increasingly smaller at high Eb/No. The reason is that, at low Eb/No, the frequency diversity allows the reinforcement of the amplitude of half of the symbols of a codeword so that the average word energy is increased (see fig. 14).
In fig. 13 the case of a Ricean channel with reflection coefficient γ = 0.5 is considered.
Also in this case the improvement due to the bandwidth spreading is clearly shown, with increasing performance improvement when $\gamma \to 1$.

6. CONCLUDING REMARKS

The basic modulation - coding design considered here, together with a FFT based demodulation, allows the simultaneous reception of several MFSK Signals with a reasonable hardware complexity.
Multipath propagation, causing frequency selective fadings, is efficiently counteracted by the coding and the suitable choice of a pseudorandom allocation of the frequency tones.
The computer results yielded information on the error rate performance and on the pull-in behaviour of the loops used for fine time and frequency adjustments.
The simulation showed that, at the signal to noise ratios required by the decoder, the final pull-in of the loops could be accomplished in less than 50 codewords with degradation of the order of 0.2 dB and for Doppler frequency of 1 KHz w.r.t. a central frequency of 300 MHz.
With a suitable choice of the DTL bandwidth, so that the r.m.s. error in the frequency unstability compensation is negligeable, the frequencies of the complex tones processed by the DFT coincides, in mean, with the basis set.
In fact, with frequencies of the complex tones shifted with respect to the basis set, it is possible a leakage of signals from one to another channel and a contribution in undue filters.
However this event can be overrided adapting the filter parameters of the DTL to the various tracking requirements.

REFERENCES

1) Wozencraft J.M. and Jacobs I.M., "Principles of communication Engineering", New York, Pegamon Press, 1968, pp. 223-228.

2) Lindsey W.C., "Error probabilities for Rician fading multichannel reception of binary and N-ary signals", IEEE Trans. on Information Theory, IT-10, pp. 339-351, 1964.

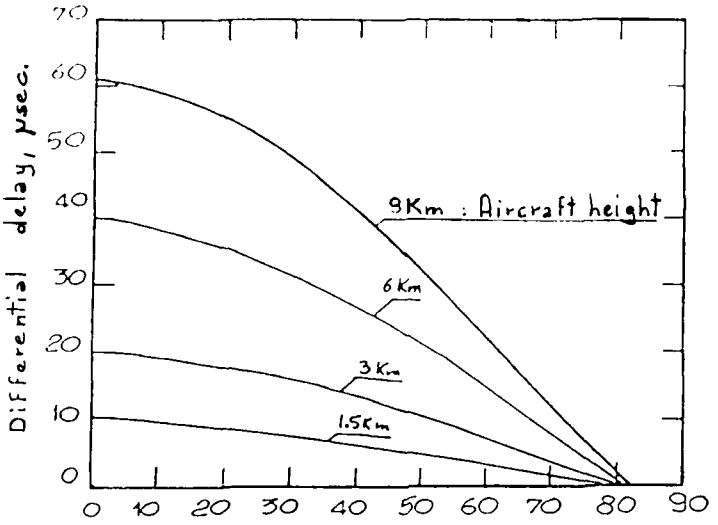

Aircraft - center of the earth - satellite angle (deg.)

Fig. 1 Differential delay of direct and indirect ray

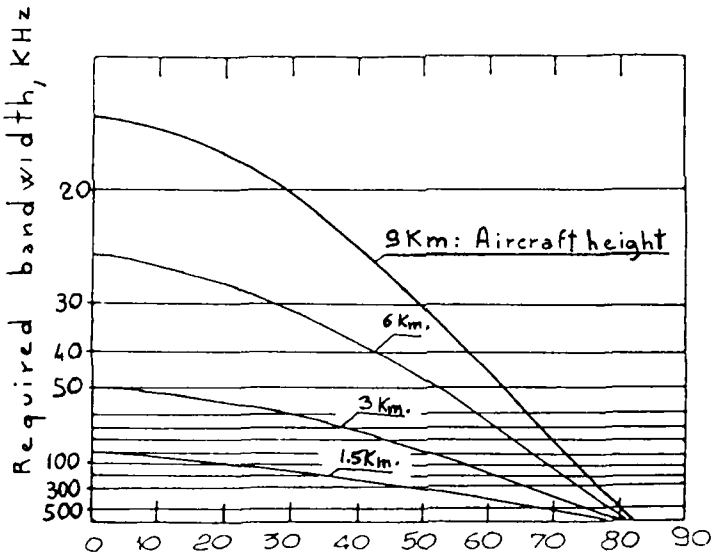

Aircraft - center of the earth - satellite angle (deg.)

Fig. 2 Bandwidth requirements

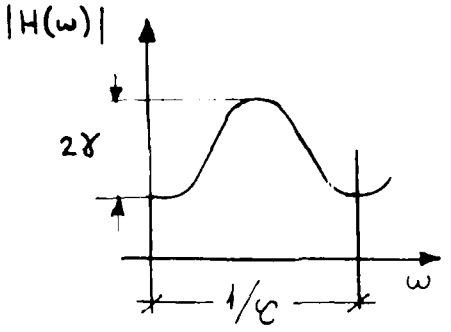

Fig. 3 2 rays channel response

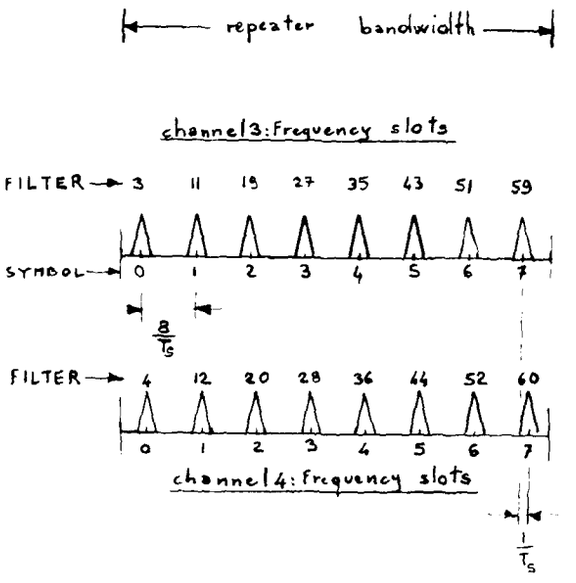

Fig. 4 Signal multiplexing

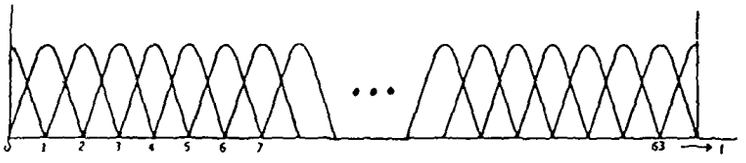

Fig. 5 - DFT spectral filters

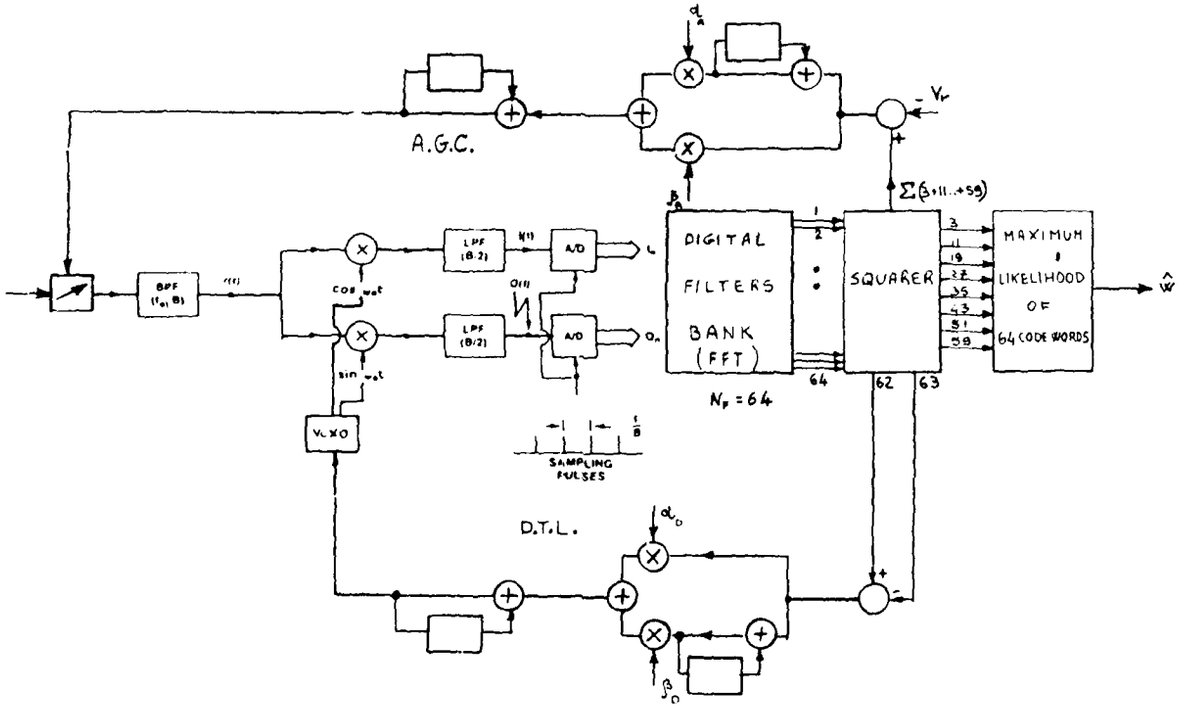

Fig. 6 - Block diagram of the demodulator / decoder

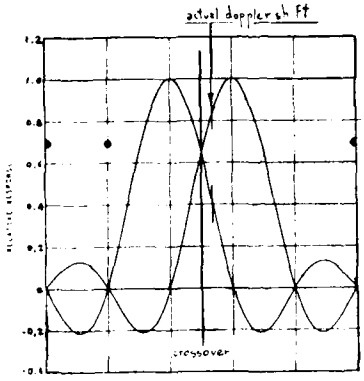

Fig. 7 Doppler shift measure

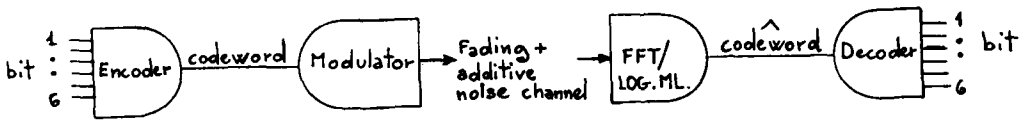

Fig. 8 Model of communication system

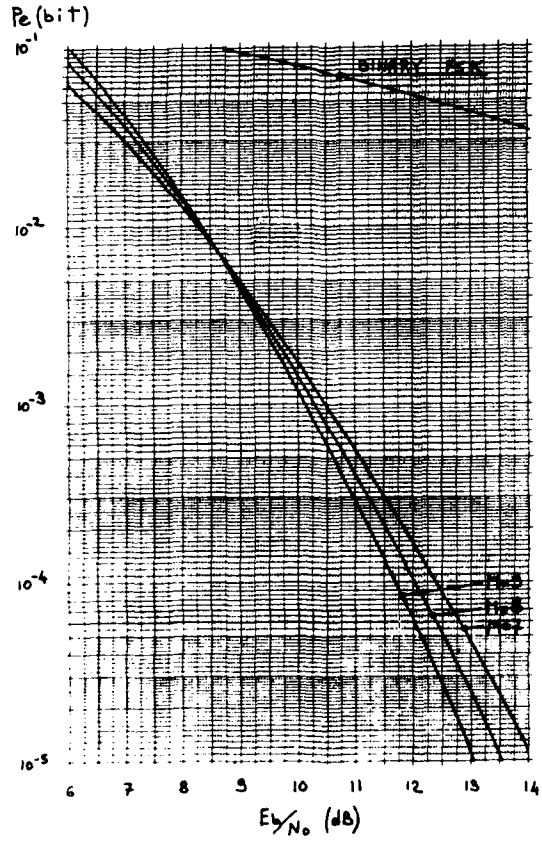

Rayleigh channel

Fig. 9 Error probability for the 64 orthogonal codeword receiver w

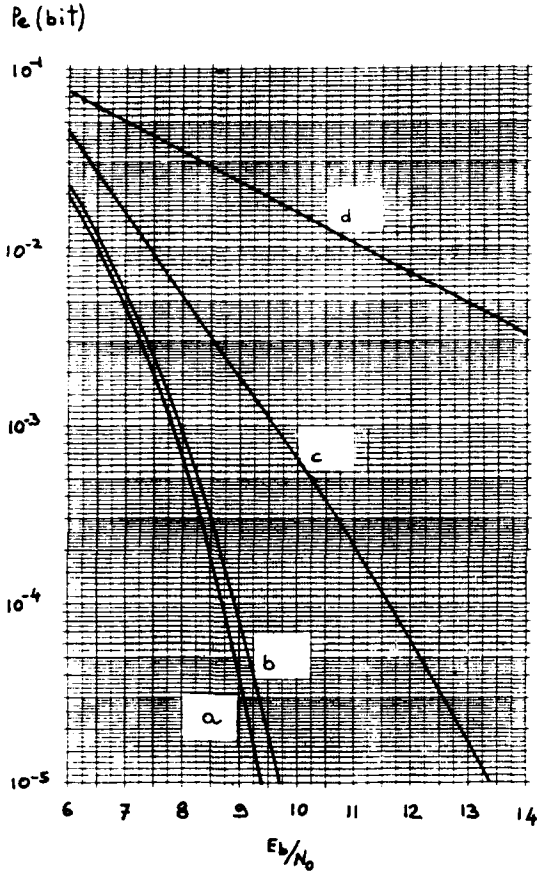

Fig. 10 Bit error rate with Gaussian noise

Parameter: r.m.s. frequency error in D.T.L./symbol rate

(Δ F/R)

(a) Δf/R = 0 (b) Δf/R = 0.1 (c) Δf/R = 0.2

(d) Δf/R = 0.3

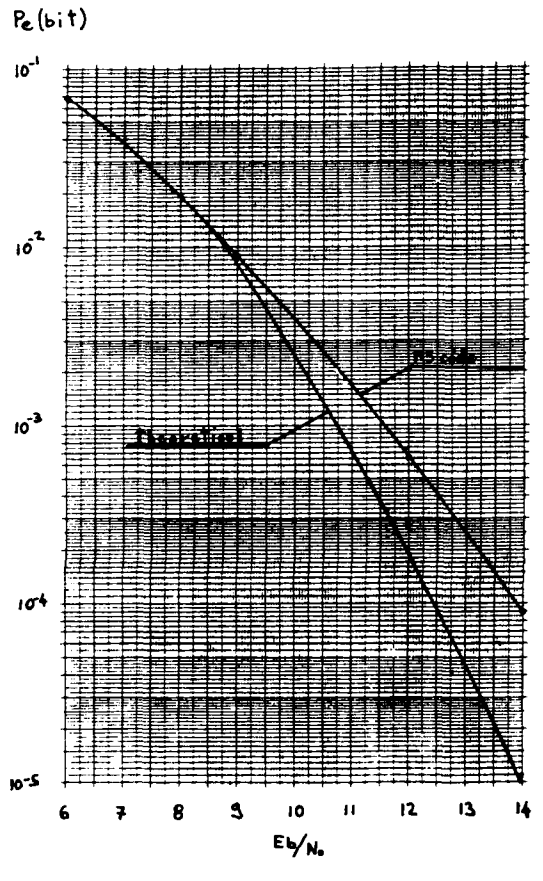

Fig. 11 Bit error rate with a Rayleigh channel

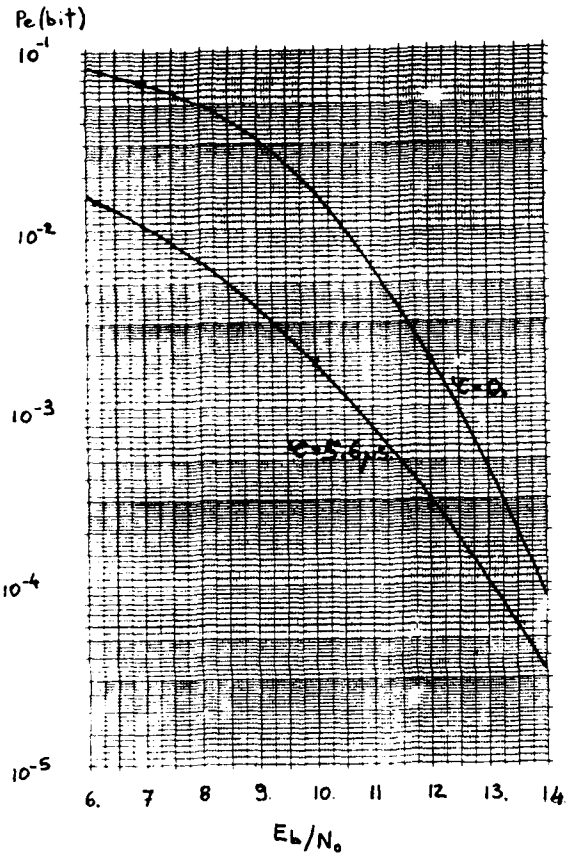

Fig. 1. Bit error rate with a 2 ray channel and reflection coefficient $\gamma = 0.5$

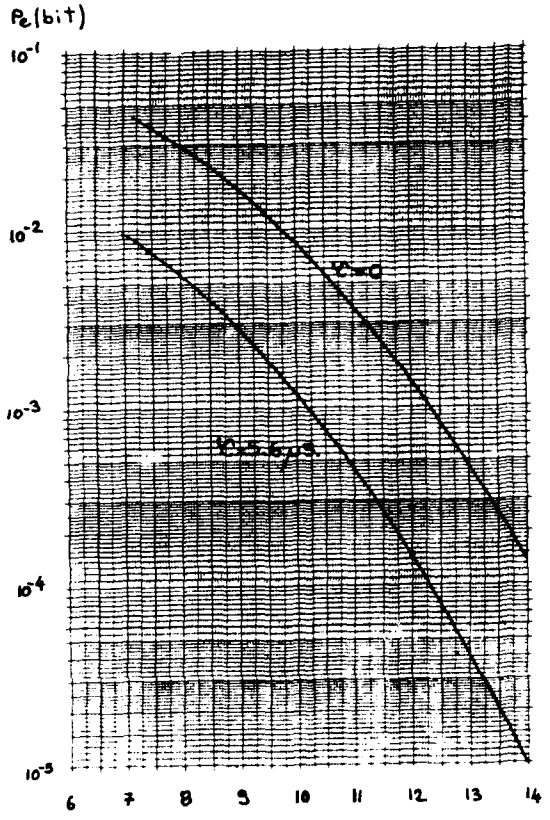

Fig. 13 Bit error rate for a rician channel and reflection coefficient $\gamma = 0.5$

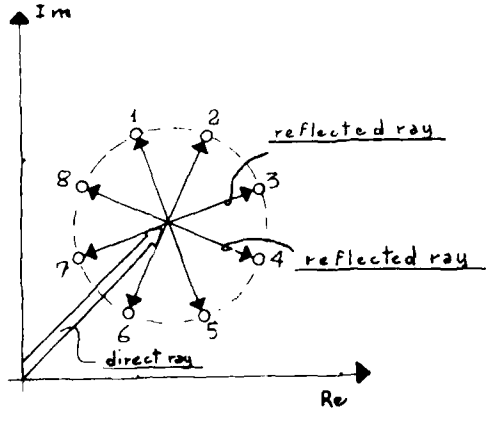

Fig. 14 Case of direct and reflected ray

TIME AND SPACE DOMAIN FILTERING FOR IMPROVED HF DETECTION

Richard N. Smith
U. S. Air Force
RADC/DCCD
Griffiss AFB, NY 13441

Randolph L. Moses
Dept. of Electrical Engineering
Virginia Polytechnic Institute
and State University
Blacksburg, Virginia 24061

SUMMARY

High speed data transfer has until recently been generally unattainable over HF channels because of the highly disturbed nature of the channel. The development of real-time signal processors has done much to mitigate effects of channel disturbances, making it possible to substantially increase throughput. Data rates as high as 9600 bits per second can be achieved by implementing signal processors as adaptive channel equalizers. Real-time processors are also being used to adapt antenna array systems to provide improvement in spatially disturbed environments.

This recent increase in data rates has rendered feasible HF spread spectrum communication systems. Spread spectrum systems are attractive in many applications because they are resistant to narrowband interference. However, channel equalizers necessary for high data rates are susceptible to narrowband interference. Spatial or temporal prefiltering has commonly been employed to prewhiten the received data, providing improved equalizer performance. It now appears possible to realize a further improvement in system performance by combining spatial and temporal techniques into a single multidimensional prefiltering process.

This paper reviews some of the more popular one-dimensional techniques for temporal and spatial prewhitening of HF communication signals. Also, combined space-time prewhitening techniques are proposed. Algorithms for designing and implementing these two-dimensional whitening filters are presented. Advantages and disadvantages of the two design strategies are discussed. Particular attention is focused on system performance, computational requirements, and cost. Computer simulated results for these signal processing algorithms are presented.

I. INTRODUCTION

In the past several years there has been a marked increase in communication systems that operate in the HF range (3-30 MHz). This increase has been spawned by advances in the understanding of the HF communication channel and by the development of effective channel equalization processors (see figure 1, 2). Data rates of as high as 9600 bits/sec have been achieved in systems incorporating these channel equalizers [1]. Adaptive receiver antenna arrays are also being used to provide improved performance in spatially disturbed environments.

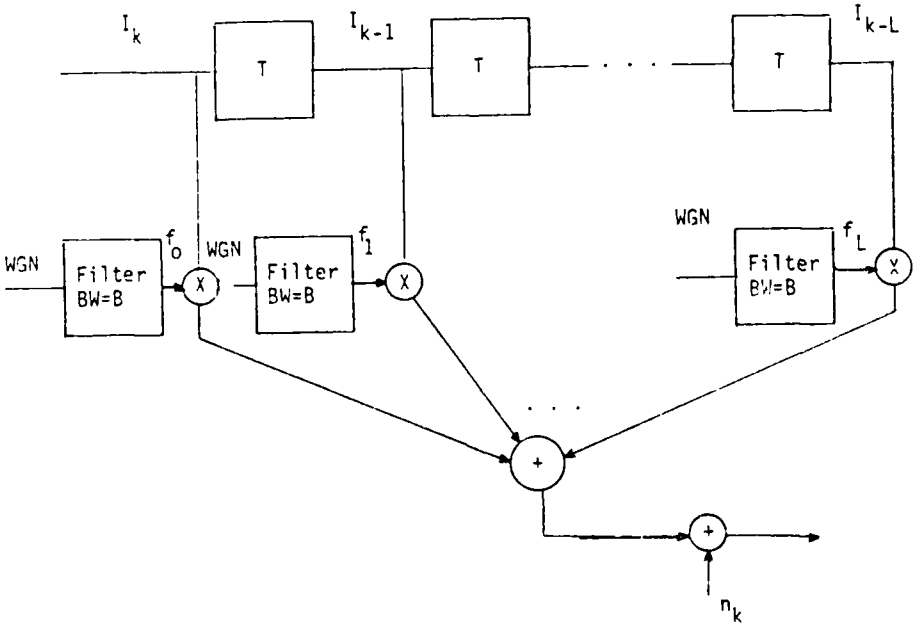

FIGURE 1. A DISCRETE CHANNEL MODEL

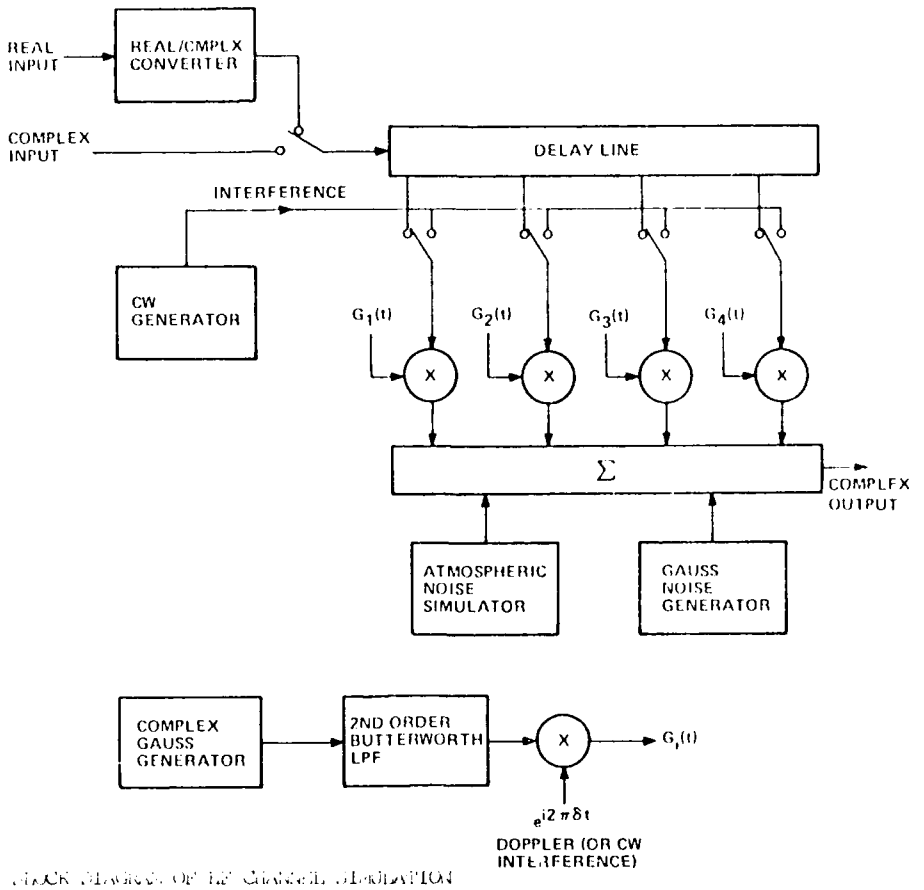

FIGURE 2. BLOCK DIAGRAM OF HF CHANNEL SIMULATION

By combining spread spectrum techniques with adaptive receiver antenna arrays, HF communication systems are potentially able to provide reliable communication links even in electromagnetically hostile environments. However, the performance of channel equalizers necessary in such systems is very sensitive to interference signals. Effective operation in this type of environment is contingent upon effective signal prefilters that attenuate these interference signals before channel equalization. Because knowledge of frequency content and source location of many interference signals are not known apriori and may vary with time, these prefilters must be adaptive.

The most common adaptive filtering technique applied to this problem consists of cascading spatial nulling algorithms with temporal spectral whitening filters. [2] However, it appears possible to realize a further improvement in interference rejection by combining the spatial and temporal filtering tasks into a single multidimensional process. Frost [3] developed one such technique that assumes the desired signal direction is known (an often impractical assumption). Godestiho, et.al. [4] have investigated maximum likelihood algorithms. Also, related algorithms have been developed for the processing of geophysical data [5], [6].

This report investigates two-dimensional signal processing algorithms for prefiltering of array element data. These algorithms do not assume known signal direction. The procedure taken is to model the received data as a two-dimensional auto-regressive moving-average (ARMA) process, then to propose particular algorithms for estimating the coefficients in the ARMA model. The AR coefficients are then used as the weights in a two-dimensional data prefilter.

II. [illegible]

A. [illegible]

1. [illegible]

Commercial and military systems for greater communication reliability, lower error rates, and higher data rates in the transmission of digital information over dispersive media, such as HF ionospheric channels, are continually increasing (see figure 3). There are two classical approaches for dealing with fading and multipath (see figure 4). The traditional configuration for an HF modem uses multitone modulation (slow-rate) with guard time inserted between adjacent symbols for avoiding the intersymbol interference. The transmitter based on multitone techniques must be capable of supporting a high peak-to-average power ratio in the range of 8-9 dB. This means that the average transmitter power is about 8-9 dB below the maximum deliverable power of the transmitter. Consequently, the power loss in a traditional multitone modem is enormous. The amount of signal energy available for bit decisions is further lowered by using the guard time since only a portion of each received signaling element is used in the integration interval. Significant spectral efficiency is lost by the requirement of separating the tones by an amount larger than 1/T, where T is the symbol interval. A spectral efficiency of 0.5 bps/Hz is typical in 4-phase multitone DPSK modems. Finally, the performance of (uncoded) multitone

transmission schemes can be seriously degraded when spectral nulls in the channel fall on or near one of the tone frequencies used. [16]

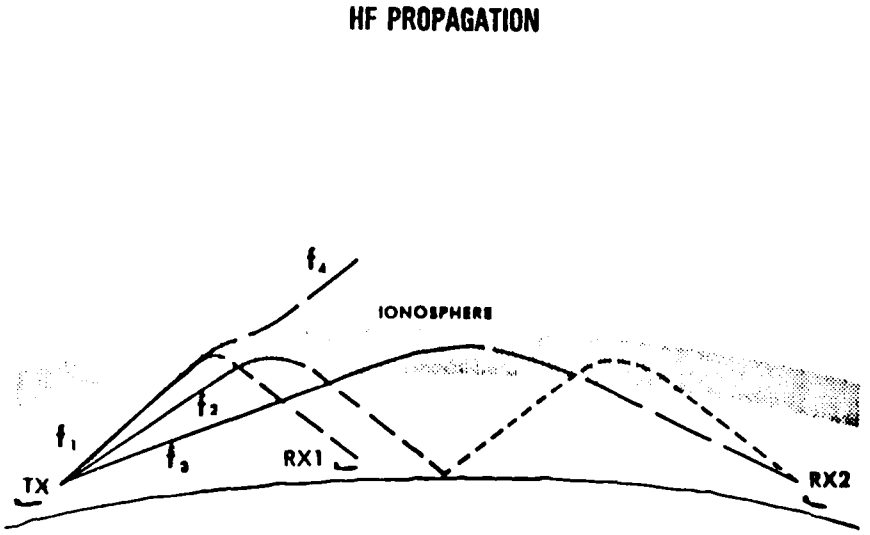

FIGURE 3. HF PROPAGATION

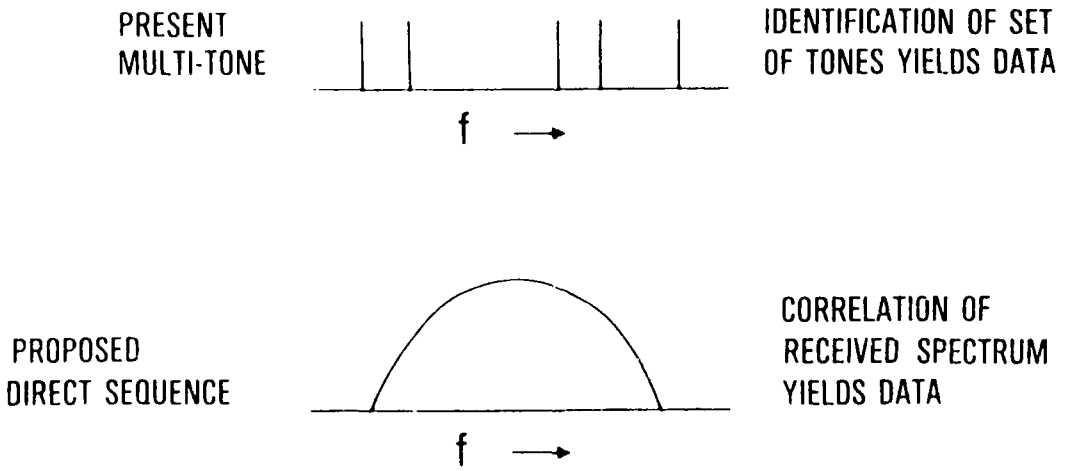

FIGURE 4. HF WAVEFORM PROCESSING

A second configuration for an HF modem uses single tone M-ary PSK modulation and a decision feedback equalizer (DFE) employing some form of recursive least-squares estimation for adjusting its tap weights [17], [18], [19], (see figure 5, and 6). In contrast to the multitone case, a single tone modem in principle suffers from none of the above consequences. Both higher data rates and low (nominally unity) peak-to-average ratio can be achieved by a single tone modem. Nevertheless, there are several drawbacks related to the DFE techniques. One disadvantage of the DFE is that, the equalizer tap weights must change more quickly than the channel does in order for the equalizer to track the channel. This implies that a fast converging algorithm for updating the DFE is needed even if the channel varies very slowly in time. The computational complexity of a fast converging algorithm such as the square-root Kalman algorithm for updating the equalizer tap weights is proportional to N^2 per symbol, where N is

the number of taps in the DFE. Consequently, a fairly complicated signal processor is required for implementing the DFE. A second disadvantage of the DFE is that an ARQ training scheme is needed for attaining high throughput and good performance. The ARQ training scheme employed assumes a full duplex link. The return link is sometimes not available or poor in quality. Frequently, the intended application provides a forward acting link only. A third disadvantage of the DFE is that the equalizer may "hang up" due to a deep channel fade. A decision-directed signal will drive the feed forward tap weights to zeros and signals with alternate signs appear in the decision. When this occurs, the decision-directed error signal goes to zero and the equalizer stays in the ill-conditioned state until the training signal is enacted again.

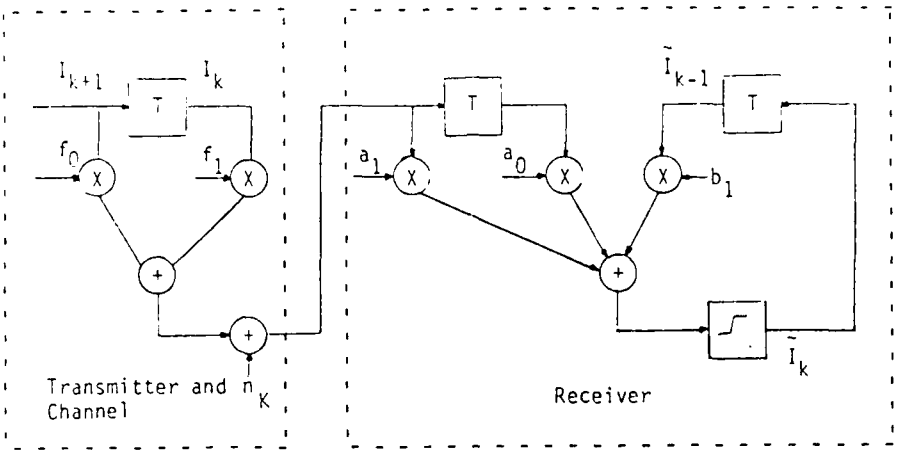

An Example of a Communication System Using a DFE Technique

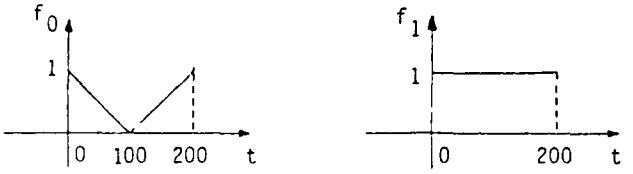

FIGURE 5. VARIATION OF CHANNEL WEIGHTS

In order to get around the three major drawbacks found in the DFE techniques, a new method called Data-Directed Estimation (DDE) was developed. The proposed scheme uses single tone (or carrier) transmission and least-squares adaptive techniques for dealing with fading and multipath. However, in contrast with the earlier method, which used Decision-Feedback Equalization (DFE) and symbol-by-symbol equalizer adaptation, the DDE is based upon direct estimation of channel parameters and data blocks. Training data is embedded into the transmission in the form of blocks of training bits alternated with blocks of source data at a fixed (though selectable) fraction of the transmission. In contrast with the DFE techniques, the DDE is forward acting only, not requiring a feedback link for retraining the equalizer.

For clarity, some possible modulation alphabets, block parameters, data rates, percentage of training, throughput and maximum allowable multipath spread for an HF modem using the DDE techniques are listed in Table 1. The block parameters, M and N, denote the sizes of the block for source data and training bits respectively. The modem proposed here uses a 2,400 keying rate and a 3 kHz bandwidth. From Table 1, it is clear that the single tone modem using the DDE techniques may achieve a data rate up to 2 bps/Hz or higher.

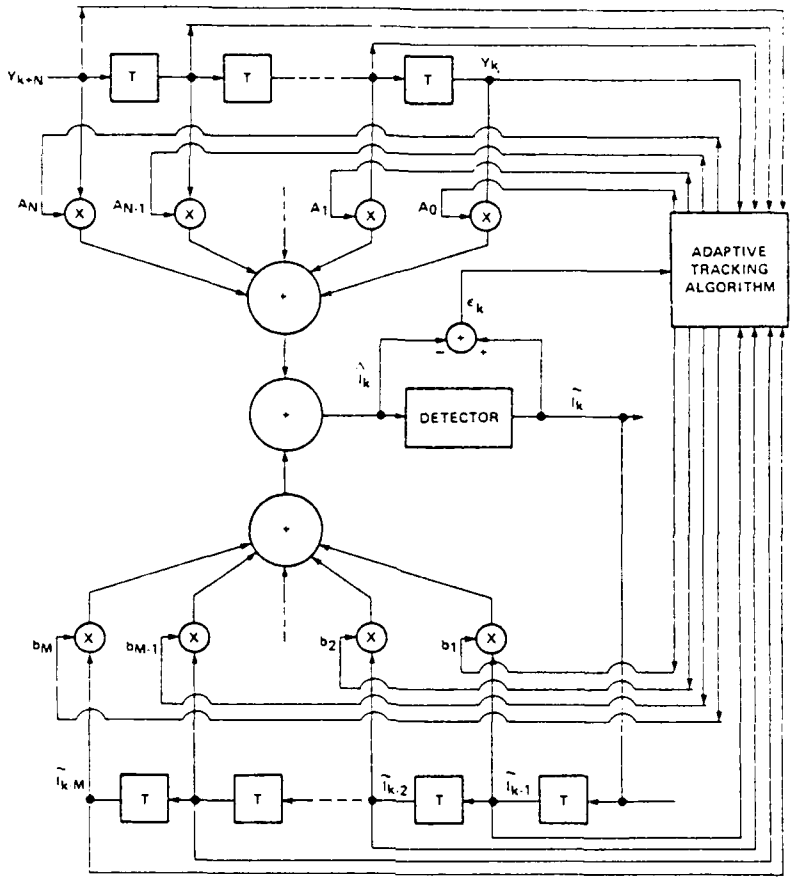

FIGURE 6. DECISION FEEDBACK EQUALIZER FOR T SECOND SPACING

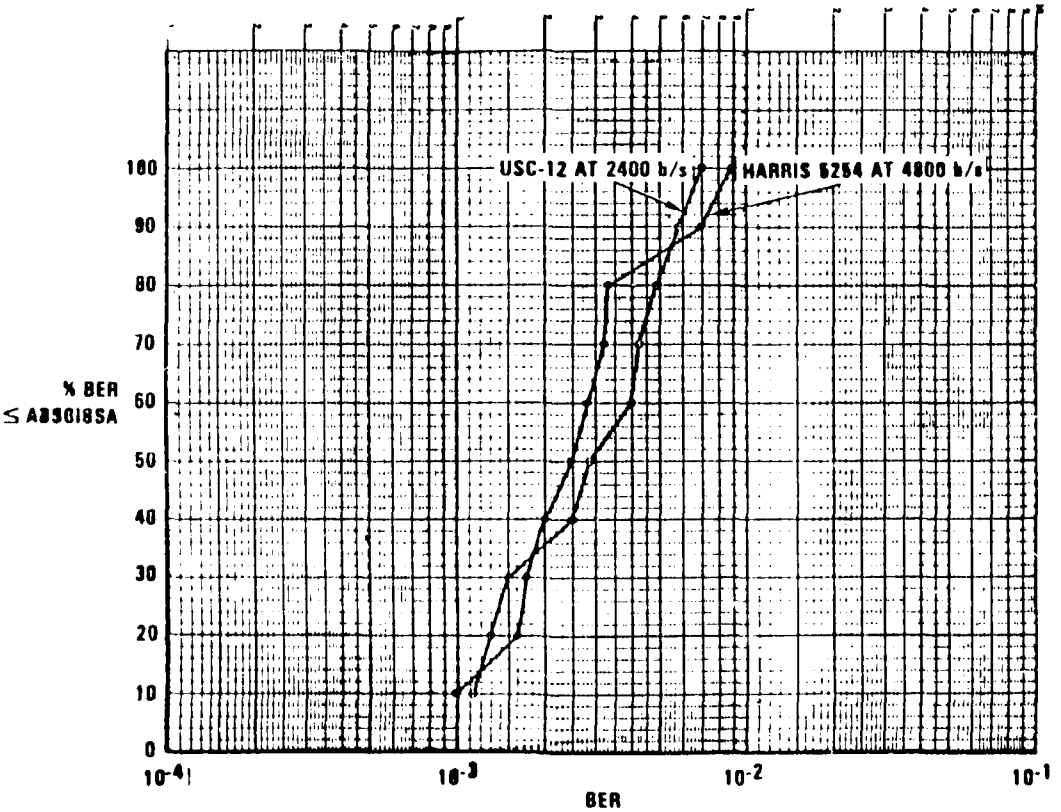

FIGURE 6A. HARRIS/USC-12 COMPARISON ASCENSION ISLAND TO CAPE CANAVERAL

3. Spatial

An adaptive array is a system consisting of an array of antenna elements and a real-time adaptive receiver-processor which, given a beam-steering command, samples its current environment and then automatically proceeds to adjust its element control weights toward optimization (usually) of the output SNR in accordance with a selected algorithm (see figure 9). These antenna systems are sometimes referred to as "smart" arrays, a term which is not inappropriate since they utilize far more of the information available in the antenna aperture than does a conventional array.

GENERAL ADAPTIVE NULL STEERER

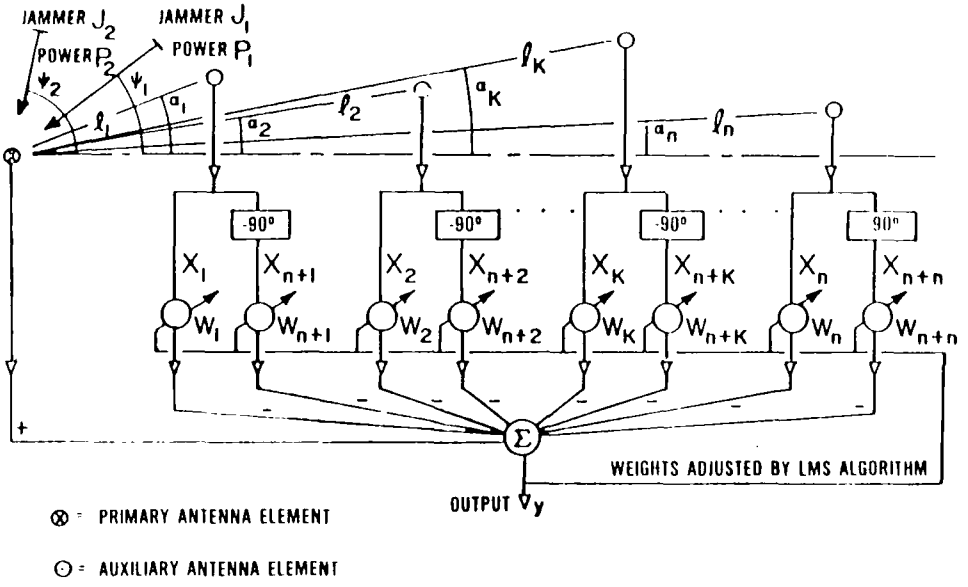

FIGURE 9.

Conventional communications and radar antenna systems are susceptible to degradation in SNR performance caused by undesired "noise" which intrudes via the antenna sidelobes and mainlobes. The noise may consist of RF interference (RFI), clutter scatterer returns, and natural noise sources. This degradation is often further aggravated by motion of the antenna, poor siting conditions, multipath, and a changing interference environment. Adaptive array techniques offer possible solutions to these serious interference problems via their flexible capabilities for automatic null steering and notching in the spatial domain, the frequency domain, and in polarization. Adaptive nulling is considered to be the principal benefit of adaptive techniques at the present time.

In addition to the automatic interference nulling, adaptive arrays can be designed to incorporate their more traditional capabilities for self-focusing on receive and the conjugate function of retrodirective transmit. Also, important side benefits are possible, such as compensation for antenna and/or scatterer distortion effects.

Adaptive antennas have been under development in various forms during the past two decades or so. Although adaptive antennas have only been used in small numbers thus far, they have proven themselves capable of rejecting interference to an extent that is unprecedented. Most high performance radar and communications systems being designed to work in these environments currently incorporate adaptive antennas. The development of spread spectrum techniques simultaneously with adaptive antennas provides a formidable set of technologies for interference resistant systems. These technologies are compatible and are frequently used in the same system. An adaptive antenna is relied upon to attenuate strong interference signals as they appear at the receiver "front end." Spread spectrum techniques are used to neutralize large numbers of interference spikes that may not be eliminated totally by the adaptive antenna.

Most advances in adaptive array technology have centered on developments in analog circuit hardware. Digital hardware technology has reached a high level of maturity in recent years, and is now being applied to adaptive arrays. In particular, the advent of high speed analog-to-digital converters and microprocessors has made digital processing feasible for adaptive array application.

Digital techniques provide greater flexibility in array processing than do conventional analog beam steering (BBS) techniques. One of the most important advantages of digital processing is the possibility of separating algorithm design and processor implementation. For example, the analyst designing an algorithm simultaneously specifies a particular weight-determining algorithm, and a particular hardware implementation. Digital processing techniques, on the other hand, allow the specification of various calculation algorithms (e.g., LMS, sample matrix inversion, recursive matrix inversion, etc.), separately from any consideration of hardware (e.g., whether the weights are to be derived by use of a general purpose computer, a special purpose digital processor, or by analog circuitry). Thus, an analyst considering alternative algorithms need not be familiar with digital hardware considerations.

TABLE 1

Modulation Alphabets, Block Parameters, Data Rates, Percentage of Training, Throughput and Maximum Allowable Multipath Spread for HF Modem Using the DDE Techniques with 2,400 keying Rate in 3 kHz Bandwidth.

Modulation Alphabets	Block Parameters	Data Rates (bps)	Percentage of Training	Through-put	Maximum Allowable Multipath Spread
4ϕ psk	N=20, N=20	2,400	50%	50%	8.3 ms
	N=32, N=16	3,200	33-1/3%	66-2/3%	6.6 ms
	N=36, N=12	3,600	25%	75%	5.0 ms
8ϕ psk	N=20, N=20	3,600	50%	50%	8.3 ms
	N=32, N=16	4,800	33-1/3%	66-2/3%	6.6 ms
	N=36, N=12	5,400	25%	75%	5.0
16ϕ psk	N=20, N=20	4,800	50%	50%	8.3 ms
	N=32, N=16	6,400	33-1/3%	66-2/3%	6.6 ms
	N=36, N=12	7,200	25%	75%	5.0 ms

With linear DDE, the source data block (b_0, b_1..., b_{M-1}) is estimated by a Levinson recursive algorithm. With non-linear DDE, only $\hat{b}_0$ and $\hat{b}_{m-1}$ obtained from a Levison algorithm are kept and $\hat{b}$ to $\hat{b}_{m-2}$ discarded in the first step of estimation. The estimates, $\hat{b}_0$ and $\hat{b}_{m-1}$ are then quantized to the nearest symbols, $\tilde{b}_0$ and $\tilde{b}_m$, respectively. The decisions, $\tilde{b}_0$ and $\tilde{b}_m$, are substracted from the simultaneous equations. The M-2 symbols (b_1, and b_2, ..., b_{m-2}) left are estimated by a Levinson algorithm again, and so forth. The procedure described here is used recursively until all the unknown symbols are obtained. In both linear and nonlinear DDE techniques, the channel is estimated by a steepest-decent algorithm or a pseudo-inverse algorithm.

As a linear equalizer, the linear DDE lacks the ability to cope with the severe fading dispersive HF radio channels. However, the nonlinear DDE works extremely well under the same severe channel conditions. The nonlinear DDE can achieve performance similar to the DFE or better.

The nonlinear DDE (NDDE) can achieve data rates up to 7,200 bps in a 3 kHz bandwidth with wide multipath spread (e.g., 5 ms).

2. Adaptive Whitening

Spread spectrum, direct sequence or pseudo-noise (PN) modulation is employed in digital communication systems to reduce the effects of interference. When the interference is narrow band the cross-correlation of the received signal with the replica of the PN code sequence reduces the level of the interference by spreading it across the frequency band occupied by the PN signal. Thus, the interference is rendered equivalent to a lower level noise with a relatively flat spectrum. Simultaneously, the cross-correlation operation collapses the desired signal to the bandwidth occupied by the information signal prior to spreading.

The interference immunity of a PN spread spectrum communication system corrupted by narrow band interference can be further improved by filtering the signal prior to cross-correlation, where the objective is to reduce the level of the interference at the expense of introducing some distorton on the desired signal. This filtering can be accomplished by exploiting the wideband spectral characteristics of the interference. Since the spectrum of the PN signal is relatively flat across the signal frequency band, the presence of a strong narrow band interference is easily recognized. Then the interference can be suppressed by means of an appropriately designed linear filter (see figure 7).

Hsu and Giordano [12] considered the problem of narrow band interference estimation and suppression by means of two linear prediction algorithms, the Burg algorithm [13], [14], and the Levinson algorithm [13], [15]. The channel through which the PN spread spectrum signal is transmitting was assured to be nondispersive. Results were presented on the effectiveness of the linear prediction filter in suppressing the interference. Performance was measured in terms of signal-to-noise ratio at the output of the PN correlator.

Proakis and Ketchum extended the results obtained by Hsu and Giordano on filter requirements and characteristics in single and multiple frequency band interference. In addition to a nondispersive channel, they consider the transmission of the PN spread spectrum signal over a channel characterized by fading and multipath (time dispersion). This serves as a model for radio channels such as HF. The existance of time dispersion in the received signal necessitates some means for dealing with this type of distortion at the receiver. We have considered the use of an adaptive decision-feedback equalizer preceding the PN correlator for mitigating the effects of time dispersion due to multipath and the linear, interference suppression filter (see figure 8).

APPLICATIONS OF SPECTRAL ESTIMATION TO HF SIGNAL PROCESSING (6.1)

(NARROWBAND INTERFERENCE EXCISION)

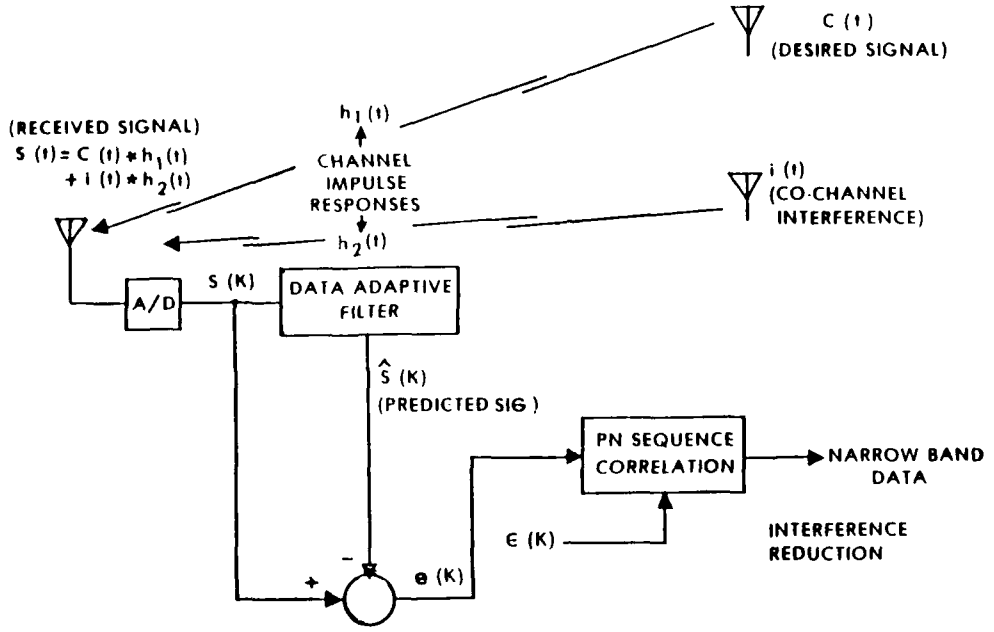

FIGURE 7.

EXCISION FILTER RESPONSE

FILTER ORDER = 29

SNR WITHOUT FILTERING = -20.000 dB PER CHIP

FOUR INTERFERENCE BANDS, 5% SIGNAL BANDWIDTH EACH

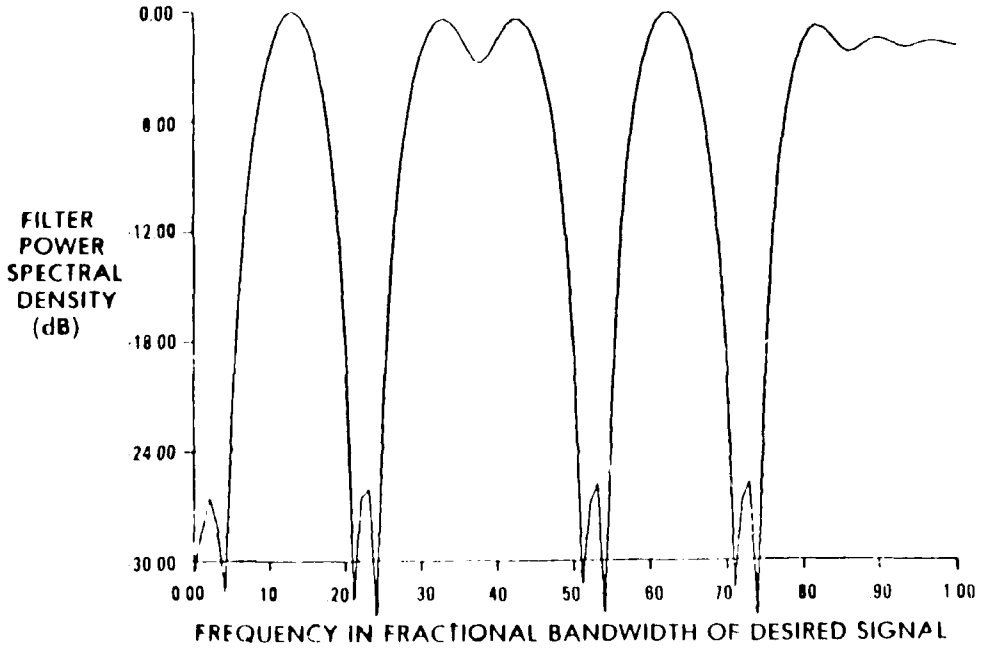

AD-A154 031 PROPAGATION INFLUENCES ON DIGITAL TRANSMISSION SYSTEMS: 5/6
PROBLEMS AND SOLU..(U) ADVISORY GROUP FOR AEROSPACE
RESEARCH AND DEVELOPMENT NEUILLY.. J H BLYTHE
UNCLASSIFIED 08 JUN 84 AGARD-CP-363 F/G 17/2 NL

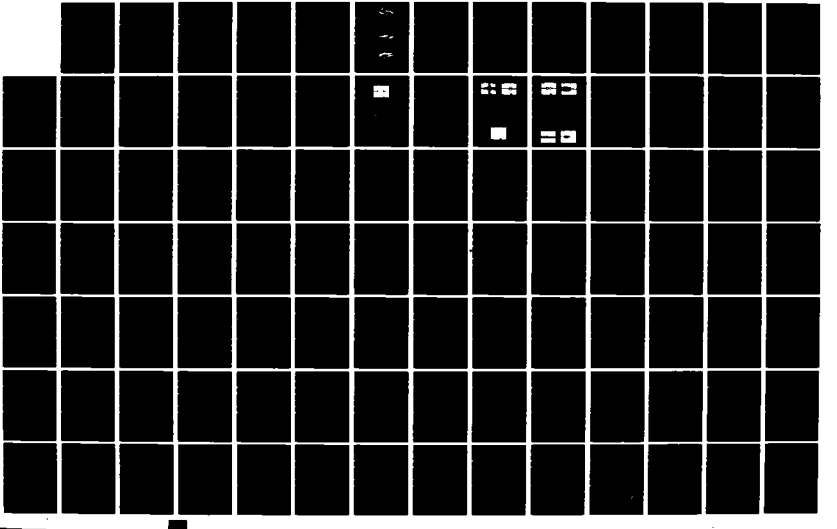

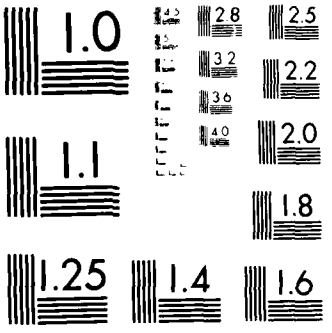

MICROCOPY RESOLUTION TEST CHART
NATIONAL BUREAU OF STANDARDS-1963-A

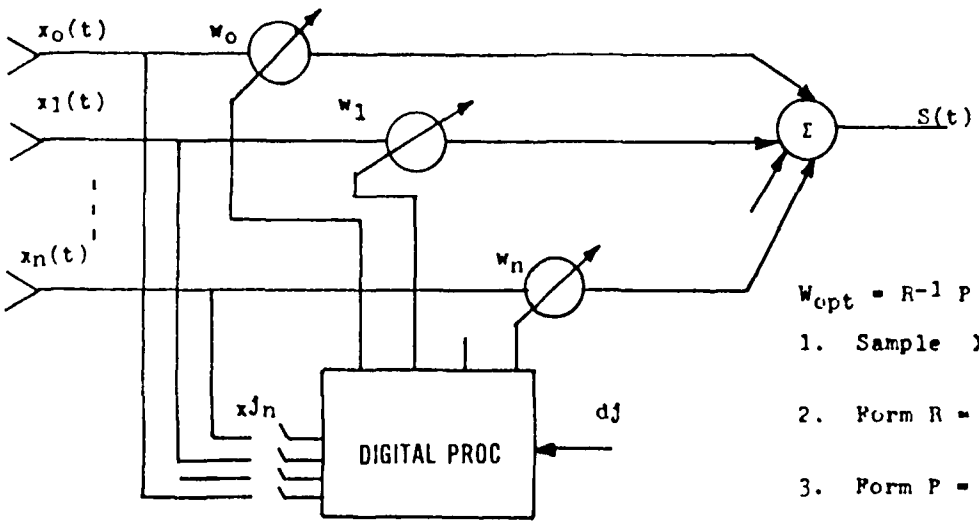

$W_{opt} = R^{-1} P$

1. Sample $X_n(t)$
2. Form $R = \frac{1}{J} \sum_{j=1}^{J} X_m^{j*} X_n^j$
3. Form $P = d_j X_j^T$
4. Invert $\underline{R}$
5. Form Product $R^{-1}P$
6. Apply Weights

FIGURE 10. MATRIX INVERSION PROCESSOR

MATRIX INVERSION PROCESSOR

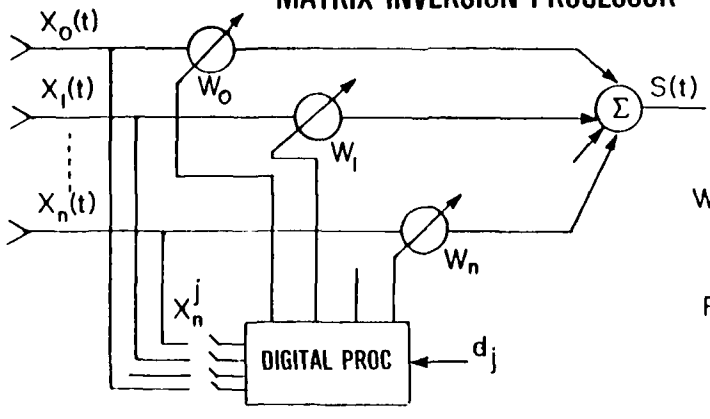

$W_{OPT} = R^{-1} P$

$R = \frac{1}{J} \sum_{j=1}^{J} X_m^{j*} X_n^j$

NUMBER OF MULTIPLES TO COMPUTE R^{-1}

ALGORITHM	PER UPDATE	PER BLOCK (2n SAMPLES)
BRUTE FORCE	$\frac{1}{2}n^3+\frac{3}{2}n^2+\frac{5}{2}n$	$\frac{3}{2}n^3+2n^2+2n$
CHOLESKY	$\frac{1}{6}n^3+2n^2+\frac{5}{6}n$	$\frac{7}{6}n^3+\frac{5}{2}n^2+\frac{2}{3}n$
SQUARE ROOT	$\frac{5}{2}n^2+\frac{9}{2}n$	$\frac{5}{2}n^3+8n^2+\frac{3}{2}n$
FACTORED SQUARE ROOT	$2n^2+6n$	$\frac{5}{3}n^3+7n^2-\frac{5}{3}n$
FACTORED INVERSE	$\frac{5}{2}n^2+\frac{7}{2}n$	$3n^3+8n^2$

FIGURE 11.

Digital processing techniques are not without disadvantages, however. The large number of computations required for typical processing applications, and the speed limitations of digital hardware, can seriously limit the processing speed or responsiveness of the array system. The dynamic range problems typically faced with analog array processing designs also appear in digital designs in the form of processor wordlength (precision). Long wordlengths result in slower processing speed.

Processor computation rate (computations/sec) may be increased using parallel computation techniques and high levels of prime power to exploit the speed-power characteristic of the digital hardware technology. These methods are not always satisfactory because they lead to physically larger, power consumptive designs.

Processing speed may also be increased by development of efficient processing algorithms and operational implementations. Efficient algorithms are those that require relatively few numerical operations per cycle and relatively imprecise calculations, i.e., short wordlength. Efficient implementations are those that permit parallel processing of high-rate and low-rate functions, such that adaptation response is relatively fast and accurate with minimum software complexity.

III. COMBINED SPACE-TIME PREWHITENING

A. Data and Filter Models

In order to propose models for the data and prefilter, it is necessary to first understand the basic receiver configuration. The basic antenna array receiver is shown in Figure 12. After amplification, the M received analog signals are shifted from the carrier frequency to baseband and lowpass filters, then sampled. The result after N samples is a complex-valued discrete time data array $x(m,n)$, for $1 \le m \le M$ and $1 \le n \le N$. This data is then passed through the two dimensional prefilter to attenuate the noise and interference. The M filter outputs are combined as a weighted sum, and this sum is sent to the channel equalizer and receiver decoding processors.

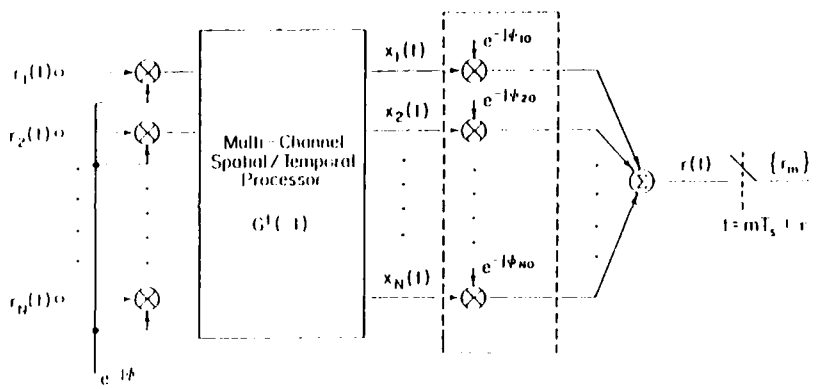

FIGURE 12. THE BASIC HF ANTENNA ARRAY RECEIVER

The received signal at each antenna consists of a desired signal s(t) incident on the array at some angle θ_S, along with any of several interference signals $i_K(t)$, each incident at some angle θ_K (see figure 12). The incident angles are assumed unknown. In addition there is additive background noise n(t). Because of possible signal and interference source movement, and because of HF channel disturbances, the amplitudes and incident angles of these signal components may vary with time at a rate that is assumed to be slow compared to the data sampling rate. These signal components are all present in the discrete data array measurements $x(m,n)$.; in addition there is a noise component $w(m,n)$ due to receiver noise, round-off, etc. Thus, we may write

$$X(m,n) = S(m,n) + \sum_{k=1}^{K} i_k(m,n) + W(m,n) + n(m,n) \qquad (1)$$

Due to the dispersive nature of the HF channel, signals arriving from point sources are spread slightly over a small spatial frequency range. We shall assume that this spreading function can be modeled by an ARMA function. An ARMA model is robust since as the spread with approaches zero, the spreading function becomes a limiting ARMA (1,1) function.

The desired signal $s(m,n)$ is a spread spectrum signal, and is well modeled as white noise in the temporal frequency domain [7]. If we assume an ARMA spatial spreading function, then a two dimensional (2-D) ARMA model results. Similarly, each interference signal is often modeled as a complex exponential or as an ARMA process in the temporal domain [7]. Since a complex exponential can be modeled as the limit of an ARMA (1,1) process, by again assuming an ARMA spatial spreading function a 2-D ARMA model is obtained for each interference signal as function a 2-D ARMA model is obtained for each interference signal as well. The noise processes can also be modeled as 2-D ARMA processes [8]. Thus we have modeled $x(m,n)$ as the sum of independent ARMA processes, which is itself an ARMA (p_1, q_1, p_2, q_2) process, where p and q are the AR and MA orders in the spatial frequency direction, and p and q are the AR and MA orders in the temporal frequency direction. The corresponding power spectral density function is given by

$$S_x(Z_1,Z_2) = \left| \frac{B(Z_1,Z_2)}{A(Z_1,Z_2)} \right|^2 \qquad (2)$$

where $B(z_1, z_2)$ is a polynomial of degree q_1 in z_1, and q_2 in z_2, and $A(z_1, z_2)$ is a polynomial of degree p_1 in z_1, and p_2 in z_2.

It is apparent that interference signals and some noise appear as areas of high power density in the 2-D frequency plane. An appropriate interference rejection filter, then, is one that spectrally whitens the data, as this flattens such peaks. If the signal power is below the background noise power (which is often the case in practice), a whitening filter has little effect on the desired signal, so SIR and SNR gains are realized at the filter output. If the signal power is substantially above the noise power level, a whitening filter attempts to attenuate the signal along with the interference. This effect is unavoidable when the signal incident angle is unknown, as the whitening filter cannot distinguish between signal and interference. However, even in this case SIR and SNR gains may be realized at the filter output.

The optimum whitening filter for $x(m,n)$, the transfer function from each input to each output of the form

$$H(e^{jw_1},e^{jw_2}) = \frac{A(e^{jw_1},e^{jw_2})}{B(e^{jw_1},e^{jw_2})} \qquad (3)$$

where A and B are given in equation (2). Since H contains a denominator term, it is an infinite impulse response (IIR) filter. IIR filters are undesirable because they pose a stability problem, (especially when the filters are time varying, as is the case here), and because the B coefficients are often difficult to estimate accurately without a large amount of data (especially when there are sharp nulls in the spectrum). Because of these problems and because spectral nulls are not formed by interference signals, there seems to be no practical reason to incorporate the coefficients into the filter. A practical alternative filter is

$$H(e^{jw_1},e^{jw_2}) = A(e^{jw_1},e^{jw_2}) \qquad (4)$$

where A is obtained by either:

1. Modeling the data with the ARMA model in equation (2) and using only the estimated AR coefficients in (4).

2. Modeling the data with an AR model and using the estimated AR coefficients in (4).

The main advance of the first alternative is that sharp spectral peaks present in the data are more effectively nulled; the main disadvantage of the second alternative is that some of the MA filtering is sacrificed because the entire spectrum is approximated by the AR model. Thus, the two filter models represent a tradeoff between effectiveness in eliminating narrowband interference and effectiveness of spectrally whitening the data.

3. Two-Dimensional ARMA Algorithms

In this section we propose one class of AR coefficient estimation algorithms derived by considering the observed data as a sample from a two-dimensional stationary ARMA process. The derivation makes use of the fact that the antenna array elements are collinear and equally spaced, which results in sufficient use of the data in generating autocorrelation estimates.

Consider the 2-D semi-causal ARMA recursion

$$\sum_{i=-P_1}^{P_2} \sum_{j=0}^{P_3} a_{ij}X(m-i,n-j) = \sum_{i=-q_1}^{q_2} \sum_{j=0}^{q_3} b_{ij}V(m-i,n-j) \ , \ a_{00}=1 \qquad (5)$$

If we follow the earlier suggestion of using only AR coefficients in the filtering operation, the corresponding prefilter outputs are given by

$$e(m,n) = \sum_{i=-P_1}^{P_2} \sum_{j=0}^{P3} a_{ij}X(m-i,n-j) \ , \ 1 \le m \le M \qquad (6)$$

It can be seen from (6) that p_1 and p_2 must be chosen so that $1 \le m-i \le M$ for $-P_1 \le i \le P_2$. In general this may require a different choice of p_1 and p_2 for each of the M filter outputs. Thus, a different set of AR coefficients is in general necessary for each of the M outputs.

An effective AR coefficient estimation procedure can be derived by appealing to the well-known Yule Walker equations, which are found by multiplying out a block of equation (5) by $x^*(m-k, n-l)$ and then taking the expected value to give

$$r_x(k,l) + \sum_{i=-P_1}^{P_2} \sum_{j=0}^{P_3} a_{ij}r_x(k-i,l-j) = 0 \ , \ \text{For } l>q_3 \qquad (7)$$

By replacing exact autocorrelations in (7) with ones estimated from the given data, we can form a matrix of approximate Yule Walker equations whose solution yields AR coefficient estimates. To this end,

getting the matrix equation

$$\hat{\underline{r}} + \hat{\underline{R}}\hat{\underline{a}} = \underline{\epsilon} \tag{8}$$

where each row is an estimate of equation (7) for a particular choice of the pair (k, l), $\hat{R}$ and $\hat{r}$ are a matrix and a vector of autocorrelation estimates, and a is a vector of (unknown) AR coefficient estimates, because autocorrelation estimates are used in equation (8), the right hand side is not in general equal to zero.

The solution to equation (8) represents the prefilter coefficient determination algorithm. If the number of rows in (8) is equal to the number of AR coefficients then ϵ can be made equal to zero and

$$\hat{a} = -\hat{R}^{-1}\hat{r} \tag{9}$$

However, choosing a greater than minimal number of rows in (8) generally results in improved AR coefficient estimates [9]. In this case the AR coefficient estimate is the least squared error solution

$$\hat{\underline{a}} = -\left[\hat{R}^{\dagger}\hat{R}\right]^{-1}\hat{R}^{\dagger}\hat{r} \tag{10}$$

The dagger system ($\dagger$) denotes complex-conjugate transposition. It can be seen from equations (9) and (10) that generally improved AR coefficient estimates are obtained at a cost of increase computational burden.

There are several standard autocorrelation estimators that may be used in generating R and r. One choice is the unbiased estimator

$$\hat{r}_x(k,l) = \frac{1}{(M-|k|)(N-|l|)} \sum_i \sum_j x(k+i, l+j)\, x^*(i,j) \tag{11}$$

where

$$i = \begin{cases} 1, 2, \ldots, M-K, & K \geq 0 \\ K+1, K+2, \ldots, M, & K < 0 \end{cases}$$

$$j = \begin{cases} 1, 2, \ldots, N-l, & l \geq 0 \\ l+1, l+2, \ldots, N, & l < 0 \end{cases}$$

It is important to note that $\hat{r}_x(k, l)$ is formed not only by summing over time lags but also by summing over spatial lags. This is a consequence of assuming collinear, equally space antennas. We shall see that this procedure uses the data more efficiently than do procedures developed in the next section.

The values of k and l in each row of equation (8) should generally be chosen small to maximize the number of data lags being summed to form autocorrelation estimates (see (11)). Equally important, however, is that by judicious selection of the (k, l) pairs, and by properly ordering the rows of (8), Toeplitz structures in the matrix R can be obtained. This can significantly reduce the computational burden of inverting $\hat{R}$ or $\hat{R}^{\dagger}\hat{R}$ [11], [12].

It can be seen that the AR coefficient estimators (9) and (10) presented in this section not only provide flexibility in model order selection, but also make efficient use of the given data in generating autocorrelation estimates. However, in order to obtain the "optimal" AR coefficients at each time n, one must perform a matrix inversion every time a new data point arrives (i.e., at each sample interval). Even though efficient matrix inversion procedures are available due to the special structure of $\hat{R}$, the computational requirements of this procedure can be very high. One way to decrease this computational burden is to update the AR coefficients at every N sample intervals, and use these coefficients in the prefilter until the next update. However, a more attractive alternative is to develop recursive versions of the algorithms. Such recursive versions determine optimal AR coefficients at every sample interval by updating the previous estimates rather than by solving for them from scratch every time.

IV. SIMULATION

This section describes the results of a computer simulation of the Two-Dimensional ARMA Algorithms. Figures A, B, C represent three different techniques for computing the spectrum of the same array data. The data, that is generated by the simulation software and consists of two sinusoids in white noise. The power in each sinusoid is 0 dB and the white noise power is -10 dB. In each case there was three antennas and 64 data points collected from each antenna. In Figure A a second order auto regressive (AR) model was used to compute the spectrum of the data. Figure B is the same as Figure A except the least squares error solution is used. In Figure C a one zero two pole auto-regressive moving-average (ARMA) model is used.

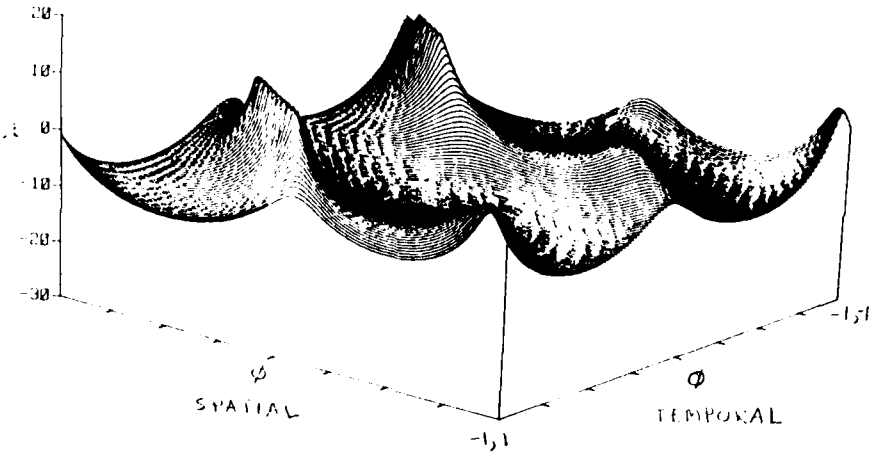

FIGURE A.

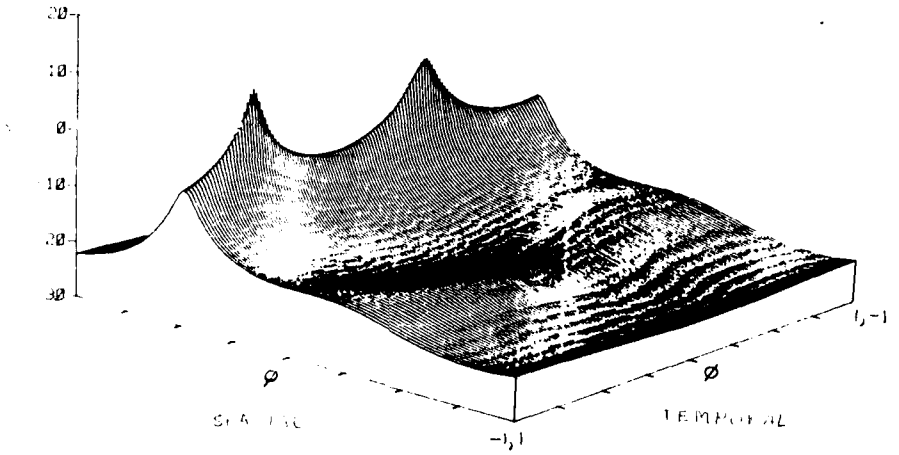

FIGURE B.

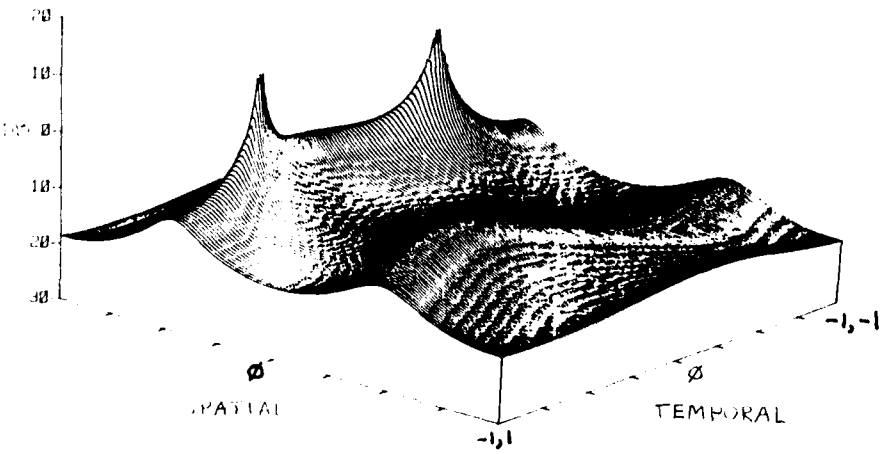

FIGURE C.

REFERENCES

1 Sylvania Systems Group, "HF Wideband Modem Program", November 1981, RADC Tech Report CDRL-A008.

2 R. A. Monzingo and T. W. Miller, Introduction to Adaptive Arrays, New York Wiley-Interscience, 1980.

3 O. L. Frost, III, "An Algoritnm for Linearly Constrained Adaptive Array Processing", Proc. IEEE, Vol. 60, No. 8, Aug 1972, pp. 926-35.

4. J. W. Modestino, et. al. "Digital Communications in Spatially Distributed Interference Channels." December 1982, Rome Air Development Center Tech. Report RADC-TR-82-151

5 R. A. Wiggins and E. A. Robinson, "Recursive Solution to the Multichannel Filtering Problem," J. Geophysical Research, Vol. 70, No. 8, Apr. 1965, pp. 1885-91.

6 M. Morf, A. Vieira, D. T. Lee, and T. Kailath, "Recursive Multichannel Maximum Entropy Spectral Estimation," IEEE Trans. Geoscience Electronics., Vol. GE-16, No. 2, Apr. 1978, pp. 85-95.

7 J. G. Proakis and J. W. Ketchum, "Suppression of Narrowband Interference in Pseudo-noise Spread Spectrum Systems," Feb 1981, Rome Air Development Center Tech. Report RADC-TRL-81-6.

8 Koopmans, The Spectral Analysis of Time Series, New York, Academic Press, 1974.

9 J. A. Cadzow and R. L. Moses, "Adaptive ARMA Spectral Estimation, Part I", Aug. 17-18, 1981, Proc. 1st IEEE Spectral Estimation Workshop, Hamilton, Ont.

10 J. A. Cadzow and R. L. Moses, "Adaptive ARMA Spectral Estimation, Part II", Aug. 17-18, 1981, Proc. 1st IEEE Spectral Estimation Workshop, Hamilton, Ont.

11 J. H. Justice, "A Levinson-Type Algorithm for Two Dimensional Weiner Filtering Using Bivariate Szego Polynomials," Proc. IEEE, Vol. 65, No. 6, pp 882-6, June 1977.

12 Hsu, F. M. and Giordano, A. A., "Digital Whitening Techniques for Improving Spread Spectrum Communications Performance in the Presence of Narrowband Jamming and Interference," IEEE Trans. Comm., Vol. COM-26, No. 2, February 1978, pp. 209-216.

13 Ulrych, T. J. and Bishop, T. N., "Maximum Entropy Spectral Analysis and Autoregressive Decomposition," Rev. Geophysics and Space Phys., Vol. 13, February 1975, pp. 183-200.

14 Burg, J. P., "Maximum Entropy Spectral Analysis," 1967, Proc. 37th Meeting of the Society of Exploration Geophysicists; also reprinted in Modern Spectrum Analysis (D. G. Childers, Ed.) 1978, pp 34-41, IEEE Press

15 Levinson, N., "The Wiener RMS Error Criterion in Filter Design and Prediction", J. Math. Phys., Vol. 25, 1947, pp. 261-278.

16 Anderson, P. E., Hsu, F. M. and Sandler, M. N., "A New Adaptive Modem for Long Haul HF Digital Communications at Data Rates Greater Than 1 bps/Hz," 17 Oct 1982, MILCOM, Boston, Mass.

17 Austin, M. E., "Decision-Feedback Equalization for Digital Communication Over Dispersive Channels," 11 Aug. 1967, Lincoln Lab. Technical Report 437.

18 Proakis, J. G., "Advances in Equalization for Intersymbol Interference," in Advances in Communication Systems, Theory and Application, edited by Viterbi, A. J., Academic Press, 1975.

19 Hsu, F. M., "Square-Root Kalman Filtering for High-Speed Data Received Over Fading Dispersive HF Channel," IEEE Trans. Inf. Thy., Sept. 1982.

20 Gabriel, W. F., "Adaptive Arrays - An Introduction", Proc. IEEE, Vol. 64, No. 2, Feb. 1976.

DISCUSSION

E.W.Lampert, Ge

What are the classes of discriminants you are using for your adaptive array system?

Author's Reply

No discriminants are used for the 2-dimensional spectral whiting filter discussed in the paper. The prefilter merely performs spectral smoothing. In terms of spatial filtering a number of discriminants are possible. They are, direction of arrival, a prior knowledge of desired signal and knowledge of receive frequency (frequency hopped).

R.W.Jenkins, Ca

Have you implemented the matrix inversion techniques yet, and if so, what are the matrix inversion times achieved?

Author's Reply

For the worst case matrix inversion would require $4n^3 + 4n^2 + 3n$ complex multiplies, where n is the number of antennas. For example, if n = 3 then $4 \times 3^3 + 4 \times 3^2 + 3 \times 3 = 34$ complex multiplies. At 100 m flops the update time is 34 μs for Cholesky $4 \times 3^2 + 18 + 3 = 26$, i.e. 2.6 μs update approx.

OVERVIEW OF RADC ADAPTIVE ANTENNA DEVELOPMENTS FOR COMMUNICATIONS

by

J.A.Graniero, C.J.Tavera and J.R.Periard
Rome Air Development Center
Griffiss Air Force Base
New York 13441
USA

ABSTRACT

Adaptive Antennas are a key technology in providing reliable communications in an interference environment.

The paper will describe key developments at the Rome Air Development Center (RADC) in areas of adaptive algorithms, experimental processors and test and evaluation. The developments are aimed at improving adaptive antenna performance such as: null depths over bandwidth and in high multipath, convergence speeds and processor size, weight and cost. A new test bed at RADC called the Flexible Adaptive Spatial Signal Processor (FASSP) will be described. The FASSP provides the capability of comparative evaluation of various adaptive algorithms in either or both of two modes: full digital beamforming/nullsteering or a hybrid mode with analog weighting and digital weight computation.

DISCUSSION

E.W.Lampert, Gc

(1) What are the constraints when using frequency hopping, especially wideband, on the antenna array (physical structure) and array processor?

(2) What does an array look like for HF (1.5 - 30 MHz) i.e. types of array elements dipoles or loop and geometrical distance between them.

Author's Reply

(1) For wideband frequency hopping adaptive arrays the main constraints associated with the aperture array are the decorrelation effects and dispersion effects as a function of the signal bandwidths and size of the aperture in wavelengths. For the array processor the constraints are in the particular implementation chosen (a frequency look ahead approaches for example) and the speed of response that the processor has to operate to perform the necessary weight updates to follow the frequency hopping roles.

(2) An array for HF frequencies may encompass a linear array of quarterwave stub antenna elements. The optimum spacing for such an array should be on the order of a half wavelength if possible. HF arrays have also been looked at incorporating combinations of linear dipoles and loops as well to achieve angular discrimination.

H.J.Albrecht, Gc

Could you comment on the minimum frequency of operation (VHF, HF, LF, ULF) of the arrays in general and the approach you described in particular.

Author's Reply

(1) In general adaptive arrays have been built at frequencies down to Hz for Sonar (Acoustics) applications. At RADC we have built and demonstrated adaptive arrays of VLF frequencies as a minimum. The processing speeds for adaptive arrays is fairly independent of the operational frequencies. For HF frequencies and below the adaptive array processor can be implemented all digitally.

(2) For the specific approach discussed (LMS processor module) the operational frequency bandwidth covers approximately 40 - 90 MHz.

TRANSMISSION ASYNCHRONE

A FORT ETALEMENT DE SPECTRE

Par M. SCHILLIGER et C. LELOUP - LMT RADIOPROFESSIONNELLE
46, Quai Alphonse le Gallo - Boulogne-Billancourt
France

RESUME

Les avantages multiples qu'apportent les systèmes de transmission à étalement de spectre rendent leur utilisation de plus en plus fréquente pour les communications militaires. Les liaisons avec étalement de spectre au moyen de séquences directes sur une très large bande peuvent, suivant les besoins, convenir pour deux types différents d'applications : avec une forte puissance à l'émission et un gain de traitement élevé, on obtient une liaison ayant une bonne résistance aux brouillages ; avec une faible puissance à l'émission, l'énergie est dispersée sur une large bande instantanée, la liaison est rendue discrète et possède une très faible probabilité d'interception du signal par l'ennemi.

Une réalisation de maquettes d'émetteur et de récepteur a permis, d'une part, d'essayer une liaison asynchrone en phonie avec une numérisation de la parole par codage delta et, d'autre part, d'effectuer des mesures.

L'étalement du spectre sur une bande de 80 MHz est effectué à l'émission au moyen de séquences pseudo-aléatoires codées en B.O.K. (Binary Orthogonal Keying) utilisant la modulation P.S.K. ou M.S.K. La démodulation à la réception est faite en mode asynchrone par un double convoluteur piézoélectrique à ondes acoustiques de surface fonctionnant à une fréquence d'entrée de l'ordre de 400 MHz. Chacun des convoluteurs est alimenté, d'une part par le signal reçu, d'autre part, par une réplique du signal attendu, à la même fréquence, et avec le même code inversé dans le temps.

En plus des avantages de l'étalement de spectre dans un environnement de guerre électronique, ce type de liaison apporte une bonne protection contre les multitrajets lorsque le retard du signal réfléchi par rapport au signal direct est supérieur à la durée d'un chip de la séquence d'étalement, (environ 10 ns) donc pour des différences de trajets extrêmement courtes.

1. INTRODUCTION

Les deux propriétés principales d'une transmission protégée utilisée pour les applications militaires, face aux actions de guerre électronique sont la résistance à la détection et à l'interception et la résistance aux interférences et aux brouillages.

Ces deux aspects différents qui d'ailleurs dans certains cas se recoupent, peuvent conduire à des choix techniques très semblables à quelques détails près.

Dans le premier cas, il s'agit d'établir une liaison qui puisse passer inaperçue à un ennemi qui effectue une radiosurveillance et cherche à détecter la présence d'émissions radioélectriques afin de pouvoir ensuite les localiser, les écouter et peut être même les brouiller ou modifier le contenu des informations qu'elles transmettent.

Pour le deuxième aspect, lorsqu'on désire que la liaison soit assurée à coup sûr, la transmission doit être capable de résister à un brouillage même intense, soit parce que l'on sait que l'émission risque d'être détectée puis ensuite brouillée, soit parce que l'on doit déjà faire face à un environnement brouillé d'une manière systématique.

Les deux propriétés énoncées au début sont très difficiles à obtenir simultanément et le choix notamment de la puissance et de la durée des émissions conduit obligatoirement à un compromis entre une liaison discrète ou une liaison résistante au brouillage. Par contre, l'utilisation des techniques d'étalement du spectre constitue une solution très efficace permettant d'apporter une amélioration dans les deux cas à la fois.

On n'envisagera dans la suite que l'étalement de spectre par séquences directes, sur une bande instantanée de l'ordre d'une centaine de mégahertz.

Des premiers essais d'une telle liaison effectués en laboratoire dans le cadre des études N.I.S. (Nato Identification System) ont permis de vérifier certaines propriétés, mais une étude plus approfondie, avec réalisation de maquettes devrait être menée prochainement. Elle permettra d'effectuer des mesures et essais en vraie grandeur et de mieux en apprécier les limites afin de bien déterminer les applications potentielles.

Ces applications peuvent concerner d'abord des liaisons bilatérales permettant de transmettre des données ou de la phonie à courte distance, soit en mode air-air entre aéronefs en formation, soit en mode air-sol ou air-mer pour fournir les informations nécessaires lors d'approches, par exemple pour des atterrissages tactiques sur aérodromes improvisés ou pour des appontages sur porte-aéronefs. L'intérêt de ce type de liaison ayant une puissance très basse à l'émission et une très faible densité spectrale de puissance est d'être pratiquement indétectable et par conséquent utilisable dans tous les cas où jusqu'à présent il est indispensable de maintenir le silence radio des équipements conventionnels (V.H.F. ou U.H.F.).

Une deuxième application possible concerne les transmissions de données numériques sur une distance de plusieurs dizaines de kilomètres, dans un milieu pouvant être fortement brouillé, entre un avion et un missile qui vient d'être largué. La liaison est alors utilisée pour fournir au missile des informations de position relatives à la cible, lui permettant de recaler son système de guidage et de poursuivre cette dernière même si elle effectue des manoeuvres d'évasion. L'avion a la possibilité avec cette transmission d'adresser des données simultanément à plusieurs missiles.

On décrira dans la suite les caractéristiques de la liaison, les possibilités de réalisation des équipements émetteurs et récepteurs et les avantages de l'utilisation de l'étalement de spectre à large bande instantanée, en particulier pour ce qui concerne la résistance aux multitrajets.

2. DESCRIPTION DE LA TRANSMISSION

L'émission est effectuée en impulsions avec un étalement du spectre de chaque impulsion par séquences directes et un codage binaire utilisant des codes orthogonaux (B.O.N.).

La réception est faite en utilisant un filtre adapté au signal à recevoir constitué par un double convoluteur piézoélectrique à ondes acoustiques de surface.

Chaque impulsion émise correspond à un symbole et les séquences d'étalement de la durée d'un symbole sont obtenues actuellement, soit directement au moyen de séquences de longueurs maximales ou de codes de Gold, soit par application des fonctions de Walsh à ces derniers. Ces types de codes linéaires ont été choisis pour leur simplicité et la facilité de leur génération, tout autre code permettant d'améliorer les performances pourra évidemment être utilisé dans l'avenir.

Le choix de la bande d'étalement doit être déterminé en fonction des possibilités technologiques de réalisation des convoluteurs et les chiffres relatifs à la première maquette, indiqués ci-après à titre d'exemple, correspondent à des composants couramment réalisés actuellement :

- Bande d'étalement : 80 MHz
- Durée de symbole : 6,4 microsecondes
- Durée de chip : 12,5 nanosecondes
- Nombre de chips par symbole : 512

Il en résulte un gain de traitement théorique de 27 dB.

La modulation H.F. utilisée actuellement pour des raisons de simplicité est le P.S.K.-P.N. Mais elle pourra avantageusement être remplacée dans l'avenir par le M.S.K.-P.N. qui, à étalement égal, permet une meilleure utilisation du spectre en concentrant mieux l'énergie dans le lobe principal et en diminuant les niveaux des lobes secondaires, ce qui facilite l'élimination des raies parasites hors bande. La possibilité d'utiliser sans problème pour les étages de puissance de l'émetteur un amplificateur transistorisé fonctionnant en classe C constitue un avantage supplémentaire de la modulation M.S.K..

Pour la réalisation de la liaison, la fréquence porteuse a été choisie en U.H.F. dans la bande L. (autour de 1 GHz) utilisée par le D.M.E./TACAN, par le J.T.I.D.S. et par l'I.F.F. ainsi que par le NIS en bande L.

Les informations à transmettre sont formattées en messages et chaque message comprend un préambule et un texte. Le préambule, formé d'une suite de plusieurs symboles avec codage temporel, permet pour chaque message reçu, d'obtenir une synchronisation utilisée ensuite pour le décodage du texte du même message. Le texte du message est suffisamment court pour que la synchronisation acquise après réception du préambule garde une précision permettant un décodage correct jusqu'à la fin de message. La liaison est dite asynchrone parce qu'il n'est pas nécessaire d'entretenir une synchronisation permanente du récepteur. Celle-ci est acquise, pour chaque message, par traitement du préambule dans un corrélateur de préambule.

Le convoluteur à ondes de surface utilisé à la réception fonctionne en mode purement asynchrone pendant la réception du préambule et ensuite en mode synchronisé pendant le décodage du texte.

3. SCHEMA D'EMISSION

Le schéma d'émission fournit à la sortie antenne les impulsions de porteuse à 1 GHz modulée [illegible] Le schéma synoptique est décrit sur la figure 1.

[illegible] sont transformés dans le générateur de codes, selon leur valeur, en [illegible] sortie du générateur de code commande en amplitude et en phase [illegible] oscillateur en anneau, alimenté par une source H.F. à une fréquence [illegible] MHz, [illegible] référence de fréquence. Après filtrage au moyen d'un filtre [illegible] sont transposées à la fréquence de sortie dans un mélangeur, [illegible] amplificateurs des faibles niveaux utilisés pour les essais, les amplificateurs de puissance sont de type linéaire. Un codeur delta auto-adaptatif fonctionnant à une fréquence de [illegible] les bits d'informations, a été utilisé pour la modulation de la liaison.

4. ENSEMBLE DE RECEPTION

L'ensemble de reception décrit sur la figure 2 se compose de quatre parties principales : la partie H.F. de reception, les modules de convolution, les generateurs de codes et les circuits de detection des pics de convolution.

4.1 Partie H.F. de reception

Elle comprend les circuits de filtrage, de mélange et d'oscillateur local, permettant d'effectuer la transposition de frequences du signal reçu (autour de 1 GHz) à la frequence nominale d'entree du convoluteur (400 MHz).

4.2 Modules de convolution

Les modules de convolution comprennent deux circuits rigoureusement identiques fournissant, pour le premier, les pics de convolution du code 1 et pour le second, les pics de convolution du code zero. Chaque module de convolution comprend deux entrées alimentees par le signal reçu, d'une part, et par le signal de reference, d'autre part. Chacun de ces signaux est amplifié et filtré dans un amplificateur lineaire et un filtre passe-bande de frequence centrale 400 MHz et de bande passante supérieure à 50 MHz. Les deux convoluteurs egalement identiques sont constitués chacun d'un substrat piezoelectrique sur lequel ont ete deposes deux transducteurs électromecaniques permettant d'engendrer des ondes de surface et une electrode se presentant sous forme d'une plaque de longueur L (voir figure 3).

Les deux ondes acoustiques générees, de même frequence porteuse F mais de modulation $S_1(t)$ et $S_2(t)$ se propagent en surface du substrat en sens contraire, à une vitesse V. Les durees de propagation sous la plaque et entre le transducteur et la plaque sont respectivement : T=L/V et T'=L'/V (L' etant la distance du transducteur a la plaque). Par effet non linéaire dans le substrat et intégration par la plaque, on recueille en sortie un signal à une frequence 2F qui est le produit de convolution $S_1(t-T-T')$ $S_2(t)$, où C(t) est donne par la relation :

$$C(t) = \int_{-T/2}^{+T/2} S1(t-\tau).S2(t+\tau).dt$$

Lorsqu'on veut obtenir l'autocorrelation d'un code de durée maximum T (mode synchrone), on applique sur une entree le signal modulé par ce code et sur l'autre entrée un signal modulé par le même code inversé dans le temps. Il faut alors que les deux signaux soient envoyés en synchronisme pour que les deux codes complets se trouvent sous la plaque au même instant. Il est à remarquer que l'intéractivité des deux ondes appliquees produit sur le signal de sortie une compression du temps dans un rapport 2, ainsi, le pic d'autocorrelation d'un code avec modulation P.S.K. aura pour largeur theorique à la base, la durée d'un chip. En realite, les mesures effectuées ont montré qu'à la sortie du convoluteur, les pics obtenus sont elargis à la base et légerement dissymétriques (voir figure 4). Ceci est dû essentiellement aux réflexions parasites du signal et de la reference, dans le convoluteur.

La caractéristique importante du convoluteur est son rendement F encore appelé facteur de conversion, qui est donné par :

$$F = \frac{C_{max}}{\sqrt{P1.P2}}$$

où C_{max} est la valeur maximum de la fonction de deux signaux de durée T et où P1 et P2 sont les puissances des signaux d'entrée sur charge adaptee de 50Ω.

La propagation parasite des ondes de surface sur les transducteurs extrêmes, entraîne la détection de signaux parasites. Les deux ondes incidentes apres réflexion peuvent se convoluer avec elles-mêmes, et engendrent ainsi les parasites dits d'autoconvolution (C auto) et de convolution double trajet (C double trajet). Les rapports C auto/C max et C double trajet/C max caracterisent également le convoluteur.

Pour une utilisation du convoluteur en mode asynchrone, l'instant d'arrivée du code d'entrée peut être quelconque, le code local doit être choisie egale à T/2. La reconnaissance du code est obtenue par corrélation avec le code dit "de reference" $S_1*(t)$, qui est en fait le code d'entrée inversé dans le temps et dont la durée T est égale à la moitie de la durée de traitement de l'information. Pour obtenir un signal codé arrivant à un temps quelconque Ta, il suffit que le signal de référence soit répétitif par la répétition avec une période T du code attendu. On aura alors toujours coïncidence des signaux d'entrée et de reference puisque les deux codes entiers seront simultanement présents sous une zone donnée de la plaque.

Le diagramme de la figure 5 relatif au mode asynchrone montre la propagation des signaux incidents et de reference par rapport à la plaque ainsi que les temps correspondants. On voit que seuls les signaux détectés pendant les tranches de temps de (2N+1)T/2 à (2N+2)T/2 correspondent à des produits de convolution complets recherchés, et que les signaux qui apparaissent pendant les autres tranches de temps doivent être éliminés au moyen d'une porte logique générée en même temps que les codes de référence.

La figure 6 représente un diagramme des temps pour la détection asynchrone de signaux de durée T, pour différentes valeurs de retard du temps d'arrivée TA par rapport au code de reference; on y voit les tranches de temps qui doivent être rejetées. Les signaux triangulaires indiqués correspondent aux cas où les codes sont constitués par des impulsions rectangulaires de porteuse pure).

A REVIEW OF TRANSMISSION AND CHANNEL EVALUATION TECHNIQUES FOR DIGITAL COMMUNICATION SYSTEMS

by

Dr M Darnell
Department of Electronics
University of York
Heslington, York, YO1 5DD
UK

SUMMARY

The paper first reviews the advantages and disadvantages of digital modes of transmission. A brief survey of the main propagation characteristics of the different types of radio systems is presented, with attention being drawn to the factors which influence the choice and performance of digital transmission techniques. The most widely used digital transmission techniques are then discussed and their applicability to various radio frequency bands considered. Finally, channel evaluation techniques yielding models of the propagation and interference environments are described and the manner in which they can be employed to enhance the reliability of digital communication systems is indicated.

1. RATIONALE FOR DIGITAL COMMUNICATION

Over the past two decades, there has been a consistent progression towards the introduction of digital technology into most forms of communication system. The main benefits of digitisation can be summarised as follows:

(a) The signal can be regenerated exactly before uncorrectable errors occur. This is in contrast to analogue transmission where signal repeaters are employed to boost the signal level; in this latter case, any noise present with the signal will also be repeated and there will be no improvement in signal-to-noise ratio (SNR).

(b) The signal can be encrypted by digital means, potentially rendering the data fully secure. With analogue signals, only limited security in the form of analogue "scrambling" can be introduced.

(c) The advances which have taken place in the field of digital signal generation and processing techniques and devices can be applied to the problems of detecting communication signals more reliably in a background of noise, interference and distortion.

(d) With signals in digital form, it is relatively simple to apply multiple access coding algorithms which allow the simultaneous use of a given communication channel by a number of different services.

One potential disadvantage of the introduction of digitisation is that the bandwidth requirements for a given service can increase substantially in comparison with analogue transmission; this may be seen with the aid of a simple example of a speech transmission system. Considering the arrangement shown in Fig. 1(a): this is typical of the basic pre-processing of an analogue signal which takes place prior to transmission over a telephone circuit. The spectrum of the baseband speech signal is limited to about 3kHz in bandwidth by means of a band-pass filter. Fig. 1(b) shows a corresponding digitised speech transmission arrangement: here the speech is again subjected to a similar band-limitation prior to analogue-to-digital (A/D) conversion and sampling. Applying the Nyquist sampling criterion gives a sampling rate, f_s, of

$$f_s = 2 \times 3.4 = 6.8 \text{ kHz} \qquad [1]$$

If allowance is made for non-ideal filtering and sampling, a sampling rate of

$$f_s = 8 \text{ kHz} \qquad [2]$$

is appropriate. In order to achieve a reasonable speech fidelity, the number of bits per sample, n, should be about 8 giving an overall data rate of, R, of

$$R = n \times f_s$$

$$= 8 \times 8000 = 64 \text{ kbits/s} \qquad [3]$$

Again, this is typical value for a pulse code modulated (PCM) system. Thus, data will be transmitted over the channel in the form of pulses of width

$$T = \frac{1}{64000} \text{ s} \qquad [4]$$

In Figs. 2(a) and (b), the waveform and spectrum of one such pulse are illustrated. The first "null" of the spectrum will occur at a frequency of 1/T or 64 kHz. Since most of the spectral energy is contained in the region out to the first spectral null, it is reasonable to take the position of the null as being indicative of the transmission bandwidth required. Therefore, in contrast to the 3 kHz bandwidth of an analogue system,

SUMMARY OF SESSION V

SIGNALLING AND SOUNDING SCHEMES FOR RELIABLE DIGITAL COMMUNICATIONS

by

E.J.Lampert
Session Chairman

The papers of Session V practically separate into two groups. In the first group on high speed HF-data transmission, in both papers Prof. Goutelard et al. discuss principal problems using m-ary signal alphabets on one hand and the complementary procedures of arithmetic coding on the other hand. J.P.van Uffelen et al. and also H.F.Buding discuss the associated equipment oriented problems.

A second group of papers deals with the different aspects of applying spread spectrum modulation to handle the multipath problem. K.H.Anneke and M.Ottka show in a principal discussion the great potential of this family of modulation methods to suppress multipath, whereas U.Schulz and G.Holgen focus on the often neglected method of chirp modulation, which may be used with success even in the UHF-band, however experimental results are still outstanding. U.Langewellpott shows that well known FHDS-pulsepattern can also successfully be used for mobile digital telephone nets, where it is of practical interest that in the detection process the total energy is used by means of a RAKE-type receiver.

In this tutorial paper however M.Darnell addresses the whole spectrum of problems associated with transmission of high speed data and shows our present knowledge, in particular that many different techniques are of great relevance, source coding, modulation, adaptive modulation techniques and error detection/correction methods. Also addressed is the important area of realtime channel evaluation showing that a multitude of different methods exist, which suggest that for future systems, thoughts of the different experimental systems have to be merged to provide reliable, automated service, i.e. oblique sounding, spectrum monitoring, adaptive modulation, ARQ-procedures and appropriate digital encoding.

The presented papers suggest that it is now practical to transmit fairly high data rates even in a severe multipath environment, however a generally accepted standard for each class of transmission task is still far away.

DISCUSSION OF SESSION IV

Dr Albrecht

I would like to ask Mr Edraos what minimum frequency of operation he considered for the antenna arrays described in the paper.

Mr Edraos

The adaptation process is of course frequently independent. The limitation is in the electromagnetics, as mentioned earlier by Mr Luvera. Approximately eight years ago we tried to go as far down as possible to find a limitation, and a company built an HF adaptive array which worked quite successfully on the bench, but when mounted in aircraft obviously it worked less successfully. Active antennas were used, exact mechanical matches for the UHF blades we use now. The company also made mechanical duplicates at frequencies of 10 kHz and 100 kHz. When these were mounted in place of the UHF antennas we again got some decent nulling — perhaps not very good but decent. So the answer depends on what size and complexity of structure, and what degree of nulling, are acceptable.

Dr Jenkins

At the Communications Research Centre in Ottawa we have been working with HF adaptive arrays, and recently we built a small square four-element array, 2 m on a side, using active elements with a metallic structure between them so as to more or less modify the patterns of the individual elements. Normally in an array it is the different phases at different elements which enable you to discriminate between signals coming in different directions. When the patterns are modified the amplitude relationships become important, and you can in fact get reasonable nulling. With the 2 m square array at 5 MHz we had nulls of the order of 20 dB.

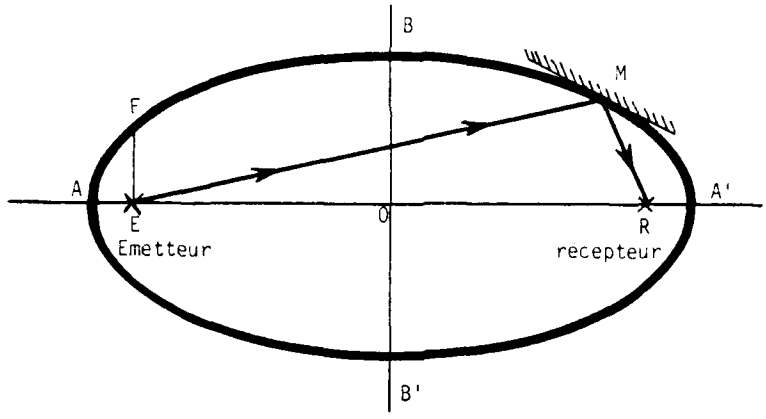

- Distance de la liaison : ER=D
- Retard du multitrajet par rapport au trajet direct : t_o
- Différence de trajet entre Signal direct et signal réfléchi : Ct_o (C = vitesse de propagation)
- Longueur du grand axe : $AA' = D + Ct_o$
- Longueur du petit axe : $BB' = \sqrt{Ct_o.(2D + Ct_o)}$
- Excentricité = $D/(D + Ct_o)$
- $AE = RA' = \frac{Ct_o}{2}$
- $EF = \frac{Ct_o}{2} \cdot \frac{2D + Ct_o}{D + Ct_o}$

FIGURE 14 MULTITRAJET PAR REFLEXION (GEOMETRIE)

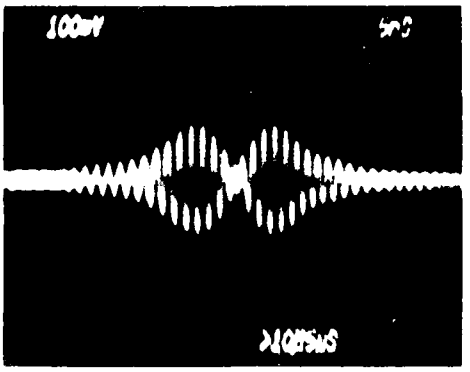

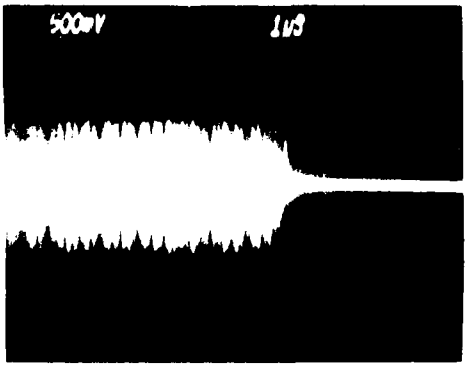

Pic de Convolution

Entree du Convoluteur

FIGURE 11 MULTITRAJET AVEC RETARD τ < t
PIC DE CONVOLUTION POUR UN MINIMUM

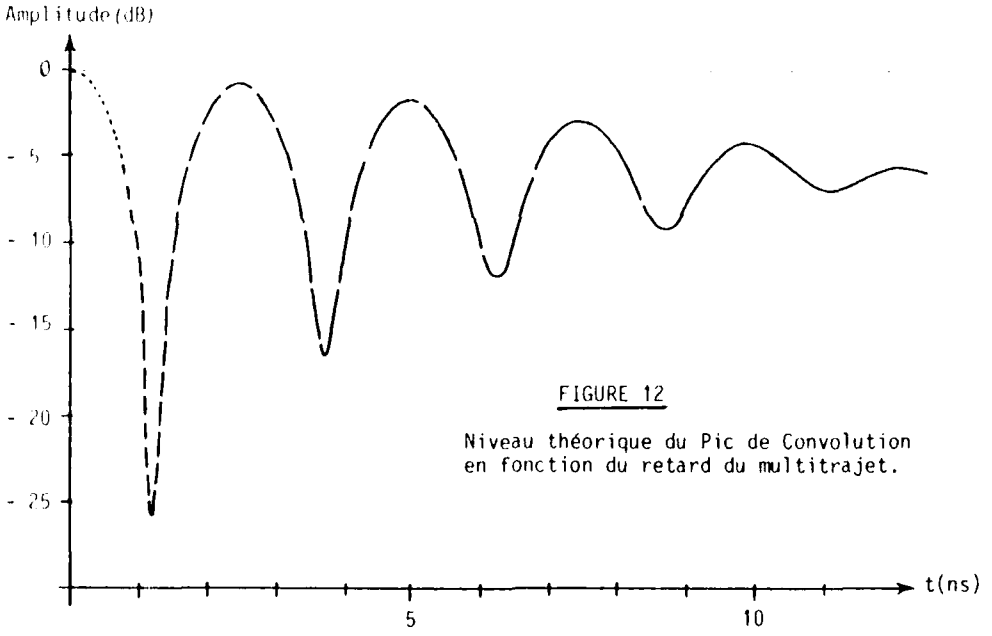

FIGURE 12

Niveau théorique du Pic de Convolution
en fonction du retard du multitrajet.

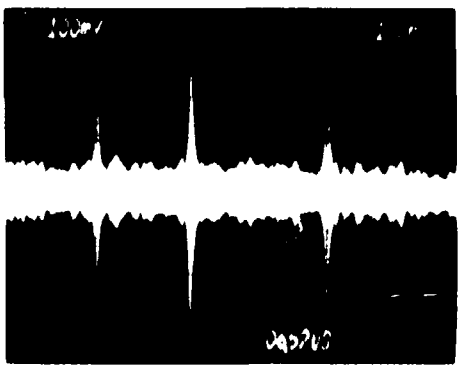

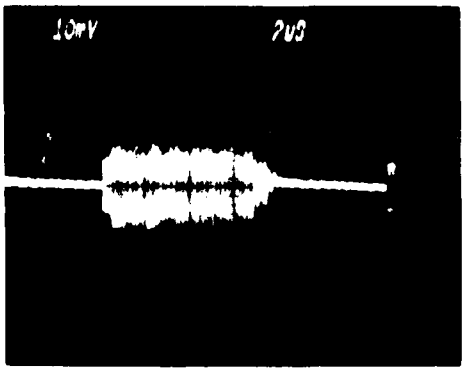

Pics de Convolution

Entree du Convoluteur

FIGURE 13 MULTITRAJETS AVEC RETARDS τ > t (210 ns et 510 ns

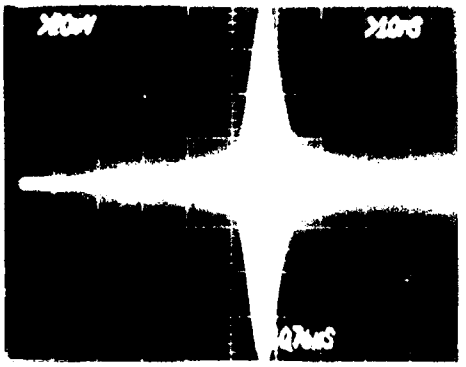

Code (9,4)

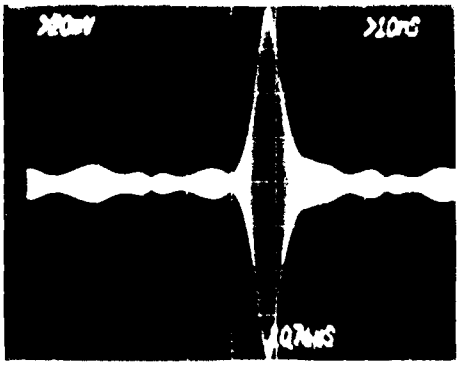

Code (9,4) + Fonction de Walsh (512,15)

FIGURE 8 PICS DE CONVOLUTION

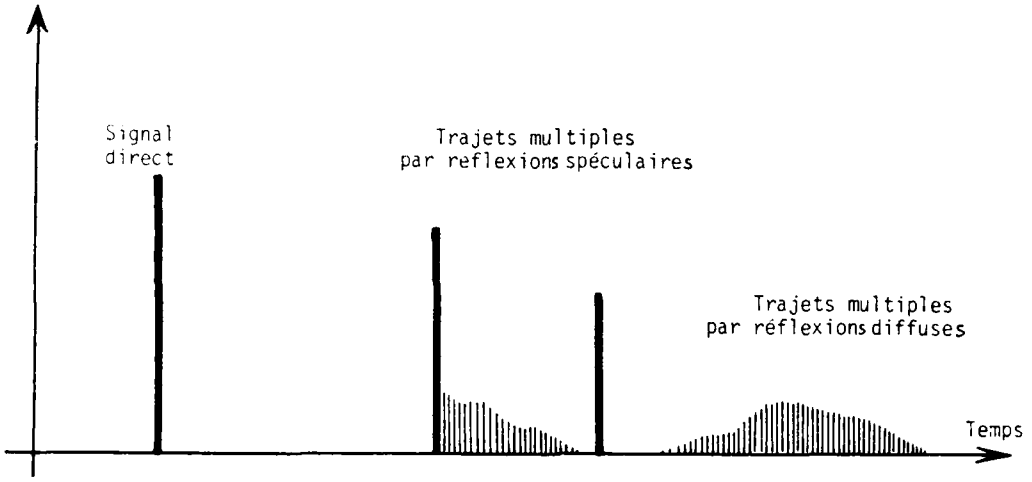

FIGURE 9 EXEMPLE DE MULTITRAJET PAR REFEXIONS

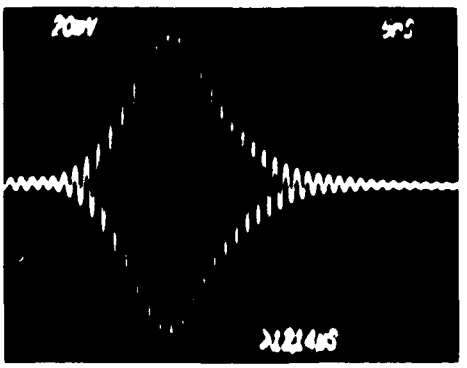

FIGURE 10 MULTITRAJET AVEC RETARD $\theta < \tau$
PIC DE CONVOLUTION POUR UN MAXIMUM

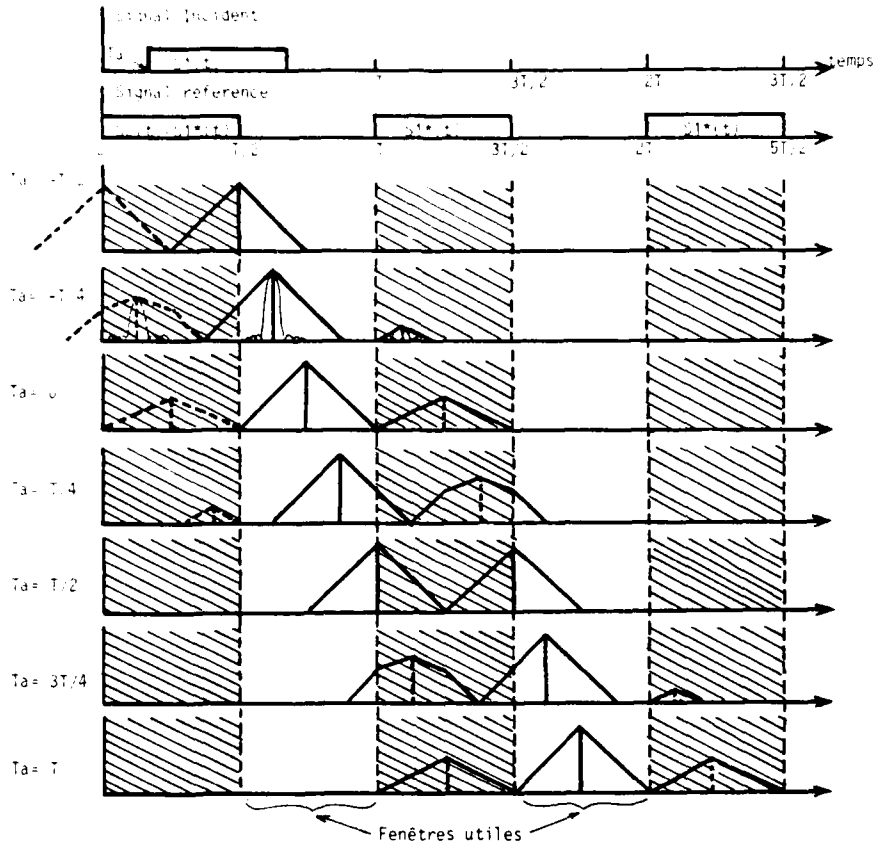

FIGURE 6 - DETECTION ASYNCHRONE D'UN SIGNAL DE DUREE T/2
DIAGRAMME DES TEMPS.

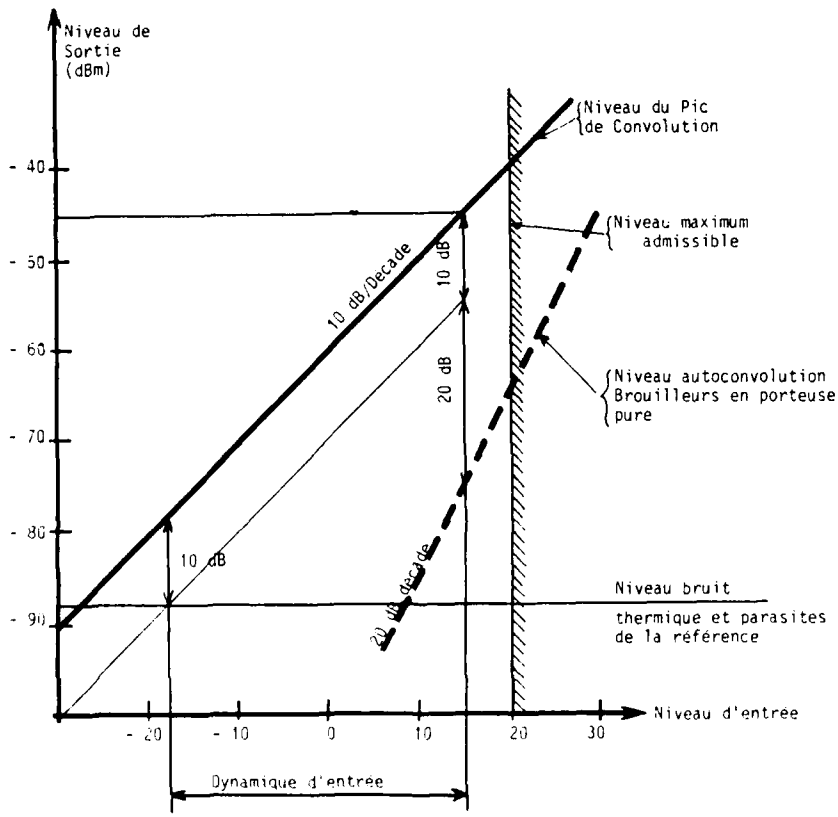

FIGURE 7 DYNAMIQUE THEORIQUE D'ENTREE DU CONVOLUTEUR.

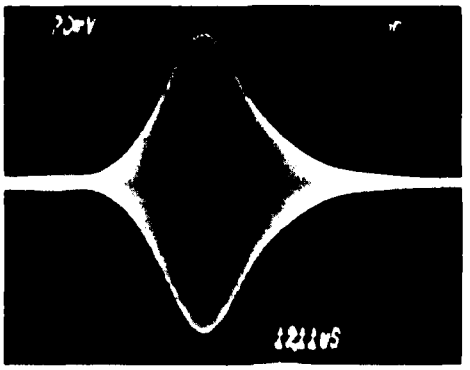

FIGURE 4 - PIC DE CONVOLUTION

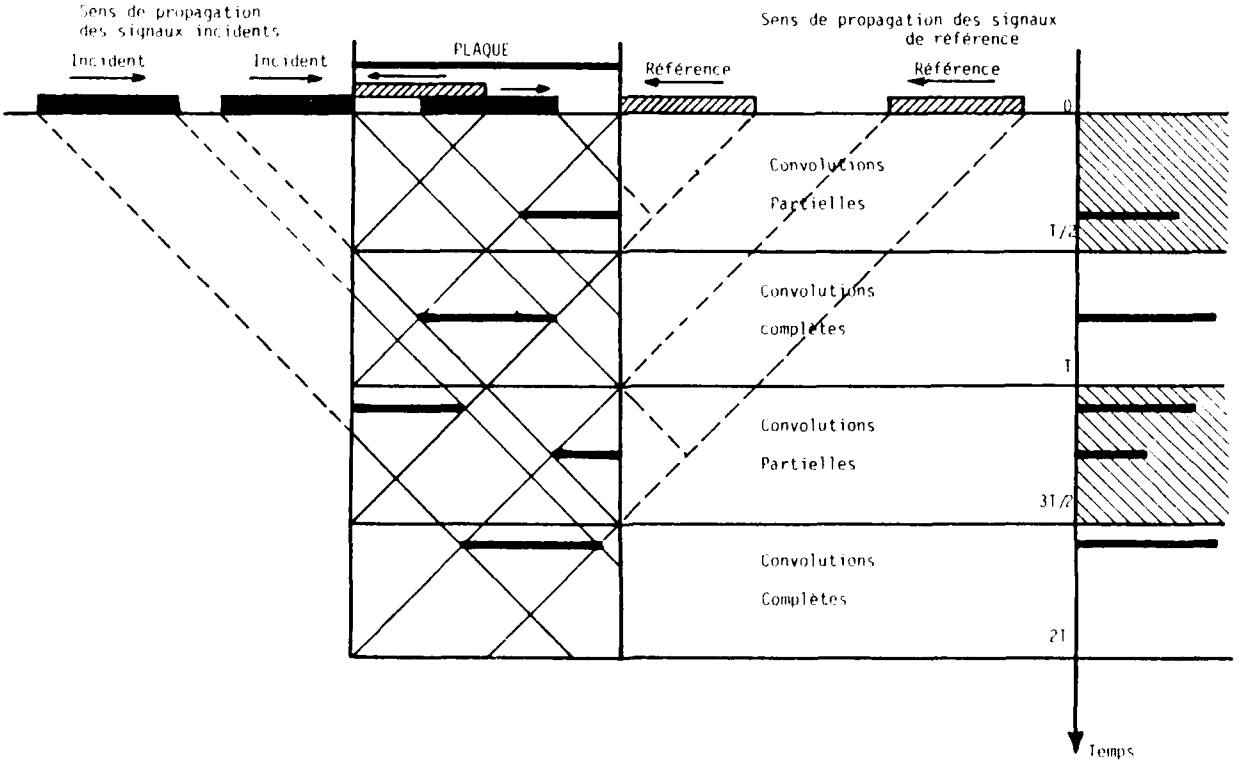

FIGURE 5 CONVOLUTEUR - DIAGRAMME DE DECODAGE EN MODE ASYNCHRONE

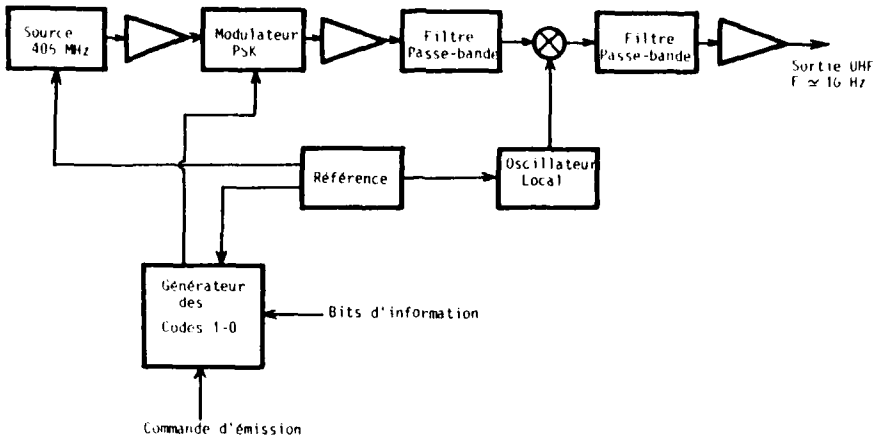

FIGURE 1 ENSEMBLE D'EMISSION - SCHEMA SYNOPTIQUE

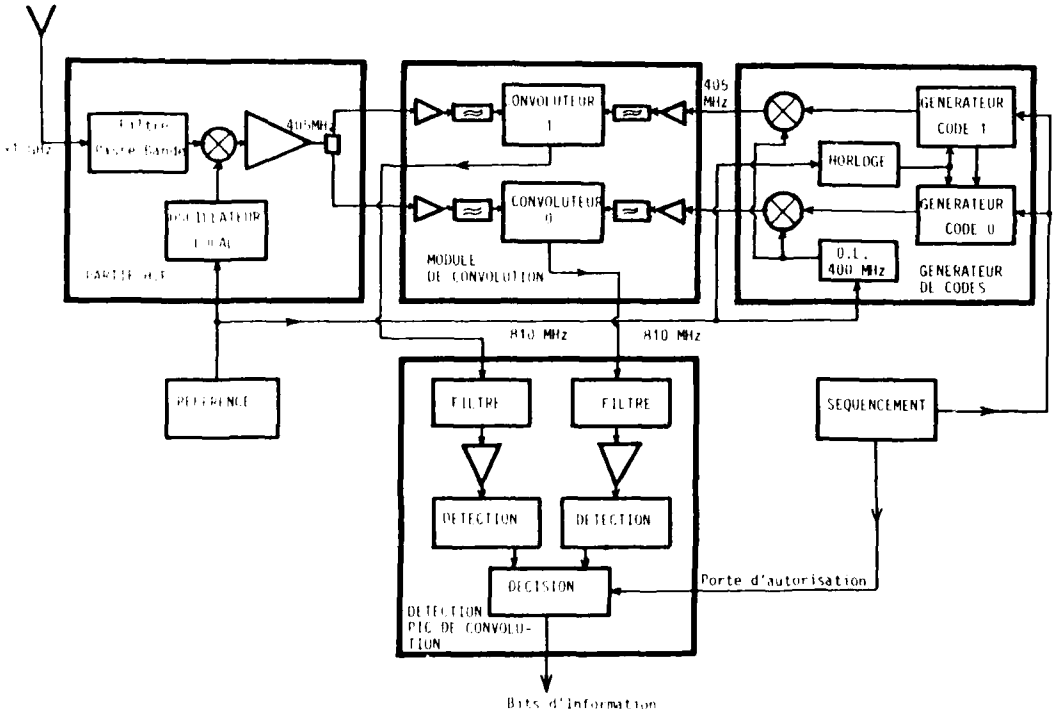

FIGURE 2 ENSEMBLE DE RECEPTION - SCHEMA SYNOPTIQUE

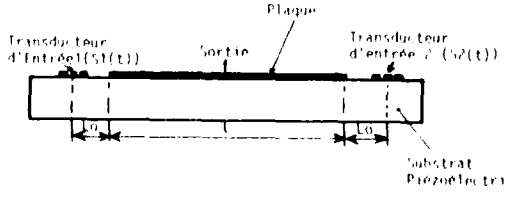

FIGURE 3 - Schéma du Convoluteur A Ondes acoustiques de surface

Pour diminuer ces effets, il suffit de reduire le plus possible la durée de chip, donc d'augmenter la bande d'étalement. Une autre solution envisageable pour les transmissions à cadence lente consiste à prévoir une redondance des messages emis.

Il faut tout de même remarquer que ces perturbations ne peuvent se produire que dans des cas assez rares de multitrajets, par refraction ou par reflexion.

Pour les multitrajets par refraction atmospherique, avec une liaison air-sol, la probabilité en est extrêmement faible car il faut à la fois que la couche refractante soit située au maximum à quelques centaines de pieds du sol et que l'aeronef vole lui-même sous la couche, donc à très basse altitude ; en liaison air-air, il faut que les deux aeronefs volent approximativement à la même altitude et tous deux sous la couche.

Pour les multitrajets par reflexion, la zone ou peut se trouver le reflecteur perturbant est extrêmement reduite et se situe à proximité immédiate des antennes d'emission ou de reception, il suffit donc de choisir avec soin leur point d'implantation. Les reflexions gênantes sur le sol ne pourront se produire que si au moins l'un des correspondants vole à très basse altitude.

- Lorsque le retard du multitrajet est superieur à la durée d'un chip, on a vu precedemment que l'on obtient en sortie du convolueur, en plus du pic de convolution desiré provenant du signal direct, des pics supplementaires correspondant aux signaux de multitrajets, et que d'autre part certains pics desirés peuvent être perturbés par des signaux de multitrajets provenant de symboles precedents. Ce type de perturbation est appelé "garbling".

Pour s'en affranchir dans le preambule, on utilise un correlateur de preambule, encore appelé correlateur de trame qui est adapté à la disposition temporelle des differents pics de convolution. Il est constitué schematiquement d'une ligne à retard avec prises et sommateur suivi d'un circuit à seuil. L'ensemble permet d'ignorer les pics supplementaires dus aux multitrajets et d'acquerir la synchronisation malgré la perte d'un ou plusieurs pics de convolution. Pour cela le preambule doit comporter un nombre suffisant de symboles.

Le decodage du texte du message fonctionne en mode synchronisé et ne prend en compte que les pics de convolution desirés situés à l'interieur d'une fenêtre de decodage. Les pics retardés dus aux multitrajets sont elimines car ils se trouvent en dehors de la fenêtre.

Les erreurs provoquées par les interferences intersymboles dues aux multitrajets peuvent être eliminées en prevoyant des redondances de symboles et en utilisant des codes detecteurs et correcteurs d'erreurs.

Pour eviter la perte d'une suite de symboles successifs par des multitrajets persistants, une distribution non recurrente des symboles du texte du message peut être envisagée.

6 CONCLUSION

La liaison asynchrone qui a été decrite presente un grand interêt pour des applications particulieres concernant certaines transmissions militaires. En plus des avantages inherents à l'utilisation de l'étalement du spectre, resistance aux brouillages et discretion, cette transmission ne necessite pas de synchronisation permanente entre emetteur et recepteur et elle présente une bonne immunité contre les multitrajets.

L'élimination des signaux de trajets multiples peut être faite par separation temporelle entre le signal direct utile et le signal perturbateur retardé. L'interêt de l'utilisation de l'étalement du spectre par sequences directes, reside dans la possibilité d'effectuer la separation après traitement dans le convoluteur, sur les pics de convolution qui sont très étroits. On peut de cette manière, s'affranchir de multitrajets ayant des retards d'autant plus courts que la cadence de la sequence d'etalement est plus rapide, donc la bande plus large.

Pour supprimer les interference intersymboles causées par les multitrajets ayant des retards assez longs, on peut également effectuer une separation temporelle. Des améliorations supplementaires peuvent encore être obtenues par un choix judicieux du format des messages et, par l'utilisation de sauts de frequence ou de changements de codes d'un symbole à l'autre, moyennant bien sûr une complication du système.

BIBLIOGRAPHIE

1. - Propagation des ondes radioelectriques dans l'environnement terrestre par J.BOITHIAS
Collection des telecommunications Editions DUNOD 1983.

2. - Low probing angle propagation measurement for the MK-XV A IFF System
par J.A. GIN Lincoln Laboratory M.I.T. Lexington Ma.

3. - [illegible] scattering multipath effect using Spread Spectrum system
par [illegible] AGARD Conferences Proceeding N° 332 Ref. 36

4. - Low-altitude tracking over rough surfaces
par [illegible] AGARD-AG-164-73 Record

5. - Radionavigation Radiolocalisation
par R.J. [illegible] Edition MASSON 1983.

5.3.2 Séparation en fréquence

Pour lutter contre les multitrajets ayant des retards importants et éviter dans ce cas les interferences intersymboles, la transmission peut être définie de manière que les symboles successifs se trouvent à des fréquences porteuses différentes(sauts de fréquence). Ainsi le signal de trajet multiple provenant d'un symbole donné, arrivant en même temps qu'un des symboles suivants ayant suivi un trajet direct, est à une fréquence différente du signal attendu et peut par conséquent être éliminé. Le convoluteur de la liaison à spectre étalé effectue cette séparation à condition que la difference de fréquence entre les symboles susceptibles de se perturber soit supérieure à 1/T (T étant la durée d'un symbole).

Dans une liaison asynchrone, ce procédé d'élimination des multitrajets par sauts de fréquence n'est pas utilisable pour le préambule dont tous les symboles doivent être à la même fréquence, dans le cas contraire, il serait nécessaire pour l'acquisition, d'utiliser simultanément plusieurs récepteurs accordés chacun sur l'une des différentes fréquences. Par contre, il peut convenir pour le texte du message qui peut être décodé en mode synchrone après acquisition du préambule. Cependant la loi de sauts de fréquence du texte doit dans ce cas être identique pour chacun des messages.

5.3.3 Séparation en codes

De la même manière que pour la séparation en fréquence, en dehors de toute considération de chiffrement, on peut changer le code d'étalement de chaque symbole pour diminuer l'effet des interférences entre symboles provoquées par les multitrajets. Pour la transmission asynchrone, ce procédé ne peut être utilisé que pour le texte du message qui peut être décodé en mode synchrone après l'acquisition du préambule ; de plus, les textes de tous les messages doivent avoir la même loi de changement de code. Le préambule devant être décodé en mode totalement asynchrone, tous les symboles qui le composent doivent posséder le même code d'étalement.

5.3.4 Séparation en temps

Un signal de trajet multiple étant toujours retardé par rapport au signal direct, pour une transmission en impulsions, lorsque son retard est supérieur à la durée de l'impulsion, le multitrajet peut être éliminé au moyen d'un traitement du signal convenable. Plus les impulsions utilisées sont brèves, meilleure est l'élimination des multitrajets, particulièrement lorsque les retards sont faibles.

Pour la transmission avec étalement de spectre considérée, on effectue cette discrimination sur les pics de convolution après traitement dans le convoluteur. Les deux pics de convolution correspondant au trajet direct et au multitrajet sont bien séparés lorsque le retard t_0 est supérieur à la durée d'un chip de la séquence d'étalement ($t_0 > 12{,}5$ ns). Ce retard *minimum* correspond à une différence de parcours entre trajet direct et trajet multiple extrêmement réduite dont la valeur est $C.t_0 = 3.75$m.

La figure 14 montre pour un multitrajet par réflexion la géométrie correspondante. Si l'émetteur E et le récepteur R sont séparés par une distance D, le lieu des points où un réflecteur R peut créer un multitrajet reçu avec un retard t est une ellipse dont les foyers sont E et R et le grand axe C.t +D.

Tous les réflecteurs possibles situés à l'extérieur de cette ellipse créent des multitrajets que l'on peut éliminer puisque leurs retards sont supérieurs à t_0.

Avec le pouvoir de discrimination indiqué ci-dessus, l'ellipse de la figure 14 à une excentricité voisine de 1 (forme très aplatie). Elle présente les dimensions suivantes : distance AE = 1.9m, distance EF = 3.8m, longueur du ½ petit axe = 306m pour une liaison sur une distance ER de 50 km et 433m pour une liaison sur une distance ER de 100 km.

On voit dans ce cas, pour des liaisons sol-air ou air-air, que les seuls multitrajets qui ne seront pas éliminés par séparation en temps auront des retards extrêmement courts. Ils pourront être produits soit par réfractions, soit par réflexions mais dans ce dernier cas, seulement sur des surfaces situées très près des antennes ou sur le porteur lui-même. Les multitrajets par réflexion sur le sol non éliminés, ne pourront se produire que pour des vols à très basse altitude.

5.4 Conséquences pour la définition des caractéristiques de la liaison

Lors de la définition complète de la liaison asynchrone, pour une application donnée, il sera nécessaire de prendre en compte les considérations indiquées précédemment afin d'améliorer la résistance aux perturbations causées par les multitrajets. Cependant, la décision d'utiliser des sauts de fréquence et des changements de codes à chaque symbole est en général motivée plutôt par la nécessité d'améliorer la résistance aux contre-mesures en augmentant la bande d'étalement et en effectuant un chiffrement, que par le besoin de diminuer les erreurs dues aux multitrajets. La séparation en temps est en fait le moyen le plus simple à utiliser et son efficacité paraît suffisante compte-tenu du pouvoir de discrimination que l'on peut obtenir avec la bande d'étalement utilisée.

On a vu que chaque message comprend un préambule et un texte. Le préambule est composé d'un certain nombre de symboles avec un codage temporel de position. Tous les symboles ont le même code d'étalement et à la réception sont décodés en mode asynchrone dans le convoluteur. L'ensemble du préambule passe ensuite dans un corrélateur de préambule qui permet d'obtenir une synchronisation utilisée pour décoder le texte, seulement pendant le message considéré. Le texte du message qui contient les bits d'informations est constitué de symboles qui sont décodés dans le convoluteur en mode synchrone.

Pour l'élimination des perturbations apportées par les multitrajets, il faut distinguer deux cas selon la valeur du retard du multitrajet :

- Lorsque le retard du multitrajet est inférieur à la durée d'un chip de la séquence d'étalement, dans le cas le plus défavorable, pour certaines valeurs de la différence de phase entre le signal direct et le multitrajet et pour une valeur élevée du niveau du multitrajet, on peut avoir purement et simplement une perte de décodage du symbole perturbé.

5.2 Effet des multitrajets sur la liaison avec étalement de spectre

5.2.1 Pics de convolution

Une liaison comportant un seul multitrajet, avec retard et niveau variables, a été simulée en laboratoire. Afin de simplifier le montage, la fréquence porteuse d'émission a été choisie à la fréquence directe d'utilisation du convoluteur de réception (405 MHz). Les signaux utilisés étaient formés d'impulsions de durée 6,4 µs, modulées en P.S.K. avec 512 chips (durée de chip : 12,5 ns). Pour ajouter le multitrajet, le signal après modulation était divisé en deux voies : la première, directe, correspondait au trajet normal, la seconde, éventuellement atténuée et retardée d'un temps θ variable au moyen d'une ligne à retard ajustable, simulait le multitrajet. Après sommation des deux voies, le signal était ensuite envoyé vers le convoluteur pour être décodé.

On peut montrer, d'une manière simplifiée, ce que devient le pic de convolution fourni par le convoluteur en présence d'un multitrajet. Si S(t) est le signal direct, S(t-θ) le signal retardé, la somme S(t) + S(t-θ) est envoyée sur l'entrée signal du convoluteur, l'entrée référence étant alimentée par un signal convenablement codé.

Pour une entrée S(t), le pic de convolution idéal est donné par :

$$\begin{cases} R(t) = (1-t/\tau)\cos 2\pi f t \text{ entre } -\tau \text{ et } +\tau \\ R(t) = 0 \qquad \text{ailleurs} \end{cases}$$

Lorsque la somme des signaux S(t)+S(t-θ) est envoyée à l'entrée du convoluteur, on a R(t)+R(t-θ) en sortie. Deux cas peuvent alors se présenter:

- Si le retard du multitrajet est inférieur à la durée d'un chip ($\theta<\tau$), la différence de phase des deux signaux varie suivant la valeur de θ et dans ce cas, le niveau du pic de convolution reste compris entre une valeur maximale et une valeur minimale.

Les maxima se produisent lorsque $\theta=k/f$, avec k entier. Dans ces conditions, la forme générale du pic de convolution n'est pratiquement pas modifiée par la présence du multitrajet.

La figure 10 montre la forme du pic de convolution obtenue au premier maximum (k=1) avec un niveau du multitrajet égal au niveau du signal direct.

Les minima ont lieu pour les valeurs $\theta = (2k+1)/2f$ avec f entier. Le pic de convolution accuse alors une forte perte d'amplitude et il se dédouble.

La figure 11 montre la forme du pic de convolution pour le premier minimum (k=1), ainsi que le signal correspondant à l'entrée du convoluteur.

La figure 12 représente la variation théorique du niveau du pic de convolution en fonction du temps de retard du multitrajet. L'amplitude de la variation de niveau indiquée par la courbe correspond au pire des cas, puisque le multitrajet a le même niveau que le signal direct. Pour un niveau de multitrajet plus faible, les minima sont moins accusés et se produisent à des instants différents.

- Si le retard du multitrajet par rapport au signal direct est supérieur à la durée d'un chip ($\theta>\tau$), la recombinaison des deux signaux se fait d'une manière aléatoire et on obtient en sortie, à la fois le pic de convolution correspondant au signal direct et le pic de convolution retardé de θ, correspondant au multitrajet. Les deux pics sont d'autant plus nettement séparés que le retard θ est plus grand. La figure 13 représente les signaux obtenus à l'entrée et à la sortie du convoluteur, avec deux multitrajets présents simultanément et ayant des retards de 210 ns et 510 ns.

5.2.2 Décodage des bits d'information

Pour un symbole reçu affecté d'un multitrajet ayant un retard inférieur à la durée d'un chip, le pic de convolution peut être, soit pris en compte, soit ignoré par le circuit de décision, selon les valeurs du déphasage et du niveau relatif du multitrajet par rapport au signal direct. Il en résulte alors une perte d'information et une augmentation du taux d'erreur de la transmission.

Lorsque le retard du multitrajet affectant un symbole est supérieur à la durée d'un chip, le pic de convolution désiré est présent et pris en compte. Mais on trouve également un pic supplémentaire retardé correspondant au multitrajet. Si aucune précaution spéciale n'est prise dans la définition des caractéristiques de la transmission, pour certaines valeurs du retard, ce pic parasite peut venir perturber la prise de décision pour l'un des symboles suivants et introduire une erreur.

5.3 Moyens permettant de lutter contre les multitrajets

Il existe plusieurs moyens, plus ou moins complexes, permettant de minimiser l'effet des multitrajets. Certains d'entre eux peuvent être appliqués d'une manière générale, quelles que soient les caractéristiques de la transmission, d'autres, plus spécifiques ne peuvent convenir que pour les liaisons avec étalement de spectre. Dans tous les cas, le but final est de séparer le signal utile des signaux parasites provenant des trajets multiples.

5.3.1 Séparation d'espace

Le trajet direct et les trajets multiples se propageant suivant des directions différentes, il est donc possible de favoriser le signal direct en utilisant, soit à l'émission, soit à la réception, ou même dans les deux cas, une antenne directive pointée vers l'autre extrémité de la liaison. A l'émission, on diminue ainsi l'illumination des réflecteurs éventuels situés en dehors de la zone de trajet direct et côté réception, on atténue les signaux provenant de directions différentes de celle de l'émetteur. Dans les deux cas, le signal direct désiré est privilégié. Cette méthode, bien adaptée à l'élimination des multitrajets par réflexion, est cependant limitée, par la directivité des antennes pour les angles faibles entre trajet direct et trajet réfléchi et par le niveau des lobes secondaires pour les angles plus importants. Elle est difficilement applicable pour les liaisons dont au moins l'une des extrémités est mobile.

5.1 Origine des multitrajets

Les divers types de multitrajets que l'on peut rencontrer dans les transmissions en hyperfrequences (vers 1 GHz) denendent essentiellement de la géométrie et du type de surface des terrains environnant la liaison, ainsi que des conditions atmosphériques. Ils proviennent de deux sources principales :

- les réflexions, par exemple sur le so. ur les bâtiments, sur les structures situées à proximite de l'une des antennes, et même sur le mobile qui supporte l'antenne (avion, navire) etc...

- les refractions atmosphériques qui peuvent créer une courbure anormale des rayons et produire entre émetteur et récepteur des chemins supplémentaires, par rapport au trajet direct.

Une troisième source de multitrajets, beaucoup moins importante, est la diffraction sur des obstacles situes à proximité immédiate de la zone de propagation directe (sommets de collines, bâtiments, ou même simplement courbure de la terre à l'horizon). Pour les liaisons en vue directe qui nous interessent, ce type de multitrajet peut être considéré comme marginal car les niveaux des signaux parasites produits restent dans tous les cas faibles par rapport au signal direct.

5.1.1 Multitrajets par réflexions

Les reflexions sur des surfaces diverses sont les sources principales de multitrajets dans la bande de fréquences considérée, d'autant plus que le type de liaison prévu, avec au moins une des extremites mobile , oblige à utiliser des antennes omnidirectionnelles et dans le cas d'une liaison sol-air, les reflexions sur le sol peuvent être importantes, particulièrement lorsque les angles de réflexion sont faibles. On distingue deux types de réflexions : les réflexions spéculaires et les réflexions diffuses.

- Réflexions spéculaires.

Ce sont des réflexions de type miroir qui se produisent lorsqu'une onde plane rencontre un changement de milieu sur une surface suffisamment plane et régulière. Le coefficient de réflexion peut être calculé, soit en utilisant les formules de FRESNEL, soit au moyen des réseaux de courbes fournis dans les références 1 et 2. Pour tenir compte de la courbure et de la rugosité de la surface terrestre qui réduisent le coefficient de réflexion sur le sol, on définit un coefficient de réflexion effectif ρ_e qui est donné par :

$$\rho_e = D.G.\rho_o$$

où D est un facteur qui tient compte de la divergence de l'énergie réfléchie dans l'espace par la surface courbe de la terre et où G prend en compte la dispersion de l'énergie due à la rugosité de surface.
Pratiquement, D est très proche de l'unité et ne diminue que pour des angles de réflexion inférieurs à 1 degré ; son influence est alors favorable pour les liaisons à grande distance lorsque le signal reçu est très faible car il apporte une réduction du niveau des multitrajets. Le facteur G peut être évalué beaucoup plus facilement sur mer que sur terre en utilisant un modèle gaussien pour la rugosité. Pour un état de la mer plus mauvais que force 4, on obtient une réduction substantielle du coefficient de réflexion sauf pour des angles de réflexion très inférieurs à 1 degré (voir référence 2).

- Réflexions diffuses.

Ce type de reflexion se produit sur des surfaces de sol irrégulières présentant des facettes qui réfléchissent l'énergie, non seulement dans la direction des réflexions spéculaires mais également dans des directions différentes. Les multiples composantes de multitrajets qui arrivent au récepteur en n'ayant pas parcouru les mêmes distances ont des phases différentes et ne s'ajoutent pas d'une maniere cohérente. Il se crée ainsi un signal analogue à un bruit. Ces réflexions, se produisant sur des zones beaucoup plus importantes que les réflexions spéculaires, ont des temps de retard beaucoup plus etalés dans le temps.

La figure 9 montre, pour comparaison, un exemple de répartition dans le temps des composantes de multitrajets provoquées par des réflexions spéculaires et diffuses, sur un signal d'origine impulsionnel très bref.

5.1.2 Multitrajets par réfraction

L'indice de réfraction de l'atmosphère, pour les ondes hyperfrequences, varie avec l'altitude, la temperature et l'humidité. Dans une atmosphère normalement claire et bien brassée, le gradient de l'indice de réfraction est négatif et quasi constant avec l'altitude. Ceci crée une legere courbure des rayons vers la terre et augmente la propagation un peu au-delà de l'horizon optique. Ce type de propagation est dit normal, il n'est pas la cause de production de multitrajets. Cependant, sous certaines conditions atmosphériques spéciales (évaporation intense apres la pluie, inversion du gradient de température), dans un air calme, le gradient de l'indice de refraction peut subir de brusques variations avec l'altitude, voire même s'inverser. Il se produit alors des courbures importantes dans certaines couches qui provoquent, en plus du trajet direct, un ou plusieurs trajets courbes supplementaires. Le nombre possible de ces multitrajets augmente avec la distance qui separe l'emetteur du recepteur. Ces multitrajets ne peuvent se produire que si l'émetteur et le récepteur a la fois, sont situés au maximum à quelques centaines de pieds de la couche refractante. Les retards entre le signal direct et les signaux réfractés reçus sont très faibles, de l'ordre de quelques nanosecondes.

Ces types de multitrajets sont très difficiles à prevoir et à mettre en evidence pour des liaisons où l'une des extrémités est mobile. Dans ce cas, ils se produisent d'ailleurs d'une maniere fugace.

Les caractéristiques principales du convoluteur utilisé pour les premiers essais sont les suivantes :

- Fréquence Centrale : 405 MHz
- Bande Passante : 80 MHz
- Durée de traitement de plaque : 12,8 µs
- Niveau maximum d'entrée : + 20 dBm
- Facteur de bilinéarité : $F = -74\ dBm^{-1}$
- Protection d'autoconvolution en porteuse pure : 30 dB

Une autre caractéristique importante du convoluteur est sa dynamique opérationnelle c'est-à-dire la plage de variation possible du niveau d'entrée pour un fonctionnement correct. Le niveau d'entrée minimum admissible est limité par le bruit thermique et par les bruits parasites provenant de la référence. Le seuil de détectivité est défini pour un rapport signal sur bruit en sortie suffisant pour traiter les pics de convolution (S/B = 10 dB). Le niveau maximum d'entrée utilisable est défini pour une protection donnée contre les brouilleurs en porteuse pure (par exemple 20 dB), de plus, il ne doit pas dépasser le niveau maximum admissible sur le transducteur (20 dBm).

La figure 7 montre comment s'obtient la dynamique opérationnelle. Les niveaux d'entrée et de sortie sont représentés en abscisse et en ordonnée. Le niveau du pic de convolution est linéaire par rapport au niveau d'entrée (droite de pente 10 dB/décade) et le niveau d'autoconvolution des brouilleurs correspond à une droite de pente 20 dB par décade. Ces courbes sont établies pour un niveau d'entrée du code de référence le plus élevé possible, compte-tenu du niveau maximum admissible sur le transducteur d'entrée (20 dBm).

On voit que la dynamique du signal d'entrée est assez limitée. Elle est de l'ordre de 35 dB sur le modèle de convoluteur utilisé et elle peut pour d'autres modèles être portée à environ 45 dB. On voit que de toute manière, pour qu'un récepteur complet utilisant ce convoluteur soit opérationnellement utilisable, il sera nécessaire d'en augmenter la dynamique. Pour cela, il faudra au niveau de l'amplificateur à fréquence intermédiaire, soit prévoir un circuit de C.A.G. avec amplificateur linéaire, soit utiliser un amplificateur limiteur, au prix d'une légère perte de niveau du pic de convolution.

4.3 Générateur de codes

Le générateur de codes est formé de registres à décalage rebouclés, fournissant des séquences de longueur maximale. Les codes de GOLD sont obtenus par addition modulo 2 de deux séquences de même longueur. L'une des séquences est initialisée d'une manière fixe et l'autre peut être initialisée par programmation, afin de pouvoir produire à la demande, des codes différents. Au lieu d'utiliser deux générateurs séparés pour le code "un" et pour le code "zéro", il est possible, à partir du premier code, de générer le deuxième au moyen de fonctions de WALSH, on obtient alors un code image, orthogonal au premier mais dont la fonction d'autocorrélation présente d'une manière générale, des pics secondaires de niveaux relatifs plus élevés par rapport au pic principal (figure 8). Le générateur de codes est déclenché par un circuit de séquencement qui fournit également, en mode asynchrone du convoluteur, la porte d'autorisation des pics de convolution.

4.4 Circuits de détection des pics de convolution

Les sorties de chacun des convoluteurs utilisés pour décoder les codes "un" ou "zéro" fournissent les pics de convolution, en U.H.F. à 800 MHz, constitués d'impulsions très brèves ayant une forme théorique de losange avec une largeur au pied d'un peu plus de 12 ns. Ces pics passent ensuite dans un filtre passe-bande, dans un amplificateur à faible bruit, puis ils sont détectés au moyen de détecteurs rapides et sensibles. Plusieurs méthodes de détection peuvent être utilisées et pour augmenter la sensibilité, il est possible de procéder avant détection, à l'élargissement des pics, au moyen d'une ligne à retard à ondes acoustiques de surface possédant des prises intermédiaires judicieusement placées. Les différents pics retardés obtenus sont ensuite sommés en phase. Le circuit de décision constitué par des comparateurs et une logique de choix, fournit les bits d'information en éliminant d'abord les pics qui correspondent à un bit à "un" et à un bit à "zéro" simultanés.

Les circuits de décodage des préambules et des textes des messages n'ont pas été représentés sur la figure 2. Ils dépendent essentiellement du format des messages qui sera choisi dans l'avenir et qui permettra d'optimiser la liaison suivant les besoins.

5 LIAISON AVEC MULTITRAJETS

On dit qu'une liaison radioélectrique, d'un émetteur vers un récepteur, est affectée de trajets multiples ou multitrajets lorsque le récepteur reçoit, en plus du signal normal se propageant suivant le trajet le plus direct (propagation optique dans la bande U.H.F.), un ou plusieurs signaux supplémentaires provenant également de l'émetteur, mais ayant suivi des trajets différents pour diverses raisons. Les signaux de multitrajets parcourant forcément des distances plus longues que le signal direct, sont affectés par rapport à celui-ci, à la fois d'un déphasage de l'onde porteuse et d'un retard d'enveloppe. Les niveaux relatifs des signaux de trajets multiples par rapport au signal direct, dépendent du phénomène qui les a provoqués.

Le signal de réception est la somme vectorielle du signal direct et des signaux retardés. Il en résulte des fluctuations de niveau et des perturbations qui sont différentes des autres types d'interférences et beaucoup plus difficiles à éviter. En effet, les signaux parasites proviennent de la même source que le signal désiré et se trouvent par conséquent sur le canal à recevoir.

the corresponding digital system will require a bandwidth of several tens of kHz, which represents a considerable expansion. In practice, the required bandwidth can be reduced significantly by the use of more sophisticated speech digitisation algorithms and signal coding schemes - a topic to be discussed in more detail in Section 3.3: however, it can be expected that, in general, digitisation of an analogue waveform will have the effect of increasing the bandwidth of the signal.

2. BRIEF OVERVIEW OF THE PROPAGATION ENVIRONMENT

In this section, a brief and non-rigorous survey of the propagation mechanisms encountered in the radio frequency spectrum will be given. For each mechanism, the influence of the propagation environment upon the characteristics of received signals will be outlined.

2.1 ELF, VF AND VLF Bands (Below 30 kHz)

At the very long wavelengths in these bands, signal propagation in many cases can be viewed as taking place via spherical waveguide modes, with the waveguide boundaries being conductors formed by the earth's surface and the D-region of the ionosphere; the transmitting antenna acts as an electric field probe in the waveguide. Because attenuation is extremely low, worldwide propagation is possible; where one mode is dominant, signal amplitude and phase are stable, but significant interference can take place between different modes of comparable amplitudes. The noise background in these bands has two main components (Watt & Maxwell, 1957):

(i) a high level Gaussian component due to a superposition of many non-Gaussian sources (the central limit theorem applies), with no dominant sources;

(ii) a component due to a few dominant sources which can be described approximately by a log-normal amplitude probability density function and which becomes significant when the overall background noise level is relatively low.

The natural noise sources are due predominantly to thunderstorm activity. In the spherical waveguide, noise energy as well as wanted signal energy will also be capable of propagating over very large distances.

From the communication system viewpoint, the frequency range below 30 kHz has the following important properties:

(a) It provides a long-range, stable propagation mechanism whose normal temporal variations can be predicted accurately. Perturbation of the ionoshpere by abnormal solar activity can give rise to sudden phase anomalies and also amplitude fluctuations.

(b) Electromagnetic (EM) signals in this frequency range have significant seawater penetration and can thus be used for communication with submersibles.

(c) Transmission tends to be of a one-way (fixed station-to-mobile) broadcast type because of the large antennas and high transmitter powers required to launch significant energy. The band is used for both communication and navigation purposes.

(d) Available bandwidths are limited and frequency assignments are carefully controlled by international agreement because of the worldwide nature of the propagation and the consequent potential for interference.

2.2 LF and MF Bands (30 kHz - 3 MHz)

In this frequency range, the dominant form of propagation is via the surface wave mechanism (Goldberg, 1966). The surface wave provides a vertically-polarised signal which within is relatively stable in amplitude and phase; the attenuation of the surface wave is dependent upon distance from the transmitting antenna, the frequency in use and the ground constants. At longer ranges and higher frequencies, especially at night, interference from ionospherically-propagated skywave signal components becomes significant and can cause severe wanted signal degradation. Surface wave propagation is particularly effective over seawater and the MF band is used extensively for ship-to-ship and ship-shore communication. Very long ranges can also be achieved by high power LF broadcast transmitters.

Atmospheric noise levels are generally lower than with ELF/VF/VLF systems, but there is still an appreciable non Gaussian component in addition to the Gaussian background. Ionospherically-refracted unwanted signals can also give rise to high levels of co-channel interference, particularly in the MF range.

In terms of communication systems, the properties of the LF/MF band can be summarised as follows:

(a) It provides a medium-range propagation medium in which signals can vary between being highly stable to exhibiting severe amplitude and phase fluctuations.

(b) Surface wave signals in this frequency range propagate efficiently over seawater and are used for maritime communications. The LF band is also used for general broadcast and navigation purposes.

(c) Large transmitting antennas are required for efficient coupling to the propagation medium.

(d) Available bandwidths are low and frequency assignments are controlled by international agreements, again because of the considerable potential for long-range interference.

2.3 HF Band (3 - 30 MHz)

The HF band is one of the most important operationally since it enables communication to take place over a range of distances from line-of-sight to world-wide; frequency values are such that efficient antenna systems need only have dimensions of a few metres, thus making them suitable for mobile mounting. The major propagation mechanism is due to signal energy refraction by the various regions of the ionosphere; surface wave propagation can still be used at the lower end of the band and, in some cases, at the upper extremes also. HF ionospherically-refracted (skywave) signals generally exhibit significant levels of multipath and time dispersion (Goldberg, 1966). Relatively transient and less predictable phenomena, such as sporadic E-layer and spread F-layer propagation, also influence signal transmission in the band.

In many regions of the world, co-channel man-made interference levels from other communications users of the spectrum are very high and indeed can be the factor limiting HF system performance (Darnell, 1984(a)) (Gott et al, 1983). Natural atmospheric noise may also be dominant in certain geographical areas and in specific frequency ranges.

The most important properties of the 3 - 30 MHz band from the communications viewpoint are:

(a) It provides a transmission medium which is effective over a wide range of distances. However, the received signals can exhibit severe fading and dispersion characteristics and considerable attention needs to be given to the type of signal generation and processing procedures employed to achieve reliable operation.

(b) Comparatively small antennas and low transmitter powers are necessary to access the medium.

(c) Available bandwidths are usually restricted to a maximum of 3kHz and a given channel may be assigned several times over on a world-wide basis. Consequently, the potential for interference is large and an HF communication system may have to operate in the presence of high-level co-channel signals generated by other spectrum users.

(d) The long-term median parameters of HF propagation paths, which are dependent upon many factors such as seasonal cycle, diurnal cycle, sunspot activity, etc, can be predicted with reasonable accuracy (Barghausen et al, 1969); the short-term (minute-to-minute/second-to-second) variability of the path is far less predictable (Rawer, 1975).

2.4 VHF Band (30 - 300MHz): Non Line-of-Sight Modes

The propagation mechanisms introduced in the context of HF systems in the previous section, i.e. ionospheric refraction, sporadic E and spread F modes, can also occur in the lower part of the VHF band. In addition, the mechanisms of meteor-burst and ionospheric scatter propagation can also give usable signals for communication purposes.

Ionospheric scatter signals (Browne et al, 1963) are propagated via the lower region of ionosphere and exhibit path attenuations which are typically 80-90 dB greater than the free-space values. Meteor-burst propagation arises as a result of signal energy being returned to earth from the ionised trails of meteors occurring at heights of between 75-120km. A given trail would normally persist for only a fraction of a second, with intervals of several tens of seconds between trails; thus the path is essentially intermittent. However, the statistical characteristics of trail occurrence are relatively well defined and can be modelled with reasonable accuracy (Oetting, 1980).

In communications terms, the properties of the above non line-of-sight modes can be summarised as follows:

(a) Meteor-burst and ionospheric scatter signals can provide usable communication at ranges of up to about 1500 - 2000 km. The primary characteristics of the scatter mode are its low signal strength and somewhat restricted bandwidth. Meteor-burst signals in contrast are at relatively high-level, persist for very short intervals, and can have a large bandwidth. Both modes can exhibit fading of various types.

(b) Directional antennas are required for both modes; because of the high path attenuation, scatter propagation transmitter powers are higher than those for meteor-burst modes.

(c) Available bandwidths for scatter modes are typically a few kHz whilst, for meteor-burst, bandwidths of several MHz are common.

(d) Meteor-burst paths are virtually unique between given transmitter and receiver locations. The incidence of meteor trails shows well-defined diurnal and seasonal variations and can be described by reasonably precise statistical models.

2.5 VHF/UHF/SHF Bands (Few 10's of MHz to few GHz): Tropospheric Scatter Modes.

In the VHF/UHF/SHF bands over the frequency range from a few 10's of MHz to a few GHz, radio waves are scattered by inhomogeneities in the troposphere some 5-11 miles above the earth's surface (Booker & Gordon, 1950). Signal attenuations are typically 60-90 dB greater than those of free-space paths. Ranges of a few hundreds of kilometers can be achieved via this propagation mechanism. Troposcatter signals exhibit both slow and rapid fading characteristics which tend to be uncorrelated for relatively small frequency and positional separations; also, there are significant multipath dispersion effects due to the finite size of the scattering volume in the troposphere.

The important communications properties of the medium are:

(a) It provides a medium-range (up to several 100's of km) means of beyond line-of-sight communication.

(b) Signal strengths are low and thus directive antennas and high transmitter powers are required. However, a received signal is always present.

(c) Both multipath and fading effects are significant; space and frequency diversity processing is effective.

(d) Usable bandwidths of several MHz are available.

(e) Atmospheric and galactic noise effects must both be considered in th analysis of troposcatter system performance.

2.6 VHF/UHF/SHF Bands (Above 30MHz): Line-of-Sight Modes

Included under this heading are terrestrial line-of-sight (LOS) propagation and propagation over earth/space paths.

Terrestrial paths may give rise to signal diffraction, atmospheric refraction, reflection, interference, re-radiation and absorption. Climatic factors, such as rainfall and water vapour in the atmosphere, can affect signal levels significantly and introduce dispersion effects (Crane, 1975). In mobile systems, the continuously changing nature of the propagation path, particularly in urban areas, causes rapid and severe signal fluctuations.

Earth/space propagation is relatively stable, although signal characteristics are affected by "near-earth" effects. Also, particularly in the UHF band, the passage of signals through certain regions of the ionosphere may impose scintillation and fading characteristics (Lawrence et al, 1964).

The important communication characteristics of line-of-sight systems are:

(a) Under most circumstances, signals are steady and only relatively low transmitter powers are required to overcome the free-space and other path losses.

(b) Re-use of frequencies is achieved by careful installation planning and directional antennas. Consequently, co-channel interference can normally be neglected except possibly in mobile systems.

(c) Available bandwidths range from several MHz in SHF systems to several kHz in VHF systems.

(d) Long-range terrestrial propagation can be achieved by tandeming line-of-sight links and using signal regenerators.

(e) At VHF, atmospheric noise and manmade noise are significant; at higher frequencies, galactic noise and noise generated within the receiving system assume a greater importance.

In the following section, the various digital transmission techniques which are used with the types of propagation media discussed above will be described and compared. The manner in which the propagation characteristics influence the choice of digital transmission techniques will be emphasised.

3. DIGITAL TRANSMISSION TECHNIQUES

From the previous discussion, it is seen that the range of propagation, noise and

interference conditions in the various frequency ranges is very great. To a large extent, it is these conditions which influence the nature of the transmission techniques used in any given digital communication system. In this section, the major digital transmission techniques will be outlined and their relevance to communication in the frequency bands introduced in Section 2 indicated.

3.1 Modulation

The factors affecting the choice of modulation technique are:

(i) available bandwidth;
(ii) EMC constraints;
(iii) time and frequency dispersion;
(iv) noise and interfering signal characteristics;
(v) rates of change of channel parameters;
(vi) requirements for interaction with other digital signal processing techniques.

The importance of these factors will now be examined.

3.1.1 Available Bandwidth

In general, increases in carrier frequency range will be accompanied by increases in the bandwidth available for any given service. Thus, in the ELF/VF/VLF bands, bandwidths of a few 10's of Hz may be assigned whilst SHF satellite or terrestrial LOS communication systems can have bandwidths of several MHz. Clearly, it is important to use bandwidth-efficient modulation schemes (i.e. those which maximise the number of bits/s/Hz) where bandwidth is limited; an example of this type of modulation is minimum-shift keying (MSK) (Pasupathy, 1979) which is now used extensively in VLF data broadcast systems.

Fig. 3 illustrates the principle of MSK modulation. Two, time-offset, quadrature sub-channels, I and Q, at the same frequency w_c, are independently phase-reversal modulated by data bit streams $a_i(t)$ and $a_q(t)$ (either +1 or -1) derived from an original single data source. The transitions between the different phase states for both I and Q sub-channel signals $m_i(t)$ and $m_q(t)$ are sinusoidally weighted so that, after combination, they form a constant amplitude MSK signal m(t). Therefore

$$m(t) = m_i(t) + m_q(t) \qquad [5]$$

$$\left.\begin{aligned} &= a_i(t) \cos\left(\frac{\pi t}{2T}\right) \cos w_c t \\ &+ a_q(t) \sin\left(\frac{\pi t}{2T}\right) \sin w_c t \end{aligned}\right\} \qquad [6]$$

which can be simplified to give:

$$m(t) = \cos\left[w_c t + b(t)\left(\frac{\pi t}{2T}\right) + \phi(t)\right] \qquad [7]$$

where

$$b(t) = -a_i(t)\, a_q(t) \qquad [8]$$

and

$$\phi(t) = \begin{cases} 0; & \text{if } a_i(t) = +1 \\ \pi; & \text{if } a_i(t) = -1 \end{cases} \qquad [9]$$

MSK may be considered as a special case of continuous-phase frequency-shift keying (FSK) with a carrier deviation equal to half the bit rate of the modulating signal - the minimum theoretically achievable.

It should be noted that:

(a) the composite MSK signal has constant envelope amplitude;

(b) the RF carrier is phase-continuous at the symbol transitions and that the phase changes linearly over the symbol intervals;

(c) MSK may be viewed alternatively as shaped offset quadrature phase-shift keying (QPSK).

The bandwidth efficiency of MSK, as compared with normal QPSK, may be evaluated by determining the corresponding bandwidth within which say 99% of the transmitted power is contained. For MSK, this bandwidth

$$B_{99} \doteqdot 1.2/T \quad \text{Hz} \qquad [10]$$

whilst for QPSK

$$B_{99} \doteqdot 8/T \quad \text{Hz} \qquad [11]$$

However, MSK has a substantially wider main spectral lobe than has QPSK.

In contrast, at higher carrier frequencies such as those employed in V/UHF tactical mobile systems and SHF satellite systems, there is an increasing trend towards the use of extended bandwidth, spread-spectrum techniques (Dixon, 1975), where the enhanced processing gain can be employed to overcome non-linearities and high-level interfering signals and to achieve a low probability of interception by unauthorised receivers. Spread-spectrum systems fall into two basic categories:

(a) direct sequence, where the carrier signal is subjected to digital phase-modulation at a high rate;

(b) frequency-hopped systems, where the signal frequency is changed rapidly over a wide spectral range.

Figs. 4(a) and (b) show diagramatically the principles of direct-sequence spread-spectrum (DSSS) processing. At the input to the spread-spectrum (correlation) receiver, the ratio of the total wanted signal power, S, to the total unwanted noise/interference power, N, is:

$$[S/N]_i \doteq S/(N_o \Delta f) \qquad [12]$$

where N_o is the average noise power spectral density. At the correlator output, the corresponding SNR is

$$[S/N]_o \doteq S/(N_o \delta f) \qquad [13]$$

Thus, the processing gain is

$$G_p = [S/N]_o/[S/N]_i \doteq \Delta f/\delta f \qquad [14]$$

Hence, in principle, large processing gains can be achieved if the ratio of spread-spectrum signal bandwidth to information bandwidth is also made large. In practice, however, receiving system noise and implementation constraints will limit performance.

In a frequency-hopped spread-spectrum (FHSS) system, assuming a uniform noise power density spectrum, the processing gain can be shown to be (Utlaut, 1978):

$$G_p = n \qquad [15]$$

where n is the total number of hopping sub-channels employed.

3.1.2 EMC Constraints

By electromagnetic compatibility (EMC) is meant the ability of a given electromagnetic (EM) system to operate in conjunction with other EM systems. In the context of communication systems, the important characteristic of a modulation technique which affects its EMC properties are its effetive occupied bandwidth and the level of sideband energy outside the immediate passband since this will form a source of co-channel interference for adjacent channel signals. In certain regions of the radio spectrum, e.g. the UHF band, channel separations are being reduced progressively which in turn places more stringent and constraints on the allowable energy overspill. Here again, spectrally-efficient modulation schemes such as MSK offer advantages.

3.1.3 Time and Frequency Dispersion

The degree of time and frequency dispersion imposed by the propagation medium on a communications transmission is possibly the most important factor influencing the choice of modulation technique. In simple terms, the intersymbol interference due to multipath and time dispersion limits the minimum symbol period. It is for this reason, for example, that HF medium-speed data modems have tended to employ multiple, low-rate, frequency-multiplexed, sub-channels for which the maximum expected multipath spread is small relative to the symbol interval.

In the frequency domain, the phase instability, or Doppler spread, of a signal has to be taken into account when selecting a modulation format. Here it must be emphasised that the rate of change of phase ϕ with respect to time, $d\phi/dt$, has the dimensions of frequency, but does not necessarily represent a steady frequency shift in either a positive or a negative sense. For instance, a phase-shift-keyed (PSK) transmission would be inappropriate for a path exhibiting large random phase perturbations, since it normally requires an accurate phase reference to be derived from the received signal. Differential phase-shift-keying (DPSK), in which the phase reference for a given symbol is derived from the phase of the previous symbol, may still be applicable where the short-term phase stability is reasonable. Frequency/phase instability and offsets may also arise due to the characteristics of the communications equipment being used and must be taken into account in the overall design. Thus, the basic choice which has to be made in a given situation is whether a synchronous (coherent) or asynchronous (non-coherent) modulation scheme should be employed; this choice will be dictated primarily by the phase and frequency stability of the medium. Clearly, stable paths such as ELF/VF/VLF and SHF ground-satellite links, can support phase-coherent modulation schemes such as MSK, PSK

and QPSK. In contrast, a relatively unstable medium, such as HF, will normally require the use of non-coherent amplitude shift-keying (ASK), non-coherent frequency-shift-keying, or DPSK.

In a situation where time and/or frequency dispersion are significant, it is normally possible to improve the quality of reception substantially by making use of one or more forms of diversity processing, eg.

- frequency diversity
- space diversity
- polarisation diversity
- time diversity
- geographical diversity

3.1.4 Noise and Interfering Signal Characteristics

The performance of a given modulation sceme will be dependent, to some extent, upon the nature of the noise and interference experienced during transmission over the communication channel. Classical comparisons of performance of different types of digital modulation assume a background of Gaussian white noise; in practice, this noise model is rarely valid. For example, in the ELF/VF/VLF bands, log-normal "thunderstorm" noise is often the mechanism giving rise to errors; at HF, man-made interference tends to be the domininant error mechanism; in VHF urban band mobile applications, noise from electrical machinery and car ignition systems often limits system performance. In each of these three examples, the noise process is certainly non-Gaussian and may well affect specific modulation types in a severe and largely unpredictable manner.

If possible, a reasonable model of the noise/interference environment should be derived from practical measurements and used in any simulations of system performance carried out at the design stage.

3.1.5 Rates of Change of Channel Parameters

The rates of change of channel parameters are related to the dispersion and noise/interference considerations discussed previously. If the frequency-selective fading characteristics or the noise profile of a given channel change with time, it may well be that a given modulation scheme, which initially had an acceptable level of performance, will subsequently provide an inadequate grade of service. Hence, it will be necessary to adapt the modulation format to allow for the changes, eg. to change the frequency separation and/or position of FSK sub-channels.

In the case of adaptive modems, see for example (Monsen, 1983), the rates of change of channel parameters will determine whether the adaptation algorithms can perform satisfactorily. Again, the need for a realistic model of the propagation path to be available during the design phase of the system becomes apparent.

3.1.6 Requirements for Interaction with other Digital Signal Processing Techniques.

It is often necessary to interface modems with other digital signal processing devices. Possibly the most important requirement of this nature is to interface a demodulator with an error control decoder of the type to be discussed in Section 3.2. Here, information from the demodulator is used to enhance the error control capability of the decoder, a technique known as "soft-decision decoding".

The principle of the technique is shown in Fig. 5. A normal binary demodulator will make a decision as to whether the received signal represents a +1 or -1 according to whether it is above or below a given threshold level; this is termed a "hard" decision. A "soft" decision associates a confidence level with a given hard decision; in Fig. 5, the soft-decision confidence levels (shown in brackets) represent the average received signal level during the hard-decision intervals, ie. the distance from the threshold.

Other parameters of the received signal, such as phase margin in a PSK or DPSK system, can also be used as soft-decision parameters. When the binary hard-decision data is applied at the input of an error control decoder, the soft-decision values may also be retained to improve the performance ot the decoder.

Modulation techniques may also interact with multiple-access coding schemes in say satellite and terrestrial LOS SHF systems. For example, in a non-linear satellite transponder, intermodulation can limit the capacity of a frequency-division multiple-access (FDMA) system; spread-spectrum multiple-access (SSMA), or code-division multiple-access (CDMA), involving DSSS modulation, can alleviate the effects of the non-linearity by effectively randomising the intermodulation products.

3.2 Error Control Coding

Error control coding, sometimes known as error protection coding or error detection and correction (EDC), involves the addition of deterministic redundancy to the source data to be transmitted. At the receiver, a knowledge of the nature of the imposed

redundancy will enable certain types of transmission errors to be detected andpossibly corrected.

Error control codes fall into two basic categories:

(a) block codes;
(b) convolutional codes.

These will now be discussed individually.

3.2.1 Block Coding

In block codes, information digits are taken k at a time; c parity check digits are then calculated giving an overall codeword length of n digits, where

$$n = k + c \qquad [16]$$

This code is termed an (n,k) code and has a code rate R, or efficiency,, given by

$$R = k/n \qquad [17]$$

An important parameter of a block code is its minimum Hamming distance, d, which is the minimum number of digits by which any two codewords differ; it is thus a measure of the uniqueness, or confusability, of codewords and is evidently related to the error detection and correction potential of a code. The greater the Hamming distance, the lower the probability that any given codeword will be transformed by errors due to noise into another valid codeword. In general, if a code is to correct e errors, its minimum Hamming distance must be at least

$$d = [2e + 1] \qquad [18]$$

Also, if a code is to detect e errors, its minimum Hamming distance must be at least

$$d = [e + 1] \qquad [19]$$

Block code designs exist for the detection and correction of many different types of error patterns, from single random errors to long error bursts (Lin and Costello, 1983). It is important that the statistical nature of errors which are likely to be encountered on a given channel is known prior to the application of error control coding, otherwise a "mismatched" coding procedure can make the situation worse and actually increase the overall error rate. As mentioned in section 3.1, soft-decision data can be used to enhance the error control capabilities of many codes.

It is possible to use block codes in an open loop (forward error correction) mode, or a closed loop configuration. When the propagation path gives rise to time-varying error statistics, as might be the case in the HF band, the closed loop mode is to be preferred; such a mode of operation is commonly termed "automatic repeat request" (ARQ) (Van Duuren, 1951). All the transmitter data is encoded using a high-rate, error detection block code. If any block is found to be in error on reception, a repeat of that block is requested via a feedback link. The system can be given a greater potential for adaptation if the power of the block code can be varied in accordance with channel conditions; eg. if the number of repeats requested in a specified time interval exceeds a certain threshold value, a lower rate code will be selected (Goodman and Farrell, 1975).

ARQ has also been applied to the meteor-burst intermittent channel where the system continuously requests repeats, except during the short periods of the bursts when data can be transmitted at high rate (Bartholomé and Vogt, 1968).

Other error control techniques, based upon block codes, have been applied in the following areas:

(a) Time-diversity modems where effectively a simple repetition code is used with majority voting, the same information being transmitted on a number of time-offset frequency sub-channels (McCarthy, 1975).

(b) The CODEM modem, where a 2-dimensional array code is used in conjunction with soft-decision data in a multiple sub-channel HF modem (Chase, 1973).

(c) Interleaving, combined with a simple random error correcting block code, to combat error bursts (Douglas & Hercus, 1971).

3.2.2 Convolutional Coding

Whereas block coding derives its c parity check digits from a single block of k information digits, convolutional encoding makes use of checks derived from several blocks of information digits.

Fig. 6(a) shows a schematic diagram of a convolutional encoder. The name convolutional encoder is derived from the fact that the output data stream may be viewed as the convolution of the input data stream and the response function of the encoder, as

is the case with a linear, time-invariant analogue system (Lee, 1960). In the case of the convolutional encoder, the system may also be considered to be linear if the encoding process involves only modulo-2 arithmetic operations.

When the input is applied to the encoder, it stores h blocks of k_o digits; as each new block of k_o digits is accepted, the oldest stored block of k_o digits is discarded. For each unique set of hk_o digits, n_o encoded digits are computed, where

$$n_o > k_o \qquad [20]$$

Thus, the encoding process can be considered to have an input constraint length

$$L_i = hk_o \qquad [21]$$

and an output constraint length of

$$L_o = hn_o \qquad [22]$$

Hence the code rate R, or efficiency, is given by

$$R = \frac{hk_o}{hn_o} = \frac{hk_o}{n} = \frac{k_o}{n_o} \qquad [23]$$

where

$$n = hn_o \qquad [24]$$

n may be viewed as being equivalent to the codeword length of a block code.

Fig. 6(b) gives an example of a simple convolutional encoder where $k_o = 1$, $h = 2$ and $n_o = 2$. For this implementation

$$R = \frac{k_o}{n_o} = 0.5 \qquad [25]$$

and

$$n = hn_o = 4 \qquad [26]$$

Ideally, in order to decode a convolutional code, all the received digits should be processed to find the most probable sequence of transmitted code digits. Certain procedures, such as sequential decoding (Wozencraft & Jacobs, 1965) and Viterbi decoding (Viterbi, 1967), have been developed in which a subset of the received digits is analysed at any time, thus making them computationally efficient in comparison with the exhaustive decoding method. The loss of performance using these sub-optimum decoding algorithms can be made practically negligible.

Convolutional codes have been applied to many different types of channels since they can be designed to control many different forms of error distribution. They have perhaps been most widely used in SHF satellite communication systems.

3.3 Speech Digitisation

One of the most important forms of communication traffic is speech. In the military context, considerable emphasis is placed upon the protection of speech transmissions from unauthorised interception; therefore, as discussed in Section 1, it is first necessary to digitise the speech signals before they can be effectively encrypted.

The main factors influencing the choice of speech digitisation techniques can be summarised as follows (Darnell, 1984 (b)):

(a) The nature of the transmission medium, eg. whether a wideband or narrowband channel is available.

(b) The speech quality required; eg. whether it is simply necessary for the speech to be intelligible, or whether the voice quality must be preserved so that the speaker is also recognisable.

(c) Whether it is necessary to tandem say wideband and narrowband systems, eg when an HF link forms a tail to a microwave LOS circuit.

(d) Whether speakers of different nationalities are required to use the system.

(e) The user environment; eg whether the speakers are situated in benign office-type environments or whether they are in mobile with high ambient noise levels.

(f) The requirements for signalling, control and adaptation, which are themselves determined by the nature of the propagation path variability.

The major operational advantage of speech is that it provides a direct user communication system interface, with no requirement for message preparation via keyboards, etc. Speech digitisation algorithms can be classified under two main

headings,

(i) wideband systems

and (ii) narrowband systems.

Each of these will now be discussed in more detail.

3.3.1 Wideband Systems

Wideband speech digitisation techniques are used in situations where transmission bandwidth is plentiful, typically a few tens of kHz per speech channel. Thus, VHF/UHF/SHF line-of-sight and SHF satellite communication systems would employ this form of speech digitisation.

Wideband systems make use of a digitisation process which is termed "waveform" encoding. Fig. 1 (b) shows a basic waveform encoding scheme in which the speech waveform, after band-limiting, is subjected to direct analogue-to-digital (A/D) conversion. No account is taken of the fundamental nature of the speech signal: in principle, the input to the waveform encoder could be any arbitrary waveform. Hence, waveform encoding can be viewed as a simple A/D conversion process.

The most important practical classes of speech digitisation algorithms based upon waveform encoding are,

(i) Pulse-code modulation (PCM);

(ii) Delta modulation (DM).

There are many variants on the basic techniques, but generally the range of digitisation rates achievable for a single speech channel with such techniques is from approximately 16-64 kbits/s (Jayant, 1974).

3.3.2 Narrowband Systems

Narrowband speech digitisation techniques are applicable in situations where transmission bandwidth is restricted, as on HF links, to a maximum of a few kHz. Narrowband systems depend upon a principle known as "parameter encoding" which is illustrated in Fig. 7.

Based upon a knowledge of the mechanisms of speech production, an appropriate model of the vocal tract and its associated excitation is derived. Typically, this model would describe the main vocal tract resonances and whether the excitation corresponds to a voiced or unvoiced sound. For a voiced sound, the excitation comprises a regular train of pitch pulses at the pitch frequency; for an unvoiced sound, the excitation is assumed to be a wideband, "white noise", signal. If h(t) is the unit impulse response function of the vocal tract, then the speech output signal is given by the convolutions

$$\left.\begin{aligned} V_o(t)_v &= h(t) \otimes V_{in}(t)_v \\ \text{and}\quad V_o(t)_{uv} &= h(t) \otimes V_{in}(t)_{uv} \end{aligned}\right\} \qquad [27]$$

for voiced and unvoiced sounds respectively.

It is found that the vocal tract descriptive parameters and excitation type tend to vary relatively slowly for the average speaker and need only be updated at about 20ms intervals. Thus, a typical narrowband speech encoder, frequently termed a "vocoder", would transmit sampled values of

- vocal tract parameters (h(t))
- voiced/unvoiced excitation indication
- pitch frequency (for voiced excitation)
- amplitude scaling

as digital data frames every 20-25ms. With this form of speech encoding, overall data rates in the range 1.2-2.4 kbits/s are achievable, representing a considerable reduction in comparison with waveform encoded systems. However, the quality of speech reproduction is also reduced considerably.

The most important practical forms of narrowband coders are linear predictive coding (LPC) devices (Markel & Gray, 1976), channel vocoders (Kelly, 1970) and formant vocoders (Holmes, 1978). Interest is also developing in mid-band encoders, operating in the bit rate range of about 6-16 kbits/s (Sambur, 1982), and in synthetic speech transmission systems (Darnell, & Chesmore, 1984). Mid-band encoding is applicable particularly to speech communication in the V/UHF bands where currently wideband systems are used, but there is considerable pressure to reduce assigned channel spacings. Synthetic speech transmission, in which the data rate can theoretically be reduced to a few tens of bits/s, is potentially applicable to the VLF/LF/MF/HF frequency bands.

3.4 Multiple-Access Techniques

With the progressive increase in the number of users in all bands of the radio requency specturm, it is essential that the available frequency resources are used as efficiently as possible. Multiple-access techniques can contribute to greater efficiency by enabling a number of communication circuits to make use of a single propagation channel. Three basic forms of multiple access procedure are available.

(a) time-division multiple-access (TDMA);
(b) frequency-division multiple-access (FDMA);
(c) code-division multiple-access (CDMA), also known as spread-spectrum multiple-access (SSMA).

Multiple-access techniques are particularly effective when a number of "tail" circuit from different users concentrate at a given point where they can be combined and subsequently transmitted via composite modulation of a single carrier, or carriers; VLF/LF/MF/HF broadcast systems are examples of this mode of operation. SHF satellite communication systems also employ multiple-access techniques to enable a number of circuits to access a single transponder simultaneously. The choice of multiple-access technique is again influenced by the nature of the propagation path. TDMA, in which different time slots are assigned to different users, is inappropriate in situations where the propagation path exhibits significant time dispersion and time-varying propagation delays, eg at HF, because of the difficulty in maintaining system synchronisation.

FDMA is widely used in broadcast systems, with different frequency sub-channels within the overall transmision bandwidth being assigned to different users. As has been mentioned previously, FDMA in conjunction with a relatively non-linear satellite transponder can give rise to high levels of intermodulation, a problem which does not occur with CDMA. The primary advantage of the latter is that it provides each user with a high, and deterministic, level of protection against interfering signals.

In the following section, attention will be turned to the topic of channel evaluation, or channel modelling. It is by this means that the parameters of a given digital transmission can be adapted optimally fo the prevailing propagation path conditions.

4. CHANNEL EVALUATION TECHNIQUES

Over the past decade, the topic of channel evaluation has received considerable attention and has been the subject of much practical experimentation - especially in the context of HF communication (Darnell, 1983).

Clearly, for a given communication channel, if it is possible to produce completely accurate and reliable predictions of channel behaviour, there is no requirement for on-line monitoring of the state of the propagation path since no uncertainty exists. Whilst the characteristics of say VLF and SHF LOS and satellite channels can be predicted with reasonable accuracy, other channels, notably HF and various V/UHF mobile paths, exhibit wide and, to some extent, unpredictable variability. It is for these latter types of paths that the availability of channel evaluation techniques can greatly enhance the reliability and effectiveness of communication.

Because work on channel evaluation has been concentrated in the HF band, the techniques discussed in this section will be those developed primarily to support HF systems. However, it is anticipated that they will potentially be applicable to a much wider range of communication scenarios.

A basic definition of real-time channel evaluation (RTCE) (CCIR, 1981) is:

"RTCE is the term used to describe the processes of measuring appropriate parameters of a set of communication channels in real-time and of employing the data thus obtained to describe quantitatively the states of those channels and hence their relative capabilities for passing a given class, or classes, of communication traffic."

RTCE techniques operate both over a set of alternative channels and over sub-channels within any given channel.

Fig. 8 is a schematic diagram of a generalised RTCE algorithm. The inputs required are:

(i) propagation information;
(ii) noise/interference information;
(iii) the objectives of the communication system;
(iv) the characteristics of the equipment used in the communication system.

Items (i) and (ii) above are obviously essential to the channel selection procedure. Item (iii) concerns the purpose of passing information over a particular propagation path, eg whether it is required to minimise transmission time, maximise data integrity, etc. The capabilities and limitations of the elements of the communication system (Item

(iv)) also influence the choice of channel, eg. factors such as maximum available transmitter power and antenna directivity.

Brief consideration will now be given to the most important forms of RTCE systems developed to date.

4.1 Sounding Techniques

One convenient method of measuring the time dispersion of a communication channel is to evaluate its impulse response function; this is the basis of RTCE systems involving path sounding. Several alternative procedures for measuring the impulse response are available. Conceptionally, the simplest is to inject a high-level, short-duration, transmitted pulse into the channel and then to examine the corresponding output signal at the receiver. If the transmitted signal is x(t) and the unit impulse response function of the channel h(t), then the received signal y(t) is given by the convolution integral

$$y(t) = \int_{-\infty}^{\infty} h(u)\, x(t - u)\, du \qquad [28]$$

where u is a time variable. Expression [28] assumes that the propagation path behaviour is linear.

An alternative to the basic pulse sounding scheme involves the use of longer-duration transmitted signals, modulated by digital sequences with impulsive autocorrelation properties. Various forms of modulating sequences have been used in practical sounding systems: these include Barker codes (Barker, 1953), Huffman sequences (Coll & Storey, 1964) and complementary sequences (Darnell, 1975). In these cases, the important relationship is that, for a linear system, the input-output crosscorrelation function (ccf), defined by,

$$\phi_{xy}(\tau) = 1/T \int_{-T/2}^{T/2} x(t)\, y(t + \tau)\, dt \qquad [29]$$

is given by the convolution (Lee, 1960):

$$\phi_{xy}(\tau) = \int_{-\infty}^{\infty} h(u)\, \phi_{xx}(\tau - u)\, du \qquad [30]$$

where τ and u are time variables, T is the correlation period, and $\phi_{xx}(\tau)$ is the input autocorrelation function (acf). Thus, if the input acf is impulsive, then the input-output ccf will be proportional to the channel impulse response function, ie.

$$\phi_{xy}(\tau) \propto h(\tau) \qquad [31]$$

The important advantage of the modulated sounding technique is that it enables lower power transmitters to be employed, since the signal energy is now distributed over a longer period T. A similar reduction in transmitter power required is also achievable with chirp sounders which employ long-duration, low-level, frequency sweeps and spectrum analysis at the receiver (Barry & Fenwick, 1965).

In HF scenarios, ionospheric sounders have been operated in vertical incidence, oblique incidence and backscatter modes. Sounders, in general, are not constrained to operate within assigned frequency channels since their short-duration and/or low-level signals are assumed to cause negligible interference to other spectrum users. However, sounding techniques undoubtedly do cause spectral pollution and the introduction of a sounding system to aid a communication link can also increase the overall system cost substantially.

In the following section, RTCE schemes operating over a limited number of assigned channels will be discussed. These clearly will not have the same spectral occupancy restrictions as sounding systems and are generally much cheaper to implement.

4. [illegible] in Assigned Channels

Two important systems in this category are listed below.

4. [illegible] Control Evaluation & Calling (CHEC)

The CHEC system, [illegible], is a system developed to enhance HF communication between [illegible] aircraft and ground stations, with emphasis on the aircraft [illegible]. The base station sends out special bi-phase probing signals in each assigned [illegible], and the level of noise interference in each of the channels at the base [illegible] the appropriate transmitted components. The aircraft, on receiving some of [illegible] transmissions, can compute a predicted signal-to-noise ratio for its [illegible] to the base in each propagation channel, taking allowances for [illegible] transmitter powers and antenna characteristics, and also assuming [illegible] reciprocity. It then selects the channel with the highest predicted signal [illegible] for transmission.

4.2.2 Pilot Tone RTCE

Pilot tone RTCE (Betts & Darnell, 1975) is based upon measurement of the phase variations of a low-level received pilot tone inserted at an appropriate position in the channel bandwidth. Both propagation and noise/interference effects can cause phase fluctuations of the pilot tone and it has been found empirically that these fluctuations can be used to provide a reasonably accurate estimate of the error probability for various classes of data transmissions using that same channel.

4.2.3 RTCE using Error Counting

In this form of RTCE, alternative assigned channels are simply probed with a short transmission of the same format as the data transmission for which the selected channel is to be used. The error counts for each of the channels are measured and the channel with the lowest count selected for communication purposes (Darnell, 1978).

4.3 RTCE within an Assigned Channel

If the bandwidth of a digital transmission is somewhat less than the assigned channel bandwidth, then there is scope for varying the position of the data transmission within that bandwidth in accordance with the channel state. Additionally, with an RTCE-controlled system involving several alternative channels, it is also necessary to measure the state of the channel carrying the traffic at any time so that a channel change can be initiated if the error rate becomes excessive. There are several methods by which this "in-channel" RTCE can be achieved eg.

(a) By examining soft-decision parameters from a modem demodulator and employing these as a measure of channel state. Phase margins in a DPSK system or received signal amplitudes in an FSK system could provide this type of data.

(b) By counting the number repeat requests per unit time in an ARQ transmission system and intitiating a channel change if a certain threshold value is exceeded.

(c) By introducing an auxiliary EDC system into the transmission process, solely for the purpose of measuring channel state. As with (b), the number of errors detected in a predetermined interval could form a channel quality indicator (Darnell, 1983). This technique is potentially useful with encrypted data transmission systems.

4.4 General Comments

Some of the RTCE techniques discussed previously incorporate measurement of noise/interference implicitly. In the HF environment, especially, it is vital that realistic account is taken of the effects of man-made, co-channel interference and that reasonable statistical models are available for system design purposes (Darnell, 1984 (a)).

The major advantage accuring from the use of channel evaluation in a communication system is that it provides a basis for improved control and adaptive operation. To use an analogy taken from the automatic control discipline: a system cannot be controlled optimally until its parameters have been identified (measured); RTCE provides the means of identification of the parameters of a propagation path which subsequently enables a communication system using that path to be controlled more effectively.

5. CONCLUDING REMARKS

In this review paper, an attempt has been made to survey the range of transmission and channel evaluation techniques applicable to digital communication in the various bands of the radio frequency spectrum. For further reading, a set of important basic references has been provided.

The future development of digital communication systems will inevitably make greater use of adaptive operation in response to changes in path parameters. Effective adaptation and control requires the availability of an accurate and reliable model of the propagation environment, obtained ideally by sophisticated off-line prediction. In many cases, however, this will never be achievable and channel evaluation techniques will be required to provide such a model. Thus, the interaction of digital transmission techniques and channel evaluation procedures is vital to the successful development of adaptive communication systems for operation in conditions where path parameters are changing rapidly with time.

6. REFERENCES

1. Watt, A. D., & Maxwell, E. L., 1957, "Characteristics of atmospheric noise from 1 to 100kc", Proc. IRE, 45, pp. 787-794.

2. Goldberg, B., 1966, "300kHz-30MHz MF/HF", IEEE Trans., Vol. COM-14, pp. 767-784.

3. Darnell, M., 1984(a), "Interference characterisation and its importance in HF

communications", Proc. IES-84, Washington D. C.

4. Gott, G. F., Dutta, S. and Doany, P., 1983, "Analysis of HF interference with application to digital communications", Proc. IEE (Part F), Vol. 130, No. 5.

5. Barghausen, A. F., Finney, J. W., Proctor, L. L. and Schultz, L. D., 1969, "Predicting the long-term operational parameters of high-frequency skywave telecommunications systems", ESSA Technical Report ERL-110 - ITS 78, US. Government Printing Office, Washington, D.C.

6. Rawer, K., 1975, "The historical development of forecasting methods for ionospheric propagation of HF waves", (Review), Radio Science, 10, 7, pp. 669-679.

7. Browne, S., Bartholomé, P. J. and Vogt, I., 1963, "VHF scatter communications: new design concepts and experimental results", SHAPE Air Defence Technical Centre Technical Memorandum TM-56.

8. Gerstel, J. D., 1980, "An analysis of meteor burst communications for military applications", IEEE Trans., Vol. COM-28, No. 9, pp. 1591-1601.

9. Booker, H. G. and Gordon, W. E., 1950, "A theory of radio scattering in the troposphere", Proc. IRE, 38, pp. 401-412.

10. Crane, R. K., 1976, "Attenuation due to rain-mini-review", IEEE Trans, Vol AP-23, No. 5, pp. 750-752.

11. Lawrence, R. S., Little, C. G. and Chivers, H. J. A., 1964, "A survey of ionospheric effects upon earth-space radio propagation", Proc. IEEE, 52, pp. 4-27.

12. Pasupathy, S., 1979, "Minimum shift keying: a spectrally efficient modulation", IEEE Communications Society Magazine, Vol. 17, No. 4, pp. 14-22.

13. Dixon, R. C., 1976, "Spread spectrum systems", Wiley (New York).

14. Utlaut, W. F., 1978, "Spread spectrum: principles and possible application to spectrum utilization and allocation", IEEE Communications Society Magazine, Vol. 16, No. 5, pp. 21-31.

15. Monsen, P., 1983, "Modern HF communications, modulation and coding", AGARD Lecture Series No. 127, "Modern HF communications", Athens/Rome/Fort Monmouth.

16. Lin, S. and Costello, D. J. (Jr), 1983, "Error control coding: fundamentals and applications", Prentice-Hall.

17. Van Duuren, H. C. A., 1951, "Typendruktelegraphie over radiooverbindigen", Tijdschrift van het Nederlands Radio Genootschap, 16, p. 53.

18. Goodman, R. M. F. and Farrell, P. G., 1975, "Data transmission with variable-redundancy error control over a high-frequency channel", Proc. IEE, Vol. 122, No. 2, pp. 113-118.

19. Bartholomé, P. J. and Vogt, I. M., 1968, "COMET - a new meteor burst system incorporating ARQ and diversity reception", IEEE Trans., Vol. COM-16, No. 2, pp. 268-278.

20. McCarthy, R. F., 1975, "Error control with time diversity techniques", Signal, May June Issue.

21. Chase, D., 1973, "A combined coding and modulation approach for communication over dispersive channels", IEEE Trans., Vol. COM-21, pp. 159-174.

22. Douglas, F. W. and Hergas, P. T., 1971, "Development of AUTOSPEC Mark II", Point-to-point Telecommunications, May.

23. Lee, Y. W., 1960, "Statistical theory of communication", Wiley.

24. Wozencraft, J. M. and Jacobs, I. M., 1965, "Communication engineering", Wiley.

25. Viterbi, A. J., 1967, "Error bounds for convolutional codes and an asymptotically optimum decoding algorithm", IEEE Trans, Vol. IT-13, pp. 260-269.

26. Tarnoli, M., 1984 (b), "Speech digitisation techniques", Proc. of IEE Conference on "Secure communication systems", London, pp. 20-31.

27. Bryant, N. S., 1974, "Digital coding of speech waveforms: PCM, DPCM and DM quantizers", Proc. IEEE, Vol. 62, pp. 611-632.

28. Markel, J. D. and Gray, A. H., 1976, "Linear prediction of speech", Springer-Verlag.

29. Kelly, L. C., 1979, "Speech and vocoders", Radio and Electronic Engineer, Vol. 40

(2), pp. 73-82.

30. Holmes, J. N., 1978, "Parallel formant vocoders", IEEE Eascon 78.

31. Sambur, M. R., 1982, "Speech algorithm advances promise toll-quality medium-band digitized speech", Speech Technology, Vol. 1(3), pp. 22-34.

32. Darnell, M. and Chesmore, E. D., 1984, "Aspects of digitised speech communication over limited capacity channels", Proc. of IEE Conference "Communications 84", Birmingham.

33. Darnell, M., 1983, "Real-time channel evaluation", AGARD Lecture Series No. 127, "Modern HF communications", Athens/Rome/Fort Monmouth.

34. CCIR, 1981, "Real-time channel evaluation of ionospheric radio circuits", Provisional Report AK/6.

35. Barker, R. H., 1953, "Group synchronising of binary digital systems", in "Communication theory", London, Butterworth, pp. 273-287.

36. Coll, D. C. and Storey, J. R., 1964, "Ionospheric sounding using coded pulse signals", Radio Science Journal of Research, Vol. 69D(10), pp. 1155-1159.

37. Darnell, M., 1975, "Channel estimation techniques for HF communications", AGARD CP-173, "Radio systems and the ionosphere", Paper 16, Athens.

38. Barry, G. H. and Fenwick, R. B., 1965, "Extra terrestrial and ionospheric sounding with synthesized frequency sweeps", Hewlett-Packard Journal, Vol. 16(11), pp. 8-12.

39. Stevens, E. E., 1968, "The CHEC sounding system", in "Ionospheric radio communications", Plenum, pp. 359-369.

40. Betts, J. A. and Darnell, M., 1975, "Real-time HF channel estimation by phase measurements on low-level pilot tones", AGARD CP-173, "Radio Systems and the Ionosphere", Paper 18, Athens.

41. Darnell, M., 1978, "Channel evaluation techniques for dispersive communications paths" in "Communications systems and random process theory", Sijthoff and Noordhoff, The Netherlands, pp. 425-460.

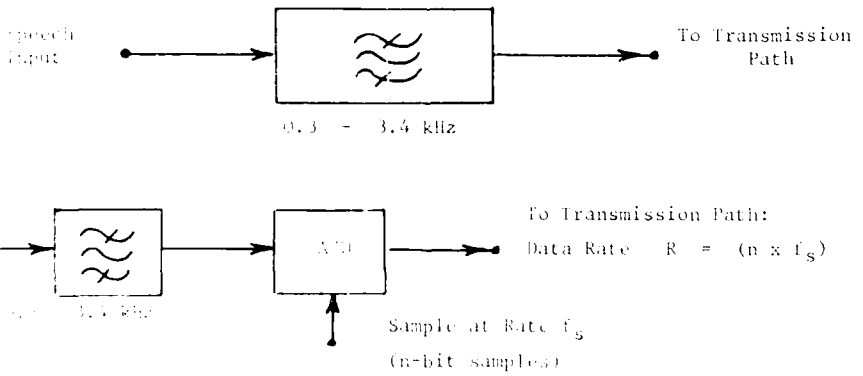

... and digital speech transmission systems

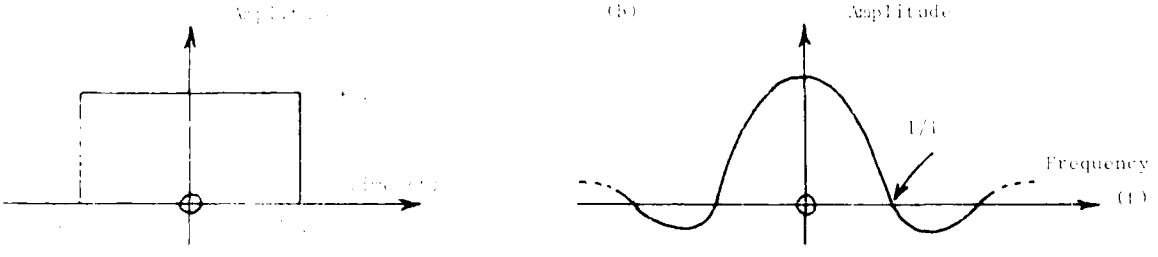

... rectangular pulse

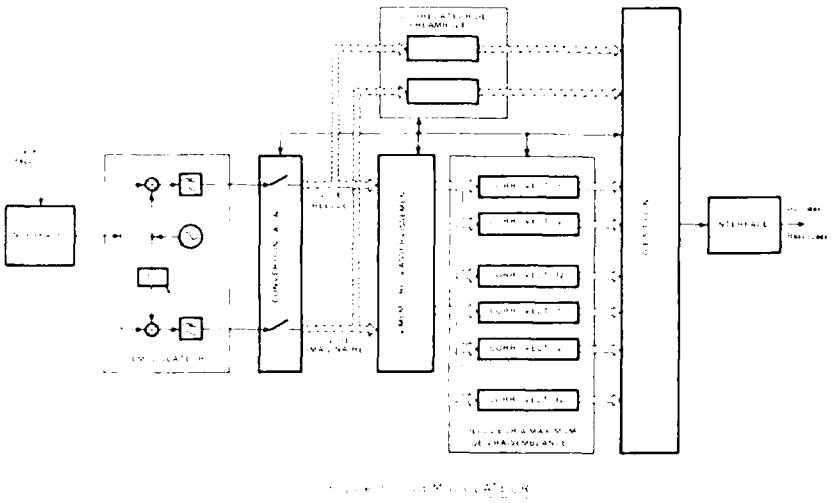

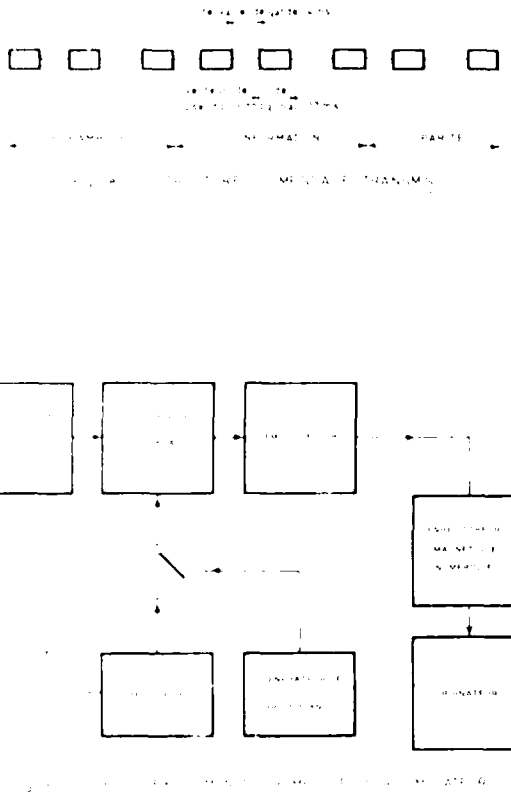

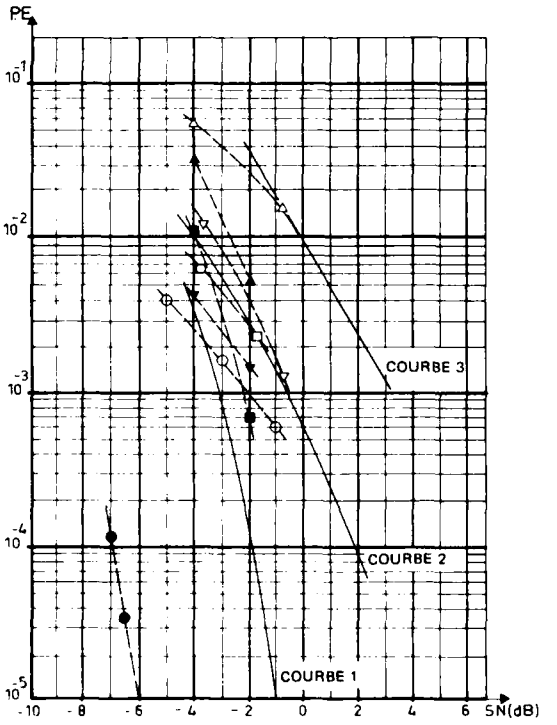

Figure 8 : TAUX D'ERREUR MESURES EN SIMULATION

	MONOTRAJET	2 TRAJETS
BRUIT BLANC	●	○
BRUIT ATMOSPHERIQUE	▼	▽
GRAPHIE	■	□
RADIODIFFUSION	▲	△

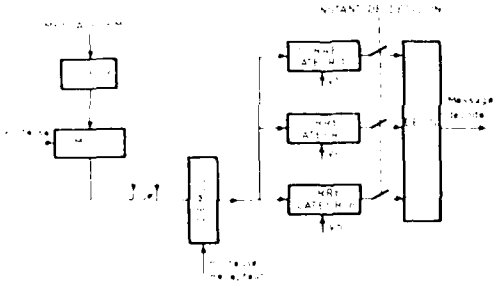

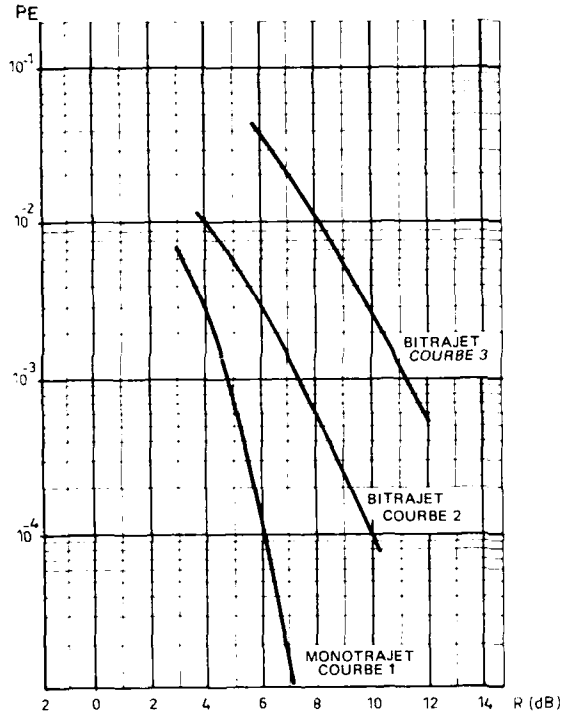

Figure 3 : PROBABILITE D'ERREUR DES CODES PSEUDO-ORTHOGONAUX

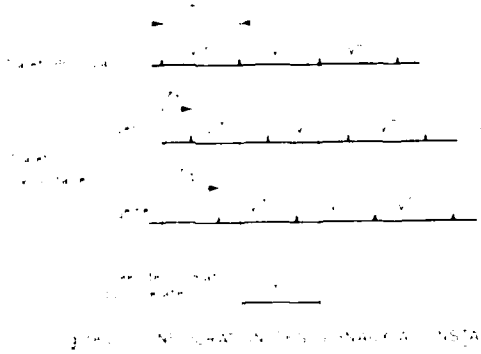

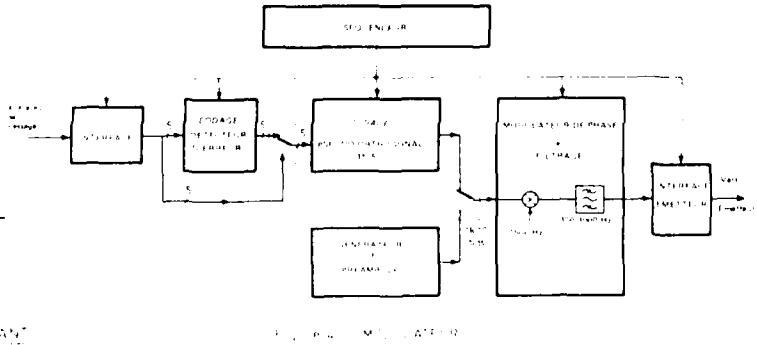

	Jour + Nuit	Jour	Nuit
Modem à codes pseudo-orthogonaux	1,2 %	1,3 %	0,9 %
Modem F.S.K. à 75 bds	9,7 %	6,5 %	16,2 %

TABLEAU 4 : Taux de perte de synchronisation moyen

TABLEAU 5

Les transmissions par ondes ionosphériques, associent la technique d'étalement de spectre aux techniques de codage, permettant d'assurer ainsi une protection contre les évanouissements sélectifs et contre les distorsions intersymboles.

Les essais expérimentaux ont été effectués sur un prototype répondant aux normes militaires.

Une première série d'essais a été effectuée en simulation de façon à caractériser les performances du modem dans des conditions de propagation et de brouillage parfaitement définies.

Dans une seconde série d'essais effectuée sur une liaison réelle, une comparaison a été faite pour des débits d'information identiques entre le comportement du modem et celui d'un modem n'utilisant pas de codage. La variabilité des conditions de propagation et de brouillage ne permet que d'effectuer des mesures comparatives qui mettent en évidence le gain apporté par le codage.

L'ensemble des résultats montre que cette technique apporte un gain notable par rapport aux procédés classiques, et est bien adaptée aux liaisons par ondes décamétriques.

BIBLIOGRAPHIE

[ ] Utilisation des codes pseudo-orthogonaux dans les canaux multitrajets non stationnaires
E. BAVARD, M.GINDRE, C.GOUTELARD
Electromagnetic wave propagation panel symposium . Athènes (Grèce) Mai 1975.

[ ] Définition et construction des codes pseudo-orthogonaux
E. BAVARD, C.GOUTELARD
Annales des Télécommunications, Tome 33, N° 65, Mai/Juin 75

[ ] Synchronisation Techniques (dans GOLOMB)
Digital Communication with space application
Prentice hall - 1964

REMERCIEMENTS

Cette étude a été réalisée dans le cadre d'un contrat de la section d'étude et de fabrication des Télécommunications de la Délégation Générale de l'Armement qui nous a aimablement accordé l'autorisation de publier cette étude.

	Jour + Nuit	Jour	Nuit
Modem à codes pseudo-orthogonaux	$3,8\ 10^{-3}$	$5\ 10^{-3}$	$2\ 10^{-3}$
Modem F.S.K. à 75 b/s	$3,2\ 10^{-2}$	$2\ 10^{-2}$	$5\ 10^{-2}$

TABLEAU 2 : Taux d'erreur moyen à long terme (mesuré pendant 98 % du temps)

Court terme

La mesure du taux d'erreur moyen à court terme est effectuée sur 20 messages consécutifs. Les résultats sont présentés sur la figure 9, en ce qui concerne les mesures réalisées de jour et sur la figure 10 pour les mesures de nuit. Chaque point sur ces graphes possède une abscisse représentant le taux d'erreur moyen associé au modem à codes pseudo-orthogonaux mesuré sur une période de 5 minutes et une ordonnée représentant le taux d'erreur moyen associé au modem F.S.K. à 75 b/s pendant les 5 minutes suivantes.

Sur ces figures, une zone se distingue particulièrement par la forte densité de points s'y rattachant. Cette zone correspond à l'ensemble des mesures où le modem à codes pseudo-orthogonaux ne fait pas d'erreur, alors que pour la même tranche de temps, le modem F.S.K. possède un taux d'erreur moyen non nul et parfois même très élevé, allant jusqu'à 20 %. Cette zone est représentative de 50 % des essais effectués le jour et de 80 % des essais effectués la nuit.

. . . Mesures effectuées au niveau de chaque message

Taux de succès

Le taux de succès représentant le pourcentage de messages reçus sans erreur, est indiqué dans le tableau 3. Ce tableau indique nettement l'aptitude du modem à codes pseudo-orthogonaux à délivrer des messages sans erreurs, malgré une puissance d'émission faible (puissance de 25 Watts). Il est intéressant de remarquer les variations des taux de succès d'un modem à l'autre, notamment la nuit où l'utilisation du code permet de passer de 62 % à [illegible].

	Jour + Nuit	Jour	Nuit
Modem à codes pseudo-orthogonaux	91 %	88,7 %	95,7 %
Modem F.S.K. à 75 b/s	69,5%	73 %	62,6 %

TABLEAU 3 : Taux de succes moyen

Un moyen supplémentaire permettant de comparer les performances en taux de succès des deux types de modem, consiste à se placer à un taux de succès donné du modem à codes pseudo-orthogonaux et de déterminer quel a été le taux de succès associé du modem F.S.K. pour les messages reçus dans les mêmes conditions. Ceci permet de bâtir des histogrammes tels que ceux représentés figures 11 et 12. Par exemple, en ce qui concerne les essais effectués le jour, lorsque le taux de succès du modem à codes pseudo-orthogonaux est compris entre 90 % et 100 % (ce qui se produit pendant 67 % du temps), la probabilité que le taux de succès du modem F.S.K. soit aussi compris entre 90 % et 100 % est seulement égale à 25 %, cette probabilité passe à 20 % pour un taux de succès du modem F.S.K. inférieur à 60 %. En ce qui concerne les essais effectués durant la nuit, cette tendance est nettement plus accentuée, en effet, pour un taux de succès du modem à codes pseudo-orthogonaux compris entre 90 % et 100 % (ce qui se produit pendant 88 % du temps), la probabilité que le taux de succès du modem F.S.K. soit compris aussi entre 90 % et 100 % tombe à 15 %, cette probabilité passant à 40 % pour un taux de succès du modem F.S.K. inférieur à 60 %. Ces considérations mettent en évidence l'efficacité du codage qui permet d'obtenir un taux de succès compris entre 90 % et 100 %, avec une forte probabilité de l'ordre de 80 %, alors que l'on obtient au mieux une chance sur quatre d'obtenir les mêmes performances pour un système de transmission non codé à débit d'information équivalent.

Taux de perte de synchronisation

Le taux de perte de synchronisation, représentant le pourcentage de messages reçus affectés d'un taux d'erreur supérieur à 30 %, est représenté dans le tableau 4. Ces résultats indiquent que le taux de perte de synchronisation du modem à codes pseudo-orthogonaux est pratiquement 10 fois plus faible que celui associé au modem F.S.K. (passage de 1 % à [illegible] %). Cette différence met en évidence l'aptitude du modem à code à résister à des conditions de propagation sévères. En particulier, lors de la période du lever du soleil, ce taux est égal à 0,2 % pour le modem à codes, alors qu'il est de 2 % pour le modem F.S.K.. Ce qui revient à dire que durant cette période, toute communication est impossible avec un modem classique n'utilisant pas le codage, pendant un quart de temps.

type d'aléas 6, restitution d'un message totalement erroné, se produit essentiellement dans le cas du brouillage par une émission de radiodiffusion. Ce type d'aléas est plus grave car il entraîne des erreurs importantes qui apparaissent clairement dans les résultats.

5. EXPERIMENTATION SUR UNE LIAISON REELLE

5.1 Conditions d'expérimentation

Une expérimentation a été effectuée sur une liaison radio-électrique dans la gamme HF, sur une distance de 500 Km, où les trajets multiples sont importants. Les essais se sont déroulés du 15 Juin au 1er Juillet 1983 avec un émetteur de puissance 25 Watts et des antennes de type fouet vertical de 10 m à l'émission et à la réception. Les fréquences utilisées lors de ces essais ont été déterminées à l'aide des prévisions de propagation établies par le C.N.E.T., et étaient comprises entre 4 et 6 MHz. La distance émission/réception étant d'environ 500 Km, il est nécessaire de rayonner au voisinage du zenith, or compte tenu du diagramme de rayonnement d'une antenne verticale, il y a atténuation de la puissance émise dans cette direction. Ces mêmes prévisions montrent que, en fonction des fréquences retenues, l'estimation des angles d'élévation du parcours radio-électrique est voisine de 70°. Sous cette élévation, les fouets présentent une atténuation de l'ordre de 10 dB par rapport à une antenne omnidirectionnelle, réduisant la puissance émise utile à 2,5 Watts. Cette atténuation de 10 dB affecte également le signal reçu réduisant ainsi le rapport signal à bruit à la prise de décision.

5.2 Méthodes d'analyse

Sachant qu'il est difficile de préciser de façon absolue les paramètres de la liaison, compte tenu de leur grande variabilité, une expérimentation du type comparatif a été retenue. Le but a été de comparer, à débit d'information équivalent, un modem utilisant les codes pseudo-orthogonaux et un modem classique n'utilisant pas de codage. Le modem classique choisi, correspond à un modem type "SEMATRANS", conforme aux recommandations publiées par le C.C.I.T.T., tome VIII du livre blanc (avis V21 et V24).

Les caractéristiques principales de ce modem sont les suivantes : mode asynchrone, débit binaire égal à 75 b/s, modulation bivalente de fréquence obtenue par déplacement de fréquence (F.S.K. 1080 ± 100 Hz). L'autre modem correspond au modem à codes pseudo-orthogonaux, précédemment décrit, le débit d'information étant égal à 237 b/s. La procédure de répétition ayant été retenue, le débit d'information réel est alors divisé par trois, soit 79 b/s.

Pour que les deux équipements soient testés sur des conditions équivalentes de propagation, un multiplexage a été établi permettant d'émettre pendant 5 minutes sur un type de modem, puis les 5 minutes suivantes sur l'autre type, etc... Le nombre d'erreurs était mesuré sur chaque bloc élémentaire de 256 éléments binaires restitués, c'est-à-dire au niveau de chaque message. Ces mesures élémentaires ont permis de déterminer le taux de succès correspondant au pourcentage de messages reçus, sans erreur, et le taux de perte de synchronisation correspondant au pourcentage de messages reçus, ayant un taux d'erreur supérieur à 30 %. Le taux d'erreur moyen a été calculé pour les deux systèmes, en effectuant une moyenne sur l'ensemble de la durée de l'expérimentation des taux d'erreur élémentaires. Cependant, la mesure de la moyenne ne reflète pas suffisamment les performances d'un système car elle englobe de trop nombreux phénomènes. Pour cette raison, il est fourni les statistiques sur le taux d'erreur moyen mesuré à court terme, c'est-à-dire sur des tranches de temps de 5 minutes.

5.3 Résultats

Pour chaque type de modem, 20 messages de 256 éléments binaires chacun ont été émis par tranche de 5 minutes, soit 5120 éléments binaires (1 seule erreur mesurée pendant cette période correspond donc à un taux d'erreur de $2\ 10^{-4}$). Sur l'ensemble de la durée de l'expérimentation 3000 messages ont été transmis de jour, et 2000 messages de nuit pour les deux systèmes de comparaison.

5.3.1 Taux d'erreur moyen mesuré à long terme et à court terme

Long terme

Le taux d'erreur moyen mesuré sur la durée globale de l'expérimentation à une signification assez imprécise, car, compte tenu de la nature du canal HF, caractérisé par de brusques variations du rapport signal à bruit, il représente en fait la moyenne des taux d'erreur les plus forts. Pour cette raison, la moyenne calculée porte sur 98 % du temps, c'est pour les deux systèmes 1 % des essais les plus mauvais et 1 % des essais les meilleurs ont été supprimés. Les résultats sont présentés dans le tableau 2. Ce tableau fait apparaître un gain de l'ordre de 10 sur la mesure du taux d'erreur moyen en faveur du modem à codes pseudo-orthogonaux par rapport au modem classique type F.S.K. (passage de $3\ 10^{-3}$ à $4\ 10^{-4}$). De plus, les performances de ce dernier se dégradent notablement la nuit ($5\ 10^{-2}$), ceci étant dû aux conditions de propagation où de nombreux évanouissements apparaissent, en particulier aux périodes correspondant aux heures de lever du soleil. L'analyse ultérieure des taux de perte de synchronisation éclairera ce phénomène.

- Cas 9 : 2 fausses alarmes successives

i	A	A	i + k

avec $k \in \{1, 2, 3, 4\}$

- Cas 10 : 3 fausses alarmes successives

i	A	A	A	i + k

avec $k \in \{1, 2, 3, 4\}$

Les résultats obtenus sont consignés dans le tableau 1 où le rapport signal/bruit est donné pour la bande passante du récepteur adapté au débit binaire de 1800 Bauds. Chaque cas traité comporte en moyenne 4800 séquences de 256 bits, soit 1200000 bits.

Type de brouillage	Nombre de séquences de 256 bits	S/N dB	Propagation monotrajet : 1 bitrajet : 2	Taux d'erreur moyen %	Type d'aléas 3	5	6	7	8	9
Bruit blanc	4485	0	1	$< 10^{-6}$	0	0	0	0	0	0
	4430	-4	1	$< 10^{-6}$	0	0	0	0	0	0
	4922	-6,5	1	0,0034	0	0	1	5	0	0
	4320	-7	1	0,0108	0	0	0	1	0	0
	4594	-1	2	0,059	0	0	1	0	0	0
	3883	-3	2	0,16	0	0	0	0	0	0
	4539	-5	2	0,40	0	0	1	1	0	0
Bruit atmosphérique	4594	-2	1	0,14	0	0	3	1	0	0
	4539	-4	1	0,43	0	0	12	10	0	0
	4922	0,8	2	0,13	0	0	0	7	0	0
	4594	-3,8	2	1,01	0	0	10	11	0	0
Morse graphie	4430	2	1	0,072	0	0	0	3	0	0
	4485	4	1	1,04	0	1	22	7	1	0
	4485	0,8	2	0,23	0	3	8	70	0	0
	4430	3,8	2	0,68	1	4	7	72	0	1
Radio diffusion	5086	2	1	0,61	0	0	4	4	0	0
	4758	4	1	3,44	0	0	55	0	1	0
	4485	0,8	2	1,3	0	0	1	0	0	0
	4539	3,8	2	5,56	0	0	70	4	1	0
	86520									
	a) (résultats d'ensemble des aléas)				1	8	195	196	3	1
	b) (probabilités d'apparition des aléas)				1,2 10^{-5}	8 10^{-5}	2,2 10^{-3}	2,2 10^{-3}	3,5 10^{-5}	1,2 10^{-5}

Tableau 1

Résultats de l'expérimentation en simulation

[illegible] type "type d'aléa" [illegible] type le nombre de fois où le type [illegible] expérimentation. Les types 1 - 2 - 4 - 10 ne [illegible].

[illegible] le graphe de la figure 8 où l'on a fait [illegible] pour faciliter la lecture du graphe, on a [illegible] même type de propagation, par un trait [illegible].

[illegible] du modem aux brouillages. Le modem [illegible] par des émissions de radiodiffusion, mais assez [illegible] acceptable, puisque les taux d'erreur [illegible] rapport signal bruit inférieurs à 0 dB.

[illegible] certains types apparaissent. Le type d'aléas 7 [illegible] n'est donc pas gênant. Il se produit essentiellement [illegible] propagation bitrajet. Par contre, le

- Un bruit atmosphérique capté par le récepteur

- Un brouilleur constitué d'un émetteur modulé en A1

- Un émetteur de radiodiffusion.

Les expérimentations ont été faites pour plusieurs valeurs du rapport signal/bruit, ce qui a conduit à un total de 18 enregistrements, représentant 216 heures d'expérimentation.

La transmission a été effectuée selon le mode décrit dans le paragraphe précédent, par l'émission d'un même message répété deux fois à des intervalles de temps aléatoire. A chaque séquence émise, le récepteur doit donc analyser le préambule et réaliser sa synchronisation.

4.3 Analyse des résultats

Pour faciliter l'analyse des résultats, on a choisi d'émettre de façon périodique quatre séquences d'information connues de 256 bits, prélevées dans une suite pseudo-aléatoire.

Les résultats, analysés par ordinateur, ont fait apparaitre les taux d'erreur et les types de non détection et de fausse alarme rencontrés. Pour ces dernières mesures on a examiné les séquences successives reçues, et on a distingué les 10 cas suivants :

- Cas 1 : Réception correcte ; la séquence i + 1 suit la séquence :

i	i + 1

- Cas 2 : Non détection de la séquence i + 1 :

i	i + 2

- Cas 3 : Non détection des séquences i + 1 et i + 2 :

i	i + 3

- Cas 4 : Non détection des séquences i + 1, i + 2, i + 3 :

i	i + 4

- Cas 5 : Fausse alarme : une séquence parasite A s'introduit dans les séquences d'information

i	A	i + 1

- Cas 6 : Fausse alarme : une séquence parasite est reçue en substitution de la séquence i + 1, ou bien la séquence i + 1 est totalement erronée

i	A	i + 2

- Cas 7 : Fausse alarme préalable : une fausse alarme intervenant entre les séquences i et i + 1 provoque la réception double de la séquence i + 1

i	i + 1	i + 1

- Cas 8 : Fausse alarme et non détection

i	A	i + 3 ou i + 4

- Décodeur

- Gestion

- Interface restitution de données.

L'interface récepteur est composé de circuits d'adaptation de niveaux et d'impédance. La démodulation du signal reçu est faite de façon quasi-cohérente sur deux voies en quadrature. La détection du préambule est effectuée par corrélation des signaux issus des 2 voies avec la copie locale de la séquence de synchronisation. Les corrélations sur les 2 voies sont ajoutées quadratiquement et comparées à un seuil fonction de la valeur moyenne du signal redressé. Les signaux démodulés sont échantillonnés à un rythme égal à 4 fois la vitesse de modulation, il en résulte une dégradation maximale de la corrélation par rapport à un échantillonnage synchrone de 1,2 dB. Une fois le seuil franchi, l'analyse de la fonction corrélation préambule se poursuit dans une fenêtre, de façon à se synchroniser sur le trajet d'amplitude principale. En effet, en cas de propagation par trajets multiples, l'organe de gestion choisit celui correspondant au niveau le plus fort, et permet ainsi la synchronisation du récepteur.

Ensuite, chaque vecteur est extrait de la trame et est démodulé par calcul des 32 modules de corrélation associés aux 32 vecteurs de code possibles. Le vecteur présumé émis est celui correspondant au module de corrélation le plus élevé. La poursuite du trajet d'amplitude maximale s'effectue en permanence, pour tenir compte des variations des conditions de propagation, en utilisant les propriétés de corrélation des codes pseudo-orthogonaux. Le message élémentaire étant émis trois fois, l'exploitation des répétitions est faite par le module de gestion en utilisant, d'une part les résultats du codage détecteur d'erreurs (décodé selon des procédés classiques), et d'autre part les résultats des corrélations. Les règles de décision sont les suivantes : si un message satisfait les relations imposées par le codage détecteur d'erreurs, il est considéré comme juste, si aucun des messages ne satisfait ces relations parmi les trois reçus la décision est prise par une technique de vote majoritaire pondéré (cette technique s'applique également dans le cas où un certain nombre de messages ne sont pas reçus).

Le système de gestion réalise plusieurs fonctions, en particulier l'exploitation des informations en provenance de la détection de préambule (pour effectuer la prise de décision de présence de message) , la poursuite du trajet d'amplitude maximale (grâce aux informations fournies par le décodeur), la décision sur la nature du vecteur émis par l'analyse des fonctions de corrélation et le traitement des répétitions. De plus, ce système de gestion assure également un rôle de supervision de la liaison, par le contrôle de qualité du signal reçu, à l'aide d'une information représentative de la marge de décision associée à chaque vecteur démodulé. L'interface de données vers l'utilisateur est conforme aux avis V24 et V28 du C.C.I.T.T. Le message de 32 octets est restitué sous forme série, en mode synchrone.

4. EXPERIMENTATION SUR SIMULATEUR

L'expérimentation menée sur simulateur a été effectuée pour obtenir des mesures absolues, les conditions de propagation et les conditions de brouillage pouvant être choisies par l'opérateur et maintenues constantes.

4.1 Dispositif expérimental

Le système de mesure utilisé est représenté sur la figure 7. Il comporte :

- Le modem à codes pseudo-orthogonaux V(31,5) décrit dans le paragraphe précédent

- Un simulateur de canal ionosphérique permettant de simuler un maximum de 4 trajets pour lesquels l'opérateur règle séparément le décalage temporel, l'amplitude et l'effet Doppler de chaque trajet. Une entrée permet d'ajouter un signal perturbateur représentant un brouillage et/ou un bruit. Pour les essais effectués, on a introduit, soit un bruit blanc, soit un signal parasite capté par un récepteur muni d'un contrôle automatique de gain, permettant de maintenir un niveau constant du signal perturbateur.

- Un enregistreur magnétique numérique sur lequel sont enregistrés les résultats traités ensuite sur ordinateur.

4.2 Conditions d'expérimentation

On a retenu des conditions d'expérimentation offrant un échantillonnage significatif des conditions de propagation et de brouillage.

Pour la propagation on a retenu :

- Une propagation monotrajet

- Une propagation à deux trajets d'égale amplitude, qui constitue le cas le plus pénalisant. On a attribué un effet Doppler de + 0,3 Hz et - 0,7 Hz aux trajets, et un écart de temps de propagation τ_1 1,66 ms.

En ce qui concerne le brouillage on a retenu comme signal :

- Un bruit blanc

3. DESCRIPTION D'UN MODEM A CODES PSEUDO-ORTHOGONAUX

3.1 Caractéristiques générales

Les codes pseudo-orthogonaux V(31,5) ont été retenus pour réaliser un modem destiné à transmettre sur canal HF des messages formatés, dont le bloc unitaire comprend 32 octets. Le débit binaire, compte tenu des contraintes imposées par le système, est de 237 b/s.

Le matériel réalisé est compatible des canaux de 3 kHz selon les recommandations du C.C.I.R. La transmission s'effectue en BLU et l'interface entre l'émetteur et le récepteur est faite en audio-fréquence (bande 300-3000 Hz), ce qui permet d'utiliser un grand nombre d'émetteurs récepteurs actuellement disponibles.

La procédure de transmission adoptée correspond à une transmission dite par paquet. Chaque paquet est constitué de vecteurs de codes, correspondant à une quantité d'information égale à 32 octets. En vue d'établir une liaison de haute qualité, l'information est émise trois fois de façon à pouvoir effectuer un décodage majoritaire sur les messages reçus. Les phénomènes provoquant les erreurs en HF, étant corrélés en fréquence et en espace, mais pas en temps, une procédure utilisant les propriétés de corrélation des codes pseudo-orthogonaux, associée à une diversité temporelle, offre de nombreux avantages en HF.

Les codes retenus sont les codes (31,5) comprenant 32 vecteurs de longueur 31 et portant 5 éléments binaires d'information. Ces codes sont nombreux et leur choix provient du fait qu'ils réalisent un bon compromis entre les performances qui croissent comme le logarithme de la quantité de bit d'information transmis, et la complexité de démodulation qui croît comme le produit de la taille des codes par la longueur des vecteurs.

3.2 Modulateur

Le modulateur, dont un bloc diagramme est représenté figure 4, comprend les fonctions suivantes :

- Interface de données avec le générateur de message
- Codage détecteur d'erreurs
- Codage pseudo-orthogonal
- Générateur de préambule
- Modulation et filtrage
- Séquenceur

L'interface avec le générateur de message comprend l'interface proprement dite, qui est conforme aux avis V24 et V28 du C.C.I.T.T., ainsi que les organes de mémorisation du message qui est fourni au modulateur par bloc de 256 éléments binaires. Le message à émettre, préalablement complété par 4 "zéros" pour constituer un message de 260 éléments binaires, est transformé en une suite de mots de 5 éléments binaires. Un codage détecteur d'erreurs est appliqué sur cette suite de mots à l'aide d'un calcul de parité effectué dans l'algèbre modulo 2^5. Un blanc, d'une longueur correspondant à 4ms, est inséré entre chaque vecteur, de façon à optimiser les performances des codes en présence de trajets multiples. La fonction codage pseudo-orthogonal consiste à associer à chaque mot de 5 éléments binaires, le vecteur de code de 31 éléments binaires correspondant. L'instant d'arrivée du message étant inconnu du récepteur, il est nécessaire d'ajouter en tête de chaque message transmis, une séquence particulière, appelée préambule. Cette séquence assure la synchronisation du récepteur, et, de sa longueur, dépendent les propriétés de détection et de fausses alarmes du système. Son insertion est effectuée dans le modulateur par le générateur de préambule.

Le message transmis est ainsi décomposé en trois parties, une partie préambule, une partie information, une partie contrôle de parité, chaque partie étant constituée de vecteurs de codes pseudo-orthogonaux, comme représenté sur la figure 5. Le flux binaire composé du préambule et du message codé, module par inversion de phase à 1800 Bauds une sous porteuse dont la fréquence est égale à 1500 Hz. Un filtrage à phase linéaire est ensuite appliqué de façon à limiter le spectre du signal modulé pour le rendre compatible avec la bande disponible. Le séquenceur engendre tous les rythmes nécessaires au fonctionnement du modulateur en fonction des signaux de commande appliqués sur la jonction avec le générateur de message.

3.3 Démodulateur

Le démodulateur, dont un bloc diagramme est donné figure 6, est composé des fonctions suivantes :

- Interface récepteur
- Démodulateur de phase
- Conversion Analogique - Numérique
- Détecteur de préambule

où A_q, τ_q, f_{dq} représentent respectivement les amplitudes, retards et fréquences Doppler du q ième trajet multiple, le premier terme représentant le trajet pris comme référence et appelé trajet principal.

La détection est effectuée par une démodulation synchrone avec la porteuse du trajet principal donnant le signal

$$r_d(t) = S_{(t)} + \sum_{q=1}^{Q} A_q \, S_{(t - \tau q)} \cos \theta_q$$

où $\theta_q = 2\pi (f_{dq} - f_d)t + 2\pi (f_{dq} + f_o) \tau_q$

qui est corrélé avec chaque vecteur du code V(n,k) (Figure 1).

La synchronisation étant effectuée sur le trajet principal, l'instant de décision correspond au moment où la corrélation du vecteur v^i, reçu sur le trajet principal avec les vecteurs de référence, est faite avec un décalage temporel nul.

L'émission étant continue, la configuration des signaux reçus par le trajet principal et les trajets secondaires, est donnée sur la figure 2. Le signal délivré par le corrélateur j vaut alors :

$$Z_j = \rho_{ij}(o) + \sum_{q=1}^{Q} A_q \cos \theta_q \left[\rho_{ij}(\tau_q) + \rho_{uj}(\tau_q) \right] + bj$$

où $\rho_{km}(\tau)$ représente la corrélation apériodique normée du vecteur v^k avec le vecteur v^m pour un décalage temporel τ.

b_j représente la corrélation du bruit avec le vecteur v^j

Le critère de décision à maximum de vraisemblance conduit à décider que v^i est reçu si Zi est supérieur à tous les Zj pour $j \neq i$.

Le code adapté à ce type de liaison est donc celui qui minimise les termes d'interférence. Les propriétés auxquelles il doit satisfaire sont uniquement liées aux propriétés d'auto-corrélation et d'inter-corrélation des vecteurs du code V(n,k) :

- l'auto-corrélation $\rho_{ii(\tau)}$ pour $\tau \neq 0$
- l'inter-corrélation $\rho_{ij(\tau)}$, $\forall \tau$

doivent être, en valeur absolue, bornées par une limite aussi faible que possible.

Les valeurs asymptotiques de la borne ont été déterminées, et la méthode de construction, ainsi que les propriétés de ces codes, ont été développées dans des publications antérieures [1] , [2] . On ne rappelle ici que les résultats généraux.

Les vecteurs des codes pseudo-orthogonaux V(n,k), sont déduits par une opération de translation interne à un code cyclique W(n,K) qui conduit à prendre un vecteur par classe d'ordre n de W(n,K). Cette construction permet d'obtenir les valeurs les plus faibles des termes d'interférence.

Les codes pseudo-orthogonaux sont des codes non linéaires qui possèdent les propriétés des codes auto-synchronisants.

Les performances les meilleures sont obtenues pour les valeurs de n de la forme $n = 2^p - 1$ ou $n = 2^p$, p entier, valeur pour laquelle les codes ont, de plus, la propriété

$$\rho_{ij(o)} = 0 \text{ pour } i \neq j$$

Les codes auto-synchronisants possèdent des propriétés similaires [3], mais présentent des termes d'interférence plus importants, et n'existent que pour des valeurs de n particulières.

Les performances des codes pseudo-orthogonaux sont illustrés sur la figure 3 qui représente la probabilité d'erreurs par bit en fonction du rapport

$$\frac{E}{N} \quad \frac{\text{Energie par bit d'information}}{\text{Densité spectrale de bruit (bruit blanc)}}$$

pour les cas de propagation suivants :

Propagation monotrajet : courbe 1

Propagation à deux trajets d'égale amplitude avec émission continue (courbe 3) ou avec une interruption de l'émission égale à T_c entre deux vecteurs (courbe 2).

MODEM A CODES PSEUDO-ORTHOGONAUX : RESULTATS EXPERIMENTAUX

P.CHAVAND (1), D.DESAGE (2), C.GOUTELARD (1), J.P. VAN UFFELEN (2)

(1) LETTI 5 Avenue de la Division Leclerc 94230 CACHAN (France)

(2) T.R.T. B.P. 21, 92350 LE PLESSIS ROBINSON (France)

RESUME

Le canal ionosphérique en ondes décamétriques est caractérisé par l'existence de trajets multiples qui introduisent des évanouissements sélectifs et des distorsions intersymboles.

Les modems à cadence lente apportent une solution aux problèmes de distorsion intersymboles, mais sont sensibles aux évanouissements sélectifs. Au contraire, les modems à cadence rapide, sont sensibles aux distorsions intersymboles, mais peu sensibles aux évanouissements sélectifs.

On présente un modem utilisant des codes pseudo-orthogonaux qui réalise une transmission rapide en assurant une bonne protection sur les distorsions intersymboles.

Les caractéristiques des codes pseudo-orthogonaux, qui constituent un codage optimum, sont rappelées et les techniques mises en oeuvre dans le modem sont décrites.

Deux types d'essais expérimentaux ont été effectués. Le premier type, effectué sur simulateur permet de mesurer les caractéristiques du modem dans des conditions de propagation et de brouillage parfaitement définies.

Le second type, effectué sur une liaison réelle, a permis de comparer les performances du modem à codes pseudo-orthogonaux avec celles d'un modem non codé de même débit. Le gain apporté par le codage est mis en évidence.

1. INTRODUCTION

Les transmissions en ondes ionosphériques sont caractérisées par la présence de trajets multiples et la non stationarité du milieu. L'interférence entre les trajets multiples, crée des évanouissements importants (fading) et l'étalement de la réponse impulsionnelle introduit une distorsion intersymboles.

Les modems utilisés se classent actuellement en deux catégories. Ceux à cadence faible et à bande étroite qui sont sensibles aux évanouissements sélectifs, et ceux à cadence rapide qui sont sensibles aux distorsions intersymboles. On combat cette distorsion, soit par des techniques d'égalisation, soit par des techniques de codage.

On présente ici un système à cadence rapide utilisant une technique de codage qui limite les effets de la distorsion intersymbole. Les codes utilisés sont optimaux et un décodage à maximum de vraisemblance est utilisé. La répétition de l'information, associée à un codage détecteur d'erreur supplémentaire, confère au système une robustesse particulière vis-à-vis des brouillages.

2. CODES PSEUDO ORTHOGONAUX

Les codes pseudo orthogonaux ont été élaborés dans le but de résoudre les problèmes rencontrés dans les transmissions, dans les canaux multitrajets à caractéristiques aléatoires.

Le principe de base retenu est celui d'une détection au maximum de vraisemblance, qui conduit au schéma de la chaine de transmission représenté sur la figure 1.

Chaque vecteur émis v^i appartient au code pseudo orthogonal binaire V(n,k), construit à partir des k-uples du message.

La modulation de type PSK conserve le caractère linéaire de la superposition des trajets multiples. Au signal s(t) émis :

$$s(t) \quad S_{(t)} \cos 2\pi f_o t \qquad \text{où} \qquad S_{(t)} \quad \pm 1$$

correspond le signal reçu $r_{(t)}$:

$$r_{(t)} \quad S_{(t)} \cos 2\pi (f_o + f_d)t + \sum_{q \quad 1}^{Q} A_q \, s(t - \tau q) \cos 2\pi (f_o + f_{dq}) (t - \tau q)$$

DISCUSSION

C.Goutelard, Fr

The presentation reminds me that nine years ago Dr Darnell also made a very interesting presentation in Athens on a subject similar to the one discussed today. We note that things have changed a lot over the past nine years. I would like to make three comments. Dr Darnell said that interleaving techniques were ancillary, but that is not perhaps entirely correct. I agree that according to information theory interleaving is bad as far as noise is concerned, but without interleaving techniques we would not know how to correct bursts of errors.

My second point refers to codes. There are some well known block codes which can be used because of their well-understood algebraic structure, but is extremely difficult to find decoding algorithms. It is interesting to mention that there are some codes which are very good for correcting errors, but which cannot be used in practice — the Gopa codes for instance. We know how to decode the so-called Class 1 codes of that type but not Class 2. If we knew how to decode them, great progress could be made in decoding.

My third point refers to multiple-access techniques, and the three techniques given in Section 3.4. You said that the first two could be used in either analogue or digital form, but not the third, which could only be used in digital and not analogue form. However, I believe that it is quite practicable; there is no theoretical reason why the spreading signal should not be an analogue signal.

Author's Reply

Thank you for your comments; I will respond to each in turn. Concerning interleaving, I did not mean to give the impression that interleaving was an ancillary technique. It tends to be a technique that is used in conjunction with conventional error protection coding, because it simplifies the type of code employed by allowing the correction of random errors rather than burst errors. I did not mean to de-emphasize the importance of interleaving. In terms of simplifying the design of a transmission system it has great value.

Concerning decoding of block codes, I accept your point that in some cases it is difficult to find efficient decoding structures. This is, of course, one of the principal advantages of convolutional codes, that the decoding structures are relatively simple. It was necessary to simplify the discussion of these aspects to fit the time available.

Concerning code division multiple access, in principle, I accept your comment, but as far as I know the systems that are used at present have the baseband data in digital form.

C.Goutelard, Fr

I also do not know of spectrum systems which use an analogue implementation, but I do not understand why it is not done. I think one should ask the question because it could be interesting. A communication in the United States described spectrum spreading with true white noise. I do think this method could be studied.

Author's Reply

Thank you very much for that comment and I do think it raises a very interesting possibility.

E.W.Lampert, Ge

Professor Goutelard, ten years ago I built a spread spectrum system using an analogue baseband signal, so some do exist.

J.A.Hoffmeyer, US

Would you consider complexity of implementation and hence cost to also be a major factor in the selection of a voice digitization technique?

Author's Reply

In many cases, the system designer is constrained by the channel characteristics to [illegible]er a wideband or narrowband algorithm. For example, at HF a narrowband 2.4 kbit/s vocoder is typically used to be compatible with a 3 kHz bandwidth, hence necessitating a rather complex implementation. However, in general, I would agree that complexity — and thus cost — should be minimised where the freedom to do this exists.

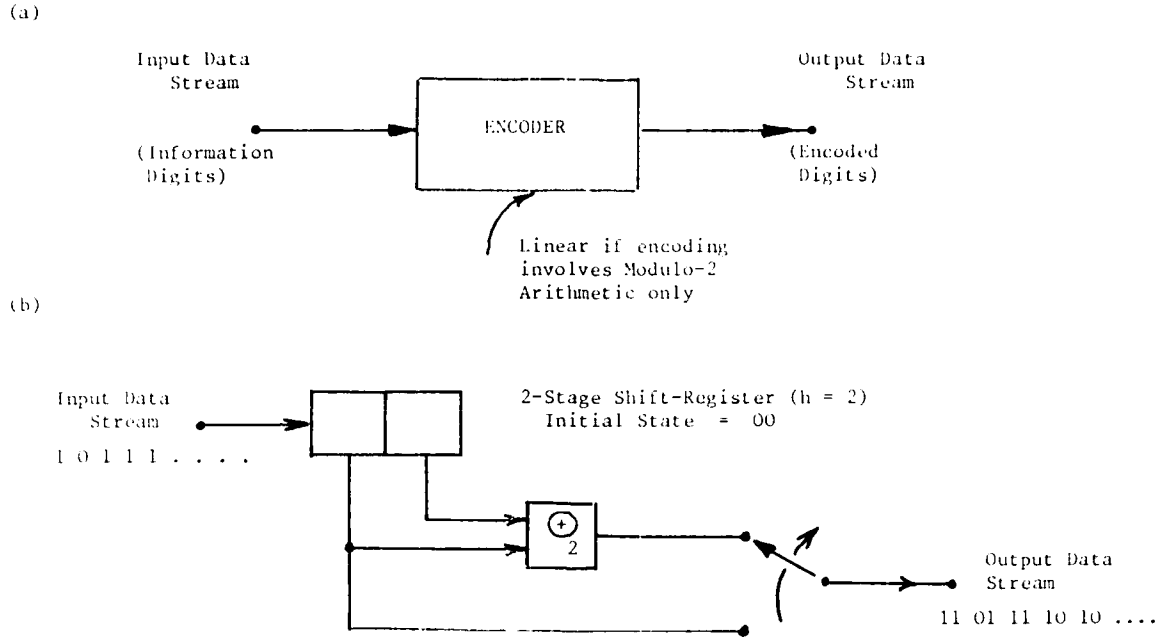

Figure 6. Schematic diagrams of convolutional encoders.

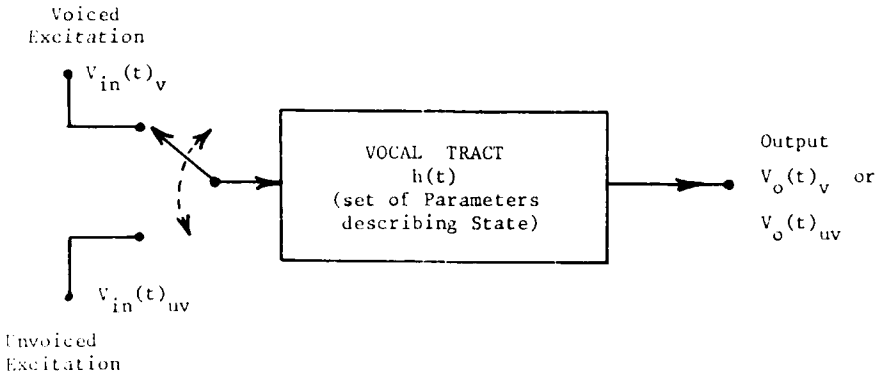

Figure 7. Principle of parameter encoding

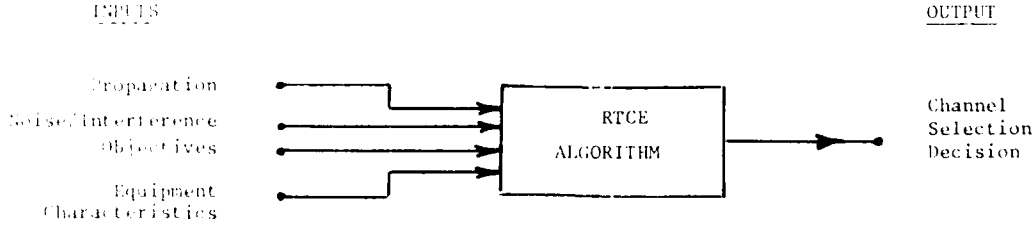

Figure 8. Generalised RTCE algorithm

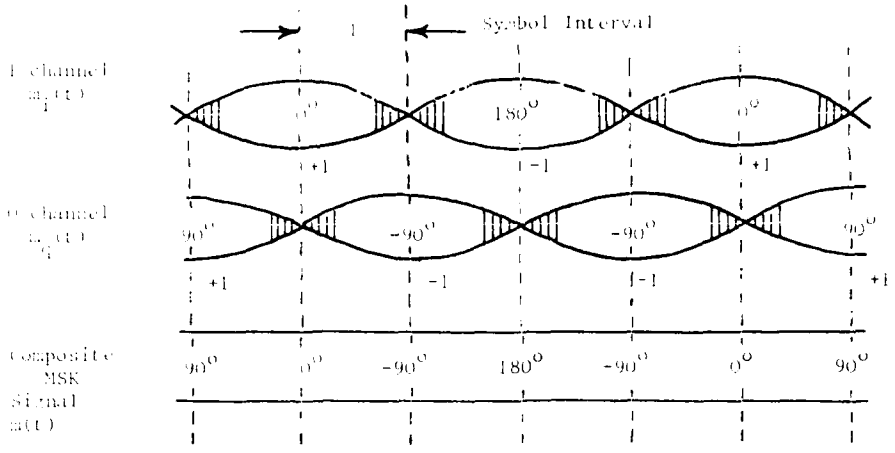

Figure 3. Principle of MSK modulation

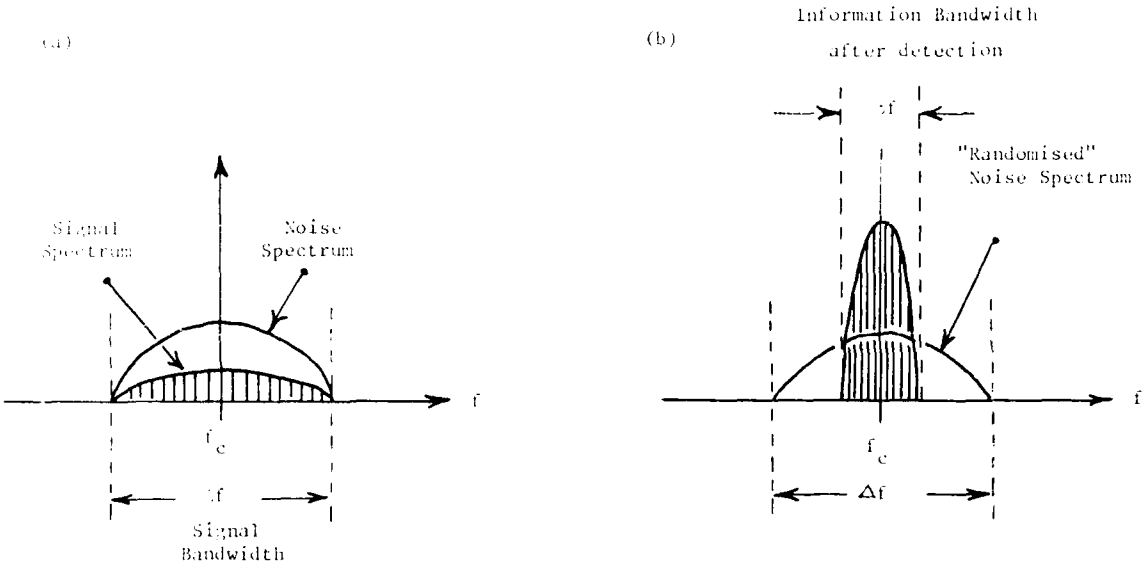

Figure 4. Principle of direct-sequence spread-spectrum processing.

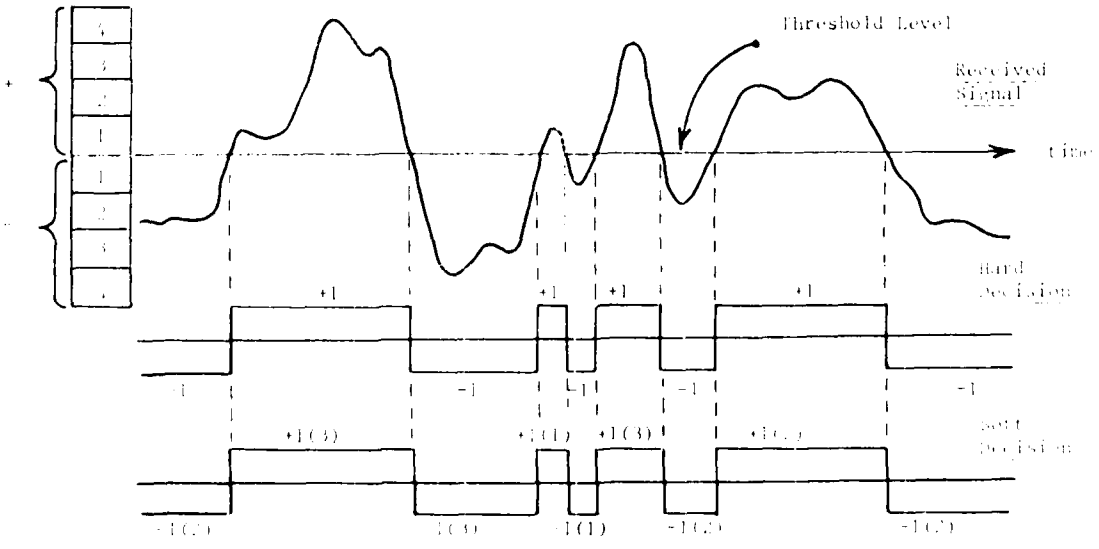

Figure 5. Principle of soft-decision decoding

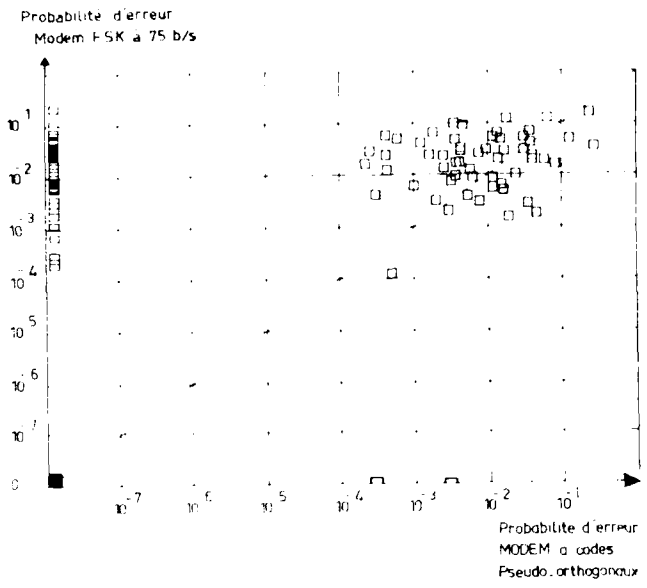

FIGURE 9 COMPARAISON EN TAUX D'ERREUR
MESURE A COURT-TERME (JOUR)

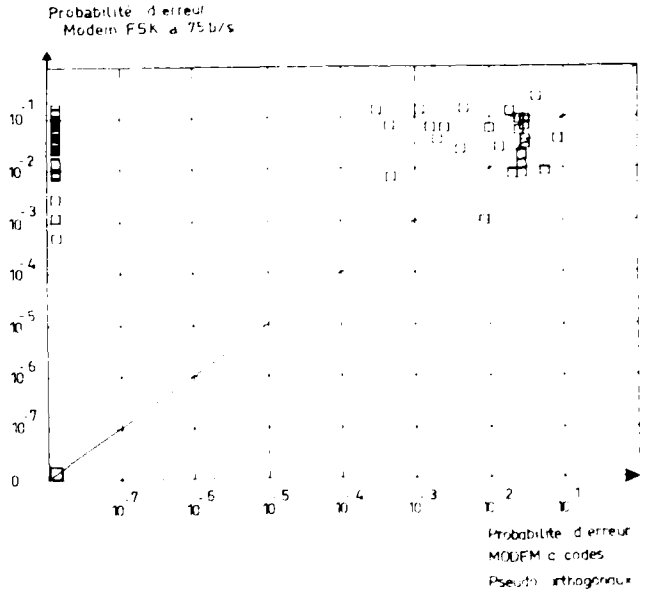

FIGURE 10 COMPARAISON EN TAUX D'ERREUR
MESURE A COURT-TERME (NUIT)

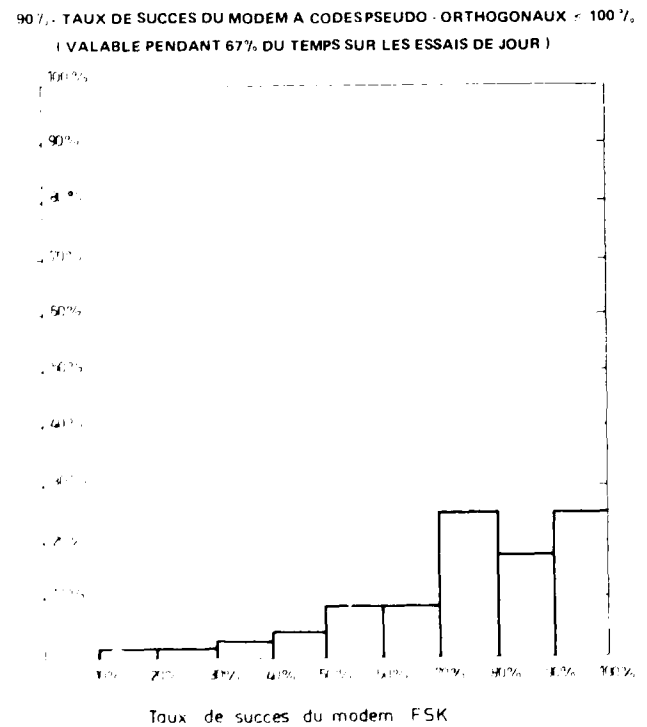

FIGURE 11 HISTOGRAMME DES TAUX DE SUCCES COMPARES
- MESURES DE JOUR -

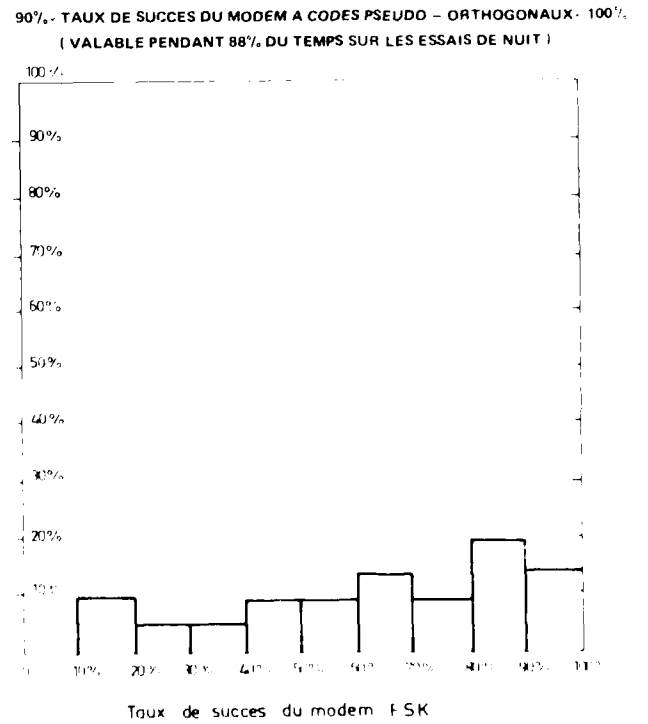

FIGURE 12 HISTOGRAMME DES TAUX DE SUCCES COMPARES
- MESURES DE NUIT -

DISCUSSION

M.Darnell, UK

Professor Goutelard at the beginning of his talk mentioned the shortcomings of the ratio $R = E_b/N_0$ for the comparison of modulation and coding systems. In his paper he overcame the problems by comparing his modem with a reference modem. I wonder if he has any suggestions for any analytical measures which could form the basis of comparison for modulation and coding schemes in a real noise environment.

Author's Reply

The ratio R is used in well-defined white noise. It is very valuable because it can be reproduced by various laboratories and I think it is the only valid element of comparison which makes it possible to compare various models, because you can compare them only in the presence of white noise. When you consider experimental results using real links, the ratio R is only an indicative element. If the noise is impulsive it will introduce bursts of errors, a completely different situation from average noise and randomly scattered errors. In our simulation we have used the ratio R to locate curves which can be used for comparison. Thus we have compared radio broadcasting with Morse, Morse with natural jamming, natural jamming with white noise. Perhaps we should define standard noise models to be able to undertake comparisons between the different systems which we are implementing, and think of setting up magnetic support libraries. We all have high-performance simulators into which we can feed data in digital form, and we could create a standard library with a repertoire of noises which could be fed into simulators. This does not exist as far as I know, and would be of great advantage to us. I expect you have similar ideas.

L.Bertel, Fr

(1) Vous avez parle de simulation effectuee avec 2 trajets pour lesquels les effets Doppler sont respectivement positifs et negatifs. Quelle est pour vous la signification exacte du terme trajet? en particulier distinguez-vous les trajets relatifs a chaque mode?

(2) Vous comparez deux modems et isolez 3 regions caractéristiques, sur les graphiques illustrant vos résultats (figures 9 et 10). Avez-vous une idée sur les origines physiques de ces trois régions caractéristiques; pourrez-vous en deduire des conclusions quant aux mesures qui doivent être effectuées dans le futur en vue d'apporter des informations utiles aux concepteurs des systèmes de transmission numérique en HF.

Author's Reply

(1) On définit un trajet en terme de réponse impulsionnelle du canal: pour une impulsion émise on distingue au lieu de reception n impulsions. On dit alors qu'il y a n trajets. Dans chaque mode de propagation, par exemple, IF, il peut y avoir un trajet correspondant au rayon bas et comprenant le mode ordinaire et extraordinaire si les délais et les dopplers ne permettent pas de les distinguer et deux trajets correspondant au rayon haut, l'un pour le mode ordinaire, l'autre pour le mode extraordinaire si les délais et les dopplers permettent de les distinguer.

(2) En ce qui concerne les trois régions qui apparaissent sur les figures 9 et 10, il est simple de les expliquer. Les points situés près des axes traduisent le fait qu'un seul des modems introduit des erreurs. On constate que le modem FSK introduit plus d'erreurs que le modem à codes pseudo orthogonaux. Il apparait à l'origine des axes les cas où aucune erreur ne s'est produite sur aucune modem. On note ensuite un ensemble de points qui traduisent l'apparition d'erreurs sur l'un et l'autre modem. Cet ensemble est distinct des autres parce que les taux d'erreurs sont mesurés sur des ensembles de 20 blocs de 256 bits d'information. Le taux d'erreurs minimum est donc de $1/(256 \times 20) \# 10^{-4}$, ce qui explique ce groupement. Voici donc les raisons des groupements et quant aux mesures qui pourraient être faites, je pense que votre question est très important, et que le réponse est difficile. Je pense qu'il faut fournir au concepteur des données complémentaires des modèles mathématiques actuels, sur les caractéristiques des canaux aux périodes de perturbation car c'est essentiellement dans ces cas qu'apparaissent les erreurs et sur le bruit peut être en dressant des catalogues comme je l'ai suggéré dans ma réponse au Dr Darnell. Il y a dans ce domaine un travail important qui, à ma connaissance, reste à faire.

I.Kiriakos, Gr

(1) What criteria did you use in order to choose the category of orthogonal codes among all the variety of codes?

(2) What were the lengths of the orthogonal codes that you have used.

(3) Did you compare the performance of the used code in the bounded and unbounded region; if yes, what were the results?

Author's Reply

(1) Nous nous sommes posés, en 1972, le problème de chercher des codes permettant de lutter contre les trajets multiples. Nous avons formulé le problème en termes d'auto et d'intercorrelation comme il est écrit dans notre communication et nous sommes arrivés à une classe de codes que nous avons appelés codes pseudo-orthogonaux. Ils présentent les meilleures performances connues et c'est la raison pour laquelle nous les avons choisis.

(2) Nous avons retenus les codes pseudo-orthogonaux (31,5) à la suite d'une étude des conditions de propagation dans une zone de 3000 km de rayon centrée sur Paris, mais les codes pseudo-orthogonaux existent pour n'importe quelle longueur.

(3) Nous avons examiné les performances des codes pseudo-orthogonaux et nous avons montré qu'elles sont très proches des bornes théoriques, notamment de la borne de Pursley et Sarwate. Ces limites sont discutées dans des publications que nous avons faites.

CODAGE CORRECTEUR D'ERREURS POUR MODEM AUTO ADAPTATIF
RESULTATS THEORIQUES ET EXPERIMENTAUX

par

F. CHAVAND - C. GOUTELARD - S. HARARI
Laboratoire d'Etude des Transmissions Ionosphériques (LETTI)
9, Ave de la Division Leclerc
94230 Cachan
France

RESUME -

L'étude présentée dans cet article porte sur une méthode de codage correcteur d'erreur adapté à un modem auto-adaptatif 1200 bits/s opérant sur une liaison ionosphérique en ondes décamétriques.
On a, dans un premier temps, mené une étude sur la répartition des erreurs à l'aide d'un simulateur sur lequel on a reproduit les caractéristiques de la propagation mesurées par une station de sondage ionosphérique par rétrodiffusion et pour des cas de brouillage divers. On a ainsi traité 27 cas différents représentant 30 millions de bits.
L'étude de la répartition des erreurs a conduit au choix des codes les mieux adaptés. Le codage retenu consiste à mettre en cascade deux codes entrelacés. L'un corrige les erreurs isolées et les petits paquets d'erreurs (code de Reed Solomon) ; l'autre, les erreurs de coupure (code de Kasami). Le rendement du système de correction est 0,55.

Une étude de l'efficacité du système de correction a été faite sur simulateur et a permis de montrer que le taux d'erreur était réduit d'un facteur égal ou supérieur à 100 dans tous les cas.
Une discussion des limites de correction que l'on peut attendre de tels systèmes est faite.

ABSTRACT -

This paper presents an error correcting system designed for a 1200 bits/s self adaptative modem operating on the HF ionospheric channel.
An analysis of error statistics has been made simulating a specific link whose characteristics had been measured before hand by a HF backscatter probe. We have treated 30 millions of bits, wich represents 27 different cases of propagation and scrambling.
The coding system wich has been chosen consists of a cascade of two codes. One corrects single error and small bursts (Reed Solomon codes), the other corrects long bursts of errors (Kasami code). The overall rate is 0,55.
An error correcting simulation has shown that in most of cases studied a ber of 10^{-4} a coding gain of a least 10^{-2} has been achieved.
Limitations of theses methods are discuted.

I. INTRODUCTION -

La transmission de données numériques par ondes décamétriques à travers le canal ionosphérique est attrayante par les avantages économiques et logistiques qu'elle offre : faibles puissances d'émission, faible coût, longueurs des liaisons, possibilités de cryptages numériques, mais par contre, les phénomènes de propagation sont la cause de complications multiples. Les variations importantes des caractéristiques du canal ionosphérique ne peuvent être prévues avec une précision suffisante pour atteindre une adaptation permanente et la part des fluctuations imprévisibles est suffisante pour laisser une grande instabilité des processus d'erreurs.

Pour pallier ces inconvénients, différentes techniques peuvent être utilisées : systèmes à débit lent, transmissions parallèles, systèmes codés. Une autre technique utilise le principe de l'auto-adaptativité que l'on retrouve sous différentes formes dans le système ADAPTICOM décrit par M.J. DITORD [1] et dans le système T.R.T. décrit par P. DAVID et J.P. VAN UFFELEN [2] qui utilisent le principe du calcul de la fonction de transfert du canal et qui conduisent à des débits importants, ou bien dans le système RAKE décrit par R. PRICE et P.E. GREEN [3] et le système KATRYN décrit par M.S. ZIMMERMAN et A.L. KIRSCH [4] qui réalisent l'adaptativité avec des principes voisins.

La présente étude porte sur la recherche de codes adaptés à un modem auto-adaptatif 1200 bits/s opérant sur une liaison à travers le canal ionosphérique. La transmission effectuée par une modulation numérique de la phase a été reproduite en laboratoire sur un simulateur. Pour définir un modèle du canal, les caractéristiques de la propagation ont été mesurées sur la liaison spécifique Rennes-Dakar par un sondeur ionosphérique à rétrodiffusion installé à Rennes.

Pour un ensemble de 27 cas de simulation échantillonnant de façon satisfaisante les conditions de propagation et de brouillage, on a étudié sur un volume de 30 millions de bits représentant 6 heures de transmission, la répartition des erreurs. Les motifs qui sont apparus ont conduit aux choix de codages possibles. Une réduction d'un facteur au moins égal à 100 de la probabilité d'erreur a été prise comme critère d'efficacité des codes. Il a conduit à l'utilisation de deux codes en cascade, Reed Solomon et Kasami, et à un entrelacement pour atteindre l'objectif fixé.

Les codages ainsi déterminés ont été réalisés au moyen d'un codeur universel qui a permis d'effectuer l'expérimentation du système complet.

Les résultats obtenus mettent en évidence l'efficacité du codage.

II. RECONSTITUTION DE LA LIAISON -

Le schéma de la figure 1 présente les éléments constitutifs de la reconstitution en laboratoire de la liaison ionosphérique.

L'analyse de la répartition des erreurs a été faite en comparant les informations issues des points B et C de la liaison. L'analyse des performances des codes est obtenue par comparaison des informations en A et D. Le fonctionnement du simulateur et du modem est présenté dans ce paragraphe. Celui du codeur décodeur sera présenté dans le paragraphe concernant l'étude du codage.

II. 1. Le modem auto-adaptatif

Le modem utilisé est celui que la société T.R.T. a construit pour ce type de liaison. Il présente les caractéristiques suivantes :

- émission en série (sur une seule porteuse),
- débit de 1200 bits/s,
- modulation par saut de phase, deux états,
- traitement du signal par égalisation auto-adaptative.

Le filtre utilisé a une structure mixte : transversale et récursive, avec décision dans la boucle (figure 2).
Les coefficients du filtre sont ajustés suivant un algorithme qui rend minimale l'erreur quadratique moyenne. Une séquence de test est émise périodiquement pour réinitialiser les coefficients en cas de désadaptation du filtre. La vitesse de modulation de 1350 bauds est donc très sensiblement supérieure au débit d'information de 1200 bits/s.

II.2. Simulation du canal ionosphérique

Soit S(t) cos 2π ft l'onde émise en modulation de phase à deux états. L'information est contenue dans la fonction S(t) qui peut prendre les deux valeurs + 1 et - 1. L'onde r(t) reconstituée par le simulateur s'écrit :

$$r(t) = \sum_i \alpha_i S(t - \tau_i) \cos \left[2\pi (f + f_{di})(t - \tau_i) \right] + n(t)$$

Dans cette expression, α_i, f_{di} et τ_i représentent respectivement l'amplitude, le Doppler et le retard de chacun des trajets ; n(t) est le bruit.
Un canal comportant trois trajets peut être reconstitué avec le simulateur. La fréquence Doppler et le retard de chacun des trajets sont programmables. La fréquence Doppler peut être réglée avec une précision de 1/100 de hertz dans la gamme 0,01 - 99Hz.
La liaison Rennes-Dakar a été choisie pour servir de base à cette étude. Les mesures du canal testé ont été faites à partir de la station de sondage du LETTI, installée à Rennes(France). Elles ont été effectuées sur trois saisons : été, équinoxe, hiver et pour quatre périodes de la journée : matin, soir, milieu de la journée et de la nuit [5].

L'analyse des résultats a conduit à retenir trois cas extrêmes de la propagation destinés à être reproduits sur simulateur en vue d'une recherche de codes pour une liaison numérique. Ces modes reproduits dans le tableau 1 sont caractérisés par les différents trajets retenus pour lesquels apparaissent les écarts de temps de groupe (retard), les décalages fréquentiels (Doppler) et les amplitudes relatives.
Le mode 1 servant de cas de référence, le mode 2 correspond à un type de propagation se produisant le matin et le mode 3 à un type de propagation se produisant le soir.

Tableau 1 : SELECTION DES MODES DE PROPAGATION

Mode de propagation	Trajet	Amplitude relative (dB)	Doppler (Hz)	Retard (ms)
Mode 1	1	0	-	-
Mode 2	1	0	0,2	0
	2	- 3	0,4	0,8
	3	- 6	0,9	1,2
Mode 3	1	0	- 0,3	0
	2	- 2	- 0,5	0,8
	3	- 4	- 0,8	2,0

Des enregistrements de 1Mbits ont été faits pour ces trois modes de propagation en introduisant des perturbations caractéristiques des ondes décamétriques

- bruits atmosphériques naturels,
- brouillages introduits par des émetteurs : brouilleurs à spectre très étroit (télégraphie manuelle) ; brouilleurs à spectre étroit (télégraphie automatique) ; brouilleurs à spectre large (liaisons phoniques BLU).

Des enregistrements ont également été faits en présence de bruit blanc stationnaire.

Le niveau de bruit a été fixé de manière telle que le taux d'erreur de chacun des enregistrements ne dépasse pas 10^{-3} (hors période de perte de synchronisation). Le but de cette étude étant de déterminer les codes correcteurs d'erreurs les mieux adaptés à ce type de liaison et le rendement demandé pour ces codes étant de 0,5, la correction d'erreur devient incertaine au-dessus d'un taux d'erreur de 10^{-3}. C'est sans aucun doute la limitation la plus sévère à l'étendue de cette étude : d'autres essais ayant montré que lorsque la liaison est mauvaise le taux d'erreur peut devenir supérieur à 10^{-3}.
Il y a lieu alors d'adopter une autre stratégie (code de rendement plus faible ou demande de répétition) dans l'utilisation du modem.

III. ETUDE DE LA REPARTITION DES ERREURS ET DU TAUX MOYEN D'ERREUR - [6]

Le dépouillement des enregistrements effectués a permis de déterminer le taux moyen d'erreur en fonction du rapport signal à bruit et la répartition des erreurs en fonction du mode de propagation et de la nature du bruit.

III.1. Taux moyen d'erreur en fonction du rapport signal à bruit (S/N)

Cette analyse ne peut être faite que lorsqu'il est possible de déterminer le rapport signal à bruit, c'est-à-dire dans le cas où le bruit est stationnaire. Le bruit est alors fourni en laboratoire par un générateur. Il a une densité spectrale constante dans la bande de fréquence utilisée par le récepteur, il est stationnaire, à distribution gaussienne.

Dans les autres cas, la puissance du bruit capté avec una antenne est très fortement fluctuante. Pour les transmissions à trajets multiples, la puissance du signal a été prise égale à celle transportée par le trajet de plus grande amplitude.

L'analyse des courbes de la figure 3 montre qu'entre le cas de trajet simple et le cas à trois trajets le plus défavorable, la probabilité d'erreur est multipliée par un facteur compris entre 20 pour (S/N) = 9 dB et 30 pour (S/N) = 10 dB.

III.2. Répartition des erreurs

Un paquet d'erreurs est un ensemble d'éléments binaires commençant et finissant par une erreur et dans lequel la densité d'erreurs est supérieure ou égale à une valeur d.
Le nombre de paquets définis ainsi est une fonction du nombre et de la répartition des erreurs dans l'enregistrement mais aussi du paramètre d. Il a donc fallu déterminer pour chaque enregistrement une densité d'erreur significative du mode de groupement des erreurs. La valeur retenue pour la plupart des enregistrements est d = 0,4.
Les figures 4, 5, 6 représentent pour chacun des modes de propagation les répartitions des paquets d'erreurs en fonction de la perturbation dominante.
Dans ces figures, pour les courbes décrivant la répartition des erreurs, les longueurs des paquets d'erreurs sont représentées :

- toutes les unités pour $1 \leqslant l \leqslant 10$
- toutes les dizaines pour $11 \leqslant l \leqslant 100$. A l'intérieur d'une dizaine le nombre de paquets d'erreurs est cumulé
- toutes les centaines pour $101 \leqslant l \leqslant 1000$

Comparaison des propagations à trajet simple et à trajets multiples

L'analyse des résultats fait apparaître que pour un taux d'erreur donné, la répartition des erreurs est plus mauvaise dans le mode 3 que dans le mode 2 et dans le mode 2 que dans le mode 1. La longueur des paquets d'erreurs peut aller jusqu'à des valeurs voisines de 1000 éléments binaires.

Le but de ce travail n'était pas d'étudier l'influence des divers paramètres (amplitude, retard, doppler) d'un canal ionosphérique, sur la qualité d'une transmission d'information numérique. En effet, pour réaliser cela, il aurait fallu que les essais soient effectués en faisant varier indépendamment l'une de l'autre chacune de ces grandeurs. Or, dans les mesures effectuées, les trois paramètres du canal changent simultanément lorsqu'on passe d'un mode à l'autre.

Néanmoins, on peut remarquer (cf. tableau 1) que dans les modes 2 et 3, les dopplers sont du même ordre de grandeur. Par contre, la différence d'amplitude entre le trajet 1 et les trajets 2 et 3 est plus grande dans le deuxième mode que dans le troisième : c'est donc dans ce dernier cas que le brouillage du trajet 1 par les trajets 2 et 3 est le plus important. Il apparaît donc logique de trouver des résultats dont l'analyse est conforme à cette constation.

Influence de la nature des brouilleurs

Si on exclut de l'analyse le mode 3 de propagation pour lequel l'interférence entre les trois trajets est l'élément primordial de la dégradation de la liaison, on constate que pour un taux d'erreur donné les paquets d'erreurs obtenus lorsque le bruit est non blanc sont nettement plus longs que lorsque le bruit est blanc. Par contre, le nombre et la diversité des enregistrements ne sont pas suffisants pour établir une différence entre les différents types de perturbations (autres que le bruit blanc).

La structure du récepteur intervient également dans la répartition des erreurs. En effet, une modification importante de la valeur des coefficients des filtres de l'égaliseur sous l'effet d'une perturbation peut entraîner la présence d'un paquet d'erreurs pendant le temps mis par le système pour converger vers une égalisation correcte.

IV. CODAGE -

L'objectif visé pour la correction a été de réduire le taux d'erreur d'un facteur au moins égal à 100 avec des codes correcteurs dont le rendement soit supérieur à 0,5.

L'adaptation du codage au système de transmission doit être effectué à partir des motifs de répartition des erreurs. De plus, il est important de réduire le délai de restitution des symboles d'information pour ne pas introduire des délais de transmission prohibitifs.

L'examen des résultats de mesure présentés dans les figures 4, 5 et 6 montre l'existence de deux types d'erreurs :

- dans tous les cas, il apparaît des erreurs isolées ou de petits paquets d'erreurs, de longueur inférieure à 10 eb (élément binaire) qui peuvent être corrigés par un premier type de code.
- Dans certains cas traités, il apparaît fréquemment de longs paquets d'erreurs, atteignant plusieurs centaines de symboles qui nécessitent un second type de code capable de corriger de grandes erreurs de coupure.

Ces deux types d'erreurs rencontrés ne peuvent être corrigés par un seul type de code avec un rendement supérieur à 0,5. Il a donc été nécessaire de cascader deux codes spécifiques.

IV.1. Codes de Kasami

Les codes de Kasami, sont des codes binaires cycliques qui assurent une protection maximale contre les paquets d'erreurs. Ils peuvent corriger un paquet d'erreurs de longueur b par bloc de n eb. Pour un code cyclique (n,k) on sait que b est borné par $(n - k)/2$, et on introduit souvent le paramètre $\gamma = n - k - 2b$ qui caractérise les performances du code. Pour un rendement donné, les codes de Kasami sont ceux qui possèdent la plus petite valeur de γ.
La capacité de correction de paquets b est de l'ordre de 6 eb pour tous les codes de Kasami. Pour atteindre la capacité de correction de paquets nécessaire on est amené à entrelacer le code N fois, de telle sorte que sur Nn bits le système corrige un paquet de Nb eb. Si l est la longueur de paquets à corriger, on choisit N de manière à avoir $Nb > l$.

L'entrelacement introduit une contrainte sur les bits à l'extérieur du paquet. Parmi les Nb eb des N blocs entrelacés les erreurs doivent être incluses dans un paquet de longueur Nb au plus. Ceci suppose qu'entre les paquets il y ait de longs intervalles sans erreurs appelés espaces de garde.
L'étude de la répartition des erreurs montre que le pas d'entrelacement nécessaire pour obtenir la correction des erreurs doit être de l'ordre de 1000.
Cet entrelacement par la méthode des 2 matrices entraîne un retard à la restitution, qui est de l'ordre de 1000 blocs.
Des méthodes utilisant des RAM permettent de diminuer sensiblement ce retard. Ce sont de telles méthodes qui devraient être utilisées dans le cas d'une implantation en vue d'une exploitation non expérimentale.

IV.2. Codes de Reed Solomon

Les codes de Reed Solomon ont été introduits pour corriger les erreurs isolées et les petits paquets d'erreurs. Ce sont des codes cycliques définis sur les extensions F_{2m} du corps F_2 (F_p désigne un corps d'ordre p). Les éléments de F_{2m} sont appelés symboles.
La représentation d'un symbole de F_{2m} est faite par un m-uplet binaire. Ces codes correcteurs de symboles erronés corrigent les paquets d'erreurs inclus dans les représentations de symboles.
Ainsi, un code de Reed Solomon corrigeant t symboles corrige, en représentation binaire toutes les erreurs sur les bits représentant au plus t symboles, c'est-à-dire t paquets d'erreurs de longueur maximale m. La compatibilité avec les codes de Kasami a conduit à prendre m = 4 ou 8 qui aboutit à une proportion importante de correction des petits paquets d'erreurs et des erreurs isolées.

IV.3. Cascade des codes et entrelacement

Les codes et l'entrelacement ont été réalisés selon le mode résumé sur la figure 7 : les données sont d'abord codées par le code de Kasami et entrelacées, puis codées par le code de Reed Solomon et entrelacées à nouveau.
A la réception après les désentrelacements, le code de Reed Solomon corrige d'abord les petits paquets d'erreurs puis le code de Kasami corrige les paquets de grande longueur.

IV.4. Discussion sur le choix des codes

Les caractéristiques des erreurs nous ont imposé ce choix, au prix d'un système de correction en cascade, et d'un fort entrelacement.

Si la contrainte sur les rendements pouvait être assouplie, un système constitué d'un seul code de bon rende ent de type Reed et Muller, entrelacé aurait été susceptible de fournir les données avec le pire en taux d'erreur souhaité. De même, certains codes convolutionnels, à condition que l'on sache conserver la synchronisation du système, tâche très ardue dans le cas présent, pourraient répondre aux besoins du problème.

V. ESSAIS EXPERIMENTAUX -

Deux séries de mesures expérimentales ont été effectuées.
La première a consisté à tester les codages dont les caractéristiques entre dans le gabarit défini dans le paragraphe précédent.
La seconde a été effectuée avec les meilleurs codes.

V.1. Codages expérimentés

Compte tenu des caractéristiques générales des codes possibles, on a retenu pour l'expérimentation :

- deux codes de Reed Solomon de longueur 32 octets corrigeant l'un 2 octets, l'autre 3 octets et entrelacés 2, 3 ou 4 fois.
- Trois codes de Kasami :
  * un code de longueur 50 corrigeant un paquet de longueur 8 entrelacé 100, 125, 150 fois ;
  * un code de longueur 34 corrigeant un paquet de 6 erreurs entrelacé 150, 175, 200 fois ;
  * un code de longueur 27 corrigeant un paquet de longueur 5 entrelacé 150, 200 et 250 fois.

Ces codes, de rendement décroissant, nécessitent un espace de garde de longueur décroissante, tous les autres paramètres restant fixes.
Les cas étudiés sont résumés dans le tableau II.

Tableau II : PARAMETRES DES CODES

	n	k	k/n	Capacité correction	Pas d'entrelacement
Reed Solomon	32	26	0,81	t = 3	2, 3, 4
Kasami	50	34	0,68	b = 8	100, 125, 150
Codage 1					
Reed Solomon	32	28	0,87	t = 2	2, 3, 4
Kasami	34	22	0,65	b = 6	150, 175, 200
Codage 2					
Reed Solomon	32	28	0,87	t = 2	2, 3, 4
Kasami	27	17	0,65	b = 5	150, 200, 250
Codage 3					

V.2. Essais des codes

Pour ces essais un codeur a été construit au LETTI. Avant d'exposer les résultats relatifs aux essais, on présente la réalisation des opérations de codage et décodage.

V.2.1. Codeur et décodeur

Les deux codes sont cycliques, l'un binaire (code de Kasami), l'autre q-aire (code de Reed Solomon), pour lequel $q = 2^p$ et $p = 8$. Le codeur réalisé permet de créer ces deux codes avec un choix très étendu de leurs paramètres.
La correction des erreurs et le décodage sont réalisés en logiciel.

V.2.2. Description et caractéristiques du codeur [7]

Les fonctions à réaliser dans le codeur sont représentées sur le schéma de la figure 8.
Les paramètres des codes et les pas d'entrelacement n'étant pas des grandeurs figées, le codeur a été conçu de façon à pouvoir les modifier de manière simple, c'est pourquoi nous nous sommes orientés vers une structure programmée à microprocesseurs.
Pour compenser le manque de rapidité de la solution retenue, le système réalisé est un multiprocesseur composé de trois microprocesseurs pouvant travailler simultanément.
L'architecture du codeur est représentée figure 9.

Les unités de calcul 1 et 2 (UC1, UC2), ainsi que l'unité de sortie (UC3) sont constituées par un micro-calculateur, ses mémoires RAM de travail et ses mémoires ROM de programme. M_{1a}, M_{1b} sont les mémoires RAM de travail du codage et entrelacement Kasami ; quand l'une est utilisée en écriture par UC1, l'autre est utilisée en lecture par UC2. M_{2a} et M_{2b} sont affectées au code Reed Solomon; leur mode de fonctionnement est le même que celui de M_{1a} et M_{1b}.
L'unité de calcul UC3 commande l'ensemble du codeur de façon que le débit d'information en sortie ne soit pas ininterrompu.

Les deux micro-calculateurs utilisés pour la réalisation du codeur ont été réalisés avec des microprocesseurs de la famille 6800 travaillant sur des mots de 8 bits. Cette technologie limite la taille des symboles utilisables à 8 éléments binaires, taille adaptée dans le cas présent pour le code de Reed Solomon. Les mémoires de codage utilisées ont une capacité de 4 096 octets, ce qui permet pour chaque code de réaliser des traitements codage-entrelacement sur des longueurs maximales de 32 768 eb.

Les possibilités de programmation permettent d'obtenir différents types de codage sur des codes binaires ou q-aires tels que $q = 2^p$ et $1 \leqslant p \leqslant 8$. Chaque bloc de calcul peut être programmé de deux façons différentes :

- pour la génération de codes binaires. Dans ce cas la longueur n du code et le pas d'entrelacement I sont limités par la relation :

(1) $\quad I.n \leqslant 32\,768$ eb

- pour la génération de codes q-aires. Dans ce cas, la longueur du code de N symboles de p éléments binaires et le pas d'entrelacement L sont limités par la relation :

(2) $\quad L.N \leqslant 4\,096$ symboles.

La longueur des symboles p est limitée à 8.

Le codeur étudié peut être utilisé dans différentes configurations. Les deux blocs de calcul peuvent être rendus indépendants et les pas d'entrelacement réglables peuvent conduire avec L ou I = 1 à supprimer l'entrelacement. Enfin tous les codes définis par un polynôme générateur et respectant les conditions (1) ou (2) sont programmables.

Les versions principales auxquelles le système peut aboutir sont donc :

- génération d'un code binaire simple ou entrelacé. Le débit binaire maximal est alors de l'ordre de 10 000 db/s ;
- génération d'un code q-aire simple ou entrelacé. Le débit binaire maximal est alors de l'ordre de 6 700 db/s ;
- génération de deux codes en cascade, entrelacés ou non.

4.4. Décodage

Pour cette expérimentation plusieurs types de codage sont utilisés afin d'en déterminer le meilleur. Dans ces conditions il ne peut être envisagé de construire un décodeur programmable compte tenu de la complexité à laquelle cette solution conduirait.
La détection des erreurs est donc effectuée par ordinateur à l'aide de méthodes conventionnelles.

La méthode de correction employée pour les codes Reed Solomon est la méthode classique commune à [illegible] [8]

Les différentes étapes en sont les suivantes :

- calcul des coefficients du syndrome ;
- détermination du polynôme localisateur d'erreur ;
- calcul de la position et de l'amplitude de chacune des erreurs.

La méthode de correction employée pour les codes de Kasami est celle du "piégeage" d'erreurs. Dans son principe, elle consiste à effectuer des rotations successives du vecteur reçu jusqu'à ce que le paquet d'erreur soit contenu dans les bits de redondance ; en pratique ces rotations sont effectuées sur le syndrome.

V.3. Résultats

Une part des résultats obtenus est résumée dans le tableau III qui représente l'estimation la plus pessimiste de la correction obtenue par les meilleurs codages appliqués aux cas présentés au paragraphe II pour l'étude des répartitions d'erreur.

On a reporté sur ce tableau le taux d'erreur avant correction, le nombre d'erreurs isolées et la longueur du bloc erroné le plus long qui donnent une idée de la distribution des erreurs.
Les deux dernières colonnes donnent le taux d'erreur après correction et le gain obtenu. Lorsqu'il est porté 0 dans la colonne probabilité d'erreur, cela signifie qu'il ne subsiste aucune erreur dans le bloc de 1 million de bits traité et que le taux d'erreur est inférieur à 10^{-6}.
L'enregistrement 12 qui comporte un paquet d'erreur de longueur 23 157, dû à une désynchronisation du modem n'a pas été pris en compte.

Sur 23 cas traités, les résultats font ressortir que :

- 20 ont une probabilité d'erreur après correction inférieure à 10^{-6} et le gain apporté par le codage est supérieur à 100 ;
- 1 cas, le cas 14, a une probabilité d'erreur après correction égale à $5\ 10^{-6}$ mais le gain du codage est encore supérieur à 100 ;
- pour 2 cas, cas 18 et 13, le gain du codage est inférieur à 100. Ces cas contiennent des paquets d'erreurs de longueur maximale voisine de 700.

Ces résultats mettent en évidence l'importance de la répartition des erreurs. En effet, le codage permet de corriger certains enregistrements comportant des paquets d'erreurs pouvant atteindre 963eb (cas 17) sans qu'on puisse cependant assurer de corriger des paquets d'erreurs de longueur inférieure (cas 14, 18 et 19).

VI. CONCLUSION -

Les résultats de cette étude montrent qu'il est possible, à partir de la répartition des erreurs, de trouver pour un modem auto-adaptatif des codages qui effectuent la correction tant que le modem demeure synchronisé.
Les codages retenus ont un rendement de 0,55 et permettent d'obtenir une liaison de qualité téléinformatique à 600 bit/s à partir d'un modem à 1200 bit/s.
La méthode présentée peut être appliquée à d'autres types de modem et les mêmes codes sont utilisables si la répartition des erreurs est identique.

Cette étude a été réalisée dans le cadre de contrats de la Direction des Recherches, Etudes et Technique de la Délégation Générale à l'Armement (Contrats 77/1083 et 80/34323) qui nous a aimablement autorisée à publier cet article.

Tableau III : Taux d'erreurs PE obtenus avant et après correction
Bite error rate PE before and after correction

N°	Type de brouillage	Mode de propagation	Avant correction			PE 10^{-6} après correct.	Gain ou PE
			PE 10^{-6}	Nbre erreurs isolées	Longueur max		
1	Bruit blanc	Mode 1	1 450	1 445	2	0	$q \geq 100$
2			439	437	2	0	$q \geq 100$
3			15	15	1	0	$Pe < 10^{-6}$
4	Parasites naturels		78	78	1	0	$Pe < 10^{-6}$
5			17	17	1	0	$Pe < 10^{-6}$
6	Graphie manuelle		247	181	5	0	$q > 100$
7	Graphie automatique		721	705	7	0	$q > 100$
8	Phonie		111	53	52	0	$q > 100$
9	Bruit blanc	Mode 2	603	296	10	2	$q > 100$
10			175	117	5	0	$q > 100$
11			128	88	15	0	$q > 100$
12	Parasites naturels		11 646	384	23 157	-	-
13			687	176	511	0	-
14	Graphie manuelle		715	138	278	5	$q > 100$
15	Graphie automatique		708	171	599	0	$q > 100$
16	Phonie		106	70	15	0	$q > 100$
17	Bruit blanc	Mode 3	923	178	963	0	$q > 100$
18			586	192	687	48	$q = 19,2$
19	Parasites naturels		793	197	732	64	$q = 12,4$
20			605	77	879	0	$q > 100$
21			726	83	875	0	$q > 100$
22	Graphie manuelle		733	271	493	0	$q > 100$
23	Graphie automatique		572	64	916	0	$q > 100$
24	Phonie		934	87	289	0	$q > 100$

R E F E R E N C E S

[1] M.J. DILORD
A new method of high speed adaptative serial communication through any time variable and dispersive medium. Design and performance of the new adaptative serial data modem on a simulated time variable multipath HF link.
First IEEE Communication convention June 1965 Réf. GCGA 2 and 3.

[2] G. DAVID, J.P. VAN HUFFELEN
Description d'un dispositif auto-adaptatif pour transmission de données sur liaisons ionosphériques.
Symposium Agard of Electromagnetic wave propagation panel on radio systems and the ionosphere
Athènes (Grèce) Mai 1975.

[3] R. PRICE, PE GREEN
A communication technique for multipath channels.
Proceeding of the IRE March 1958

[4] M.S. ZIMMERMAN, A.L. KIRSCH
The AN/GSC-10 (Katryn) variable rate data modem for HF radio
IEEE Com. Vol Com. 15 N° 2 April 1967

[5] C. GOUTELARD
Caractérisation du canal ionosphérique dans les transmissions numériques hautes fréquences.
Revue du CETHEDEC, Fr (4ème trimestre 1979) NS. 79. 2

[6] F. CHAVAND, C. GOUTELARD, S. HARARI
Système de protection contre les erreurs pour la liaison ionosphérique.
Annales des Télécommunications tome 37 N° 5-6 Mai-juin 1982

[7] F. CHAVAND, R. GALLO, C. GOUTELARD
Codeur programmable pour codes cycliques binaires et q-aires.
Revue du CETHEDEC, 4° trimestre 1981 NS 81. 2

[8] E.R. BERLEKAMP
Algebraic Coding Theory
New-York, Mc Graw-Hill 1966

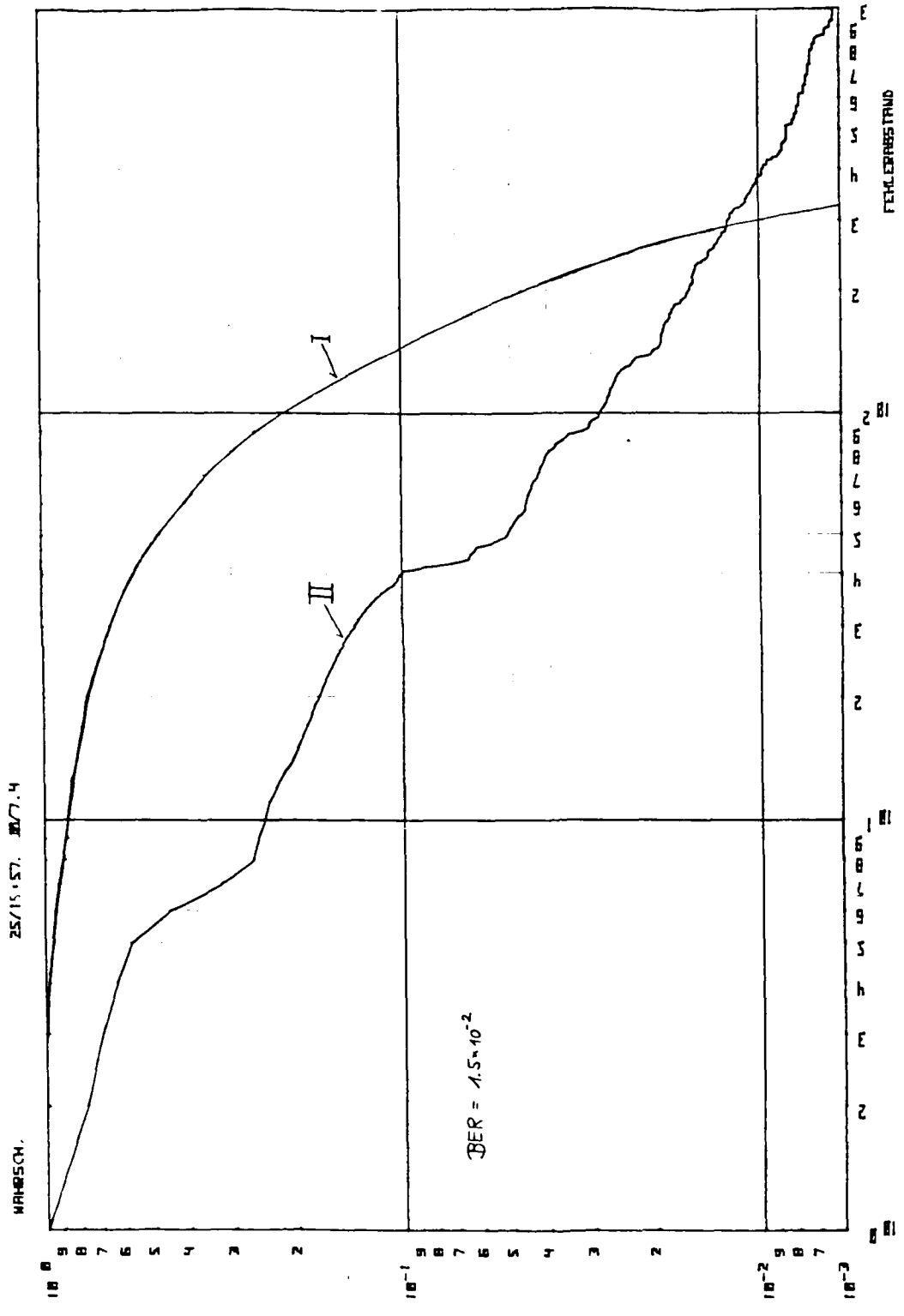

Fig.7 Error rate gap distribution

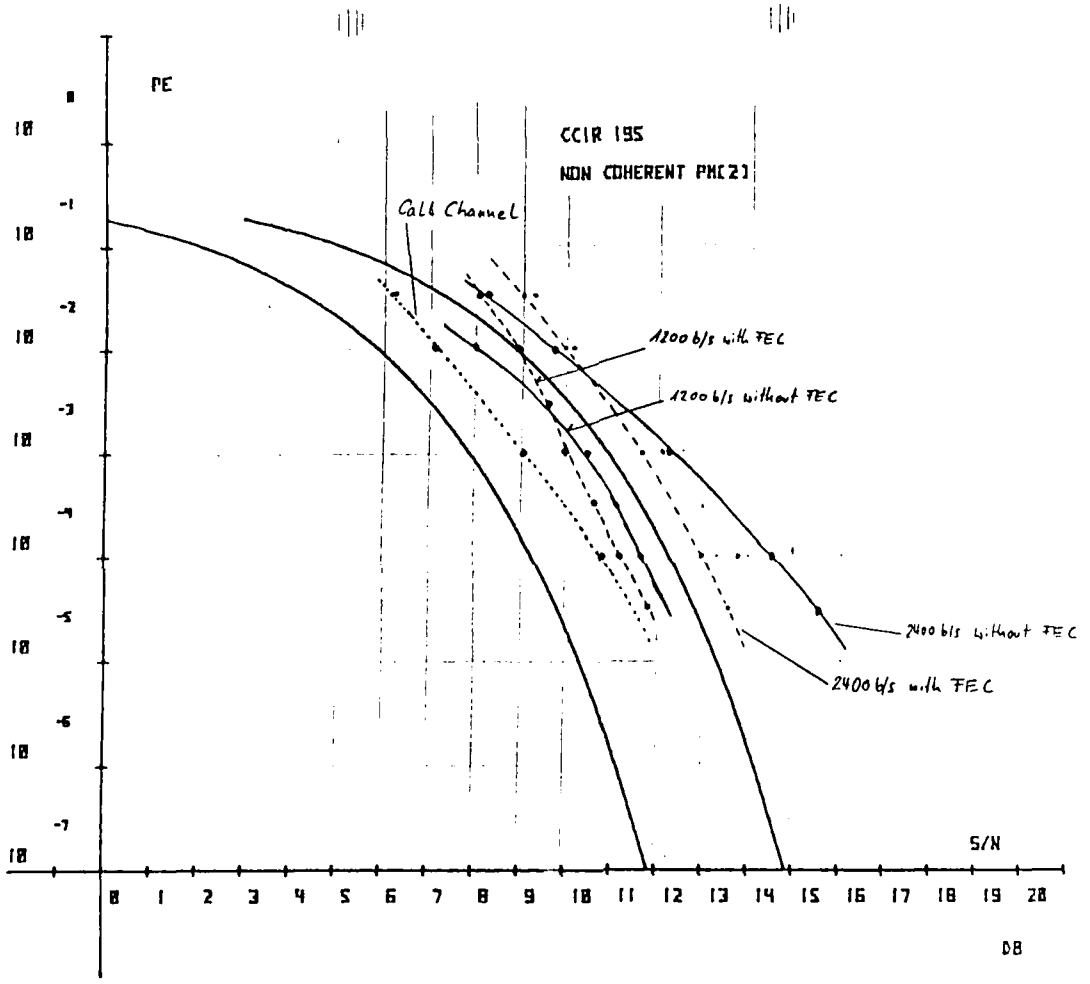

Fig.6 Error rate versus signal noise ratio

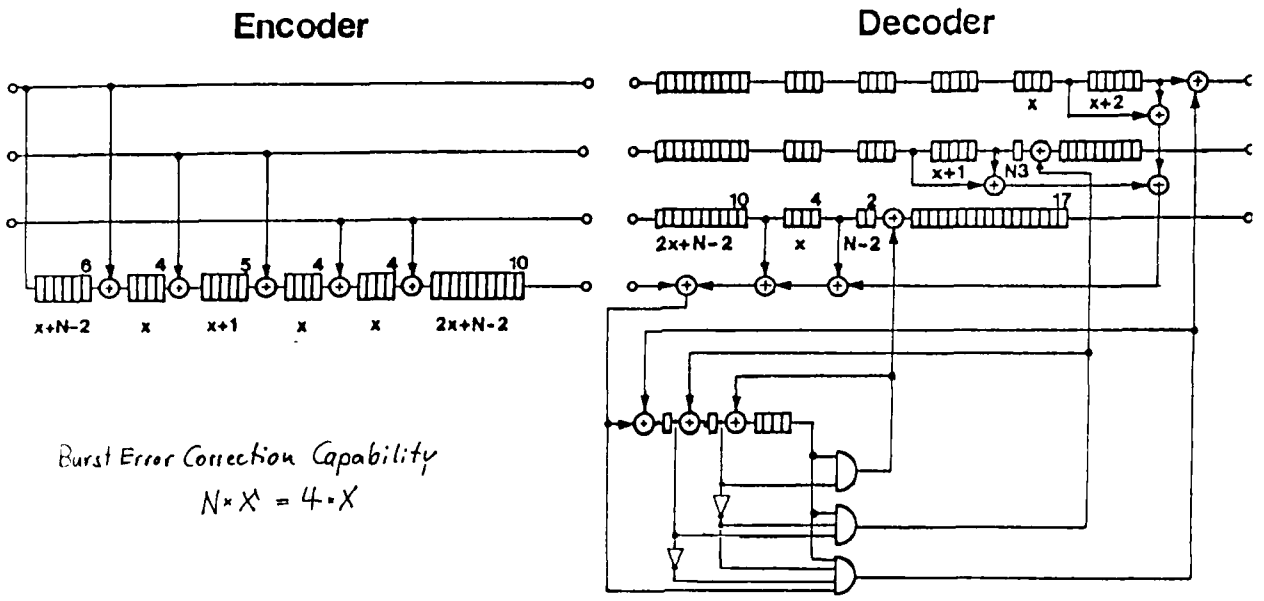

Fig.4 Convolutional code with rate 3/4 for burst error correction

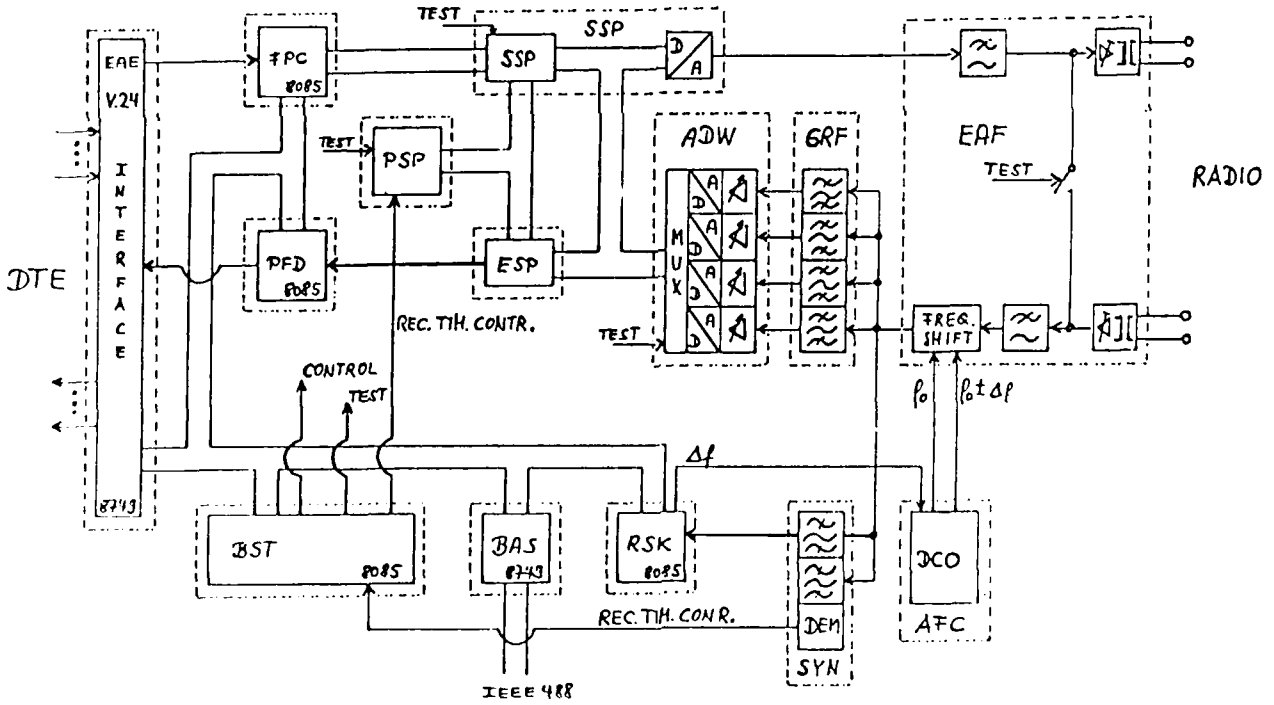

Fig.5 Block diagram HF – Modem 2400

KW-Modem 2400
Korrelation über orthogonale Frequenzen

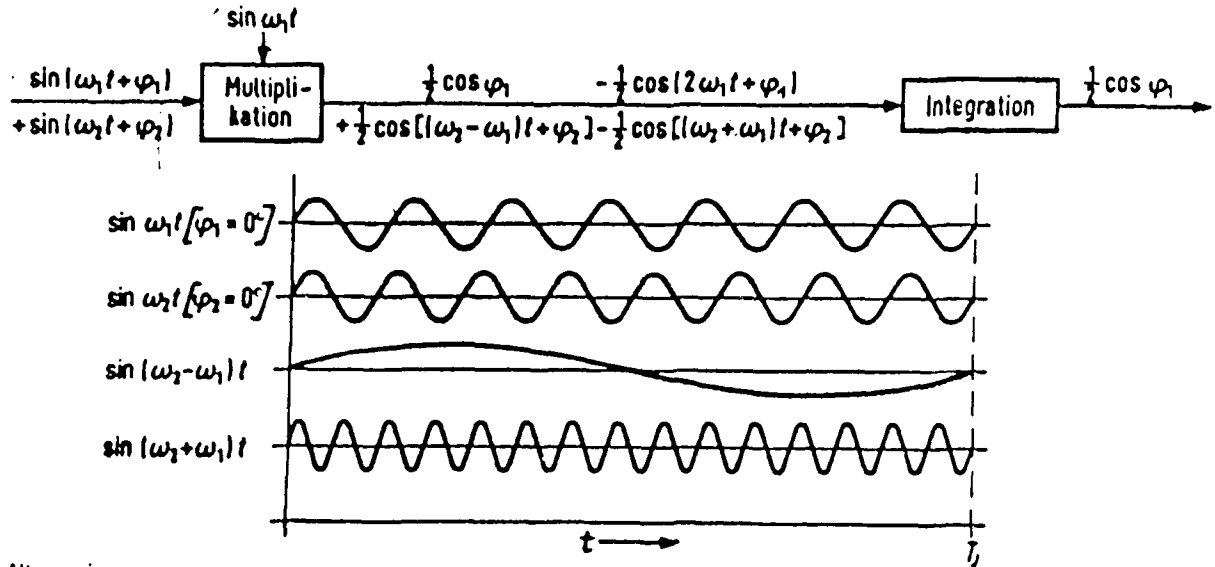

Allgemein:

Multiplikation:

$$v(t)=\sum_{i=1}^{k} u_i(t)=\sum_{i=1}^{k}\left\{\sin(\omega_1 t+\varphi_1)\cdot\sin\omega_2 t\right\}=$$
$$=\sum_{i=1}^{k}\left\{\tfrac{1}{2}\cos[(\omega_1-\omega_2)t+\varphi_i]-\tfrac{1}{2}\cos[(\omega_1+\omega_2)t+\varphi_i]\right\}$$

$$i=k:\quad u_i(t)=\tfrac{1}{2}\cos\varphi_2-\tfrac{1}{2}\cos(2\omega_2 t+\varphi_2)$$

Integration

$$U_j=\frac{1}{T_j}\int_0^{T_j} v(t)\,dt=\tfrac{1}{2}\cos\varphi_i$$

$$\omega_i=m\cdot\frac{2\pi}{T_j}\qquad i,k,m=1,2,\ldots n$$

Fig.2 Principle of demodulation

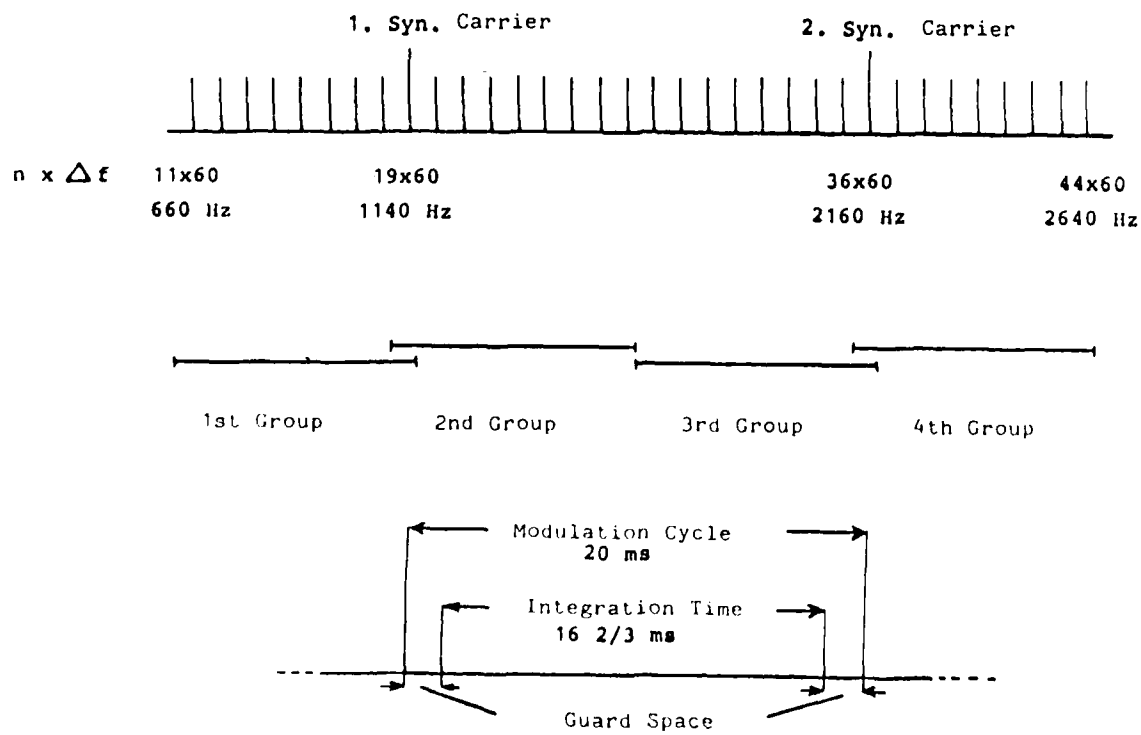

Fig.3 System parameters

TDPSK

receiver : $\phi_R(n) = \phi_T(n) + \phi_E(n)$

$\phi_R(n+1) = \phi_T(n+1) + \phi_E(n+1)$

information : $\phi_I = \phi_R(n+1) - \phi_R(n) = \phi_T(n+1) + \phi_E(n+1) - \phi_T(n) - \phi_E(n) = \underbrace{\phi_T(n+1) - \phi_T(n)}_{\text{unknown}} + \underbrace{\phi_E(n+1) - \phi_E(n)}$

ϕ_T transmitted phase

ϕ_R received phase

ϕ_E error phase

ϕ^R reference phase

ϕ^D data phase

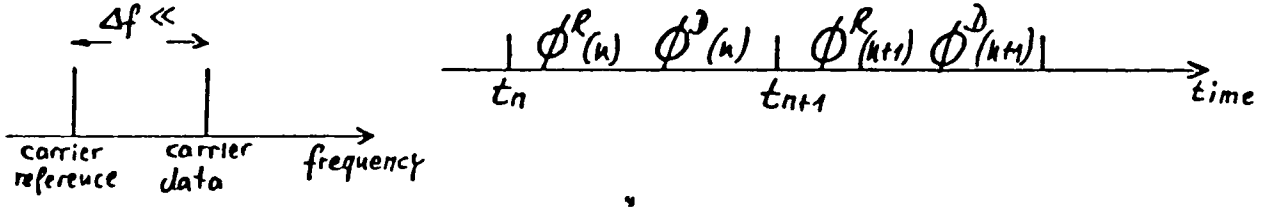

receiver : $\phi_R^D(n) = \phi_T^D(n) + \phi_E^D(n)$

$\phi_R^R(n) = \phi_T^R(n) + \phi_E^R(n)$

information : $\phi_I = \phi_R^R(n) - \phi_R^D(n) = \underbrace{\phi_T^R(n) - \phi_T^D(n)}_{\approx \text{zero}} + \underbrace{\phi_E^R(n) - \phi_E^D(n)}$

FDPSK

Fig.1 TDPSK – FDPSK

in Fig. 8 + 9 error rates per block are seen. These measurements are very interesting in the light of data transmission protocol, for example HDLC. A HDLC protocol with a maximum data length of 128 bytes (normally found in data exchange networks) would never work satisfactorily if the bit error rate comes from statistically independent errors in the order of 10exp(-3) hampering the throuput. From the measurements can be seen that up to 80 percent throughput are possible although the bit error rate is 10exp(-2). That is because of the greater channel capacity of burst error channels (c) than that of gaussian channels. Fig. 10 + 11 give an overwiew of the measurements with error rates per block.

Conclusion

From the results is seen that a parallel modem with FDPSK and FEC is capable of transmitting bitrates up to 2400 b/s over HF links. Further studies are needed to investigate suitable data transfer protocols for such links.

Literature

1) Porter, J.C. Error Distribution and Diversity Performance of a Frequency Differential PSK HF Modem IEEE Trans. Comm. COM-16(1968)p.p. 567-575

2) Walker, J.F. The Error Performance of a Class of Binary Communications Systems in Fading and Noise IEEE Trans. Comm. Syst. Vol CS-12,p.p. 28-45, Mar 1964

3) MIL-STD-188C

4) Heitmann, J., Siglow, J. and Tannhaeuser, A. Digitale Signalsynthese für Datenübertragung auf Kurzwelle ntz 34(1981) Heft 8, p.p. 504-507

5) Van Duuren, H.C.A. Error Probability and Transmission Speed on Circuits using Error Detection and Automatic Repetition of Signals IRE Trans. on Comm. Syst. (1961) p.p. 38-50

6) Markwitz, W. Automatische Fehlerkorrektur auf zeitig gestörten Verbindungen in Daten- und Funknetzen ntz 31(1978) Heft 4, p.p. 274-280

7) Filter, J.H.J., Arazi, B. and Thomson, R.J.W. The Fadeogram, a Sonogram-like Display of the Time Varying Frequency response of HF-SSB Radio Channels IEEE Trans. on Comm. Vol COM-26, No 6, June 1978

8) Büding, H. and Markwitz, W. Wirksamkeit gespreitzter, rekurrenter Codes bei Störungen eines realen Kanals und eines entsprechenden Kanalmodells AEÜE 34(1980) Heft 6, p.p. 238-242

9) Hagenauer, J. Zur Kanalkapazität bei Nachrichtenkanälen mit Fading und gebündelten Fehlern AEÜE 34(1984) Heft 6, p.p. 229-237

To do this in every modulation cycle, 16 samples of the 2nd synchronization carrier are taken to approximate a sinusoid. The approximated values are filtered and used to compute the frequency difference. A digital controlled oscillator (DCO) uses this difference to automatically compensate for the frequency error.

5 of the samples are taken for a FFT to compute the phase (0 or 180 degrees) of the synchronization carrier bearing the call information. The interpretation of the call information and the corresponding call procedure is realized in the central mode control processor.

The measuring of frequency and phase for the AFC and call procedure is implemented in a microprocessor 8085.

FEC - Forward Error Correction

In HF channels the bit error rate is considerably higher than in other channels, for example wire links. This is the reason for introducing error correction procedures in the modem. There are in principle two solutions to this problem, the first is ARQ and the second FEC (5,6). The ARQ is more related to the procedure in the DTE (data terminating equipment) and normally implemented there, therefore FEC was chosen for the modem. The needed redundancy is accomodated in added carriers. The HF channel is a typical burst error channel resulting from fadings. A suitable FEC code has to counteract this. The used FEC code is able to correct burst errors. It is a convolutional code with rate R = (N-1) / N = 3/4 with a burst error correction capability of N * X = 4 * X. X is a variable parameter (diffusing factor) and controls the costrainth length. The information and redundancy bits used in decoding and correction are diffused in time. A schematic representation of the coder and decoder is seen in Fig. 4. Each of the parallel channels is provided with FEC, that means the error correction is not done in the high data rate of 2400 b/s but in the modulation rate of 50 b/s. In this case the correcting ability is better because of the shorter bursts in the slow channels. The advantage exists due to the behaviour of the selective fadings which sweep through the transmission band and have shorter influence on each channel (7).

Remote Control

The modem is programmable via an IEEE 488 bus. It is possible to control all front panel and internal switch settings. Furthermore internal modem status can be transmitted to the bus controller. This enables the modem to operate in controlled radio stations, where a change of internal parameters and remote control are needed.

Blockdiagram of the Modem

A blockdiagram of the modem is hown in Fig. 5. The Interface to the DTE corresponds to CCITT V.24.

Firstly the transmission path is described. From the interface (EAE) the data is fed to the FEC and phase coder (FPC). On the EAE module a processor (8749) controls the V.24 interface and the control to the HF equipment and contains various functions for BITE (Built in Test Equipment). The FEC and phase coder is implemented in a microprocessor 8085 and controls the transmission signal processor (SSP) providing this processor with the computed phases through DMA in every modulation cycle. Through a D/A-converter and a low pass filter with matching to the radio transmitter (EAF) the signal leaves the modem.

The received signal is passed from the matching circuit and AFC (EAF) to the group filters with delay time compensation (GRF) and then to the gain control amplifiers and A/D-converters (ADW). The division of the voice band into four groups takes a burden off the correlators and decreases the effects of selective fadings. In the reception signal processor (ESP) the correlation is done (multiplication and integration). The computed phases are transferred to the phase and FEC decoder (FPD) through DMA in every modulation cycle. This is also implemented in a 8085. The decoded data are transmitted to the DTE via the V.24 interface (EAE).

The signal for the synchronization is fed through a narrow band filter and demodulator (SYN) to the digital low pass filter in the central mode control processor (BST). This processor controls the reception clocks in the main clock generator (TGT). The carrier in the 2nd narrow band filter (SYN) is modulated with the call information and is also used for AFC. The demodulation of the call is done by means of a FFT (BSK), implemented in a 8085. The frequency difference delta f controls a digital oscillator (DCO) on the AFC module for the frequency shift (SAF).

All the control functions (the various modes etc.) and the call procedures are also realized in a 8085 (BST).

Laboratory Measurements

Fig. 6 shows the bit error rate with and without FEC (additive white gaussion noise) at various data rates and for the call channel.
These bit error rates correspond to other modems, for example on wire links. The theoretical curve is taken from CCIR Rep. 146.

Field Tests

The results are from two distinct links, 40 and 1200 km. The transmitter power was switchable between 75 and 400 watt. The used antennas were wide band dipole, frame antenna and whip antenna. The average bit error rate was between 1oexp-2 and 1oexp-3. The results are divided into error structure measurements and measurements of average bit error rate. The figures show a selection of the measurements.

From the diagram of the error free gap distribution (Fig. 7) it is seen that the channels are fading channels with burst errors, i.e. the errors are statistically dependent (7); curve I shows the statistically independent distribution with the same bit error rate. The steep declinations in curve II are from the often or too often occuring error free gaps. From this behaviour the diffusing factor of the FEC can be derived. In the development phase of a modem such measurements are useful to determine the behaviour of distinct carriers or of the demodulation procedure.

The Principle of Demodulation

For decoding the information bits the phases of the carriers must be measured and the phase difference between two adjacent carriers computed. Filtering of the carriers is too complicated because of the small difference in frequency. Therefore a correlation technique is introduced, needing orthogonal carriers, i.e. the carriers have to be a multiple of a common fundamental frequency. This fundamental frequency is also the difference between the carriers, see Fig. 3.

In the demodulator the incoming sum of carriers is mulitplied by the quadrature components of the reference carriers and then integrated. The multiplication causes sums and differences of the different frequencies which are also orthogonal and disappear through the integration, when the integration time is equal to the period of the fundamental frequency, see Fig. 2.

Parameters of the Modem

34 carriers (orthogonal frequencies), 50 Hz difference (Fig. 3)

29 information channels, 4 synchronization channels, 1 FSK channels

4-ary PSK/DPSK when 4800 b/s
2-ary PSK/DPSK when 1200 b/s and 600 b/s (600 b/s always with FEC)

50 baud modulation rate (data and call channel)

Internal sample rate 19.2 kHz

1st synchronization carrier for timing, 4-ary PSK
2nd synchronization carrier for AFC and selective call, 2-ary PSK

FEC convolutional coding in the parallel channels
Code rate: R = 3/4 Interleaving factor M: 7 programmed values

Interface to data terminal equipment: CCITT V.24/X.21 bis
Interface to radio equipment: Signal : 0 dB, 600 ohm, balanced
Control: open collector

Generation of the Carriers

The carriers are generated digitally in a signal processor. In time intervals of 51 microseconds (sample rate 19.2 kHz) the phases of all 34 carriers are computed and the corresponding amplitudes added. The different values of the amplitude are stored in a look-up table, a ROM with 320 addresses. The signal processor as well as the processor for the correlation is realized in discrete TTL integrated circuits. A further description is found in (4).

Selective Call

In a network every subscriber has to be selected. One solution is to have as many frequencies as subscribers. This is not economical because of the limited number of channels and the many users in the air band. Before data transmission commences the receiving station has to be synchronized, for example with a preamble. If this preamble carries subscriber information (a calling number), a network can operate with only one frequency. The selective call in the modem can be used in broadcast mode as well as in duplex and halfduplex links. With duplex and halfduplex an ARQ protocol is used (automatic repeat on request). In the call procedure transmission of control data is possible, in order that the called modem can be programmed to the mode setting of the calling modem.

The calling procedure uses only two of the carriers, the synchronization carriers. The transmission data rate is 50 b/s (see Fig. 3). Because of the separate call channel the data channel remains transparent. As in data transmission the one carrier is used to synchronize the timing of the modulation cycle. The other carrier is 2-ary phase modulated with the call information. The decoding is done with FFT (Fast Fourier Transformation) in a microprocessor 6809.

Synchronization of the Modulation Cycle

With FDM in a parallel system the synchronization could be done with every two adjacent carriers, but this would be technically complicated and is not necessary. The guard space (Fig. 3) between modulation cycles is sufficient for the carriers to be stable when measurement commences. To decode without errors the cycle synchronization has to be approximately in the centre of the guard space, therefore the synchronization with only one carrier is sufficient.

The synchronization carrier, binary phase shift keyed, is filtered in a narrow band pass with 5 Hz bandwidth. The envelope is then decoded. The zero crossings of this envelope is very distorted because of the phase shift of the other carriers and the distortion in the HF medium. This is compensated in a low pass filter with a large delay time (t ≈ 10 s). The low pass filter is realized in software in the central signal processor.

Automatic Frequency Correction

The demodulation principle relies on the orthogonality of the carriers. It is thus important that in the receiver part of the modem an AFC (Automatic Frequency Correction) compensates for the frequency shift of the local oscillator and the frequency changes in the HF medium.

A MICROPROCESSOR CONTROLLED PARALLEL MODEM WITH FDPSK

by Holger E. Buding
Siemens-Aktiengesellschaft
Hofmannstraße 51
8000 München 70, FRG

SUMMARY

Within the frequency band of a HF-channel (3 kHz) the phase distortion is timevariable and of a considerable size. In this environment it is advantageous to use FDPSK (frequency differential phase shift keying) for transmission instead of TDPSK (time differential phase shift keying). In FDPSK the information is transmitted as the phase difference between two synchronized carries of different frequency. When they only have a small frequency difference (e.g. 60 Hz) both are exposed to the same phase distortion of the HF-channel. With an appropriate demodulation method this phase error therefore can be cancelled.

The modem described uses for transmission 2400 bit/s, which are modulated on 24 + 2 parallel subcarriers. With the addition of the FEC Code (convolutional code R = 3/4), the number of subcarriers is increased by 8. Two channels are used for synchronization - one for the synchronization of the Modulation Cycle (50 Baud = 20 ms Modulation cycle) and one for the AFC (Automatic Frequency Control) in 1/7 Hz increments. The frequencies are a multiple of 60 Hz and are also spaced at 60 Hz which means that they are orthogonal. This is important for the method of decoding in the receiver.

On the transmitting side the different frequencies are generated by means of a Look-up Table. The oscillators are represented by memory positions which contain the momentarily phase changes of the respective frequencies. The calculation of the phases of all frequencies is done constantly at a sample rate of 19,2 kHz.

On the receiving side several synchronisation and control loops are required. Firstly a possible frequency offset due to frequency changes over the HF-link or because of the radio equipment themselves, must be cancelled out. Then, by means of a Software low pass filter, the modulation cycles (20 ms) are synchronised. The received signal is subdivided into 4 groups so that independant amplitude regulation could be done in each group (selective fadings) and to take the burden off the correlators.

The phases of the respective frequencies are detected by means of correlation. The sum of frequencies in each group is multiplied with a reference frequency which is generated internally and then integrated. Because of the orthogonality of the frequencies, all products dissapear after integration (T = 1/60 = 16 2/3 ms) except the cosine of the wanted frequency. This calculation has to be done for each frequency in every modulation cycle (20 ms).

For the operation in networks, the modem has got a selective calling feature. The calling procedure is either Simplex of Halfduplex and is a special "calling channel" with phase modulation and a data rate of 50 Bit/s (also 50 Baud). The decoding of this calling channel is done by means of a FFT (Fast Fourier Transform) in a 8085 microprocessor. The AFC (Automatic Frequency Control) values are at the same time calculated in this 8085.

Measurements were done over two different HF links (40 km and 1200 km). Wideband dipole antennas and a frame antenna were used. The power output of the HF radio equipment was switchable between 70 and 400 Watt. The measured error rates were in the order of magnitude 1 X 10exp-02 to 1 X 10exp-03. With the inclusion of the FEC these error rates could be improved to 1 X 10exp-03 to 1 X 10exp-05.

Introduction

The HF medium is known to be very unfavourable for transmission of information, esspecially digital information. The changing ionisation of the ionosphere causes multipath propagation. The receiver in a HF link has to cope with great changes in propagation delay time, fadings and phase shifts of the signal. Therefore until today these effects were solved with a corresponding modulation rate, i.e. a modulation rate up to 200 baud. For higher bitrates the transmission in parallel channels was used. Modems had been constructed for 2400 b/s with FDPSK (frequency differential phase shift keying) (1,2) or alternatively with TDPSK (time differential phase shift keying) (3). The latter are used for example in LINK 11. In recent times single tone modems are in developement. They operate with special adapting algorithms to counteract the influence of the HF medium. In this paper a parallel modem is introduced with FDPSK and FEC (forward error correction).

TDPSK-FDPSK

In TDPSK the information is coded in the change in phase of any carrier from modulation cycle to modulation cycle. This application (normally named DPSK) is often used in modems for wire links and gives good results. On HF links there are phase changes of the carriers from the known effects. These phase changes cause errors in the information bits if they exceed a specific value. Fig. 1 shows the behaviour.

In FDPSK the information is coded in the phase difference of two carriers in the same modulation cycle. If the adjacent carriers are close enough to each other (a frequency difference of some 10 Hz) they would have the same distortion, the same phase changes. Since these absolute phase errors are approximately the same in the two adjacent carriers they are cancelled by the computation of the difference. This is the advantage of FDPSK above TDPSK, in which case the phase errors are not compensated for. In FDPSK n+1 carriers are needed to transmit n information channels in a parallel system, one data carrier being the reference for the next.

DISCUSSION

A.Schneider, US

Why did you choose Kasami codes rather than Fire codes? The Fire codes are known to be highly effective burst error correcting codes and reasonably simple to decode. In retrorespect, was the choice justified?

Réponse d'Auteur

Cette question est très interessante. Les codes de Fire sont effectivement bien connus pour leurs propriétes de correction de paquets d'erreurs, mais si on compare la valeur du paramètre que j'ai introduit on constate qu'il est plus petit pour les codes de Kasami que pour les codes de Fire. Les codes de Kasami possèdent les plus petit z parmi les codes connus, ce sont donc les meilleurs. Les codes de Fire sont utilisés parce que leur décodage est relativement simple. Les codes de Kasami sont des codes cyclíques raccourcis qui se décodent beaucoup plus difficilement. La méthode dite du piegeage d'erreurs est applicable en utilisant le polynome de recurrence réciproque, mais cela conduit de toutes façons a des calculs importants. On s'est orienté, finalement vers une méthode de decodage statistique. Nous avons donc retenu les codes de Kasami pour deux raisons: la première parce que ce sont les plus puissants que nous connaissons, et le seconde parce que le débit à travers le canal HF est relativement lent, ce qui laisse aux techniciens suffisamment de temps pour effectuer les calculs de décodage.

Figure 6 : REPARTITION DES ERREURS / ERRORS DISTRIBUTION
TROISIEME MODE DE PROPAGATION : TROIS TRAJETS / 3rd MODE - 3 PATCHES

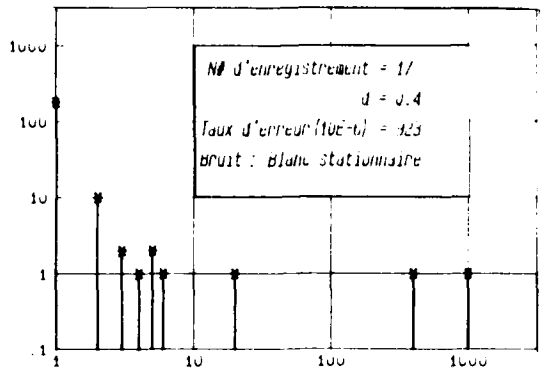

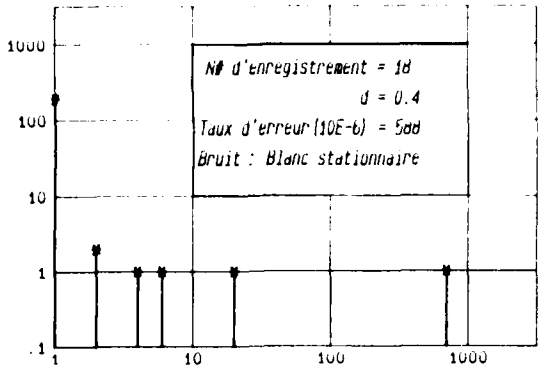

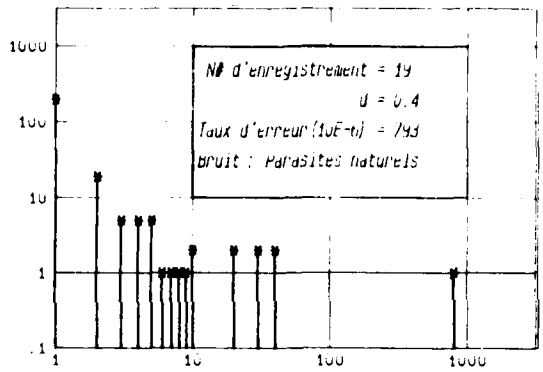

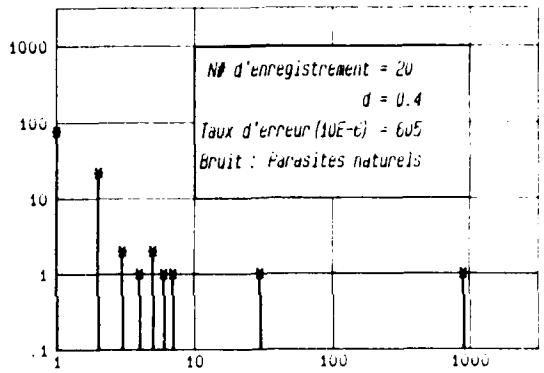

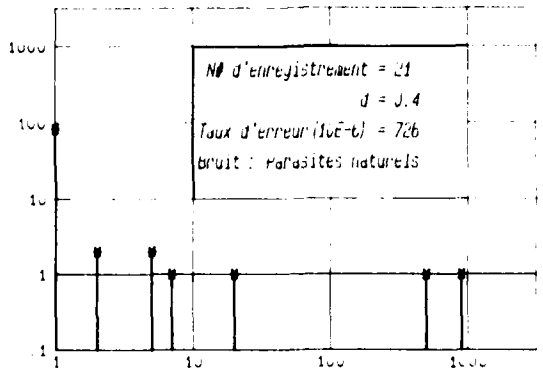

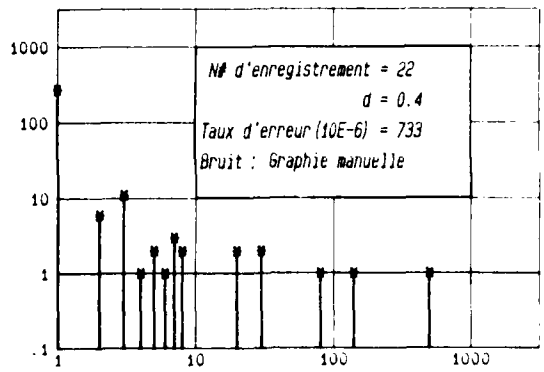

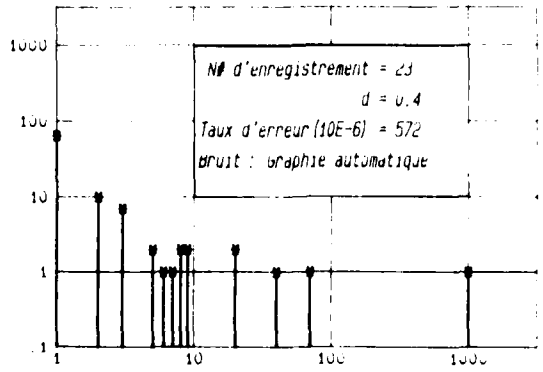

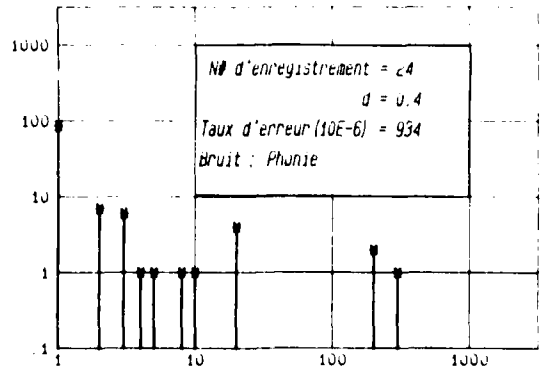

Figure 5 : REPARTITION DES ERREURS / ERRORS DISTRIBUTION
DEUXIEME MODE DE PROPAGATION : TROIS TRAJETS / 2nd MODE - 3 PATCHES

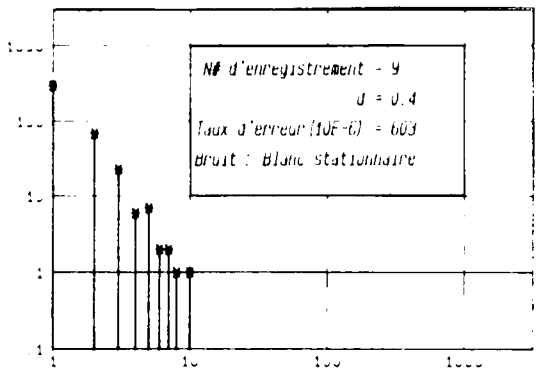

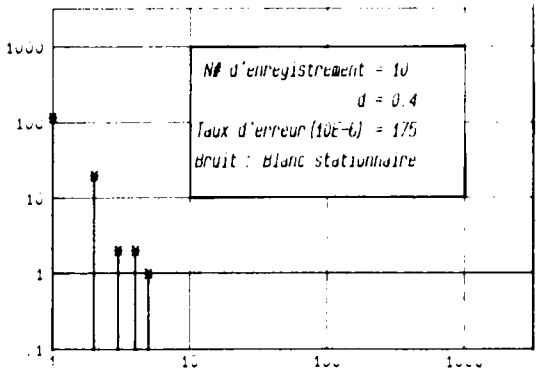

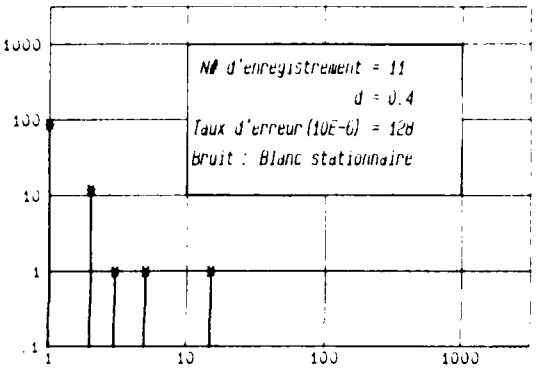

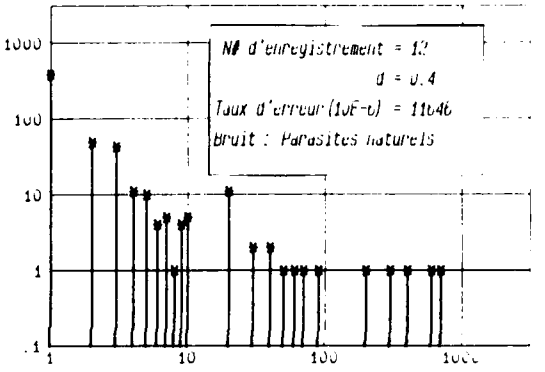

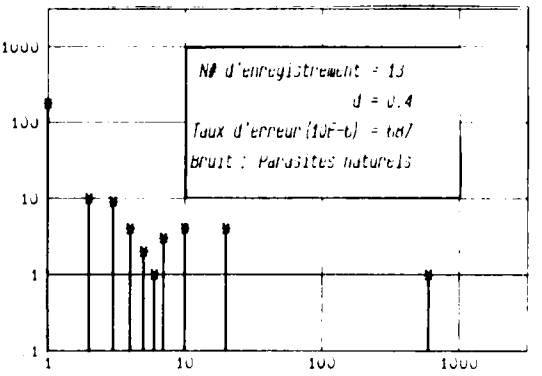

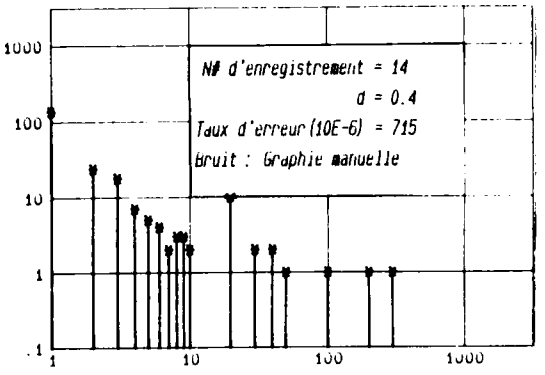

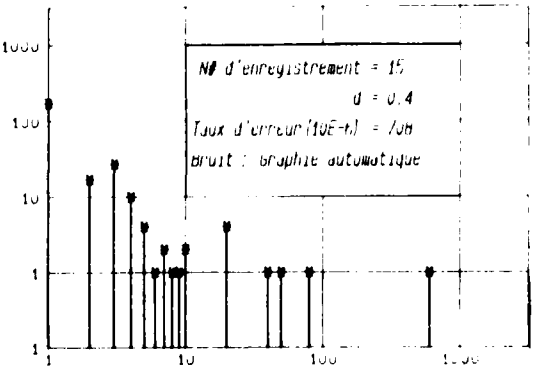

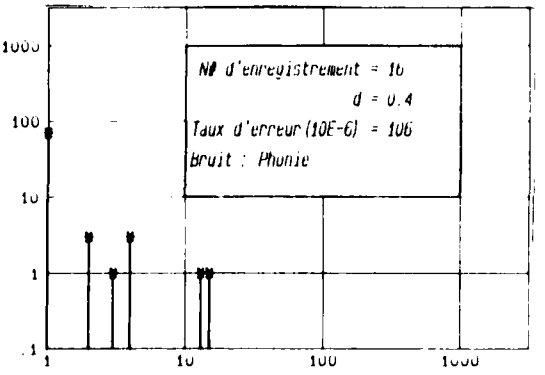

Figure 4 : REPARTITION DES ERREURS / ERRORS DISTRIBUTION
PREMIER MODE DE PROPAGATION : UN SEUL TRAJET / 1nd MODE - 1 PATH

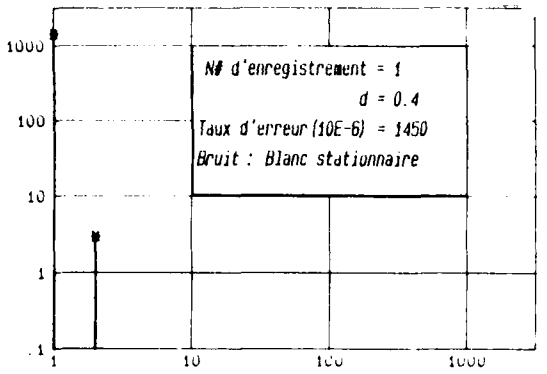

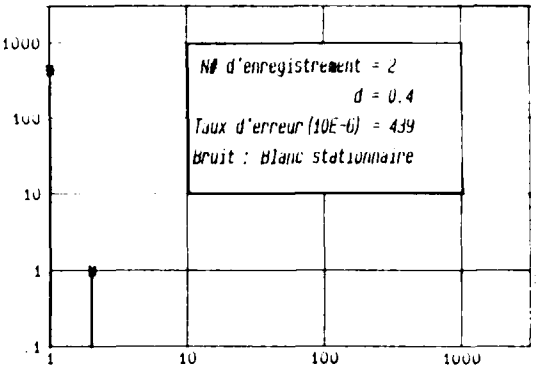

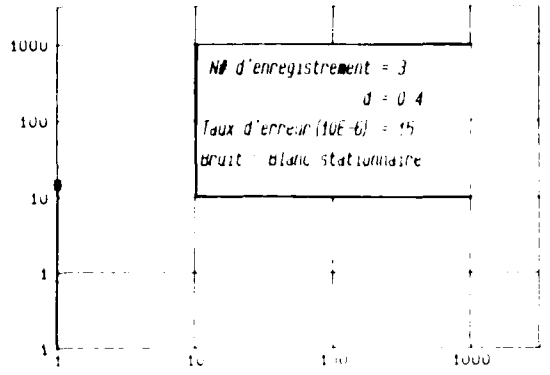

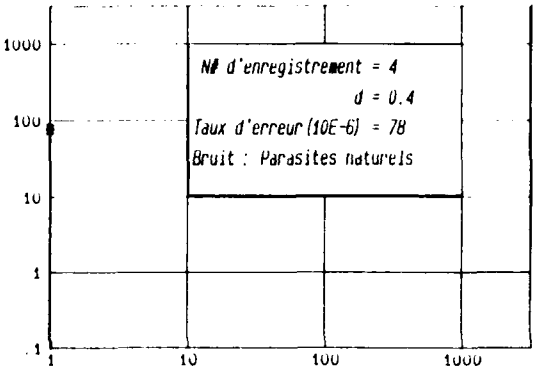

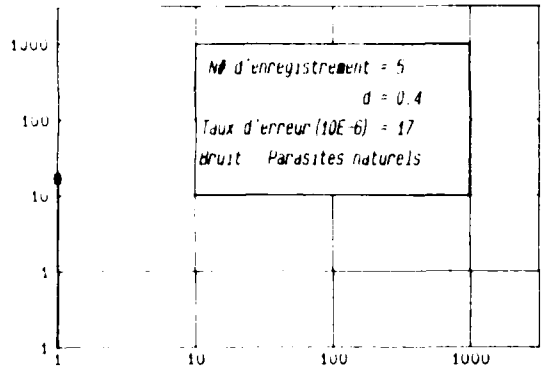

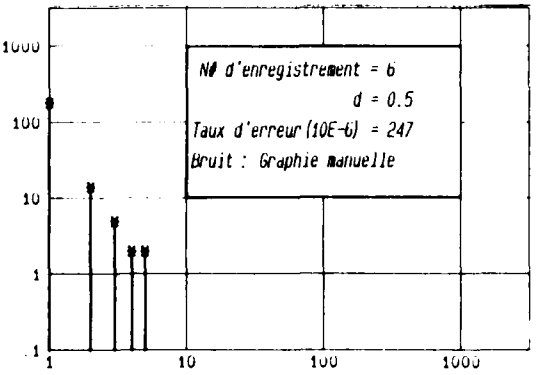

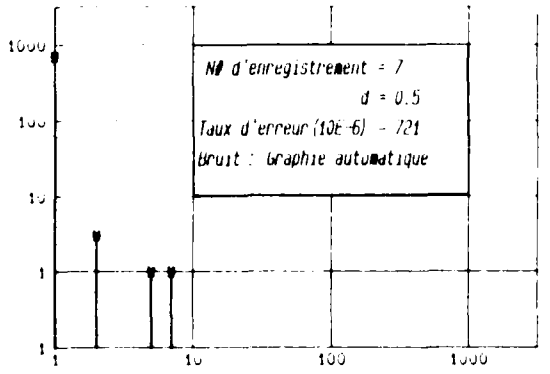

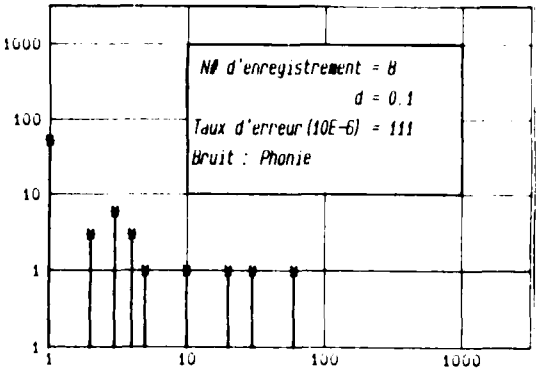

Figure 1 : RECONSTITUTION DE LA LIAISON
SIMULATION OF LINK

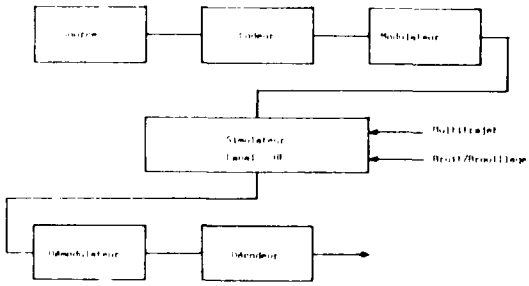

Figure 2 : FILTRE AUTO ADAPTATIF
SELF ADAPTATIVE FILTER

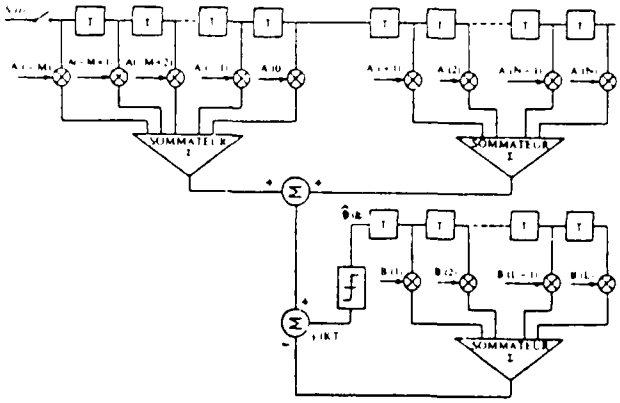

Figure 3 : TAUX MOYEN D'ERREUR
BIT ERROR RATE

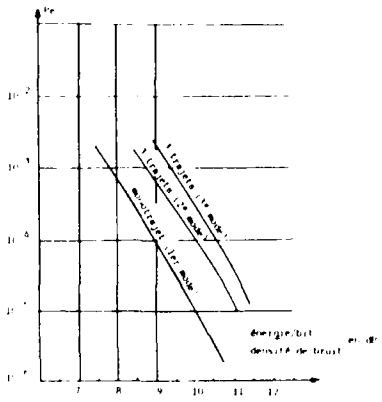

Figure 7 : ORDRE DE CODAGE ET DECODAGE
CODAGE AND DECODAGE

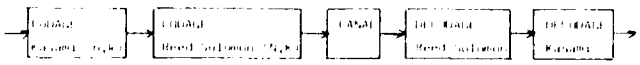

Figure 8 : SCHEMA SYNOPTIQUE DU CODEUR
SYNOPTIC OF CODER

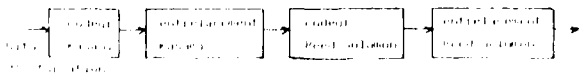

Figure 9 : STRUCTURE DU CODEUR
CODER STRUCTURE

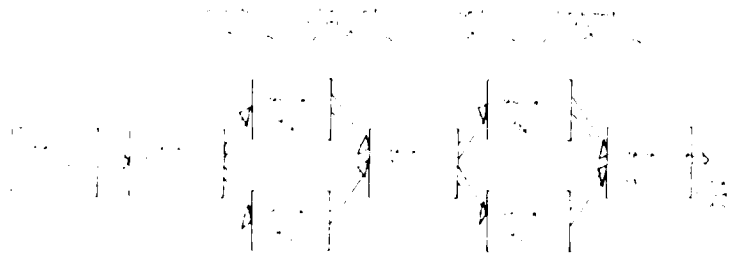

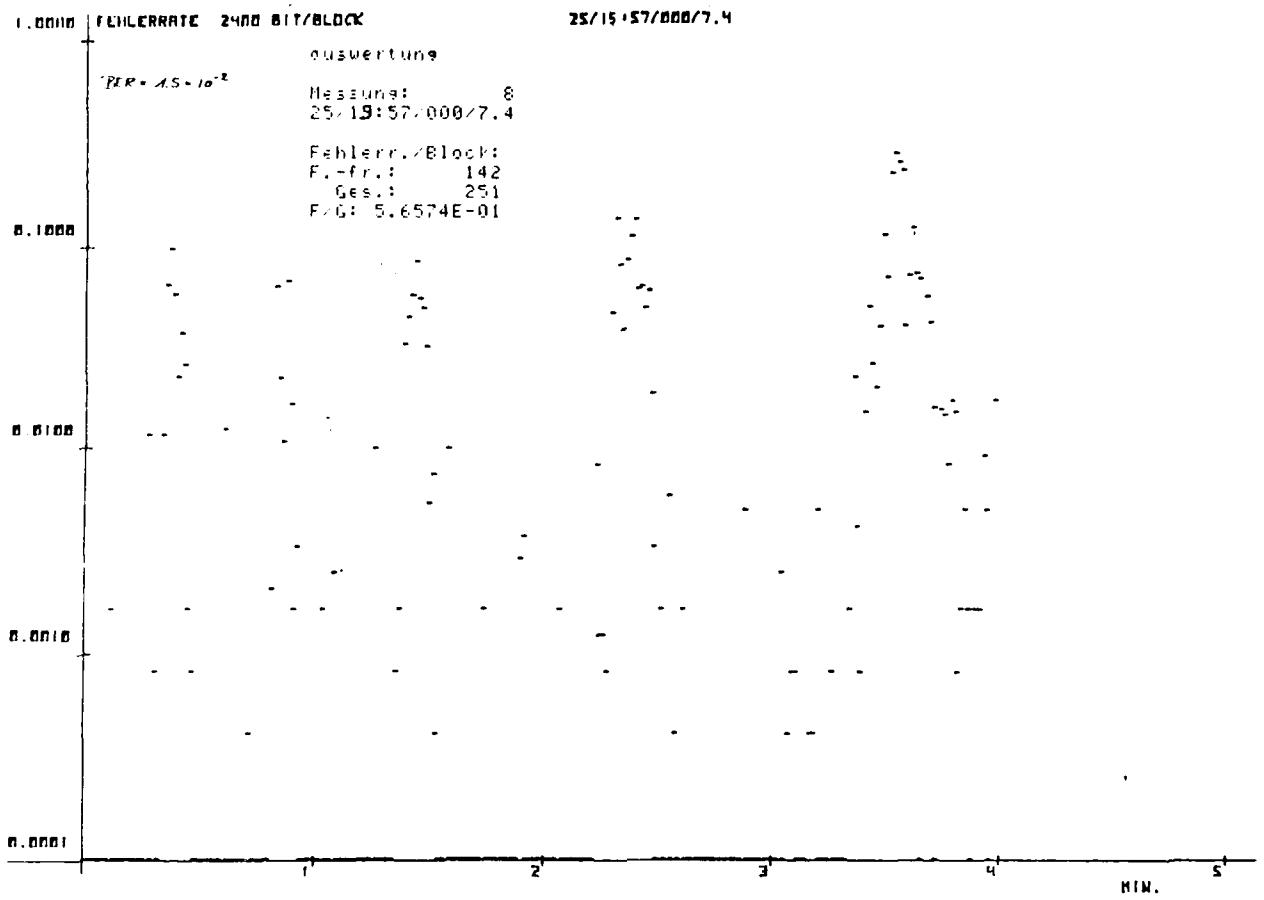

Fig.8 Error rate per block

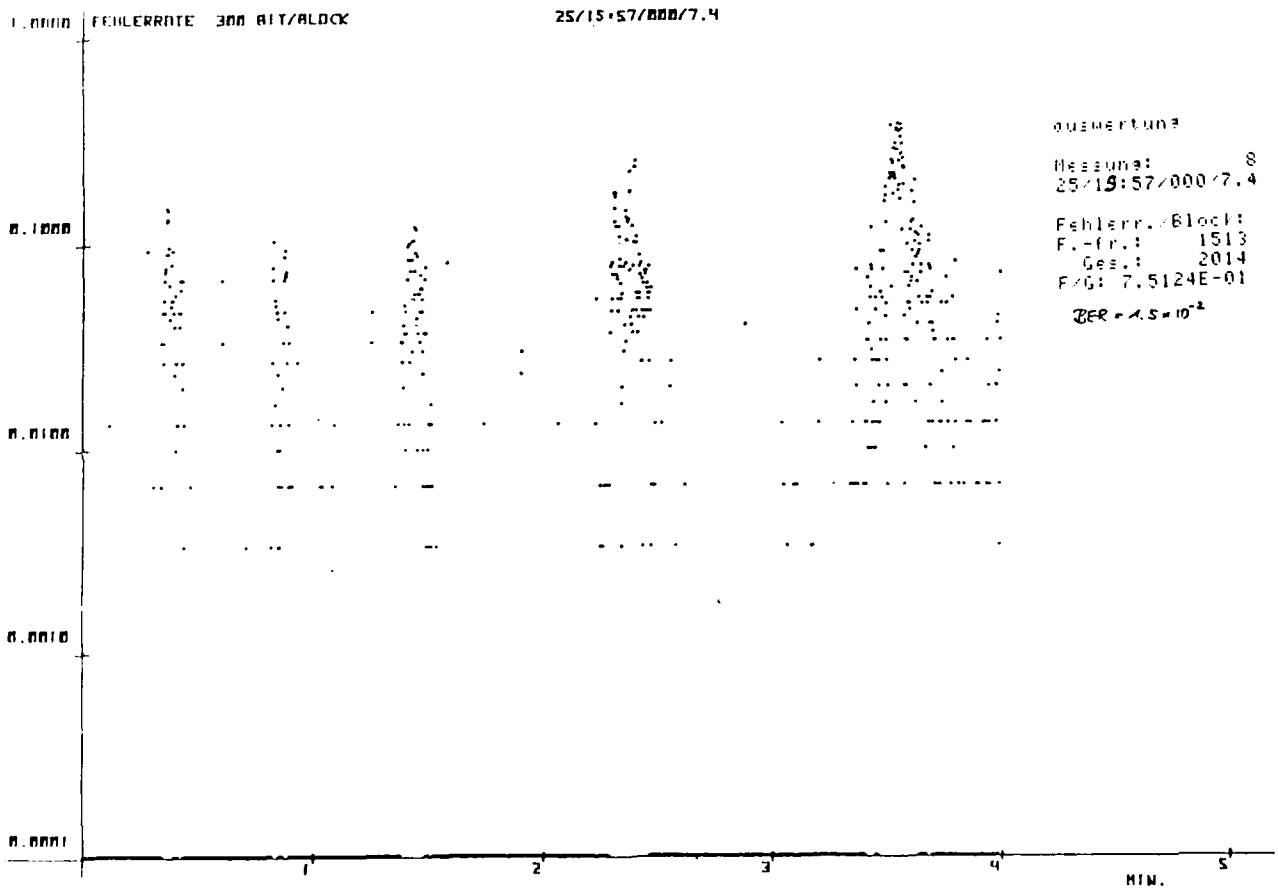

Fig.9 Error rate per block

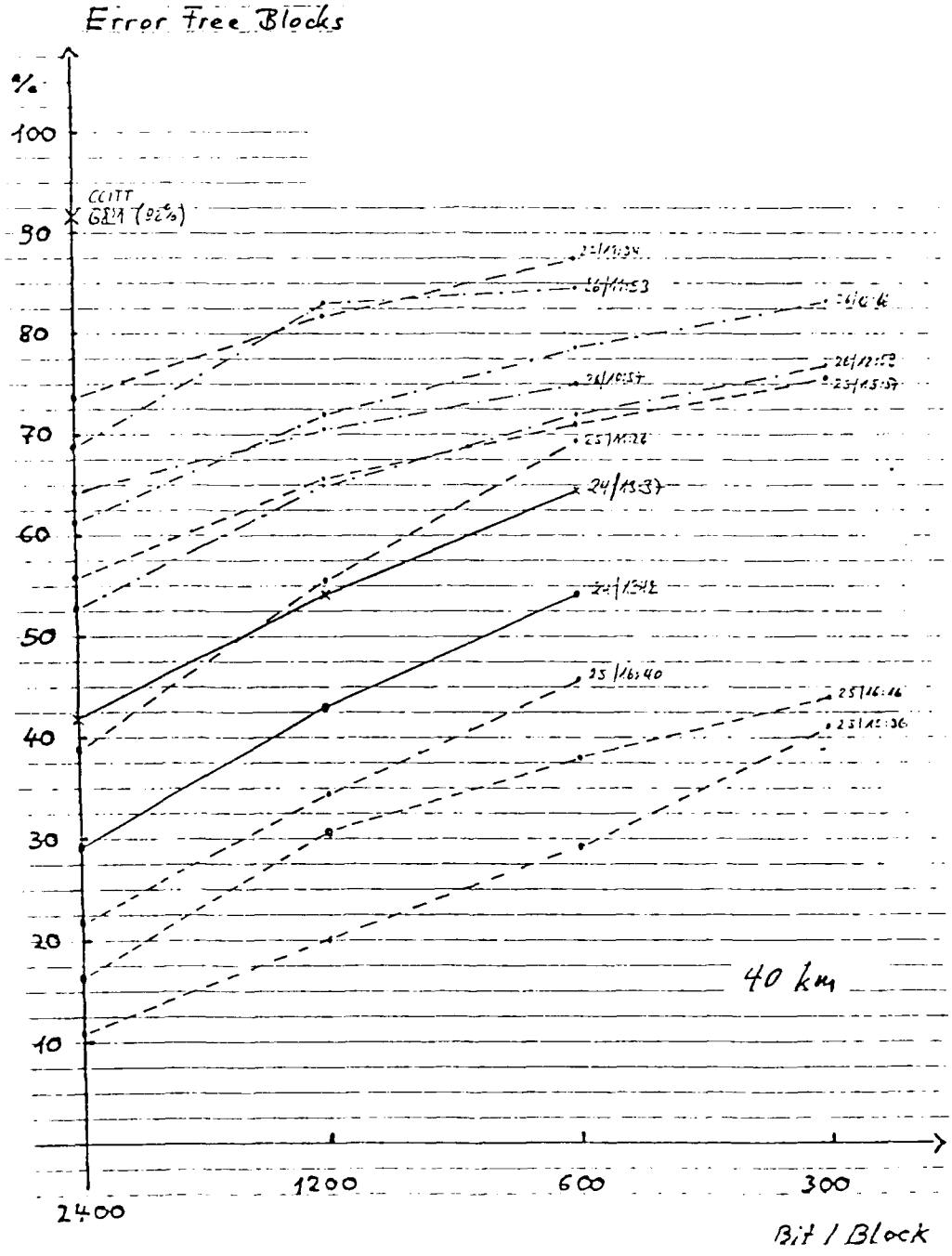
Error Free Blocks
%
100
90
80
70
60
50
40
30
20
10
CCITT
G821 (92%)
24/13:37
24/13:42
25/16:40
40 km
2400
1200
600
300
Bit / Block

Figure 10

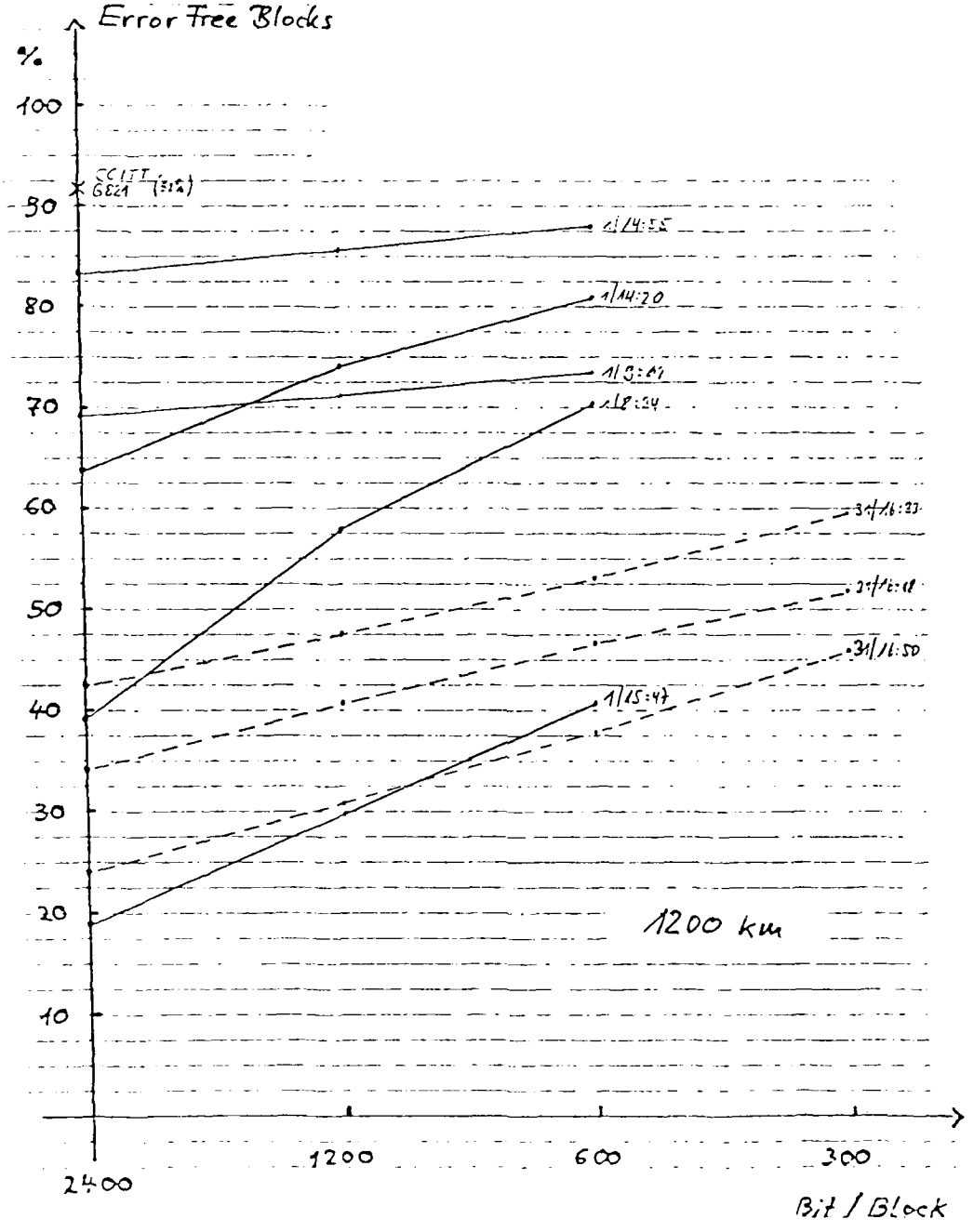
Error Free Blocks
%
100
90
80
70
60
50
40
30
20
10
CCITT G621 (3:2)
1/14:55
1/14:20
1/13:41
1/12:34
31/16:33
31/16:11
31/11:50
1/15:47
1200 km
2400
1200
600
300
Bit / Block

Figure 11

DISCUSSION

E.W.Lampert, Ge

You pointed out that you intended to use FEC on the single carrier instead of on the total bit stream. Do you feel that this is a most promising way to go?

Author's Reply

Yes, I think so, because selective fading over 100 Hz or 200 Hz will be smaller and will travel through the band, and the influence in a slow bit stream of 50 bits/s will not be so long in bit times.

E.W.Lampert, Ge

Can you give your personal feeling how much improvement there will be.

Author's Reply

Two weeks ago we started measurements on a 300 kms link, and we saw the improvement due to FEC. The results are too few to give statistically reliable answers.

TRANSMISSION DE DONNEES SERIE A GRAND DEBIT SUR CANAL HF

J.P. VAN UFFELEN
A DECONCHE
Société TRT, BP 21, 92350 LE PLESSIS ROBINSON, France

Résumé

Le modem décrit utilise une transmission série et un égaliseur auto-adaptatif pour corriger les distorsions de propagation. Il permet des transmissions de données au débit maximal de 2400 b/s aussi bien en mode continu qu'avec des messages brefs de durée nominale 1 seconde.

La communication proposée comprend 3 parties :

. La première est une description des caractéristiques du modem et des traitements de signal appliqués.

. La seconde partie correspond à l'évaluation des performances en laboratoire. Les mesures effectuées se rapportent à des essais en propagation multi-trajet simulée ou avec décalage de fréquence.

. La dernière partie est consacrée aux essais effectués sur une liaison de 500 Km. Les résultats de ces essais sont analysés sur calculateur, ce qui permet de présenter les résultats sous forme de statistiques à court et long terme.

1. INTRODUCTION

Les distorsions dues à la propagation ionosphérique (interférences entre symboles, évanouissements sélectifs), limitent la vitesse de modulation des transmissions de données dans la gamme de 2 à 30 MHz. L'obtention d'un débit élevé nécessite l'utilisation de traitements aptes à tolérer les effets des trajets multiples.

Cet exposé décrit un modem capable de transmettre des données jusqu'à un débit de 2400 b/s avec un spectre radioélectrique dont la largeur est inférieure à 3 kHz.

La transmission est du type série et la vitesse de modulation est de 1350 bauds. Les distorsions introduites par les trajets multiples sont compensées par un égaliseur automatique. La mise en oeuvre d'une démodulation cohérente rendue possible par le traitement auto-adaptatif, permet d'accroître de 3 dB la protection du modem vis à vis du bruit.

Ce modem est conçu pour des liaisons effectuées avec réfraction ionosphérique et dispose de 2 modes d'exploitation :

- un premier mode permet de transmettre des données à un débit moyen de 600 - 1200 ou 2400 bits/s avec des messages brefs de durée nominale 1 seconde.

- un second mode permet la transmission continue de données à un débit de 600 - 1200 ou 2400 bits/s ; ce mode est utilisable en particulier pour la transmission de la phonie numérisée par un vocodeur.

2. TRANSMISSIONS DE DONNEES EN HF

2.1 Problèmes

Dans la gamme des ondes décamétriques, la propagation s'effectue par réfraction des ondes dans les couches ionisées, principalement les couches E et F2. La multiplicité des couches et les caractéristiques d'ionisation font qu'il existe fréquemment plusieurs trajectoires susceptibles d'assurer simultanément la liaison radioélectrique entre l'émetteur et le récepteur. Ces trajectoires étant de longueurs différentes, la réponse du canal à une impulsion comporte plusieurs impulsions dont la dispersion peut atteindre 5 ms. Ces trajets multiples provoquent en transmission de données le phénomène d'interférences entre symboles et peuvent engendrer des évanouissements sélectifs.

La mobilité des couches ionisées rend les conditions de propagation non stationnaires et affecte le signal reçu d'un effet Doppler dont la fréquence est de l'ordre de quelques dixièmes à quelques Hertz.

2.2 Solution proposée

Pour exploiter au mieux un canal de transmission affecté par des évanouissements sélectifs, il importe de répartir l'information à transmettre dans la bande passante disponible. Ainsi une dégradation localisée du spectre n'entraine pas la perte irrémédiable

d'une partie de l'information transmise. Une transmission de données sous forme série avec une vitesse de modulation de l'ordre de la moitié de la bande disponible réalise la dilution de l'information sur la totalité de la bande disponible.

Les trajets multiples provoquent des interférences entre symboles qui limitent sévèrement la qualité du signal reçu. La dégradation du taux d'erreur est d'autant plus importante que la vitesse de modulation est plus élevée. Ces interférences peuvent être réduites en utilisant la technique de l'égalisation du canal de transmission.

2.3 Caractéristiques fonctionnelles du modem

Les principes de base concernant la modulation, la démodulation, la structure de l'égaliseur et l'insertion d'une séquence de test pour assurer la convergence de l'algorithme, ont déjà été décrits dans un article précédent (1), ainsi que les performances obtenues (2).

Les caractéristiques nouvelles apportées à ce modem, outre l'augmentation du débit à 2400 bits/s et les deux modes de fonctionnement proposés, proviennent de l'accroissement de la rapidité des prises de synchronisation et de la diminution du temps de convergence de l'égaliseur.

Ceci a été rendu possible grâce à l'utilisation d'un microcalculateur spécifique qui permet de réaliser les principales fonctions complexes du démodulateur.

Principe de la synchronisation

Le modem auto-adaptatif comporte trois types de synchronisation :

- la synchronisation message qui détermine la position de la séquence de test,

- la synchronisation primaire qui reconstitue l'horloge à partir des données reçues,

- la synchronisation en fréquence qui permet de corriger en fréquence les données reçues.

La séquence de test est un message pseudo-aléatoire. La phase de celle-ci est retrouvée par corrélation qui détermine la position de la séquence qui correspond au trajet maximal de la réponse percussionnelle.

Un suréchantillonnage d'ordre 4 permet d'augmenter la précision dans l'estimation initiale de la phase de la séquence de test, et permet aussi d'augmenter la rapidité de la synchronisation primaire.

La synchronisation en fréquence est assurée par un asservissement entièrement numérique traitant les signaux reçus après égalisation. L'écart en fréquence maximal admissible, entre la porteuse émission et la porteuse réception, peut atteindre 75 Hz.

2.4 Caractéristiques techniques du modem

Les caractéristiques techniques du modem sont les suivantes :

Débit : 600/1200/2400 bits/s
Modes : transmission continue/transmission de messages brefs
Modulation : PSK (2 ou 4 phases)
Vitesse de modulation : 1350 Bauds
Démodulation cohérente
Egalisation adaptative
Ecart de fréquence admissible : $\pm$ 75 Hz
Interface avec Emetteur-Recepteur : fréquence audio (300 - 3000 Hz)
Interface avec Terminal de Données : Avis V24 - V11 du CCITT

3. EVALUATION DES PERFORMANCES EN LABORATOIRE

3.1 Méthode de mesure

L'évaluation des performances du modem en laboratoire, a été faite avec un banc de mesure simulant une propagation ionosphérique dont les perturbations sont engendrées par :

- du bruit additif blanc et gaussien

- des trajets multiples additifs

- l'adjonction d'un décalage en fréquence

Les performances sont évaluées par la mesure du taux d'erreurs moyen sur la liaison, et comparées avec la courbe théorique d'une transmission de données en modulation PSK à 2 ou 4 états de phase.

Les différentes configurations de propagation choisies pour tester les performances sont les suivantes :

- canal monotrajet avec bruit additif, avec et sans décalage en fréquence

- canal fixe avec 2 trajets d'amplitude égale et bruit additif (sans décalage en fréquence).

Le retard différentiel valant 2 ms dans le cas d'une transmission continue, et une demi-période de modulation (T/2 = 0,37 ms) pour la transmission de messages brefs.

- canal variable avec 2 trajets (l'amplitude du 2ème trajet variant entre 0 et l'amplitude du 1er trajet selon une loi sinusoïdale de fréquence 1 Hz). Les retards différentiels sont les mêmes que pour le canal fixe.

3.2 Résultats

Les courbes montrant la variation du taux d'erreurs en fonction du rapport signal à bruit, sont données dans chacun des cas d'utilisation du modem (transmission continue ou messages brefs, vitesses : 600 - 1200 ou 2400 bits/s).

Les courbes obtenues pour chacune des configurations de propagation proposée, sont données figures 1 à 3.

Il est à noter que la mesure du rapport signal à bruit a été effectuée en fréquence intermédiaire ; donc dans le cas d'un canal à 2 trajets, la puissance mesurée correspond à la somme des puissances de chacun des trajets.

Pour chacun des cas d'utilisation, la qualité d'égalisation vis à vis du bruit, est mesurée par l'écart entre la courbe théorique (courbe 0) et la courbe expérimentale (courbe 1).

La dégradation apportée par la présence d'un trajet secondaire d'égale amplitude est déterminée par l'écart entre la courbe expérimentale obtenue dans le cas d'un canal fixe à 2 trajets (courbe 2) et la courbe 1.

La dégradation supplémentaire résultant de la variation en amplitude du trajet secondaire correspond à l'écart entre la courbe expérimentale obtenue dans le cas d'un canal variable à 2 trajets (courbe 3) et la courbe 2.

Ainsi, pour une transmission continue, on constate les résultats suivants :

- la qualité de l'égalisation est voisine de 0,5 dB pour les débits 1200 et 2400 bits/s.

- la dégradation apportée par la présence d'un trajet secondaire d'amplitude égale (retardé de 2 ms) est voisine de 4 dB, pour les 3 débits 600 - 1200 et 2400 bits/s. La puissance prise en compte pour mesurer le rapport signal à bruit étant celle des 2 trajets, cela signifie que, ramené à la puissance d'un seul trajet, la dégradation est de 1 dB, où que l'égaliseur a été capable d'annuler l'effet de ce 2ème trajet en apportant une dégradation supplémentaire de 1 dB.

- lorsque le canal est variable, on peut voir que pour les 3 débits, l'égaliseur n'apporte aucune dégradation supplémentaire puisque les courbes 2a et 3a des figures 1 à 3 sont confondues.

Pour une transmission de messages brefs, on constate que :

- la qualité de l'égalisation est comprise entre 0,5 et 1 dB pour un débit de 1200 bits/s et entre 1 et 2 dB pour un débit de 2400 bits/s dans la zone de taux d'erreurs située entre 10^{-4} et 10^{-2}.

- la dégradation apportée par la présence d'un trajet secondaire d'égale amplitude (retardé de T/2) est voisine de 1 dB pour les 3 débits 600 - 1200 - 2400 bits/s.

- lorsque le canal est variable, on peut voir que pour les 3 débits, l'égaliseur apporte une dégradation supplémentaire de 3 dB, si l'on se réfère à la puissance du signal due aux 2 trajets. Cela montre ainsi que la présence d'un tel trajet secondaire variable apporte une dégradation totale de 4 dB, comme dans le cas de la transmission continue avec un trajet secondaire retardé de 2 ms. En d'autres termes, l'égaliseur s'est comporté comme s'il y avait 2 trajets indépendants, et a pu éliminer le trajet dont l'amplitude est variable en apportant une dégradation supplémentaire de 1 dB (la puissance étant mesurée sur un seul trajet).

En ce qui concerne la qualité de la correction en fréquence, les mesures effectuées dans le cas d'un canal monotrajet, ont montré qu'en transmission continue, les performances sont inchangées lorsqu'il y a un écart de 10 Hz entre les porteuses émission et réception. Par contre, pour la transmission des messages brefs, ce même écart de fréquence apporte une dégradation voisine de 0,5 dB.

4. EXPERIMENTATION DU MODEM SUR UNE LIAISON REELLE

4.1 Description de la liaison

Le modem a été testé sur une liaison radioélectrique dans la gamme HF, sur une distance de 500 Km.

Les essais se sont déroulés courant Juillet 1983, avec un émetteur de puissance 400 Watts et des antennes de type fouet vertical de 10 m à l'émission et à la réception.

Les fréquences utilisées lors des essais ont été déterminées à l'aide des prévisions

de propagation, compte tenu d'un indice d'activité solaire IR5 égal à 77 et pour une atténuation de 100 dB sur une distance de 500 Km.

Dans la mesure ou 80% des essais se sont effectués sur des fréquences voisines de la LUF, ces mêmes prévisions montrent que l'estimation des angles d'élévation du parcours radioélectrique est voisine de 70°, c'est-à-dire que le trajet est dû à la réfraction sur la couche F2.

Sous cette élévation les fouets présentent une atténuation voisine de 10 dB réduisant à 40 Watts la puissance utile ; l'antenne réception apporte la même atténuation, réduisant ainsi le rapport signal à bruit.

4.2 Méthode de mesure

Les performances du modem ont été évaluées pour les 2 modes de fonctionnement à la vitesse de 2400 bits/s.

Le taux d'erreurs était mesuré, dans chacun des cas, pendant la transmission de 10^6 éléments binaires (e.b.). Le message de test utilisé était la séquence pseudo-aléatoire de longueur 511.

Chacune des mesures de taux d'erreurs sur 10^6 e.b. transmis, est décomposée en 20 mesures sur 50 000 e.b., elles-mêmes décomposées en mesures élémentaires portant sur des blocs courts de 1022 e.b. pour une transmission continue ou 1533 e.b. pour une transmission de messages brefs.

Les mesures portant sur 50 000 e.b. sont représentatives des performances du modem lors de la transmission des messages longs. Les mesures effectuées sur les blocs courts permettent d'évaluer l'aptitude d'un modem à la transmission de messages courts ou à la transmission de la phonie numérisée par vocodeur. En effet, l'aptitude d'un modem à transmettre la phonie numérisée, est caractérisée par le pourcentage du temps pendant lequel le taux d'erreurs est localement inférieur à 10^{-2} (limite de taux d'erreurs acceptable par le vocodeur).

Cette caractéristique est accessible en mesurant le taux d'erreurs sur les blocs courts.

Pour chacune des mesures sur 10^6 e.b. ont été effectués les deux histogrammes suivants :

- le premier (histogramme à long terme) indique le pourcentage de blocs de 50 000 e.b. pour lesquels le taux d'erreurs appartient à une tranche donnée. Les taux d'erreurs mesurés sont regroupés en 10 tranches définies par les bornes :

  $0 \quad 5.10^{-5} \quad 10^{-4} \quad 5.10^{-4} \quad 10^{-3} \quad 5.10^{-3} \quad 10^{-2} \quad 5.10^{-2} \quad 10^{-1} \quad 5.10^{-1}$

  De cet histogramme, on peut déduire la fonction de répartition associée donnant le pourcentage de blocs longs reçus avec un taux d'erreurs inférieur à une valeur donnée.

- le second (histogramme à court terme) indique le pourcentage de blocs courts pour lesquels le taux d'erreurs local (égal au nombre d'erreurs mesuré, divisé par la longueur d'un bloc) est nul ou supérieur à 10^{-2}.

A partir des histogrammes à long terme, effectués pour chaque séquence de 10^6 e.b., a été établi un histogramme global pour l'ensemble des essais.

A partir des histogrammes à court terme, effectués pour chaque séquence de 10^6 e.b., il est possible de représenter graphiquement le pourcentage du nombre de blocs courts reçus sans erreur en fonction du taux d'erreurs moyen observé sur la séquence de 10^6 e.b.. Il est également possible de représenter le pourcentage du nombre de blocs courts reçus avec un taux d'erreurs local supérieur à 10^{-2}.

4.3 Résultats

Les résultats d'ensemble donnant la probabilité d'obtention d'une tranche de taux d'erreurs, et la fonction de répartition associée, sont présentés en figures 4 et 5.

Les pourcentages du nombre de blocs courts reçus sans erreur, ou avec un taux d'erreurs local supérieur à 10^{-2}, sont donnés figures 6 et 7.

L'analyse de l'ensemble des mesures obtenues pendant ces essais, permet d'en déduire les moyennes globales pour chacun des 2 modes d'utilisation.

Pendant la transmission continue :

- taux d'erreurs moyen : 3%

- pourcentage moyen des blocs de 1022 e.b. reçus sans erreur : 69%

- pourcentage moyen des blocs de 1022 e.b. reçus avec un taux d'erreurs local supérieur à 10^{-2} : 20%

Pendant la transmission de messages brefs :

- taux d'erreurs moyen : 3,5%
- pourcentage moyen de blocs de 1533 e.b. reçus sans erreur : 57%
- pourcentage moyen de blocs de 1533 e.b. reçus avec un taux d'erreurs local supérieur à 10^{-2} : 18%

On peut voir également sur la figure 7, que lorsque le taux d'erreurs moyen est inférieur à 10^{-2}, 95% des blocs courts sont transmis avec un taux d'erreurs local inférieur à 10^{-2}.

5. CONCLUSIONS

Les essais effectués sur ce modem montrent que la transmission série associée à l'égalisation automatique permet d'obtenir, en propagation ionosphérique, une transmission de données à grand débit fiable tant pour les messages courts (typiquement une seconde) que pour les messages dont la durée est de l'ordre de la minute.

En particulier, il est montré que la technique de synchronisation est bien adaptée puisqu'il apparaît que les probabilités d'erreurs sont voisines, que les messages soient courts ou longs.

Le signal modulé à amplitude quasi constante, permet d'exploiter au mieux la puissance de l'émetteur. Cette caractéristique a permis au mieux de compenser l'atténuation apportée par les antennes fouet sur cette liaison courte qui imposait des angles d'élévation élevés.

Références

1 VAN UFFELEN, J.P., 1975, "Description d'un dispositif auto-adaptatif pour transmission de données sur liaisons ionosphériques", AGARD CP-173 "Radio systems and the ionosphere", Paper 24, Athens.

2 PENNINGTON, J., 1982, "Comparative measurements of parallel and serial 2.4 kbps Modems", IEE Conference Publication Number 206 "HF Communication Systems and techniques", 141-144.

PERFORMANCES DU MODEM

SIMULATIONS EN LABORATOIRE

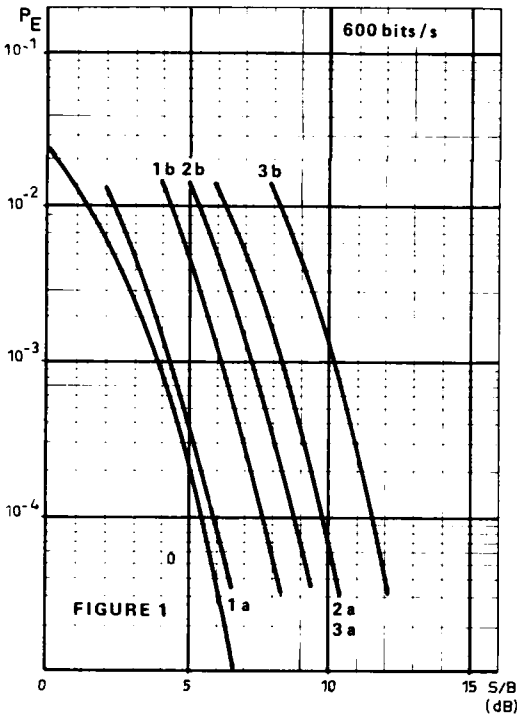

FIGURE 1

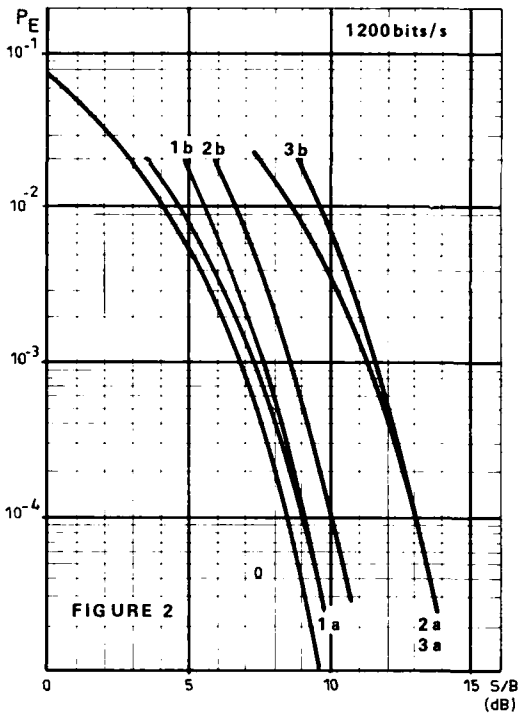

FIGURE 2

Courbe théorique

0 canal monotrajet

Courbes expérimentales

1a canal monotrajet - transmission continue

1b canal monotrajet - messages brefs

2a canal fixe, 2 trajets (2ms) - transmission continue

2b canal fixe, 2 trajets (T/2) - messages brefs

3a canal variable (1 Hz), 2 trajets (2 ms) transmission continue

3b canal variable (0,9 Hz), 2 trajets (T/2) messages brefs

S/B = rapport signal à bruit, mesuré en FI.

La puissance mesurée correspond à la somme des puissances de chacun des trajets.

P_E = taux d'erreurs

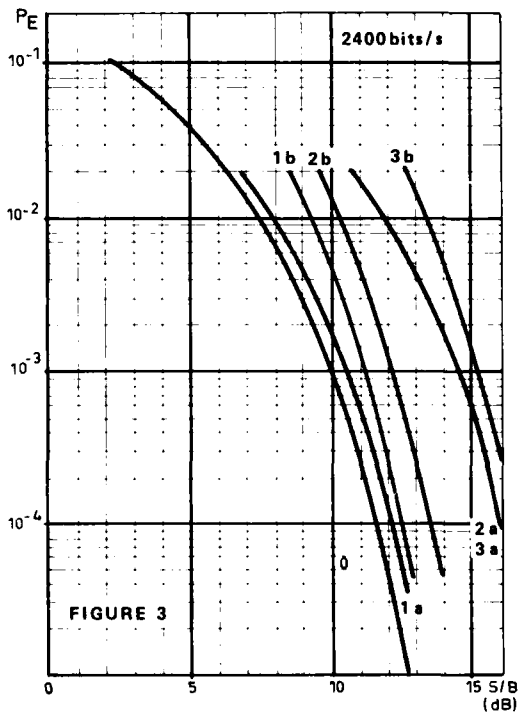

FIGURE 3

EXPERIMENTATION DU MODEM
LIAISON REELLE DE 500 KM

Débits : 2400 bits/s

Modes : transmission continue/messages brefs

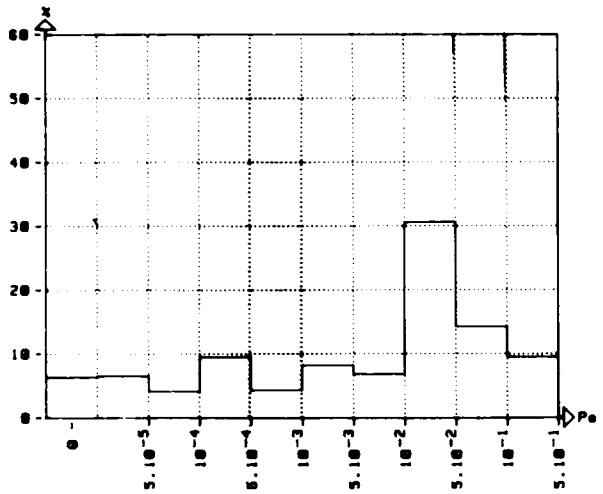

Figure 4 : Histogramme des taux d'erreurs sur 50.000 e.b.

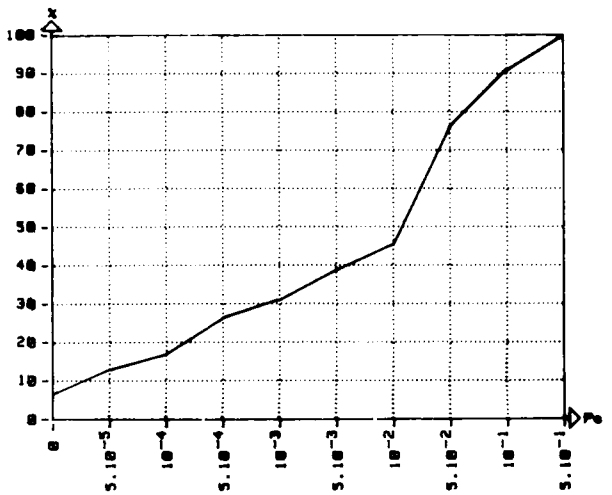

Figure 5 : Fonction de répartition des taux d'erreurs sur 50.000 e.b.

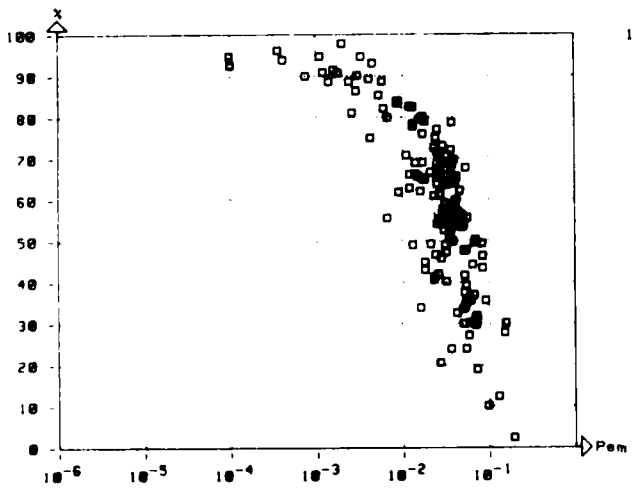

Figure 6 : Pourcentage des blocs courts reçus sans erreur

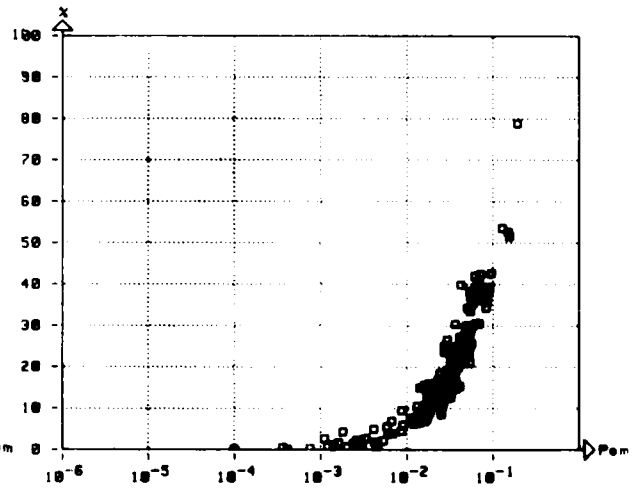

Figure 7 : Pourcentage des blocs courts reçus avec un taux d'erreurs local supérieur à 10^{-2}.

Pe = Taux d'erreurs sur les blocs de 50.000 e.b.

Pe_m = Taux d'erreurs moyen sur les séquences de 10^6 e.b.

DISCUSSION

J.H.Blythe, UK

Can the speaker tell us what measurements were made of the impulse response of the channel. Was multipath present during the observation periods?

Réponse d'Auteur

Durant la transmission, il a été mis en place un système qui permettait d'observer la réponse impulsionnelle du canal, mais seulement de façon visuelle. Nous n'avons pas effectué une analyse statistique des conditions de propagation rencontrées durant ces essais, le système mis en place nous a permis de voir que la propagation s'effectuait souvent pour multitrajets.

C.Goutelard, Fr

Pour compléter la réponse de Monsieur Deconche je peux signaler que nous effectuons sur la même liaison des mesures de temps de groupe et de doppler. Nous avons constaté que de jour et de nuit les modes de propagation sur E et sur F sont en général bien définis. Par contre il apparaît souvent aux transitions Jour-Nuit de nombreux trajets à évolutions rapides avec des délais courts qui arrivent à former un continuum. On arrive, sur cette distance si courte — 500 km — à dénombrer cinq ou six trajets qui ne correspondent pas à des modes successifs sur E ou F. La liaison étant nord-sud, nous les avons attribués à des propagations hors du grand cercle créées par des gradients d'ionisation horizontaux perpendiculaires au plan orthodromique.

Fast Data and Voice Transmission for Mobile Services with High Immunity Against Multipath and Co-channel Interference

by
U. Langewellpott
Standard Elektrik Lorenz AG
Hellmuth-Hirth-Strasse 42
7000 Stuttgart 40
FRG

SUMMARY

Wideband transmission over multipath channels usually causes problems because of intersymbol interference in addition to fading and shadowing. A novel wideband transmission scheme, developed for mobile telephone and data services, is suited not only to cope with but also to utilize multipath effects by moderate but effective spectrum spreading. As a result high levels of reception performance and, in addition, immunity against co-channel interference are achieved.

INTRODUCTION

This paper deals with a scheme for high rate data and voice transmission over multipath channels which has been developed and evaluated during the design of a wideband cellular mobile telephone and data system operating at 900 MHz /1/, /2/. The transmission bandwidth in the order of 5 MHz is a consequence of the time division multiple access (TDMA) architecture having been selected for cost savings and advantages in system organization. In TDMA time is divided into a contiguous stream of short time slots and individual channels consist of different subsets of time slots. All time slots use the same frequency, so no synthesizer is required. In addition, there is no need for a diplexer at the mobile because the transmit and receive time slots can be separated in time. For the same reason the base stations only need one transmitter and one receiver tuned to the transmit and receive frequency respectively. So the complexity is favourably reduced. The highest potential for cost savings stems from digital transmission which, in conjunction with a forecast number of more than one million subscribers, fulfills the prerequisite to low production cost. System organization is facilitated by the TDMA approach because the mobiles only need to be active during the short transmit and receive time slots. So they can easily monitor all surrounding base stations and decide to initiate hand-off to the one offering the best propagation conditions.

PROPAGATION EFFECTS

The high bandwidth is a consequence of the fact that the information having been collected in the period between two time slots of a channel must be compressed in time in order to be put out during the transmit slot in a burst-like manner. High rate transmission, however, introduces some additional problems in a multipath propagation environment.

It is well known that narrowband systems in multipath propagation conditions suffer from shadowing and fading reducing the margin required to suppress interference such as noise and co-channel signals. In the case of shadowing the direct path between the communicating parties is obstructed by buildings or other obstacles and the link can be used because of the paths arriving at the receiver via reflectors. Spatially fast changing (Rayleigh-) fading arises from the field strengths of all paths being summed up at the receiver antenna. The resulting signal may be extremely weak depending on the respective amplitudes and phase angles.

On a link with fixed users the constellation which leads to fading is frequency dependant, the frequency difference with high correlation between the influences on signals being called the coherence bandwidth /3/. As far as digital transmission over multipath channels is concerned wideband systems are those whose bit rates approach or even exceed the coherence bandwidth of the channel. In this case the interpath delays of the propagation field become as large as one or several bit durations and at the receive antenna the phasors of different information bits overlap producing intersymbol interference in addition to fading which, as usual, is caused by paths with short interpath delays.

While it is possible to decrease the effects of fading on reception performance by augmenting the transmit power, this is useless as far as intersymbol interference is concerned. Any change of the transmit power simultaneously changes the strengths of the overlapping symbols and the so called irreducible bit error probabilities may be substantial /4/.

In a multipath environment like urban area delays between paths of relevant power often amounts to several microseconds resulting in coherence bandwidths down to several hundreds of kHz. Thus, systems with transmission rates in the order of or beyond 1 MHz are likely to be affected by intersymbol interference.

MULTIPATH UTILIZATION

Signals of propagation paths with small delays as compared to the signalling period melt together at the receiver and fadings will occur as happens in narrowband transmission. Paths with long interpath delays, however, allow to revert the channel dispersion by appropriate signal processing and thus utilize multipath, i. e. take advantage from the fact that every path conveys signal energy. One well known method is equalization /5/. As far as land mobile radio transmission is concerned applicability of adaptive equalization, however, is limited because of the rapidly changing propagation field.

The approach which subsequently will be described is based on correlation techniques which will be explained based on figure 1. A signal arrives at the receiver on two paths with a time separation τ. Both receive signals can be separated from each other because (1) the width of the autocorrelation peaks is

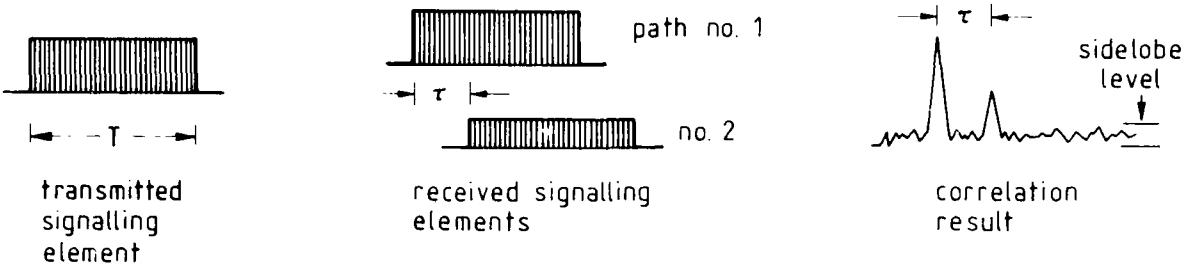

Figure 1: Signal separation by correlation

narrower than the time separation and (2) the sidelobe level is low enough as to not suppress the peaks. These conditions are satisfied if e. g., as signalling elements, pseudorandom sequences are selected such that the time-bandwidth-product TB becomes markedly greater than unity with T being the signalling period. In otner words: Signal separation by correlation can be achieved by application of spread spectrum techniques which by means of an appropriate processing gain are suited to suppress the effects of intersymbol interference.

As far as multipath utilization is concerned the correlation technique offers several options. The simplest one is to evaluate only those samples of the correlation results belonging to the strongest path. As there may be numerous paths which can be separated, selecting the strongest one already introduces a considerable reserve against the residual path fadings. A much more powerful method, however, is to take samples at the arrival times of all paths of the multipath profile and form a complex weighted sum of the samples. So the different path phase angles can be equalized which, in conjunction with appropriate amplitude weighting, yields an optimum output signal-to-noise ratio. This procedure, known as coherent integration, effectively makes use of the signal energy conveyed by the multipath propagation field.

Now some questions arise about how to get the knowledge about path arrival times, amplitudes and phases and how to effectively transfer information by the signalling elements. These questions will be covered in the following paragraph.

SIGNAL FORMAT AND SIGNAL PROCESSING

In order to be more specific and to give the reader a realistic idea of how multipath utilization by correlation can be achieved in a spectrally efficient way the following discussion is based on the newest version, called CD 900, of the aforementioned mobile telephone system. CD 900 is an evolution of a system named AUTOTEL which was developed under sponsorship of the German Ministry of Research and Technology (BMFT) in order to prove the feasibility of high rate transmission over multipath channels.

The time slot and channel structure of CD 900 are depicted in figure 2.

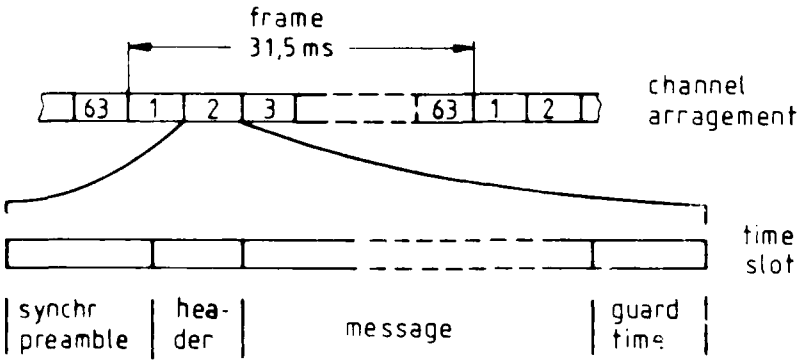

Figure 2: Time slot and channel structure of CD 900

The system supports 60 communications channels for 16 kbit/s digital voice and 3 control channels. Each time slot of 500 µs length is repeated after a period of 31.5 ms. The transmitted signal commences with a preamble which contains in essence an M-sequence of 127 chips (codebits) for synchronization with a chip duration of 250 nanoseconds or a chip rate of 4 MHz. As soon as the synchronization preamble has totally entered an accordingly programmed correlator in the receiver a peak occurs from which the path amplitude and, by processing in quadrature components, the phase angle can be derived. Thus, reception of the sync-preamble in a multipath environment reveals all path properties required for multipath utilization: time of arrival, amplitudes and phases. During the short time slot a vehicle will travel only a small fraction of a wavelength. So amplitude changes and doppler phase shifts can be neglected although a scheme has been developed which is suited to track the multipath profile. A description of this scheme and of the procedure for tracking oscillator frequency offsets as well would, however, be beyond the scope of this paper.

AD-A154 031 PROPAGATION INFLUENCES ON DIGITAL TRANSMISSION SYSTEMS: 6/6
PROBLEMS AND SOLU..(U) ADVISORY GROUP FOR AEROSPACE
RESEARCH AND DEVELOPMENT NEUILLY.. J H BLYTHE
UNCLASSIFIED 08 JUN 84 AGARD-CP-363 F/G 17/2 NL

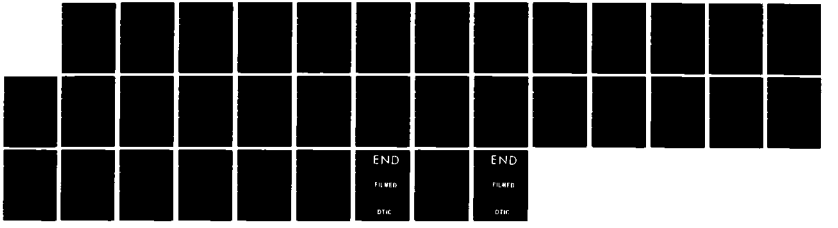

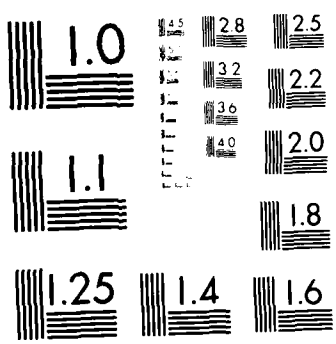

MICROCOPY RESOLUTION TEST CHART

The information part of a time slot begins with a header containing control information. The message itself is followed by a guard period in order to avoid overlaps of two subsequent time slot emissions at the receiver caused by different propagation delays.

As was pointed out earlier the signalling elements in the information part of a time slot need a time-bandwidth-product significantly greater than unity. Our investigations have shown that a processing gain of at least 16 should be selected for cellular mobile radio applications. The signalling elements of CD 900 consist of 32 chips producing a processing gain of 32. This results in an excellent capability of multipath utilization and, in addition, establishes a margin to suppress strong co-channel interference. A bandwidth spreading factor of 32, however, cannot be accepted for civil applications like mobile telephony where spectral efficiency plays a dominant role. An elegant way to maintain the processing gain and not to substantially degrade performance is to use an M-ary signalling alphabet. In this case there exists a set of M unique signalling elements or symbols one out of which is going to be transmitted in every signalling interval. For CD 900 M equals 32. So each symbol carries an information content of 5 bits because there are 32 different 5-bit sequences.

Receiver operation can be understood by imagining 32 symbol correlators to be available. When a received symbol totally has entered the correlators the "correct" correlator shows up a high peak while at the "wrong" correlators only small sidelobes occur which even vanish in the case of an orthogonal signalling alphabet and no interference. Thus the receiver strategy is to decide in favour of the correlator with the strongest outcome.

By introducing a 32-ary alphabet the bandwidth spreading ratio is decreased from 32 down to 32/5 = 6.4. Actually in CD 900 the bandwidth spreading ratio has a value of 2.67 altering the TB-product. This was achieved within two steps. One additional bit per symbol was introduced which determines the symbol sign; as the receiver performs coherent integration the sign can be detected. Similarly the receiver can distinguish between two 6 bit-/32 chip-symbols being simultaneously transmitted in phase quadrature. So, during one symbol interval ($32 \cdot 250$ ns = 8 µs) an information content of 12 bits is conveyed.

Undoubtedly these steps lead to a performance degradation which, however, can be tolerated. So co-channel interference with power equal to the wanted signal still can be tolerated in most of the multipath situations.

As far as receiver implementation is concerned nearly all signal processing is performed digitally and off-line during the period between two receive time slots. In course of the receive slot only a sequence of complex-valued samples is generated which subsequently can be processed by appropriate algorithms.

PERFORMANCE EVALUATION

Based on the experiences gained during the AUTOTEL program comprising theoretical investigations as well as successful field measurements predictions of the CD 900 system performance could be generated taking changes of the design into account. So, e. g., sectoral antennas will be used instead of omnidirectional antennas because of implementation reasons where each one of three antennas illuminates a hexagonal sector as depicted in figure 3. In order to minimize mutual interference different time slots are used in adjacent sectors with the exception of channel borroughing being allowed to some extent between adjacent sectors or cells in case of a capacity bottleneck.

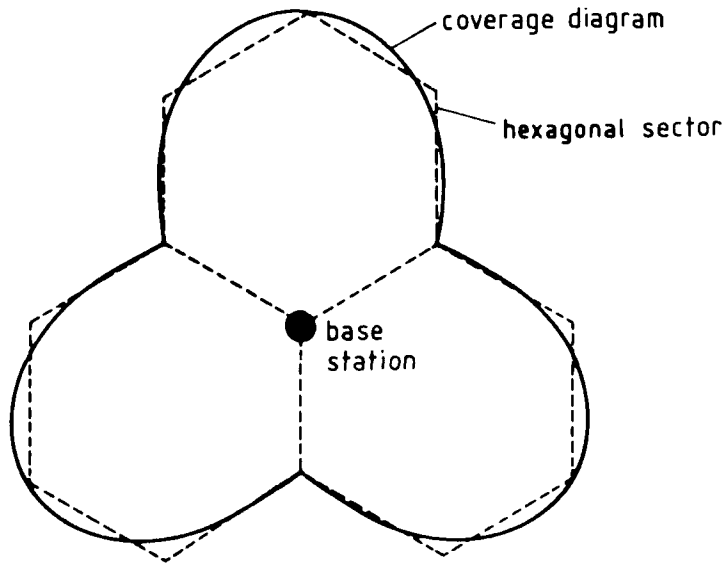

Figure 3: Cell configuration (3 sectors) of CD 900

For performance predictions realistic data about multipath profiles must be used as have been collected by various researchers in the USA and Great Britain, e. g. Cox /6/, Nielson /7/, Turin et al. /8/ or Bajwa and Parsons /9/. Based upon Turin's measurements in and around San Francisco a simulation program has been developed by Hashemi /10/ which now is used in our investigations. The program generates sequences of multipath profiles for different types of propagation characteristics, ranging from the most severe scenario of the financial district in San Francisco to the residential area of Berkeley. These sequences are incorporated in another program simulating a cellular system, where for various strategies for cell and channel selection as well as for power control statistical parameters of channel quality and loss rates can be computed. Figures 4 to 6 may give an impression of system performance. So figure 4 shows that an average traffic demand of 0.8 erlangs per channel can be realized with a loss probability of below 0.5 percent while conversation quality keeps on a high level. The diagram of figure 4 was generated for large city propagation conditions with clusters of skycrapers interspersed with lower buildings such that often there is no line-of-sight connection between transmitter and receiver.

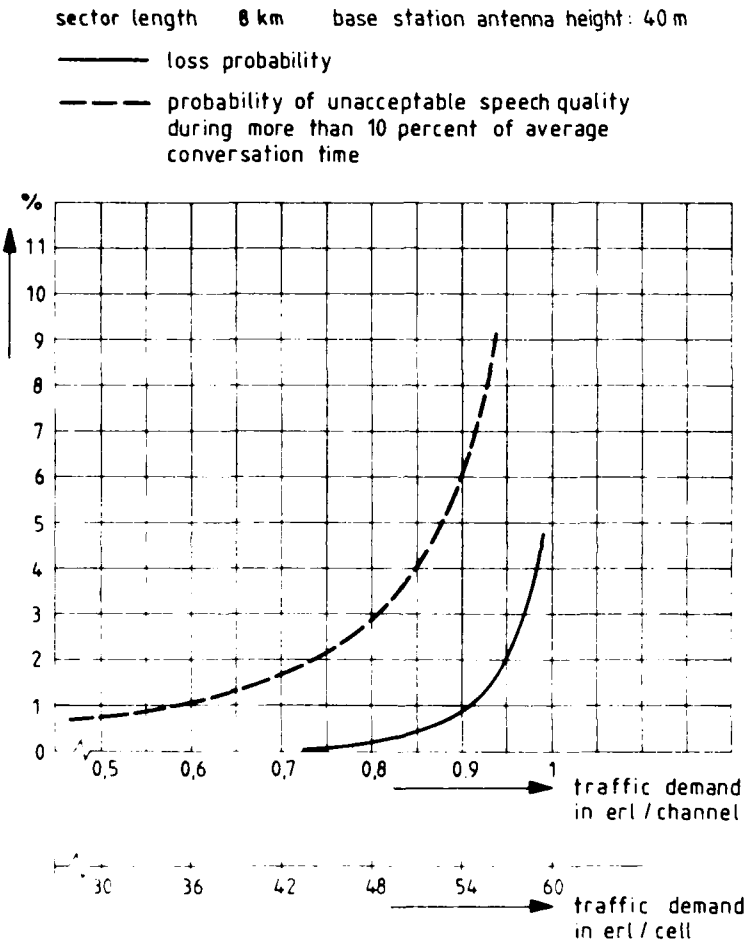

Figure 4: Traffic handling capability in a large city

As a performance measure the probability of voice degradation beyond an acceptable level for more than 10 percent of the average conversation time was selected. For subband coded (SBC) voice a bound of at least 1 percent symbol error probability according to a bit error probability of 0.5 percent is acceptable.

The cumulative distribution of symbol error probability in large city propagation conditions averaged over location and time is depicted in figure 5. For a traffic demand as high as 0.8 erlangs per channel at most one percent symbol error probability is achieved on a 99 percent reliability level.

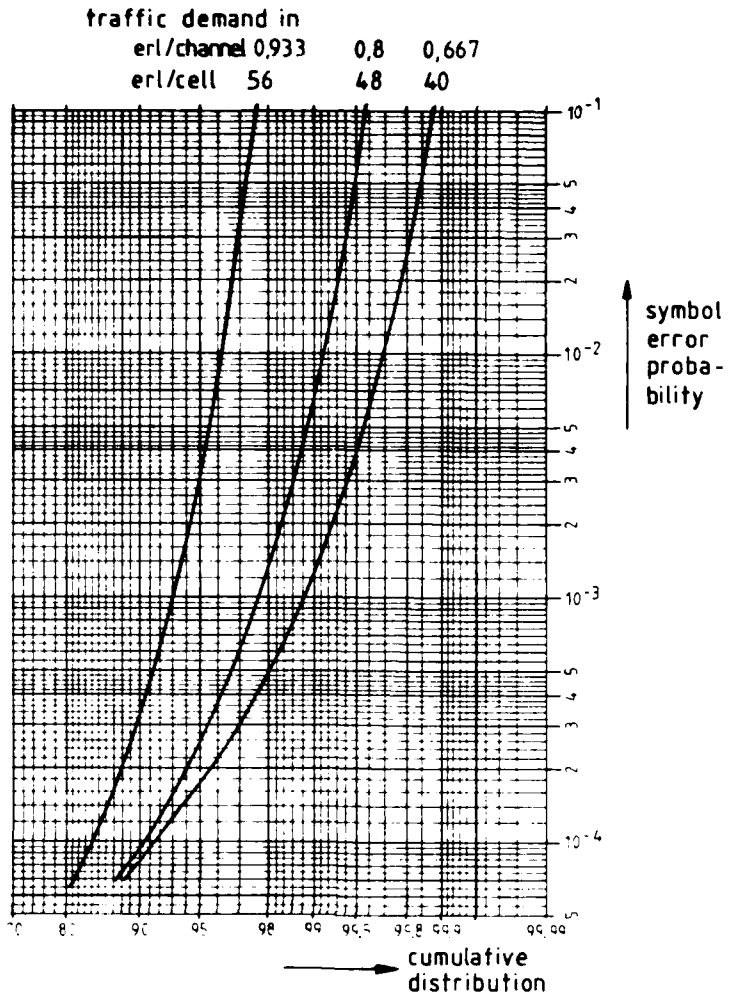

Figure 5: Cumulative distribution of symbol error probability averaged over location and time in a large city

Although only 4 W transmitter peak power on the mobile side was selected the system range reserves are considerable as can be seen from figure 6. As the peak power of 4 W is required only during a transmit time slot, the average transmitter power has a value of about 0.064 W. This very low figure demonstrates a substantial advantage also for inclusion of portable phones in the system. So, not only system operation but also equipment cost take benefit from multipath utilization.

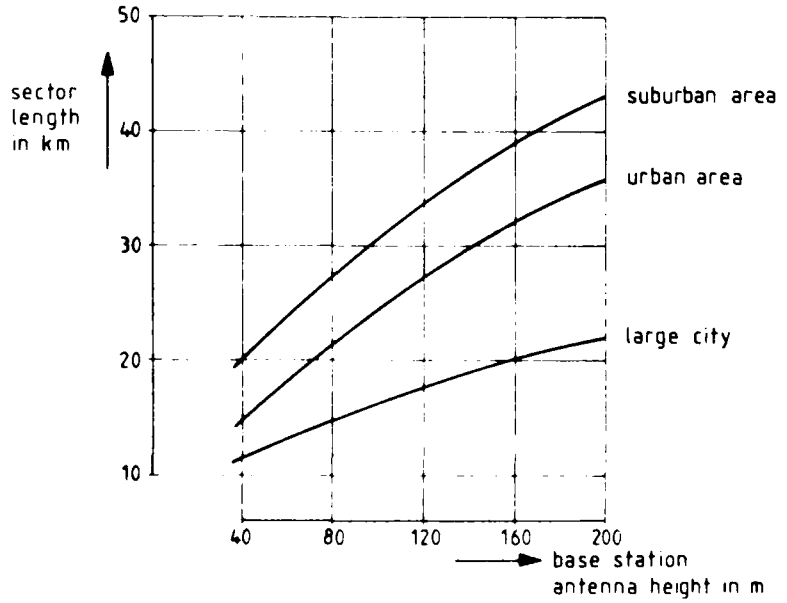

Figure 6: Maximum sector length for area coverage in flat terrain

CONCLUSION

Multipath propagation does not only cause problems for radio transmission. Wideband systems can be designed in a way not only to cope with but to utilize multipath for improvement of link availability and reception performance. A combination of spread spectrum techniques with M-ary signalling allows for spectrally efficient and interference resistant system implementation. Digital transmission and signal processing provide a basis for favourably low equipment cost.

REFERENCES

/1/ Langewellpott, U.: Mehrwegeresistente Datenübertragung mit hohen Raten im Mobilfunk bei 1 GHz, Frequenz 36 (1982) 4/5, pp. 105-109

/2/ Langewellpott, U.: AUTOTEL, a Novel Wideband Mobile Telephone and Data System at 900 Megahertz, 1983, IEE Conf. on Radio Spectrum Conservation Techniques, pp. 85-88

/3/ Jakes, W. C. Jr.: Microwave Mobile Communications, New York, John Wiley & Sons, 1974

/4/ Bajwa, A. S., Parsons, J. D.: Small-area Characterisation of UHF Urban and Suburban Mobile Radio Propagation, Proc. IEE, 129, 2, 1982, pp. 102-109

/5/ Monsen, P.: Feedback Equalization for Fading Dispersive Channels, IEEE Trans. IT-17 (1971), pp. 56-64

/6/ Cox, D. C.: 910 MHz Urban Mobile Radio Propagation: Multipath Characteristics in New York City, IEEE Trans. VT-22 (1973) 4, pp. 104-110

/7/ Nielson, D. L.: Microwave Propagation Measurements for Mobile Digital Radio Application, IEEE Trans. VT-27 (1978) 3, pp. 117-132

/8/ Turin, G.L. et al.: A Statistical Model of Urban Multipath Propagation, IEEE Trans. VT-21 (1972) 1, pp. 1-9

/9/ Parsons, J. D., Bajwa, A. S.: Wideband Characterisation of Fading Mobile Channels, IEE Proc., 129, 2, 1982, pp. 95-101

/10/ Hashemi, H.: Simulation of the Urban Radio Propagation Channel, Ph. D. thesis, Dep. Elec. Eng. Comput. Sci., Univ. California, Berkeley, 1977

DISCUSSION

A.Maloberti, Fr

Was your link tested under impulsive noise conditions? We find this very often in urban propagation, when communicating with mobile stations. It may become a predominant noise for a large bandwidth transmission. I would like to know the views of the author on that, and if any attempts were made to test your system under that condition.

Author's Reply

My answer has several aspects. Initially we foresaw a potential problem, and examined the literature for information on impulsive noise at 900 MHz, and found a very disappointing level of available information. During our experimental investigations which are still proceeding, we did not detect any serious impact on our system from impulsive noise. I think there are two factors. One is that the spectral density of these effects decreases substantially with frequency, and the other is that our system has some inherent capability to suppress these effects through the use of spread spectrum.

J.C.Arnbak, Ne

It was interesting to see the measurements you have been doing in the Stuttgart area on fading changes from narrowband to wideband. Can you indicate what kind of statistics you found in the wideband case. Did the Rayleigh statistics change into something else, did the log-normal statistics normally assumed for shadowing change into something else?

Author's Reply

In the wideband measurements shadowing is still there, but the fading changes, the fading depths are significantly reduced, by the order of 10 dBs or even more.

J.C.Arnbak

That was not really my question: did the statistics change?

Author's Reply

It is no longer Rayleigh statistics, which go down to zero sometimes. But on the other hand we must look at the statistics of the multipath profiles. Because of the limited spreading ratio we have some intersymbol interference in the system which is reduced. We have developed an analytical model to incorporate all of these effects and it is very close to the real nature.

"Narrowband" Spread Spectrum Systems

Karl Heinz Annecke, Manfred Ottka
ANT Nachrichtentechnik GmbH
Gerberstrasse 33
D-7150 Backnang
Federal Republic of Germany

Summary

The available military radio frequency bands are covered very densely by the already existing conventional systems and therefore the application of bandwidth widening procedures as antijam measures will be allowed only with small spreading factors within these RF-bands.
In this paper the problems arising from the random code selection for spread spectrum systems with small spreading factors are discussed. The calculations show the dependence between certain statistical properties of classes of codewords and the number of codewords available in these classes.
The bit error probabilities in case of jamming by white gaussian noise, narrowband and cw-jammers are calculated in comparison with the error probability of the class of codewords with ideal correlation properties.

Introduction

In recent years the discussions regarding the introduction of spread spectrum systems into military communication systems have become more and more intensive. In this paper the influences of small spreading factors on the process gain and anti-jam capability of direct sequence (DS) and frequency hopping (FH) systems will be discussed.
The anti-jam capability of spread spectrum systems is based on the use of a bandwidth much greater than necessary for the data-transmission in an unjammed environment. Information theory shows that the channel capacity, i.e. the theoretically faultless transmissionable bitrate is only a function of the available bandwidth and the signal to noise ratio within this bandwidth in case of white gaussian noise.

$$C = B \cdot \mathrm{ld}\,(1+S/N) \approx B \cdot S/N \cdot 1.4 \quad \text{for} \quad S/N \ll 1 \tag{1}$$

Regarding this the process gain of a system using additional bandwidth efficiently should be in the order of the bandwidth widening factor or greater for noise or jammers better predictable than white gaussian noise. A good strategy to fight unknown or unpredictable jammers in symbol by symbol transmission systems is the random spreading of the energy available for the transmission of each symbol over the whole transmission bandwidth, that means filling the available bandwidth with a flat power density spectrum. For best results it is necessary to do so for each individual symbol and not only in an average over the transmitted signal.
The best known systems with these features are direct sequence and frequency hopping spread spectrum systems, both assigning each transmitted symbol a codeword consisting of a sequence of different phases or frequencies. In this paper we are not discussing the behaviour of so called slow frequency hopping systems with one or more symbols transmitted per frequency hop. Figure 1 shows a blockdiagram of a simple 2-PSK/2-PSK data transmission/direct sequence spread spectrum system and figures 2 and 3 examples of frequency hopping systems with coherent and noncoherent demodulation.
In the following firstly well known results calculated for DS systems with spreading factors much greater than 1 will be reported. Secondly some computations done for DS systems with small spreading factors jammed by continuous wave or gaussian narrowband jammers will be shown. Based on these results a class of codewords optimized to fight these jammers is described. Thirdly the calculations are done for FH systems.

Direct Sequence Systems with large spreading factors

The codegenerator shown in figure 1 must generate a set of codewords which spectrum is as flat as possible within the available bandwidth. Therefore the aperiodic autocorrelation function of the codeword $c_i(t)$ must have sidelobes as low as possible.

$$c_i(t) = \sum_{k=0}^{m_c-1} a_{k,i} \cdot \mathrm{rect}\left(\frac{t-kT_c}{T_c}\right)$$

$$\mathrm{rect}\left(\frac{t}{T_c}\right) = \begin{cases} 0 & , \ |t| > T_c/2 \\ 1 & , \ |t| \le T_c/2 \end{cases} \tag{2}$$

$$a_{i,k} \in \{-1, +1\}$$

$$\varphi_{c_i,c_i}(\tau) = \int_{-\infty}^{+\infty} c_i(t) \cdot c_i(t+\tau)\, dt$$

The fourier transform of the autocorrelation function is the energy-density spectrum of the codeword.

$$\Phi_{c_i c_i}(f) = \mathcal{F}\left\{\varphi_{c_i c_i}(\tau)\right\} \qquad (3)$$

The number of spreading bits (called chips in the following) per data bit is the so called spreading factor m_c. The problems of the existence and generation of sets of binary codewords with limited absolute sidelobes or sidelobe to main ratios of the autocorrelation function have been discussed extensively /4, 5/. Using only these ideal codewords in case of gaussian noise + jammer the error probability at the output of a matched filter receiver can be approximated very well by the error function complement of the energy per transmitted symbol E_S, the noise and jammer spectral densities (Φ_N, Φ_J) and the spreading factor.

$$p_e = 0.5\ \mathrm{erfc}\ (E_S, \Phi_{t_s}, \Phi_J, m_c)$$

The use of so called pseudo noise (PN) sequences as codewords or as spreading sequences sections of which are used as codewords in direct sequence spread spectrum systems with spreading factors much greater than 1 are discussed in /1,2,3/. It is shown that for large m_c and continuous wave jammers (because of the rule of great numbers and the central limit theorem) the behaviour of the system can be described approximately by the error function complement assuming a wideband gaussian distributed jammer of the same power.

In the following all calculations of the error probability are done under the assumption of a signal to noise ratio much better than the signal to jammer ratio. The actual signal to noise ratios have of course to be taken into consideration so that the error probability of the systems approaches asymptotically the value given by the signal to noise ratio for increasing signal to jammer ratios. Moreover an additional gaussian white noise causes a smoothing of the steps existing in some of the curves calculated for the signal and jammer alone.

The error probability of a system with arbitrary codewords and white gaussian noise jammers is given by the error function complement as follows

$$p_e = 0.5\ \mathrm{erfc}\ (\sqrt{S/J \cdot m_c})$$

$$\mathrm{erfc}\ (x) = \frac{2}{\sqrt{\pi}} \int_x^\infty e^{-y^2}\, dy \qquad (4)$$

The formula is also relevant as an approximation in case of ideal wideband codewords and gaussian bandpass jammers tuned to the centre frequency of the system. In most cases certain assumptions concerning the statistics of the jammers to be expected can be made with high probability. In this paper only continuous wave jammers and narrowband jammers with a gaussian amplitude distribution and a centre frequency offset smaller than the information signal bandwidth will be considered in the following.

Narrowband Spread Spectrum Systems

The application of spread spectrum signal processing methods to single channel communication links in the tactical area with spreading factors and therefore process gains in the order of up to 100 or more leads to a transmission bandwidth for one speech channel of a few MHz which may be acceptable in the used frequency region for low range communications. Widespread communication nets partly based on microwave links have transmission capacities of up to a few Mbit/s or even 34 Mbit/s. Additional spreading of these signals with spreading factors in the order mentioned above will lead very fast to problems in bandwidth consumption and technical feasibility of mixers and codegenerators. Therefore only small bandwidth spreading factors probably in the order of 5 to 50 will be acceptable for microwave links.

Nevertheless the gain implemented by these signal processing procedures may be just enough to hold the line against a jammer's attack. Especially in combination with error correction coding procedures or other nonlinear signal processing methods with threshold effects known from frequency modulation/demodulation the introduction of spread spectrum systems gaining enough dB to hold the system just above the threshold may be of great interest.

Investigations of ECCM for microwave systems showed that a combination of a spread spectrum system with a moderate spreading factor, an error correction coding procedure, an adaptive notch filter to fight narrowband jammers and a null steering antenna can generate a very high degree of anti-jam capability for microwave systems with acceptable expenditure and expense.

In the next chapters the behaviour of DS and FH spread spectrum systems with small spreading factors (called narrowband spread spectrum systems) will be discussed.

Narrowband Direct Sequence Spread Spectrum Systems

Optimal white wideband codewords for these systems are codewords with low sidelobes or low sidelobe to main value ratios of the aperiodic autocorrelation function. The number of these codewords is a very limited one for each length, for example for codelengths of 7 to 42 exist only 4 to 1000 different codewords with these properties dependent on the bit width sidelobe level.

Apart from the storage and randomly generated access to these codewords in the transmitter and receiver will be a minor problem the susceptibility to imitating jammers becomes very high with increasing codeword length and number. On the other side purely random generated bit set codewords with a generation rule only known to the receiver have the known disadvantage of missing codes with good autocorrelation properties and poor autocorrelation properties. In special case of a jammer tuned on the centre frequency of the system figure 4 and 5 show the error probabilities calculated for spreading factors of 1 - 100 with random codes for sinewave and narrowband gaussian jammer.

The calculation of these error probabilities is as follows.
The signal $s(t)+j(t)$ at the input of the receiver (Fig. 1) is given by

$$s(t) = d(t-iT_d) \cdot c(t-iT_d) \cdot \cos \omega_0 t$$

with $$d(t) = b \; \mathrm{rect}(t/T_d), \qquad b_i \in \{-1, +1\} \quad \text{as informations bits} \tag{5}$$

and

$$j(t) = n_j(t) \cdot \cos(\omega_0 t + \varphi(t))$$

is a narrowband jamming signal, uncorrelated to $s(t)$. Herein the ratio of the bit clock time T_d and the chip duration T_c defines the band spreading factor m_c.
It is assumed that the amplitude of the demodulated jammer signal is constant during one information bit (narrowband jammer tuned on centre-frequency) and furthermore that a continuous wave jammer after demodulation into the baseband has the amplitude distribution of a cosine function because of the unknown or randomly varying phase.

$$p_{CW}(x) = \frac{1}{\pi \sqrt{J/2 - x^2}} \tag{6}$$

J is the power of the jammer-signal.
In case of a narrowband gaussian jammer the demodulated baseband signal is also gaussian distributed

$$p_{NG}(x) = \sqrt{\frac{2}{\pi \cdot J}} \cdot e^{-\frac{2x^2}{J}} \tag{7}$$

The error probability of a codeword containing i "ones" and $m_c - i$ "zeros" follows as

$$p_{i,CW} = \begin{cases} \frac{1}{2} - \frac{1}{\pi} \arcsin\left(\frac{m_c}{|2i-m_c|}\sqrt{\frac{S}{J}}\right) & , \text{ for } \frac{m_c}{|2i-m_c|}\sqrt{\frac{S}{J}} < 1 \\ 0 & , \text{ otherwise} \end{cases} \tag{8}$$

and

$$p_{i,NG} = \frac{1}{2} \operatorname{erfc}\left(\frac{m_c}{|2i-m_c|}\sqrt{\frac{S}{J}}\right)$$

For random codes or short sequences taken from much longer PN-sequences there are existing

$$\binom{m_c}{i} = \frac{m_c!}{i!\,(m_c-i)!} \tag{9}$$

codes containing exactly i "ones" and $m_c - i$ "zeros".
The resultant average error probability for a DS system with randomly chosen codes now is

$$p_E = \frac{1}{2^{m_c}} \sum_{i=1}^{m_c} \binom{m_c}{i} \cdot p \tag{10}$$

with

$$p = \begin{cases} p_{i,CW} & \text{for cw - jammers} \\ p_{i,NG} & \text{for gaussian jammers} \end{cases}$$

In case of cw-jammers figure 4 shows that only for large spreading-factors ($\approx$100) the error probability curves tend to 0.5 erfc($\sqrt{S/J}$) relevant for white gaussian noise. For gaussian narrowband jammers randomly diced codes result in a degradation compared with the erfc relevant for $m_c = 1$ as shown in figure 5. This degradation is in the order of 4 to 6 dB for error probabilities of 10^{-3} to 10^{-5} and spreading factors of 5 to 100.

Strategies for excluding poor codes

In order to get a better system performance one should exclude the codes with the highest contribution to the resulting error probability. Eq. 8 obviously shows that the unbalancy $\chi = |2i-m_c|$ of a code which is the absolute value of the difference between the number of "ones" and "zeros" is a measure for its degradation of anti-jam-capability in the cases discussed here. Beginning with $|2i-m_c| = m_c$ it is possible to exclude step by step poor codes and increase the system performance. This procedure results in the error probability for a code set which excludes all codes with more than $m_c - k$ "zeros" or "ones"

$$p_k = \frac{\sum_{i=k}^{m_c-k} \binom{m_c}{i} \cdot p_i}{\sum_{i=k}^{m_c-k} \binom{m_c}{i}} \tag{11}$$

where the denominator is the number of remaining codes.
One possibility to establish a code generator with such a behaviour may be the combining of a common random-code-generator with a supervising unit counting the "ones" and "zeros" in each codeword in order to start the codegenerator for another try if the counter exceeds a given bound. Figures 6 and 7 show some representative results.
For example by using a spreading factor $m_c = 10$ there are existing totally $2^{10} = 1024$ codes. If the number of codes is reduced to $n = 672$ by excluding all codes with a high degree of "unbalancy" $\chi = |2i-m_c|$ much better system performance can be achieved. For error probabilities of less than 10^{-3} the maximum gain is about 12 to 14 dB in case of cw-jammers.

Although the accessible S/J-gains are lower (maximal 9 to 10 dB for error probabilities of 10^{-3} to 10^{-4}) for narrowband gaussian jammers the strategy of excluding poor codes is a powerful tool to increase the anti-jam-capability (Fig. 7).

Narrowband Frequency Hopping Spread Spectrum Systems

A similar severe problem is the selection of codes for narrowband frequency hopping spread spectrum systems with n_c different available frequencies and m_c frequency hops per bit.
To increase the ability in fighting intelligent jammers the aim is using as much different codes as possible. For a fixed product $m_c \cdot n_c = M$ the largest amount of different codes $N_c = n_c^{m_c}$ is obtainable by choosing $m_c = 3$.
Because of problems in technical feasibility this desirable high rate of $m_c = M/n_c$ chips per bit (fast frequency hopping) often can't be achieved, so higher numbers n_c of frequencies and lower numbers m_c of hops per bit are realized. Figures 8 to 10 show the error probabilities for cw- and gaussian jammers by using randomly all N_c codes for $n_c = 10$ and 100 and different m_c. The results are based on a coherent demodulation system model (Fig. 2) and on an incoherent system model (Fig. 3) consisting of two different signal processing paths. One path is tuned on frequencies used for the transmission of binary "ones", whereas the other one is tuned on frequencies used for the transmission of binary "zeros".
The transmitted signals are either given by

$$s(t) = d(t - iT_d) \cdot c_i(t - iT_j)$$

$$d(t - iT_d) = b_i \operatorname{rect}\left(\frac{t - iT_d}{T_d}\right), \quad b \in \{-1, +1\}$$

$$c(t - iT_j) = \sum_{k=0}^{m_c - 1} \operatorname{rect}\left(\frac{t - kT_c}{T_c}\right) \cdot \cos \omega_{i,k} t \qquad (12)$$

$$\omega_{i,k} \in \{\Omega_0, \Omega_1, \ldots, \Omega_{n_c - 1}\}$$

for the coherent receiver model, or in the incoherent case by

$$s(t) = \begin{cases} c_i^{(0)}(t - iT_j) & \text{for } d_i = \text{binary "0"} \\ c_i^{(1)}(t - iT_j) & \text{for } d_i = \text{binary "1"} \end{cases}$$

$$c(t) = \sum_{k=0}^{m_c - 1} \operatorname{rect}\ \frac{t - kT_c}{T_c} \quad \cos \omega_{i,k} t \qquad (13)$$

and $c_i^{(0)}(t)$ and $c_i^{(1)}(t)$ have no common $\omega_{i,k}$.

The calculations are carried out under the assumption of a single channel narrowband jammer (J), with the following post demodulation amplitude distribution:

coherent demodulation

$$p_x(x) = \frac{1}{\pi\sqrt{J/2 - x^2}} \quad \text{for cw-jammers}$$

$$p_x(x) = \sqrt{\frac{2}{\pi J}}\ e^{-} \quad \text{for gaussian jammers} \qquad (14)$$

incoherent demodulation

$$p_x(x) = \left\{ \begin{array}{ll} 1 & \text{, for } x = \sqrt{J/2} \\ 0 & \text{, otherwise} \end{array} \right\} \quad \text{for cw-jammers}$$

$$p_x(x) = \left\{ \begin{array}{ll} \frac{2}{\sqrt{\pi J}}\ e^{-} & \text{, } x > 0 \\ 0 & \text{, otherwise} \end{array} \right\} \quad \text{for gaussian jammers} \qquad (15)$$

For random codes the probability of jamming a total of i frequency slots during one bit interval is

$$\binom{m_c}{i} p_c^{\,i} \cdot p_c^{\,m_c - i} \tag{16}$$

where $p_c = 1/n_c$ is the apriori "to be jammed probability" for each frequency.

By averaging over all possible codes the above abbreviations and assumptions are resulting in the following error probabilities.

$$p_e = \sum_{i=1}^{m_c} \binom{m_c}{i} p_c^{\,i} \cdot p_c^{\,m_c - i} \cdot p_i$$

for cw-jammers and coherent demodulation:

$$p_i = \begin{cases} \frac{1}{2} - \frac{1}{\pi} \arcsin \frac{m_c}{i}\sqrt{S/J} & , \text{ for } \frac{m_c}{i}\sqrt{S/J} < 1 \\ 0 & , \text{ otherwise} \end{cases} \tag{17}$$

for gaussian jammers and coherent demodulation:

$$p_i = \frac{1}{2}\,\mathrm{erfc}\left(\frac{m_c}{i}\sqrt{\frac{S}{J}}\right) \tag{18}$$

for cw-jammers and incoherent demodulation:

$$p_i = \begin{cases} 1 & , \text{ for } S/J < i/m_c \\ 0 & , \text{ otherwise} \end{cases} \tag{19}$$

for gaussian jammers and incoherent demodulation:

$$p_i = \frac{1}{2}\,\mathrm{erfc}\left(\sqrt{\frac{m_c}{i}} \cdot \sqrt{\frac{S}{2J}}\right) \tag{20}$$

Figures 8 to 10 show the calculated error probabilities for different n_c and m_c.

Strategy for excluding poor codes

For a given number of frequencies n_c and a total of m_c hops per bit the random usage of all $n_c^{m_c}$ possible codes has the great disadvantage of generating also codes with maximal up to m_c equal frequencies. To be sure that a jammer of arbitrary frequency can cause in worst case only k jammed slots one has to eliminate all codes containing any of the possible frequencies more than k times. Therefore one should exclude step by step codes with m_c, m_c-1,...,2 equal frequencies. Considering this last chapter's resulting error probabilitites can be rewritten as

$$p_e = \frac{\sum_{i=1}^{k} \binom{m_c}{i} p_c^{\,i} \cdot p_c^{\,m_c - i} \cdot p_i}{\sum_{i=0}^{k} \binom{m_c}{i} p_c^{\,i} \cdot p_c^{\,m_c - i}} \tag{21}$$

Although this formula gives correctly the error probability under the above assumptions the calculation of the number of remaining codes is a difficult task for $\varrho \neq 1$ and $\varrho \neq m_c$.

In principle the above problem can be solved calculating the sum of all possible variations of the multinomial expression

$$\sum \frac{m_c}{k_0! \cdot k_1! \cdot k_2! \cdot \ldots \cdot k_n!}$$

with the marginal condition $\sum k_i = m_c$. Only for greater bandspreading factors (for example $m_c > 10$, $n_c \geq 10$) the calculation and counting of all possible permutations becomes very complicate. But nevertheless the construction of a device seems to be possible, which counts the number of used frequencies for each data interval and resets the codegenerator for another independent trial if a given bound for multiple frequency usage is exceeded. Some calculations for the two types of narrowband jammers and the coherent and noncoherent frequency hopping receivers are carried out. Figures 11 to 14 are showing the results. The highest system performance is obviously obtained, if each frequency is taken only one time in each bit interval ($\varrho = 1$). With this method gains up to about 11 dB (for cw-jammers) or up to 6 dB (for gaussian jammers) are possible.

The usage of envelope detectors in the noncoherent receiver results in rectangular curves for the cw-jammer's case. For gaussian jamming signals it is well known, that the noncoherent slow-frequency hopping system ($m_c = 1$) degrades 3 dB against the coherent system. Beside this additional degradations for higher hopping rates ($m_c \approx 5...10$) are observed.

4 Conclusion

In this paper results have been presented for the performance of coherent direct sequence, coherent fast frequency hopping and incoherent fast frequency hopping systems. The assumed jamming signals are wideband gaussian noise, narrowband gaussian noise and cw-signals. The calculations show that by very simple algorithms classes of spreading codes with increased anti-jam capability can be generated from random codes. Especially in spread spectrum systems with low spreading factors this code-generation method is of greater interest to get a higher variety of used codewords and therefore lower susceptibility to intelligent jammers than in case of using well known sets of ideal wideband codewords.

References

1 L.B.Milstein, S.Davidovici, D.L.Schilling, The Effect of Multiple-Tone Interfering Signals on a Direct Sequence Spread Spectrum Communication System, IEEE Trans. on Communications, Vol. COM-30, No.3, March 1982, 436-446.

2 D.L.Schilling, L.B.Milstein, R.L.Pickholtz, R.W.Brown, Optimization of the Processing Gain of an M-ary Direct Sequence Spread Spectrum Communication System, IEEE Trans. on Communications, Vol. COM-28, No.8, Aug.1980, 1389-1398.

3 S.S.Lichtevich, Performance of a Direct Sequence Spread Spectrum System with Long Period and Short Period Codes Sequences, IEEE Trans. on Communications, Vol. COM-31, No.3, March 1983, 412-419.

4 H.Ipatov, Binary Sequences up to Length 40 with Best Possible Autocorrelation Function, Electronics Letters 11 (1975), 507.

5 H. Ipatov, Synthese zeitdiskreter Binärsignale mit speziellen Auto- und Kreuzkorrelationsfunktionen, PhD-Dissertation, RWTH Aachen, 1977.

6 R.C. Dixon, Spread Spectrum Systems, Wiley, New York 1976.

This work was partly supported by the "Bundesministerium für Verteidigung" of the Federal Republic of Germany.

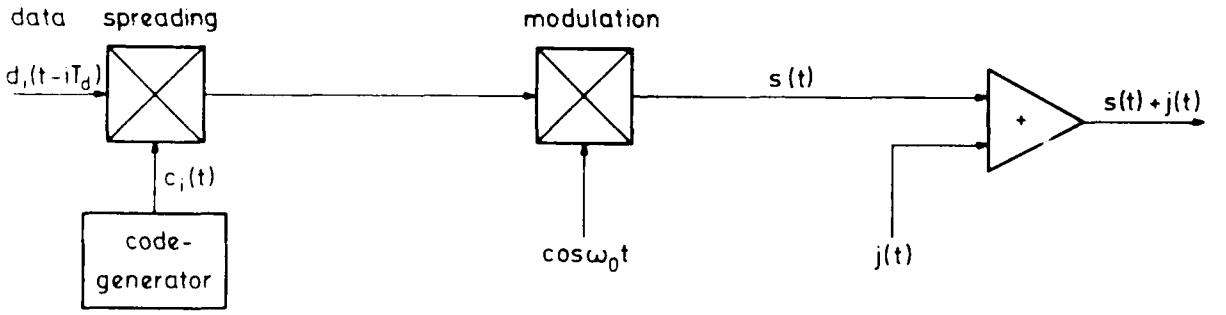

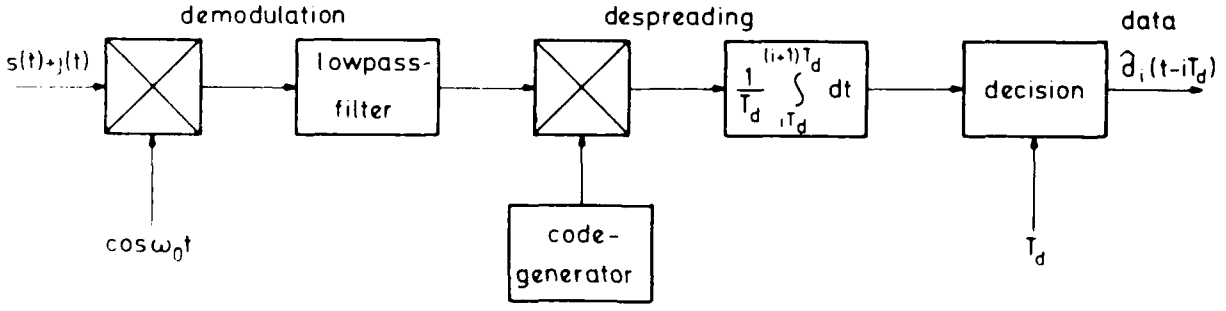

Fig. 1: Model of a direct sequence spread spectrum system

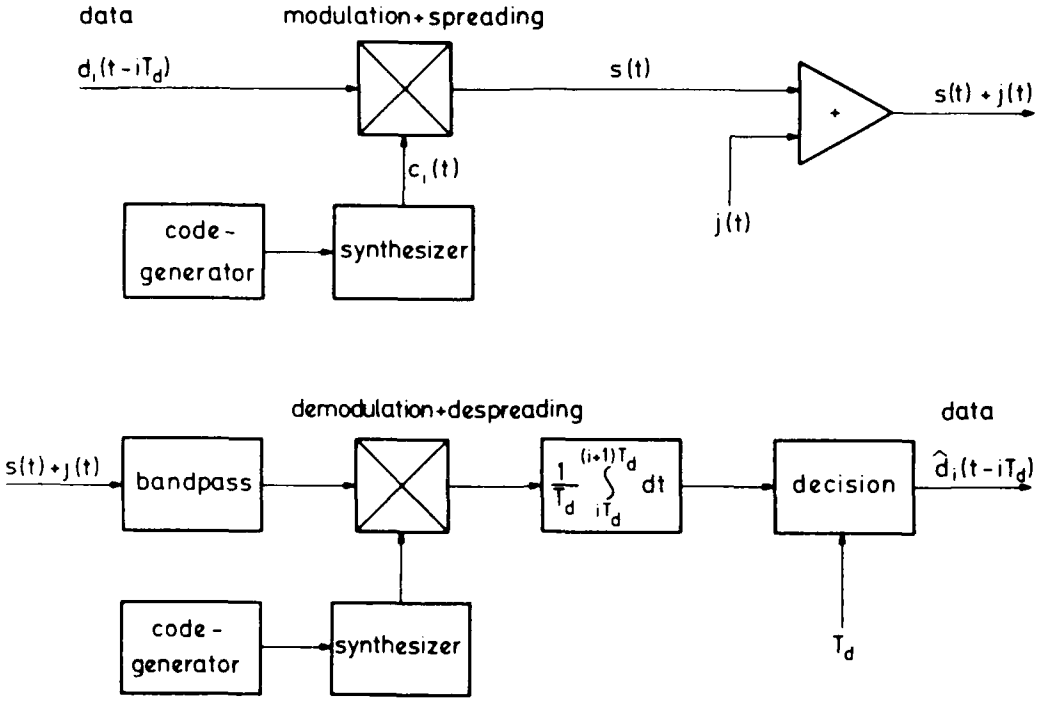

Fig. 2: Model of a coherent frequency hopping spread spectrum system

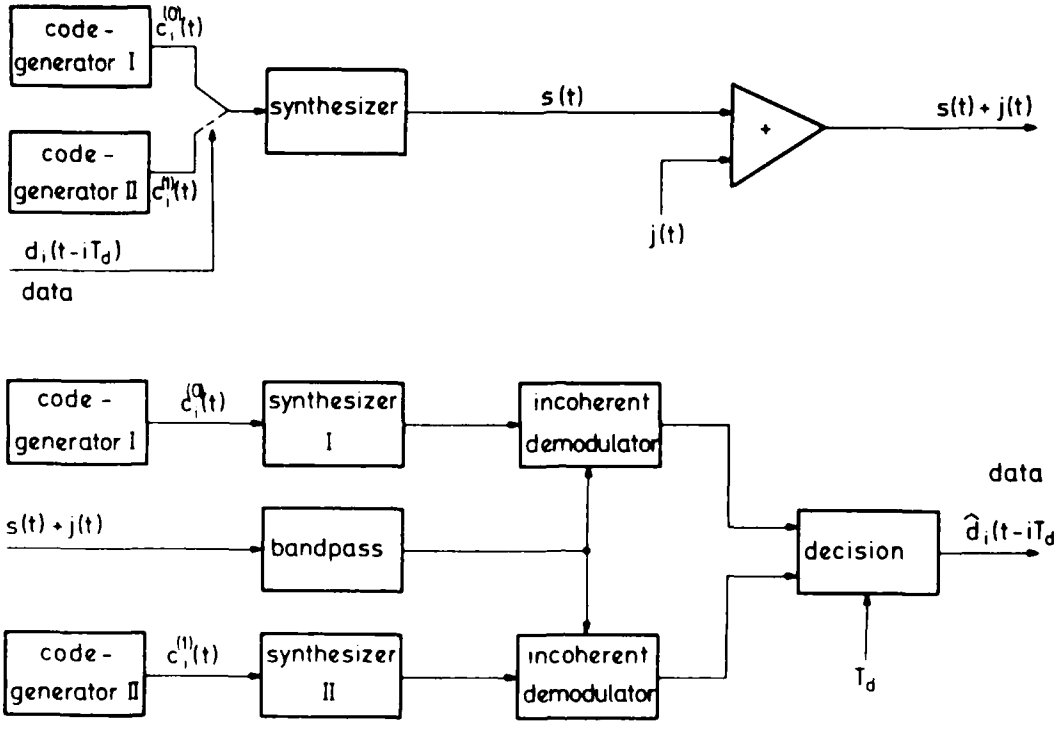

Fig. 3: Model of a incoherent frequency hopping spread spectrum system

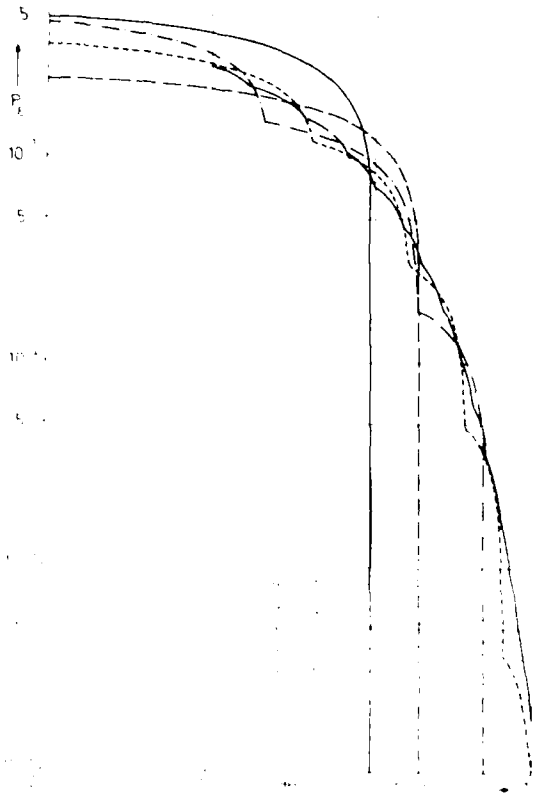

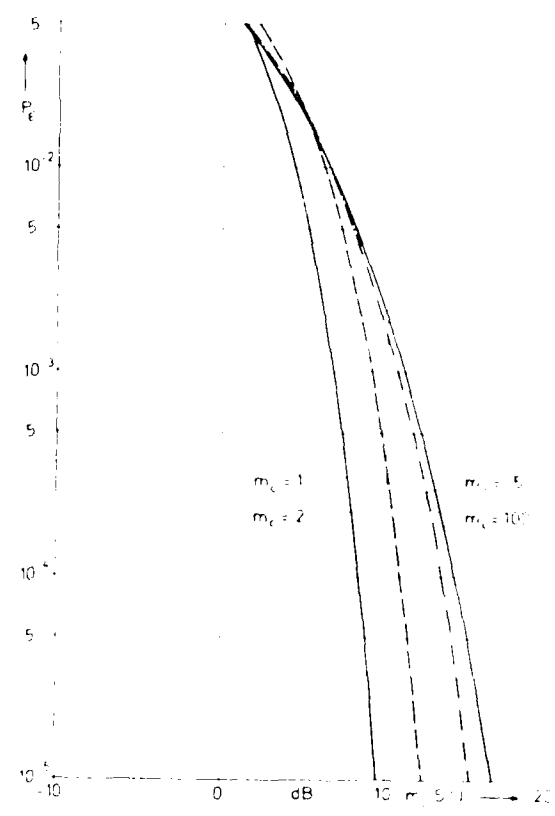

Fig. 5: DS systems, gaussian

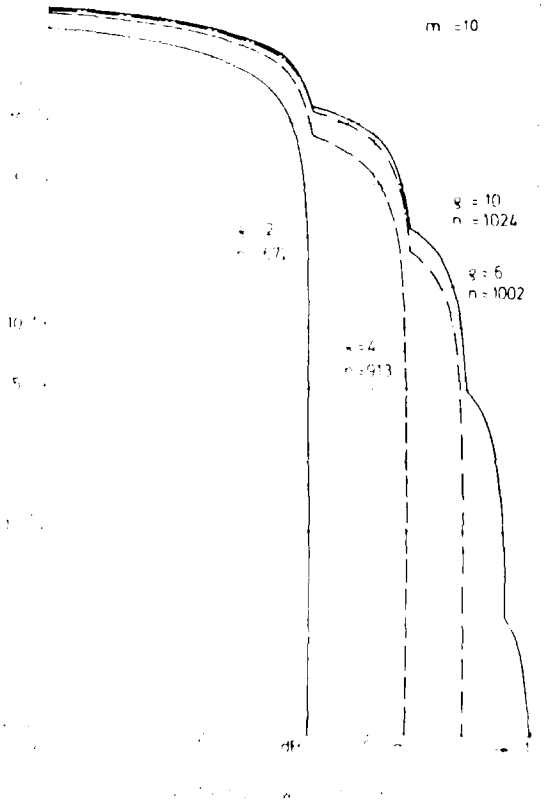

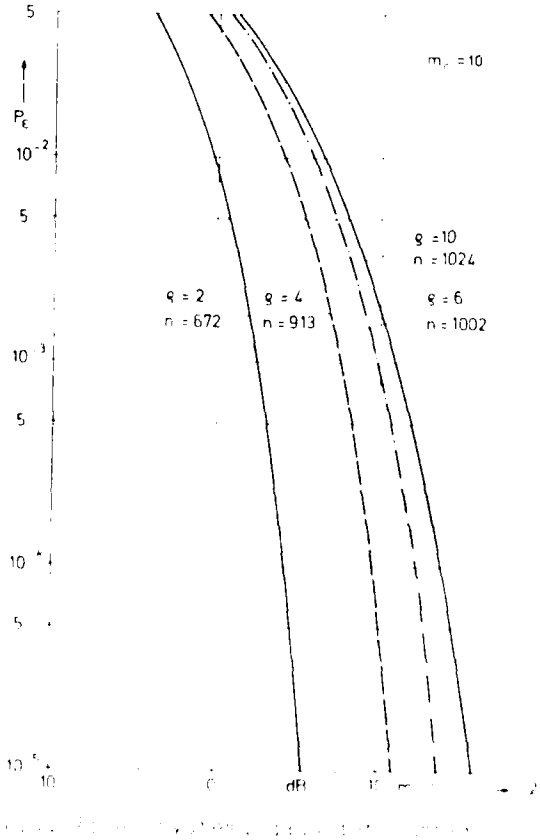

P.3

DEVARENNE, Mr	Electronique Serge Dassault, 55 Quai Carnot, 92 St Cloud, France
DOBBEL, J.E. Mr*	R.6.3.4, British Telecom Research Lab., Martlesham Heath, Ipswich, IP5 7RE, United Kingdom
EDRAOS, P.N. Mr*	Rome Air Development Center (DCCD), Griffiss Air Force Base, NY 13441, United States
FABBRI, F. Dr*	C/o Telettra S.p.a., Via Trento 30, 059 Vimercate, Milano, Italy
FIMERELIS, C. Mr	Hellenic Navy General Staff, Research Centre GEETEN, Holargos, Athens, Greece
GAROYEALIAS, C. Mr	HAF, 202 KEAT-H, Hellinicon, Athens, Greece
GEORGE, P.E. Mr	Andrews Antennas, Suite 1, 1st Floor, Innovation House, Technology Park, The Levels, S.A 5095, Australia
GEORGE, A.M. Mr	Marconi Avionics, Air Radio Div., Christopher Martin Road, Basildon, Essex SS14 3EL, United Kingdom
GHIOCPOULOS, B. Dr	Hellenic Air Force, KETA, Delta Falirou, Palaion Faliron, Greece
GOUIFFARD, C. Prof*	Universite de Paris-Sud, LEETI, 9, Avenue de la Division Leclere, 94230 Cachan, France
GREEN, A.E. Mr	British Aerospace plc, Aircraft Group, Weybridge Div., Chester Road, Woodford, Bramhall, Stockport, Cheshire SK7 1QR, United Kingdom
HABER, F. Prof.*	Moore School of Electrical Eng., University of Pennsylvania, Philadelphia, PA 19104, United States
HARDING, C.R. Mr	PD 109 RSRE, St Andrews Road, Malvern, Worcs, United Kingdom
HATZITHEODOROU, E. Dr	OTE, Department R.H. 3 September St 7, Athens, Greece
HAVEL, G. Dr*	CNET, 38, 40 Avenue du General Leclerc, 92131 Issy-le-Moulineaux, France
HOFMEYER, J.A. Dr	US Department of Commerce, NTIA/ITS, N4, 325 Broadway, Boulder, CO 80303, United States
HOFGEN, R.G. Dr	Standard Elektrik Lorenz AG, 7000 Stuttgart 40, Federal Republic of Germany
HOLTZMAN, J.C. Prof*	Electrical Engineering Dept., University of Kansas, Lawrence, Kansas 66045, United States
HUBAL, M. Mr	FABG, Abt. WIS, Einsteinstrasse 20, D-8012 Ottobrunn, Federal Republic of Germany
HUBBARD, R.W. Dr*	US Department of Commerce, NTIA/ITS.N4, 325 Broadway, Boulder, CO 80303, United States
INCE, A.N. Prof	Science and Engineering Council, Burumcuk Sok 7/10, Ankara, Turkey
JENKINS, R.W. Dr	Communications Research Centre, P.O. Box 11490, Station H, Ottawa, Ont. K2H 8S2, Canada
JOURNET, A.R.	THOMSON CSF, 16, rue du Fosse Blanc, B.P. 156, 92231 Genevilliers, France
JUETTER, A.E.R. Mr	ONERA, 29 Avenue de la Division Leclerc, 92320 Châtillon sous Bagneux, France
KALTANDERIS, E. Mr	Hellenic Navy General Staff, Research Centre GEETEN, Holargos, Athens, Greece
KALOYPSIDIS, N. Dr	University of Athens, University Cambus, Electronic Physics Labs., Zografou, Athens, Greece
KAPBEZIDIS, N. Mr	National Observatory, Thision, Athens, Greece
KAPELIANAKIS, N. Mr	HAF, 202 KEAT-H, Hellinicon, Athens, Greece
KAROYBALOS, C. Prof	University of Athens, University Cambus, Electronic Physics Labs., Zografou, Athens, Greece
KATELOZOS, D. Major	HAF, 202 KEAT-H, Hellinicon, Athens, Greece
KERN, F. Mr	BWB/ME, Dachauerstrasse 128, D-8000 Munchen 19, Federal Republic of Germany
KLINKERT, F. Mr*	National Aerospace Laboratory, NLR, P.O. 90502, NL-1006 BM Amsterdam, The Netherlands
KOOB, K.A. Dr	MBB, Dept. AE 32, Postfach 801149, D-8000 Munchen 80, Federal Republic of Germany

* Author of paper presented at the meeting
Member of Electromagnetic Wave Propagation Panel

LIST OF PARTICIPANTS

AARONS, J Dr*	Department of Astronomy, Boston University, 725 Commonwealth Avenue, Boston, MA 02215, United States
AGOURAS, P Mr	115 Macedonomachon St., Thracomacedones, Athens, Greece
AIVAZIS, K Mr	National Defence Research Centre, Hippocratus and Diogenus St, Galatsi, Athens, Greece
ALBRECHT, H-J Dr	FGAN, Konigstrasse 2, D-5307 Wachtberg-Werthhoven, Federal Republic of Germany
ANAGNOSTOU, E Mr	National Defence Research Centre, Hippocratus and Diogenus St, Galatsi, Athens, Greece
ANESTOPOULOS, C Mr	Ministry of Res. and Technology, Ermou St 2, Athens, Greece
ANNECKE, K H Dr*	ANT Nachrichtentechnik GmbH, Gerberstrasse 33, D-7150 Backnang, Federal Republic of Germany
APOSTOLOU, N Mr	ERT-1, Department of Technical Research, Mesogion 402, Athens, Greece
ARGYROPOULOS, G Mr	OTE, Department of Technical Programming, E Negri 3 and Patision St, Athens, Greece
ARNBAK, J C Prof. Dr	Telecom Division, EH 1233, Eindhoven University, P.O. Box 513, 5600 MB Eindhoven, The Netherlands
BAKATSIS, A P Mr	Hellenic National Defence Res. Centre, Hippocratus and Diogenus St, Galatsi, Greece
BELROSE, J S Dr	Communications Research Centre, P.O. Box 11490, Station H, Ottawa, Ont. K2H 8S2, Canada
BENGER, E Mr	FGAN/IEF, Konigstrasse 2, D-5307 Wachtberg-Werthhoven, Federal Republic of Germany
BERTEL, E Dr*	LAB MER-GER, CNET, 22300 Lannion, France
BESSERUDHAGEN, K Mr*	N.D.R.E., P.O. Box 25, N-2007 Kjeller, Norway
BLATSIOS, J Mr	ERT-1, Department of Technical Research, Mesogion 402, Athens, Greece
BLYTHE, J H Dr (Panel Chairman)	Marconi Research Centre, West Hanningfield Road, Great Baddow, Chemlsford, CM2 8HN, United Kingdom
BOITHIAS, L Mr	C.N.E.T., 38, Rue du General Leclerc, 92131 Issy-les-Moulineux, France
BOSSY, D Prof.	University Cath. Louvain, 174, Av. W. Churchill, B-1180 Bruxelles, Belgium
BOUKIS, D Mr	HNDGS, Branch COM and Electronics, Holargos, Athens, Greece
BRADLEY, P Mr	Rutherford and Appleton Lab., Chilton, Didcot, Oxon, United Kingdom
BUDING, H Mr*	Siemens AG, Postfach 70 00 60, 8000 München 70, Federal Republic of Germany
BURGESS, B Dr	Radio and Navigation Dept., Royal Aircraft Establishment, Farnborough, Hants GU14 6TD, United Kingdom
BURSHTEIN, I Mr*	THOMSON CSF, 55, rue Greffulhe, 92301 Levallois-Perret, France
CHRISTODOYLOY, C Mr	OTE, Department of International Comm., Veranjerou St 1, 106 77 Athens, Greece
COYNE, V E Mr	Rome Air Development Center, Strategic Surveillance Branch, Griffiss AFB, N.Y. 13441, United States
CUTOLO, M Prof.	Universita di Napoli, Istituto di Fisica, Via Monteolivetо 3, 80134 Napoli, Italy
DARNELL, M Dr*	Department of Electronics, University of York, Heslington, York, YO1 5DD, United Kingdom
DAWSON, J Mr*	Department of Electronics, University of York, Heslington, York, YO1 5DD, United Kingdom
DECONCHE, A Mr*	TRT, B.P. 21, 92350 Le Plessis Robinson, France

* Author of paper presented at the meeting
Member of Electromagnetic Wave Propagation Panel

Dr Lampert, Session Chairman

I agree that a lot of ideas have been presented, but when addressing again the question posed by Dr Blythe I recall a diagram shown by Dr Salz, showing improvements with adaptive filtering, and I hope people won't be too cross but my interpretation was that it is irrelevant what type of adaptive filtering you use as long as you do use one. Somehow I feel that that is also true for our different modems. If we want to make a further major step we have to think of something else, not only modems.

Before ending the discussion we should touch on the problem of real time channel evaluation in a broad sense, which was referred to by Dr Darnell. What I think Dr Darnell has in mind is to optimise the complete system adaptively to the instantaneous conditions.

Dr Darnell

Your interpretation of what I said is correct. I was not envisaging that real time channel evaluation would be used to optimise just one particular aspect of the system, but rather that it would be used to control several different components of the system in order to produce an improvement in performance.

Dr Lampert, Session Chairman

I feel however that each of us has a different interpretation of real time channel evaluation. Some people feel they have been using real time channel evaluation for some decades because they use ARQ systems. Isn't that enough? How do you feel about that?

Dr Darnell

One of the techniques for channel evaluation I mentioned yesterday was in fact the frequency of ARQ requests. What does one do with that information? One thing you could do, assuming the data is formatted in blocks, is to vary the coding redundancy applied to these blocks to reduce the number of requests should they go above a certain threshold, at the expense of course of data throughput rate. In principle ARQ requests can certainly be used as a source of channel evaluation.

Dr Lampert, Session Chairman

A source, so up to now we still have no concise picture of what is the complete tool of channel evaluation, or do we?

Dr Darnell

No I think not. In a given communication system there may well be several sources of channel evaluation information. One might use the impulse response of the medium, one might use the phase stability of the received signal, and one might use ARQ requests, all to contribute to a basic channel evaluation decision.

DISCUSSION OF SESSION V

Dr Lampert, Session Chairman

Several authors have used an average bit error probability because they can do wonderful calculations with it. Some others used diagrams showing error-free intervals, and a multitude of other sorts of diagrams have been used. It is not clear to me, up to now, how close we can get to a standardised display, such as is available with normal additive Gaussian channels, in order to be able to compare these methods with ease. I think that it is a general problem we are faced with when looking at the papers of the last session, the different ways used to present the error characteristics. What should we do here?

Mr Harding

Can we standardise not only the presentation but also the measurement techniques? Returning to the comment of Professor Goutelard made after his Paper 36, and points raised by many other speakers during this conference, it would appear that we now have the capability with modern technology to provide workers, certainly in the HF field, with sophisticated real time channel simulators. I would like to know whether data exist that fully characterise these channels, particularly HF channels, including propagation parameters, interference and noise structures that we have heard are so important, and if this data does not exist do the members of the conference feel that it should exist so that we can have these standard techniques. Can anybody suggest a way forward so that this data might be gathered and disseminated to those interested?

Dr Lampert, Session Chairman

I fully agree with you and I think that is a specific question to those people who designed error correcting codes and modems in particular systems — what was the reason they chose a certain way of displaying for example bit error characteristics or specific quality characteristics.

Professor Goutelard

I can't reply to the suggestion which has just been put forward, but I can provide some information. For about two years now we have conducted a lot of measurements on HF noise, and have proceeded by receiving well-known transmissions at different distances between Paris and Moscow. We have examined different types of modulation, and we have seen what was the amplitude distribution of the fading, and we have conducted Doppler frequency analysis.

Concerning the field of coding and ways in which we might envisage to study the error distribution, it is not just the average error rate which matters, it is an important parameter of course, but the distribution law of errors is prerequisite to the study of codes for use. You have to construct codes for the worst case, and very often there is too much power and hence a reduction of the efficiency of transmission. We could perhaps do two things. Many papers have presented adaptive systems, and it is a path we should follow in the future. Also we should go a little further and use real time network management systems, in order to adapt the codes to the transmission system.

Dr Bertel

We at CNET have also tackled the problem of modelling the HF channel, and have made a lot of measurements, as I mentioned in my presentation. There were two equipments allowing channels to be characterised – a link analyser, enabling very refined studies, and a surveillance system. There is a reason for this. Given the large number of data which we can obtain it is sometimes quite difficult to perform correlations, for example to correlate fading with other things. We have developed a mathematical study of fading taking into account the link geometry, antenna effects, and individual mode Doppler effects. I think that because of the mathematical formulation we can make simulations different from those which exist, in more diversified and refined situations, and this is planned in the same programme.

Dr Blythe

I would like to return to a precise and pertinent question posed by Professor Goutelard in the first session, when he asked, for a given multipath channel, could we specify the optimum modulation and coding to be used, and nobody replied. I would like to ask him whether he feels we have advanced in that regard. My own impression from this symposium is that a number of different schemes have been presented, but not in a form in which their performance can be compared. It is not merely desirable to have a standard environment — multipath, interference and so on — without it we won't make progress.

Professor Goutelard

Dr Blythe said there was no reply to our question. It would be marvellous if we had a reply. Systems have been proposed but propagation conditions vary so much that there is no unique solution. There has been great evolution. I have been amazed and extremely interested by certain papers, and I go back to my country with many ideas, and I hope this is true for every one of us.

DISCUSSION

R.Valentin, Cie

What is the transmitting power envisaged for this system, and what is the sensitivity of the receiver. At this frequency if you do not have a line of sight path there is a large diffraction loss and so you must provide a sufficient margin.

Author's Reply

I think the transmitted power was about 2 watts; I cannot answer the question on noise figure. We do have a line of sight path.

E.W.Lampert, Cie

You mentioned that you can reduce the sensitivity to multipath to about 0.5 metres, and that means the area round the antenna, but in millimetre communications that 0.5 metre area round the antenna is most critical. How did you realise a uniform radiation within that region?

Author's Reply

I must say that it is only a two-path model and further tests are necessary.

plotted in fig.5c and d, once without noise and once with SNR = 0 dB . As can be seen, there is now the effect of cycle slipping, as long as Δf_s will be zero, after which the actual phase control begins.

Figs.5a - d show the results for worst case conditions. Nevertheless, this is very important in order to establish the limitations for system applications.
The transient responses for average start-conditions are illustrated in fig.5e and f, where the time difference between the two modulation functions is only $T_s/4$. As can be seen, the acquisition time is essentially smaller than in the previous cases of fig.5a - d.

Another example, dealing with further practical inaccuricies shall be finally considered. It is assumed, that the difference $f_{M1} - f_{M2}$ has a drift of 10 MHz compared with the centre frequency of the discriminator. In addition, the sweep width of the transmitted signal shall differ from the sweep width of the receiver oscillator by 4 MHz. The transient responses of the relative phase difference and the corresponding frequency error Δf_{IF} respectively are plotted in fig.6a and b. Whereas the drift of the difference $f_{M1} - f_{M2}$ will be completely compensated by the control loop with $G_1(p)$, the different sweep widths lead to a remaining oscillating error Δf_{IF}. But in most practical applications, the error due to different sweep widths can be accepted.

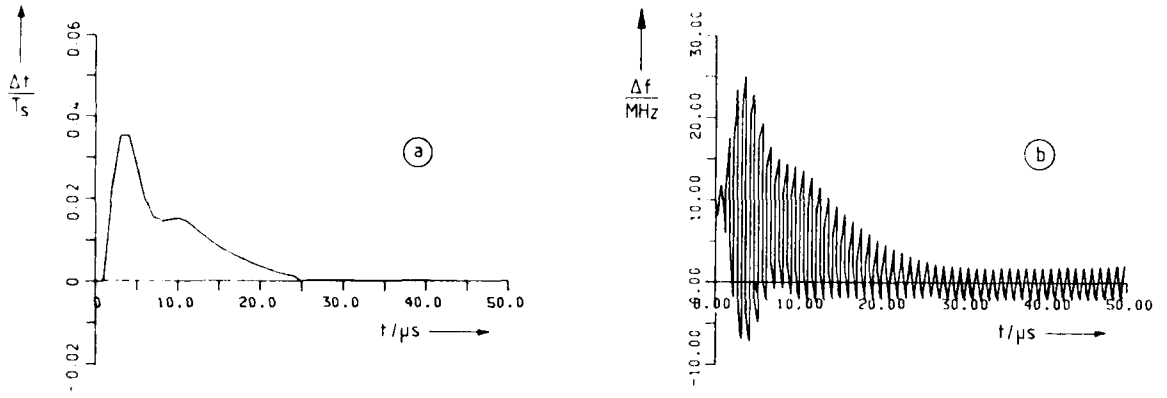

Fig.6 Transient responses of the relative phase a) , and the frequency error b) ; H = 200 MHz , B_D = 20 MHz , f_s = 1 MHz , ΔH = 4 MHz , Δf_M = 10 MHz .

Conclusion

It has been proven, that radio transmission on millimeter waves under strong fading conditions can be significantly improved by chirp modulation. The needed sweep width for relevant path differences of more than 1m is about 150 MHz ··· 200 MHz. The acquisition time of the receiver tracking loop mainly depends on the discriminator bandwidth. Respectable tracking performance can be obtained even for a relative small discriminator bandwidth of e.g. 20 MHz (for a sweep width of 200 MHz !). The transient responses of the control loop are hardly affected by the influence of noise.

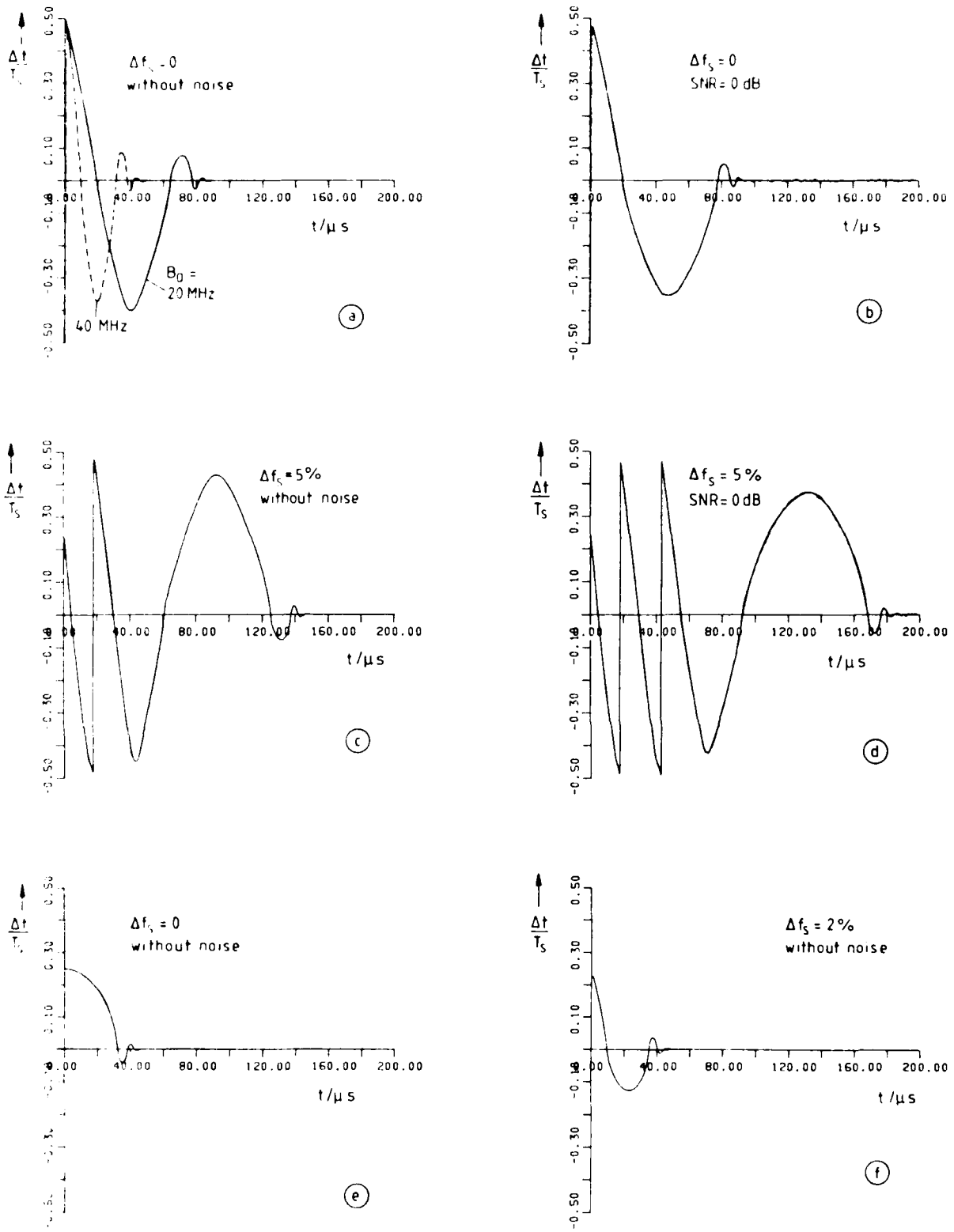

Fig. 7 Transient responses of the relative phase between the two modulation waveforms; B = 200 MHz, B_D = 20 MHz, f_s = 1 MHz

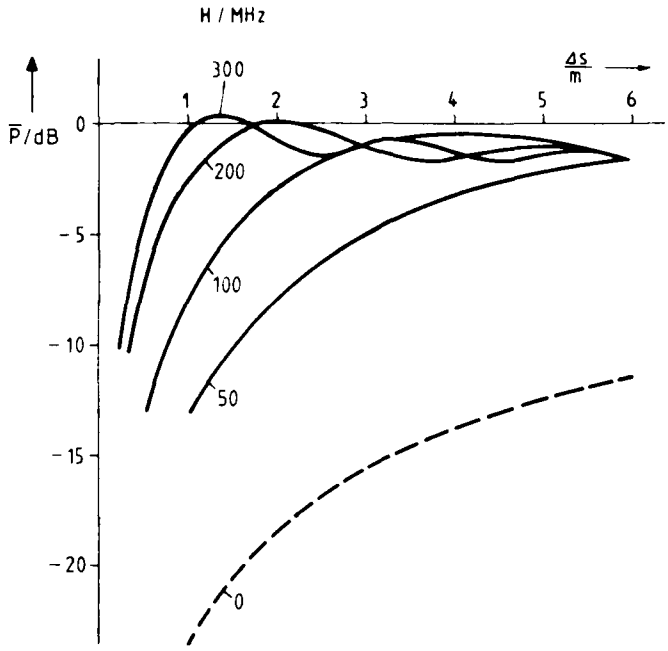

Fig.4 Average power of the received signal level in dependence of the sweep width H and the path-difference Δs of the reflected wave with a reflection coefficient of $|\rho| = 1$.

Acquisition

The behaviour of the control loop in the locked condition is well described by linear control theory. In the first step the loop filters $G_1(p)$ and $G_2(p)$ were designed for this case. In the next step, the filter parameters had to be further optimized using computer simulations based on a complex receiver model. In this way, some special effects could be taken into account, such as the nonlinear characteristic of the discriminator and the synchroneously controlled switch.
For such an optimized receiver some examples of transient responses are presented, which give a good insight into the characteristic behaviour of the control loop. All results are related to a system with the following data :

centre frequency	$f_{M1} = 37$ GHz
sweep width	$H = 200$ MHz
sweep frequency	$f_s = 1$ MHz
bit rate	$f_{Bit} = 300$ kHz
IF-frequency	$f_{IF} = 100$ MHz
discriminator - bandwidth	$B_D = 20$ MHz

The acquisition time mainly depends on the discriminator-bandwidth B_D. For technical reasons the bandwidth B_D for an analog discriminator must be smaller than the sweep width H. Hence, for certain time differences Δt between the modulation waveforms $g_1(t)$ and $g_2(t)$ the nonlinear part of the discriminator characteristic is effective. This means, that the control voltage u_D is no longer proportional to the frequency deviation Δf, but considerably smaller. As a consequence, the corresponding acquisition time will be greater than for the ideal linear case.

Fig.5a shows the transient response for the worst case $\Delta t = 0.5\,T_s$. The acquisition time takes about 80 sweep periods for a bandwidth of 20 MHz. As demonstrated by the dashed shape, the acquisition time can be reduced with increasing bandwidth of the discriminator.

The next figure 5b illustrates the influence of noise on the acquisition behaviour. A signal to noise ratio of SNR = 0 dB of the IF-signal is assumed. In spite of this noisy IF-signal, the acquisition is hardly affected, as a comparison with fig.5a shows.

The assumption in fig.5a,b has been $\Delta f_s = 0$, that is, the sweep frequencies of the transmitter- and the receiver-modulation functions $g_1(t)$ and $g_2(t)$ are exactly the same. However, it is realistic to take a deviation of about 0.1%...1% into account As a consequence, the loop filter $G_2(p)$ should include an integral-controlled behaviour, in order to yield no offset in the loop.
For a comparatively large sweep frequency deviation $\Delta f_s = 5\%$ the transient responses are

is now accomplished by means of a synchroneously controlled switch S, which is on during the positiv slope and off during the negative slope of the modulation waveform $g_2(t)$. Thus, the output voltage of the following low-pass filter is proportional to the time difference Δt between $g_1(t)$ and $g_2(t)$. The output voltage u_2 of the loop filter $G_2(p)$ controls the sweep frequency of the triangular-VCO until the control deviation Δf will be close to zero.

because the centre frequencies of the RF-oscillators can easily drift by about some MHz, an additional control loop is necessary to keep the difference $f_{M1} - f_{M2}$ constant at f_{IF}. A suitable control variable is obtained by low-pass filtering the output voltage of the discriminator - before the switch S - , because the average value $\bar{u}_D$ is a measure of the drift deviation $|f_{M1} - f_{M2}| - f_{IF}$. By means of an integrating loop filter $G_1(p)$ an offset u_1 is obtained and added to the modulation function $g_2(t)$. Through this the centre frequency f_{M2} of the RF-oscillator is always controlled in such a way, that the difference $f_{M1} - f_{M2}$ is constant and equal to f_{IF}.

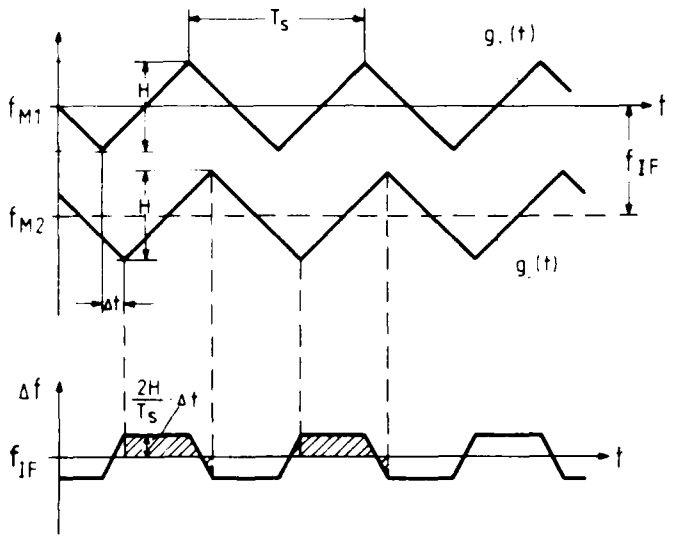

Fig. 3 Modulation waveforms and frequency error

Fading analysis with a two-path model

In order to obtain an estimation of the required sweep width H to avoid deep fadings, a two-path model is assumed. The receiving waveform $s_1(t)$ is now a superposition of the direct path and a reflected path with a time delay τ:

$$s_1(t) = a(t)\cos\left[\omega_{M1}t + 2\pi\int g_1(t)\right] + \sqrt{\gamma}\,a(t-\tau)\cos\left[\omega_{M1}(t-\tau) + 2\pi\int g_1(t-\tau)\,dt + \beta\right] \quad (6)$$

where γ stands for the power ratio of the reflected signal to the direct signal. The time delay $\tau = \Delta s/c$ for relevant path-differences Δs of some meters is very small compared with the sweep period T_s. E.g. for $\Delta s = 3m$ one gets a time delay of $\tau = 10$ ns , but the sweep period T_s has a range of about some µs. As on the other hand the bit duration T_{Bit} is greater than T_s, $a(t)$ and $a(t-\tau)$ in Eq.(6) are practically identical. Thus, there is no intersymbol interference but frequency-selective interference which produces fadings.

The following expression gives the normalized power of the signal in Eq.(6), valid for the two-path model :

$$\bar{P} = 1 + \gamma + 2\sqrt{\gamma}\,\frac{\sin H\tau\pi}{H\tau\pi}\cos\beta \quad (7)$$

β is a random angle between 0 and 2π. For the worst case, $\beta = \pi$ and reflection coefficient $\gamma = 1$, the fadings are calculated. Fig.4 shows the corresponding curves depending on the sweep width H and the path-difference Δs. It has been taken into account that an additional amount of free-space attenuation for the reflected path is caused by an increasing Δs. Accordingly, the power ratio γ is decreasing with increasing Δs.
As a result of fig.4, fadings can be reduced considerably with a suitable sweep width H. E.g., with H = 200 MHz fadings are limited to no more than -5dB, if the path-differences are at least 0.5 m .

System description

Fig.2 shows the basic configuration of the receiver in form of a block diagram. For technical reasons a simple On-Off-Keying (OOK) is used, i.e., the amplitude a(t) of the transmitted carrier is switched between two levels, full on and full off. It must be emphazised, that the concept described is not only restricted to OOK but may also be applied to the general amplitude modulation.
Generally, the received signal can be described as

$$s_1(t) = a(t)\ \cos\left[\omega_{M1}t + 2\pi \int g_1(t)\,dt\right] \qquad (1)$$

In addition to the amplitude modulation, the carrier frequency is swept periodically about the centre frequency f_{M1} with a triangular function $g_1(t)$ between $f_{M1} - H/2$ and $f_{M1} + H/2$ (see fig.3). The larger the sweep width H, the more resistant against fading the radio transmission will be. On the other hand, a large sweep width H leads to a large bandwidth. In order to utilze the whole sweep width H during one bit duration, the sweep period T_s should not exceed twice the bit duration T_{Bit}.

The RF - oscillator in the receiver is likewise modulated by a triangular function $g_2(t)$:

$$s_2(t) = 2\ \cos\left[\omega_{M2}t + 2\pi \int g_2(t)\,dt + \varphi\right] \qquad (2)$$

Basically, the modulation waveforms $g_1(t)$ and $g_2(t)$ are the same. However, the relative phase difference between these two functions is arbitrary when turning the receiver on (see fig.3). The centre frequency f_{M2} of the receiver oscillator deviates from the transmitting centre frequency f_{M1} by the IF - frequency f_{IF} :

$$f_{M2} = f_{M1} \pm f_{IF} \qquad (3)$$

Recovery of the baseband signal a(t) may be accomplished by using a mixer, as illustrated in fig.2. The purpose of the following low-pass filter is to remove undesired spectral components which are produced by the mixer. The resulting IF - waveform at the output of the amplifier is

$$y(t) = a(t)\ \cos\left[\omega_{IF}t + 2\pi \int [g_1(t) - g_2(t)]\,dt - \varphi\right] \qquad (4)$$

The modulation function $g_2(t)$ generated in the receiver has now to be automatically controlled in such a way, that the IF-frequency deviation

$$\Delta f(t) = g_1(t) - g_2(t) \qquad (5)$$

vanishes. As a result the IF-waveform y(t) will have the constant frequency f_{IF}.
In order to obtain a suitable control signal a FM-discriminator with a centre frequency equal to f_{IF} is used. Its output voltage u_D is proportional to the frequency deviation $\Delta f(t)$. However, as illustrated in fig.3, this deviation is periodic and has an average value of zero. The desired phase detection between the modulation waveforms $g_1(t)$ and $g_2(t)$

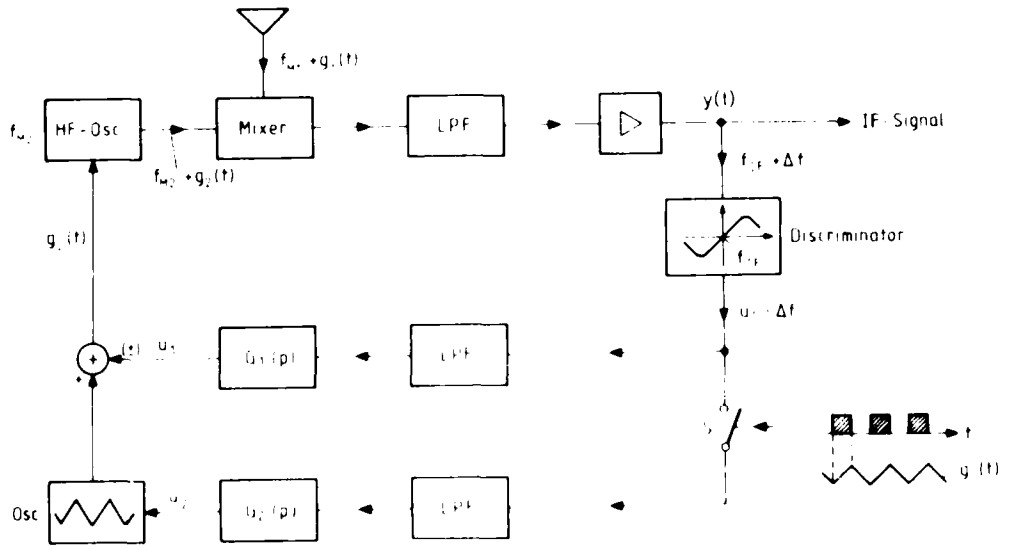

Fig.2 Block diagram of the receiver

EFFECTIVE MILLIMETER WAVE TRANSMISSION UNDER SEVERE MULTIPATH CONDITIONS

by
U. Schulz and G. Höfgen
Standard Elektrik Lorenz AG
7000 Stuttgart 40, FRG

Summery

Radio transmission on millimeter waves substantially suffers from multipath propagation as long as obstacles cannot be avoided in the propagation path. A novel system concept to overcome the fading problem will be presented. This concept uses a broadband RF-transmission by chirp modulation and a respective correlation technique in the receiver. This paper describes the transmission principle and the basic equipment functions. In addition, the results of the theoretical investigations on the receiver signal processing are presented.

Introduction

Wireless data transmission over short distances can be accomplished either by radio or by infrared links. Unfortunately, the infrared solution is sensitive against optical interference (e.g. sunlight) and other influences (e.g. fog).
An attractive solution of this task is the radio transmission on millimeter waves, e.g. 37 GHz , because the microwave integrated technology has made great progress with regard to a low cost realisation in the last few years (e.g. finline structures). In contrast to the MHz-range, where already many services are established, the range about 37 GHz is available in most cases. Moreover, this range guarantees sufficient bandwidth for digital data transmission with good performance. A further advantage is the comparatively strong free - space attanuation at 37 GHz . Thus, the probability of detection or interference with other services respectively is significantly reduced.

However, radio transmission on millimeter waves substantially suffers from multipath propagation as long as obstacles cannot be avoided in the propagation terrain. That is especially true for omnidirectional transmission close to the earth surface which may easily generate fadings of more than 30 dB .
As an example, fig.1 shows a section of the measured signal pattern at the receiving antenna for two different frequencies. The transmitting antenna is fixed, whereas the orientation : of the receiving antenna is varied. As can be seen, there are many fadings in several directions. However, the fading angles move, when the frequency is changed. The frequency selectivity can now be utilized to improve the reception quality under fading conditions. If the carrier frequency is swept periodically about a certain centre frequency, the fadings or signal nulls are overrun and in this way the averaged receiver signal power can be kept at an acceptable level. Of course, the receiver must be able to compensate for the transmitted sweeps. For this purpose the receiver contains a control loop to track the transmitting sweeps.
The basic configuration of such a receiver and the obtained tracking performance will be presented in the following sections.

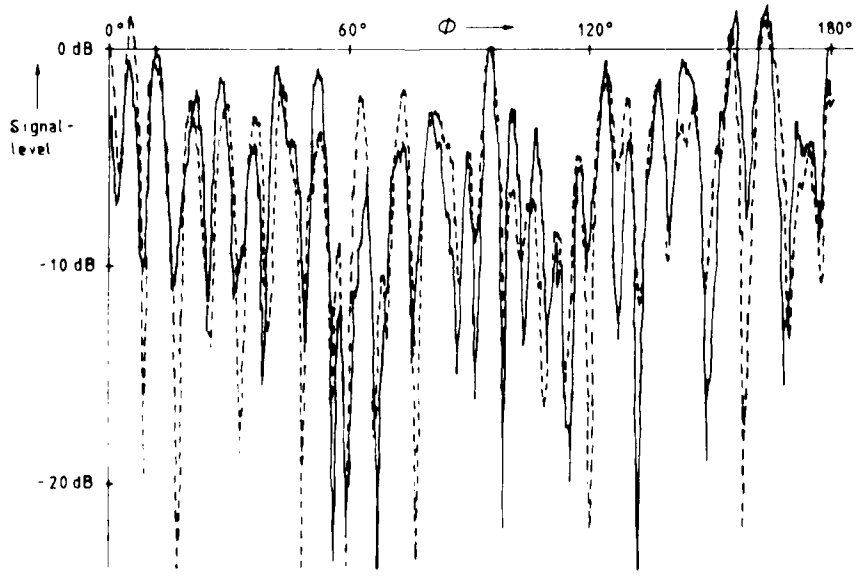

Fig.1 Measured signal pattern versus orientation ; of the receiving antenna with fixed transmitting antenna.
—— f = 37 GHz ; - - - f = 37.02 GHz

DISCUSSION

J.S.Belrose, Ca

A comment rather than a question. Of course, narrow band spread spectrum is useful for combatting multipath as well as coping with jamming problems. Canadian industry has in fact developed, through guidance of Sherman Chow, an engineer at CRC, an in-band spread spectrum modem, at 75 baud rate in 3 kHz. This modem is currently being evaluated for HF digital ground to air communications. An alternative way of combatting multipath, which has been used on a number of other developments stimulated by Sherman Chow, is in-band diversity frequency shift keying, in other words two channels in band are used in a diversity arrangement to combat multipath. This modem is used in a number of applications for digital communications, and also for control of audio processing in the Lincompex system.

C.Goutelard, Fr

I would like to ask the author if he is contemplating other techniques in order to combat jamming and intereception. There are two problems for those making discreet transmissions. The enemy can either jam us, or listen in on what we are saying. The narrowband spread spectrum system that you present is very interesting because using different words makes intereception difficult, but with a very good computer it may be possible. What is the merit of your system compared with higher spreading factors, say one thousand or even one million, which makes the transmission very discreet since it is far below the noise level and hard for the enemy to detect.

Author's Reply

On the first part of your question, I think that to have a system with good anti-jam capability and perhaps also good anti-multipath capability it is necessary to combine the different kinds of techniques that have been described, such as coding, null-steering antennas, spread spectrum, etc. We have considered complete systems in which none of these features is too expensive, so each feature gives us say 10 dB or so, in that order. It is much more difficult for a hostile jammer to jam an equipment whose anti-jam capability is based on a variety of techniques and can react flexibly.

The second part was the spreading factor. I think it is a problem for these microwave systems. I pointed out that if you had a very crowded frequency band, and if you now use spreading factors to bring your system power density just below the noise level, then noise from all the systems you have in this bandwidth will add up and so you will jam yourself, in effect.

C.Goutelard

What you say is quite correct. On the other hand a much broader spread spectrum can give much better protection against intereception. However, synchronisation becomes a major problem. What do you think about that?

Author's Reply

We have done some research on synchronisation systems but there is not time to discuss it here. I agree with you that we always have to find a reasonable balance between synchronisation problems, bandwidth considerations, anti-jam capability, and perhaps a few other factors. It is a problem to find a reasonable balance between these different factors.

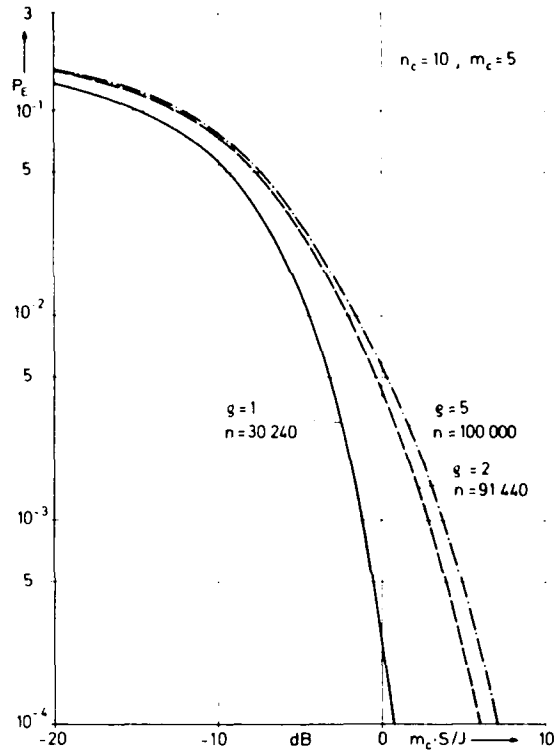

Fig. 12: Coherent FH system; gaussian jammer

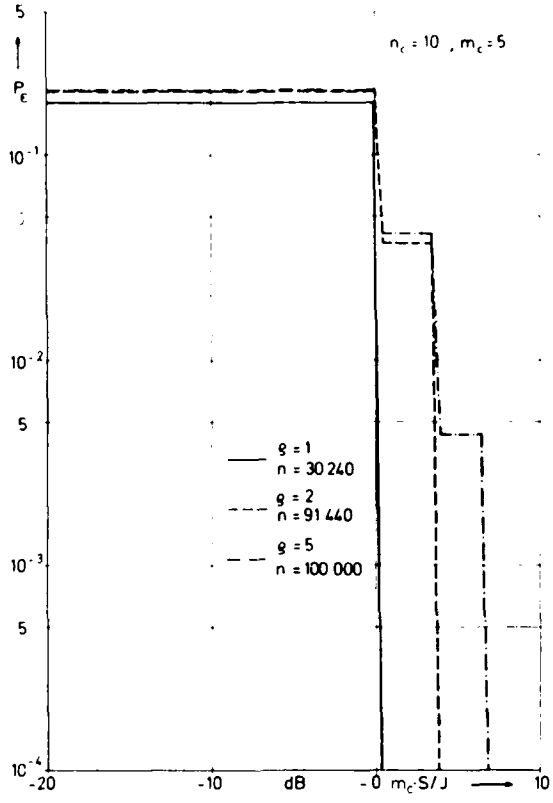

Fig. 13: Noncoherent FH system; CW-jammer

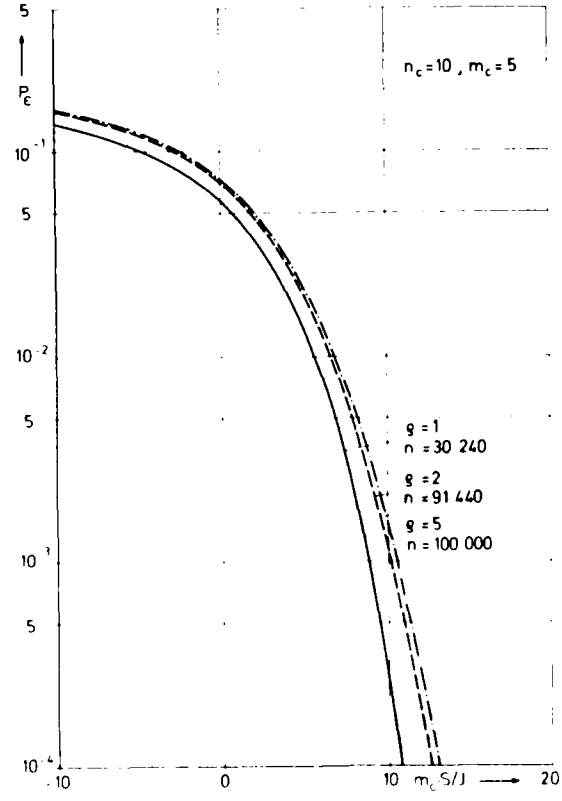

Fig. 14: Noncoherent FH system; gaussian jammer

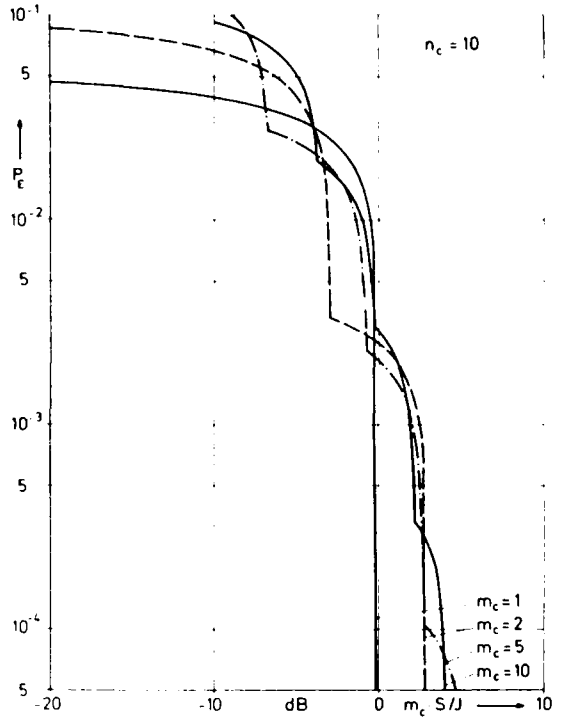

Fig. 8: Coherent FH system; CW-jammer

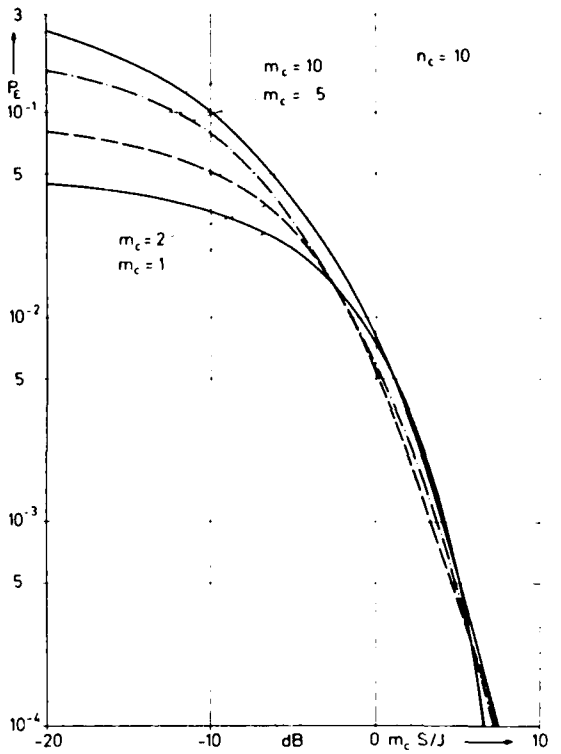

Fig. 9: Coherent FH system; gaussian jammer

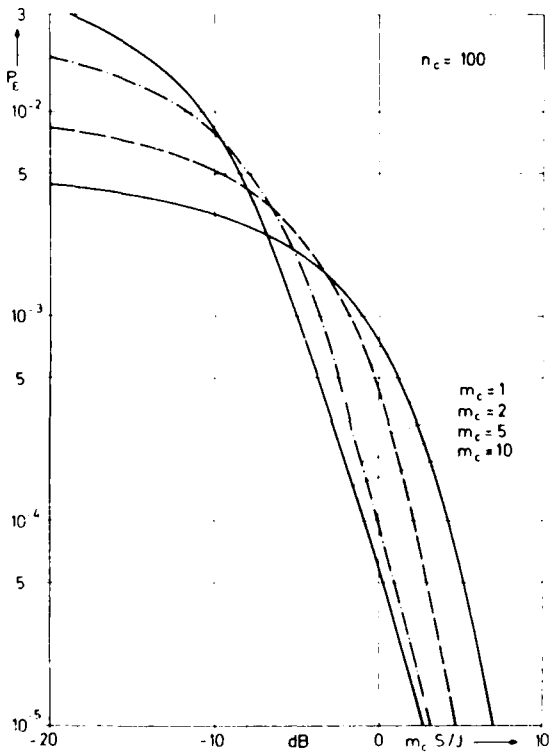

Fig. 10: Coherent FH system; gaussian jammer

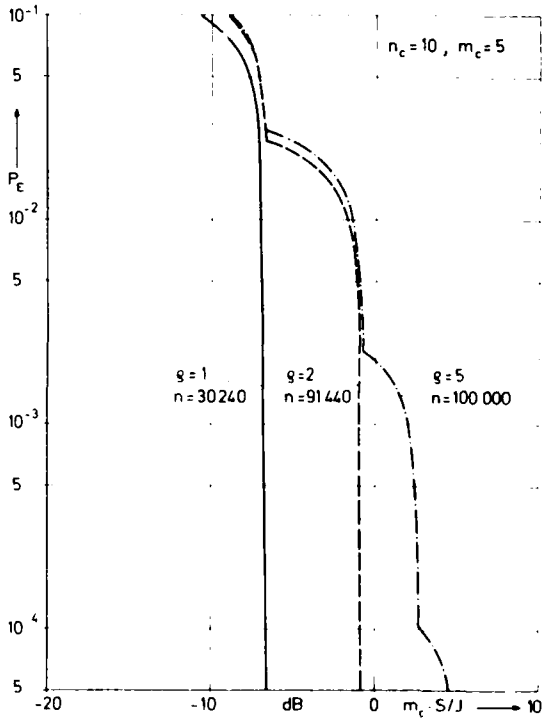

Fig. 11: Coherent FH system, CW-jammer

KOUROGONIS, C. Prof.	Air Academy, Dekelia, Athens, Greece
LAMBRAKIS, M. Mrs	Hellenic Air Force, KETA, Delta Falirou, Palaion Faliron, Greece
LAMBROPOULOS, D. Mr	Hellenic Aerospace Industry, P.O. Box 23, Sximatari, Tanagra, Greece
LAMPERT, E.W. Dr Ing.†	Siemens AG, Postfach 70 00 60, 8000 München 70, Federal Republic of Germany
LANGEWELLPOTT, C. Dr*	Standard Elektrik Lorenz AG, Dep. CS ERGP2, Hellmuth-Hirth-Str. 42, D-7000 Stuttgart 40, Federal Republic of Germany
LARSEN, R. Mr*	Marconi Research Centre, West Hanningfield Road, Great Baddow, Chelmsford, Essex CM2 8HN, United Kingdom
LEOVARIS, A. Mr	Hellenic Air Force, KETA, Delta Falirou, Palaion Faliron, Athens, Greece
LEUTKE, E. Dr	EGAN-IFE, Neuenahrer Str. 20, D-5307 Wachtberg-Werthhoven, Federal Republic of Germany
LIGTHART, L.P. Ir.*	Delft University of Technology, Dept. of EE, Microwave Laboratory, Mekelweg 4, P.O. Box 5031, 2600 GA Delft, The Netherlands
LINDER, J. Dr	AEG Telefunken, A12E253, Postfach 1730, D-7900 Ulm, Federal Republic of Germany
LINOS, A. Dr	HDGS, Branch TEL/3, Holargos, Athens, Greece
LINTZ CHRISTENSEN, E. Prof.	Electromagnetics Inst., B. 348 Techn., University, DK-2800 Lyngby, Denmark
LOSQUADRO, G. Mr*	Selenia Space, Via Tiburtina 12400, Roma, Italy
LUCAS, M.R.Y. Mr	THOMSON CSF, 178 Bld Gabriel Peri, 92240 Malakoff, France
LUND, T. Mr	N.D.R.E., P.O. Box 25, 2007 Kjeller, Norway
LUVERA, C.J. Mr*	Rome Air Development Center, Griffiss AFB Code DCDD, N.Y. 13441, United States
MAGOS, J. Major	Hellenic Navy General Staff, D3 Directorate 6,Cholargos, Athens, Greece
MAGOULAS, P. Capt.	Air Academy, Scholi Ikaron, Dekelia, Greece
MALOBERTI, A. Mr*	CNET PAB/ETR, 38—40, rue du Général Leclerc, 92131 Issy-les-Moulineaux, France
MANESI, P. Lt. Col.	HAFGS/3, Holargos, Athens, Greece
MASTROGIANNIS, M. Mr	National Defence Research Centre, Hippocratus and Diogenus St, Galatsi, Athens, Greece
MATSOUKAS, D. Mr	TEI, Athens, Greece
MAVROKOUKOULAKIS, N. Dr†	Hellenic Air Force, KETA, Delta Falirou, Palaion Faliron, Greece
METZGER, K. Dr*	Research Institute of the Deutsche Bundespost, Am Kavalleriesand 3, D-6100 Darmstadt, Federal Republic of Germany
MICHAILIDIS, N. Mr	ERT 1, Department of Technical Research, Mesogion 402, Athens, Greece
MILLMAN, G.H. Dr*	General Electric Company, Bldg 5, Room B4, Court St Plant, Syracuse, New York 13221, United States
MITRAKOS, D. Sec. Lieut.	HDGS, Staff C/3, Holargos, Athens, Greece
MONSEN, P. Dr*	Signatron, Inc., 12 Hartwell Avenue, Lexington, MA 02173, United States
MORAITIS, G. Dr	Ionospheric Institute, P.O. Box 20048, 118 10 Athens, Greece
NEESSEN, J.T.A. Ir.†	PTT, Dr Neher Labs., St Paulusstraat, 4, 260 AK Leidschendam, The Netherlands
NOODT, L.E. Mr	Elektrisk Bureau, div NERA, Kokstadvn 23, 5061 Kokstad, Norway
OLAISEN, H. Mr*	N.D.R.E., P.O. Box 25, N-2007 Kjeller, Norway
OTTKA, M. Mr*	ANT Nachrichtentechnik GmbH, Gerberstrasse 33, D 7150 Backnang, Federal Republic of Germany
PALMER, F. Dr†	DREO NDHQ, Ottawa, Ontario K1A 0Z4, Canada
PAMPOUKAS, T. Mr	Air Academy, Dekelia, Athens, Greece
PANDIS, A. Mr	ERT 1, Department of Technical Research, Mesogion 402, Athens, Greece
PAPADAKIS, J. Mr	National Defence Research Centre, Hippocratus and Diogenus St, Galatsi, Athens, Greece
PAPADOPOULOS, G. Dr	OTE, Department R/H, 3 September St 7, Athens, Greece

*Author of paper presented at the meeting.
†Member of Electromagnetic Wave Propagation Panel.

PAPAGEORGIOU, A. Mr	National Defence Research Centre, Hippocratus and Diogenus St, Galatsi, Athens, Greece
PAPASCHALIS, A. Capt.	Air Academy, Dekelia, Athens, Greece
PATRICIO, J.F. Mr†	Direccao dos Servicos de Radiocomunicacões dos CTT, R. Conde de Redondo 79, 1189 Lisboa Codex, Portugal
PAVLIDIS, P. Mr	44, Achilleos Street, 175 62 P. Phaliro, Greece
PERDICARIS, P.D. Mr	Civil Aviation Authority, King George 1, Hellinicon, Athens, Greece
REINISCH, B.W. Prof.*	University of Lowell, Center for Atmospheric Research, 450 Aiken Street, Lowell, MA 01854, United States
REMY, C.J.P. Mr†	DRET/SDR, 26 Bld Victor, 75996 Paris Armées, France
RITCHIE, R.P. Mr	BBC Research Dept., Kingswood Warren, Tadworth, Surrey KT20 6NP, United Kingdom
ROOME, S.J. Mr	Thorn EMI Central Research Lab., Trevor Road, Hayes, Middx UB3 1HH, United Kingdom
ROSSOTTI, M.L. Dr	Aeritalia S.A.I.P.A., GEQ, 10072 Caselle Torinese (TO), Italy
SALZ, J. Dr*	Bell Laboratories, Crawford Hill Laboratory, Box 400 Holmdel, N.J. 07733, United States
SARANTARIDIS, E. Sgt	Hellenic Air Force, KETA, Delta Falirou, Palaion Faliron, Greece
SCHILLIGER, M. Mr*	LMT Radio Professionnelle, 46, Quai A. Le Gallo, 92103 Boulogne-Billancourt, France
SCHNEIDER, A. Dr*	Cyber Com Corp, 4105 North Fairfax Dr, Arlington, VA 22203, United States
SCHULZ, U. Dr*	Standard Elektrik Lorenz AG, 7000 Stuttgart 40, Federal Republic of Germany
SIAGAS, J. Mr	National Defence Research Centre, Hippocratus and Diogenus St, Galatsi, Athens, Greece
SIDERIS, E. Mr	National Defence Research Centre, Hippocratus and Diogenus St, Galatsi, Athens, Greece
SKOYEAS, Z. Dr	Hellenic Navy General Staff, D3 Directorate 6, Cholargos, Athens, Greece
SMITH, R.N. Mr*	Laboratory Contract Manager, RADC/DCCD, Griffiss Air Force Base, Rome, NY 13441, United States
SOICHER, H. Dr† (Deputy Chairman)	US Army Communication-Electronic Cmd, Centre for Communications Systems, Attn: DRSEL-COM:RN-1, Fort Monmouth, N.J. 07703, United States
SPANOS, A. Mr	Direction of Technical Services, Mesogion 432, Athens, Greece
SPENNING, J.H. Mr	Oslo Mil/Akershus, Oslo 1, Norway
SPITHAS, E. Dr	Ministry of Res. and Technology, Ermou St 2, Athens, Greece
SPRENKELS, R.C. Colonel†	Etat Major de la Force Aerienne, Section Communications & Electronique, (VDM) Quartier Reine Elisabeth, B-1140 Bruxelles, Belgium
STACHEOS, D. Dr	OTE, Department R/H, 3 September St 7, Athens, Greece
STARON, M. Mr	ONERA, B.P. 72, F-92322 Châtillon Cedex, France
STAVRAKAKIS, J. Mr	Civil Aviation Authority, King George 1, Hellinicon, Athens, Greece
STRATIGOULAKOS, Mr	Ministry of Communications, 49 Syngrou Avenue, GR-11780 Athens, Greece
SUNDAL, G.I. Mr	Norwegian Telecommunication, Adminstr. Research Establishment, P.O. Box 83, 2007 Kjeller, Norway
TEIGLAND, I. Mr	Oslo Mil/Akershus, Oslo 1, Norway.
THANOPOULOS, TH. Mr	OTE, Technical Planning Division, E. Negri 3 and Patision St, Athens, Greece
TSAKIRIS, C. Mr	HRT 1, Department of Technical Research, Mesogion 402, Athens, Greece
TSALAMEGAS, I. Mr	Air Academy, Dekelia, Athens, Greece
TSAOUSI, I. Mr	National Defence Research Centre, Hippocratus and Diogenus St, Galatsi, Athens, Greece
TSAVDARIS, S. Major	Hellenic Air Force, KETA, Delta Falirou, Palaion Faliron, Greece
TSIGIROGLOU, C. Mr	Office (SOENE), Hellenic Navy General Staff, Holargos, Athens, Greece
TSITOMENEAS, S. Dr	University of Athens, University Cambus, Building Typa, Zografou, Athens, Greece

* Author of paper presented at the meeting
† Member of Electromagnetic Wave Propagation Panel.

TZERBINOS, B. Mr	Hellenic Aerospace Industry, P.O. Box 23, Sximatari, Tanagra, Greece
UTLAUT, W.F. Dr†	Director, Institute for Telecommunication Science, National Telecommunications and Information Adminstration, Department of Commerce, Boulder, CO 80303, United States
UZUNOGLU, N.K. Mr*	Hellenic Navy General Staff, Research Centre/GETEN, Cholargos, Athens, Greece
VALENTIN, R. Dr*	Research Institute of the Deutsche Bundespost, Am Kavalleriesand 3, D-6100 Darmstadt, Federal Republic of Germany
VAN, L. Ir.	Dr Neher Laboratorium PTT, P.O. Box 421, 2260, AK Leidschendam, The Netherlands
VASAKIOTIS, S. Captain	HAE, 202 KEA/T-H, Hellinicon, Athens, Greece
VON GROOTE, H. Dr	MBB LKE 411, Postfach 80 11 60, D-800 München, Federal Republic of Germany
WHITE, M.B. Dr†	Office of Naval Research, E-C Region, Bldg 114 Section D, 666 Summer St, Boston, MA 0221, United States
XATZOPOULOS, G. Dr	OTE, Department R/H, 3 September St 7, Athens, Greece
YEH, Kung Chie Prof.†	Department of Electrical Engineering, University of Illinois, 1406 W. Green Street, Urbana, Il 61801, United States

*Author of paper presented at the meeting.
†Member of Electromagnetic Wave Propagation Panel.

REPORT DOCUMENTATION PAGE

1. Recipient's Reference	2. Originator's Reference	3. Further Reference	4. Security Classification of Document
	AGARD-CP-363	ISBN 92-835-0367-8	UNCLASSIFIED

5. Originator Advisory Group for Aerospace Research and Development
North Atlantic Treaty Organization
7 rue Ancelle, 92200 Neuilly sur Seine, France

6. Title
PROPAGATION INFLUENCES ON DIGITAL TRANSMISSION SYSTEMS — PROBLEMS AND SOLUTIONS

7. Presented at
the 34th Symposium of the Electromagnetic Wave Propagation Panel held at the War Museum, Athens, Greece, 4—8 June 1984.

8. Author(s)/Editor(s)	9. Date
Edited by Dr John H.Blythe	October 1984
10. Author's/Editor's Address	**11. Pages**
Marconi Research Centre Great Baddow Chelmsford, CM2 8HN, UK	534

12. Distribution Statement This document is distributed in accordance with AGARD policies and regulations, which are outlined on the Outside Back Covers of all AGARD publications.

13. Keywords/Descriptors

Digital transmission	Adaptive systems
Multipath effects	Communication systems
Radio noise	Digital communications
Man-made interference	Propagation models
Signalling schemes	Channel simulation
Sounding schemes	Signal processing

14. Abstract

These Proceedings for the 34th Symposium/Meeting of the AGARD Electromagnetic Wave Propagation Panel contain the papers presented, session summaries, session chairmen reports, and discussions that followed the presentations of papers. Nine papers were presented in the session on propagation constraints to reliable digital communications. A total of eleven papers were presented in the two sessions devoted to recent progress in propagation measurements and propagation models. The channel simulation session presented five papers. The Avionics Panel helped organize seven papers for the session on signal processing technology. During the final session on signalling and sounding schemes for reliable digital communications eight papers were presented.

The Symposium reviewed propagation effects which have an influence on the performance of digital systems, including: noise levels, and system sensitivities to noise; man-made interference types and system sensitivities to man-made interference; and multipath effects, dispersion, fading rates, medium coherent bandwidth, channel models, and system sensitivities to these effects. The meeting also reviewed systems designed to counter the above effects, including the various kinds of adaptive systems, and assessed the performance improvements which can be provided.

AGARD Conference Proceedings No.363
Advisory Group for Aerospace Research and Development, NATO
PROPAGATION INFLUENCES ON DIGITAL TRANSMISSION SYSTEMS – PROBLEMS AND SOLUTIONS
Edited by Dr John H.Blythe
Published October 1984
534 pages

These Proceedings for the 34th Symposium Meeting of the AGARD Electromagnetic Wave Propagation Panel contain the papers presented, session summaries, session chairmen reports, and discussions that followed the presentations of papers. Nine papers were presented in the session on propagation constraints to reliable digital

P.T.O.

AGARD-CP-363

Digital transmission
Multipath effects
Radio noise
Man-made interference
Signalling scheme
Sounding schemes
Adaptive systems
Communication systems
Digital communications
Propagation models
Channel simulation
Signal processing

AGARD Conference Proceedings No.363
Advisory Group for Aerospace Research and Development, NATO
PROPAGATION INFLUENCES ON DIGITAL TRANSMISSION SYSTEMS – PROBLEMS AND SOLUTIONS
Edited by Dr John H.Blythe
Published October 1984
534 pages

These Proceedings for the 34th Symposium Meeting of the AGARD Electromagnetic Wave Propagation Panel contain the papers presented, session summaries, session chairmen reports, and discussions that followed the presentations of papers. Nine papers were presented in the session on propagation constraints to reliable digital

P.T.O.

AGARD-CP-363

Digital transmission
Multipath effects
Radio noise
Man-made interference
Signalling scheme
Sounding schemes
Adaptive systems
Communication systems
Digital communications
Propagation models
Channel simulation
Signal processing

AGARD Conference Proceedings No.363
Advisory Group for Aerospace Research and Development, NATO
PROPAGATION INFLUENCES ON DIGITAL TRANSMISSION SYSTEMS – PROBLEMS AND SOLUTIONS
Edited by Dr John H.Blythe
Published October 1984
534 pages

These Proceedings for the 34th Symposium/Meeting of the AGARD Electromagnetic Wave Propagation Panel contain the papers presented, session summaries, session chairmen reports, and discussions that followed the presentations of papers. Nine papers were presented in the session on propagation constraints to reliable digital

P.T.O.

AGARD-CP-363

Digital transmission
Multipath effects
Radio noise
Man-made interference
Signalling scheme
Sounding schemes
Adaptive systems
Communication systems
Digital communications
Propagation models
Channel simulation
Signal processing

AGARD Conference Proceedings No.363
Advisory Group for Aerospace Research and Development, NATO
PROPAGATION INFLUENCES ON DIGITAL TRANSMISSION SYSTEMS – PROBLEMS AND SOLUTIONS
Edited by Dr John H.Blythe
Published October 1984
534 pages

These Proceedings for the 34th Symposium Meeting of the AGARD Electromagnetic Wave Propagation Panel contain the papers presented, session summaries, session chairmen reports, and discussions that followed the presentations of papers. Nine papers were presented in the session on propagation constraints to reliable digital

P.T.O.

AGARD-CP-363

Digital transmission
Multipath effects
Radio noise
Man-made interference
Signalling scheme
Sounding schemes
Adaptive systems
Communication systems
Digital communications
Propagation models
Channel simulation
Signal processing

communications. A total of eleven papers were presented in the two sessions devoted to recent progress in propagation measurements and propagation models. The channel simulation session presented five papers. The Avionics Panel helped organize seven papers for the session on signal processing technology. During the final session on signalling and sounding schemes for reliable digital communications eight papers were presented.

The Symposium reviewed propagation effects which have an influence on the performance of digital systems, including: noise levels, and system sensitivities to noise; man-made interference types and system sensitivities to man-made interference; and multipath effects, dispersion, fading rates, medium coherent bandwidth, channel models, and system sensitivities to these effects. The meeting also reviewed systems designed to counter the above effects, including the various kinds of adaptive systems, and assessed the performance improvements which can be provided.

Papers presented at the Electromagnetic Wave Propagation Panel Symposium held in Athens, Greece, 4—8 June 1984.

ISBN 92-835-0367-8

communications. A total of eleven papers were presented in the two sessions devoted to recent progress in propagation measurements and propagation models. The channel simulation session presented five papers. The Avionics Panel helped organize seven papers for the session on signal processing technology. During the final session on signalling and sounding schemes for reliable digital communications eight papers were presented.

The Symposium reviewed propagation effects which have an influence on the performance of digital systems, including: noise levels, and system sensitivities to noise; man-made interference types and system sensitivities to man-made interference; and multipath effects, dispersion, fading rates, medium coherent bandwidth, channel models, and system sensitivities to these effects. The meeting also reviewed systems designed to counter the above effects, including the various kinds of adaptive systems, and assessed the performance improvements which can be provided.

Papers presented at the Electromagnetic Wave Propagation Panel Symposium held in Athens, Greece, 4—8 June 1984.

ISBN 92-835-0367-8

communications. A total of eleven papers were presented in the two sessions devoted to recent progress in propagation measurements and propagation models. The channel simulation session presented five papers. The Avionics Panel helped organize seven papers for the session on signal processing technology. During the final session on signalling and sounding schemes for reliable digital communications eight papers were presented.

The Symposium reviewed propagation effects which have an influence on the performance of digital systems, including: noise levels, and system sensitivities to noise; man-made interference types and system sensitivities to man-made interference; and multipath effects, dispersion, fading rates, medium coherent bandwidth, channel models, and system sensitivities to these effects. The meeting also reviewed systems designed to counter the above effects, including the various kinds of adaptive systems, and assessed the performance improvements which can be provided.

Papers presented at the Electromagnetic Wave Propagation Panel Symposium held in Athens, Greece, 4—8 June 1984.

ISBN 92-835-0367-8

END

FILMED

6-85

DTIC

NATO ✈ OTAN
7 RUE ANCELLE 92200 NEUILLY SUR SEINE
FRANCE
Telephone 745 08 10 · Telex 610176

DISTRIBUTION OF UNCLASSIFIED AGARD PUBLICATIONS

AGARD does NOT hold stocks of AGARD publications at the above address for general distribution. Initial distribution of AGARD publications is made to AGARD Member Nations through the following National Distribution Centres. Further copies are sometimes available from these Centres, but if not may be purchased in Microfiche or Photocopy form from the Publication Agencies listed below.

NATIONAL DISTRIBUTION CENTRES

BELGIUM
Coordonnateur AGARD – VSL
Etat-Major de la Force Aérienne
Quartier Reine Elisabeth
Rue d'Evere 1140 Bruxelles

CANADA
Defence Scientific Information Services
Dept of National Defence
Ottawa, Ontario K1A 0K2

DENMARK
Danish Defence Research Board
Ved Idraetsparken 4
2100 Copenhagen Ø

FRANCE
O.N.E.R.A. (Direction)
29 Avenue de la Division Leclerc
92320 Chatillon

GERMANY
Fachinformationszentrum Energie,
Physik, Mathematik GmbH
Kernforschungszentrum
D-7514 Eggenstein-Leopoldshafen

GREECE
Hellenic Air Force General Staff
Research and Development Directorate
Holargos, Athens

ICELAND
Director of Aviation
c/o Flugrad
Reykjavik

ITALY
Aeronautica Militare
Ufficio del Delegato Nazionale all'AGARD
3 Piazzale Adenauer
00144 Roma/EUR

LUXEMBOURG
See Belgium

NETHERLANDS
Netherlands Delegation to AGARD
National Aerospace Laboratory, NLR
P.O. Box 126
2600 AC Delft

NORWAY
Norwegian Defence Research Establishment
Attn: Biblioteket
P.O. Box 25
N-2007 Kjeller

PORTUGAL
Portuguese National Coordinator to AGARD
Gabinete de Estudos e Programas
CLAFA
Base de Alfragide
Alfragide
2700 Amadora

TURKEY
Department of Research and Development (ARGE)
Ministry of National Defence, Ankara

UNITED KINGDOM
Defence Research Information Centre
Station Square House
St Mary Cray
Orpington, Kent BR5 3RE

UNITED STATES
National Aeronautics and Space Administration (NASA)
Langley Field, Virginia 23365
Attn: Report Distribution and Storage Unit

THE UNITED STATES NATIONAL DISTRIBUTION CENTRE (NASA) DOES NOT HOLD STOCKS OF AGARD PUBLICATIONS, AND APPLICATIONS FOR COPIES SHOULD BE MADE DIRECT TO THE NATIONAL TECHNICAL INFORMATION SERVICE (NTIS) AT THE ADDRESS BELOW

PURCHASE AGENCIES

Microfiche or Photocopy

National Technical
Information Service (NTIS)
5285 Port Royal Road
Springfield
Virginia 22161, USA

Microfiche

ESA Information Retrieval Service
European Space Agency
10, rue Mario Nikis
75015 Paris, France

Microfiche or Photocopy

British Library Lending
Division
Boston Spa, Wetherby
West Yorkshire LS23 7BQ
England

Requests for microfiche or photocopies of AGARD documents should include the AGARD serial number, title, author or editor, and publication date. Requests to NTIS should include the NASA accession report number. Full bibliographical references and abstracts of AGARD publications are given in the following journals:

Scientific and Technical Aerospace Reports (STAR)
published by NASA Scientific and Technical
Information Branch
NASA HQ (CR-1) (STAR-10)
Washington DC 20546, USA

Government Reports Announcements (GRA)
published by the National Technical
Information Services, Springfield
Virginia 22161, USA

Printed by Specialised Printing Services Limited
40 Chigwell Lane, Loughton, Essex IG10 3TZ

END

FILMED

6-85

DTIC